REPORT AOK 63-0001
31 JANUARY 1963

A STUDY OF EARLY MANNED INTERPLANETARY MISSIONS
FINAL SUMMARY REPORT

CONTRACT NO. NAS 8-5026

Prepared for
GEORGE C. MARSHALL SPACE FLIGHT CENTER
(FUTURE PROJECTS OFFICE)
HUNTSVILLE, ALABAMA

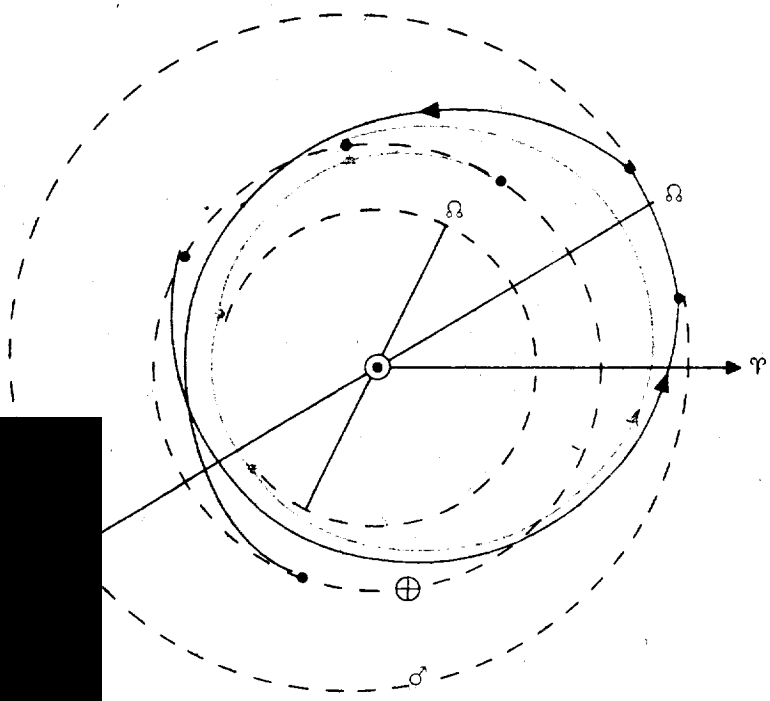

[redacted]

Prepared by
GENERAL DYNAMICS | ASTRONAUTICS
(ADVANCED STUDIES OFFICE)
SAN DIEGO, CALIFORNIA

FOREWORD

This report documents the results of work performed under Contract NAS 8-5026. Work was initiated in March 1962 and continued through January 1963. Definitive conclusions are presented, based upon the ground rules established. Included in this report is a developmental cost breakdown as required by the contractual work statement. This report has a classified addendum, under the same report number, which contains the results of a radar mapping system study and a nuclear propulsion system study.

TABLE OF CONTENTS

1	Introduction and Principal Conclusions (K. A. Ehricke)
PART I	MISSION ORIENTED STUDIES
2	Interplanetary Mission Profile Survey (K. A. Ehricke)
3	The Target Planets (Dr. D. Garber)
4	The Interplanetary Environment (D. Robey)
5	Mission Objectives (K. A. Ehricke)
6	Mission Analysis (K. A. Ehricke)
7	Performance Analysis (K. A. Ehricke)
PART II	VEHICLES AND CREW
8	The Vehicles (F. D'Vincent, K. A. Ehricke, B. Evans, Dr. D. Garber W. Mitton, B. Oman, E. Spier, B. Strobl)
9	Crew and Life Support (K. A. Ehricke)
10	Ecological Life Support System (T. J. Linzey, W. A. Johnson)
11	Artificial Gravity for Interplanetary Ships (F. D'Vincent)
12	Crew Radiation Protection (D. Robey)
PART III	SYSTEMS INTEGRATION, OPERATIONS, PLANNING
13	Mission Modes (K. A. Ehricke)
14	Pre-Launch and Launch Operations (B. Brown)
15	Space Mating (F. D'Vincent)
16	Sequence of Events (K. A. Ehricke)
17	Emergency and Rescue (K. A. Ehricke)
18	Principal Development Tasks, Schedules and Cost Estimates (K. A. Ehricke)
19	References

SECTION 1

INTRODUCTION

1.1 DEFINITION OF EMPIRE STUDY. The EMPIRE study is concerned with Early Manned Planetary-Interplanetary Roundtrip Expeditions. The purpose of the study is to provide deeper insight into the problems involved in the tremendous undertaking of manned missions to the vicinity, and where possible to the surface, of other planets. Since missions of this kind may be only 10 to 12 years away, it is quite realistic to start considering them seriously at this time. Therefore, General Dynamics/Astronautics welcomed the opportunity to participate in this study.

Primary emphasis was to be placed on capture missions. The practical feasibility of undertaking such missions was to be investigated, assuming chemical and nuclear heat exchanger engines and defining the propulsion systems required. Operational aspects, including emergency conditions, and a variety of mission modes were to be considered. Vehicle design considerations were to include all important subsystems, specifically propulsion structure, life support system, Earth entry vehicle, cryogenic storage, communications, power supply, and guidance. The scientific mission aspects were to be investigated. Finally, a development plan and a funding plan were to be included.

In relation to other key development programs, it is the objective of the EMPIRE study to contribute to a definition of requirements for a Post-Saturn Earth Launch Vehicle (ELV), to furnish potential goals for operational nuclear engines and to investigate the requirements and lead times, in general, for the development of an initial manned planetary exploration.

1.2 PRINCIPAL CONCLUSIONS. The following study conclusions are presented:

a. Particularly favorable mission periods to Mars exist in 1973 and 1975. Thereafter conditions become less favorable from the standpoint of mission energy requirement as well as solar activity. Conditions become favorable again in 1984 on both counts.

b. With nuclear powered vehicles having specific impulses in the lower 800-sec region, roundtrip missions can be flown which permit a planetary capture period of 30 to 50 days at a total mission period which most frequently lies between 400 and 450 days for Mars and between 350 and 400 days for Venus missions.

c. The orbital departure weights of the nuclear ships for these missions vary in comparatively wide limits, because of the many variables involved. Given a crew of eight and an initial payload of the order of 100,000 lb, the orbital departure weight of the complete ship tends to fall into the 1200 to 1400 metric ton (t) region

(2.5 to 3 $\times 10^6$ lb) for Mars and into the 500 to 700 t category (1.2 to 1.5 $\times 10^6$ lb) for Venus.

d. The energy requirement for capture missions can be reduced considerably (20 to 33 percent) by entering an elliptic rather than a circular capture ellipse. Ellipticities of interest range from $n = r_A/r_P = 4$ to $n = 20$. Most of the energy (hence, departure weight) saving is realized between $n = 1$ (circular capture) and $n = 4$ (about 25 percent).

For Venus, for which manned surface excursion during the capture period would not be considered, and where planetary surface reconnaissance must rely on high-resolution radar measurements, elliptic capture orbits up to $n = 20$ are of potential interest. The azimuth resolution of the radar system can be independent of altitude so that essentially only the power requirement, which increases rapidly with altitude, appears to be the limiting factor.

For Mars, with consideration preserving the manned surface excursion capability, the region $1 < n \lesssim 4$ is of interest.

In all cases, when elliptic capture orbits (especially for large n-values) are used, separate predeparture maneuvers might have to be carried out for the purpose of rotating the major axis of the ellipse in such a manner that departure near the periapsis is assured (this is above and beyond a possible plane change maneuver which preferably is combined with the departure maneuver proper for reasons of propellant economy). Departure near the apoapsis, or significantly ($>90^\circ$) off the periapsis, should be avoided since it tends to reduce or offset the energy advantage gained by using an elliptic capture orbit in the first place.

e. Compared to capture orbit ellipticity, all other means of reducing the orbital launch weight are less effective. For example, eliminating the Earth capture retromaneuver (whose purpose it is to replace the planetary entry conditions by Apollo entry conditions) and entering hyperbolically was found to reduce the launch weight by only 10 to 15 percent for the mission profiles and propulsion system (high-p_c O_2/H_2 for the capture engines). Reduction in crew size (standard size is 8 persons) from 8 to 6 or 4 is comparatively even less effective because the heavy radiation shield weight is not very sensitive to variation in crew size.

Nevertheless, by combining high-eccentricity capture orbits with drastic reduction in crew size, very low departure weights can be obtained, even for all chemical ships. For example, a four-man Venus ship (1973 mission) capturing in an $n = 20$ orbit has an orbital departure weight of 436 t (962,000 lb) although it is chemically propelled (high-p_c O_2/H_2, $I_{sp} = 455$ sec) for all maneuvers). An all-chemical two-man Venus ship for the same conditions weighs 320 t (700,000 lb) at departure.

f. It is concluded that the crew number should not be reduced below six and that the preferred minimum is eight, because it leaves the flight commander and the flight surgeon outside the duty cycle and retains therewith a reserve capability. Interplanetary ships with four or two men aboard definitely must travel in crew vehicle convoys for mutual support; even then, it must be accepted that for several hours in a particular ship nobody is on control room duty. Depending on the degree of surface excursion effort planned and on the length of the capture period, the crew size is more likely to grow beyond eight than to decrease.

g. When nuclear vehicles are used it is advantageous to concentrate the crew in one vehicle. The convoy consists in this case of a crew vehicle and one or two service vehicles carrying auxiliary vehicles, spares and contingency fuel and serving as emergency crew vehicles. The reason for this is crew safety against side radiation from the reactors of ships in the convoy. If only one ship contains the crew, this vehicle takes the lead. The others, which are far less radiation sensitive, are lined up behind it. Engine ignition sequencing makes sure that a service vehicle cannot pass the crew vehicle.

h. The convoy vehicles (crew and service vehicles) are strictly modularized, standardized and designed to be as easily exchangeable as possible under given conditions. Thereby the crew is offered maximum flexibility to cope with emergencies in a variety of ways (parts exchange, propellant transfusion, or weight reduction). Even the crew section is modularized and orbital equipment arranged so that part of it can be sacrificed if necessary. The crew modules as a whole can be transferred from the crew ship, if it has to be abandoned, to any one of the service vehicles (the "head" which is most heavily protected can be placed on a new "body" to improve crew survival probability).

i. Nuclear propulsion is most important for missions of this type. It is most desirable from the systems engineer's viewpoint to have a mission engine (engine attached to the planetary ship proper, in distinction from the engines attached to the escape booster) which 1) has a long operational life (order of 10-20 hours) and 2) ready restart capability at any time following an engine shut-off. These two characteristics in an engine of 820 to 850 sec specific impulse are more important than an I_{sp} gain of 20 to 30 seconds.

j. If the engine operational life is restricted to one hour or less, the pacing criterion for engine thrust selection is no longer gravitational loss, but staying within the lifetime limitations. This requirement imposes in any case a thrust level at which gravitational losses are no longer significant.

With a short-life engine, the most desirable thrust level lies at 200 to 250 k. The reason for this specification is that it assures compatibility between a, say, one-hour engine life, and duration of a given individual maneuver for all practical mission profiles. It is also a good size for clustering three to four engines to

drive the escape booster. On the other hand, if the engine can be throttled by 30 to 50 percent, this engine is still not yet to heavy to be used on M-3 (target planet escape propulsion section).

k. Even though the total mission velocity requirement for two missions may be similar or alike, the departure weights may be noticeably different, because the velocity distribution over the four major maneuvers (two escape, two capture maneuvers) are different. A comprehensive (but not yet sufficiently exhaustive) investigation showed that it is best to have a fairly even velocity distribution, because of several mutually counteracting factors involved which are discussed in Paragraph 7-14. It turns out that if any maneuver should require a higher mass ratio it is best to be M-3 (target planet escape maneuver).

l. Cometary and meteoritic matter still represent unknown hazards to interplanetary missions (perhaps the least known ones). For this reason a study of cometary distribution is included which may serve as the starting point for more extensive investigations by NASA's Space Sciences Office. It was found that the chance for the convoy to pass through the coma of a new comet (i.e., one whose elements are not yet known) is no more than about 1/6000 per year. The distribution of comet perihelion on the celestial sphere (Figure 4-12) suggests that new comets may come from almost any direction.

   The lack of knowledge about meteor streams which do not intersect the Earth's orbit is perhaps the most critical aspect of the question of hazards from extra-terrestrial debris. The fact that Mariner II fared so well on its way to Venus is reassuring, but by no means conclusive. It is here where the NASA Space Sciences Office can contribute most significantly to a higher confidence level in the design and probability-of-success analysis of the manned convoy, by sending long-term probes into heliocentric orbits in cis-Martian and cis-Venusian space. This need has been taken into consideration in the EMPIRE Program Schedule (Figure 18-3).

m. Preliminary schedule analysis strongly indicates that a 1975 mission to Venus or Mars is in the realm of realistic technological planning; the most critical technical item is the nuclear engine (cf. its schedules in the classified addendum to this report).

n. The most critical nontechnical item is money. A preliminary cost analysis which included the development of a 10^6-lb payload Post-Saturn Earth Launch Vehicle ($4 Billion) indicates a total funding requirement between FY-65 and FY-75 of close to $18.5 billion; i.e., an average of almost $2 billion per annum. Peak funding requirements of around $2.5 billion per annum occur in the FY-period of 1968-70 (CY 1969-71). By eliminating the Post-Saturn ELV development and the nuclear engine development the development cost can be cut by at least $6 billion,

albeit at the price of a severe reduction in mission capability. The interplanetary ship would have to operate chemically. Several crew ships would be required because the individual vehicle crew would likely be too small. Capture orbit would have to be fly-by. The latter offers no significant performance reduction over an n = 20 capture ellipse.

o. An initial mission mode analysis has been performed (Section 13) which will be extended considerably during follow-on investigations to carefully appraise each combination of mission modes. The investigation shows how much further reduction in orbital launch weight is possible at the price of additional mating or fuel transfer activities en route. It is too early at this point in the investigation to present a firm conclusion.

PART I

MISSION ORIENTED STUDIES

SECTION 2

INTERPLANETARY MISSION PROFILE SURVEY

2.1 DYNAMICS OF EARTH AND TARGET PLANETS. The improvement of the value of the astronomical unit (A.U.), by the JPL radar reflection measurements on Venus, permits a more accurate computation of the orbital velocities of Earth and the planets. Table 2-1 summarizes these for Venus, Earth and Mars.

Table 2-1. Planetary Velocity Data Based on a Solar Gravitational Parameter $K_\odot$, Computed from 1 A.U. = $149.598845 \cdot 10^6$ km (JPL, 1962)

		KM^3/SEC^2	FT^3/SEC^2	$A.U.^3/SEC^2$
	$K_\odot$	13.27154×10^{10}	$46,8677079 \times 10^{20}$	3.964027×10^{-14}
PLANET	VELOCITY	KM/SEC	10^4 FT/SEC	10^{-7} A.U./SEC
Venus	U_a	35.0209	11.4898	2.3410
	U_P	35.2597	11.5681	2.3569
	U_A	34.7838	11.4120	2.3251
Earth	U_a	29.7849	9.7719	1.9910
	U_P	30.2872	9.9367	2.0246
	U_A	29.2907	9.6098	2.5271
Mars	U_a	24.1295	7.9165	1.6129
	U_P	26.4981	8.6936	1.7713
	U_A	21.9726	7.2088	1.4688

$U_a = \sqrt{K_\odot/a}$ = mean orbital velocity of planet

U_P = perihelion velocity

U_A = aphelion velocity

The ephemerides of Venus, Earth and Mars have been extended to the year 2000, using the 7090 computer, defining the heliocentric elliptic coordinates, referred to the equinox of 1 January 1960. This leads to slight errors, of the order of 0.25 degree in position for the 1990-2000 period, but permits the definition of nodal passages, inferior conjunction (Venus) and oppositions (Mars) with adequate accuracy for the

purposes of this study. The machine-interpolated dates for the above events are presented in Tables 2-2 through 2-5 and in Figures 2-1 and 2-2. Figures 2-3 through 2-8 show the variation of transfer time, transfer angle and position angles as functions of the eccentricity of transfer orbit to Venus and Mars for the simplified case of coplanar circular planet orbits, which is adequate to illustrate the trends discussed in this and the subsequent section. Comparison of the position angles at departure ($\psi_2 \gtrless 0$, depending on whether target planet leads or trails) and at arrival ($\psi_2 \gtrless 0$, depending on whether target planet leads or trails) shows that during these transfers, which are representative of those considered in this study, inferior conjunctions or oppositions take place. In fact, for short transfer orbits, departure to Venus may occur while Venus and Earth are near an inferior conjunction ($\psi_1 \rightarrow 0$), or arrival at Mars may occur while the two planets are near opposition ($\psi_2 \rightarrow 0$). The heliocentric longitude at which these events occur is, therefore, indicative of the orientation of the nodal line of the transfer orbit relative to that of the target planet. If the angle between these two nodal lines is small, most transfer orbits (especially the shorter ones) are little inclined. If the angle between these nodal lines approaches 90 degrees, most transfer orbits, particularly the short ones, are steeply inclined and require a correspondingly larger amount of transfer energy. Therefore, if the inferior conjunction or the opposition takes place near the nodes, transfer will generally be less expensive than if it occurs at points near 90 degrees off the nodal line of the planet.

Therefore, the position of the target planet with respect to the nodes at arrival (or departure) time has an important influence on the transfer energy requirement. This is generally true, independent of target orbit inclination; if the arrival point is located at 90 degrees off one of the nodes and the transfer angle is to be a maximum, then the transfer orbit plane must be normal to the ecliptic, no matter what the target orbit inclination. To be a maximum, certain constellational requirements must be satisfied at departure. As the departure constellation differs, the transfer orbit becomes shorter or longer. In these cases the absolute value of the inclination becomes a significant factor, since it determines the change in celestial latitude (heliocentric ecliptic system) which is associated with the particular transfer orbit. The higher the inclination, the larger the variation in celestial latitude during one target-planet revolution and the larger the potential change in latitude during a transfer; hence, the greater the potential variation in transfer energy. Transfer energies to Venus are governed primarily by the changes in celestial latitude during transfer, since the Venus orbit is inclined by 3° 23.9′ with respect to the ecliptic. The variation of the celestial latitude of Venus during periods of interest between 1970 and 1980 is plotted in Figure 2-9. Transfer orbits selected for either low hyperbolic excess velocities at Earth departure ($v^*_{\infty 1}$) or for low values at Venus arrival ($v^*_{\infty 2}$) values close to minimum are tabulated in Table 2-6 for the corresponding time period. A few of the transfer orbits are drawn into Figure 2-9. Of the two transfer time values given in the third column, the first one belongs to the low $-v^*_{\infty 1}$ transfer orbit, the second to the low $-v^*_{\infty 2}$ transfer. The effect of the latitude

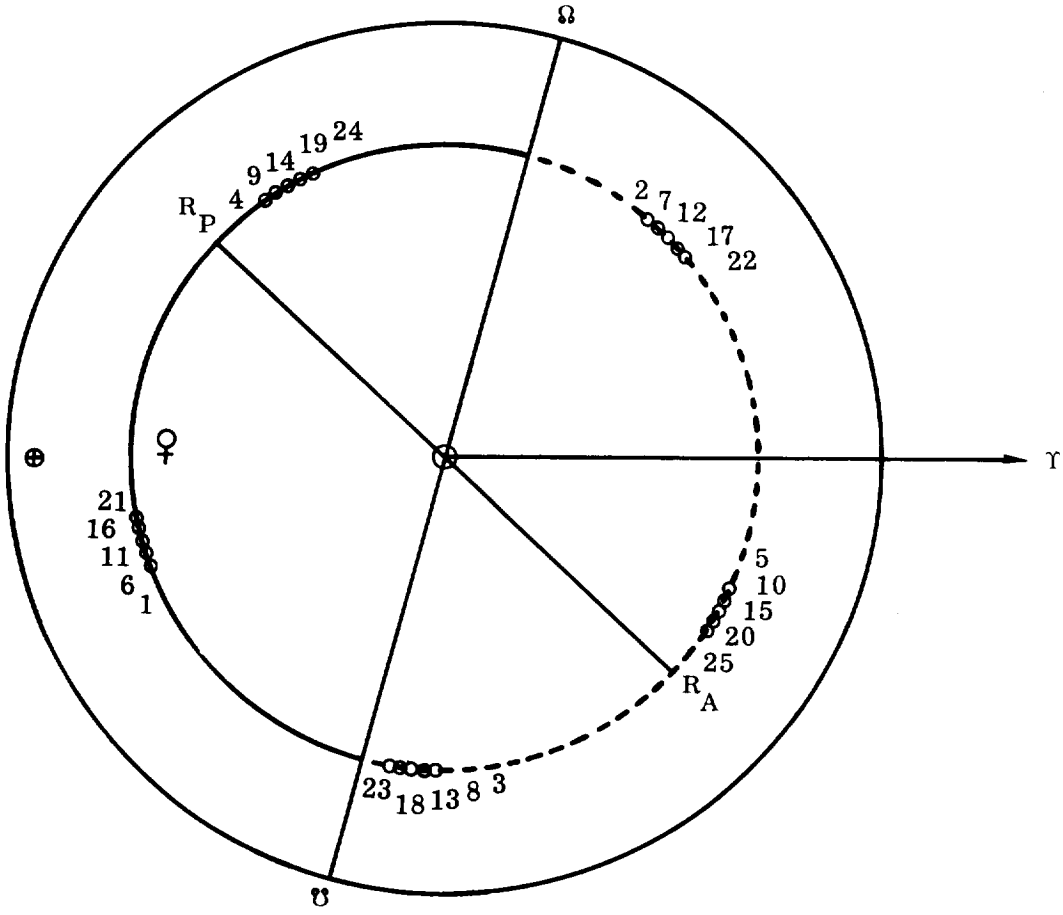

Figure 2-1. Venus Inferior Conjunctions 1961-1999

change during the transfer is clearly apparent in the case of the 1975 transfer where the transfer orbit inclination is very low and the transfer period indicates a near-Hohmann transfer. (The Hohmann transfer period between coplanar circular Earth and Venus orbit is 146 days.) In other instances (1970, for example) the effect of the comparatively low-inclination transfer is masked by the capture energy requirement, which is high because intersection angle with the Venus orbit is large due to the fast transfer. Therefore, the effect of the latitude change is more clearly apparent when comparing only the $v^*_{\infty_1}$ values.

The orbit of Mars is less inclined ($i \sim 1° 51'$), but it has a higher eccentricity (0.0934 compared to 0.0068 for Venus). Thus, for Mars, one faces a combination of the effect of latitude and of heliocentric distance. During the second half of the 1960's the celestial latitude of Mars at arrival increases while the heliocentric distance at arrival decreases. These two opposing effects keep the variation in minimum $v^*_{\infty_1}$ small, although minimum $v^*_{\infty_1}$ decreases slightly during the Sixties (Ref. 2-3). Figure 2-10 shows the variation of the celestial latitude of Mars for interesting time intervals during the 1971-1980 period. Figure 2-11 shows the corresponding variation

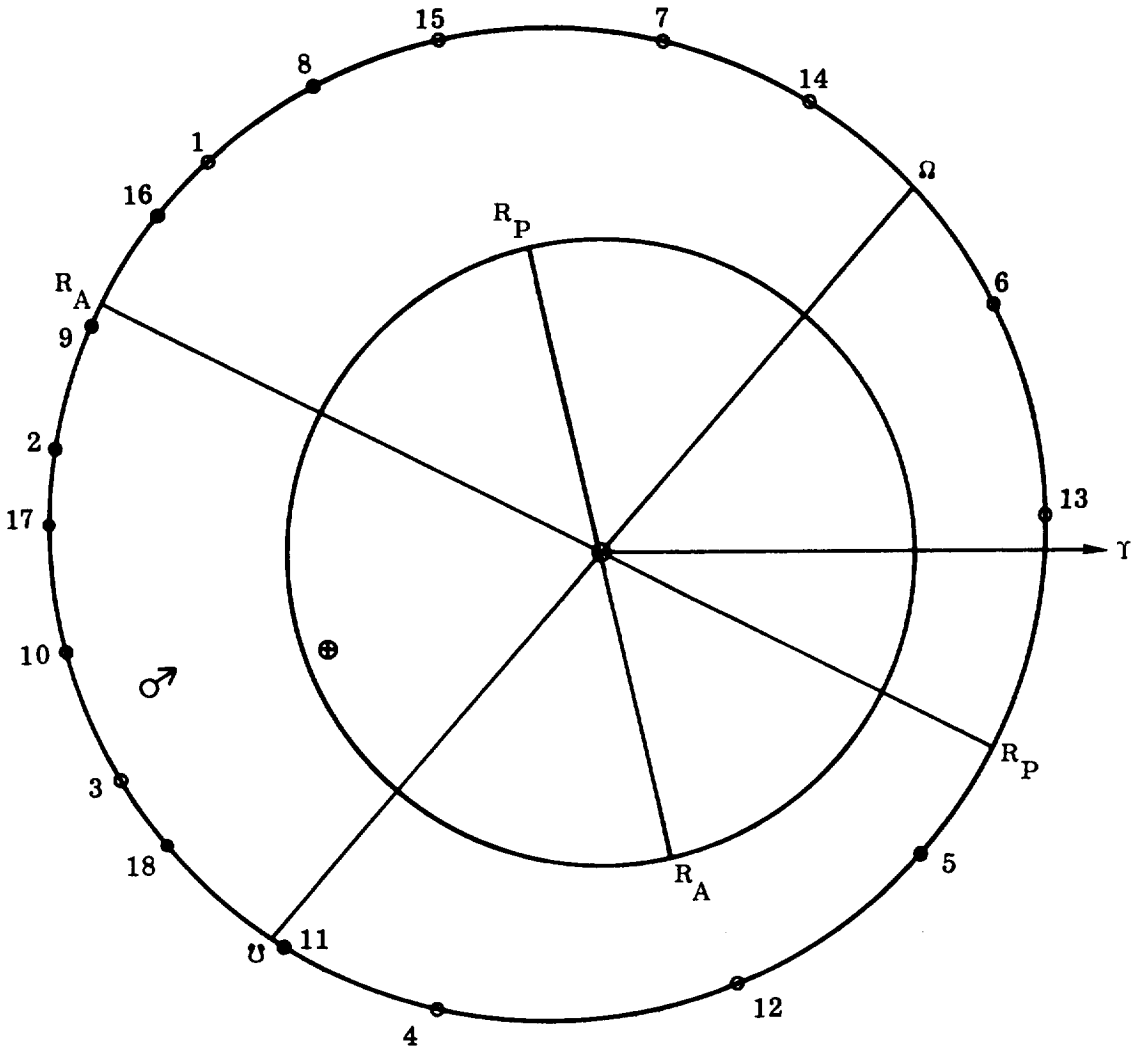

Figure 2-2. Mars Oppositions 1963-1999

in heliocentric distance. Table 2-6 lists low $-v^*_{\infty 1}$ and low $-v^*_{\infty 2}$ transfer missions. The year 1971 is seen to be exceptionally good, since the latitude of the arrival point is only b = -0.443° and the distance at arrival is $R_{♂}$ = 1.443 A.U. (perihelion distance 1.381 A.U.). In 1973, 1975 and 1977, both latitude and distance increase, causing the transfer energy to rise. In 1980 short transfer orbits are likewise quite expensive and a reduction in transfer energy can be achieved only by resorting to long transfer periods. This cannot be regarded as desirable from the viewpoint of a balanced mission evaluation.

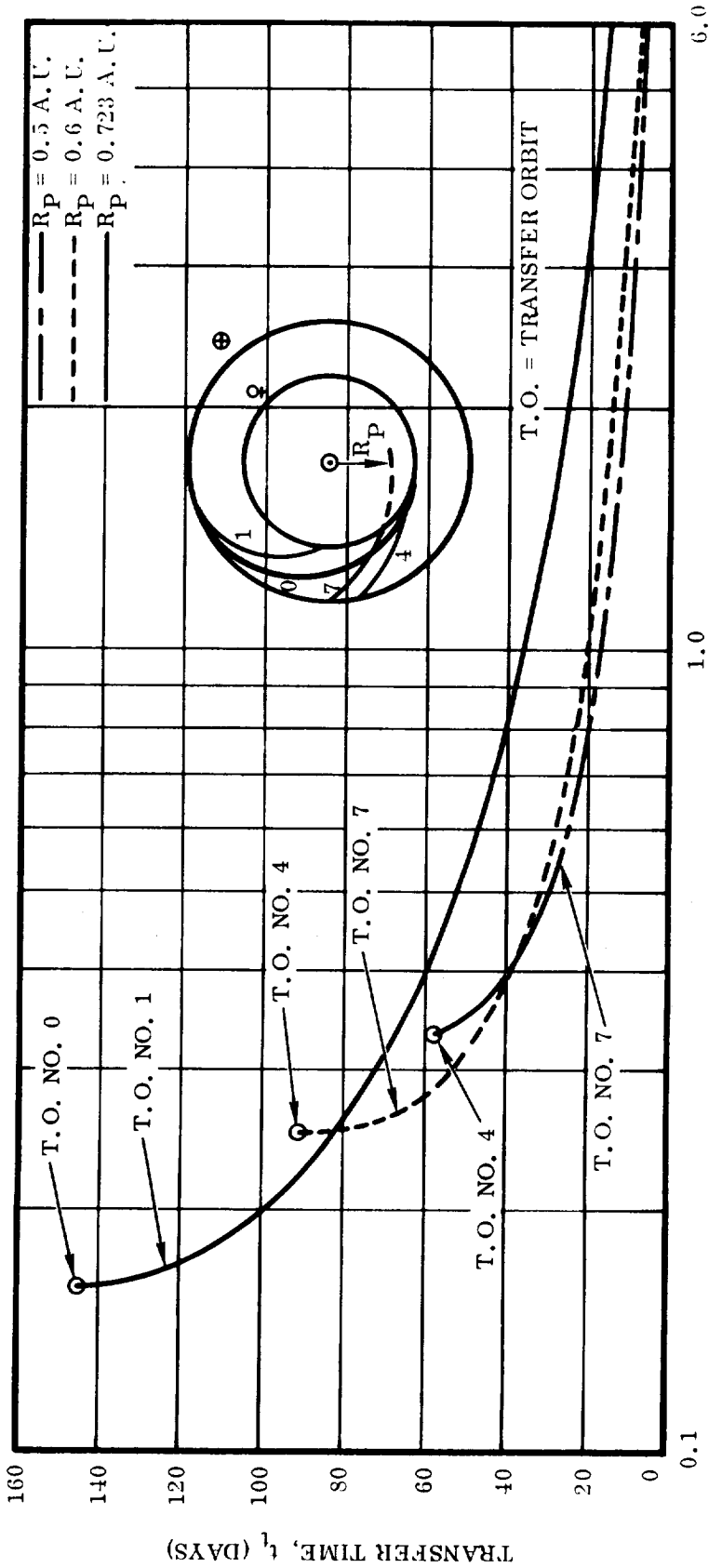

Figure 2-3. Earth – Venus Transfer Orbits No. 0, 1, 4 and 7: Heliocentric Transfer Period, t_t

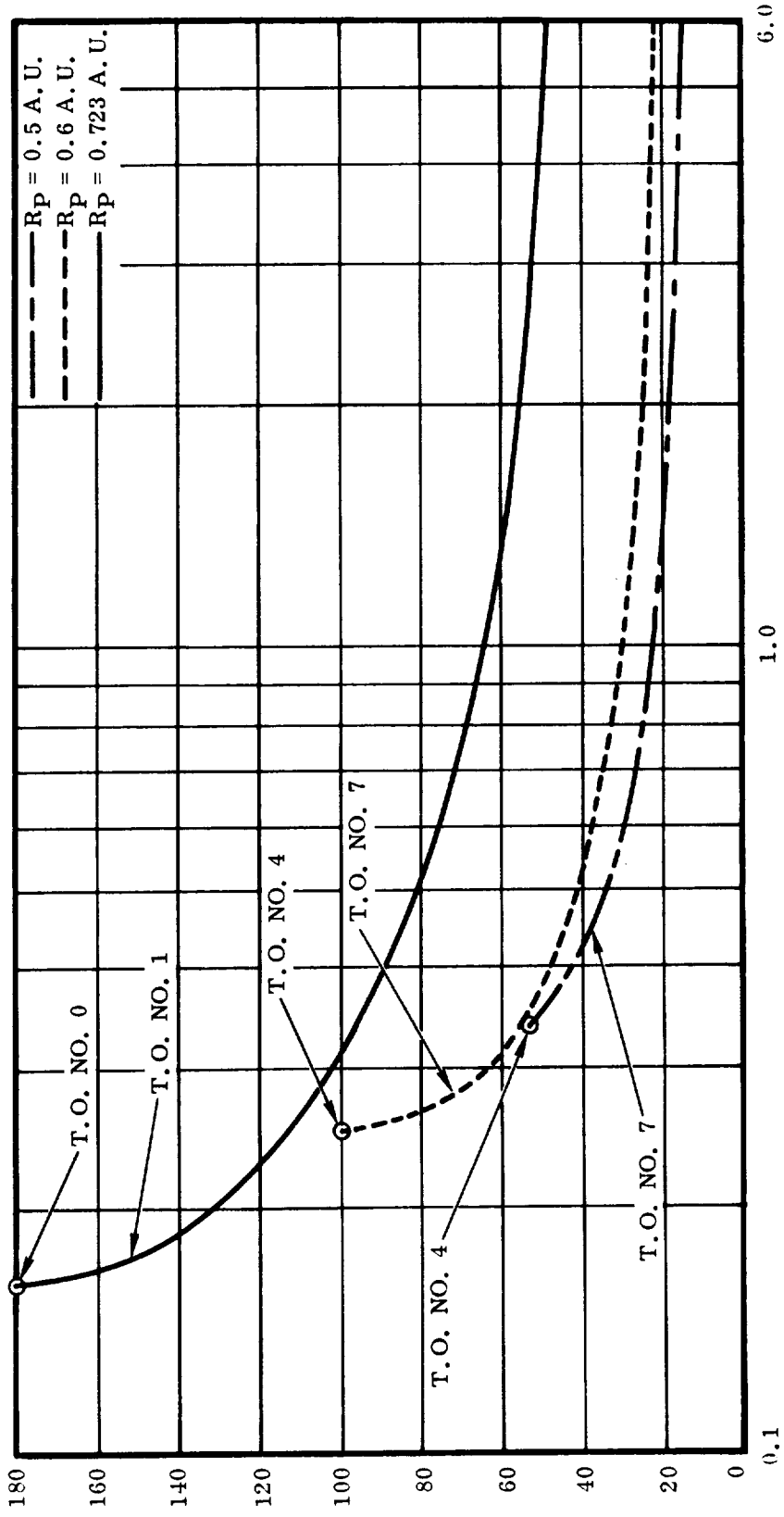

Figure 2-4. Earth – Venus Transfer Orbits No. 0, 1, 4 and 7: Heliocentric Transfer Angle, η_t

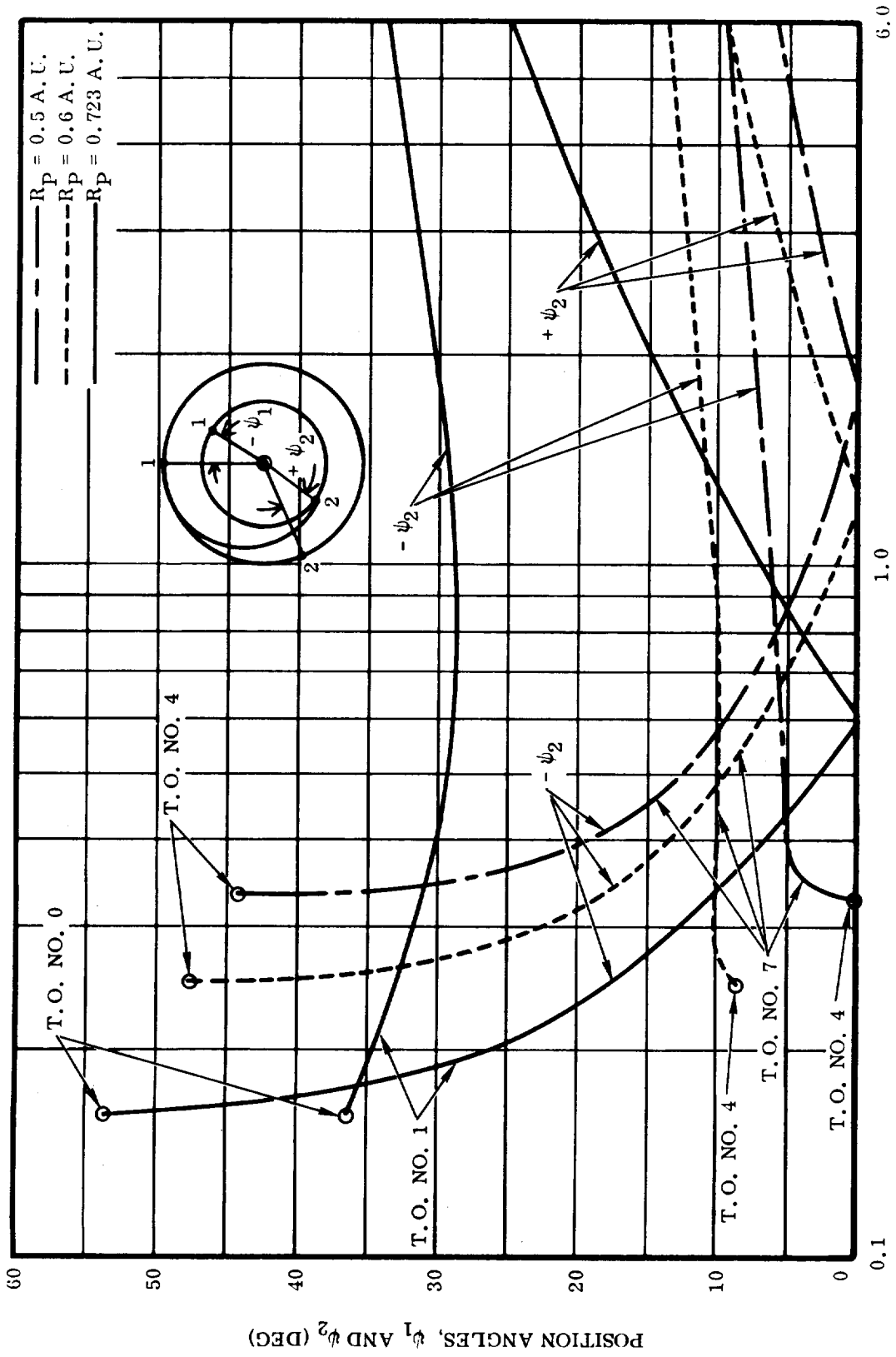

Figure 2-5. Earth = Venus Transfer Orbits No. 0, 1, 4 and 7: Target Planet Position Angles at Departure and Arrival, ψ_1 and ψ_2 (For Earth-Target Planet Transfers Angle is Positive if Target Planet Leads Earth, Negative if Target Planet Trails Earth; Signs are Reversed in Case of Target Planet-Earth Transfers)

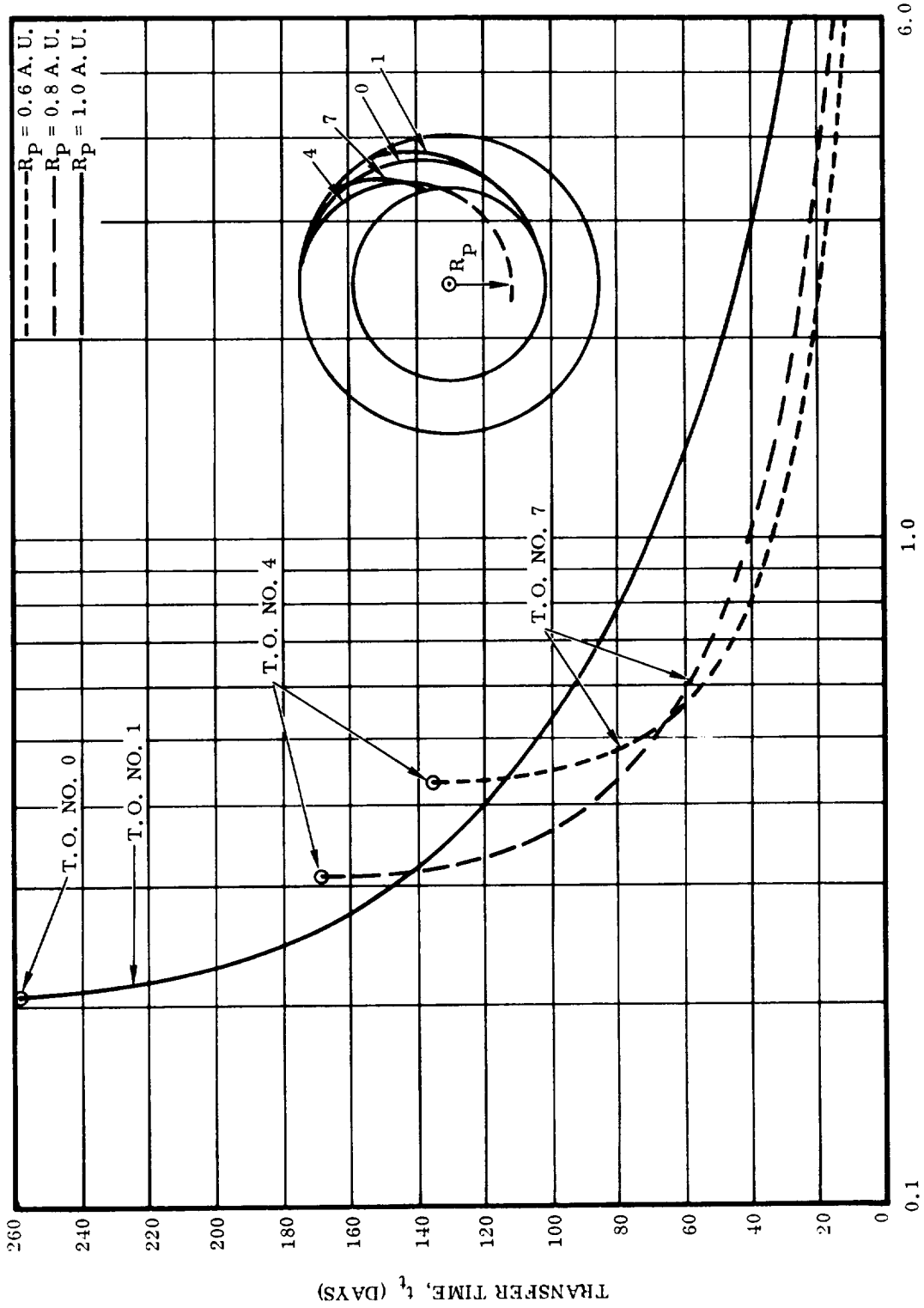

Figure 2-6. Earth ⇄ Mars Transfer Orbits No. 0, 1, 4 and 7: Heliocentric Transfer Period, t_t

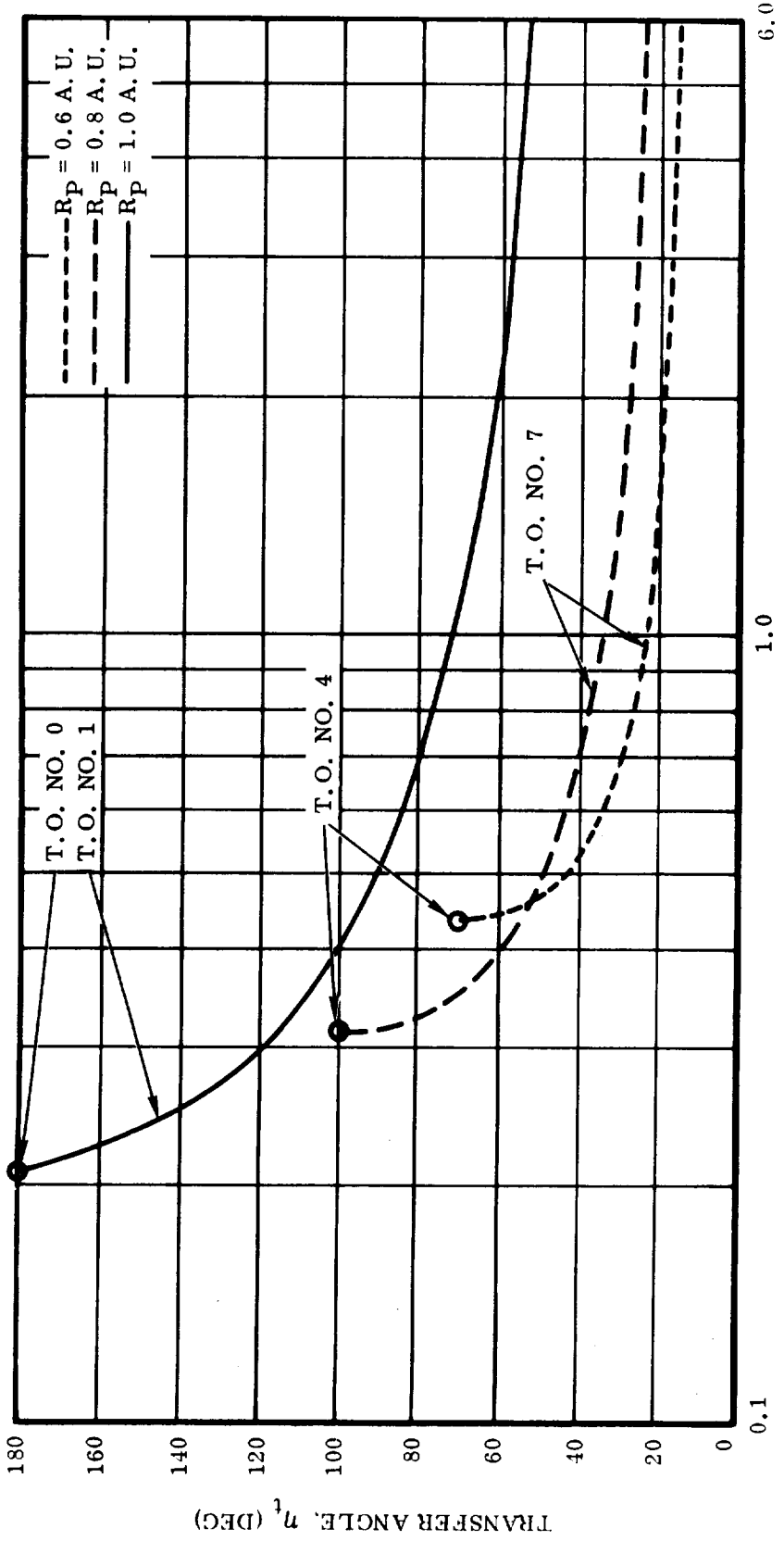

Figure 2-7. Earth ⇄ Mars Transfer Orbits No. 0, 1, 4 and 7: Heliocentric Transfer Angle, η_t

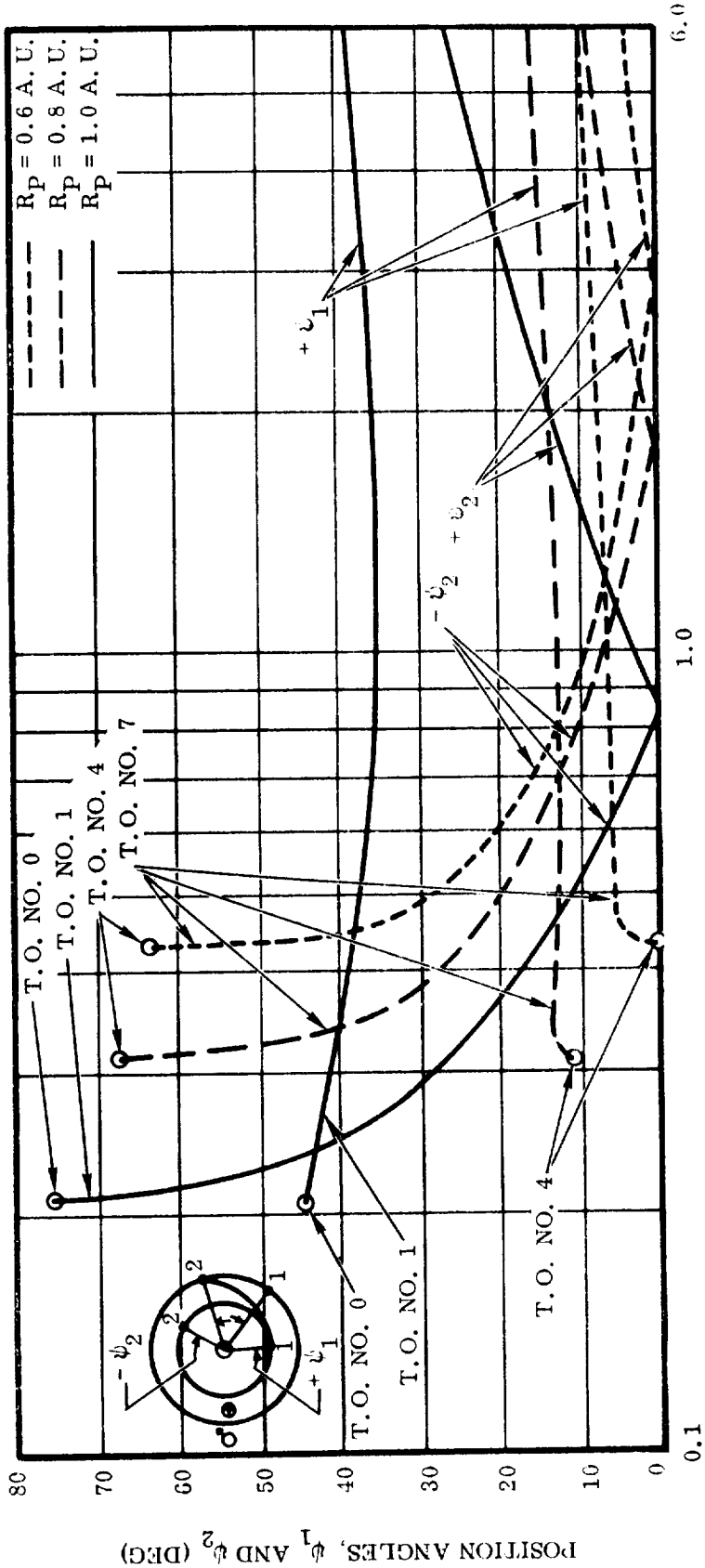

Figure 2-8. Earth ⇄ Mars Transfer Orbits No. 0, 1, 4 and 7: Target Planet Position Angles at Departure and Arrival, ψ_1 and ψ_2 (For Earth-Target Planet Transfers Angle is Positive if Target Planet Leads Earth, Negative if Target Planet Trails Earth; Signs are Reversed in Case of Target Planet-Earth Transfers)

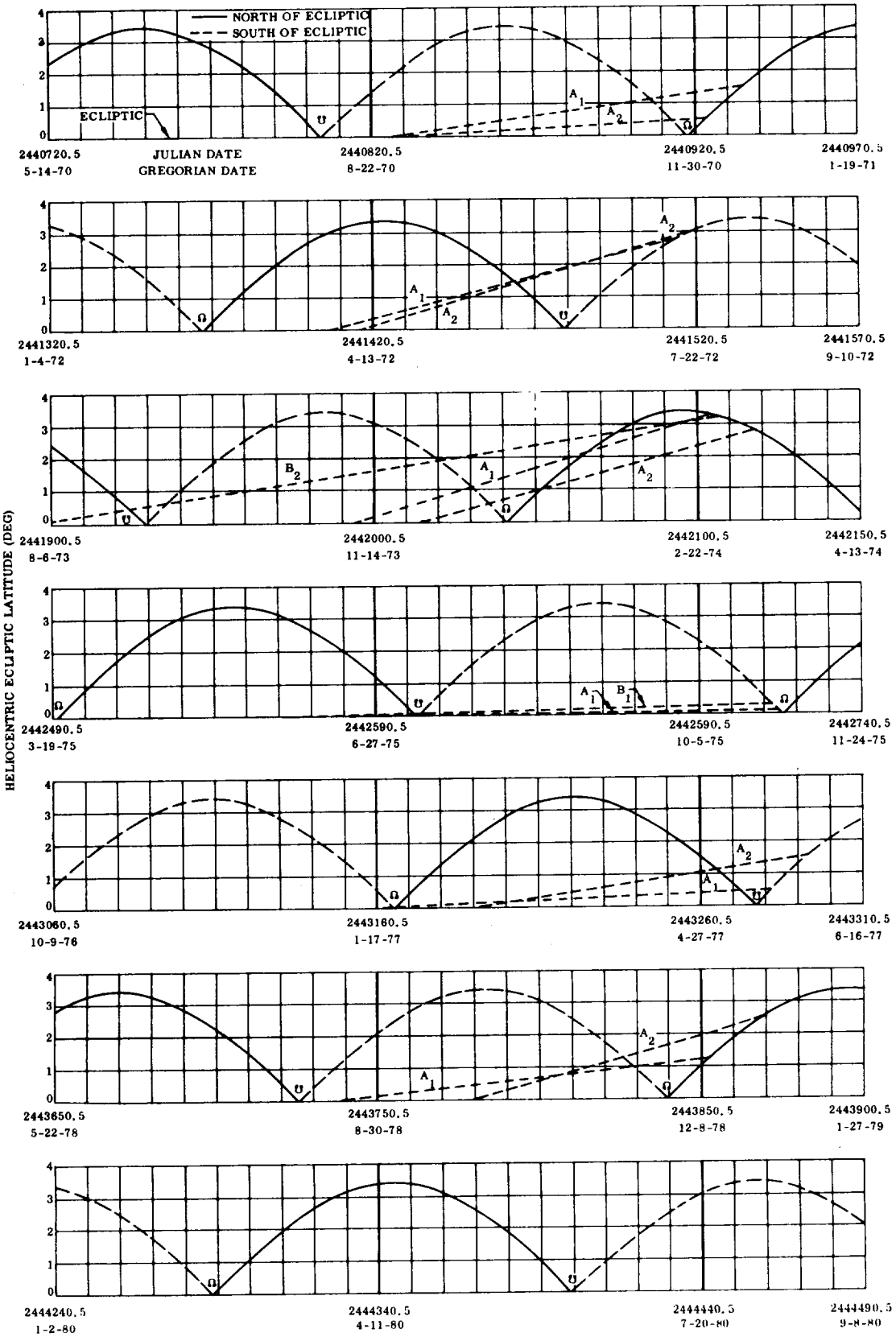

Figure 2-9. Variation of Celestial Latitude of Venus During Transfer Periods in 1970-1980 Time Period

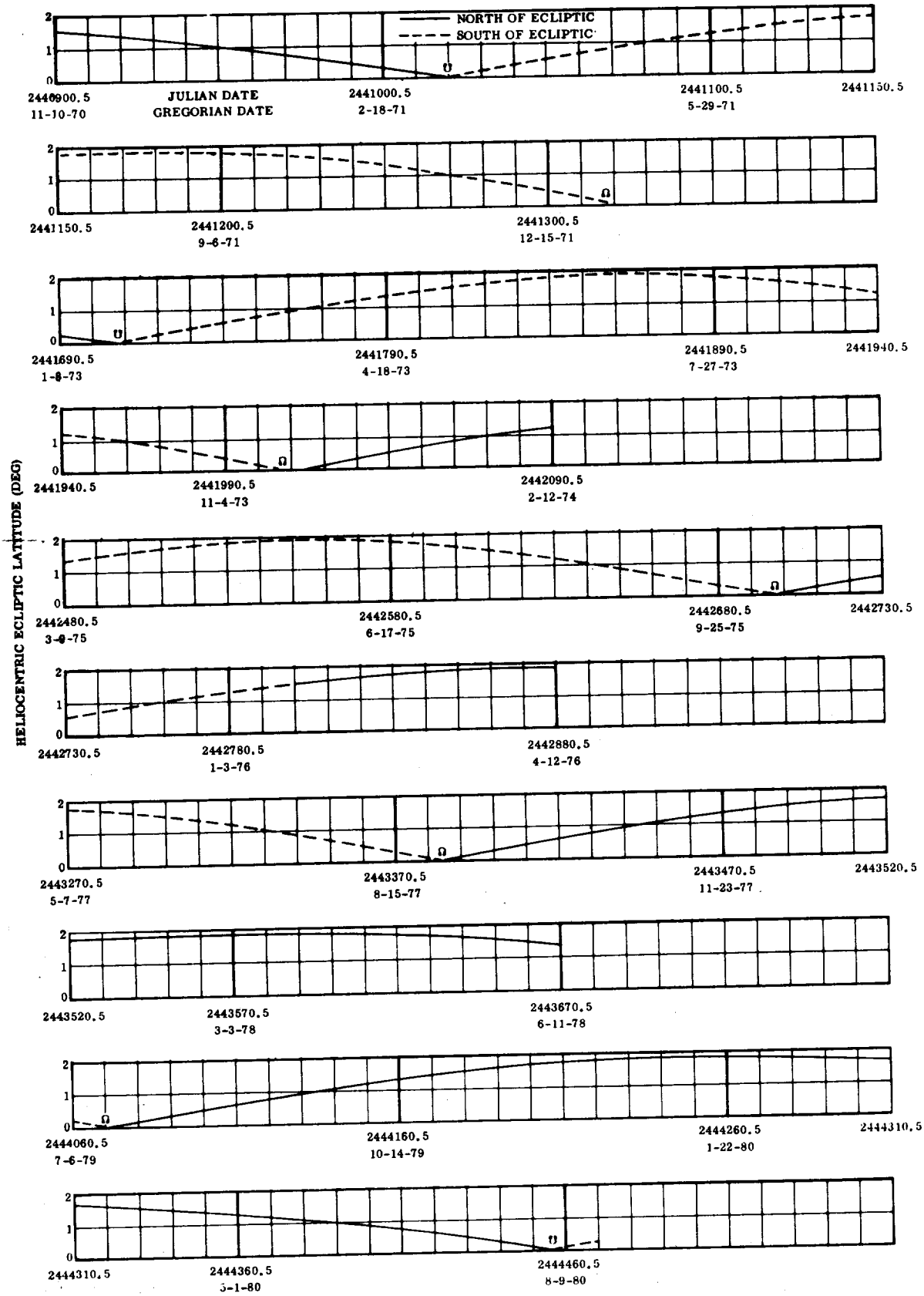

Figure 2-10. Variation of Celestial Latitude of Mars During Transfer Periods in 1970-1980 Time Period

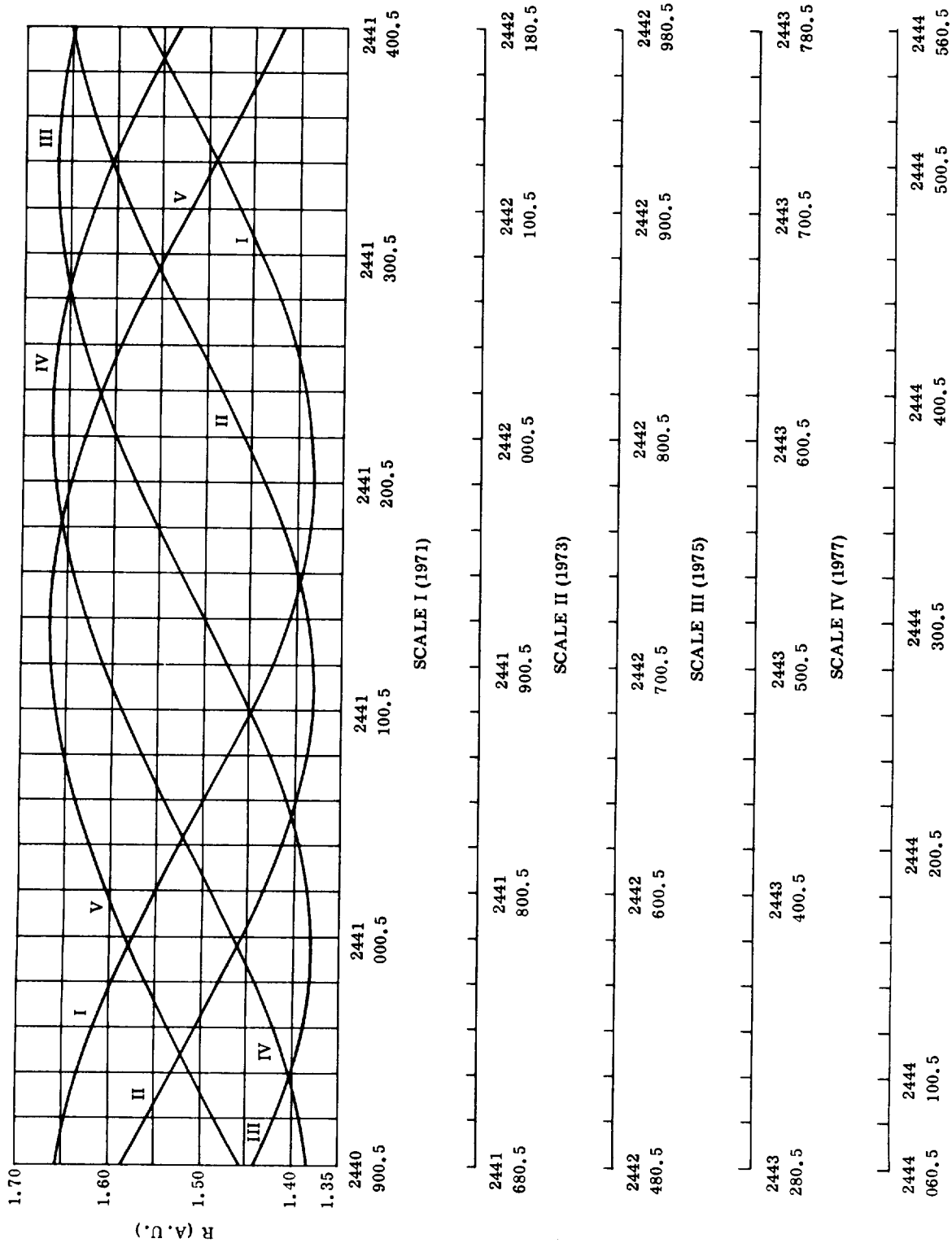

Figure 2-11. Variation of Heliocentric Distance of Mars Versus Julian Date

Table 2-2. Nodal Passages of Planet Venus for the Period 1963-1999

ASCENDING NODE, ☊				DESCENDING NODE, ☋			
Mo.	Day	Year	Julian Date	Mo.	Day	Year	Julian Date
7	11	63	2438222.45	3	20	63	2438109.31
2	21	64	8447.15	10	31	63	8334.01
10	3	64	8671.85	6	12	64	8558.71
5	16	65	8896.55	1	22	65	8783.41
12	26	65	9121.25	9	4	65	9008.11
8	8	66	9345.95	4	17	66	9232.81
3	21	67	9570.65	11	28	66	9457.51
10	31	67	9795.35	7	10	67	9682.21
6	12	68	2440020.05	2	20	68	9906.91
1	23	69	0244.76	10	2	68	2440131.62
9	4	69	0469.46	5	14	69	0356.32
4	17	70	0694.16	12	25	69	0581.02
11	28	70	0918.86	8	7	70	0805.72
7	11	71	1143.56	3	19	71	1030.42
2	20	72	1368.26	10	30	71	1255.12
10	2	72	1592.96	6	11	72	1479.82
5	15	73	1817.66	1	22	73	1704.52
12	25	73	2042.36	9	3	73	1929.22
8	7	74	2267.06	4	16	74	2153.92
3	20	75	2491.77	11	27	74	2378.63
10	30	75	2716.47	7	9	75	2603.33
6	11	76	2941.17	2	19	76	2828.03
1	22	77	3165.87	10	1	76	3052.73
9	4	77	3390.57	5	13	77	3277.43
4	16	78	3615.27	12	24	77	3502.13
11	27	78	3839.97	8	6	78	3726.83
7	10	79	4064.67	3	19	79	3951.53
2	19	80	4289.37	10	29	79	4176.23
10	1	80	4514.07	6	10	80	4400.93
5	14	81	4738.78	1	21	81	4625.63
12	24	81	4963.48	9	2	81	4850.33
8	6	82	5188.18	4	15	82	5075.03
3	19	83	5412.88	11	26	82	5299.74
10	30	83	5637.58	7	8	83	5524.44
6	10	84	5862.28	2	18	84	5749.14
1	21	85	6086.98	9	30	84	5973.84
9	3	85	6311.68	5	13	85	6198.54

Table 2-2. Nodal Passages of Planet Venus for the Period 1963-1999, Cont

ASCENDING NODE, ☊				DESCENDING NODE, ☋			
Mo.	Day	Year	Julian Date	Mo.	Day	Year	Julian Date
4	15	86	2446536.38	12	23	85	2446423.24
11	26	86	6761.08	8	5	86	6647.94
7	9	87	6985.79	3	18	87	6872.64
2	18	88	7210.49	10	28	87	7097.34
9	30	88	7435.19	6	9	88	7322.04
5	13	89	7659.89	1	20	89	7546.74
12	24	89	7884.59	9	1	89	7996.14
8	5	90	8109.29	4	14	90	7996.14
3	18	91	8333.99	11	25	90	8220.84
10	29	91	8558.69	7	8	91	8445.54
6	9	92	8783.39	2	17	92	8670.24
1	20	93	9008.09	9	29	92	8894.94
9	2	93	9232.80	5	12	93	9119.64
4	14	94	9457.50	12	22	93	9344.34
11	25	94	9682.20	8	4	94	9569.04
7	8	95	9906.90	3	17	95	9793.74
2	18	96	2450131.60	10	27	95	2450018.45
9	29	96	0356.30	6	8	96	0243.15
5	12	97	0581.00	1	19	97	0467.85
12	23	97	0805.70	9	1	97	0692.55
8	4	98	1030.40	4	13	98	0917.25
3	17	99	1255.10	11	24	98	1141.95
10	28	99	1479.81	7	7	99	1366.65

Table 2-3. Inferior Conjunctions of Planet Venus for the Period 1961-1999

NO.	MONTH	DAY	YEAR	JULIAN DATE	HELIOCENTRIC LONGITUDE (DEG)
1	4	11	61	2437400.50	200.71
2	11	12	62	7981.34	49.79
3	6	19	64	8566.45	268.45
4	1	26	66	9151.86	125.72
5	8	29	67	9732.39	335.61
6	4	8	69	2440320.13	198.34
7	11	10	70	0900.86	47.25
8	6	17	72	1486.03	266.19
9	1	23	74	2071.38	123.15
10	8	27	75	2652.05	333.30
11	4	6	77	3239.77	195.96
12	11	7	78	3820.39	44.72
13	6	15	80	4405.82	263.92
14	1	21	82	4990.92	120.75
15	8	25	83	5571.56	331.02
16	4	4	85	6159.60	193.98
17	11	5	86	6739.92	42.33
18	6	12	88	7325.49	261.80
19	1	18	90	7910.47	118.17
20	8	22	91	8491.37	328.85
21	4	1	93	9079.22	191.57
22	11	2	94	9659.46	39.81
23	6	10	96	2450245.42	259.99
24	1	16	98	0830.00	115.55
25	8	20	99	1411.01	326.52

Table 2-4. Nodal Passages of Planet Mars for the Period 1964-2000

ASCENDING NODE, ☊				DESCENDING NODE, ☋			
Mo.	Day	Year	Julian Date	Mo.	Day	Year	Julian Date
6	30	64	2438576.91	8	31	63	2438272.60
5	18	66	9263.89	7	18	65	8959.58
4	4	68	9950.87	6	5	67	9646.56
2	20	70	2440637.85	4	22	69	2440333.54
1	8	72	1324.83	3	10	71	1020.52
11	25	73	2011.81	1	25	73	1707.50
10	13	75	2698.79	12	12	74	2394.48
8	30	77	3385.77	10	29	76	3081.46
7	18	79	4072.75	9	16	78	3768.44
6	4	81	4759.73	8	3	80	4455.42
4	22	83	5446.71	6	21	82	5142.40
3	9	85	6133.69	5	8	84	5829.38
1	25	87	6820.67	3	26	86	6516.36
12	12	88	7507.65	2	11	88	7203.34
10	30	90	8194.63	12	29	89	7890.32
9	16	92	8881.61	11	16	91	8577.30
8	4	94	9568.59	10	3	93	9264.28
6	21	96	2450255.57	8	21	95	9951.26
5	9	98	0942.55	7	18	97	2450648.24
3	26	2000	1629.53	6	5	99	1335.22

Table 2-5. Oppositions of Planet Mars for the Period 1963-1999

NO.	MONTH	DAY	YEAR	JULIAN DATE	HELIOCENTRIC LONGITUDE (DEG)
1	2	3	63	2438064.31	134.22
2	3	9	65	8829.03	168.67
3	4	15	67	9596.01	204.73
4	5	31	69	2440373.18	249.89
5	8	11	71	1173.78	316.84
6	10	25	73	1980.61	31.99
7	12	15	75	2762.07	82.74
8	1	22	78	3530.50	121.36
9	2	26	80	4294.74	155.50
10	3	31	82	5059.92	190.06
11	5	11	84	5831.22	230.51
12	7	10	86	6621.74	287.33
13	9	28	88	7432.64	4.83
14	11	27	90	8223.32	64.88
15	1	7	93	8995.42	107.17
16	2	12	95	9760.60	142.40
17	3	18	97	2450524.84	176.25
18	4	24	99	1293.23	213.55

2.2 MISSION PROFILE CLASSES. Interplanetary mission profiles can be divided into three principal classes which are defined as follows:

a. Capture Mission: Reduction to a selected level of negative planetocentric orbit energy in the target planet's activity sphere. Re-escape, following a planned capture period. A surface excursion capability, that is, a limited landing effort capability (few days, small crew size) may be included in a capture mission; however, this capability is optional and not a prerequisite for a successful capture mission whose primary objective is detailed planetary reconnaissance from orbit in preparation for future large-scale landings.

b. Fly-By Mission: Passage through the target planet's activity sphere at positive planetocentric orbit energy, using a combination of gravitational and powered maneuver to enter (in the case of manned missions) the desired heliocentric return orbit.

c. Landing Mission: A capture mission followed by landing and re-ascent maneuvers. The prime objective is to carry out a comparatively extensive surface exploration of the target planet. Landing becomes a prerequisite for mission success. The landing effort is commensurate with stay time and surface travel of a crew of 20 to 100 persons for a period of 360 to 500 days.

Table 2-6. One-Way Capture Transfer Orbits to Venus and Mars Selected Either For Low $v^*_{\infty 1}$ or For Low $v^*_{\infty 2}$ (A = short transfer orbits, $\eta_t < 180°$; B = long transfer orbits, $\eta_t > 180°$)

	TRANSFER SELECTED FOR LOW $v^*_{\infty 1}$							TRANSFER SELECTED FOR LOW $v^*_{\infty 2}$						
	Depart ⊕	$v^*_{\infty 1}$	$v^*_{\infty 2}$	Σv^*_{∞}	Transf. Time (d)	Arrive ♀	Latitude (deg)	Depart ⊕	$v^*_{\infty 1}$	$v^*_{\infty 2}$	Σv^*_{∞}	Transf. Time (d)	Arrive ♀	Latitude
A	8-29-70 2440827.5	0.101	0.178	0.279	108	2440835.5	+1.54	9-28-70 2440857.5	0.168	0.142	0.310	96	2440953.5	+2.784
B	9-8-70 2440837.5	0.112	0.212	0.324	174	2441011.5	+1.74	5-2170 2440727.5	0.157	0.115	0.272	210	2440937.5	+1.62
A	3-31-72 2441407.5	0.118	0.210	0.328	108	2441515.5	-2.83	4-10-72 2441417.5	0.125	0.191	0.316	102	2441519.5	-3.03
B	4-10-72 2441417.5	0.097	0.182	0.291	168	2441585.5	-0.703	1-1-72 2441317.5	0.178	0.113	0.291	204	2441521.5	-1.31
A	11-9-73 2441995.5	0.123	0.166	0.289	108	2442103.5	+1.337	11-29-73 2442015.5	0.140	0.099	0.239	102	2442117.5	+2.88
B	11-9-73 2441995.5	0.091	0.145	0.236	156	2442151.5	+0.27	8-1-73 2441895.5	0.179	0.134	0.313	210	2442105.5	+1.33
A	6-19-75 2442582.5	0.096	0.108	0.204	132	2442714.5	-0.1	6-9-75 2442572.5	0.101	0.095	0.196	138	2442710.5	-0.56
B	5-30-75 2442562.5	0.082	0.115	0.197	156	2442712.5	-0.33	6-9-75 2442572.5	0.101	0.102	0.203	150	2442722.5	+0.59
A	1-19-77 2443162.5	0.095	0.148	0.243	120	2443282.5	-0.55	2-18-77 2443192.5	0.158	0.141	0.299	102	2443294.5	-1.54
B	2-8-77 2443182.5	0.120	0.209	0.329	174	2443356.5	-2.75	12-10-76 2443122.5	0.124	0.093	0.217	168	2443290.5	-1.21
A	8-19-78 2443739.5	0.097	0.182	0.279	114	2443853.5	+1.27	9-28-78 2443779.5	0.177	0.144	0.321	90	2443869.5	+2.5
B	9-18-78 2443769.5	0.110	0.222	0.332	168	2443937.5	+1.1	6-10-78 2443669.5	0.143	0.104	0.247	192	2443861.5	+1.937
A	3-31-80 2444329.5	0.118	0.199	0.317	108	2444437.5	-2.87	4-30-80 2444410.5	0.180	0.125	0.305	102	2444512.5	+3.33
B	4-10-80 2444390.5	0.097	0.186	0.283	168	2444558.5	+3.22	1-1-80 2442390.5	0.175	0.112	0.287	204	2444543.5	+2.32
						Arrive ♂	Lat. (deg) Dist.(AU)						Arrive ♂	Lat. (deg) Dist.(AU)
A	5-29-71 2441100.5	0.095	0.096	0.191	200	2441300.5	-0.441 1.443	5-29-71 2441100.5	0.096	0.095	0.191	220	2441310.5	-0.258 1.455
A	7-27-73 2441890.5	0.128	0.106	0.234	190	2442080.5	+1.095 1.560	2441920.5	0.159	0.081	0.240	210	2442130.5	+1.607 1.615
B	9-5-73 2441930.5	0.137	0.124	0.261	400	2442330.5	+0.945 1.621	6-17-73 2441850.5	0.179	0.085	0.264	280	2442130.5	+1.607 1.615
A	9-15-75 2442670.5	0.145	0.124	0.269	210	2442880.5	+1.849 1.658	10-15-75 2442700.5	0.193	0.080	0.273	240	2442940.5	+1.677 1.664
B	9-25-75 2442680.5	0.123	0.108	0.231	390	2443070.5	+0.173 1.564	10-15-75 2442700.5	0.191	0.079	0.270	260	2442960.5	+1.538 1.658
A	10-24-77 2443440.5	0.141	0.151	0.292	210	2443650.5	+1.514 1.657	11-13-77 2443460.5	0.176	0.089	0.265	250	2443710.5	+0.864 1.615
B	10-14-77 2443430.5	0.111	0.083	0.194	330	2443760.5	+0.124 1.560	9-24-77 2443410.5	0.211	0.082	0.293	270	2443680.5	+1.227 1.640
B	11-3-79 2444180.5	0.101	0.102	0.203	280	2444460.5	-1.870 1.544	11-13-79 2444190.5	0.105	0.088	0.193	300	2444490.5	-0.582 1.505

2.3 CAPTURE MISSION PROFILES. Due to the relative proximity of Venus and Mars, their synodic periods are particularly long, as can be seen from the time intervals between inferior conjunctions (about 585 days) or between oppositions (740 to 806 days, the variation being due to the ellipticity of the Martian orbit). Therefore, flying the same transfer orbit out and back involves extraordinarily long waiting times near the planet (450 to 480 days for Venus or Mars). Actually, because of the inclination of the planet orbit planes relative to the ecliptic, the transfer orbit is not only dependent upon recurrence of the same planetary constellation, but also on the heliocentric longitude at which it occurs. To repeat a given transfer orbit, therefore, a given planetary constellation must be repeated at the same heliocentric longitudes (of Earth and target planet). These two conditions are met only in very long time intervals. They are approximately met in intervals of 16 years (Venus) and 15 years (Mars).

For this reason and because the long waiting time imposes severe constraints on mission flexibility, only mission profiles which involve different transfer orbits out and back are of practical interest. Most mission profiles that are attractive from the standpoints of mission period (total time of absence from Earth) and energy look approximately as shown in Figure2-12. They consist of a short transfer orbit (1-2; transfer angle $\eta_t < 180°$) and a long "lag" (3-4; $\eta_t \gtrsim 180°$). The short lag is often, but not always, the outgoing orbit. In Venus mission profiles the long lag is caused by "overshooting" the Earth orbit; in Mars missions by "undershooting" the Earth orbit. Therefore, paradoxically, the problem of avoiding dangerously close perihelion distances is often more acute for Mars missions than for Venus missions.

The reason for the characteristic trends of these mission profiles is easily recognized (cf. also Figures 2-3 to 2-8). At Venus arrival the Earth trails Venus ($\psi_2 > 0$). Since motion inside the Earth orbit is faster than in the Earth orbit, Earth should lead at return departure from Venus. To wait until Venus is "approaching" Earth "from behind" involves long waiting times (capture periods) at Venus. If one wants to depart after a briefer capture period, the only alternative is to insert a "slow-motion" section into the return transfer orbit to permit Earth to catch up. This "slow-motion" section is provided by overshooting the Earth orbit. Around the aphelion of its return transfer orbit, the space ship moves at lower angular velocity that Earth. Although this leads to return orbits which are significantly longer than the outgoing orbits, the overall mission period is nevertheless significantly shorter than if the capture period had been extended to allow Venus to approach Earth from behind until Earth was given the required lead angle of approximately 30 degrees (Figure 2-5, $-\psi_2$ becoming $+\psi_1$ for the return trip).

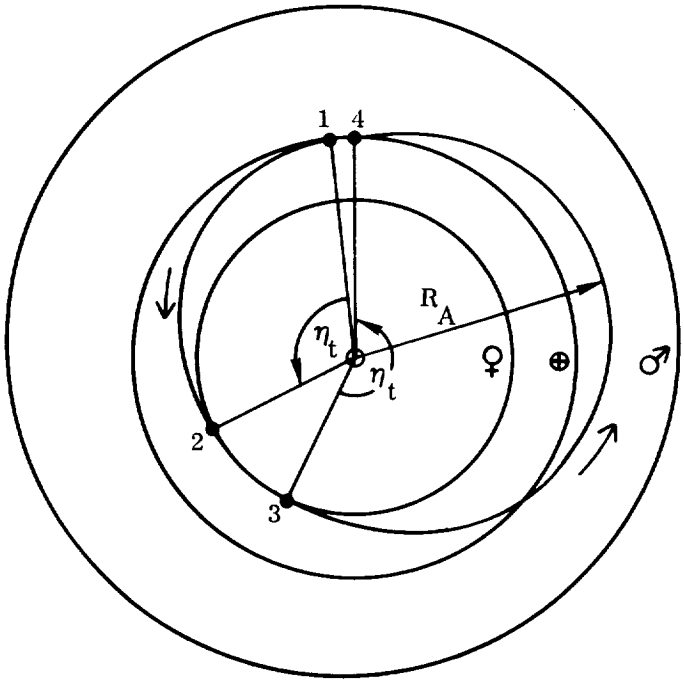

(a) Earth-Venus Mission

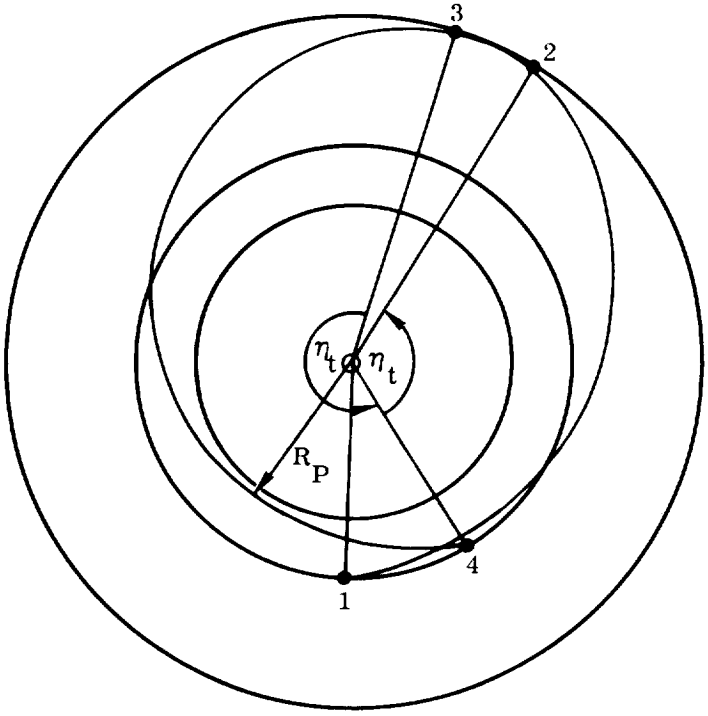

(b) Earth-Mars Mission

Figure 2-12. Characteristic Profiles for Mars and Venus Capture Missions

If the trailing position angle of Earth at Venus arrival is to be reduced, the outgoing orbit must be long (T.O. No. 2 or No. 8, Figure 2-13). In this case, Earth is given an opportunity to pass the space ship while it coasts through its aphelion. After crossing the Earth orbit for a second time, with the Earth ahead of it, the space ship starts catching up with Earth while approaching Venus. It may pass Earth during this part of the transfer, in which case ψ_2 remains positive at Venus arrival (although ψ_2 will generally be smaller than in the case of the transfer orbit shown in Figure 2-12); or it may just catch up with Earth at Venus arrival, in which case $\psi_2 = 0$; or, finally, it may not catch up completely, in which case $\psi_2 < 0°$. Figure 2-14 shows these three conditions graphically (for the simplified case of circular, coplanar planet orbits, which is adequate for displaying the trend) and indicates on the abscissa the aphelion distances involved. It is seen that, for tangential approach to the Venus orbit (T.O. No. 2) an aphelion of 1.15 A.U. is required to catch up ($\psi_2 = 0$ at Venus arrival). Still greater aphelion distances are required to give Earth the lead required for a short return trip, even for zero capture period. Aphelion distances beyond 1.27 A.U. are required to provide the proper Earth lead for a fast return and to provide time for a capture at the average rate of 1.599-0.986 = 0.613 deg/day, corresponding to the capture at the average rate of 1.599-0.986 = 0.613 deg/day, corresponding to the difference in angular velocity between Venus and Earth. Figure 2-15 shows that the resulting transfer times become very long. If ψ_2 at Venus arrival remains positive, a long return orbit is required, resulting in a mission profile as shown in Figure 2-16(a). The principal objection to these profiles is the long mission period involved, as can easily be deduced from Figures 2-14 and 2-15. A positive position angle ψ_2 at Venus arrival can be attained more easily with T.O. No. 8 if small perihelion distances are selected, as can be seen in Figure 2-14. In this case the transfer orbit is short ($\eta_t < 180°$). Therefore, the mission profile may consist of two short transfer orbits (Figure 2-16(b)) at a great reduction in mission period. The principal problem with this mission profile is that the outgoing lag is very expensive, because of strong directional changes involved at stations 1 and 2. Thus, in the case of Venus one has essentially a choice between the following mission profiles:

a. long-short transfer orbits,

b. long-long transfer orbits,

c. short ($R_A > 1$ A.U.) - short transfer orbits.

Of these, b involves very low mission profiles; c is very expensive, but yields mission periods well under a year at 10-30 day capture periods; a generally represents a missle-of-the road compromise in terms of mission period and mission energy.

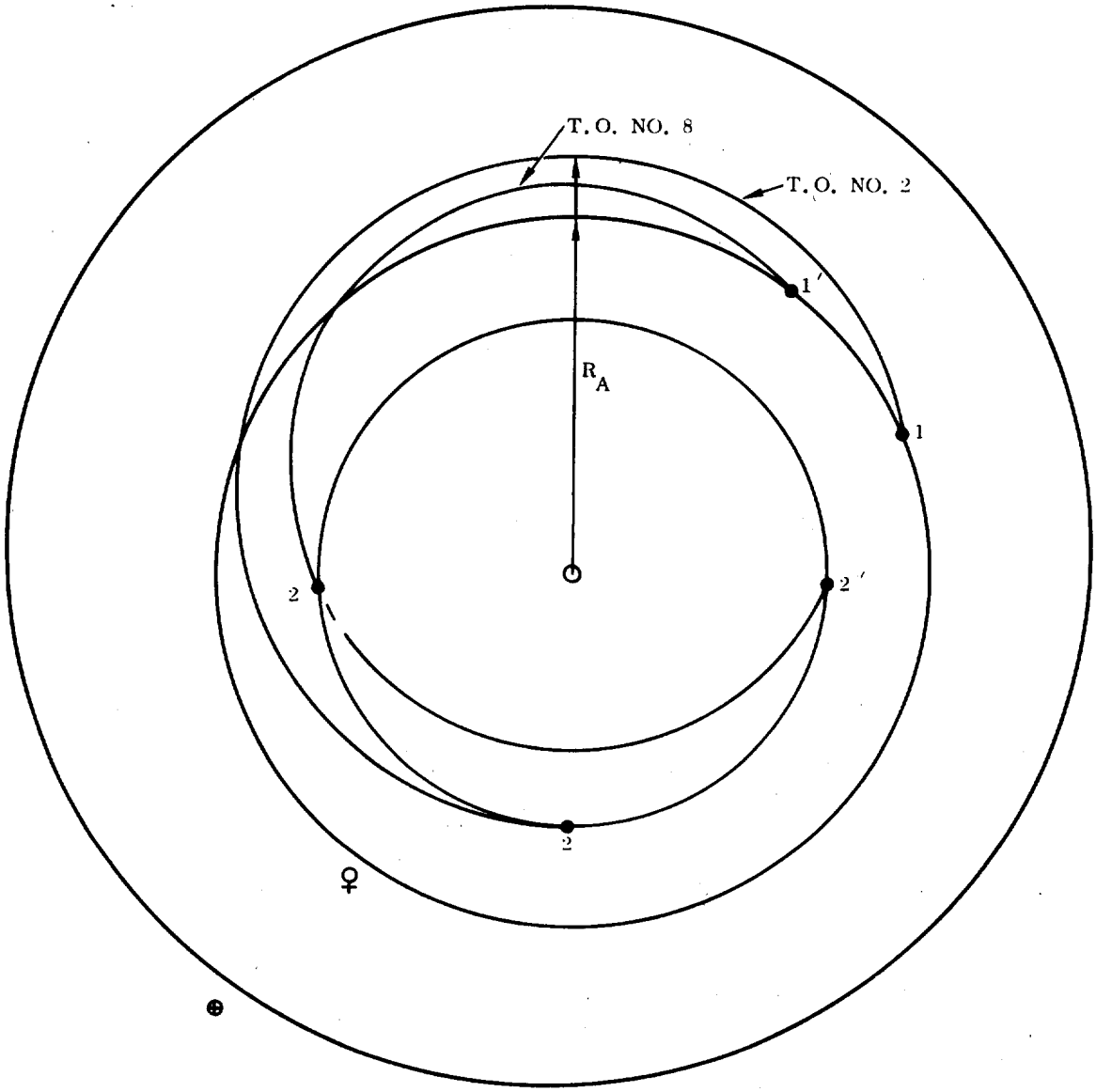

Figure 2-13. Long Outgoing Transfer Orbits to Venus

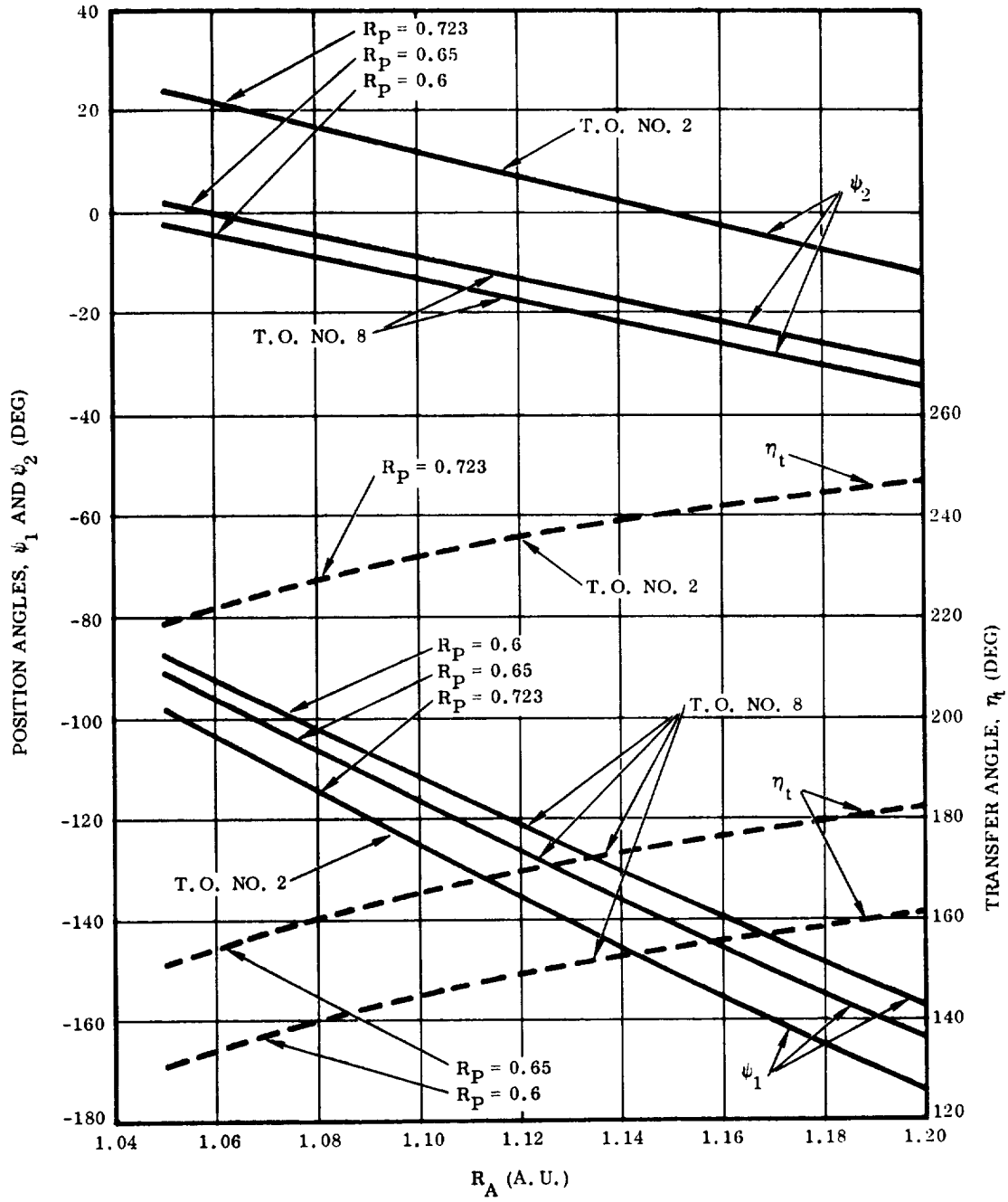

Figure 2-14. Earth ⇄ Venus Transfer Orbits No. 2 and 8: Heliocentric Transfer Angle, η_t, and Target Planet Position Angles at Departure and Arrival, ψ_1 and ψ_2 (For Earth Venus Transfers ψ is Negative if Venus Trails Earth; Signs are Reversed in Case of Venus → Earth Transfer)

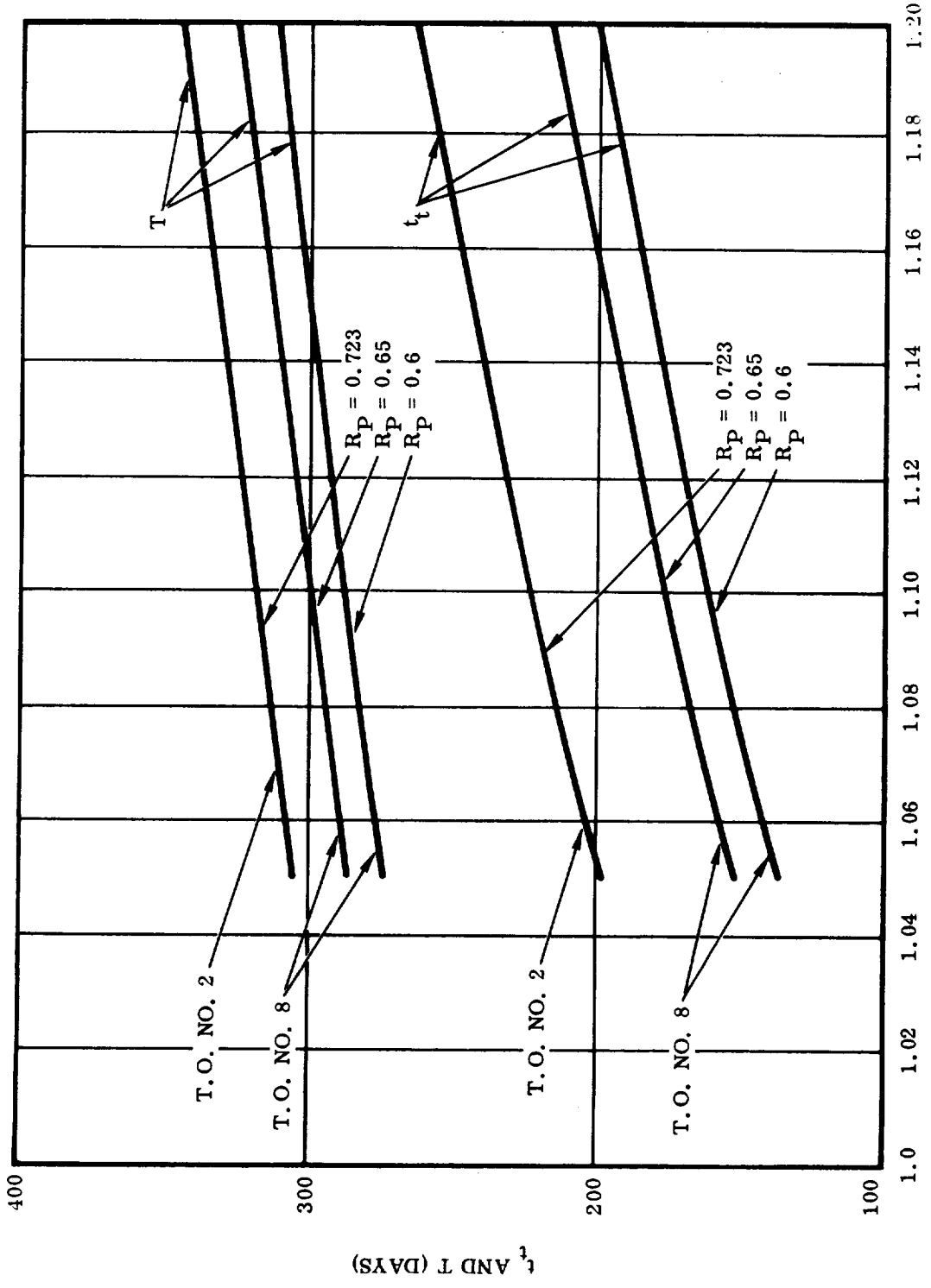

Figure 2-15. Earth ⇌ Venus Transfer Orbits No. 2 and 8: Heliocentric Transfer Period, t_t, and Period, T, of One Revolution in Transfer Ellipse as Function of Aphelion Distance for Several Transfer Perihelion Distances (Coplanar Circular Terminal Orbits)

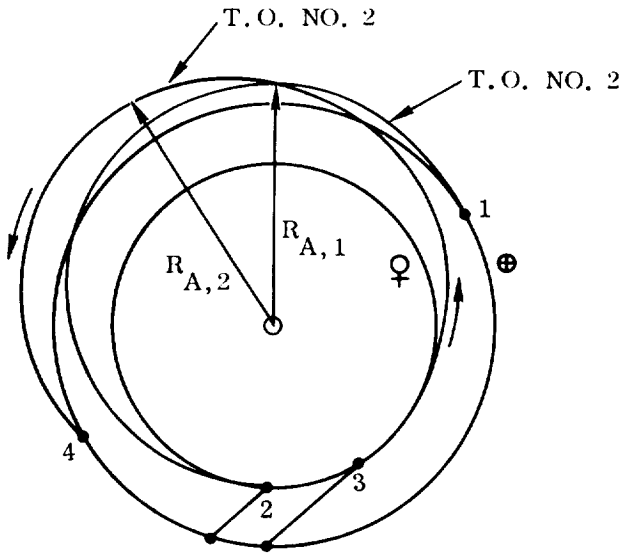

(a) Mission Profile (M.P.) Consisting of Two Long Transfer Orbits With Different Aphelion Distances (M.P. 22 or 88 or 28 or 82)

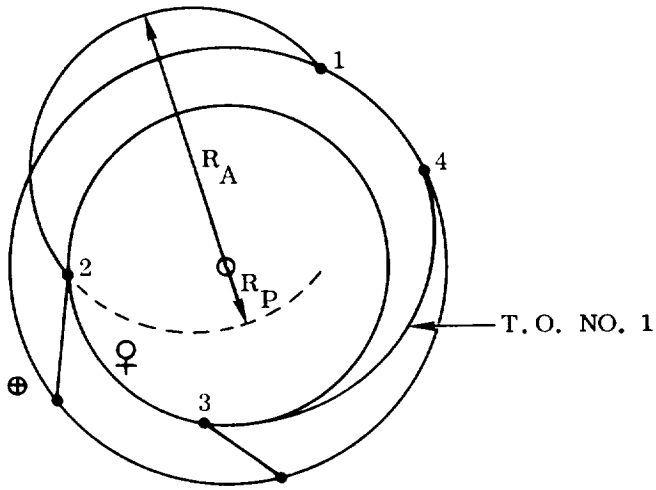

(b) Mission Profile (M.P.) Consisting of Two Short Transfer Orbits (e.g. M.P. 81)

Figure 2-16. Alternate Profiles for a Venus Capture Mission.

At Mars arrival, following a short transfer as shown in Figure 2-12(b), Earth leads ($\psi_2 < 0$, Figure 2-8). The space ship's angular velocity outside the Earth orbit is less than the angular velocity of Earth. Therefore, in order to meet Earth on return, Mars should lead at the time the space ship departs. One could wait until the faster Earth approaches Mars from behind, thereby providing the required lead for Mars. However, this involves a long capture period. In order to depart after a short capture period, the slower motion of the space ship outside the Earth orbit must be compensated by a faster motion inside the Earth orbit. By taking a "short cut" at closer vicinity to the Sun, the space ship can catch up with Earth at the second orbit intersection.

Figure 2-8 shows that for very fast (high eccentricity) transfer orbits, Mars can lead Earth at arrival of the space ship ($\psi_2 > 0$). However the lead angle is small, namely about 3 degrees for T.O. No. 1 at e = 1 (parabolic transfer orbit). For large lead angles, hyperbolic transfer orbits, which are quite expensive, are required. Even so, a perihelion distance of less than 1 A.U. is required in most cases. Nevertheless, the return orbit must also be fast. The longer the capture period, the longer must be the return orbit and the closer must be the perihelion distance. A typical mission profile resulting from this approach is shown in Figure 2-17(a). It yields short mission periods, but is unacceptably expensive for propulsion systems such as are considered in this study. The other alternative is to make the outgoing orbit so long that Earth has time to complete one revolution and part of the next. Earth then approaches Mars from behind so that, after the desired capture period, Mars has the proper lead for a space ship-Earth rendezvous at station 4 following a short return orbit. This mission profile is shown in Figure 2-17(b). The outgoing transfer orbit is fairly inexpensive, unless high inclination is required. The main objectives against this mission profile is the long mission period (approaching 2 years). Thus, the mission profile shown in Figure 2-12(b) represents middle-of-the-road compromise with respect to mission energy and mission period. For a given outgoing transfer orbit, increasingly long capture periods mean decreasing perihelion distance during return. For a given capture period, shorter outgoing transfer means greater perihelion distance during return.

Practical considerations lead to a layout for a given mission plan in such a manner as to provide an Earth departure window (i.e., the possibility for the space vehicles to depart during a period of, say, one month) while retaining a constant arrival point. Thereby, the capture period is kept independent of Earth launch delays. In this manner, the fuel requirement for the return flight does not have to be changed every time there is a change in Earth launch date, provided this change takes place within the Earth departure window. This is shown in Figure 2-18, where the Earth launch window (1a-1b) transfer orbits all lead to a fixed arrival point (2). The nominal capture period is 2-3a. Again, for practical reasons which in this case are even

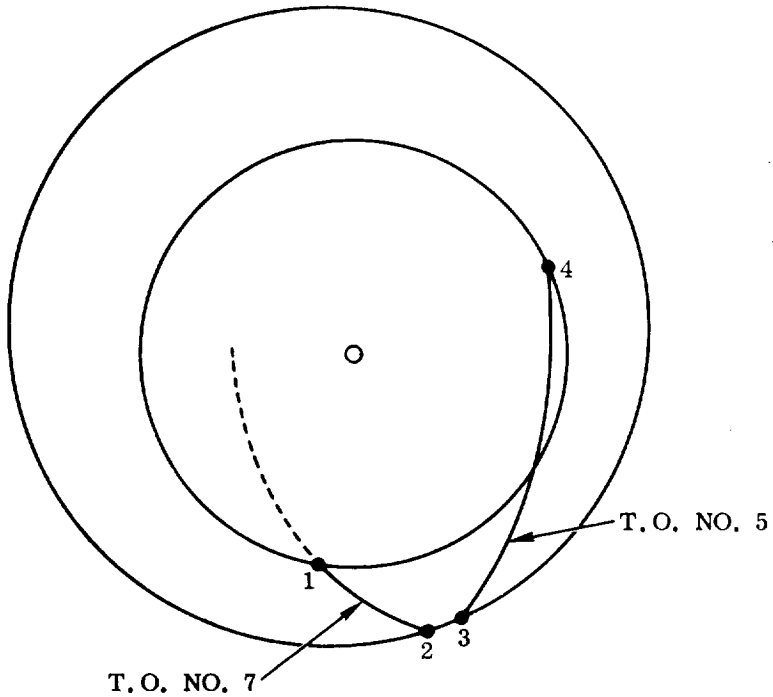

(a) Mission Profile (M.P.), Consisting of Two Short Transfer Orbits (M.P. 75 or 15 or 51)

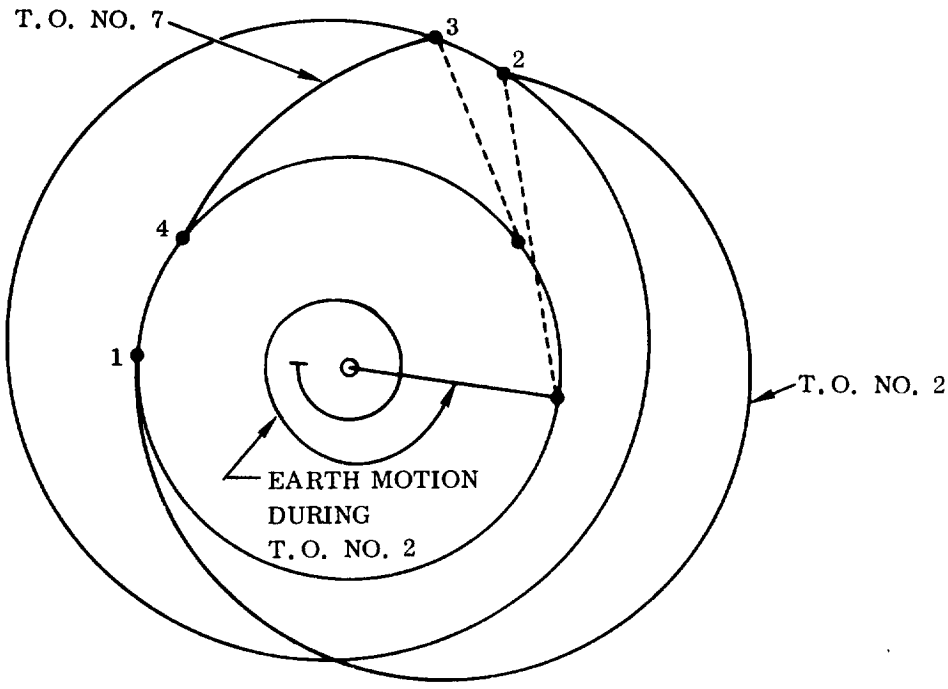

(b) Mission Profile Consisting of One Long and One Short Transfer Orbit (e.g. M.P. 27)

Figure 2-17. Alternate Profiles for a Mars Capture Mission

more vital than during Earth departure, a tolerance should be built into the capture period to allow for possible delays at target planet departure. This tolerance is the target planet departure window 3a-3b. A typical Mars or Venus capture mission profile with built-in Earth departure window and target planet departure window looks. therefore, as shown in Figure 2-18.

2.4 FLY-BY MISSION PROFILES. From the discussion in the preceding section it follows that for a Venus mission profile as shown in Figure 2-12(a) the aphelion distance of the return orbit increases with increasing capture period. Consequently, for a fly-by mission this aphelion distance becomes a minimum.

Analogously, the perihelion distance of the return orbit in a Mars mission profile of the type shown in Figure 2-12(b) becomes a maximum.

In both cases, the deflection from outgoing to return transfer orbit becomes a minimum. This is fortunate, since some deflection is obtained by the hyperbolic encounter with the target planet's gravitational field. Thus, the powered maneuver to complement planetary assistance becomes a comparative minimum. The deflection of the heliocentric velocity vector by passage through the planet's activity sphere is illustrated schematically in Figure 2-19.

2.5 LANDING MISSION PROFILES. From the present uncertainty in our knowledge of the conditions in the atmosphere and on the surface of Venus, it is apparent that some very basic information must still be gathered before one can begin to plan a manned descent to the surface of this planet. In particular, period of rotation, orientation of the Venus polar axis (if any), atmospheric composition, pressures and winds on the surface and at altitude, surface temperatures and their variation with location and time, surface composition and the amount of relief on the surface remain to be investigated.

Therefore, Mars is the principal target planet, at this time, when a manned planetary landing mission is considered. By definition, the landing mission involves extended stay of most or all of the crew on the Martian surface. The period between two approximately equal transfer orbits (not counting differences in transfer orbit inclination) was stated at the beginning of Section 2.3 to range from 450 to 480 days (namely, synodic period minus twice the time required for Earth to cover the position angle, ψ_2, between Earth (in the lead) and Mars at Mars arrival of the space ships). This time interval corresponds to 65 to 72 percent of a Martian sidereal year (686.98 days). A typical mission profile for capture periods in excess of 450 days is shown in Figure 2-20 (1-2-3'-4'). If shorter capture periods are desired (350-400 days), the space ships must leave Mars before Earth has caught up sufficiently with Mars. Therefore, a long transfer orbit leading into trans-Martian space is required (1-2-3-4). that a return flight does not appear feasible with the propulsion systems under consideration; also, very small perihelion distances are likely to be encountered.

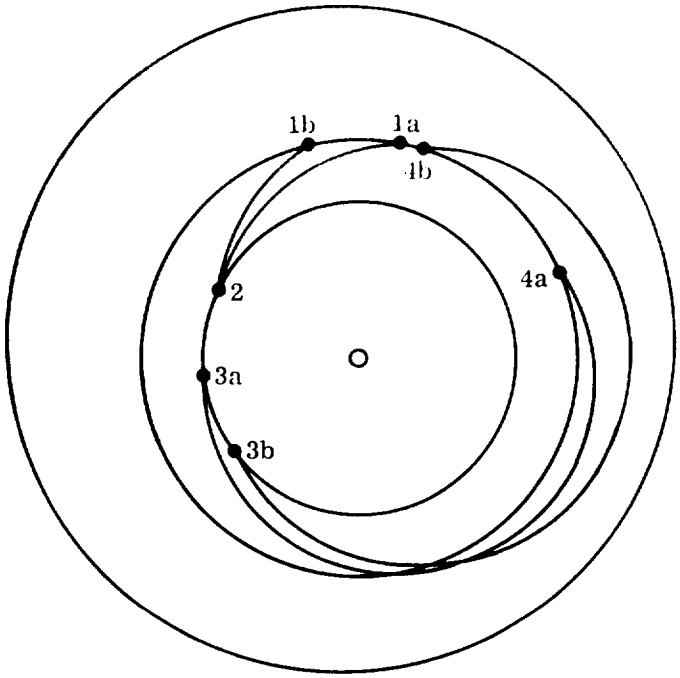

(a) Venus Mission

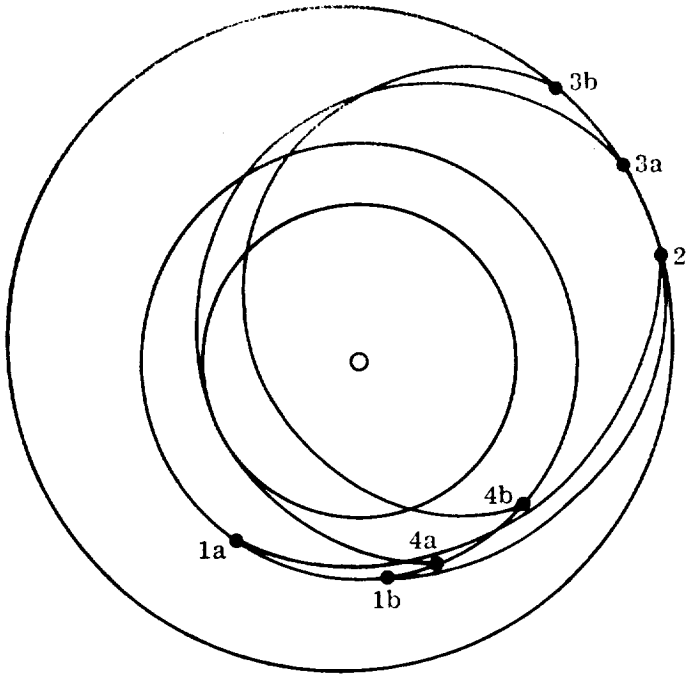

(b) Mars Mission

Figure 2-18. Earth Departure and Target Planet Departure Windows

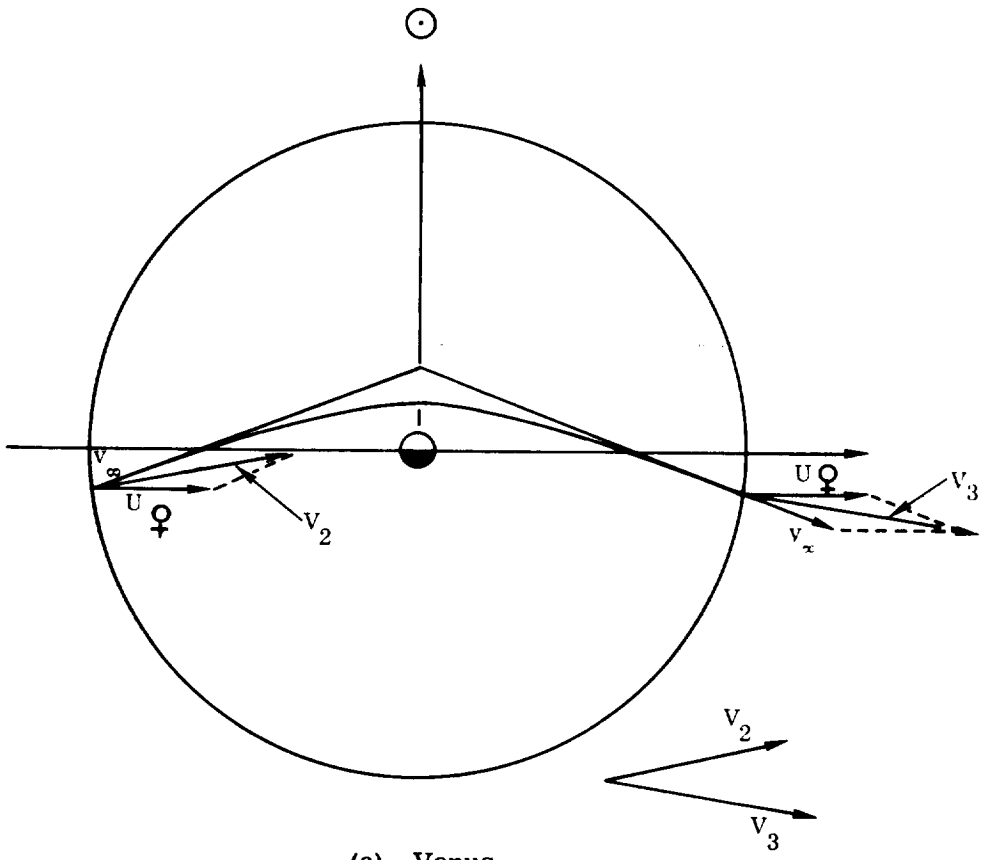

(a) Venus

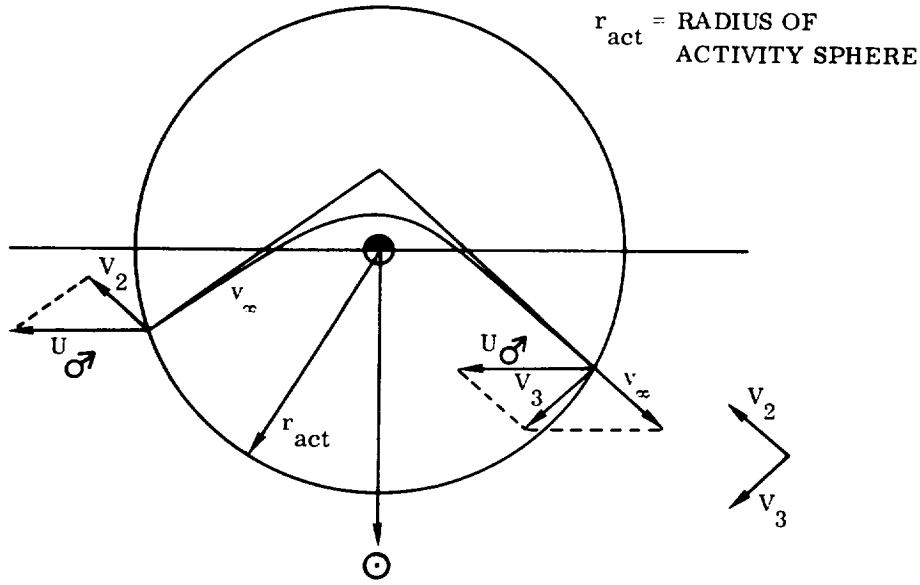

(b) Mars

Figure 2-19. Deflection of Heliocentric Velocity Vector by Hyperbolic Encounter in Mission Profiles Figure 2-9

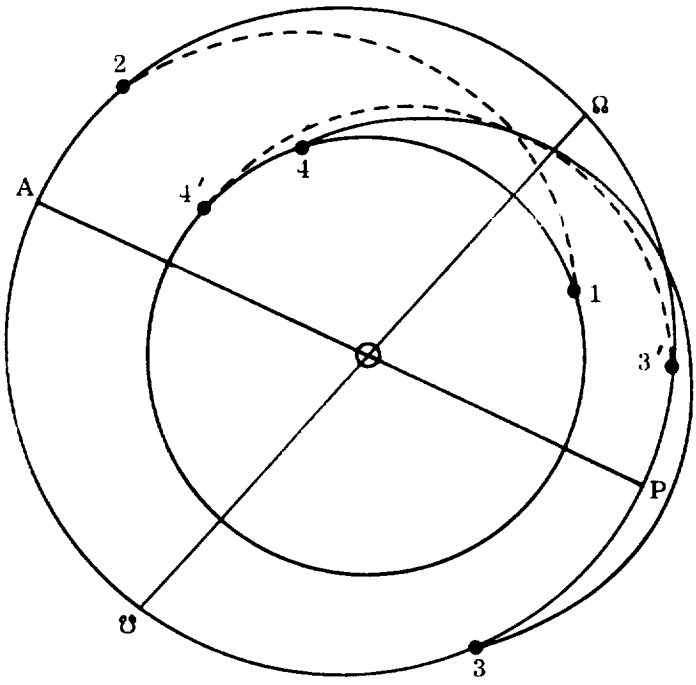

Figure 2-20. Typical Profiles for a Manned Landing Mission to Mars (Extended Surface Stay Time) (Schematic)

SECTION 3

TARGET PLANETS

Next to the Moon, the planets Mars and Venus are highest on the list of extraterrestrial bodies for reconnaissance by man in his exploration of space. The planetology of Mars and Venus, as currently known and conjectured, is briefly summarized in this section. The interaction between the nature of the planetary environment and the Empire mission is discussed in Sections 2, 5, and 6.

The planetology data discussed here are necessarily preliminary; the literature search and evaluation are continuing. It is emphasized that current knowledge of Martian and Venusian environments is insufficient for many requirements of the present study and that some decisions on the mission analysis must be made on the basis of extrapolation and conjecture concerning Mars and Venus.

3.1 GENERAL SOURCES OF DATA. A compact summary of general data on Mars and Venus is conveniently available in a book by Ehricke (Ref. 3-1). Kuiper reviews atmospheric data of a decade ago (Ref. 3-2) and also presents a modern analysis of physical observations (Ref. 3-3). Another useful general study is by Urey (Ref. 3-4), who also has published a more recent summary (Ref. 3-5). Moore (Ref. 3-6) gives a general discussion of planetary characteristics.

A recent compilation of Mars data is by Hess (Ref. 3-7). Moore (Ref. 3-8) gives a nontechnical history of Martian study. An excellent book by de Vaucouleurs (Ref. 3-9) presents detailed analysis of data available eight years ago. Slipher (Ref. 3-10) has published an extensive collection of photographic studies of Mars.

Much of the published so-called data on Venus consists of extrapolation and speculation, largely because of the masking cloud cover which obscures the surface. Sagan (Ref. 3-11) summarizes current views on Venus. A nontechnical discussion is given by Moore (Ref. 3-12).

3.2 PLANETARY PARAMETERS. Table 3-1 presents values for selected planetary parameters for Mars and Venus, with Earth for comparison. Much of the data comes from Ehricke (Ref. 3-1). Some values come from other sources or have been computed for the present compilation.

The value 149,598,845 ±250 (p.e.) kilometers for the astronomical unit (A.U.) is adopted from the 1961 Jet Propulsion Laboratory radar reflection measurements (Ref. 3-13). It agrees well with the value 149,597,850 ±400 kilometers reported by the Massachusetts Institute of Technology Lincoln Laboratory (Ref. 3-14).

Table 3-1. Selected Planetary Data

	VENUS	EARTH	MARS
1. Symbol	♀	⊕	♂
2. Radius, equatorial	6,200 km 0.973 (⊕ = 1)	6,378.39 km	3,310 km 0.520 (⊕ = 1)
3. Angular diameter from Earth	9.9 to 64.5 sec		3.5 to 25.1 sec
4. Oblateness	0	1/297 = 0.00337	1/192 = 0.00521
5. Mass	4.86×10^{24} kg 0.8136 (⊕ = 1)	5.975×10^{24} kg	6.43×10^{23} kg 0.1077 (⊕ = 1)
6. Density, average	4.90 gm/cm^3 0.8877 (⊕ = 1)	5.52 gm/cm^3	4.20 gm/cm^3 0.7609 (⊕ = 1)
7. Orbital semi-major axis	108,209,600 km 0.723332 A.U.	149.598,845 km 1.000000 A.U.	227,942,400 km 1.523691 A.U.
8. Perihelion	107,474,500 km 0.718418 A.U.	147,096,500 km 0.983273 A.U.	206,660,500 km 1.381431 A.U.
9. Aphelion	108,944,800 km 0.728246 A.U.	152,101,200 km 1.016727 A.U.	249,224,300 km 1.665951 A.U.
10. Orbit eccentricity	0.0067935	0.0167272	0.0933654
11. Orbit inclination to ecliptic	3°23'39"1		1°50'50"8
12. Orbital period	0.6156 y 224 d 17 h	1.0 y 365 d 6 h	1.8822 y 687 d 0 h
13. Equator inclination to orbit	Not known	23°26'59"	25°12'
14. Spin period	Not known	23 h 56 m 4.09 s	24 h 37 m 22.58 s
15. Spin rate	Not known	73.1958 microrad/sec	70.8821 microrad/sec
16. Mass gravitational acceleration at 45° latitude	8.434703 m/sec^2 0.85805 (⊕ = 1)	9.830080 m/sec^2	4.019938 m/sec^2 0.40894 (⊕ = 1)

Table 3-1. Selected Planetary Data, Cont

	VENUS	EARTH	MARS	
17. Centrifugal relief acceleration at 45° latitude	Rotation not known	0.017067 m/sec^2	0.008315 m/sec^2	
18. Apparent gravitational acceleration at 45° latitude	Rotation not known	9.813013 m/sec^2	4.011623 m/sec^2	
19. Circular velocity at equator	7,231.54 m/sec	7,909.59 m/sec	3,600.36 m/sec	
20. Parabolic velocity at equator	10,726.20 m/sec	11,185.90 m/sec	5,091.67 m/sec	
21. Satellites	None	Moon	Phobos	Deimos
22. Satellite diameter		3,476 km	~15 km	~8 km
23. Satellite distance from planet center, average		384,400 km	9,350 km	23,500 km
24. Satellite orbital period		27 d 7 h 43.19 m	7 h 39.23 m	1 d 6 h 17.92 m
25. Satellite orbit inclination to planet equator		18° 19' to 28° 35'	1° 8'	1° 46'
26. Satellite orbit eccentricity		0.05490	0.021	0.003

Mars opposition occurs about every 780 days (synodic period: 26 months or 2.14 years). At perihelic opposition, which occurs about every 17 years, Mars approaches to about 56 million kilometers (35 million miles or 0.37 A.U.) from Earth. Recent perihelic oppositions were in 1924, 1939, and 1956; the next will be approximately August 1971 and October 1988.

The Martian day is the only one in the solar system known to be approximately equal in length to that of Earth (1 Mars day = 1.026 Earth days).

Venus inferior conjunction occurs about every 584 days (19 months or 1.60 years), at which time the distance to Earth is about 39 million kilometers (24 million miles or 0.26 A.U.).

The Venusian day is unknown at the time of the present writing. Speculation ranges from very short to one Venusian year (224.7 days), with increasing indirect evidence favoring the long (synchronous) period. A recent unpublished report of the Mariner 2 Venus encounter on 14 December 1962 indicates a magnetic field considerably less than that of Earth, which implies a spin rate similarly less than that of Earth.

3.3 MARS ENVIRONMENT

3.3.1 Mars Atmosphere. Current estimates of the composition of the Mars atmosphere are listed in Table 3-2. The sources include Ehricke (Ref. 3-1, pp. 122-123, 166), Kuiper (Ref. 3-2), and Kellogg and Sagan (Ref. 3-15). Comparative distributions of atmospheric temperature and density for Earth and Mars are presented by Chamberlain (Ref. 3-16). Schilling has evaluated realistic limits to possible values of atmospheric parameters (Ref. 3-17).

The surface pressure of the Martian atmosphere, about 85 millibars, is equivalent to the terrestrial atmosphere at an altitude of about 18 kilometers (60,000 feet) (Ref. 3-18).

Only CO_2 has been clearly identified spectroscopically in the Martian atmosphere. After elimination of many other possible components by search (upper limits are indicated in Table 3-2) or by theoretical considerations, the balance is assumed to be N_2 plus Ar. That 1% Ar is present in the Martian atmosphere is an ad hoc assumption by analogy with Earth's 0.93% Ar, using the argument that the planets were probably all formed in a similar manner and that Ar^{40} comes from radioactive decay of K^{40} in the planetary crust. Neither H_2 nor He is expected on Mars because of their low molecular weights.

Table 3-2. Planetary Atmospheric Composition

COMP. (Dry Air)	VENUS		EARTH		MARS	
	Percentage by Volume	Absolute Quantity, NPT*	Percentage by Volume	Absolute Quantity, NPT*	Percentage by Volume	Absolute Quantity, NPT*
N_2	95		78.09	6,246 m	96.8	1,360 m
O_2			20.95	1,676 m	< 0.18	< 2.5 m
Ar	1		0.93	74.4 m	1	14 m
CO_2	4		0.03	2.2 m	2.2	31 m
Ne			0.0018	0.14 m		
He			0.00052	0.042 m		
CH_4		< 0.2 m	0.00015	0.012 m	< 0.007	< 0.1 m
Kr			0.0001	0.008 m		
N_2O		< 1 m	0.00005	0.004 m	< 0.14	< 2 m
H_2			0.00005	0.004 m		
O_3			0.00004	0.003 m	< 0.000036	< 0.0005 m
Xe			0.000008	0.0006 m		
CO		< 1 m			< 0.007	< 0.1 m
NH_3		< 0.04 m			< 0.0014	< 0.02 m
C_2H_4		< 0.03 m			< 0.0014	< 0.02 m
C_2H_6		< 0.01 m			< 0.0007	< 0.01 m
SO_2					< 0.0000021	< 0.00003 m
CH_2O		< 0.003 m				
H_2O		< 0.088 m < 0.07 kg/m^2	0.1 to 1	10 to 100 m	< 0.031	< 0.44 m < 0.35 kg/m^2
Surface Pressure	≧ 10 atm ≧ 150 lb/in.^{2}		1.0000 atm 1.0133 bar 760 mm mercury 14.7 lb/in.^{2}		0.084 atm 0.085 bar 64 mm mercury 1.2 lb/in.^{2}	

*NPT = Normal Pressure (1 atmosphere) and Temperature (0°C). Height of equivalent layer in meters.

3.3.2 Mars Irradiance and Albedo. Solar irradiance data are presented in Table 3-3, based on a report by Strughold and Ritter (Ref. 3-19). The average solar irradiance of Mars is less than half that for Earth. Because Mars has a greater orbital eccentricity (exceeded only by Pluto and Mercury among the planets), its solar irradiance varies substantially from perihelion to aphelion. Mars has an axis inclination with the normal to its orbital plane slightly in excess of that for Earth, so seasonal changes are similar. The combination of axis tilt and orbit eccentricity produces unequal seasons; northern summer and southern winter occur at aphelion. Consequently, the southern summer is shorter and hotter than northern summer, and the southern winter is longer and colder than the northern winter. (A similar condition prevails for Earth but the differences are small because its orbit is less eccentric than that of Mars (Table 3-1)). Table 3-4 lists the approximate length of Martian seasons (Ref. 3-1).

Table 3-3. Optical Planetary Data

	VENUS	EARTH	MARS
1. Solar constant (irradiance) above atmosphere at perihelion	3.88 cal/(cm^{2}min) 2,706 watt/m^2	2.07 cal/(cm^{2}min 1,444 watt/m^2	1.047 cal/(cm^{2}min) 730 watt/m^2
2. Solar constant (irradiance) above atmosphere at distance of semi-major axis	3.82 cal/(cm^{2}min) 2,664 watt/m^2	2.00 cal/(cm^{2}min) 1,395 watt/m^2	0.861 cal/(cm^{2}min) 600 watt/m^2
3. Solar constant (irradiance) above atmosphere at aphelion	3.77 cal/(cm^{2}min) 2,630 watt/m^2	1.935 cal/(cm^{2}min) 1,350 watt/m^2	0.720 cal/(cm^{2}min) 502 watt/m^2
4. Surface albedo, average visible	0.76	0.39	0.148

Table 3-4. Martian Seasons

SEASON		LENGTH
NORTHERN HEMISPHERE	SOUTHERN HEMISPHERE	
Spring	Autumn	199 days
Summer	Winter	182 days
Autumn	Spring	146 days
Winter	Summer	160 days

The diffuse spherical reflectivity (albedo) of Mars is near 0.3 at λ7000 (red) but declines rapidly to about 0.04 below λ4500 (Ref. 3-15, p. 22). Thus, Mars has an overall reddish coloration. The low albedo in the blue and violet is an atmospheric effect associated with the blue haze. In yellow light, the dark areas of Mars have an albedo of about 0.05; in the bright areas the albedo is about 0.15. It is probable that low O_2 content in the Martian atmosphere also requires low O_3 content, with resultant high transparency to ultraviolet radiation which reaches the ground.

3.3.3 Mars Surface Temperature. Table 3-5 summarizes some data on Martian surface temperatures and temperature ranges (Refs. 3-15 and 3-20). Direct observation from Earth of Mars night temperatures is difficult because of the relative positions with respect to the sun. Maximum temperatures are probably not maintained for long because of rapid cooling of the surface by radiation. The average daytime temperature is in fair agreement with microwave brightness measurements.

The maximum temperature of the near-surface Mars atmosphere (at a few meters elevation) may be 50°K (90° F) less than the maximum ground temperature at a given equatorial location. This difference is smaller at higher latitudes and at times other than near local midday.

3.3.4 Mars Surface Features. The surface of Mars contains the following types of features (Figure 3-1) which are recognizable telescopically:

a. White polar caps

b. Dark areas, predominantly colored gray, blue-gray, or green-gray

c. Light areas, colored ochre, orange, or buff.

The surface is frequently obscured by clouds or haze, as discussed later.

Table 3-5. Martian Surface Temperatures

	TEMPERATURE		
1. Average entire surface, daytime	240°K	-33°C	-27°F
2. Maximum, noon summer, equatorial	300°K	27°C	81°F
3. Maximum, noon summer, equatorial, light areas	293°K	20°C	68°F
4. Maximum, noon summer, equatorial, dark areas	306°K	33°C	91°F
5. Minimum, night, most of surface, estimated	203°K	-70°C	-94°F
	TEMPERATURE RANGE		
6. Daylight range at given region, estimated	80 K°	80 C°	144 F°
7. Diurnal range at given region, estimated (night surface mostly not observed at earth)	100 K°	100 C°	180 F°
8. Seasonal range, noon, equatorial, estimated	40 K°	40 C°	72 F°

The polar caps are probably thin coatings of solid H_2O (snow, frost), which appear to be formed during autumn in each hemisphere while obscured by clouds or fog. Toward the end of winter the clouds recede and reveal maximum development of the cap, around which appears a dark fringe. The cap recedes (melts? sublimes?) during late winter and spring, the dark fringe being widest when the "melting" rate is greatest. The south cap is centered at longitude 40°, latitude 83°. It extends to 45° latitude at its maximum; it can disappear entirely. The north cap extends to 57° latitude at its maximum; its minimum size is 300 kilometers (1° = 57 km). The cap centers do not coincide with the geographic poles (similarly, the ice caps of Earth are not centered at their respective geographic poles).

The dark areas are generally believed to represent vegetation regions, although the literature includes alternative suggestions (e.g., hygroscopic salts, volcanic ash). A crucial factor was the discovery by Sinton (Ref. 3-21) of C-H bond resonance absorption bands from the dark areas only (not the light areas). Dark areas cover about 0.38 of the surface and appear to be mostly stable regions, but additional dark areas appear from time to time and persist for up to a few years. Seasonal color changes occur, with darkening appearing first near the poles and advancing toward the equator in the spring. Dark areas are interconnected by a network of several hundred narrow strips or "canals", some of which also cross dark areas. Their nature (and detailed description) and even existence has been highly controversial. It is, however, generally agreed that the "canals" are not open channels through which liquid water flows.

Bright areas cover about 0.75 of the Martian surface. They are generally interpreted as deserts. The yellow-orange or ochre color has been ascribed to limonite (an iron oxide) and to felsite (an aluminum potassium silicate). Because of wide surface-temperature variations, surface rocks are presumed to have become sandy or dusty (pulverized by daily expansion and contraction).

No abrupt heights on Mars exceed 760 meters (2500 feet) (Ref. 3-15).

3.3.5 Mars Clouds and Haze. Three classes of Martian clouds have been recognized: yellow, white, and blue. The so-called blue haze or violet haze may cover all or parts of Mars so as to obscure surface features photographed in blue light ($<\lambda$ 4330) (Ref. 3-15).

Yellow clouds are probably dust storms. They are frequently widespread at perihelic opposition and may obscure our view of the entire planet. They may also cover limited areas and are seen to move with the winds. They usually occur at low altitudes, up to several kilometers, but have been reported as high as 30 kilometers (98,000 feet) (Ref. 3-22).

White clouds are probably ice clouds although solid CO_2 particles have also been proposed. Blue clouds appear to be somewhat similar in occurrence to white clouds. White clouds may be somewhat thicker or more dense blue clouds. White clouds or blue clouds have been observed on all parts of Mars but are more prevalent toward the limb. They may form in a few hours and last up to several weeks. White clouds occur at altitudes up to about 20 kilometers (66,000 feet).

The blue haze dissipates from time to time, particularly near oppositions. It can form or dissipate in three or four hours. Clearings may be planet-wide or as small as 0.12 of the visible surface. The blue haze has been ascribed to small (0.2 to 1 micron diameter) ice crystals or possibly CO_2 particles, at heights of 30 to 35 kilometers (98,000 to 115,000 feet). Urey and Brewer (Ref. 3-23) suggest that solar protons may ionize upper atmosphere molecules to CO_2^+, CO^+, and N_2^+, all of which have absorption bands which occur in the spectral region where surface obscuring is observed. Sagan (Ref. 3-24) concludes that a combination of the known atmospheric distribution, solar proton flux, and planetary and interplanetary magnetic fields cannot produce the observed blue haze and its clearing at times of opposition with Earth (assuming terrestrial magnetic interaction with the path of solar protons en route toward Mars).

3.3.6 Mars Winds. General circulation of the Martian atmosphere appears to be similar to that of Earth. Transfer of heat from equatorial to polar regions imposes a heat load on the atmosphere which is relatively light compared with that on Earth (Ref. 3-15). However, seasonal changes are probably large because of the low heat

capacity of the surface. In winter instability waves are probably in the general circulation pattern.

A theoretical estimate predicts surface winds between 1 meter per second (2 knots, stable circulation) and 10 meters per second (20 knots in parts of a cyclonic system). For comparison, on Earth a wind of about 6 meters per second (12 knots) is required to raise dust on the ground, so that dust storms are more likely during the winter season of unstable circulation waves (Ref. 3-15). Upper air winds are generally larger than surface winds at all seasons.

3.3.7 Mars Magnetic Field. The magnitude of the Martian magnetic field, or even whether it exists, is not known. Literature search to date has revealed no significant data and very little speculation. A realistic approach is to observe that the small diameter and density of Mars, relative to Earth (Table 3-1), implies a much smaller liquid iron-nickel core than Earth, if indeed Mars has any such core at all. Urey (Ref. 3-4) concludes that Mars probably has a uniform chemical composition throughout. The absence or small size of such an inner core, together with a spin rate of about 1.02 times that of the Earth, would imply a smaller magnetic field for Mars than for Earth.

3.3.8 Mars Radiation Belt. The magnitude and nature of the Martian radiation belt, or even whether it exists, is not known. Because of the dependence of charged-particle trapping on planetary magnetic field, the same argument used above implies that the Martian radiation belt is probably of smaller extent and lower energy content than that of Earth. A supporting argument is the fact that Mars is further from the sun and would probably tend to intercept a smaller number of solar charged particles than would Earth.

3.4 VENUS ENVIRONMENT

3.4.1 Venus Atmosphere. Current estimates of the composition of the Venus atmosphere are listed in Table 3-2. Noteworthy is the CO_2 value of only 4 percent, which is reported by Spinrad (Ref. 3-25) with a probable uncertainty factor of 2. Earlier estimates (Ref. 3-10) of CO_2 fraction were larger than this value by factors of about 4 to 20.

The balance of the atmosphere is essentially unidentified and assumed to be N_2^+ and Ar by elimination, with 1 percent ascribed to Ar by analogy with Earth, as in the case of Mars.

In 1954, N.A. Kozysev (Crimean Observatory, USSR), reported from a single low dispersion spectrogram the detection of λ3914 which he attributed to N_2^+, presumably observed as an auroral feature (Refs. 3-26 and 3-27). Subsequently Newkirk reported somewhat similar but questionable results (Ref. 3-28). In later attempts Weinberg and Newkirk (Ref. 3-29) got negative results. Warner (Ref. 3-30) later analyzed these experiments and concluded that N_2^+ had probably been observed; perhaps the incidence can be related to variations in solar activity.

Spinrad (Ref. 3-25) estimates surface pressures of the order of 10 atmospheres, but Sagan (Ref. 3-31) gives values greater than 30, with "an outside chance" of being as high as several hundred atmospheres.

The limiting value of H_2O shown in Table 3-2 is based on the negative results of a search by Spinrad (Ref. 3-32). Negative results have also been reported for H_2 and CH_2O by Spinrad (Ref. 3-31) and for CO, N_2O, NH_3, CH_4, C_2H_4 and C_2H_6 by Kuiper (Ref. 3-2).

3.4.2 Venus Irradiance and Albedo. Solar irradiance data are presented in Table 3-3. The average solar irradiance of Venus is almost twice that for Earth. The value remains almost constant throughout the year because of the very low eccentricity of the Venus orbit (less than for any other planet).

The very high albedo is caused by the persistant cloud layer, the nature of which is not known (conjectures have included H_2O, CO_2, and hydrocarbons). Colors for the clouds have been reported including yellow and brown, with occasional markings, both bright and dark.

Because of the absence of knowledge about inclination of the planetary axis or spin rate, no seasonal or diurnal irradiance data are available. Inclinations ranging from 0° to 90° have been reported (Ref. 3-11). The radiation balance of Venus has been analyzed by Sagan (Ref. 3-33).

3.4.3 Venus Surface Temperature. Spinrad (Ref. 3-25) has estimated surface temperatures of the order of 600°K; Sagan (Ref. 3-31) has calculated a dark-side temperature of the order of 640°K and a bright-side value of about 750° K. However, earlier observations do not reveal substantial temperature differences between dark and bright sides (Ref. 3-10), which implies either short-period diurnal rotation or substantial atmospheric mixing to keep temperatures equalized.

3.4.4 Venus Surface Features. A considerable range of speculation has been exercised in estimating Venus surface conditions, with insufficient data to provide direct evidence.

3.4.5 Venus Magnetic Field. A recent unpublished report of The Mariner 2 Venus encounter on 14 December 1962 indicates a magnetic field considerably less than that of the Earth.

3.4.6 Venus Radiation Belt. From the observation of the small Venus magnetic field it follows that there should be a weaker trapped radiation belt, if any. The Mariner 2 Venus encounter also provided a measurement of no substantial increase in radiation level compared with interplanetary data, at about 6.6 Venus radii from the center of Venus.

SECTION 4

THE INTERPLANETARY ENVIRONMENT

Phenomena considered here as potentially hazardous to man in space include: a) high energy solar protons, b) cosmic radiation, c) trapped particle radiations, d) meteoroid streams, e) comets, and f) meteorites.

An attempt is made to forecast mean annual solar proton fluxes for the next two solar cycles, 20 and 21. Because of the many assumptions that are necessary for this work the results can only be heuristic. However, if the next peak in solar activity should occur 7 years after the 1957-58 peak, rather than 11 years later, it is not disastrous because the long range predictions can be improved accordingly. The basic intent is to make an initial attempt at establishing working methods for solar flare prediction, associated flare-particle flux intensity probability, flare-particle encounter probability, probable fluxes which filter through radiation shields, and shield selections.

No attempt is made to shield the crew from cosmic radiation (CR). The philosophy used is to provide a storm shelter for solar flare and trapped particle radiations, and essentially no additional shielding for cosmic radiation. An exception to this occurs when an abundant supply of hydrogen is available for shielding. In this case, if desired, the crew might sleep in a shield within the hydrogen tank, thereby obtaining some relief from the heaviest CR primaries. Since, when interacting with H_2, the heavy primaries are replaced by more numerous particles with lower atomic weights, the shielding is impractical unless compelling reasons are found for eliminating heavy primaries.

Linear polyethylene was selected for dry shielding against protons and neutrons when liquid H_2 was not preferred. It has advantages over natural polyethylene because of its 3.8 percent greater H content (8.2×10^{22} H atoms/cm^3). Some 19 gm/cm^2 was used for Martian interplanetary missions, with the inner portion filled with 6 percent boron.

Trapped particles offer no significant hazard because of the polyethylene flare shelter. If the crew is forced to remain within the intense part of the Van Allen belt for several days the dose rate is no more than 3.8 rad/day.

It is believed that meteoroid streams, as well as comet orbits, should be avoided, especially near comets where the space density of debris would be expected to increase significantly. For example, intense Draconid meteor showers were observed on the afternoon of 9 October 1952 when Earth crossed the orbit 195 days ahead of the comet (Giacobini-Zinner). Showers have also been observed on occasion when Earth passed 170 days behind the comet.

Out of some 39 known, active, short period comets, three were found that had nodes between Mars and Venus in the 1973 to 1976 period. Their locations and dates are printed out in detail.

4.1 SOLAR CORPUSCULAR RADIATION. The charged particle flux in interplanetary space is governed by, and consists largely of, expanding gases from the Sun. According to Parker (Ref. 4-1) the corona appears to consist of hot and cool striations, with temperatures $>10^6$ °K and $<10^6$ °K, respectively, directed outward along magnetic flux lines. The Doppler width of coronal emission lines continually suggests temperatures of 2×10^6 °K whereas temperatures of $<10^6$ °K are indicated by relative emission line intensities of Fe_{XI} and Fe_{XIV}. The solar magnetic field presumably serves to partially insulate and isolate the hot and cold regions from each other.

However, within a given striation the thermal conductivity is extremely high and, as a consequence, the radial temperature gradients are probably not more than a few (≈ 3) degrees per kilometer near the Sun (Ref. 4-2). It follows that the hot lower corona heats the outer corona by thermal conduction, thereby enhancing the evaporation process. Consequently, at distances of a few solar radii, the corona is expanding at velocities of several hundred km/sec, i.e., in excess of solar escape velocity. Parker calls this escaping plasma the solar wind and identifies it with "solar corpuscular radiation" (Ref. 4-1).

A consequence of the solar wind model for the interplanetary medium is the dragging-out of the solar dipole field into a radial configuration in interplanetary space. This should be most evident at lower latitudes where the electrically conducting plasma flows perpendicular to the unperturbed magnetic flux lines. Indeed, Bachman (Ref. 4-3) was able to simulate the observed directions of polar streamers in the solar corona by assuming a dipole magnetic field with poles located on the axis of rotation at distances of 0.6 solar radii from the Sun's center. The representation fails at latitudes below 50° to 60°, presumably, because of the stretching out of the 1-gauss solar dipole field. This results in an interplanetary magnetic field which varies more as the inverse square of the distance than the inverse cube associated with dipoles. The field will actually have a spiral configuration because of solar rotation.

Preliminary study of Mariner II magnetometer data suggests interplanetary magnetic field values ranging from 2 to 10 gamma (Ref. 4-4).

In further support of Parker's theory, Mariner II (Ref. 4-5) consistently detected a measurable flow of plasma from the direction of the Sun. Ten ranges of plasma current were monitored, corresponding to proton velocities ranging from 314 to 1250 km/sec. These two extremes were observed only occasionally, whereas there were almost continuous plasmas moving at speeds of 563 and 690 km/sec which correspond, in Parker's theory, to isothermal corona temperatures of 0.75×10^6 °K and 1.8×10^6 °K, respectively (Ref. 4-1).

4.1.1 Solar Flares. The solar wind does not appear to present radiation hazards to man in space. The solar flare is thought to be the principle source and indicator of intense, high energy proton fluxes which are potentially hazardous.

In general, major solar flares are explosive outbursts of light and ionized matter in the vicinity of sunspots, and rarely occur more than 10^5 km from the center of a spot group. The flash of red hydrogen-alpha light (6562.8 A) may cover as much as 0.1 percent of the Sun's surface. Subflares, which are minor, short-lived outbursts, may occur without associated sunspots. They are not considered hazardous, although during periods of solar activity there may be one or two dozen every day. When seen on the limb (in profile) a flare may resemble a bright little mound directly above the photosphere. Since loop prominences often appear with flare intensities, it is thought that they too might be flares on the limb.

After, or during the initiation of a flare, some of the spot facular, or plage, regions may brighten considerably. Also, occasionally one of the dark hydrogen atom clouds (filaments), which float above the photosphere and become prominences when seen in profile, may be observed to brighten and temporarily vanish or blend with the background hydrogen-alpha light following a flare. Since intermediate filaments may remain dark and undisturbed, the phenomenon must not be caused by direct radiation but rather by ions moving along magnetic flux tubes. It may be possible that the heating, or increase in ionization required to produce transparency, is caused by fast-moving, electromagnetic shock fronts traveling in curved paths or undergoing focusing.

Moreton (Ref. 4-6) and co-workers discovered flare-initiated disturbances moving through the solar atmosphere at speeds of 1000 km/sec. They also found that some filaments were activated at distances as great as 500,000 km.

It is safe to assume that flare energy is supplied by sunspot magnetic fields. Sunspots with irregular, or disordered, magnetic fields are more likely to produce great flares. A hint at this is illustrated in Table 4-1, where eight flares are listed which produced solar cosmic rays (protons in the Gev energy range) along with the associated sunspot (SS) magnetic field types. It is seen that four of the SS magnetic fields were complex (γ), three were semi-complex ($\beta\gamma$) and only one was bipolar (β). None were uncomplicated unipolar (α) spots.

In studying the flare of 23 February 1956, Parker (Ref. 4-7) found an energy of about 2×10^{32} ergs of which 0.6×10^{32} ergs were in hydrogen-alpha light. About 2×10^{30} ergs were spent in generating protons with energies greater than 2 Gev. At the Earth this gives about 10^4 ergs/cm^2 if the particles are spread over a solid angle of 1 steradian. Diffusion of this flux by interplanetary magnetic fields would effectively double the flux passing through a unit volume. Assuming an inverse square law, it is approximately doubled again as close to the Sun as Venus.

Table 4-1. Solar Cosmic Ray Flares

DATE	MAGNETIC TYPE OF ASSOCIATED SPOT	DISK POSITION OF FLARE	SUBSEQUENT GEOMAGNETIC ACTIVITY
28 February 1942	γ	4°E 7°N	Great Storm
7 March 1942	γ	90°W 7°N	Small Storm
25 July 1946	$\beta\gamma$	15°E 22°N	Great Storm
19 November 1949	β	70°W 2°S	No Storm
23 February 1956	γ	80°W 23°N	Great Storm
4 May 1960	γ	90°W 12°N	Moderate Storm
12 November 1960	$\beta\gamma$	~10°W 25°N	Very Great Storm
15 November 1960	$\beta\gamma$	~50°W 25°N	Great Storm

X-ray radiation from a class 2+ flare was measured by Friedman (Ref. 4-8) who found an integrated flux of 7100 erg/cm^2 at the Earth's distance. Assuming that this energy was spread over 2π steradians one obtains 10^{31} ergs at the flare site.

Total flare-associated radio noise energy has been as great as 10^{22} ergs (Ref. 4-9).

4.1.2 Procedures for Predicting Annual Solar Flare Fluxes to Interplanetary Spaceships. It is well known that solar flare data obtained by different observatories are frequently inconsistent. For example, the number of flares reported depends on the longitude of the observatory, or in other words, on universal time! Three times as many flares of class ≥ 1 are reported between 7^h and 8^h UT than are reported around 18^h UT. Secondly, twice as many flares of class ≥ 2 are reported near the center of the solar disk than near the limb. Finally, different observatories frequently disagree on the importance of the same flare.

Fortunately, the IGY flare data for the last six months of 1957 and for the entire year 1958 have been analyzed and modified to remove understandable conflicts of the types just mentioned (Ref. 4-10). This work was done by Constance Warwick of the NBS in Boulder, Colorado. Flare areas were also corrected to yield more realistic importance values.

The year 1958 was, therefore, selected as a model year to represent the last peak in solar activity (1957-1958). Since major flares are always associated with sunspots, flare activity in future years is estimated from predicted sunspot (SS) numbers.

In Figure 4-1 the predicted smoothed SS numbers for solar cycle 20, with expected peak in 1968, are superimposed on cycle 19, with a peak in 1957-1958. The average value of 11 cycles (8 to 18) is also shown, taken from Ref. 4-11.

The next SS number peak in 1968 is assumed to be around 135, which is about 2/3 of the 1957-58 peak. This is based on the work of Minnus who calculated that there was a 0.75 chance of the peak lying between 110 and 160 (Ref. 4-12).

Solar conditions identical to the model year 1958 were used for all interplanetary trajectories. Future years are weighted with respect to the model year on the basis of predicted smoothed SS numbers. Thus, the anticipated SS number peak of 135 in 1968 has a weight of 0.675, based on a SS number of 200 for 1958.

During the anticipated period of minimum activity from 1973 to 1976 the mean annual SS number may range between 10 and 20. Mean annual solar fluxes would therefore be expected to drop to 5 or 10 percent of their 1958 values. However, because of the many assumptions needed to make these predictions and to remain conservative, the annual flux at solar minimum is assumed to remain at 1/3 of the value at the

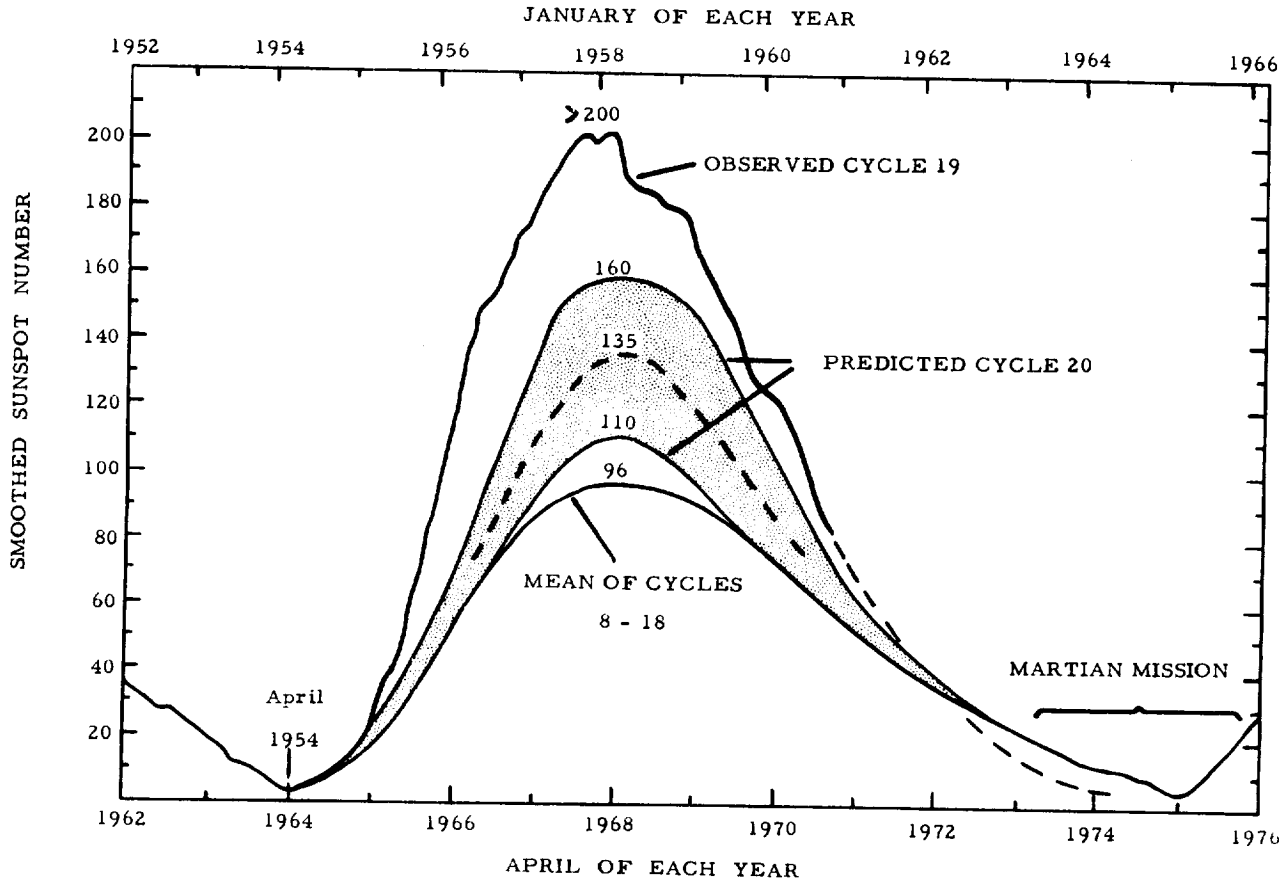

Figure 4-1. Predicted smoothed SS numbers showing cycle 19 (top scale), predicted cycle 20 (bottom scale), and the mean of cycles 8 to 18 (bottom scale). It is assumed that the incidence of major solar flares will occur approximately in proportion to the smoothed SS number.

preceding solar maximum. Since the forthcoming SS number in 1968 is expected to be 1/3 less than the 1957-1958 peak, the working value for the 1973-1976 minimum period might be taken as 1/3 × 2/3 or about 2/9 of the 1958 annual flux. One-third of the 1958 value is probably well on the conservative side.

4.1.2.1 Net Solar Flare Flux Per Mission. The calculation of the net flux encountered per mission by an interplanetary vehicle is a statistical problem since the solar distance is a variable, and the flares effectively occur at random. Also, there is not a one-to-one correspondence between flare incidence and particle encounter.

For representative computational purposes, the probabilities of occurrence of flares of various types are inferred from the frequency of their occurrence in the model year 1958. If the flare importance is limited to class ≥ 2, there is a total of 112 flares to consider. The probability of particle encounter from these flares must also be introduced, which effectively reduces the number of flares to 12, based on polar cap absorption (PCA), as explained in Section 4.1.2.2.

The total flux encountered per mission is calculated as follows:

a. For each trajectory of interest, the inverse square of the solar distance, normalized at 1 AU, is calculated for 10-day intervals. Thus, for a 410-day trip there are 41 points along the trajectory where solar conditions can be sampled (Figure 4-2).

b. The probability of occurrence of a specified number of flares of any given class is assumed to obey a Poisson distribution. Thus, a constant probability per unit time is used and the mean of the distribution corresponds to the average flare incidence for the corresponding flare class. Effectively, the various Poisson distributions are compounded with the weight factors discussed below, and a single resulting distribution is obtained. The justification for this simplifying approximation is that the probability of occurrence of each type of flare per unit time is small. In the actual computation, the simultaneous occurrence of more than one flare is excluded, and overlap between successive time intervals is ignored. The use of discrete time intervals instead of a continuous time base does not lead to any significant error.

c. When a flare occurs a flux is calculated, based on a normalized flux at 1 AU from a model class 3+ flare, and corrected for inverse-square effects. A weighting factor is then introduced which takes into account the flare class.

   Total flux, or source strength, from flares of different classes are weighted according to the product of average duration, hydrogen-alpha brightness, and corrected area. The relative weights used for flares of each class are indicated in Table 4-2.

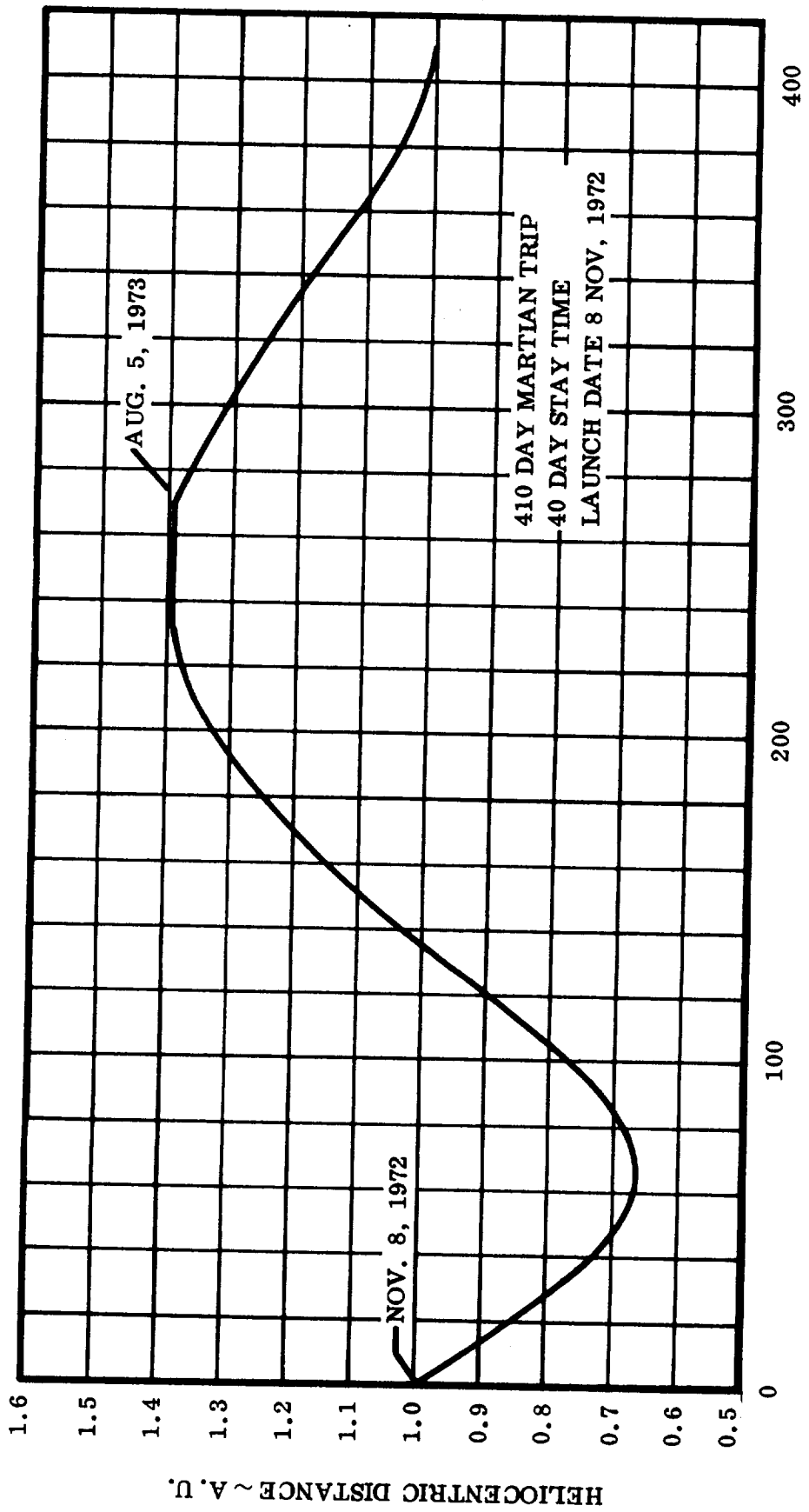

Figure 4-2. A plot of solar distance versus time for a 410 day Martian mission which comes fairly close to the Sun.

Table 4-2.

FLARE CLASS	WEIGHT
3+	1.0
3	0.2
2+	0.05
2	0.02

d. The net flux (which may be zero) associated with each sampling is stored in an integrating circuit and read out at the end of the trip.

e. This process is repeated several hundred times until the dose distribution is well defined. About 500 round trips are sufficient. Both the dose mean and the standard deviation are calculated in the program.

In making these calculations, both the probability of encountering flare particles from flares of each class, and a suitable model for class 3+ solar flares were required. A brief discussion of the analog computer program is given in Section 4.1.2.4.

4.1.2.2 Flare-Particle Encounter Probability. Polar cap absorption (PCA) events were assumed to be the most reliable indicators of the arrival of intense solar proton beams with energies in the 10 to 100 Mev range or higher. Also, since PCA events correlate well with flare-associated dekametric radio bursts, the latter are believed to provide evidence that flare particles have left the Sun (Ref. 4-13). Proton fluxes with insufficient intensity to produce PCA were assumed harmless. The number of PCA/year for flares of each class from 1956 to 1960 is plotted in Figure 4-3.

Table 4-3. Solar Flare and Polar Cap Absorption Data For 1958

FLARE CLASS	3+	3	2+	2	1+	1, 1-
NUMBER OF FLARES (1958)	4	9	43	56	550	9007
ASSOCIATED PCA EVENTS	3	2	3	4	--	--
PCA/FLARE	0.75	0.22	0.07	0.07	--	--
APPARENT ANGULAR BEAM WIDTH-STERADIANS	5.7	1.38	0.44	0.44	--	--

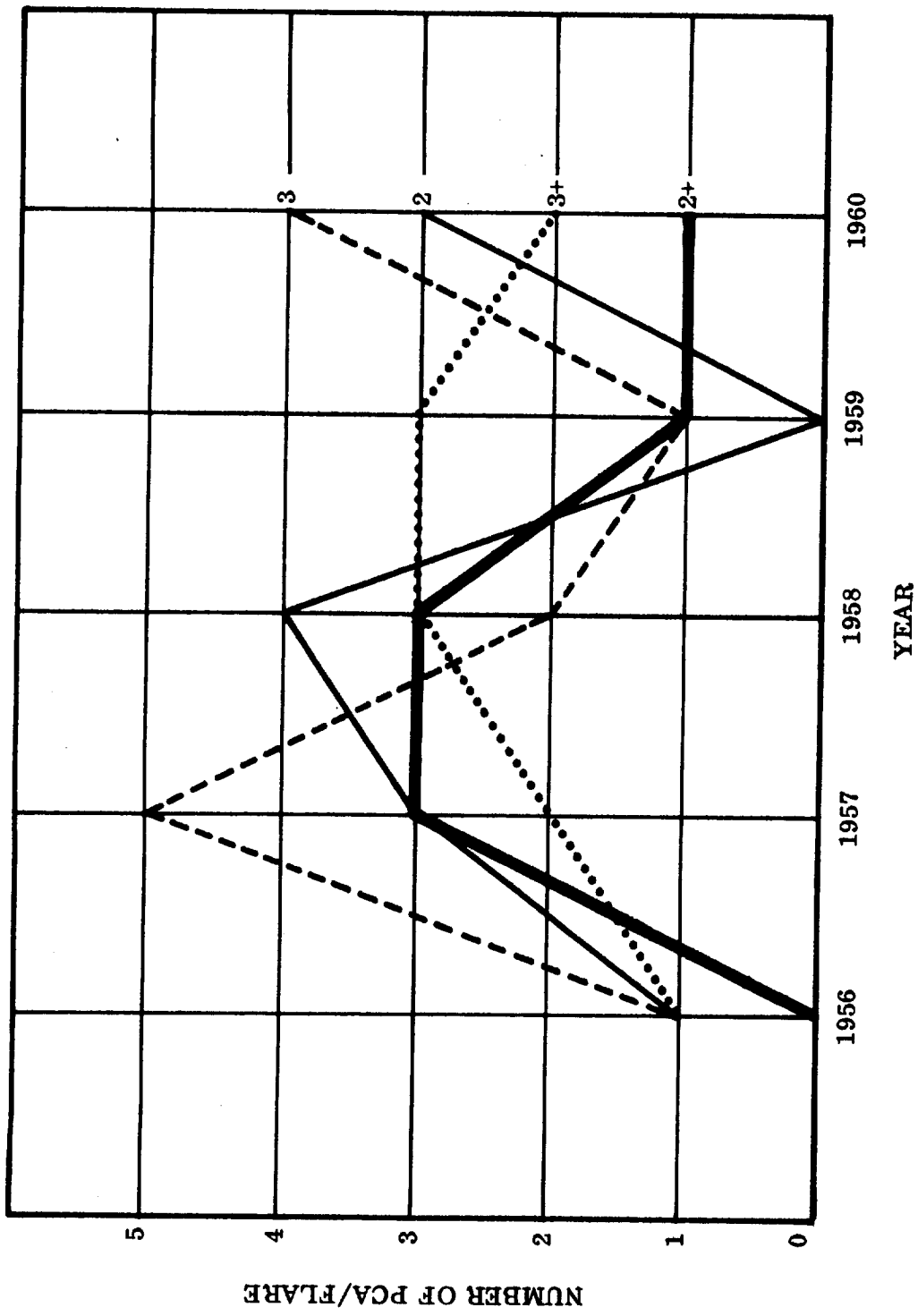

Figure 4-3. The number of PCA's/flare/year for flares of class 2, 2+, 3 and 3+, and for the years 1956 through 1960. When more than one flare could be associated with a given PCA the largest flare was selected.

The data in Table 4-3 were calculated from references 4-10 and 4-13 to determine the effective number of hits on space vehicles from flares of different class. It is assumed that a PCA is synonymous with a vehicle "hit." This is believed to be justified because both Earth and the space vehicle are small compared to flare particle beamwidths.

The spiraling of high energy particles will introduce an error when vehicles are at great solar distances where the particles will be arriving almost from the West. Another source of error which also underestimates fluxes is the trapping mechanism in interplanetary space. This is not yet understood, and although the slow decay of flare flux can be integrated into the total normalized flux at 1 AU, the modification to the inverse-square-law decrease with distance may be significant. For example, the dependence may be closer to an inverse cube between Earth and the Sun, and closer to being linear between Earth and Mars (Ref. 4-14).

A plot of flare class versus PCA per flare class (from Table 4-3) for the year 1958 is shown in Figure 4-4. It shows that larger flares produce more PCA's, or more "hits" on space vehicles, per flare than small flares. If this is interpreted as a geometrical phenomenon dependent on angular beamwidth, then (from Table 4-3) flares of greater importance have larger beamwidths. This may be interpreted another way by assuming that flares of greater importance are more likely to produce intense particle beams. Whether particles are released might be determined by criteria such as strength and duration of decimetric or dekametric radio emission.

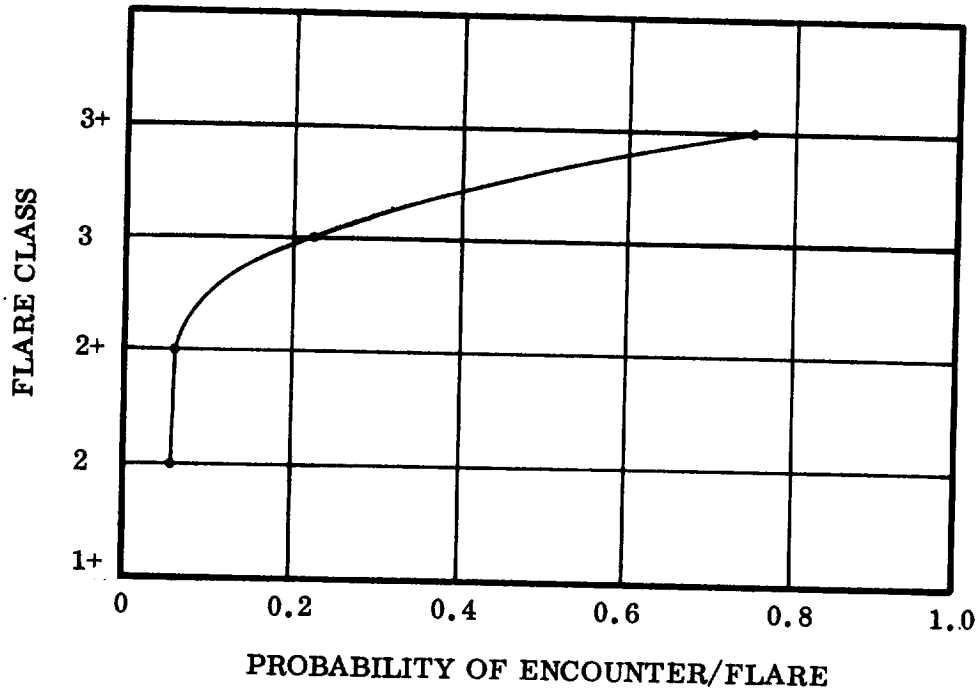

Figure 4-4. Probability of particle encounter/flare as a function of flare class. The probability of encounter/flare of a given class is defined as the number of PCA absorptions per year from flares of the given class divided by the number of flares per year of the given class.

4.1.2.3 Model Class 3+ Solar Flare. The flare of 10 May 1959 was used as a model for normalizing the radiation dose from class 3+ flares at a distance of 1 AU. This selection was made for the following reasons: a) a considerable amount of good data was available; b) the flare was analyzed from several viewpoints including the consequences of flare energy limitations (Ref. 4-15), and probable secondary particle productions in shields (Ref. 4-16 and 4-17); and c) the flare was larger in area (45 square degrees) and longer in duration (4.3 hours) than other flares of the last solar cycle (number 19).

It was therefore considered to be one of the more hazardous flares on record, although it could have been worse since there was a paucity of particles with energies above a few hundred Mev. It also occurred 50 degrees East of the central solar meridian, which suggests that Earth was not in a position to receive the most hazardous flux component from this flare.

It is well known that cosmic-ray-type flares tend to occur in the northwestern quadrant of the solar disk. The flare of 23 February 1956, which produced particles with energies as high as 15 Gev, was on the NW limb. Other flares through 1960 which produced Gev particles are listed in Table 4-1.

The tendency for high energy flares to occur in the West can hardly be attributed to chance. The most reasonable explanation appears to be that the very high energy proton fluxes are greatly charged (lacking electrons) and are therefore steered by the solar magnetic field lines which spiral because of solar rotation. This is shown in Figure 4-5, where the accompanying low-energy plasma is expected to be less influenced by the solar magnetic field because of over-all neutrality and high inertia.

It is possible, therefore, if the 10 May 1959 and 23 February 1956 flares could have been interchanged, that Gev particles might have been detected from the very large May flare while they might have been missing from the February flare.

There is probably a most hazardous location for a great flare with respect to a space vehicle, where both high and medium energy fluxes deliver an over-all maximum dose, but this has not been determined.

4.1.2.4 Flare Simulation. A simple, yet adequately rigorous, probabilistic model is used to duplicate solar conditions during interplanetary missions. The random-event process is simulated on the analog computer by use of an electronic white-noise generator. Pulses which are random in time are used to sample on a repetitive sawtooth waveform varying linearly from 0 to 100 volts. Thus, random voltages are sampled which are uniformly distributed in the range 0 to 100. Voltage intervals within this range are assigned widths which are proportional to probabilities of flare-flux encounter and the remaining interval corresponds to the absence of flux.

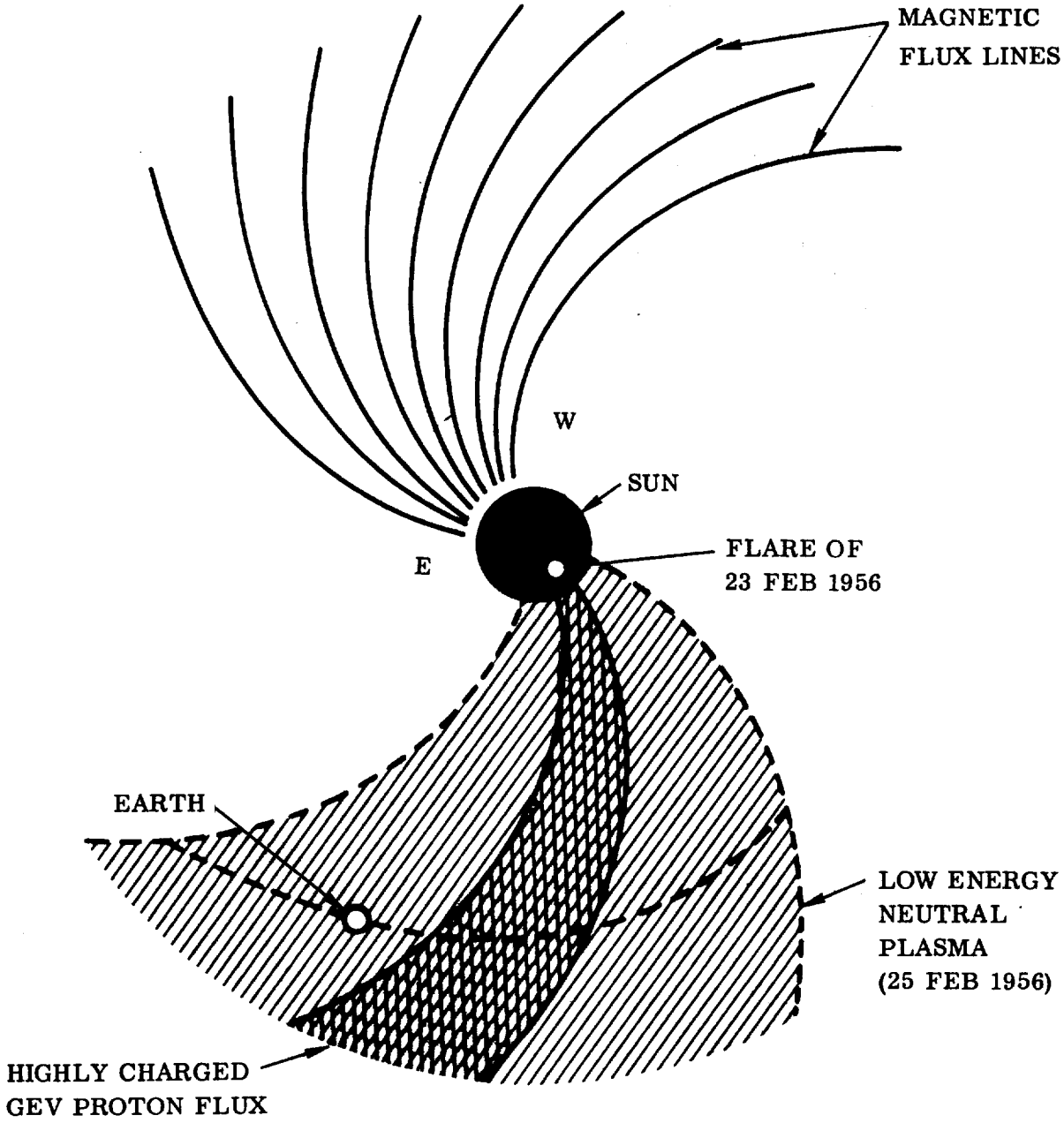

Figure 4-5. Representation of the solar magnetic field as seen from above, or north of, the solar equator, parallel to the axis of rotation. The flux lines are expected to be spiraled and may serve as guides for high energy flare particles.

Each sampled voltage level is classified according to the interval within which it lies. Whenever a given interval is thus triggered, a flare of that type is said to have occurred. A gate is then opened momentarily to a voltage accumulator circuit and a voltage is added which is proportional to the product of the flux for that type of flare at unit solar distance and the inverse square law correction factor for the actual position in the orbit. At the end of the mission, the accumulator thus registers the total dosage contributed from all flares. This value may be read out on a meter, plotted on a graph, or simply transferred automatically to another register which is part of a circuit for cumulative computation of both the mean dose and the standard deviation.

The prototype analog computer block diagram is shown in Figure 4-6. Standard analog computer symbols are used. The "intensity function," namely, $1/R^2$ versus time, is set up on a diode function generator. The function is approximated satisfactorily with a number of straight line segments. Each individual simulated mission requires a matter of seconds on the computer.

The computer used is an Electronic Associates Model 16-special, operated in the repetitive operation mode. Several dozen operational amplifiers are employed, along with a modest array of relay comparators, servo-multipliers, and a white-noise generator. The simulation technique is regarded as cheap, flexible, and easy to program and run on short notice.

4.2 PRIMARY COSMIC RADIATION. Cosmic rays are believed to consist of elementary nuclei with atomic numbers ranging up to 27 or higher. Primary cosmic ray electrons have been discovered (Ref. 4-18 and 4-19) in the energy range 0.3 to 3.0 Gev. More recently (Ref. 4-20), primary electrons in the rigidity range 10 to 1000 Mv were observed to undergo a 40 percent Forbush decrease in flux while the primary protons underwent a simultaneous 9 percent decrease for $E > 350$ Mev. The omnidirectional electron flux, with $E > 1.3$ Gev, may be of the order of $0.1/cm^2/sec$. The fluxes appear to be omnidirectional in space and are assumed to originate within our galaxy.

The particle energies range from the order of 10^2 Mev to over 10^{12} Mev. Ionization losses increase rapidly for energies below 10^2 Mev and it is not realistic to extend the spectrum any lower. Minimum particle energies measured during the recent cycle of solar maxima and minima were > 420 Mev and > 230 Mev, respectively (Ref. 4-21).

The various nuclei found in galactic radiation and their relative abundances are indicated in Table 4-4 from a compilation by E.P. Ney.

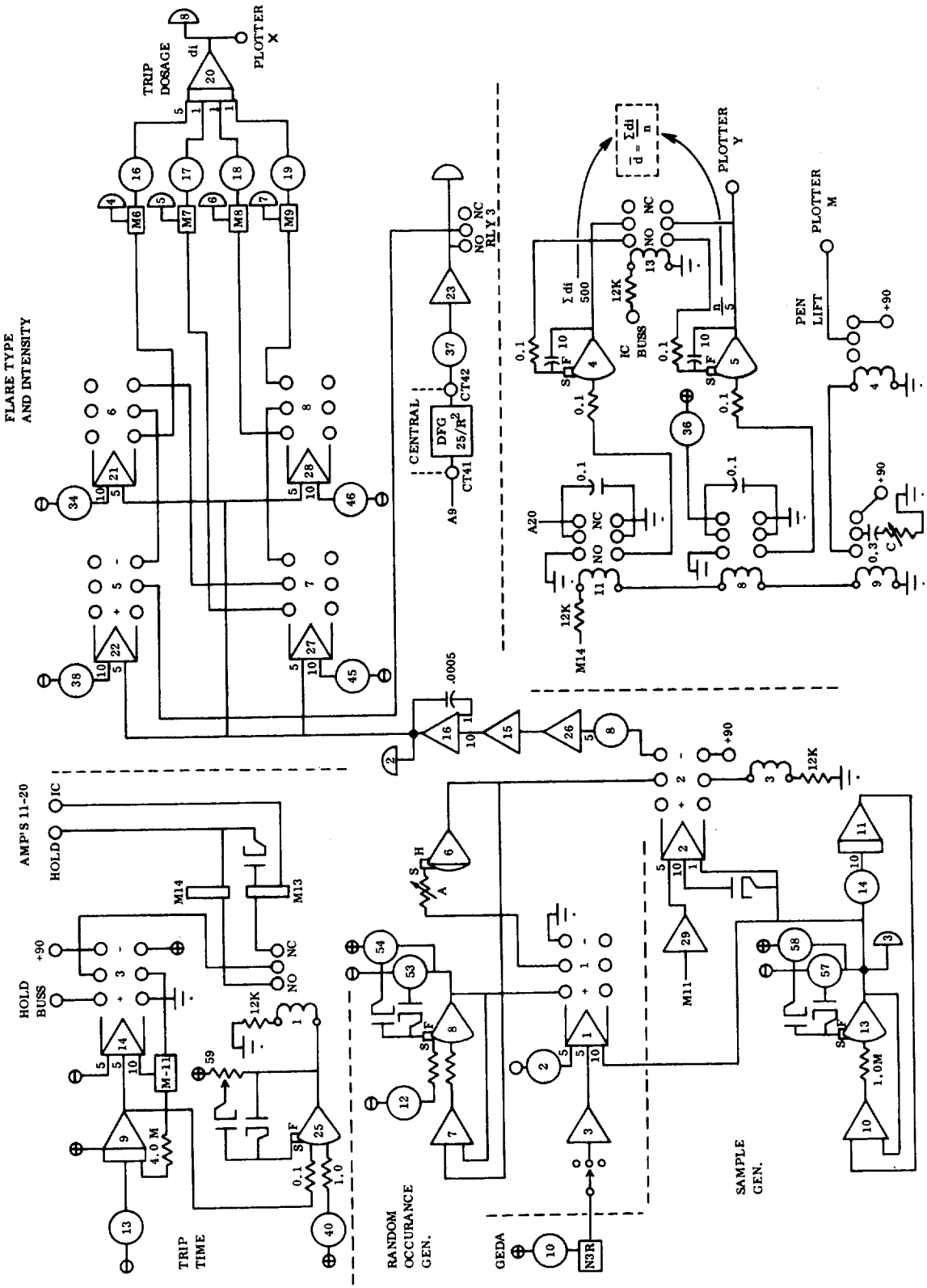

Figure 4-6. Prototype Analog Computer Block Diagram for Solar Flare Simulation

Table 4-4. Abundance of Cosmic Ray Particles

NUCLEI	ABUNDANCE
Hydrogen	1000
Helium	155
Li, Be, B	0.24
C, N, O, F	1.2
$10 \leq Z \leq 22$	0.3
$23 \leq Z \leq 30$	0.1
$Z > 30$	0.0001

The mean energy of charged particles in the inner solar system can be estimated from the cosmic ray exposure ages of meteorites; e.g., by determining the steepest helium-3 gradients (Ref. 4-22). The average energy, when determined in this manner, ranges from 4 to 6 Bev for protons, and is constant within a factor of three (private communication from E.L. Fireman).

The proton energy spectrum is given approximately by

$$N(>E) = \frac{0.3}{1+E^{1.5}} \text{ p/cm}^2\text{/sec/steradian}$$

which is valid over the energy range 500 Mev $\leq E \leq 2 \times 10^4$ Mev (Ref. 4-23).

Heavier nuclei have similar spectral shapes but with somewhat lower average energies.

Cosmic ray intensities are known to vary 180 degrees out of phase with the general solar activity. Presumably, this is caused by outgoing magnetized plasmas which turn incoming charged particles away from the Sun. Collectively, the outgoing plasmas constitute an ionized wind, referred to as the "solar wind," caused by enhanced coronal evaporation (Ref. 4-24). It is probably reinforced at solar latitudes below 60 degrees or so, where flares, plages, prominences (spicules), and sunspots are more plentiful.

Forbush discovered that geomagnetic storm producing plasmas from major solar flares could also modulate the cosmic ray background, the changes (decreases) being transient in nature, short-lived (Ref. 4-25) and as great as 30 to 40 percent.

Forbush decreases can be attributed to magnetic fields carried with solar plasmas rather than to disturbances in the geomagnetic field. This concept received considerable support when cosmic ray decreases were registered by both Pioneer V and the Earth, while the former was well beyond the terrestrial magnetosphere.

The fact that cosmic ray intensities decrease when solar activities increase was established by Forbush from measurements of secondary neutrons at sea level. Sea level neutron intensity changes between 1955 and 1958 amounted to 20 to 30 percent. Cosmic ray primaries with energies below 2 Bev do not produce sea level neutrons except possibly over the geomagnetic poles. However, they undergo greater intensity variations than the higher energy components (about a factor of two between solar maximum and minimum), based on measurements of the over-all ionization near the top of the atmosphere at high latitudes (Ref. 4-23).

4.2.1 Cosmic Ray Radiation Dose. Measurements by three different space probes far from Earth agree within 20 percent on CR particle intensities; e.g., Mechta: 2.4 particles /cm^2/sec; and Pioneer V: 2.5 particles/cm^2/sec. These measurements were made near the peak period of the last solar cycle (1959) and are therefore expected to be an underestimate of the cosmic ray flux at either solar minimum or at greater solar distances than 1 AU where solar modulations should be less effective. It is, therefore, probably justifiable to assume twice this flux for the expected solar minimum period from 1973 to 1976.

If the flux density is taken to be 5 particles/cm^2/sec with a mean particle energy of 4 Bev, the power passing through a unit volume is 0.032 ergs/cm^2/sec or an energy density of 1.0×10^{-12} erg/cm^3. This compares favorably with Woltjer's estimates (Ref. 4-26) of energy densities in the galaxy; e.g.,

Magnetic energy density = 4×10^{-12} erg/cm^3

Kinetic energy density of random motion = 1×10^{-12} erg/cm^3

Energy density of cosmic rays = 1×10^{-12} erg/cm^3

Kinetic energy density of galactic rotation = 5×10^{-10} erg/cm^3

The optical radiation in the galactic plane is about 0.5×10^{-12} erg/cm^3.

If the entire flux were absorbed by a mass of 1 gram, the radiation dose would be 10^4 rad/year. However, there is no material with this capability. High energy protons, for example, give up about 1.8 Mev per gram in tissue, or in materials of low atomic number, while low energy protons relinquish about 6 Mev/gram based on Berkeley bevatron data.

The presence of heavier nuclei in cosmic rays slightly increases these values. For example, Pioneer V, while measuring the free-space flux of 2.5 particles/cm^2/sec inside a volume shielded by roughly 1 gm/cm^2 of material having a low atomic number, recorded an ionization rate of 5×10^{-4} rad/hr, or 3.5 Mev/gm/particle.

The walls of the Mars vehicles, as presently conceived, provide about 0.4 gm/cm^2 of aluminum/fiberglass insulation, which wipes out protons with energies below 16 Mev, but has little effect on cosmic rays. Since 1 gm/cm^2 of shielding does not offer any significant additional protection against cosmic radiation, the ionization rate data for Pioneer V can be used in making radiation dose estimates. This gives 12 mrad/day or 4.32 rad/year. If the rate is doubled, as explained previously, the net CR dose for a 410-day mission is 10 rad. Secondary radiation from the surrounding vehicle mass will increase the dose rate over Pioneer V. An increase of 50 percent is assumed. This increase is believed to be realistic but it could be higher, depending on vehicle mass location. The last two Soviet astronauts averaged 12 mrad/day but they were partly shielded by both the Earth and its magnetic field.

The physical effects of continuous low level radiation in humans have not been adequately defined. Some data exist; e.g., Carter and Knowlton (Ref. 4-27) found a statistically significant drop in total white count and absolute neutrophile and lymphocyte counts, in a study lasting 77 weeks, where 10 human beings received a gamma radiation dose rate of 0.2 roentgens/week. However, part of the cosmic ray dose results from heavy primaries where the rad concept is of little value. The rad is normally used as a measure of absorbed dose per gram of material, or tissue. The damage produced by heavy cosmic ray nuclei is limited to tracks less than about 440 microns wide but sometimes several 1000 microns long. Iron primaries can produce as many as 10^5 ion pairs/micron in tissue as shown in Figure 4-7. The dashed lines show the various energy levels along the path of each kind of particle as it terminates in water. The resultant dose to the region within the ionization track can be very high. This is illustrated in Figure 4-8 which is taken from Ref. 4-28.

The number of hits from heavy nuclei and associated "thin downs" on radiosensitive regions, such as the sensory cells of the inner ear, the retinal cells, etc., can be calculated to assess the hazard involved. However, quantitative data establishing the relation between hits in sensitive cells, or nerve tracks, and resulting catastrophies have not been obtained. It is probably necessary to use an experimental manned space station for providing such information.

It is known that the pigment cells (melanocytes) of hair follicles have a high radiosensitivity, and the loss of three to six pigment cells can turn the whole hair white. The sensitive melanocytes are about 30 microns wide and twice as deep.

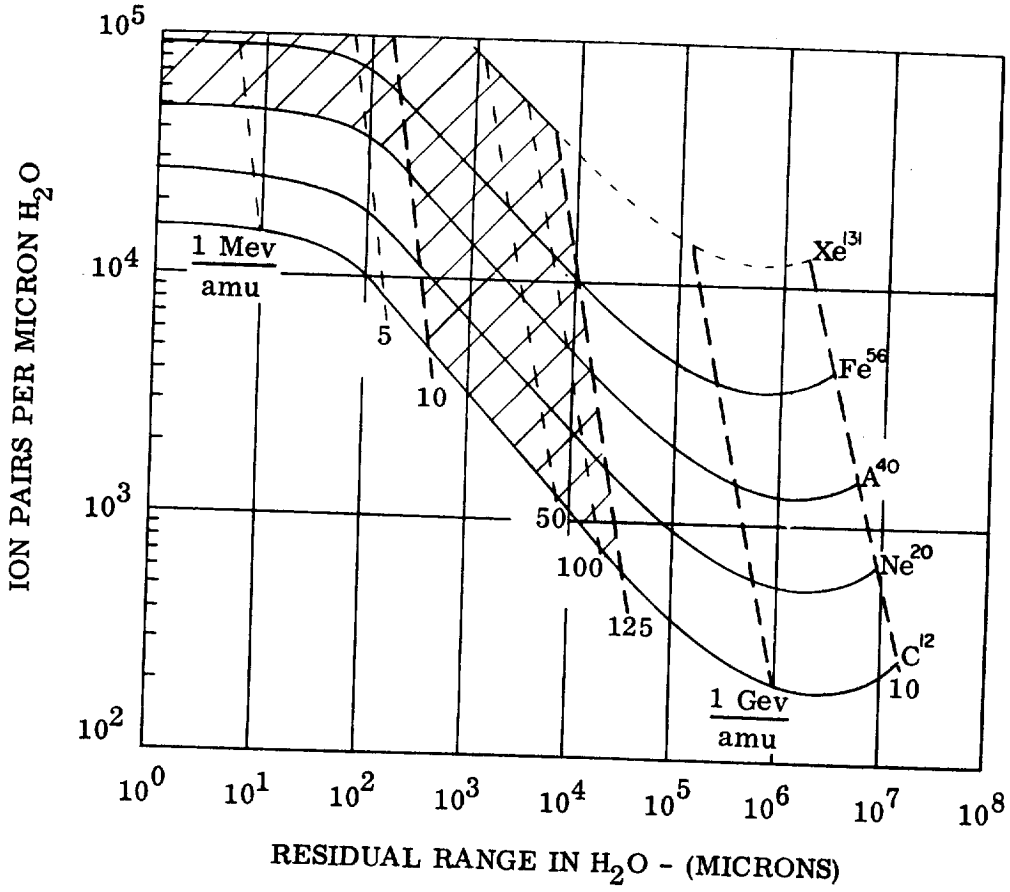

Figure 4-7. A plot of residual range for nucleons having atomic weights between 12 and 131 and the associated number of ion pairs per micron (10^{-3} mm) of water. Particle energies corresponding to various residual ranges are also shown. Courtesy of Dr. Roger Wallace, UCRL, Berkeley.

It is not known at this time to what extent heavy nuclei could initiate cataracts in the lens of the eye. There is evidence that radiation with a high rate of energy loss (LET) may be very effective in producing cataracts (Ref. 4-29). The minimum time for a cataract to form in rats after exposure to radiation is about six months. The epithelial cells which cover the anterior portion of the lens are sensitive. The cataracts result after the damaged (not killed) cells migrate to the posterior (rear) part of the lens. About 200 rads from 100 Kv X-ray radiations have caused cataracts after 3 to 5 years in humans.

However, Curtis (Ref. 4-30) concludes that heavy cosmic-ray particles do not pose serious problems for man in space based on laboratory studies of mice exposed to deuteron microbeams to simulate heavy particle ionization patterns. It was deduced that a) brain tissue is very insensitive to the radiation, b) only minute abnormalities and possibly minute cataracts are formed in the eyes, and c) hair follicles, when hit, will probably turn grey.

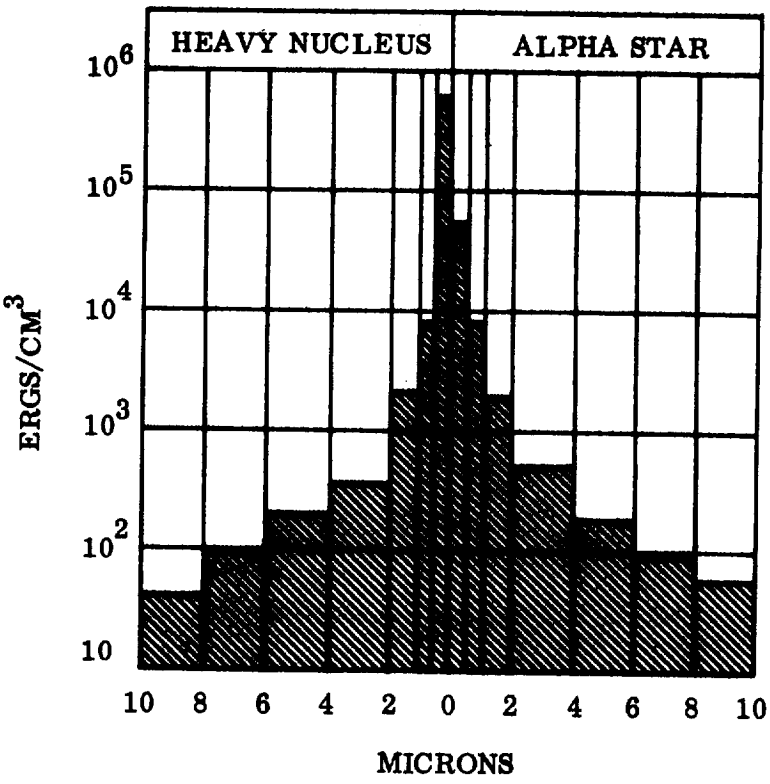

Figure 4-8. Showing the high energy deposition in tissue from heavy nuclei as a function of track width.

Two other problems which need further scrutiny in connection with cosmic rays are: a) the effects from extremely fast dose delivery rates uniquely characteristic of cosmic primaries, and b) the fact that there appears to be no clear low-level tolerance limit for cosmic radiations.

4.2.2 Nuclear Shielding. The mass of shielding that a charged particle can penetrate is given by its range in the shield material, unless it has a nuclear interaction. Protons with energies of a few Mev (less than 20 Mev) have little chance of nuclear interactions, except in beryllium which has a loosely bound neutron. As the proton energy increases the probability of a nuclear interaction increases, and for proton energies of a Bev or more there is hardly any chance of penetrating to their full range. Cosmic ray protons have average energies of 4 to 6 Bev where penetrations are governed solely by collisions. The concept of mean free path (mfp) is therefore of more interest. The mfp is defined as the range of mass traversed by a nucleon before undergoing a collision, and is the reciprocal of the total cross section. In carbon the mfp is approximately constant for proton energies over 180 Mev.

At high energies the inelastic nuclear cross section (σ_i) is related to the mean free path by

$$\lambda = \frac{1}{N\sigma_i} \tag{4-1}$$

where N = number of nuclei/gm. Now, a mass in grams, equal numerically to its atomic weight (A), contains N_o atoms or, if N is the number of atoms/gm, then

$$N = N_o/A \qquad \text{atoms/gm} \tag{4-2}$$

Hence, from the above equations,

$$\lambda = \frac{A}{N_o \sigma_i} \tag{4-3}$$

The nuclear cross section for high energy nuclear interactions is essentially the inelastic cross section. The total cross section (σ_t) is defined as the sum of the elastic (σ_e) and inelastic cross sections. The effective "removal cross section" lies between σ_i and σ_t and coincides with σ_i at high energies. This is illustrated in Figure 4-9.

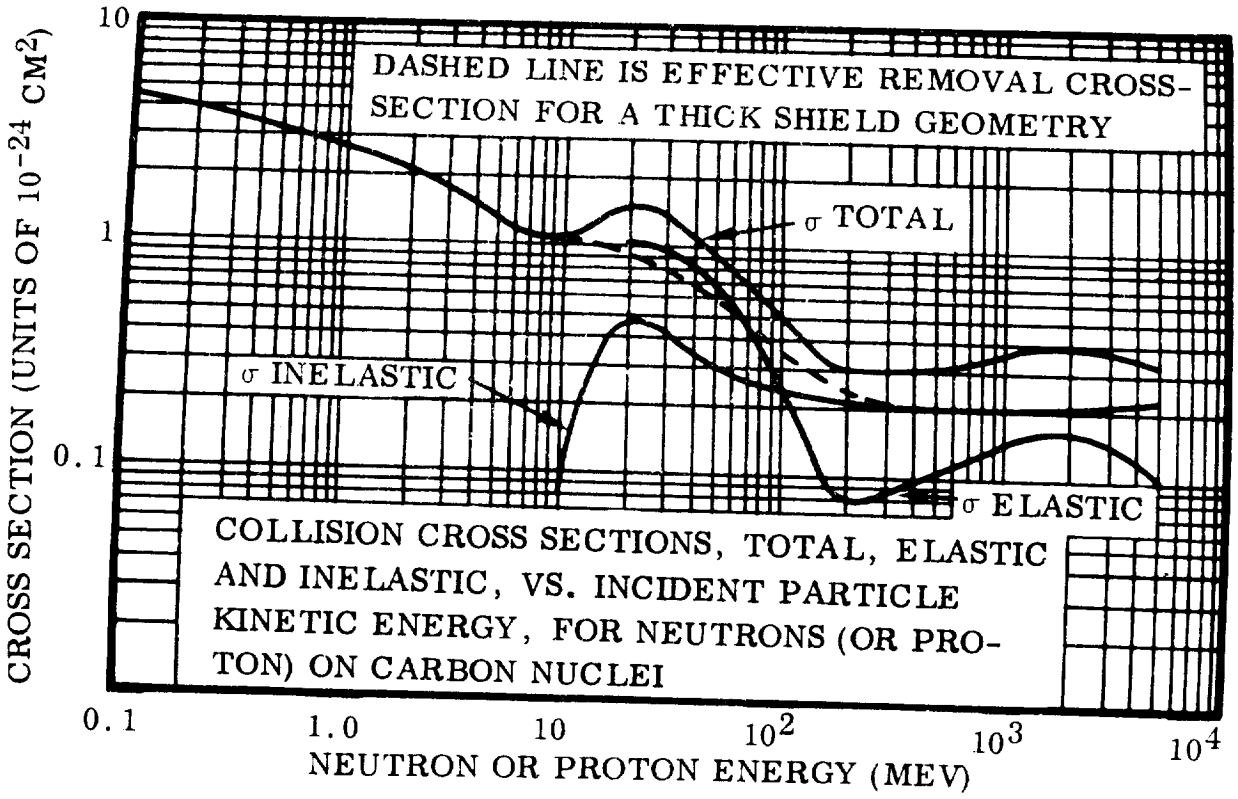

Figure 4-9. Cross Sections for Protons and Neutrons in carbon.

The inelastic cross section is related to the geometric cross section (σ_o) through a small correction for nuclear transparency. Transparency is defined as the probability of a neutron or proton traversing a nucleus without interaction when averaged over all possible paths. For example, Kocharian, et al (Ref. 4-31), found that the graphite nucleus was semitransparent to protons and π mesons at proton energies $E \leq 6$ Gev. For carbon,

$$\sigma_i = 0.65\, \sigma_o \tag{4-4}$$

The transparency decreases with increasing atomic number (Z) and, accordingly, they found that $\sigma_i = 0.75\, \sigma_o$ for copper, and 0.9σ for lead.

The collision cross sections for neutrons and protons are about equal at energies above 20 Mev. The coulomb forces affect charged particles at lower energies, and tend to produce strong scattering in the forward direction.

The inelastic cross section and mfp can be calculated as follows. Equation 4-4 is written as

$$\sigma_i = 0.65\, \pi R^2 \tag{4-5}$$

where R is a good measure of the size of the nucleus. In using Equation 4-5 it is necessary to use the coefficient 1.4 in the expression for R, viz.,

$$R = 1.4 \times 10^{-13}\, A^{1/3} \tag{4-6}$$

The coefficients in Equations 4-5 and 4-6 depend on the experiment. For example, the latter may vary between 1.1 and 1.5. However, the coefficient 1.4 is the proper one to use with 0.65. Now for carbon, from Equations 4-5 and 4-6

$$\begin{aligned} \sigma_i &= 0.65\, \pi\, (1.4)^2\, (2.29)^2 \times 10^{-26}\ \text{cm}^2 \\ &= 210 \text{ millibarns.} \end{aligned} \tag{4-7}$$

The corresponding mean free path is found from Equation 4-3) to be

$$\lambda = \frac{12 \times 10^{27}}{6.03 \times 10^{23} \times 210} = 95\ \text{gm/cm}^2.$$

It was also found that the inelastic nuclear interactions of π mesons and protons for energies ≥ 1 Gev were equal and independent of energy within the limits of experimental errors.

4.2.2.1 Hydrogen Shielding. Hydrogen appears to provide the maximum amount of protection against CR nuclei with the least mass. That is, the collision cross section (σ_i) varies as $A^{2/3}$ while the mass varies as A. Thus the ratio σ_i/m varies as $A^{-1/3}$ and is greatest for hydrogen. A comparable carbon shield would be more than twice as massive, although there is a weight problem in containing hydrogen. Hydrogen, boron, lithium, polyethylene, water and other low-Z materials are therefore of great interest for CR shields. These materials also have the advantage of contributing no heavy recoils when nuclear stars occur.

Hydrogen does not yield secondary neutrons until the incident nuclei are energetic enough to produce reactions such as

$$p + p \rightarrow \pi^+ + n + p \quad \text{and}$$

$$p + p \rightarrow \pi^+ + \pi^o + n + p.$$

Star formation is a very important phenomenon in reducing the heavy primary hazard. It eliminates a heavy nucleus, along with the associated high specific ionization that it creates just before stopping, and replaces it with lighter nuclei.

In a typical fragmentation, an iron primary may produce 7 neutrons, 6.2 protons, 1.1 deuterons, 1.2 tritons, 0.75 He^3 nuclei, and 2.3 He^4 nuclei (Ref. 4-32). A magnesium nucleus (12 protons and 12 neutrons) is all that remains. The ionization density is proportional to Z^2. Prior to the collision it was 676 as compared to 162 ($6.2 + 1.1 + 1.2 - 2.3 \times 2^2 + 12^2$) following the collision, a reduction of 75 percent.

4.2.2.2 Mean Free Path of Heavy Nuclei. The collision cross section for nuclei i and k of atomic weights A_i and A_k is given by (Ref. 4-33)

$$\sigma = \pi (r_i + r_k - 2\Delta r)^2$$

where

$$r_{i,k} = 1.45 \times 10^{-13} A_{i,k}^{1/3} \text{ cm}$$

and

$$\Delta r = 0.85 \times 10^{-13} \text{ cm}.$$

For Fe nuclei on hydrogen

$$\sigma = \pi \left[1.45 \times 10^{-13} (1) + 1.45 \times 10^{-13} (3.825) - 1.7 \times 10^{-13} \right]^2$$

$$= 0.88 \times 10^{-24} \text{ cm}^2.$$

The mfp is then given by

$$\lambda = \frac{A}{N\sigma_i} = \frac{1}{6.03 \times 10^{23} \times 0.88 \times 10^{-24}}$$

$$= 1.9 \text{ gm/cm}^2.$$

The mfp in an iron shield is about 18 times as great (34.5 gm/cm^2), from which it is concluded that large metal masses such as generators and electronic equipment do not provide much additional protection against very high energy particles and may do more harm than good.

The curves in Figure 4-10 show the mfp for various nuclei in hydrogen and air. Brass is also shown as an example of a heavy material.

4.2.2.3 Thermal Neutrons. Since very low energy neutrons can be quite dangerous, especially to the eyes, materials have been selected to absorb them. This problem could become serious if a nuclear engine did not shut off properly, for example.

Boron and gadolinium are of particular interest for covering inside walls of shielding. Boron, hydrogen, and gadolinium cross sections are shown in Figure 4-11. Boron was chosen for a filler material on the inside walls of polyethylene shielding because: a) natural boron provides a high concentration of B^{10} isotope (about 18.5 percent) which has a very large capture cross section for thermal neutrons, surpassing H at energies below 1000 ev; b) it gives no capture γ radiation, yielding only low energy α particles which can be stopped by paper, and c) it has been added to polyethylene successfully.

Some properties of commercial linear polyethylene with 6 percent amorphous boron (Trona) are listed in Table 4-5. Data were supplied by Phillips Chemical Company.

Table 4-5. MARLEX 6000, Type 9 Plus 6 Percent Amorphous Boron (Trona)

Softening Temperature	260° F
Thermal Expansion	0.6×10^{-4} in./in./° F
Tensile Strength (2 in./min)	3930 psi
Tensile Elongation (2 in./min)	150 percent
Compressive Stress (Yield or stress at 1 percent offset)	2700 psi
Shear Stress (2 in./min)	3560 psi
Density	1.0 gm/cc
Appearance	Rigid Brown Solid

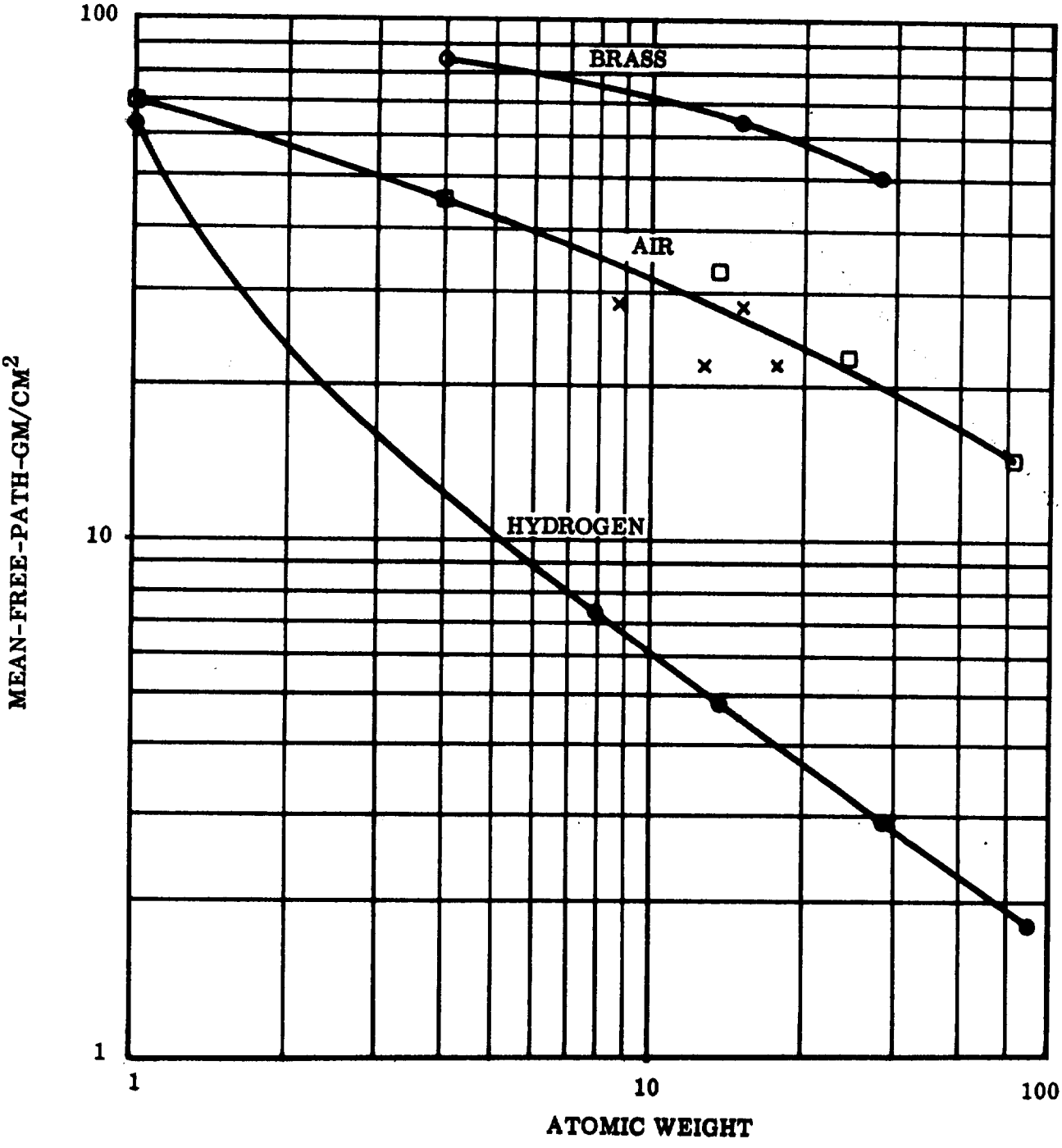

Figure 4-10. Mean-Free-Paths for Various Nuclei in Hydrogen, Brass and Air

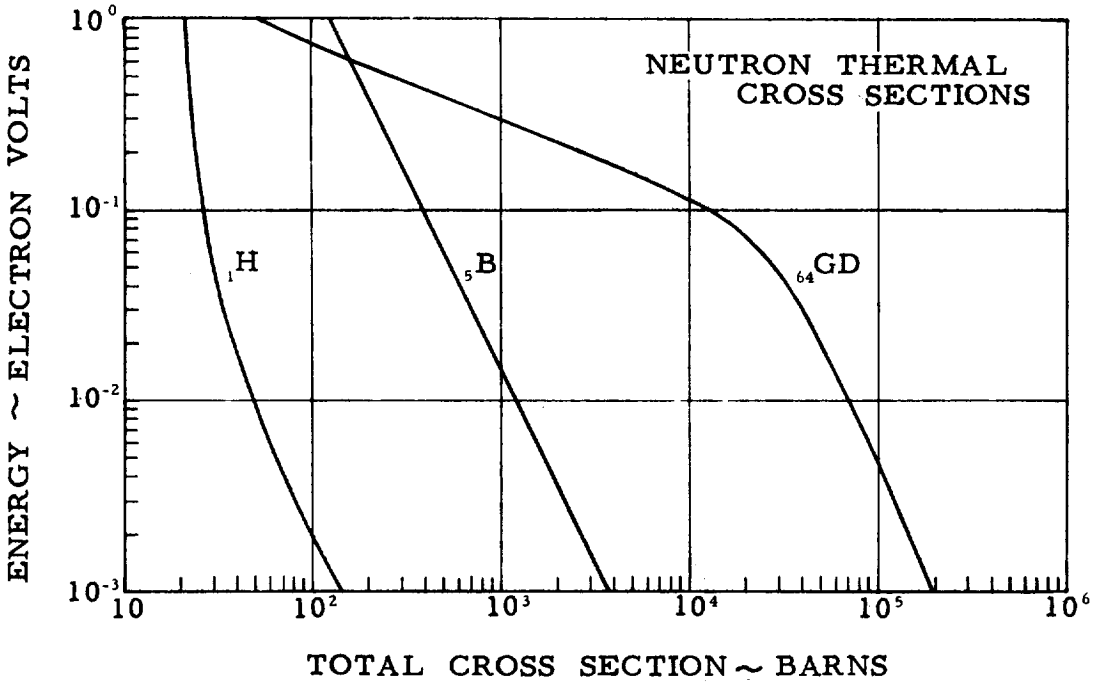

Figure 4-11. Total Cross Sections for Thermal Neutrons in Boron, Hydrogen and Gadolinium

4.3 TRAPPED PARTICLE RADIATION. Data from Explorer XII, Energetic Particles Satellite (8/16/61), indicates that there is a single large trapped particle region around Earth with different characteristics within the region (Ref. 4-34), rather than an inner and outer belt as formerly thought.

Older space probe measurements, suggesting 20 kev electron fluxes of 10^{11} particles/cm^2/sec, were based on the incorrect assumption that only bremsstrahlung, not electrons, penetrated the shielding; this made the flux about 10^3 times too high and the Mev electron flux far too low. O'brien, et al (Ref. 4-35), using Explorer XII data found the maximum electron flux to be closer to 10^8 particles/cm^2/sec. This effectively eliminates trapped electrons as a hazard to interplanetary spaceflight, since the solar flare shielding which must be provided is adequate for direct passage through the region. However, because of the larger number of electrons in the Mev energy range (Table 4-6), the outer part of the belt may give a bremsstrahlung dose rate of the order of 0.1 rad/hr. This has not been quantitatively evaluated up to this time, but it could influence emergency orbital operation procedures. The same is true for the artificial trapped particle belt.

The electron intensities in Table 4-6 were taken from Ref. 4-2. The Freden and White spectrum (Ref. 4-36) was used in estimating trapped proton intensities.

Table 4-6. Electron Intensities in Outer Portion of Trapped Particle Belt

ENERGY RANGE	ELECTRONS/CM^2/SEC
45 < E < 60 Kev	$\approx 1.4 \times 10^8$
80 < E < 110 Kev	$\approx 1.3 \times 10^8$
0.110 < E < 1.60 Mev	$< 10^8$
1.6 < E < 5 Mev	$\approx 2 \times 10^5$
5.0 < E Mev	$< 10^3$

4.4 COMETS AND METEOR STREAMS. Cometary nuclei and streams of meteoritic matter each constitute potential hazards to manned spaceflight. The nuclei, in themselves, present no serious problems because of their small sizes and scarcity. Cross-sectional areas are thought to be less than a few hundred km^2, while the majority are probably less than a few km^2 (Ref. 4-37). However, comet heads range in diameter from 10^4 to 10^6 km, while the tails have been as long as 2 AUs. Comet heads are more likely to contain larger size debris than the tails since they remain in the vicinity of the nuclei and move along the orbits. The tails are believed to be more feathery, consisting of gases and micron-sized dust particles blown out of the heads by solar wind and radiation pressure. In fact, larger sized debris, such as chips from nuclei (cometoids), must tend to lie along the orbits since at least a dozen meteor streams can be associated with known comets.

The appearances of new comets or re-appearances of comets observed more than about 200 years ago cannot be reliably predicted. However, from the comet discovery rate for the year 1959 it appears that there is about one chance in 6000 of a new comet coming within 10^{-2} AU of a space vehicle traveling between Mars and Venus. That is, the chance of a space vehicle passing through a new comet's coma is no more than about 1/6000 per year.

The distribution of comet perihelia on the celestial sphere is shown in Figure 4-12, where it is strongly suggested that new comets may come from almost any direction.

At least one comet is known to have struck the Earth during recorded history; i.e., the object which blew down an estimated 80 million trees in the Siberian taiga on 30 June 1908 (Ref. 4-32). The net energy of the explosions may have been as great as 10^{26} ergs and the total mass of the disintegrating objects about 10^{13} grams (Ref. 4-33). This is considered to be a small, faint comet whereas a great comet might have a mass of up to 10^{21} grams (Ref. 4-34).

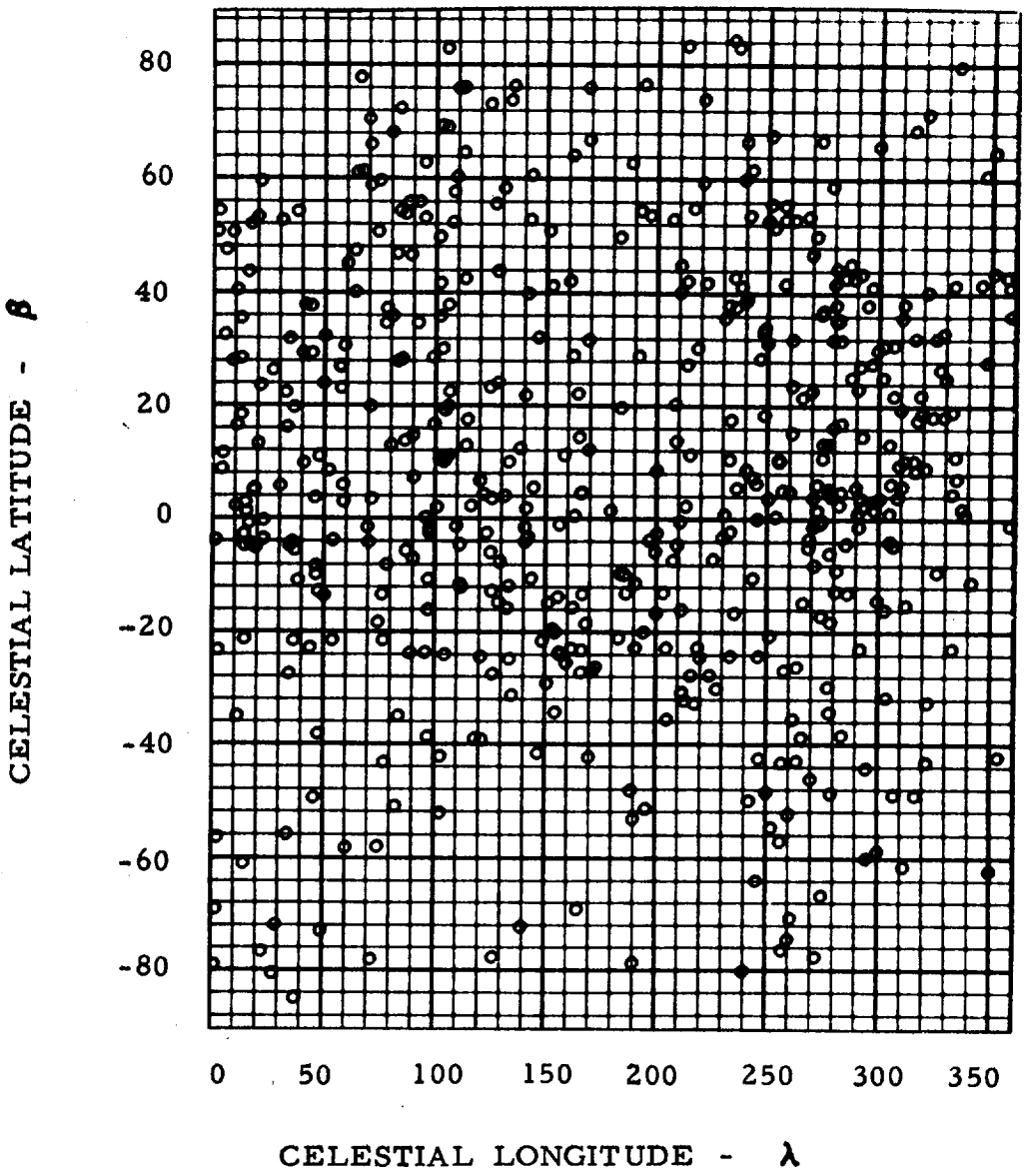

Figure 12. Distribution of 566 comet perihelia on the celestial sphere. This includes all comets recorded up to the year 1961.

The appearance of short-period comets can be predicted with a fair degree of accuracy, although we cannot say "all is well" regarding them. For example, orbital elements have been computed for 94 comets, with periods less than 165 years, observed between 239 BC and 1961 AD. Sixty-four of these were discovered during the latter 100 years. Thirty-two were lost after the first appearance, eight have not had time to make a second appearance, and fifteen others were missed after two or more appearances (Ref. 4-35). Thus, only 39 of the 94 recorded short-period comets may be expected to appear on their predicted returns.

Very little is known about meteor streams which do not intersect Earth's orbit. However, an idea of what might be expected can be obtained by noting how the perihelion distances of comets vary with numbers of comets. This is illustrated in Figure 4-13, where the perihelia of 566 different comets of all periods are plotted against the number of comets. There is a peak between 0.7 and 0.8 AUs. The nodal distances would be more significant but they have not been calculated for all of these comets. The inner nodes would be expected to peak somewhat under 1 AU. Because the orbits converge near the Sun, the meteor-stream encounter hazard should be greater on a Venusian mission than on a Martian mission. However, hazards from sporadic meteoroids were found by Mariner II to be small.

The expected number of nodes between Venus and Mars from March 1974 to January 1976 is three, as shown in Table 4-7. Because of the low inclination, comet Finlay presents the greatest hazard although, if properly avoided, it may offer the crew a rare opportunity for close observations during a Martian trip.

The location of the node in question is given by R_1 (solar distance), Ω_1 (longitude), and T_1 (time of node). The remaining symbols are: a (semi-major axis), P (period), e (eccentricity), q (perihelion distance), ω (argument of the perihelion), Ω (longitude of ascending node), and i (inclination).

Not all meteor streams carry equally hard objects; i.e. the, friability or crushing strength of shower meteors seems to be a characteristic of the particular stream. The Geminids, for example, have harder cores, are larger, and may be a degree more hazardous than most meteoroids. Jachia (Ref. 4-36) finds that Geminid densities are roughly 2.4 times as great as average meteoroids. He also notes that Taurid meteoroids do not fragment and appear to be unusually tough, although of average density (Ref. 4-37). On the other hand, the Draconids are exceptionally fragile and have been observed (on radar) to break up before being visible telescopically.

Orbital information relating to 24 meteor streams, adapted from reference 4-36, is given in Tables 4-8 and 4-9.

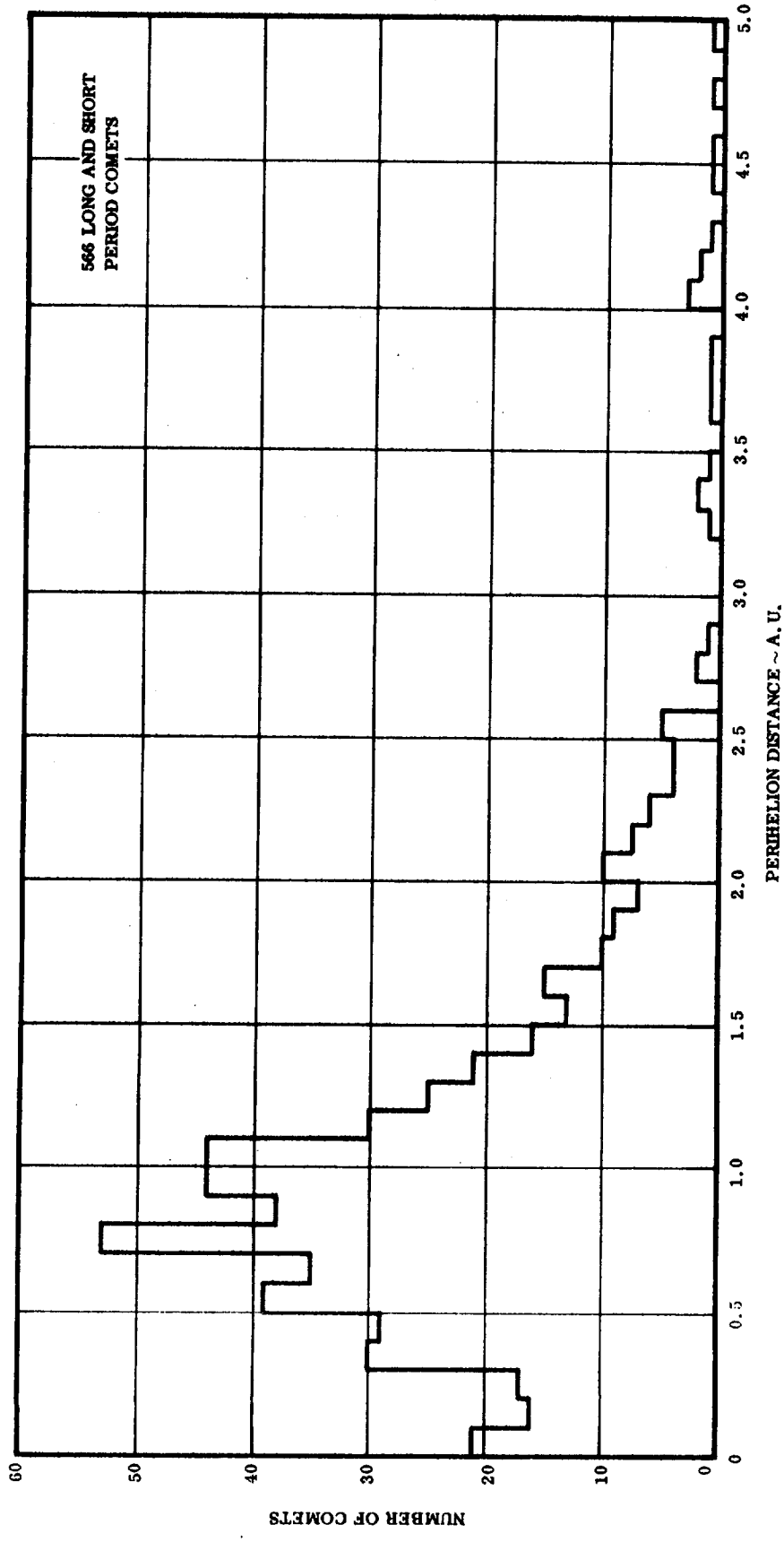

Figure 4-13. Perihelion distances for 566 short and long period comets. One comet with a perihelion distance of 5.5 was omitted.

Table 4-7. Cis-Martian Comet Nodes, 1973-1976

	a (AU)	P	e	q (AU)	ω	Ω	i	R_1 (AU)	Ω_1	T_1
Tuttle (1973.27)	3.109	5.48	0.641	1.117	37.9	165.6	13.8	1.2172	165.6	1973.12
Finlay (1974.47)	3.624	6.90	0.703	1.077	321.6	42.1	3.6	1.1826	42.1	1974.57
Perrine (1975.15)	3.472	6.47	0.667	1.154	167.8	242.6	15.9	1.1645	62.6	1975.18

Table 4-8. Meteor Stream Orbital Elements

STREAM	ω	Ω	i	a (AU)	e	q (AU)
Quadrantids	167.9°	282.6°	73.8°	3.42	0.715	0.974
Virginids	285.8	353.7	5.2	2.82	0.857	0.403
II	187.1	27.3	11.0	2.67	0.626	0.999
Lyrids	213.9	31.8	79.9	29.6	0.969	0.918
η Aquarids	83.0	43.1	160.0	5.0	0.91	0.47
Daytime, Arietids	29	76.8	21	1.6	0.94	0.09
Daytime, ζ Perseids	59	77.8	0.4	1.6	0.79	0.34
Daytime, β Taurids	246	276.4	6	2.2	0.85	0.34
Southern, δ Aquarids	154	302	29.3	2.60	0.976	0.062
Northern, δ Aquarids	332.6	138.9	20.4	2.62	0.973	0.070
Southern, ι Aquarids	127.5	311.0	6.0	2.88	0.920	0.230
Northern, ι Aquarids	308.0	150.9	4.7	1.75	0.842	0.265
α Capricornids	270.5	132.8	4.0	2.57	0.779	0.568
Perseids	151.2	138.1	113.7	20.8	0.955	0.936
κ Cygnids	204.2	144.3	37.0	4.09	0.762	0.973
Draconids	171.8	196.3	30.7	3.51	0.717	0.996
Orionids	86.8	29.8	163.2	7.70	0.930	0.539
Southern, Taurids	111.9	45.1	5.4	2.30	0.835	0.380
Northern, Taurids	298.4	221.8	3.2	2.14	0.849	0.323
Andromedids	242.4	224.4	6.0	3.34	0.776	0.748
Leonids	173.7	235.0	162.5	12.76	0.924	0.970
Geminids	324.3	261.2	24.0	1.39	0.899	0.140
χ Orionids	105.4	79.8	0.8	2.92	0.859	0.412
Monocerotids	128.2	81.6	35.2		1.002	0.186
Ursids	212.2	264.6	52.5	5.91	0.845	0.916

Table 4-9. Meteor Stream Observed Data

STREAM	U.T. Date at Maximum	Extreme Limits	Radiant 1950 R.A. Dec.	V_∞ km/sec	Radiant Transit (Local Time) Midnight = 00 hr
Quadrantids	Jan 3	Jan 1 4	230 + 48	42.7	08 hr 28 min
Virginids	Mar 13	Mar 5 21	183 + 4	30.8	00 49
II		Mar 13 Apr 21	157 + 56	15.2	20 49
Lyrids	Apr 21	Apr 20 23	270 + 33	48.4	03 59
η Aquarids	May 4	May 2 6	336 + 0	64	07 36
Daytime, Arietids	June 8	May 29 June 18	44 + 23	39	09 51
Daytime, ζ Perseids	June 9	June 1 16	62 + 23	29	10 59
Daytime, β Taurids	June 30	June 24 July 6	86 + 19	32	11 12
Southern, δ Aquarids	July 30	July 21 Aug 15	339 - 17	43.0	02 14
Northern, δ Aquarids		July 14 Aug 19	339 - 5	42.3	02 08
Southern, ι Aquarids		July 16 Aug 25	338 - 14	35.8	02 04
Northern, ι Aquarids		July 16 Aug 25	331 - 5	31.2	01 36
α Capricornids	Aug 1	July 17 Aug 21	309 - 10	25.5	00 00
Perseids	Aug 12	July 29 Aug 17	46 + 58	60.4	05 43
κ Cygnids		Aug 19 22	289 + 56	26.6	21 25
Draconids	Oct 10	Oct 10	264 + 54	23.1	16 13
Orionids	Oct 22	Oct 18 26	94 + 16	66.5	04 12
Southern, Taurids	Nov 1	Sept 15 Dec 15	51 + 14	30.2	00 42
Northern, Taurids	Nov 1	Oct 17 Dec 2	52 + 21	31.3	00 46

Table 4-9. Meteor Stream Observed Data, Cont

STREAM	U.T. Date at Maximum	Extreme Limits	Radiant 1950 R.A. Dec.	V_∞ km/sec	Radiant Transit (Local Time) Midnight = 00 hr
Andromedids	Nov 7	Nov 7	22 + 27	21.3	22 hr 23 min
Leonids	Nov 17	Nov 14	152 + 22	72.0	06 22
		20			
Geminids	Dec 14	Dec 7	113 + 32	36.5	02 01
		15			
χ Orionids		Dec 9	87 + 21	30.6	00 25
		14			
Monocerotids		Dec 13	103 + 8	44.0	01 21
		15			
Ursids	Dec 22	Dec 17	206 + 80	35.2	08 24
		24			

Additional streams mentioned by Millman (Ref. 4-38) are given in Table 4-10.

Table 4-10.

STREAM	SHOWER MAXIMUM	RADIANT (1950) α	δ
Aurigids	Feb 9	75	+ 42
Cetids	May 20	30	- 3
Scorpio-Sagittarius	June 14	260	- 26
Draconids	June 28	220	+ 58
Northern Arietids	Nov 12	50	+ 22
Beilids	Nov 14	24	+ 44

4.5 METEORITES. Asteroids are seldom seen at angular distances greater than about 35 degrees from the ecliptic. Meteorites are assumed to be asteroidal debris and consequently are expected to populate the same regions of space. Work which supports this assumption includes that by Wood (Ref. 4-28) who made a study of stony meteorite orbits and concluded that "stony meteorites pursue asteroid-like orbits and are not derived from the surface of the Moon as suggested by Urey".

Because of their apparent paucity, meteorites and asteroids are not expected to be encountered very often in cis-Martian space.

The following list of cis-Martian asteroids is of general interest for interplanetary flight (Ref. 4-39).

Table 4-11. Cis-Martian Asteroids

NAME	t_o	M_o	ω	Ω	i	e	q (AU)
Eros	18 Jan 1931	0.586	177.930	304.071	10.831	0.2398	1.1084
Albert	2 Oct 1911	7.929	151.940	186.094	10.825	0.5406	1.1876
Alinda	31 Jan 1942	358.049	348.119	111.029	9.024	0.5398	1.1602
Atami	19 June 1941	96.784	205.517	213.215	13.102	0.2552	1.4503
Amor	3 June 1948	22.165	25.549	171.202	11.924	0.4346	1.0850
Icarus	7 Aug 1950	53.499	30.912	87.746	22.979	0.8266	0.1869
Betulia	14 Dec 1952	291.862	158.888	61.874	52.037	0.4928	1.1135
Geographos	24 Dec 1954	195.077	276.211	336.999	13.325	0.3352	0.8271
1948 Oa	7 Oct 1948	0.000	126.314	274.191	9.397	0.4360	0.7715
Apollo	25 Apr 1932	319.984	284.878	36.077	6.422	0.5663	0.6445
Adonis	25 Feb 1936	22.086	39.537	352.538	1.480	0.7792	0.4348
Hermes	7 Nov 1937	327.038	90.687	35.367	4.685	0.4746	0.6780

t_o = Epoch
M_o = Mean anomaly at epoch t_o
ω = Longitude of the perihelion
Ω = Longitude of the ascending node
i = Inclination of orbital plane to ecliptic
e = Eccentricity

SECTION 5

MISSION OBJECTIVES

5.1 INTRODUCTION. Mission objectives were defined and evaluated in terms of their effect on scientific payload weight and power requirements, auxiliary vehicle requirements, and operational mission requirements.

The mission objectives were divided into general and specific objectives. The general objectives are based on the philosophy that the manned fly-by mission phase can be leap-frogged and that manned missions, at least to Mars, will occur in the capture-landing mission sequence, with optional Mars surface excursion capability already built into the first capture mission to Mars. It is realized that a precise definition of the specific objectives, and the establishment of priorities, in particular, must be the subject of intense study by the scientific and engineering community. It has been attempted here to set up a model that will serve as a starting point for future investigations and priority specifications which, no doubt, will lead to many modifications of the original model. The basic aspects of the mission objectives for the first manned flight to Venus or Mars are surveyed in Table 5-1.

Table 5-1. Early Manned Planetary Mission Objectives

GENERAL OBJECTIVES
1. Demonstrate the feasibility of manned round-trip missions to Venus and Mars, with temporary capture in the target planet's activity sphere and a manned surface excursion where feasible.
2. Mars: Conduct detailed reconnaissance of the planet surface and its environment in preparation for future landings and surface explorations.
3. Venus: Conduct reconnaissance of the surface and atmosphere to determine whether, and under what conditions, future manned landings might be feasible and to further the understanding of the physical characteristics of Venus, its history, and its part in the evolution of the solar system.
SPECIFIC OBJECTIVES
1. Astronautic Mission Objectives: Space technology Planetary/interplanetary operations
2. Scientific Mission Objectives: Planetary/interplanetary exploration Planeto-biological exploration Astro-clinical research

5.2 GENERAL OBJECTIVES. In defining the general objectives, the ultimate purpose of manned planetary flight, namely, surface exploration of the planets proper (primarily Mars) has been considered. Before this can be accomplished at the scale commensurate with the task, a capture mission capability, the prerequisite for a landing mission, must be demonstrated; and proper planetary (Martian) reconnaissance from orbit must be accomplished, providing detailed information in the form of a high-resolution map of the major part of the surface and in the form of atmospheric and surface data, so that a realistic choice of future landing sites can be made.

These two general objectives are not necessarily coupled (Figure 5-1). One is a technological objective, demonstrating the feasibility of manned flights from the activity sphere of our planet into that of the other. For the achievement of this objective man's participation is mandatory, since proving himself on a mission of this kind is part of the feasibility demonstration. The second objective is in the nature of space exploration and could, in principle, be handled by instrumented probes.

The advantages of combining these two objectives in one mission are obvious. However, since Mars appears to be the only planet for which an extended surface operation can be seriously planned, such combination of objectives ties the capture mission to Mars as target planet.

If the two objectives are not combined, one is free to consider demonstration of the feasibility of a planetary capture mission by a flight to Venus. If this flight is successful, a repetition in the form of a fast capture mission to Mars appears not warranted. For the planning of an extended surface operation, detailed Mars reconnaissance must then be carried out by instrumented probes of the Voyager or advanced Voyager type. Since a landing mission can hardly be planned realistically before the second half of the seventies, the number of opportunities for carrying out such reconnaissance is not inadequate, if planned in time (Figure 5-2). However, it must be assured that, in terms of capability and reliability, the probes can carry out the task. The photo-reconnaissance requirements in preparation for a manned landing mission are higher than those required for initial scientific information. The probe must be able to attain a reasonably accurate capture orbit and to transmit fairly high resolution pictures (10 to 30 meters) for at least one to two months. To the extent to which redundancy and ruggedness (hence, weight) contribute to the probe's reliability, launch vehicle capability sets practically no limits, if one is willing to accept the cost, since with the use of Saturn C-5 the escaping probe weight may be as high as 50,000 to 70,000 lb. The launch windows shown in Figure 5-2 for the probes are so selected that the hyperbolic excess velocities for Earth departure as well as Mars arrival do not exceed 0.2 EMOS (Earth Mean Orbital Speed). For capture in a circular orbit at 1.3 Mars radii distance, the impulsive velocity change lies, therefore,

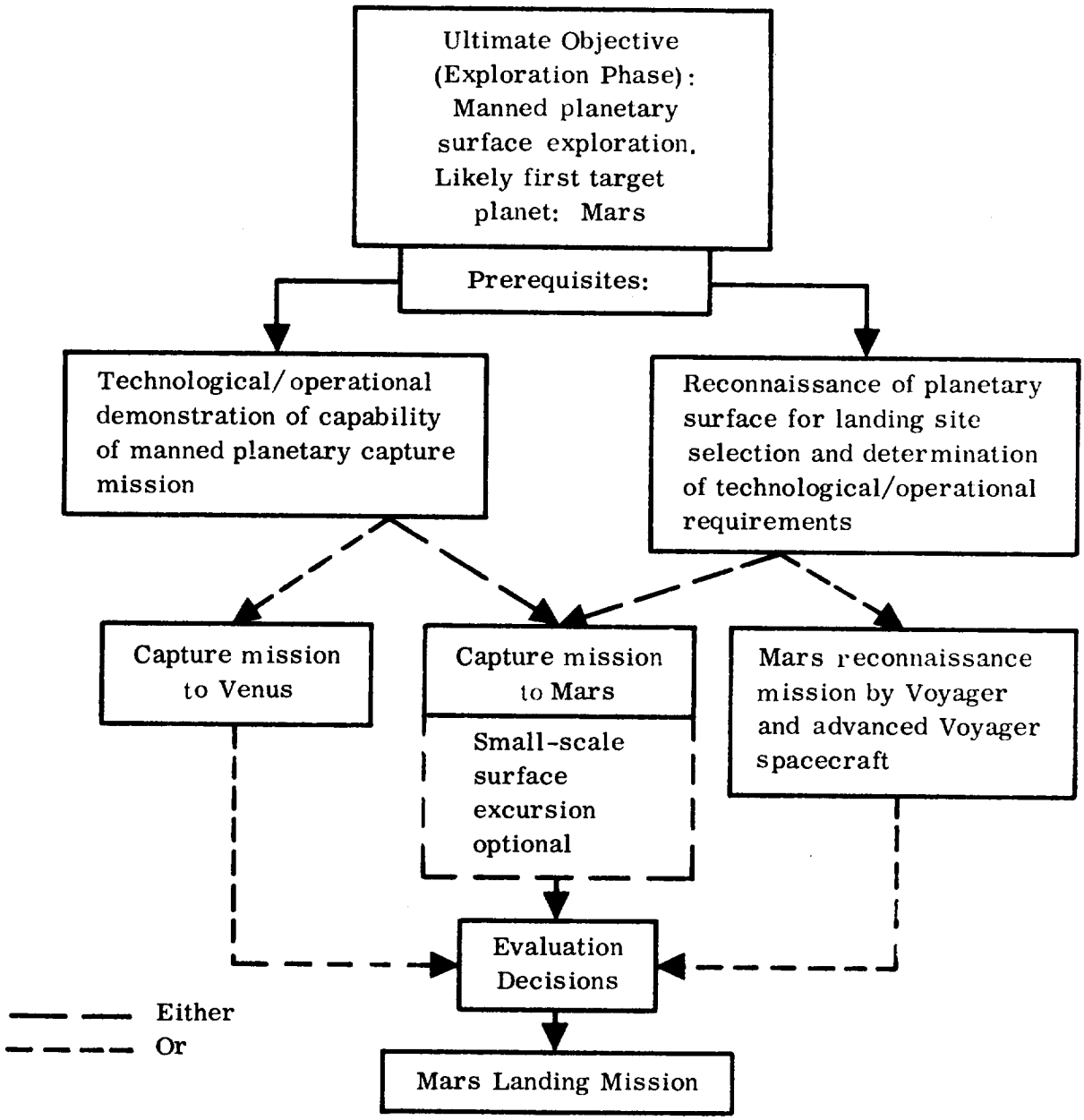

Figure 5-1. Two Alternatives in Preparing for the Capability of a Mars Landing Mission

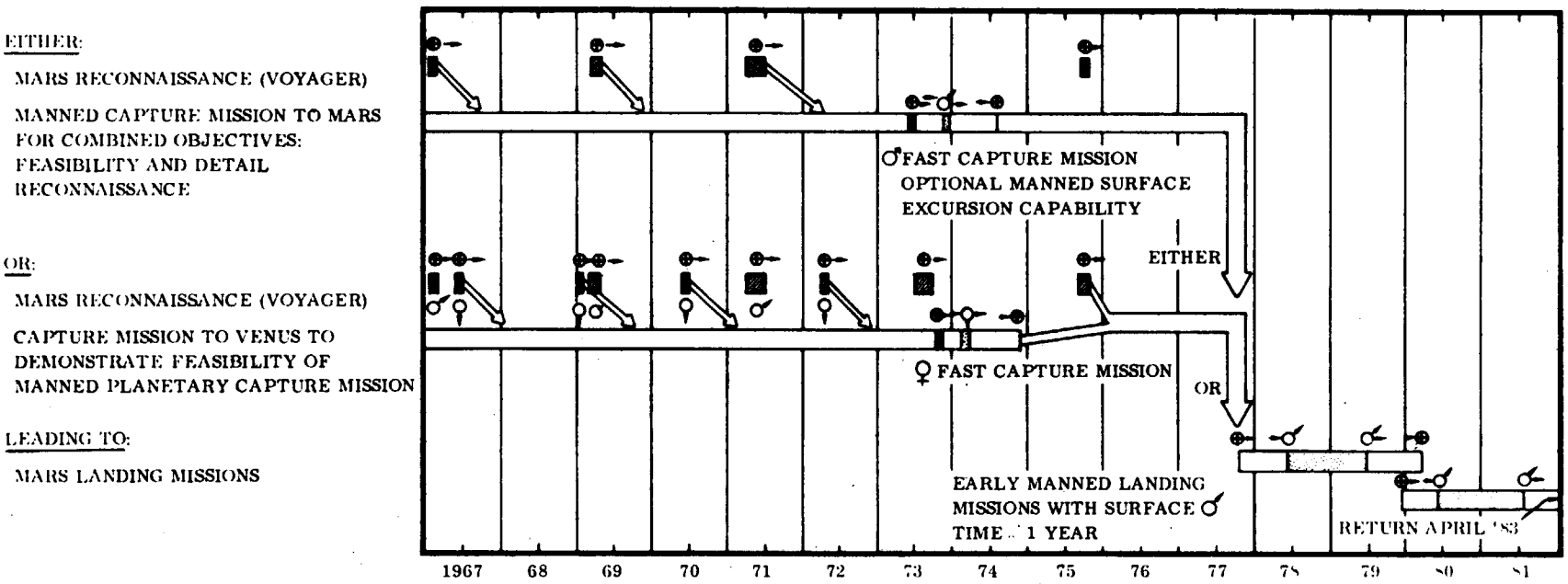

Figure 5-2. Two Possible Basic Alternatives of Development Progress Toward Mars Landing Missions With Extensive Surface Exploration

Adamas A2
Aethiopis A2
Aethiops A2
Agathodaemon C3
Amenthes A2
Aquae Calidae A1
Argyre I C4
Arsia Silva D3
Astaboras B2
Astusapes B2
Atlantis D3
Aurora Sinus C3
Bathys D3
Biblis Fons D2
Casius A1
Cimmerium A3
Corax C3
Daemone C3
Dawes Bay B3
Deucalion B3
Deucalionis R B3
Eden B2
Elysium A2
Eumenides D3
Eunostos A2
Euphrates B2
Fastigium Aryn B2
Ferentinae Lucus D2
Gehon C2
Hadriaticum B3
Hellas B4
Hellespontus B4
Hesperia Strait A3
Hydraotes C2
Ionium B3
Isidis-Libya A2
Isidis Regio A2
Jamuna Canal C2
Lacus Phoenicis D3
Laestrygon A3
Laestrygonum Sinus A3
Libya A2
Libya-Syrtis B2
Lucus Moeris B2
Maeisia Silva C3
Mare Acidalium C1
Mare Australe B4 C4
Mare Cimmerium A3
Mare Erythraeum C3
Mare Sirenum D3
Mare Tyrrhenum A3
Margaritifer Sinus C3
Meridiani Sinus B3
Mts. of Mitchel B4
Nectar C3
Nepenthes-Thoth A2
Noachis B3
Nodus Lacoontis A2
Nuba Lacus A2
Ophir C3
Pandorae Fretum B3
Phoenicis Lacus D3
Poras A3
Sabaeus Sinus B3
Sinus Gomer A3
Solis Lacus C3
Syrtis Major B2
Tharsis D3
Thaumasia C3
Thoth A2
Thoth-Nepenthes A2
Thoth-Nepenthes-Triton A2
Tithonius C3
Tithonius Lacus C2

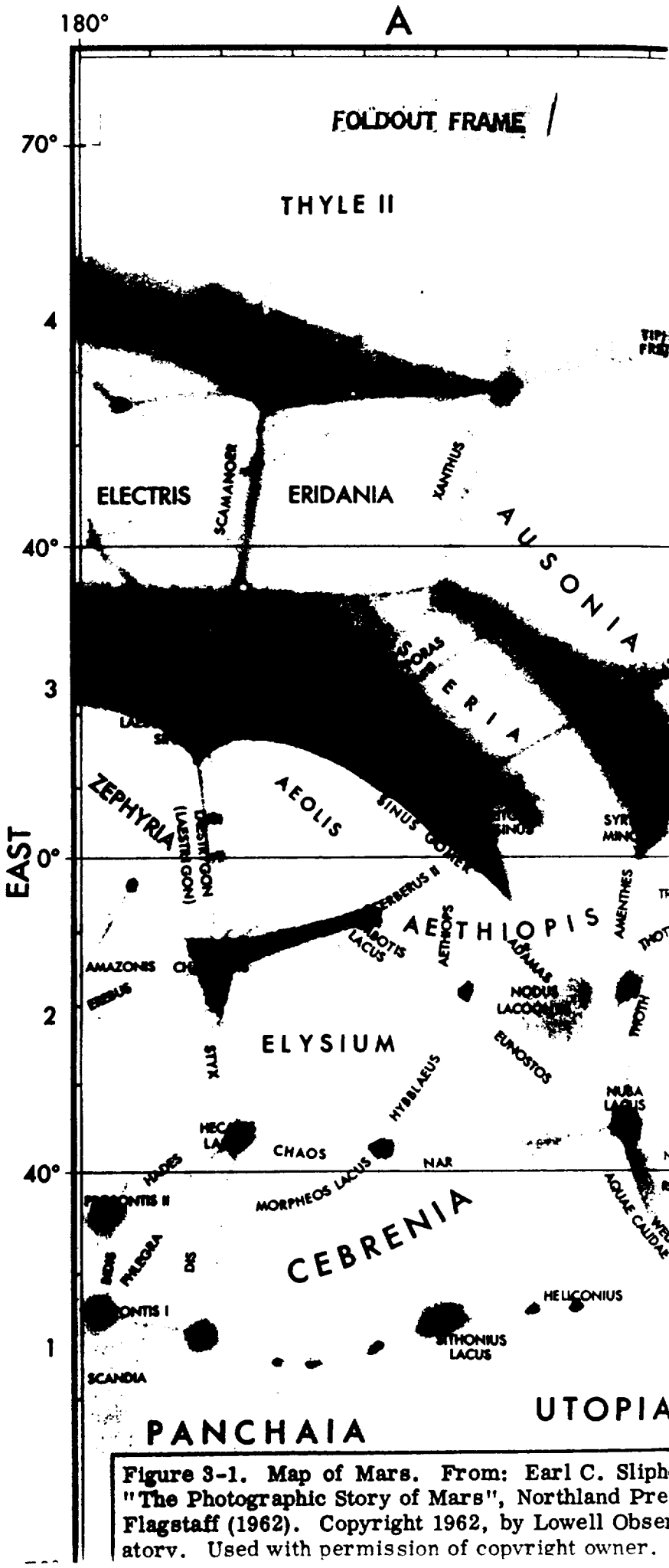

Figure 3-1. Map of Mars. From: Earl C. Sliph "The Photographic Story of Mars", Northland Pre Flagstaff (1962). Copyright 1962, by Lowell Obser atory. Used with permission of copyright owner.

MARS - KEY MAP

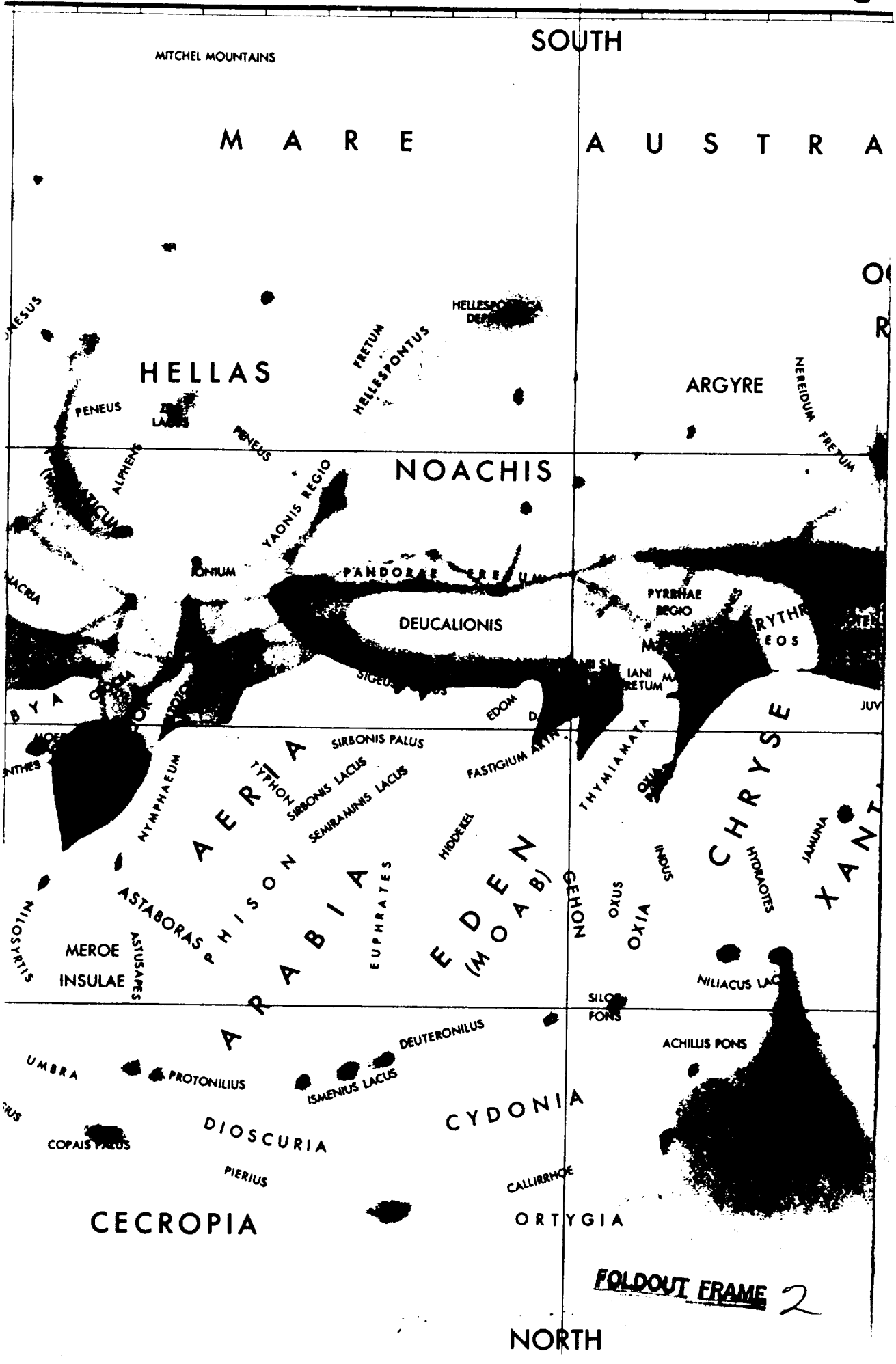
270°
B
0°
C
SOUTH
MITCHEL MOUNTAINS
M A R E
A U S T R A
HELLAS
FRETUM HELLESPONTUS
PENEUS
ARGYRE
NEREIDUM FRETUM
NOACHIS
ALPHEUS
YAONIS REGIO
PANDORAE FRETUM
PYRRHAE REGIO
DEUCALIONIS
SIRBONIS PALUS
SIRBONIS LACUS
SEMIRAMINIS LACUS
TYPHON
NYMPHAEUM
AERIA
FASTIGIUM ARYN
THYMIAMATA
HIDDEKEL
EUPHRATES
ARABIA
EDEN (MOAB)
GEHON
OXUS
OXIA
INDUS
HYDRAOTES
JAMUNA
CHRYSE
MEROE INSULAE
ASTABORAS
PHISON
NILOSYRTIS
ASTUSAPES
NILIACUS LAC
SILOS FONS
ACHILLUS PONS
DEUTERONILUS
PROTONILIUS
ISMENIUS LACUS
UMBRA
CYDONIA
DIOSCURIA
COPAIS PALUS
PIERIUS
CALLIRRHOE
CECROPIA
ORTYGIA
FOLDOUT FRAME 2
NORTH

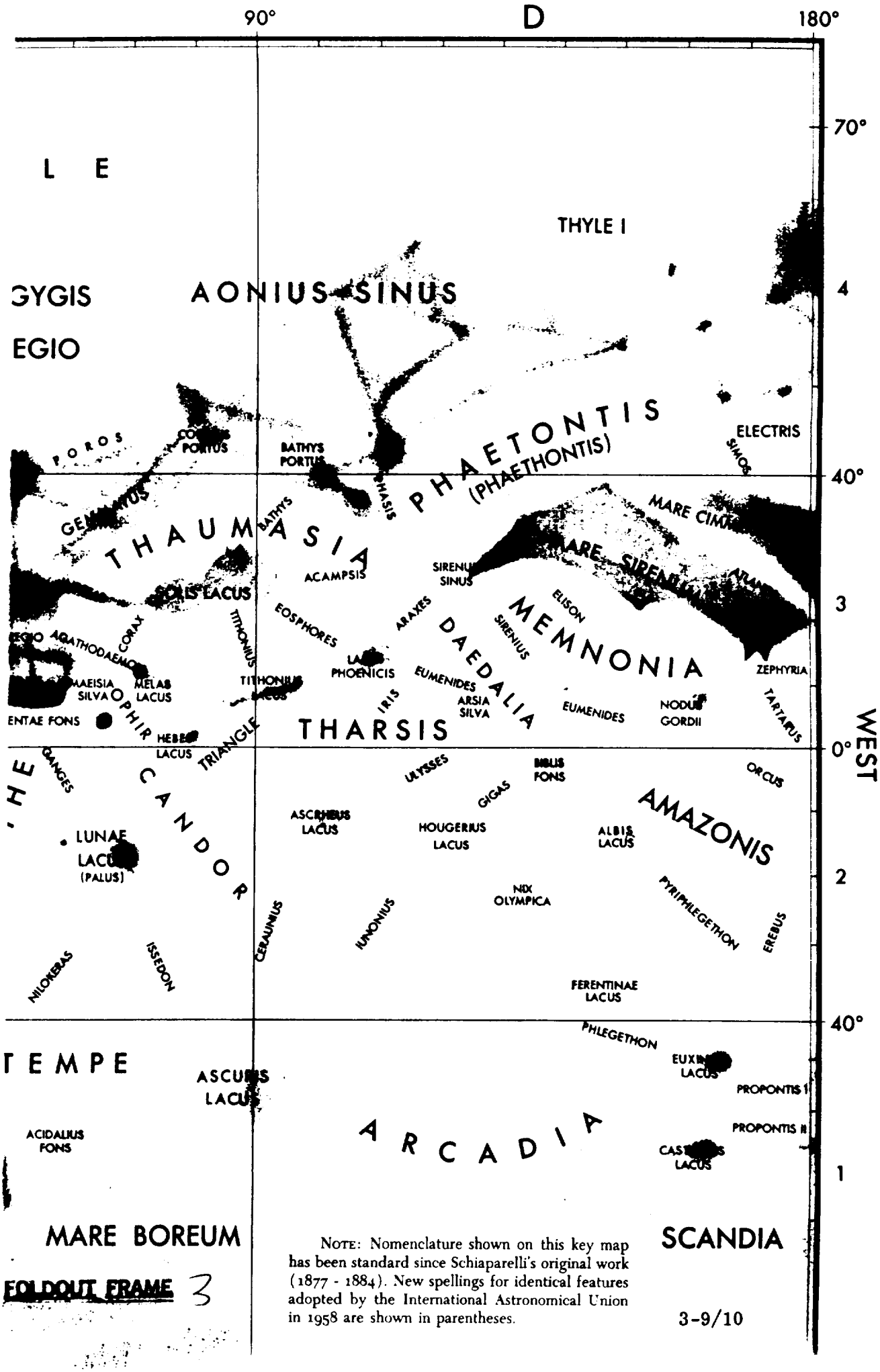

NOTE: Nomenclature shown on this key map has been standard since Schiaparelli's original work (1877 - 1884). New spellings for identical features adopted by the International Astronomical Union in 1958 are shown in parentheses.

FOLDOUT FRAME 3

3-9/10

between 0.1 to 0.15 EMOS (3 to 4.5 km/sec). Thus, for a specific impulse of 350 sec, the probe weight after capture is approximately 0.43 to 0.28 of its arrival weight (which is not very different from the above mentioned hyperbolic escape weight), that is, 14,000 to 28,000 lb.

The alternatives of combining or separating the two basic mission objectives of early manned planetary flights are left open at this point, to retain freedom of choice between Venus or Mars as first target planets.

5.3 CLASSIFICATION OF SPECIFIC MISSION OBJECTIVES. The number of specific mission objectives for a manned planetary expedition is very large. Therefore, it is useful to separate the comparatively more important from the comparatively less important mission objectives by affixing a priority to them.

The purpose of the classification is to:

a. Correlate payload and mission performance requirements,

b. Derive and define specific requirements, especially with respect to the payload,

c. Provide a guide for establishing system and component reliability requirements,

d. Justify the degree of redundancy on the system and component level,

e. Determine the relative importance of supporting research and development programs in relevant areas.

In order to meet the specific objectives, the crew vehicle and a number of auxiliary vehicles are required (Table 5-2). They are discussed in further detail in Section 9.

Table 5-2. Auxiliary Vehicles for Mars or Venus Mission

DESIGNATION	DESCRIPTION	TASK
MEV	Mars Excursion Vehicle	Landing men on Mars
C^2	Convoy Companion	Instrumented probe which can be detached from convoy to carry out sensitive space physical experiments during transfer in heliocentric space and in planetocentric space
Mapper	Mars: Optical Surveyance and Altimeter System, operating while attached to crew vehicle during capture period; and as independent mapping satellite following convoy re-escape.	Surveyance of Mars, preferably from polar orbit, in visual, infrared, and ultraviolet light. While attached to crew vehicle, a resolution of the order of 10 meters (33 ft) or less should be achieved.

Table 5-2. Auxiliary Vehicles for Mars or Venus Mission, Cont

DESIGNATION	DESCRIPTION	TASK
Mapper (Cont)	Venus: Radar Mapping System operating while attached to crew vehicle or to a secondary manned scout vehicle, penetrating to low altitude; and as independent mapping satellite following convoy reescape.	Surveyance of Venus in the 10 kmc frequency range; frequency variation to determine atmospheric characteristics through radar wave absorption.
Floater	Balloon probes of different buoyancy altitudes.	Vertical as well as horizontal (winds) exploration of the planetary atmosphere. They carry omnidirectional transmitters emitting code signals, in addition to data transmission, by which the individual probe can be identified by the crew vehicle on the day or night side of the planet.
Lander	Soft landing instrumented surface probe (Surveyor-type).	Soft landing at selected sites. Reports environmental conditions and search-for-life results to crew vehicle.
Returner (Mars)	Soft landing instrumented surface probe, capable of returning to the orbiting crew vehicle.	Furnish soil and air samples to the crew
Marens Venens	Mars or Venus environmental satellites.	Planeto-physical measurements. Satellites preferably are placed into highly elliptical orbits about the planet in equatorial, 45° inclined, and polar orbits.
Phopro Deipro	Phobos probe and Deimos probe (Ranger-type)	Attempts hard or rough landing on Mars moons Phobos and Deimos. Is equipped to carry out and report useful experiments even when missing the moon.

5.4 OBJECTIVES FOR MARS CAPTURE MISSION

5.4.1 Class I Objectives

5.4.1.1 Convoy-to-Earth communication and data transmission. During transfer, Class I objectives include data gathering and transmission on corpuscular radiation and meteoroids. Space medical data will also be gathered and transmitted. Pictures will be transmitted from inside and outside the space ship.

5.4.1.2 Mars mapping in maximum possible detail from low-altitude (approximately 1.3 Mars radaii) polar orbit; polar or near-polar orbit desired for maximum surface coverage during capture period.

It is assumed that the mappers will remain connected with the crew vehicle during the capture period, to retain maximum control over the mapper's activity, to provide additional reliability by keeping the mapper accessible for repair or adjustments, and to simplify the data transmission between the mapper's optical equipment and the convoy vehicle's storage system. Prior to re-escape, the mappers will be released to remain in orbit and continue sending information to the departing convoy (and eventually to Earth, at reduced resolution).

5.4.1.3 Lander surface mission.

5.4.1.4 Returner mission to surface and back.

5.4.1.5 Floater mission to various levels of the Mars atmosphere.

5.4.2 Class II Objectives. During transfer the Class II objectives include gathering and transmitting data on magnetic fields, soft corpuscular radiation, and interstellar wind, as well as making incidental astronomical observations. During Mars capture the Class II objectives are to perform the MEV Mission, Marens Mission, Phopro Mission, and Deipro Mission.

5.4.3 Description and Requirements

5.4.3.1 Convoy - Earth Communication and Data Transmission

5.4.3.1.1 Earth - Mars Transfer. Generally, the sampling rate is low. Much time is available. Relative peak bandwidth and power requirements will be connected with picture transmissions.

5.4.3.1.2 Capture Period. The data influx rate to the space ship is very high. In deciding whether data should be stored in the space ship or passed on immediately to Earth for storage, the following must be considered:

For some mission profiles, distance between Earth and Mars varies between 0.7 and 0.9 A.U. during the capture period. For other mission profiles, the distance during capture period varies between 0.35 and 0.7 A.U.

The optimum from the standpoints of data-handling weight and power requirement is a judicious combination of on-board data storage and passing on of data to Earth without more than the minimum storage required by limitations in the capacity of the ship-to-Earth data transmission system. These two alternatives are supplemented by a third alternative of direct data transmission from auxiliary vehicle to Earth.

The primary mission assignment of the crew is to observe and report, not to analyze and explain. Thus, only those data should be stored for more than minimum time which (a) are needed by the crew during the capture period as basis for local decisions affecting the deployment of landers, returners, floaters and MEV, or (b) exceed a reasonable capacity limit of the transmission system and therefore should be transmitted following Mars escape.

Direct transmission from auxiliary vehicle to Earth only should be provided for Marens.

Combined transmission capability (i.e., auxiliary vehicle to Earth and auxiliary vehicle to convoy) should be provided for Landers and Mappers in the sense that alternation between directional transmission to Earth and directional (Mapper)/ omnidirectional (Lander) transmission for the convoy is possible. Landers do not need a very high sampling and transmission rate; hence, they should be equipped with a storage capability which does not need a very high capacity. The mappers should possess a picture storage capability of up to one hour. The power requirements and information bit sampling rate of the mapper are determined by the high-resolution requirements for Mapper-to-Convoy transmission. A resolution between 25 and 50 feet is desired for this transmission. From these pace-setting requirements, the Mapper-to-Earth capability, which in this case represents the dependent rather than the independent variable, can be derived.

The mappers automatically cease their activity when entering the night side of the planet. Thus, if in the circular low-altitude polar orbit, the mapper will have a total duty cycle of approximately 13 hours out of 24 hours. In the elliptic orbit, the duty cycle will involve at least 75 percent of 24 hours (estimated only). The Mapper is to observe the Martian surface in the visible(high-resolution), ultraviolet (low resolution),

and infrared (low resolution) spectra. As a rule, the ultraviolet and infrared information should go to Earth directly, with an override option by the convoy for occasional information. Following its use by the crew, this information is transmitted from the convoy to Earth. In the interest of obtaining the highest possible resolution map of Mars, the information in the visible light should be directed primarily to the convoy for storage and slow transmission to Earth following Mars escape. No display requirements exist for these Mapper visible-light pictures. It is assumed that the convoy ships themselves have a capacity for selected high and low resolution observation which will be used as the basis for local decisions. The reason for storing these pictures in the space ship rather than transmitting them directly from Mapper to Earth is not use of these pictures by the crew, but to obtain highest resolution with the available Mapper power.

It is assumed that attempts will be made to land at least three landers in predetermined areas; e.g.,

a. North or South Pole

b. Syrtis Major or Sinus Meridians (typical dark green areas)

c. Solis Lacus area (green to desert features; changing).

One or two landers should be reserved for destinations decided upon by the crew after initial surface observations.

In order to eliminate unnecessary data transmission, the following philosophy is tentatively adopted:

a. Following touchdown, the lander transmits (or stores for transmission) an initial set of measurements.

b. Subsequently, it will record and transmit only changes of the original set of data, such as changes in wind intensity and direction, atmospheric pressure, temperature (ground and air), humidity or precipitation, light intensity, collimated light intensity, and sounds.

c. After a few (2 to 5) days of initial monitoring by the convoy, the particular lander can be "turned over" to Earth, with most or all of its data transmissions, except pictures.

Transmission from auxiliary vehicle to convoy only should be provided for Returners, MEV's, Floaters, Phopro, and Deipro.

Returners and MEV's should have sizeable storage systems and less powerful transmission systems. If the returner lands intact and capability of re-ascent is not impaired, most (say 75 percent) of the data collected will be returned in stored form to the convoy. If return capability is impaired, the returner becomes a lander but can transmit its information at a slow rate, since it has a better storage system than the lander.

In order to keep the floaters light in weight, they have only limited data objectives:

a. Wind direction and magnitude (obtained by observing the motion of the floater optically and/or by radio signals, which should be omnidirectional).

b. Air pressure and density.

c. Air composition at buoyancy altitude.

d. Air temperature.

e. Relative humidity.

f. Sky and ground brightness and clouds.

g. Spectral absorption of sunlight (especially ultraviolet intensity) at buoyancy altitude.

h. Corpuscular radiation intensity.

i. Altitude above ground (day and night).

Again, the technique of recording and transmitting changes from initial data should be applied.

Phopro and Deipro are encounter probes, or, at best, impact probes. Their primary assignment is to provide close-up pictures of the moons. Because of possible impact, no storage device can be employed. Regular space-physical measurements are made enroute to the moons.

5.4.3.1.3 Return transfer. Full scale transmission of all stored data in the convoy begins following Mars escape. Most of the return-transfer time period is available for data transmission. Fundamentally, transmission is desired as quickly as possible, but within the limits of the transmission capacity available. This capacity is determined by capture period requirements (or less, so that the vehicle weight can be reduced, if possible, prior to the Mars escape maneuver).

Earth is never more than 0.9 A.U. away. Available return transfer periods range from 170 to 270 days.

5.4.4 Capability Versus Capture Period Matrix. Table 5-3 shows a capability versus capture-period matrix, ranging from zero days (fly-by) to 50 days.

The whole spectrum of auxiliary vehicles can be deployed safely at capture periods of 20 days or more and probably, although marginally, at capture periods down to 10 days. Thus, below 10 days, certain tasks cannot be accomplished at all. Those which can be accomplished can be done increasingly better with increasing time. As the capture period becomes very long, the gain with time is expected to decrease. Time would then be better utilized by a larger share of manned surface excursion activities.

5.5 OBJECTIVES FOR VENUS CAPTURE MISSION.

5.5.1 Class I Objectives

5.5.1.1 Convoy-to-Earth communication and data transmission. During transfer, Class I objectives are the same as given in 5.4.1.1.

5.5.1.2 Venus surface mapping in maximum possible detail by means of radar from the highest orbital altitude consistent with available electric power.

5.5.1.3 Lander mission to the Venus surface.

5.5.1.4 Floater mission to various levels of the Venus atmosphere.

5.5.2 Class II Objectives. During transfer, Class II objectives are the same as given in 5.4.2. During capture the Class II objective is performance of the Venens mission.

5.5.3 Description and Requirements

5.5.3.1 Convoy-Earth communication and data transmission

5.5.3.1.1 Earth-Venus transfer. Same as given in 5.4.3.1.1.

5.5.3.1.2 Capture period. Similar to 5.4.3.1.2. Distance between Earth and Venus during the capture period varies within limits similar to those for Mars. Inasmuch as radar is employed for surface mapping, the mappers continue operating over the planet's night side.

Unless more is known about the Venus surface by the time the first manned expedition arrives, no specific target areas can be designated for Landers.

Table 5-3. Capability Versus Capture Period During Mars Mission

Capture Period (d)	TASK OR OBJECTIVE: Convoy to Earth Communication	Mapper	Lander	Returner	Floater	MEV	Marens	Phopro/ Deipro
0 (fly-by)	X	X	X				X	
1	X	X	X		X		X	
5	X	X	X	X	X	X	X	X
10	X	X	X	X	X	(X)	X	X
20	X	X	X	X	X	X	X	X
30	X	X	X	X	X	X	X	X
40	X	X	X	X	X	X	X	X
50	X	X	X	X	X	X	X	X
	Increasing capacity required with longer capture period because of added tasks. Data transmission density, however, can be reduced as capture period is increased.	Improving quality attainable with time.	Increasing capacity attainable with time.	Increasing capacity attainable with time.	Increasing capture period has little effect on capacity of probe; only on duration of observation.	Limited to maximum surface stay time of 8-10 days. No effect of capture period beyond this time.	Unaffected by capture period.	Beyond 5 days not affected by capture period except for possible celestial mechanical reasons.

5.5.3.1.3 Return transfer. Similar to 5.4.3.1.3. Return transfer times generally tend to be longer than for Mars, namely, 220 to 280 days.

5.5.4 Capability Versus Capture Period Matrix. Because so very little is known firmly about the atmospheric and surface conditions of Venus, prime emphasis will be directed toward the determination of atmospheric pressure, temperature, and surface winds, as well as toward the observation of surface features. Assuming synchronous rotation of Venus, strong surface winds should, according to calculations (Ref. 5-1), occur only if the atmospheric surface pressure is small. If, on the other hand, the air temperature at the surface is high and the pressure of the order of 50 atmospheres, the observed variation of the atmospheric temperature with the phase of Venus can be accounted for by low wind velocities ($\lesssim$ 0.5 mph) across the terminator. These temperature variations between daylight and night side seem to amount to only 80 K° to 150 K° according to radar measurements of the change in brightness temperature between superior and inferior conjunctions (Ref. 5-2 and 5-3). The dark side must, therefore, be heated primarily by atmospheric convection. However, according to Ref. 5-1, the violence of this convective process depends primarily on atmospheric pressure and temperature.

The observation of surface features should show the existence of mountain ranges; i.e., the magnitude, location and orientation of fold belts in general which will offer an insight into the planet's thermal history and present as well as past plutonic activity. Radar measurements made by the Jet Propulsion Laboratory (Ref. 5-4) indicate that the surface roughness of Venus is comparable to that of the Moon, which renders unlikely the existence of large bodies of water or of molten material on the surface.

Verification of some of the basic assumptions regarding the surface, and information on atmospheric surface pressures, temperatures, and wind magnitudes should be provided by instrumented probes in advance of the first manned flight. This will provide a firmer foundation for the design and operation of Landers and Floaters to be carried along by the Convoy.

Table 5-4 shows a capability versus capture-period matrix, ranging from 0 days (fly-by) to 20 days. It is of importance to note that, aside from the Mapper activities, less gain appears desirable from an extension of the capture period than in the case of Mars. If the Venusian atmospheric pressures are comparatively low (1-10 atm), and if the rotation is synchronous, the resulting severe storms will cause the operational life of Floaters and Landers to be far shorter than on Mars. A dust-filled atmosphere will further aggravate matters from an engineering point of view. Whether the atmosphere is thin and stormy or thick and sluggish, the conditions are, in either case, very unfavorable for the re-ascent of Returners.

Table 5-4. Capability Versus Capture Period During Venus Mission

Capture Period (d)	TASK OR OBJECTIVE: Convoy to Earth Communication	Mapper	Lander	Floater	Venus
0 (fly-by)	X	X	X		X
1	X	X	X	X	X
5	X	X	X	X	X
10	X	X	X	X	X
20	X	X	X	X	X
	Communication capacity does not change much with increasing capture period.	Improving surface coverage with time.	Increasing capacity attainable with time.	Increasing capture period has little effect on capacity of probe; only on duration of observation leading to improved determination of wind patterns. Floaters may be destroyed much faster than on Mars.	Unaffected by length of capture period.

The principal incentive for an extended capture period during a Venus mission appears, on the basis of present knowledge, to be the radar mapping of all parts of the planet.

5.5.5 Specific Tasks. A break-down of typical specific mission tasks for a mission to Mars or Venus, their relative priorities, and associated vehicle assignments has been worked out and is presented in Table 5-5.

Table 5-5. Specific Mission Objectives, Relative Priority and Associated Vehicle Assignments

OBJECTIVE OR SUBJECT	PRIORITY CLASS	CREW VEHICLE	MEV	C^2	MAPPER	FLOATER	LANDER	RETURNER	MARENS/VENENS	PHOPRO	DEIPRO
1. Astronautic Mission Objectives:											
1.1 Carrying men into target planet capture orbit	1	*									
1.2 Orbital reconnaissance of target planet	1	*			*	*			*		
1.3 Convoy-to-Earth communication and data transmission	1	*									
1.4 Floating and landing of instrumented probes	1					*	*				
1.5 Landing and return of instrumented probes (Mars)	1							*			
1.6 Manned excursion to surface (Mars)	2		*								
1.7 Exploration of Mars Moons	2									*	*
1.8 Return to Earth	1	*									
2. Scientific Mission Objectives:											
2.1 Planetography											
2.1.1 Visual mapping (high-resolution (Mars))	1	*			*						
2.1.2 Infrared (IR) mapping (Mars)	1	*			*						
2.1.3 Radar mapping (Venus)	1	*									
2.1.4 Altimetry	1	*			*						
2.1.5 Planetary mass, shape, dimensions	1	*			*				*		
2.2 Planetology (Surface)											
2.2.1 Landscape photography (Mars) (Venus?)	1		*				*	*			
2.2.2 Surface and soil investigation	1		*				*	*			
2.2.3 Seismographic measurements	1		*				*	*			
2.2.4 Sound measurements	2		*				*	*			
2.2.5 Corpuscular radiation	1	*	*			*	*	*			
2.2.6 Magnetic field	2		*			*	*	*			
2.2.7 Thermal surface radiation	1	*	*				*	*			
2.3 Climatology/Meteorology											
2.3.1 Atmospheric composition	1		*			*	*	*			
2.3.2 Wind measurements	1	*	*			*	*	*			
2.3.3 Temperature (air/ground)	1		*			*	*	*			
2.3.4 Pressure and density	1		*			*	*	*			

Table 5-5. Specific Mission Objectives, Relative Priority and Associated Vehicle Assignments, Cont

OBJECTIVE OR SUBJECT	PRIORITY CLASS	CREW VEHICLE	MEV	C^2	MAPPER	FLOATER	LANDER	RETURNER	MARENS/VENENS	PHOPRO	DEIPRO
2.3.5 Sky brightness (day/night)	2		*			*	*	*			
2.3.6 Surface brightness and colors	2	*	*			*	*	*			
2.3.7 Solar constant	1		*				*	*			
2.3.8 Sunlight intensity (overall and spectral distribution)	1		*			*	*	*			
2.3.9 Relative humidity	1		*			*	*	*			
2.3.10 Sky photos	2		*				*	*			
2.4 Planeto-Biology (possibly Mars only)											
2.4.1 Organic soil analysis	1		*				*	*			
2.4.2 Biochemical soil analysis	1		*				*	*			
2.4.3 Soil microscopy	1		*				*	*			
2.4.4 Ultraviolet (UV) mapping	1	*			*						
2.4.5 UV surface examination	1		*				*	*			
2.4.6 Culture studies	1		*				*	*			
2.4.7 Planetary biological contamination studies	1		*				*	*			
2.4.8 Chemistry of planetary organisms	1		*				*	*			
2.4.9 Sound/noise studies	2		*			*	*	*			
2.4.10 Search for moving objects	2		*								
2.4.11 Search for plant life	1		*				*	*			
2.5 Planetary Environment											
2.5.1 Corpuscular radiation	1	*		*					*	*	*
2.5.2 Meteorites	1	*		*					*	*	*
2.5.3 Magnetic field	2			*					*	*	*
2.5.4 Outer atmosphere characteristics	2	(*)		(*)					*	*	*
2.6 Mars Moons											
2.6.1 Size, shape, surface features	1	*								*	*
2.6.2 Thermal radiation	2	*								*	*
2.6.3 Search for unknown moons (Venus, Mars)	1	*								*	*
2.6.4 Albedo	2	*								*	*
2.6.5 Search for colors	2	*								*	*

SECTION 6

MISSION ANALYSIS

6.1 INTRODUCTION. The analysis of planetary round-trip missions can be divided into two major categories: heliocentric transfer and planetocentric orbits. For precision navigation, these two regions must be combined by including perturbation calculations. For performance analysis and for a preliminary guidance and navigational analysis, the two areas can remain separated (Figure 6-1).

6.2 HELIOCENTRIC TRANSFER ANALYSIS. Considering heliocentric space as a central force field (i.e., no perturbations), a transfer ellipse between two planets is determined as to orientation and size in its orbit plane if the three elements, longitude of perihelion (ω), eccentricity (e), and semi-latus rectum (p) are known. Therefore, three equations are required, relating these elements to other, known parameters. The theories of orbit determination indicate that radii vectores from the focus (Sun) to specified positions in the ellipse are the natural choice for use as known parameters, if they are given with respect to magnitude and direction. Their correlation with the forementioned elements yields equations of the form

$$\frac{p}{r} = 1 + e \cos (\mu - \omega) \qquad (6\text{-}1)$$

where $\mu = \omega + \eta$, the argument of the latitude, and η is the true anomaly. Accordingly, three pairs of known values of μ and r would be required in order to formulate the required three equations for the determination of p, e, and ω. If one of these three elements were known, only two pairs of μ, r would be required for determination of the ellipse. These two pairs, therefore, would also enable one to compute the time required by the radius vector to move from one given position to the other (transfer time). From this follows, conversely, that from two known radii vectores $\bar{r}_1 (r_1, \mu_1)$ and $\bar{r}_2 (r_2, \mu_2)$ and the intermediate time interval, it is possible to determine the one element assumed above to be known, and thereafter the two other elements, hence the transfer orbit.

The semi-latus rectum (p) is the element which usually is determined first. Then e and ω are found from p, $\bar{r}_1$ and $\bar{r}_2$. A particularly interesting method of determining p, devised by Lambert (Ref. 6-1), uses the ratio of the sector between $\bar{r}_1$ and $\bar{r}_2$ to the associated triangle formed by the focus and the two end points of $\bar{r}_1$ and $\bar{r}_2$. This method has later been expanded by Gauss (Ref. 6-2), Encke and Hansen. Using Lambert's ratio and the method of Gauss, the elements of the transfer orbit can be determined between the two planets involved and for a given transfer, as has been done in Ref. 6-3 and in Ref. 6-4 where the application of the Gauss method to elliptic and hyperbolic transfer orbits is described.

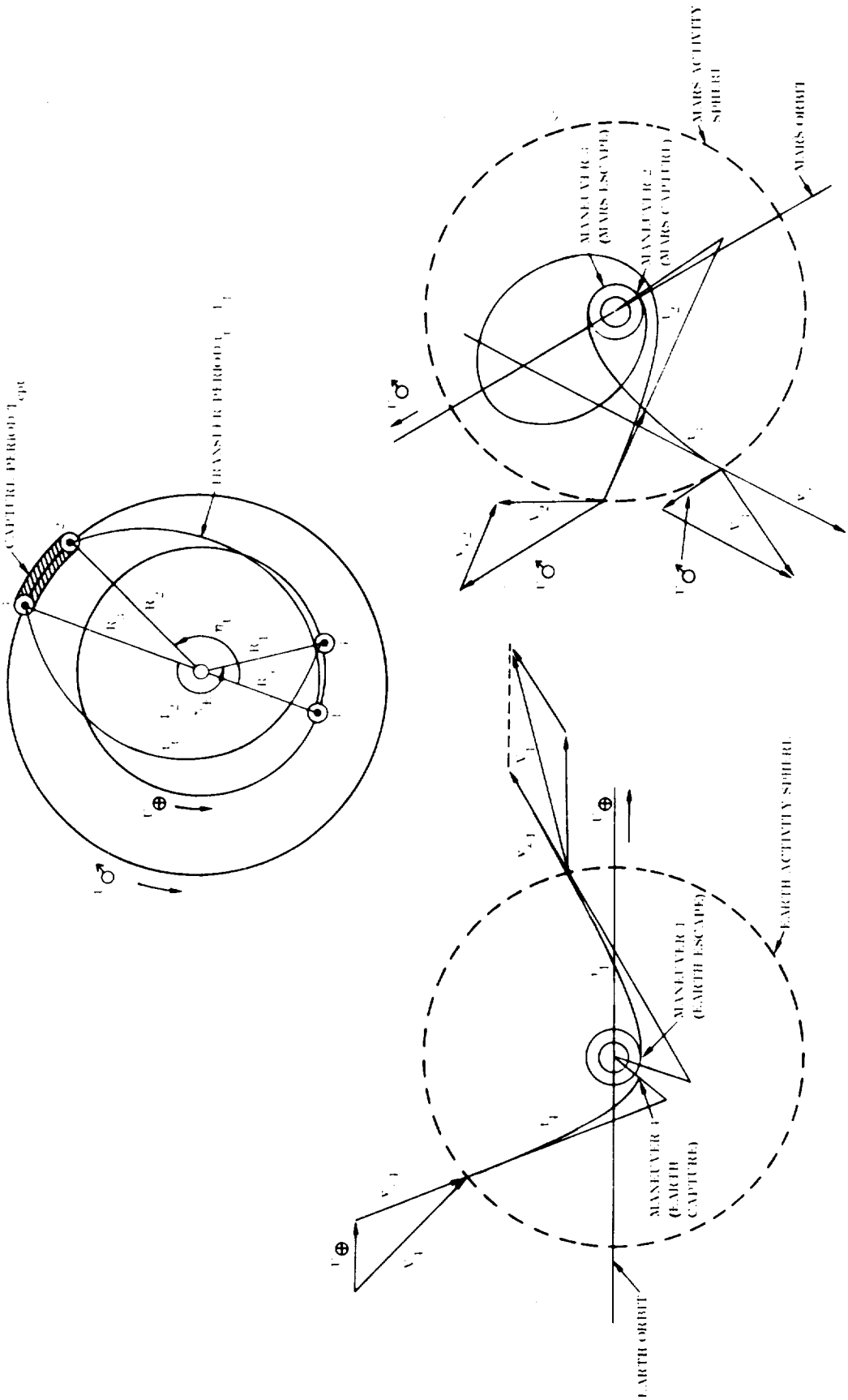

Figure 6-1. Nomenclature of a Capture Mission

The analysis, which can be divided into seven principal steps, is summarized in the computation flow chart (Table 6-1), which refers to transfer from Earth (Maneuver 1) to a target planet (Maneuver 2). The return transfer (Maneuvers 3 and 4) are treated analogously. Only three initial information items are required: target planet (hence, its orbital elements), departure date, D_1, and transfer period, t_t. From these a set of 11 additional data inputs is derived by use of the ephemeris of Earth and target planet and by analysis. With this initial information, a set of four parameters, which assure compliance of the transfer orbit with all established boundary conditions, is determined. From these follow the elements and other characteristic data of the transfer orbit and, finally, its dynamic characteristics leading to the hyperbolic velocity excess values which are a key parameter in the computation of the velocity requirements for the respective escape or capture maneuver.

Table 6-1. Computation Flow For Computation of Transfer Orbit Between Earth (⊕) and Target Planet (pl), Taken as Transfer Orbit Connecting to Points in the Heliocentric Control Force Field

1. Initial information

   D_1 = departure date
   t_t = transfer period

2. Derivative initial information

   U = planet orbital velocity
   θ = path angle relative to normal to radius vector
   R = heliocentric distance
   ℓ, b = longitude, latitude (heliocentric ecliptic system)
   η_t = central transfer angle
   ⊕ = Earth
   pl = target planet
   1 = departure (initial)
   2 = arrival (terminal)

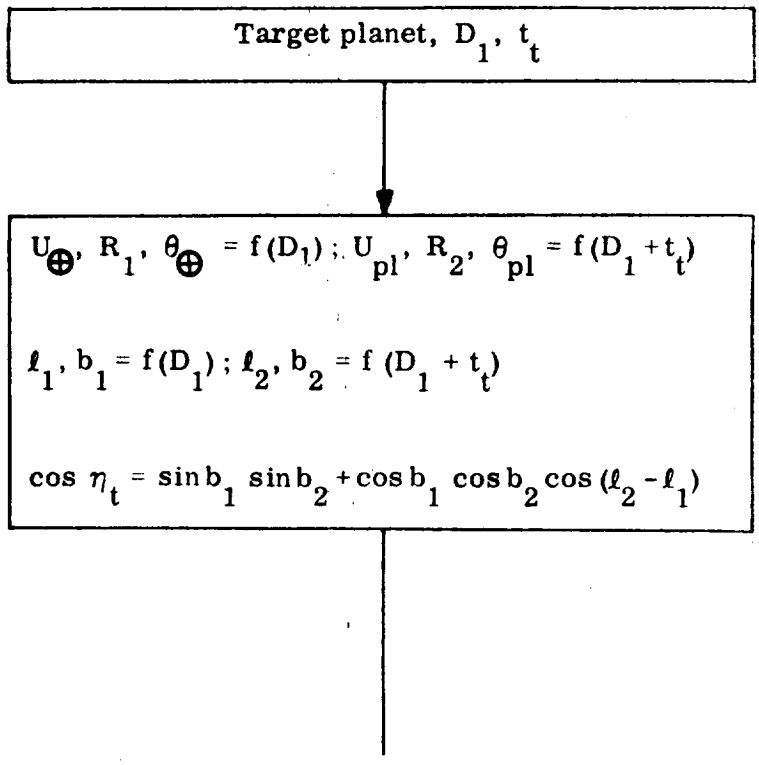

Table 6-1. (Cont)

3. Determination of first and second parameters: m, j

$K_\odot$ = gravitational parameter of Sun

$$m = \frac{\sqrt{K_\odot}\, t_t}{\left[2 \cos f \sqrt{R_1 R_2}\right]^{3/2}} \qquad (0 < \frac{1}{2}\eta_t < 180^\circ)$$

$$j = \frac{R_1 + R_2}{4 \cos f \sqrt{R_1 R_2}} - \frac{1}{2} \qquad (0 < \frac{1}{2}\eta_t < 180^\circ)$$

$$(f = \frac{1}{2}\eta_t)$$

4. Iterative determination of third parameter: g

$$m = \sqrt{j + \sin^2 \frac{1}{2} g} + \sqrt{(j + \sin^2 \frac{1}{2} g)^3} \left(\frac{2g - \sin 2g}{\sin^3 g}\right)$$

5. Determination of fourth parameter: y

$$y^2 = \frac{m^2}{j^2 + \sin^2 \frac{1}{2} g}$$

6. Determination of transfer orbit elements

p = semi-latus rectum
a = semi-major axis
η = true anomaly
E = eccentric anomaly
M = mean anomaly
μ = mean angular motion
ω = longitude of perihelion
i_1 = inclination relative to ecliptic
i_2 = inclination relative to target planet orbit
1 = departure (initial)
2 = arrival (terminal)

$$p = y^2 \frac{R_1^2 R_2^2}{K_\odot t_t^2} \sin^2 \eta_t$$

$$a = \frac{2 (j + \sin^2 \frac{1}{2} g) \cos f \sqrt{R_1 R_2}}{\sin^2 g}$$

$$e^2 = 1 - p/a$$

$$\cos \eta_1 = \frac{p/R_1 - 1}{e}$$

Table 6-1. (Cont)

$$\eta_2 = \eta_1 + \eta_t$$

$$E_\nu = 2 \tan^{-1}\left[\frac{e-1}{e+1} \tan \frac{1}{2} \eta_{1,2}\right] \quad (\nu = 1, 2)$$

$$M_\nu = E_{1,2} - e \sin E_{1,2} \quad (\nu = 1, 2)$$

$$\mu = \sqrt{K_\oplus / a^3} = (M_2 - M_1)/t_t$$

$$\omega = \eta_t - \eta_2 = -\eta_1$$

$$\sin i_1 = \frac{\sin b_2}{\sin \ell_2}$$

$$\sin i_2 = \frac{\sin (\Omega_{pl} - \ell_1)}{\sin \eta_t}$$

7. Determination of dynamic characteristics of transfer orbit

V = heliocentric velocity
θ = path angle relative to normal to radius vector
β = intersection of planar angle with planet orbit
B = three-dimensional intersection angle
v_∞ = hyperbolic excess velocity (velocity of space ship relative to planetary activity sphere

$$V_\nu^2 = \frac{K_\oplus}{R_\nu}\left(2 - \frac{R_\nu}{a}\right) \quad (\nu = 1, 2)$$

$$\theta_\nu = \tan^{-1}\left(\frac{R_P}{R_\nu} \frac{e}{1+e} \sin \eta_\nu\right) \quad (\nu = 1, 2)$$

$$\beta_\nu = |\theta_\nu - \theta_x| \quad \begin{matrix}(\nu = 1,\ x = \oplus) \\ (\nu = 2,\ x = pl)\end{matrix}$$

$$B_\nu = \cos \beta_\nu \cos i_\nu \quad (\nu = 1, 2)$$

$$v_{\infty,\nu}^2 = U_x^2 + V_\nu^2 - 2 U_x V_\nu \cos B_\nu \quad \begin{matrix}(\nu = 1,\ x = \oplus) \\ (\nu = 2,\ x = pl)\end{matrix}$$

6.3 INTERPLANETARY MISSION MAPS. The data resulting from a large number of transfer orbit calculations can be arranged in different ways, e.g., as v_∞, V, B, etc., as functions of time for constant transfer periods (Ref. 6-4). In Ref. 6-3 the computer results were presented in the form of lines of constant v_∞ in the departure date/arrival date plane. In Ref. 6-5 these charts have been developed through 1975. A modification of this contour chart was developed in Ref. 6-6.

A different mission map was constructed to serve the particular information requirements of interplanetary round-trip mission and system information. The principle is illustrated in Figure 6-2. The abscissa shows Earth departure and arrival dates; the ordinate shows target planet arrival and departure dates. The latter are offset with respect to the dates on the abscissa by the minimum transfer orbit (Earth to target planet) considered. The two date scales are matched along the equal date line. On the left side of the equal date line is a set of parallel lines, representing lines of constant transfer time from Earth to target planet; on the right side are lines of constant return transfer times. At the dots (Figures 6-3 through 6-11), which represent individual transfer orbits, can be shown the various parameters of interest. Thus, one chart shows the hyperbolic excess velocities, $v^*_{\infty 1}$ and $v^*_{\infty 2}$, at the points left of the equal-date-line and the values $v^*_{\infty 3}/v^*_{\infty 4}$ at points to the right of this line. Another chart may show associated perihelion distances; a third, inclination angles, and so forth. Shown in Figures 6-3 through 6-11 are regions of different hyperbolic excess velocities for Earth departure ($v^*_{\infty 1}$), target planet arrival ($v^*_{\infty 2}$), target planet departure ($v^*_{\infty 3}$), and Earth arrival ($v^*_{\infty 4}$) for four Venus constellations and three Mars constellations in the seventies. In some of the charts are shown lines of constant perihelion distance of the heliocentric transfer orbits. These "iso-perihelion" lines are a bit difficult to see on the right hand side of the Venus maps, because they run in the same general direction as the v^*_∞ lines. The letters "NPT" stand for "no perihelion transit"; i.e., the space ships do not pass through the perihelion of the heliocentric transfer orbits in the respective region.

The map is divided into two areas: the left refers to the Earth-target planet transfer, the right refers to the return flight. Each area is characterized by a two-digit number. The first of these refers always to the target planet, the second to Earth. A given individual number designates the second digit of the hyperbolic excess velocity given in terms of the Earth mean orbital speed (EMOS); e.g., 1 means the hyperbolic excess velocity lies between 0.1 and 0.199 (i.e., roughly $3 \leq v_\infty < 6$ km/sec or $10,000 < v_\infty \leq 20,000$ ft/sec) and so forth. The number 21 on the left side of the map means that in this region the Earth-departure hyperbolic excess is in the region $0.1 \leq v^*_{\infty 1} \leq 0.199$ (the asterisk on v^*_∞ indicates EMOS as unit) and the hyperbolic excess at target planet arrival is $0.2\ v^*_{\infty 2} \leq 0.299$. The number 12 on the left hand side of the map means $0.2 < v^*_{\infty 1} \leq 0.299$ and $0.1 \leq v^*_{\infty 2} \leq 0.199$; analogously, the number 32 on the right side means $0.3 \leq v^*_{\infty 3} \leq 0.399$, $0.2 \leq v^*_{\infty 4} \leq 0.299$; and so forth. The symbols T_1 and T_2 designate the transfer period in the outgoing and return orbit, respectively.

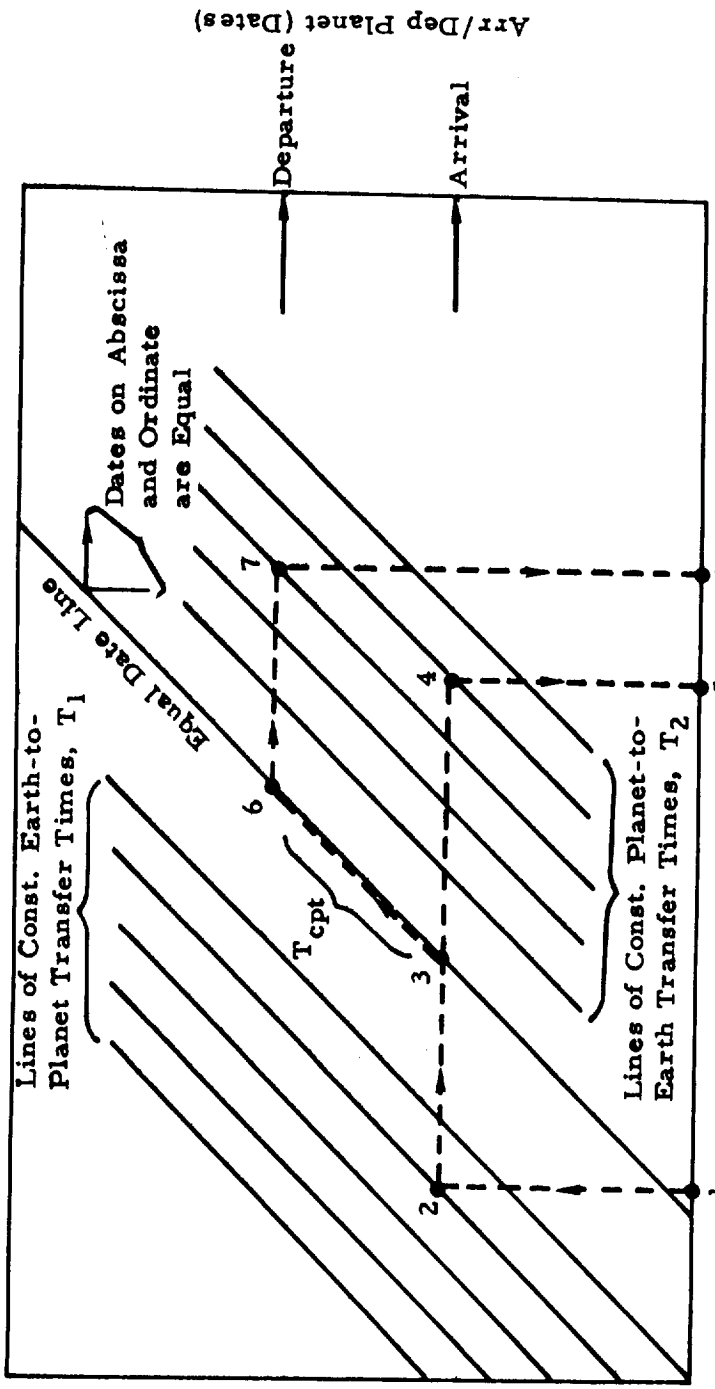

1. Select Earth departure date
2. Select Earth-planet transfer time T_1 (days)
3. Move horizontally to Equal Date Line (EDL) Date on ordinate on right hand side shows planet arrival date
4. For-Fly-By Mission select planet-Earth transfer time, T_2 on same date as arrival
5. Earth arrival date for fly-by mission
6. For Capture Mission select capture period T_{cpt} (3-6)
7. Select planet-Earth transfer time, T_2
8. Earth arrival date for capture mission

Figure 6-2. Method of Presentation of Interplanetary Mission Profile Data (Mission Map)

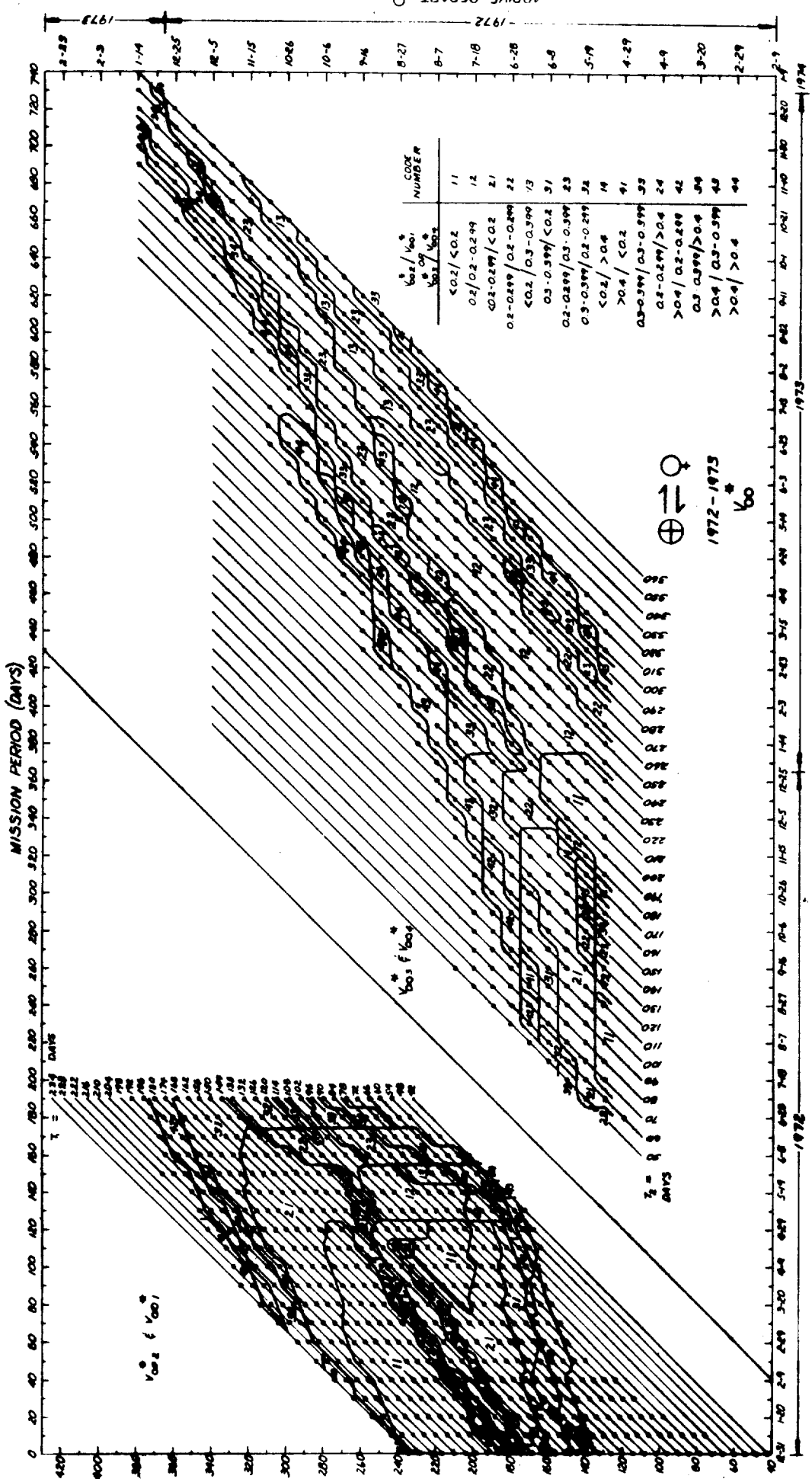

Figure 6-3. Earth-Venus Hyperbolic Excess Mission Map 1972-1973 (Outgoing Transfer Periods in 6-day Intervals)

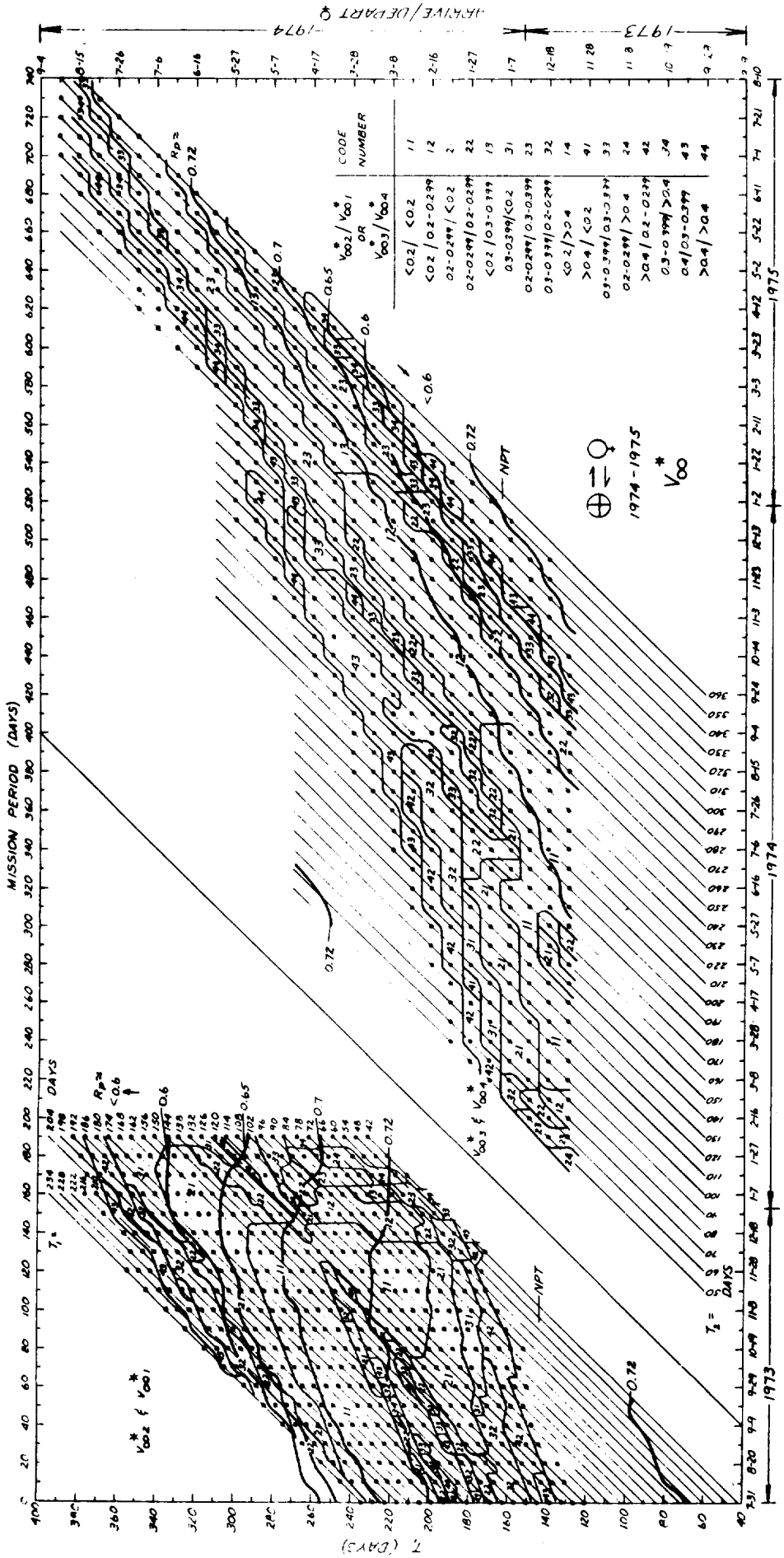

Figure 6-4. Earth-Venus Mission Map 1974-1975: Hyperbolic Excess and Iso-Perihelion Lines (Outoging Transfer Periods in 6-day Intervals)

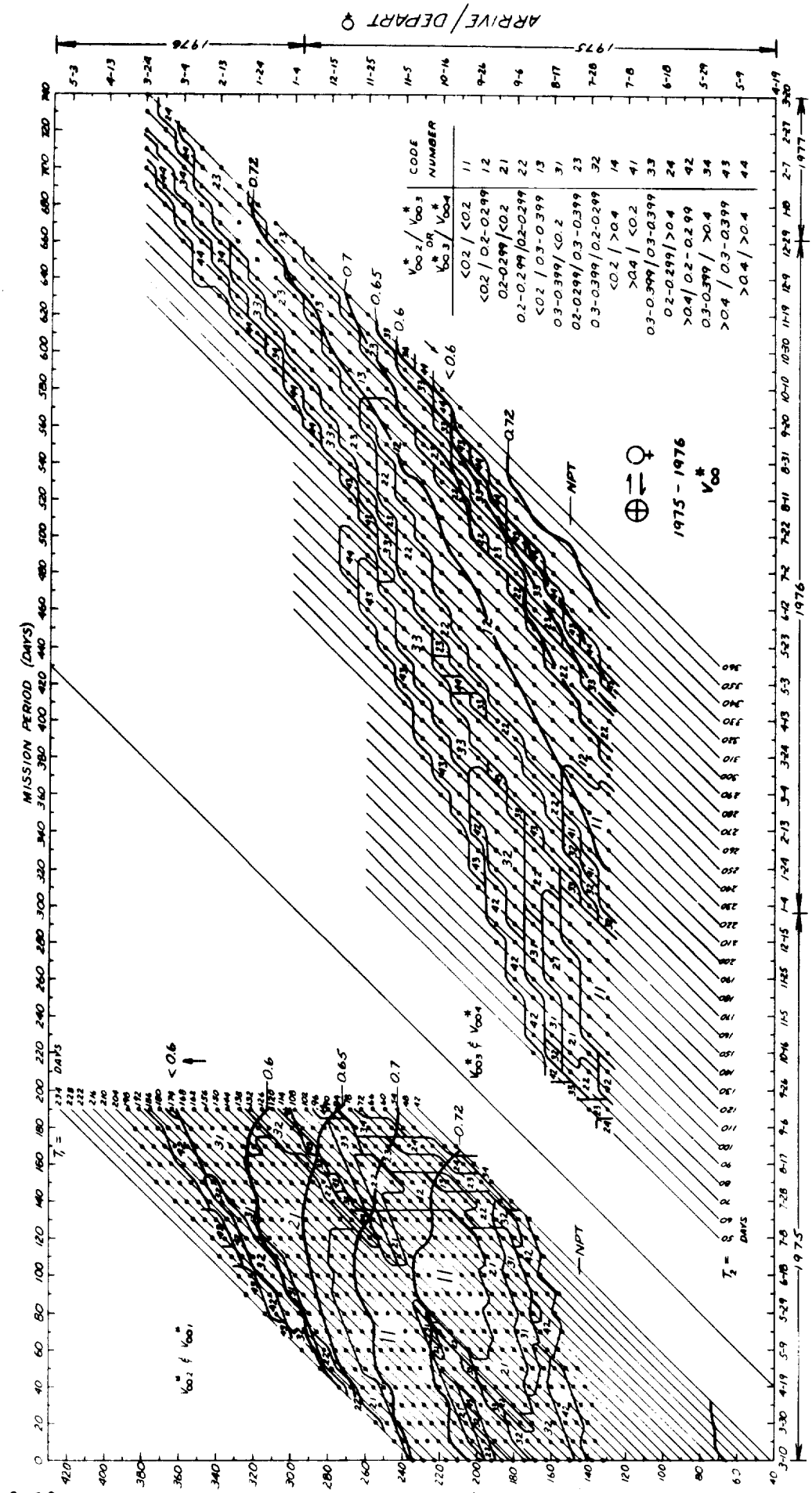

Figure 6-5. Earth-Venus Mission Map 1975-1976: Hyperbolic Excess and Isoperihelion Lines (Outgoing Transfer Periods in 6-day Intervals)

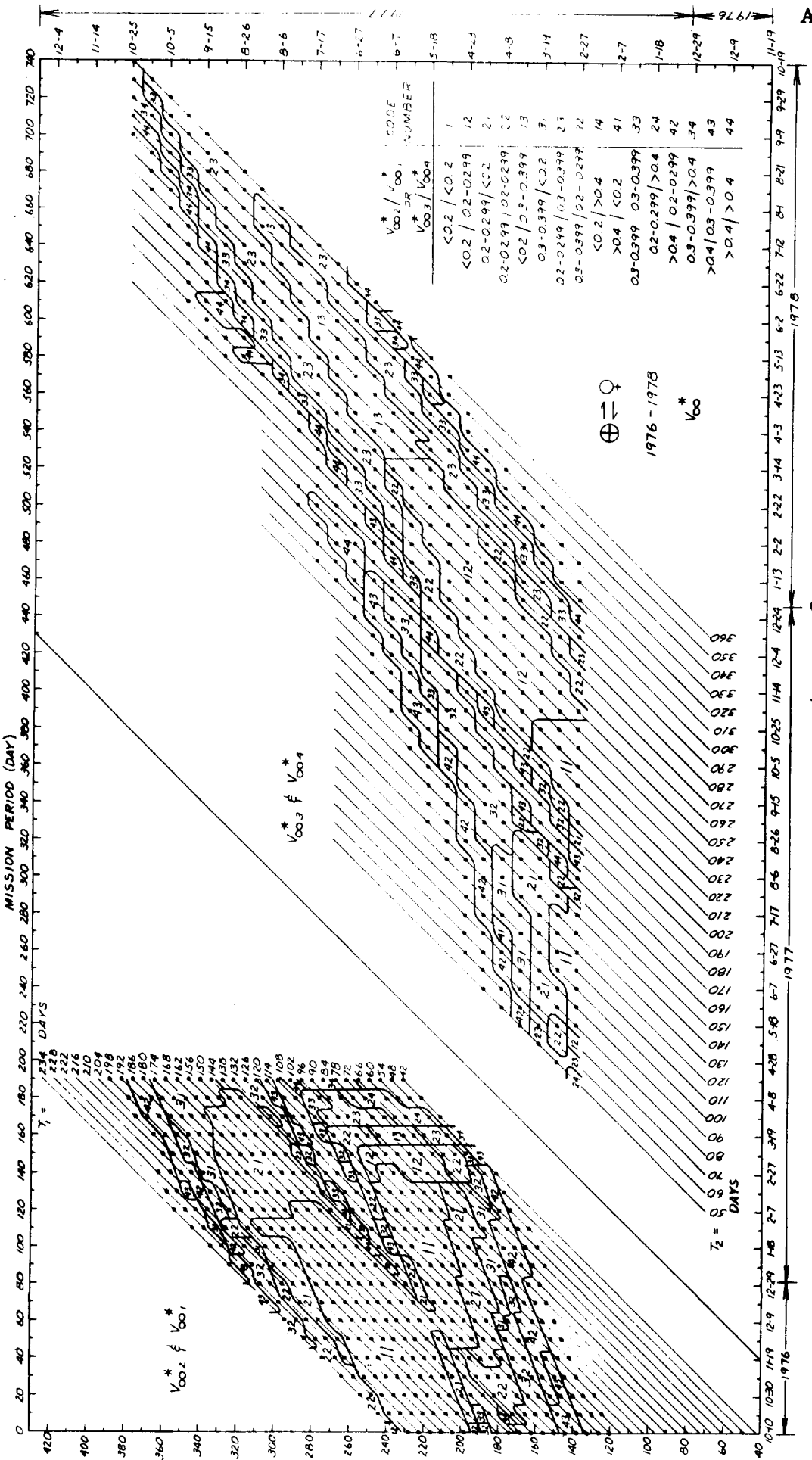

Figure 6-6. Earth-Venus Hyperbolic Excess Mission Map 1976-1978 (Outgoing Transfer Periods in 6-day Intervals)

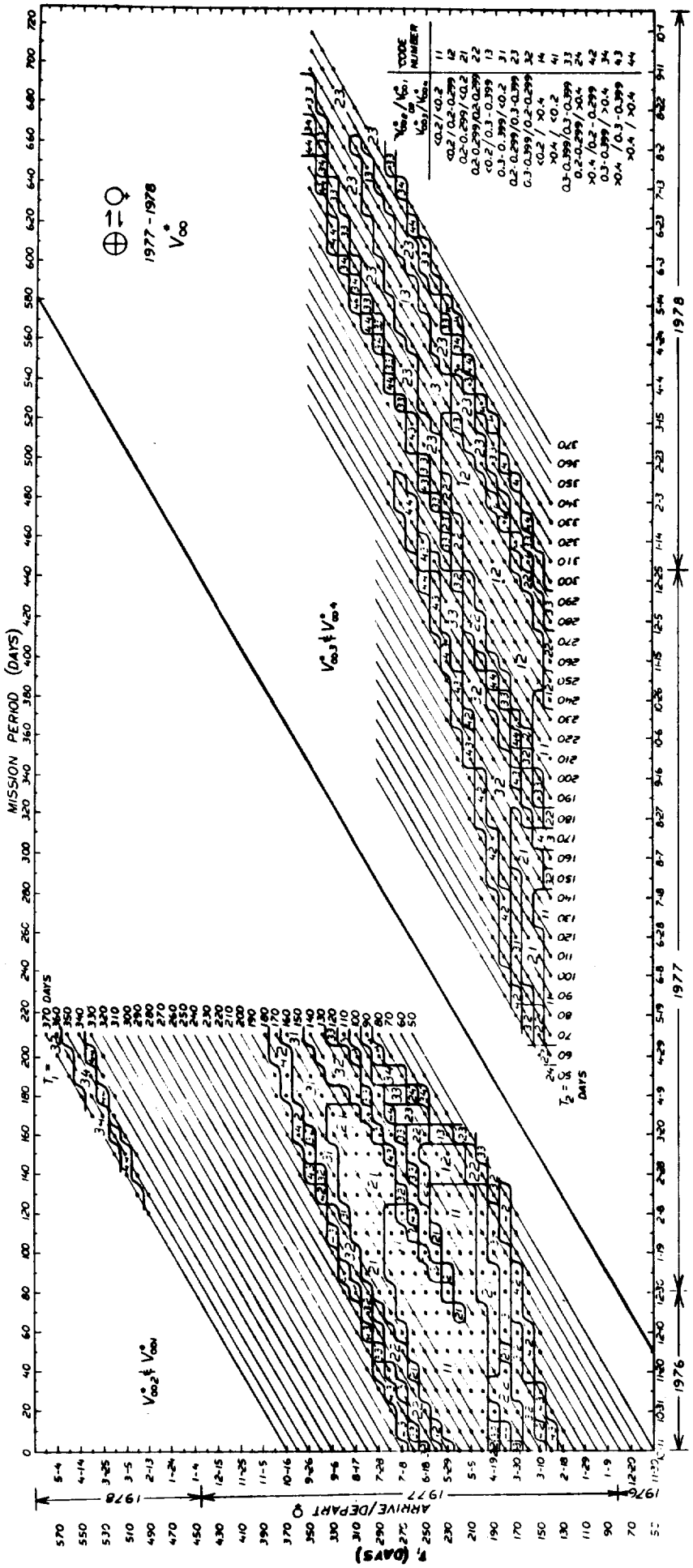

Figure 6-7. Earth-Venus Hyperbolic Excess Mission Map 1976-1979 (10-day Intervals)

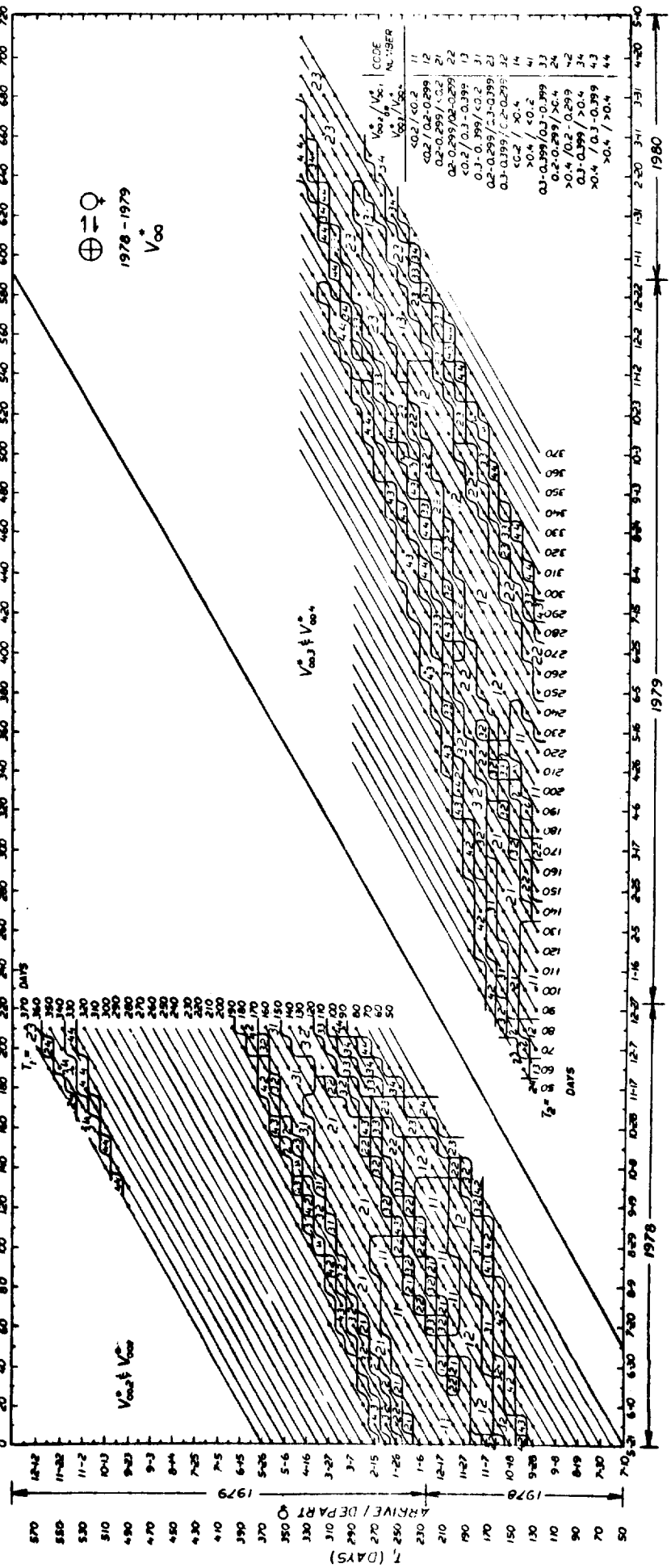

Figure 6-8. Earth–Venus Hyperbolic Excess Mission Map 1978–1980 (10-day Intervals)

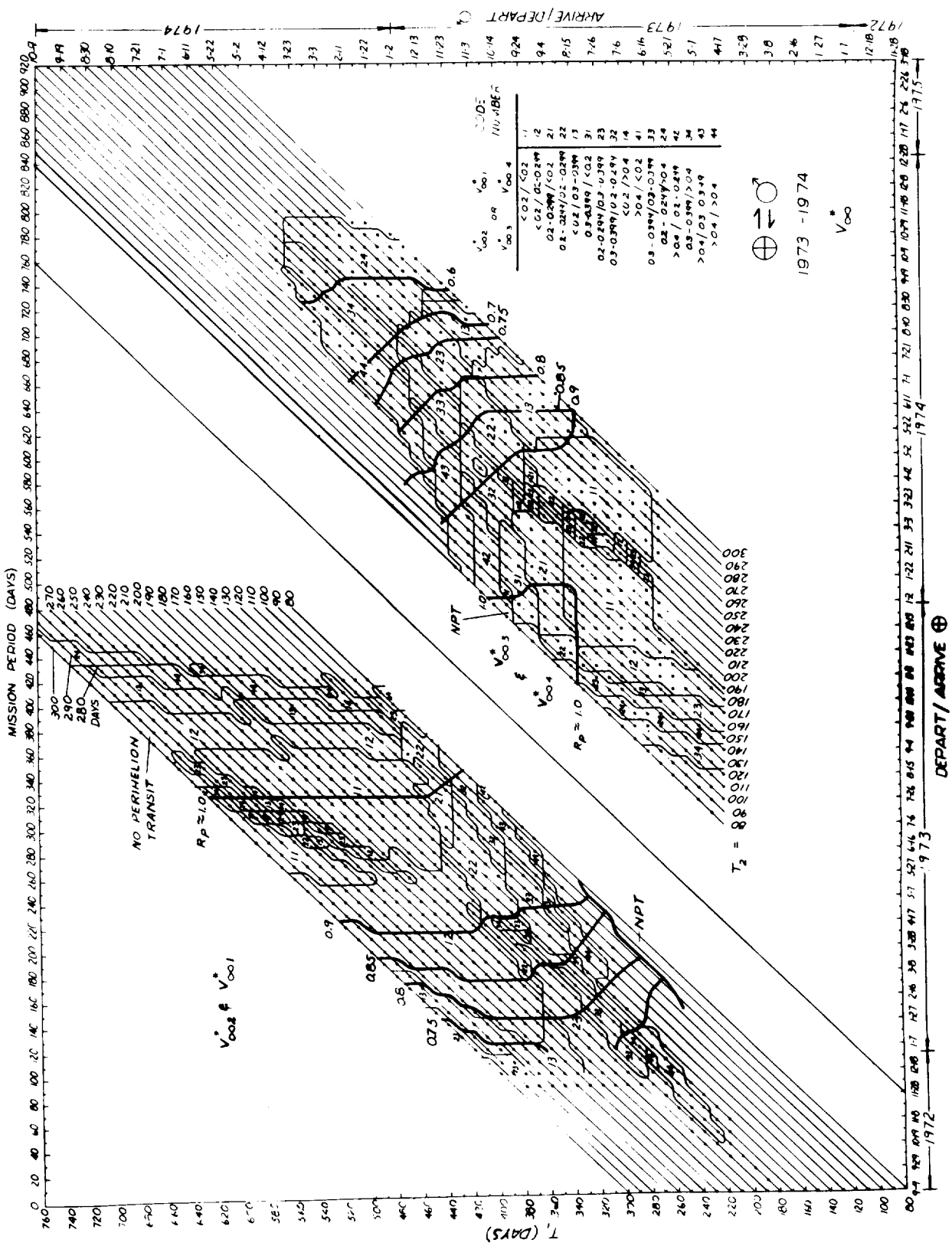

Figure 6-9. Earth-Mars Mission Map 1973-1974: Hyperbolic Excess and Iso-Perihelion Lines (10-day Intervals)

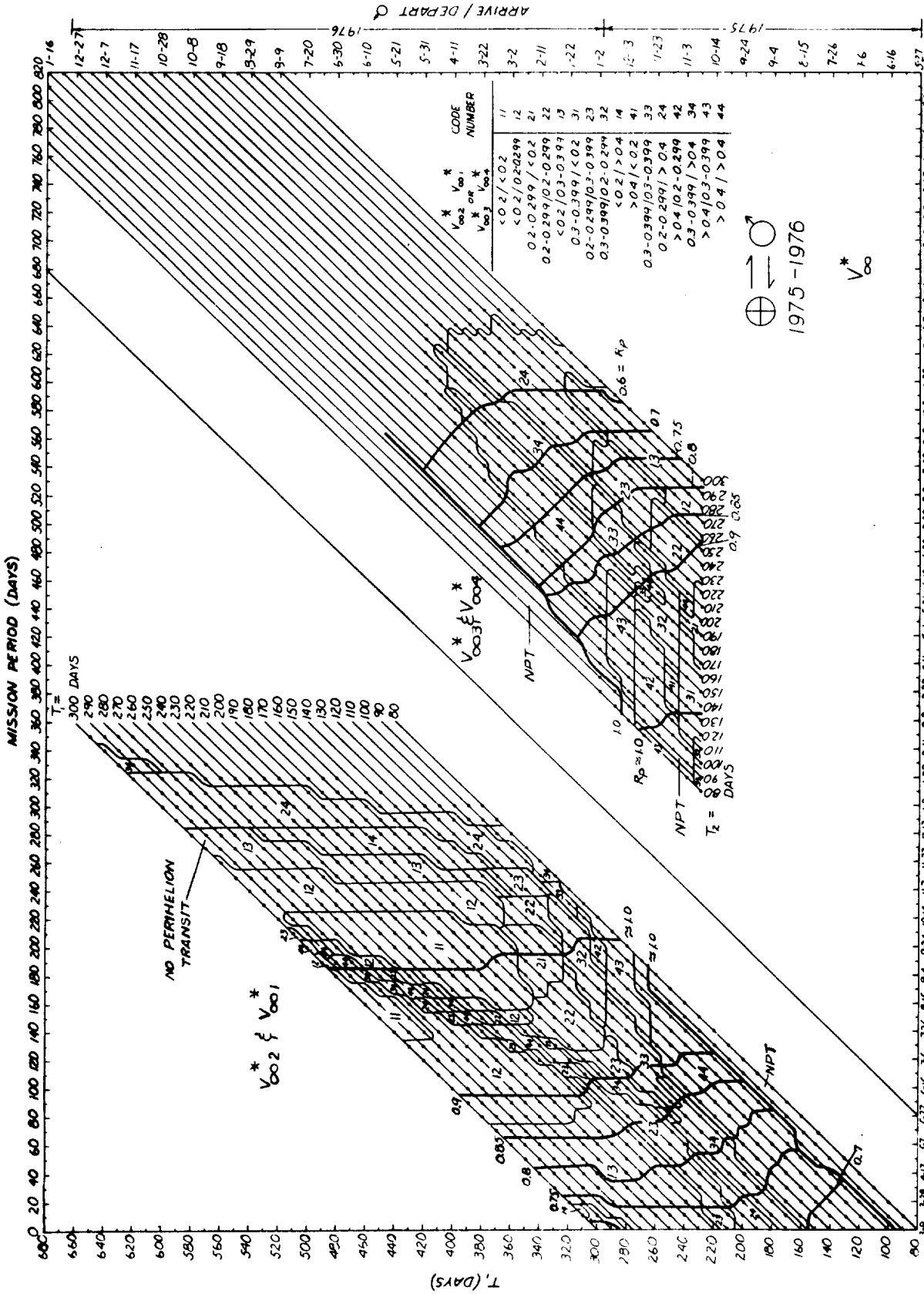

Figure 6-10. Earth-Mars Mission Map 1975-1976: Hyperbolic Excess and Iso-Perihelion Lines (10-day Intervals)

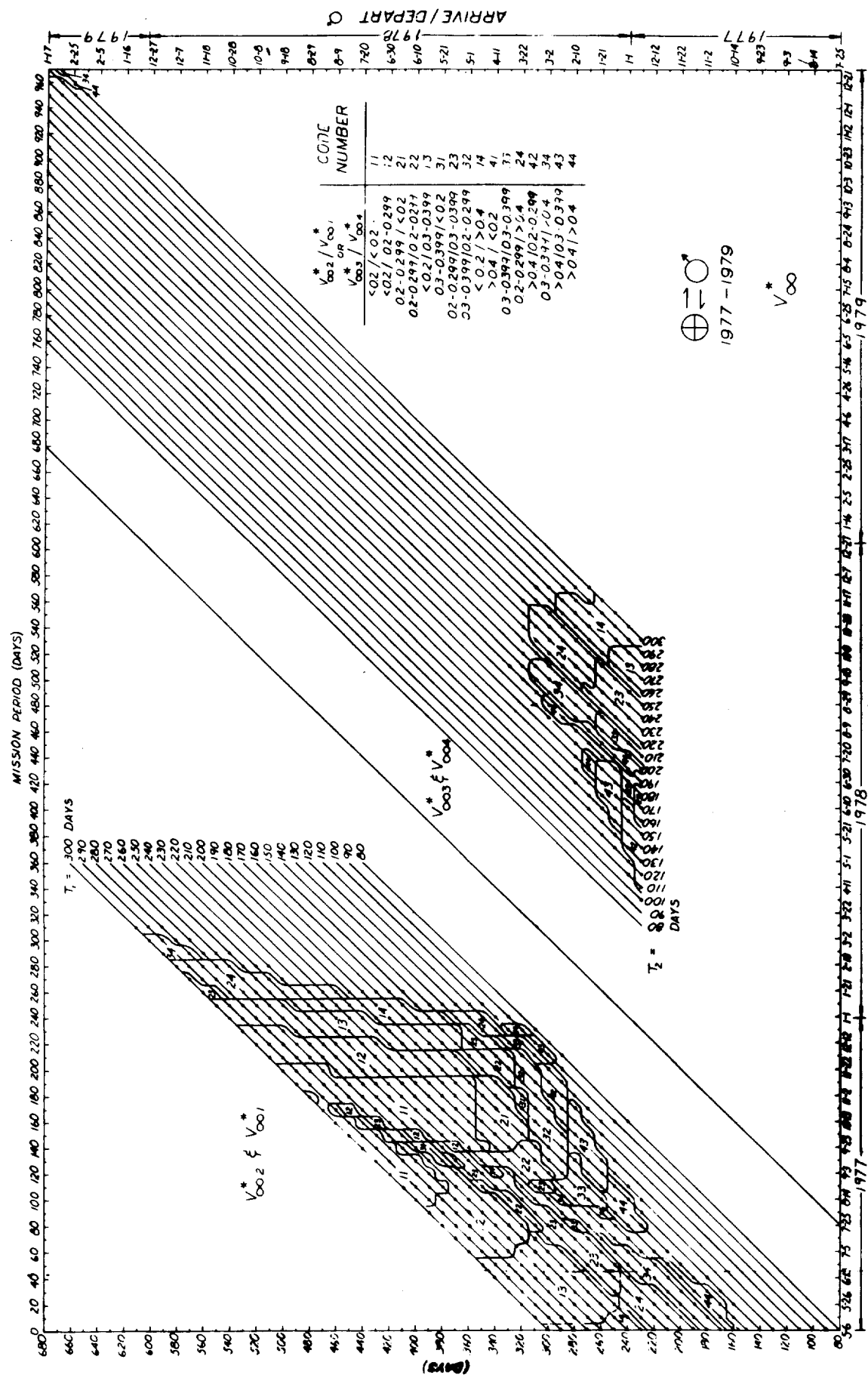

Figure 6-11. Earth-Mars Hyperbolic Excess Mission Map 1977-1979 (10-day Intervals)

Although comparatively coarse, these maps provide the basis for a first-order definition of suitable mission windows (i.e., combinations of Earth departure window, capture period and target planet departure window, as well as the associated transfer periods, which, together with the capture period, yield the overall mission period). Within the range of selected windows, refined mission maps can be, and presently are being, constructed.

The most important transfer orbit parameters for round trips to Venus and to Mars are presented in mission map arrangement for the period 1972 to 1982 in References 6-7 and 6-8.

Figures 6-12 and 6-13 show iso-perihelion lines and a number of transfer orbits whose plane is inclined 25 degrees or more with respect to the ecliptic. These transfer orbits are particularly expensive and should either be avoided or flown with an intermediate plane change in heliocentric space. In this case, three major maneuvers are required for the transfer (cf. Paragraph 6.4).

Figure 6-14 shows the positions of Venus and Mars during probable capture period in the years indicated. Comparison with the mission maps shows the influence of these positions, relative to the planet's nodal line, on the hyperbolic excess velocities involved. Conditions are in general more favorable when the target planet is in the vicinity of one of its nodes. Whenever the position of Venus is far off the nodal line, as in 1972 and 1974, low hyperbolic excess velocities during the return flight are associated with longer transfer times (long transfer orbits, $\eta_t > 180^\circ$) to avoid more highly inclined transfer orbits (Figure 6-15).

In the case of Mars, long transfer orbits ($\eta_t > 180^\circ$) are more difficult to accept, because of the associated very long transfer periods. Therefore, the position of Mars relative to the nodal line, during the capture period, has a far stronger influence on the hyperbolic excess than does the position of Venus. In addition, the higher eccentricity of the Mars orbit augments this effect, because the apsidal line (PA) happens to be almost at a right angle to the nodal line. Around the aphelion, the Martian angular velocity is particularly low, therefore prolonging the duration of the unfavorable position of Mars. The fact that the mission conditions are considerably less favorable in 1977 than in 1975 or 1973 is clearly reflected in the mission map, Figure 6-20. The 1975 mission conditions are slightly less favorable than those existing in 1973.

For the 1973 and 1975 constellations which are of primary interest in this study, the orbital positions of Venus and Mars as function of the dates are shown in Figures 6-16 through 6-19.

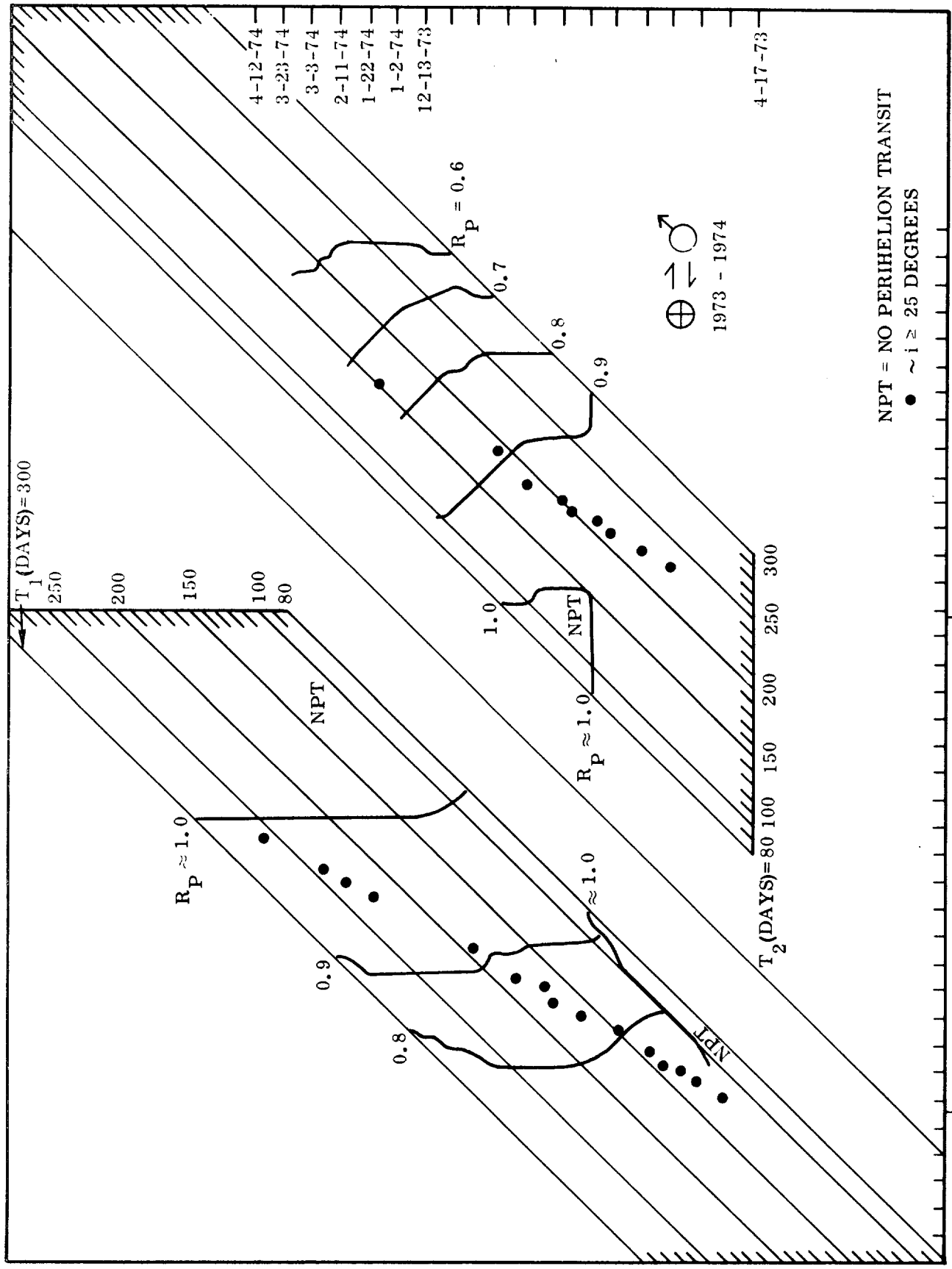

Figure 6-12. Iso-Perihelion Lines and Location of Transfer Orbits of ≥ 25° Inclination

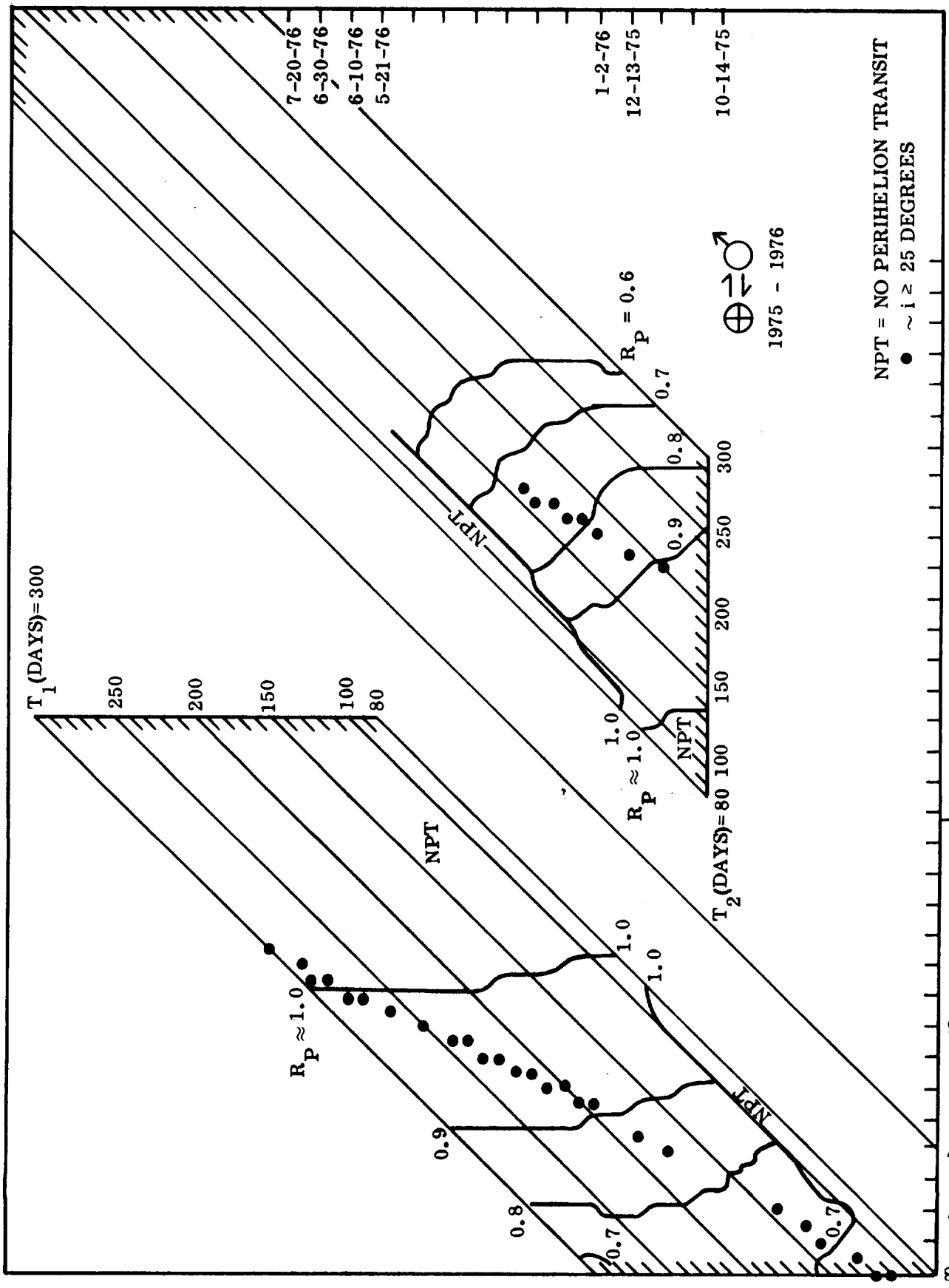

Figure 6-13. Iso-Perihelion Lines and Location of Transfer Orbits of ≥ 25° Inclination

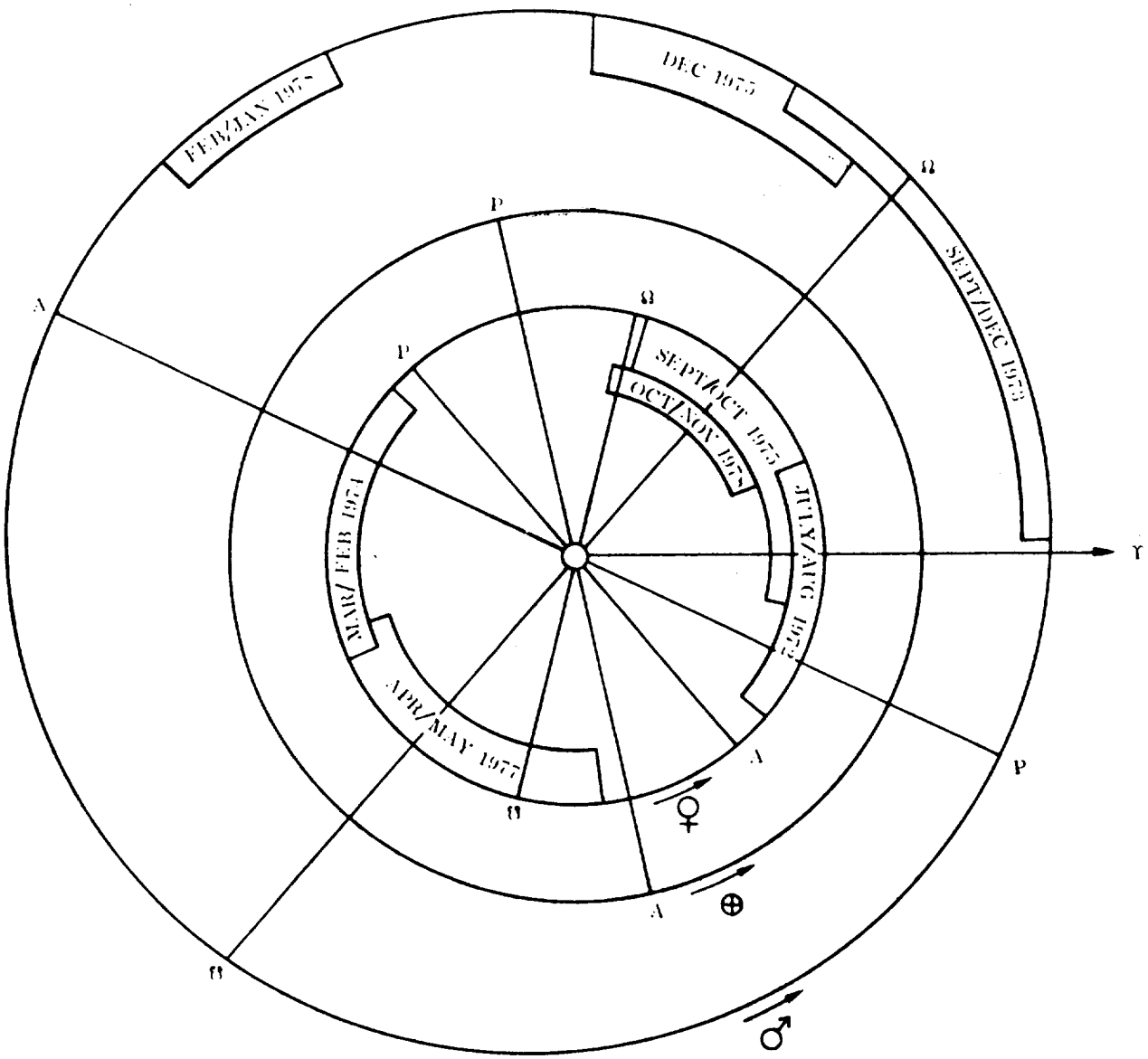

Figure 6-14. Positions of Venus and Mars During Likely Capture Periods, 1972/1978

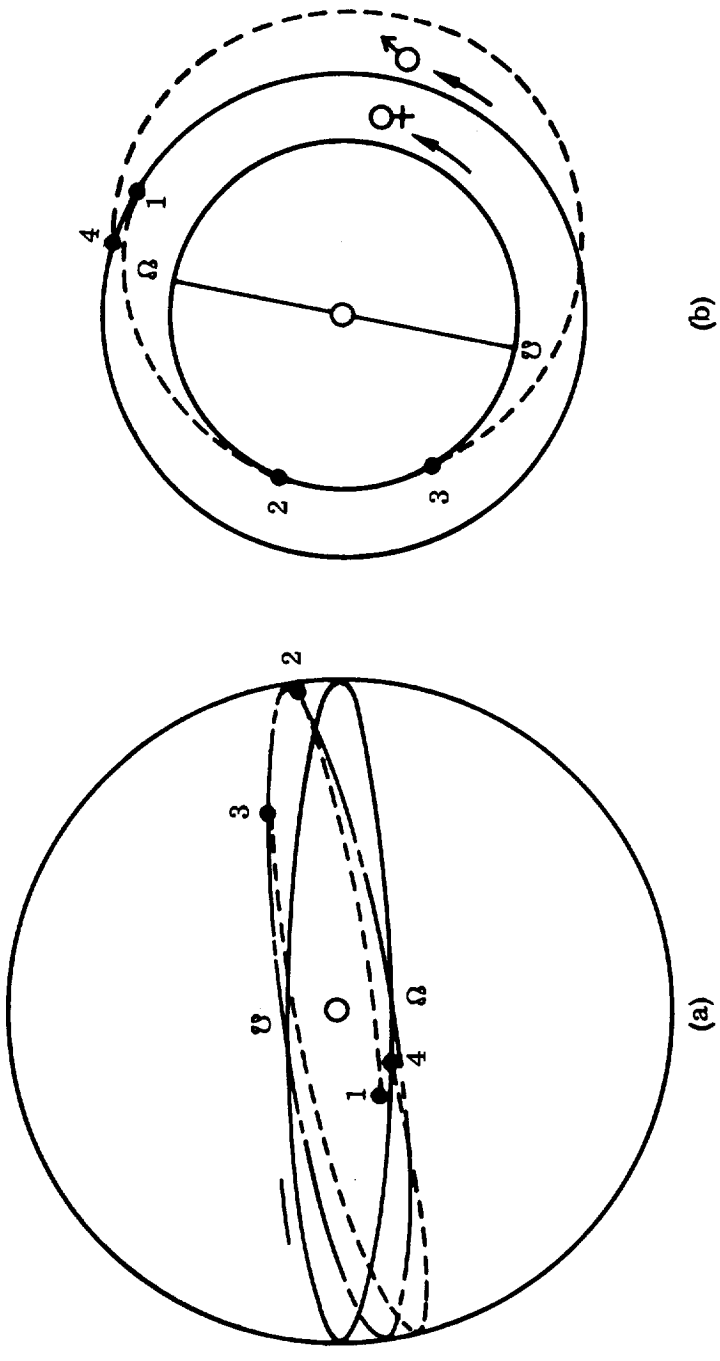

Figure 6-15. Venus Capture Mission in the Ecliptic Plane (b) and in the Plane Normal to it (a)

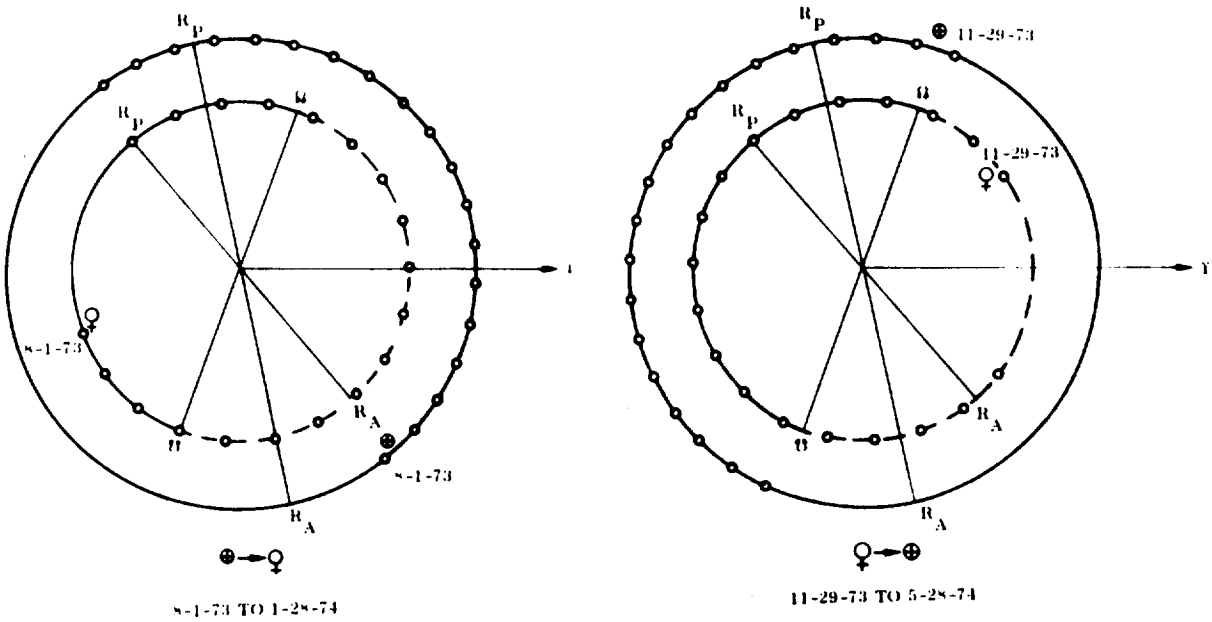

Figure 6-16. Orbital Positions of Earth and Venus During Indicated Periods

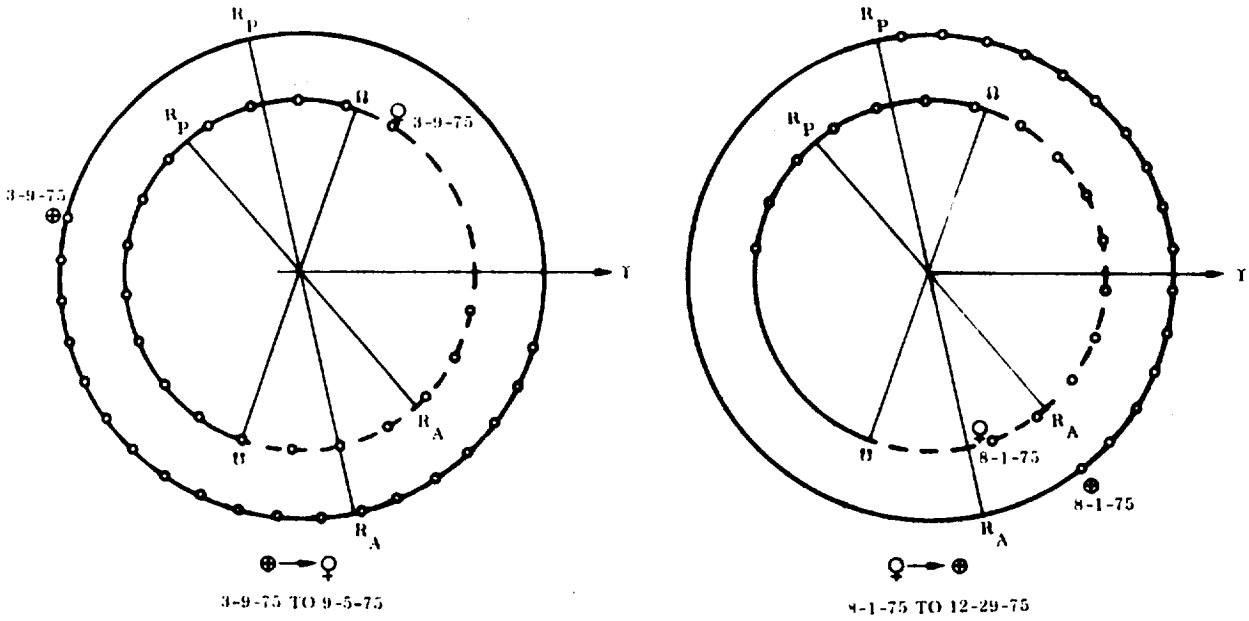

Figure 6-17. Orbital Positions of Earth and Venus During Indicated Periods

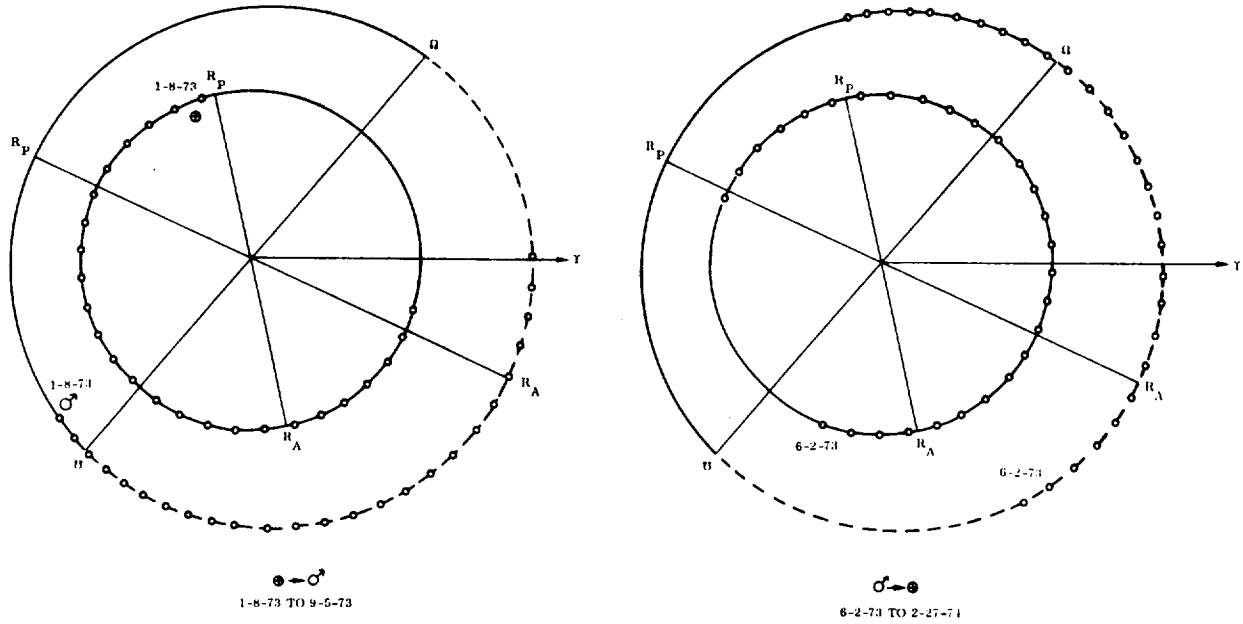

Figure 6-18. Orbital Positions of Earth and Mars During Indicated Periods

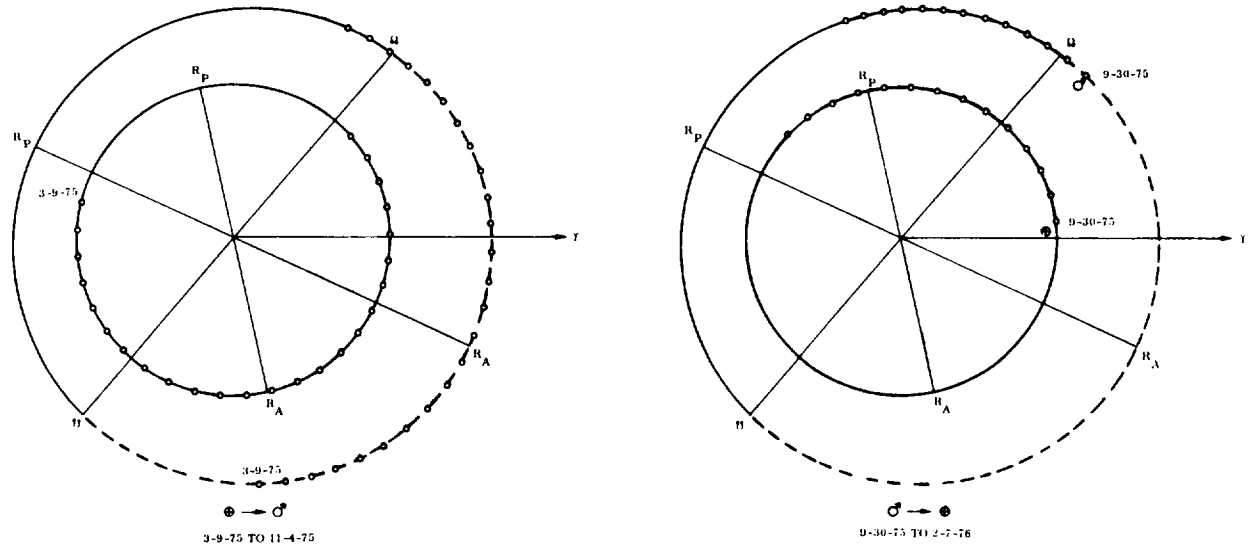

Figure 6-19. Orbital Positions of Earth and Mars During Indicated Periods

6.4 MISSION WINDOW SELECTION. Although the hyperbolic excess velocity is an indicator of the mission energy requirement (subject to modifications determined by the distance and eccentricity of the capture orbit and by the thrust accelerations involved, cf. below), mission energy is but one of the criteria for mission window selection. A summary of these criteria is listed in Table 6-2.

Table 6-2. Criteria for Mission Window Selection

1. Flight Dynamic Criteria
   - 1.1 Mission energy
   - 1.2 Energy distribution over the principal maneuvers
   - 1.3 Perihelion distances (outgoing and return)
   - 1.4 Variation of energy requirement with time, $\partial E/\partial$ (Date), especially for the return flight.
2. Mission and Systems Criteria
   - 2.1 Mission period
   - 2.2 Capture period
   - 2.3 Number of principal maneuvers during mission
   - 2.4 Specific impulse available at each particular principal maneuver
   - 2.5 Capture orbit shape

Criterion 1.2 recognizes the fact that, due to the interaction of performance and design criteria, the same total mission velocity may lead to greatly different departure weights for a vehicle of given designs and engines, dependent upon how the velocity changes are distributed over the individual principal maneuvers.

Criterion 1.3 takes into account the effect which the closest proximity to the Sun has on vehicle design, on possible hydrogen evaporation losses, and on the radiation shield requirements for the crew. Since both Venus and Mars are considered target planets, and since the Venus mission windows selected did not require perihelion distances closer than about 0.7 A.U., this value was tentatively chosen as the limiting perihelion distance for Mars mission, also, at the same time attempting to keep Mars mission perihelions above this value, wherever possible. A more detailed analysis of the limiting perihelion distance is planned. Restricting the minimum perihelion distance for Mars missions to 0.8 A.U., or higher values, imposes considerable constraints on the 1975/1976 and 1977/1978 mission windows in terms of mission energy levels and capture periods comparable to those for 1973/1974.

Variation of energy requirements with time refers to the fact that overall minimum energy or the energy level of a particular transfer (two maneuvers), or of a particular individual maneuver, may vary greatly with the departure date. This imposes certain restrictions on the Earth departure window, but it can have far more critical

consequences for the target planet departure window. Here, the crew is committed and must return or face either a very dangerous (close perihelion) return flight path or a very long "hold-over" period in which the expedition is "frozen" in the target planet's activity sphere until a new departure window arrives which permits them to return. The capture period must therefore be located in such a region of the mission map that involuntary delay in departure does not jeopardize the chances for return. In other words, the probability of success of the mission is enhanced if a limited target planet departure window tolerance (10-20 days) is built into the mission profile.

Mission period and capture period are obviously mission-oriented criteria. Generally, mission periods to Venus are shorter than those to Mars, with lower mission energy requirements. Most of the Mars missions with periods of 380-560 days involve Σv_∞^* of 1.0 to 1.18 for 20-60 day capture periods (circular capture orbit). Venus mission periods lie between 200 and 300 days for energy levels comparable to those required for Mars, or involve Σv_∞^* of 0.7-0.85 for periods of 360-420 days (Figure 6-20). For comparison, the conditions for extended Mars landing missions are also shown.

The number of principal maneuvers during the mission may vary between four and six, depending upon whether a major orbit change enroute is required to avoid excessive heliocentric inclination of the outgoing or return transfer orbit. Transfer orbits are highly inclined when the nodal line of the transfer orbit forms an angle in the vicinity of 90 degrees with the nodal line of the target planet's orbit, relative to the ecliptic plane of Earth. The location of high-inclination transfer orbits (taken as $i \geq 25^\circ$) is shown in Figures 6-12 and 6-13 for Mars missions in 1973 and 1975. In a few areas where these high-inclination regions interfere with otherwise desirable departure windows, an incentive is provided for considering a three-maneuver transfer. Operationally, a plane change en route does not add much complexity, if a chemical or a nuclear space ship with adequate engine life is used. However, if an extra stage is needed the mission complexity is increased, perhaps significantly. An analysis of the optimization of the location of the intermediate maneuver during a three-maneuver transfer has recently been presented (Ref. 6-9). It is noted that the opportunities for two-maneuver transfers (i.e., unchanged heliocentric transfer orbit, except for navigational corrections) are frequent enough so that the three-maneuver transfers could be temporarily disregarded without causing a significant constraint.

The final two criteria mentioned in Table 6-2 are self-evident. Capturing in planetocentric orbits or increasing eccentricity leads to decreasing capture- (hence, mission-) energy requirements and either reduces the vehicle weight or the mission period, or increases the payload or capture period. Increasing the eccentricity of the capture orbit is one of the most effective means of reducing the energy requirement of a capture mission. In order to retain some energy reserves, a circular capture orbit was assumed as the standard case. The effect of increasing the eccentricity is shown below.

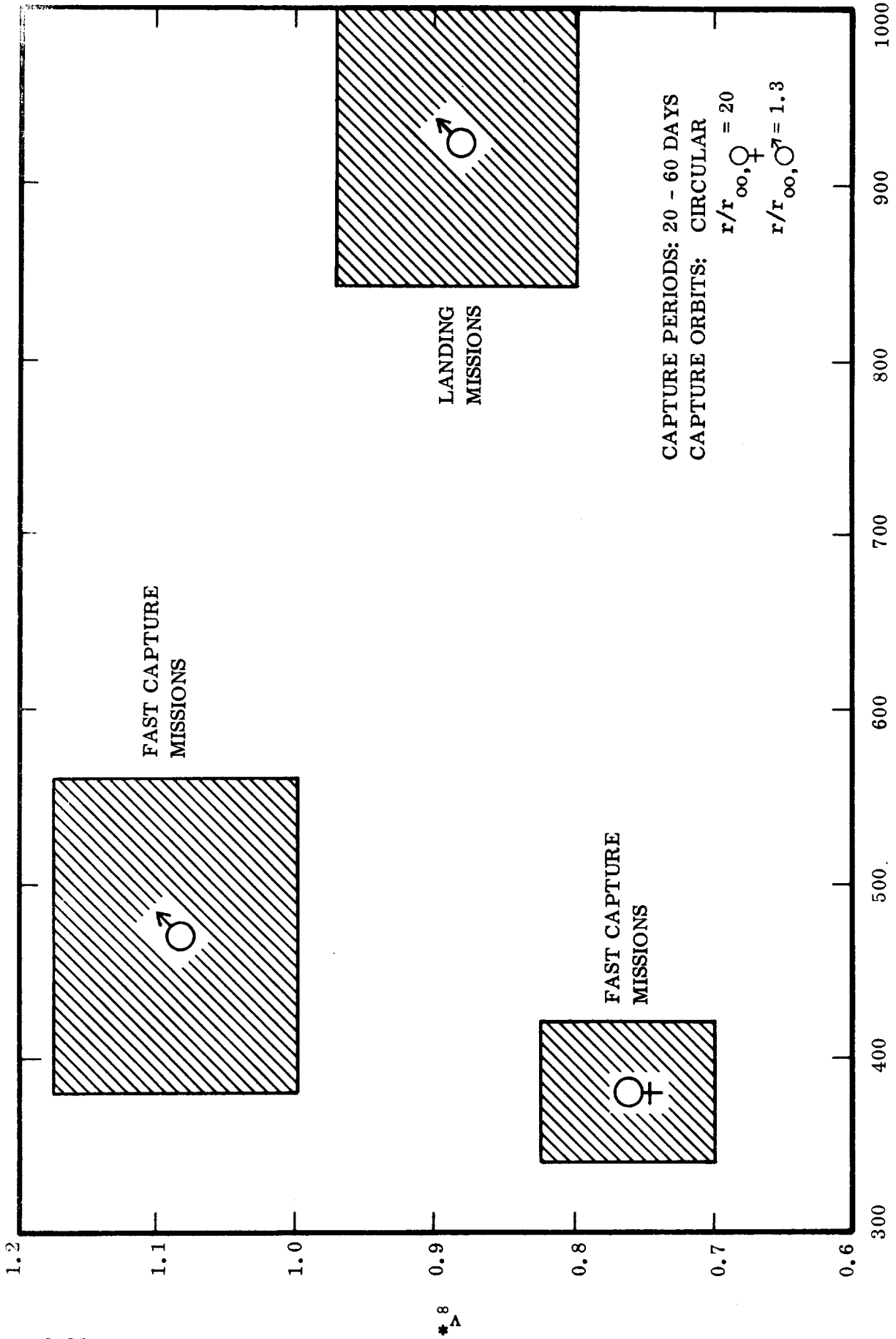

Figure 6-20. Comparison of Energy and Period for Missions to Venus and Mars

6.5 SPECIFIC MISSION WINDOWS. With these criteria in mind, a number of mission windows have been defined for the 1973/1974 mission to Venus and the 1973/1974 and 1975/1976 missions to Mars. They are listed in Tables 6-3 through 6-7. For discussion of the maneuvers listed in the tables, see Section 7. Detailed charts of v_∞^* and, where relevant, of perihelion distance R_p, are presented versus dates and transfer periods in Figures 6-21 through 6-30 for the selected mission windows.

In Figures 6-31 through 6-41 are presented plots of the transfer orbits for the 1973 mission windows to Venus and Mars and for the 1975 window to Mars. The flight paths shown represent the first and the last date of Earth and target planet departure windows listed in Tables 6-3 through 6-6. Although the return transfer periods from Venus are long, they at least do not lead closer to the Sun, but rather beyond the Earth orbit, so that the departing space ships, following Venus departure, quickly gain heliocentric distance. Unfortunately, as shown in Figure 6-31, Mars is not in the "vicinity" when the returning Venus convoy passes through its aphelion.

The terminal departure from Mars is the same (12-24-73) for mission windows 73-2 and 73-3 and leads through a perihelion of approximately 0.7, which was the reason for making this the terminal date. Again, unfortunately, $V_e$nus is not close by when the returning Mars convoy passes through its perihelion (Station 11).

The specification of particular flight profiles during the mission window has been based on the following considerations:

a. During the Earth departure window, the transfer time (T_1) is varied such that the arrival date at the target planet remains unchanged. Therefore, if a delay occurs in departure from Earth, it is not necessary to change the propellant load for the return flight. Only the tankage for Earth escape and target planet capture may have to be changed. For this reason, the detail charts (Figures 6-28, 6-30 through 6-32 and 6-36, showing Earth to target planet transfer conditions) are all laid out for one or several discrete arrival dates which remain constant as the departure date changes.

b. Having assured a fixed target-planet-arrival date, a maximum capture period is tentatively specified. Inside this maximum capture period lies an effective capture period (usually 10-20 days shorter) during which all planned operations, observations, and research are completed if everything goes according to schedule. The end of the effective capture period thus represents the earliest planned departure date from the target planet. The difference between this date and the end of the maximum capture period represents the target planet departure window, that is, a time reserve to absorb delays without critical effect. Therefore space ship performance is specified for the maximum capture period, the end of which constitutes the latest departure date. If this date is exceeded,

Table 6-3. Earth-Venus Mission Window 1973-1

Earth Dep. Window	10-25-73 through 11-16-73
Arr. Venus	2-17-74
Transfer Periods	$115 \geq T_1 \geq 93$ d
Venus Dep. Window	2-17-74 through 3-25-74
Transfer Periods	$244 \leq T_2 \leq 280$ d
Maximum Capture Period, T_{cpt}	36 d
Mission Periods	115 + 36 + 280 = 431 (Maximum)
	93 + 36 + 280 = 409 (Min. for Max. T_{cpt})
	115 (93) + 30 + 269 = 441 (392) d
	115 (93) + 20 + 259 = 394 (372) d
	115 (93) + 10 + 244 = 369 (347) d
Perihelion Distances:	Outgoing T. O. : No perihelion transits
	Return T. O. : $R_P > 0.7$

Maneuver	M-1	M-2	M-3	M-4
v^*_∞	0.13	0.21	0.18	0.29
ϵ	-1.0	-1.0	-1.0	-0.04
Orbit Distance	1.05 r_{oo},	20 r_{oo},	20 r_{oo},	y_P = 60 km
F/W	0.3	0.8	0.8	3.0
Engine	Nuclear	Nuclear	Nuclear	O_2/H_2
I_{sp}	846	846	820	455
Δ v (km/sec)	3.85	4.7	3.78	3.25
(ft/sec)	12,600	15,400	12,400	10,660
μ	1.59	1.76	1.6	2.02
μ_ℓ	1.005	1.02	1.025	1.03
μ corr				1.071^2
μ pl			1.21	
μ'	1.597	1.795	1.984	2.44

Table 6-4. Earth-Mars Mission Window 1973-1

Earth Dep. Window	2-17-73 through 3-7-73
Arr. Mars	9-25-73
Transfer Periods	$220 \geq T_1 \geq 202$ d
Mars Dep. Window	9-25-73 through 11-3-73
Transfer Periods	$170 \leq T_2 \leq 210$ d
Maximum Capture Period, T_{cpt}	39 d
Mission Periods	220 + 39 + 210 = 469 d (Maximum)
	202 + 39 + 210 = 451 d (Min. for Max. T_{cpt})
	220 (202) + 30 + 203 = 453 (435) d
	220 (202) + 20 + 196 = 436 (418) d
	220 (202) + 10 + 191 = 421 (403) d
Perihelion Distances:	Outgoing T. O. : $0.82 \leq R_P \leq 0.85$
	Return T. O. : $0.9 \geq R_P \geq 0.835$

Maneuver	M-1	M-2	M-3	M-4
v_∞^*	0.20	0.29	0.29	0.29
ϵ	-1.0	-1.0	-1.0	-0.04
Orbit Distance	1.05 r_{oo},	1.3 r_{oo},	1.3 r_{oo},	$y_P \doteq 60$ km
F/W	0.3	0.3	0.4	0.3
Engine	Nuclear	Nuclear	Nuclear	O_2/H_2
I_{sp}	846	846	820	455
Δ v (km/sec)	4.78	7.06	6.70	3.25
(ft/sec)	15,710	23,160	22,000	10,660
μ	1.78	2.34	2.3	2.07
μ_ℓ	1.005	1.01	1.015	1.02
μ corr				1.071[2]
μ pl			1.21	
μ'	1.79	2.361	2.825	2.424

Table 6-5. Earth-Mars Mission Window 1973-2

Earth Dep. Window			5-18-73 through 6-17-73		
Arr. Mars			11-4-73		
Transfer Periods			$170 \geq T_1 \geq 150$ d		
Mars Dep. Window			11-4-73 through 12-24-73		
Transfer Periods			$205 \geq T_2 \leq 223$		
Maximum Capture Period, T_{cpt}			50 d		
Mission Periods			170 + 50 + 223 = 433 d (Maximum)		
			150 + 50 + 223 = 413 d (Min. for Max. T_{cpt})		
			170 (150) + 40 + 222 = 432 (412) d		
			170 (150) + 30 + 219 = 419 (389) d		
			170 (150) + 20 + 216 = 406 (386) d		
			170 (150) + 10 + 211 = 391 (371) d		
Perihelion Distances:		Outgoing T. O. :	$0.9 < R_P < 1.0$		
		Return T. O. :	$0.7 \leq R_P \leq 0.81$. Specifically:		
Dep ♂	12-24	12-14	12-4	11-24	11-14
R_P (A.U.)	0.7	0.74	0.762	0.79	0.81

Maneuver	M-1	M-2	M-3	M-4
v_∞^*	0.24	0.24	0.3	0.4
ϵ	-1.0	-1.0	-1.0	-0.04
Orbit Distance	1.05 $r_{oo,}$	1.3 $r_{oo,}$	1.3 $r_{oo,}$	y_P = 60 km
F/W	0.3	0.3	0.4	3.0
Engine	Nuclear	Nuclear	Nuclear	O_2/H_2
I_{sp}	846	846	846	455
Δ v (km/sec)	5.54	5.75	7.01	5.68
(ft/sec)	18,150	18,850	24,000	18,630
μ	1.95	2.0	2.32	3.57
μ_ℓ	1.005	1.01	1.015	1.02
μ corr				1.071[2]
μ pl			1.21	
μ'	1.96	2.02	2.85	4.181

Table 6-6. Earth-Mars Mission Window 1973-3

Earth Dep. Window	6-6-73 through 7-6-73
Arr. Mars	12-3-73
Transfer Periods	$180 \geq T_1 \geq 150$ d
Mars Dep. Window	12-3-73 through 12-24-73
Transfer Periods	$218 \leq T_2 \leq 223$ d
Maximum Capture Period, T_{cpt}	21 d
Mission Periods:	180 + 21 + 223 = 424 d (Maximum)
	150 + 21 + 223 = 394 d (Min. for Max. T_{cpt})
	180 (150) + 10 + 211.5 = 401.5 (371.5) d

Perihelion Distances: Outgoing T. O. : $0.9 < R_P < 1.0$
Return T. O. : Like 1973-2

Maneuver	M-1	M-2	M-3	M-4
v_∞^*	0.20	0.20	0.30	0.40
ϵ	-1.0	-1.0	-1.0	-0.04
Orbit Distance	1.05 r_{oo},	1.3 r_{oo},	1.3 r_{oo},	y_P = 60 km
F/W	0.3	0.3		
Engine	Nuclear	Nuclear		
I_{sp}	846	846	As 1973-2	As 1973-2
Δ v (km/sec)	4.78	4.68		
(ft/sec)	15,170	15,350		
μ	1.78	1.7		
μ_ℓ	1.005	1.01		
μ_{corr}				
μ_{pl}				
μ'	1.079	1.717		

Table 6-7. Earth-Mars Mission Window 1975-1

Earth Dep. Window	3-9-75 through 3-29-75
Arr. Mars	11-4-75
Transfer Periods	$240 \geq T_1 \geq 220$ d
Mars Dep. Window	12-4-75 through 12-24-75
Transfer Period	260 d
Maximum Capture Period, T_{cpt}	50 d
Mission Periods:	240 + 50 + 260 = 550 d (Maximum)
	220 + 50 + 260 = 530 d (Min. at Max. T_{cpt})
	240 (220) + 30 + 260 = 530 (510) d
	240 (220) + 10 + 260 = 510 (490) d

Perihelion Distances: Outgoing T. O. : $0.71 \leq R_P \leq 0.82$
Return T. O. : $0.79 \leq R_P \leq 0.71$

Maneuver	M-1	M-2	M-3	M-4
v_∞^*	0.3705	0.1774	0.2082	0.3842
ϵ	-1.0	-1.0	-1.0	-0.04
Orbit Distance	1.05 $r_{oo,}$	1.3 $r_{oo,}$	1.3 $r_{oo,}$	y_P = 60 km
F/W	0.3	0.3	0.4	3.0
Engine	Nuclear	Nuclear	Nuclear	O_2/H_2
I_{sp}	846	846	820	455
Δ v (km/sec)	8.44	4.06	4.55	5.24
(ft/sec)	27,700	13,310	14,950	17,200
μ	2.76	1.63	1.76	3.23
μ_ℓ	1.005	1.01	1.015	1.02
μ corr				1.071[2]
μ pl			1.21	
μ'	2.774	1.646	2.162	3.778

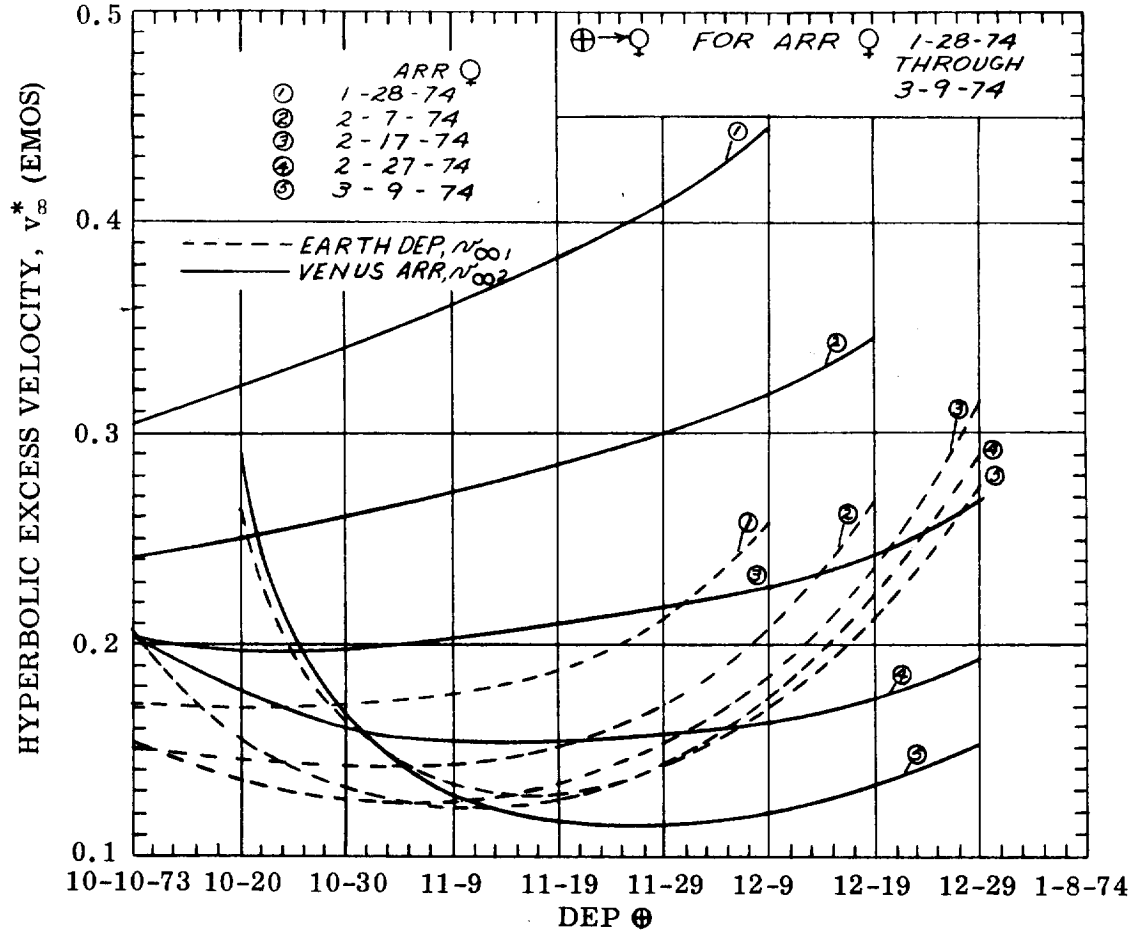

Figure 6-21. Earth-Venus Departure Window Oct/Dec 1973

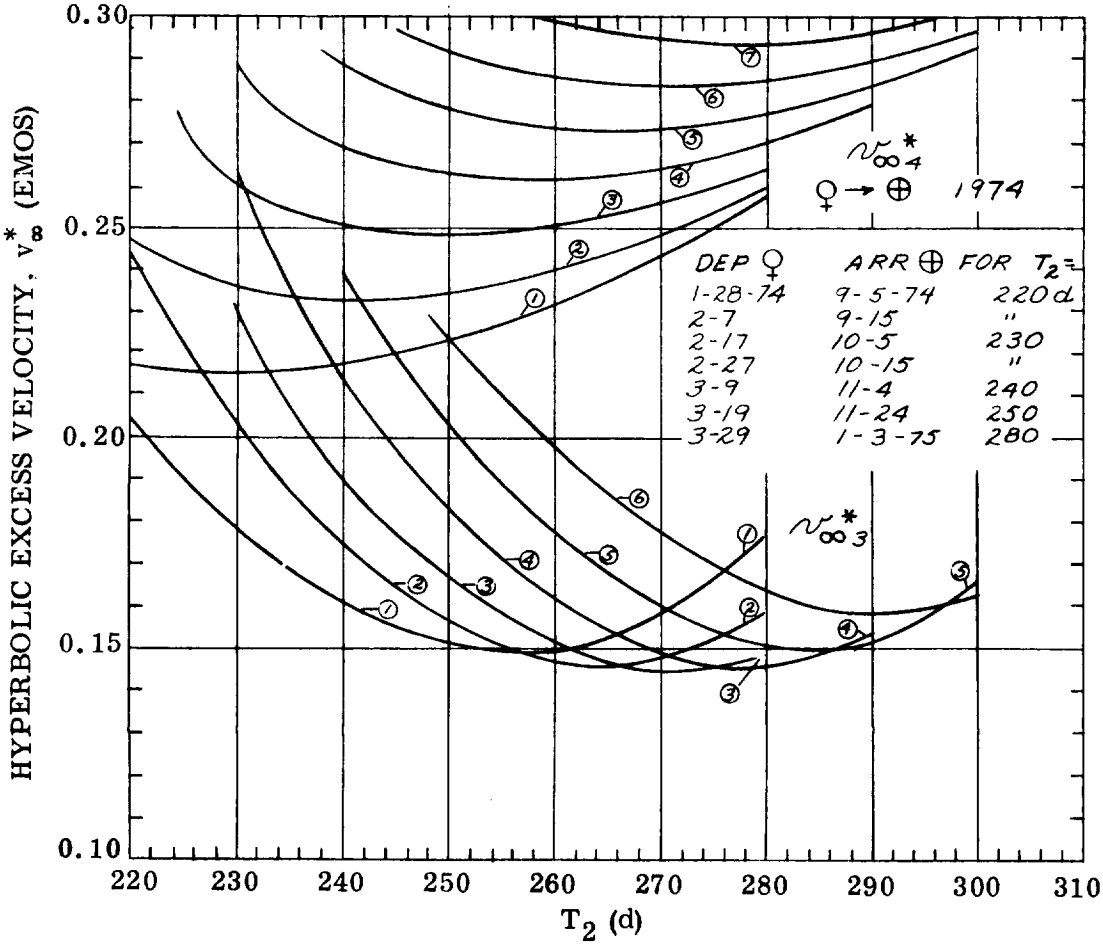

Figure 6-22. Venus-Earth Departure Window Jan/March 1974

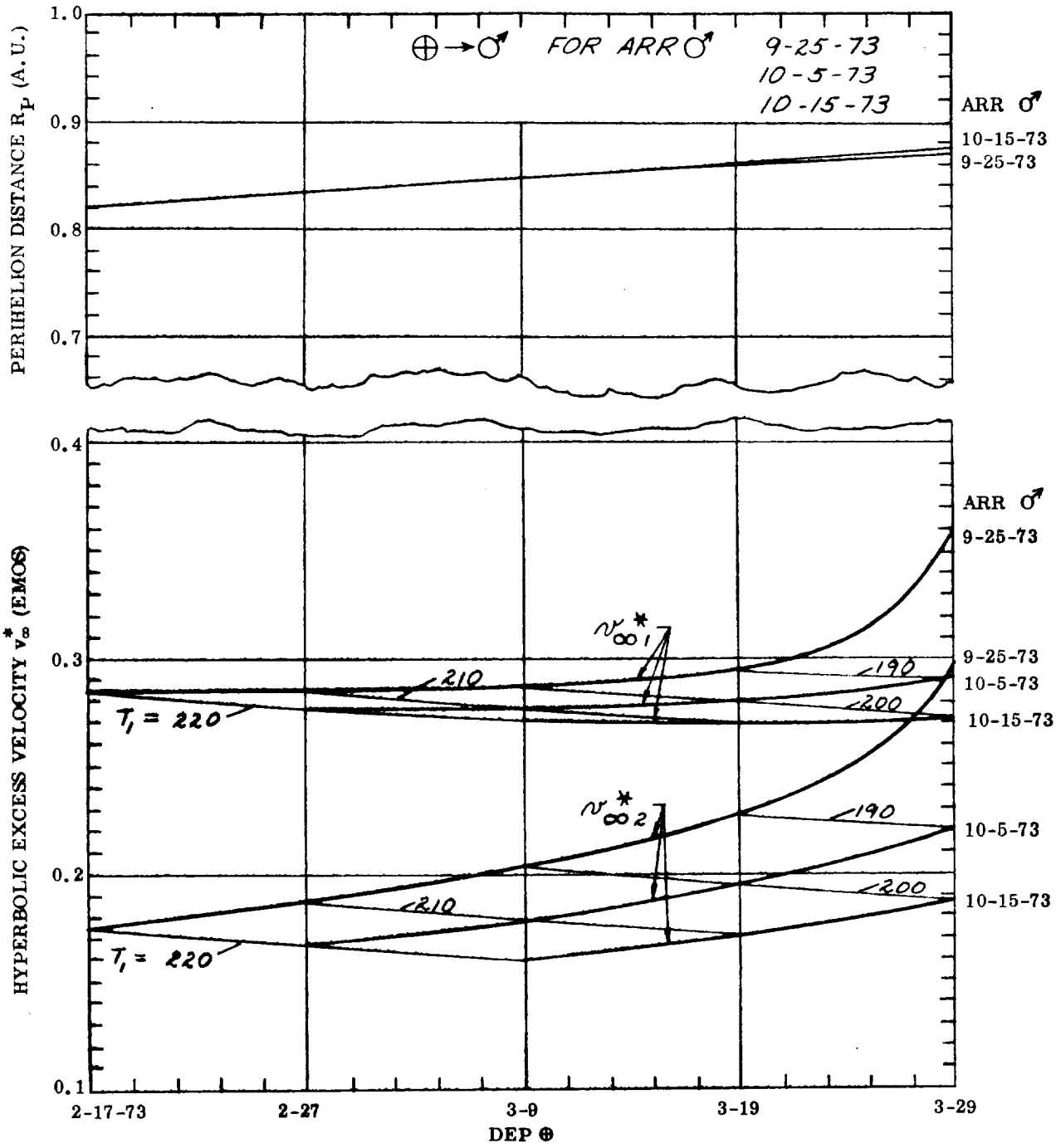

Figure 6-23. Earth-Mars Departure Window, Feb/March 1973

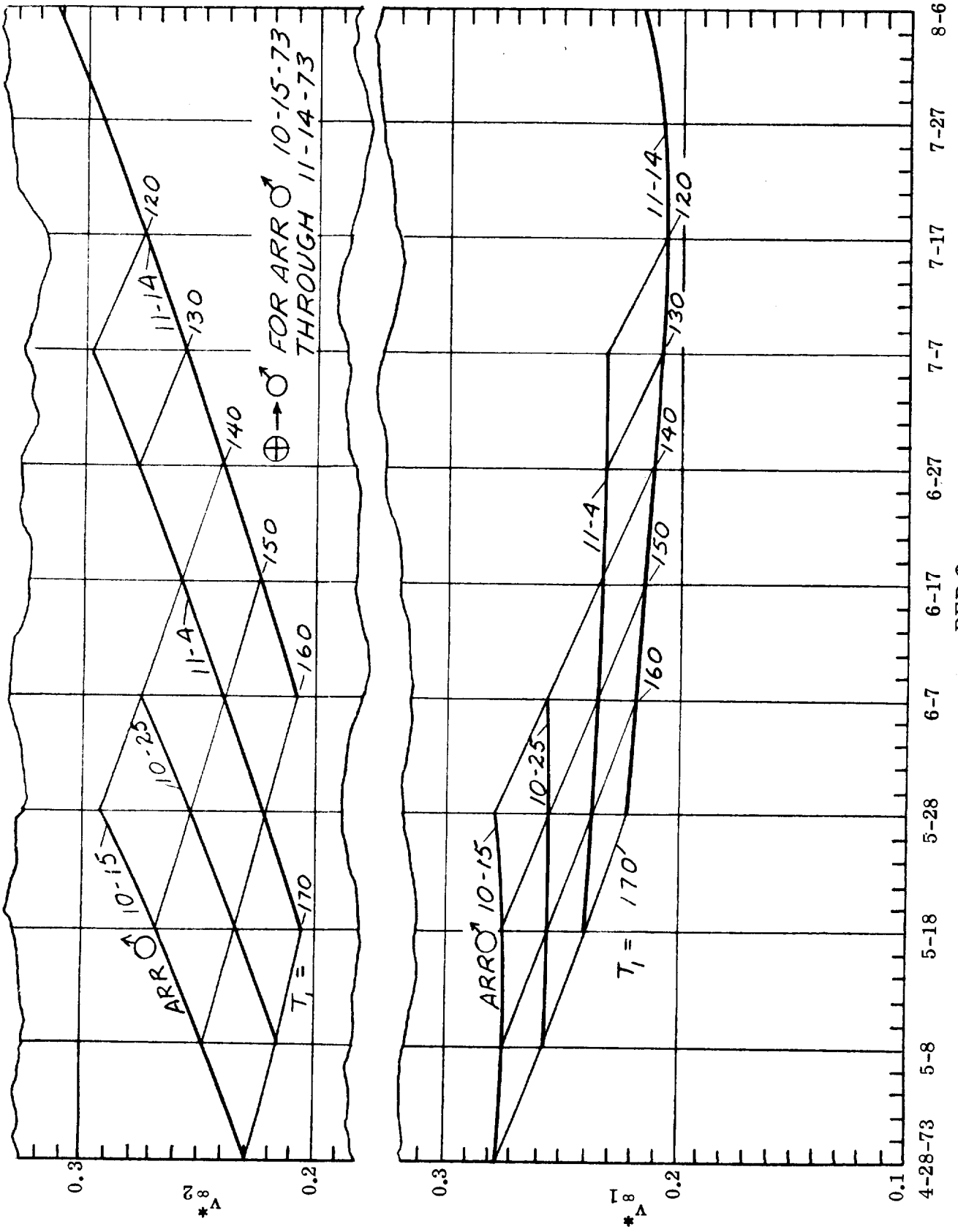

Figure 6-24. Earth-Mars Departure Window May/July 1973

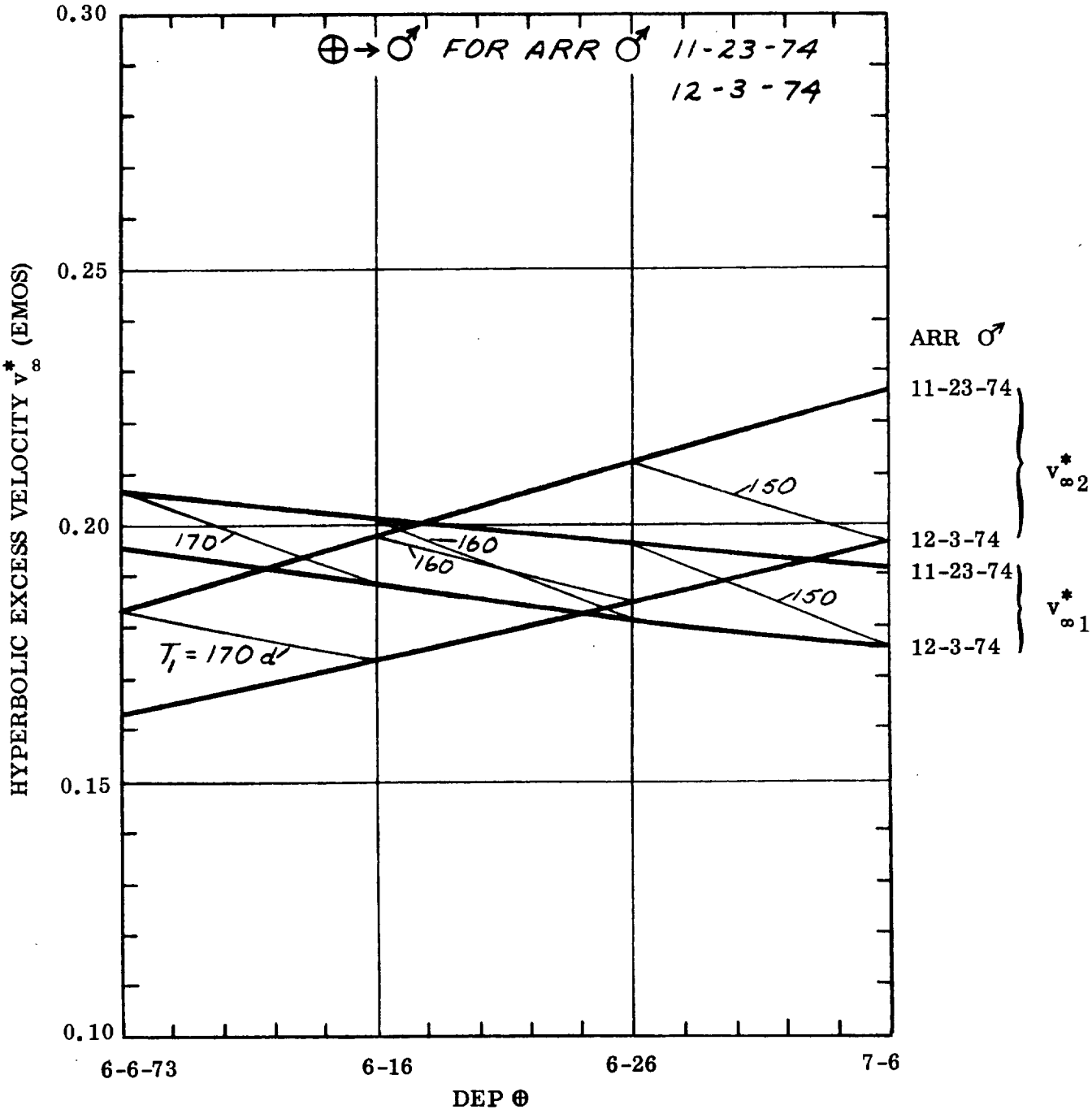

Figure 6-25. Earth Departure Window, June/July 1973

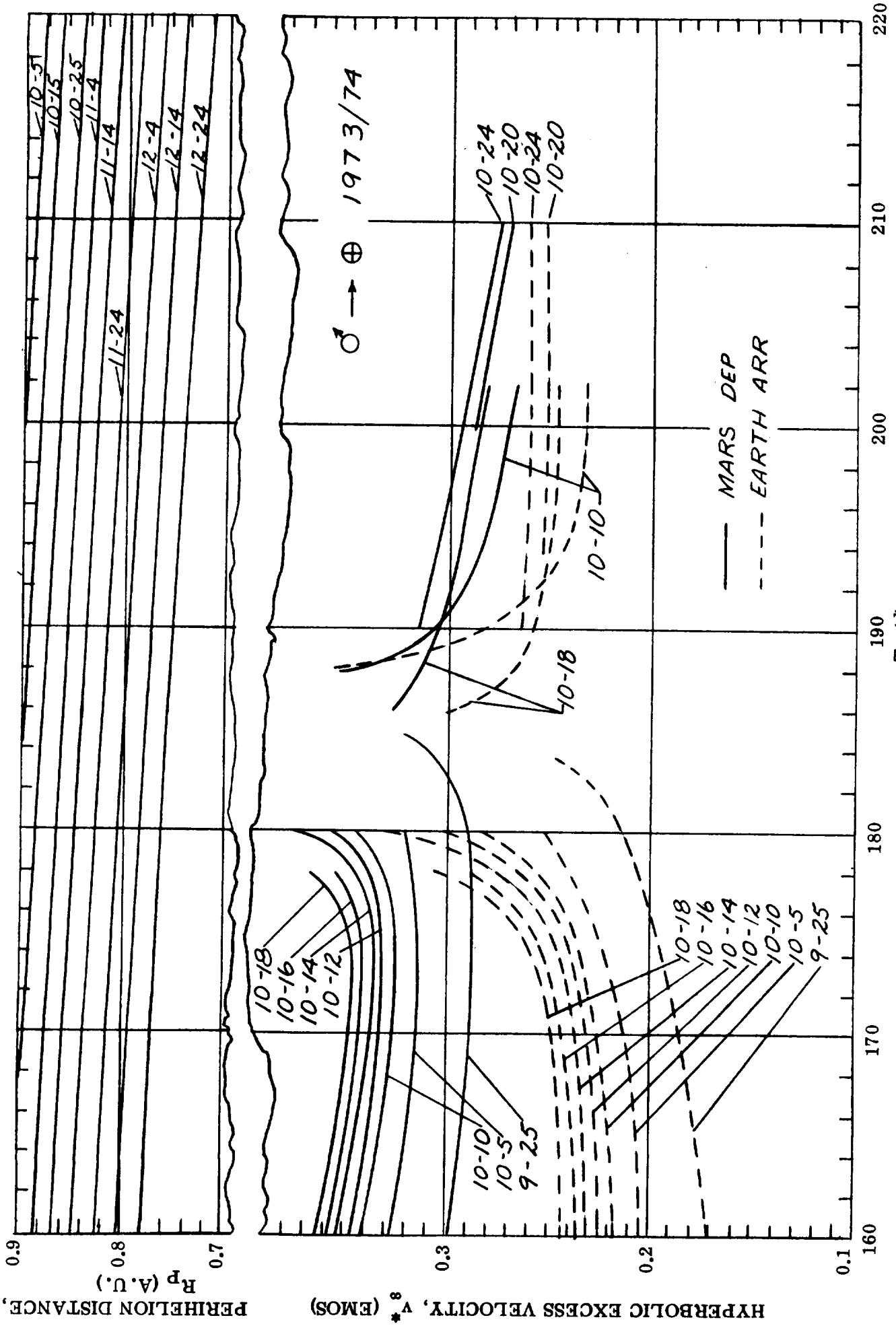

Figure 6-26. Mars Departure Window, Sept/Oct 1973

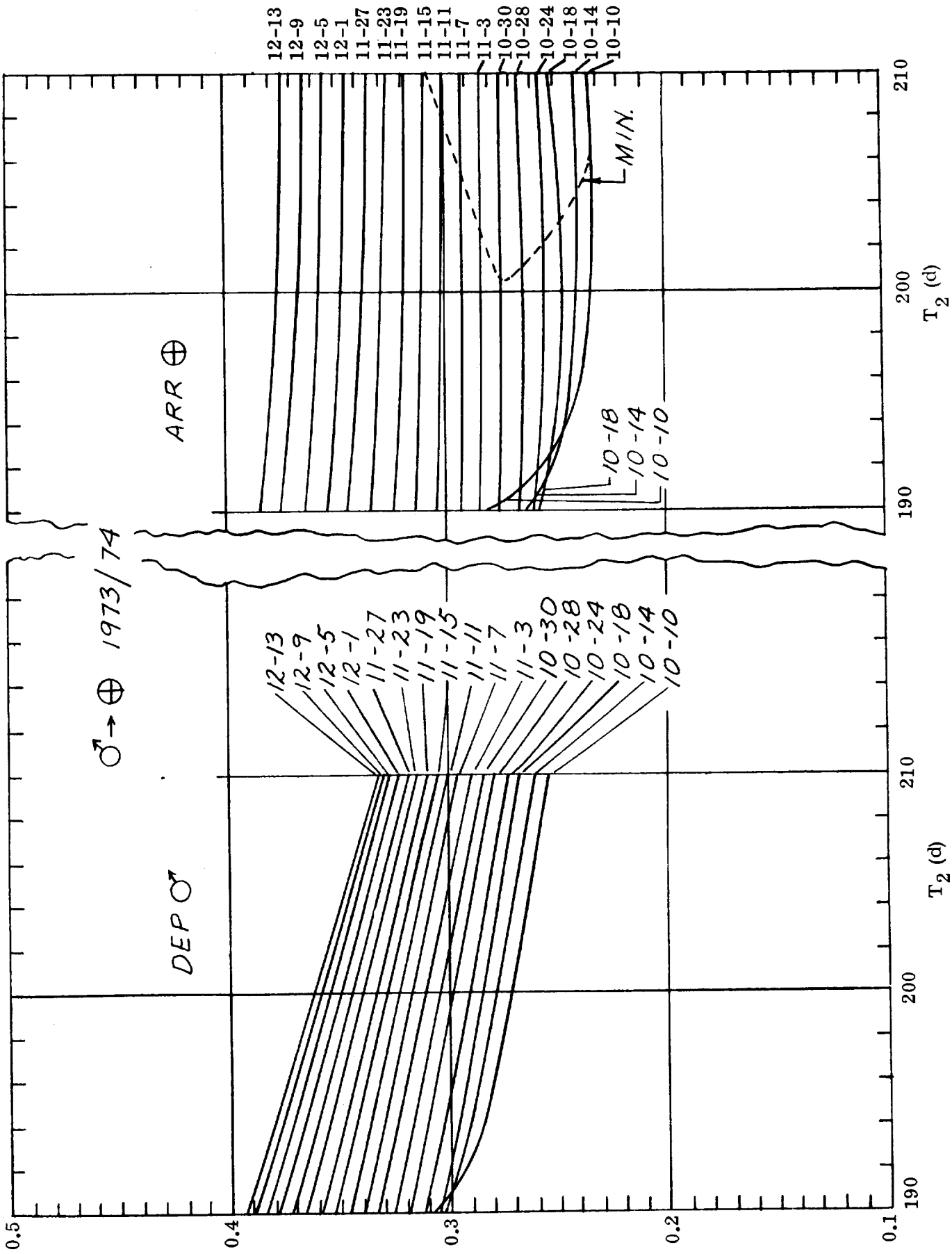

Figure 6-27. Mars Departure Window, Oct/Dec 1973

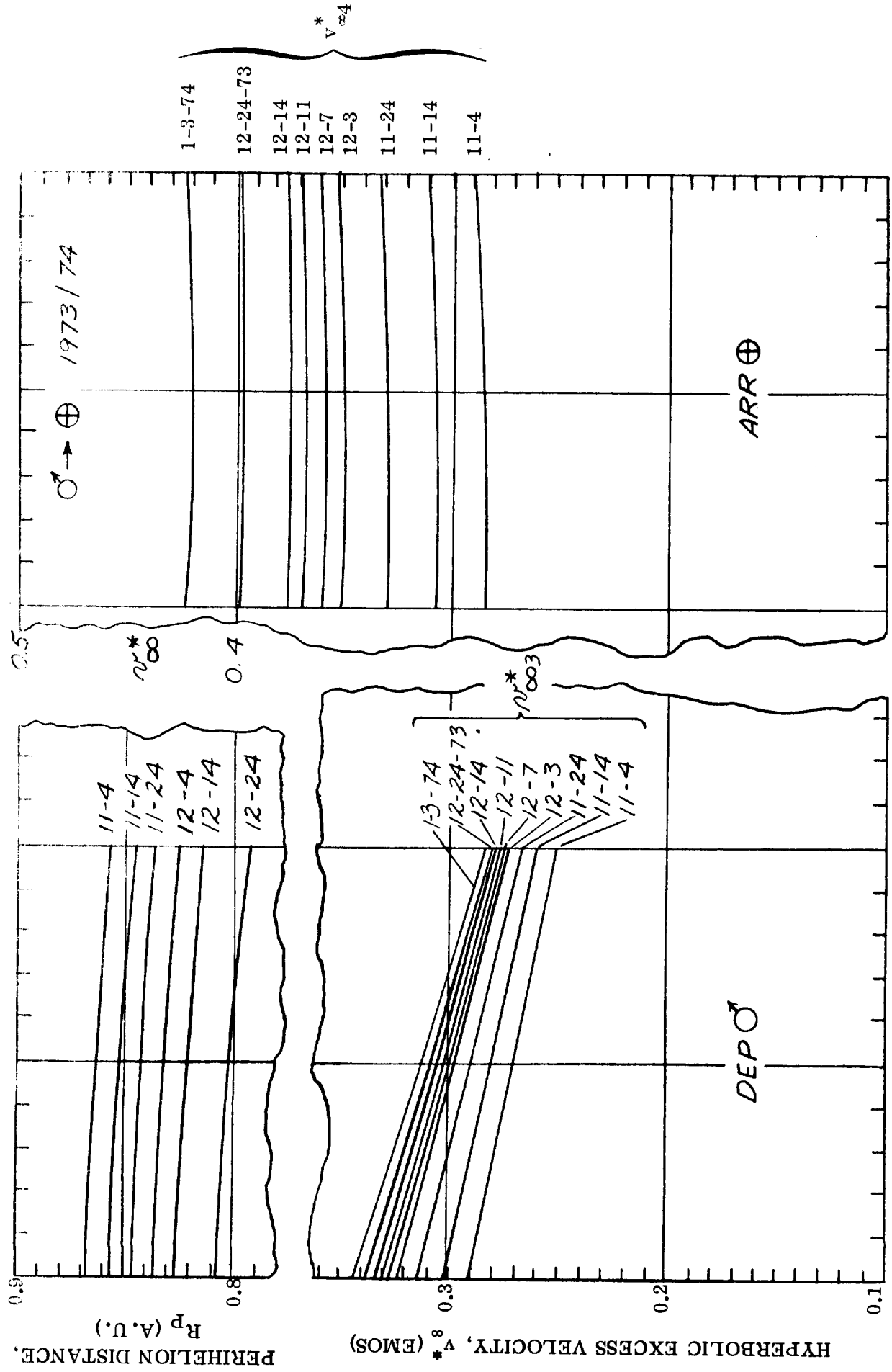

Figure 6-28. Mars Departure Window, Nov 1973/Jan 1974

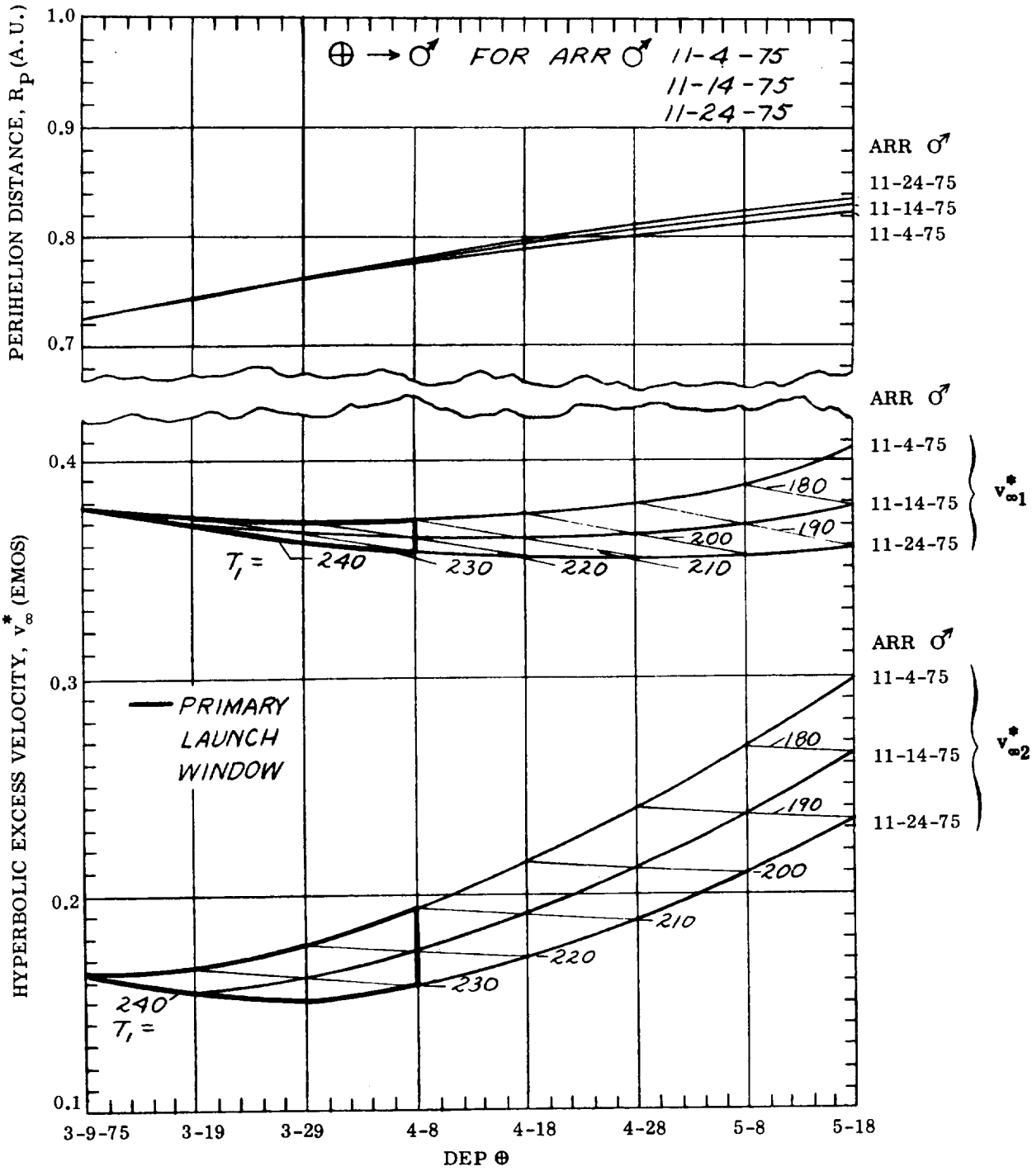

Figure 6-29. Earth-Mars Departure Window March/May 1975

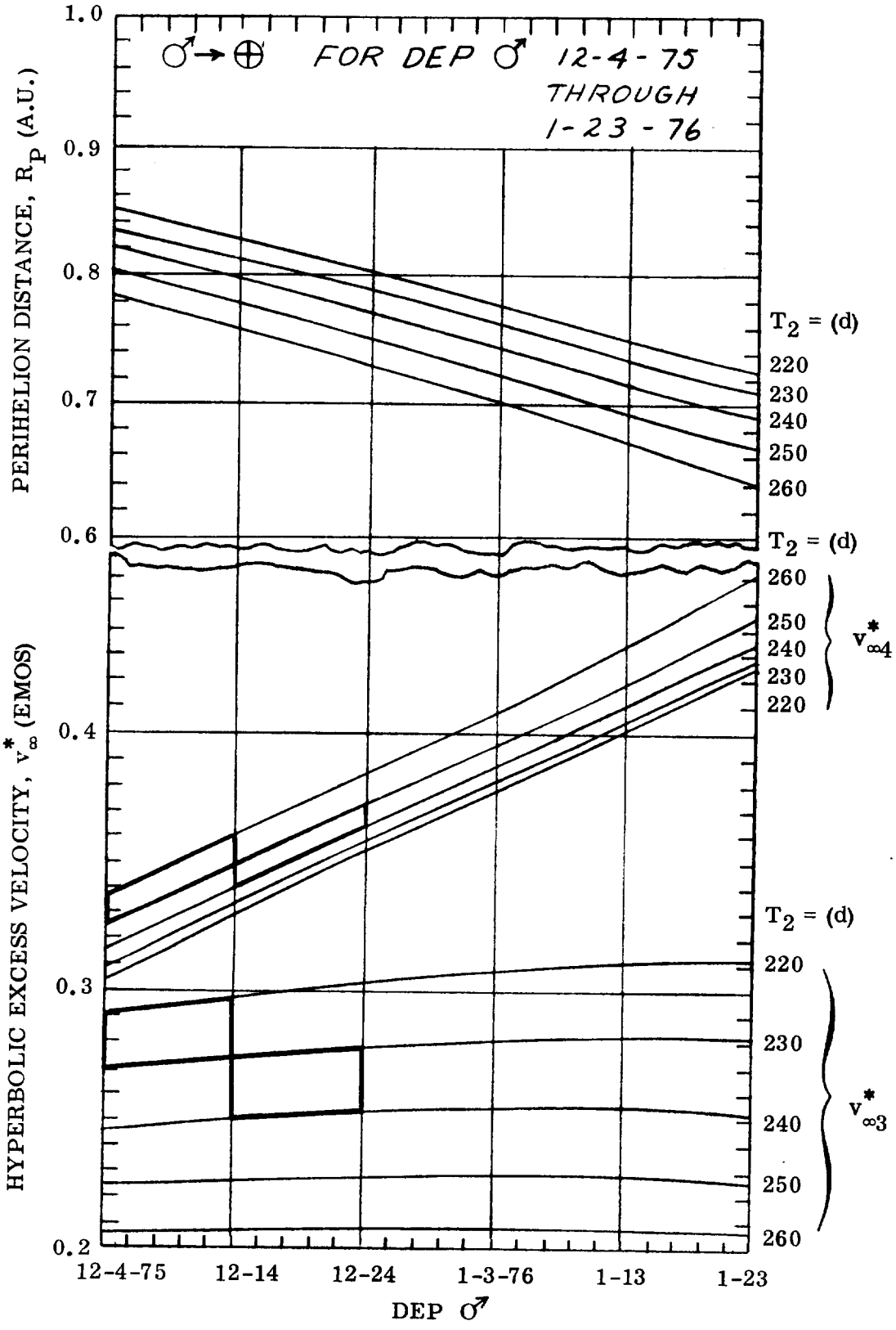

Figure 6-30. Mars-Earth Departure Window Dec 1975/Jan 1976

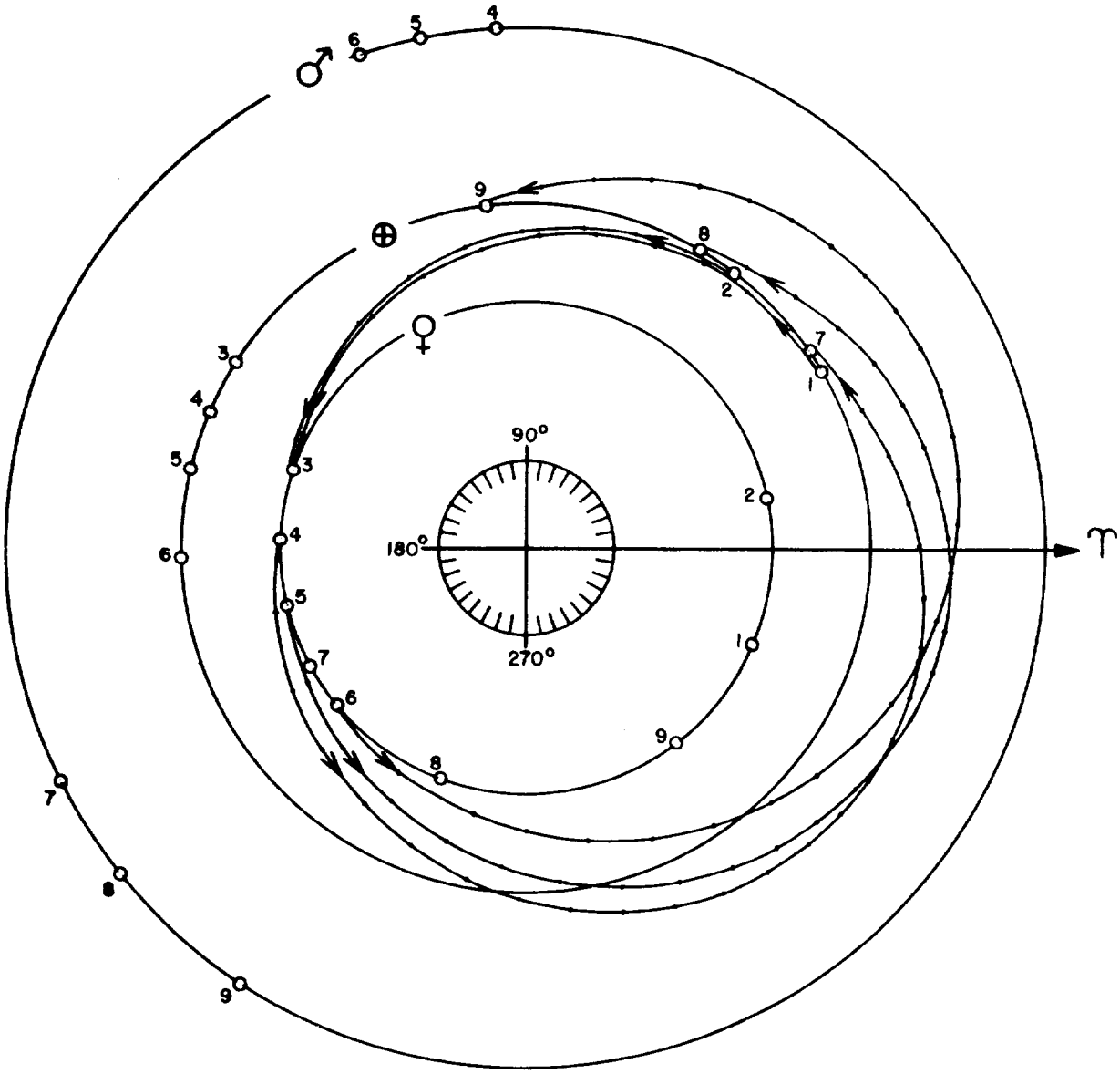

PLANET POSITION	CALENDAR DATE	EVENT	FLIGHT TIME (DAYS)
1	10-25-73	Earth Departure	115
2	11-16-73	Earth Departure	93
3	2-17-74	Venus Arrival	
4	2-27-74	Venus Departure	244
5	3-9-74	Venus Departure	259
6	3-25-74	Venus Departure	280
7	10-29-74	Earth Arrival	
8	11-23-74	Earth Arrival	
9	12-29-74	Earth Arrival	

Figure 6-31. Transfer Orbit Earth-Venus Mission Window 1973-1

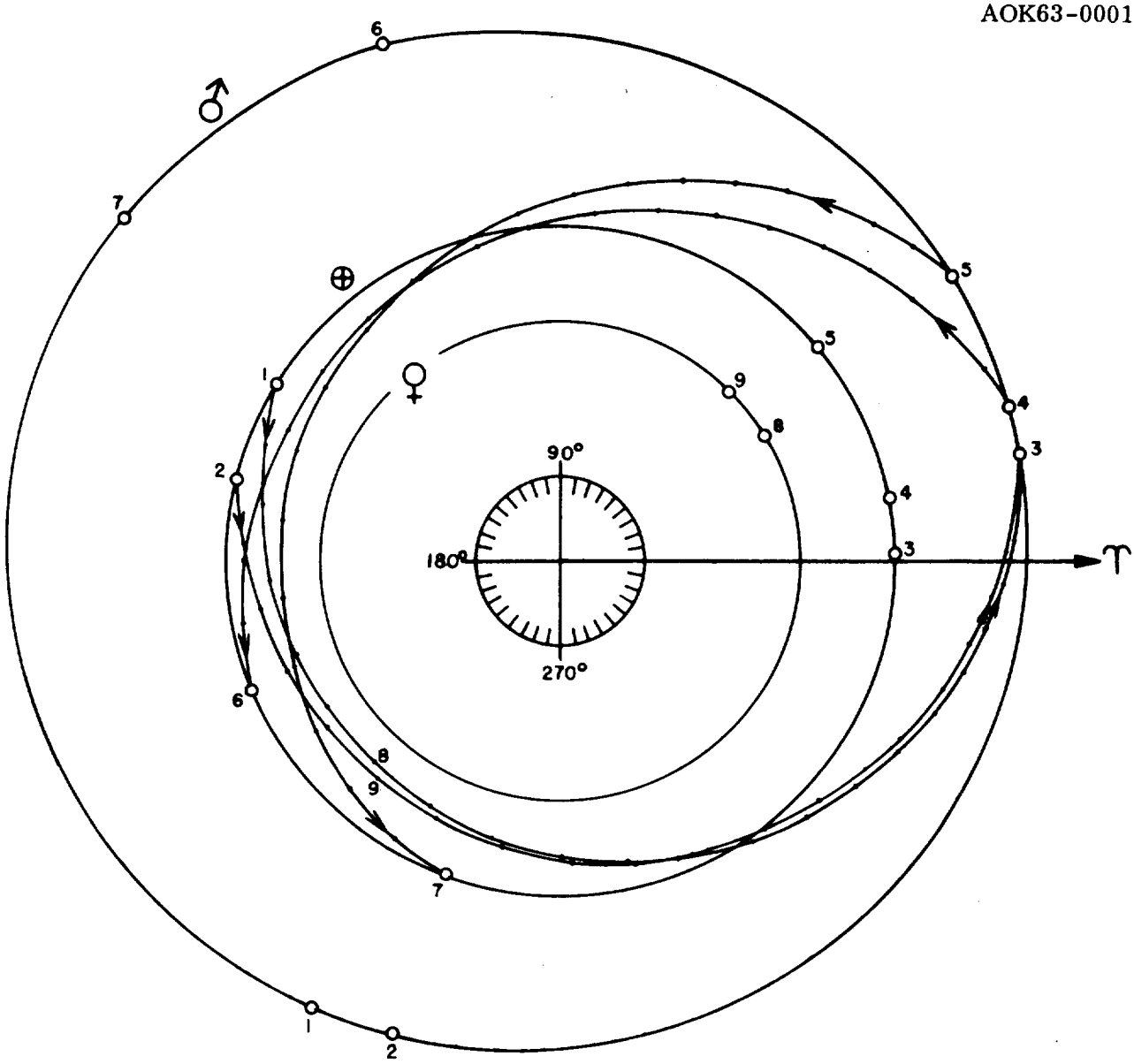

PLANET POSITION	CALENDAR DATE	EVENT	FLIGHT TIME (DAYS)
1	2-17-73	Earth Departure	220
2	3-7-73	Earth Departure	202
3	9-25-73	Mars Arrival	
4	10-5-73	Mars Departure	191
5	11-3-73	Mars Departure	210
6	4-14-74	Earth Arrival	
7	6-1-74	Earth Arrival	
8	4-18-73	Perihelion of Earth Departure Flight Path	
9	4-26-73	Perihelion of Earth Departure Flight Path	

Figure 6-32. Transfer Orbit Earth-Mars Mission Window 1973-1

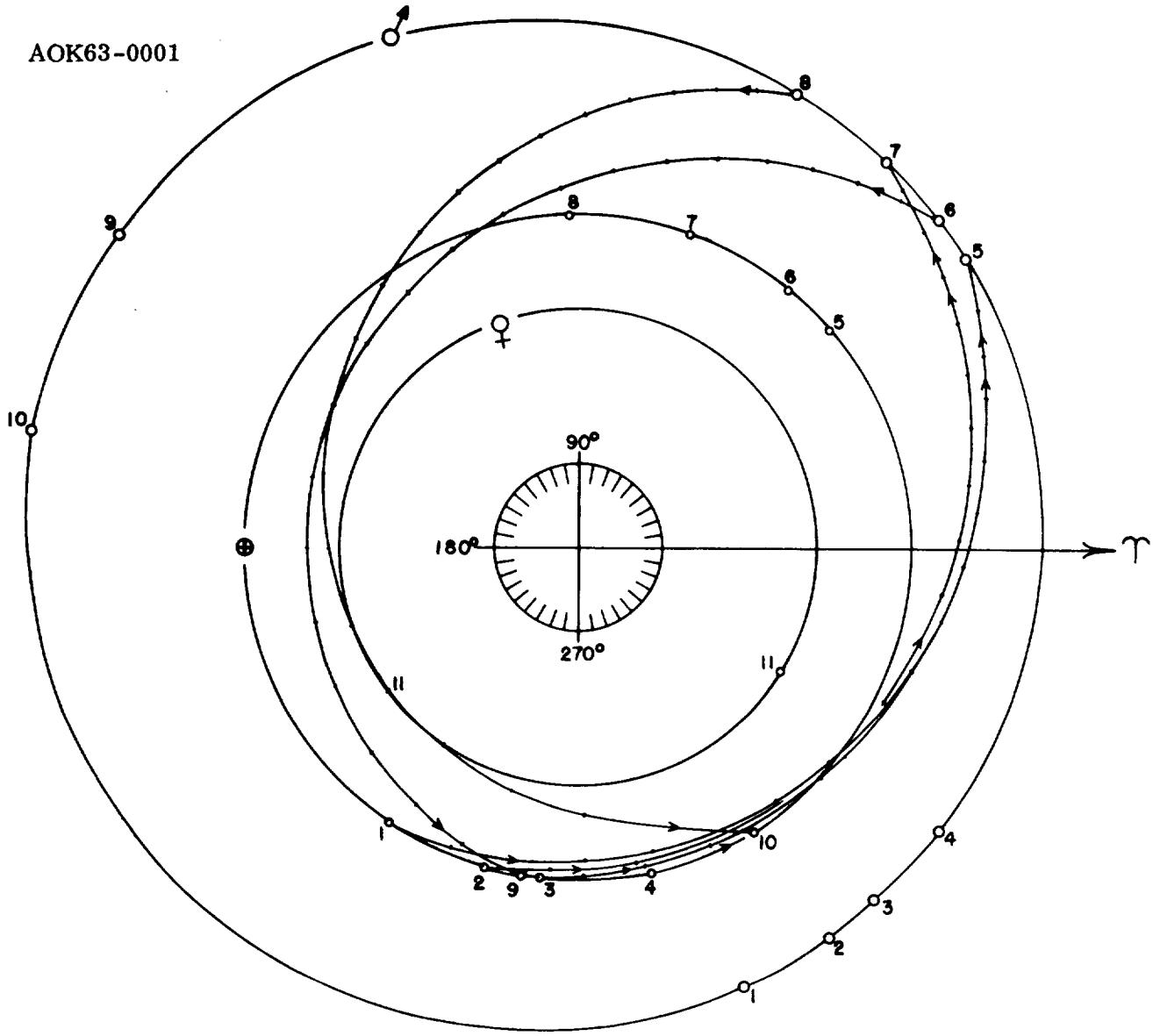

PLANET POSITION	CALENDAR DATE	EVENT	FLIGHT TIME (DAYS)
		WINDOW 2	
1	5-18-73	Earth Departure	170
3	6-17-73	Earth Departure	150
5	11-4-73	Mars Arrival	
6	11-14-73	Mars Departure	211
8	12-24-73	Mars Departure	223
9	6-13-74	Earth Arrival	
10	8-4-74	Earth Arrival	
		WINDOW 3	
2	6-6-73	Earth Departure	180
4	7-6-73	Earth Departure	150
7	12-3-73	Mars Arrival	
8	12-24-73	Mars Departure	223
10	8-4-74	Earth Arrival	
11	6-2-74	Perihelion of Mars	
		Departure Flight Path	

Figure 6-33. Transfer Orbit Earth-Mars Mission Window 1973-2 and 1973-3

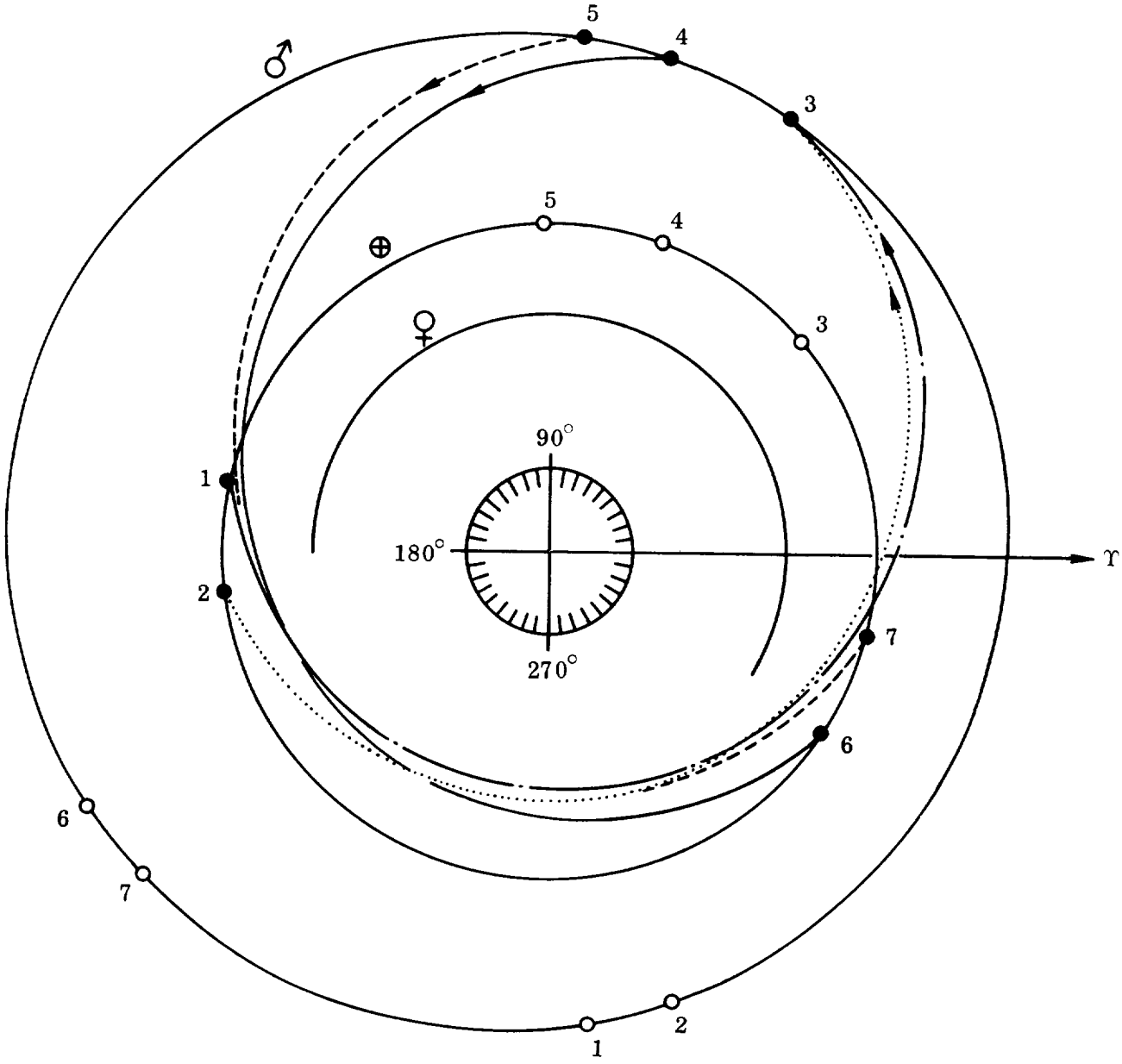

PLANET POSITION	CALENDAR DATE	EVENT	FLIGHT TIME (DAYS)
1	3-9-75	Earth Departure	240
2	3-29-75	Earth Departure	220
3	11-4-75	Mars Arrival	
4	12-4-75	Mars Departure	260
5	12-24-75	Mars Departure	260
6	9-20-76	Earth Arrival	
7	10-10-76	Earth Arrival	

Figure 6-34. Transfer Orbit Earth-Mars Mission Window

emergency weight reductions or other emergency measures are required (e.g., reducing the number of returning ships) to provide the necessary performance capability.

c. For the return flight, the energy requirement, flight time and (possibly) minimum perihelion distance are more significant parameters than the Earth arrival date. Figures 6-29, 6-33 through 6-35 and 6-37 show, therefore, the return flight time, T_2, as a parameter.

6.6 EARTH DEPARTURE. Earth departure takes place by a high-thrust (> 0.2g) launch from a rendezvous orbit, assumed to be very nearly circular, at 325 km altitude. In line with the ground rule described in Section 6.1, the Earth escape path is taken as a hyperbola to a distance equal to the Earth's activity sphere, $r_{act} = 144.9\, r_{oo,\oplus} = 920,000$ km = 498,765 n.mi. At that distance the hyperbolic path is very nearly merged with its asymptote and the relative velocity of the space ship with respect to Earth becomes very nearly invariant with time; i.e., it very nearly is equal to the hyperbolic excess velocity. The space ship "enters" heliocentric space. Its hyperbolic velocity is added vectorially to the Earth's orbit velocity, $U_\oplus$. The resulting heliocentric departure velocity of the space ship is V_1.

Let the geocentric ecliptic coordinate system be projected on the activity sphere (Figure 6-35) with the lead meridian, pointing in the direction of the Earth's motion, being the zero meridian, $\lambda' = 0$. The latitude is β', with $\beta = 0$ in the Earth's orbit plane. Then, for a given V_1, and with departure path angle β_1 (between $U_\oplus$ and V_1) known from the heliocentric transfer calculations, the hyperbolic excess is given by

$$v_\infty = \left[U_\oplus^2 + V_1^2 - 2 U_\oplus V_1 \cos \beta_1 \right]^{\frac{1}{2}} \qquad (6\text{-}1)$$

This equation applies to the planar case; i.e., v_∞ and V_1 lie in the ecliptic and $\beta_1^1 = 0$. The longitude of the exit point (E) on the activity sphere is

$$\lambda_1' = \alpha_1 + \beta_1 + \gamma_1 \qquad (6\text{-}2)$$

where

$$\sin \alpha_1 = \frac{\delta}{r_{act}} \sin (\beta_1 + \gamma_1) \qquad (6\text{-}3)$$

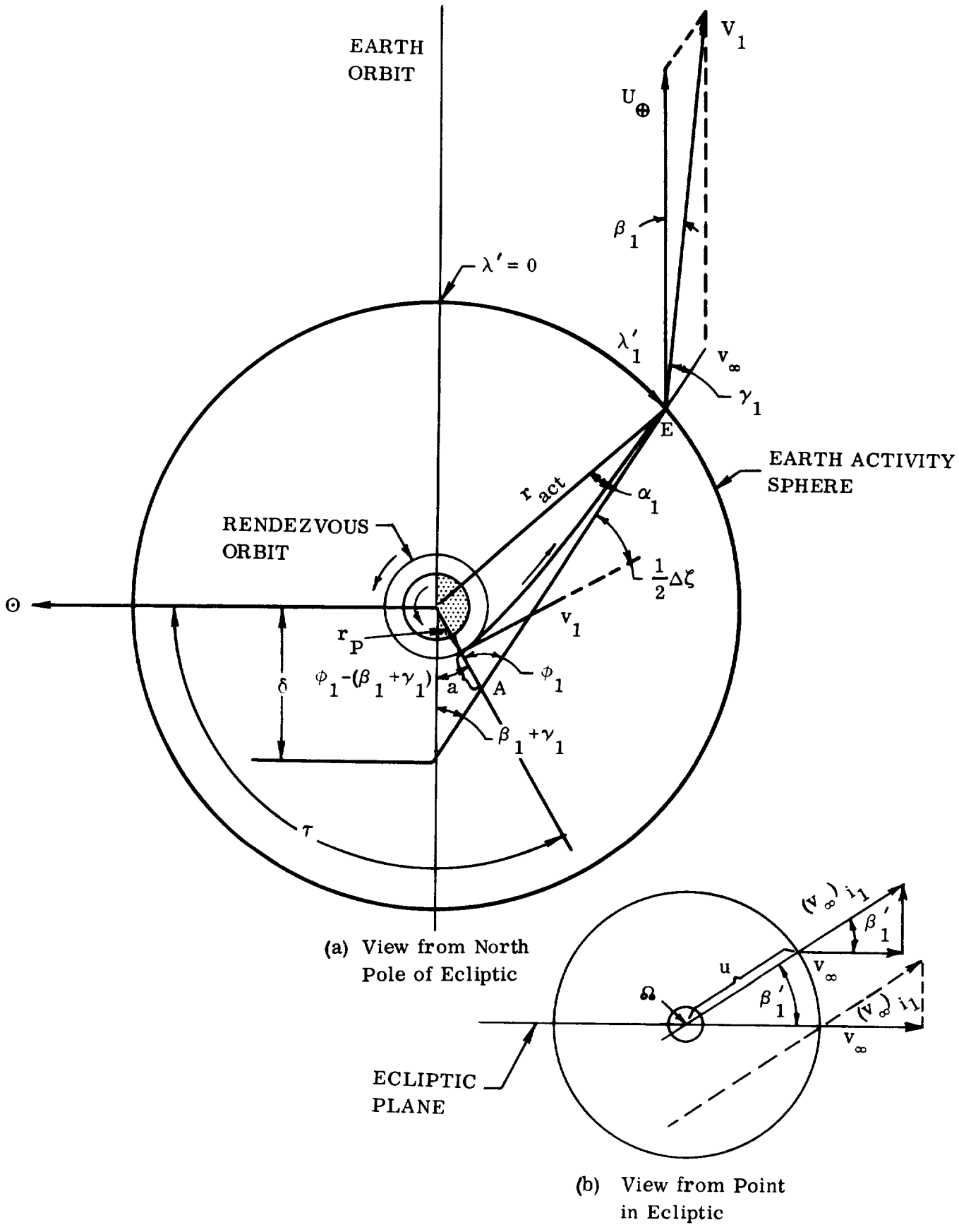

Figure 6-35. Earth Departure Maneuver on a Mars Mission

with

$$\delta = \frac{a}{\sin(\beta_1 + \gamma_1)} \sqrt{e^2 - 1} \tag{6-4}$$

$$e = 1 + \frac{r_P}{K_\oplus} v_\infty^2 \tag{6-5}$$

$$a = \frac{K_\oplus}{v_\infty^2} \tag{6-6}$$

The perigee distance equals the distance of the rendezvous orbit in the case of an impulsive departure maneuver, and

$$\sin \gamma_1 = \frac{U_\oplus}{v_\infty} \sin \beta_1 \tag{6-7}$$

The planetocentric departure velocity

$$v_1 = \left[\frac{2K_\oplus}{r_P} + v_\infty^2 \right]^{\frac{1}{2}} \tag{6-8}$$

points in the direction

$$\lambda_1'' = \lambda_1' + \frac{1}{2} \Delta\zeta - \alpha_1 \tag{6-9}$$

where

$$\sin \frac{1}{2} \Delta\zeta = \frac{1}{e} \tag{6-10}$$

is one-half of the angle by which v_∞ would be turned if the vehicle flew the entire hyperbola through the activity sphere, as is the case of a hyperbolic encounter (fly-by).

The angle between the Earth-Sun radius vector and the Earth-spacecraft radius vector at the moment of impulsive departure (i.e., at the vertex of the hyperbola) is

$$\tau = 90 + \phi_1 - (\beta_1 + \gamma_1) \tag{6-11}$$

where the semi-vertex angle (ϕ_1) follows from

$$\cos \phi_1 = \frac{1}{e} \tag{6-12}$$

At the sub-perigee meridian of Earth the time is $\tau/15$ hours past high noon. The flight time (t_{P_r}) from perigee to distance r from Earth is shown in Figure 6-36 as a function of r for a series of v_∞^* (EMOS) values.

At nonplanar departure, the plane of the hyperbolic orbit no longer coincides with the ecliptic (Figure 6-35, bottom). If i_1 is the inclination of the heliocentric transfer orbit with respect to the ecliptic (i_1 is known from the heliocentric transfer orbit calculations, Section 6.3), the hyperbolic excess velocity becomes larger than the value given by Equation 6-1 for otherwise the same conditions (i.e., same β_1 and planar v_∞):

$$(v_\infty)_{i_1} = \left[U_\oplus^2 + V_1^2 - 2 U_\oplus V_1 \cos \beta_1 \cos i_1 \right]^{\frac{1}{2}} \tag{6-13}$$

Thus, the ratio $(v_\infty)_{i1}$ to v_∞ (Equation 6-1) must be equal to the cosine of the angle formed by the two vectors. However, the orbit must now be tilted; i.e., rolled about the axis OA = r_P + a (if the perigee was previously located in the $\beta' = 0$ plane) or about the axis OΩ (if the perigee was above or below the $\beta' = 0$ plane) until $(v_\infty)_{i_1}$ lies in the plane which passes through the center of attraction as required by Newton's law of gravitation. This, however, means that the angle between $(v_\infty)_{i_1}$ and v_∞ is equal to β_1' ; whence,

$$\cos \beta_1 = \frac{(v_\infty)_{i_1}}{v_\infty} = \frac{\left[U_\oplus^2 + V_1^2 - 2 U_\oplus V_1 \cos \beta_1 \cos i_1 \right]^{\frac{1}{2}}}{\left[U_\oplus^2 + V_1^2 - 2 U_\oplus V_1 \cos \beta_1 \right]^{\frac{1}{2}}} \tag{6-14}$$

However, the inclination of the hyperbolic orbit plane, i_h, is not necessarily equal to β_1'. This would be the case only if the center angle u (argument of the longitude, measured from the ascending node) is 90 degrees, since

$$\sin i_h = \frac{\sin \beta'}{\sin u} \tag{6-15}$$

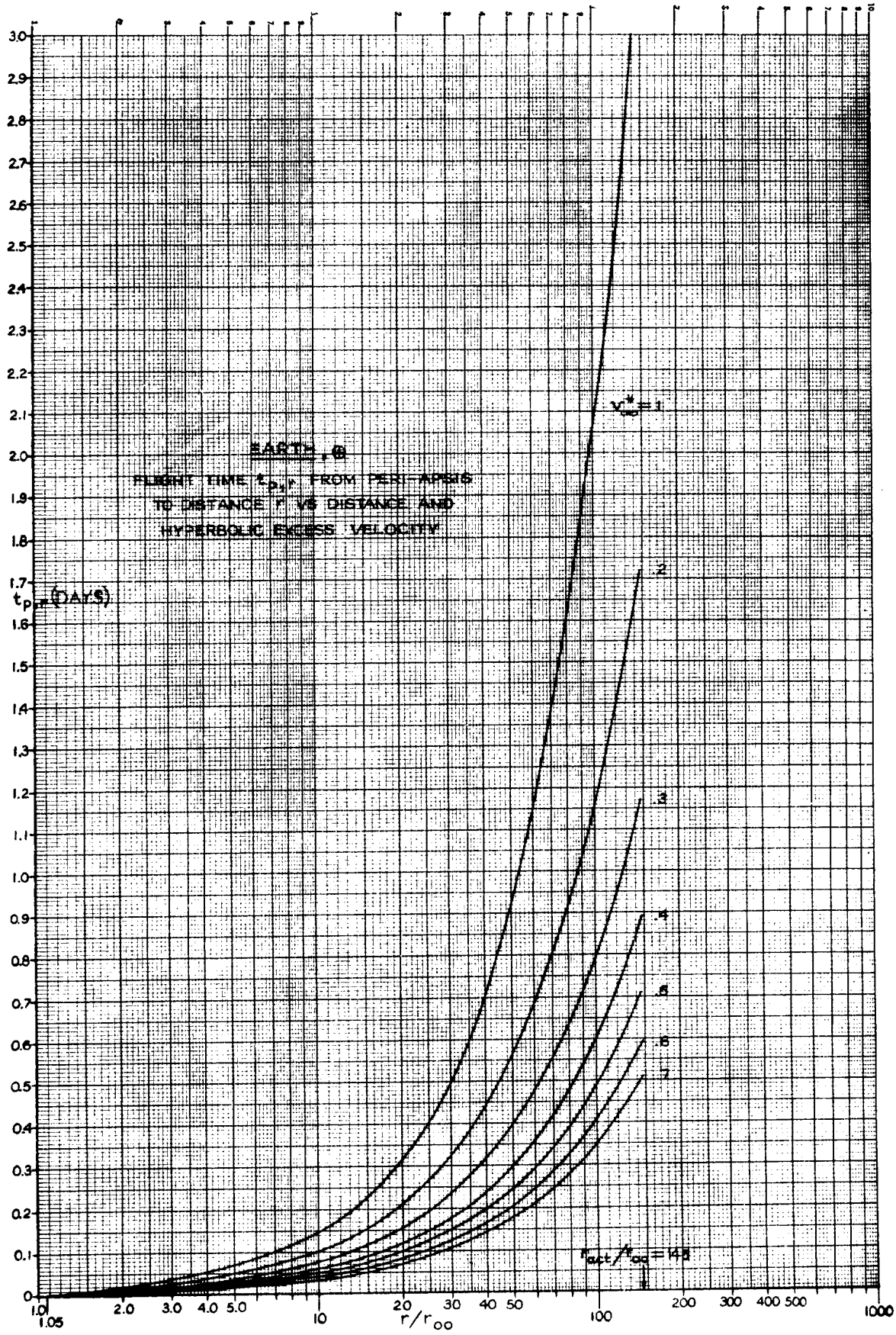
EARTH → θ
FLIGHT TIME $t_{p_2 r}$ FROM PERI-APSIS TO DISTANCE r VS DISTANCE AND HYPERBOLIC EXCESS VELOCITY
$t_{p_2 r}$ (DAYS)
$V_{\infty}^2 = 1$
2
3
4
5
7
$r_{act}/r_{oo} = 145$
r/r_{oo}
1.0
1.05
2.0
3.0
4.0
5.0
10
20
30
40
50
100
200
300
400
500
1000

Figure 6-36.

If the ascending node coincides with the perigee (i.e., if the perigee of the hyperbola lies in the ecliptic), then u = η (true anomaly), or more specifically,

$$\cos u = \cos \measuredangle (AOE) \equiv \cos \eta_\ell = -\frac{1}{e} \tag{6-16}$$

where η_ℓ is the limiting true anomaly of the hyperbola, i.e, the true anomaly of a point at infinity (point E, Figure 6-35 approaches this condition); and $\eta_\ell > 90^\circ$. Therefore, i_h must, in this case, be larger than β'_1.

For a discussion of the performance aspects of distance and precession of the rendezvous orbit, see Section 7.

6.7 PLANET CAPTURE. A space ship approaching a target planet in such a manner that the approach asymptote intersects the target-planet orbit at a distance δ from the center of the target planet, will reach a periapsis distance r_p which is given as a function of v_∞, β_2, γ_2 and δ (Figure 6-37) by the relation (Ref. 6-10)

$$r_P = K_{pl} \frac{\left[1 + \left(\frac{\delta \sin(\beta_2 + \gamma_2)}{K_{pl}/v_{\infty,2}^2}\right)^2\right]^{\frac{1}{2}} - 1}{v_{\infty,2}^2} \tag{6-17}$$

All parameters have been defined in the preceding paragraph.

In order to achieve the correct planetocentric approach conditions defined above, the heliocentric transfer orbit must intersect the activity sphere at a certain longitude λ_2 (Figure 6-38) which, for the planar (two-dimensional) case, is found as follows: Figure 6-38 shows that λ_2 is measured counterclockwise from the meridian pointing in the direction of the planet's motion. It is seen that

$$\lambda_2 = 180 + \alpha_2 - (\beta_2 + \gamma_2) \tag{6-18}$$

where

$$\sin \alpha_2 = \frac{\delta}{r_{act}} \sin(\beta_2 + \gamma_2) \tag{6-19}$$

$$\sin \gamma_2 = \frac{U_{pl}}{v_{\infty 2}} \sin \beta_2 \tag{6-20}$$

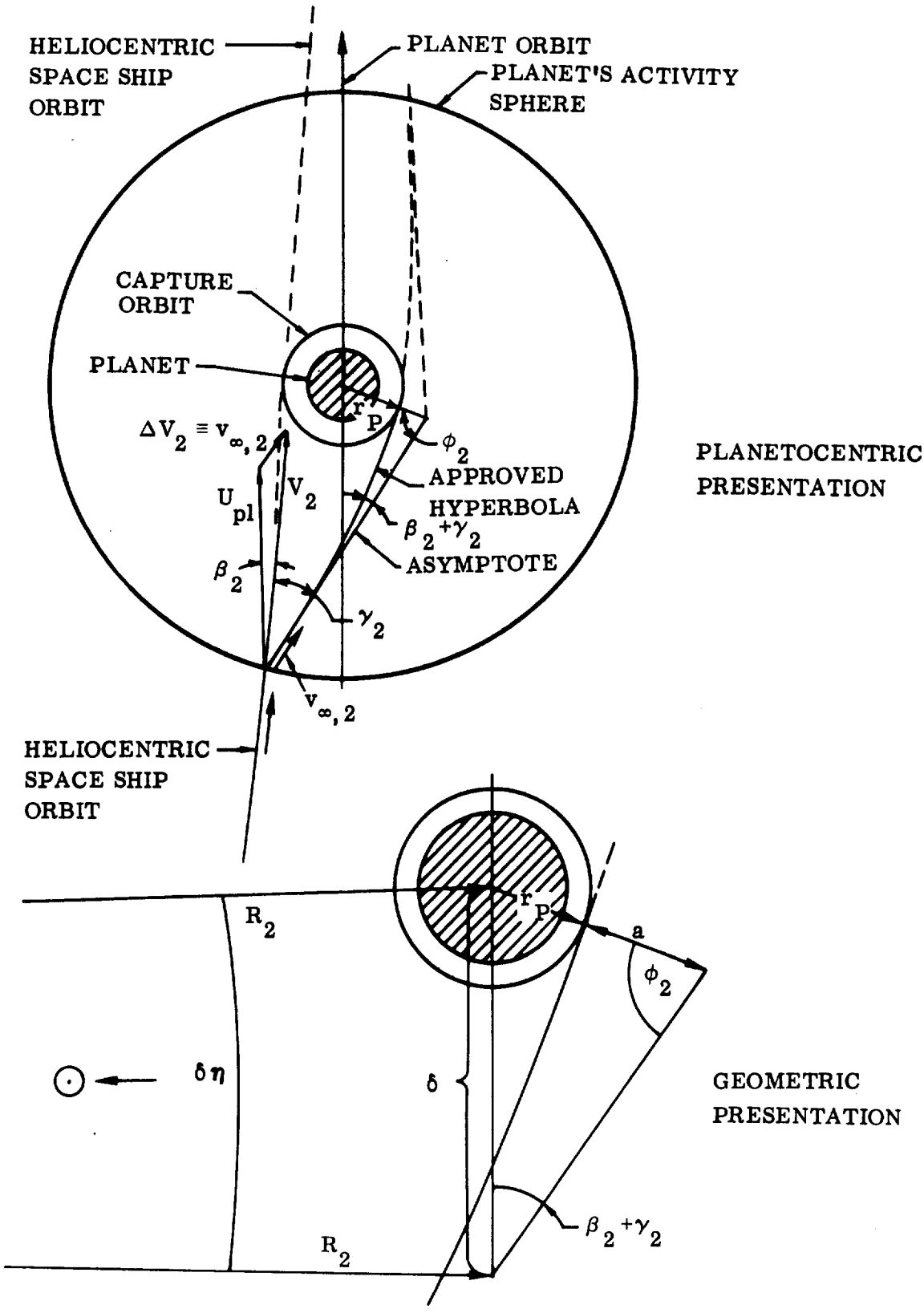

Figure 6-37. Planetocentric Geometry of Capture

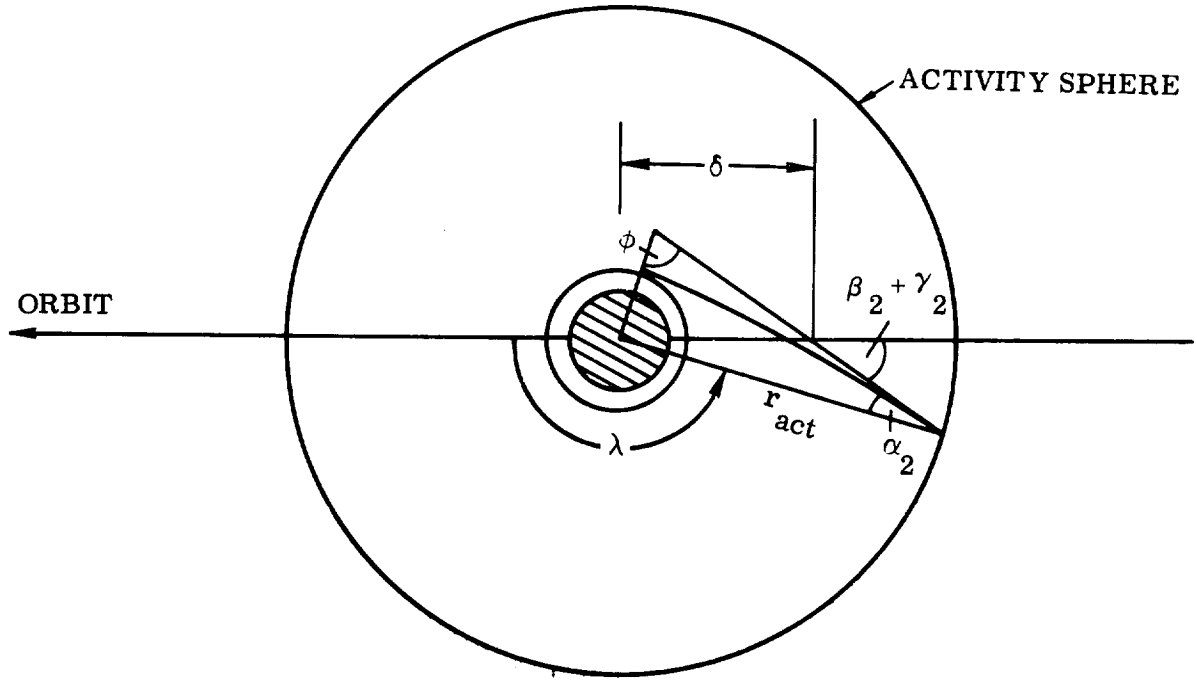

Figure 6-38. Determination of the Impact Point on the Planet's Activity Sphere

From the fact that the hyperbolic orbit passing through the activity sphere has two branches, symmetrically oriented with respect to the semi-major axis, it is obvious that the same periapsis distance can be approached from two "entry points" into the activity sphere. In one case the orbit is direct, in the other retrograde.

For a capture mission not involving landing and return of a probe or a manned excursion vehicle, it makes little difference whether the orbit is direct or retrograde. Re-escape is not affected. In view of the approach to the Venus capture mission presented in Section 5, there would, therefore, exist two possible entry points. This is not true for Mars because of the mission philosophy adopted for this target planet, since at least instrumented Returners would be deployed to the Martian surface. For reasons of energy management the Mars capture orbit must therefore be direct, leaving only one permissible entry point.

The third important parameter is the orientation of the orbit plane. Capture orbit inclination control is necessary, to assure the planned capture orbit inclination with respect to the equator for reconnaissance purposes, and to minimize plane changes prior to departure from the target planet. While the periapsis is a function of the longitude of the entry point, among other parameters, the inclination of the capture orbit is affected by the latitude of the entry point. It is possible to meet the distance

accuracy requirement in many planetocentric orbit planes, depending upon the location of the entry point on the correct meridian of the planet's activity sphere, or, in other words, on the latitude and longitude of that point on the planet's celestial sphere at which the ship's orbit-reference system changes from heliocentric to planetocentric. In Figure 6-39 the reference plane is the planet's orbit plane. If the ship passes into the activity sphere through the heading meridian (pointing in flight direction), the planetocentric orbit plane must be orthogonal to the reference plane (point 1), if no lateral velocity vector exists at the moment of entry. Point 2 exemplifies an arbitrary entry point with arbitrary velocity vector orientation at impact.

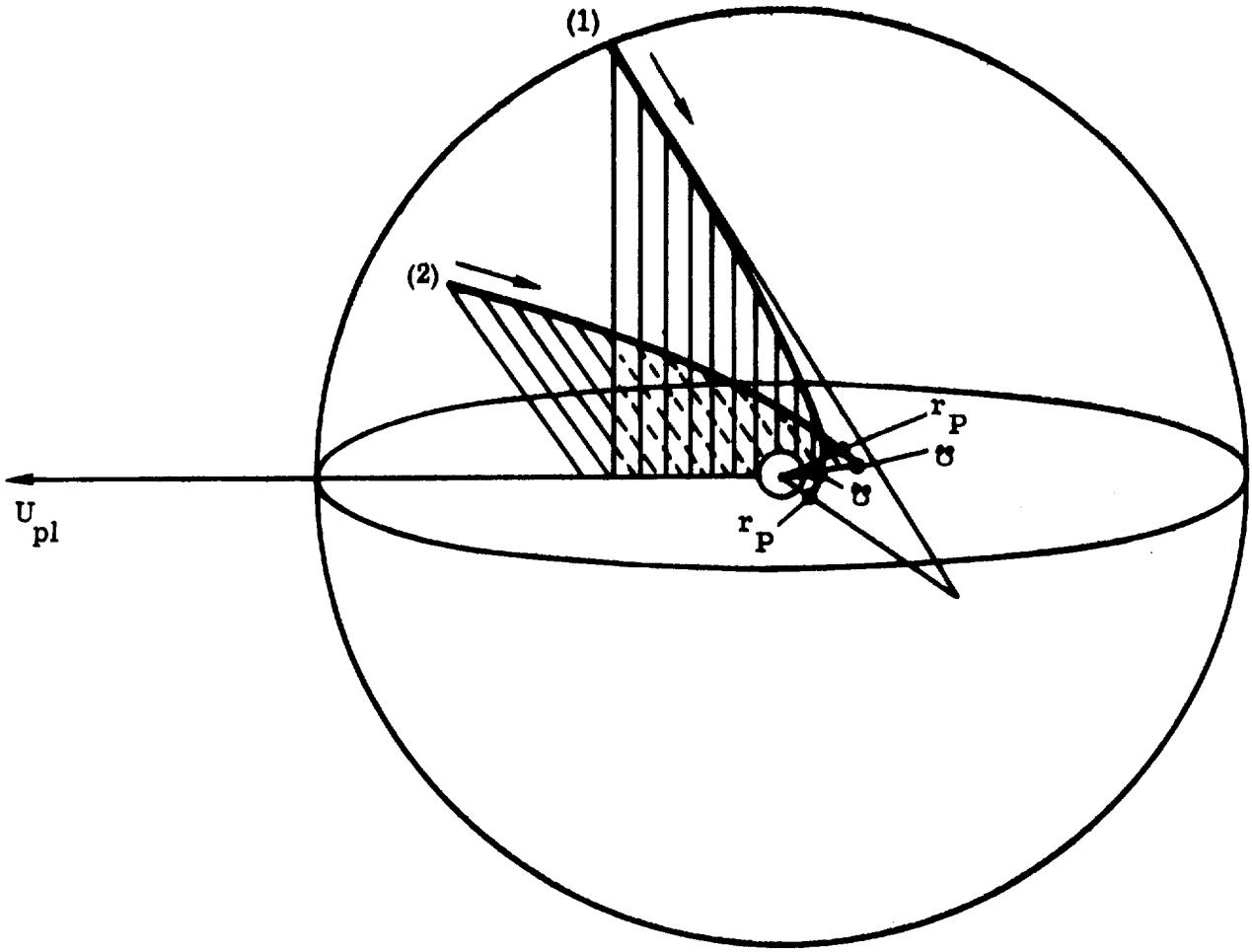

Figure 6-39. Effect of "Entry Point" into Planet's Activity Sphere on Capture Orbit Inclination

Therefore, the independent variable, from the standpoint of guidance and navigation, is the plane of the hyperbolic orbit inside the activity sphere of the planet. This plane determines the plane of the capture orbit in the absence of a plane change during the capture maneuver. The inclination (i) of this hyperbolic orbit plane is determined by the entry coordinates (λ and $\pm\beta$) on the activity sphere, and by the aximuth angle (A):

$$\cos i = \cos \beta \sin A \tag{6-21}$$

whence (Figure 6-40),

$$\sin u = \frac{\sin \beta}{\sin i} \tag{6-22}$$

$$\cos (\lambda - \Omega) = \frac{\cos u}{\cos \beta} \tag{6-23}$$

so that, for given β, λ and A, the values of i, u and Ω are determined. The angle A is a function of the projection of the vector v_∞ on the activity sphere. This projection is a function of the entry angle (I):

$$v_\infty' = v_\infty \sin I \tag{6-24}$$

and A is equal to δ, the angle of deviation from the meridian plane through entry longitude λ.

If the plane of the capture orbit can be controlled effectively, it is possible to determine an orbit properly inclined with respect to the planet's equator so that no (or only a small) plane change is required at departure. This can be achieved with or without the aid of orbital precession during the capture period near Mars. For example, if the capture orbit is polar it does not precess but, for a given departure orbit, there exists a desirable plane orientation at capture which places the orbit plane in the right position at departure time due to the curvature of the planet orbit (Figure 6-41).

These orbit plane orientation requirements must be compatible with the need to cover a maximum of illuminated surface for optical mapping during the comparatively brief Mars capture period. As pointed out in Section 5, the Mappers would, of course, be left behind when the manned vehicles depart, so that more time than the capture period would be available for mapping. However, because of the superior data handling and power supply conditions on board the manned ships, it is likely that the Mapper will operate at inferior resolution after being left behind. Thus, there is important incentive to accomplish as much optical mapping as possible during the capture period.

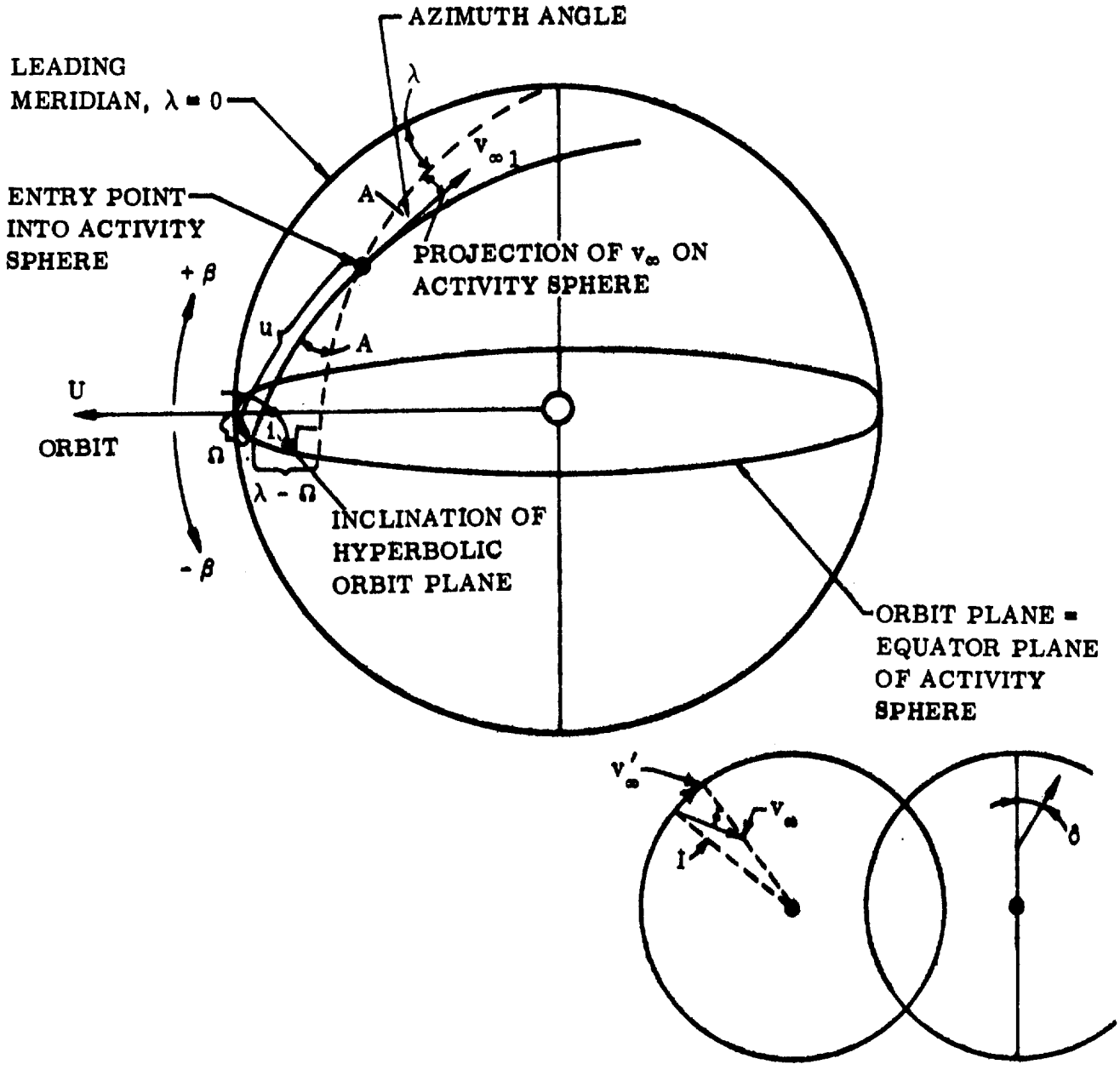

Figure 6-40. Determination of the Inclination of the Hyperbolic Orbit Plane in the Planetary Activity Sphere

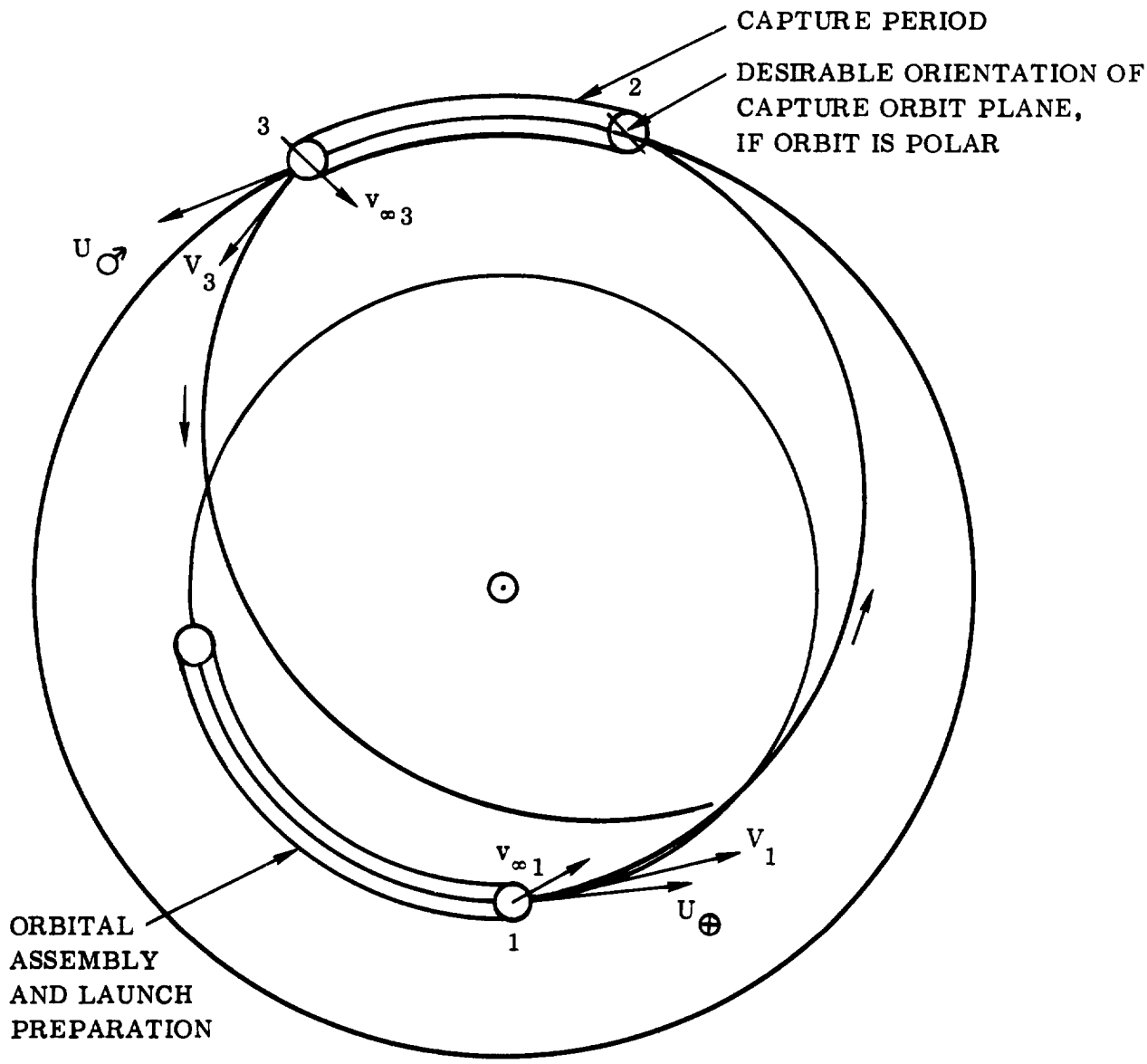

Figure 6-41. Determination of Desirable Capture Orbit Inclination for Target Planet Departure Without Plane Change (Dual-Constraint Navigation With Capture Distance and Orbit Inclination Fixed)

A polar capture orbit certainly is highly compatible with requirements for extensive coverage, since polar or near-polar orbits provide geometric access to the entire planetary surface even from low altitudes. This is desirable for the Floater, Lander, Returner, and MEV. However, the wrong plane orientation may maximize the shadow periods. Fortunately, it turns out that for the Mars positions and the Mars departure directions required in Mars Missions 1973-1, -2, -3, and 1975-1, the daylight viewing conditions are quite favorable. This is illustrated in Figure 6-42 for the example of Mission 1973-1. Neglecting the inclination of the Mars equator plane with respect to the Mars orbit plane, and assuming that a capture orbit plane normal to the Mars orbit plane is at the same time a polar orbit, then the orbit would not precess. The orientation of the plane would be as indicated in Figure 6-42, if it were controlled by the departure conditions. There is, however, little if any conflict with the optical requirements. The observer would initially pass over the daylight side at its mid-afternoon. Due to the motion of Mars about the Sun at the rate of some 0.52 degrees per day, the (non-precessing) orbit plane rotates clockwise (i.e., into the daylight side toward high noon) at the rate of 0.52 degrees per day. During the maximum capture period of 39 days, the plane will have rotated about 20 degrees toward high noon.

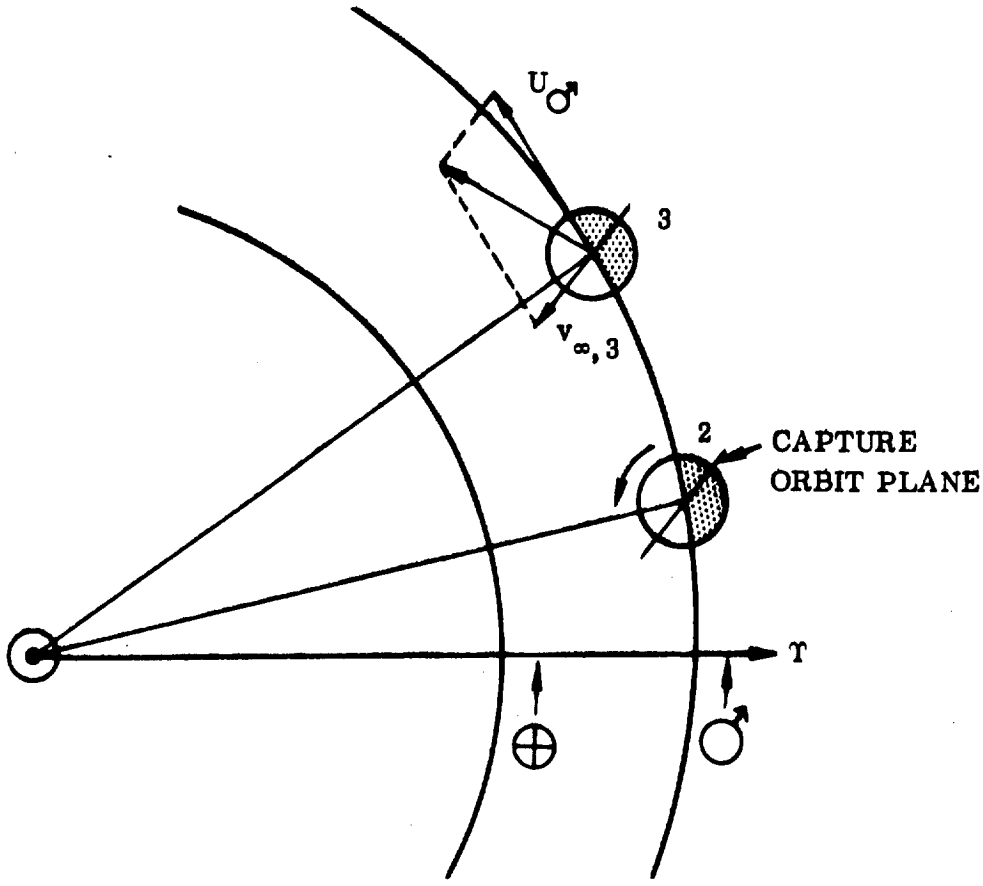

Figure 6-42. Daylight Viewing Conditions During Capture Period of Mars Mission 1973-1

Rotation of the observer toward high noon reduces the contrasts and the relief. Therefore it might be desirable to start somewhat closer to the evening terminator. This can be done relatively simply by tilting the orbit slightly out of the polar plane and letting precession provide the somewhat higher rate of rotation required.

Thus, the conditions for optical observation from a polar or highly inclined orbit are favorable during the capture periods of the 1973 and 1975 Mars missions. Nevertheless, a high-resolution radar system might be profitably included in the Mars Mapper instrumentation because the optical duty cycle comprises hardly more than one-half of each revolution at the orbit altitudes of 1000-1065 km which have been considered to provide coverage overlap and resonance conditions for Returners and MEV. Power requirements are moderate because of the low altitude (cf. Addendum, Confidential Restricted Data).

A careful comparison of optical versus optical-radar Mars Mapper is recommended for a future study phase, with consideration given to weight and power requirements.

Figure 6-43 shows the circular orbit velocity versus distance and the period versus mean distance from Venus and Mars.

The period of nodal precession is approximately given by

$$T_{pr} \approx \frac{T_{sid}}{\gamma \cos \iota} \left(\frac{a}{r_o} \right)^2 \tag{6-25}$$

where T_{sid} is the sidereal period of the (near-circular) orbit at mean distance, a, from the primary whose equatorial radius is r_o; ι is the inclination of the satellite orbit with respect to the equator plane and

$$\gamma = \epsilon_{\sigma'} - \frac{1}{2} m \tag{6-26}$$

is the coefficient of the second harmonic of the equation describing the gravitational field of an oblate body; $\epsilon_{\sigma'}$ is the oblateness (optical flattening of Mars and

$$m = \frac{r_o \omega^2}{g_o} \tag{6-27}$$

is the ratio of centrifugal to gravitational acceleration at the equator. Using, for a rough estimate, $g_o = 402$ cm/sec^2, $r_o \omega^2 = 0.83$ cm/sec^2, and $\epsilon_{\sigma'} \approx 1/100$, it follows that

$$\begin{aligned} m &\approx 0.002062 \\ \gamma &\approx 8.99 \cdot 10^{-3} \end{aligned} \tag{6-28}$$

(Earth value of γ is $(1.62341 \pm 0.004) \times 10^{-3}$, from Vanguard I.)

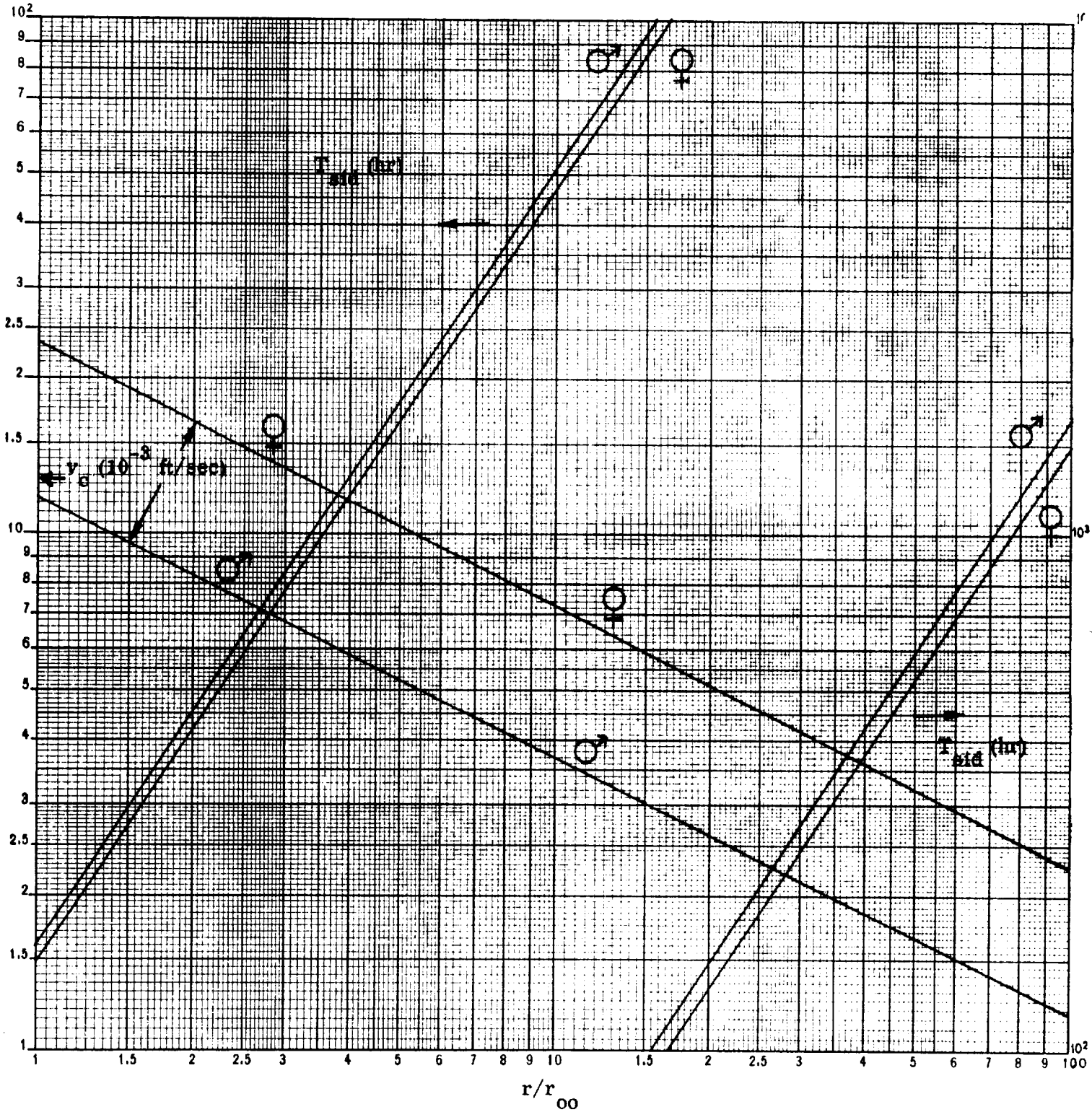

Figure 6-43. Sidereal Period and Circular Orbit Velocity Versus Distance in Planet Radii for Venus and Mars

For the case of $a/r_o = 1.32$ (y = 1070 km) and $T_{sid} = 2.38$ hrs, it follows that

$$T_{pr} \approx \frac{461}{\cos \iota} \quad \text{hrs.} \tag{6-29}$$

This approximation serves to show that, in spite of its greater oblateness, the weak Martian field causes the precession periods to be very long. Even for a near-equatorial orbit ($\cos \iota \sim 1$) the precession period of about 19 days represents a significant fraction of the capture period. For near-polar orbits, very long periods are indicated. The precession period relative to the daylight side of Mars is

$$\frac{1}{T'_{pr}} = \frac{1}{T_{pr}} + \frac{1}{686.98} \left[\frac{1}{\text{days}}\right] \tag{6-30}$$

where 686.98 days = 1 Mars year.

A considerable amount of additional analytical and data-research work is required to arrive at more precise precession periods and to combine all the factors affecting the Martian capture orbit into a harmonious system.

The visible disk of Venus has no perceptible oblateness. During the initial study phase no direct evidence (aside from that which could be inferred from the possibility that Venus may have synchronous rotation) was available that Venus has no radiation belt. Greater proximity to the Sun, size similar to Earth, and a suggestion by Houtgast (Ref. 6-11) which interpreted certain data as indication that Venus has a strong magnetic field, made it advisable not to dismiss entirely the possibility that Venus has a strong radiation belt. This has not been verified by Mariner 2. However, making the conservative assumption of a strong field which might have to be avoided by the interplanetary ships, two modes of operation in the Venusian activity sphere were carried along in parallel:

a. The interplanetary ships stay outside the radiation belt, in a near-circular orbit at 15 radii; a two-man heavily shielded Venus Scout Vehicle (VSV) enters the belt and approaches the Venusian surface to an altitude just outside the atmosphere for radar reconnaissance operations.

b. With the other modus operandi, the main vehicles approach Venus to a mean distance of 1.1 radii and carry out radar and other reconnaissance (Floaters, Landers). As in the case of Mars, the Mapper stays connected with the main vehicle, but is left behind to continue operation.

For either mode, no preferred capture-orbit plane can be defined for the reconnaissance activity; capture-orbit inclination control was, in this case, considered to be determined solely by the requirements for minimizing plane changes at Venus escape.

Figures 6-44 and 6-45 show the flight time (t_{p_r}) in hyperbolic orbits from periapsis to distance r for a range of hyperbolic excess velocities, v^*_∞ (EMOS).

The vehicles may be captured in elliptic, rather than in circular orbits. This may lead to considerable energy savings, but imposes certain additional constraints on the escape operations. This subject is discussed in Section 7.

6.7 EARTH RETURN. The work statement specified that whenever possible the state-of-the-art should not exceed those of the Apollo mission. For this reason, particular attention was given to the limited retrothrust return mode, in which, at a suitable distance from the surface, the planetary (hyperbolic) approach conditions are erased by means of retrothrust which acts just long enough to reduce the velocity to slightly sub-parabolic (i.e., negative orbital energy) flight conditions closely matching Apollo conditions. This return mode was considered attractive and practical for the following reasons:

a. Use of a (by then) tried and proven technique.

b. Capture in the Earth's activity sphere is attained prior to the entry maneuver. This offers additional safety for the crew, which is protected against re-escape in case entry is too high, and it greatly facilitates rescue operations.

c. If nuclear propulsion is used. the hydrogen carried along for the final maneuver can, if carried in sufficient quantity, serve as a radiation shield for the crew, thereby saving shield weight in addition to the added weight required for the hyperbolic entry vehicle.

d. The retrothrust offers a comparatively greater mission flexibility. If very high return approach velocities are involved, more propellant is taken along or, if a mission profile change en route becomes necessary, the available propellant can be made to buy a larger velocity change by greater mass reduction, prior to M-3 or even M-2. To achieve the same flexibility with hyperbolic entry, entry velocities to the order of $v^*_{entry} \sim 0.5$ or 16 km/sec must be mastered.

On the other hand, it is realized that hyperbolic entry offers advantages:

a. If restricted to relatively low hyperbolic velocities, entry conditions are not radically different from Apollo conditions.

b. If a comparatively low specific impulse (400-420 sec) is postulated for the retro-system, it quickly becomes much heavier than a hyperbolic entry system, especially at low hyperbolic velocities.

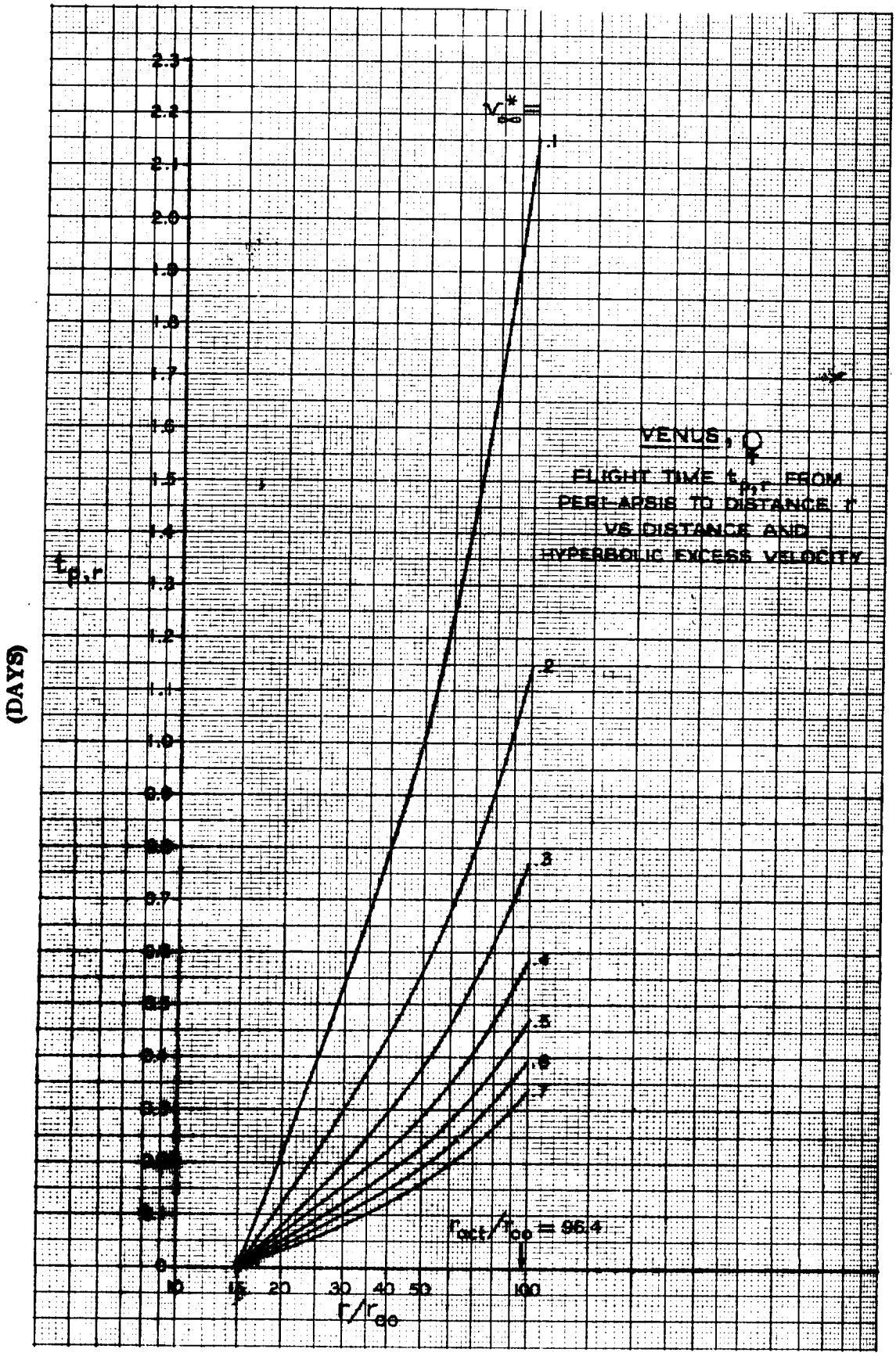
VENUS, ♀
FLIGHT TIME $t_{p,r}$ FROM PERI-APSIS TO DISTANCE r VS DISTANCE AND HYPERBOLIC EXCESS VELOCITY
V_∞^* =
.1
.2
.3
.4
.5
.6
.7
$t_{p,r}$
(DAYS)
$r_{act}/r_{\infty} = 96.4$
r/r_{∞}
10
15
20
30
40
50
100

Figure 6-44.

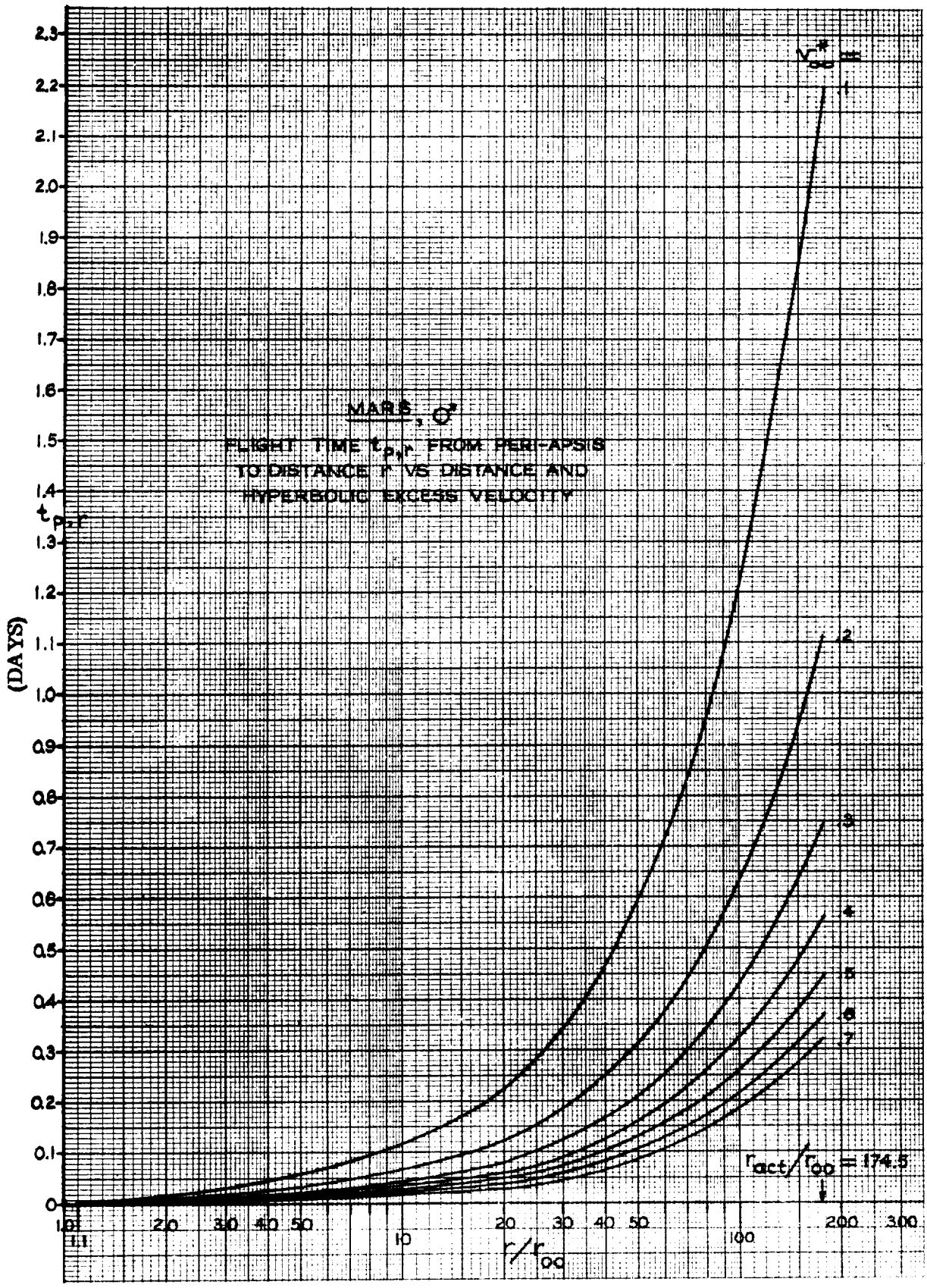
MARS, C³
FLIGHT TIME $t_{p,r}$ FROM PERI-APSIS TO DISTANCE r VS DISTANCE AND HYPERBOLIC EXCESS VELOCITY
$t_{p,r}$ (DAYS)
V_{∞}^{*} atu
1
2
3
4
5
6
7
$r_{act}/r_{\infty} = 174.5$
r/r_{∞}

Figure 6-45.

c. A terminal weight reduction is augmented by the mass-ratio factor when its effect on the initial weight is considered.

In compliance with the work statement, alternate return modes were investigated; however, investigation so far has been only in the lower hyperbolic entry velocity regime (up to $v^*_\infty \sim 0.3$, i.e., $v^*_{entry} \sim 0.45$ or $\sim$ 14 km/sec) because conditions in this regime do not exceed the expected technological state of the art in the early 1970's. A combination of retro- and hyperbolic entry system was also considered, as well as a Hohmann entry maneuver (skip).

The retro-thrust return mode was used on the following basis: Retrothrust was applied early enough so that, at an altitude of 1000 km, the vehicle was slowed down to a velocity equal to 1.4 local circular velocity ($\nu = 1.4$). The osculating orbit at cut-off was to have an unperturbed perigee at approximately 60 km altitude. From the defined terminal condition, the powered flight path was computed backward to various values of v^*_∞ (cf. Section 7).

6.8 ERROR ANALYSIS AND GUIDANCE TECHNIQUE. Errors at orbital departure inject the space vehicles into an erroneous escape orbit which in turn delivers them into an incorrect heliocentric transfer orbit. Errors in departure velocity direction and magnitude affect the heliocentric orbit to a different degree. Displacement of the heliocentric distance of the exit point E, for example, are in any case so small (maximum value would be the radius of the activity sphere) that their effect on the heliocentric orbit is practically negligible. Of greater importance is that, in the case of an error in launch time or in geocentric departure velocity v_1, or both, the latitude λ_1 of E is displaced. This changes the heliocentric departure velocity V_1 and the departure angle β_1 with respect to the Earth orbit, aside from the direct effect of an error in v_1 on V_1 and β_1. Assuming that injection occurs at the periapsis, then $v_1 \equiv v_p$ and the effect of an error Δv_p is

on the semi-major axis (see Figure 6-46):

$$\Delta a = -\frac{2a^2}{K_O} \; v_p \; \Delta v_p \qquad (6\text{-}31)$$

on the eccentricity

$$\Delta e = \frac{2}{v_p} \; (1 + e) \; \Delta v_p \qquad (6\text{-}32)$$

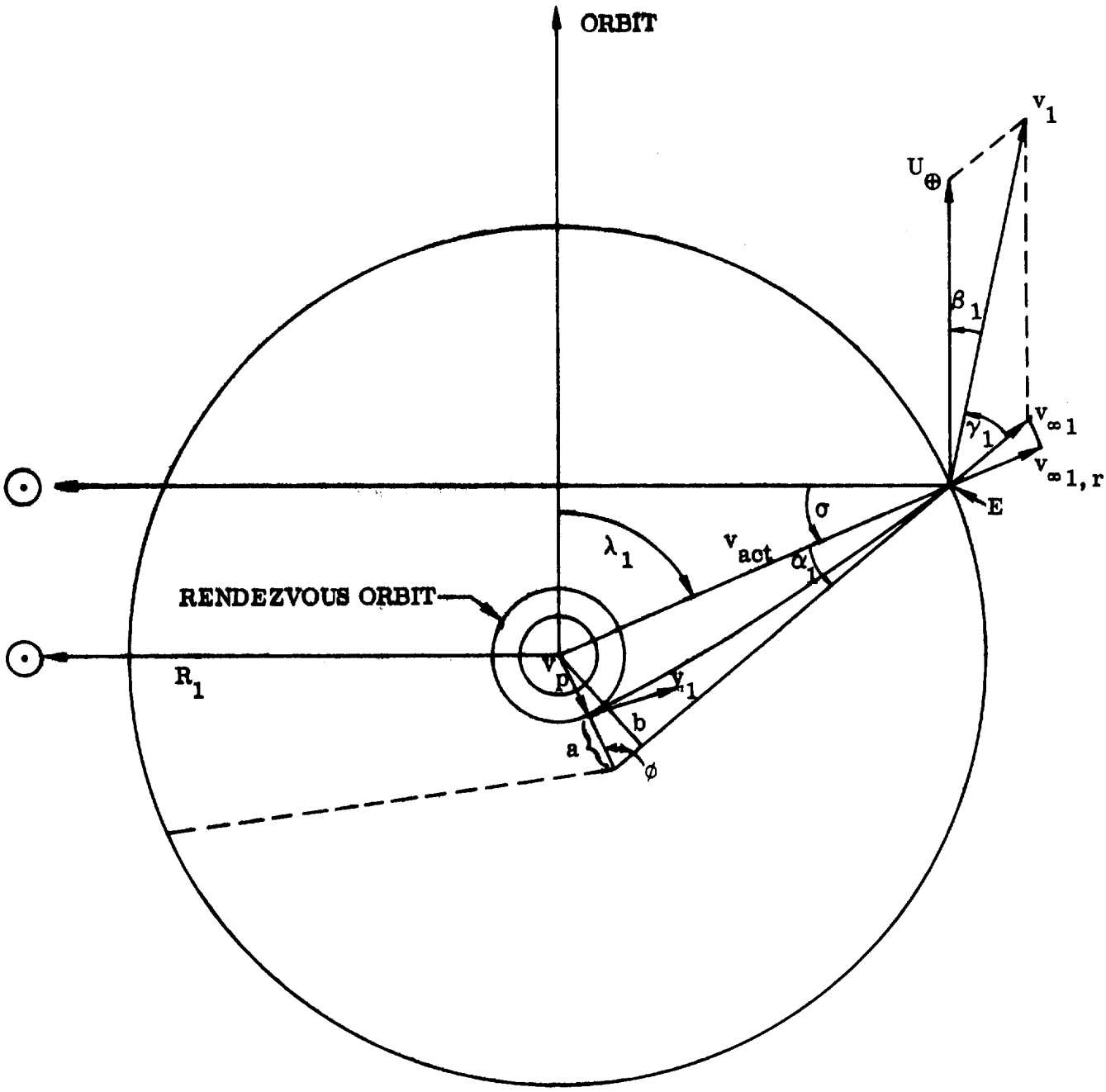

Figure 6-46. Earth Departure

and on the hyperbolic excess velocity

$$\Delta v_\infty = \frac{v_p}{v_\infty} \Delta v_p \tag{6-33}$$

changing the semi-vertex angle to

$$\tan \phi' = \frac{(v_p \pm \Delta v_p)(v_\infty \pm \Delta v_\infty)}{K/r_p} \tag{6-34}$$

and the semi-major axis to

$$b' = (a \mp \Delta a) \tan \phi' = b \pm \Delta b.$$

The angle α_1 is changed by

$$\Delta \alpha_1 = \frac{\Delta b}{r_{act} \cos \alpha_1} \tag{6-35}$$

The associated change of the radial component $v_{\infty 1,r}$ of the hyperbolic excess velocity is

$$\Delta v_{\infty 1,r} = (v_{\infty 1} \pm \Delta v_{\infty 1}) \cos (\alpha_1 \pm \Delta \alpha_1) \tag{6-36}$$

The change in the radial component of the heliocentric departure velocity is

$$\Delta V_{1,r} = (v_{\infty 1} \pm \Delta v_{\infty 1}) \sin (\Delta \phi) \tag{6-37}$$

$\Delta \phi = \phi' - \phi$, is usually entirely negligible, at least as far as its effect on the heliocentric transfer orbit is concerned. Primarily affected will be the scalar magnitude of V_1.

The errors at beginning of heliocentric coast lead to a heliocentric miss distance (d) of the planet, taken in this case as a mass-less point in space-time. The resulting periapsis distance in the actual planetary activity sphere is plotted in Figure 6-47. It is seen that r_p/d is more closely equal to one for Mars than for Venus, due to the stronger gravitational field of the latter. The assumptions underlying Figures 6-47 and 6-48 and the subsequent discussion are:

a. the planets move in circular orbits at mean distances, and
b. their orbits are coplanar in the ecliptic.

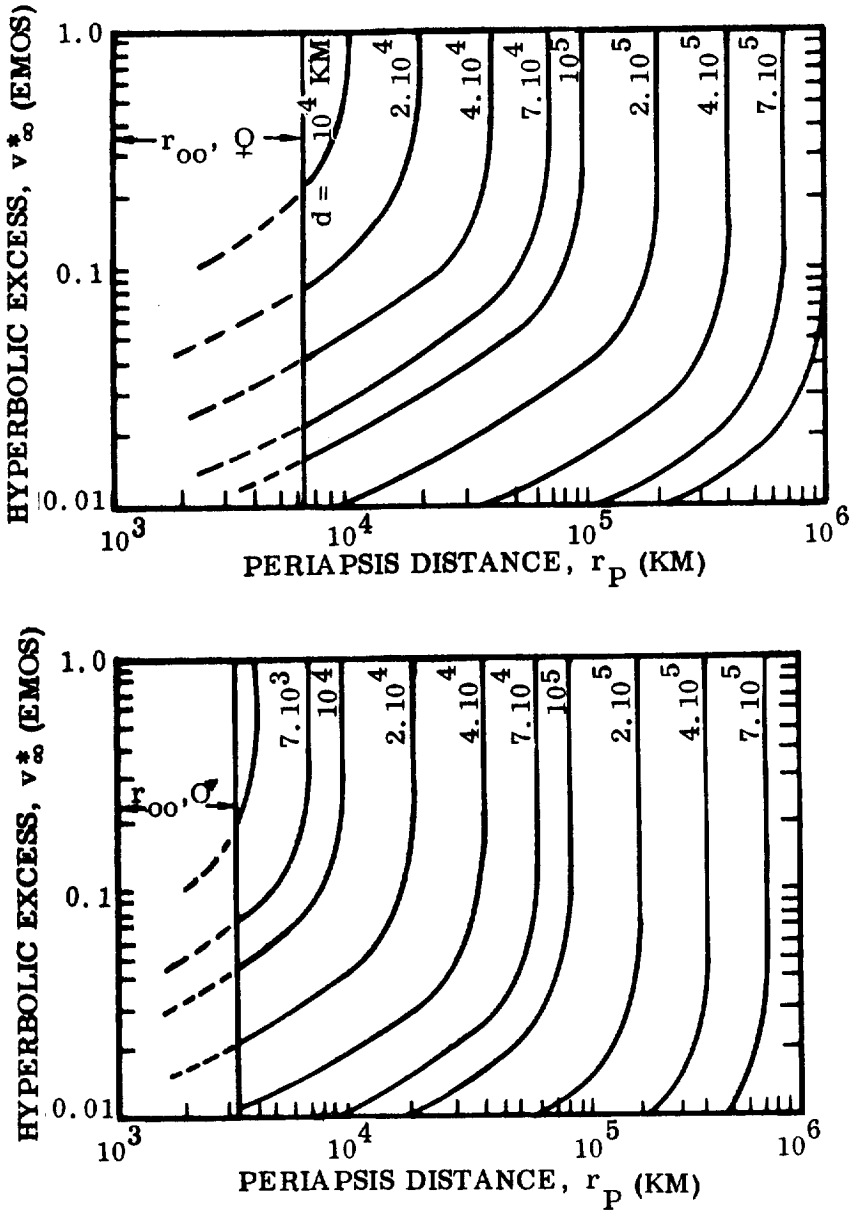

Figure 6-47. Periapsis Distance from Venus and Mars as Function of Hyperbolic Excess Velocity and Heliocentric Miss Distance

The effect of the first assumption on the conclusions obtained from the error analysis is negligible. The effect of the second assumption is that a cross-coupling effect between the planar and the nonplanar components of the miss distance is neglected. In reality, the transfer orbit plane will almost always be inclined. It is designed to intersect the target orbit plane when the distance of the vehicle is equal to the instantaneous distance of the target planet. However, if the transfer orbit plane or the transfer angle or both deviate from the reference value, the vehicle will intersect the target plane at a different distance. That is, it will reach the target planet's distance at a point of northern or southern deviation from the heliocentric ecliptic latitude b by the amount

$$\Delta d_b = \eta_t \tan i \tag{6-36}$$

where d_b is the miss distance in heliocentric latitude (i.e., the latitude of the space vehicle at the point of closest approach to the mass-less target point occupied by the center of the target planet), η_t is the transfer angle and i is the inclination of the transfer orbit plane relative to the target orbit plane. The two cross-coupling terms are therefore, in the case of non-planar transfer,

$$\left.\begin{aligned} \frac{\partial}{\partial x}(d_b) &= \frac{\partial \eta_t}{\partial x} \tan i \\ \frac{\partial}{\partial y}(d_b) &= \frac{\partial \eta_t}{\partial y} \tan i \end{aligned}\right\} \tag{6-37}$$

where x and y are two quantities measured parallel to the transfer orbit plane (angles or distances, cf. below). For practical reasons (energy limitation) the angle i will generally be small and, therefore, these terms will generally be small compared to the error coefficients to be discussed below. For this reason, they are presently neglected for reasons of simplicity. It is recognized, however, that they must be considered in the precision analysis of specific mission profiles and in the design of the actual midcourse guidance system.

Miss distance d is resolved into two components, d_ℓ and d_b, which, in the planar case, are measured in the plane of the ecliptic and normal to it, respectively. If θ is the intersection angle between target planet orbit and transfer orbit, $U_{p\ell}$ and V_2 are the target planet's orbit velocity and the vehicle's velocity at target orbit intersection, then (Figure 6-48)

$$\sin \zeta = \frac{V_r}{v_\infty} \tag{6-38}$$

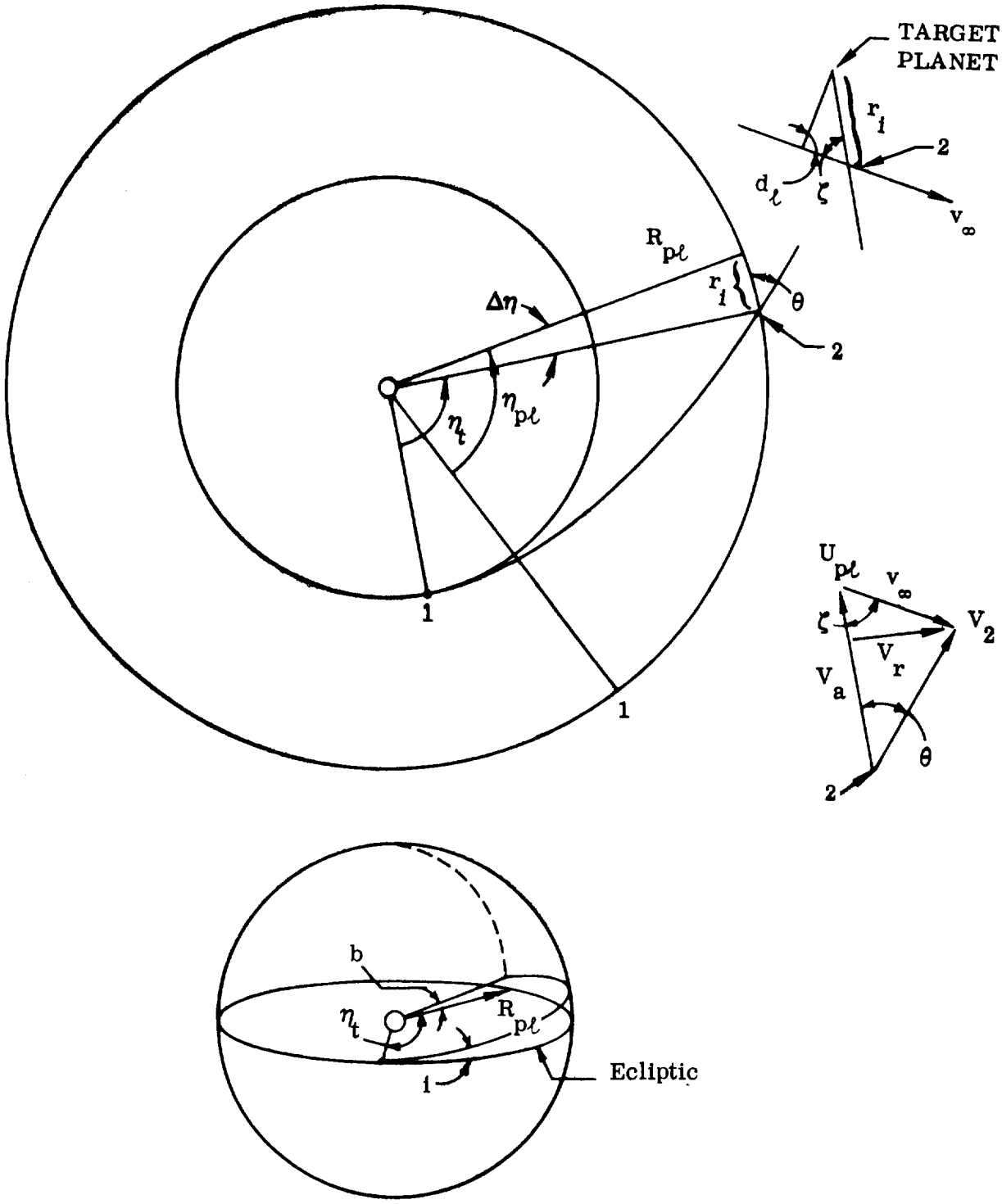

Figure 6-48. Nomenclature of Miss Distance

where V_r is the radial component of V_2. The distance between vehicle and planet (mass-less) at intersection of the planet's orbit is

$$r_i = R_{p\ell} (\eta_t - \eta_{p\ell}) = R_{p\ell} \Delta\eta \tag{6-39}$$

The planar component of the miss distance is related to the angle ζ by the relation

$$\sin \zeta = \frac{d_\ell}{r_i} \tag{6-40}$$

$$d_\ell = r_i \sin \zeta = \frac{V_r}{V_\infty} r_i = R_p \Delta\eta \sin \zeta \tag{6-41}$$

The orthogonal miss distance is (Figure 6-49),

$$d_b = R_{p\ell} b_2 \tag{6-42}$$

where b_2 is the heliocentric ecliptic latitude of the vehicle at the time when the vehicle's distance is equal to that of the target planet ($R_v = R_{p\ell}$). The miss distance is given by

$$d = \sqrt{d_\ell^2 + d_b^2} \tag{6-43}$$

It is now possibly to establish a correlation between initial and terminal errors, which would apply to the case of a purely ballistic transfer; or between initial and midcourse errors; or between midcourse and terminal errors. The first case is of little significance presently, since a midcourse correction capability is assumed to be available to the convoy vehicles. For the errors between departure and midcourse it holds that

$$\left.\begin{aligned} \Delta R &= \frac{\partial R}{\partial V_{r,1}} \Delta V_{r,1} + \frac{\partial R}{\partial V_{a,1}} \Delta V_{a,1} \\ \Delta\eta_t &= \frac{\partial \eta}{\partial V_{r,1}} \Delta V_{r,1} + \frac{\partial \eta}{\partial V_{a,1}} \Delta V_{a,1} \\ \Delta b &= \frac{db}{dV_{w,1}} \Delta V_{w,1} \end{aligned}\right\} \tag{6-44}$$

where R, η_t and b are the heliocentric distance, transfer angle and latitude, respectively, of the space vehicle; $V_{r,1}$, $V_{a,1}$, and $V_{w,1}$ are the heliocentric departure values of the radial, azimuthal and orthogonal component, respectively, of the vehicle's heliocentric departure velocity, V_1. The partials and the differential in the third equation are the error coefficients which are determined by differentiating the appropriate equations of the conic orbit in a central force field. The variation of the partials with V_1 follows from

$$\frac{\partial R}{\partial V_1} = \sqrt{\left(\frac{\partial R}{\partial V_{r,1}}\right)^2 + \left(\frac{\partial R}{\partial V_{a,1}}\right)^2}$$

$$R\frac{\partial \eta_t}{\partial V_1} = R\sqrt{\left(\frac{\partial \eta_t}{\partial V_{r,1}}\right)^2 + \left(\frac{\partial \eta_t}{\partial V_{a,1}}\right)^2} \qquad (6\text{-}45)$$

For equal transfer periods to a given transfer angle, the error coefficients turn out to be almost independent of the numerical value of the transfer angle. The error coefficients are plotted in Figure 6-49 for a Mars flight. The latitude error reaches a maximum at 90° and then decreases to zero at 180°, while the error in distance and transfer angle grow monotonously with time. The longer the midcourse correction is delayed, the more the vehicle is off course and the more expensive is the correction maneuver likely to be.

On the other hand, the earlier during the transfer the midcourse correction is made, the greater is the potential post-midcourse error. This leads to the discussion of the error sensitivity of the terminal coordinates to a midcourse correction. The error equation can be written in the form

$$\Delta d_\ell = \frac{\partial}{\partial x}(d_\ell)\ \Delta x + \frac{\partial}{\partial y}(d_\ell)\ \Delta y \qquad (6\text{-}46)$$

$$\Delta d_b = \frac{\partial}{\partial z}(d_b)\ \Delta z \qquad (6\text{-}47)$$

where x, y and z are measurements made in the ecliptic plane (x, y) and orthogonally to it (z). The two alternatives which have been considered are: a) angular position measurements only, such as the angular positions and two planets or of one planet and the Sun; b) range and two angular position measurements. Since the equations of motion of the vehicle in the transfer

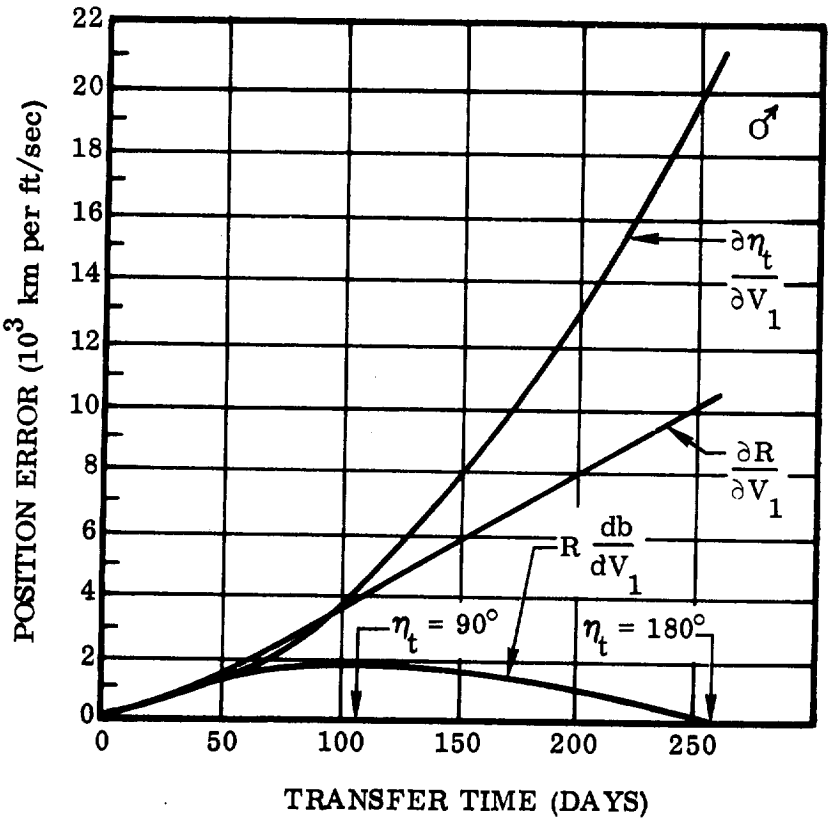

Figure 6-49. Position Error During Transfer to Mars Due to an Error in Departure Velocity V_1

orbit contain six constants, six values are required to define the orbit (namely, three positions and three velocities). The most accurate position measurement is the one which can be made near Earth at the departure cutoff point. Subsequent very accurate position measurements can be made from Earth-based tracking facilities by means of radar or, even better, optically (the vehicle can easily and very accurately be tracked in cislunar space by carrying along an inflated sphere) or by laser. Therefore, the midcourse guidance system of a vehicle, which is not propelled by more or less continuous thrust, must measure only three quantities. As pointed out above, these are either angles or range and two angles.

Angular sightings of two solar-system objects with known positions relative to inertial space (fixed stars) extablish two lines of position. Their intersection determines the location of the vehicle. In order to avoid over-determination, the position of two objects in the ecliptic plane is determined, but the position of only one of these objects (preferably the nearer one) is measured normal to the ecliptic. If the position normal to the ecliptic of both objects is measured, a least-square solution may be employed, yielding higher accuracy, but requiring somewhat greater computer complexity. This is not considered a problem, though, in a manned space vehicle 10 to 13 years hence. The objects to be considered are the Sun, Earth, target planets and finally other objects (planets or asteroids if their ephemerides are

well established). The usefulness of the latter group depends upon their position during transfer of the convoy. The first three objects are more reliably available. The Sun, in particular, is both plainly visible and at comparatively close distance for the missions considered here ($0.7 \leq R \leq 1.6$ A.U.). Moreover, it is the only body which always is in the same plane as the convoy, in heliocentric space. It is therefore a likely choice as one of the objects, at least at certain periods during the transfer. In the case of a flight to Mars, the other object is preferably Mars. By observing the target planet which is practically a "full Mars", except for the very first and last portion of the flight, difficulties connected with observing a body of varying crescent shape are avoided. In a Venus flight the Earth should be used as much as possible, for the same reason.

It is presently assumed that all three angular measurements are made with the same accuracy. In this case the planar error coefficients can be combined in the root-sum-square term

$$\Delta d_\ell = \sqrt{\left[\frac{\partial}{\partial \ell_1}\ (d_\ell)\right]^2 + \left[\frac{\partial}{\partial \ell_2}\ (d_\ell)\right]^2}\ \Delta V_1 \qquad (6\text{-}48)$$

If the nominal value of the miss distance d is zero, it is approximately

$$\Delta d \approx\ 0.8726\ (\Delta d_\ell + \Delta d_b) \qquad (6\text{-}49)$$

provided the ratio of the two error coefficients is in the range $0.146 \leq \Delta d_\ell / \Delta d_b \leq 1/0.146$. Thus

$$\Delta d = \frac{\partial d}{\partial V_1}\ \Delta V_1 \qquad (6\text{-}50)$$

The ratio $\partial d/\partial V_1$ is plotted in Figure 6-50 for Venus and Mars. The orthogonal angular measurement has been assumed to be made on the nearer of the two planets; (i.e., during the Mars flight, first on Earth and then on Mars). The values of $d\,(d_b)/db_{\odot,\oplus,\sigma^*}$ with respect to Sun, Earth and Mars, plotted in Figure 6-51 show that the orthogonal error coefficient for the Sun is always larger than that of both planets. The orthogonal error coefficient for Earth has the smallest value of all three bodies up to about the 105th day of the 200-day transfer to Mars. Thereafter, the orthogonal error coefficient for Mars becomes smaller and Mars should be used. In the case of the transfer to Venus, the crossover point occurs at about the 81st day of the 140-day transfer. Figure 6-50 shows that, for the transfer to Mars, if Earth and Sun are used, the midcourse correction should be made around the 30th day of flight. Shortly thereafter and through the 60th day, the Mars-Sun combination yields the smallest error coefficient for practically the rest of the flight. For the transfer

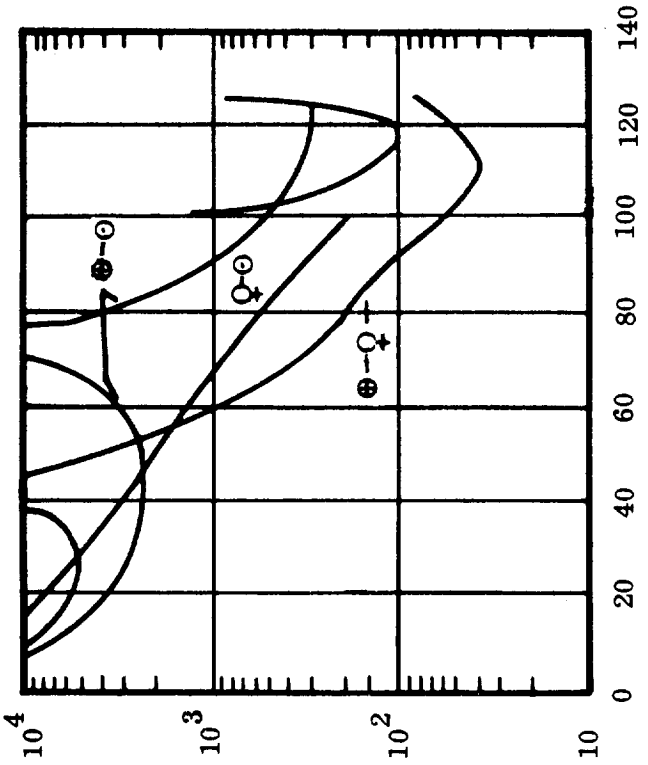

(b) 130-DAY EARTH-VENUS TRANSFER

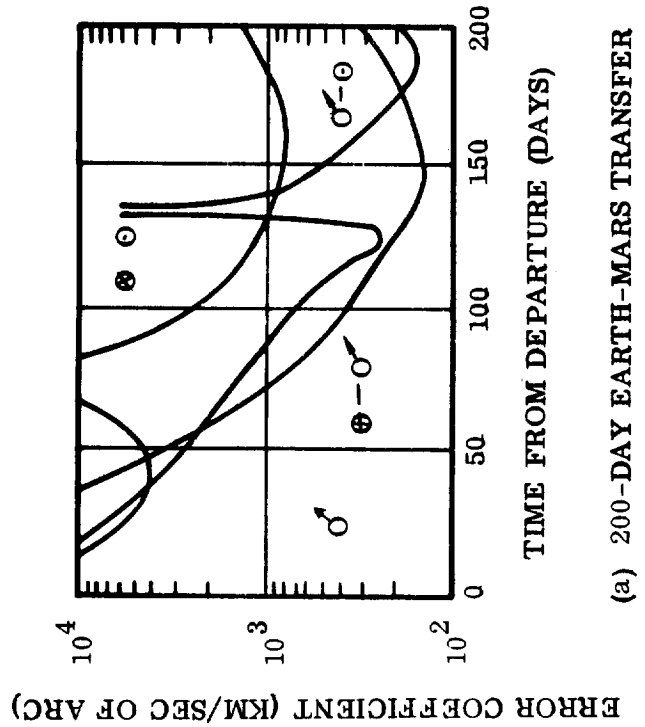

(a) 200-DAY EARTH-MARS TRANSFER

Figure 6-50. Error Coefficients for Planet-Planet or Planet-Sun Guidance

to Venus, the Venus-Sun combination yields a first minimum at about the 40th day. Thereafter, the Earth-Venus combination is best for almost the entire flight.

Generally, the error coefficients decrease with time, due to the gradual increase of the position error, as shown in Figure 6-50. Each curve becomes infinite at a particular time, at which the vehicle passes through the line connecting the two bodies when the sightings were made. In a nonplanar transfer this is less likely to occur.

For the alternate case of two angular measurements and a range measurement, the error equations are

$$\Delta d_\ell = \frac{\partial}{\partial r} (d_\ell) \quad \Delta r + \frac{\partial}{\partial \ell} (d_\ell) \quad \Delta \ell \tag{6-51}$$

$$\Delta d_b = \frac{d}{db} (d_b) \quad \Delta b \tag{6-52}$$

The individual error coefficients are shown in Figures 6-51 and 6-52 for the same transfers to Venus and Mars as before. Since the range measurement is dimensionally different from the angular measurements, the error coefficients cannot be combined into a single coefficient, unless each error coefficient is multiplied by probable error of the corresponding guidance measurement. The main difference, in comparison to the three angular measurements, is the low value of $\partial (d_\ell) / \partial \ell$ and $\partial (d_b) / db$ for Earth while the vehicle is near the Earth and for the target planet during the terminal phase of the flight. This renders the combined range and angle measuring technique particularly attractive for departure and early midcourse guidance, using Earth; and for late midcourse and terminal guidance, using the target planet. Since the position angles of the vehicle as seen from Earth are simply the reverse of the position angle as seen from the vehicle, these error coefficients may also be used for an Earth-based guidance and control system which measures r, ℓ, and b to the vehicle.

Comparison of both the angle and the range-plus-angle method shows that, for minimum guidance error coefficients, an Earth-based technique should be applied, for greatest accuracy, during the hyperbolic and the early heliocentric flight phase. During heliocentric midcourse a Sun-planet angle measuring technique appears most attractive. During final approach to the target planet, the guidance method should revert back to the r, ℓ, b technique using range (and range rate) radar measurements.

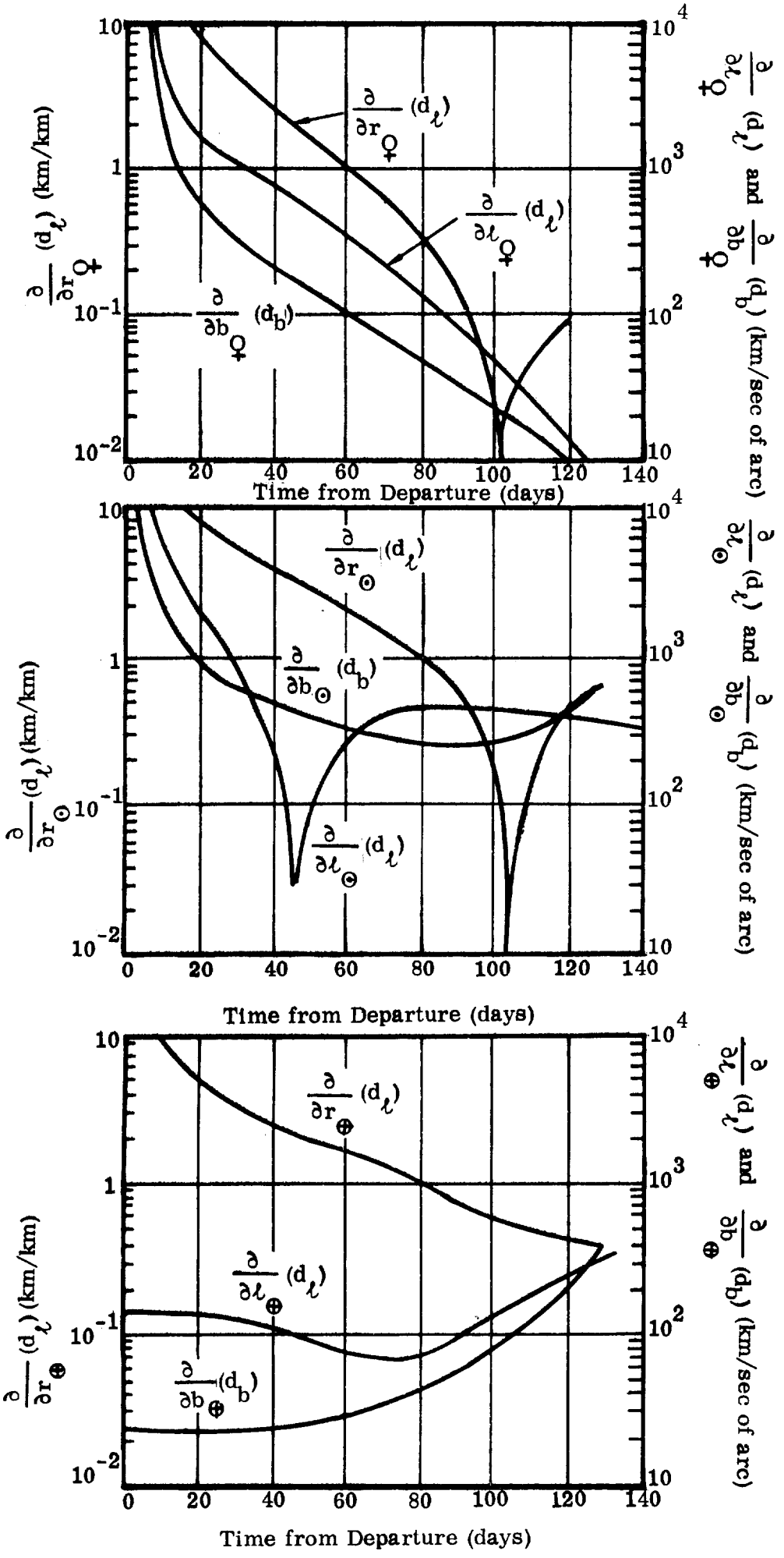

(a) Measurements on Venus

(b) Measurements on Sun

(c) Measurement on Earth

Fig. 6-51. Error Coefficients for Range and Angle Measurements During a 130-Day Earth-Venus Transfer.

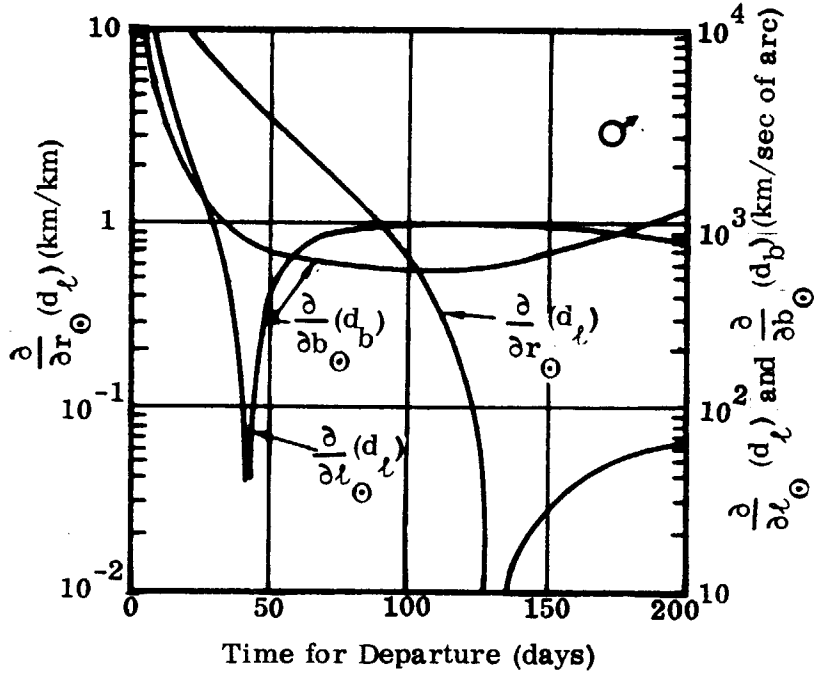

(a) Measurements on Sun

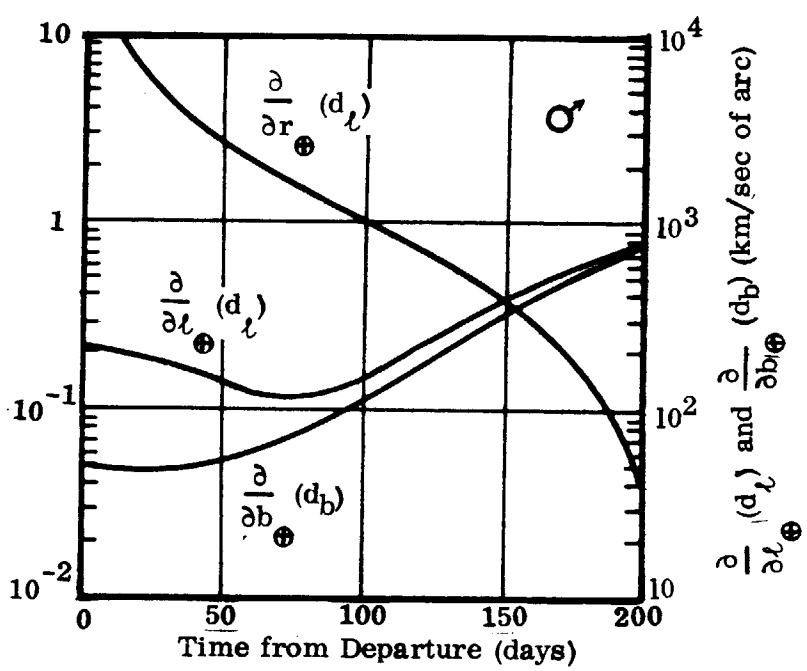

(b) Measurements on Earth

Figure 6-52. Error Coefficients for Range and Angle Measurements During a 200-Day Earth-Mars Transfer.

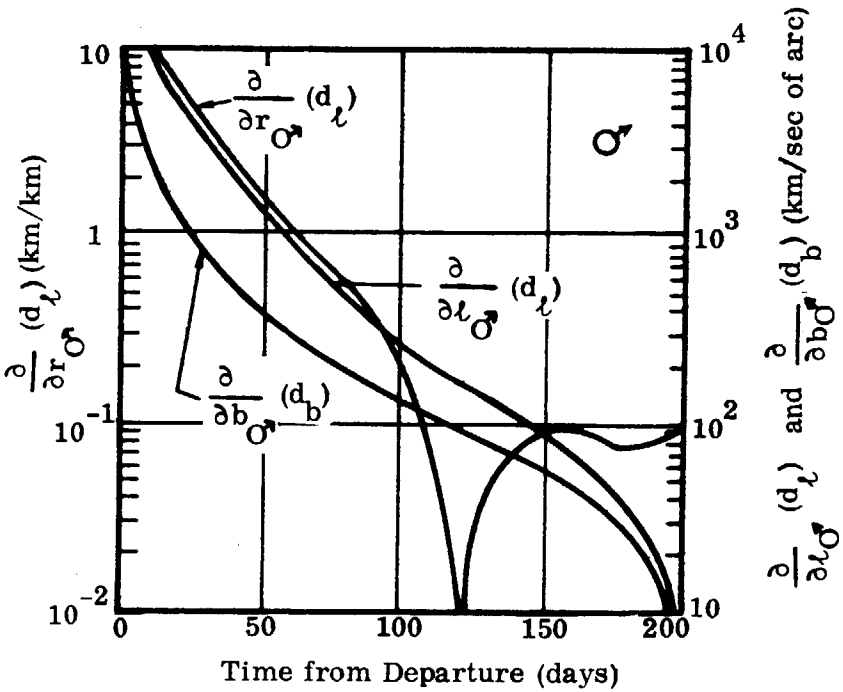

(c) Measurements on Mars

When a powered correction maneuver is carried out, the change in position (x, y, z) as well as in velocity ($V = \sqrt{V_x^2 + V_y^2 + V_z^2}$) will be measured accurately by means of a stellar-monitored all-inertial guidance system. Therefore, a new set of position data is accurately available and the guidance technique of measuring only three quantities is retained after the correction maneuver. Theoretically, a new set of error coefficients must be computed, since the convoy now follows a different transfer orbit. However, if the orbit change is small (velocity change 50 to 100 m/sec), the error sensitivity will be changed very little, so that for preliminary or comparative studies the same error coefficients can be retained.

6.9 NAVIGATION. Errors at orbital departure are propagated through the hyperbolic excape orbit to the heliocentric transfer orbit. The latter shows a wide range of sensitivities to individual launch errors. Any error will affect the exit point position on the activity sphere. Among other changes there is likely to be a change in heliocentric distance of the exit point. Such displacement is an example for an error which has a negligible effect on the heliocentric orbit. Of far greater importance are: failure to launch on time, resulting in an error in the launch azimuth; an error in departure velocity, v_1; and an error in the initial flight path angle. At no given launch date or departure velocity are all three error sensitivities minimized. The cause which can be least controlled with the navigational equipment on hand may therefore tend to become a controlling factor. Figure 6-53 shows the miss distance of Venus as the result of launch errors from a 325-km rendezvous orbit. In this orbit the space ship travels at approximately 0.066 deg/sec. A launch azimuth error of 0.1 deg corresponds, therefore, to an error of 1.65 seconds in burnout time. It is seen that in this case (and in most others) it is precisely the launch-on-time error which has the strongest effect. Because of the high angular velocity in orbit, and because of the fact that a convoy of several vehicles may have to be launched simultaneously, the launch-on-time requirement may not be fulfilled to the degree of precision desired. Selecting a departure velocity at which this particular error sensitivity is a minimum, however, imposes constraints on the mission profile selection which are hardly acceptable. Gordon (Ref. 6-14) has shown that there exists a value of coast arc in the parking or the rendezvous orbit for which the effect of guidance errors (gyro and accelerometer errors) is minimized, because the correlations between the coordinate deviations vary as function of the parking orbit coast angle. Certain errors may cancel each other. This coast arc lies between 100 and 140 degrees from the point of injection, or from the point of the last powered correction maneuver in the orbit. As a result of errors in departure, post-injection correction is necessary. The presence of human intelligence on both ends, in the planet ship as well as on Earth, will be of great benefit in terms of reliability and precision of interplanetary navigation.

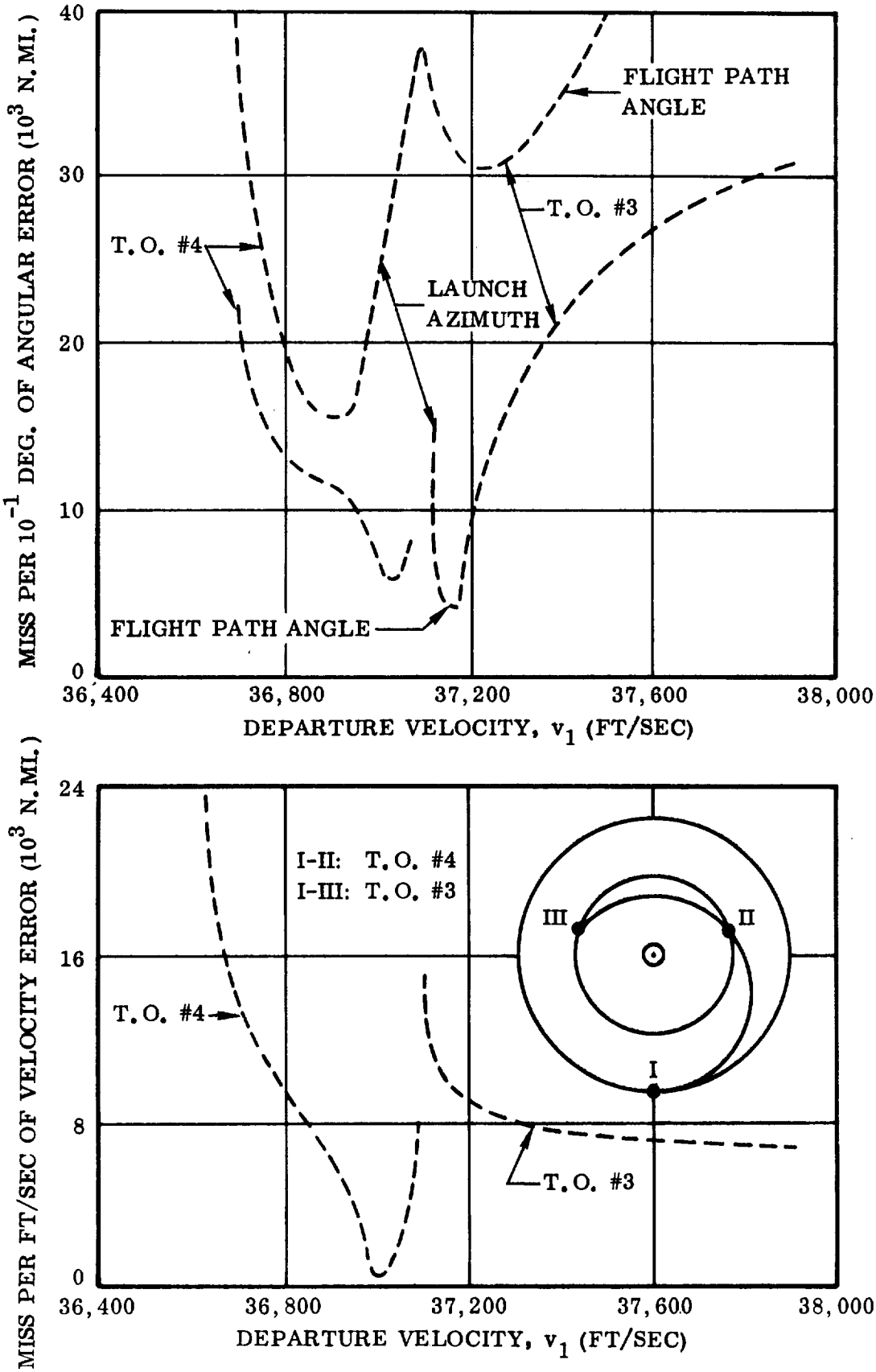

Figure 6-53. Miss Distance of Venus as Result of Launch Errors on 6-19-1973 (Low Error Sensitivity Case; No Midcourse Corrections)

The preferred methods of guidance and navigation during the various flight modes are listed in Table 6-2.

Because of the variety of locations above the Earth's surface at which the ignition and burnout points may be located, the guidance system for orbital launch through to injection into the hyperbolic escape orbit should be a self-contained all-inertial system, using a four-gimbal, all-attitude platform which is space stabilized for the duration of the powered maneuver by three single-degree-of-freedom gyros. On the four gimbal axes of the inertial platform, a resolver chain is provided which is used for transforming vectors from the guidance inertial corrdinate system to the pitch, yaw and roll axes of the vehicle. This transformation is used for autopilot functions and provides an attitude reference for steering the vehicle during powered flight and for orienting the vehicle during coast periods and prior to powered maneuvers. The second major component of the inertial guidance system is the computer. The flexibility allowed in changing the computer program is a major factor in the overall flexibility of the guidance system. Program changes which might have to be made in a short time, if an Earth departure date is postponed by a few days, require far greater computer-program-change flexibility than is available in most, if not all inertial systems presently in use. The computer must be digitalized and capable of orbit computations as well as of other functions, including logical commands, information pick-up and storage, and input-output. The computer accepts the three accelerometer inputs which are in the form of pulse trains, each pulse being equivalent to about a 1/10-ft/sec velocity increment. In addition, the computer accepts time impulses from a crystal oscillator which serves as precision time source. The continuous outputs from the computer are six analog signals, three for vehicle steering and three for gyro torquing during alignment and calibration, and for gyro drift compensation in flight. These analog outputs are provided by six digital-to-analog converters. Discrete outputs are provided for initiation of ignition, thrust cutoff, and staging sequences. Additional discrete inputs to the computer are used for mode switching during in-orbit prelaunch operation of the computer and for autopilot commands to the guidance computer during powered flight. Along with the main computer, a computer control unit is required to keep track of time during the prolonged coast periods during which the computer may be shut off to conserve vehicle power, or during emergencies when sufficient power is temporarily unavailable.

In applying an all-inertial system to planetary missions, certain limitations must be overcome. The system accuracy is affected by (among other factors)the shifting of gyro drift rates which occur from run-up to run-up of the inertial platform when the storage environment of this unit is not closely controlled. Also, there are possible accelerometer bias and scale factor shifts under storage conditions. If the system operates in free space, the typical oscillatory characteristics of an inertial guidance system are absent, so that a constant acceleration error, for example, propagates as

Table 6-2. Guidance and Navigation During the Principal Flight Modes

NO.	FLIGHT MODE	GUIDANCE AND NAVIGATION
1	Orbital launch and injection into departure hyperbola	Vehicle-based all-inertial guidance system with four-gimbal all-attitude inertial platform, digital guidance computer and associated equipment.
2	Hyperbolic coast	Earth-based radio-command guidance system based on range and position measurements. Vehicle-based inflatable tracer bodies could assist to perform precise optical position determination by Earth stations. First powered correction maneuver in cislunar space (0.5-1 day following launch) to improve heliocentric injection accuracy.
3	Initial heliocentric coast	As No. 2. During midcourse correction maneuvers thrust acceleration is integrated by all-inertial guidance system to obtain new position and initial velocity data for new transfer orbit.
4	Intermediate heliocentric coast	Vehicle-based three-angle measuring technique (cf. Section 6.8) using Earth and target planet (especially advantageous for transfer to Venus) or Sun and target planet.
5	Terminal heliocentric coast (approach of target planet's activity sphere)	Revert back to combined range and two-angle measurements, using vehicle-based radar for range measurements.
6	Hyperbolic approach	As No. 5
7	Capture maneuver	Vehicle-based all-inertial guidance system.
8	Capture-orbit coast and attitude control	Horizon scanner and all-inertial platform as back-up.
9	Maneuvers to change capture orbit	As No. 7
10	Preparation of return flight	Exphemerides of suitable alternative heliocentric return orbits and associated capture-orbit plane orientation, launch azimuth, and hyperbolic orbit elements precalculated. Associated error coefficients also precalculated. Independent on-board backup capability provided by vehicle-based computer.
11	Return flight	Analogous to outgoing flight.
12	Earth capture	Earth-based radio-command system; for powered maneuvers: vehicle-based all-inertial guidance system.

(1/2) (a) (t^2) instead of as a bounded oscillatory function. An acceleration bias error of $t \times 10^{-5}$ g, for example, would produce during a 2000 sec powered flight a position error of 1000 m (3280 ft) and a velocity error of 1 m/sec (3.28 ft/sec). If these factors are not taken into account in applying the system to the planetary mission, its usefulness would be greatly limited. A major limitation of the computer could be a too-slow computation rate. It is important that the arithmetic unit contain an adequate number of accumulators. It should also be possible to load the computer in an unmanned companion ship (service vehicle) from the control room of the manned ship (crew vehicle). In order to overcome the accuracy problem in the inertial components (caused by shifts in their parameters over extended storage periods in the rendezvous orbit prior to departure) it is necessary to carry out a thorough calibration of the inertial components shortly before launch, after the guidance system has settled into a steady-state operating condition. During this prelaunch calibration mode, the accelerometer bias and scale factors are determined again, for use in correcting the position and velocity calculations in flight. Also, gyro drift parameters are redetermined, including the measurement of gyro-fixed restraint drifts and the mass unbalance drift coefficients for mass shifts along the input axes of the three platform gyros. The drift parameters determined during this calibration mode are used to generate torquing rates as a function of measured acceleration, which are fed into the platform gyros during flight, in order to compensate for their internal drifts. These drifts continue (although at a lesser rate) after cutoff, if artificial gravity is generated for biological reasons. Therefore, it would be advantageous, from the viewpoint of minimizing drift rates during the long coast periods, to install the system in a service vehicle, which would not rotate and would, in fact, be likely to be attitude controlled, in order to minimize propellant evaporation or possibly for other reasons (e.g., to shield the crew module from nuclear radiation emanating from the service vehicle). The mass unbalance coefficients for the spin reference axes have not been determined in the above-mentioned calibration mode. They must be determined prior to placing the system into the vehicle to determine an optimum platform orientation for which the errors caused by shifts of these parameters prior to launch are not severe.

Calculations which require high iteration rates by the computer and which might, therefore, be impeded by low computer solution rates are: a) the integration of vehicle acceleration due to variations in thrust direction (if any); b) the double integration of the resulting acceleration vector to velocity and position; c) the generation of attitude error signals; d) the precise determination of engine cutoff commands. High iteration rates are required for the steering loop, if the guidance system is to provide the basic vehicle attitude error information to the autopilot during powered flight (i.e., if there are no independent attitude reference sources, such as integrating rate gyros in the autopilot during powered flight).

The parameters describing the interplanetary transfer orbit (hence, also those describing the associated hyperbolic paths) change continuously with respect to the guidance platform coordinate system prior to launch. In order to avoid continual updating of the guidance parameters with every change of launch time (escpecially in the systems on the service vehicles) from the control room of the crew vehicle, it is desirable to develop guidance equations whose parameters and equation-form are as much independent of time as possible; i.e., to express only a minimum number of quantities in terms of launch time (these alone would then have to be changed if the launch time is changed) and then calculate the other guidance parameters explicitly from these launch time dependent parameters. For instance, for interplanetary missions, it is possible to express in platform coordinates the three components of the hyperbolic excess velocity vector $\bar{v}_\infty$ in terms of the launch time, measured from a reference time t_o. All other guidance parameters are then computed explicitly from this quantity and from the vehicle velocity and position measured in the platform coordinate system. The components of $\bar{v}_\infty$ can be computed as functions of launch time in the computer by expressing them in polynomial form. During the injection phase into the hyperbolic escape orbit for a Mars mission, for example, the following computation must be performed:

$\bar{v}$ = vehicle velocity vector

$\bar{v}_\infty$ = hyperbolic excess velocity vector

$\bar{v}_R$ = velocity vector which, together with $\bar{r}$, defines the escape hyperbola with the specified $\bar{v}_\infty$ for every point along the powered flight path (required velocity)

$\bar{r}$ = vehicle position vector

$\bar{v}_R$ is the basic guidance vector and is given in terms of magnitude v_R, radial component v_{Rr} and a component orthogonal to the required orbital plane, $v_{Rw} = 0$.

$$v_R^2 = \bar{v}_\infty \cdot \bar{v}_\infty + \frac{2K}{r}$$

$$v_{Rr} = \frac{\frac{K}{rv_\infty}(v_\infty + \bar{\ell}_r \cdot \bar{v}_\infty) - (\bar{\ell}_r \cdot \bar{v})^2 + v_\infty(\bar{\ell}_r \cdot \bar{v}_\infty)}{v_\infty - \bar{\ell}_r \cdot \bar{v}_\infty}$$

$$v_{Rw} = 0$$

$$\bar{\ell}_r = \frac{\bar{r}}{r} \quad r = |\bar{r}| \; ; \; v_\infty = |\bar{v}_\infty|$$

The expression for v_{Rr} is an approximation to the radial component of the required velocity which converges to the exact value as the vehicle approaches cutoff. The outline of the computation is presented in Table 6-3.

Table 6-3. Computation Sequence During Powered Departure Mode for a Mars Mission

For cutoff: Compare the magnitude of the vehicle velocity ϵ (cutoff parameter) to the magnitude of the required velocity:

$$\epsilon^2 = v_R^2 - \bar{v} \cdot \bar{v}$$

Generate desired steering attitude vector from the radial and crossrange velocity errors:

$$\epsilon_r = v_{Rr} - \bar{\ell}_r \cdot \bar{v}_m$$

$$\epsilon_w = -\bar{\ell}_w \cdot \bar{v} \cdot \bar{\ell}_w = \bar{\ell}_r \times \frac{v_\infty}{v_\infty}$$

The desired vector now follows from

$$\bar{f} = f_a \bar{\ell}_a + f_w \bar{\ell}_w + f_r \bar{\ell}_r$$

where the subscript a stands for azimuthal (circumferential) components and where

$\bar{\ell}_a = \bar{\ell}_w \times \bar{\ell}_r$ (computed only once at the beginning of the thrust period)

f_a = constant

$f_w = f_w(\epsilon_w, \epsilon)$

$f_r = f_r(\epsilon_r, \epsilon)$

f_w and f_r are made functions of the cutoff parameter ϵ, so that they may be modified to prevent excessive maneuvering during powered flight. The desired attitude vector $\bar{f}$ is the steering output from the computer and is computed in the platform coordinate system. This vector can then be transformed to vehicle coordinates by the resolver chain and forms the attitude error signals for the autopilot.

Analogous considerations apply to all other powered phases during the mission.

A planetary departure involves two injection processes, from rendezvous orbit into planetocentric hyperbola and from there into the heliocentric orbit. Conversely, a capture process involved injection from heliocentric orbit into planetocentric hyperbola and from there into the capture orbit. The sooner a correction is made following injection, the more economic, in terms of propellant consumption, will it be; but greater is the uncertainty that the correction was adequate. Causes of errors fall into three groups:

a. Uncertainty of masses and orbital elements of the celestial bodies involved.

b. Equipment inaccuracies during powered flight (e.g., accelerometer bias, etc.) and during thrust determination.

c. Uncertainties in the determination of the vehicle orbit proper.

Causes in group a are diminishing rapidly. The accuracy of the astronomical unit has been improved by two orders of magnitude. Evaluation of the Mariner 2 experiment will lead to improved knowledge of the mass of Venus.

Equipment inaccuracies are unavoidable. On the basis of JPL studies reported in Reference 6-15, typical root mean square (rms) variations in injection conditions are

velocity, magnitude	1.22 m/sec
velocity vector orientation	2 milliradians
altitude variation	1 km

On the basis of these tolerances, Reference 6-14 estimates that the midcourse correction maneuver during heliocentric transfer would require an impulsive velocity change of the order of 60 m/sec (~200 ft/sec). Since the above variations in injection conditions will probably be improved by the time an EMPIRE convoy is launched (particularly the velocity vector orientation), this corrective velocity requirement may be regarded to be conservative. Nevertheless, in the preliminary performance specification of the convoy ships (cf. Section 7) an impulsive velocity change of 305 m/sec (1000 ft/sec) was set aside, since the following considerations were included: a) corrective maneuvering of individual convoy vehicles relative to the lead (or reference) vehicle; b) losses due to chilldown, if cryogenic propellants are employed; c) midcourse maneuver in the hyperbolic departure orbit, at entry into the target planet's activity sphere and in the hyperbolic approach orbit to the target planet are included; and, finally, (d) special requirements not only for accuracy in capture distance but also in the capture orbit plane might impose larger midcourse energy requirements which remain to be investigated. Therefore, it is believed that a higher equivalent corrective velocity change should, at this point of the study, be realistically regarded as representative for each leg of the manned capture mission.

SECTION 7

PERFORMANCE ANALYSIS

7.1 INTRODUCTION. The performance analysis conducted during the study period was entirely based on a patched conic approach with the "surface" of the planet's activity sphere of radius

$$r_{act} = R_{p\ell}\left(\frac{m_{p\ell}}{m_O}\right)^{\frac{2}{5}} \qquad (7\text{-}1)$$

separating the planetocentric conic from the heliocentric conic. The radii of the relevant planetary activity spheres are listed, in various units, in Table 7-1.

Table 7-1. Radius of the Activity Spheres of Venus, Earth and Mars

RADIUS	VENUS	EARTH	MARS
Kilometers	610,000	920,000	580,000
Nautical miles	332,160	498,765	311,627
Planet radii	99.2	144.9	174.4
Astronomical units	0.00408	0.00615	0.00388

7.2 DEFINITION OF WEIGHTS AND MASS RATIOS. An interplanetary round-trip mission is a very complex combination of large and small powered maneuvers, of stagings and various other weight changes of larger or smaller magnitude. Therefore, it is necessary to first establish one or several performance-related mission models which contain the principal events and can be refined in further studies. Three mission models are shown in Figures 7-1 through 7-3. Figure 7-1 represents a capture mission with four main maneuvers: M-1, Earth escape; M-2, target planet capture; M-3, target planet escape; and M-4, Earth capture. Figure 7-2 shows the same mission, but with a heliocentric plane change maneuver in the outgoing transfer orbit. Figure 7-3 shows a fly-by mission with one powered maneuver during the hyperbolic encounter.

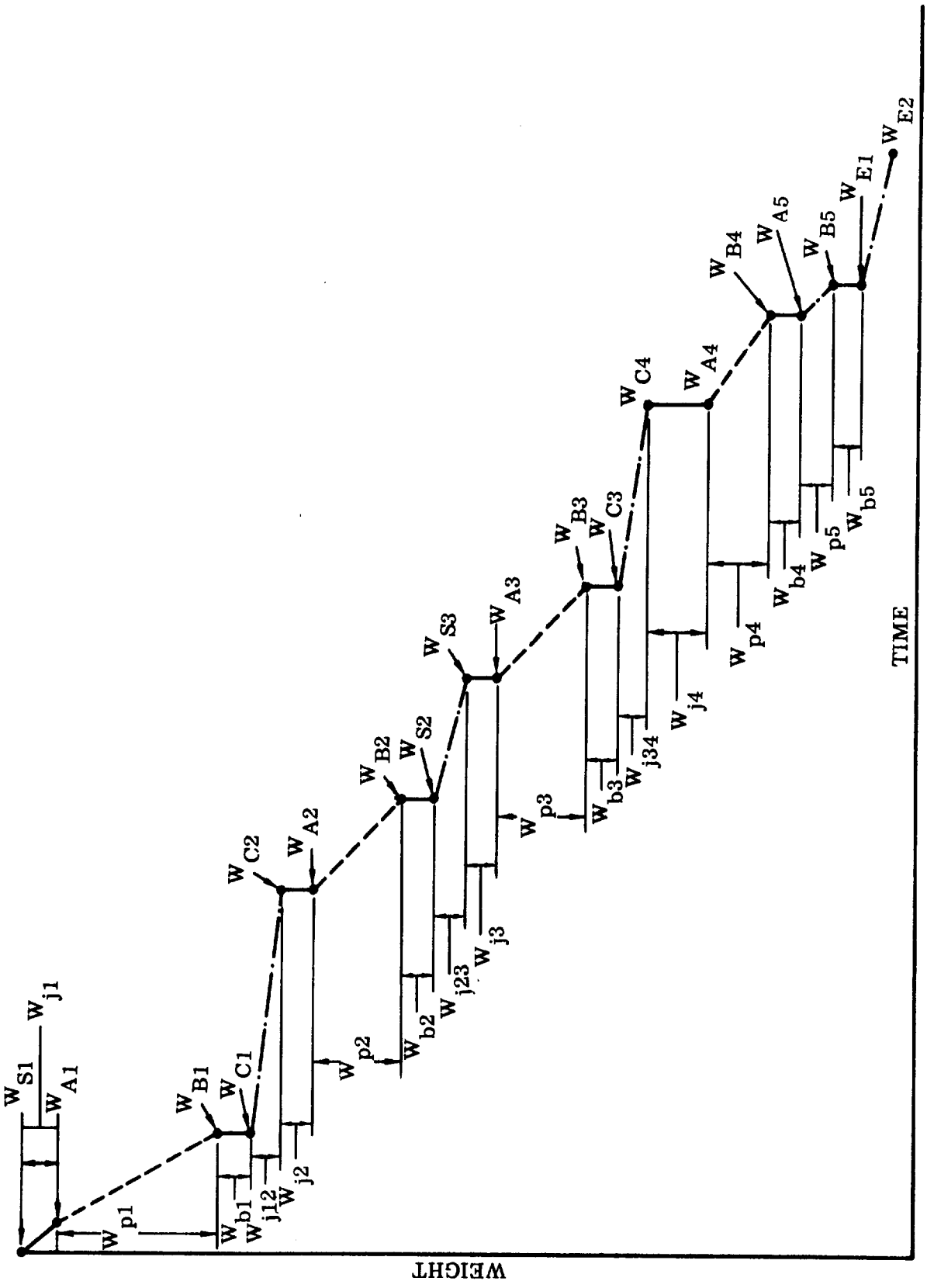

Figure 7-1. Weight Change During Planetary Capture Mission (Self-Sufficient Vehicle; 2-Maneuver Transfers)

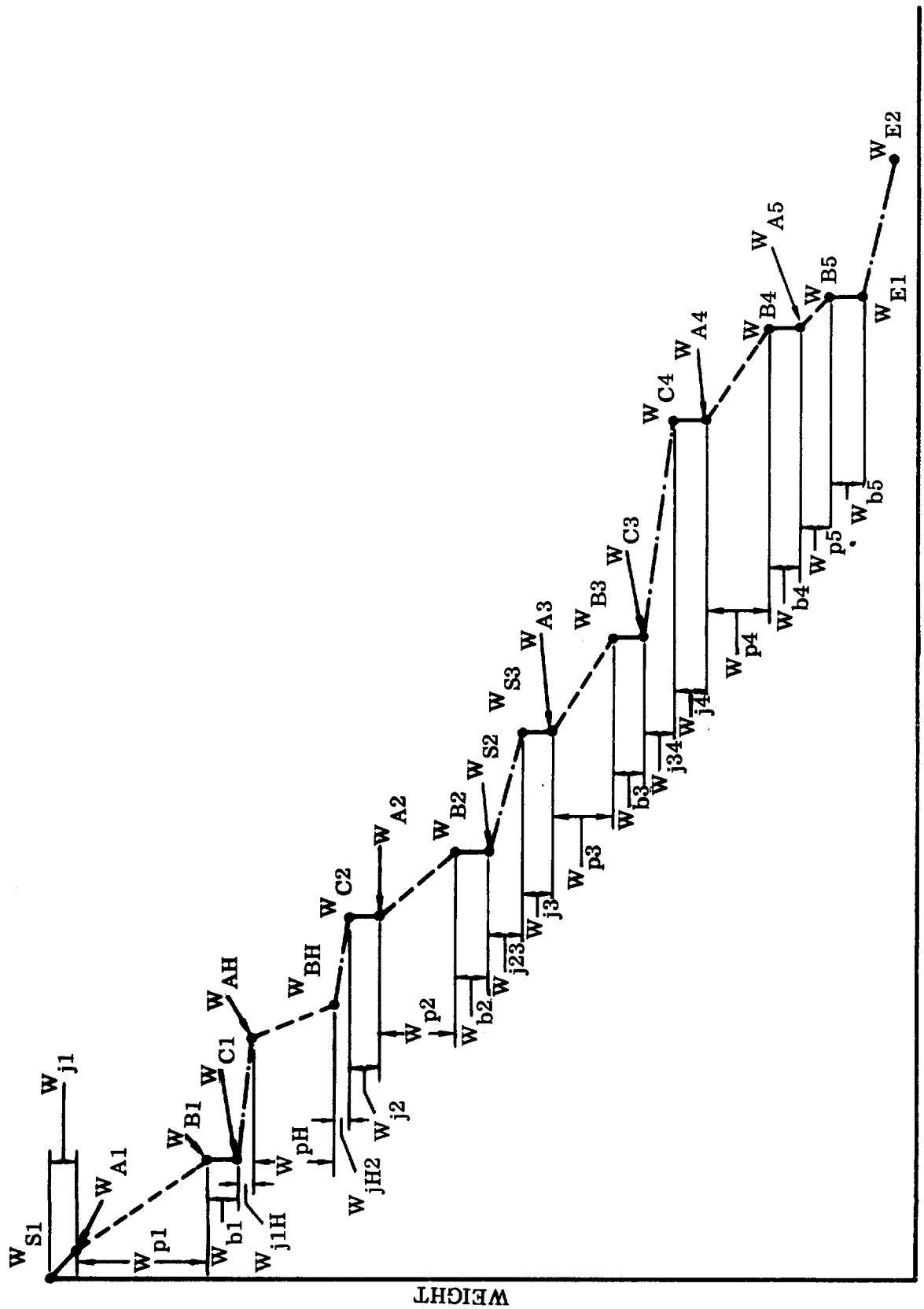

Figure 7-2. Weight Change During Planetary Capture Mission (Self-Sufficient Vehicle; Heliocentric Plane Change)

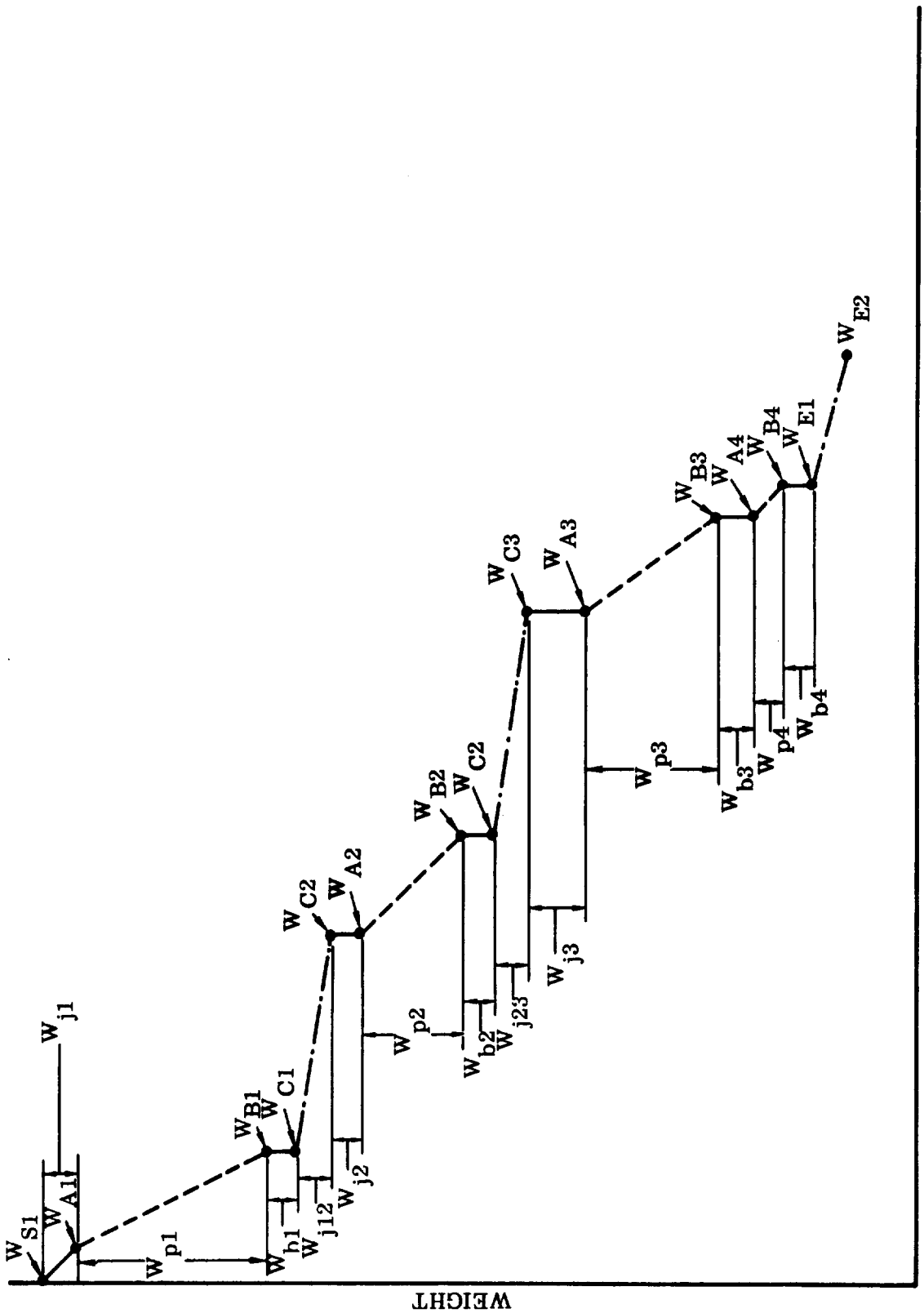

Figure 7-3. Weight Change During Planetary Fly-By Mission (Self-Sufficient Vehicle; No Heliocentric Plane Change)

The principal performance-related events during the capture mission with four principal maneuvers are listed in Table 7-2. The associated weights (or weight losses) are grouped as follows:

Principal Weights

W_S = weight in satellite orbit (of Earth or target planet)

W_A = ignition weight

W_B = burnout weight

W_C = transfer coast weight

W_E = Earth entry weight

Principal Weight Eliminations

W_p = useful propellant weight consumed during a given powered maneuver

W_b = wet inert weight of propulsion unit jettisoned following the given maneuver

W_j = weight consumed or jettisoned during coast or capture periods and prior to powered maneuvers (i.e., weight eliminated between the principal powered maneuvers).

Principal Subscripts

1 = first maneuver (M-1); initial satellite orbit weight; initial outbound coast weight

12 = between maneuvers M-1 and M-2

2 = terminal outbound coast weight; second maneuver (M-2); initial weight in capture satellite orbit

23 = between maneuvers M-2 and M-3

3 = terminal weight in capture satellite orbit; third maneuver (M-3); initial return coast weight

34 = between M-3 and M-4

4 = terminal return coast weight; fourth maneuver (M-4)

5 = final correction maneuver (M-5) prior to Earth entry

Table 7-2. Principal Events in Capture Mission Depicted in Figure 7-1

Weight of vehicle fully assembled in satellite orbit (initial weight)	W_{S1}
Weight consumed prior to launch	W_{j1}
Weight, following mission readiness test, at ignition (launch weight)	W_{A1}
Burnout weight following M-1	W_{B1}
Propellant weight consumed during M-1	$W_{p1} = W_{A1} - W_{B1}$
Wet inert weight of vehicle section (escape booster) staged following M-1	W_{b1}
Weight at the beginning of coast (initial outbound coast weight)	W_{C1}
Weight consumed or jettisoned during planetocentric coast and heliocentric coast, including weight consumed for correction or spin and de-spin maneuvers, boiloff losses etc.	W_{j12}
Weight at termination of transfer coast, at the beginning of preparations for the M-2 maneuver (terminal outbound coast weight	W_{C2}
Weight eliminated in preparation of capture maneuver M-2; "house cleaning", i.e., jettisoning of all items no longer needed at the end of the outbound coast. This measure is taken to ensure that no unnecessary weight is accelerated	W_{j2}
M-2 ignition weight	W_{A2}
M-2 burnout weight	W_{B2}
M-2 useful propellant weight	$W_{p2} = W_{A2} - W_{B2}$
Wet inert weight (M-2 propulsion unit) staged following M-2	W_{b2}
Weight at beginning of capture period in target planet satellite orbit (initial capture weight)	W_{S2}
Weight consumed or jettisoned during capture period, including propellant consumed for whatever adjustment maneuvers are necessary	W_{j23}
Weight at termination of capture period (terminal capture weight)	W_{S3}
House cleaning in preparation of M-3	W_{j3}

Table 7-2. Principal Events in Capture Mission Depicted in Figure 7-1 (Continued)

M-3 ignition weight	W_{A3}
M-3 burnout weight	W_{B3}
M-3 useful propellant weight	$W_{p3} = W_{A3} - W_{B3}$
Wet inert weight (M-3 propulsion unit) staged following M-3	W_{b3}
Weight at beginning of coast (initial return coast weight)	W_{C3}
Weight consumed or jettisoned during planetocentric and heliocentric coast, including weight consumed for correction, or spin and de-spin maneuvers, boiloff losses, etc.	W_{j34}
Weight at termination of transfer coast, at the beginning of preparations for the M-4 maneuver (terminal return coast weight)	W_{C4}
House cleaning in preparation of M-4, including jettisoning of the entire LSS except the EEM	W_{j4}
M-4 ignition weight	W_{A4}
M-4 burnout weight	W_{B4}
M-4 useful propellant weight	$W_{p4} = W_{A4} - W_{B4}$
Wet inert weight (M-4 propulsion unit) staged following M-4	W_{b4}
Ignition weight for correction maneuver M-5 prior to Earth entry	W_{A5}
M-5 burnout weight	W_{B5}
Wet inert weight jettisoned following M-5 and prior to Earth entry	W_{b5}
Initial Earth Entry Module (EEM) weight	W_{E1}
Terminal EEM weight (terminal mission weight)	W_{E2}

Payload definitions are listed in Table 7-3. Principal events in the capture mission depicted in Figure 7-2 are listed in Table 7-4.

Table 7-3. Payload Definitions

W_λ	= payload weight
$W_{\lambda 1}$	= payload of escape booster (the planet ship of nominal initial weight W_{C1})
λ_1	= W_{C1}/W_{A1} = Earth departure payload ratio
$W_{\lambda 2}$	= payload of M-2 propulsion unit
λ_2	= W_{S2}/W_{A2} = capture payload ratio
$W_{\lambda 3}$	= payload of M-3 propulsion unit
λ_3	= W_{C3}/W_{A3} = target planet departure payload ratio
$W_{\lambda 4}$	= payload of M-4 propulsion unit
λ_4	= W_{A5}/W_{A4} = Earth capture payload ratio

Table 7-4. Principal Events in Capture Mission Depicted in Figure 7-2

Sequence of events and weight designations are the same as in the mission of Figure 7-1 with the exception of a heliocentric plane change maneuver. If the plane change occurs during the outgoing transfer coast:

Weight consumed or jettisoned while coasting to the heliocentric maneuver point	W_{j1H}
Ignition weight for heliocentric maneuver	W_{AH}
Burnout weight (or cutoff weight) at termination of heliocentric maneuver	W_{BH}
Weight consumed during remaining portion of outgoing coast	W_{jH2}

Designations are altered correspondingly if heliocentric maneuver occurs during return transfer coast.

For each main maneuver it holds that $\lambda + b + \Lambda = 1$. (7-2)

Where λ is the payload fraction of the given stage (cf. Table 7-2), b the wet inert weight fraction and Λ the useful propellant fraction of the given stage,

$$\lambda \equiv \frac{W_\lambda}{W_A} = \frac{1}{x}\left(\frac{1}{\mu} - 1\right) + 1 = 1 - \frac{1}{x}\left(1 - \frac{1}{\mu}\right) = 1 - \frac{\Lambda}{x} \qquad (7\text{-}3)$$

$$b \equiv \frac{W_A - W_B}{W_A} = \frac{1 - x}{x} \quad \frac{\mu - 1}{\mu} \tag{7-4}$$

$$\Lambda \equiv \frac{W_p}{W_A} = \frac{\mu - 1}{\mu}$$

$$x \equiv \frac{W_p}{W_b + W_p} \tag{7-5}$$

is the mass fraction of the given stage and

$$\mu \equiv \frac{W_A}{W_B} = 1 + \frac{W_p}{W_\lambda + W_b} = \exp\left(\frac{\Delta v_{id}/g}{I_{sp}}\right) = \exp\left(\frac{\tau}{I_{sp}}\right) \tag{7-6}$$

is the mass ratio based on the ideal velocity change, Δv_{id} (i.e., actual velocity change plus velocity losses), of the given stage and

W_p = useful propellant weight of the given stage,

W_λ = payload weight of the given stage,

W_b = wet inert weight of the given stage, and

$$\tau \equiv \Delta v_{id}/g. \tag{7-7}$$

Burnout (or cutoff) weight of the stage is

$$W_B = W_b + W_\lambda. \tag{7-8}$$

Initial weight

$$W_A = W_B + W_p. \tag{7-9}$$

The mission payload ratio is defined as

$$\lambda_{tot} = \frac{W_{A5}}{W_{A1}} = \prod_{n=1}^{4} \lambda_n \quad \text{or} \quad \frac{W_{A4}}{W_{A1}} = \prod_{n=1}^{3} \lambda_n \tag{7-10}$$

for capture or fly-by missions, respectively.

The mission mass ratio is defined as

$$\mu_{tot} = \mu_1 \cdot \mu_{12} \cdot \mu_2 \cdot \mu_{23} \cdot \mu_3 \cdot \mu_{34} \cdot \mu_4 \cdot \mu_5 \qquad (7-11)$$

for the capture mission with four main maneuvers, as

$$\mu_{tot} = \mu_1' \cdot \mu_{1H} \cdot \mu_H \cdot \mu_{H2} \cdot \mu_2 \cdot \mu_{23} \cdot \mu_3 \cdot \mu_{34} \cdot \mu_4 \cdot \mu_5 \qquad (7-12)$$

for the capture mission with heliocentric plane change maneuver, and as

$$\mu_{tot} = \mu_1' \cdot \mu_{12}' \cdot \mu_2' \cdot \mu_{23}' \cdot \mu_3' \cdot \mu_4' \qquad (7-13)$$

for the fly-by mission.

For the principal maneuvers μ_1', μ_2', μ_3', μ_4', it holds (n = 1,2,3,4) that

$$\mu_n' = \mu_n \cdot \mu_\ell \cdot \mu_{corr} \cdot \mu_{p\ell} \qquad (7-14)$$

Where

$$\mu_n = e^{\tau_n / I_{sp,n}} \qquad (7-15)$$

is the mass ratio based on the ideal velocity change during the maneuver,

μ_ℓ = equivalent mass ratio due to losses (residuals, boiloff losses, make-up for expected leakage losses, contingencies, etc.),

μ_{corr} = equivalent mass ratio for navigational corrections, and

$\mu_{p\ell}$ = equivalent mass ratio for plane change maneuver(s) in the capture orbit or prior to departure.

Generally, μ_n is the mass ratio for which the tanks of the particular propulsion section are laid out. Not all propulsion sections are determined by Equation 7-14. For example, for the escape booster it holds

$$\mu_1' = \mu_1 \cdot \mu_\ell . \qquad (7-16)$$

Correction manuevers are normally charged to the propulsion section associated with the main maneuver following the coast period during which navigational correction maneuvers are carried out. This presupposes that it is desirable or feasible to start the particular main engines for such a comparatively small maneuver as a

navigational correction. Where this is not the case, the correction maneuvers must be charged to another propulsion system and do not appear in the main propulsion section that is to operate at the termination of the coast period in which the correction maneuvers took place. The value of μ_{pl} will generally affect only the layout of the M-3 propulsion section.

It should be noted that the mass ratio (μ') based on the actual velocity charge does not necessarily represent one single maneuver, but may be the product of several maneuvers. For example, target planet departure may consist of several separate maneuvers, as is shown below in connection with elliptic capture orbits. In this case,

$$\mu_3 = \mu_{3.1} \cdot \mu_{3.2} \cdot \mu_{3.3} \cdots \tag{7-17}$$

In addition, there are mass ratios associated with a number of smaller maneuvers such as spin and de-spin (μ_{sp}) and intra-convoy maneuvers (μ_{icm}) by which the path of convoy vehicles is adjusted relative to that of the lead or reference vehicle. These will be carried out by small auxiliary engine systems and are not charged to the main systems, unless one propellant component (e.g., the hydrogen) is drawn from the main tank of a given propulsion section.

Launch abort energy requirements (μ_{abort}) are charged to the spin/de-spin propulsion section. This section is laid out for the higher energy requirement. If the launch abort energy requirement is the determining factor, provisions are made to jettison tanks containing excess propellants after a successful launch and prior to the subsequent main maneuver.

7.3 ESCAPE AND CAPTURE MANEUVERS. The relative orbital energy is defined by the relation

$$\epsilon = -\frac{2}{n+1} \tag{7-18}$$

where $n = r_A/r_p$, the ratio of apoapsis to periapsis distance. Thus, for a circular orbit, $\epsilon = -1$ and for a parabolic orbit, $\epsilon = 0$. The value of ϵ is always negative, $0 \geq \epsilon \geq -1$. This concept of the relative orbital energy provides correlations between ellipticity of the capture orbit

$$n = -\frac{2+\epsilon}{\epsilon} \tag{7-19}$$

periapsis velocity

$$v_P = \sqrt{(2+\epsilon)\frac{K}{r_P}} = \sqrt{\left(1+\frac{n-1}{n+1}\right)\frac{K}{r_P}} \tag{7-20}$$

and numerical eccentricity

$$e = 1 + \epsilon \tag{7-21}$$

which are convenient for capture calculations. The term K in Equation 7-20 designates the gravitational parameter ($K = gr^2$) of the central force field in question. Figure 7-4 shows the correlation between n and ϵ.

For thrust accelerations approximately equal to or higher than the surrounding gravitational acceleration, the concept of impulsive velocity changes provides a good initial approximation. Thus, the well-known relation for impulsive velocity for escape from, or capture into, a circular planetocentric orbit at distance r is, for a given v_∞,

$$\Delta v = \sqrt{\frac{2K}{r} + v_\infty^2} - \sqrt{\frac{K}{r}} \tag{7-22}$$

Or, in terms of v_∞,

$$\frac{\Delta v}{v_\infty} \equiv \frac{\Delta v^*}{v_\infty^*} = \sqrt{1 + \frac{1}{v_\infty^2}\,\frac{2K}{r}} - \frac{1}{v_\infty}\sqrt{\frac{K}{r}} \tag{7-23}$$

where the asterisk indicates that Earth mean orbital speed (EMOS) is used as unit. More generally, Equation 7-23 can be written in the form

$$\frac{\Delta v^*}{v_\infty^*} = \sqrt{1 + \frac{1}{v_\infty^2}\,\frac{2K/r_{oo}}{r/r_{oo}}} - \frac{1}{v_\infty}\sqrt{2 + \epsilon}\sqrt{\frac{K/r_{oo}}{r/r_{oo}}} \tag{7-24}$$

where r_{oo} is the radius of the planet in question and r is the radius or the periapsis distance of the capture orbit.

Equations 7-23 and 7-24 provide a convenient correlation between v_∞^* (as it follows from the heliocentric mission calculations), the capture impulse, and the capture distance in units of the planet's radius. Figures 7-5 through 7-8 provide graphs for rapid determination of Δv^* for, respectively, Earth escape, Venus capture or escape, Mars capture or escape--all with respect to circular planetocentric orbits--and for Earth capture to slightly subparabolic velocity ($\epsilon = -0.04$).

The thrust/weight ratio is based on expected thrust values of the nuclear or chemical engines involved. For various finite values of $(F/W)_o$ the powered escape flight path was determined on the electronic computer using, for the sake of simplicity, the well-known equations for powered flight at tangential thrust in a central force field rather

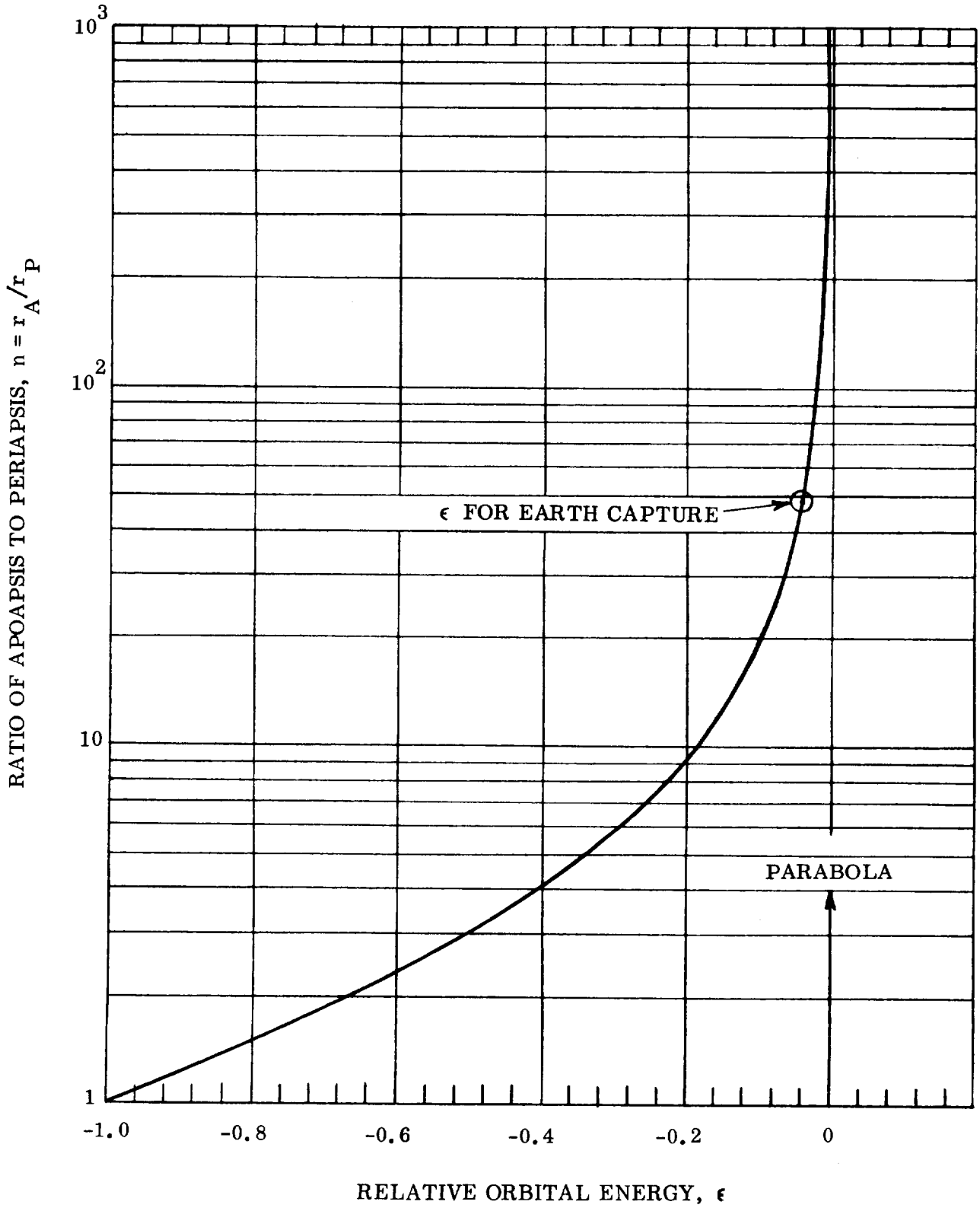

Figure 7-4. Correlation Between n and ϵ

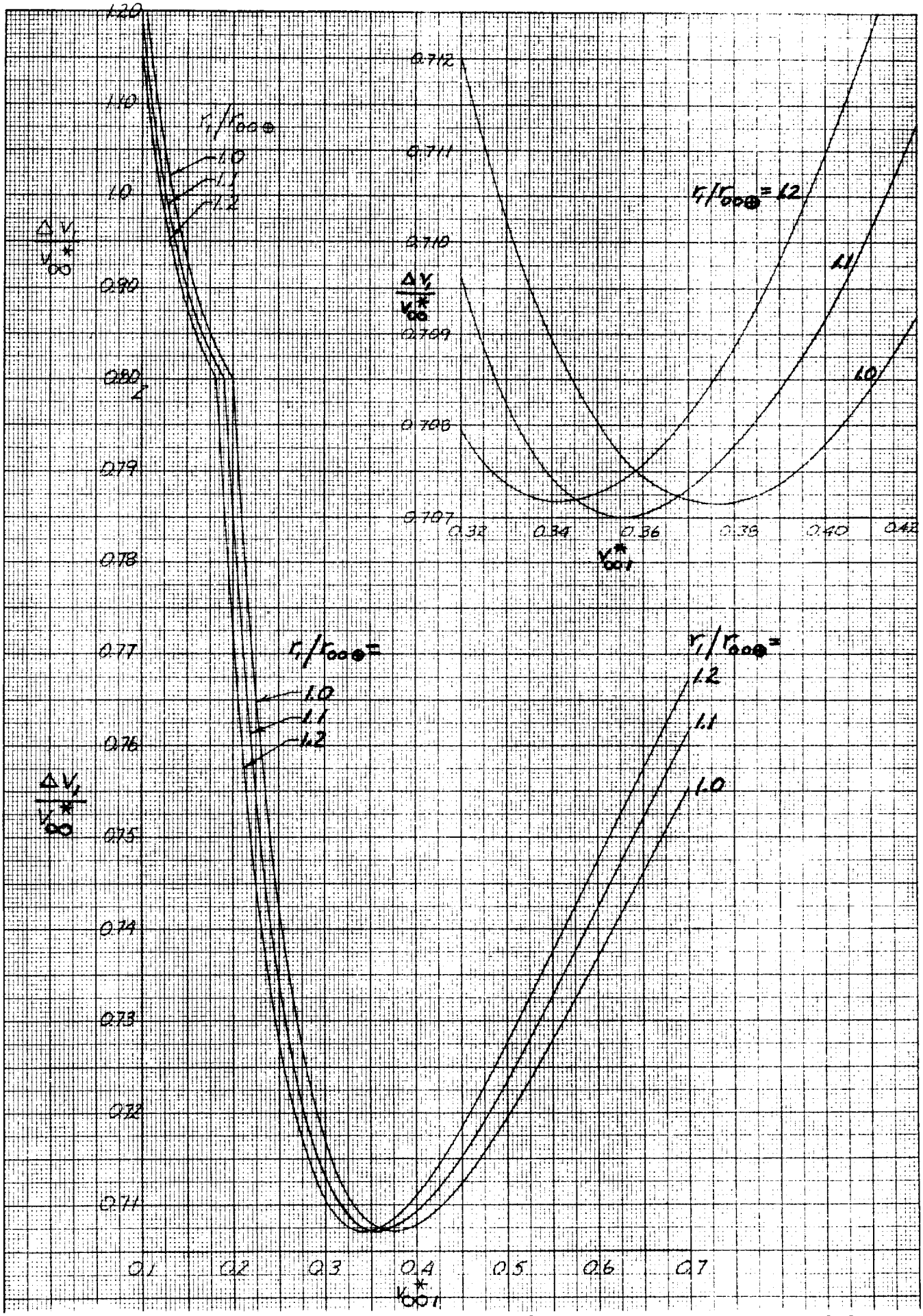

Figure 7-5. Non-dimensional Earth Departure Velocity Increment Versus Hyperbolic Excess Velocity for Several Earth Orbit Distances

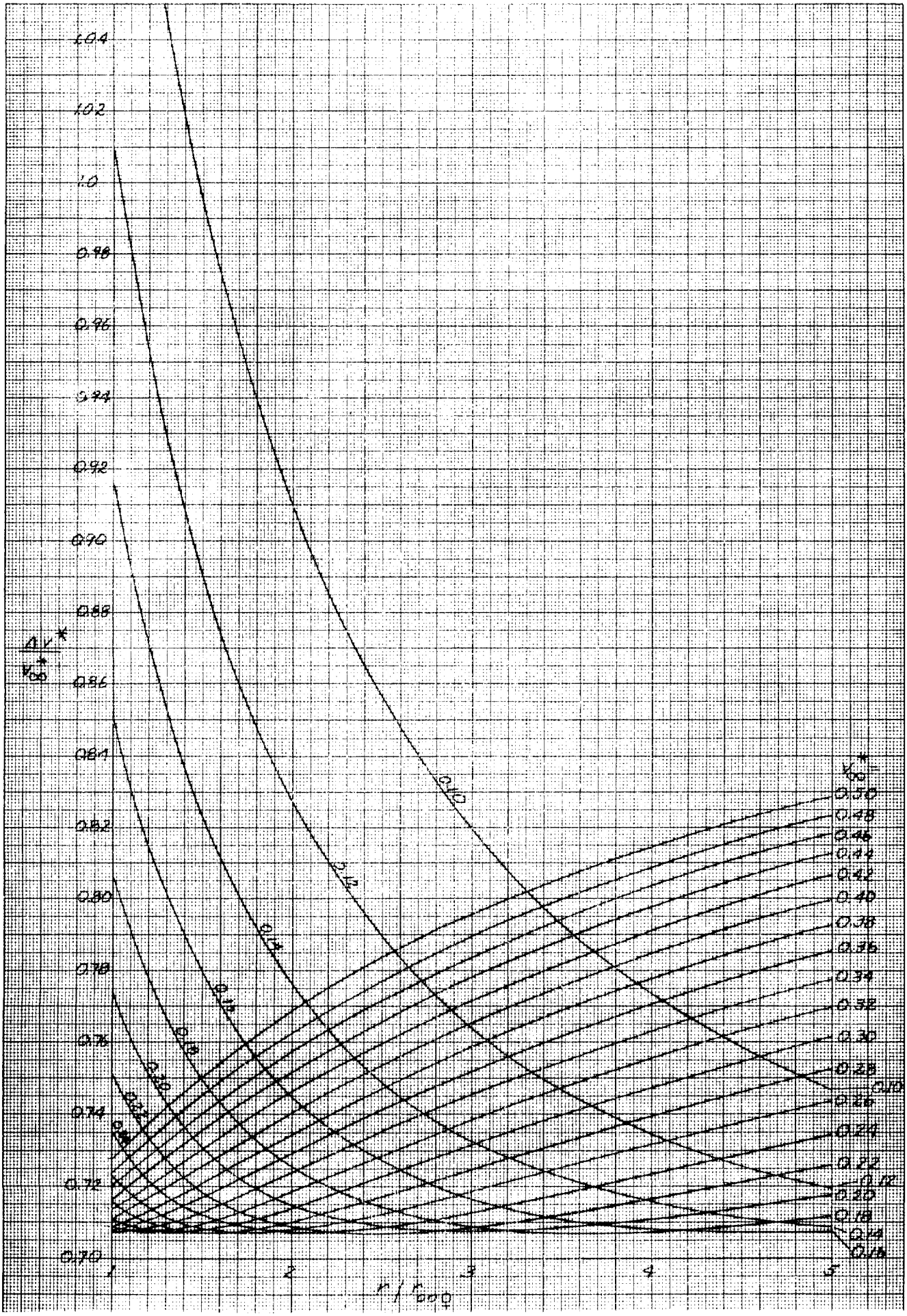

Figure 7-6. Capture and Escape Impulse Requirement for Venus To and From Circular Satellite Orbits as a Function of Orbit Distance and Hyperbolic Excess Velocity

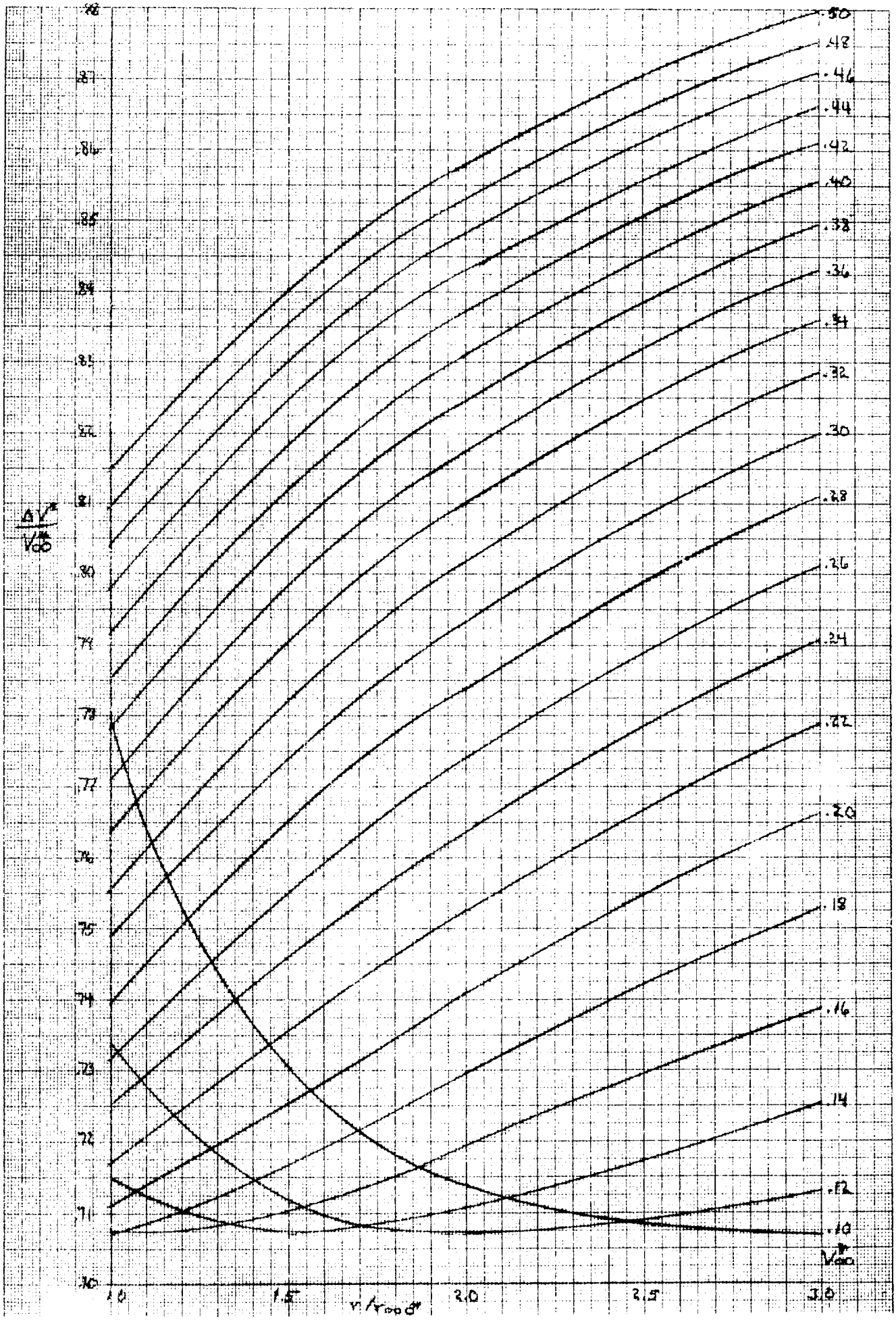

Figure 7-7. Capture and Escape Impulse Requirement for Mars To and From Circular Satellite Orbits as a Function of Orbit Distance and Hyperbolic Excess Velocity

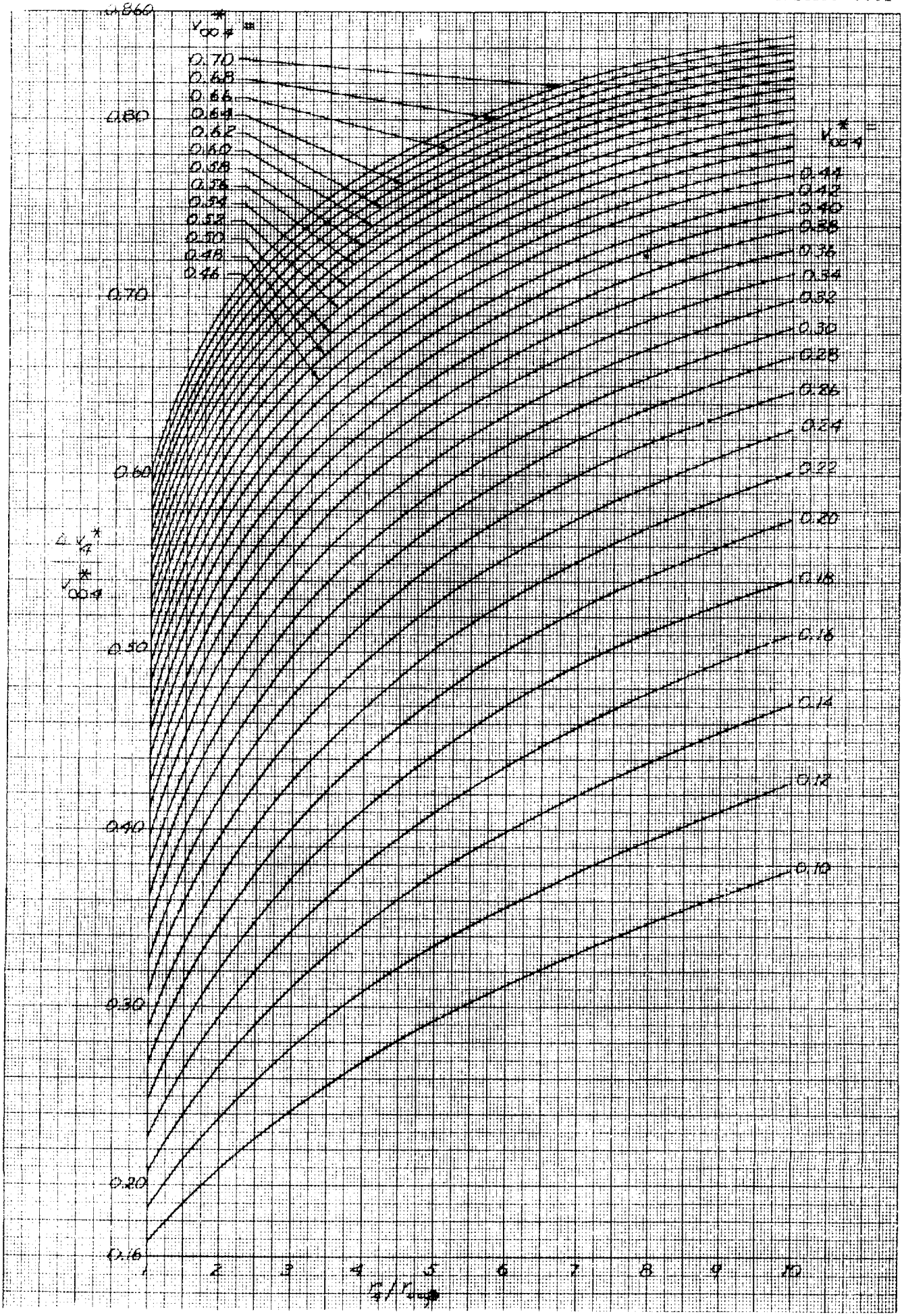

Figure 7-8. Impulse Requirement for Near-Paeabolic Earth Capture as a Function of Distance of Capture Maneuver and Hyperbolic Excess

than optimized thrust direction. A large variety of thrust-to-weight ratios, of specific impulses, and of relative orbital energies was used in these computations. The resulting value of mass ratio and powered flight time were plotted against the hyperbolic excess to provide an immediate correlation between the mission map data and the performance data. A number of results are plotted in Figures 7-9 through 7-65, which have been grouped at the end of this section (pages 7-59 through 7-115). In order to facilitate the use of these charts, a survey is presented in Table 7-5.

For capture, the powered flight phase slows the vehicle down to the planetocentric velocity

$$v = \sqrt{(2 + \epsilon)\ \frac{K}{r + y}} \qquad (7\text{-}25)$$

In the case of Venus and Mars, this terminal velocity was attained at horizontal flight direction at the prescribed altitude and for $\epsilon = -1$. In the case of Earth, terminal velocity (i.e., burnout) of the near-parabolic orbit ($\epsilon = -0.04$) was placed at a 1000-km altitude. The burnout angle was determined by the requirement that the osculating orbit entered at the cut-off point should have a perigee altitude of 60 km, if it were unperturbed by drag. In all cases of capture, the powered flight path was computed backward from the fixed burnout conditions to a wide range of hyperbolic excess velocities, using tangential thrust for reasons of simplicity. Since, for capture, the burnout thrust/weight ratio $(F/W)_1$ was fixed, the initial acceleration was thus obtained as a function of the hyperbolic excess velocity.

During the initial phase of the study (Mariner II information not yet available), the possibility of a strong circum-Venusian radiation belt was considered more probable and therefore two capture conditions were studied for Venus. One capture orbit was close to the Venus surface, the other was outside a hypothetical radiation belt at a capture distance of 20 Venus radii (128,000 km). Since the latter case requires somewhat more energy in most cases than capture at close Venus distance (cf. Figure 7-6), the values for capture to and escape from 128,000 km distance from Venus are presented in the charts. For Mars, a distance of 1.3 radii, corresponding to an altitude of about 1000 km, was selected.

The mass ratio required for the main maneuver can therewith be computed on the basis of Figures 7-5 through 7-8 or with the aid of Figures 7-9 through 7-65, either directly or by interpolation. Nuclear propulsion systems were assumed in all charts, except for the Earth capture maneuver, where nuclear and chemical systems are covered.

Table 7-5. Survey of Powered Maneuver Charts, Figures 7-9 through 7-65

FIGURE	MANEUVER	(F/W)	ϵ	I_{SP} (SEC)
7-9	Earth escape	$(F/W)_o = 0.3$	-1.0	829, 836, 843, 850
7-10	Earth escape	0.4	-1.0	829, 836, 843, 850
7-11	Earth escape	0.5	-1.0	829, 836, 843, 850
7-12	Venus capture	$(F/W)_1 = 0.2$	-1.0	820, 860, 900
7-13	(128,000 km = 20 $r_{oo,♀}$)	0.2	-0.9	820, 860, 900
7-14	(128,000 km = 20 $r_{oo,♀}$)	0.2	-0.8	820, 860, 900
7-15	(128,000 km = 20 $r_{oo,♀}$)	0.2	-0.7	820, 860, 900
7-16	(128,000 km = 20 $r_{oo,♀}$)	0.4	-1.0	820, 860, 900
7-17	(128,000 km = 20 $r_{oo,♀}$)	0.4	-0.9	820, 860, 900
7-18	(128,000 km = 20 $r_{oo,♀}$)	0.4	-0.8	820, 860, 900
7-19	(128,000 km = 20 $r_{oo,♀}$)	0.4	-0.7	820, 860, 900
7-20	(128,000 km = 20 $r_{oo,♀}$)	0.8	-1.0	820, 860, 900
7-21	(128,000 km = 20 $r_{oo,♀}$)	0.8	-0.9	820, 860, 900
7-22	(128,000 km = 20 $r_{oo,♀}$)	0.8	-0.8	820, 860, 900
7-23	(128,000 km = 20 $r_{oo,♀}$)	0.8	-0.7	820, 860, 900
7-24	Venus escape	$(F/W)_o = 0.2$	-1.0	820, 860, 900
7-25	(128,000 km = 20 $r_{oo,♀}$)	0.2	-0.9	820, 860, 900
7-26	(128,000 km = 20 $r_{oo,♀}$)	0.2	-0.8	820, 860, 900
7-27	(128,000 km = 20 $r_{oo,♀}$)	0.2	-0.7	820, 860, 900
7-28	(128,000 km = 20 $r_{oo,♀}$)	0.4	-1.0	820, 860, 900
7-29	(128,000 km = 20 $r_{oo,♀}$)	0.4	-0.9	820, 860, 900
7-30	(128,000 km = 20 $r_{oo,♀}$)	0.4	-0.8	820, 860, 900
7-31	(128,000 km = 20 $r_{oo,♀}$)	0.4	-0.7	820, 860, 900
7-32	(128,000 km = 20 $r_{oo,♀}$)	0.8	-1.0	820, 860, 900
7-33	(128,000 km = 20 $r_{oo,♀}$)	0.8	-0.9	820, 860, 900

Table 7-5. Survey of Powered Maneuver Charts, Figures 7-9 through 7-65 (Continued)

FIGURE	MANEUVER	(F/W)	ϵ	I_{SP} (SEC)
7-34	(128,000 km = 20 $r_{oo,♀}$)	$(F/W)_o$ = 0.8	-0.8	820, 860, 900
7-35	(128,000 km = 20 $r_{oo,♀}$)	0.8	-0.7	820, 860, 900
7-36	Mars capture	$(F/W)_1$ = 0.2	-1.0	820, 860, 900
7-37	(1.3 $r_{oo,♂}$)	0.2	-0.8	820, 860, 900
7-38	(1.3 $r_{oo,♂}$)	0.2	-0.6	820, 860, 900
7-39	(1.3 $r_{oo,♂}$)	0.2	-0.4	820, 860, 900
7-40	(1.3 $r_{oo,♂}$)	0.4	-1.0	820, 860, 900
7-41	(1.3 $r_{oo,♂}$)	0.4	-0.8	820, 860, 900
7-42	(1.3 $r_{oo,♂}$)	0.4	-0.6	820, 860, 900
7-43	(1.3 $r_{oo,♂}$)	0.4	-0.4	820, 860, 900
7-44	(1.3 $r_{oo,♂}$)	1.2	-1.0	820, 860, 900
7-45	(1.3 $r_{oo,♂}$)	1.2	-0.8	820, 860, 900
7-46	(1.3 $r_{oo,♂}$)	1.2	-0.6	820, 860, 900
7-47	(1.3 $r_{oo,♂}$)	1.2	-0.4	820, 860, 900
7-48	Mars escape	$(F/W)_o$ = 0.2	-1.0	820, 860, 900
7-49	(1.3 $r_{oo,♂}$)	0.2	-0.8	820, 860, 900
7-50	(1.3 $r_{oo,♂}$)	0.2	-0.6	820, 860, 900
7-51	(1.3 $r_{oo,♂}$)	0.2	-0.4	820, 860, 900
7-52	(1.3 $r_{oo,♂}$)	0.4	-1.0	820, 860, 900
7-53	(1.3 $r_{oo,♂}$)	0.4	-0.8	820, 860, 900
7-54	(1.3 $r_{oo,♂}$)	0.4	-0.6	820, 860, 900
7-55	(1.3 $r_{oo,♂}$)	0.4	-0.4	820, 860, 900
7-56	(1.3 $r_{oo,♂}$)	0.8	-1.0	820, 860, 900
7-57	(1.3 $r_{oo,♂}$)	0.8	-0.8	820, 860, 900
7-58	(1.3 $r_{oo,♂}$)	0.8	-0.6	820, 860, 900
7-59	(1.3 $r_{oo,♂}$)	0.8	-0.4	820, 860, 900

Table 7-5. Survey of Powered Maneuver Charts, Figures 7-9 through 7-65, (Continued)

FIGURE	MANEUVER	(F/W)	ϵ	I_{SP} (SEC)
7-60	Earth capture	$(F/W)_1 = 0.3$	-0.04	820, 860, 900
7-61	(ϵ = -0.04)	0.4	-0.04	820, 860, 900
7-62	(ϵ = -0.04)	0.8	-0.04	820, 860, 900
7-63	(ϵ = -0.04)	3.0	-0.04	440, 460, 480
7-64	(ϵ = -0.04)	4.0	-0.04	440, 460, 480
7-65	(ϵ = -0.04)	5.0	-0.04	440, 460, 480

If computed on the basis of Figures 7-5 through 7-8, the implication that velocity change is impulsive (i.e., low gravitational losses) must be reasonably well fulfilled. For example, the initial thrust-to-weight ratio should be at least 0.3 (in local g's at the departure point) if $0.1 < v_\infty^* < 0.4$; for larger v_∞^*, the minimum initial thrust-to-weight ratio should be higher if it is to qualify for approximation as an impulsive maneuver. Requirements for specific cases can easily be established by comparing the mass ratios as functions of initial thrust/weight ratio. For capture maneuvers the initial thrust/weight ratio follows from $(F/W)_1 \times \mu$. The mass ratio is given by

$$\mu_n = \exp\left(\frac{\Delta v_n^*}{v_{\infty n}^*} \quad \frac{U_{\oplus,a}\, v_{\infty n}^*}{g_{oo}\, I_{sp,n}}\right) \qquad (n = 1,2,3,4) \qquad (7\text{-}26)$$

Where $\Delta v^*/v_\infty^*$ follows from Figures 7-5 through 7-8 for the desired circular capture distance, v_∞^* follows from the selected mission profile, Earth mean orbital speed, $U_{\oplus,a}$, is listed in Table 2-1 and g_{oo} is the Earth-based mass-force conversion factor.

Even if near-impulsive conditions are not given, Figures 7-5 through 7-8 are useful for comparative purposes.

If Figures 7-9 through 7-65 are used, the mass ratio contains, of course, the gravitational losses. The corresponding ideal velocity, characterizing the particular maneuver, is

$$\Delta v_{id,n} = g_{oo}\, I_{sp,n}\, \ell n\, \mu_n \qquad (n = 1,2,3,4) \qquad (7\text{-}27)$$

If it is desired to estimate the effect of a different specific impulse than those associated with the curves shown, the following relation can be used for the difference in burning time:

For escape

$$\frac{t_1}{t_2} = \frac{I_{sp\,1}}{I_{sp\,2}} \frac{1 - \exp\left(-\frac{\sqrt{K/a_o}}{g_{oo}\, I_{sp\,1}}\right)}{1 - \exp\left(-\frac{\sqrt{K/a_o}}{g_{oo}\, I_{sp\,2}}\right)} \qquad (7\text{-}28)$$

and for capture

$$\frac{t_1}{t_2} = \frac{I_{sp\,1}}{I_{sp\,2}} \frac{\exp\left(-\frac{\sqrt{K/a_1}}{g_{oo}\, I_{sp\,1}}\right)^{-1}}{\exp\left(-\frac{\sqrt{K/a_1}}{g_{oo}\, I_{sp\,2}}\right)^{-1}} \qquad (7\text{-}29)$$

where K is the gravitational parameter of the respective planetocentric field, and a_o and a_1 are the semi-major axes of the near-circular initial or terminal capture orbits, respectively. From the new burning time, and the known mass flow rate, the new mass ratio can be computed.

7.4 EQUIVALENT MASS RATIO FOR LOSSES AND CONTINGENCIES. To provide a contingency for losses until a more refined analysis is made, the following mass ratio equivalents for losses were assumed for maneuvers M-1 through M-4. Roughly, μ_ℓ = 1.005, 1.01, 1.02, 1.025 and 1.03, corresponds to losses of 0.5, 1, 2, 2.5 and 3 percent of useful propellant in the tank systems associated with each of these maneuvers. Because the vehicles are assumed to be equipped with a hydrogen re-liquefaction capability, the assumptions for the M-2, M-3 and M-4 tanks appear to be conservative (aside from possible losses due to meteorite damage) since, in the case of a convoy vehicle equipped with a metal-carbide reactor which is started repeatedly, even the post-cutoff cooling hydrogen for the engine is not lost but is planned to be recycled into the nearest loaded hydrogen tank whose heat capacity acts as buffer for the liquefaction unit.

The velocity equivalent of these mass ratios depends on the specific impulse. Figure 7-66 correlates μ with τ/I_{sp} where $\tau = \Delta v_{id}/g_{oo}$ is correlated with Δv_{id} (in m/sec or ft/sec) in Figure 7-67. For mass ratios of less than 1.03 it is, with good accuracy,

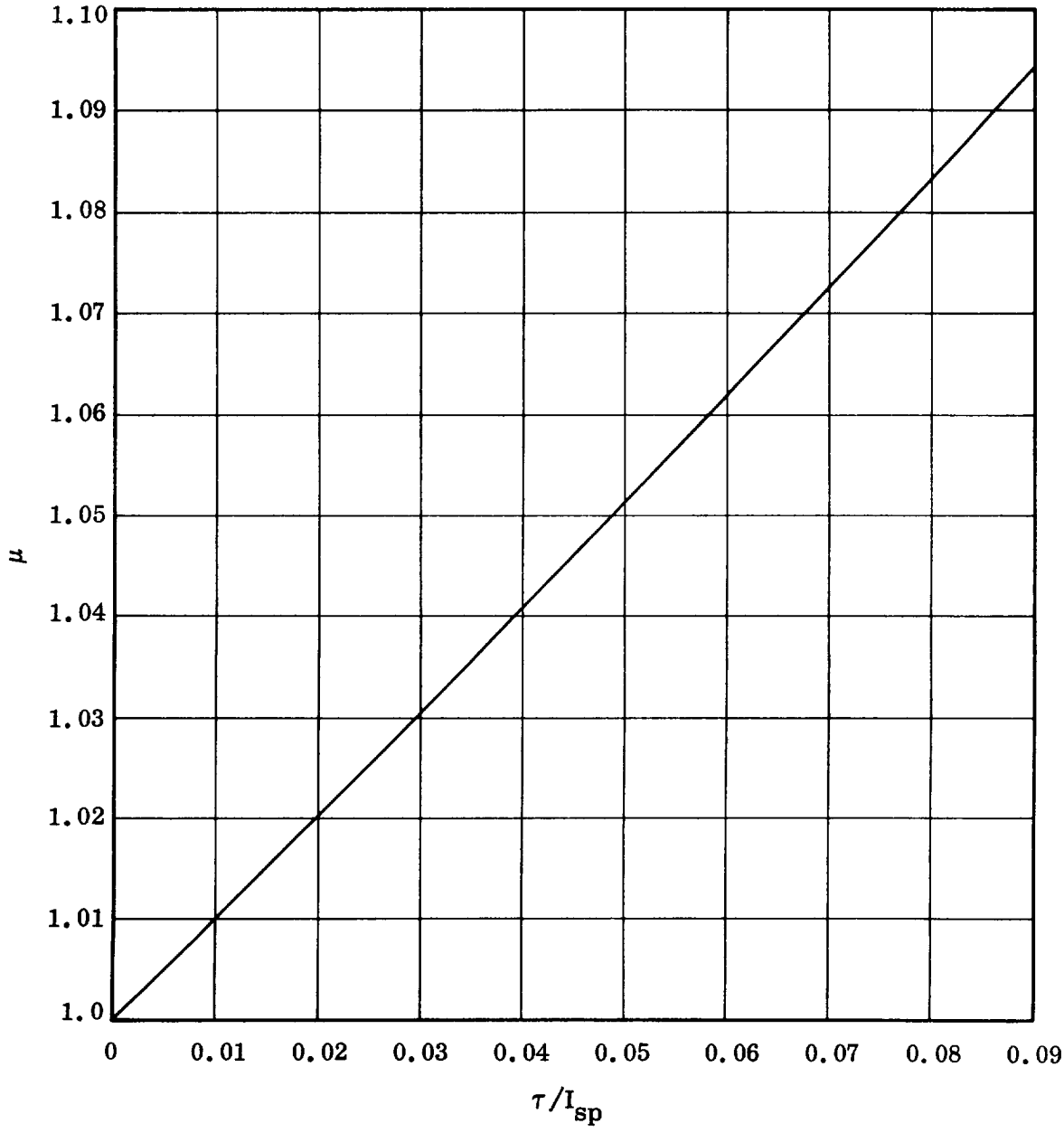

Figure 7-66. Mass Ratio Versus τ/I_{sp} for Small Velocity Changes

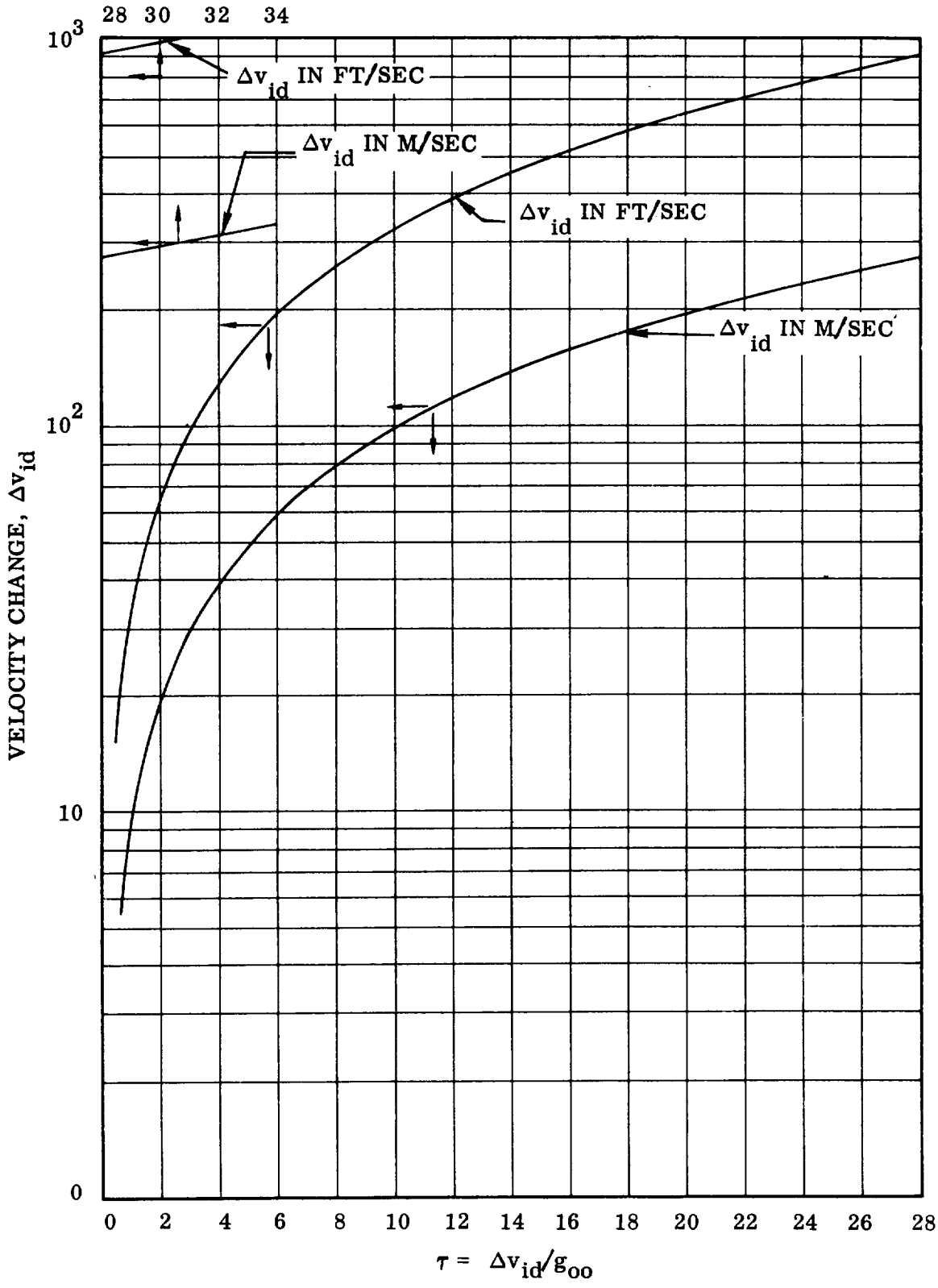

Figure 7-67. Correlation Between Δv_{id} and τ

$\tau = \mu - 1$. For a nuclear vehicle with $I_{sp\,1} = 846$ sec and $I_{sp\,2} = I_{sp\,3} = I_{sp\,4} = 900$ sec, the above values of μ_ℓ correspond to a total velocity loss of 807 m/sec (2650 ft/sec). For a chemo-nuclear vehicle with $I_{sp\,1} = I_{sp\,2} = 846$ sec, $I_{sp\,3} = 820$ sec, and $I_{sp\,4} = 455$ sec, the total equivalent velocity loss is 623 m/sec (2050 ft/sec). These velocities correspond to two to three percent of the total mission velocity.

7.5 MASS RATIO FOR NAVIGATIONAL CORRECTIONS. Pending a more accurate computation of navigational requirements for specific missions, a total velocity of 305 m/sec (1000 ft/sec) has been set aside for all navigational path corrections during the mission. This includes, primarily, navigational corrections during outbound and return transfer (approximately 100 m/sec each) and post-cutoff corrections in the capture orbit. Not included are propellant expenditures for potential plane changes in the capture orbit. These are covered by $\mu_{p\ell}$ (discussed below). The velocity mentioned above corresponds to a mass ratio of 1.035 for $I_{sp} = 900$ sec and to $\mu_{corr} = 1.071$ for 455 sec. The velocity change set aside for path-correction maneuvers corresponds to 1.2 to 1.5 percent of the total mission velocity.

7.6 MASS RATIO FOR PLANE CHANGES IN THE SATELLITE ORBIT. To establish a given inclination of the heliocentric transfer orbit plane with respect to the Planet's orbit plane, first consider the orbit plane of the planet, of which the space ship is a satellite, as the reference plane. Let β be the planar intersection angle of the heliocentric departure vector V with the planet's velocity vector U, and let i_t be the inclination of the heliocentric transfer orbit (Figure 7-68a). The associated hyperbolic excess velocity is

$$v_\infty = \sqrt{U^2 + V^2 - 2UV \cos\beta \cos i_t} \qquad (7\text{-}30)$$

In order to assure correct magnitude of the hyperbolic excess velocity, a departure velocity

$$v_1 = \sqrt{v_p^2 + v_\infty^2} \qquad (7\text{-}31)$$

must be attained (v_p is the local parabolic velocity). To assure correct orientation of the hyperbolic excess vector, v_1 must originate at a particular true anomaly in the satellite orbit whose plane must be properly oriented (Figure 7-68b). If the plane deviated by an angle δ, there would be only two points (a and a 180°-opposite point) where the effect of δ would not be noticeable. These points are 90 degrees off the nodal line along which the correctly and the incorrectly oriented orbits intersect. It is very improbable that these points are at the correct true anomaly. As a result, wrong orientation of the satellite orbit plane and departure at the wrong true anomaly will cause β and i_t to change. It can be assumed that departure at the correct true

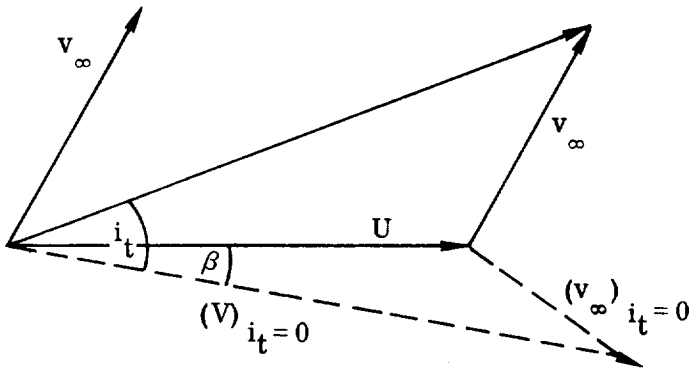

(a)

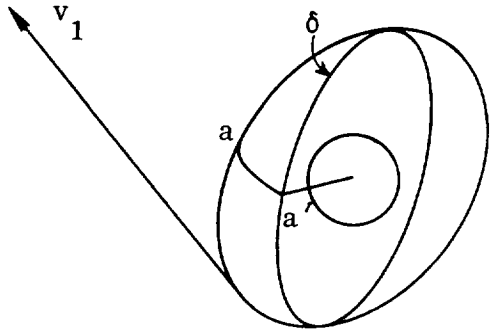

(b)

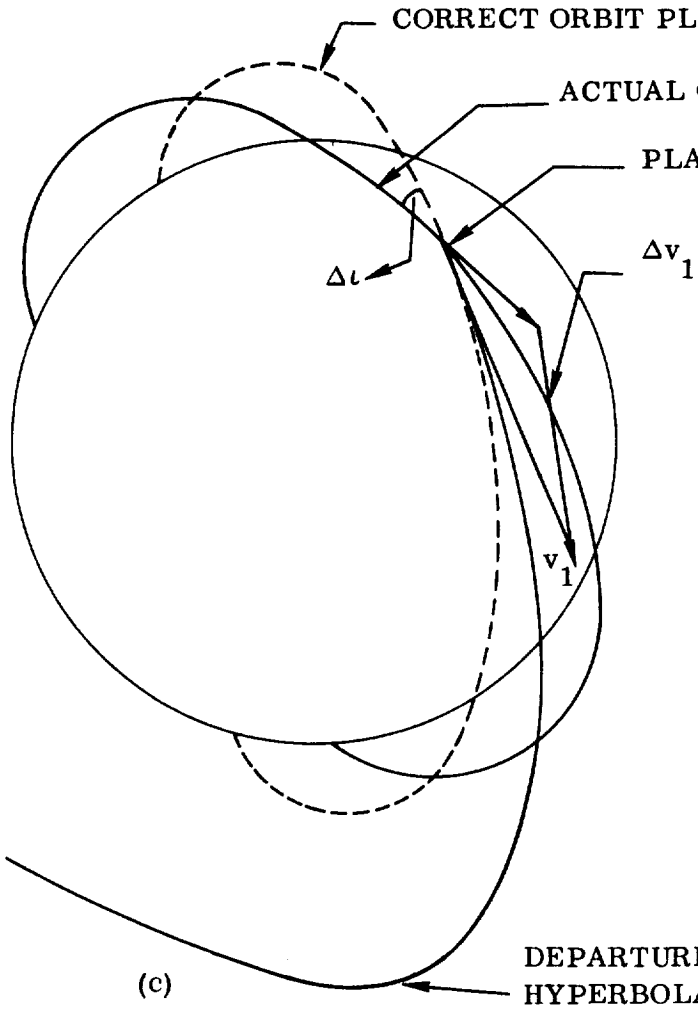

(c)

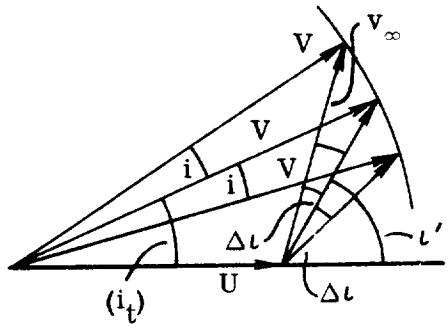

(d)

Figure 7-68. Nomenclature for the Analysis of Plane Change Requirements at Planet Departure

anomaly can be achieved with high accuracy. It is, however, less certain that the satellite orbit plane is correctly oriented. This is true not only for the Earth launch orbit, but particularly for the target planet capture orbit.

Now consider the instantaneous satellite orbit plane as the reference plane, and the associated values of β and i_t as reference values. Then, if the orbit plane orientation is in error, β and i_t (or either one of them alone) are incorrect if the space ship is launched in the plane of the satellite orbit. Therefore, the instantaneous plane of the satellite orbit must be changed during departure to coincide with the correct plane of the satellite orbit, which is the plane in which the departure hyperbola lies (Figure 7-68c). The resulting departure impulse is

$$\Delta v_1 = \sqrt{v_0^2 + v_1^2 - 2v_0 v_1 \cos \Delta\iota} \tag{7-32}$$

The actual velocity by which the vehicle's mass ratio is penalized, compared to departure from the correct orbit plane ($\Delta\iota = 0$), is

$$\begin{aligned} \Delta\Delta v_\iota &= \sqrt{v_0^2 + v_1^2 - 2v_0 v_1 \cos \Delta\iota} - (v_1 - v_0) \\ &= \Delta v_1 - (\Delta v_1)_{\Delta\iota = 0} \end{aligned} \tag{7-33}$$

For a given value of $\Delta\iota$, the penalty decreases with decreasing v_0/v_1 (i.e., with increasing v_∞).

Equation 7-33 requires that $\Delta\iota$ and v_1 be known. If (i_t) is the incorrect transfer inclination (Figure 7-68d), and ι' the associated satellite-orbit inclination with respect to the planet's orbit plane, then

$$\tan \iota' = - \frac{V \sin (i_t)}{U - V \cos (i_t)} \tag{7-34}$$

The correct transfer inclination may be $(i_t \pm i)$. The resulting satellite orbit inclination is

$$\tan (\iota' \pm \Delta\iota) = - \frac{V \sin (i_t \pm i)}{U - V \cos (i_t \pm i)} \tag{7-35}$$

The corresponding values of v_∞ are

$$\left.\begin{aligned} (v_\infty)_{(i_t)} &= \frac{V - U}{\cos \varphi} \\ \varphi &= \tan^{-1}\left[\frac{2\sqrt{UV}}{V-U} \sin\frac{1}{2}(i_t)\right] \end{aligned}\right\} \quad (7\text{-}36)$$

and

$$\left.\begin{aligned} (v_\infty)_{(i_t \pm i)} &= \frac{V - U}{\cos \varphi} \\ \varphi &= \tan^{-1}\left[\frac{2\sqrt{UV}}{V-U} \sin\frac{1}{2}(i_t \pm i)\right] \end{aligned}\right\} \quad (7\text{-}37)$$

Thus, for the case of (i_t),

$$\left.\begin{aligned} (\Delta v_1)_{(i_t)} &= v_1 - v_0 \\ v_1 &= \sqrt{v_p^2 + (v_\infty^2)_{(i_t)}} \end{aligned}\right\} \quad (7\text{-}38)$$

and for the case of $(i_t \pm i)$

$$\left.\begin{aligned} (\Delta v_1)_{(i_t \pm i)} &= \sqrt{v_0^2 + v_1^2 - 2 v_0 v_1 \cos \Delta\iota} \\ v_1 &= \sqrt{v_p^2 + (v_\infty^2)_{(i_t \pm i)}} \end{aligned}\right\} \quad (7\text{-}39)$$

Therewith $\Delta\Delta v_\iota$ can be found from Equation 7-33.

The velocity associated with a change in the transfer plane can be found by the angle in a more direct manner, without determining $\Delta\iota$. Again using the transfer inclination obtained by launching in the instantaneous satellite orbit plane as the reference value, and i as the transfer plane change which requires non-planar launch from the satellite orbit, the velocity increment due to plane change i is

$$\Delta v_i^* = \sqrt{v_p^{*2} + U^{*2} + V^{*2} - 2\,U^*\,V^*\cos\beta\cos i}$$

$$- \sqrt{v_p^{*2} + U^{*2} + V^{*2} - 2\,U^*\,V^*\cos\beta} \qquad (7\text{-}40)$$

$$= \sqrt{v_p^{*2} + v_\infty^{*2}} - \sqrt{v_p^{*2} + \left[v_\infty^{*2}\right]_{i=0}}$$

The value Δv_i^* has been computed for Earth, Venus and Mars for a large number of conditions (Figures 7-69 through 7-88 located at the end of Section 7). These graphs can be used to rapidly determine the amount of plane change which a given Δv_i^* buys. For example, on 12-24-1975, the Mars departure conditions for T_2 = 220 d are:

$$V_3^* = 0.7182 \qquad \text{and} \qquad \beta_3 = -15.54°.$$

For these values, Figure 7-85 shows that for $\Delta v_i^* = 0.05$ ($\Delta v_i \approx 1.64$ km/sec = 5000 ft/sec) the capture orbit plane could be allowed to be off by as much as 23° from its correct position. The effect of the heliocentric departure velocity V_3^* on this value is small for otherwise similar conditions. For a high-altitude orbit about Venus (Figure 7-71), the same velocity yields a smaller tolerance ($i \sim 11°$ for $\beta \sim 15°$); but, here again, this value is fairly characteristic for practical variations of V_3^*. Without pre-judging, at this point, the significance of the guidance aspects involved, a velocity change of 1.64 km/sec (5000 ft/sec) has tentatively been allowed for plane-change maneuvers in the capture orbits around Venus and Mars. These velocity changes correspond to the mass ratios

$$\mu_{p\ell} = 1.202 \text{ for } I_{sp} = 846 \text{ sec}$$

$$= 1.21 \text{ for } I_{sp} = 820 \text{ sec.}$$

7.7 MASS RATIOS FOR MISSION WINDOWS EARTH-VENUS 1973-1 AND EARTH-MARS 1973-1, 1973-2, 1973-3 AND 1975-1. With the previously defined mass ratios, the mass ratios for the four main maneuvers (determining the fuel tank layout for the individual propulsion sections) were obtained and are listed in Tables 7-6 through 7-10. A shortened version of these tables appears in Section 6.

Table 7-6. Earth ⇄ Venus Mission Window 1973-1

Earth Departure Window	10-25-73 through 11-16-73
Arrive Venus	2-17-74
Transfer Periods	$115 \geq T_1 \geq 93$ d
Venus Departure Window	2-17-74 through 3-25-74
Transfer Periods	$244 \leq T_2 \leq 280$ d
Maximum Capture Period, T_{cpt}	36 d
Mission Periods	115 + 36 + 280 = 431 (Maximum)
	93 + 36 + 280 = 409 (Min. for Max. T_{cpt})
	115 (93) + 30 + 269 = 441 (392) d
	115 (93) + 20 + 259 = 394 (372) d
	115 (93) + 10 + 244 = 369 (347) d

Perihelion Distances: Outgoing T. O.: No perihelion transits
Return T. O.: Rp > 0.7

MANEUVER	M-1	M-2		M-3		M-4		TOTAL (MISSION)	
v_∞^*	0.13	0.21		0.18		0.29		0.81	
	-1.0	-1.0		-1.0		-0.04			
F/W	0.3	0.2	0.8	0.4	0.8	0.8	3.0		
I_{sp}	846	900	846	900	820	900	455		
Δv (km/sec)	3.85	4.79	4.7	4.16	3.78	3.37	3.25	16.17	15.58
(ft/sec)	12,600	15,700	15,400	13,630	12,400	11,070	10,660	53,000	51,060
μ	1.59	1.721	1.76	1.6	1.6	1.43	2.02	6.261	9.044
μ_ℓ	1.005	1.02	1.02	1.025	1.025	1.03	1.03	1.0225	1.0225
μ_{corr}		1.035				1.035	1.071[2]	1.0612	1.1470
μ_{pl}				1.19	1.21			1.19	1.21
μ'	1.597	1.817	1.795	1.95	1.984	1.56	2.44	8.827	13.877
Nucl. Eng. Reactor	Graph.	Metal	Graph.	Metal	Graph.	Metal	(O_2/H_2)		
Vehicle	A_1, B_1	A_2	B_2	A_3	B_3	A_4	B_4	A_{tot}	B_{tot}

Table 7-7. Earth ⇄ Mars Mission Window 1973-1

Earth Departure Window	2-17-73 through 3-7-73
Arrive Mars	9-25-73
Transfer Periods	$220 \geq T_1 \geq 202$
Mars Departure Window	9-25-73 through 11-3-73
Transfer Periods	$170 \leq T_2 \leq 210$ d
Maximum Capture Period, T_{cpt}	39 d
Mission Periods	220 + 39 + 210 = 469 d (Maximum)
	202 + 39 + 210 = 451 d (Min. for Max. T_{cpt})
	220 (202) + 30 + 203 = 453 (435) d
	220 (202) + 20 + 196 = 436 (418) d
	220 (202) + 10 + 191 = 421 (403) d

Perihelion Distances: Outgoing T.O.: $0.82 \leq R_p \leq 0.85$
Return T.O.: $0.9 > R_p \geq 0.835$

MANEUVER	M-1	M-2		M-3		M-4		TOTAL (MISSION)	
v_∞^*	0.20	0.29		0.29		0.29		1.07	
ϵ	-1.0	-1.0		-1.0		-0.04			
F/W	0.3	0.08	0.3	0.1	0.4	0.8	0.3		
I_{sp}	846	900	846	900	820	900	455		
Δv (km/sec)	4.78	7.54	7.06	6.63	6.70	3.37	3.25	22.32	21.79
(ft/sec)	15,710	24,760	23,160	21,780	22,000	11,070	10,660	73,320	71,530
μ	1.78	2.35	2.34	2.12	2.3	1.46	2.07	12.947	19.831
μ_ℓ	1.005	1.01	1.01	1.015	1.015	1.02	1.02	1.0509	1.0509
μ_{corr}		1.035				1.035	1.071[2]	1.0612	1.1470
$\mu_{p\ell}$				1.19	1.21			1.19	1.21
μ'	1.79	2.455	2.361	2.56	2.825	1.541	2.424	17.336	28.940
Nucl. Eng. Reactor	Graph.	Metal	Graph.	Metal	Graph.	Metal	(O_2/H_2)		
Vehicle	A_1, B_1	A_2	B_2	A_3	B_3	A_4	B_4	A_{tot}	B_{tot}

Table 7-8. Earth ⇄ Mars Mission Window 1973-2

Earth Departure Window	5-18-73 through 6-17-73
Arrive Mars	11-4-73
Transfer Periods	$170 \geq T_1 \geq 150$ d
Mars Departure Window	11-4-73 through 12-24-73
Transfer Periods	$205 \leq T_2 \leq 223$
Maximum Capture Period, T_{cpt}	50 d
Mission Periods	170 + 50 + 223 = 433 d (Maximum)
	150 + 50 + 223 = 413 d (Min. for Max. T_{cpt})
	170 (150) + 40 + 222 = 432 (412) d
	170 (150) + 30 + 219 = 419 (389) d
	170 (150) + 20 + 216 = 406 (386) d
	170 (150) + 10 + 211 = 391 (371) d

Perihelion Distances: Outgoing T. O.: $0.9 < R_p < 1.0$

Return T. O.: Dep ♂	12-24	12-14	12-4	11-24	11-14
R_p	0.7	0.74	0.762	0.79	0.81

MANEUVER	M-1	M-2		M-3		M-4		TOTAL (MISSION)	
v_∞^*	0.24	0.24		0.3		0.4		1.18	
ϵ	-1.0	-1.0		-1.0		-0.04			
F/W	0.3	0.08	0.3	0.1	0.4	0.8	3.0		
I_{sp}	846	900	846	900	846	900	455		
Δv (km/sec)	5.54	6.12	5.75	7.83	7.01	5.97	5.68	25.46	23.98
(ft/sec)	18,150	20,150	18,850	25,700	24,000	19,600	18,630	83,600	79,630
μ	1.94	2.0	2.0	2.36	2.32	1.96	3.57	18.040	32.301
μ_ℓ	1.005	1.01	1.01	1.015	1.015	1.02	1.02	1.0509	1.0509
μ_{corr}		1.035				1.035	1.071[2]	1.0612	1.1470
$\mu_{p\ell}$				1.19	1.21			1.19	1.21
μ'	1.96	2.091	2.02	2.85	2.85	2.075	4.181	24.237	47.878
Nucl. Eng. Reactor	Graph.	Metal	Graph.	Metal	Graph.	Metal	(O_2/H_2)		
Vehicle	A_1, B_1	A_2	B_2	A_3	B_3	A_4	B_4	A_{tot}	B_{tot}

Table 7-9. Earth ⇄ Mars Mission Window 1973-3

Earth Departure Window	6-6-73 through 7-6-73
Arrive Mars	12-3-73
Transfer Periods	$180 \geq T_1 \geq 150$ d
Mars Departure Window	12-3-73 through 12-24-73
Transfer Periods	$218 \leq T_2 \leq 223$ d
Maximum Capture Period, T_{cpt}	21 d
Mission Periods:	180 + 21 + 223 = 424 d (Maximum)
	150 + 21 + 223 = 394 d (Min. for Max. T_{cpt})
	180 (150) + 10 + 211.5 = 401.5 (371.5) d

Perihelion Distances: Outgoing T. O.: $0.9 < R_p < 1.0$

Return T. O.:

Dep ♂	12-24	12-14	12-4	11-24	11-14
R_p	0.7	0.74	0.762	0.79	0.81

MANEUVER	M-1	M-2		M-3		M-4		TOTAL (MISSION)	
v_∞^*	0.20	0.20		0.3		0.4		1.10	
ϵ	-1.0	-1.0		-1.0		-0.04			
F/W	0.3	0.08	0.3	0.1	0.4	0.8	3.0		
I_{sp}	846	900	846	900	846	900	455		
Δv (km/sec)	4.78	4.68	4.68	7.83	7.01	5.97	5.68	23.26	22.15
(ft/sec)	15,170	15,350	15,350	25,700	24,000	19,600	18,630	75,820	73,150
μ	1.78	1.7	1.7	2.36	2.32	1.96	3.57	13.997	25.063
μ_ℓ	1.005	1.01	1.01	1.015	1.015	1.02	1.02	1.0509	1.0509
μ_{corr}		1.035						1.0612	1.1470
$\mu_{p\ell}$				1.19	1.21			1.19	1.21
μ'	1.079	1.775	1.717	2.85	2.85	2.075	4.181	11.326	22.076
Nucl. Eng. Reactor	Graph.	Metal	Graph.	Metal	Graph.	Metal	(O_2/H_2)		
Vehicle	A_1, B_1	A_2	B_2	A_3	B_3	A_4	B_4	A_{tot}	B_{tot}

Table 7-10. Earth ⇄ Mars Mission Window 1975-1

Earth Departure Window	3-9-75 through 3-29-75
Arrive Mars	11-4-75
Transfer Periods	$240 \geq T_1 \geq 220$ d
Mars Departure Window	12-4-75 through 12-24-75
Transfer Periods	260 d
Maximum Capture Period, T_{cpt}	50 d
Mission Periods:	240 + 50 + 260 = 550 d (Maximum)
	220 + 50 + 260 = 530 d (Min. at Max. T_{cpt})
	240 (220) + 30 + 260 = 530 (510) d
	240 (220) + 10 + 260 = 510 (490) d

Perihelion Distances: Outgoing T.O.: $0.71 \leq R_p \leq 0.82$
Return T.O.: $0.79 \geq R_p \geq 0.71$

MANEUVER	M-1	M-2		M-3		M-4		TOTAL (MISSION)	
v_∞^*	0.3705	0.1774		0.2082		0.3842		1.1403	
ϵ	-1.0	-1.0		-1.0		-0.04			
F/W	0.3	0.08	0.3	0.1	0.4	0.8	3.0		
I_{sp}	846	900	846	900	820	900	455		
Δv (km/sec)	8.44	4.54	4.06	4.68	4.55	5.55	5.24	23.21	22.29
(ft/sec)	27,700	14,890	13,310	15,000	14,950	18,200	17,200	75,790	73,160
μ	2.76	1.67	1.63	1.76	1.76	1.875	3.23	15.210	25.575
μ_ℓ	1.005	1.01	1.01	1.015	1.015	1.02	1.02	1.0509	1.0509
μ_{corr}		1.035				1.035	1.071[2]	1.0612	1.1470
$\mu_{p\ell}$				1.19	1.21			1.19	1.21
μ'	2.774	1.746	1.646	2.126	2.162	1.979	3.778	20.378	37.295
Nucl. Eng. Reactor	Graph.	Metal	Graph.	Metal	Graph.	Metal	(O_2/H_2)		
Vehicle	A_1, B_1	A_2	B_2	A_3	B_3	A_4	B_4	A_{tot}	B_{tot}

The mass ratios are given for two types of vehicles: Vehicle A consists of an escape booster with a graphite reactor system, and a planetary ship with a metal reactor engine of 30,000 to 50,000 lb thrust and 900 sec specific impulse. Vehicle B consists of the same escape booster and a planetary ship which is powered by graphite engines for M-2 and M-3 and by a chemical engine for M-4. In the latter case corrections are assumed to be made by the chemical system, yielding the comparatively large value $\mu_{corr} = 1.147$.

It is of interest to note that the metal reactor, in a number of cases, does not yield a lower mass ratio (μ). This is because higher gravitational losses are accumulated due to the comparatively low thrust/weight ratio and the fairly high values of v_∞^*. These losses nearly balance the gain due to higher specific impulse. Nevertheless, the launch weight of vehicle A is significantly lower than that of vehicle B, because only one comparatively light engine is needed for Maneuvers M-2, M-3, and M-4, in contrast to vehicle B which requires a separate engine (of greater weight than the metal-reactor engine) for each maneuver (cf. Section 8). A discussion of engine selection is presented in the classified Addendum of this report.

7.8 MASS RATIOS FOR AUXILIARY MANEUVERS. Important auxiliary maneuvers not specifically covered above are the spin-up and de-spin maneuvers, the intra-convoy maneuvers by which the path of convoy vehicles is adjusted relative to that of the lead or reference vehicle, and terminal maneuver M-5.

The spin-up and de-spin propellant requirements depend on the vehicle configuration (c.g. location) as well as its mass (both of which determine its moment of inertia), and on the specific impulse. A preliminary determination of propellant weights is presented in Section 11 (cf. Table 11-1) for a particular configuration (8M-14) which is described and depicted in Section 8.

A determination of propellant requirements for intra-convoy maneuvers and for M-5 have not yet been made, but they are small enough to be considered within the general accuracy tolerance of weight determinations at this point of the study.

7.9 HELIOCENTRIC PLANE CHANGE MANEUVER. Transfer orbits which involve a plane change during heliocentric transfer have not been considered in this study.

Figures 7-69 through 7-88 present an estimate of the "cost" (Δv_i^*) of a heliocentric plane change in the activity sphere of a planet. It is important to note that the larger the angle β and the greater the difference between V^* and U^* (i.e., generally, the faster the transfer orbit), the greater can be the plane change i for a given fraction of v_∞.

Generally, it is considerably more efficient to change the transfer orbit inclination in a planetary activity sphere, rather than in heliocentric space. For example, a $\Delta v_i^* = 0.05$ expended during the departure maneuver from Earth, Venus, or Mars "buys" a heliocentric plane change between 20 and 30 degrees in most cases; in heliocentric space it buys a plane change of 4 to 7 degrees. However, if conditions arise in which a planetocentric plane change is several times as large as the plane change to be accomplished at a later point in the heliocentric transfer orbit, it can become energetically more advantageous to carry out a plane change en route. This is generally the case when, by the planetocentric maneuver, a transfer plane change of more than 30 degrees is to be attained.

7-10. REDUCTION OF MISSION PERFORMANCE REQUIREMENTS. The mass ratios for the missions presented in Tables 7-6 through 7-10 are based on capture in circular orbits and comparatively long capture periods. As a result, the mass ratios (hence, the orbital departure weight) are fairly high, considering the high specific impulses used. Measures to reduce performance are discussed in Paragraphs 7-11 through 7-14.

Fly-by missions are a means of reducing the orbital departure weight. However, in this case, important mission objectives, such as optional surface excursion and certain aspects of planetary reconnaissance from orbit, must be sacrificed or curtailed severely (cf. Table 5-3). The stay time in the vicinity of the planet is reduced to a few hours (cf. Figures 6-44 and 6-45).

7.11 PLANAR HELIOCENTRIC MANEUVERS. One alternate heliocentric maneuver should be mentioned. Conditionally, it can result in a reduction in the overall mission energy. It is applicable to cases where a perihelion passage is involved (e.g., during an Earth-Mars return, as illustrated in Figure 7-89). Such orbits may lead to large intersection angles with the Earth orbit and result in correspondingly large v_∞ values (dashed line). By a retro-maneuver during perihelion passage, the intersection angle (θ_4) as well as the heliocentric arrival velocity (V_4) are reduced, leading to a rapid reduction in $v_{\infty 4}$ (hence in the capture energy) or to a corresponding alleviation of hyperbolic entry conditions.

This approach is only conditionally effective, for a number of reasons. First, a penalty has to be paid in terms of a perihelion retro-maneuver. Heliocentric maneuvers are easily (but not necessarily) more expensive than maneuvers in the planetary activity sphere, and must always be approached with caution. Second, the maneuver, as shown in Figure 7-89 is planar. In reality, the transfer orbits are always inclined. Thus, unless the perihelion of the transfer orbit coincides with one of the nodes (i.e., lies in the Earth's ecliptic plane), the perihelion retro-maneuver must also include a plane change to retain a rendezvous course with Earth. This additional requirement could easily wipe out any savings which may be indicated on the basis of the planar maneuver. Another factor is that the decision to carry out a perihelion retro-maneuver

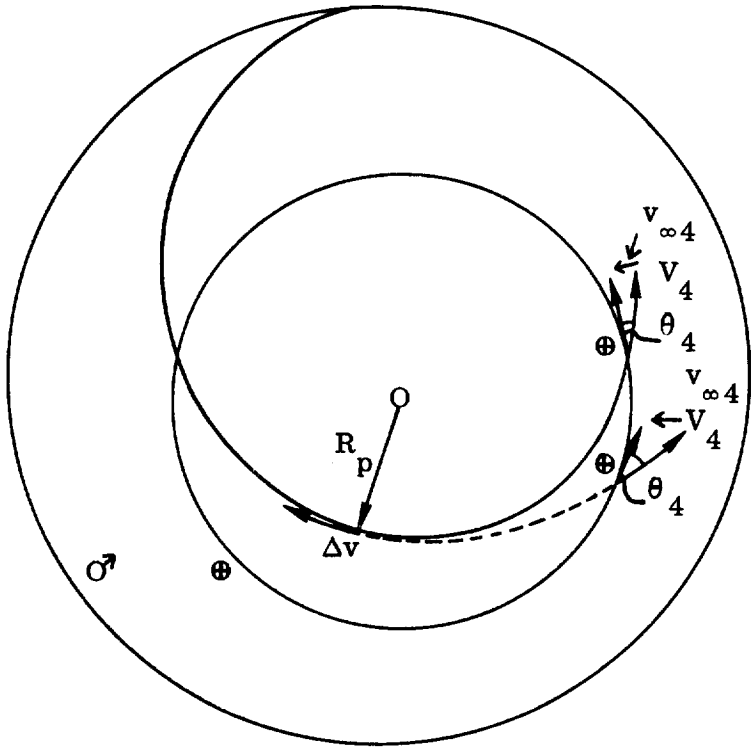

Figure 7-89. Perihelion Retro-Maneuver to Reduce Hyperbolic Excess at Earth Return (Schematic)

must be made prior to leaving Mars, because, if the vehicle was on a rendezvous course with Earth prior to the perihelion maneuver, it is unlikely to be on one following the maneuver. Thus, if a perihelion maneuver is intended, the Mars departure time must be changed so that the space ships will be on Earth-rendezvous course after the maneuver. This change can affect (increase or decrease) the Mars departure energy requirements.

It is, therefore, not possible to definitely associate a mission energy reduction with a perihelion retro-maneuver; but wherever return orbits of the type shown in Figure 7-89 are encountered with large Earth-orbit intersection angles, it is worthwhile to investigate the merits of a perihelion retro-maneuver.

7.12 EFFECT OF ELIMINATION OF THE EARTH CAPTURE MANEUVER (M-4) BY RELIANCE ON ATMOSPHERIC BRAKING ONLY. A reduction in mission energy (hence, in orbital launch weight) might be achieved by not using retro-thrust for recapture near Earth prior to atmospheric entry and using the atmosphere directly for slowing down from hyperbolic to suborbital speed. The aerothermodynamic and technological feasibility of entry at 40,000 to 70,000 ft/sec would have to be verified by actual flight experience -- an expensive and time consuming project. The capability of the crew to withstand the associated acceleration which would exceed the

already high acceleration at near-parabolic speed (lunar return, Project Apollo) if a drag body is used can probably be assured even at the end of a prolonged existence at low g-level as during an interplanetary mission, by stepping up muscle-building exercises on-board during the return coast. Perhaps the most critical aspect of this approach is that in the case of a "miss" the crew does not have a second chance and would re-escape Earth, unless the velocity were reduced to at least near-parabolic. Finally, in order to enter at hyperbolic speeds, the drag parameter ($C_D A/W$) of the Earth entry module (EEM) must be increased greatly over that of a capsule entering at near-parabolic velocity; or, variable negative and positive lift has to be applied and the proper lifting surfaces have to be provided. These provisions, too, cost weight and must be carried through the entire mission at corresponding propellant expense in the individual stages. On the other hand, by reducing the systems weight prior to the Earth recapture maneuver to the utmost (e.g., jettisoning the entire life support system and housing the crew in the EEM, and jettisoning all no longer needed equipment), and by reducing the velocity to a value no less than slightly sub-parabolic, the (chemical) propellant expenditure can be kept comparatively low. Figure 7-90A shows a plot of atmospheric entry velocity v^*_{entry} in the absence of any retro-thrust braking, retro-impulse $(\Delta v^*/v^*_\infty)_{2r_{oo},\ \epsilon = -0.04}$ for impulsive slow-down to an orbital energy $\epsilon = -0.04$ at two-Earth-radii distance, and propellant consumption W_p required to negotiate retro-impulse Δv^* if $I_{sp} = 455$ sec (high - p_c O_2/H_2) and if $I_{sp} = 900$ sec (all quantities as function of hyperbolic velocity excess $v^*_{\infty 4}$ at Earth arrival).

It is found that at $v^*_{\infty 4} = 0.29$ (Venus 1973-1, Mars 1973-1, cf. Tables 7-6 and 7-7) a propellant weight of about 17,000 lb ($I_{sp} = 455$ sec) or of about 12,000 lb ($I_{sp} = 900$ sec) is required. If this maneuver could be eliminated without any other weight penalty, the departure weight of the graphite - O_2/H_2 (chemonuclear) Venus vehicle would be reduced to about 85 percent of its original weight, from 550 t (1,214,000 lb) to 470 t (1,031,000 lb); the metal or metal carbide reactor vehicle departure weight would also be reduced to about 82 percent, from 479 t (1,054,000 lb) to 394 t (866,000 lb). For the Mars 1975-1 mission ($v^*_{\infty 4} = 0.3842$) the reduction of the Earth departure weight is about 22 percent, from 1108 t (2,435,000 lb) to 867 t (1,908,000 lb) for the chemonuclear vehicle and 26 percent, from 987 t (2,166,000 lb) to 725 t (1,596,000 lb) for the metal reactor vehicle. (For a weight breakdown of the vehicles for the standard mission profiles with Earth capture maneuver M-4, see Section 8.)

Generally, for the 1973 and 1975 mission windows, the gross reduction in Earth departure weight indicated by elimination of M-4 lies between 15 and 27 percent. Of course, the net savings are lower because more structural and heat shield weight has to be carried along on the trip as the Earth entry velocity is increased. The dashed curve indicates the approximate excess weight of a high-drag entry vehicle over that of the modified (for 8 persons) Apollo capsule (about 10,000 lb) as a function

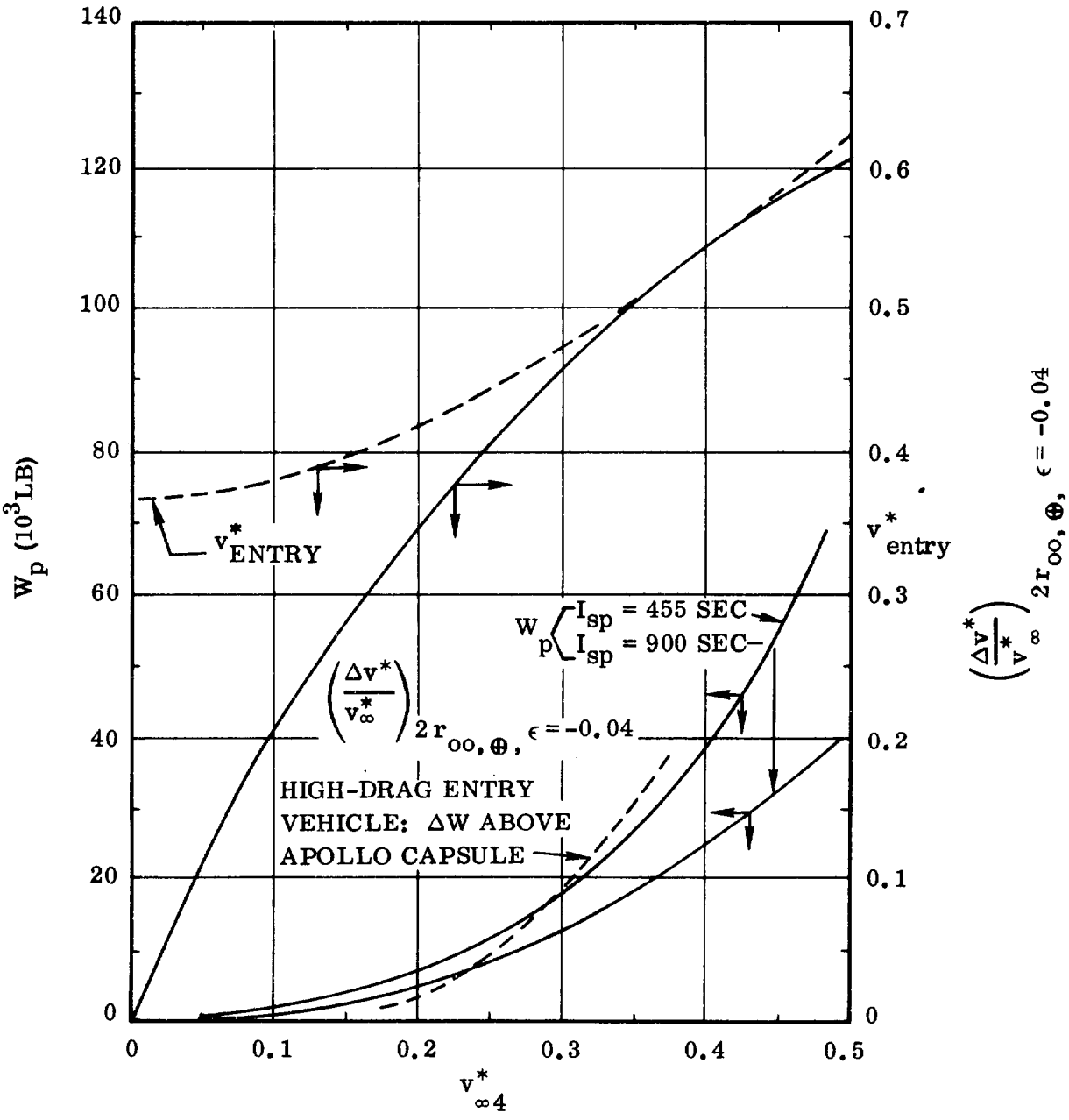

Figure 7-90A. Propellant Requirements for Earth Capture to $\epsilon = -0.04$ as Function of v^*_∞ and v^*_{entry} for a Terminal Payload Weight of 9400 Pounds

of $v^*_{\infty 4}$ (cf. Figure 7-90B). This curve indicates a weight superiority, over a capture maneuver, of up to $v^*_{\infty 4} \sim 0.25$ ($v_{entry} \sim$ 12 km/sec $\sim$ 43,000 ft/sec) if the I_{sp} of the M-4 system is 900 sec and up to $v^*_{\infty 4} \sim 0.3$ ($v_{entry} \sim$ 14.5 km/sec $\sim$ 47,500 ft/sec). At higher values of $v^*_{\infty 4}$ a capture maneuver, or possibly a combination of retro-maneuver (without "capture", i.e., remaining in the $\epsilon > 0$ regime) and high-drag body, are superior. These conclusions are tentative and based on the configuration and weight data shown in Section 8 for the Earth Entry Vehicle.

Two entry paths can be flown with a high-drag vehicle, either direct entry with attitude control or a two-step Hohmann braking maneuver, reducing the velocity, during the first step, from hyperbolic to $\epsilon \sim -0.04$ and during the second step entering the Earth's atmosphere permanently (Figure 7-91). The latter maneuver requires a less-stringent control of the first and second entry corridor. This is especially important with respect to the first entry corridor because of the very high speed and the associated possibility of high deceleration and high temperatures. An analysis of entry corridor tolerances as functions of entry velocity, W/A and deceleration during the atmospheric passage has been started, but could not be completed during the study period.

If the above result remains valid after further study, it must be concluded that a modest reduction in Earth departure weight can be achieved in the region of approach velocities $0.1 \lesssim v^*_{\infty 4} \lesssim 0.2$ by adopting the method of atmospheric capture, and in the high-velocity region ($v^*_{\infty 4} \gtrsim 0.35$) by applying the retro-thrust capture maneuver. The reason why the gain is modest lies in the fact that the drag method is compared with retro-thrust at fairly high specific impulses and, for this reason, the propellant weight in the region $0.1 \lesssim v^*_{\infty 4} \lesssim 0.2$ is small also. The resulting reduction in Earth departure weight is of the order of 10 percent.

7.13 ELLIPTIC CAPTURE ORBITS. If the capture orbit is not circular, $\Delta v^*/v^*_\infty$ decreases with increasing ellipticity until, for $\epsilon = 0$ (i.e., for impulsive slow-down to parabolic speed), $\Delta v^*/v^*_\infty$ reaches its lowest value. The reduction of $\Delta v^*/v^*_\infty$ is a function of hyperbolic excess and capture distance, as well as of the gravitational field (K) of the target planet. Generally, one can define a correction factor κ with which to multiply $\Delta v^*/v^*_\infty$ for circular capture orbits (where $n \equiv r_A/r_P = 1$).

$$\left(\frac{\Delta v^*}{v^*_\infty}\right)_{n>1} = \kappa \left(\frac{\Delta v^*}{v^*_\infty}\right)_{n=1} \qquad (7\text{-}41)$$

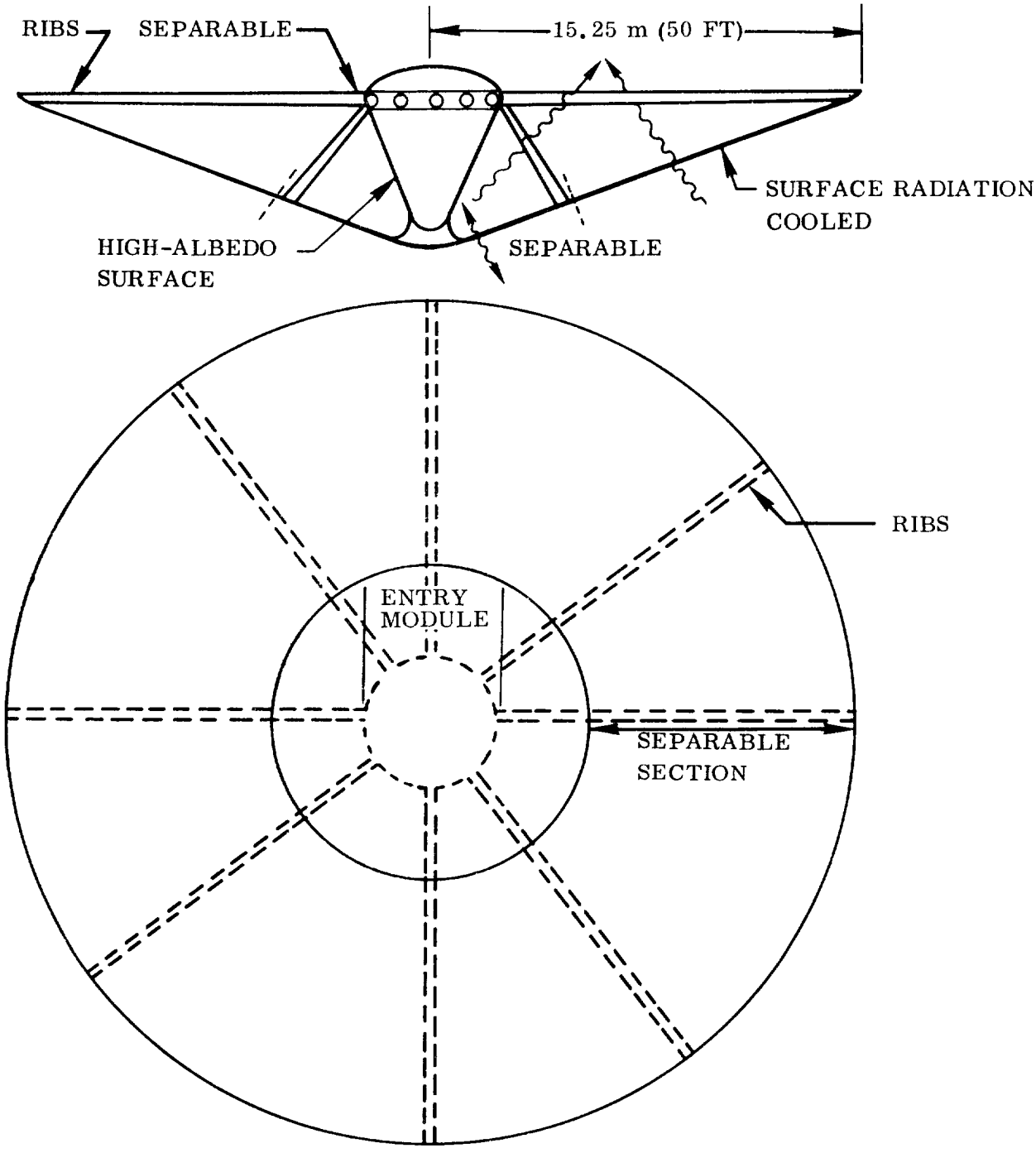

Figure 7-90B. Earth Entry Module

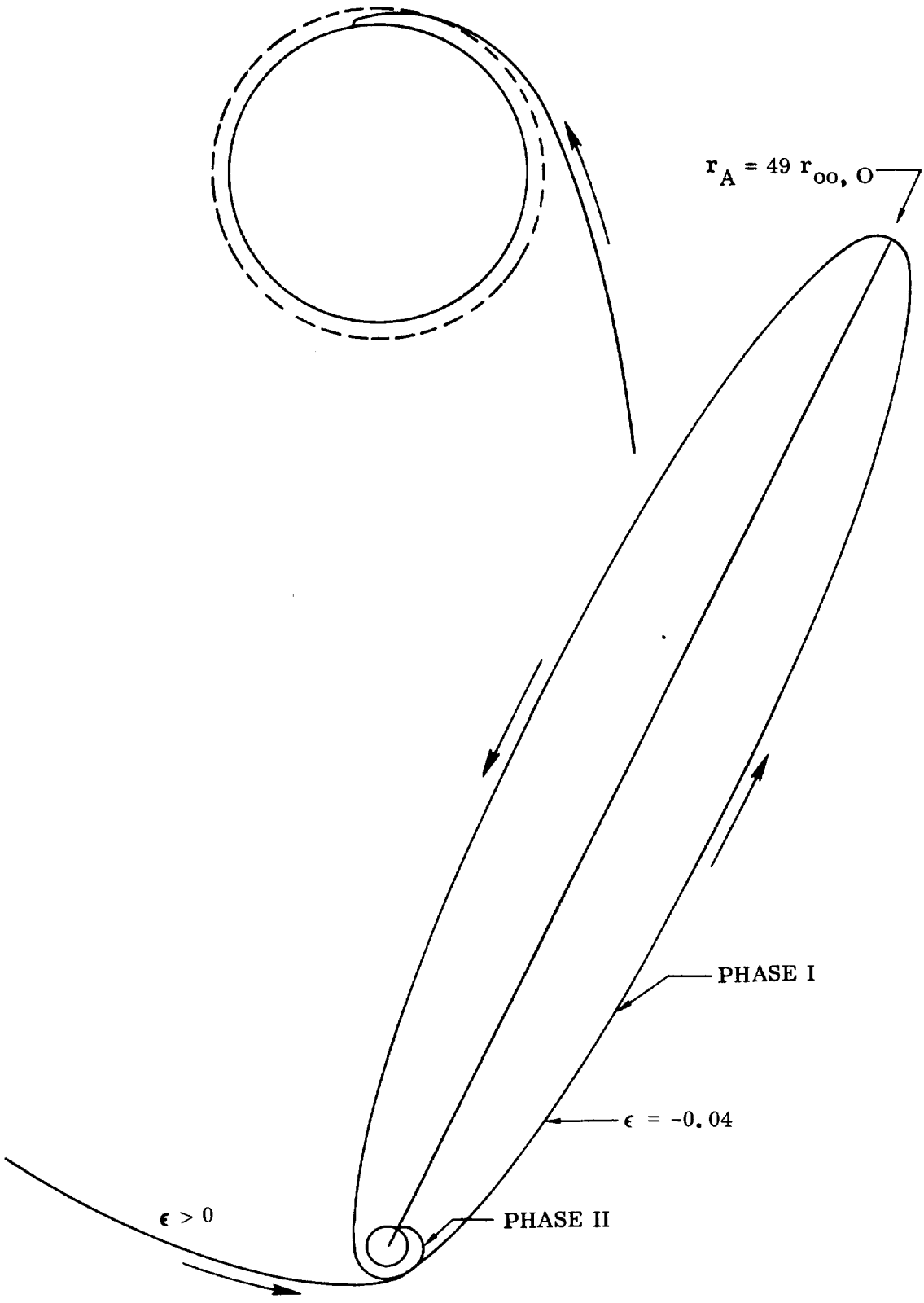

Figure 7-91. One- and Two-Step Atmospheric Capture Maneuver

where

$$K = \frac{\sqrt{1 + \frac{1}{v_\infty^2}\frac{2K/r_{oo}}{r/r_{oo}}} - \frac{1}{v_\infty}\sqrt{2+\epsilon}\sqrt{\frac{K/r_{oo}}{r/r_{oo}}}}{\sqrt{1 + \frac{1}{v_\infty^2}\frac{2K/r_{oo}}{r/r_{oo}}} - \frac{1}{v_\infty}\sqrt{\frac{K/r_{oo}}{r/r_{oo}}}} \qquad (7\text{-}42)$$

To show the effect of capture (or departure) orbit ellipticity on the impulsive capture (or escape) velocity change to (or from) the periapsis, Figure 7-92 shows the correction factor versus ϵ for two Venus distances and one Mars distance and each for two hyperbolic excess velocities which correspond to values found in the foregoing mission windows.

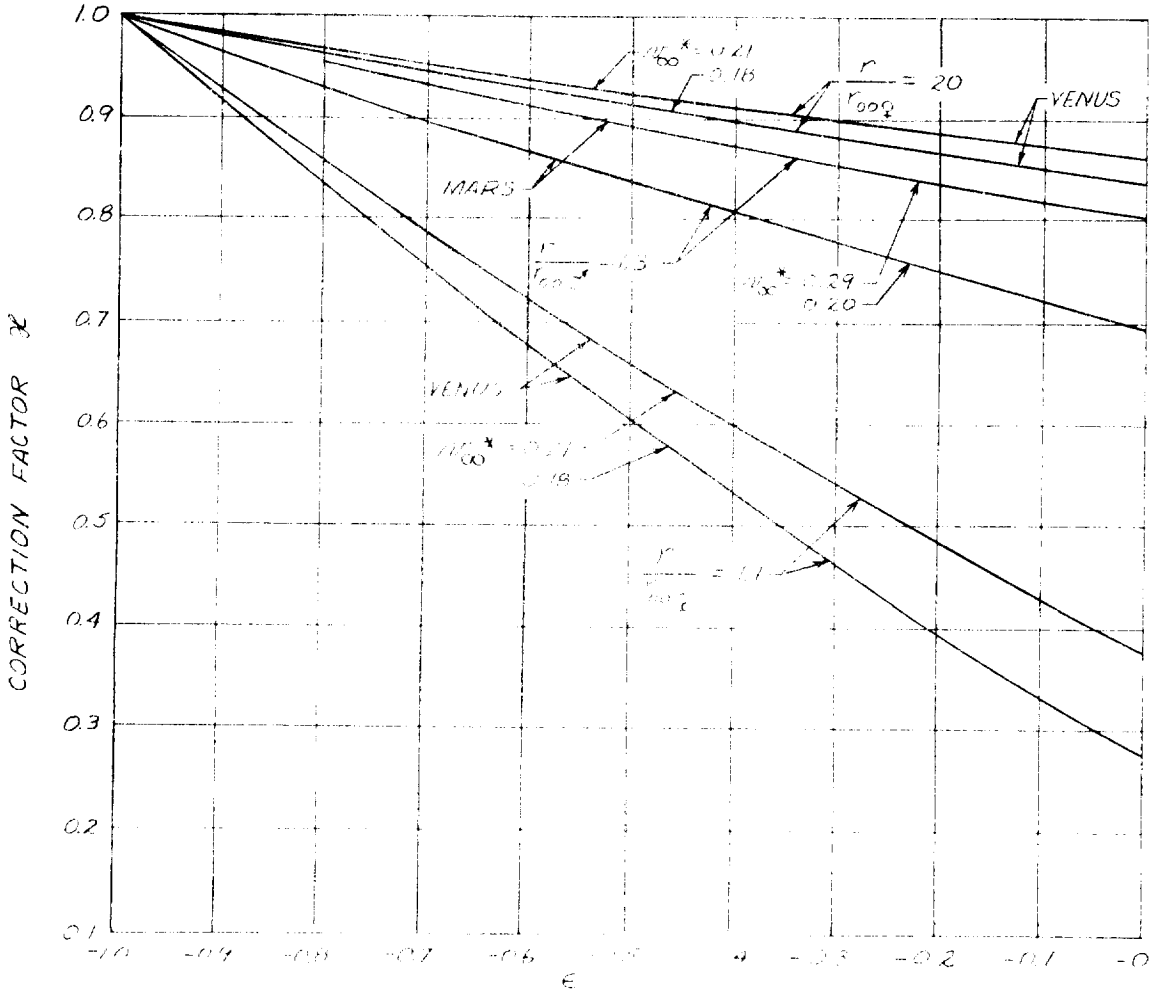

Figure 7-92. Correction Factor K for Ellipticity of Capture Orbit Versus Relative Capture Orbit Energy ϵ

The effect of ellipticity of the capture orbit on the orbital departure weight of a given planetary vehicle is shown in Figures 7-93 and 7-94. On the example of the Venus ship, it is shown that the elliptic capture method is more effective for a given n-value when the periapsis distance is kept small (cf. also Section 8).

It must be emphasized that the reduction in orbital departure weight indicated in Figures 7-93 and 7-94 is based on the premise that the escape as well as the capture maneuver takes place at the periapsis of the capture orbit. This is the most favorable case. Assuming correct approach of the target planet, the capture maneuver will occur at the periapsis. However, the orientation of the hyperbolic departure vector may prevent the departure maneuver from taking place at the periapsis. The weight savings are reduced when departure occurs at any other point of the ellipse -- in the worst case, at the apoapsis. For this case Equation 7-42 becomes

$$\left.\frac{\Delta v^*}{v_\infty^*}\right|_{r=r_A} = \sqrt{1 + \frac{1}{v_\infty^2}\,\frac{K/r_{oo}}{n\,r_p/r_{oo}}} - \frac{1}{v_\infty}\sqrt{2 + \epsilon\,\frac{1}{n}}\sqrt{\frac{K/r_{oo}}{r_p/r_{oo}}} \qquad (7\text{-}43)$$

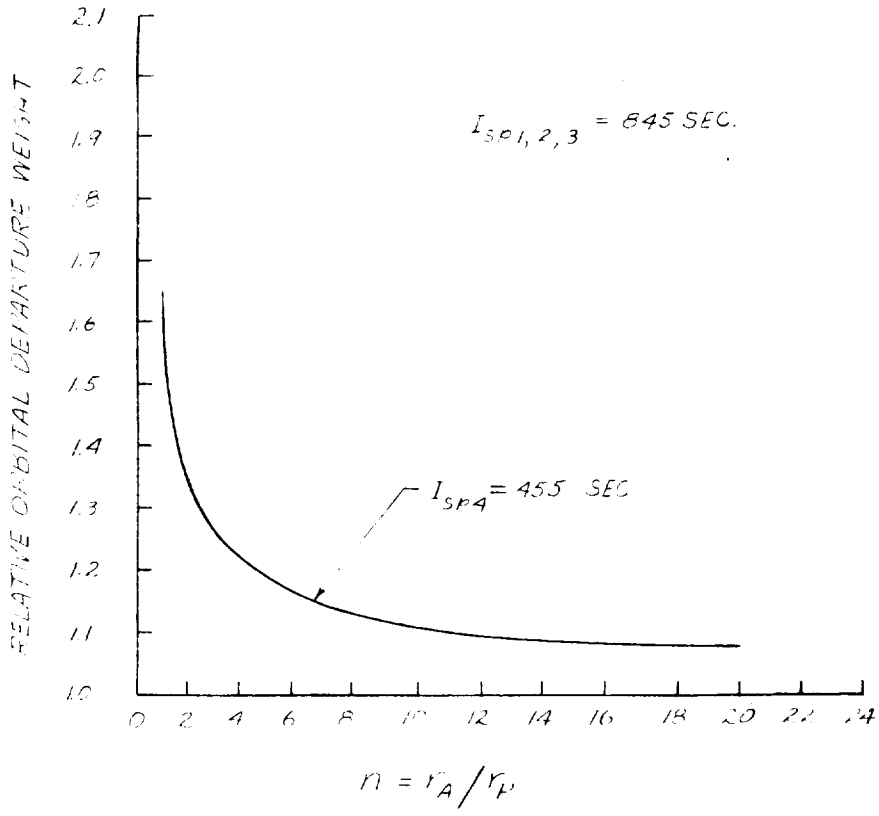

Figure 7-93. Relative Gross Weight Versus n Value
Four Person Mars Ship

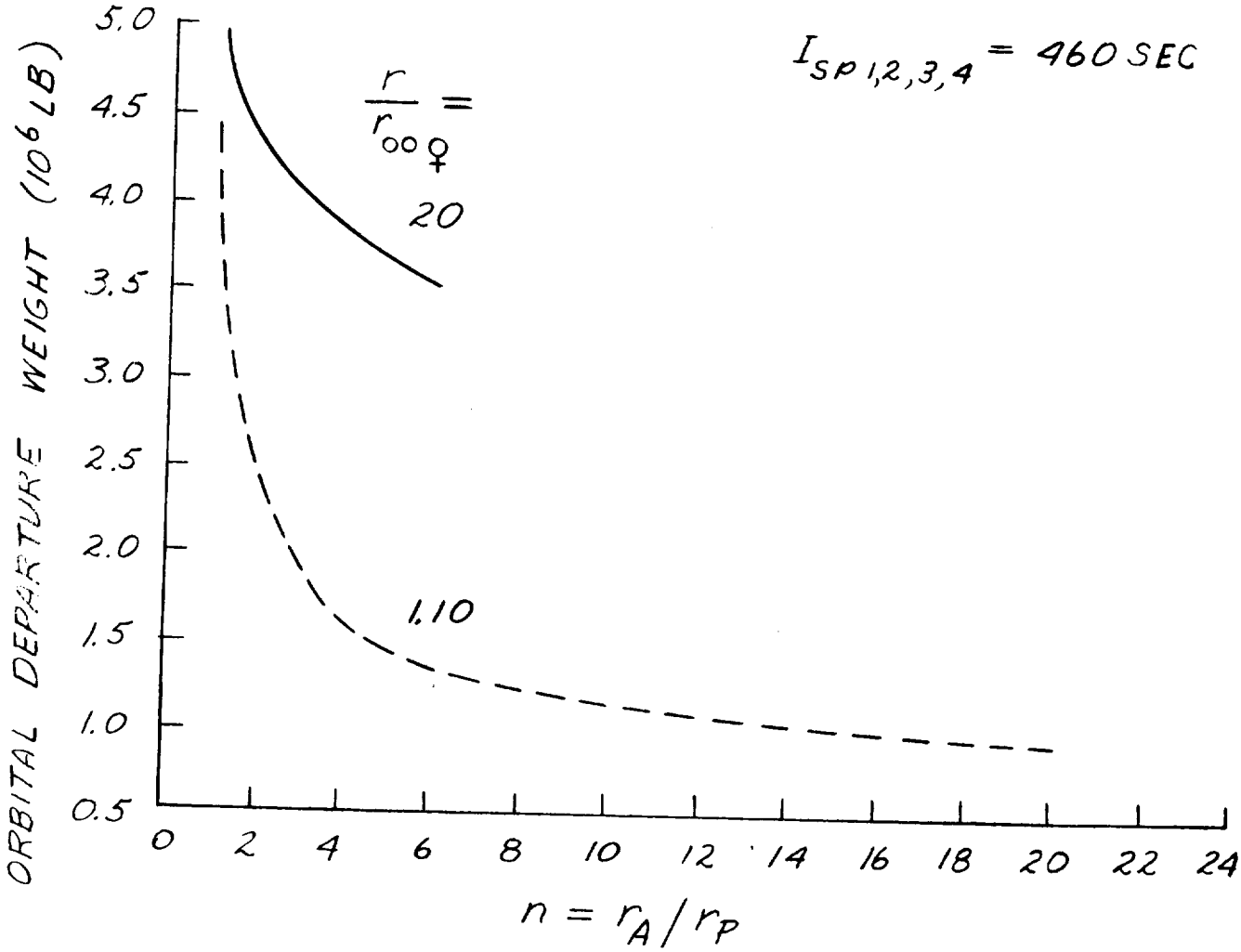

Figure 7-94. Gross Weight Versus n Value 4-Person Venus Ship

The effect of 1/n in the second term outweighs that of 1/n in the first term. Figure 7-95 shows the variation of $(\Delta v^*/v_\infty^*)_{r_P}$ and $(\Delta v^*/v_\infty^*)_{r_A}$ as functions of n for $v_\infty^* = 0.1$ and 0.5. It is seen that the effectiveness of the elliptic capture orbit can be seriously reduced, or even negated entirely, if conditions require departure near the apoapsis. This can be avoided by a four-impulse elliptic capture maneuver (Figure 7-96) in which the hyperbolic velocity is first reduced (impulse 1) to the periapsis velocity of a highly eccentric ellipse which, in turn, is changed (impulse 2) to a distant circular orbit, converted back (impulse 3) to the former elliptic orbit and finally (impulse 4) turned into the desired elliptic capture orbit whose periapsis is now in the correct location for the departure maneuver at termination of the capture period. Plane changes, if needed, can be incorporated most effectively in maneuver 2 or 3. Maneuvers 2 and 3 are the less expensive the farther out the apoapsis. The maximum distance of the intermediate circular orbit, however, is limited by the requirement that the coast period between maneuvers 2 and 3 should not exceed a specified fraction of the capture period. At 19 Mars radii, for example, the circular orbital velocity is already down approximately 2.4 deg/hr. Assuming, for example, arrival and departure at $v_\infty^* = 0.1$ EMOS and a four-impulse capture maneuver with an intermediate circular orbit at

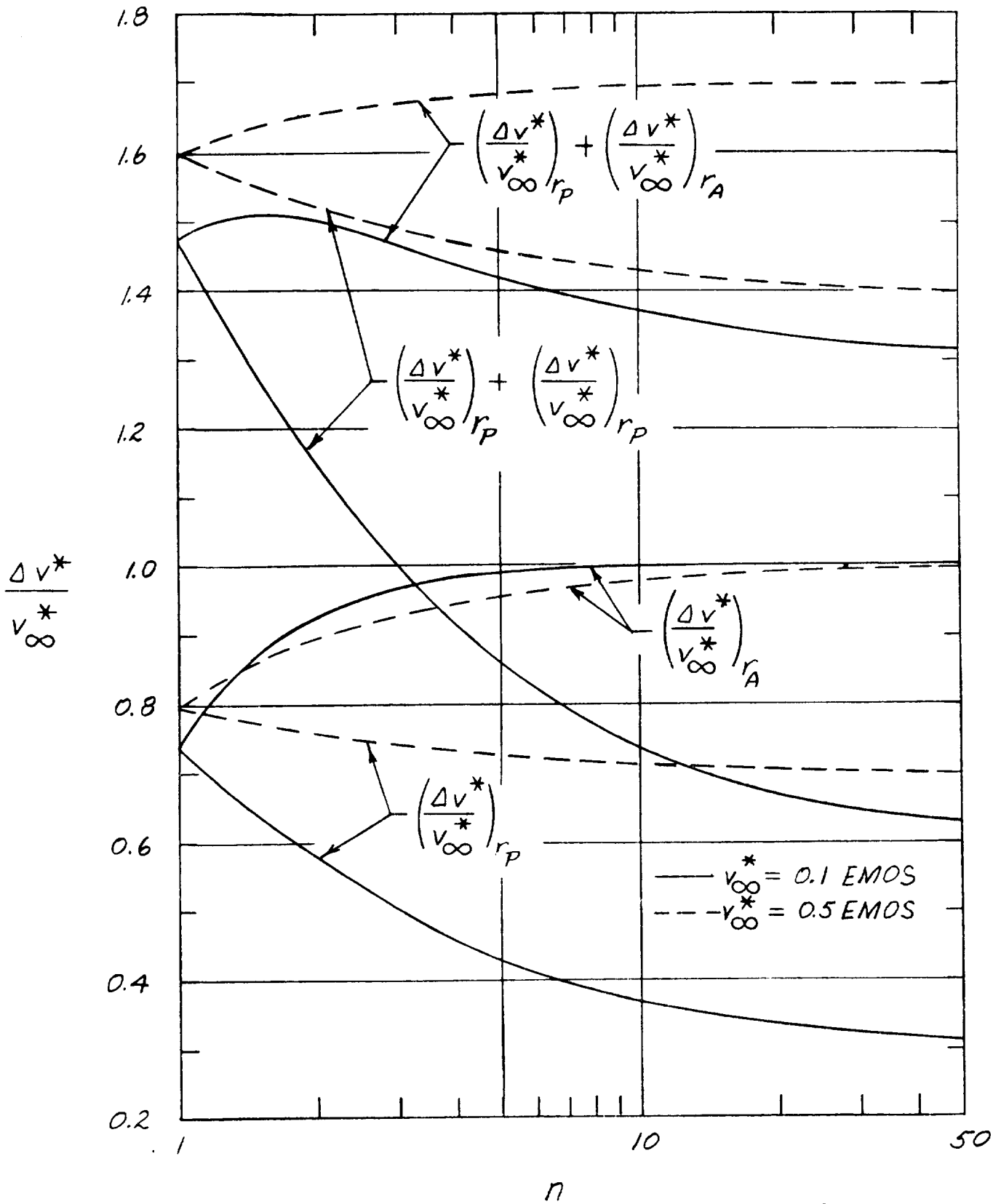

Figure 7-95. Perigee and Apogee Impulses in an Elliptic Orbit for Capture or Escape Versus n for Two Values of v_∞^*

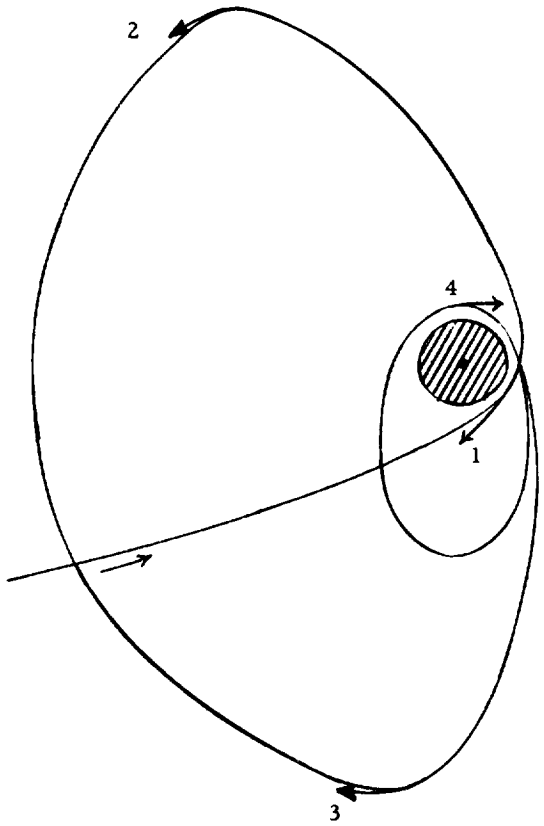

Figure 7-96. Four-Impulse Elliptic Capture Maneuver or Escape Maneuver (Reverse Sequence)

19 r_{oo} and a terminal elliptic capture orbit of n = 4 ($r_P = 1.31\ r_{oo}$), the four maneuvers and the departure maneuver (taking place at the periapsis) amount to:

$$\frac{\Delta v^*}{v^*_\infty} = 0.338 \text{ (Fig. 7-95)} + 0.016 + 0.016 + 0.119 + 0.457 \text{ (Fig. 7-95)} = 0.946$$

(or $\Delta v^* = 0.0946$ EMOS). By comparison, for arrival and departure from the n = 4 capture orbit without intermediate maneuver, $\Delta v^*/v^*_\infty = 0.914$ (Figure 7-95); for arrival at the periapsis and departure at the apoapsis of the n = 4 orbit, $\Delta v^*/v^*_\infty = 1.44$ (Figure 7-95); and for arrival and departure from a circular capture orbit at 1.31 r_{oo} distance, $\Delta v^*/v^*_\infty = 1.474$. The example, which represents a typical case, shows that by means of the four-impulse capture technique the weight reductions offered by the elliptic capture orbit can essentially be maintained.

The process can be reversed by capturing directly in the n = 4 orbit and going through a four-impulse departure maneuver. This has three added advantages: First, the capture orbit period does not have to be a sub-multiple of the capture period; the position of the periapsis can be determined when the exact departure time (which may be different from the original target value) is specified. Second, the correct orbit plane for departure can be established when the exact departure date is specified. Third, the departing vehicles will be lighter, because much equipment will be abandoned at termination of the capture period, so that the intermediate maneuvers require less propellant.

7.14 EFFECT OF MASS RATIO DISTRIBUTION ON EARTH DEPARTURE WEIGHT. The principal factor determining the mass ratio of the planet ship is the product of the mass ratios resulting from the four main maneuvers (M-1 through M-4) of the capture mission. This product is of course independent of the mission velocity distribution, i.e., the distribution of the overall velocity requirement over these four maneuvers; but the Earth departure weight is not independent of it due to the effects of mass fraction and specific impulse, which are not necessarily the same for each propulsion section ("stage"). The propellant weight for a given stage follows from the mass fraction (X), the mass ratio (μ) and the payload weight (W_λ). The propellant weight for a given stage is

$$W_p = \frac{W_\lambda}{\frac{1}{\mu - 1} - \frac{1 - X}{X}} \tag{7-44}$$

The wet inert weight is

$$W_b = \frac{1 - X}{X} \quad W_p . \tag{7-45}$$

The burnout weight is

$$W_B = W_b + W_\lambda \tag{7-46}$$

and the ignition (gross) weight is

$$W_A = W_B + W_P . \tag{7-47}$$

Thus, the factors affecting the gross weight (W_A) of the vehicle, prior to a given maneuver, are seen to be μ (velocity change, specific impulse), X and, of course, W_λ. The mass fraction depends upon the size of the propellant tanks and upon whether a separate engine is needed for each propulsion section.

In the interest of keeping Earth departure weight as low as possible consistent with the type and objectives of the mission, it is important to understand how the mission velocity distribution affects the Earth departure weight of a planetary ship of given terminal payload weight (i.e., the payload weight left at the beginning of the Earth capture maneuver, M-4), of given specific impulse for each propulsion section, of consistent variation of the mass fraction (i.e., similarity of basic design) and of given weight variation during the mission coast periods. Knowledge of "favorable"

and "unfavorable" mission velocity distribution is an important factor in the comparative evaluation of interplanetary mission profiles.

In order to obtain a "first-cut" answer to this question, an analysis was made to determine the Earth departure weight W_{A1} of a four-stage planet ship for a large variety of specific impulses and ideal velocity changes during the mission, distributed in various combinations. The analysis started during the initial phase of the study by assuming a limited variation of the mass fraction with stage size of stage 4, while holding the other mass fractions constant. The payload fraction

$$\lambda_{1234} = \frac{W_{\lambda 4}}{W_{A1}} \tag{7-48}$$

was determined for various combinations of a total mission velocity of 100,000 ft/sec (30.5 km/sec), which corresponds to $\Sigma_1^4 v_\infty^*$ of the order of 1.2 to 1.4. This is on the high side, but the trends shown are representative for lower mission velocities also, if the mass fractions and specific impulses are similar. Specific impulses corresponding to nuclear and to chemonuclear vehicles were used. In this first analysis, no allowance was made for weight changes during coast periods. Therefore

$$\lambda_4 = \Pi_1^4 \lambda \equiv \Pi_1^4 \frac{W_\lambda}{W_A} \tag{7-49}$$

The results are shown in Figure 7-97. First, it is noted that the trend is constant, i.e., the mission velocity distribution yielding highest payload fraction at I_{sp} = 900 sec also yields the comparatively highest value at lower specific impulses. Secondly, it is seen that the highest payload weight fraction is consistently obtained when large velocity changes occur at M-2 and M-3, and between these two, when the largest velocity change is required at M-3 (target planet departure). This result is strongly affected by the high values used for mass fractions X_2 and X_3.

To account more precisely for the variation of the mass fraction with the size of the propulsion unit, the more or less continuous variation of X with the stage size must be taken into consideration. Figure 7-98 shows a plot correlating the values of X with the stage gross weight for nuclear vehicles only. The top curve is for stages 2 and 3 on the basis that the same engine is used for both maneuvers and that this engine is small, weighing approximately 3000 pounds and producing a thrust of 30,000 pounds. The same engine was assumed for M-4, but here the propellant load is so much smaller for the Earth capture maneuver to ϵ = -0.04, that a smaller mass fraction is obtained. For the escape booster a single nuclear engine of 700-k thrust was assumed. (For detailed engine data, which are classified, cf. Addendum of this report.) Assuming individual engines of 200-k thrust each for maneuvers M-2 and M-3, the mass fractions X_2 and X_3 are reduced to values similar to X_1. Therefore,

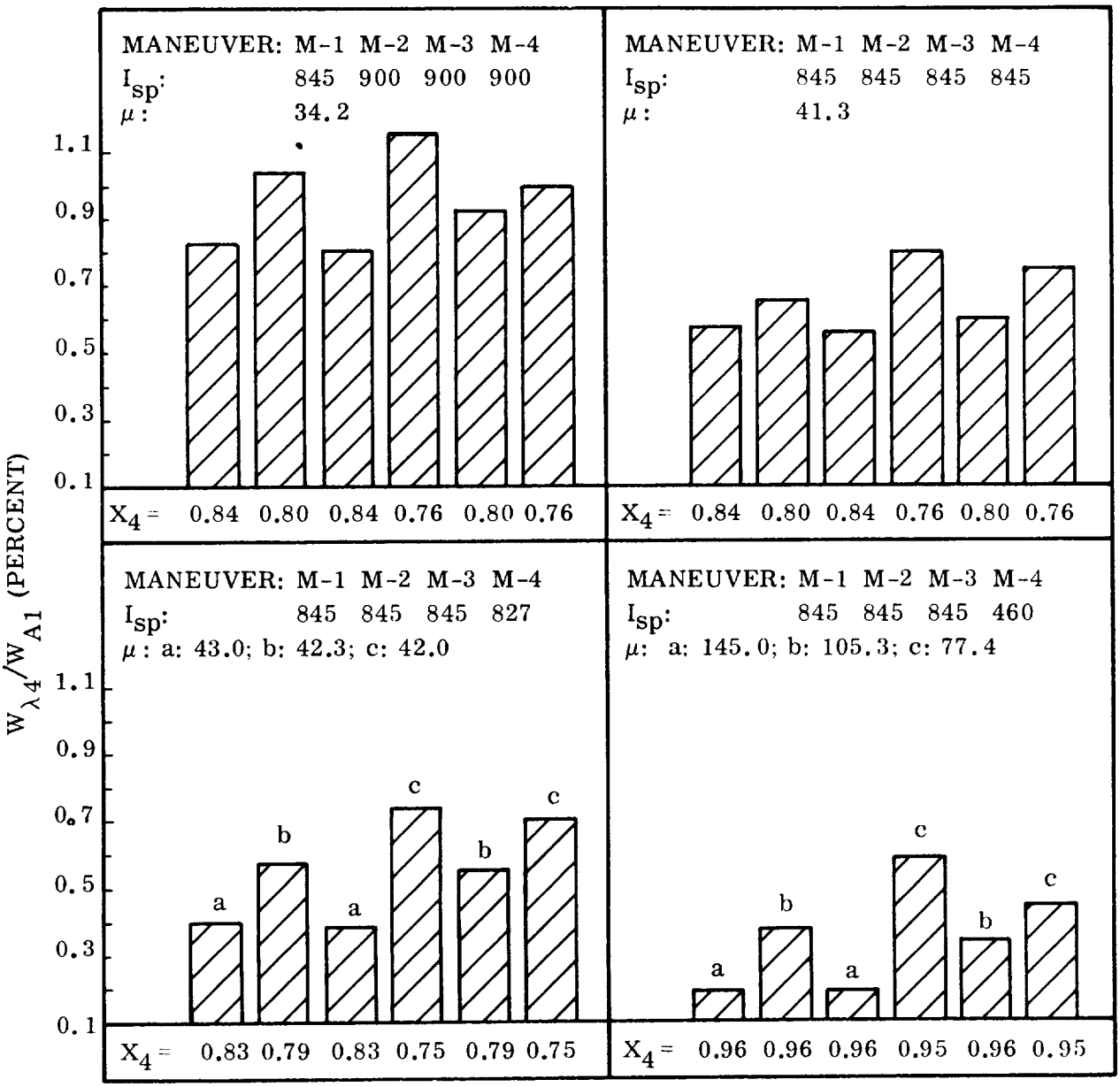

MISSION VELOCITY DISTRIBUTION (10^3 FT/SEC)

MASS FRACTIONS OF STAGE 1, 2, 3: $X_1 = 0.86$, $X_2 = 0.90$, $X_3 = 0.92$

Figure 7-97. Payload Fraction as Function of Mission Velocity Distribution and Specific Impulses for Given Mass Fractions

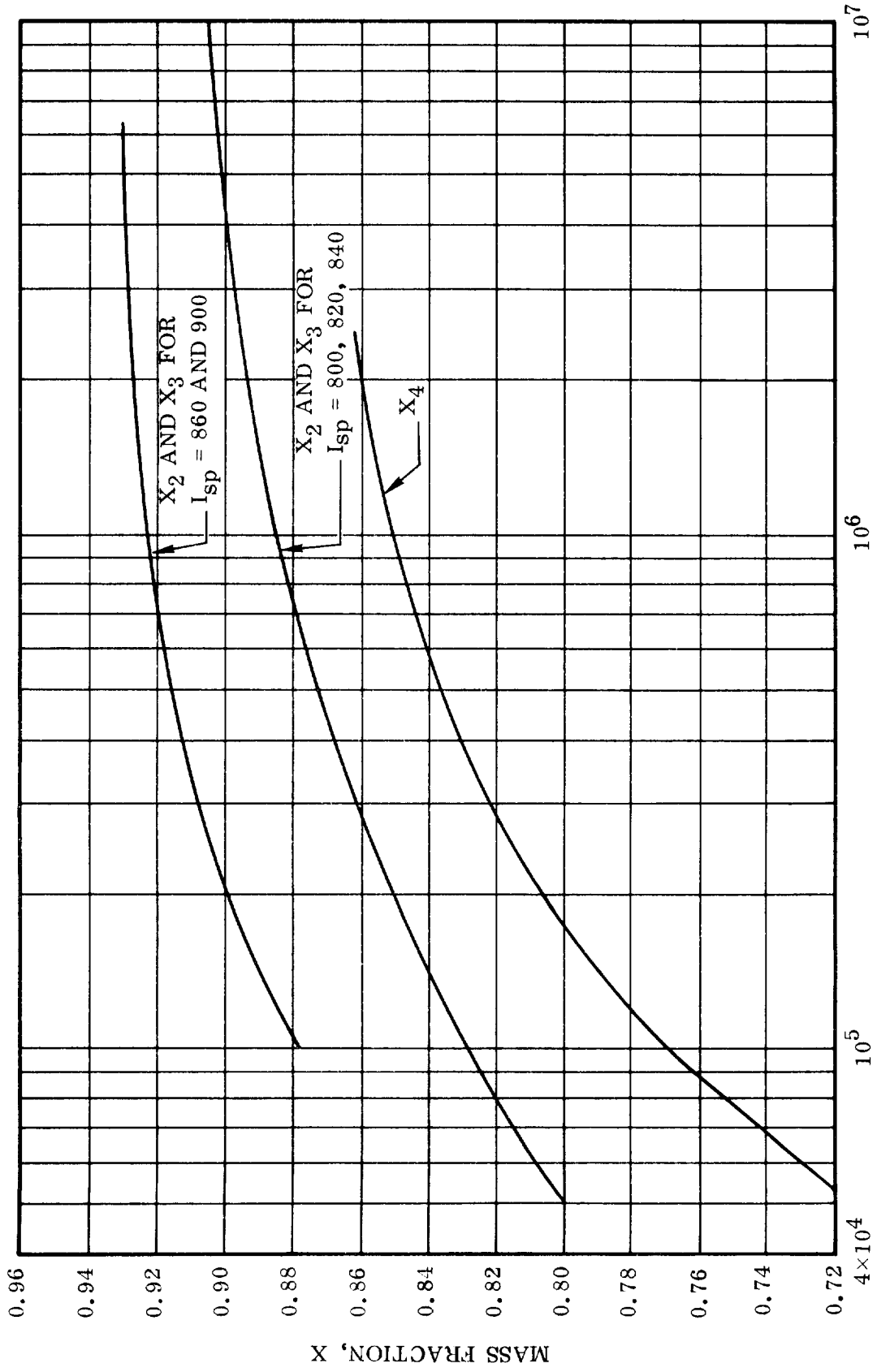

Figure 7-98. Mass Fractions for Propulsion Sections for the Maneuvers M-1 through M-4

they were combined with X_1 in one curve. It should be noted that refinements in weight analyses during the second half of the study phase have led to improved mass fraction curves, which are shown in Section 8 of this report.

Since a value of X is needed to compute W_A and since, on the other hand, X is a function of W_A, the use of the curves in Figure 7-97 involves a trial-and-error procedure for the computation of each of the four ignition weights. As a further refinement, certain weight reductions during coast phases have been fed into the computation process. Therefore, Equation 7-49 is no longer valid. Each of the four stage weights has to be computed for each of the many combinations, and the M-4 payload weight ($W_{\lambda 4}$) divided by the W_{A1} obtained, in order to obtain the desired payload fraction $\lambda_4 = W_{\lambda 4}/W_{A1}$. As before, $W_{\lambda 4}$ represents the terminal payload, defined as the sum of Earth Entry Module plus its associated propulsion system for M-5 (cf. Figures 7-1 through 7-3). As before, the absolute values of W_{A1} or λ_4 are not of prime interest (since no specific mission is assumed here), but rather the change in λ_4 with varying mission velocity distribution and specific impulse. A round value of 10,000 pounds (4.545 t) was assumed for the terminal payload. Because of the considerable computational effort involved, a computer program was set up. The computation process and the associated specifications are presented in Table 7-11. The symbols W_C and W_S have the same meaning as defined in Table 7-2. The large weight reduction (90,000 lb) prior to M-4 is due to the jettisoning of the entire LSS module, except for the Earth entry module.

The results of those computations are shown in Figures 7-99 through 7-101, for a total mission velocity of 60,000 ft/sec (18.3 km/sec), 70,000 ft/sec (21.4 km/sec) and 90,000 ft/sec (27.4 km/sec), respectively. For these total mission velocities, 9, 10, and 7 velocity combinations, respectively, are shown. For each combination, four different combinations of specific impulses are presented. The mission velocity distributions show the effect of large velocity changes at M-1, M-2, or M-3. The specific impulse distributions show the effect of low I_{sp1}, low I_{sp4}, and equal I_{sp} for all maneuvers. From these figures the following conclusions can be drawn.

First, the interesting fact stands out that without exception the payload fraction is highest when the M-3 velocity change is large.

Second, the payload fraction is consistently low when the M-1 velocity change is high. This goes so far as to yield a (comparatively) significantly higher payload fraction for velocity distribution 5 in Figure 7-100 (where M-1 = 10,000 ft/sec, M-4 = 15,000 ft/sec) than for velocity distribution 3 (where the situation is reversed). This appears contrary to what one would intuitively be inclined to assume, especially since X_4 is smaller than X_1. The result can be understood, however, if one considers the fact that a higher μ_4 mass ratio involves a far smaller mass increase than is caused by

Table 7-11. Computation Process for Determining the Effect of Mission Velocity Distribution on the Earth Departure Weight

Given

$W_{\lambda 4}$ = 10,000 lb (constant)
I_{sp4} = 800, 840, 860 sec
Δv_{id4} = 10,000, 15,000, 30,000 ft/sec

↓

Determination of W_{p4}, W_{b4}, W_{B4}, and W_{A4} by successive approximation using Figure 7-98

↓

$W_{C4} = W_{A4} + 0.1\, W_{p4}$ + 90,000 lb
$W_{C3} = W_{C4}$ + 20,000 lb = $W_{\lambda 3}$
I_{sp3} = 800, 840, 860, 900 sec
Δv_{id3} = 10,000, 15,000, 25,000, 30,000 ft/sec

↓

Determination of W_{p3}, W_{b3}, W_{B3}, and W_{A3} by successive approximation using Figure 7-98

↓

$W_{S3} = W_{A3} + 0.1\, W_{p3}$ + 10,000 lb
$W_{S2} = W_{S3}$ + 30,000 lb = $W_{\lambda 2}$
I_{sp2} = 800, 840, 860, 900 sec
Δv_{id2} = 10,000, 15,000, 25,000, 30,000 ft/sec

↓

Determination of W_{p2}, W_{b2}, W_{B2}, and W_{A2} by successive approximation using Figure 7-98

↓

$W_{C2} = W_{A2} + 0.1\, W_{p2}$ + 2000 lb
$W_{C1} = W_{C2}$ + 50,000 lb = $W_{\lambda 1}$
I_{sp1} = 760, 800, 840, 900 sec
Δv_{id1} = 10,000, 15,000, 20,000, 25,000, 30,000 ft/sec

↓

Determination of W_{p1}, W_{b1}, W_{B1}, and W_{A1} by successive approximation using Figure 7-98

↓

$\lambda_4 = 10,000/W_{A1}$

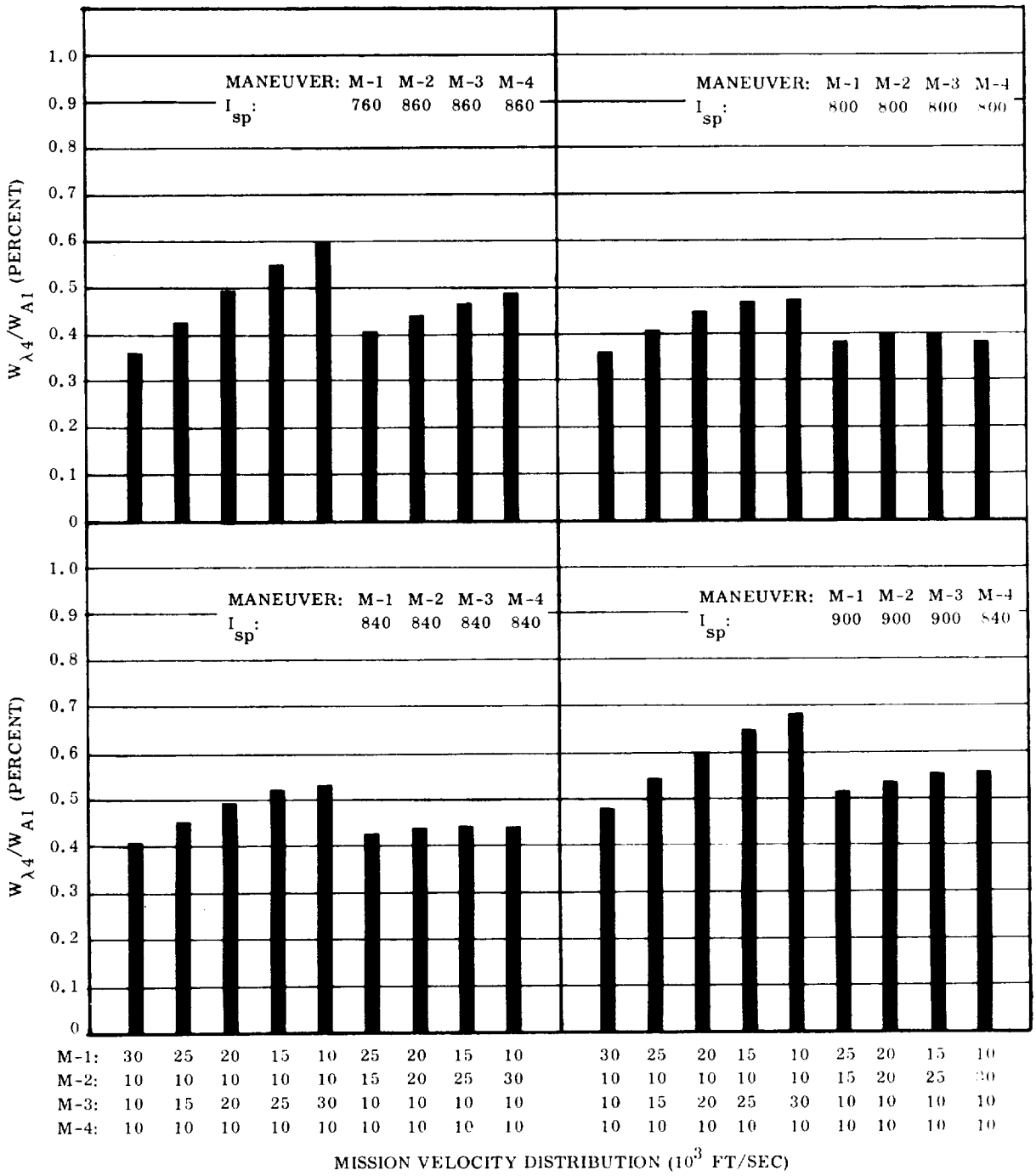

Figure 7-99. Payload Fraction as a Function of Mission Velocity Distribution and Specific Impulses
($\Sigma_1^4 \Delta v$ = 60,000 ft/sec = 18.3 km/sec)

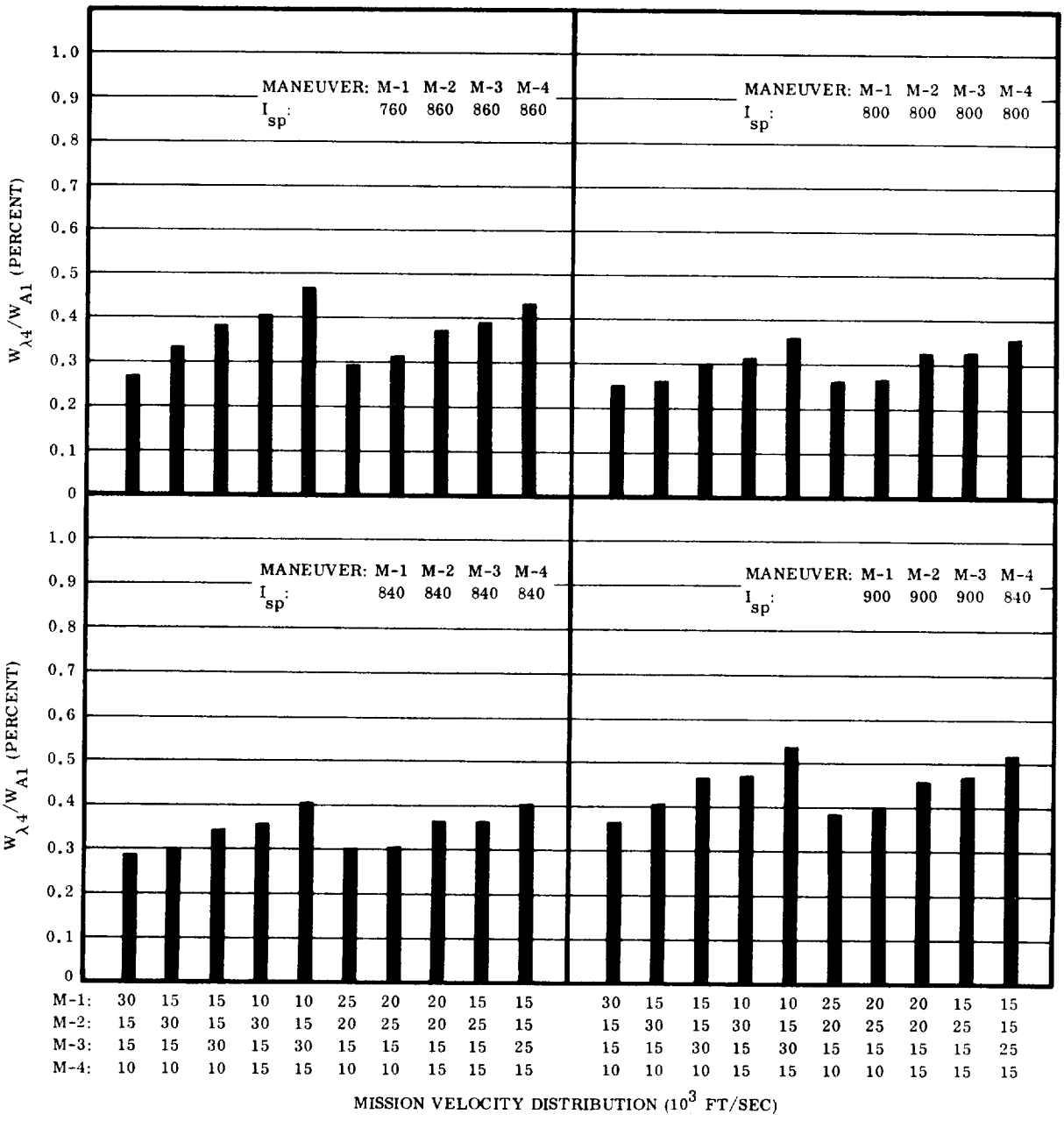

Figure 100. Payload Fraction as a Function of Mission Velocity Distribution and Specific Impulses
($\Sigma_1^4 \Delta v$ = 70,000 ft/sec = 21.4 km/sec)

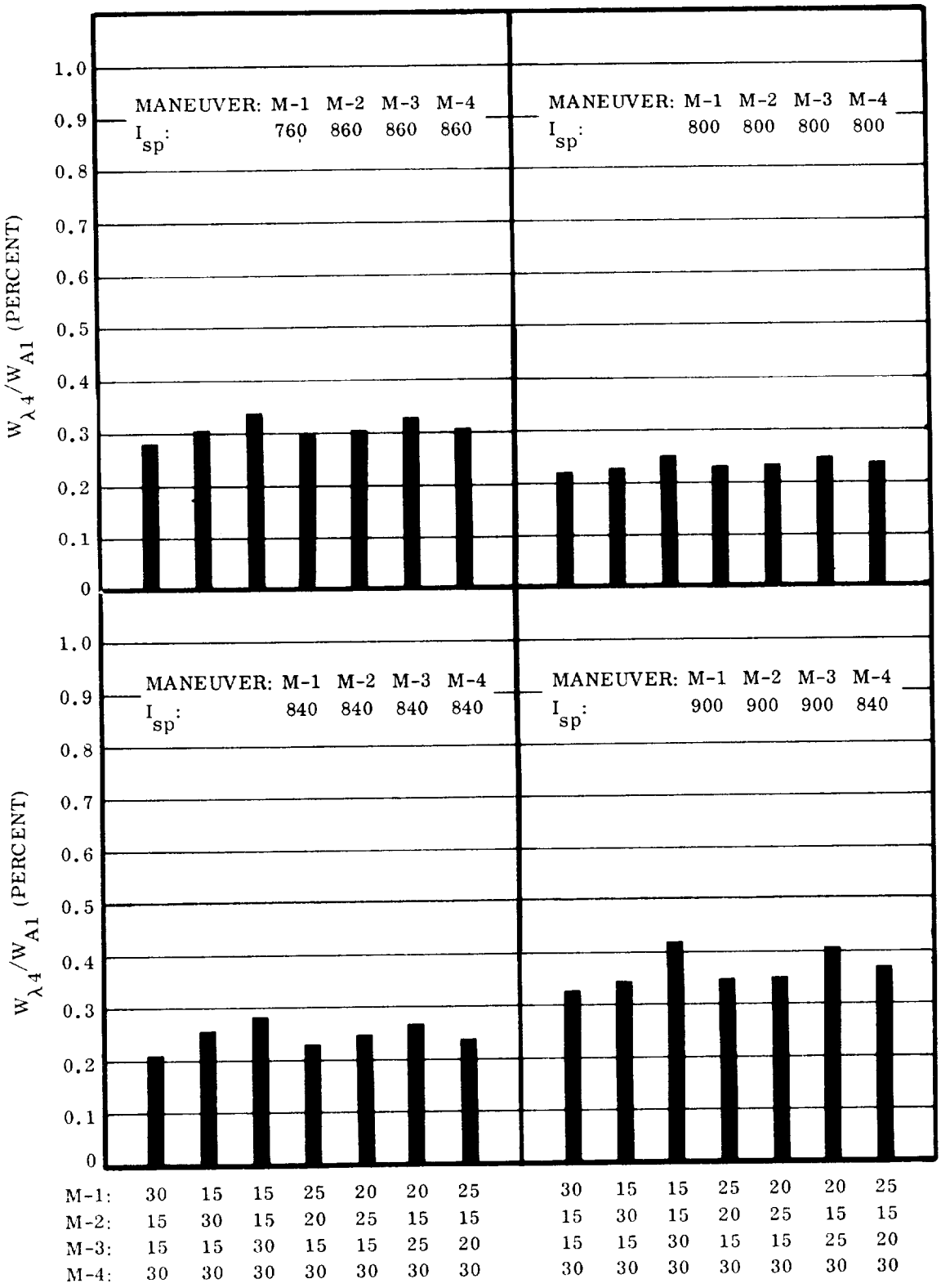

Figure 7-101. Payload Fraction as a Function of Mission Velocity Distribution and Specific Impulses ($\Sigma_1^4 \Delta v$ = 90,000 ft/sec = 27.4 km/sec)

the same increase in mass ratio μ_1. The difference is large enough so that even the augmentation of the M-4 mass ratio increase through the multiplication by μ_3, μ_2, and μ_1 does not change the picture. In other words, an increase in μ_1 is more critical (within limits) than an increase in μ_4, even though the trade-off factor for the first stage is much smaller than that for the fourth stage.

Third, it is found that the most favorable mission velocity distribution is generally characterized by evenly distributed velocity changes for M-1, M-2, and M-4, and a peak velocity change at M-3. Extremes at either end of the mission result in lower payload fractions. However, if a choice is to be made between a higher velocity change at M-1 than at M-4, or vice versa, the advantage of higher payload fraction goes to the higher velocity change at M-4.

Fourth, concerning the effect of specific impulse, it is of interest (and perhaps somewhat surprising) to note than an I_{sp} reduction of 20 seconds for M-2 through M-4 (from 860 to 840 sec) overcompensates the effect of an I_{sp} increase of 80 seconds (760 to 840 sec) for M-1.

Fifth, an across-the-board increase of 5 percent in I_{sp} (from 800 to 840 seconds) tends to raise the overall payload fraction by about 0.05 percent for mission velocities of 60,000 to 70,000 ft/sec.

Sixth, an increase in mission velocity from 60,000 to 70,000 ft/sec reduces the overall payload fraction by 0.12 to 0.15 percent for the specified mission conditions. It takes an I_{sp} increase of the order of 100 sec to compensate for a 10,000 ft/sec increase in overall mission velocity.

From the first and third conclusion it follows that any additional adjustment maneuvers required during the capture period to attain correct return flight conditions (cf. Section 7-13) should be changed to the M-3 propulsion section rather than to the M-2 propulsion section; i.e., any maneuvers required to adjust the inclination or major axis orientation of the capture orbit should be carried out as part of departure maneuver M-3, rather than part of arrival maneuver M-2. Thus, keeping the Earth departure weight low is an additional reason for associating target planet pre-departure maneuvers with M-3, aside from those reasons mentioned in Paragraph 7-13.

From the fourth conclusion it follows that emphasis on development of high specific impulse for the engine or engines of the interplanetary ship proper (mission engine) pays off more, in terms of terminal payload fraction (hence, of low Earth departure weight), than spending much effort on raising the specific impulse but at some expense to the mission engine.

The studies reported in this paragraph are only the beginning of an extensive systematic study of the influence of a large number of factors which influence the payload effectiveness of the interplanetary ships. A computer program which ties an increasingly detailed weight analysis and weight error analysis directly into the celestial mechanical part of the mission and performance analysis, as part of refining the determination of mission windows, has been prepared for future studies.

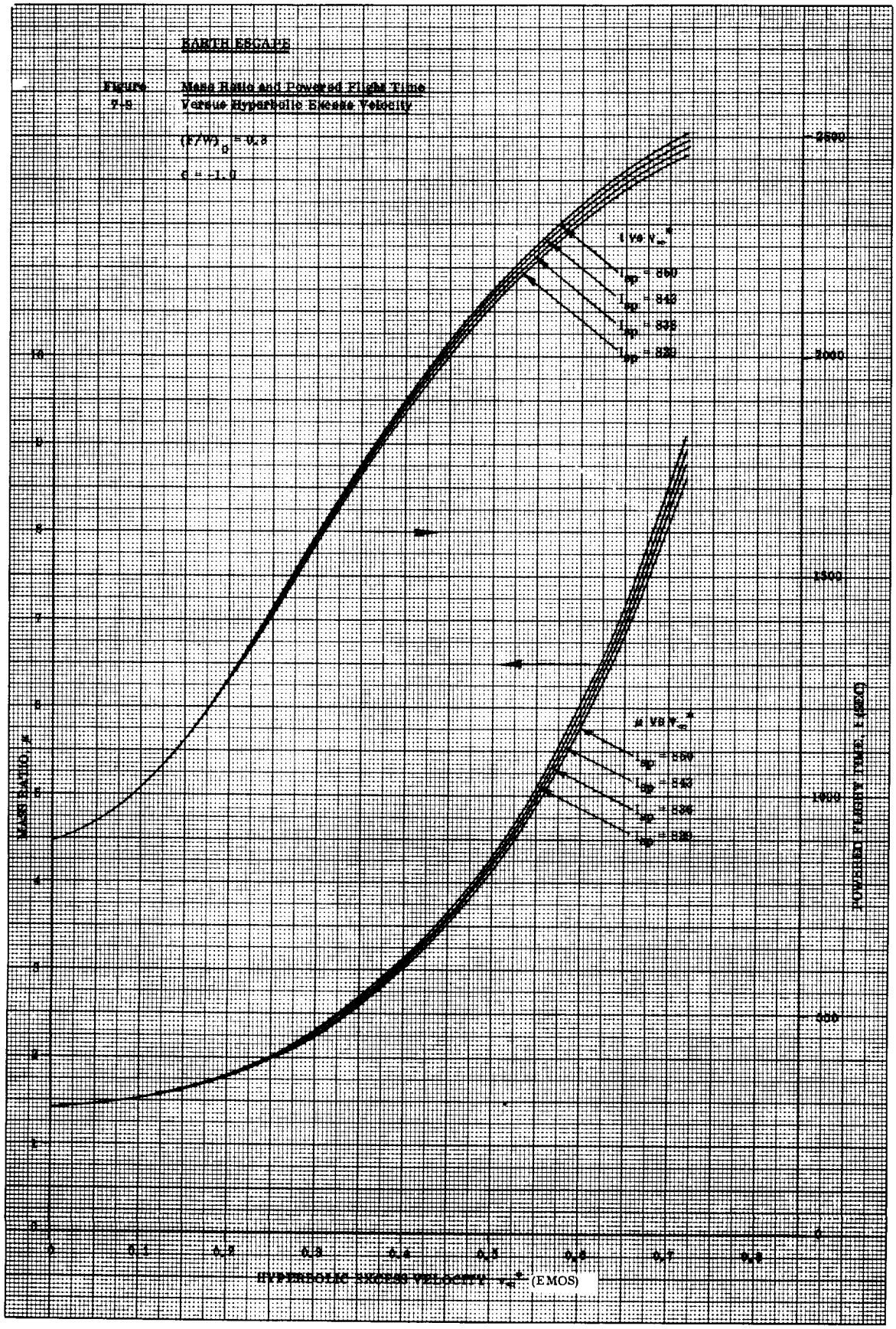
EARTH ESCAPE
Figure 7-8 Mass Ratio and Powered Flight Time Versus Hyperbolic Excess Velocity
$(T/W)_0 = 0.8$
$\epsilon = -1.0$
I_{sp} = 860
I_{sp} = 843
I_{sp} = 835
I_{sp} = 820
I_{sp} = 860
I_{sp} = 843
I_{sp} = 835
I_{sp} = 820
MASS RATIO, R
POWERED FLIGHT TIME, t (SEC)
HYPERBOLIC EXCESS VELOCITY, V_∞^+ (EMOS)

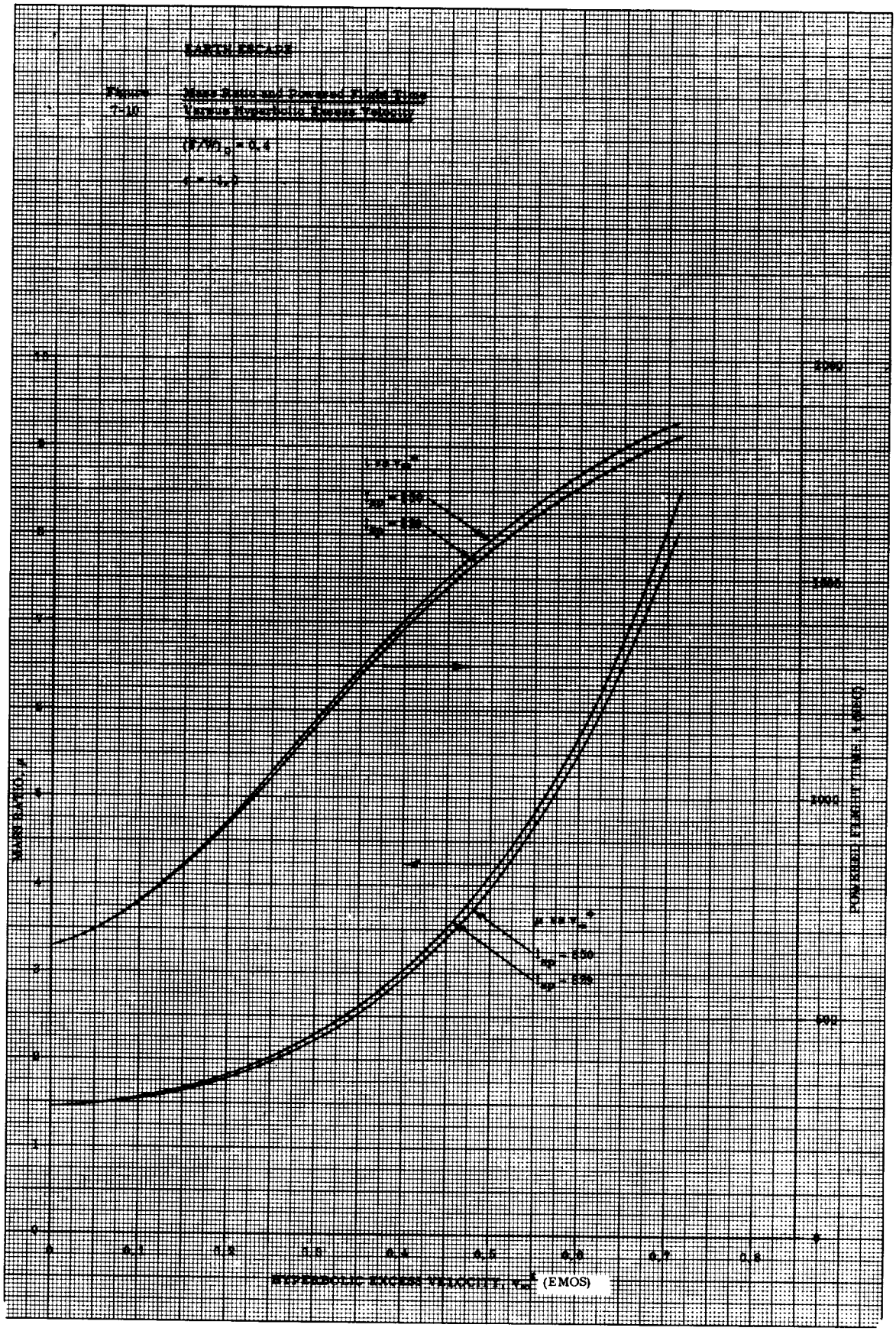
EARTH ESCAPE
Figure 7-10
Mass Ratio and Powered Flight Time Versus Hyperbolic Excess Velocity
$(T/W)_0 = 0.4$
$\delta = -3.7$
MASS RATIO, R
POWERED FLIGHT TIME, t_{pf} - SEC
HYPERBOLIC EXCESS VELOCITY, V_{∞}^2 (EMOS)

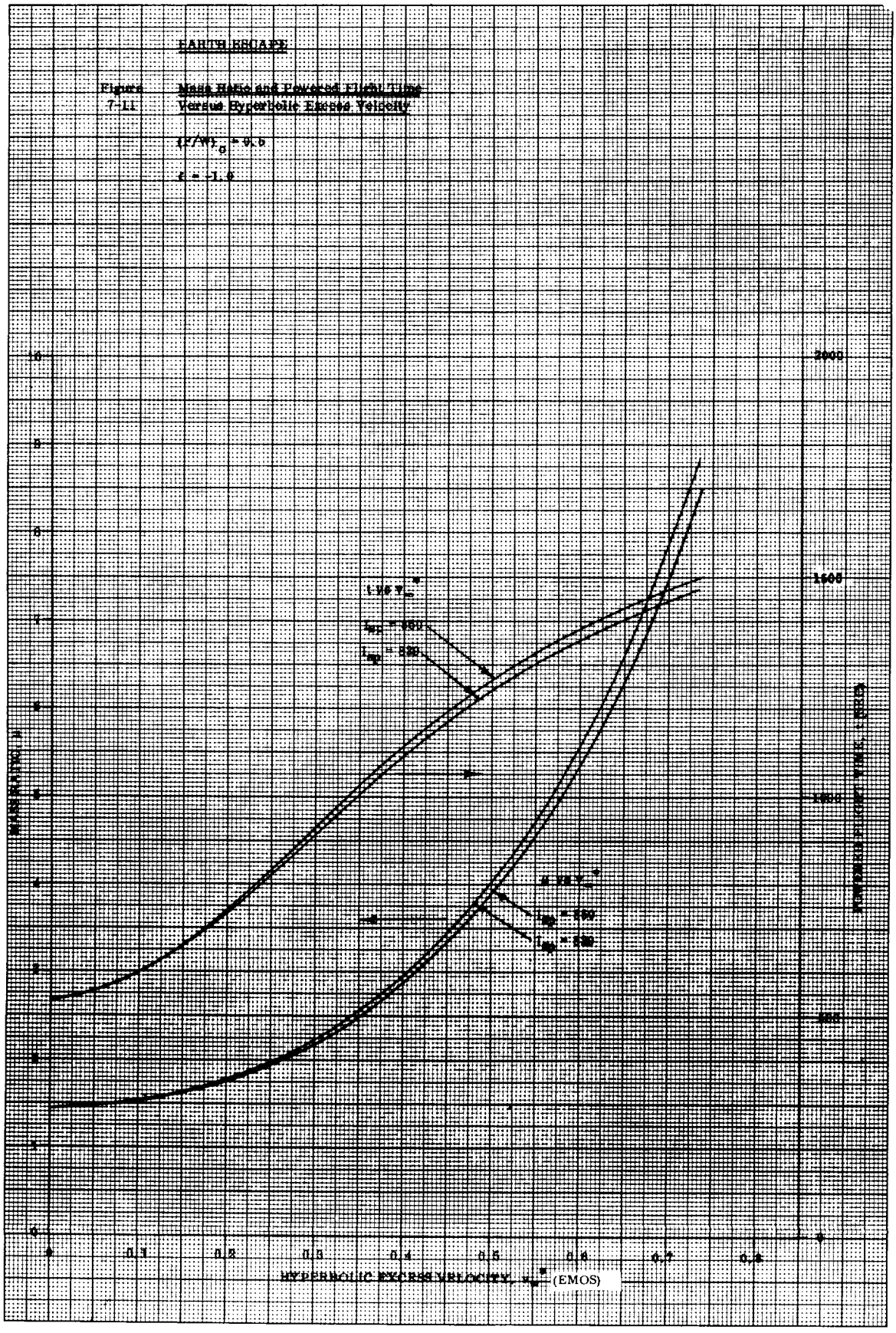
EARTH ESCAPE
Figure 7-11 Mass Ratio and Powered Flight Time Versus Hyperbolic Excess Velocity
$(T/W)_0 = 0.6$
$\zeta = -1.6$
1.05 V_{∞}^*
$I_{sp} = 480$
$I_{sp} = 530$
0.95 V_{∞}^*
$I_{sp} = 480$
$I_{sp} = 530$
MASS RATIO, R
POWERED FLIGHT TIME, SEC
HYPERBOLIC EXCESS VELOCITY, V_{∞}^* (EMOS)

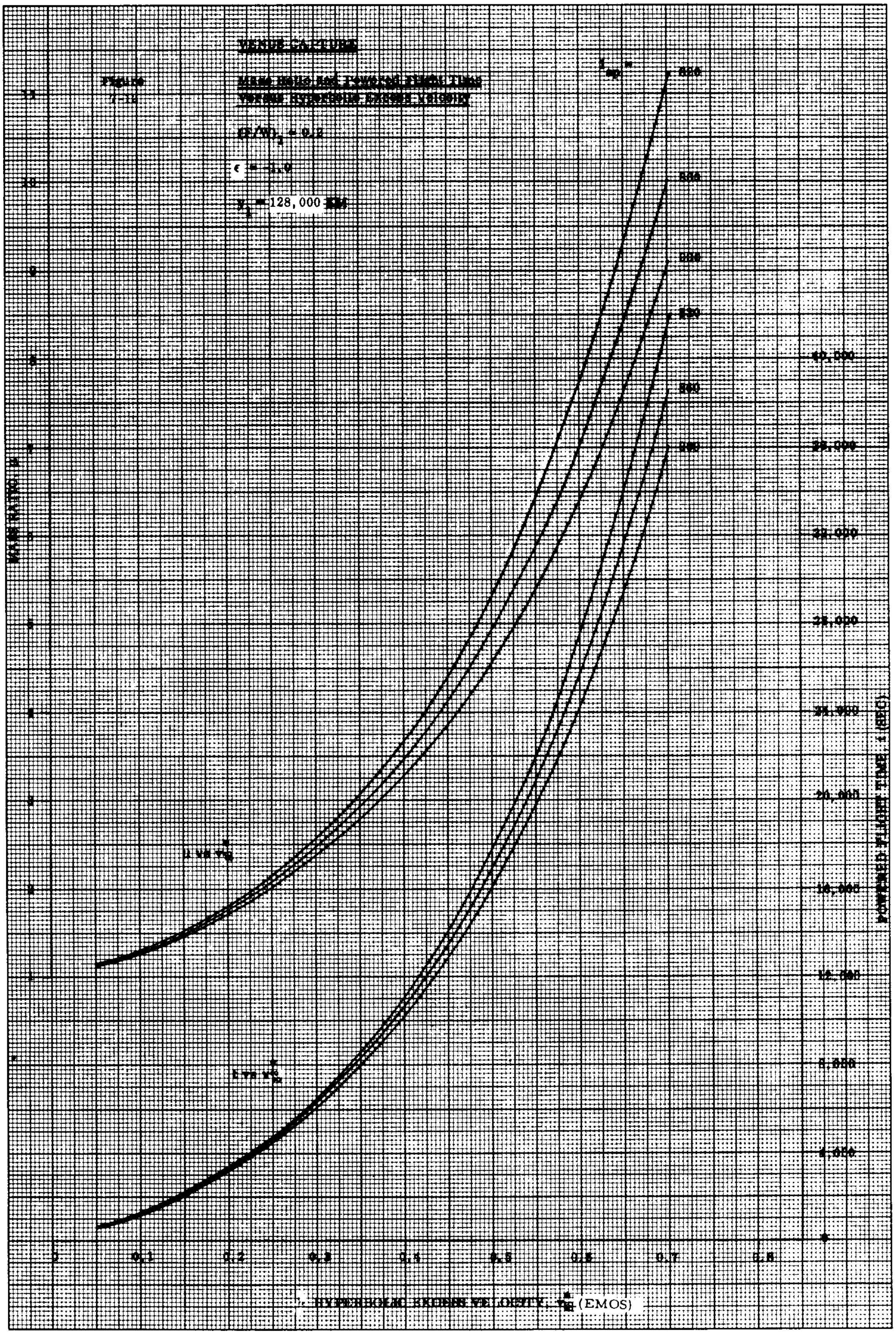
VENUS CAPTURE
128,000
0.1
0.2
0.3
0.4
0.5
0.6
0.7
0.8
(EMOS)

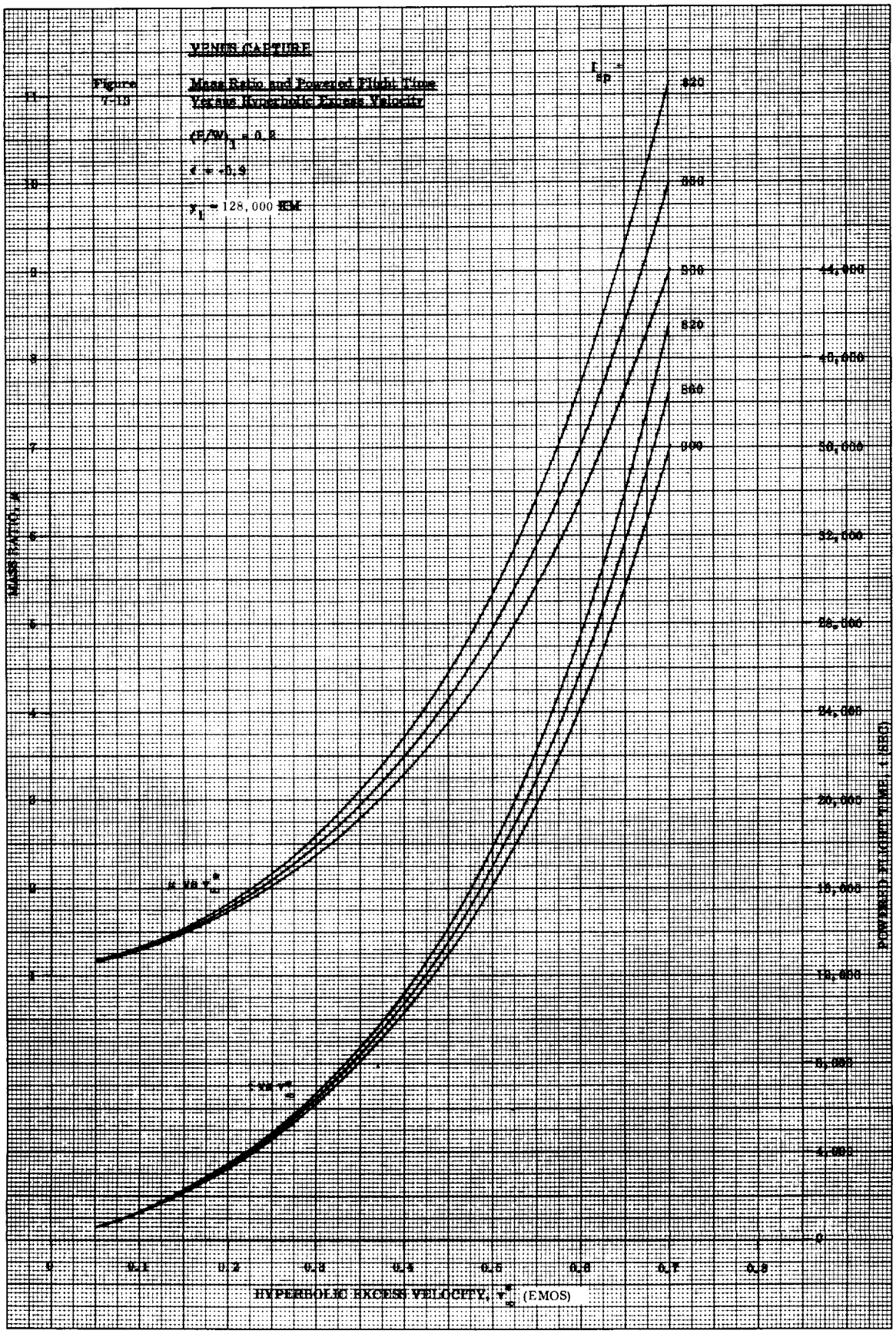
VENUS CAPTURE
Mass Ratio and Powered Flight Time Versus Hyperbolic Excess Velocity
$(T/W_0)_1 = 0.2$
$\epsilon = -0.2$
$r_1 = 128,000$ KM
I_{sp} =
820
800
780
760
740
MASS RATIO, R
POWERED FLIGHT TIME, T (SEC)
44,000
40,000
36,000
32,000
28,000
24,000
20,000
16,000
12,000
8,000
4,000
0
0.1
0.2
0.3
0.4
0.5
0.6
0.7
0.8
HYPERBOLIC EXCESS VELOCITY, $v_{\infty_1}^*$ (EMOS)

Figure 7-13

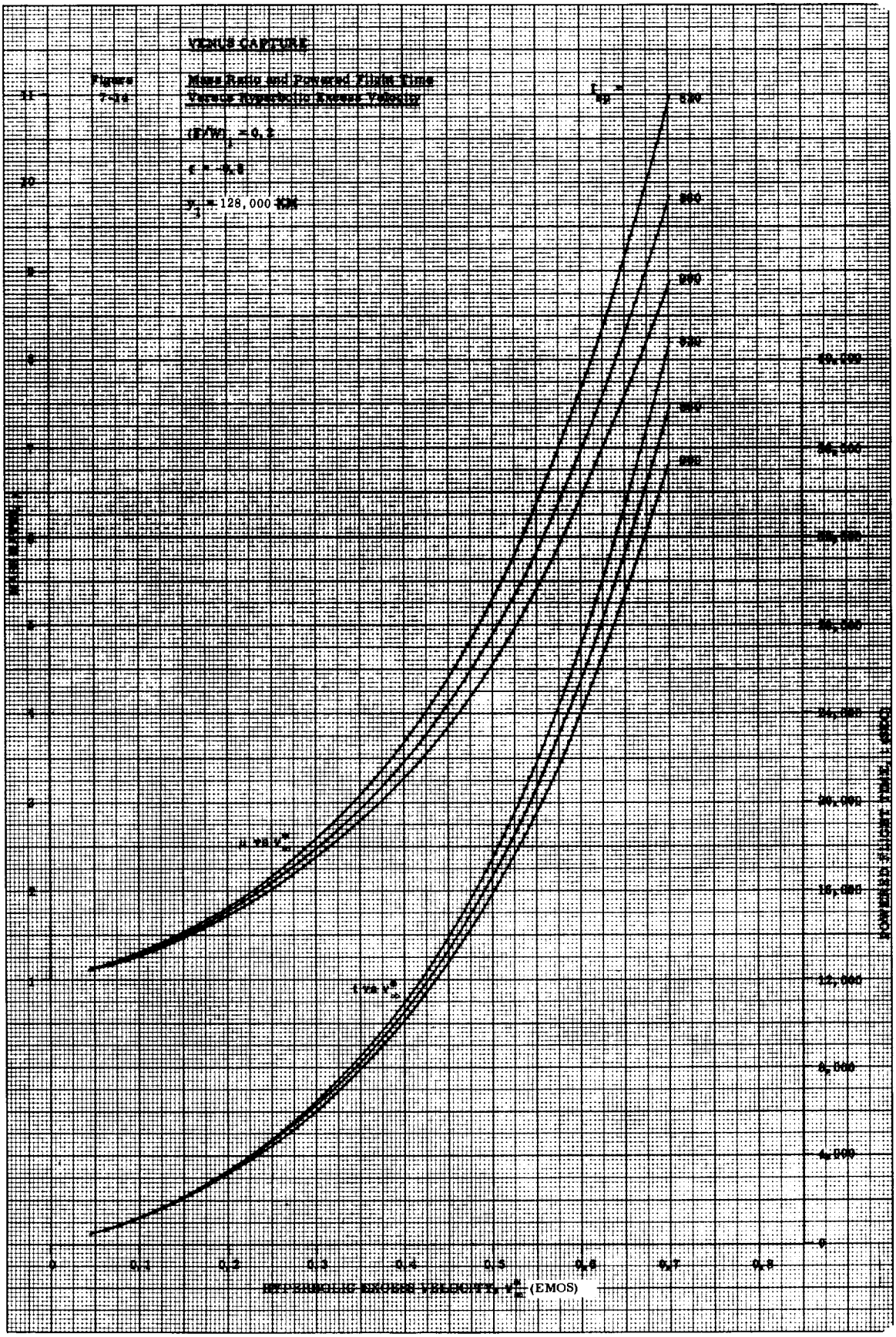
VENUS CAPTURE
Figure 7-14
Mass Ratio and Powered Flight Time Versus Hyperbolic Excess Velocity
$(E/W)_1 = 0.2$
$\epsilon = 0.8$
$r_3 = 128,000$ KM
$t_{FB} =$
μ vs V_∞^*
t vs V_∞^*
HYPERBOLIC EXCESS VELOCITY, V_∞^* (EMOS)

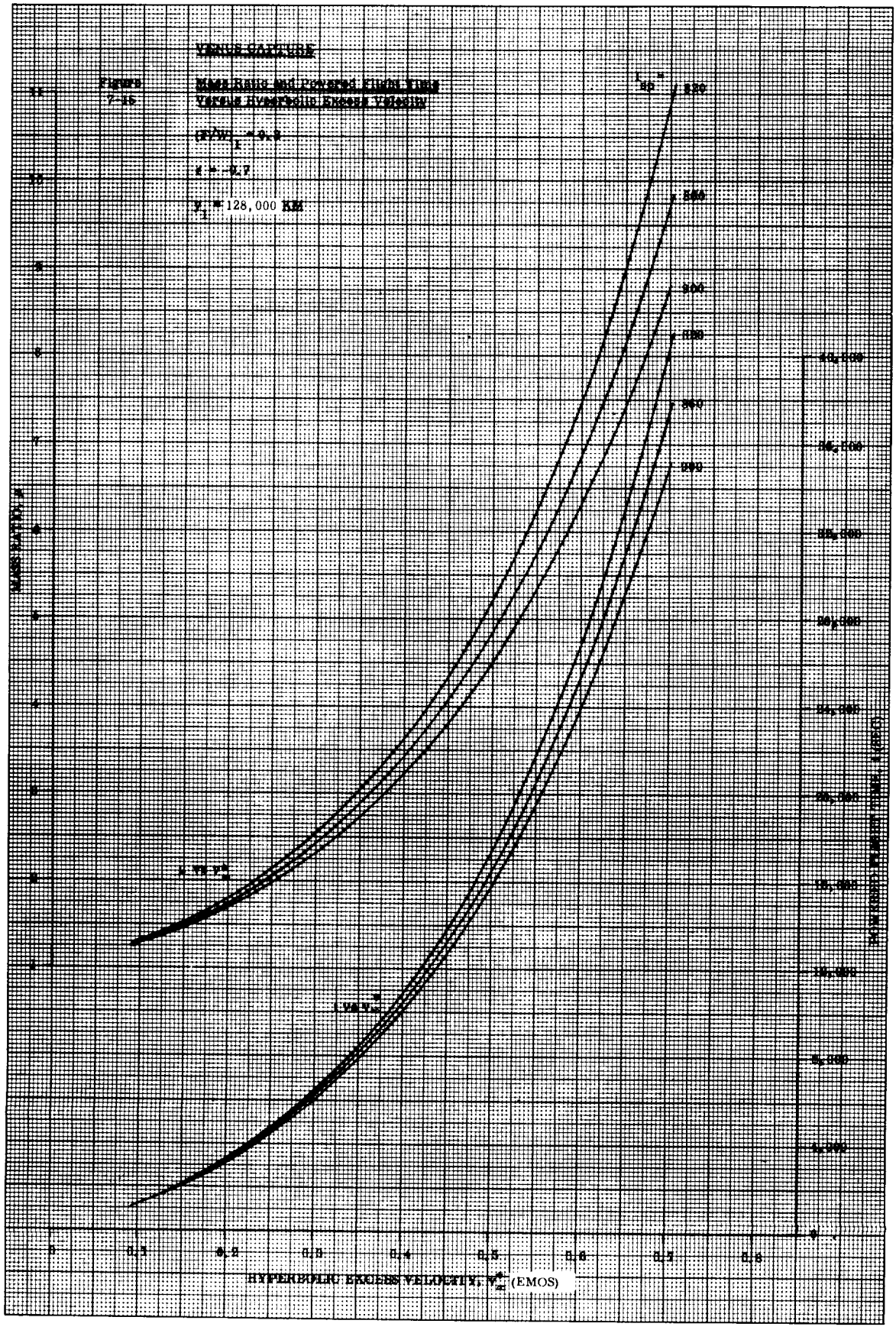
VENUS CAPTURE
Figure 7-15
Mass Ratio and Powered Flight Time Versus Hyperbolic Excess Velocity
$(R/W)_I = 0.9$
$\epsilon = -0.7$
$r_I = 128,000$ KM
$t_{BO} =$ 520
560
600
640
680
720
MASS RATIO, R
POWERED FLIGHT TIME, t_{BO} (SEC)
HYPERBOLIC EXCESS VELOCITY, V_∞^* (EMOS)

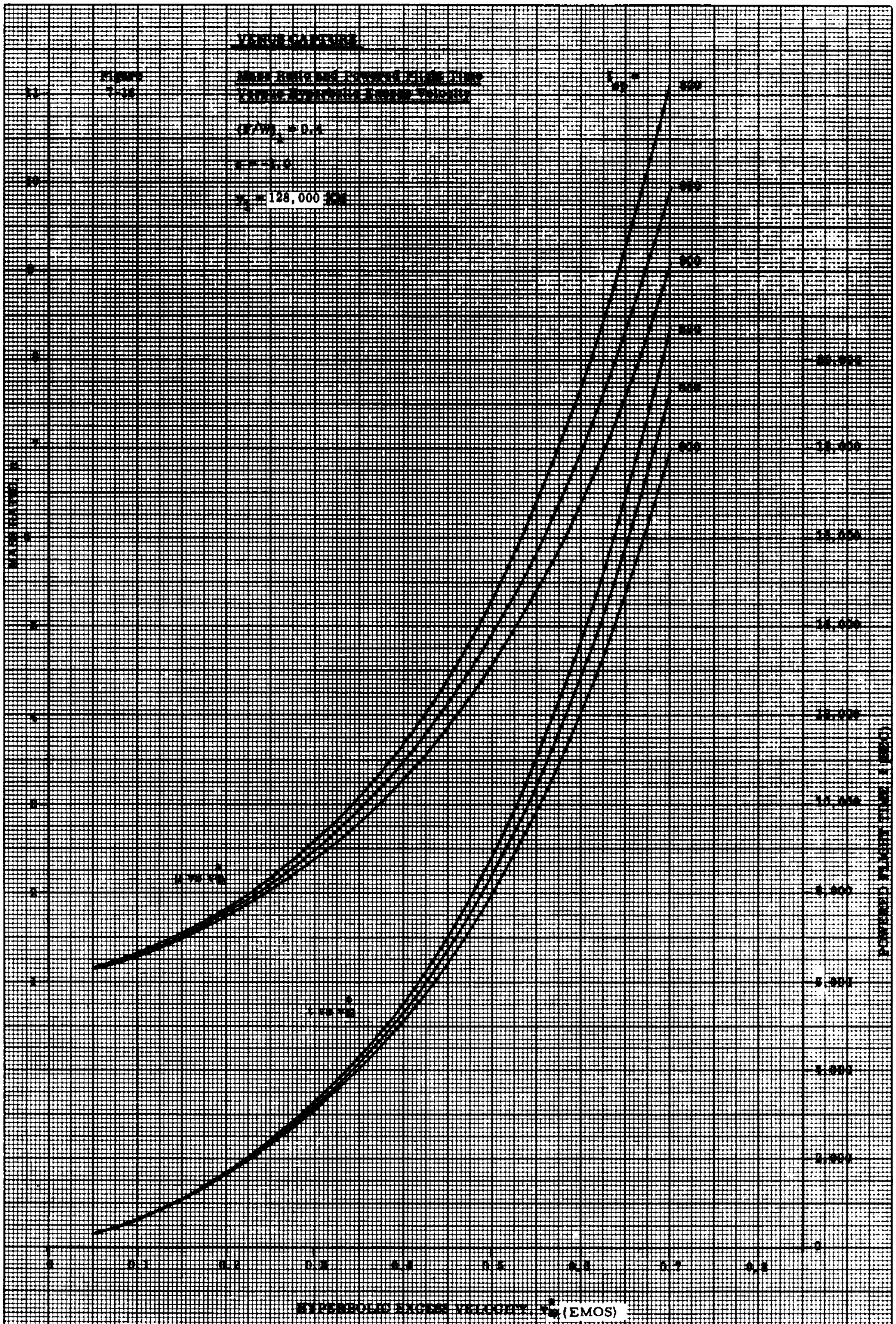
VENUS CAPTURE
128,000
HYPERBOLIC EXCESS VELOCITY
(EMOS)

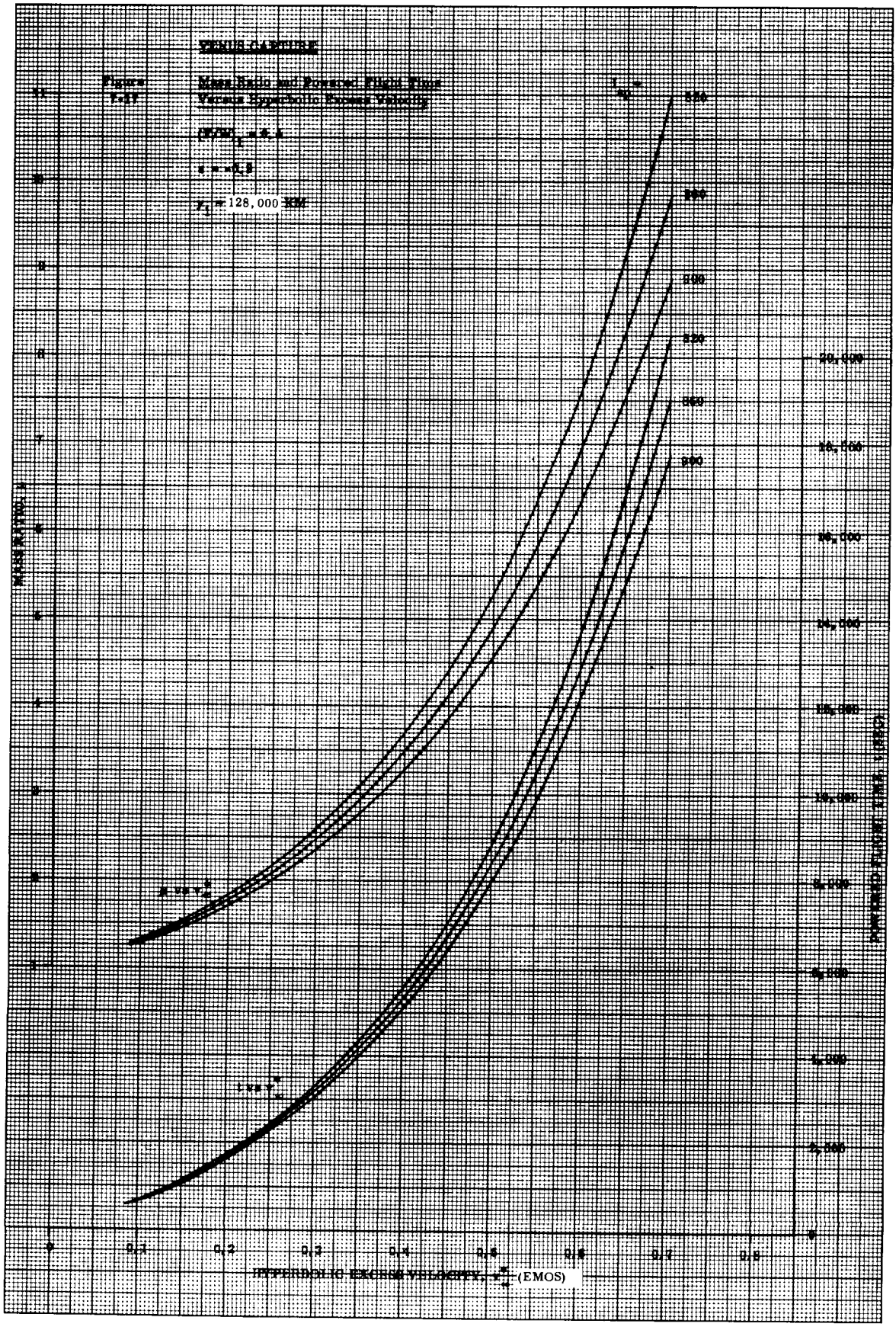
VENUS CAPTURE
Figure
Mass Ratio and Powered Flight Time
Versus Hyperbolic Excess Velocity
HYPERBOLIC EXCESS VELOCITY, V_∞^* (EMOS)

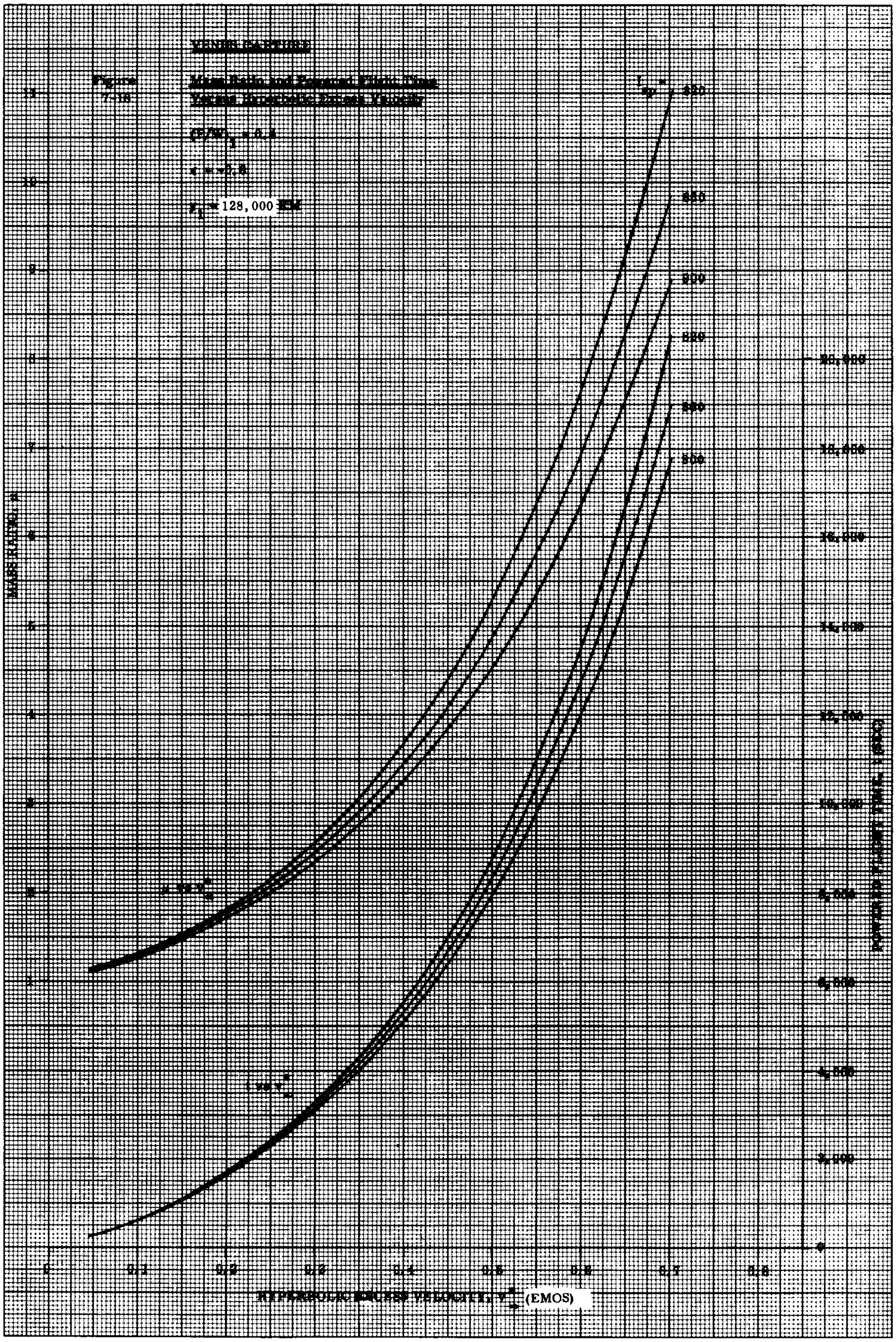
128,000
(EMOS)

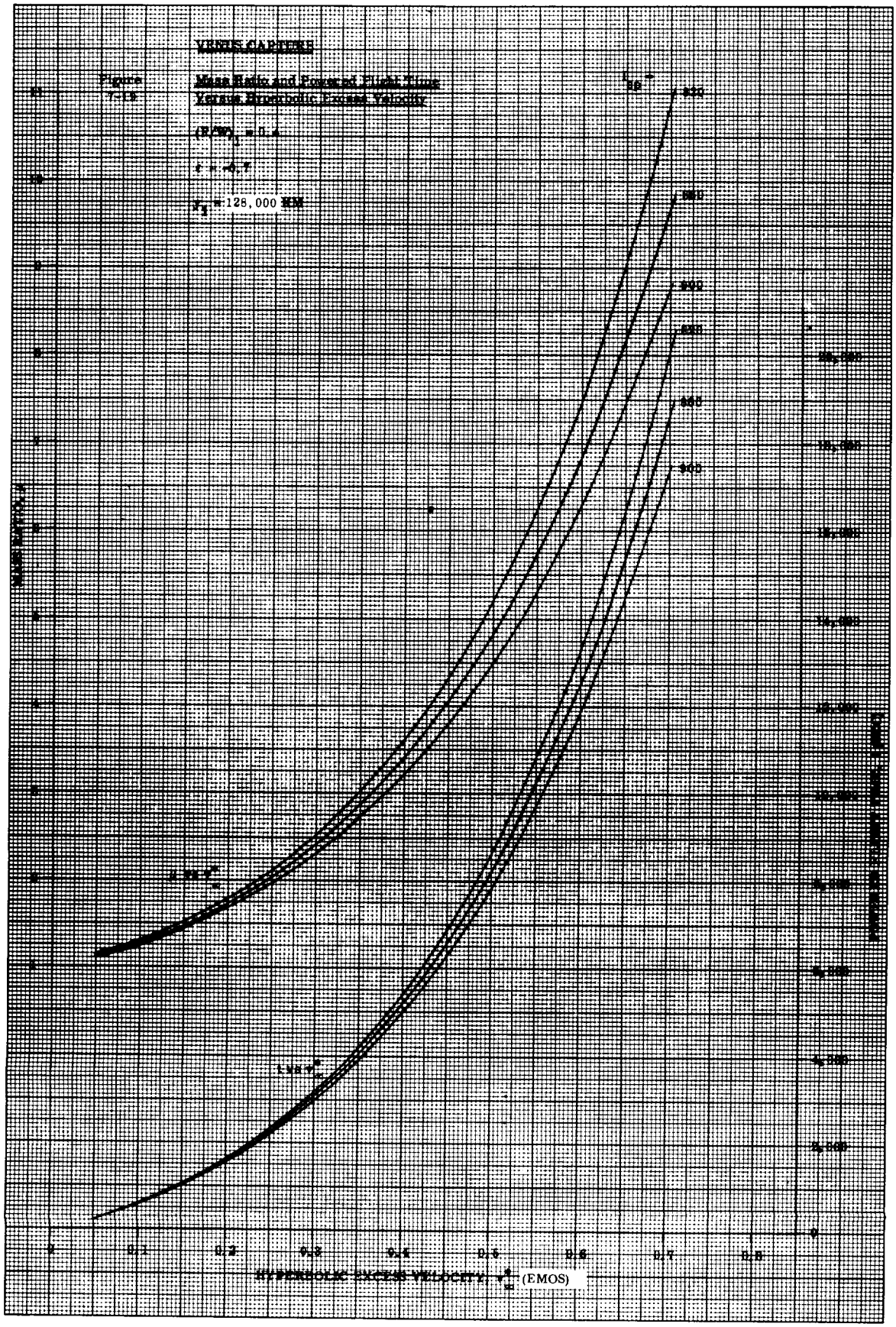
VENUS CAPTURE
Figure 7-19
Mass Ratio and Powered Flight Time Versus Hyperbolic Excess Velocity
$(R/W)_i = 0.4$
$r = 4.7$
$r_p = 128,000$ KM
HYPERBOLIC EXCESS VELOCITY, V_{∞}^* (EMOS)

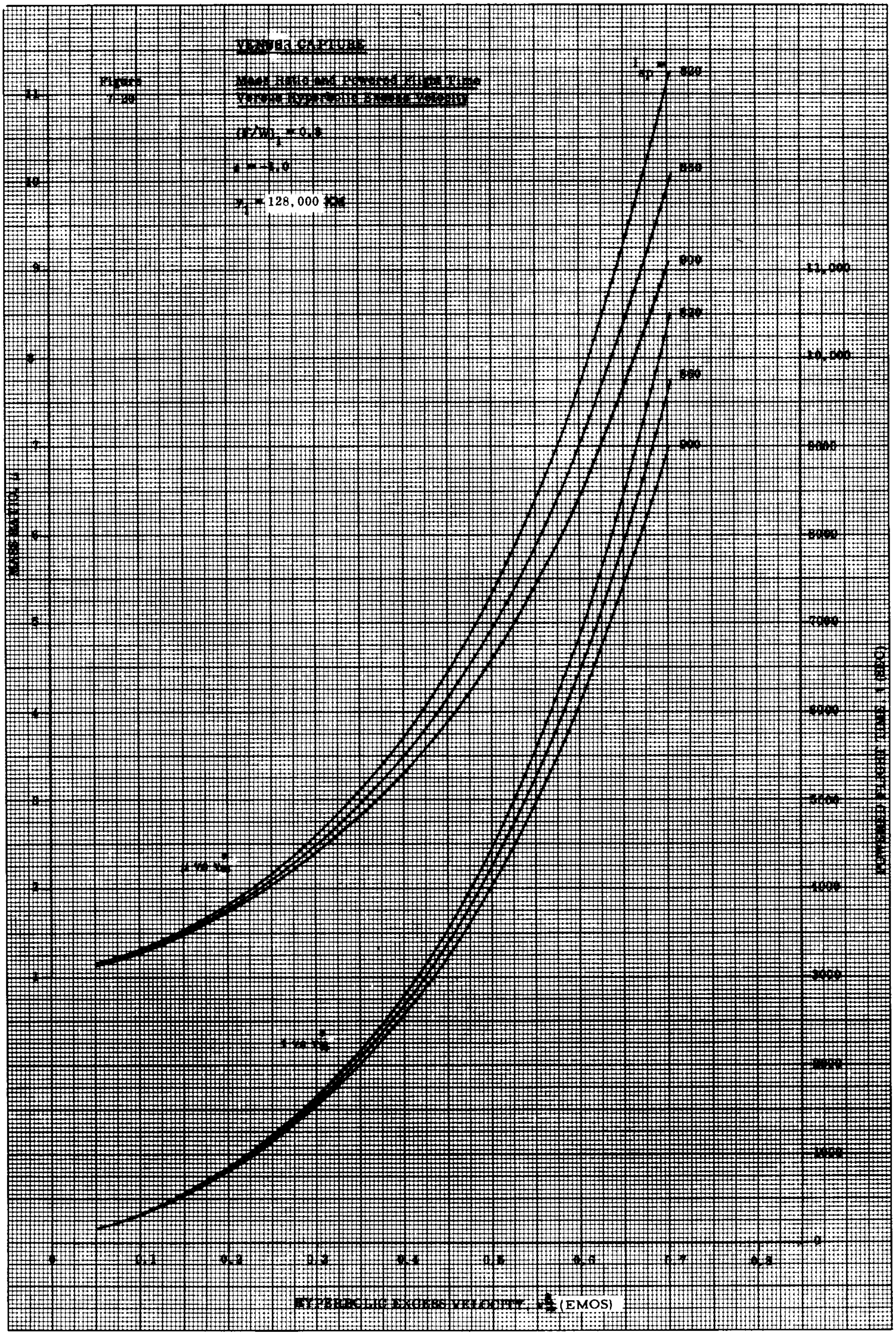
Figure 7-20
VENUS63 CAPTURE
Mass Ratio and Powered Flight Time Versus Hyperbolic Excess Velocity
128,000 KM
11,000
10,000
(EMOS)

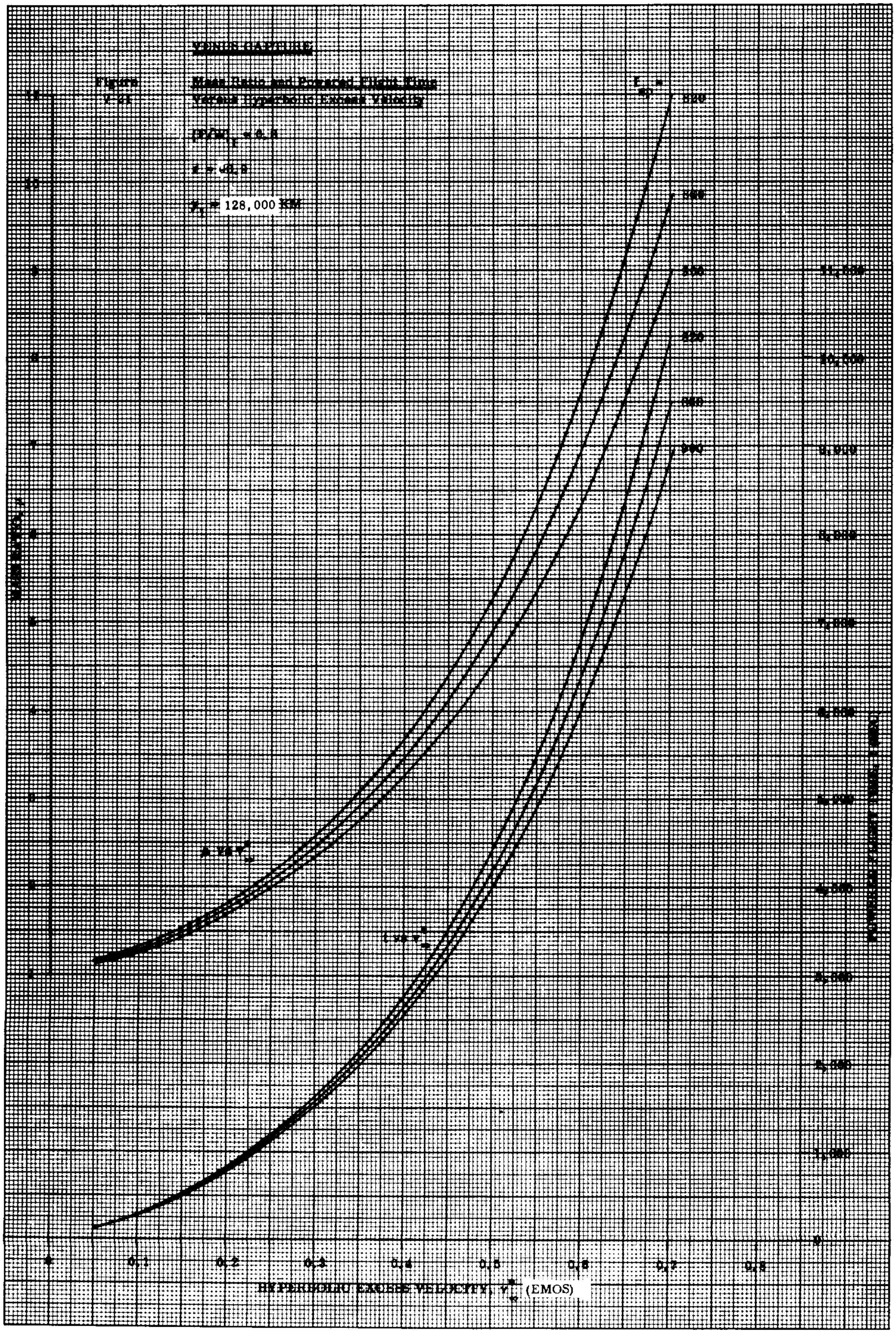
VENUS CAPTURE
Mass Ratio and Powered Flight Time
Versus Hyperbolic Excess Velocity
128,000 KM
0
0.1
0.2
0.3
0.4
0.5
0.6
0.7
0.8
HYPERBOLIC EXCESS VELOCITY, V∞* (EMOS)

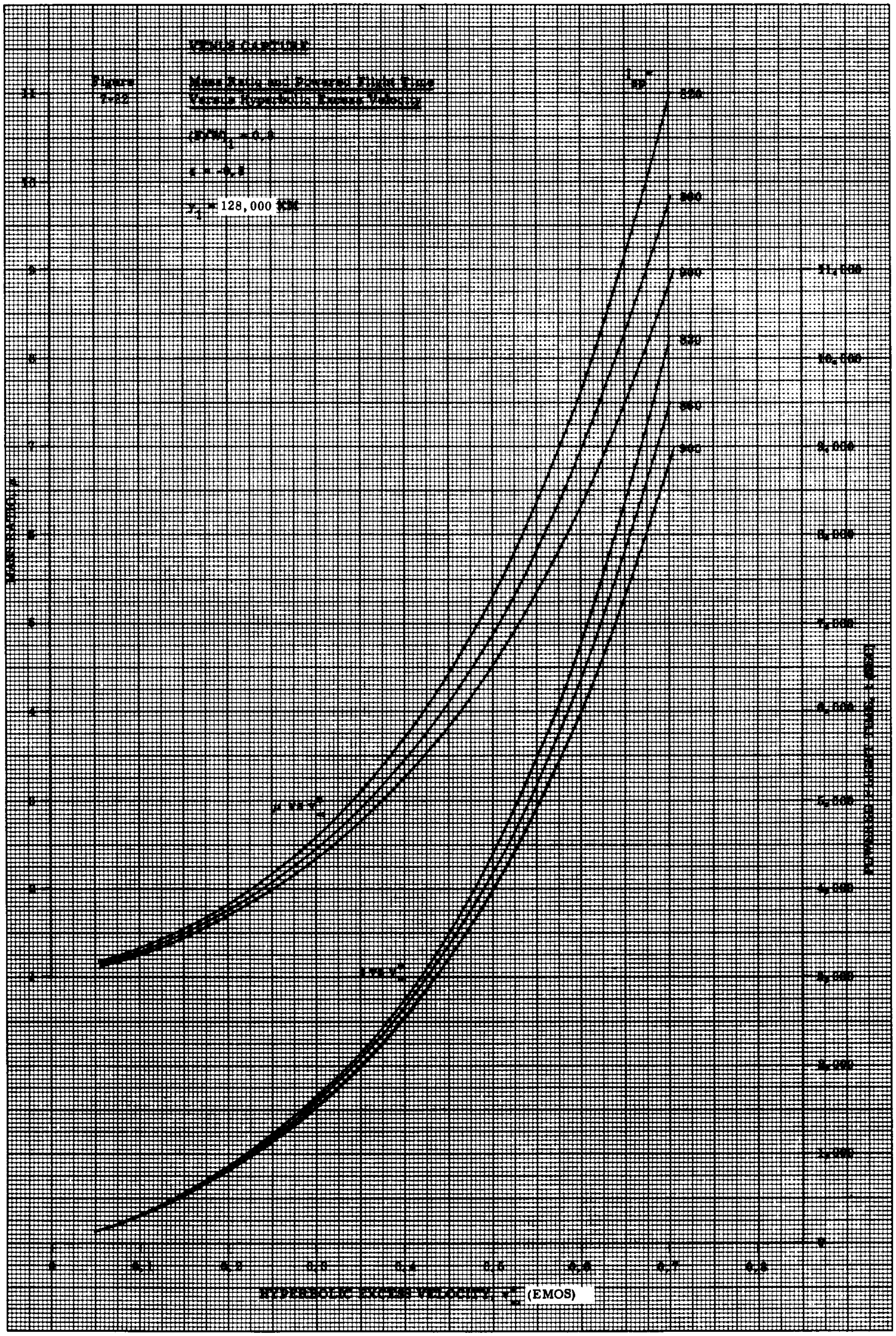
VENUS CAPTURE
y_1 = 128,000 KM
HYPERBOLIC EXCESS VELOCITY, v_∞^* (EMOS)

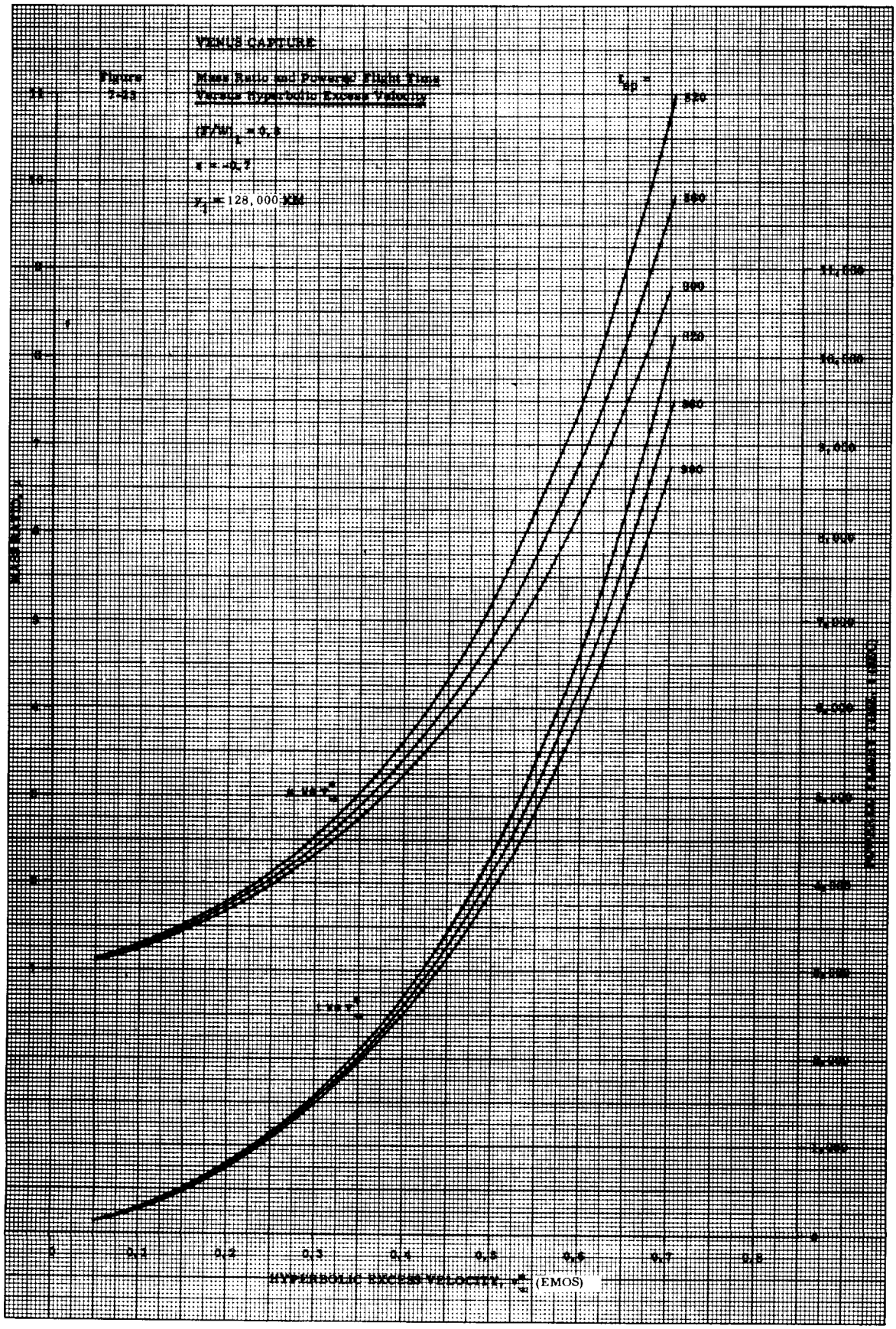
VENUS CAPTURE
Figure 7-43
Mass Ratio and Powered Flight Time Versus Hyperbolic Excess Velocity
$(R/W)_i = 0.8$
$\epsilon = -0.7$
$r_1 = 128,000$ KM
$t_{pf} =$
HYPERBOLIC EXCESS VELOCITY, v_{∞}^{*} (EMOS)

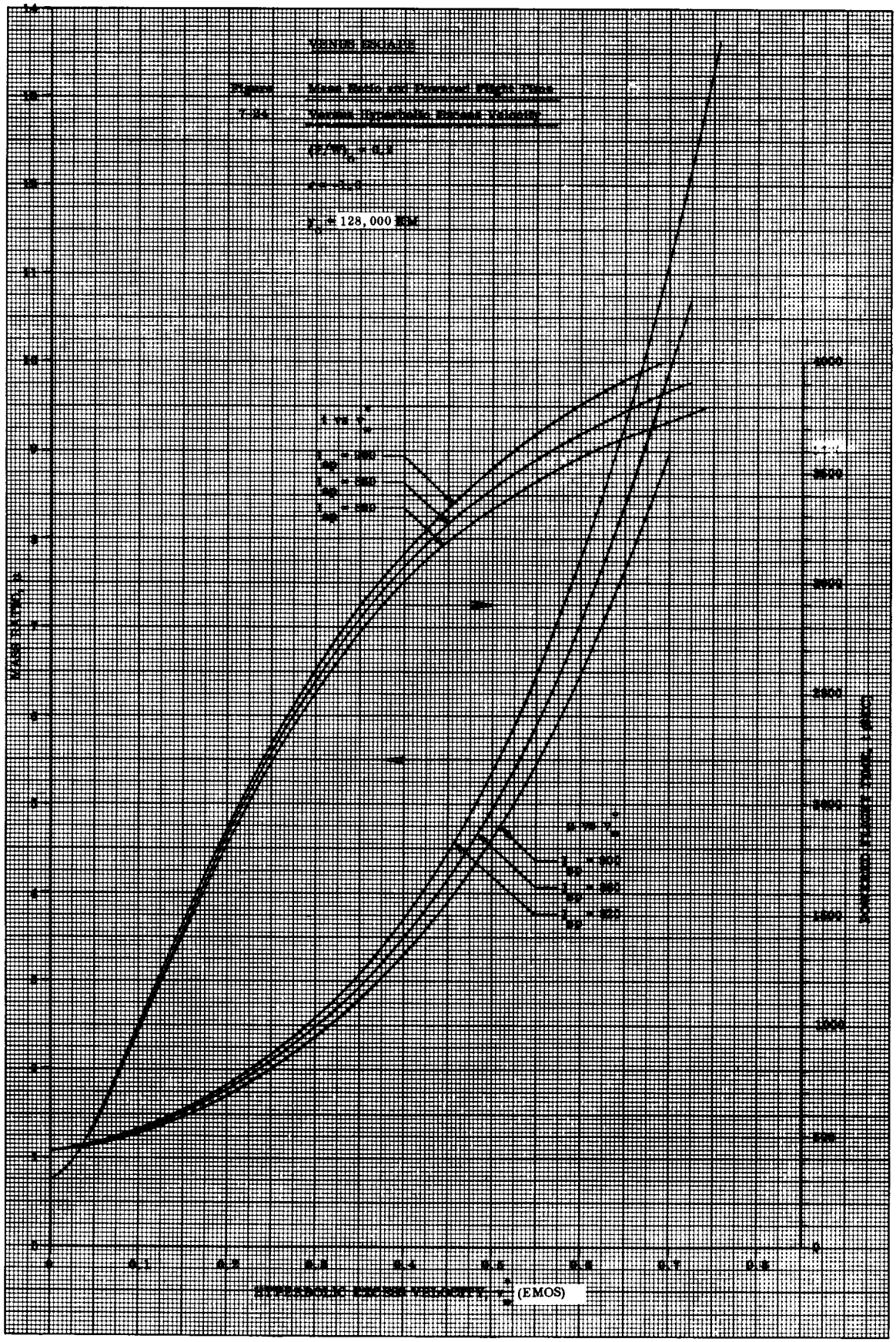

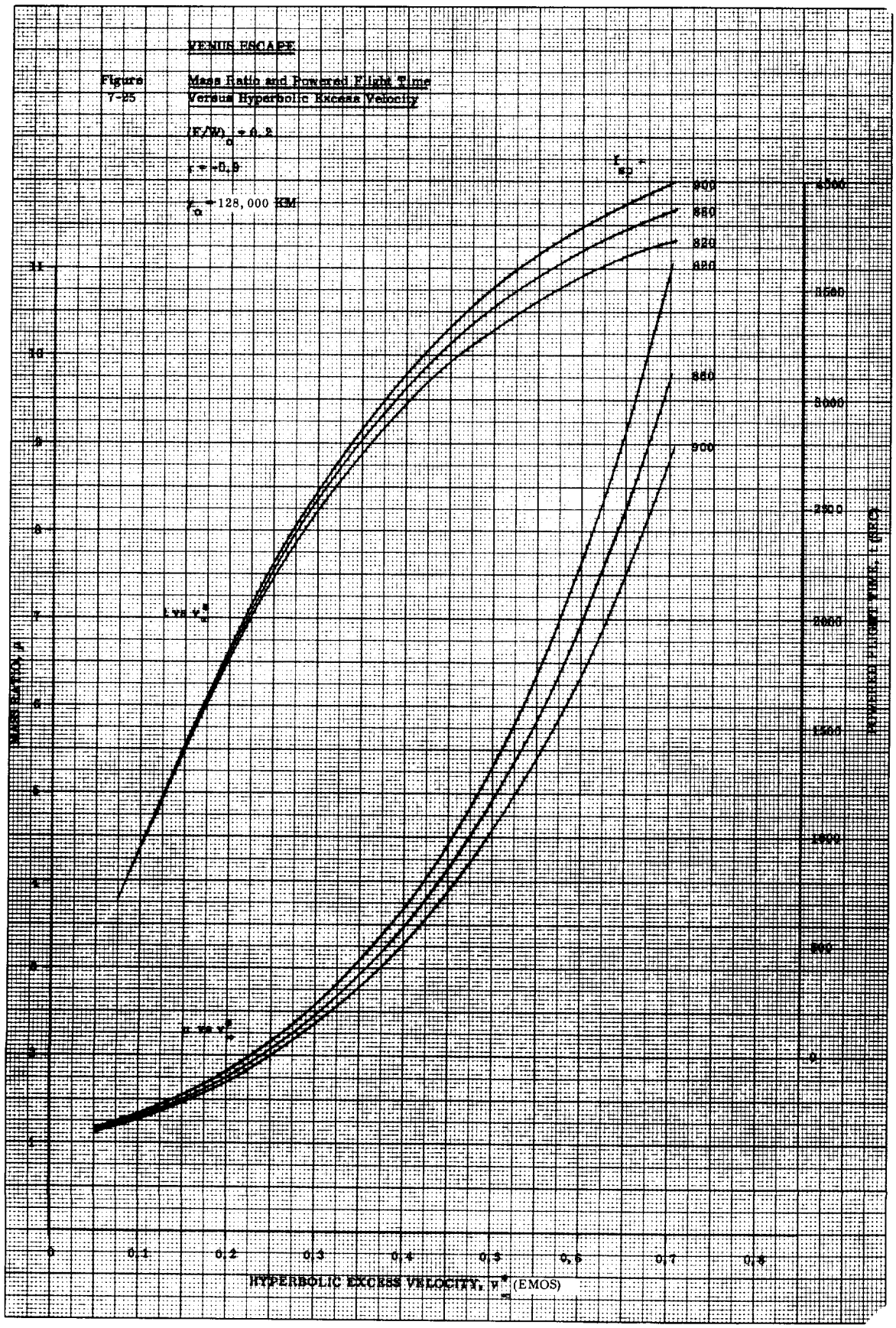
VENUS ESCAPE
Figure 7-25
Mass Ratio and Powered Flight Time Versus Hyperbolic Excess Velocity
$(F/W)_o = 0.2$
$i = +0.9$
$r_o = 128,000$ KM
$t_{BO} =$
900
880
860
850
900
MASS RATIO, R
POWERED FLIGHT TIME, t (SEC)
t vs v_∞^*
R vs v_∞^*
0
0.1
0.2
0.3
0.4
0.5
0.6
0.7
0.8
HYPERBOLIC EXCESS VELOCITY, v_∞^* (EMOS)

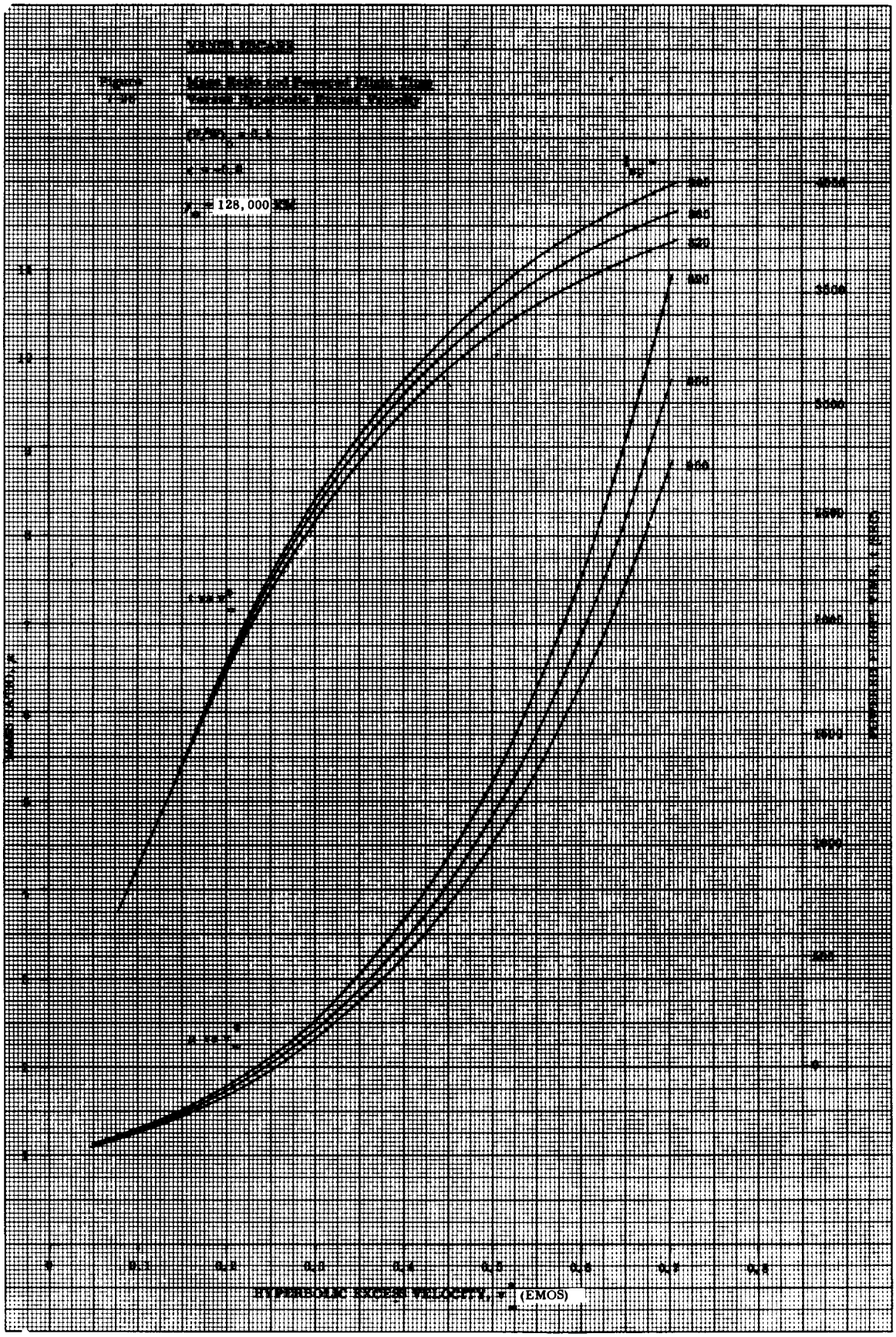

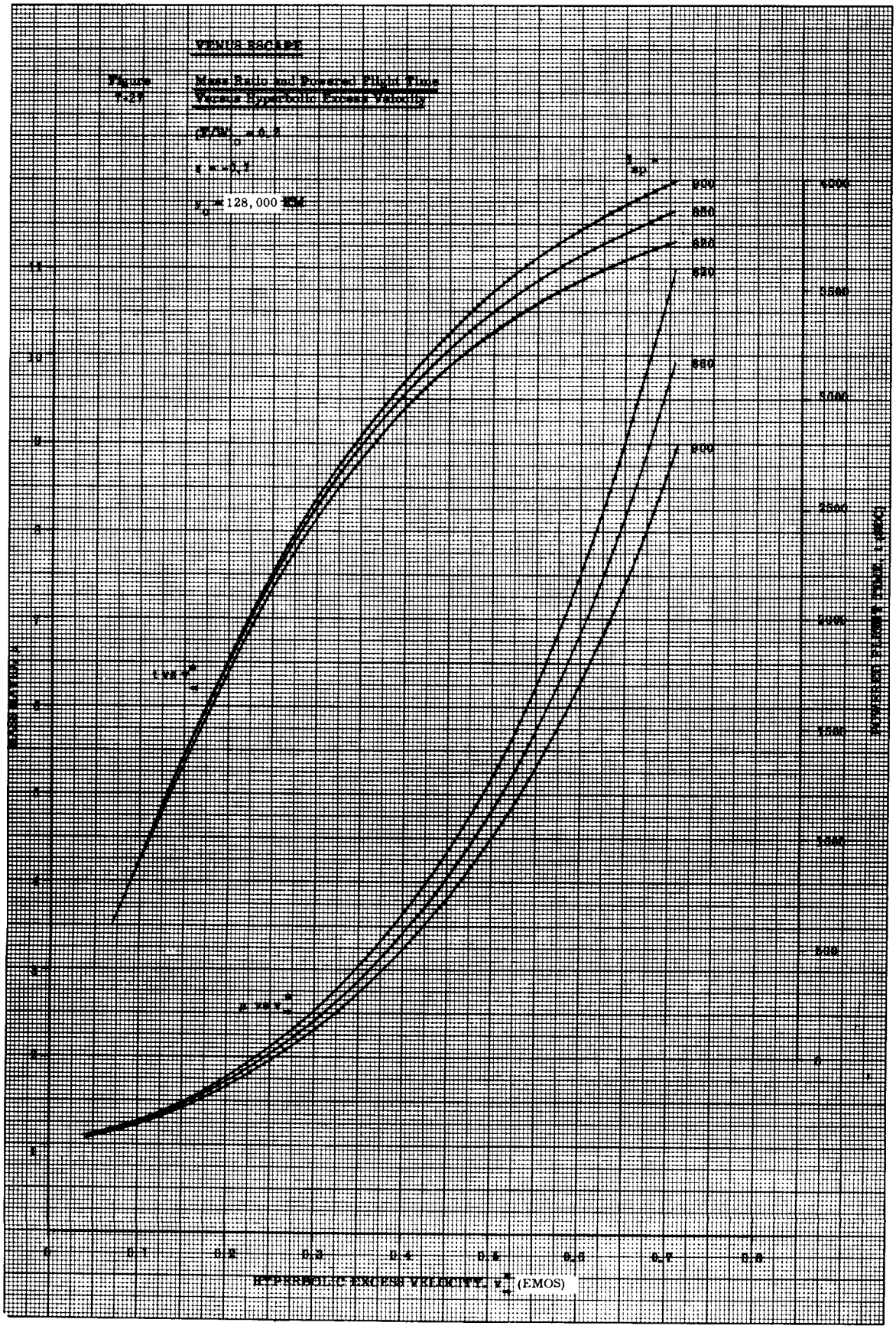
VENUS ESCAPE
Figure V-27
Mass Ratio and Powered Flight Time
Versus Hyperbolic Excess Velocity
$(W/W)_0$ = 6.2
ϵ = -0.2
r_0 = 128,000 KM
t_{BO} =
900
850
800
750
700
650
600
550
500
450
400
350
300
250
200
150
100
50
0
MASS RATIO, W_0/W_{BO}
POWERED FLIGHT TIME, t_{BO} - SEC
0
0.1
0.2
0.3
0.4
0.5
0.6
0.7
0.8
HYPERBOLIC EXCESS VELOCITY, V_∞^* (EMOS)

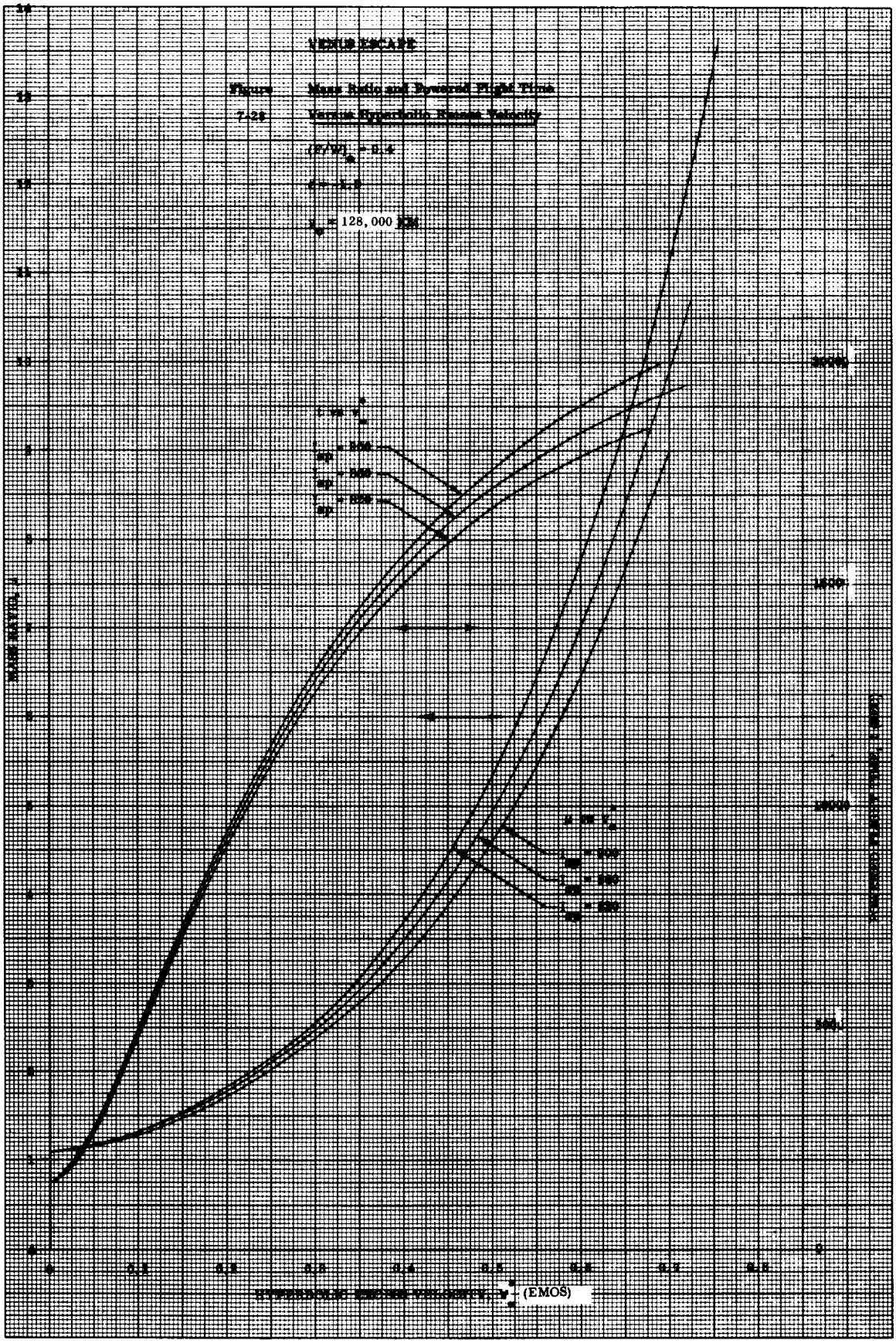
VENUS ESCAPE
Figure 7-23 Mass Ratio and Powered Flight Time Versus Hyperbolic Excess Velocity
(EMOS)

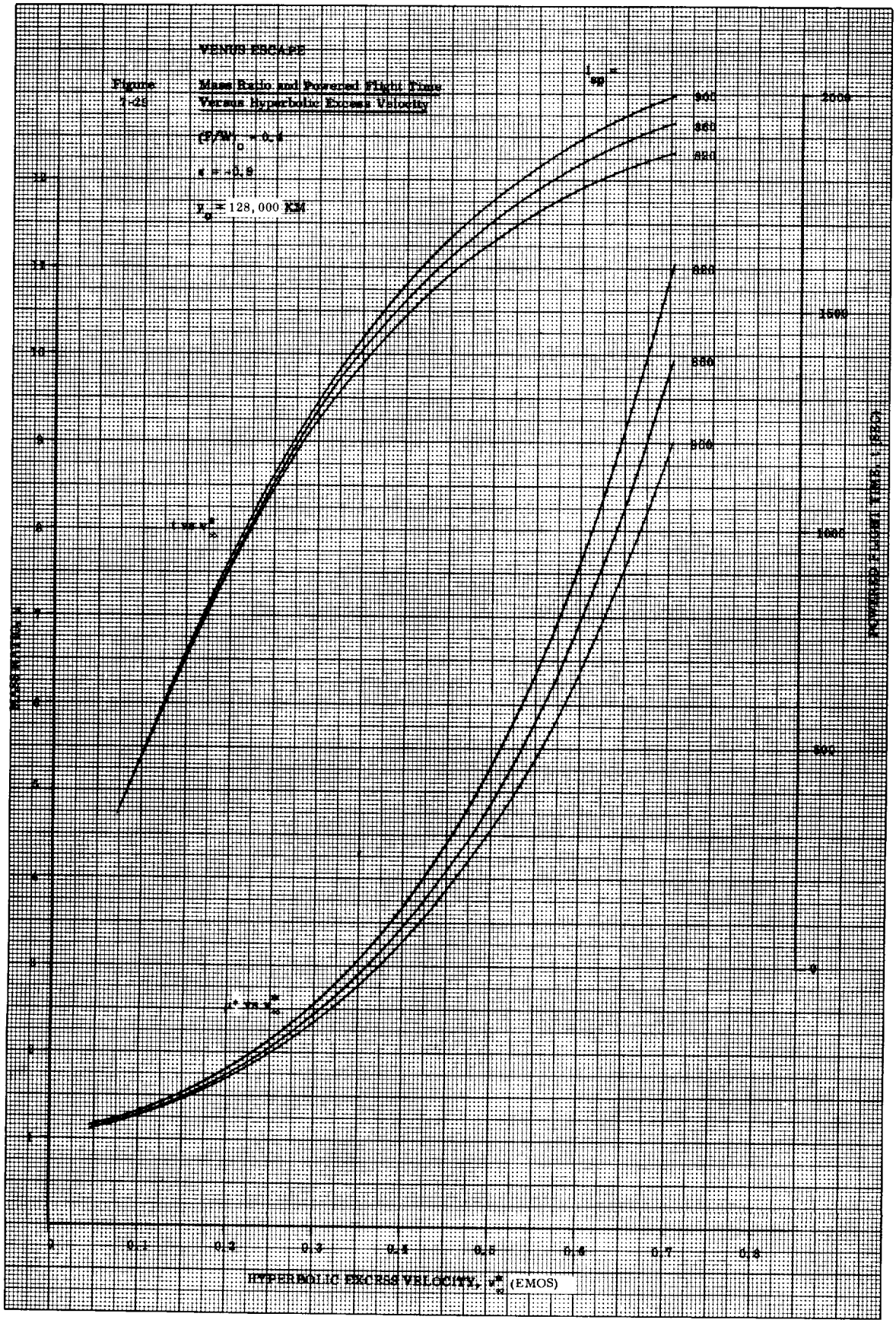
VENUS ESCAPE
Mass Ratio and Powered Flight Time Versus Hyperbolic Excess Velocity
$(P/W)_o$ = 0.4
ϵ = -0.9
r_o = 128,000 KM
t_{pp} =
900
860
820
MASS RATIO
POWERED FLIGHT TIME, t (SEC)
2000
1500
1000
500
0
0.1
0.2
0.3
0.4
0.5
0.6
0.7
0.8
HYPERBOLIC EXCESS VELOCITY, v_∞^* (EMOS)

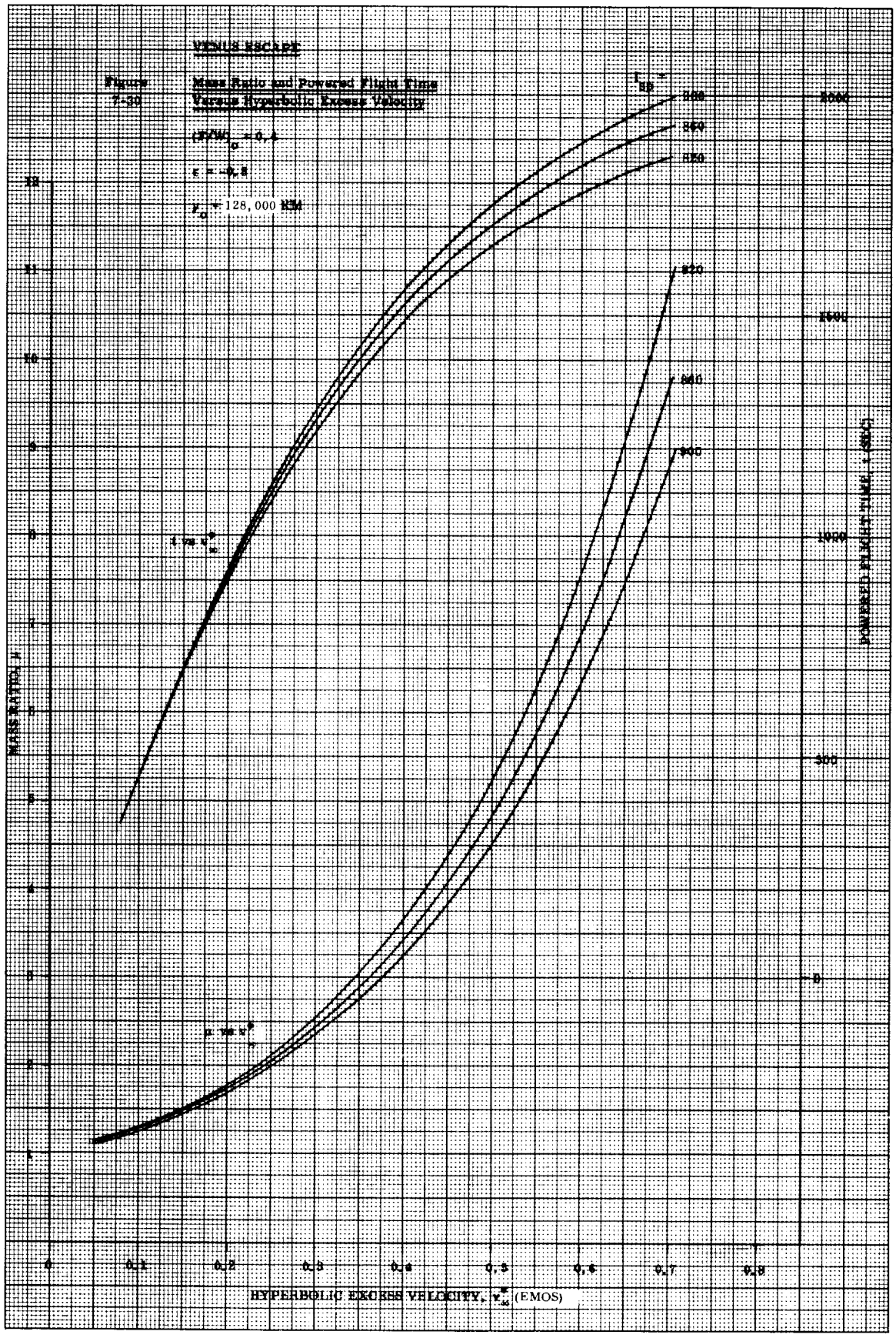
VENUS ESCAPE
Mass Ratio and Powered Flight Time
Versus Hyperbolic Excess Velocity
$(W/W_0)_0 = 0.4$
$\epsilon = -0.8$
$r_0 = 128,000$ KM
$t_{BB} =$
800
850
850
820
840
860
1000
500
0
MASS RATIO, R
POWERED FLIGHT TIME, t (SEC)
HYPERBOLIC EXCESS VELOCITY, v_∞^* (EMOS)

Figure 7-30

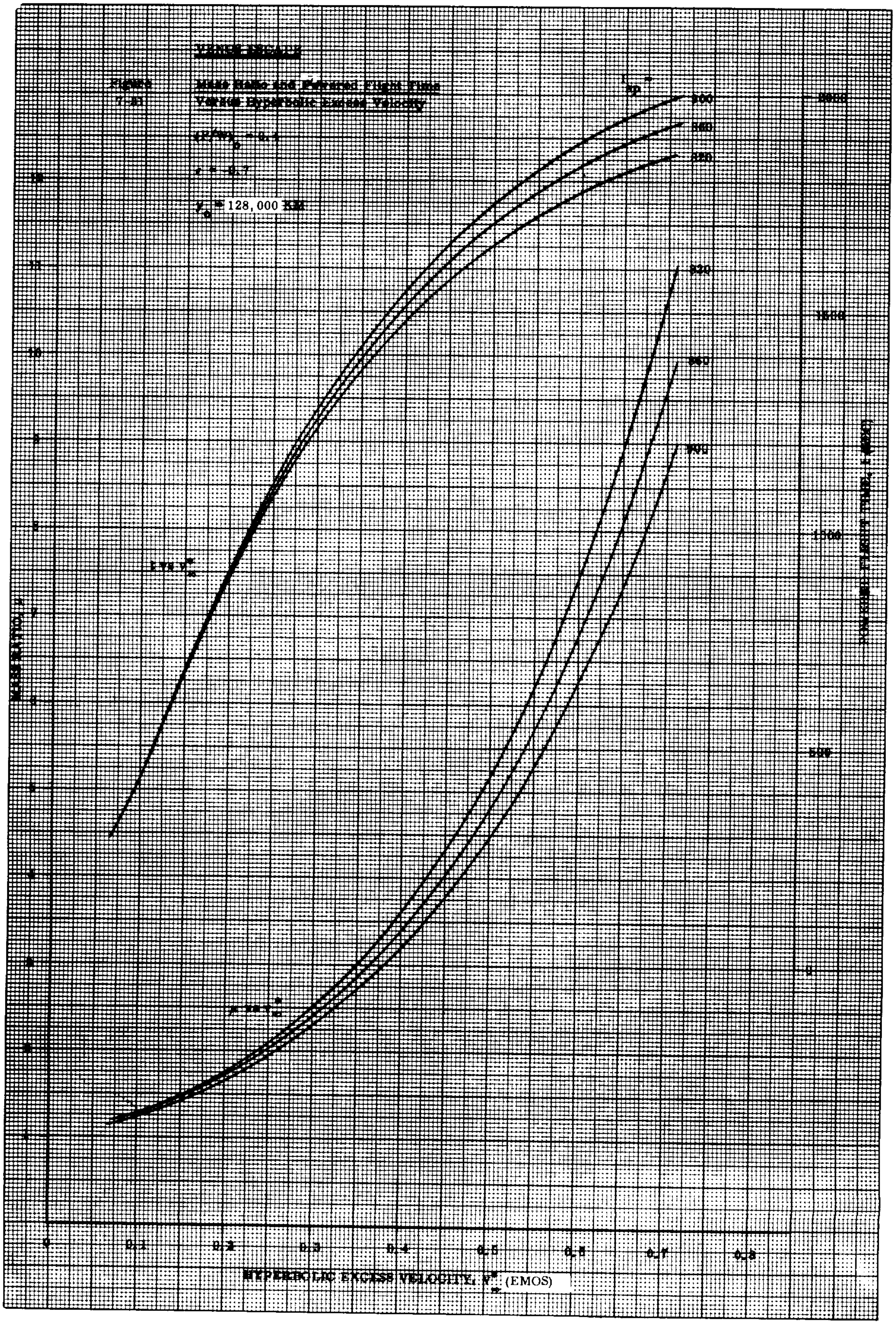
Figure
7-81
Mass Ratio and Powered Flight Time
Versus Hyperbolic Excess Velocity
r = 0.7
128,000 KM
0
0.1
0.2
0.3
0.4
0.5
0.6
0.7
0.8
(EMOS)

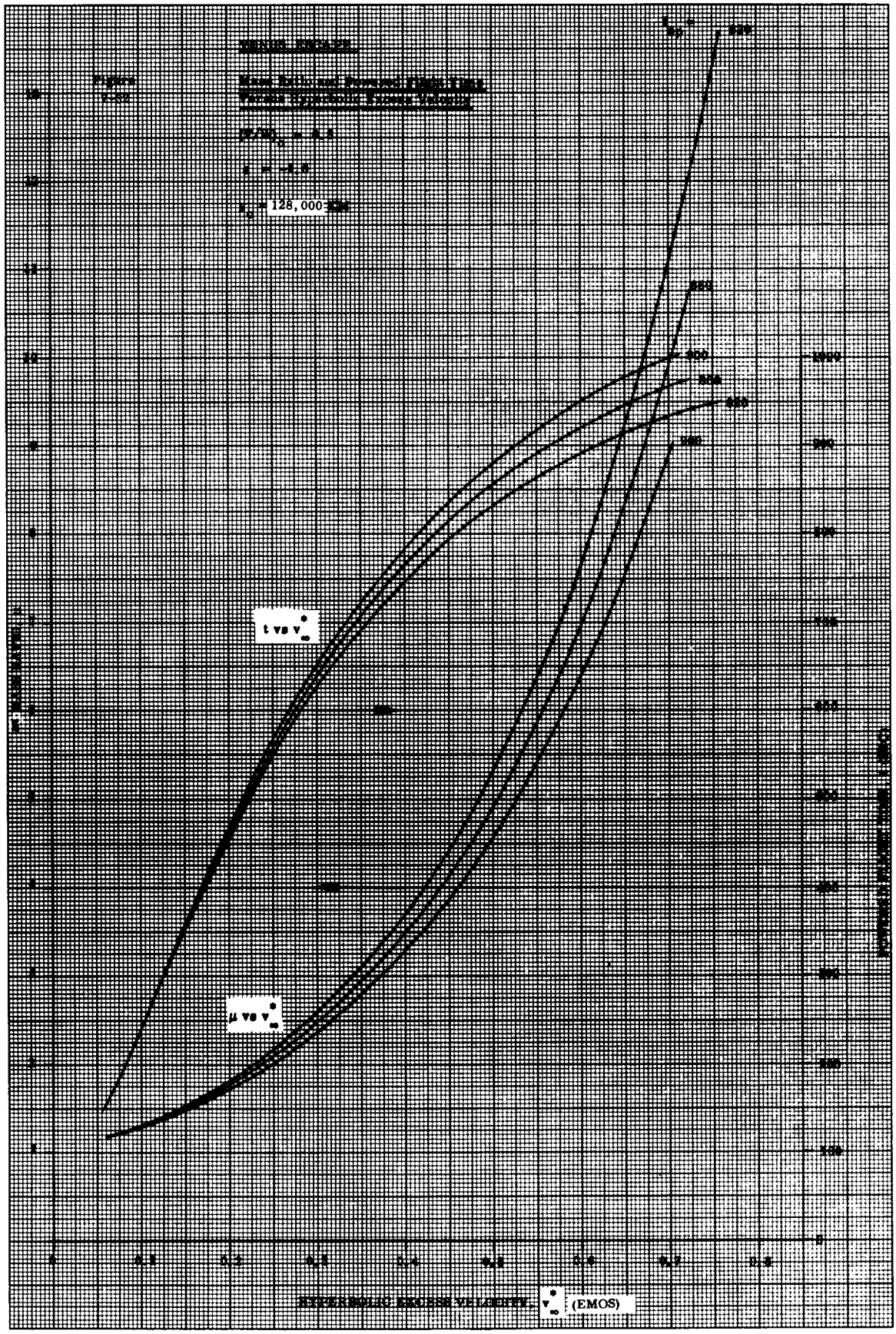
t vs V_∞^*
μ vs V_∞^*
HYPERBOLIC EXCESS VELOCITY, V_∞^* (EMOS)

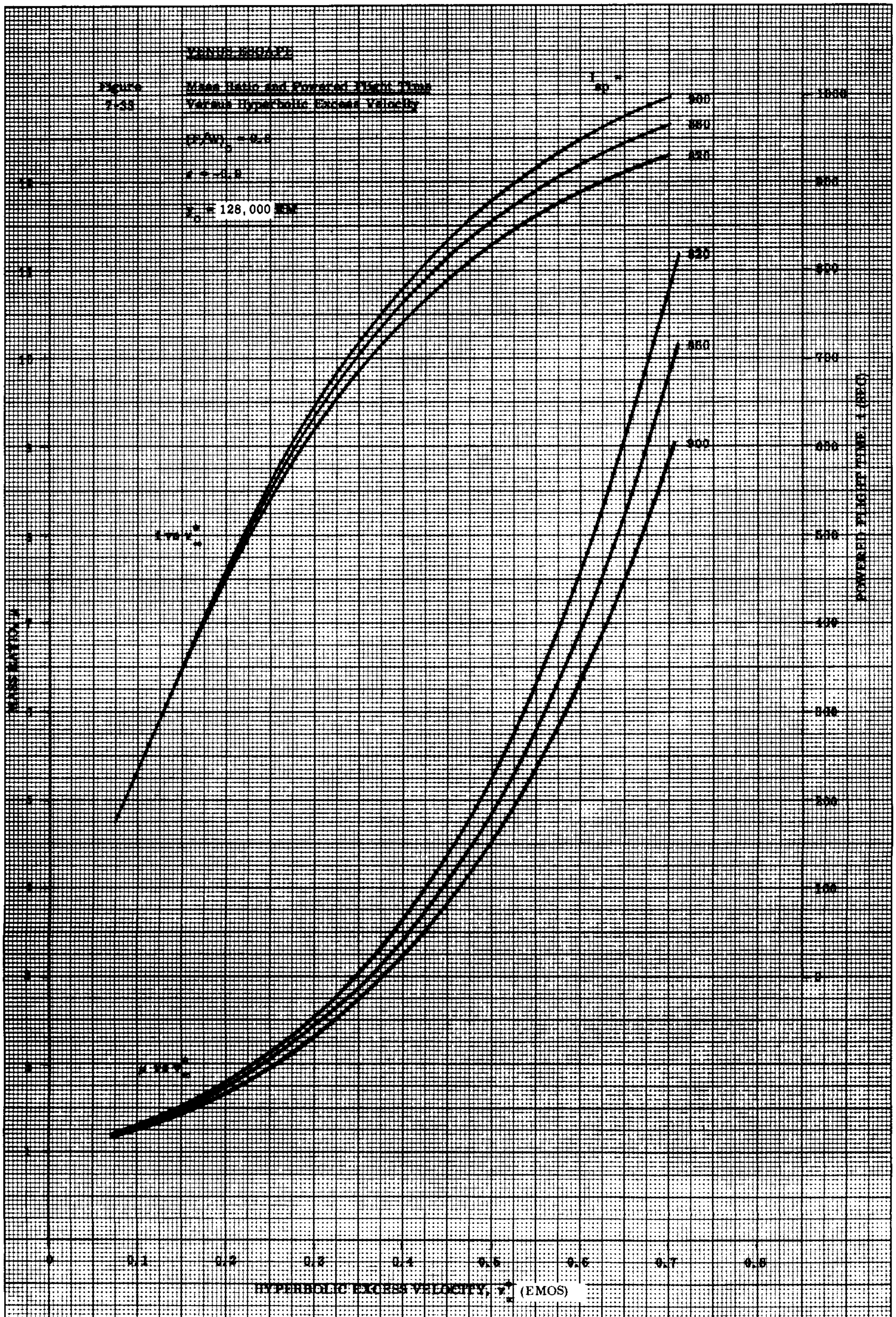
VENUS ESCAPE
Mass Ratio and Powered Flight Time
Versus Hyperbolic Excess Velocity
128,000
HYPERBOLIC EXCESS VELOCITY, (EMOS)
POWERED FLIGHT TIME
MASS RATIO

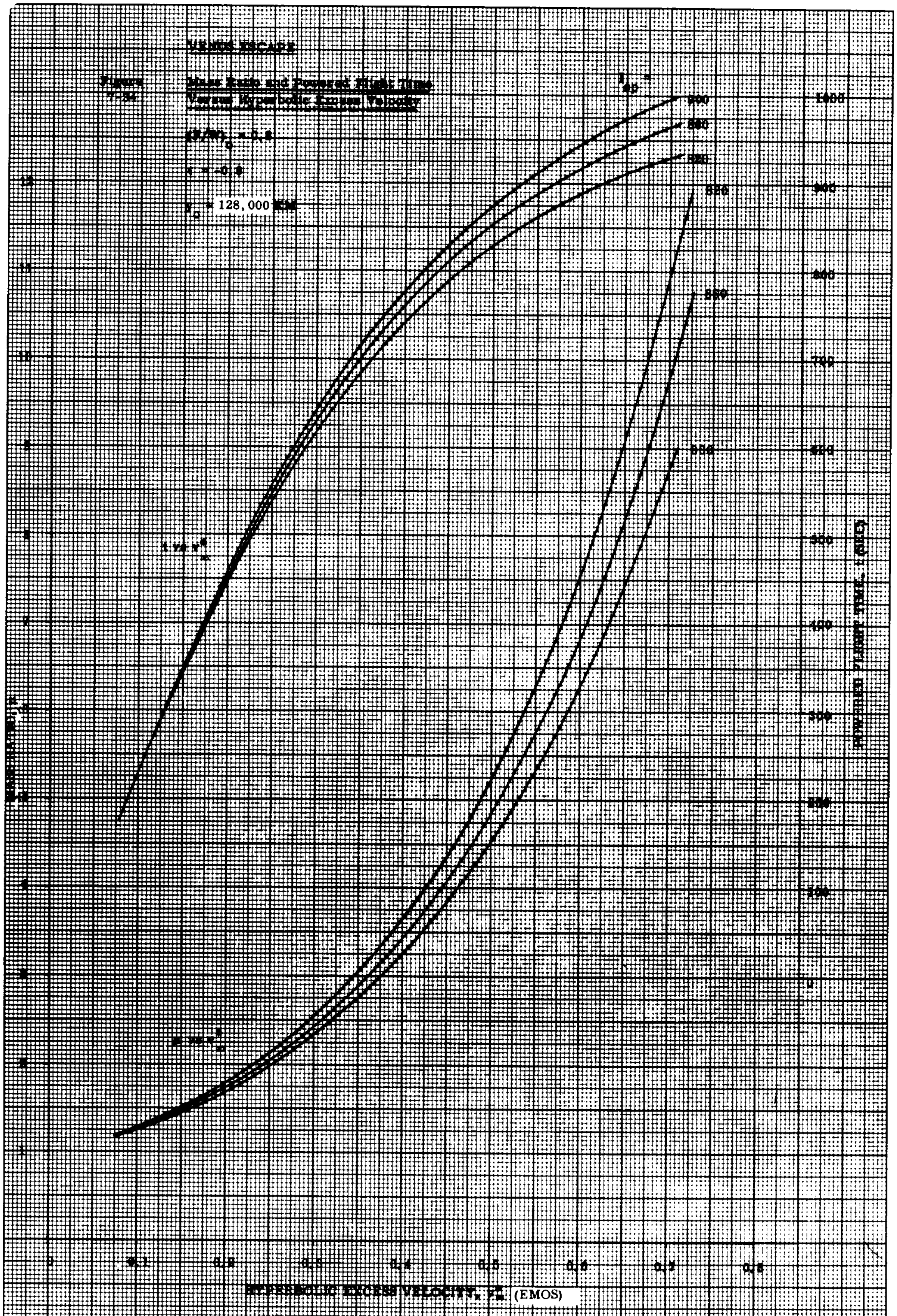
VENUS ESCAPE
Mass Ratio and Powered Flight Time
Versus Hyperbolic Excess Velocity
128,000 KM
900
860
820
0
0.1
0.2
0.3
0.4
0.5
0.6
0.7
0.8
HYPERBOLIC EXCESS VELOCITY
(EMOS)
1000
900
800
700
600
500
400
300
200
100
0

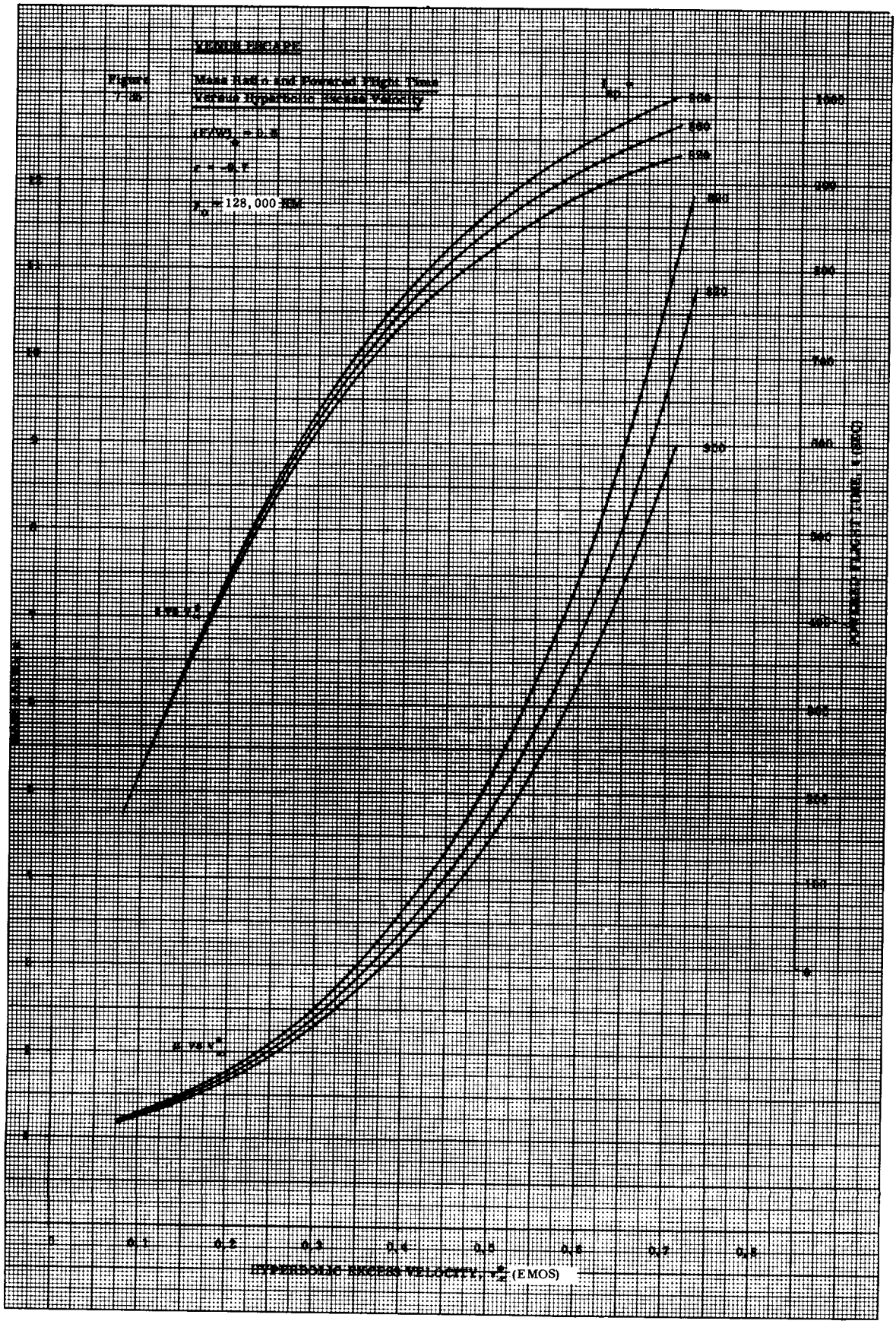
VENUS ESCAPE
Figure 7-36
Mass Ratio and Powered Flight Time Versus Hyperbolic Excess Velocity
$(T/W)_0 = 0.5$
$\gamma = -0.1°$
$R_0 = 128,000$ KM
HYPERBOLIC EXCESS VELOCITY, v_∞ (EMOS)

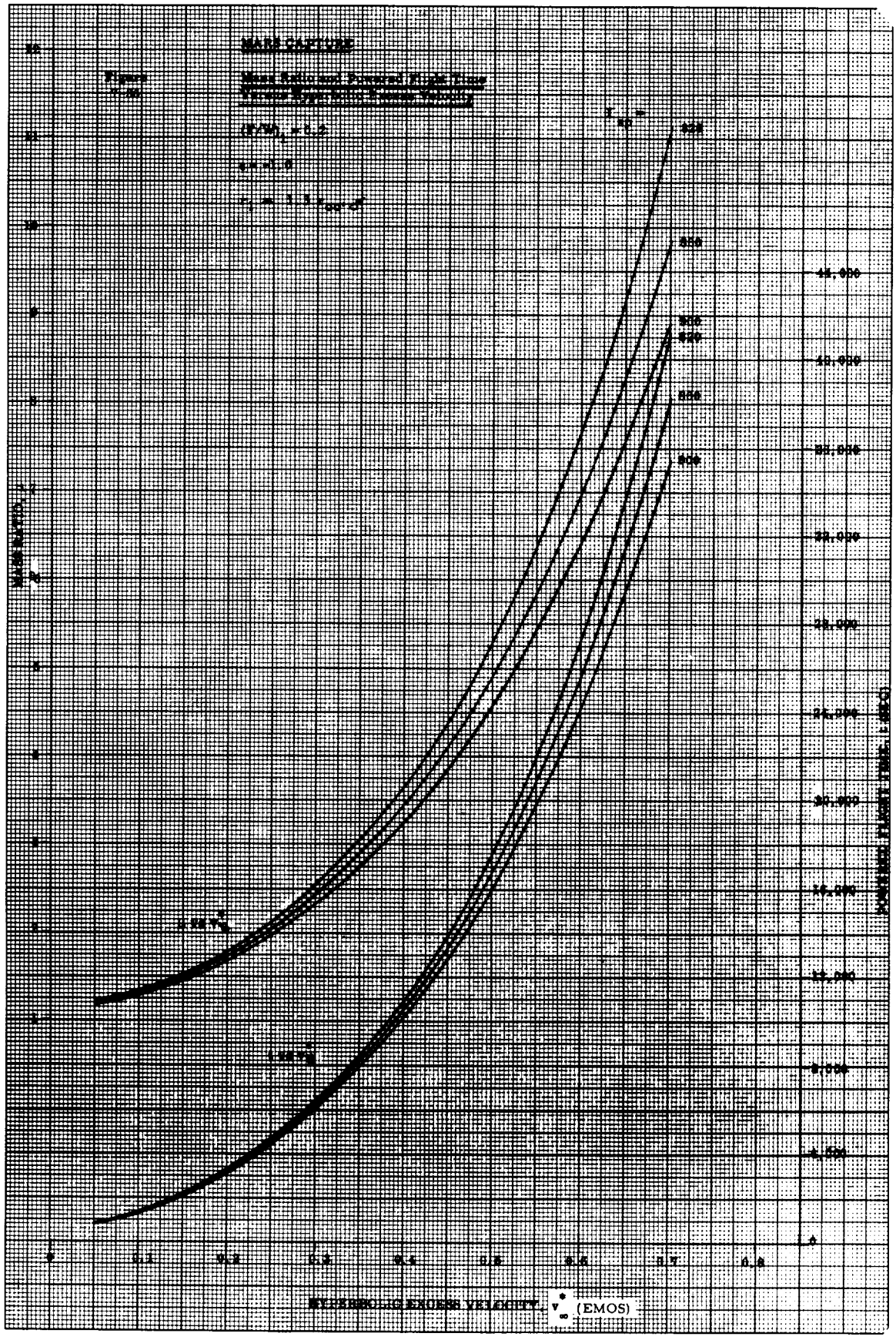
MARS CAPTURE
(EMOS)

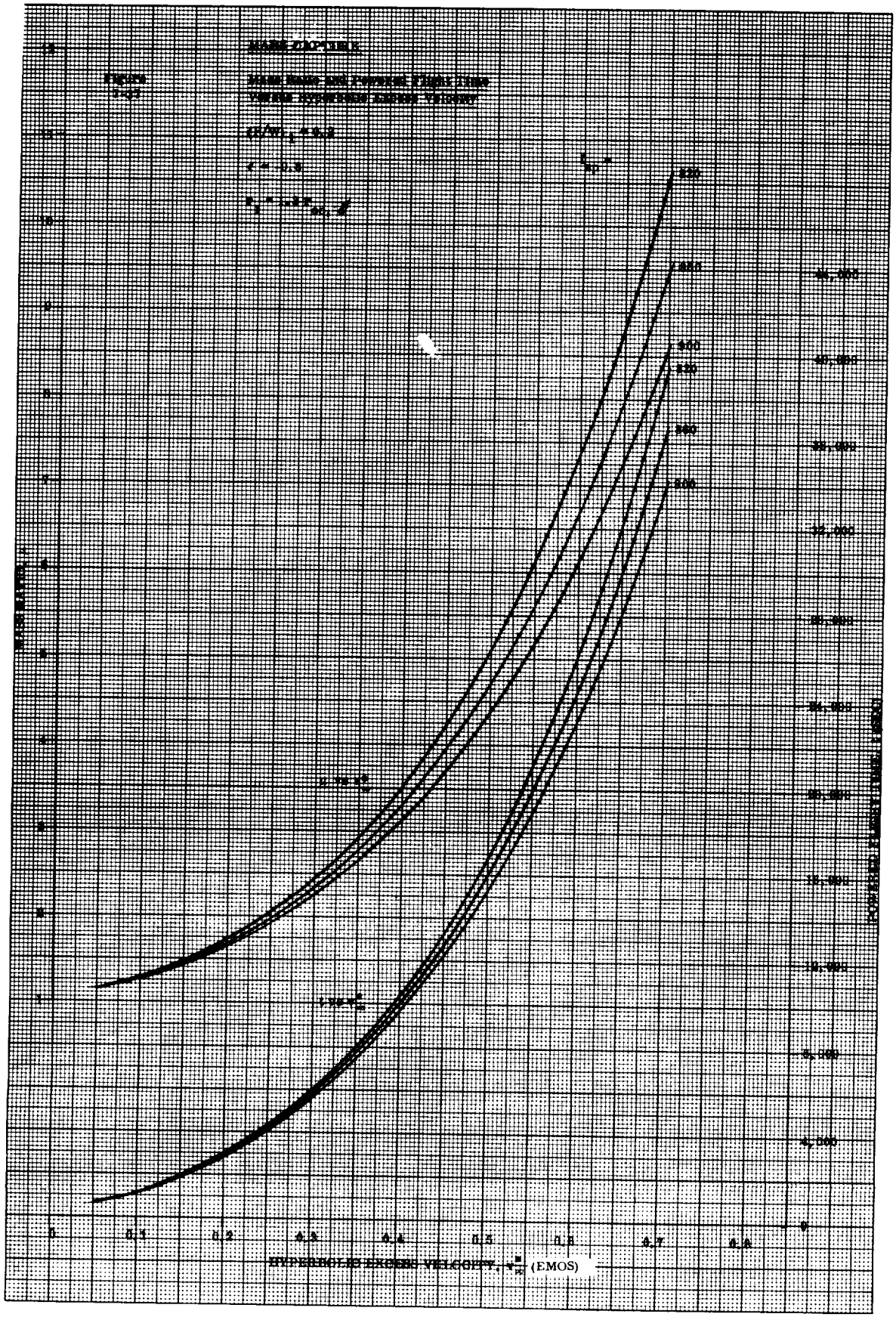
MARS CAPTURE
HYPERBOLIC EXCESS VELOCITY, v_{∞}^{*} (EMOS)

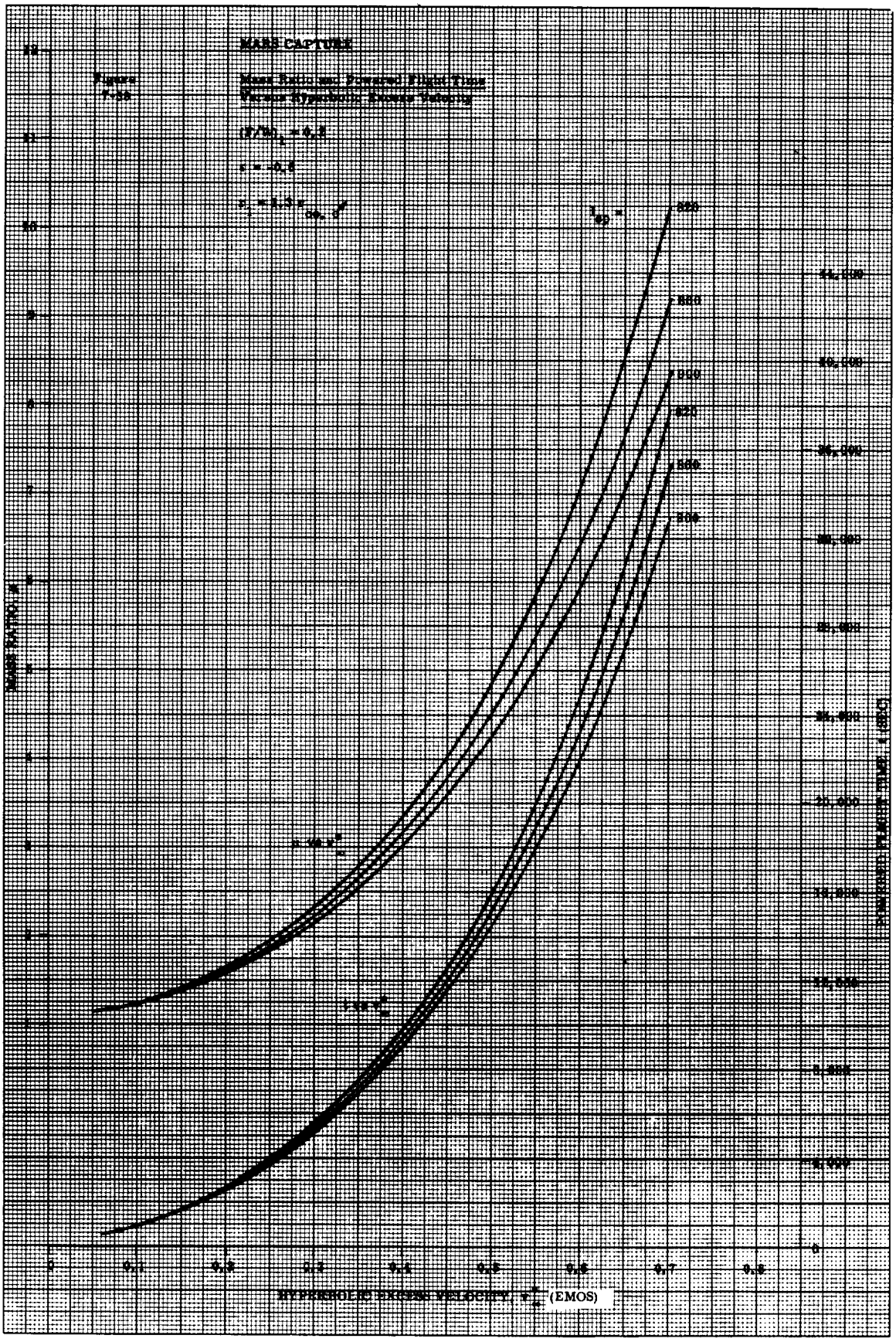
MARS CAPTURE
Figure 7-58
Mass Ratio and Powered Flight Time Versus Hyperbolic Excess Velocity
HYPERBOLIC EXCESS VELOCITY, V_∞^* (EMOS)

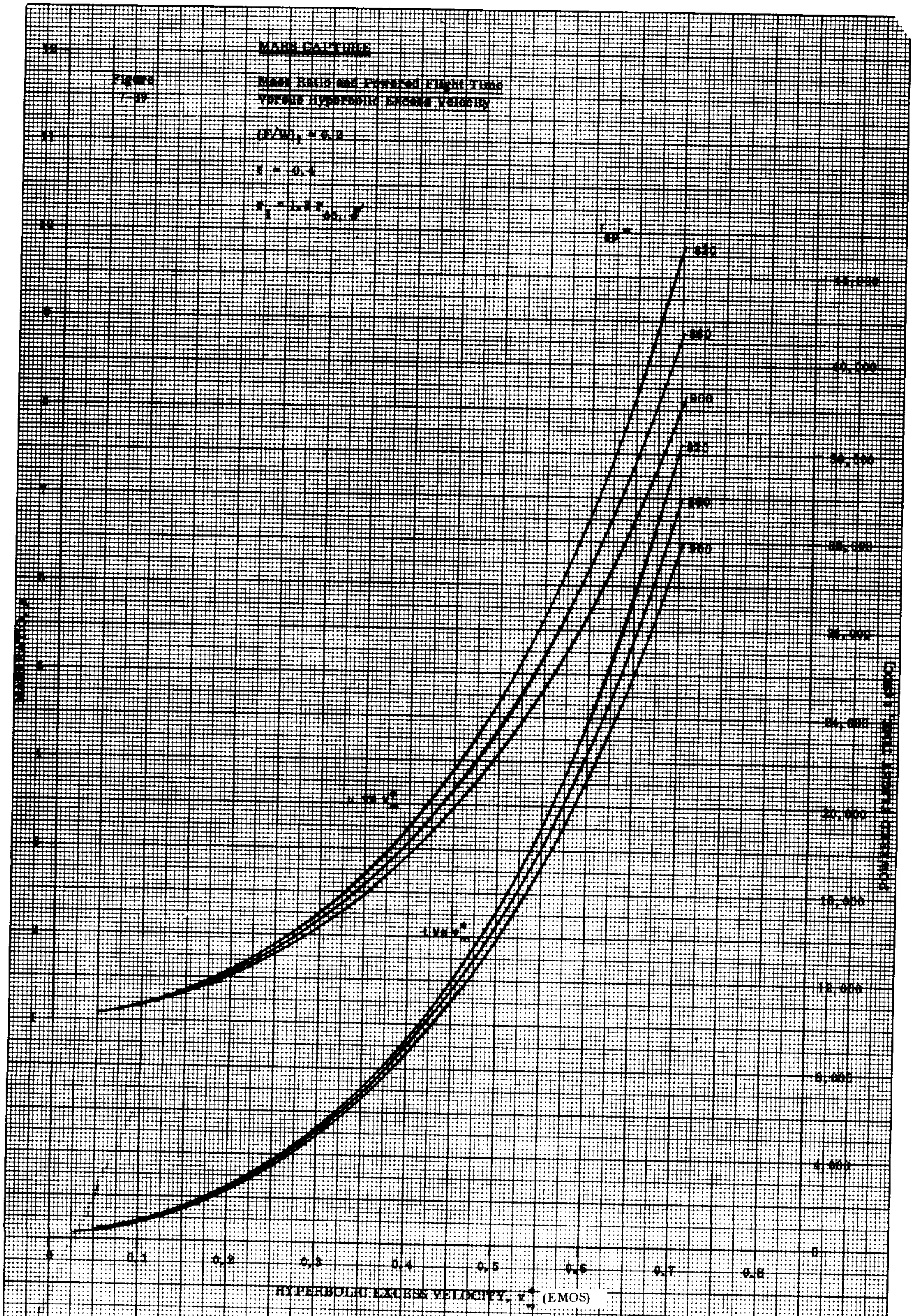
MASS CAPTURE
Figure 7-97
Mass Ratio and Powered Flight Time
Versus Hyperbolic Excess Velocity
(F/W)₁ = 0.2
ε = -0.4
HYPERBOLIC EXCESS VELOCITY, v (EMOS)
POWERED FLIGHT TIME (SEC)
MASS RATIO
0
0.1
0.2
0.3
0.4
0.5
0.6
0.7
0.8
300
350
400
40,000
20,000
16,000
12,000
8,000
4,000
0

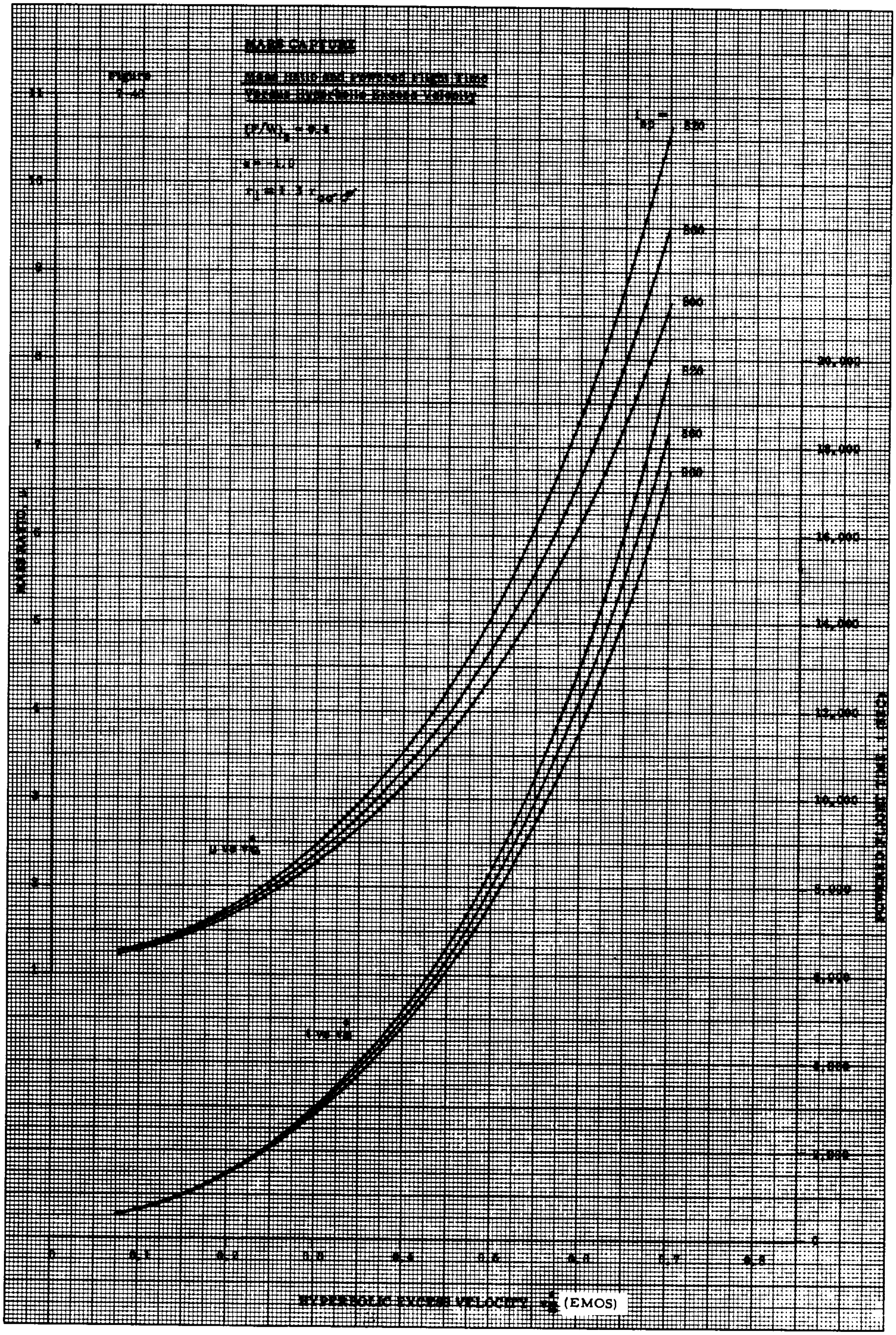
MARS CAPTURE
(EMOS)

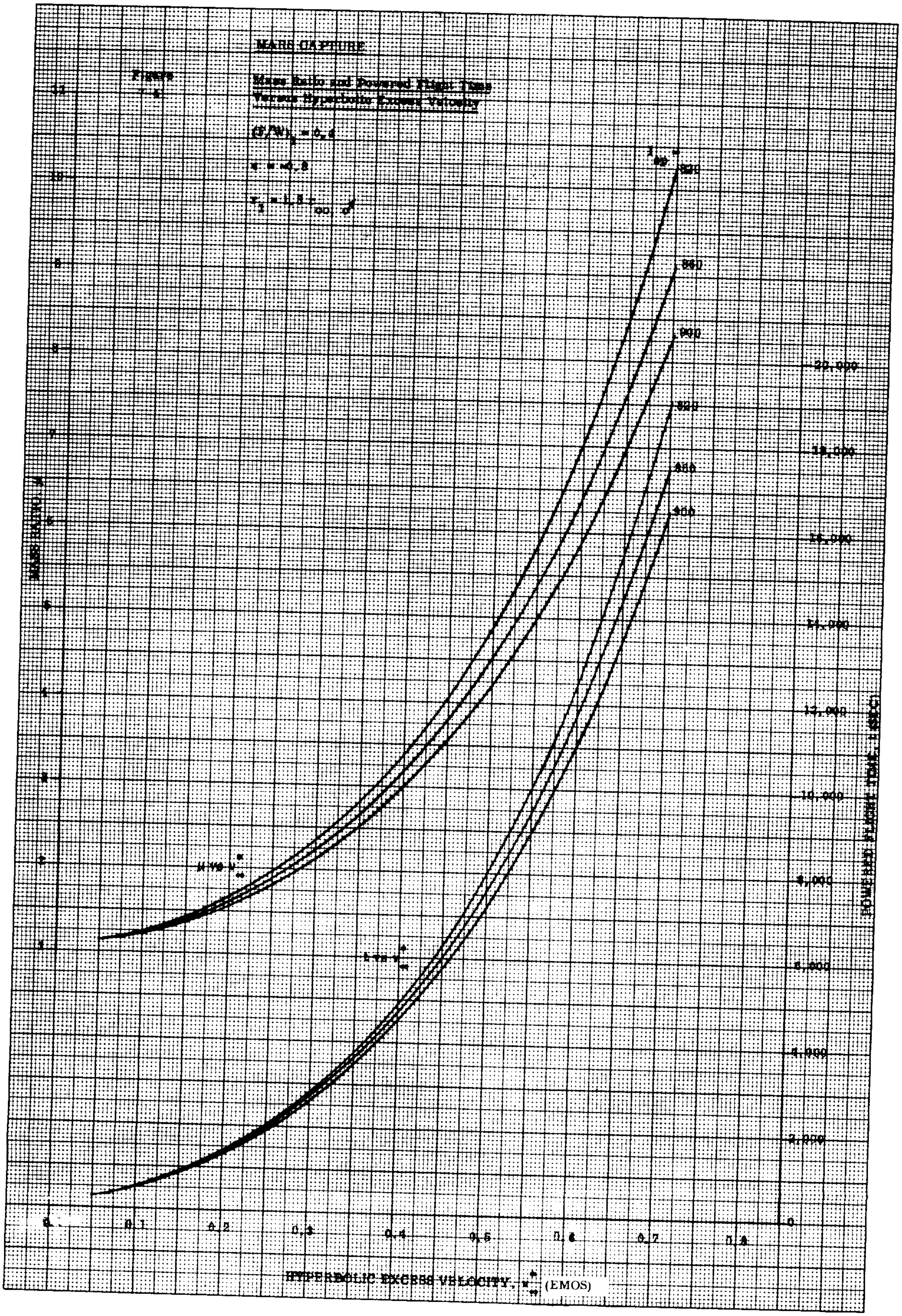
MARS CAPTURE
Mass Ratio and Powered Flight Time
Versus Hyperbolic Excess Velocity
MASS RATIO
POWERED FLIGHT TIME
20,000
18,000
16,000
14,000
12,000
10,000
8,000
6,000
4,000
2,000
0
0.1
0.2
0.3
0.4
0.5
0.7
HYPERBOLIC EXCESS VELOCITY
(EMOS)

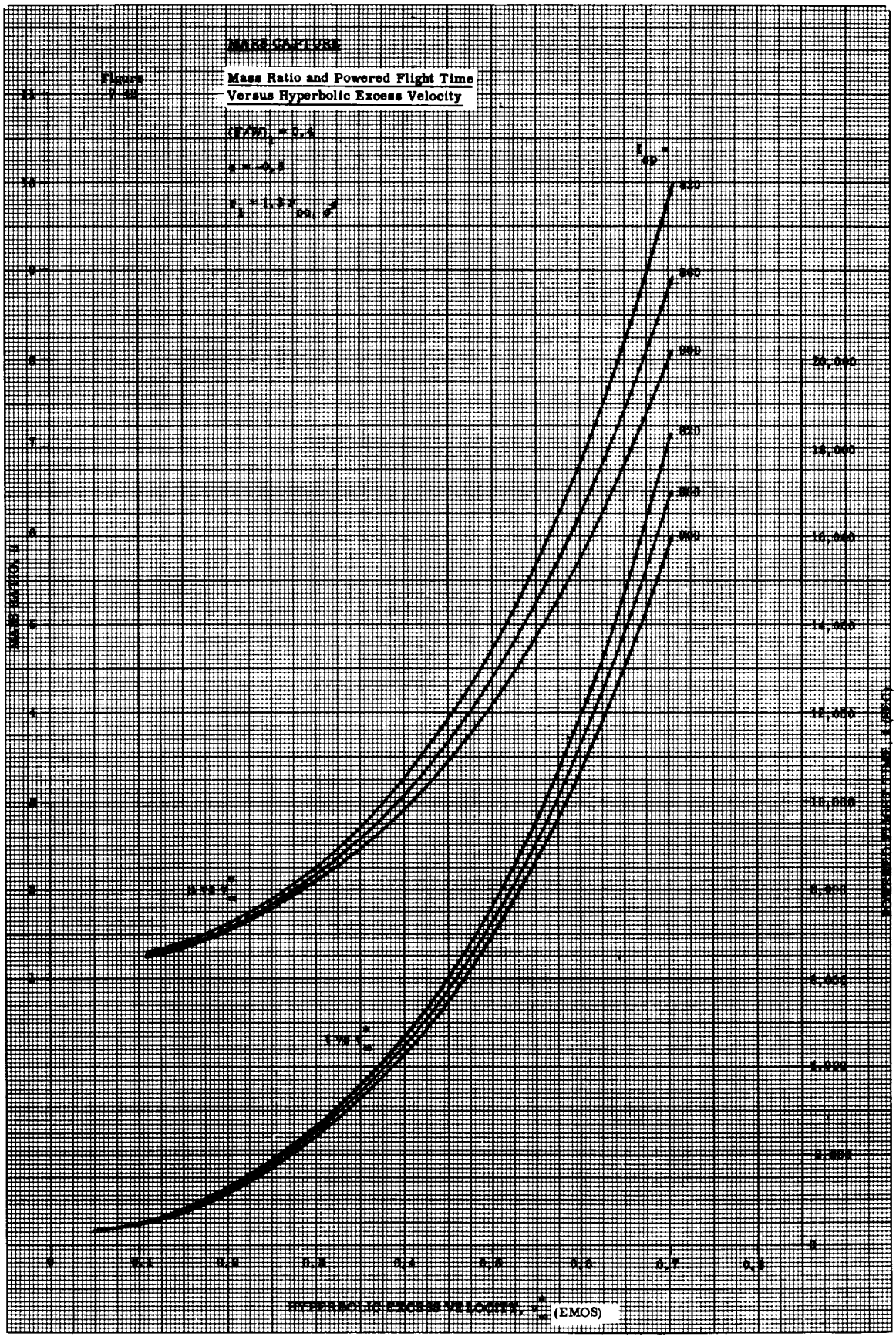
MARS CAPTURE
Figure 7-92
Mass Ratio and Powered Flight Time Versus Hyperbolic Excess Velocity
$(T/m)_i = 2.4$
$g = -0.3$
$I_{sp} = 320$
$I_{sp} = 330$
$I_{sp} = 340$
$I_{sp} = 350$
$I_{sp} = 360$
20,000
16,000
14,000
12,000
10,000
8,000
6,000
4,000
2,000
0
0.2
0.4
0.6
0.8
1.0
1.2
1.4
HYPERBOLIC EXCESS VELOCITY, V_{∞} (EMOS)

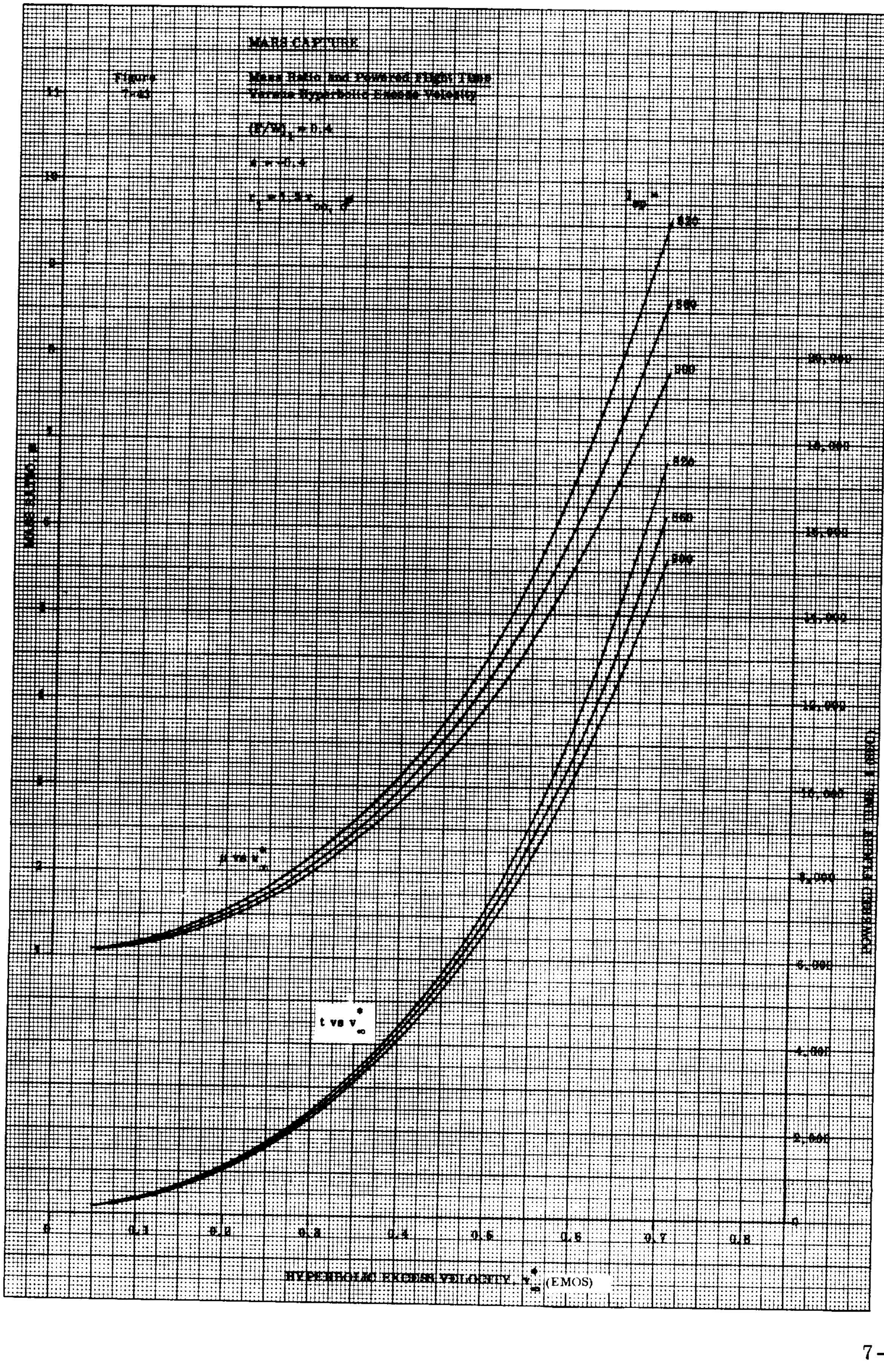
MARS CAPTURE
Figure
Mass Ratio and Powered Flight Time
Versus Hyperbolic Excess Velocity
μ vs v*∞
t vs v*∞
0
0.1
0.2
0.3
0.4
0.5
0.6
0.7
0.8
HYPERBOLIC EXCESS VELOCITY, v*∞ (EMOS)

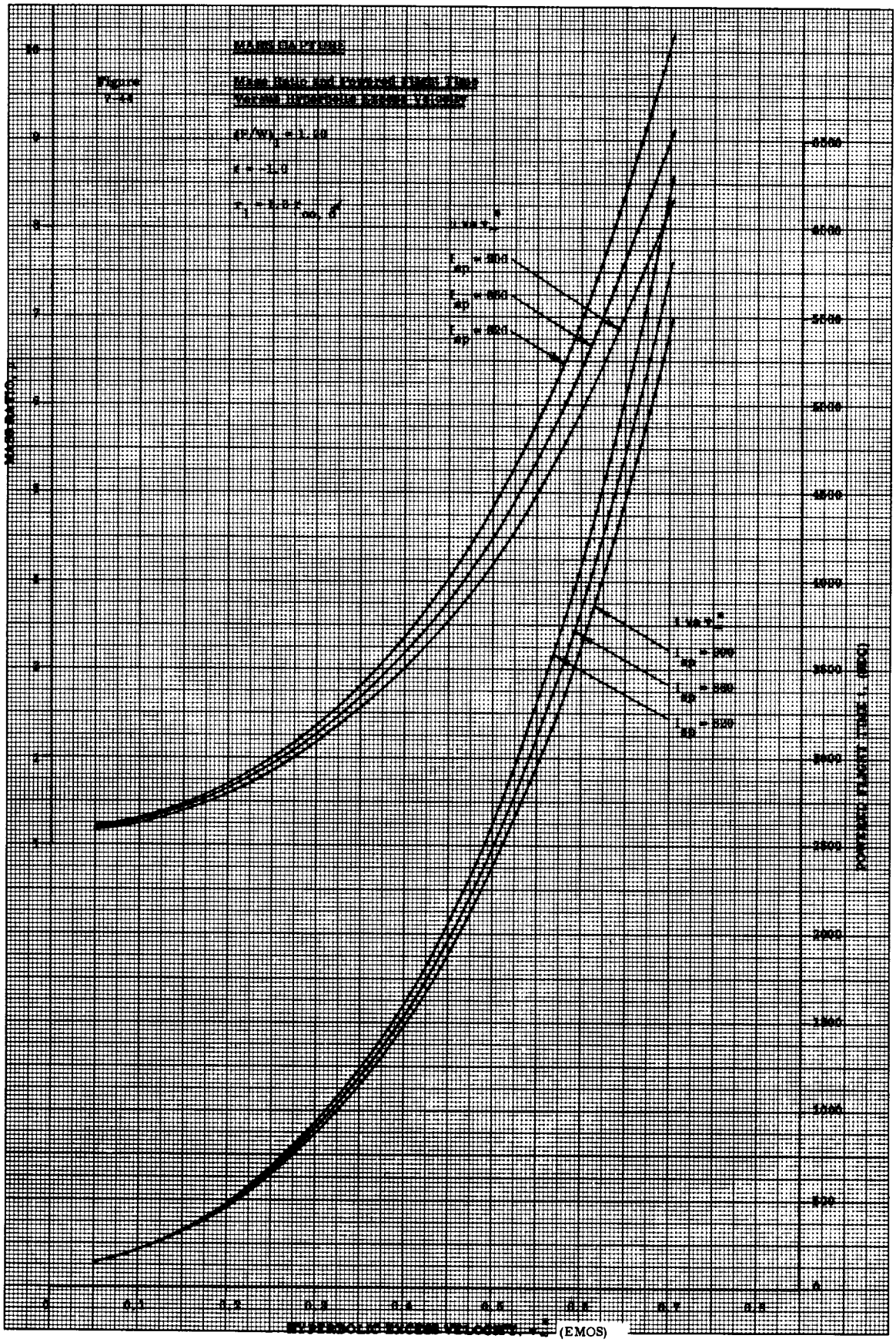

7-94

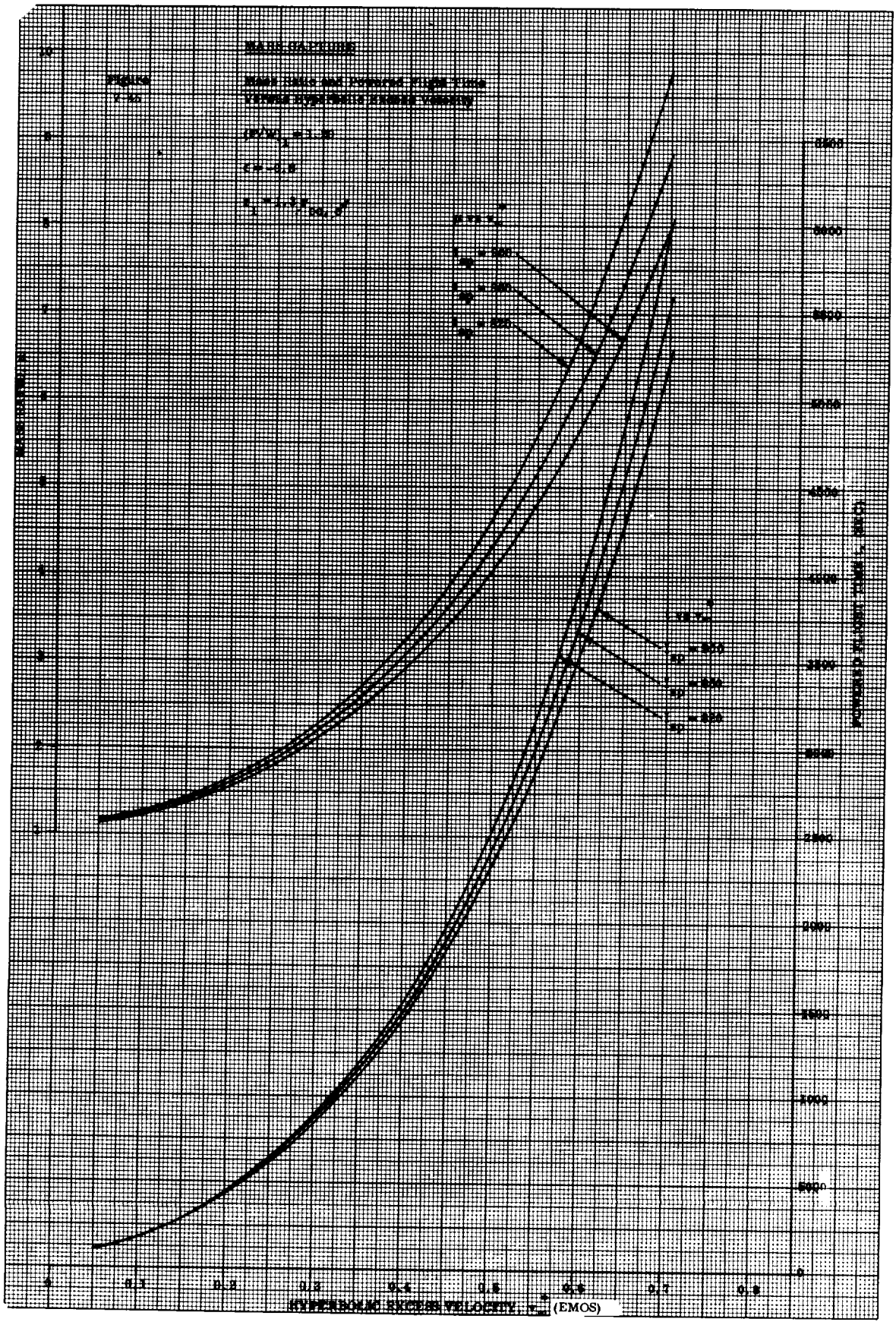
MARS CAPTURE
Figure
7-95
(EMOS)

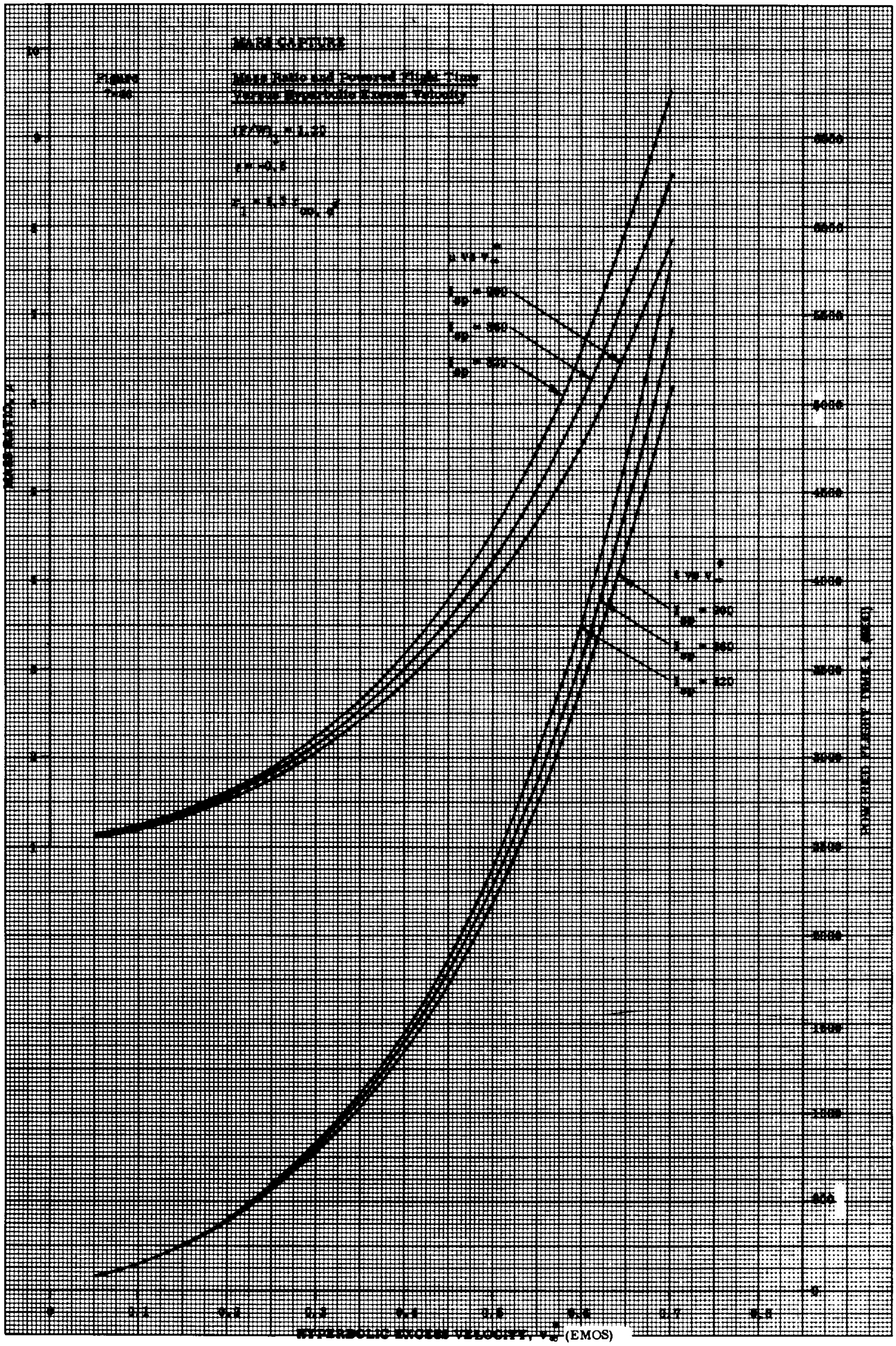
MARS CAPTURE
Mass Ratio and Powered Flight Time
Versus Hyperbolic Excess Velocity
HYPERBOLIC EXCESS VELOCITY
(EMOS)

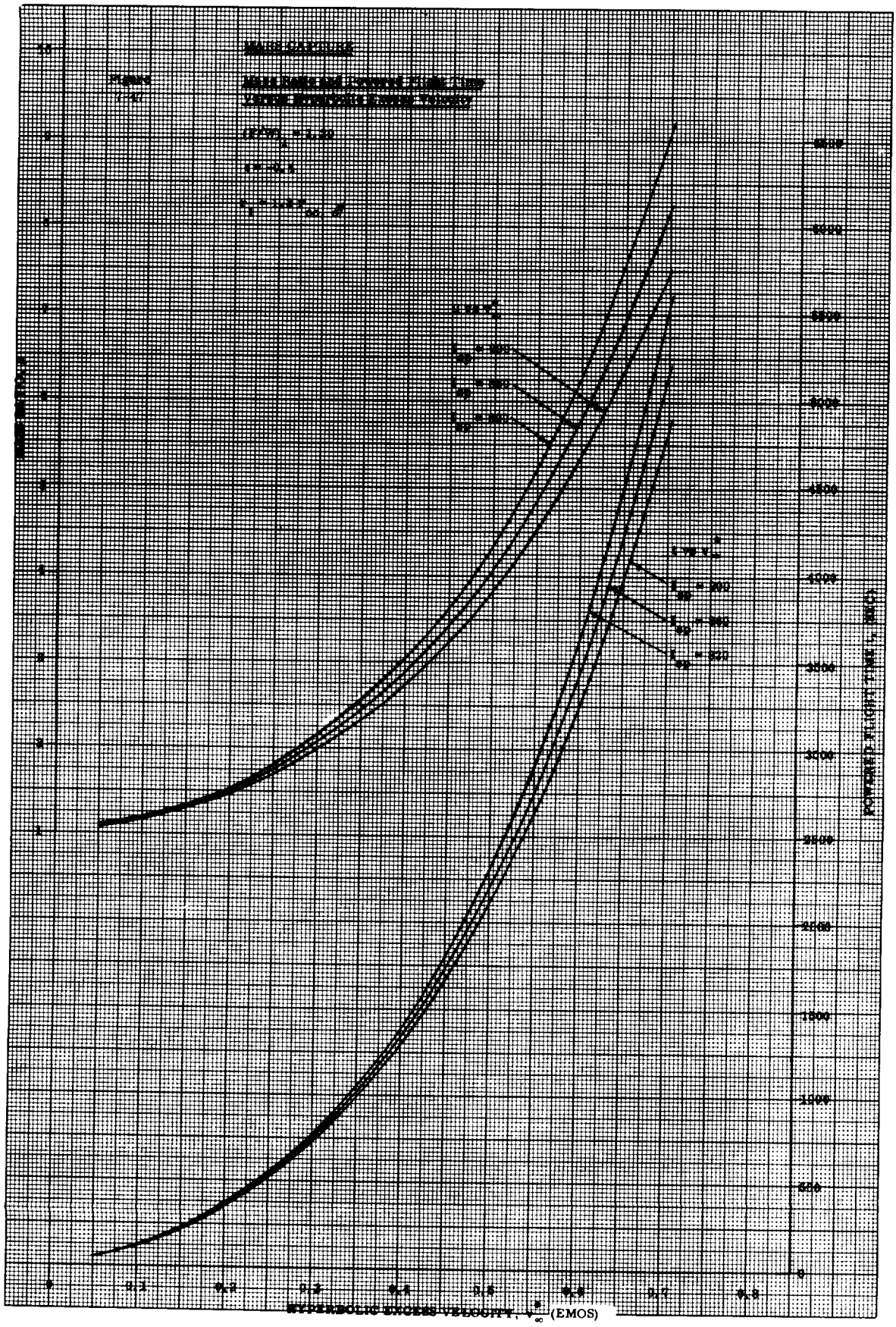
POWERED FLIGHT TIME, T, SEC
HYPERBOLIC EXCESS VELOCITY, V_∞^* (EMOS)

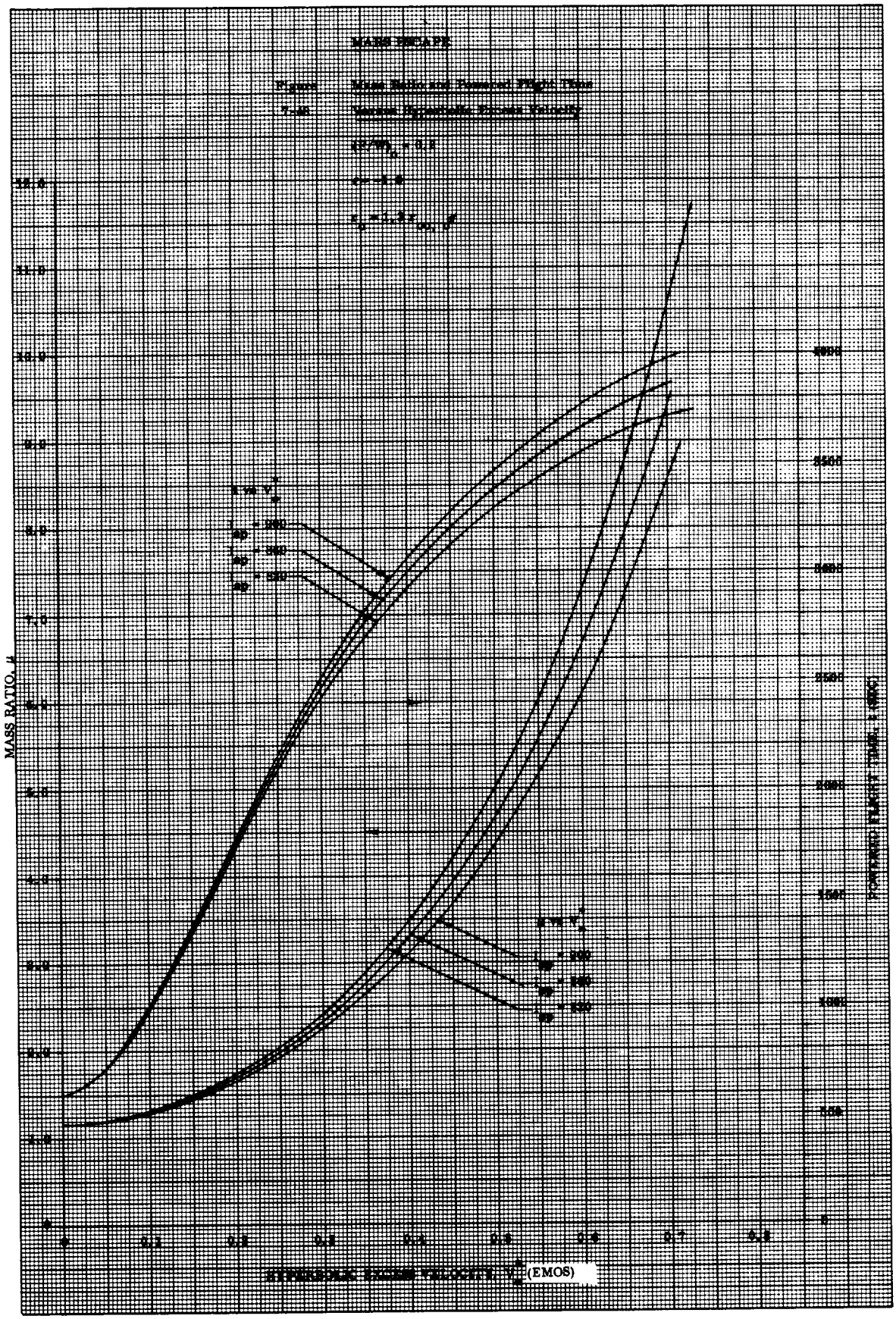
MASS RATIO, μ
POWERED FLIGHT TIME, t (SEC)
HYPERBOLIC EXCESS VELOCITY, V_∞ (EMOS)

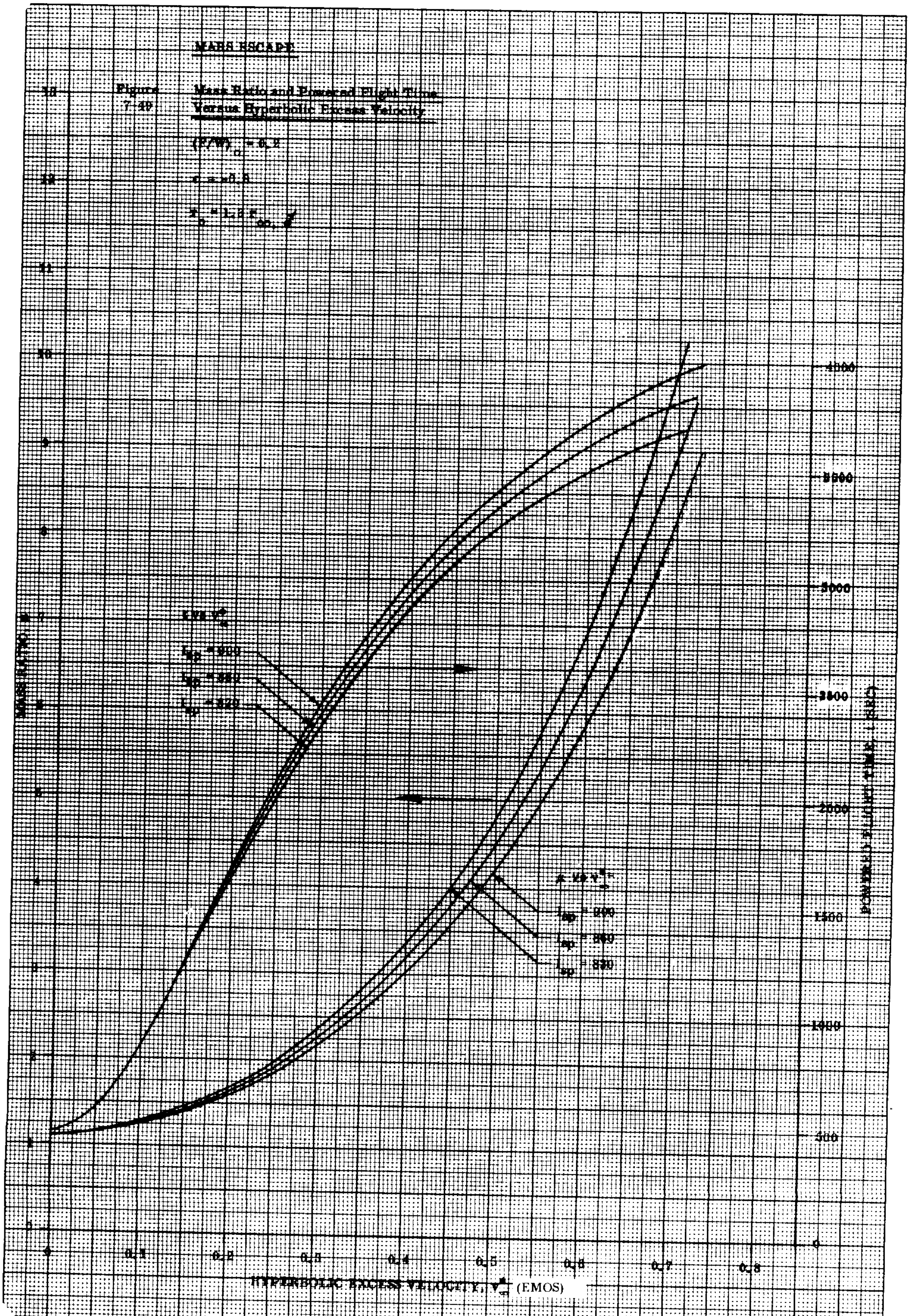

Figure 7-49 Mass Ratio and Powered Flight Time Versus Hyperbolic Excess Velocity

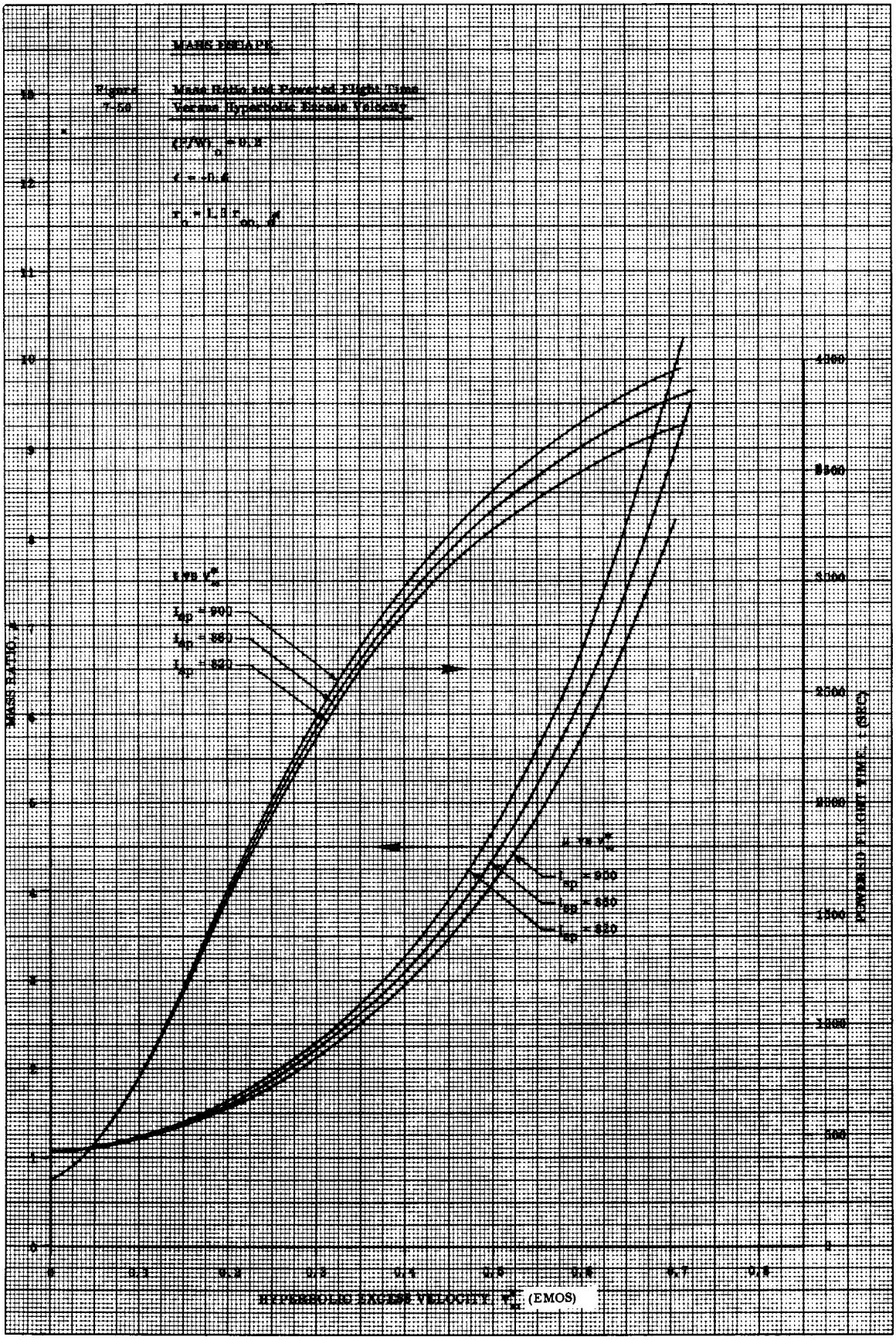

Figure 7-58 Mass Ratio and Powered Flight Time Versus Hyperbolic Excess Velocity

MASS RATIO

$(T/W)_o$ = 0.2

ϵ = -0.6

τ_o = 1.2 $\tau_{co,\epsilon}$

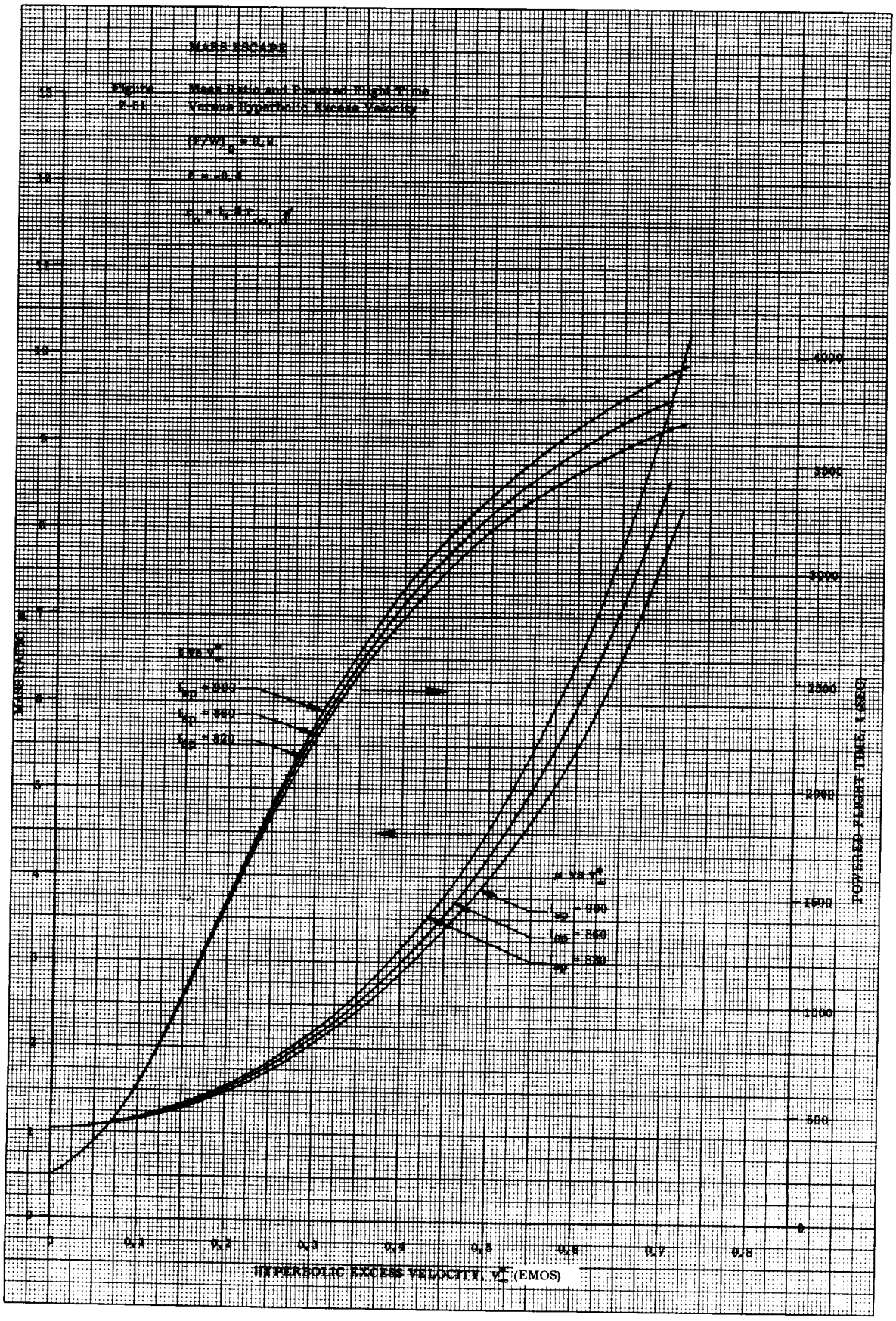
MARS ESCAPE
Figure 2.7.1
Mass Ratio and Powered Flight Time Versus Hyperbolic Escape Velocity
MASS RATIO
POWERED FLIGHT TIME, SEC
HYPERBOLIC EXCESS VELOCITY, V_∞^* (EMOS)
0
0.2
0.3
0.4
0.5
0.6
0.7
0.8
500
1000
1500
2000
2500
3000

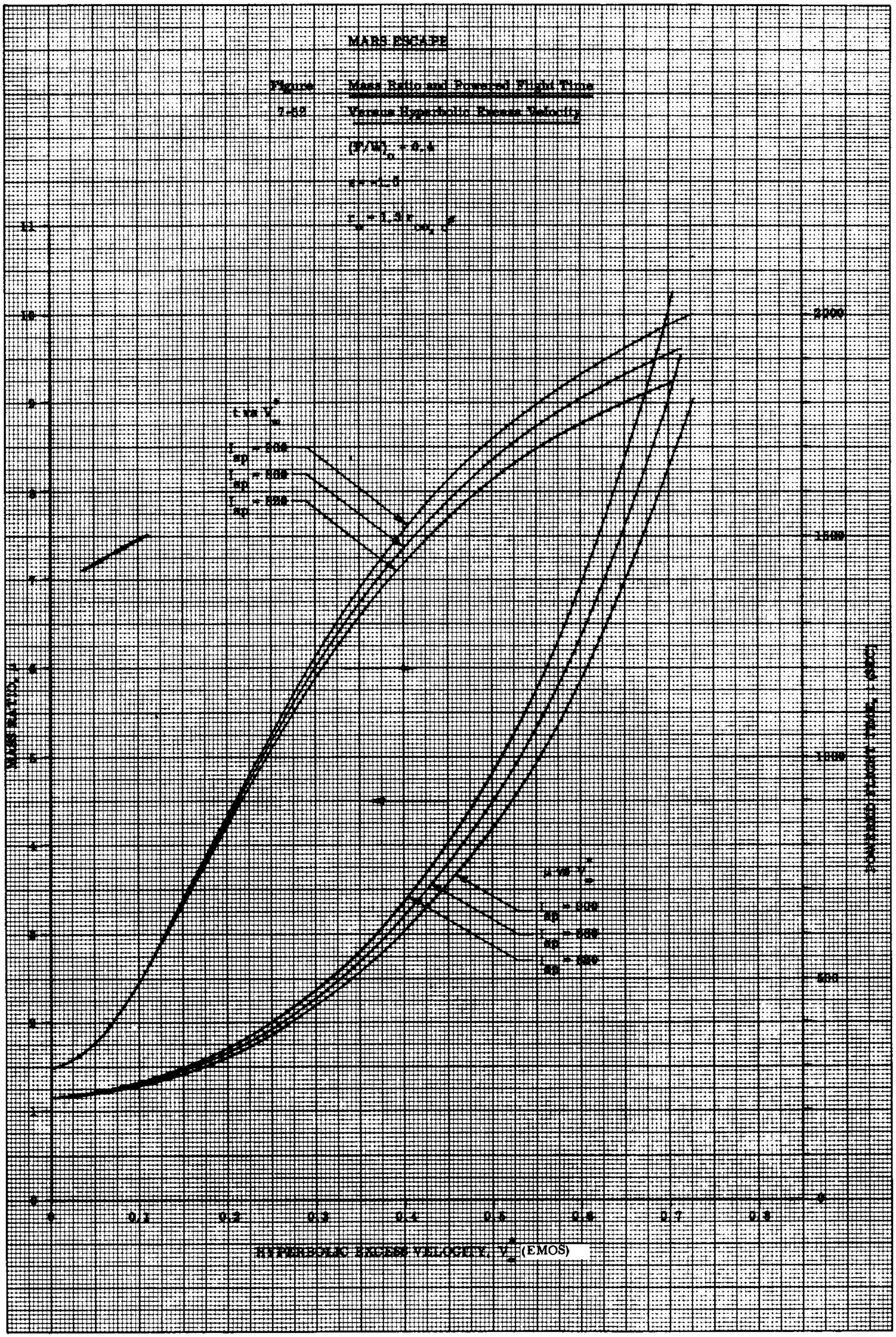
MARS ESCAPE
Figure 7-52
Mass Ratio and Powered Flight Time
Versus Hyperbolic Excess Velocity
0
0.1
0.2
0.3
0.4
0.5
0.6
0.7
0.8
2000
1500
1000
500
0
HYPERBOLIC EXCESS VELOCITY, V∞* (EMOS)

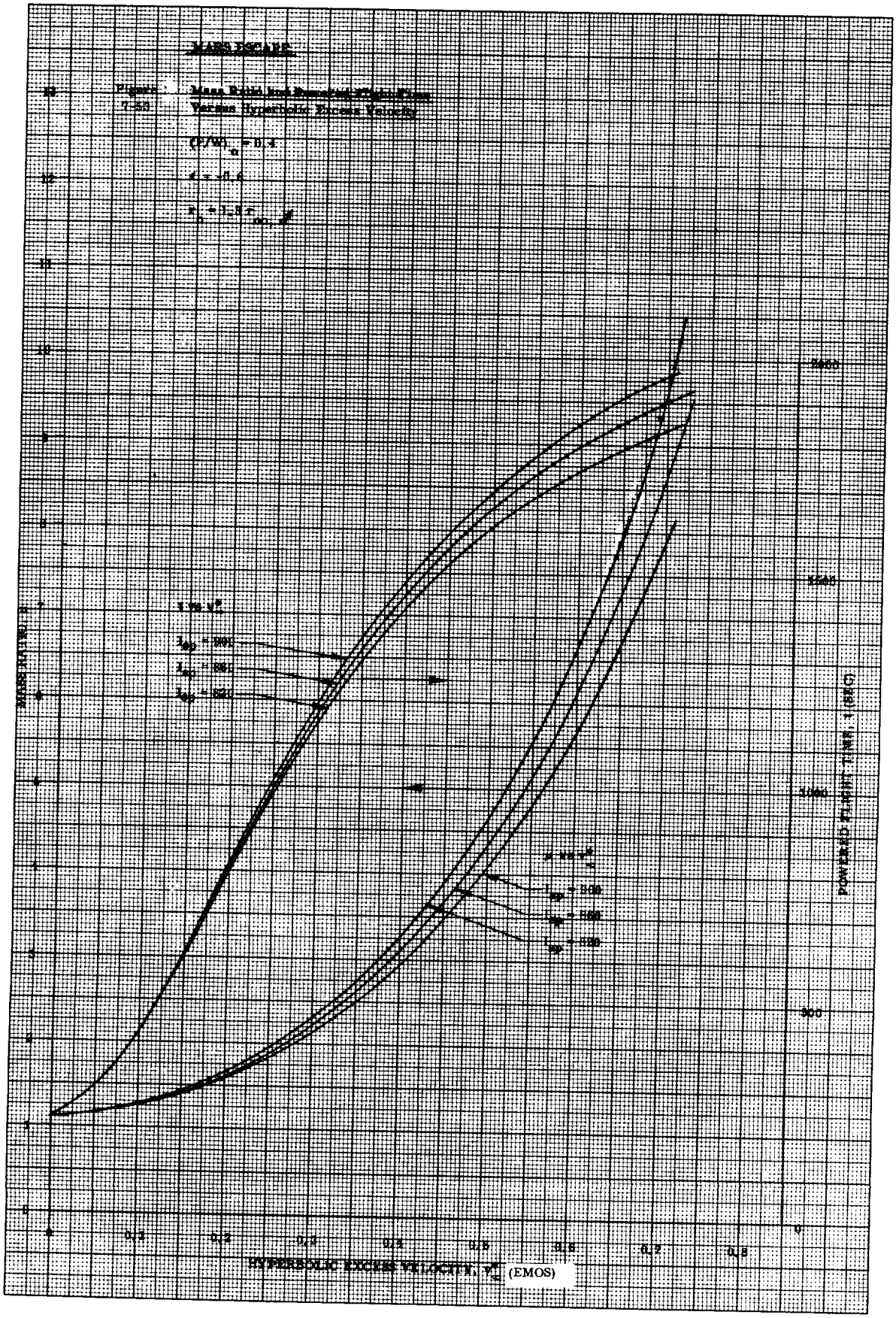
MARS ESCAPE
Figure 7-53
Mass Ratio and Powered Flight Time Versus Hyperbolic Excess Velocity
$(T/W)_o = 0.4$
$\epsilon_1 = -0.6$
$r_o = 1.3 r_{oc}$
MASS RATIO, R
POWERED FLIGHT TIME, t (SEC)
HYPERBOLIC EXCESS VELOCITY, V_∞ (EMOS)

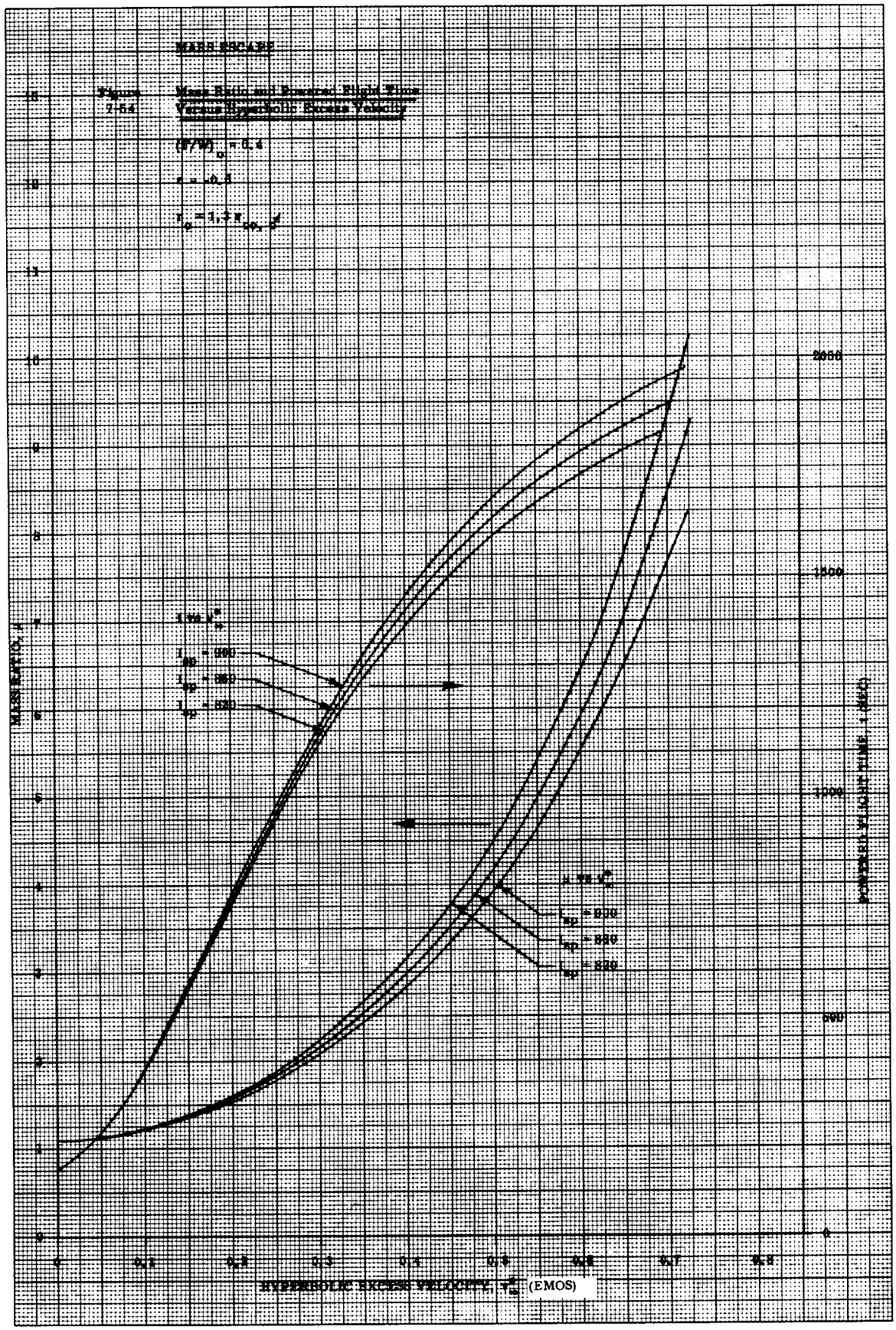
MARS ESCAPE
Figure 7-64
Mass Ratio and Powered Flight Time Versus Hyperbolic Excess Velocity
$(T/W)_o = 0.4$
$\epsilon = -0.5$
$r_o = 1.2 r_{SOI}$
MASS RATIO, $\frac{W_o}{W_{BO}}$
POWERED FLIGHT TIME, t (SEC)
HYPERBOLIC EXCESS VELOCITY, V_{∞}^2 (EMOS)
$I_{sp} = 900$
$I_{sp} = 880$
$I_{sp} = 820$

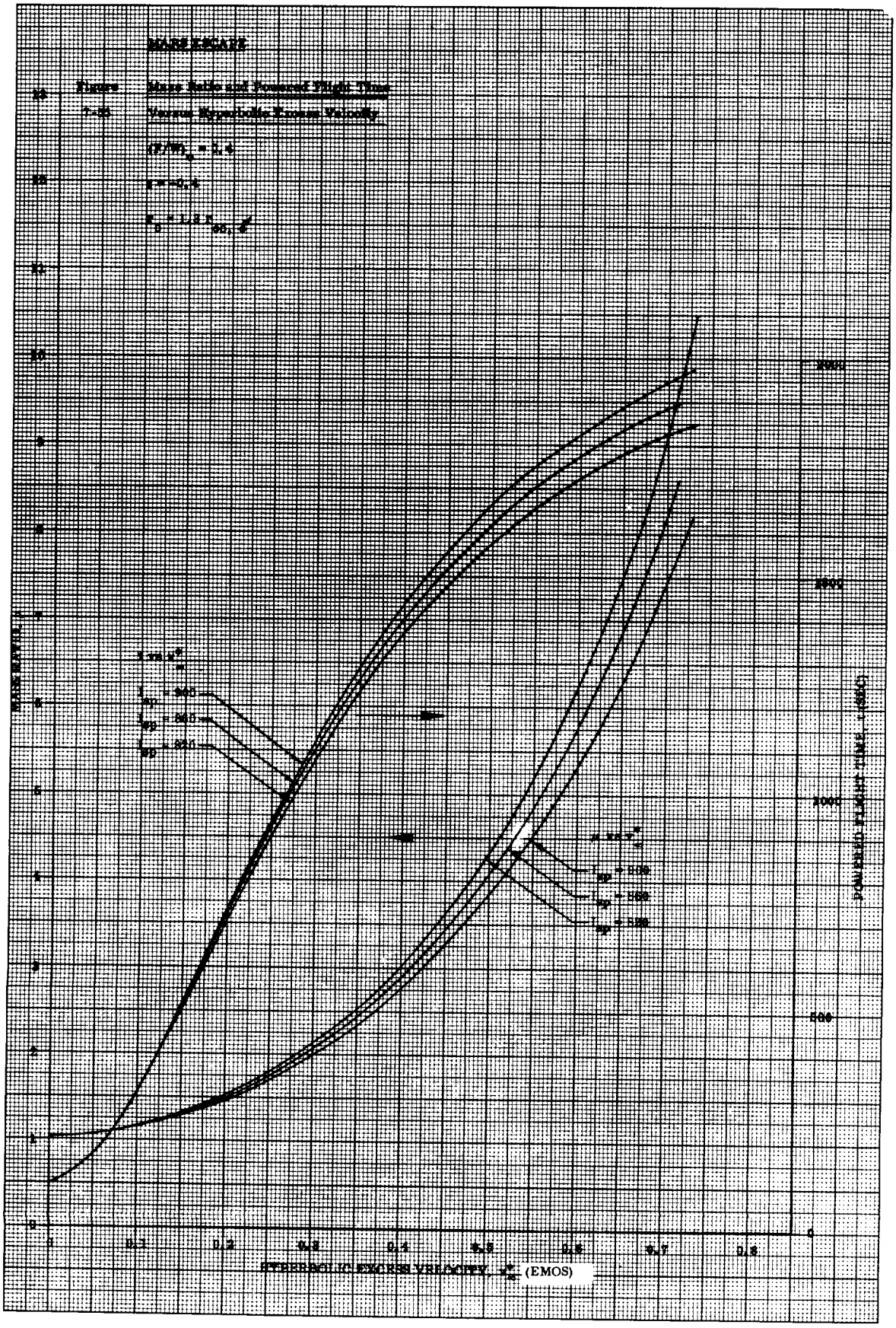
MARS ESCAPE
Figure
Mass Ratio and Powered Flight Time
Versus Hyperbolic Excess Velocity
HYPERBOLIC EXCESS VELOCITY, v_{∞}^2 (EMOS)

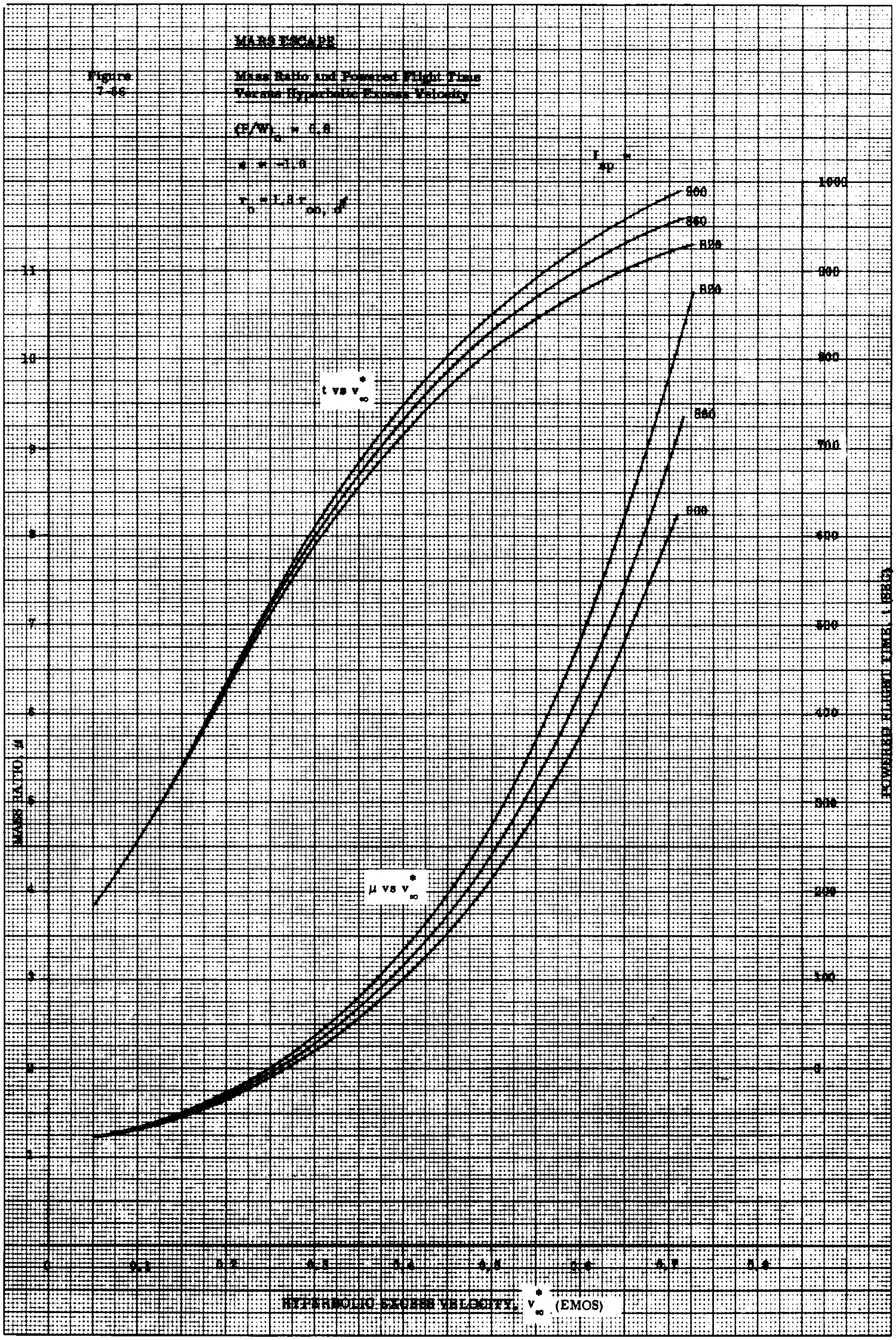
MARS ESCAPE
Figure
Mass Ratio and Powered Flight Time
Versus Hyperbolic Excess Velocity
t vs v∞*
μ vs v∞*
MASS RATIO, μ
POWERED FLIGHT TIME (SEC)
HYPERBOLIC EXCESS VELOCITY, v∞* (EMOS)

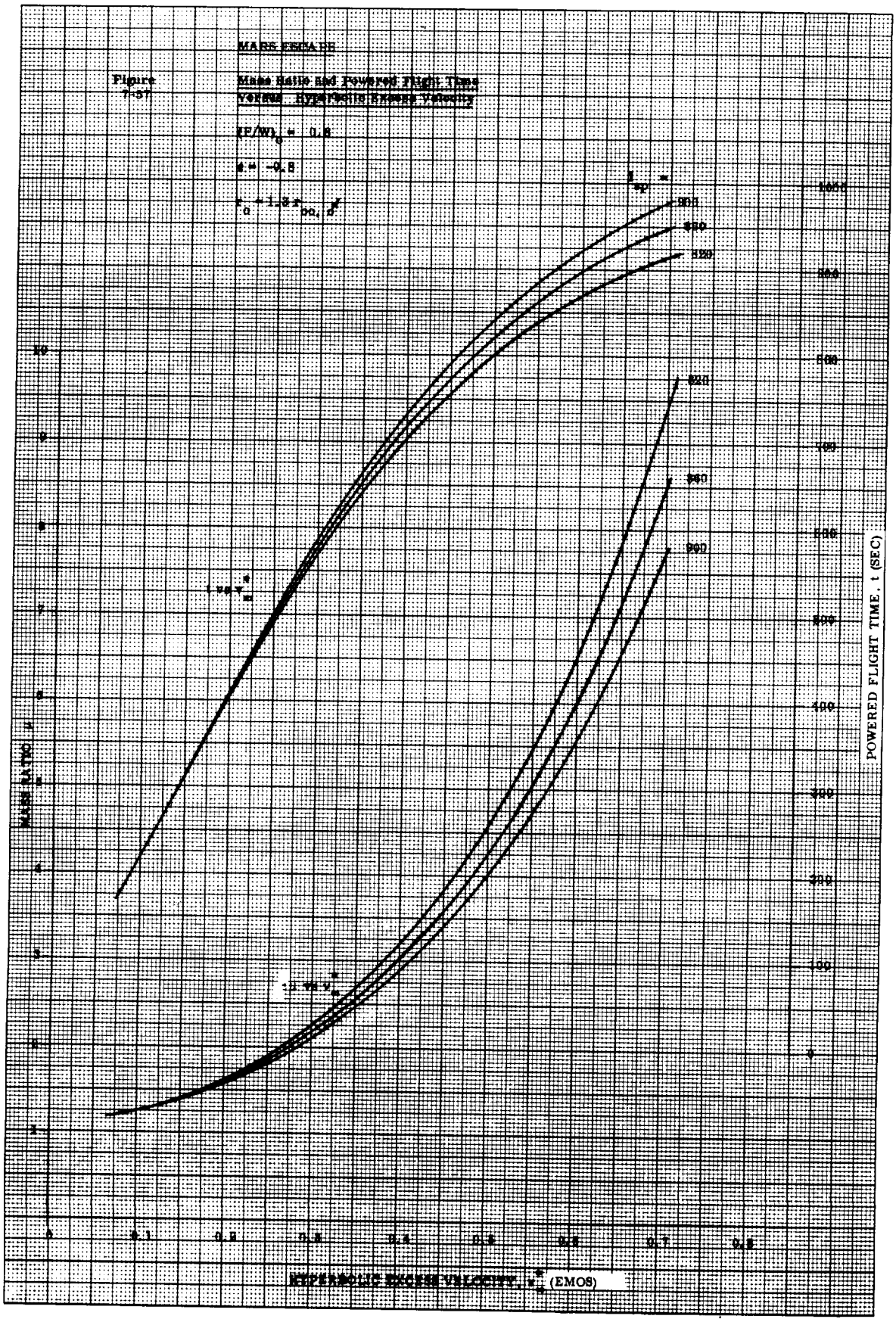
MARS ESCAPE
Mass Ratio and Powered Flight Time
versus Hyperbolic Excess Velocity
$(F/W)_0$ = 0.8
$\dot{\epsilon}$ = -0.8
$\tau_0 = 1.2\tau_{50,0}$
I_{sp} =
MASS RATIO, $\frac{m_0}{m_f}$
POWERED FLIGHT TIME, t (SEC)
HYPERBOLIC EXCESS VELOCITY, v_∞^* (EMOS)

Figure 7-51

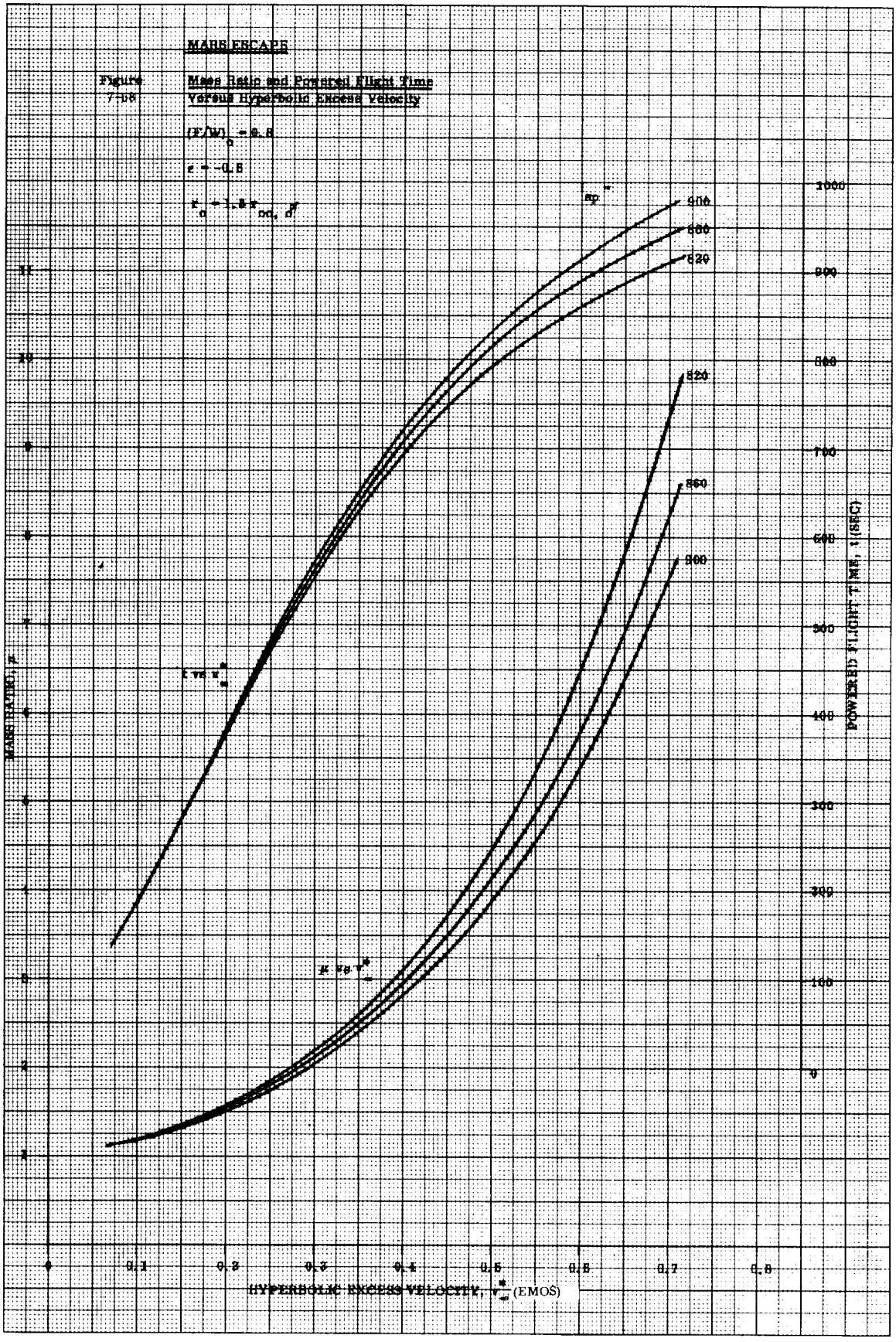
MARS ESCAPE
Figure 7-58
Mass Ratio and Powered Flight Time Versus Hyperbolic Excess Velocity
(F/W)o = 0.8
ε = -0.8
ro = 1.5 rmo, d
mp =
900
880
820
820
860
800
t vs v*∞
μ vs v*∞
MASS RATIO, μ
POWERED FLIGHT TIME, t (SEC)
0
0.1
0.2
0.3
0.4
0.5
0.6
0.7
0.8
HYPERBOLIC EXCESS VELOCITY, v*∞ (EMOS)

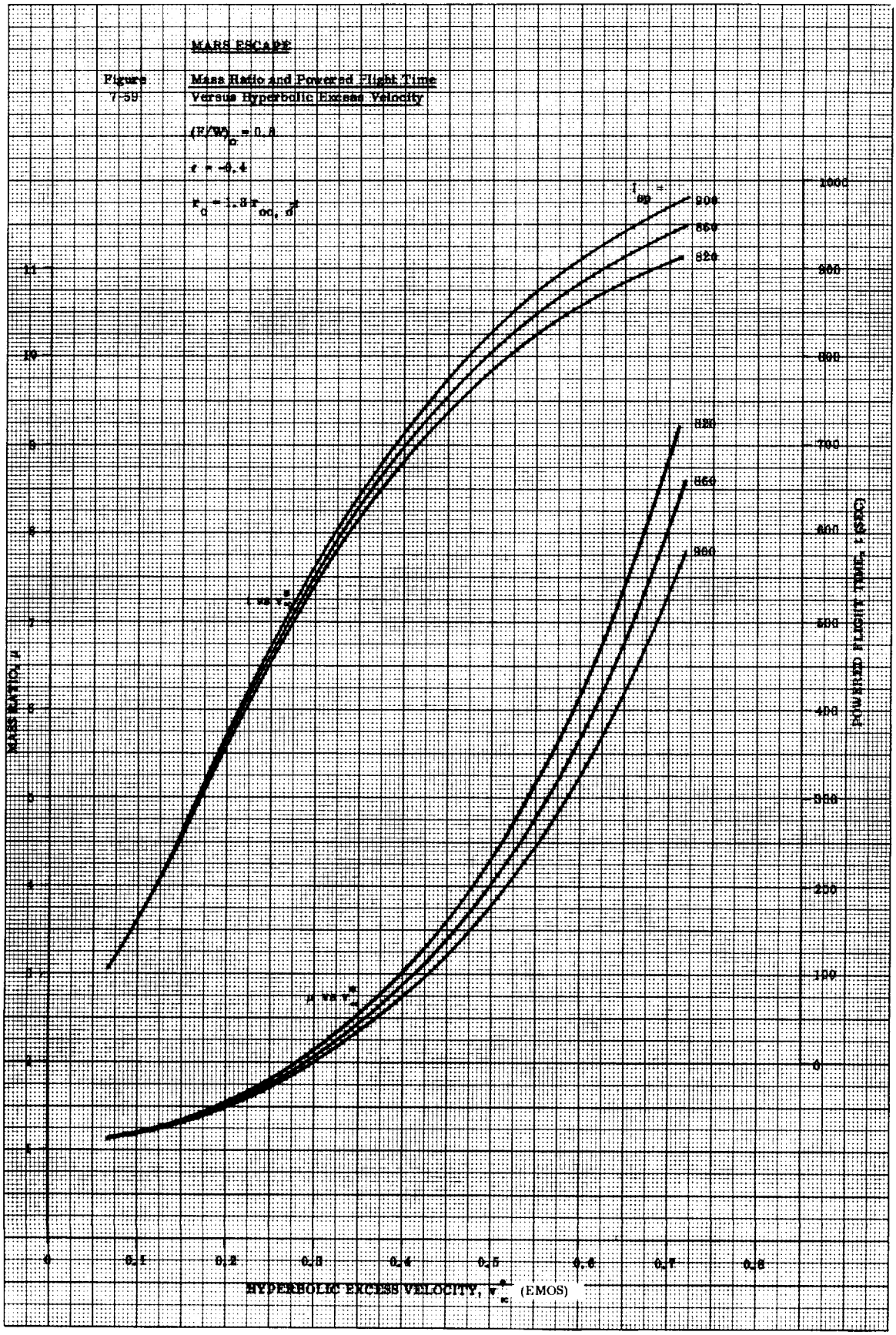
MARS ESCAPE
Figure 7-59
Mass Ratio and Powered Flight Time Versus Hyperbolic Excess Velocity
$(F/W)_o = 0.8$
$\epsilon = -0.4$
$r_o = 1.8 r_{oc, \oplus}$
MASS RATIO, R
POWERED FLIGHT TIME, t (SEC)
HYPERBOLIC EXCESS VELOCITY, v_∞^* (EMOS)
0
0.1
0.2
0.3
0.4
0.5
0.6
0.7
0.8
1000
800
600
400
200
0

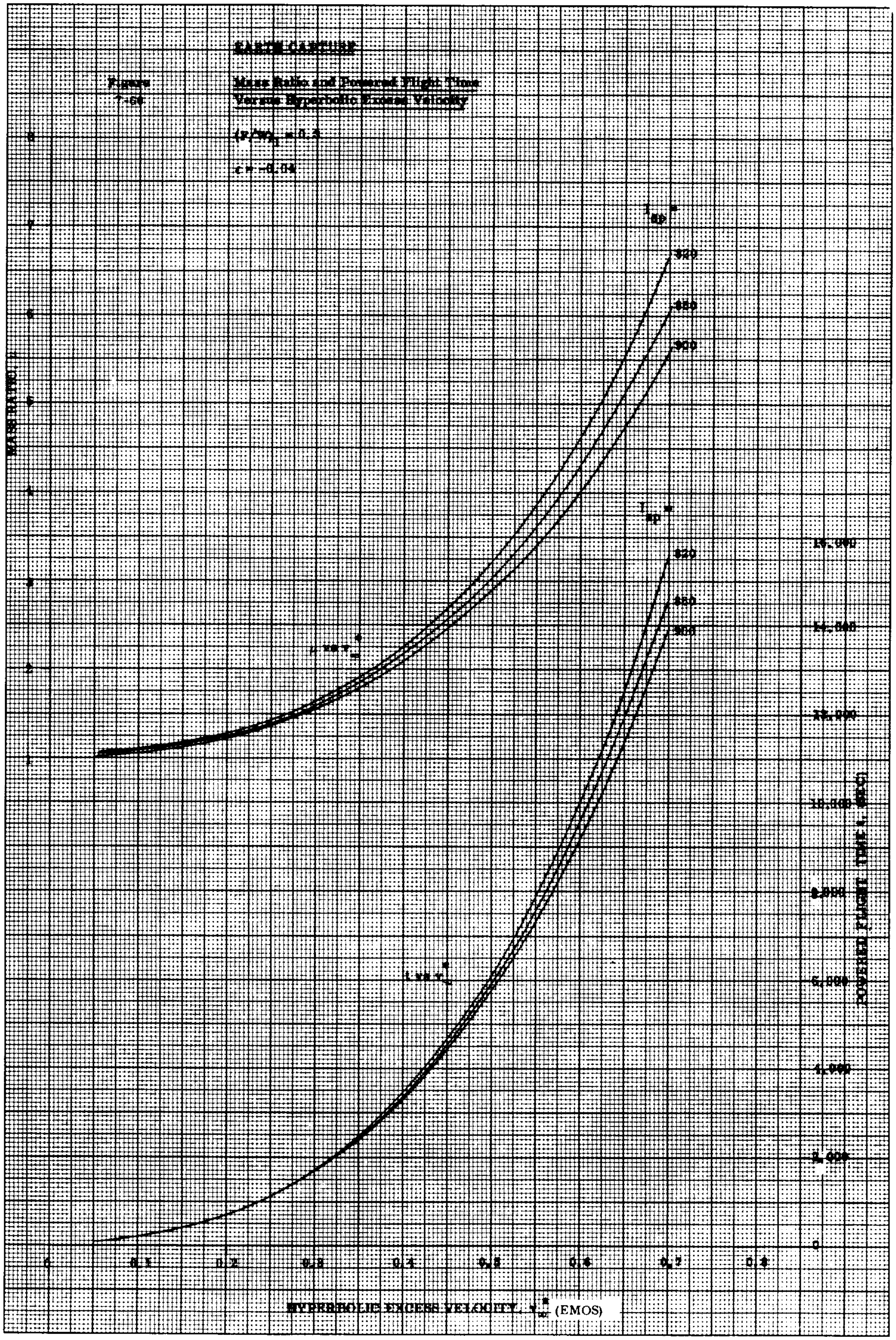
EARTH CAPTURE
Figure
Mass Ratio and Powered Flight Time
Versus Hyperbolic Excess Velocity
c = -0.04
MASS RATIO
POWERED FLIGHT TIME
0.1
0.2
0.3
0.4
0.5
0.6
0.7
0.8
2,000
4,000
6,000
8,000
HYPERBOLIC EXCESS VELOCITY
(EMOS)

Figure 7-61

EARTH CAPTURE

Mass Ratio and Powered Flight Time Versus Hyperbolic Excess Velocity

$(F/W)_i = 0.4$

$\epsilon = -0.04$

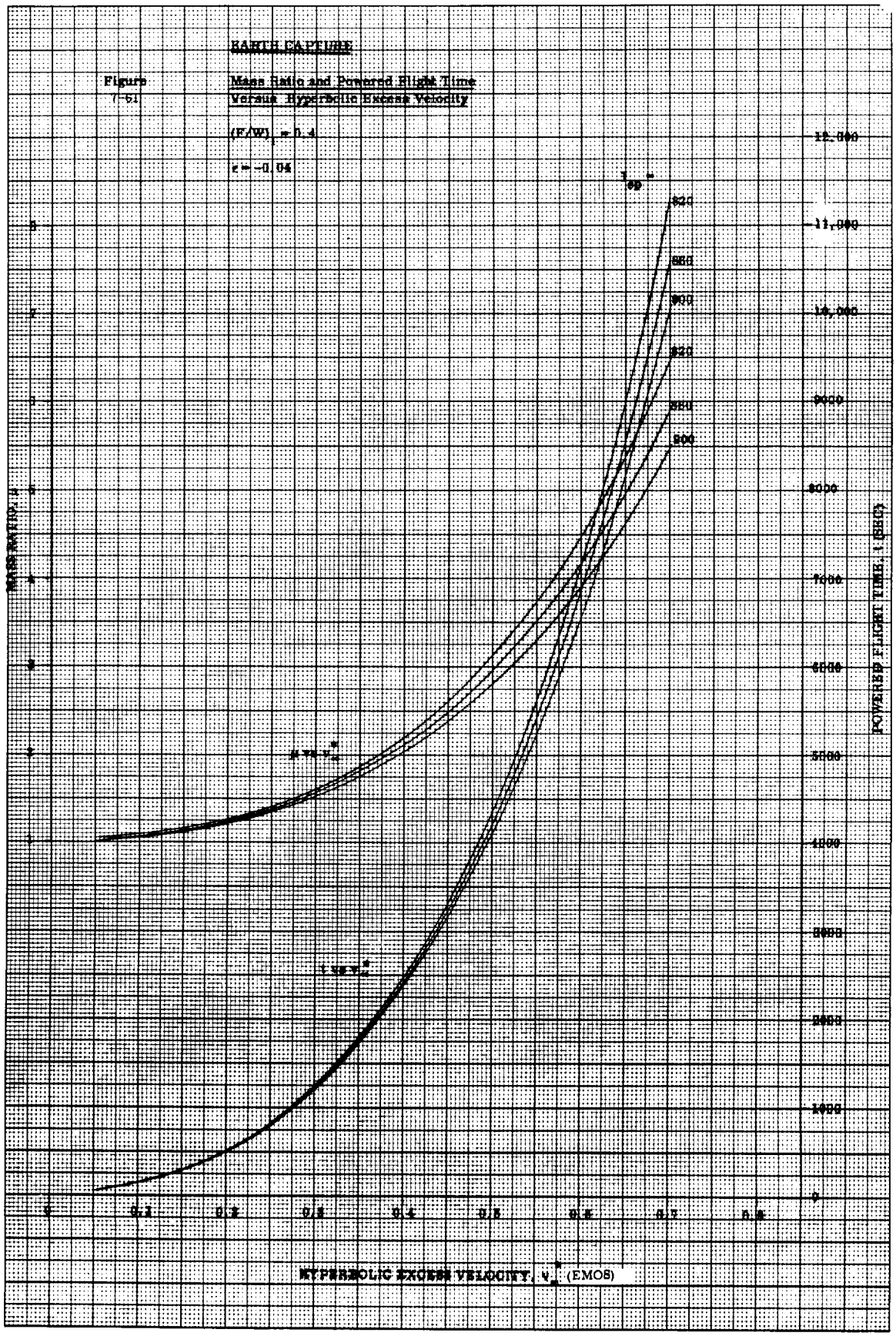

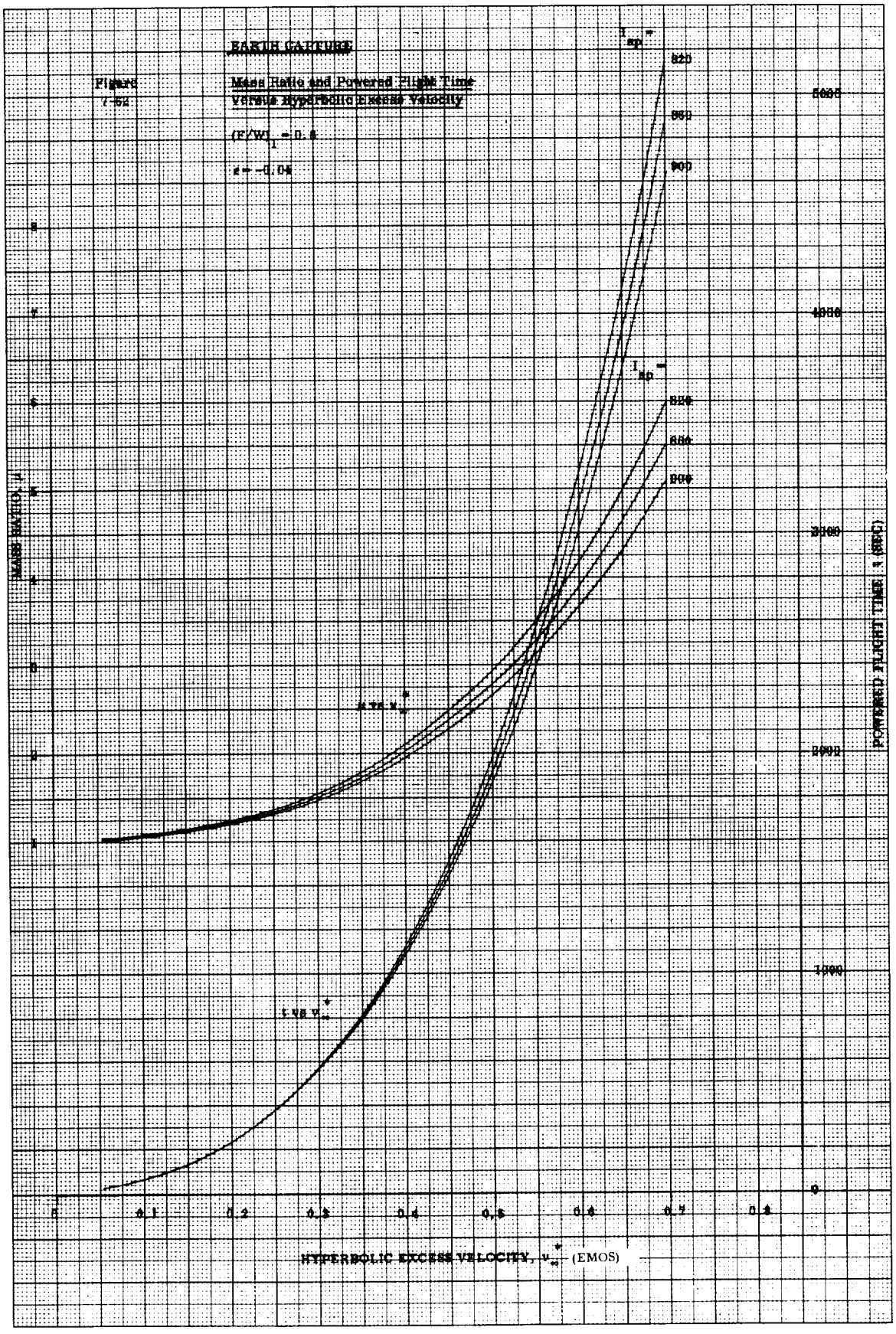
EARTH CAPTURE
Mass Ratio and Powered Flight Time
Versus Hyperbolic Excess Velocity
$(F/W)_1 = 0.6$
$\epsilon = -0.04$
$I_{sp} =$
820
860
900
820
860
900
MASS RATIO, J
POWERED FLIGHT TIME, t (SEC)
4.76 v_∞^*
1.48 v_∞^*
0
0.1
0.2
0.3
0.4
0.5
0.6
0.7
0.8
HYPERBOLIC EXCESS VELOCITY, v_∞^* (EMOS)

Figure 7-52

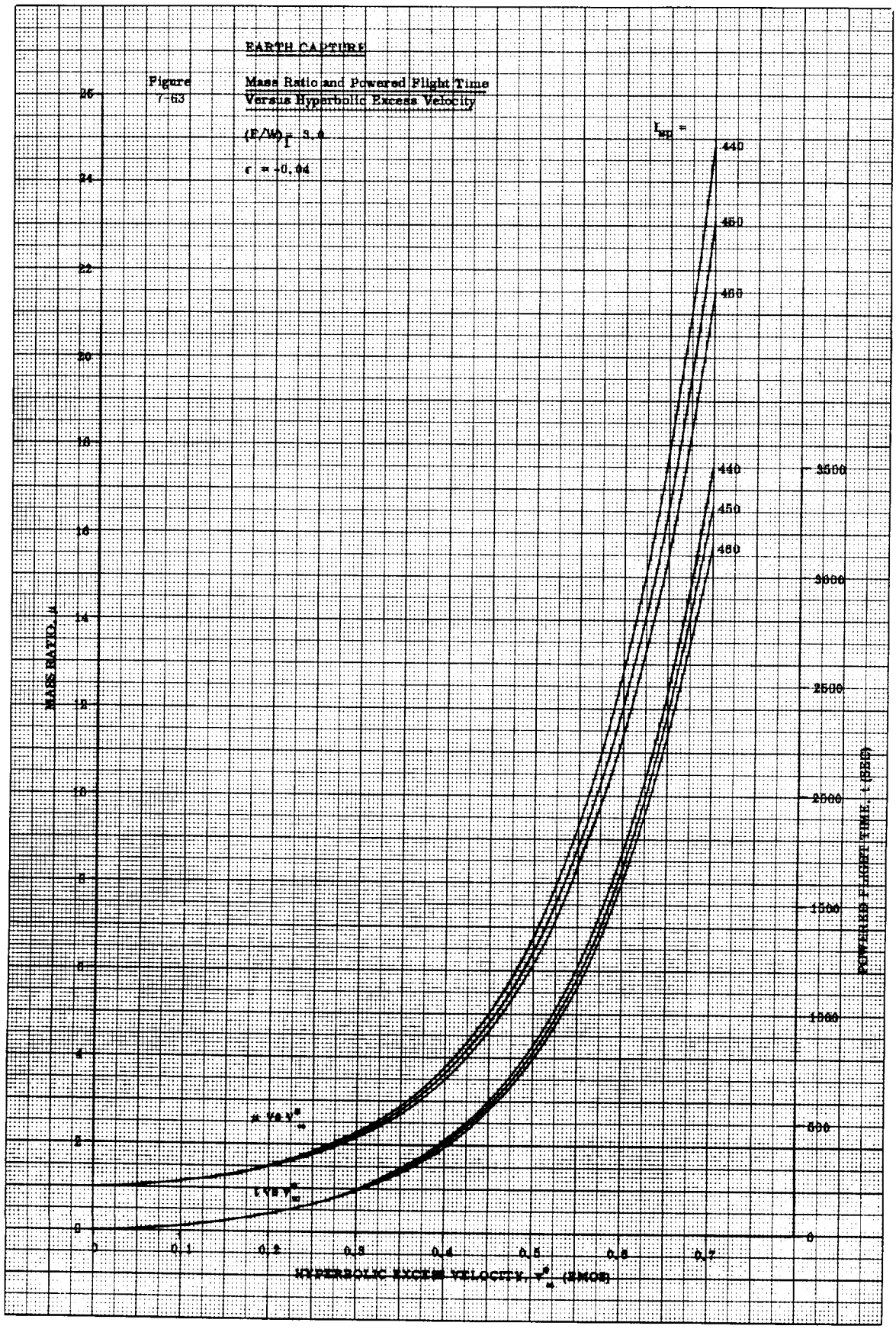
EARTH CAPTURE
Figure 7-63
Mass Ratio and Powered Flight Time Versus Hyperbolic Excess Velocity
$(F/W_0)_I$ = 3.0
ϵ = -0.04
I_{sp} =
440
450
460
MASS RATIO, R
POWERED FLIGHT TIME, t (SEC)
HYPERBOLIC EXCESS VELOCITY, V_∞^* (ER/SEC)

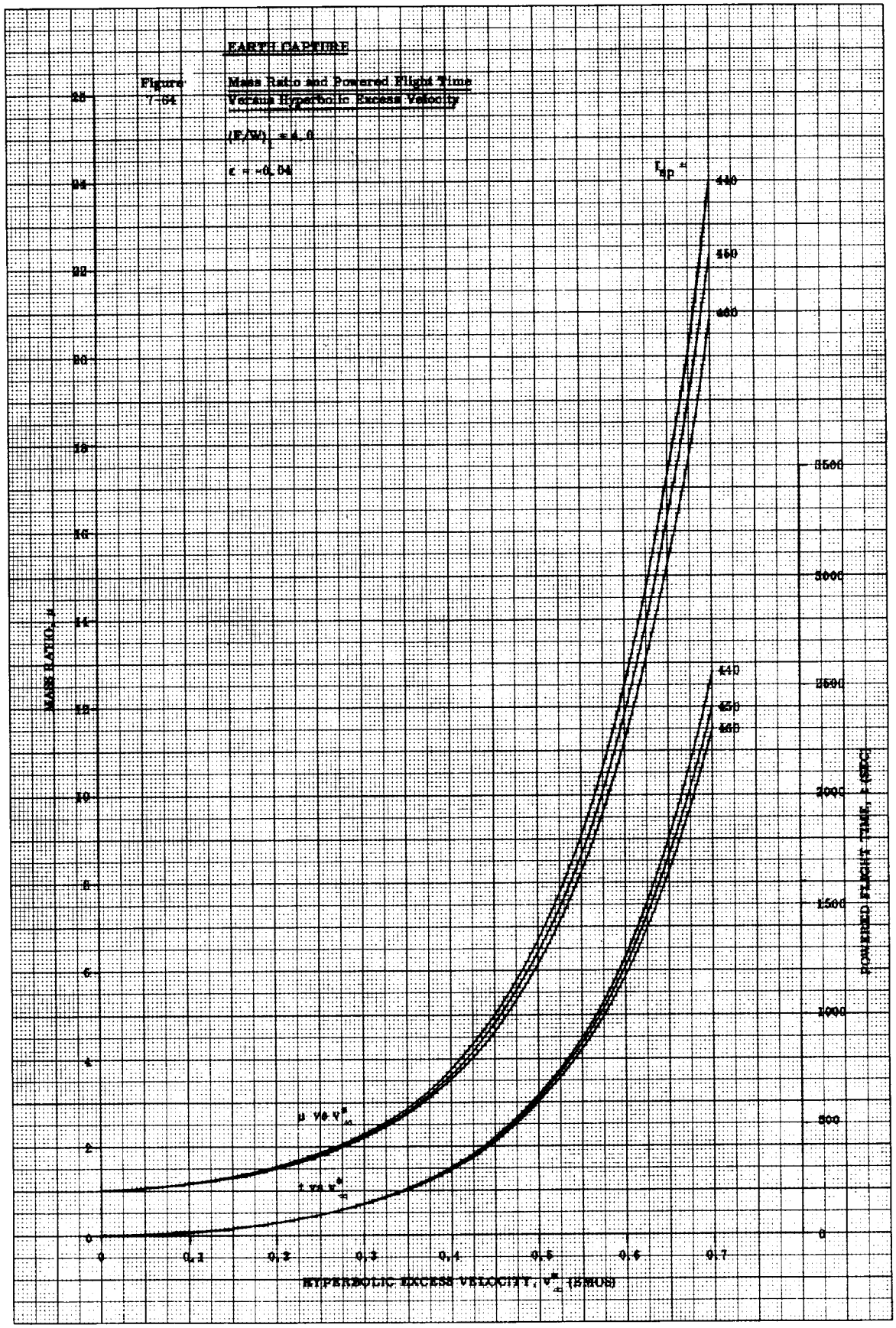
EARTH CAPTURE
Figure 7-64
Mass Ratio and Powered Flight Time Versus Hyperbolic Excess Velocity
$(F/W)_1 = 4.0$
$\epsilon = -0.04$
I_{sp}
440
450
460
MASS RATIO, R
POWERED FLIGHT TIME, SEC
μ Via V_{∞}^2
τ via V_{∞}^2
HYPERBOLIC EXCESS VELOCITY, V_{∞}^2 (ERUS)

AOK63-0001

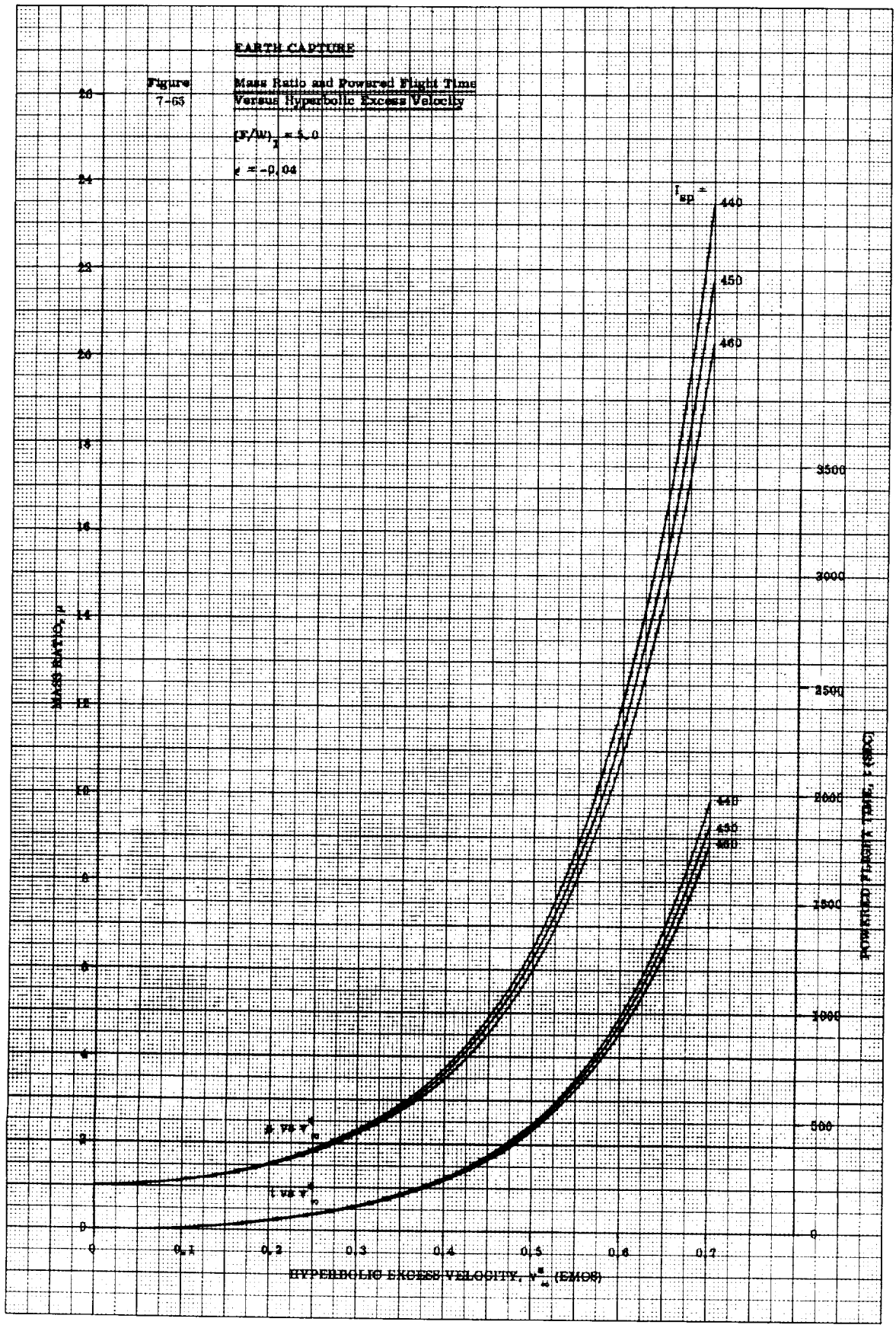
EARTH CAPTURE
Figure 7-65
Mass Ratio and Powered Flight Time Versus Hyperbolic Excess Velocity
$(F/W)_I = 1.0$
$\epsilon = -0.04$
I_{sp} =
440
450
460
MASS RATIO, R
POWERED FLIGHT TIME, t (SEC)
HYPERBOLIC EXCESS VELOCITY, V_∞ (EMOS)

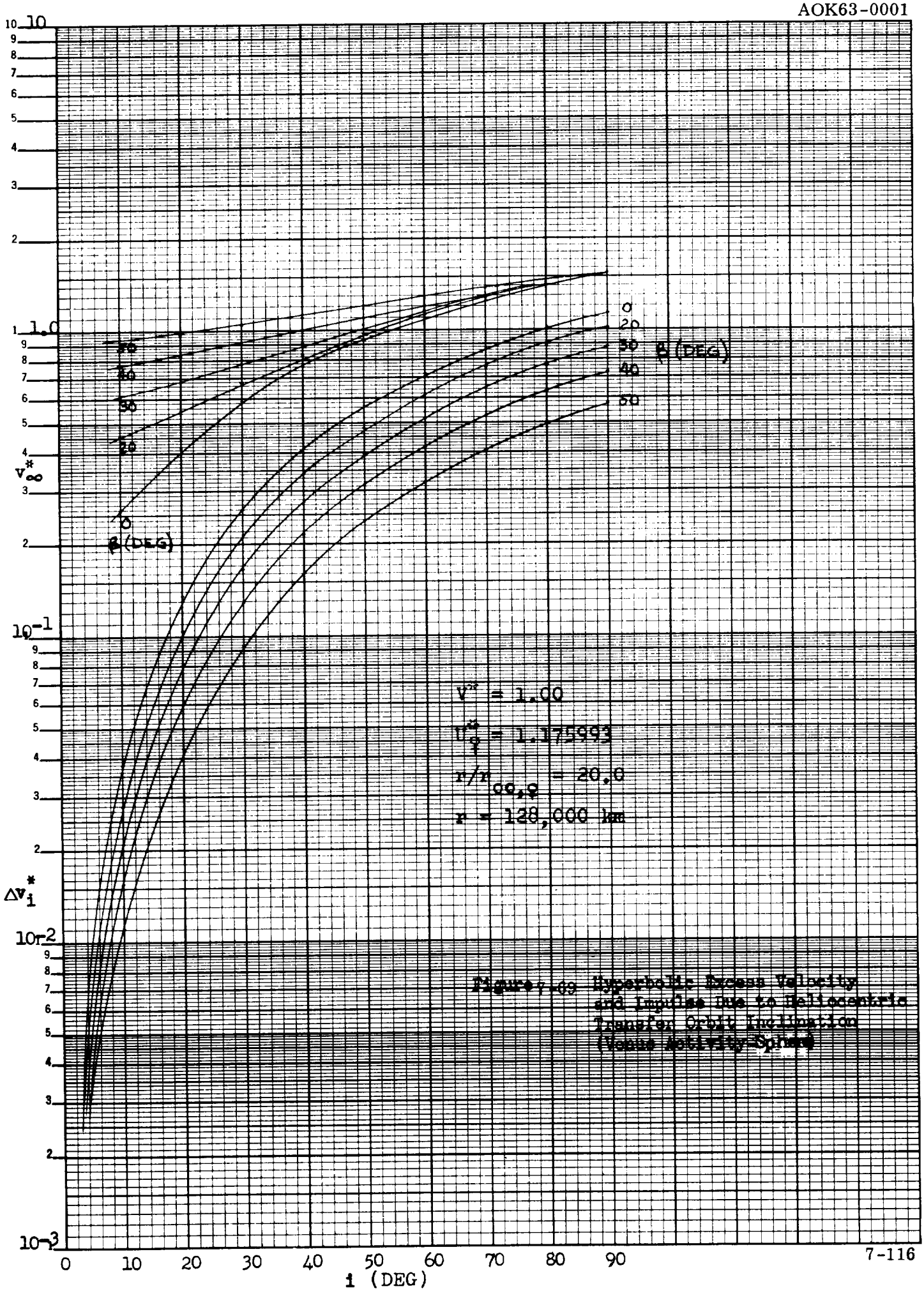

Figure 7.69 Hyperbolic Excess Velocity and Impulse Due to Heliocentric Transfer Orbit Inclination (Venus Activity-Sphere)

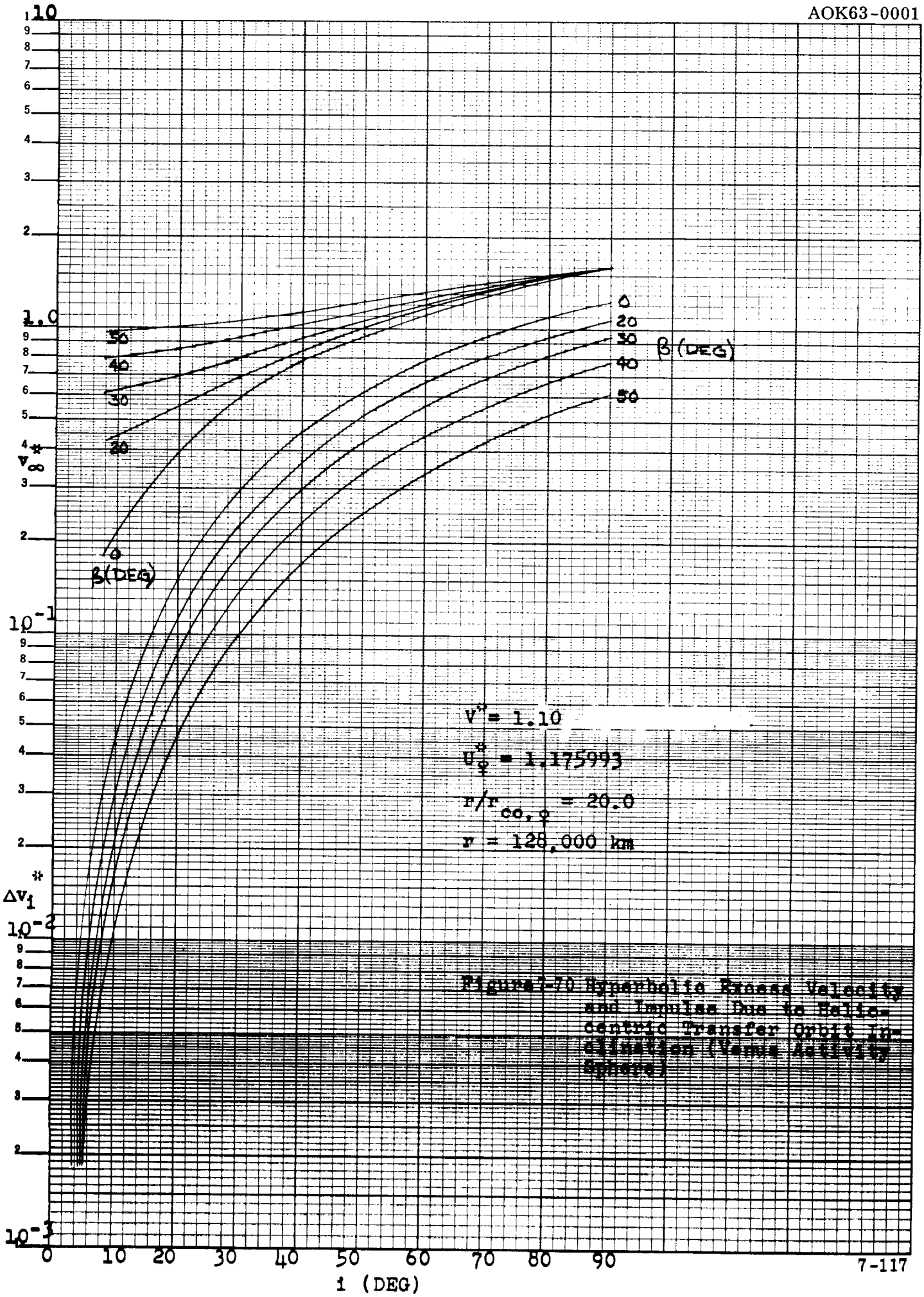

Figure 7-70 Hyperbolic Excess Velocity and Impulse Due to Heliocentric Transfer Orbit Inclination (Venus Activity Sphere)

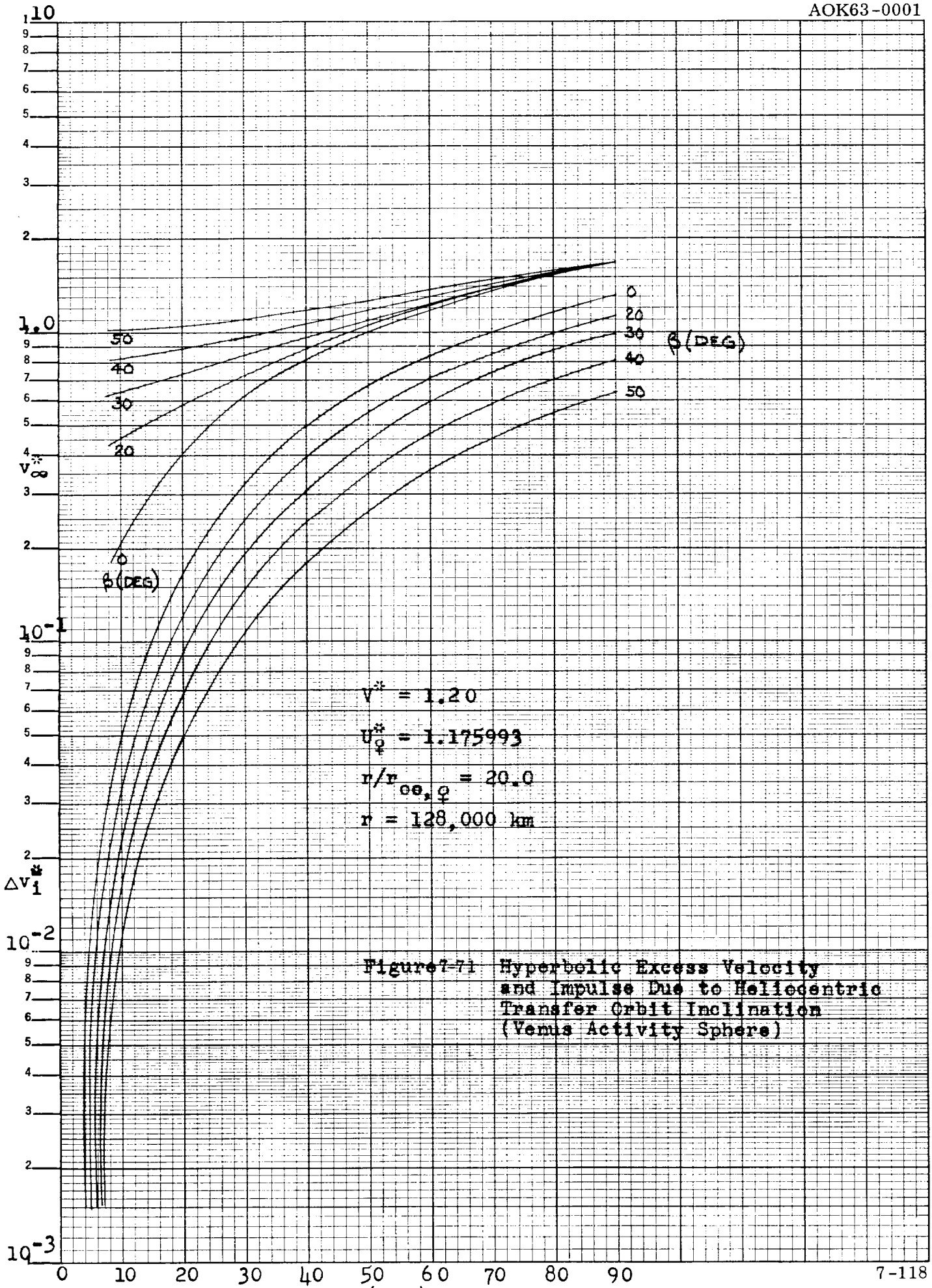

Figure 7-71 Hyperbolic Excess Velocity and Impulse Due to Heliocentric Transfer Orbit Inclination (Venus Activity Sphere)

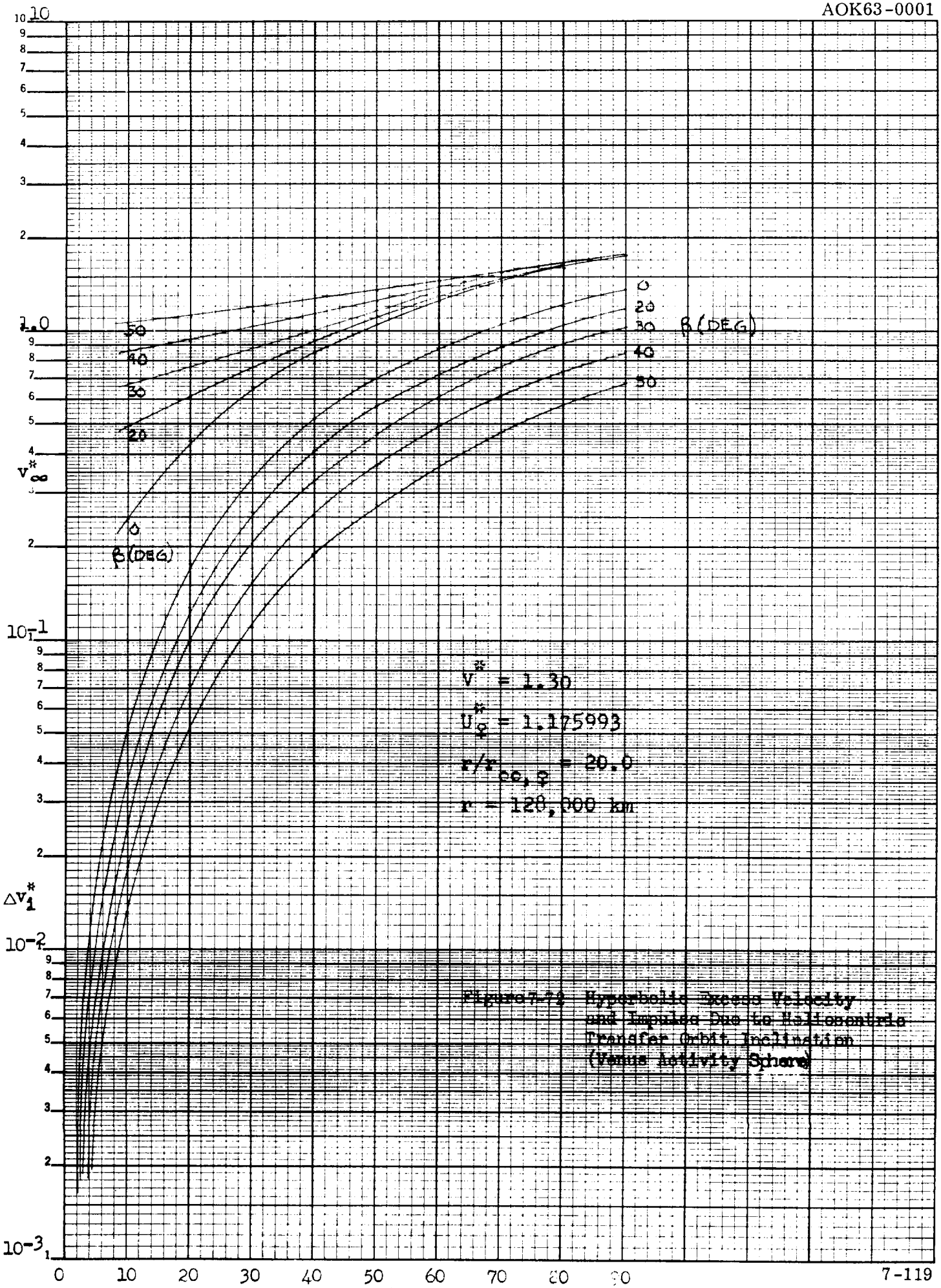

Figure 7.72 Hyperbolic Excess Velocity and Impulse Due to Heliocentric Transfer Orbit Inclination (Venus Activity Sphere)

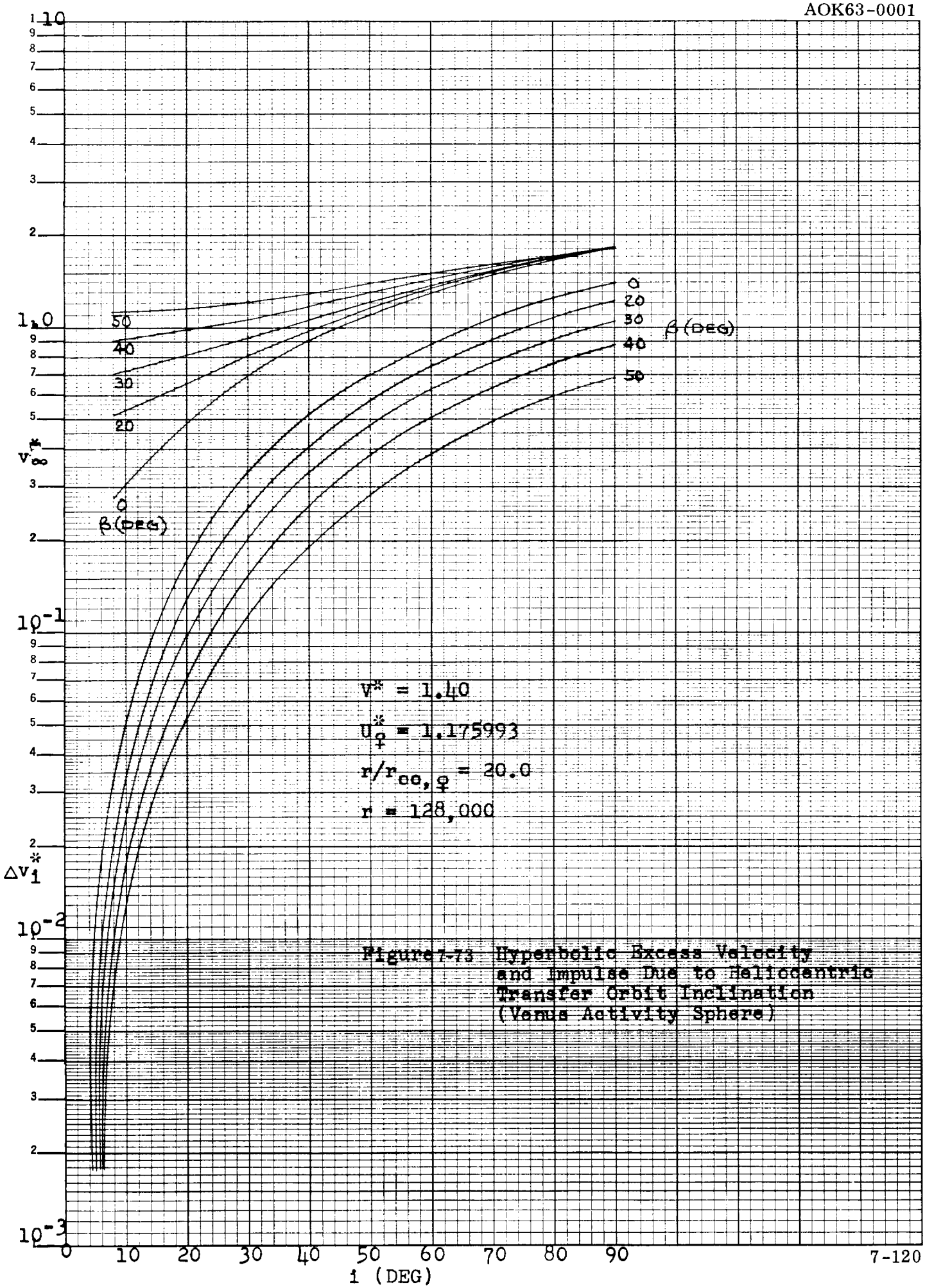

Figure 7-73 Hyperbolic Excess Velocity and Impulse Due to Heliocentric Transfer Orbit Inclination (Venus Activity Sphere)

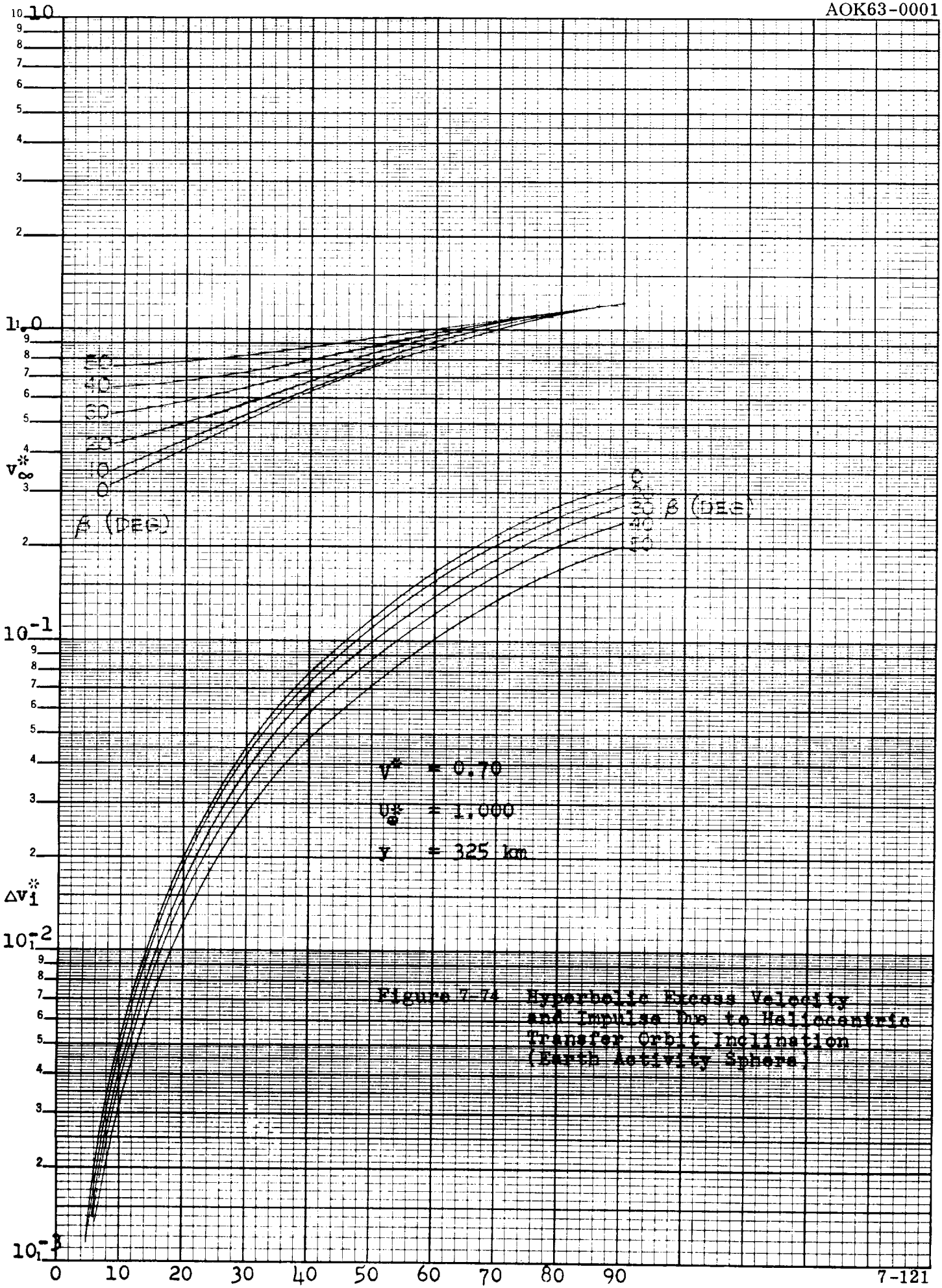

Figure 7-74 Hyperbolic Excess Velocity and Impulse Due to Heliocentric Transfer Orbit Inclination (Earth Activity Sphere)

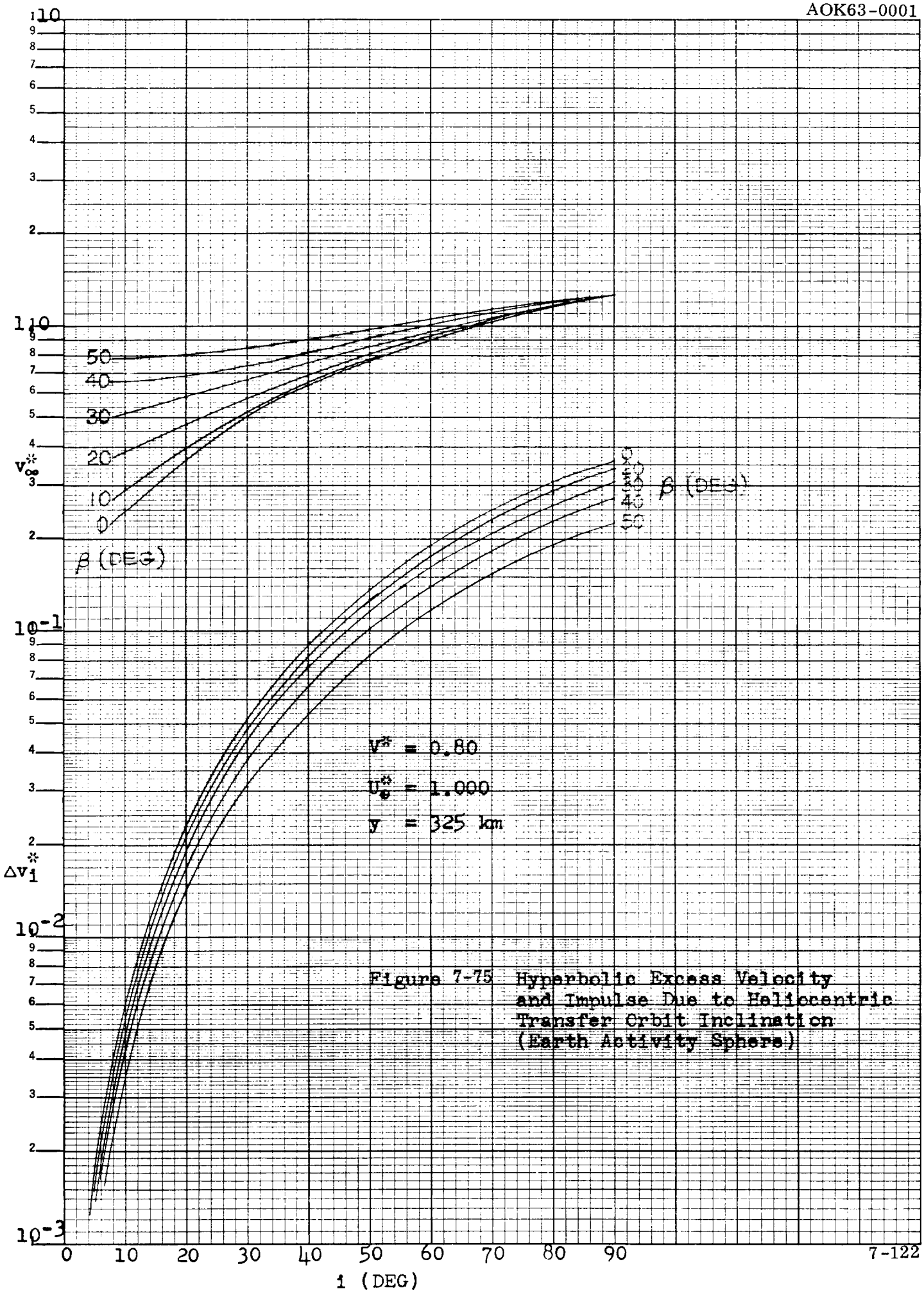

Figure 7-75 Hyperbolic Excess Velocity and Impulse Due to Heliocentric Transfer Orbit Inclination (Earth Activity Sphere)

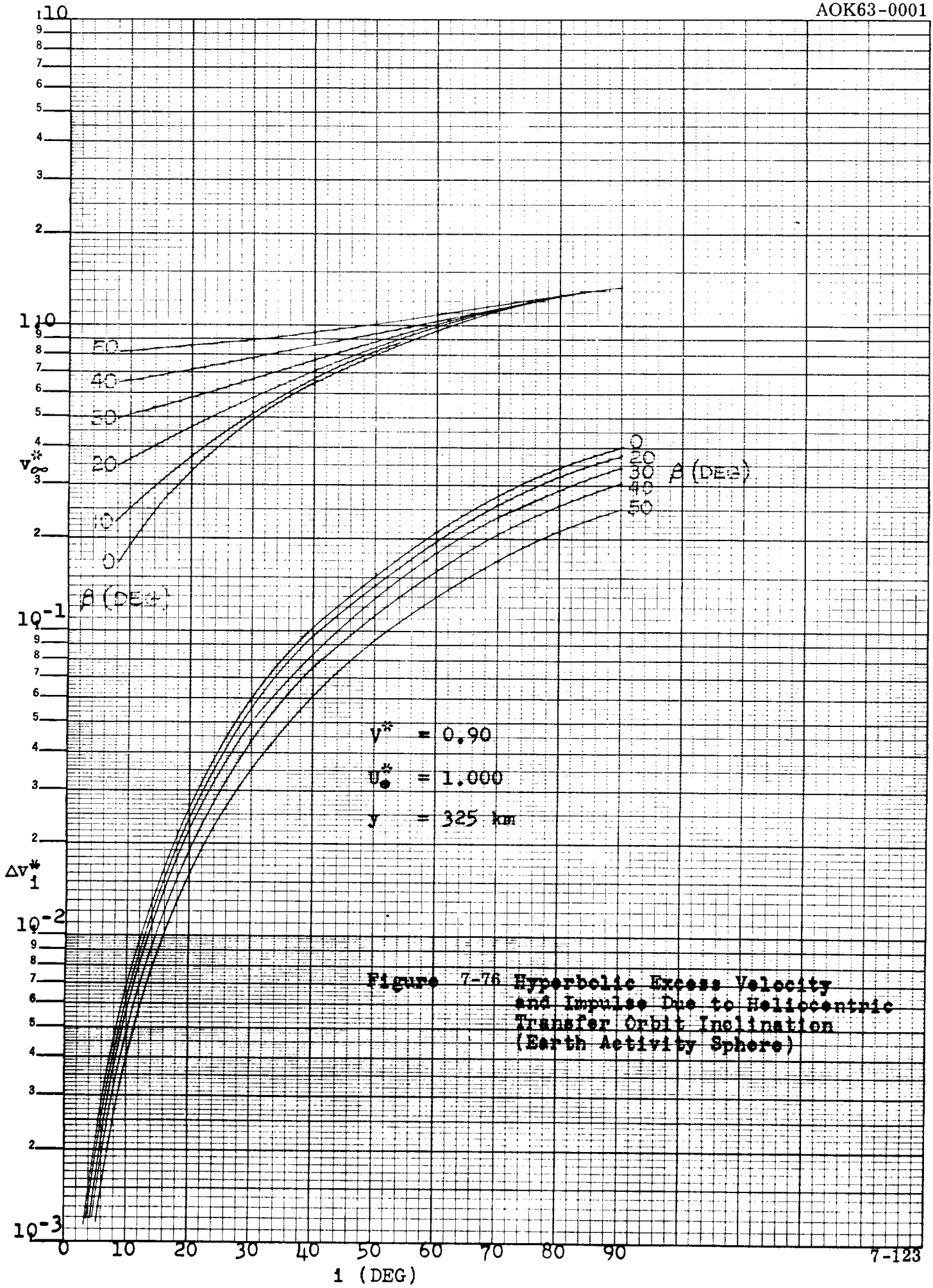

Figure 7-76 Hyperbolic Excess Velocity and Impulse Due to Heliocentric Transfer Orbit Inclination (Earth Activity Sphere)

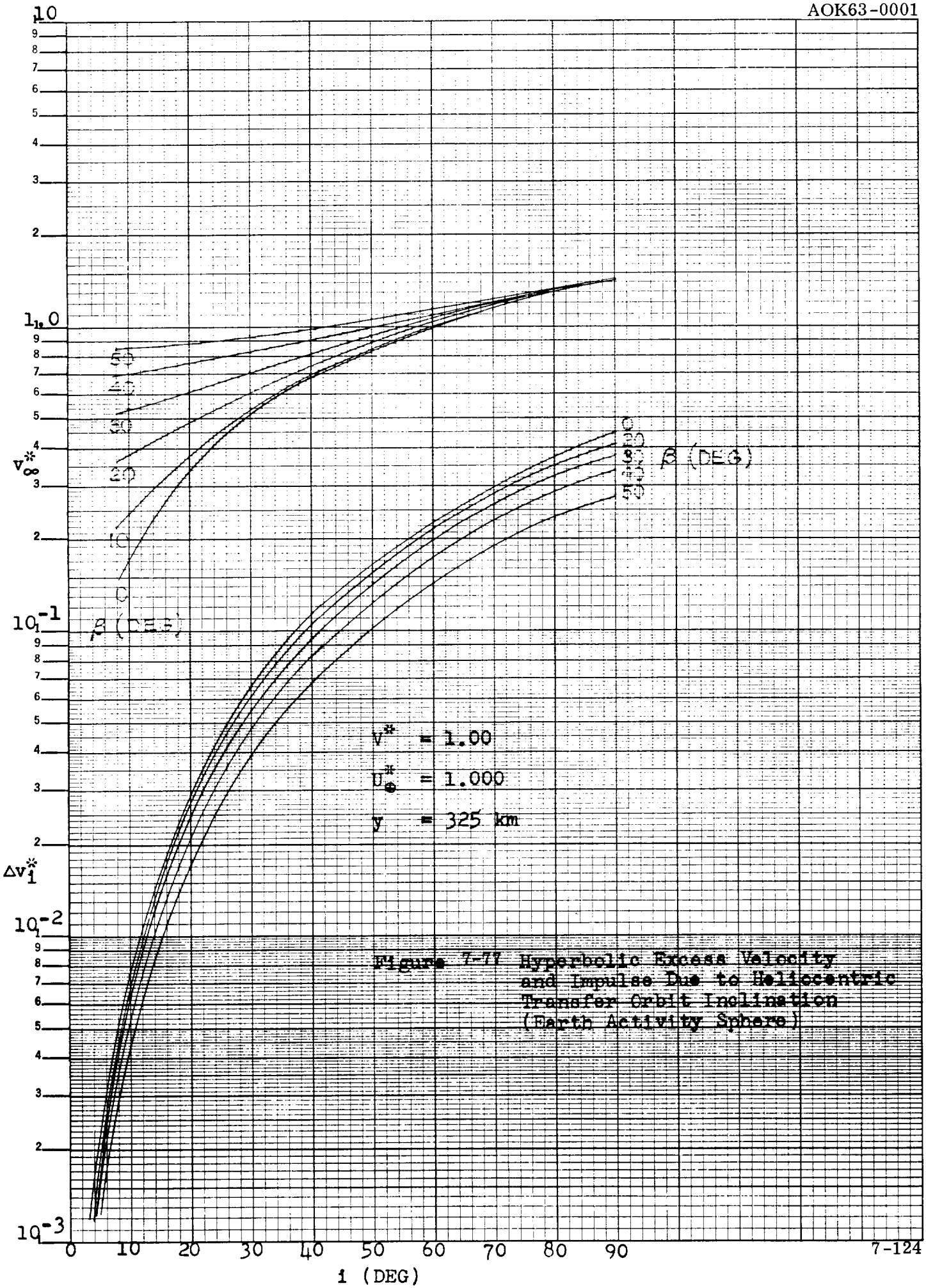

Figure 7-77 Hyperbolic Excess Velocity and Impulse Due to Heliocentric Transfer Orbit Inclination (Earth Activity Sphere)

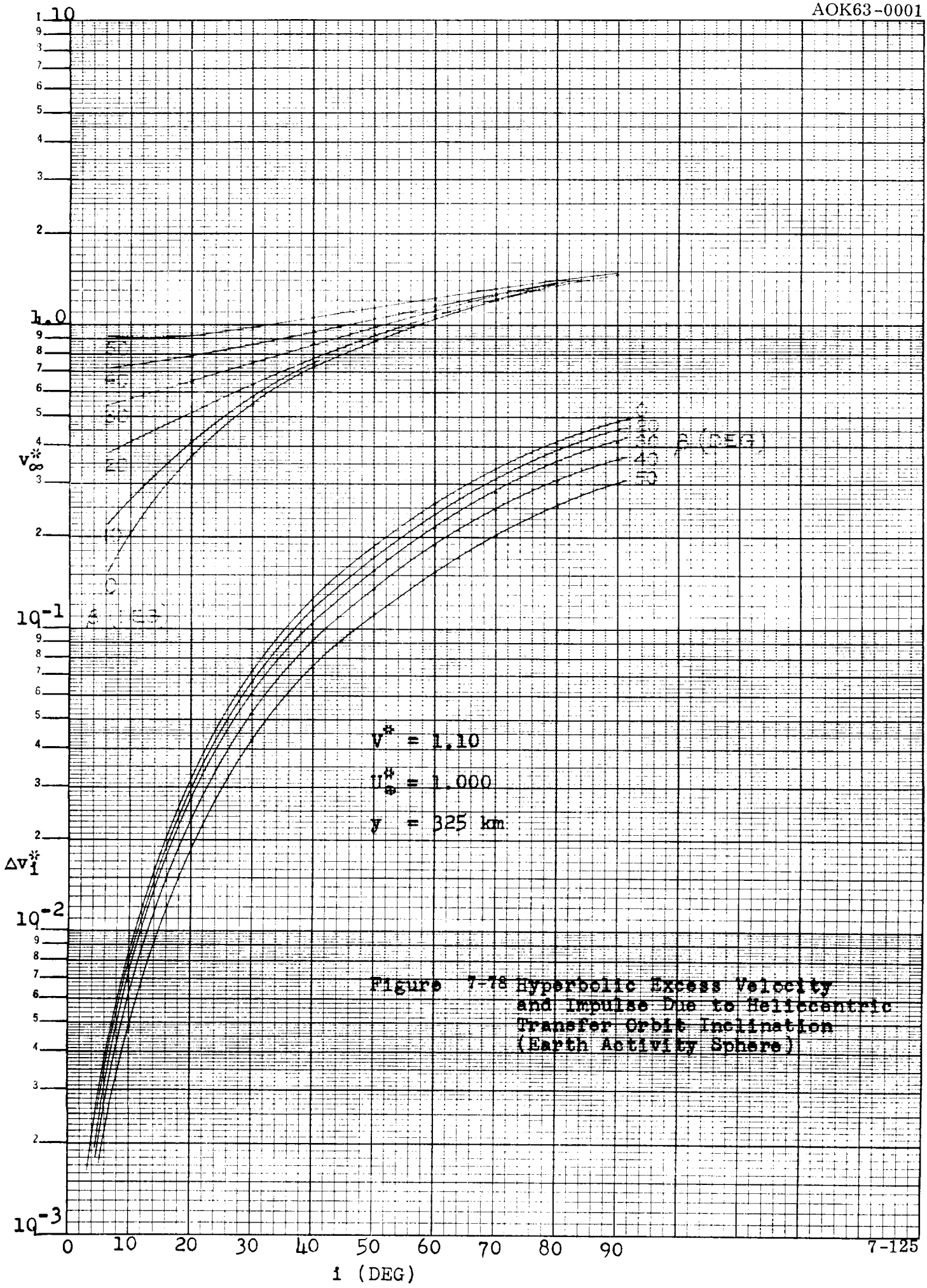

Figure 7-78 Hyperbolic Excess Velocity and Impulse Due to Heliocentric Transfer Orbit Inclination (Earth Activity Sphere)

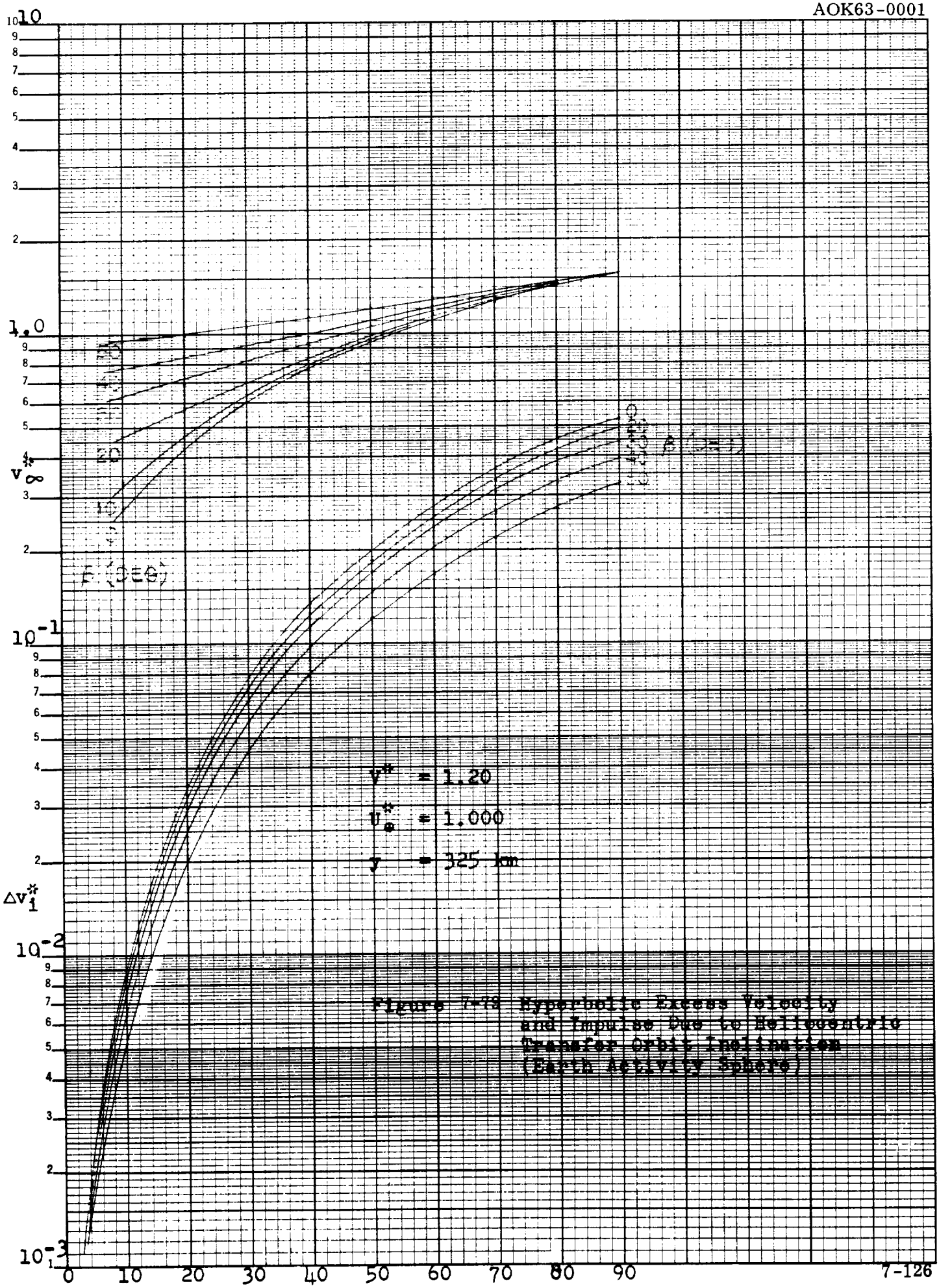

Figure 7-18 Hyperbolic Excess Velocity and Impulse Due to Heliocentric Transfer Orbit Inclination (Earth Activity Sphere)

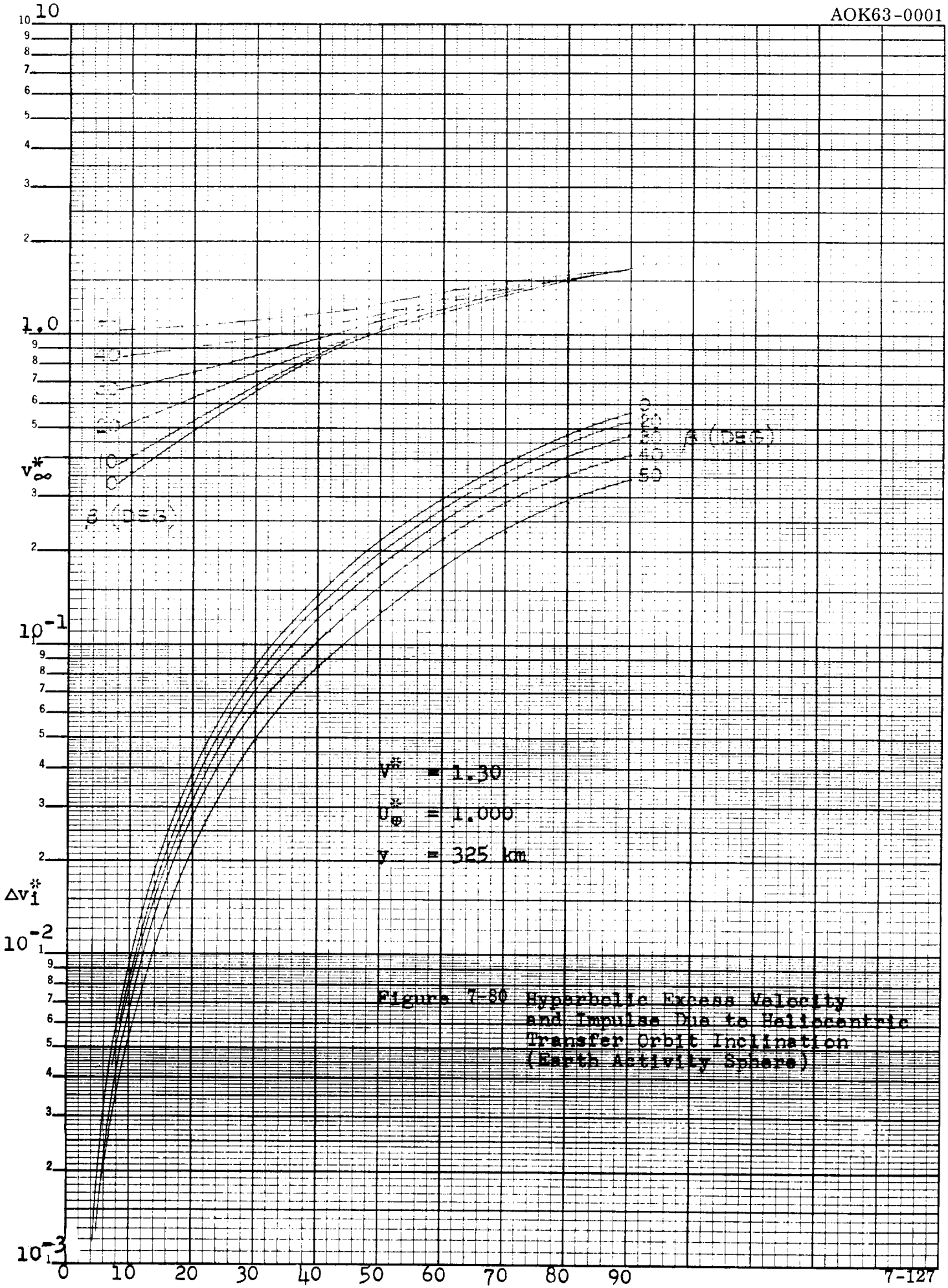

Figure 7-80 Hyperbolic Excess Velocity and Impulse Due to Heliocentric Transfer Orbit Inclination (Earth Activity Sphere)

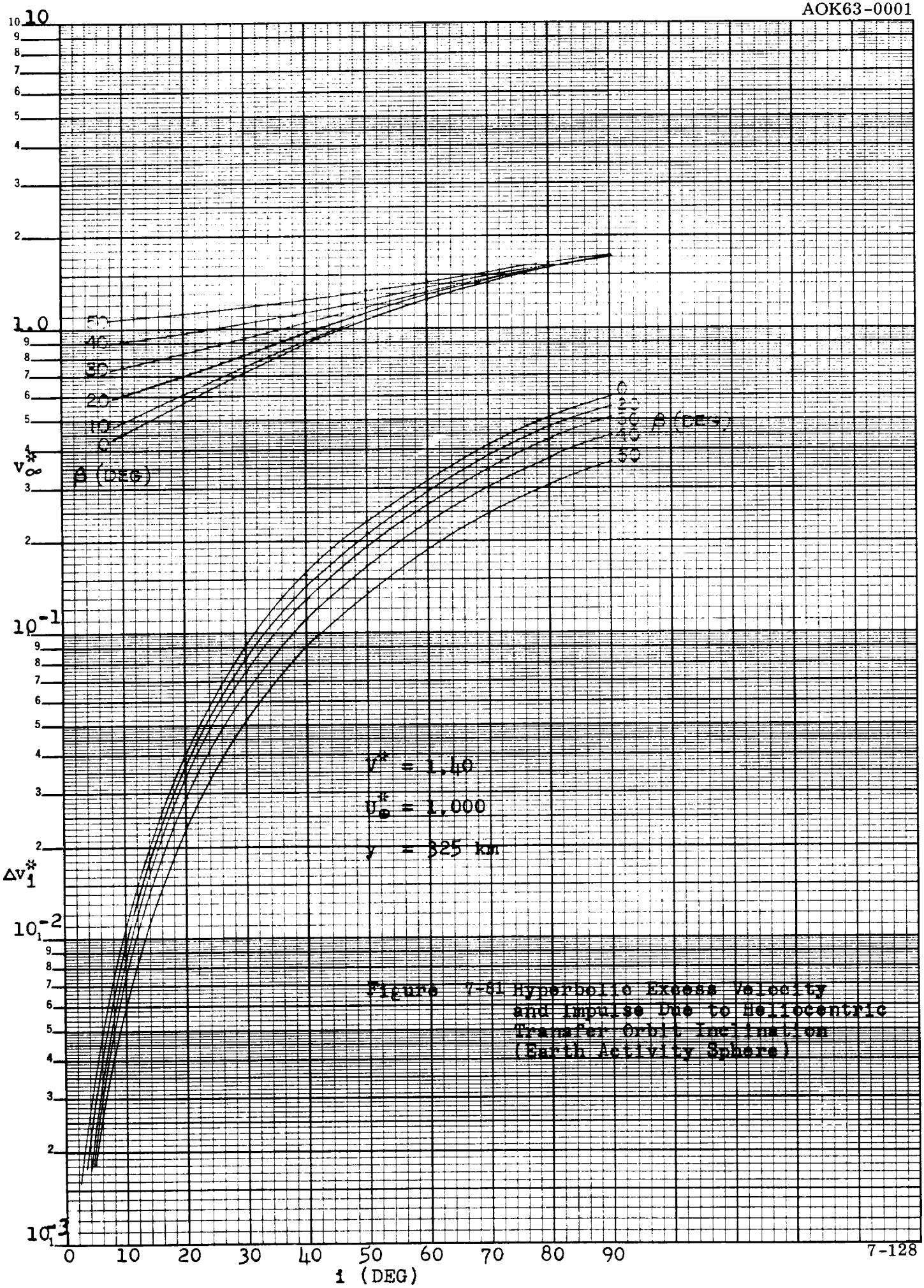

Figure 7-61 Hyperbolic Excess Velocity and Impulse Due to Heliocentric Transfer Orbit Inclination (Earth Activity Sphere)

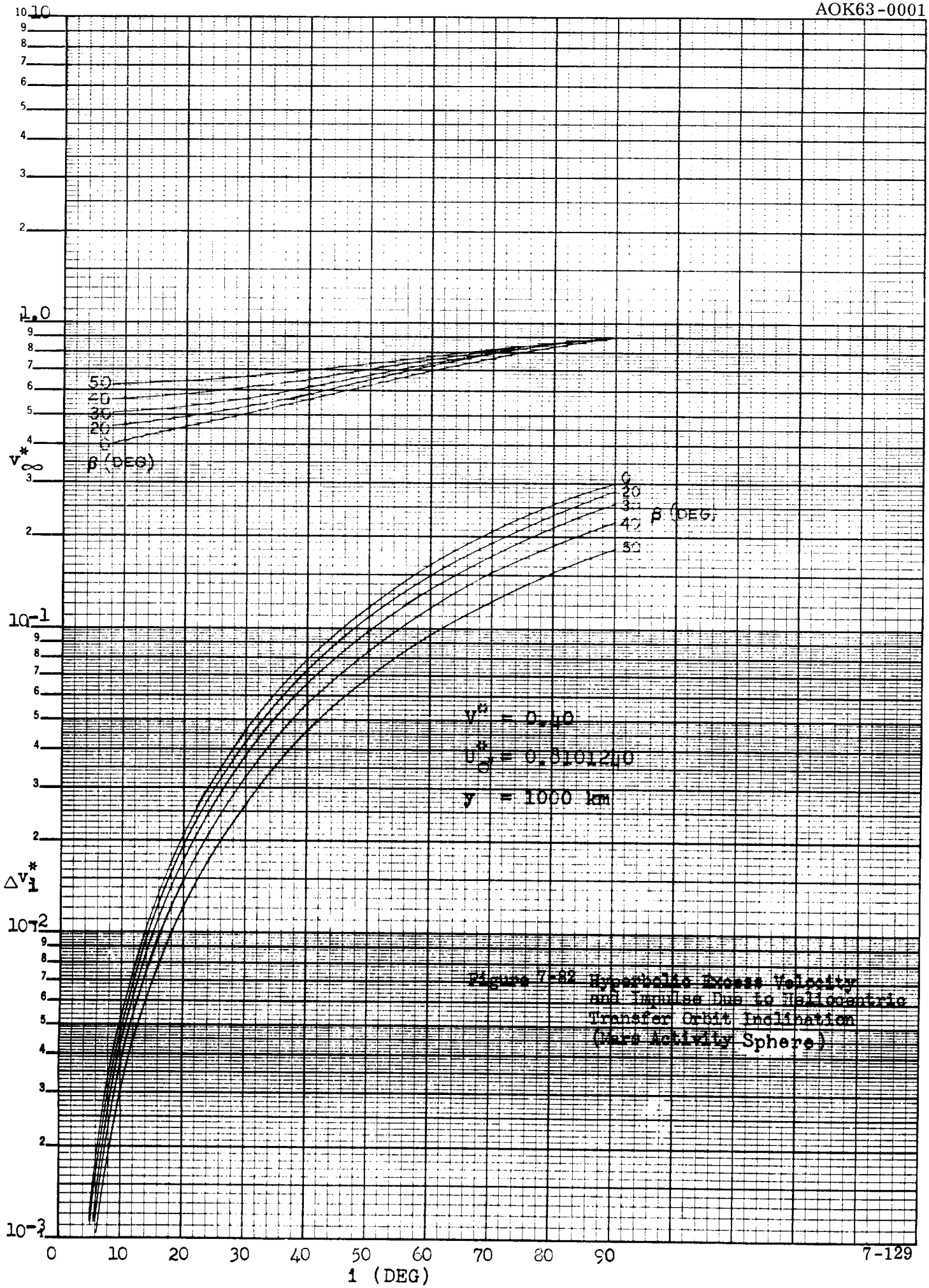

Figure 7-82 Hyperbolic Excess Velocity and Impulse Due to Heliocentric Transfer Orbit Inclination (Ares Activity Sphere)

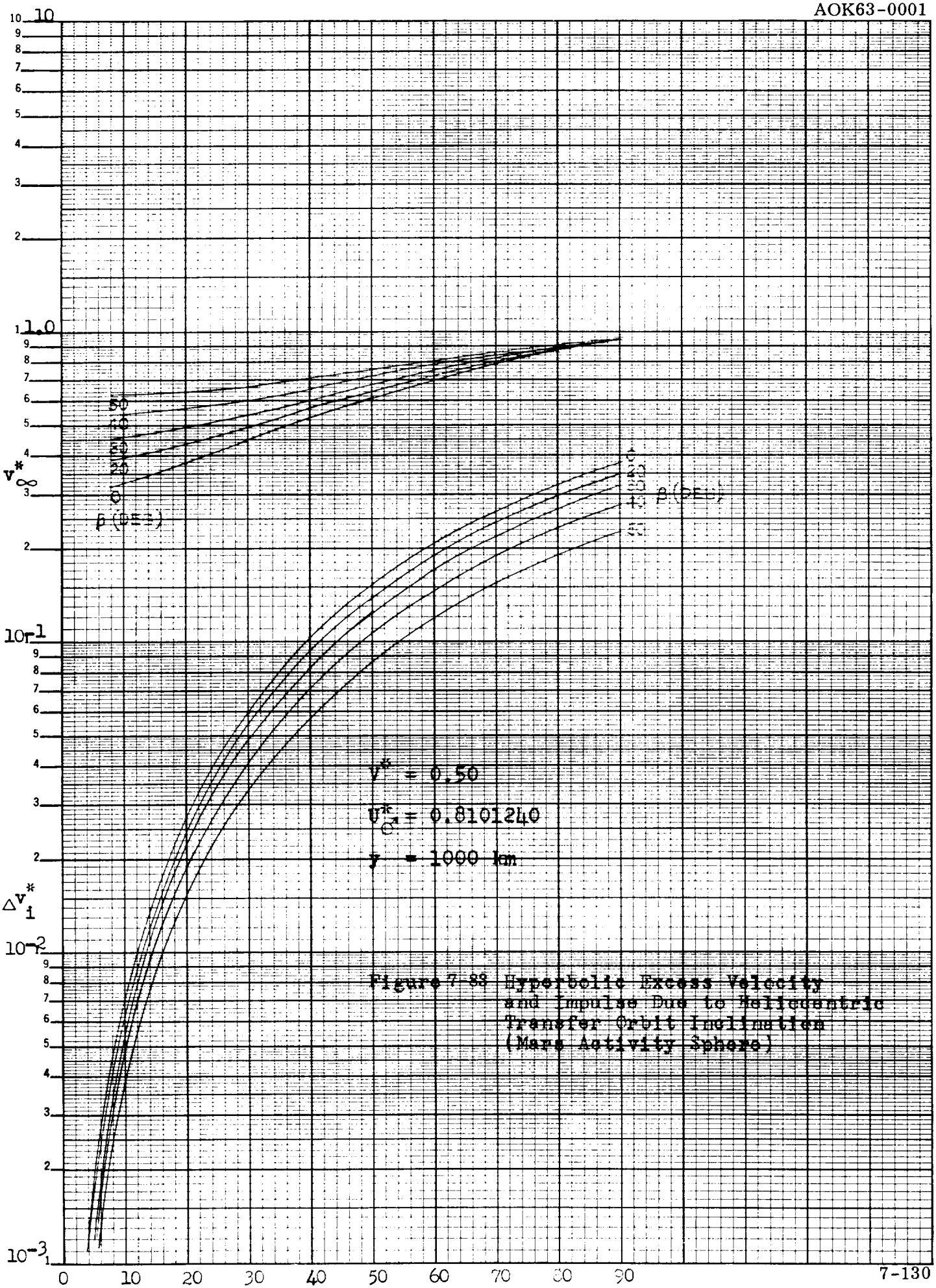

Figure 7-88 Hyperbolic Excess Velocity and Impulse Due to Heliocentric Transfer Orbit Inclination (Mars Activity Sphere)

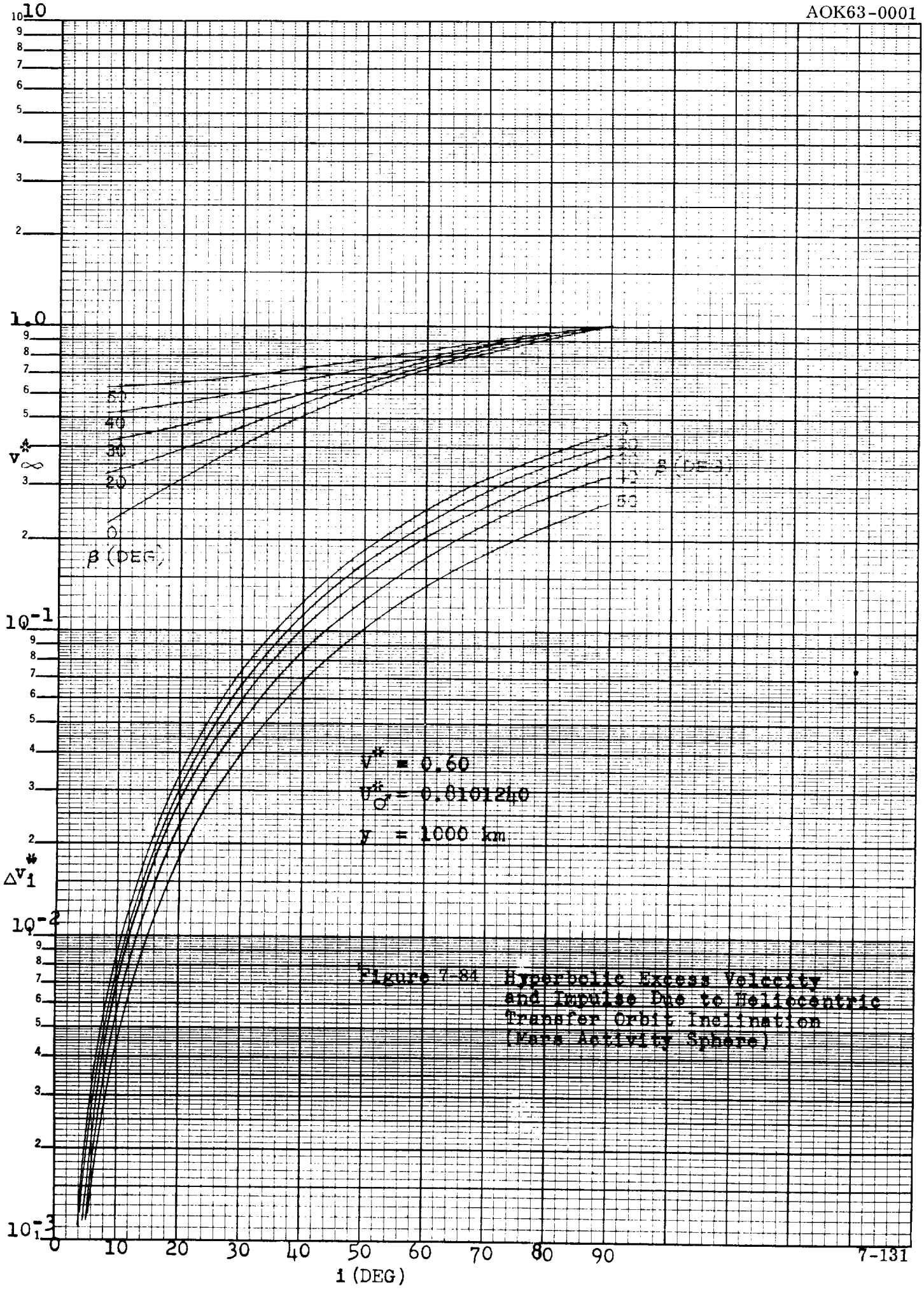

Figure 7-84 Hyperbolic Excess Velocity and Impulse Due to Heliocentric Transfer Orbit Inclination (Mars Activity Sphere)

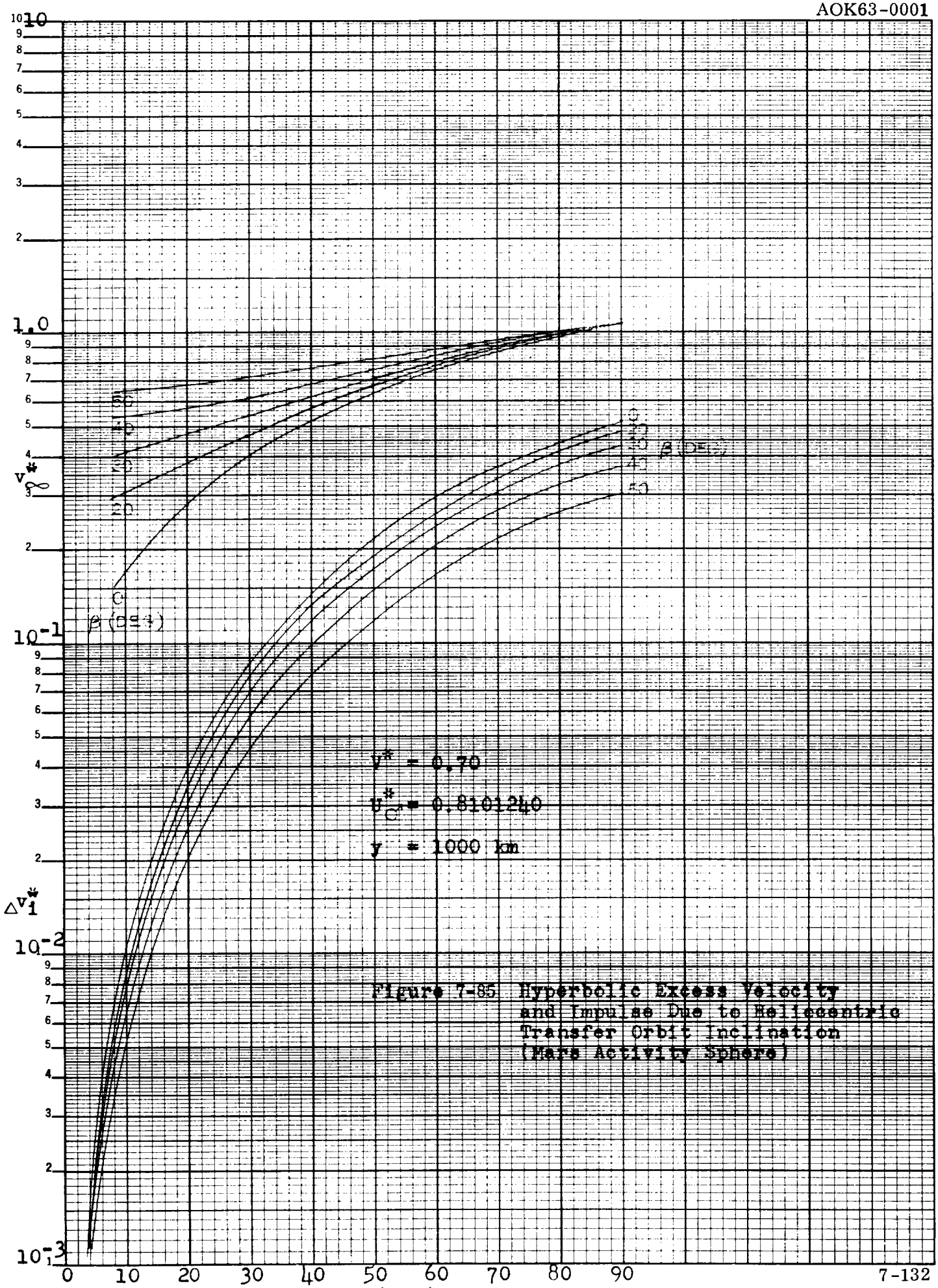

Figure 7-85 Hyperbolic Excess Velocity and Impulse Due to Heliocentric Transfer Orbit Inclination (Mars Activity Sphere)

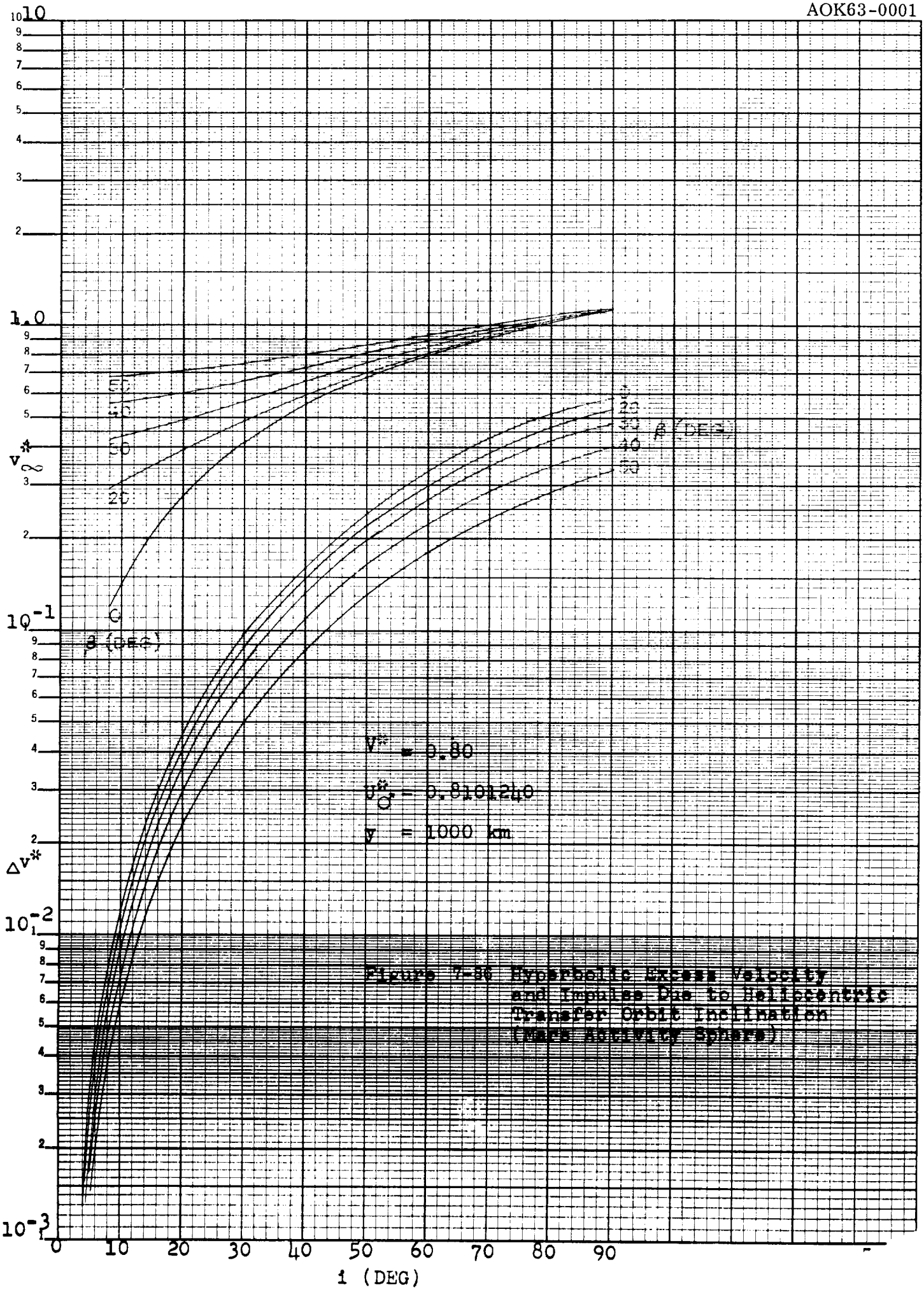

Figure 7-86 Hyperbolic Excess Velocity and Impulse Due to Heliocentric Transfer Orbit Inclination (Mars Activity Sphere)

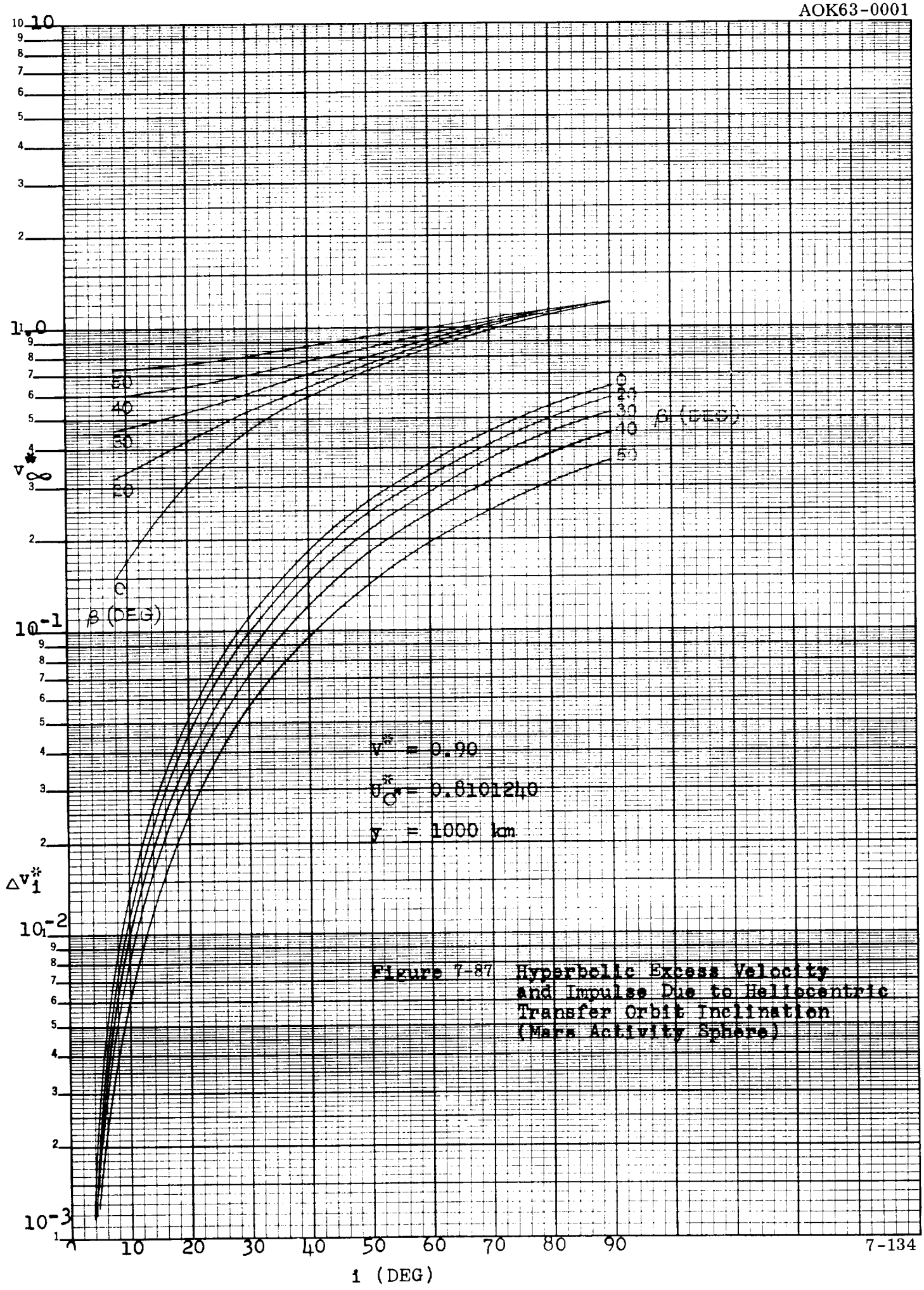

Figure 7-87 Hyperbolic Excess Velocity and Impulse Due to Heliocentric Transfer Orbit Inclination (Mars Activity Sphere)

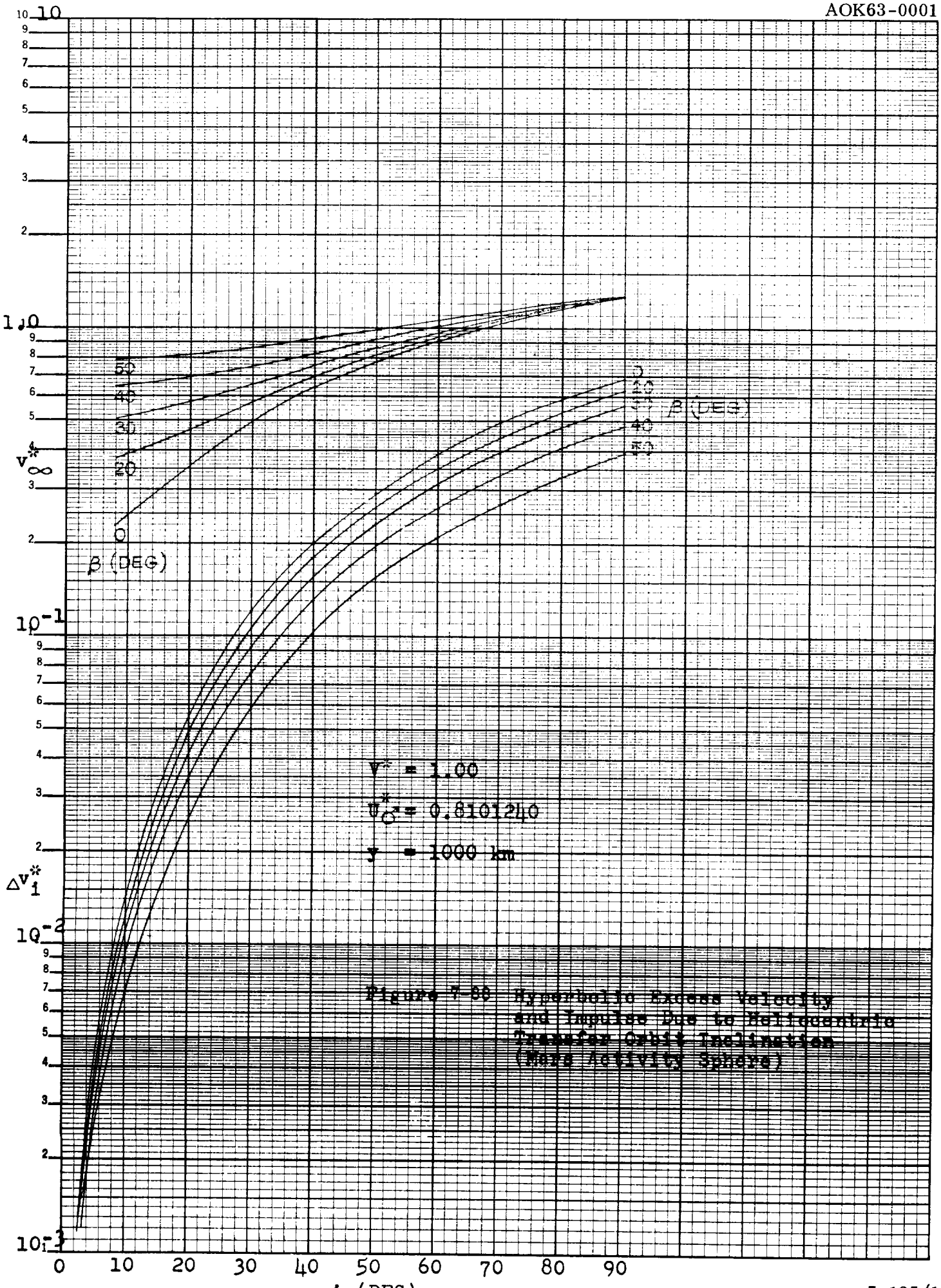

Figure 7-86 Hyperbolic Excess Velocity and Impulse Due to Heliocentric Transfer Orbit Inclination (Mars Activity Sphere)

PART II

VEHICLES AND CREW

SECTION 8

THE VEHICLES

8.1 INTRODUCTION. This section surveys the results of the vehicle and systems studies. The primary objective of these studies was to solve, by selective elimination of various alternatives, certain key design problems and thereby to arrive at a degree of conceptual standardization which forms the frame of reference for a large number and variety of planet ships and which is the basis of future more detailed design and systems integration. This objective has been met. Two preferred life support section designs were evolved, one using the M-4 liquid hydrogen as the essential part of the LSS radiation shielding system ("wet" LSS), the other being based entirely on boron-filled polyethylene and the drinking water ("dry" LSS). A preferred fuel tank arrangement was evolved for propulsion sections with the same engine system for M-2 through M-4, as well as for sections with a separate engine system for each maneuver.

8.2 SURVEY OF VEHICLE TYPES. A large number of vehicles is involved in a manned planetary capture mission. They are classified as main vehicles or convoy vehicles and as auxiliary vehicles. The main vehicles carry the crew and the auxiliary vehicles into the activity sphere of the target planet. Some of them transport the crew and selected payload weight back to Earth. The auxiliary vehicles operate in the activity sphere of the target planet and do not return.

The main vehicles travel in a convoy. The number of convoys is not necessarily one (cf. Section 13); however, since each convoy would be governed by essentially the same principles, only one convoy needs to be considered at this point.

The convoy vehicles are classified as crew vehicles and service vehicles. The vehicle is termed self-sufficient if it is capable, under planned conditions, of carrying out its mission without transfer of fuel tanks or of fuel en route. An alternate approach is to carry vehicle modules along separately and mate them en route as required (cf. Section 13). The main difference between the two types of convoy vehicles is that the crew vehicle carries a life support system, and the other does not. The six principal tasks of the crew and the service vehicle are listed in Table 8-1. The crew vehicle is so designed that all its capabilities outside of propulsion and, possibly, major electrical power generation are concentrated in the command module and service module of the life support section (LSS). The entire LSS, in turn, is separable from the crew vehicle and can be mated with the front section of the service vehicle, thereby turning the latter into a crew vehicle, in case the propulsion sections of the crew vehicle are incapacitated. Therefore, except for the front section, crew vehicle and service vehicle are standardized as much as practical.

Table 8-1. Convoy Vehicle Assignments

(CONVOY VEHICLES SELF-SUFFICIENT)	
CREW VEHICLE TASK:	SERVICE VEHICLE TASK:
1. Crew transport	1. Transport of auxiliary vehicles
2. Navigation	2. Transport of spares
3. Data processing and storage	3. Transport of make-up fuel
4. Communication	4. Transport of a spare Earth Entry Module
5. Control of auxiliary vehicles	5. Navigation assist
6. Injection of Earth Entry Module into correct atmospheric entry orbit	6. Back-up crew vehicle

The auxiliary vehicles and their tasks are listed in Section 5, Table 5-2. Two systems must be added here, namely, the taxis and the Earth Entry Module (EEM). The EEM is not designated as a "vehicle", but rather as a module, because during the mission it is part of the service vehicle in the sense that it serves as crew abode during powered maneuvers and is used as abort system in case separation of the crew from the service vehicle becomes necessary. This is of particular importance during Earth departure. The purpose of the taxis (taxi capsules) is to serve as commuter between convoy vehicles, and as "tugboat" for conveying fuel tanks or bulky spare material between convoy vehicles.

The principal vehicle sections and the major systems which they contain are listed in Table 8-2. The forward section of both vehicles contains the M-5 propulsion section for abort, spin-up and de-spin, attitude control and, possibly, navigational correction maneuvers (depending on the design). The M-5 propulsion section is attached to the EEM, which is located at the forward end of the life support section and with access to it. In the service vehicle the EEM is attached to the service module section (SMS) which represents the counterpart to the LSS of the crew vehicle. The LSS and the SMS are attached to a column (spine) to provide adequate distance from the nuclear engines and to keep the c.g. sufficiently aft to permit the generation of artificial gravity by tumbling. For the latter reason, chemical vehicles are also equipped with the spine. The attachments between spine and LSS or SMS are alike, so that the LSS can be attached to the spine of the service vehicle. Both LSS and SMS are detachable from their respective vehicles, At the aft end of the spine follow the propulsion sections for the various maneuvers, M-2 through M-4. The entire convoy vehicle (if self-sufficient) is launched from orbit and injected into the departure hyperbola by an escape booster which represents the propulsion section (M-1).

Depending on the propulsion system used, the convoy vehicles are designated briefly as "metal vehicles" or "metal carbide vehicles", "graphite vehicles" and "chemical

vehicles". The metal or metal carbide vehicles are based on a single fast-neutron reactor engine which is used for maneuvers M-2 through M-4, as well as for navigational correction maneuvers. The graphite vehicles use a separate nuclear engine with a primarily thermal neutron reactor for each of the maneuvers, M-2 and M-3. For M-4 a high-pressure O_2/H_2 system was found to yield a lower departure weight than a nuclear engine. Both the metal carbide and the graphite vehicle use an escape booster with a graphite reactor engine or engines. (The engines are discussed in detail in the classified Addendum of this report.) The chemical vehicle is based on a high-pressure O_2/H_2 system with a vacuum specific impulse of 455 sec.

Table 8-2. Principal Sections and Systems of the Convoy Vehicles

SECTION	SYSTEM	VEHICLE CREW	VEHICLE SERVICE
M-5	Propulsion	*	*
	Spin	*	*
	Attitude control	*	*
Earth Entry Module	Earth entry	*	*
	Abort	*	*
	Navigation	*	*
	Emergency communication	*	*
Life Support Section	Ecological life support	*	
	Radiation protection	*	
	Navigation	*	
	Communication	*	
	Emergency power	*	
	Mapper dock	*	
Service Module Section	Docks and storage bins for MEV, Returner, Lander, environmental satellites, Phopro, Deipro, and spare parts		*
Spine	H_2 liquefaction	*	*
	Electric power generation	*	*
M-2, M-3, M-4	Fuel tank docks	*	*
	Meteoroid protection	*	*
	Thermal shield	*	*
	Fuel control	*	*
	Engine	*	*
Earth Escape Booster (M-1)	Fuel control	*	*
	Engine	*	*
	Attitude control	*	*

8.3 DESIGN AND DEVELOPMENT PHILOSOPHY AND DESIGN CRITERIA. If manned planetary flights are to be conducted in 1973 or 1975, the following design principles are mandatory:

a. The simplest and most reliable approach, based on a conservative and carefully balanced extrapolation of the expected state of the art, must be used.

b. New developments should be kept at a minimum; but where they are necessary, they should be initiated soon and/or pursued vigorously. Principal areas in which new developments are very important include:

1. nuclear engines (preferably) or, alternately, high-p_c O_2/H_2 engines,
2. long-duration ecological life support systems (inorganic as well as organic),
3. reliable nuclear or solar electric power generation systems of 30 ekw or higher,
4. hydrogen reliquefaction system as part of the vehicle's fuel conservation system,
5. orbital testing and crew training facility for long-duration operations to satisfy durability and reliability criteria for interplanetary missions,
6. development of an Earth-orbital rendezvous and mating technology, especially if no larger Earth launch vehicle (ELV) than the Saturn C-5 is available; the development of this technology has been postponed because of the particular mission mode selected for Apollo. If Saturn C-5 is the available ELV, some extent of orbital mating or fuel transfer is unavoidable, no matter what mission mode is selected. If a Post-Saturn ELV is available, it is possible to avoid the requirement for mating or fueling very massive modules (order of 300 to 500 tons) in orbit by choice of the proper mission module (cf. Section 13)
7. development of a suitable data compaction and transmission system from convoy ship to Earth.

There are other areas in which a more advanced state of the art than can be expected is desirable, but not mandatory. These include Earth entry vehicles for higher velocities than those needed for Apollo.

c. Utmost standardization and modularization of the convoy vehicles to give maximum versatility and usefulness to each vehicle, and maximum flexibility and safety to the crew.

The following is a summary of the principal design criteria which form the basis for the vehicle design and systems studies carried out during this study phase:

8.3.1 Performance. Although a variety of mission profiles was initially considered for design studies, the designs and weight analyses, done after a certain measure of conceptual standardization (referred to in Paragraph 8-1) was attained, are all based on the mission windows Venus 1973-1, Mars 1973-1, -2, -3 and Mars 1975-1 (tabulated in Section 7).

8.3.2 Crew Size. Mostly eight persons; for purposes of comparison the crew sizes considered ranged from two to sixteen persons.

8.3.3 Environment. Shirtsleeve environment. Atmospheric pressure 5.5 psia. Atmosphere: $O_2 + N_2$. Artificial gravity of the order of 0.1 to 0.4 g provided. However, since vehicle tumbling is not desired or feasible during certain periods of the mission, the crew and all equipment are expected to operate continuously at zero-g (or near-zero-g) for up to 30-50 days. Radiation shielding is laid out for a maximum dosage of 0.75 rad/day. Since the reference missions occur in 1973 and 1975, the shielding is designed for a quiet period of the solar cycle.

8.3.4 Thermal Control. In comparing insulation control with hydrogen reliquefaction or refrigeration, it was found, as in earlier studies, that the latter system is lighter for the mission durations under consideration. A combination of thermal and meteoroid shield and hydrogen refrigeration/liquefaction system is presently considered.

8.3.5 Meteoroid Protection. The meteoroid protection shield is made part of the heat shield surrounding the fuel tanks.

8.3.6 Electrical Power Generation. The standard system assumed presently is the SNAP-8 system. For Venus missions, solar power generator systems would be highly desirable, at least for power requirements in excess of 30 ekw. Power requirements during a Venus mission tend to be greater, because more intense solar irradiation requires a more powerful refrigeration/liquefaction system and because of large power requirements for the radar surface reconnaissance system (cf. Addendum).

8.3.7 Modularization. The modularization concept employed is based on one fundamental premise: The nucleus of the LSS which contains the ecological life support system, navigation, communication and control system and in which the entire crew can live for the entire mission period, if necessary, is practically indestructible because of heavy radiation-shielding walls and because of mechanical protection furnished by equipment and modules surrounding the nucleus.

This means that destruction of the nucleus, should it occur, implies destruction of the crew as well. The nucleus consists of the command module and the "spine modules" A, B, and C (Figure 8-1). The mission modules are expendable, if necessary.

Based on this premise, there is no need for the backup service vehicle to contain a spare LSS. The only reason which would force the crew to abandon the ship would be irreparable (at least for the crew) damage to the propulsion system. If abandoning the ship, the crew does so in its entire LSS, transplanting it from crew vehicle to service vehicle. If damage is done to individual tanks, these can be replaced by tanks from

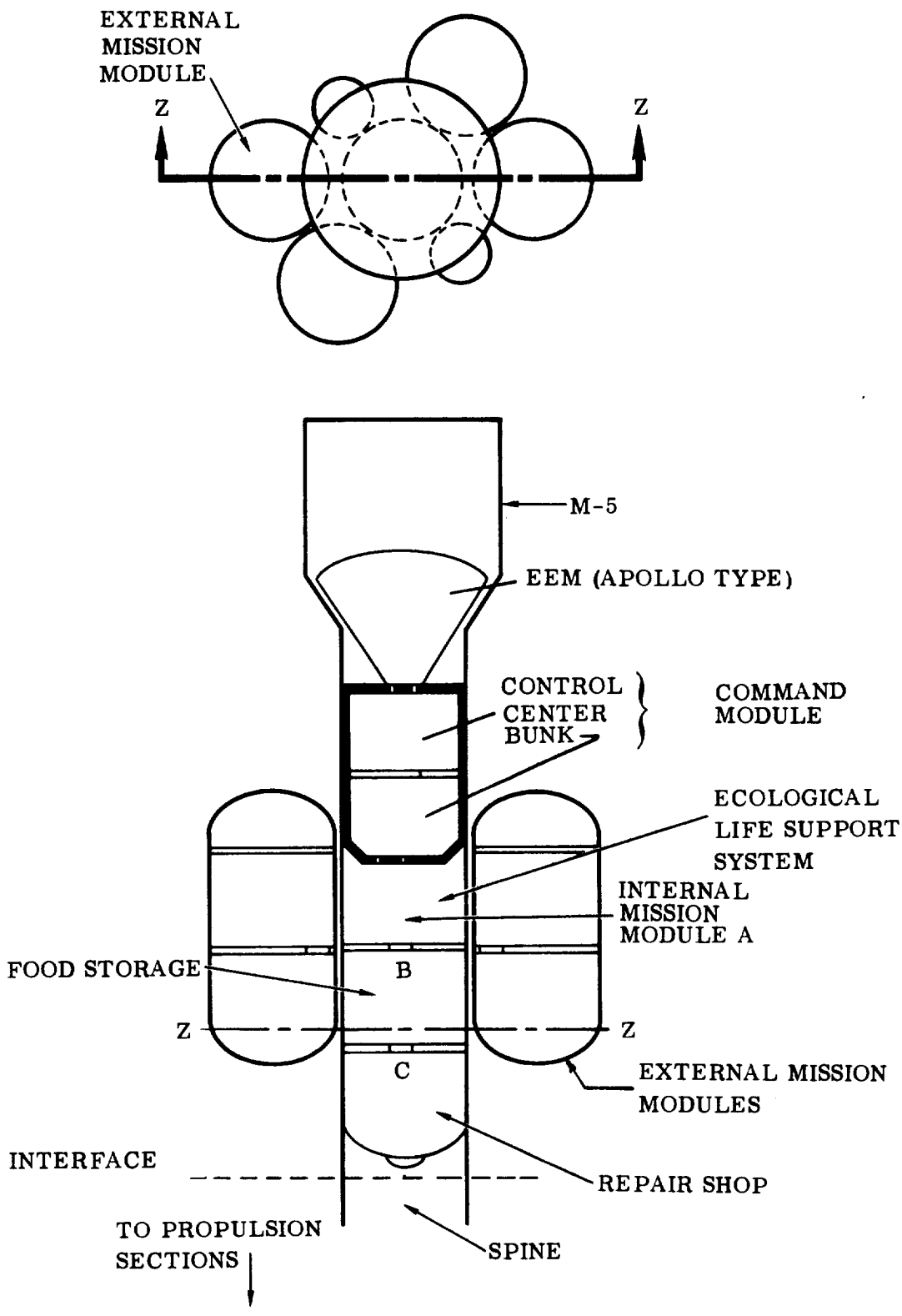

Figure 8-1. Crew Modules (Life Support Section)

the service vehicle. The propulsion system tank arrangement is always such that a larger center tank is surrounded by a ring of smaller tanks which protect the center tank. Meteoritic damage will most likely affect one of the smaller outside tanks. The losses are smaller. The tank is more easily replaceable. The overall system is more flexible in adjusting fuel quantities prior to departure, should a launch delay require addition or reduction of fuel.

A data digest on the convoy vehicles is presented in Table 8-3.

Table 8-3. Data Digest - Interplanetary Crew Vehicles

A.	WEIGHTS		
1.	Gross Weight W_{A1} (Graphite)		1.906 M to 3.057 M lb
2.	Gross Weight W_{A1} (Metal)		1.574 M to 2.8 M lb
3.	Propellant		See Propellants (23 through 25)
4.	Engines:		
	700K	46,500 lb	845 I_{sp}
	Phoebus	20,000	845
	Nerva	14,000	820
	Chemical	1,000	456
5.	LSS Total (includes all life support systems less EEM):		
	L-27 Standard Wet		68,250 lb
	L-28 Standard Dry		84,900
	L-36 Alternate		85,400
6.	Earth Entry Module		7,800 lb
7.	LSS Meteoroid Shield		No Weight (Structure Serves as Shield)
8.	Command Module Radiation Shield		17,000 lb
9.	Abort Propulsion		18,150 lb (MMH/OF_2) I_{sp} = 404
10.	Abort Engine		300 lb (10 K Thrust) Ablative Cooled 300 Pc
11.	Spin Propellant		9,500 lb (MMH/OF_2) I_{sp} = 404
12.	Water		1,200 lb
13.	Ecological System		28,560 lb (350 Days + 150-Day Res.
14.	Food and Containers		8,800 lb

Table 8-3. Data Digest - Interplanetary Crew Vehicles (Continued)

15. Crew (8)	1,600 lb
16. Taxi and Propellant	1,350 lb each
17. Spine	17 lb/ft (10 ft diameter × 75 ft)
18. Ext. Mission Modules (4)	5,700 lb
19. Wrap Around Mission Modules (1)	9,300 lb
20. Mission Module Floors:	
Ext. Modules (8)	2,150 lb
Wrap Around (3)	3,540 lb
Weight = 2.10 lb/ft^2	
21. Pressure Bulkheads (Wrap Around Module)	1,500 lb
Weight = 2.10 lb/ft^2	
B. PROPULSION	
22. Booster (M_1):	
Propellant	400 K to 1400 K Hydrogen
Engines	Four 200 K or One 700 K Graphite Reactor
Tanks	One 60-ft Dia. to One 60-ft Dia. plus Two 25-ft Dia. or Two 33-ft Dia. Tanks
23. Into Mars Orbit (M_2):	
Propellant	244 K to 730 K Hydrogen
Engines	One Phoebus 200 K or One 30 K Fast Reactor
Tanks	One 20-ft Dia. Tank Surrounded by Six 20-ft Dia. Tanks or One 30-ft Dia. Tank Surrounded by Nine 14-ft Dia. Tanks
24. Out of Mars Orbit (M_3):	
Propellant	138 K to 275 K Hydrogen
Engines	One 30 K Fast Reactor, or One 75 K Nerva, or One 200 K Phoebus
Tanks	One 20-ft Dia. Tank Surrounded by Seven 14-ft Tanks, or One 30-ft Dia. Tank Surrounded by Nine 14-ft Dia. Tanks

Table 8-3. Data Digest - Interplanetary Crew Vehicles (Continued)

25. Earth Capture (M_4):	
Propellant	16.8 K to 33 K O_2/H_2 or 11.8 K to 21.4 K Hydrogen
Engines	One 75 K O_2/H_2 or One 30 K Fast Reactor
Tanks	One 20-ft Dia. Tank (H_2) or One 10-ft Dia. O_2 Tank and One 14-ft Dia. H_2 Tank
C. LIFE SUPPORT SECTION	
26. Crew Size	Eight Men
27. Compartment Size:	
Standard	Twelve 10-ft Dia. Compartments
Alternate	Two 10-ft Dia. plus Nine 7-ft × 20-ft Compartments
28. Floor Area:	
Standard	Approx. 1,000 ft^2
Alternate	Approx. 1,850 ft^2
29. Volume:	
Standard	Approx. 8,500 ft^3
Alternate	Approx. 10,700 ft^3

30. General Arrangement:

Standard Dry (L-28) - Command module plus life support equipment, food storage, and shop modules arranged vertically in a 10-ft diameter cylinder, and surrounded by four individual cylindrical mission modules, 10-ft in diameter, with two floors each.

Standard Wet (L-27) - Command module plus life support equipment and food storage modules arranged vertically and immersed within the M_4 hydrogen tank. Shop module and re-entry vehicle surrounded by four individual cylindrical mission modules having two floors each.

D. ARTIFICIAL GRAVITY

31. Crew vehicle is rotated at 4 rpm about its center of mass to provide a 0.3 g level. Minimum radius of 55 ft results from return coast configuration where LSS is balanced by M_4 propellant, empty M_3 tank and nuclear engine.

Table 8-3. Data Digest - Interplanetary Crew Vehicles (Continued)

E. METEOROID SHIELDING

32. External Mission Modules:
    Aluminum honeycomb sandwich structure.
    0.020-in. Faces 1-in. apart with 6 lb core
    Good for one penetration/100 missions/compartment
    Maximum particle size - 0.006 gm.
    Particle velocity - 28 Kilometers/sec (92,000 ft/sec)
    Visual Magnitude - 6.7 0.06-in. Dia. at 3.5 gm/cc.

33. Internal Mission Modules:
    Aluminum Honeycomb as above plus shielding due to external modules.

34. Command Module:
    7.6-in. of Polyethylene

35. Propellant Tanks:
    Aluminum Honeycomb Sandwich
    0.032-in. Faces 1-in. apart
    4 lb Core filled with 4 lb glass wool
    Good for one penetration/100 missions/maneuver tankage
    Maximum particle size - 0.8 gm.
    Particle velocity - 28 Kilometers/sec (92,000 ft/sec)
    Visual Magnitude - 1.2 - 0.30-in. Dia. at 3.5 gm/cc.
    Weight - 2.30 lb/ft^2 to 3.75 lb/ft^2

36. One penetration will cause propellant loss of from 5 to 15 percent for any one maneuver.

37. Remedy for Tank Penetration:

M_2	Change Tank or Alter Mars Orbit
M_3	Change Tank, Jettison Weight, Alter Stay Time or Return Mission
M_4	Repair or Change Tank

F. THERMO SHIELDING

38. Space Insulation:
    Reflective Shielding plus liquefaction unit
    Fiberglass honeycomb in meteoroid shield
    External reflective coating
    Two inner reflective shields

39. Ground Insulation -Helium Atmosphere within meteoroid shield envelope

Table 8-3. Data Digest - Interplanetary Crew Vehicles (Continued)

G. MATERIALS

40. All tanks and stem - Welded Titanium (t = 0.010 to 0.040)

41. Shielding and Crew Modules - Aluminum Honeycomb (t = 0.020 to 0.064)

H. STRUCTURE

42. All tanks will be designed to withstand 7-g launch load without internal pressure.

Tanks	Skin Stringer Structure
Spine	Skin/Stringer/Frame Structure
LSS	Honeycomb Structure

I. RADIATION SHIELDING

43. Allows maximum dosage of 3/4 rad/day.
Shielding designed for quiet part of solar cycle.
Command module shielded on sides and top by 7.6-in. boron filled polyethylene and on floor by 4-in. poly and 4-in. water.

8.4 LIFE SUPPORTING SECTION (LSS). The LSS is the living space of the vehicle, housing the crew, life support equipment and supplies. It is comprised of a command module, mission modules, and an Earth Entry Module.

8.4.1 Command Module. The required functions of the command module were established as follows:

a. Provide an ultimate emergency life support area, including adequate radiation shielding.

b. House the vehicle flight control center.

A number of arrangements were studied, ranging in capacity from two to eight men with emergency accommodations for up to 16 men. The latter arrangement applied to a convoy having two crew vehicles of eight men each, where either vehicle might become inoperable. This module (Figure 8-2) had two compartments. The upper compartment was used as a flight control or command station; the lower had accommodations for five men, including two bunks and most of the life support equipment. In a rescue operation, eight additional men could be crowded into this configuration.

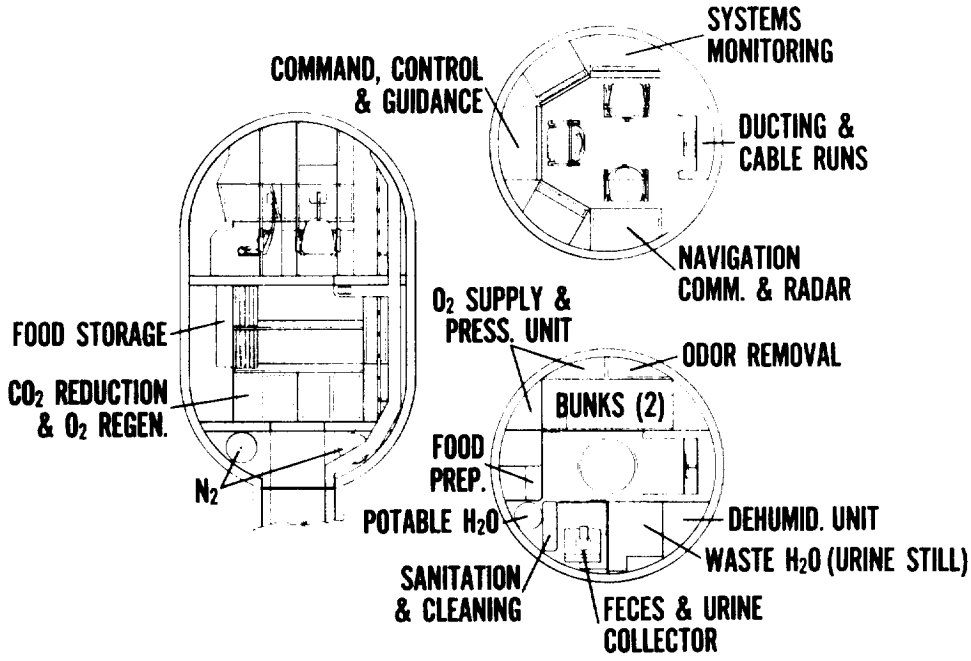

Figure 8-2. Command Module, Interior Arrangement

A study was also made of minimum two-man and four-man arrangements to reduce the shield weight to a minimum. To achieve this objective, the size of the flight station was reduced and the bunks and some of the life support equipment were removed.

Finally an eight-man module, without rescue accommodations, was established as a standard. This configuration (Figure 8-3) includes a control room which seats three operators and has provisions for emergency ration storage. The lower compartment accommodates four bunks, a folding seat, and a feces collector. Though only five feet high, the lower compartment provides standing room through a large passageway leading to the upper level. In order to minimize the size of the module (and thereby the shield weight), the life support equipment was removed from the command module. Normally all seats and bunks are arranged with respect to the artificial gravity direction, which is opposite to the engine thrust loads. To accommodate the engine thrust, the three operator seats are designed to rotate until seat backs parallel the ceiling. Due to the size and burning time limits of the graphite engines, the extent of such acceleration is no more than 1.0 g for 30 minutes.

8.4.1.1 Solar Corpuscular Radiation Shielding. Studies were made comparing hydrogen, carbon, boron filled polyethylene, and water as solar radiation shields. Of these, the hydrogen and/or polyethylene proved best on a weight basis (see Figure 8-4). From these studies two versions resulted: a "wet" version where the command

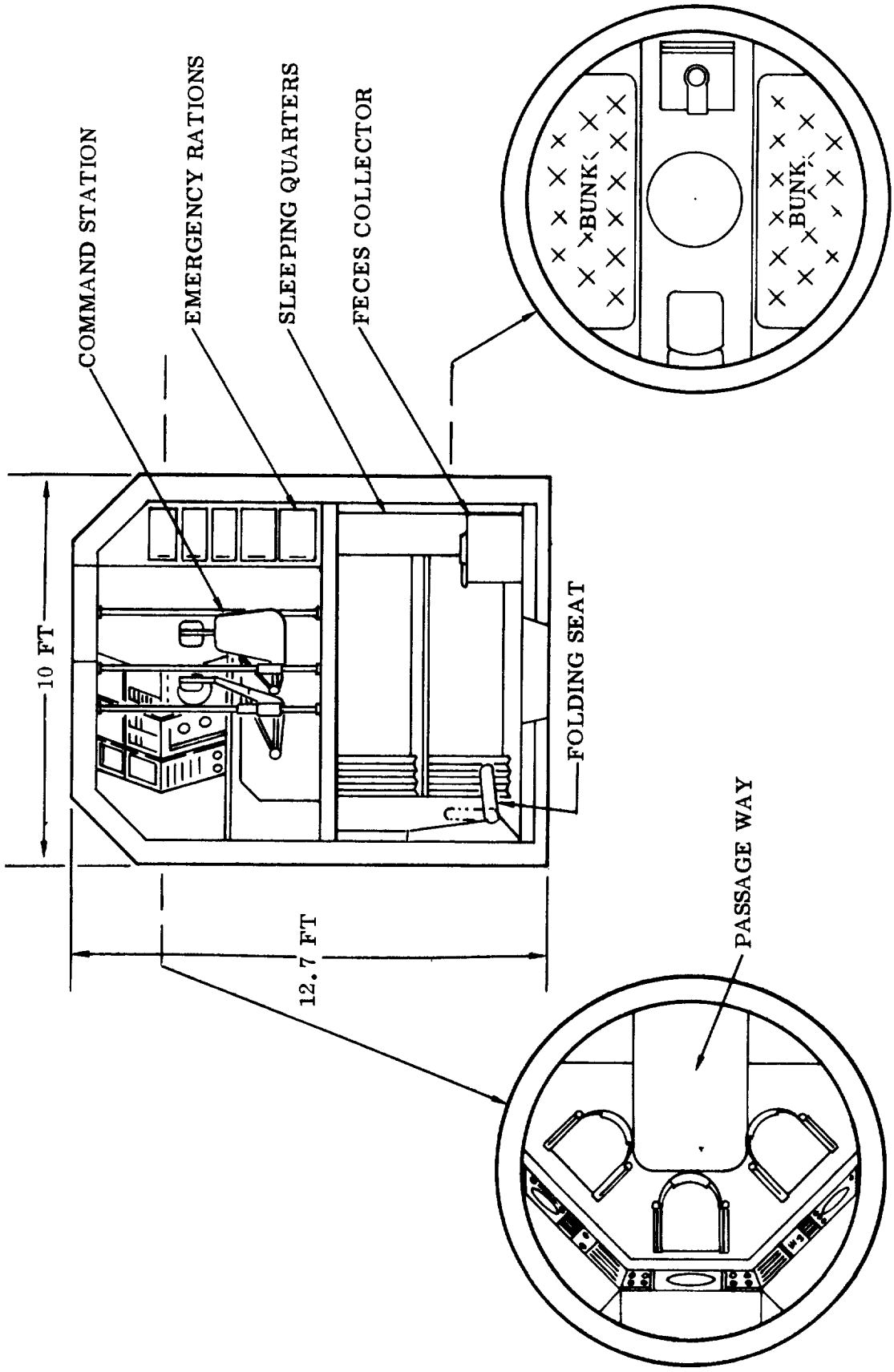

Figure 8-3. Eight-Man Module

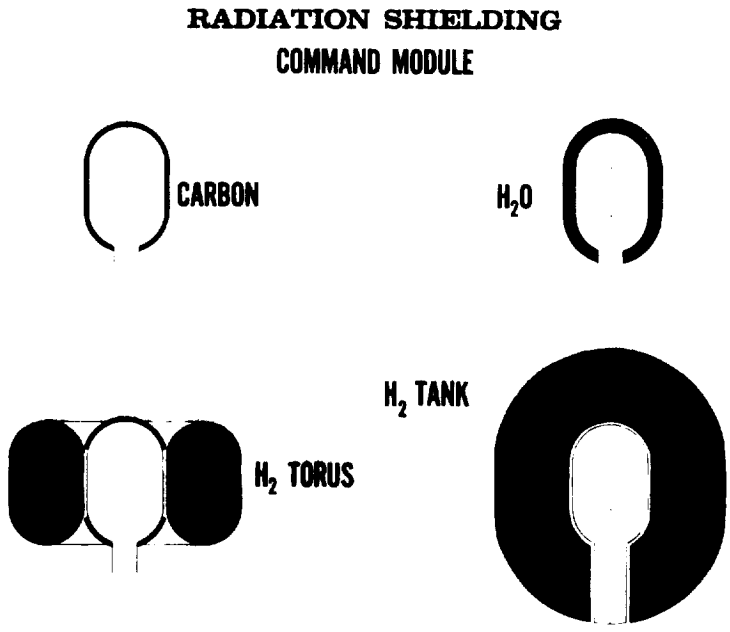

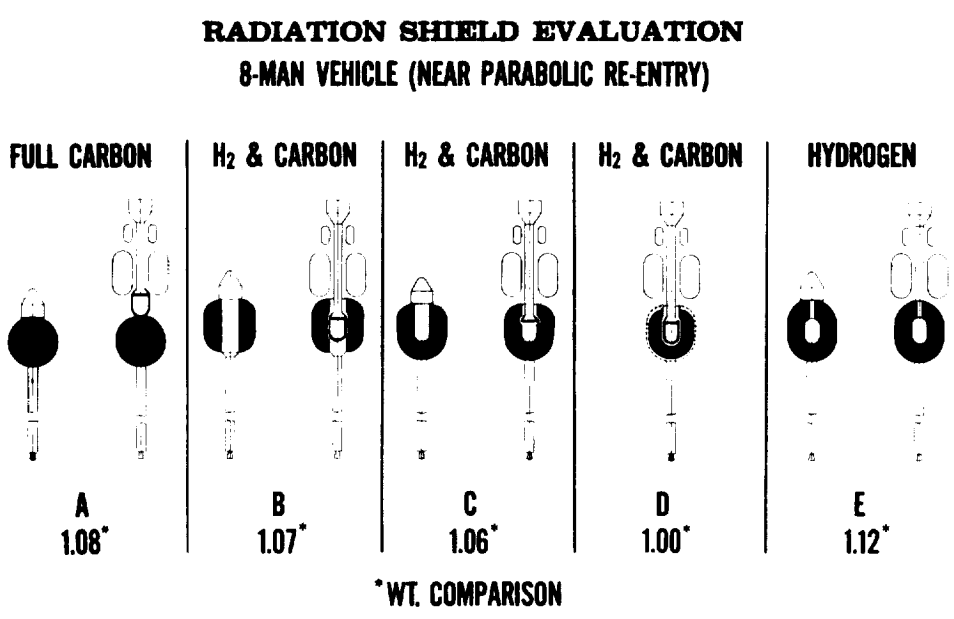

Figure 8-4. Radiation Shielding

module is immersed within the hydrogen tank, and a "dry" version utilizing a polyethylene wall. For an eight-man module, the wet version is always much the lightest since it shields with hydrogen already onboard for other reasons. Unfortunately, the over-all lightest Mars missions do not carry enough hydrogen during return coast to make the wet version feasible. For such missions, the dry version produces the lightest over-all vehicle. During the early part of the study, no allowance was made for the quiet part of the Solar period and a polyethylene wall of 10.7 inches was used. Later this requirement was reduced to 7.6 inches with appreciable weight saving. This thickness if used all over the command module with the exception of the floor which is 4 inches of polyethylene and 4 inches of water. This floor tank also serves as the ecological water-storage facility.

8.4.1.2 Water Management of the LSS. Providing for water storage in the command module floor will cause such water to double as a radiation shield resulting in a net weight saving equal to the weight of the polyethylene replaced. This saving is approximately equal to the mission water requirement since H_2O and polyethylene are about equal in weight and shielding ability.

Assuming a maximum total water requirement of 10.0 lb/man-day (7.0 for food and drink, and 3.0 for personal sanitation), and an emergency water supply (recovery system out) for a crew of eight for seven days, the mission water requirement is almost 600 pounds. Doubling this for a safety margin of 100 percent, 1200 pounds of water must be carried. In order to remove this amount of polyethylene, the water is stored in a 3.5 inch thick tank covering the module floor. A similar waste water tank is installed over the first. Normally, the second tank is not used since waste is processed continuously, but any repair of the recovery system will require storage of waste water during this period, and such waste must be stored in the command module so as to maintain the shielding system. This arrangement will provide an 8-man crew with 15 days of maximum water requirements in the event of recovery failure and with no loss of shielding. The average water requirement of 6 lb/man-day would extend this period to 25 days.

The normal management cycle will be from potable water tank to man to small waste tank to reprocessing still and back to potable tank. The emergency arrangement leads from potable tank to man to small waste tank to floor waste tank (Figure 8-5).

A reprocessing unit of 10.0 lb/man-day capacity is used plus a smaller redundant stand-by unit. These are either vacuum distillation units or vapor compression stills which utilize centrifugal boilers for zero-g operation. In operation, urine and wash water are mixed prior to processing. The estimated weight, including accessories, of both stills is 300 pounds. Plumbing, pumps, and tanks will be additional.

Atmospheric condensate may be reclaimed directly from the air dehumidifier and passed through activated charcoal and bacterial filters, or even through the main reprocessing unit.

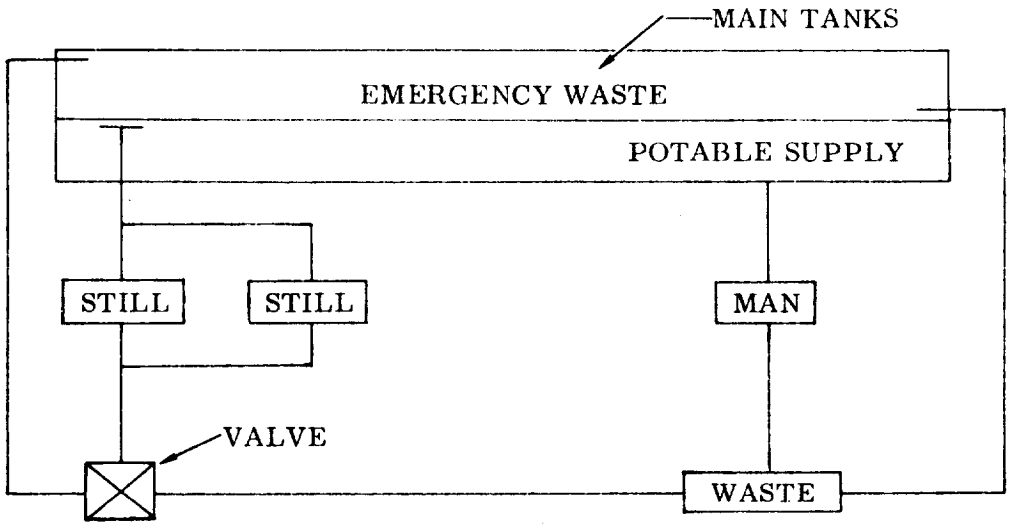

Figure 8-5. Water Management Schematic

8.4.1.3 Reactor Radiation Shielding. The study revealed that an extremely heavy shielding penalty resulted from the use of a carbon reactor for the earth capture, Maneuver 4. Radiation dosage becomes particularly severe toward the end of burning when the shielding due to the hydrogen is expended. To overcome this, it was necessary to carry heavy shielding in the form of polyethylene or unexpended hydrogen, or remove the radiation source by going to a chemical engine for Maneuver 4. The latter approach proved to be by far the better choice. Shielding from the Maneuver 1, 2, and 3 reactors is provided by the hydrogen tanks and spine length. Shielding from the reactors of the service vehicle is done by maneuvering it in line behind the crew vehicle (cf. Section 9).

8.4.2 Mission Modules. These are defined as all of the crew compartments other than the command module and re-entry vehicle. The mission modules are separated into two categories: Internal and external.

8.4.2.1 Internal Mission Modules (Spine Modules). Internal Mission Modules acquire their designation because they are surrounded by the external modules. Because of their location they are more heavily shielded from meteoroids and are therefore used to house the more critical equipment and supplies. In the wet version, L-27, (Figure 8-6), the compartments housing the life support equipment and food are immersed within the hydrogen tank. A third internal compartment is surrounded by external modules and serves as an access-way and shop. In the dry version, L-28, (Figure 8-7), the two internal modules are used for food and life support equipment. The top center module is used as a shop.

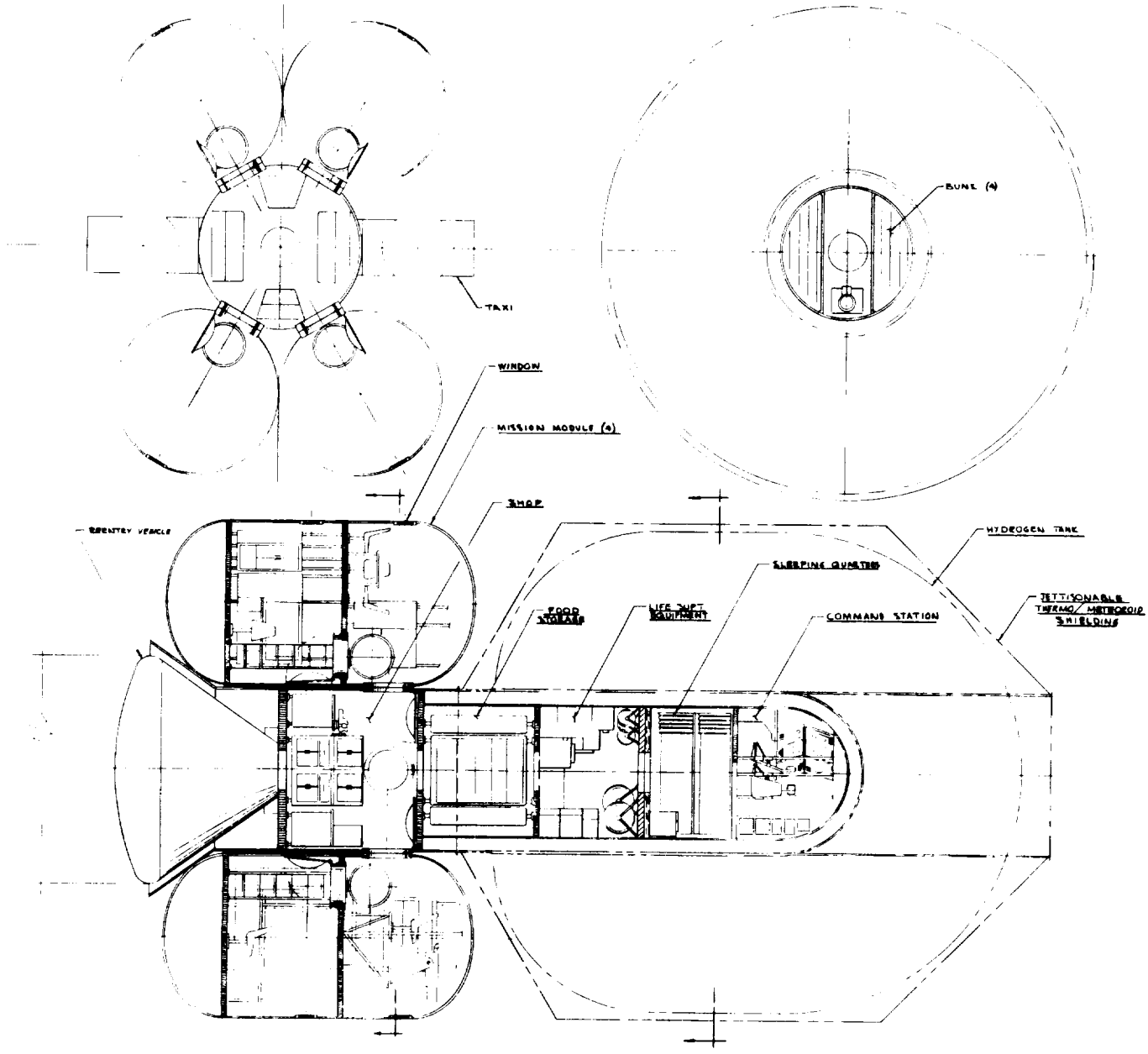

Figure 8-6. L-27 Interior Arrangement

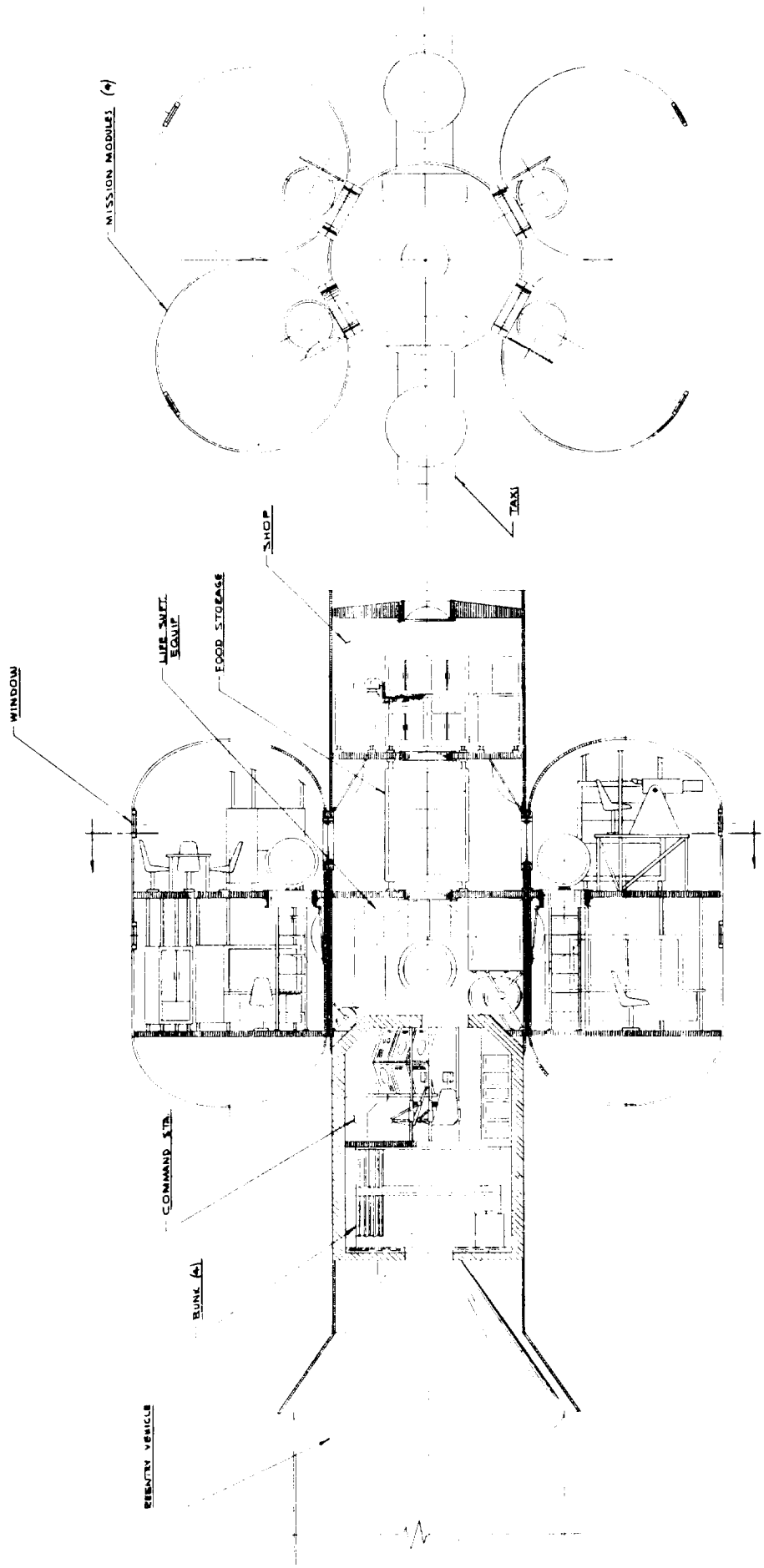

Figure 8-7. L-28 Interior Arrangement

8.4.2.2 Outer Mission Modules. The external cylindrical modules which are individually attached to the center LSS assembly constitute the major part of the living space. Each is divided into two levels by honeycomb sandwich floors. These floors are acapable of withstanding the internal pressure so that no more than one compartment is affected by a meteoroid penetration. Two opposing pressure doors are provided in the floors for this purpose. Each of the external modules are designed to be jettisonable in any mission emergency where their weight means the difference between mission success or failure.

8.4.3 LSS Configuration Study. During the study some 36 other arrangements (a number of these are shown in Figures 8-8A and 8-8B) were investigated which lead to the selection of the wet and dry standard versions. Of the others, two possessed sufficient merit to be discussed briefly. In arrangement L-18, all modules were stacked within the spine and surrounded by the vehicle space radiator for additional shielding. This made a neat appearing configuration, but did not adapt to the artificial gravity spin plan since it would have resulted in an appreciable g-level change for the crew in going from one end of the LSS to the other. The other configuration derived from a study of wrap-around versions where the external compartments completely encircle the internal in the form of a torus is shown in Figure 8-9. The chosen version is shown in Figure 8-10. It is a "D" shaped torus wrapped around the command and inner mission module. The three floor levels are each divided into three compartments by pressure bulkheads. Salient features are: a) the protection afforded to the command module and re-entry vehicle; b) the spaciousness of the external compartments (7 × 20 feet); c) the large floor area (almost 75 percent more than the standard versions with little increase in weight); and d) the simplicity of all wiring and ducting due to the common wall construction. In spite of these favorable features, it appears to sacrifice an important degree of flexibility inherent in the standard versions since one cannot jettison the external modules in a mission emergency.

8.4.4 Meteoroid Shielding. The approach has been to design structure that will double as a thermo/meteoroid shield. The result is aluminum sandwich with a fiberglass honeycomb core for all mission modules. An evaluation of this structure as a meteoroid shield is made using Whipple's flux estimates and a modification of Bjorke's impact equation which incorporates a multi-sheet factor of 5. This approach indicates a shielding capability in excess of 100 missions per penetration for a single external compartment. Should more protection be required, it can be vastly improved by blowing fiberglass wool into the honeycomb core prior to bonding. The internal compartments of course have a much higher degree of shielding due to being surrounded by the external modules. The command module is protected by 7.6 inches of polyethylene or by immersion within the hydrogen tank. (See Section 8.4.7 for the analysis used.)

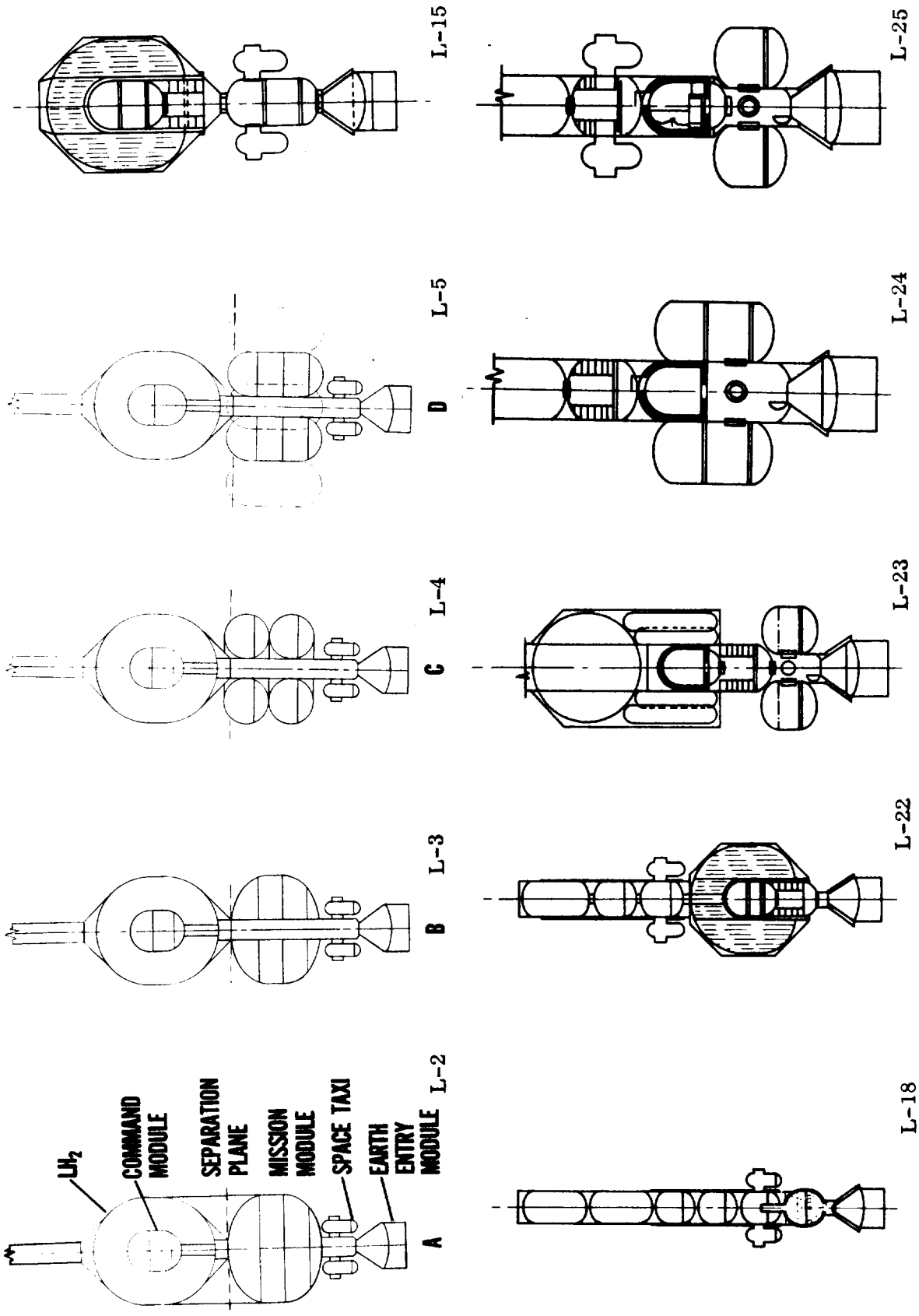

Figure 8-8A. Configurations Studied

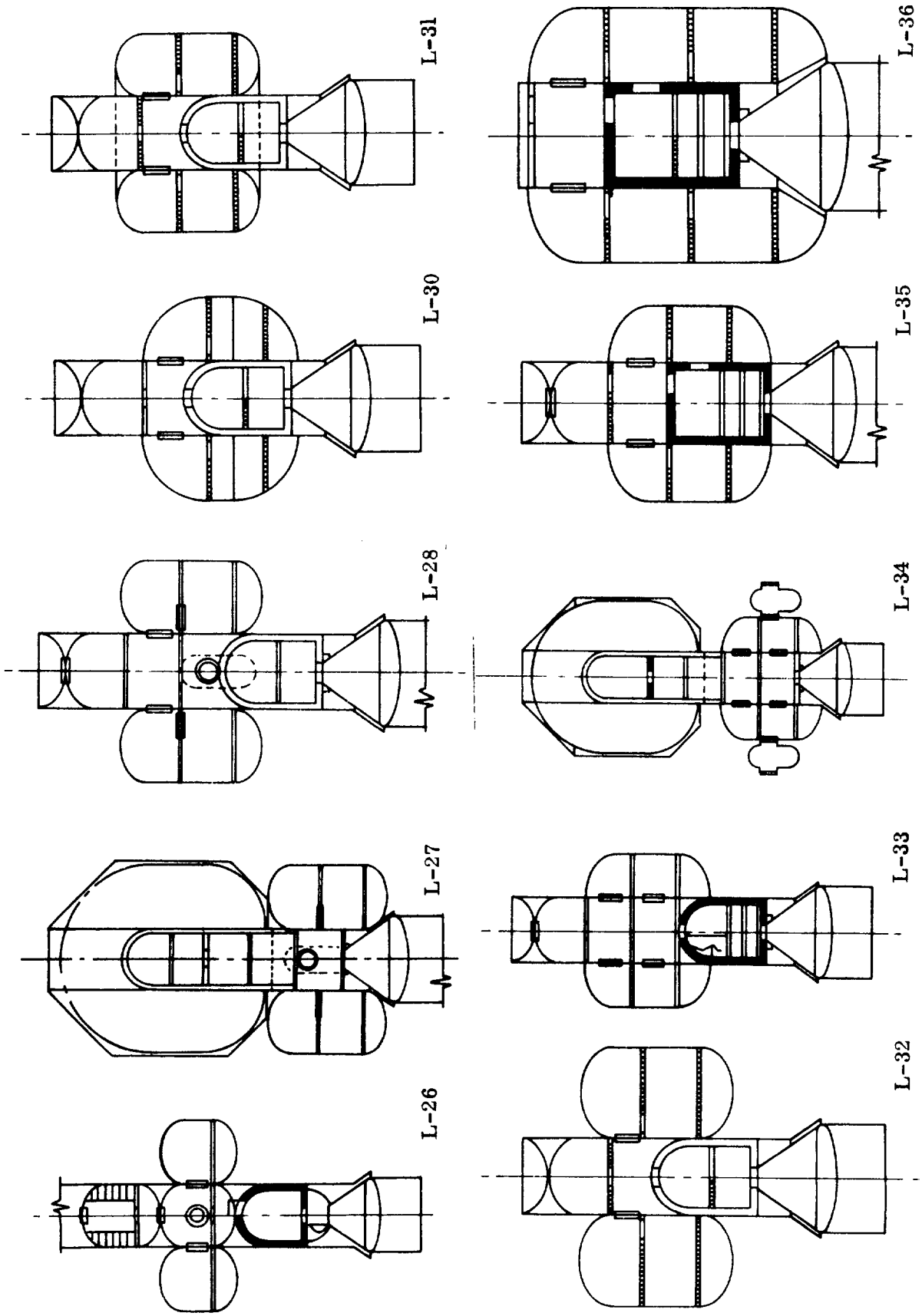

Figure 8-8B. Configurations Studied (Continued)

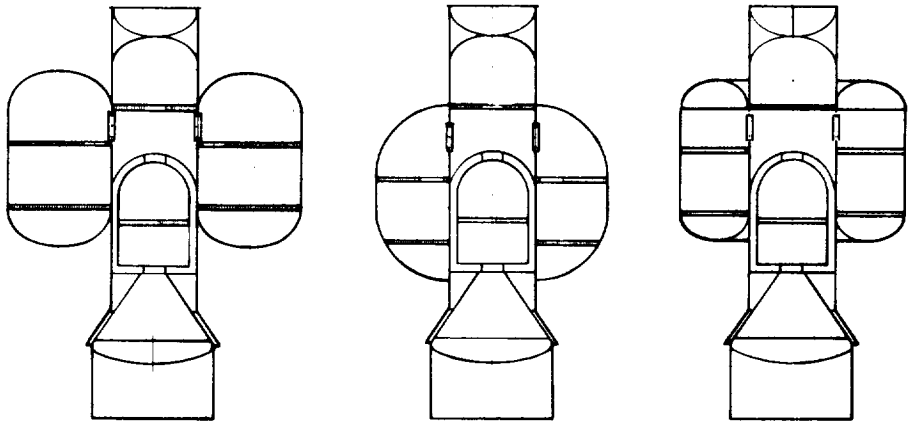

	L-32	L-30	L-31
FLOOR AREA	1,200 FT.^{2}	1,200 FT.^{2}	1,200 FT.^{2}
VOLUME	9,580 FT.^{3}	9,650 FT.^{3}	9,950 FT.^{3}
WT.	95,000 LB.	95,600 LB.	95,950 LB.

Figure 8-9. Mission Module Comparison

8.4.5 Structural Design and Analysis. For the dry version command module, it is proposed to use a fiberglass-reinforced polyethylene laminate. The wet version would use this only in the floor, the remainder being aluminum sandwich. All mission modules are proposed as sandwich construction using aluminum faces bonded to fiberglass honeycomb core. This type of structure appears good as a structural thermo/meteoroid shield since the fiberglass honeycomb serves both as insulator and structure, while the spaced aluminum faces serve both as structure and multi-layer meteoroid shield. Some testing of bonding agents subjected to long time space environment will be required, but there is no evidence to indicate an insurmountable problem area here.

One structural area pin-pointed for study during this period was the mission module floors. It was considered desirable to design these as pressure bulkheads so that a meteoroid penetration would only affect the compartment penetrated. An analysis of a ten-foot-diameter floor tapered from nine inches in the middle to four inches at the edge disclosed a 0.58-inch maximum deflection under a load of 5.0 psi. Edge rotation amounted to 0.8 degrees. This structure had a 4.5-pound aluminum core with aluminum face thicknesses tapered from 0.40 inch at the center to 0.25 inch at the edge. The mathematical analysis used follows in Section 8.4.6.

8.4.6 Design Conclusions. Of the configurations studied, the dry standard version appears best from the standpoint of flexibility. For example, its feasibility is not dependent on mission hydrogen requirements as is the wet version. The integrated wrap-around version cannot jettison its external compartments, while the modularized dry version can. An obvious safety consideration is involved in the external modular

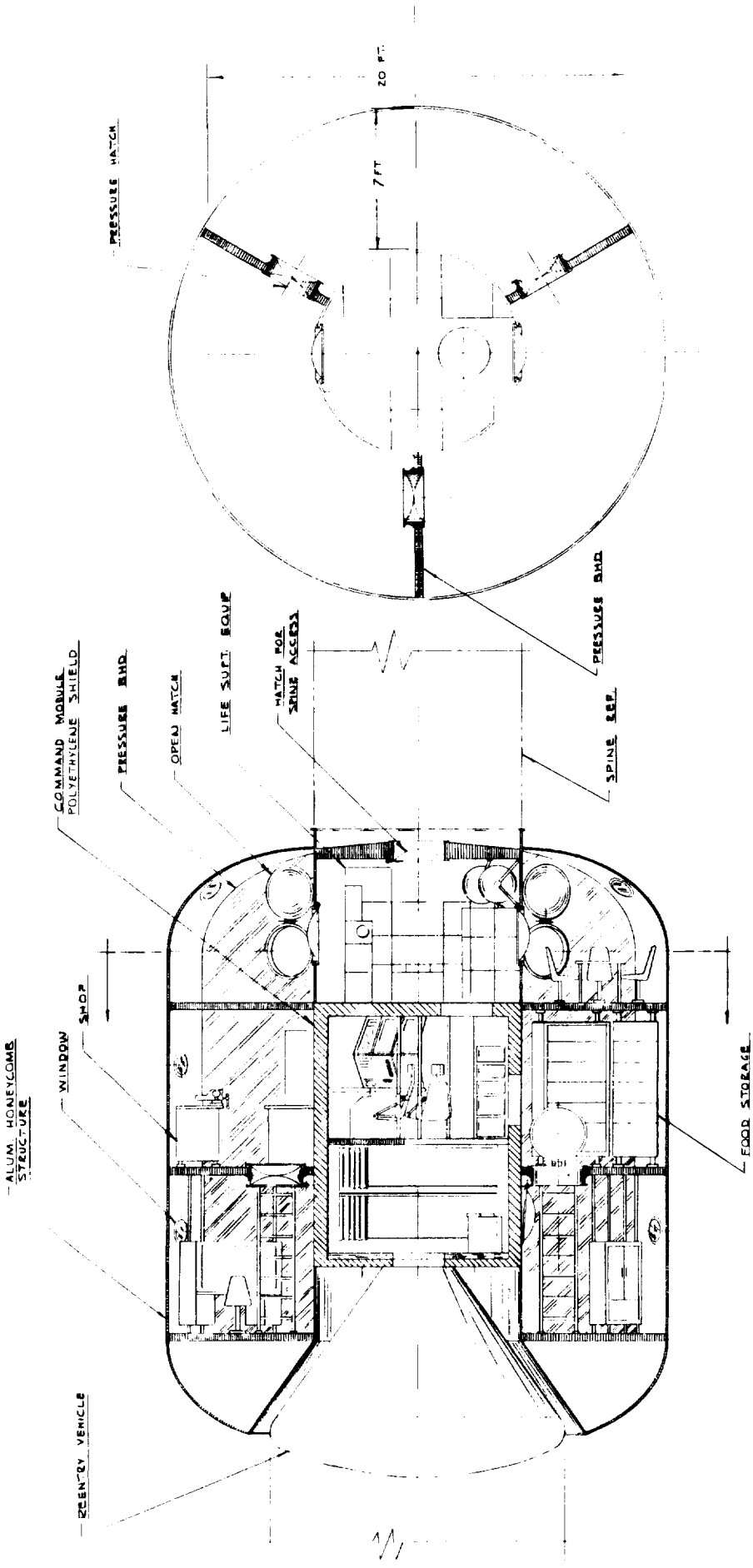

Figure 8-10. L-36 Interior Arrangement

design since these units can be jettisoned during any mission emergency where the weight savings and associated fuel savings involved would mean the difference between mission completion or failure. This configuration can also adapt itself to a wide variety of missions by carrying larger, smaller, or fewer external modules to satisfy crew size and mission duration. Finally, its flexibility allows tailoring to an evolutionary program covering long-term orbital and cislunar missions and leading to interplanetary flight applications.

8.4.7 Structural Analysis of Mission Module Floors. The mission module floors are designed for an emergency pressure condition of q = 5 psi. A tapered cross section of sandwich construction is chosen for minimum weight, and the edge is pinned to prevent discontinuity bending in the supporting structure. A stress analysis of the ten-foot-diameter mission module floor is obtained by an approximate numerical method utilizing finite difference equations and neglecting shear deflections. The radius "a" of the plate is divided into a number of points spaced a distance "h" apart as shown in Figure 8-11.

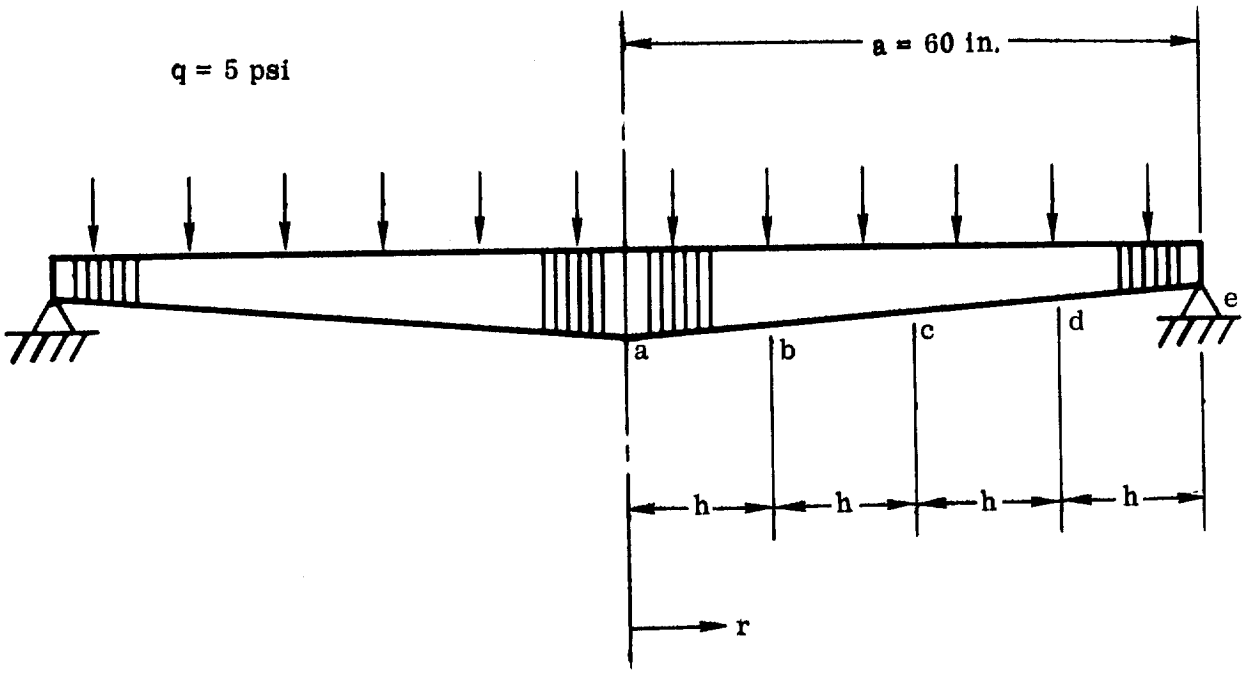

Figure 8-11. Module Floor Structural Analysis

From Theory of Plates and Shells, by Timoshenko and Woinowsky-Krieger, Chapter 3, pages 52 to 54, McGraw-Hill, 1959, the differential equation

$$\frac{d^2\varphi}{dr^2} + \frac{1}{r}\frac{d\varphi}{dr} - \frac{\varphi}{r^2} = \frac{qr}{2D} \qquad (8\text{-}1)$$

governs the deflection of an axisymmetrically loaded circular plate. The equation for the bending moment in the radial direction is

$$M_r = D\left(\frac{d\varphi}{dr} + \frac{\nu}{r}\varphi\right) \qquad (8\text{-}2)$$

where

$\varphi = \frac{dw}{dr}$ (slope in radians)

w = transverse deflection

$D = \frac{EI}{1-\nu^2}$ (flexural rigidity)

E = modulus of elasticity

I = moment of inertia

ν = Poisson's ratio

The boundary conditions are

$\varphi_a = 0$ (zero slope at Point a)

$$\left(\frac{d\varphi}{dr} + \frac{\nu}{r}\varphi\right)_e = 0 \quad \text{(zero radial moment at Point e)} \qquad (8\text{-}3)$$

In solving for the unknowns (φ_b, φ_c, φ_d, φ_e), the differential equation (8-1) is put in finite difference form at each interior point by substituting first-order central differences, and the boundary equation (8-3) is put in finite difference form by using first-order backward differences. From Numerical Methods in Engineering, by Salvadori and Baron, pages 74, 77, and 78, Prentice-Hall, 1061, the first order finite equations needed here are

Central Difference Equations

$$\left(\frac{d\varphi}{dr}\right)_n = \frac{1}{2h}\left(-\varphi_{n-1} + \varphi_{n+1}\right)$$

$$\left(\frac{d^2\varphi}{dr^2}\right)_n = \frac{1}{h^2}\left(\varphi_{n-1} - 2\varphi_n + \varphi_{n+1}\right)$$

Backward Difference Equations

$$\left(\frac{d\varphi}{dr}\right)_e = \frac{1}{h}\left(-\varphi_d + \varphi_e\right)$$

$$\left(\frac{d^2\varphi}{dr^2}\right)_e = \frac{1}{h^2}\left(\varphi_c - 2\varphi_d + \varphi_e\right)$$

Forward Difference Equation (for M_r at Point a)

$$\left(\frac{d\varphi}{dr}\right)_a = \frac{1}{h}\left(-\varphi_a + \varphi_b\right)$$

The resulting matrix of the simultaneous difference equations at Points n = b, c, d, e becomes

$$\begin{bmatrix} -6 & 3 & 0 & 0 \\ 3 & -9 & 5 & 0 \\ 0 & 15 & -38 & 21 \\ 0 & 0 & -4 & 4.3 \end{bmatrix} \begin{Bmatrix} \varphi_b \\ \varphi_c \\ \varphi_d \\ \varphi_e \end{Bmatrix} = -qh^3 \begin{Bmatrix} 1/D_b \\ 4/D_c \\ 27/D_d \\ 0 \end{Bmatrix} \qquad (8\text{-}4)$$

where the right hand side depends on the material property E, the pressure q, and the moment of inertia I at each interior point. The following material and cross section dimensions are tentatively chosen to be:

Face Material

Aluminum Alloy

At the Center

Core thickness = 9 inches
Face thickness = 0.040 inch

At the Edge

Core thickness = 4 inches
Face thickness = 0.025 inch

After substituting the calculated values in the righthand side of Equation 8-4 the unknowns are found to be

$\varphi_b = 0.00569$ radian

$\varphi_c = 0.01093$ radian

$\varphi_d = 0.01450$ radian

$\varphi_e = 0.01349$ radian

The rotation at the edge is approximately

$$\varphi_e = 0.01349 \times 57.3$$
$$= 0.8 \text{ degree}$$

Now the deflection at the center is obtained by the quadrature

$$w_a = \int_a^e \varphi dr$$

which can be found approximately by Simpson's rule

$$w_a = \frac{h}{3} (\varphi_a + 4\varphi_b + 2\varphi_c + 4\varphi_d + \varphi_e)$$

After substitution,

$w_a = 0.58$ inch

Reducing Equation 8-2 to difference form at point a by using forward differences, the approximate bending moment at the center becomes

$$M_a = \frac{1}{h} \varphi_b$$

from which the approximate bending stress at the center is found to be

$$\sigma_b = 19,000 \text{ psi}$$

Based on a core density of 4.5 lb/ft^3, the total weight of the floor is found to be 235 pounds.

8.4.8 Meteoroid Shielding Analysis. For a single external mission module compartment:

Exposed Area = 25 meters

Mission Time = 34×10^6 seconds

Penetration Probability = 1 per 100 missions (No Hit = 0.99)

(a) Frequency (Particles/M^2-sec) = $\frac{1.0}{25\ (34 \times 10^6)} = 1.34 \times 10^{-10}$

(b) Entering Whipple's Flux Chart (Figure 8-12): Maximum Particle Mass = 5×10^{-4} gram

(c) Using Bjork's equation (ARS Journal, June 1961, Page 803) Modified for a multi-lay factor of 5.0 (NASA TN-D-1039):

$$P = 1.09\ (1.5)\ (MV)\frac{1}{3}$$

where P = Penetration Depth (cm)

M = Particle Mass (gm)

V = Impact Velocity (KM/sec)

1.5 = Thin Plate Factor

P = Inches = $1.64\ (MV)\frac{1}{3}$/(2.54 cm/in.) (5 multi-lay)

$$P = 0.129\ (MV)\frac{1}{3}$$

$$= 0.129\ (0.0005 \times 26)\frac{1}{3} = 0.129\ (0.235) = 0.31$$

t/sheet = 0.031/2 = 0.016

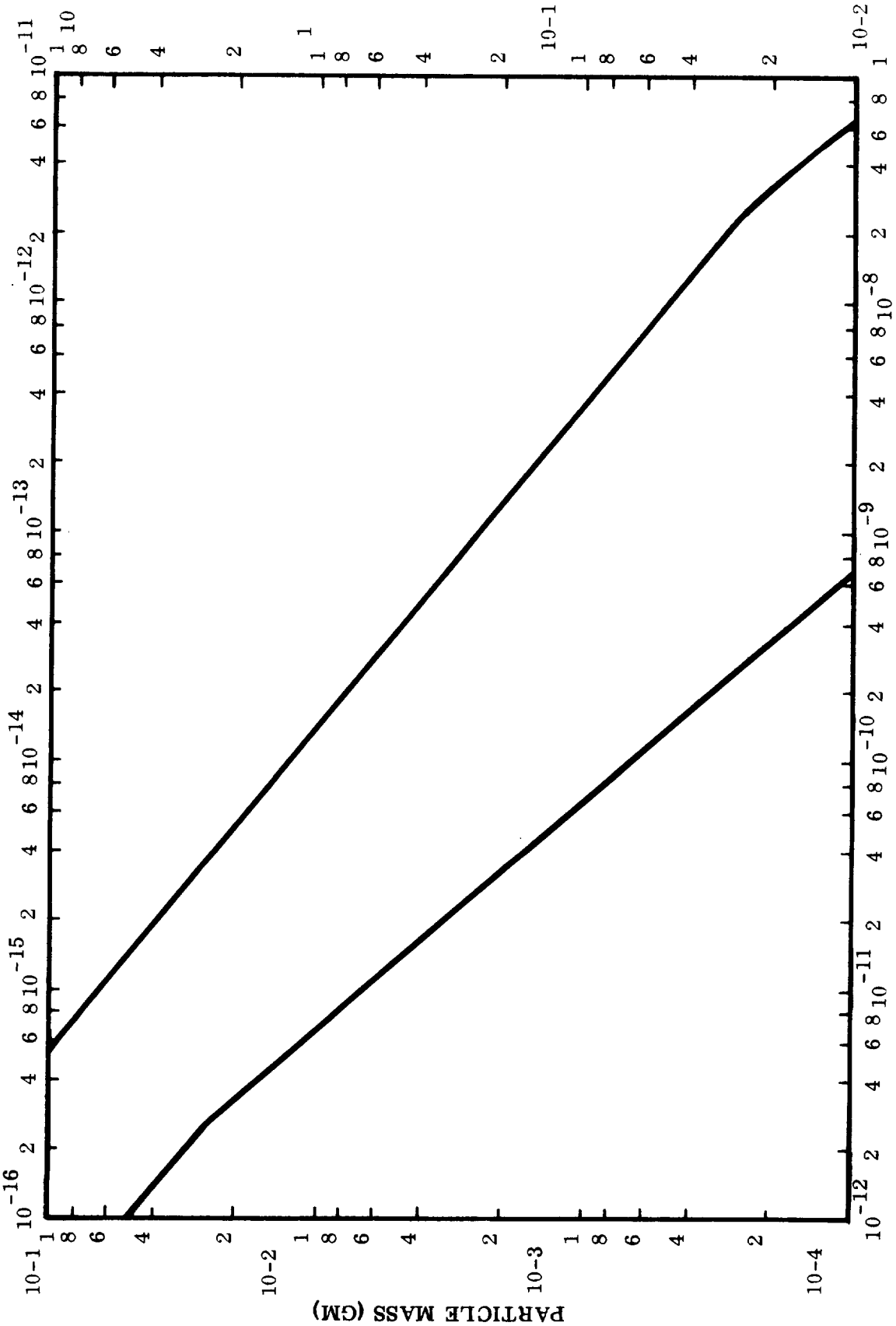

Figure 8-12. Whipple's Mass-Flux Distribution for Sporadic Meteoroids

8.5 SERVICE MODULE SECTION (SMS). The SMS provides a form of auxiliary vehicle hanger. Its final size and shape will depend on the size, shape, and numbers of auxiliary vehicles carried. One requirement, based on the convoy plan, is that the SMS be readily interchangeable with the LSS so that the propulsion section of the service vehicle can serve as a redundancy for the crew vehicle. Another provision is that the SMS carry a spare re-entry vehicle and a stellar navigation unit. Since the service vehicle will not spin, it may be selected as the platform for convoy navigational sightings.

One possible SMS concept takes the form of a cylindrical canister having a hinged cover which is opened for auxiliary vehicle removal (see Figure 8-13). The spare re-entry vehicle and navigation unit are carried in the cover with the navigation unit at the forward extremity of the vehicle. This location provides a maximum sighting sweep without the need for vehicle reorientation.

8.6 CREW VEHICLE PROPULSION STRUCTURE. Propulsion structure design requirements were determined and different vehicle configurations were developed to meet these requirements. Vehicle structural materials and associated hardware components were chosen according to their availability and reliability by 1973 to 1975. Structural and systems analyses were based upon present-day state-of-the-art methods.

8.6.1 Design Requirements. The design requirements for an interplanetary vehicle fall into two categories: 1) launch to Earth-orbit and 2) interplanetary flight.

The launch to Earth-orbit requirements to be considered are:

a. Liquid hydrogen and liquid oxygen insulation
b. Fail-safe structure
c. Dynamic and acoustic vibrations
d. Launch acceleration
e. Aerodynamic heating and loading
f. Orbital rendezvous and assembly
g. Propellant tank interchangeability
h. Weight
i. Manned safety (1.4 factor based on ultimate strength)

The interplanetary requirements to be considered are:

a. Meteoroid protection
b. Fail-safe structure
c. Acceleration loading which is much lower than the launch accelerations
d. Propellant tank interchangeability (during any coast portion of the mission)
e. Orbital and interplanetary rendezvous and assembly

NOTE: Only half of views A-A, B-B, and C-C are shown. The missing halves are symetrical with those shown.

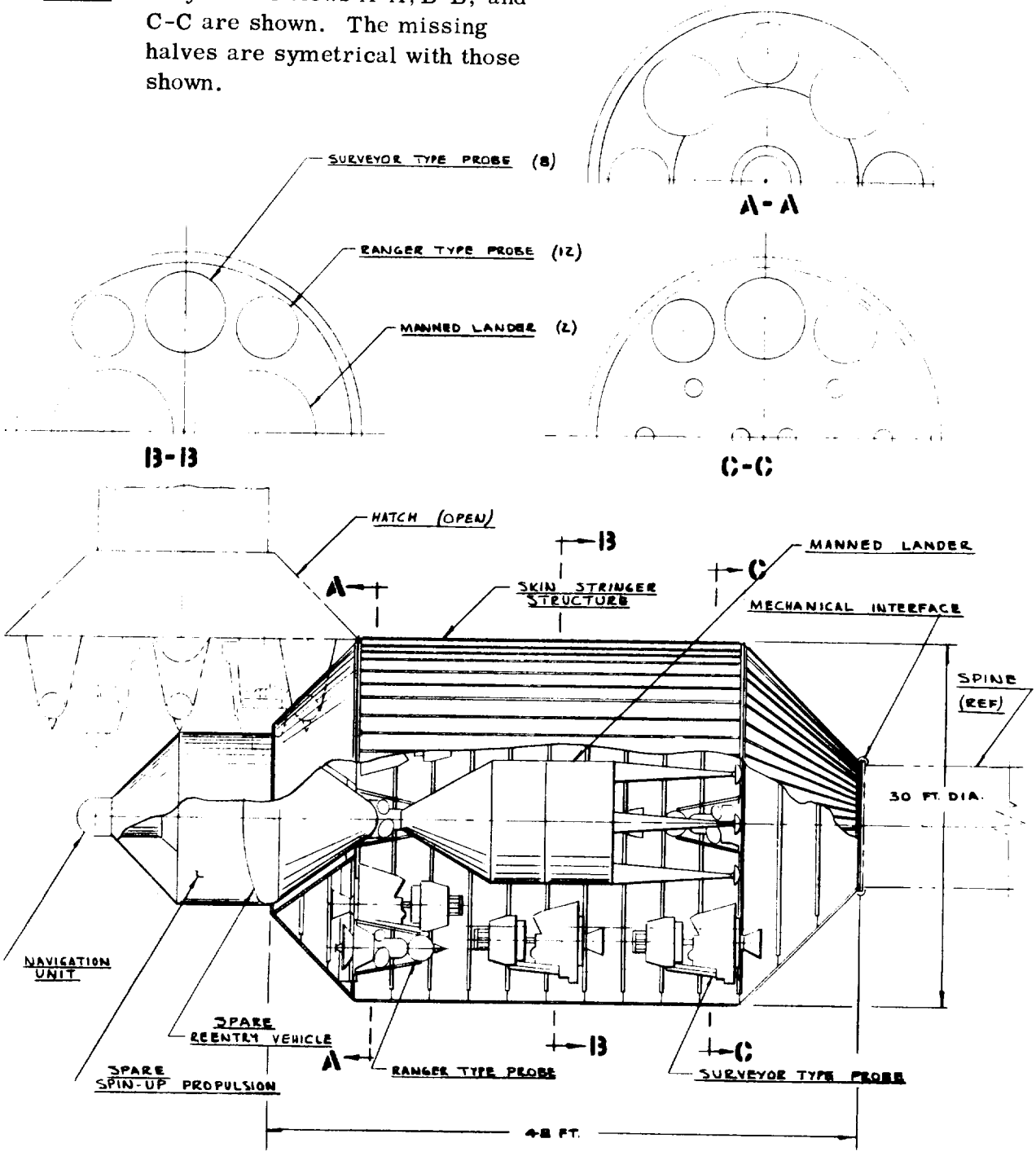

Figure 8-13. Mars Service Module

f. Thermal radiation
g. Engine burning time
h. Weight
i. Manned safety (1.4 factor based on ultimate strength)

Some of the design requirements in both categories were grouped together when the structure being evaluated could efficiently satisfy them. As an example, an analysis was performed on a structure to satisfy liquid hydrogen insulation, aerodynamic heating and loading, radiation, meteoroid shielding, and launch to Earth-orbit acceleration requirements.

8.6.2 Vehicle Design Survey. Beginning with the Mars Interplanetary Vehicle as described in AZM-072, studies were performed and results yielded the 8M-14 vehicle shown in Figure 8-14. The 8M-14 vehicle is composed of an Earth-orbital escape booster and an interplanetary vehicle. The Earth-orbital escape booster consists of one 60-ft diameter tank and a single 700-K nuclear engine. The interplanetary vehicle provides propulsion for the remainder of the mission -- Mars capture (M-2), Mars escape (M-3), and Earth capture (M-4) -- employing a metal nuclear engine with a 30-K thrust. The nuclear engine is separated from the crew by a 150-ft spine. The M-4 propellant tank surrounds the command module and serves as protection during a solar storm. The propellant tanks for M-2 and M-3 are clustered around the central spine, and are jettisoned after depletion of propellant.

Further studies of missions, engines and engine arrangements, propellant tanks and supporting structural arrangements, and crew sizes resulted in more desirable configurations. Two vehicles, 8M-22 (Figure 8-15) and 8M-23 (Figure 8-16), were chosen because of nuclear engine availability. The 8M-22 vehicle is shown in two configurations regarding the escape booster. The metal nuclear reactor used in 8M-23 may not be available, whereas the Nerva and Phoebus engines used in 8M-22 are assumed to be operational in time for a Mars expedition. These vehicles were modified and applied to a Venus mission, resulting in 8V-2 (Figure 8-17) and 8V-3 (Figure 8-18). Therefore, the 8V-3 could grow into the 8M-23 and the 8V-2 could grow into the 8M-22 with a slight change in tank size. Both Mars and Venus vehicles are composed of an Earth-orbital escape booster and an interplanetary vehicle.

The 8M-22 employs a chemical liquid oxygen/liquid hydrogen system with a 75-K engine for M-4. M-3 and M-2 each use one 30-ft diameter tank surrounded by nine 14-ft diameter tanks. M-3 uses an advanced Nerva nuclear engine while M-2 employs a Phoebus nuclear engine. M-1 uses two 60-ft diameter tanks and four Phoebus engines. The 8M-23 employs a metal nuclear engine for M-4, M-3, and M-2. M-4 propellant tank is 20 ft in diameter and is surrounded by the M-2 tanks which are also 20 ft in diameter. M-3 has one 20-ft diameter tank surrounded by seven 14-ft diameter tanks. The Earth-orbital escape booster is composed of a 60-ft diameter tank, two 33-ft diameter side tanks and a single 700-K graphite nuclear engine or four Phoebus engines.

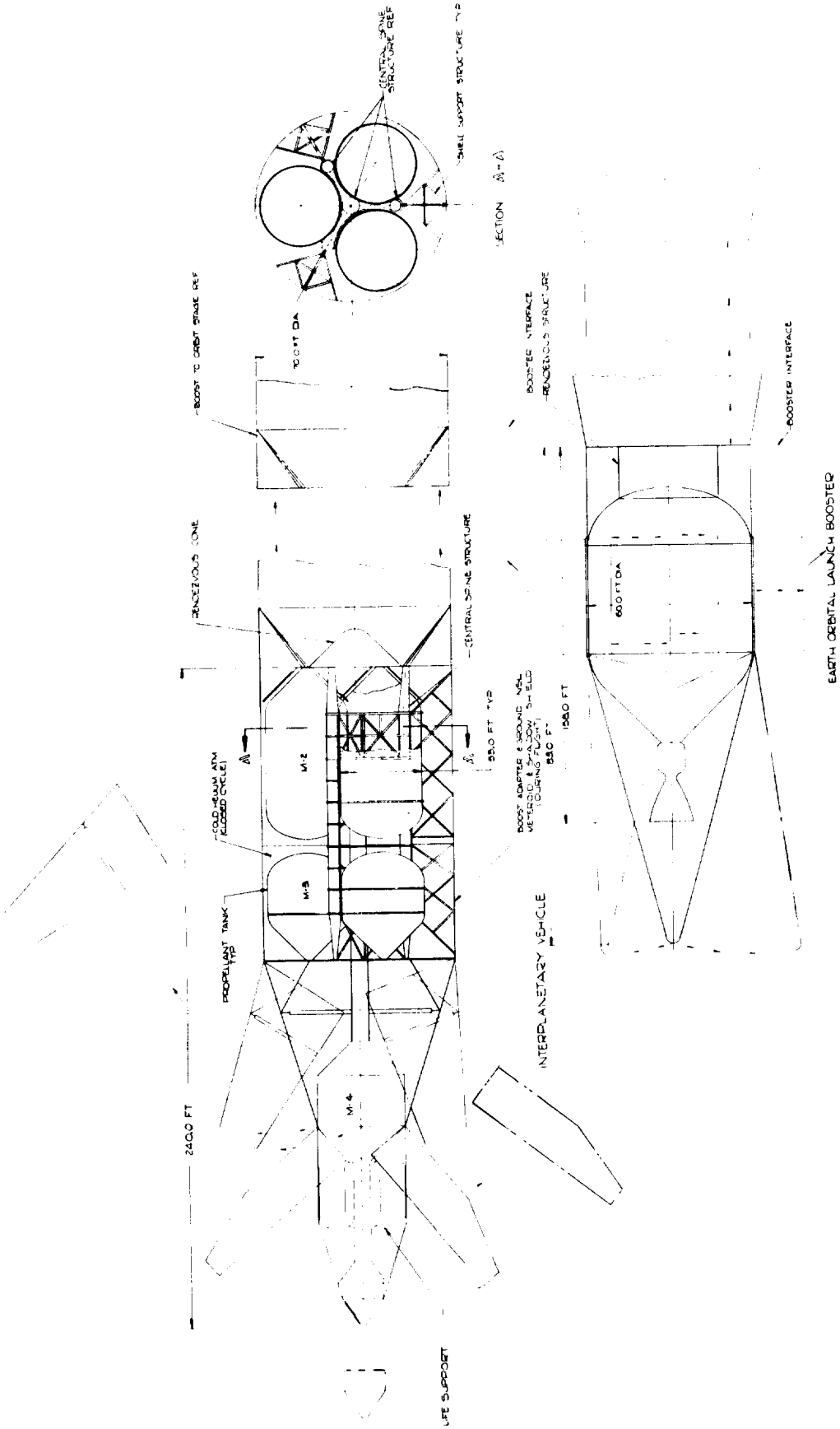

Figure 8-14. Mars Vehicle 8M-14

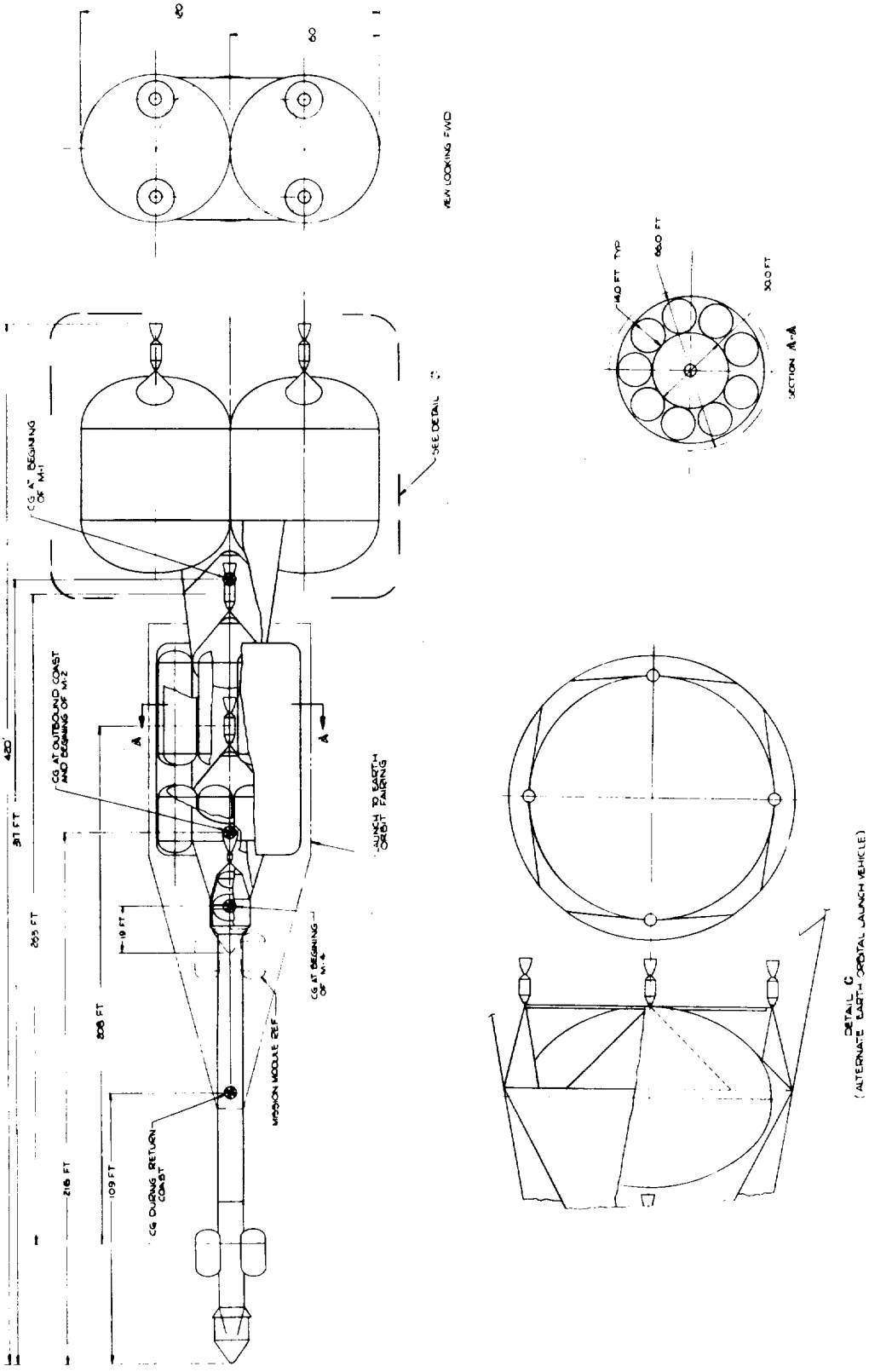

Figure 8-15. Mars Interplanetary Vehicle 8M-22

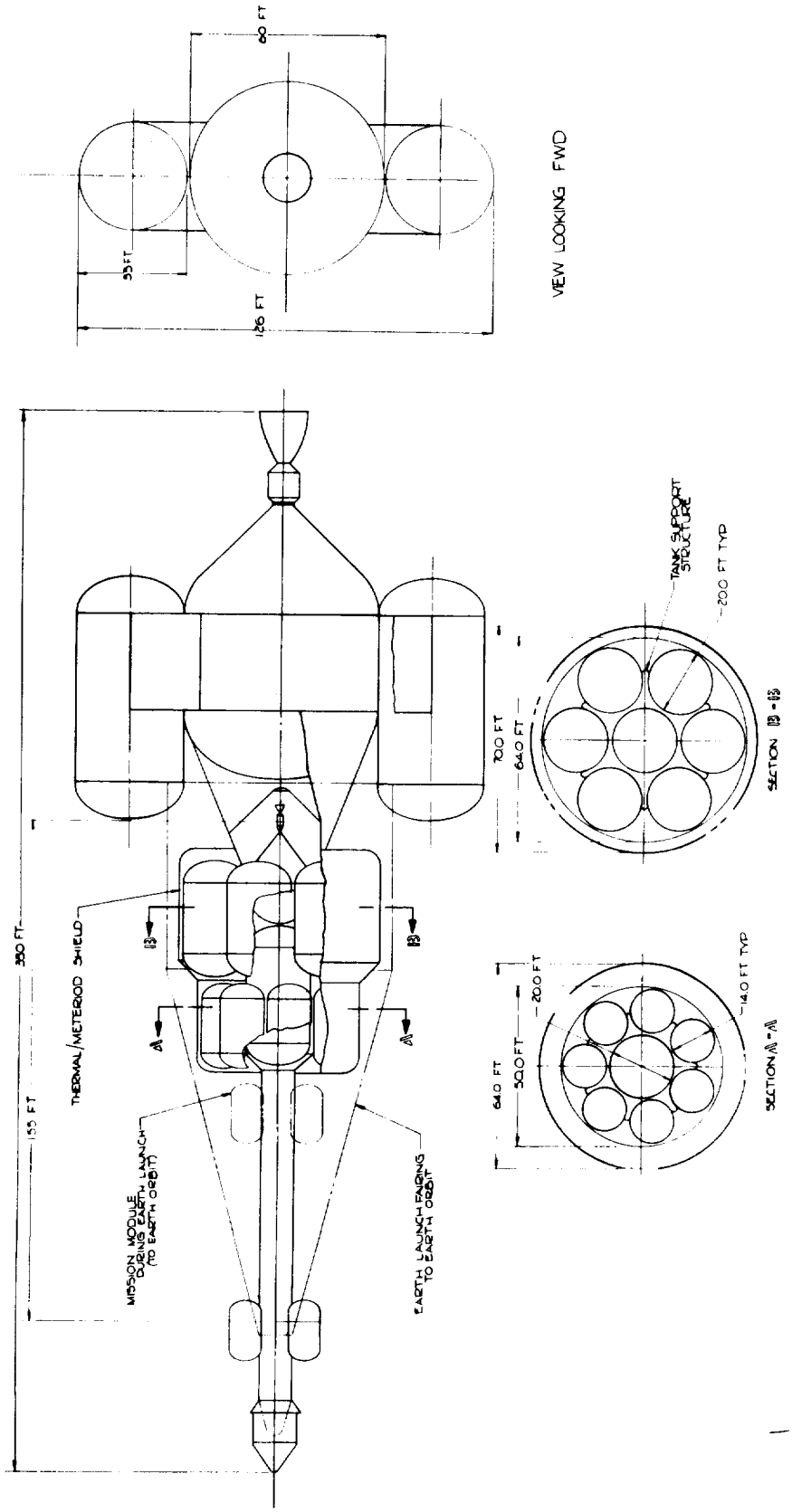

Figure 8-16. Mars Interplanetary Vehicle 8M-23

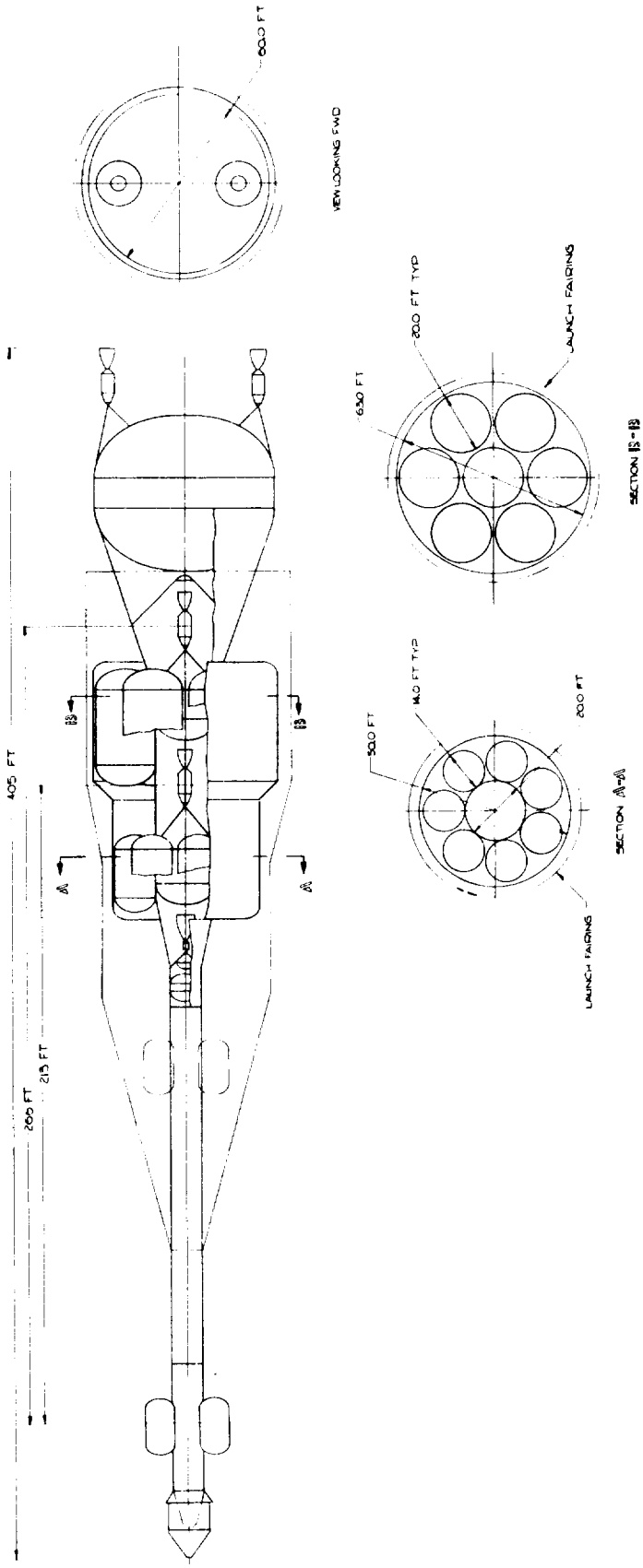

Figure 8-17. Venus Interplanetary Vehicle 8V-2

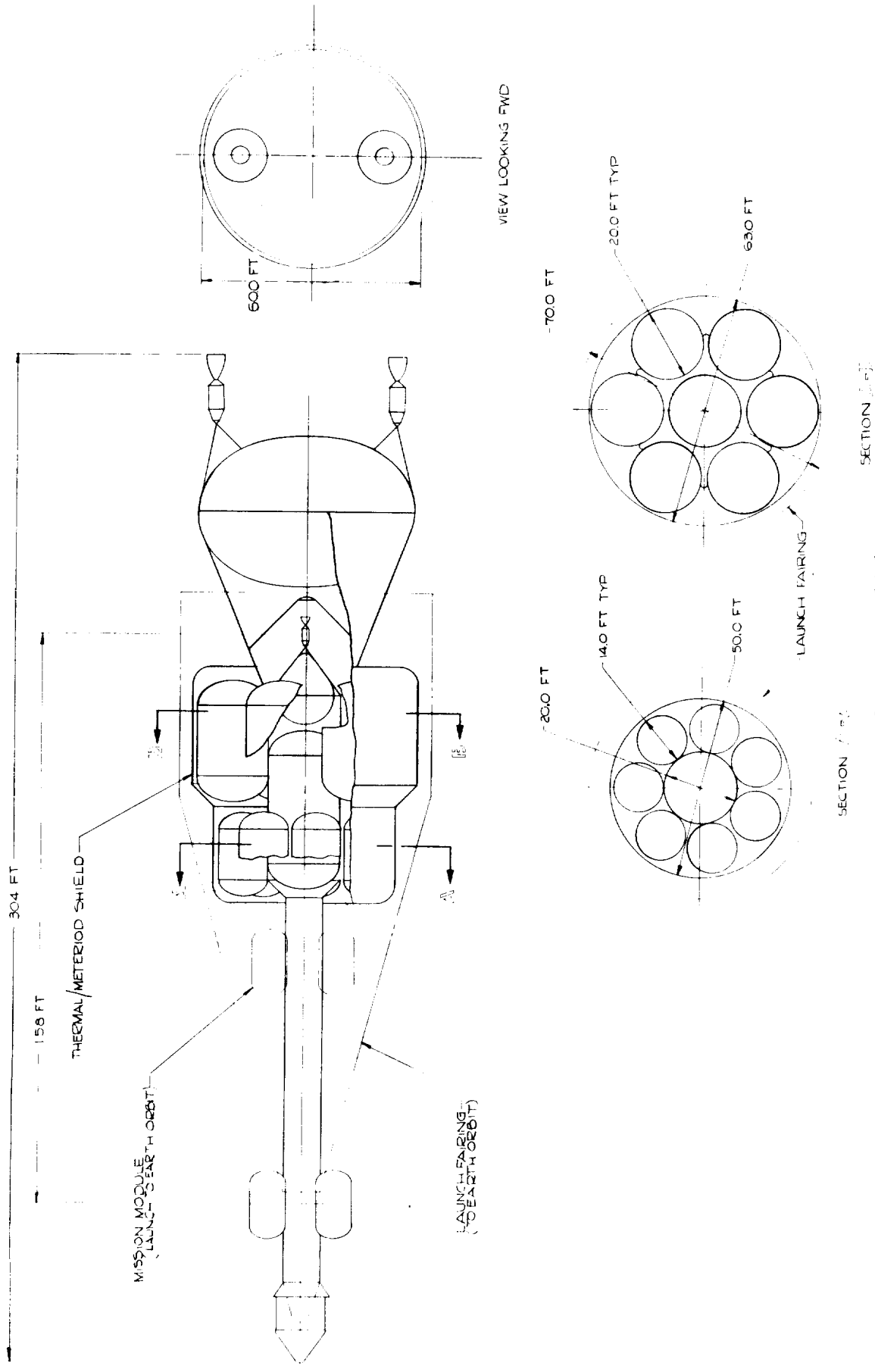

Figure 8-18. Venus Interplanetary Vehicle 8V-3

8.6.2.1 Propellant Tank Arrangements. Different propellant tank arrangements were studied to determine preferred vehicle configurations. Tanks clustered around a central spine, tanks clustered around tanks, tanks clustered around the life support system, single tanks in vertical and horizontal lines, and torus tanks (Figures 8-19 and 8-20) were investigated. Propellant tanks clustered around a central spine provided a simple and accessible arrangement for exchange of tanks and a lightweight structure. Therefore, this arrangement was chosen for the 8M-14 vehicle. However, when other factors (meteoroid shield and thermal reflectors) were included, an arrangement that employed a tank surrounded by several other tanks proved to better satisfy design requirements. This configuration had the following desirable characteristics:

a. Lightest gross weight.

b. Adaptability to vehicles using metal or graphite nuclear engines.

c. Growth potential for use to explore other planets with only slight modifications.

d. Provision for additional meteoroid protection. Each small tank contains from 5 to 16 percent of the total propellant for that maneuver and thus, if the tank were punctured, only a small amount of propellant would be lost. The mission could continue with a change in trajectory or a jettisoning of some excess weight.

e. The outermost ring of tanks can be exchanged before and during coast flight.

f. Simpler and smaller tank attachments.

Thus, the propellant tank arrangements were developed for 8M-22 (M-2 and M-3) and 8M-23 (M-4, M-3, and M-2).

For vehicles employing graphite nuclear engines, a study was performed for the Earth entry propulsion, comparing a chemical and a nuclear system. Figure 8-21 illustrates different chemical and nuclear configurations. The relative weight values presented on this figure indicate that a chemical liquid hydrogen/liquid oxygen system is lightest by 15.5 percent (refer to Figure 8-22 for a chemical M-4 configuration.)

The two main reasons contributing to heavier nuclear systems are: a) crew radiation shielding and b) high Nerva-engine weight. The liquid oxygen difloride/monomethylhydrazine engine system was heavier because of inferior specific impulse. Therefore, the chemical liquid hydrogen/liquid oxygen system was chosen for those vehicles using a graphite nuclear system.

A single 60-ft diameter propellant tank, with the possibility of adding smaller side tanks, was chosen for the Earth-orbital escape booster. The advantages of a single tank are:

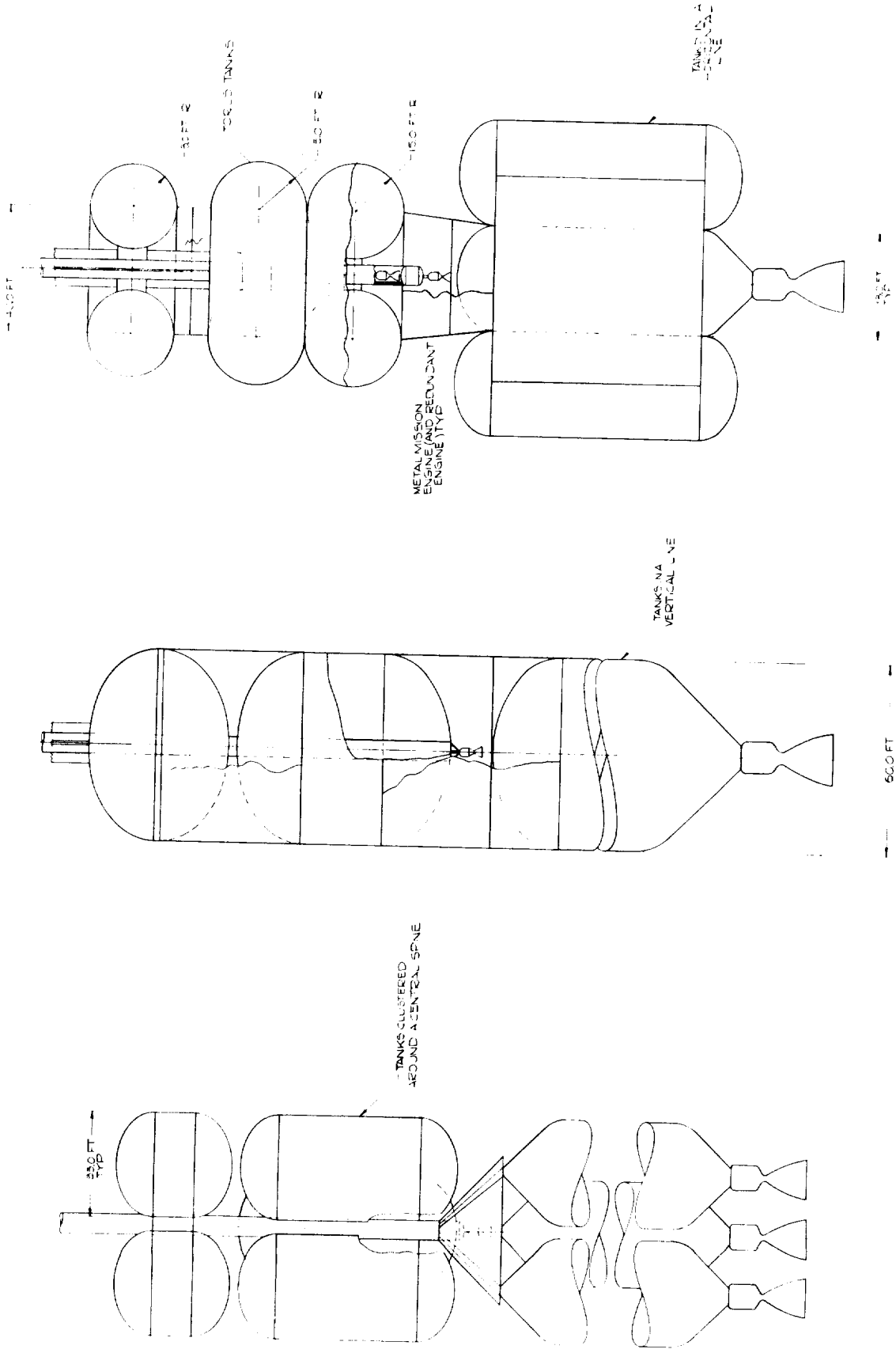

Figure 8-19. Propellant Tank Arrangements

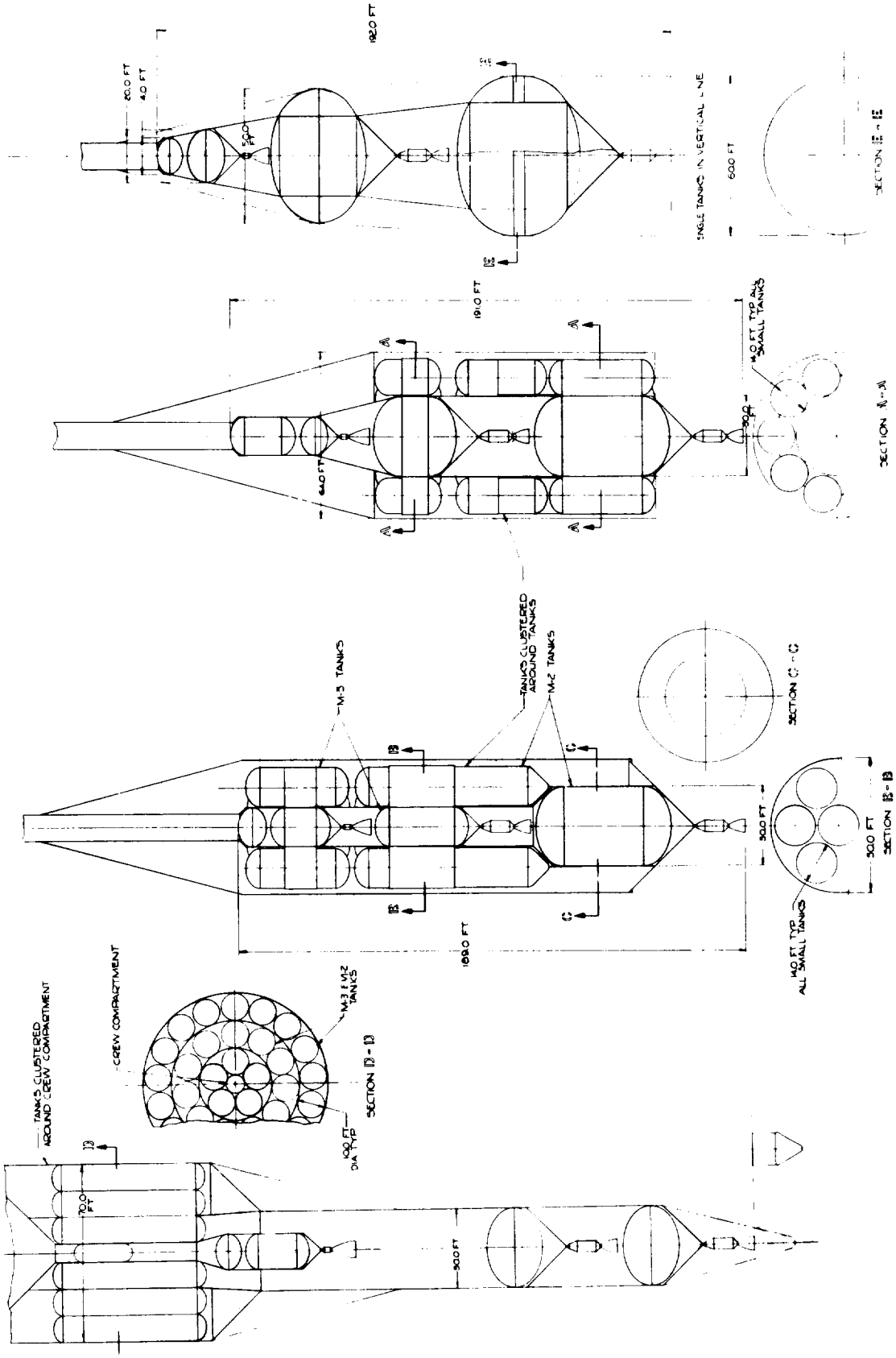

Figure 8-20. Propellant Tank Arrangements (Multi-Engines)

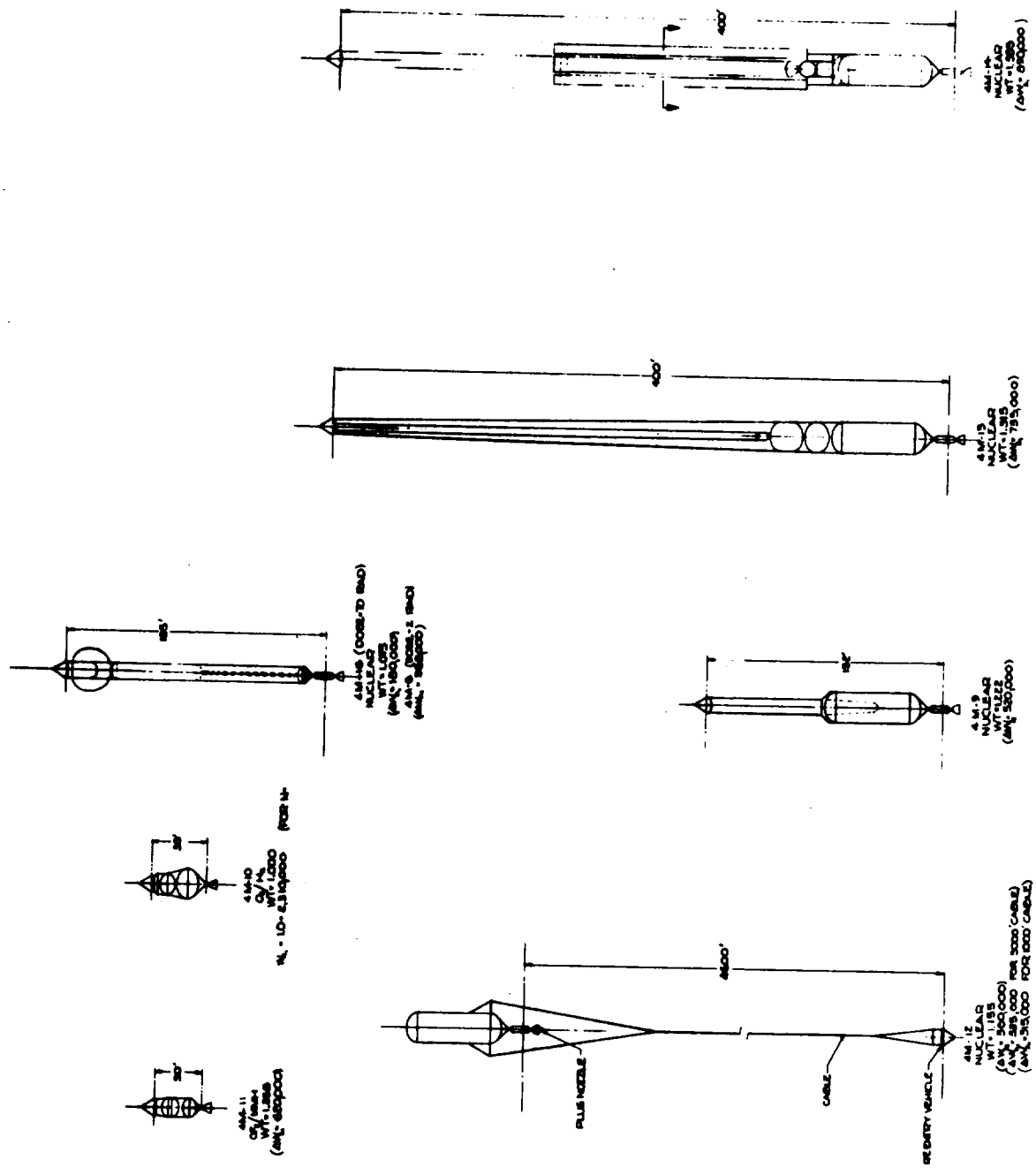

Figure 8-21. Maneuver IV Propulsion Comparison

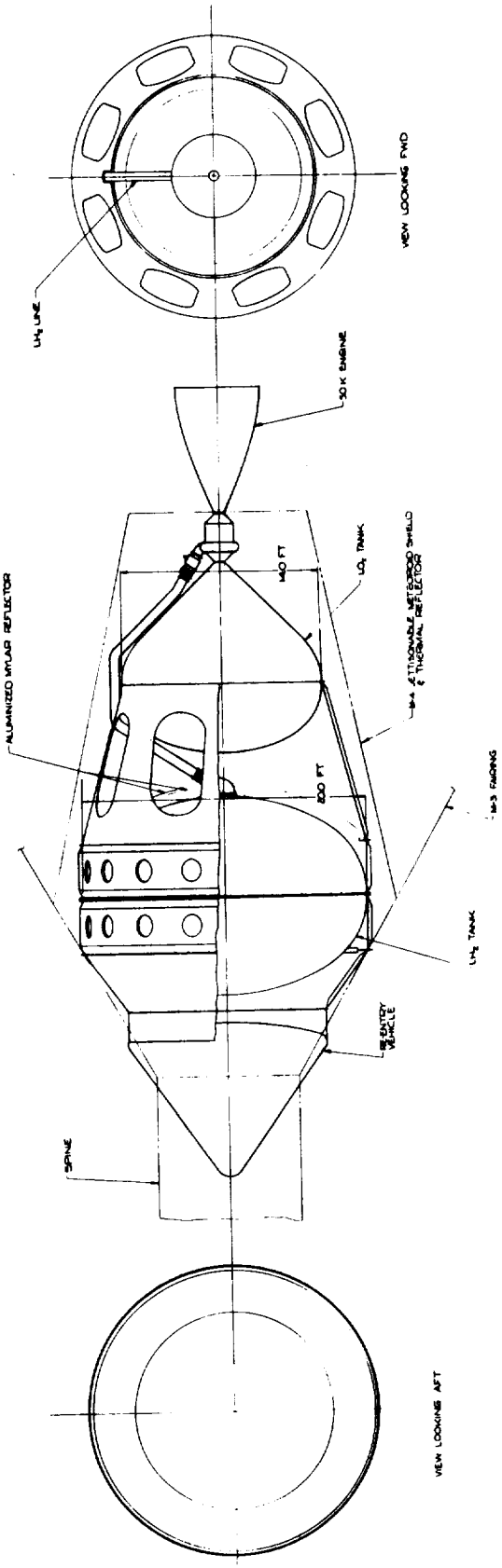

Figure 8-22. LO_2/LH_2 M-4 Configuration

a. Lightest weight

b. Growth potential (side tanks could be added for missions requiring additional propellant.)

c. Adaptability to use of a single 700-K engine or a cluster of Phoebus engines.

8.6.2.2 Fail-Safe Structure. The Mars and Venus vehicles are composed of a multitude of propellant tanks. Pressurization of these tanks results in a structure capable of supporting acceleration loadings during and prior to launch. However, loss in pressure would result in tank or (possibly) vehicle failure. Therefore, these propellant tanks must be designed as a fail-safe structure capable of resisting maximum acceleration loads (assume 7 g's) without pressure. Propellant tank wall thicknesses were determined by the maximum pressure (Δp = 10 psi) occurring in the tank. The tanks were then stiffened by stringers and frames. This arrangement is lighter than a skin/honeycomb-core structure because of the relatively low pressure differential across the tank wall and low acceleration loads. (Side tanks contain hydrogen, which is a light material: multiplying the hydrogen weight by the acceleration, then dividing by the tank circumference results in a small load per inch.) With this condition existing, a minimum gauge skin-core is heavier than required.

8.6.2.3 Thermal and Meteoroid Protection. The propulsion tanks of an interplanetary vehicle will be exposed to possible impacts by meteoroids. Whipple's Flux Estimates and information from NASA report TN D-1039 was used as a basis for analysis (cf. Section 8.4.8 for a sample problem).

The two thermal requirements are a) launch insulation and b) space radiation. A closed-cycle helium atmosphere was chosen to satisfy ground launch conditions. This solution was compared to evacuated super insulations, thick solid insulations, and layers of reflectors with a helium purge. The latter solutions consisted of placing the insulation around each invididual tank and attaching it to the tank wall. Some maneuver configurations consist of a multitude of propellant tanks; therefore, it is almost impossible to shed the insulation. The insulation around each tank also causes difficult ground handling problems. The helium atmosphere method uses the meteoroid shield as an enclosure for the helium, leaving the tanks clean. This shield can be jettisoned.

A combination of thermal reflectors and a hydrogen liquefaction unit is most advantageous as a solution to the space radiation problem. Along with the insulation methods presented for the launch condition, attitude control was investigated. The same reasons disqualifying the launch insulation methods are valid for attitude control, which is insufficient for long time periods in space, and would therefore require additional insulation of the "launch from Earth" type.

A preliminary analysis was performed on the use of the Earth launch fairing as a multi-purpose structure combining a) launch fairing (to withstand aerodynamic loading and heating), b) meteoroid shield, c) thermal radiation reflector, and d) launch-to-orbit enclosure for a helium atmosphere insulation. This method was chosen for the 8M-14 vehicle; however, a more detailed study (Figure 8-23) proved that separating a) from b), c) and d) would be 18 percent lighter (2.30 lb/ft^2 versus 2.85 lb/ft^2). The propellant tank arrangements chosen for the 8M-22 and 8M-23 reduce the area exposed to meteoroid impacts, and thus reduce meteoroid shield thickness. (The 2.30 lb/ft^2 would be reduced to about 2.00 lb/ft^2). The latter method is employed in the 8M-22, 8M-23, 8V-2 and 8V-3 vehicles.

8.6.2.4 Effect of Crew Size and Capture Orbit Eccentricity. Crew sizes ranging from two to eight people were investigated. The vehicle weight varies about 18 percent and the length varies about 15 percent in going from two to eight persons. Refer to Section 8.9 for further weight discussions.

An elliptical orbit compared to a circular orbit around a target planet can reduce vehicle weight as much as 33 percent (for Venus, $r_A/r_P = 20$). The elliptical orbits require less energy to enter and leave. (Refer to Section 7.13 and 8.9.)

8.6.2.5 Engine Arrangements. A single 30-K to 50-K metal nuclear engine for the interplanetary section (M-4, M-3, and M-2) and a single 700-K graphite nuclear engine for the orbital escape booster is the most desirable combination. Compared to this, using an advanced Nerva and a Phoebus engine, the vehicle will increase in weight and size, but could still perform the mission far better than a chemical vehicle. A burning time of 30 minutes was assumed for all graphite nuclear engines. The earth orbital escape booster shown in Figure 8-24 employs a cluster of four Phoebus engines at a minimum distance of 25 feet. These Phoebus engines would require clustering ability incorporated into their design.

8.6.2.6 Materials. The material for all propellant tanks is 5 Al-2.5 Sn titanium alloy. The central spine and associated structure uses 13V-11Cr-3 Al titanium alloy. The meteoroid shield, launch fairing and reflectors use 2014-T6 aluminum alloy.

8.7 SERVICE VEHICLE PROPULSION STRUCTURE. The propulsion requirements for the interplanetary service vehicle are identical to those of the crew vehicle except, perhaps, for differences in the propellant load. To provide a back-up for the crew vehicle, the service vehicle propulsion structure is identical to that of the crew vehicle. Propellant tanks, engines, etc., have the same specifications. If the crew vehicle is damaged beyond repair, the crew could transfer to the service vehicle and continue the mission. Portions of the crew vehicle that are only partially damaged could be replaced by those from the service vehicle. Manufacturing costs and problems will be effectively reduced by keeping the propellant tanks to a minimum number of sizes.

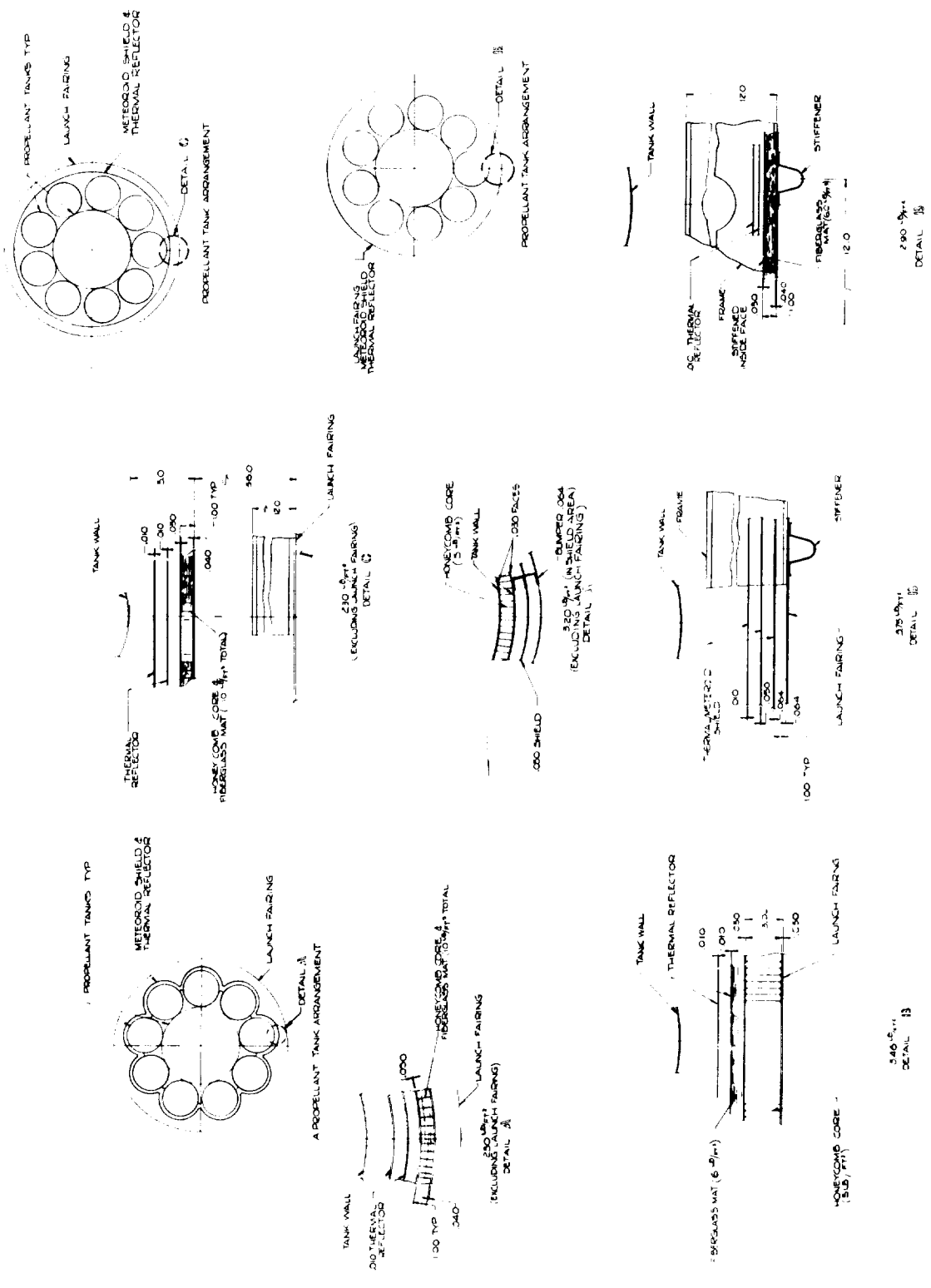

Figure 8-23. Meteroid Shield and Thermal Reflector Comparison

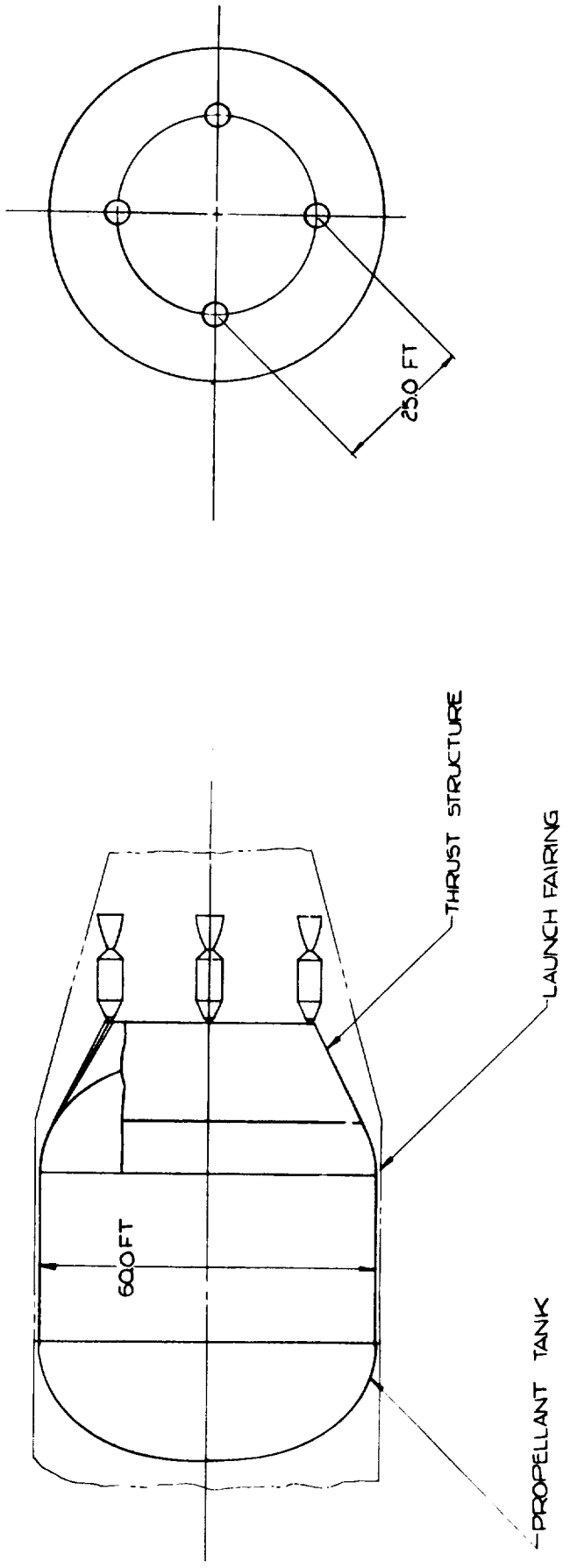

Figure 8-24. The Phoebus Cluster

8.8 STRUCTURAL ANALYSIS OF THE M-4 HYDROGEN TANK CONTAINING THE COMMAND MODULE.

8.8.1 Stability of Stiffened Cylinders. In the structural analysis of stringer-frame stiffened cylinders subjected to axial compression, the most controversial method of analysis is that for frame design. On the basis of tests sponsored by NACA some years ago on small scale stiffened-cylinders subjected only to bending, Shanley has proposed the equation

$$I = \frac{6.25 \times 10^{-5} D^2 M}{EL} \qquad (8\text{-}5)$$

for the design of frames where

I = moment of inertia of frame

M = maximum bending moment on cylinder

L = frame spacing

E = modulus of elasticity of frame

D = diameter of cylinder.

This equation presupposes the condition that the stringers are on the threshold of collapse by elastic or inelastic column buckling between frames and that, with a frame of this moment of inertia, general instability is just as likely to occur.

After evaluating the compressive stability test results of the first three stiffened cylinders shown in Figure 8-25A, B, and C of a structures research test program at General Dynamics/Astronautics, a tentative modification of Shanley's equation for axial compression is proposed as

$$I = \frac{25 \times 10^{-5} R^3 P}{EL} \qquad (8\text{-}6)$$

where

P = total axial load on cylinder

R = radius of cylinder.

In the first test, buckling occurred between frames; in the second test, buckling occurred over two frames; and in the third test, buckling occurred over four frames.

The cylinder must also be checked for long column (Euler) buckling and for discontinuity failures due to pressure.

Figure 8-25a Compressive Stability Test 1

Figure 8-25b Compressive Stability Test 2

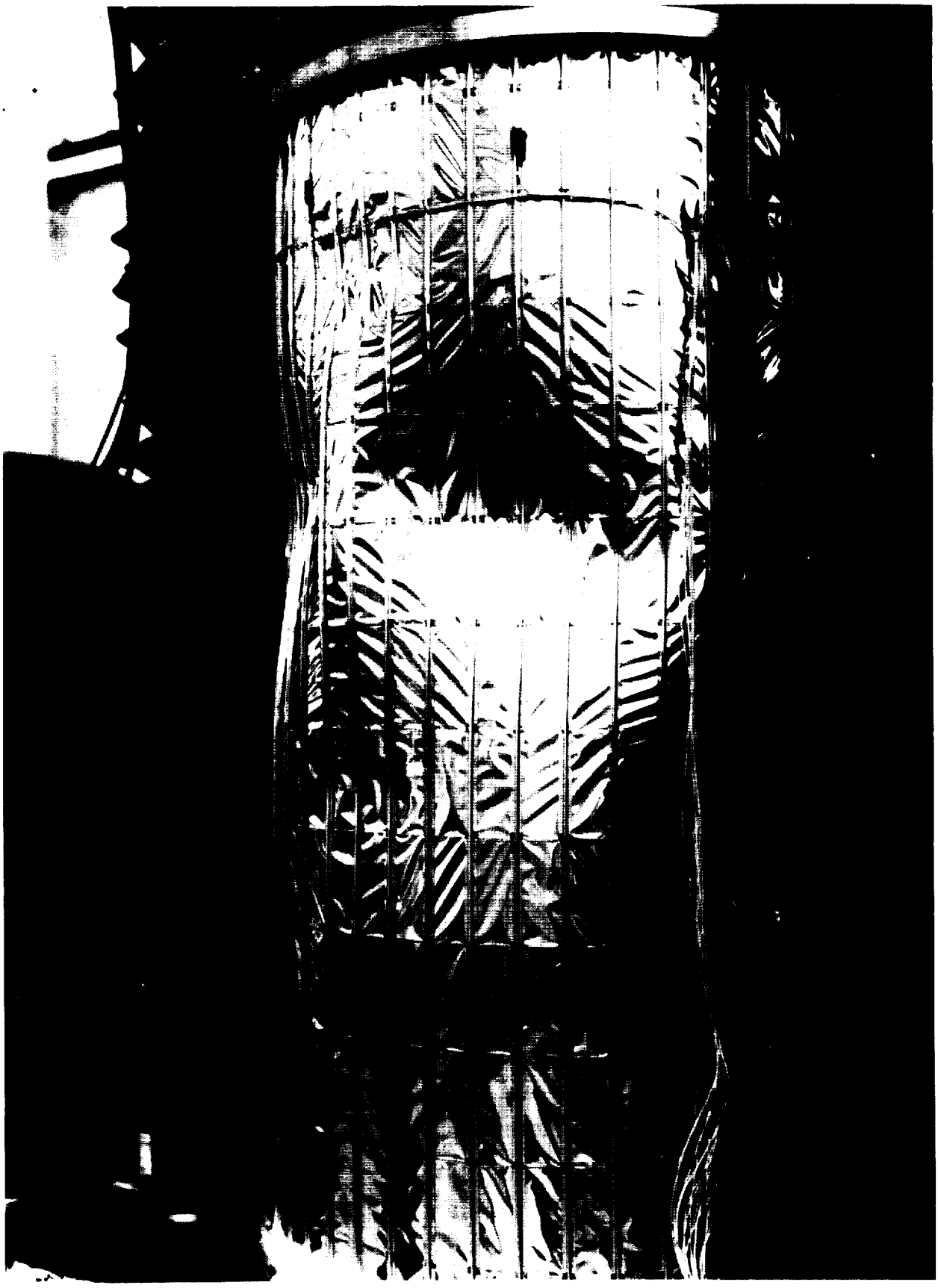

Figure 8-25c Compressive Stability Test 3

8.8.2 Stability of Sandwich Structures. At present we are depending on available General Dynamics/Astronautics test data for designing externally pressurized sandwich spherical shells and sandwich cylinders subjected to axial compression. The latter contain liquid hydrogen. As more test data become available, the design procedures will be revised accordingly. Some future testing is contemplated on hydrostatically loaded ring-stiffened sandwich cylinders similar to that in the M-4 liquid hydrogen tank shown in Figure 8-26.

8.8.3 Spherical Shell Junctures in Maneuver 4 LH_2 Tank. Large-deflection theory for axisymmetrically loaded thin-walled spherical shells has been incorporated into a computer program for the IBM 7090. Surface loading, temperature, and shell thickness may vary along a meridian and, in addition, temperature may vary through the thickness. Discontinuity analyses of the thin-shell junctures in the M-4 liquid hydrogen tank shown in Figure 8-26 will be performed by this program.

8.9 NUCLEAR ENGINE SYSTEMS FOR CREW AND SERVICE VEHICLE. Nuclear propulsion is necessary for all but the very minimum manned planetary mission capabilities. Although chemical systems have been taken into consideration (cf. Section 8-10), main emphasis has been given to nuclear-powered vehicles. For this reason, Rocketdyne, a Division of North American Avaiation, Inc., was invited, through a subcontract, to participate in the evaluation of high-thrust nuclear engines (200 to 700 k) using graphite reactors and of a low-thrust nuclear engine (30 to 50 k) using a metal reactor. Aerojet General was contacted for information on the NERVA engine and on a NERVA follow-on. General Dynamics/General Atomics was consulted on the material problems connected with fast-neutron metal and metal-carbide reactors. Rocketdyne's contribution and other detailed discussions, such as schedules, are presented in the classified Addendum of this report. The following conclusions can be stated here.

8.9.1 Earth Departure Weight. The use of graphite-reactor ships with chemical M-4 propulsion reduces the Earth departure weight by a factor of 4 to 5 below that of a chemical vehicle using O_2/H_2 at 460 seconds specific impulse. The reduction factor is 5 to 7 if the chemical vehicle is compared to a metal-reactor vehicle. Table 8-4 presents a summary of Earth departure weights for Venus crew vehicles which shows the effectiveness of nuclear propulsion. The chemical vehicle can compensate for this disadvantage only by entering an extremely elliptic capture orbit ($n = 20$, $e = (n-1)/(n+1) = 0.905$) or by a combination of less extreme capture orbit ($n = 4$, $e = 0.6$) and reduction in crew size (eight to four). Of these two, the latter is far less effective so that the main contributor to a reduction in departure weight is the high eccentricity of the capture orbit. This option is, of course, also available to the nuclear vehicle whose weight for $n = 20$ would reduce from 550.6t to approximately 354 t or to about 400 t for $n = 4$.

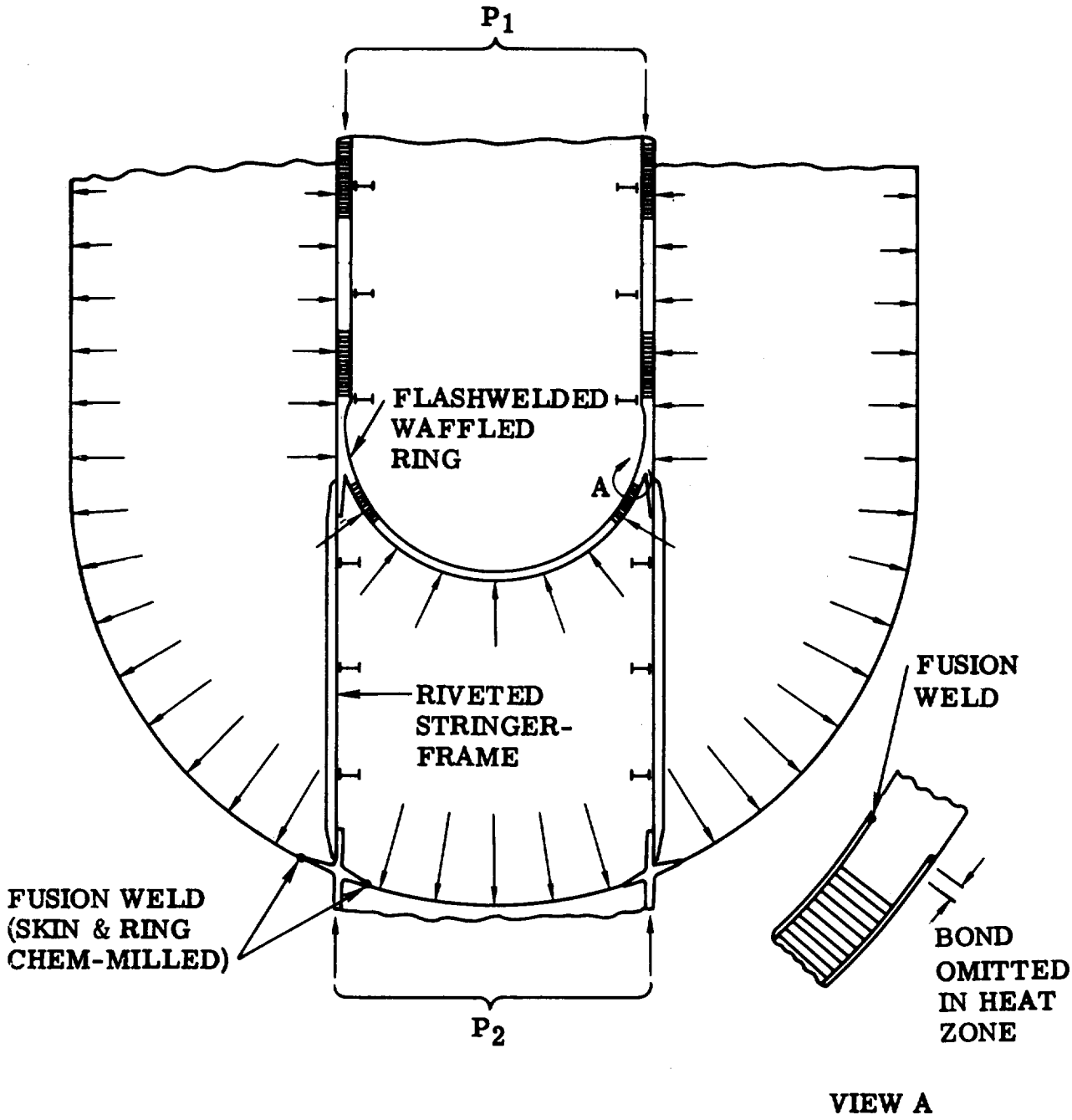

Figure 8-26. Maneuver 4 Hydrogen Tank

Table 8-4. Effect of Propulsion System, Crew Size and Capture Orbit Ellipticity on the Earth Departure Weight of Venus Crew Vehicles

MISSION	VENUS 1973-1										
COLUMN	1	2	3	4	5	6	7	8	9	10	11
CREW NUMBER	8	8	8	4	2	4	2	8	8	4	4
Propulsion	O_2/H_2	Graphite	Metal	O_2/H_2	O_2/H_2	O_2/H_2	O_2/H_2	O_2/H_2	O_2/H_2	O_2/H_2	O_2/H_2
M-1 I_{sp} =	460	845	845	460	460	460	460	460	460	460	460
M-2 I_{sp} =	460	845	900	460	460	460	460	460	460	460	460
M-3 I_{sp} =	460	845	900	460	460	460	460	460	460	460	460
M-4 I_{sp} =	460	455	900	460	460	460	460	460	460	460	460
Capture Orbit $n = r_A/r_P$	1	1	1	1	1	1	1	20	4	20	4
Capture Distance $r/r_{oo,♀}$	20	20	20	20	20	1.1	1.1	1.1	1.1	1.1	1.1
Earth Departure Weight (tons)	2785	550.6	478	2220	1690	1998	1540	553	866	436.3	684.4

For Mars, the superiority of the nuclear drive is even more striking, because the Mars mission energy requirement is usually higher, and capture-orbit ellipticity brings comparatively less relief due to the weaker gravitational field of Mars.

This superiority of nuclear propulsion is long recognized. The quantitative data presented in Table 8-4 substantiate this superiority more precisely. They also show how the capture orbit must be modified to approach nuclear-vehicle departure weights with chemical ships. Column 8 shows that the chemical ship would have to capture in an n = 20 orbit in order to approximate the departure weight of the graphite ship (Column 2). This is probably more acceptable for a Venus capture mission (and quite superior to a fly-by mission) than for a Mars mission where an optional surface excursion capability is desirable. A surface excursion from an n = 20 orbit is very difficult. However, orbits up to n = 4 could be considered and, as a comparison between Columns 1 and 9 shows, most of the savings already are obtained at n = 4. Nevertheless, the weight increase from Column 8 to 9 is not negligible and will appreciably influence the orbital assembly and launch operations. For these reasons, during this study an all-chemical alternate has been considered only for Venus missions.

However, the chemical approach to manned planetary flight remains quite unattractive although it offers a certain minimum capability for the 1973-1975 period. A Venus capture mission in 1973 or 1975 with an eccentric capture orbit using an all-chemical vehicle (if nuclear propulsion should not be ready, which appears likely) is strongly suggested, in preference to attempting no planet mission at all.

8.9.2 Combination of Nuclear and Chemical Engines. In the case of the graphite ship, it was found that the use of a chemical engine for M-4 is superior to that of a nuclear engine (an engine of 75-k thrust and 827 sec specific impulse was considered). The greater hardware weight (especially the long spine) which has to be carried through M-4 overcompensates the effect of higher specific impulse for the velocity changes involved in M-4 for mission profiles 1973-1, -2, -3 and 1975-1 to such an extent that the Earth departure weight is increased by about 100 tons compared to the use of a high-p_c O_2/H_2 system.

In Paragraph 7.14, it was found that the departure weight is particularly sensitive to increases in mass ratio of the escape booster (M-1 system). Conversely, the application of nuclear propulsion to the Earth departure maneuver is particularly effective. In other words, if nuclear propulsion is considered for any particular maneuver, with chemical propulsion for all other maneuvers, application to M-1 should be particularly effective in reducing the departure weight for three reasons: a) the reduction factor is multiplied by the largest mass, i.e., the entire convoy vehicle proper, b) the M-1 system requires the highest thrust of all stages and therefore the engine weight per pound of thrust should be lowest (comparing single engines for each stage), and c) the M-1 system requires the largest propellant mass and

therefore the higher weight of nuclear engine systems (compared to chemical systems of equal thrust) is less detrimental to the mass fraction of the escape booster than it would be to that of other stages.

With reference to reason a), it whould be noted that, for I_{sp} = 845 sec and $0.2 \leq v_{\infty}^{*} \leq 0.3$, the mass ratio is about one-half that required for a chemical escape booster (Figure 8-27), therefore causing a reduction in departure weight by a factor of two. This is between 40 and 50 percent of the total reduction.

Therefore, the most effective individual maneuver to which to apply nuclear propulsion is the Earth departure maneuver (M-1). This, at the same time, determines the desired thrust level to be of large magnitude, that is, of the order of 700 K.

8.9.3 Desirable Characteristics of the Nuclear Engines. Performance analysis shows that for interplanetary missions, even with nuclear heat-exchanger drives, vehicle staging is required. The most logical staging point is following Earth escape. This produces two basic sets of requirements for the nuclear engines:

a. Earth Escape Booster Engine:

   1) High thrust, sufficient to produce an initial thrust/weight ratio, F/W_o, of 0.3 to 0.4.

   2) A specific impulse between 750 and 850 sec; Figure 8-27 shows that it is not very important to reach the upper limit of this bracket, so far as the superiority of this drive over chemical drives is concerned.

   3) Comparatively short operational life -- of the order of 30 to 40 minutes.

   4) No restart required.

   5) Singular application only, since the escape booster will be staged at hyperbolic speed and not recovered.

b. Interplanetary Convoy Ship Engines (Mission Engines):

   1) Low thrust in the sense that specific impulse in comparatively more important, provided thrust/weight ratios are not too low (e.g., $\gtrsim$ 0.06 for Mars capture or escape (Figure 8-28), $\gtrsim$ 0.1 for Venus capture at close distance for $v_{\infty}^{*} \lesssim 0.3$ and $<$ 0.03 for Venus capture at 20 radii distance (Figure 8-29)); this implies thrust levels of 30 to 50 K, except for close Venus capture (ϵ = - 1.0) where a thrust level in the 50 to 100-K range is required.

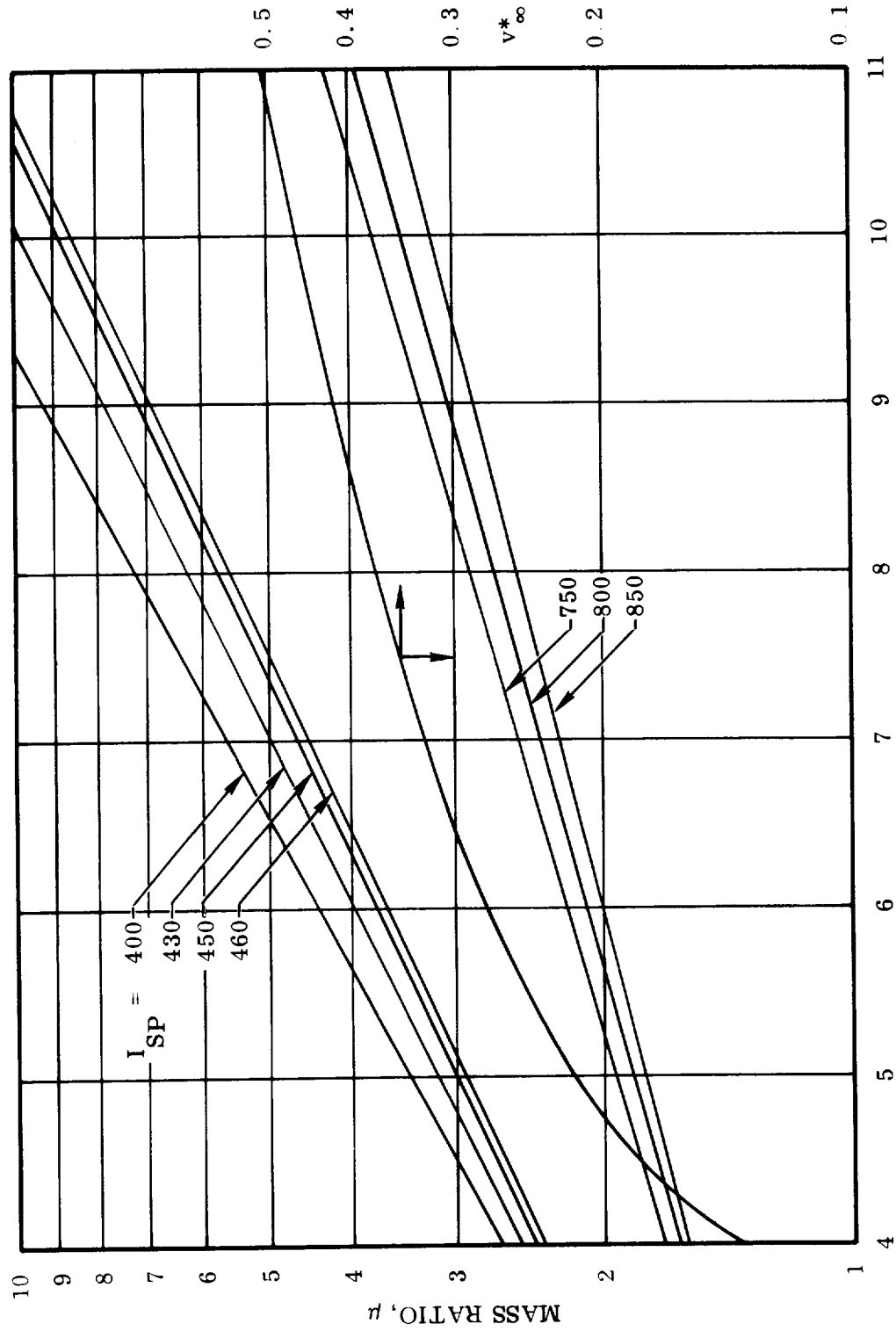

Figure 8-27. Mass Ratio Versus Earth Departure Velocity Increment

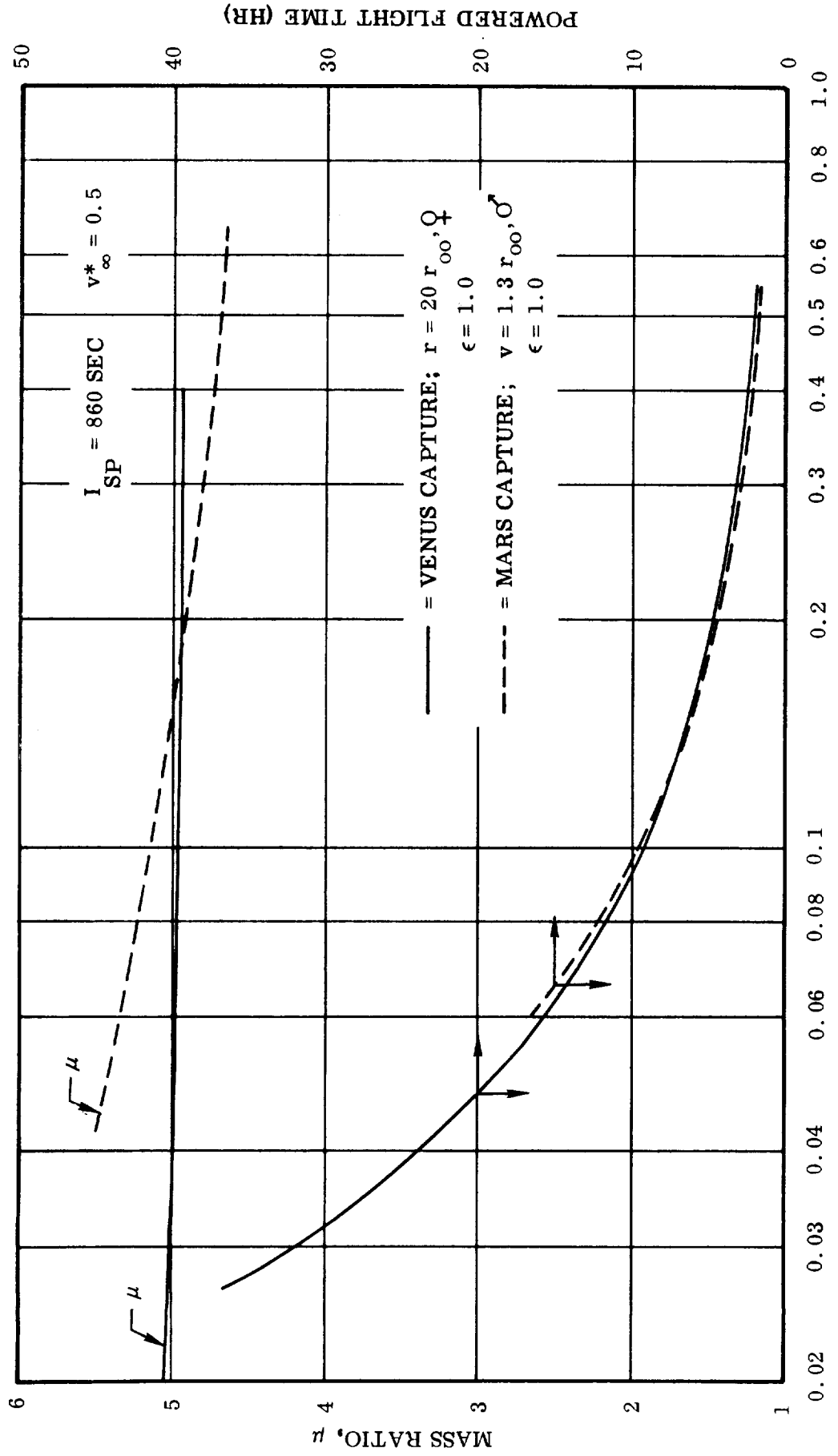

Figure 8-28. Variation of Mass Ratio and Powered Flight Time With Terminal Thrust/Weight Ratio for Venus and Mars Capture Maneuver (M-2)

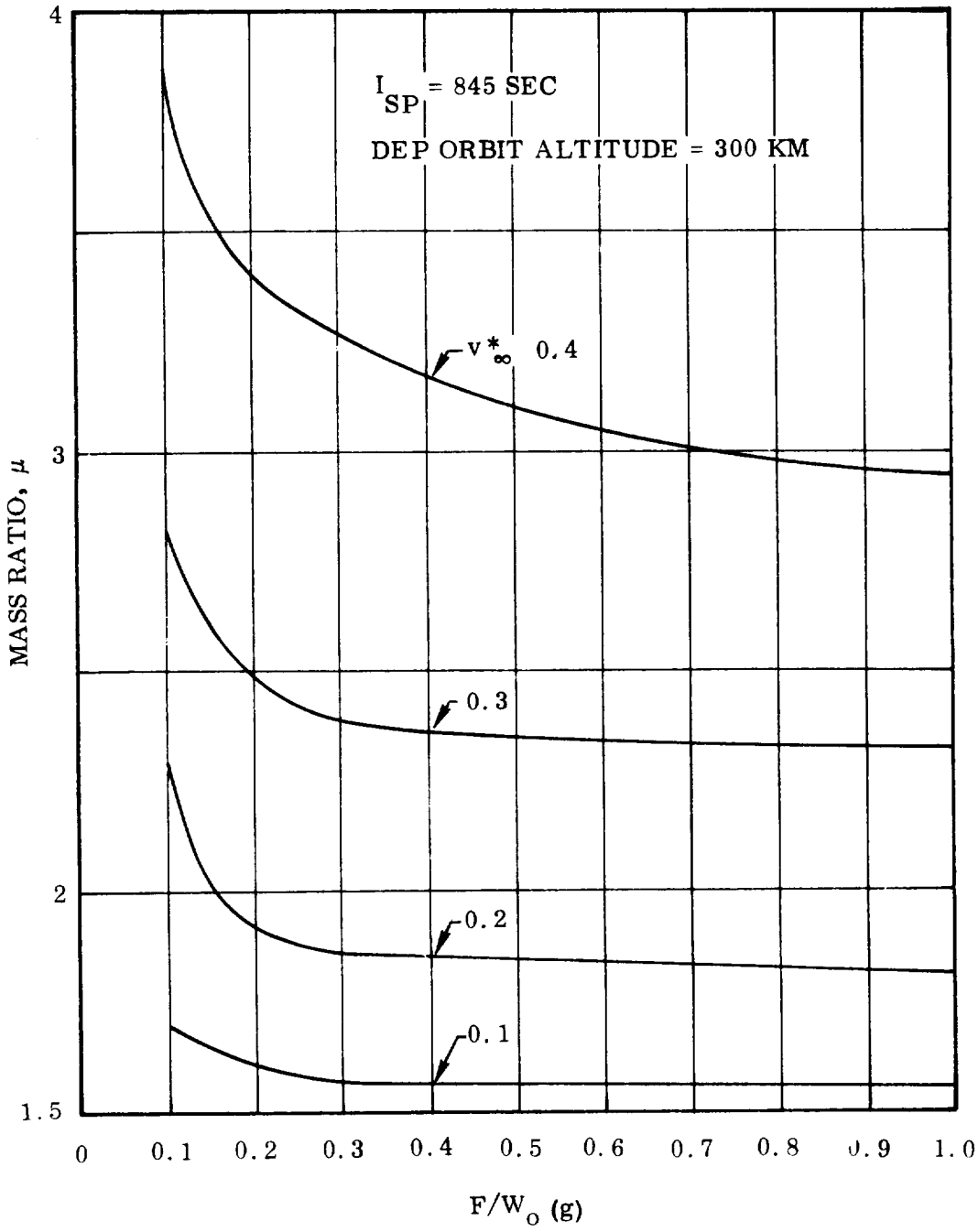

Figure 8-29. Gravitational Losses During Venus Escape as a Function of Thrust Acceleration and Hyperbolic Excess Velocity

2) High specific impulse; it was pointed out in the conclusions of Paragraph 7.14 that a small increase in the specific impulse of the mission engine (e.g., 20 sec) pays off more than a large increase in specific impulse of the escape booster engine (e.g., 80 sec).

3) Long operational life (the length depending upon the accelerations involved). Figure 8-28 shows that the powered flight time varies to a far greater extent than the mass ratio.

4) Restart capability, since for full mission flexibility the crew should be able to negotiate certain maneuvers in steps (e.g., an escape maneuver from an elliptic orbit about the target planet, cf. Paragraph 7-13) with intermediate coast periods of minutes or hours.

5) Multiple application, since the engine should be reusable for all maneuvers following Earth escape, so that only fuel tanks and associated structure have to be jettisoned.

From the view point of vehicle systems weight, a single large escape booster engine of the order of 700-k thrust is most desirable. From the view point of reliability a cluster of four engines at 200 to 250 k thrust would be more desirable, because this arrangement provides an engine-out capability during escape.

Interplanetary vehicles need, in the long run, a nuclear mission engine with ready restart capability, and long operational life (measuring a significant fraction of a day rather than an hour). The great importance of present nuclear engine development notwithstanding, it is the duty of the systems engineer to emphasize the importance of these two operational characteristics which eventually must be provided by the nuclear engine developer.

It appears that fast-neutron reactor engines are better able than thermal neutron engines to furnish ready restart capability and longer lifetime. When considering fast-neutron reactors, many experts look at certain metals and metal carbides as the most promising structural materials.

As an additional benefit, the high melting point of these materials may permit higher operating temperatures, thereby raising the specific impulse beyond the level attainable with the earlier engines. Development of the metal or metal-carbide reactor poses new problems and requires time - perhaps as much as 12 to 14 years - starting from the present level of limited experience with reactor components of this type. However, unless advancements in graphite reactor technology can provide these two vital operational characteristics for manned deep-space ships, efforts to determine the practicability of metal or metal-carbide reactor engines are worthwhile.

8.9.4 Thrust Selection for NERVA. Follow-On Engines. It is clearly evidenced by Figure 8-28 and by Figures 7-9 through 7-65 that, within the accelerations under consideration, the determining criterion for thrust selection for the nuclear engines for M-1 through M-3 is not mass ratio variation but the variation in powered flight duration, briefly referred to as "burning" time. If the burning time of the engine is limited to one-half hour (or even to 1-2 hours), the thrust generated is large enough to automatically satisfy the requirement for low gravitational losses during powered maneuvers. Figure 8-30 shows the required initial thrust/weight ratios for 30 minutes of powered maneuver during Earth escape and for 30 and 60 minutes burning time during Mars capture and escape. It is seen that increase of operational life from 30 to 60 minutes greatly reduces the F/W_0 value required. However, even in this case, F/W_0 values between 0.15 and 0.175 are required. Mars capture weights lie between 600,000 and 1,200,000 pounds. Thus, the thrust level required ranges roughly from 100 to 200 K for a 60-minute burning-time limit. The thrust level ranges from 200 K to 300 K if the burning-time limit is 30 minutes.

Thus, if the development effort were concentrated on one NERVA follow-on engine to be operationally available for the EMPIRE mission, and if the operational life of this engine were 30 minutes, then, all things considered, the thrust level of this engine should be 200 to 350 K. If the operational life were 60 minutes the engine thrust should also be in the 200 to 250-K range. In this range, there is a slight preference for the 250-K level over the 200-K level for the following reasons:

a. Four engines form a suitable cluster for the escape booster with a quite adequate engine-out capability. With 200 K, this engine-out capability would be marginal, at least from the performance (if not from the control) viewpoint.

b. If the engine operational life is one hour, a 250-K thrust level would make it possible in many missions to use the same engine for M-2 and M-3. As to failure of this engine to start on the crew vehicle, refer to the discussions in Section 9. No spare engine needs to be carried along, since the engine of the service vehicle acts as spare engine (cf. also Paragraph 8.3.7). If an engine-out occurs on the crew vehicle after both crew and service vehicle powered flight (target planet capture or escape) has begun, the crew must abort its vehicle, shut the service vehicle engine off by remote control and thereafter rendezvous with the service vehicle, board it, and continue the flight. (The abort would in this case involve not only the EEM, but also the nucleus of the LSS).

In summary:

a. The development of one 50 to 75-K engine of 30 to 60 minutes operational life time is of little value to the manned planetary mission capability.

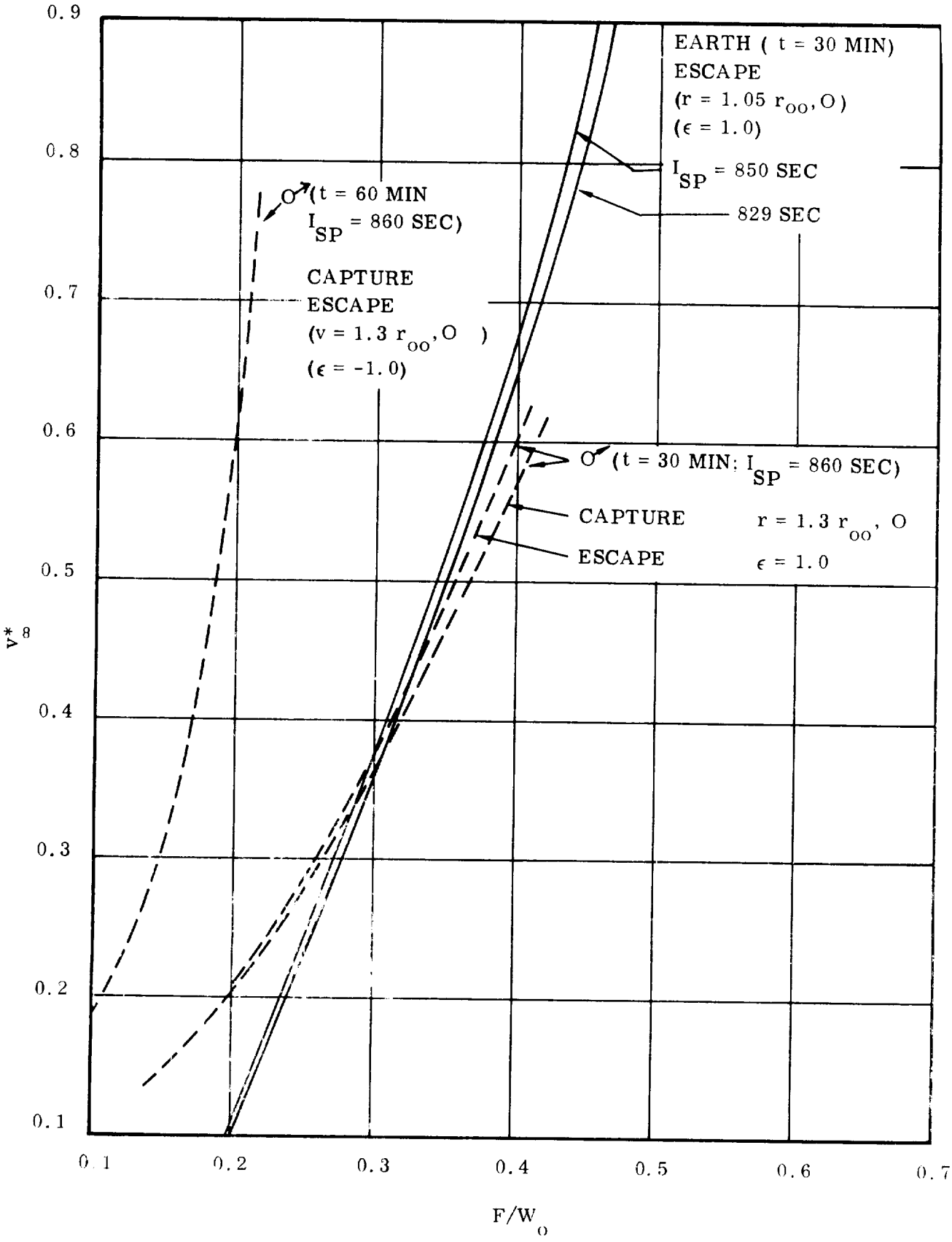

Figure 8-30. Required Initial Thrust/Weight Ratio Versus Hyperbolic Excess Velocity for Powered Operation of 30 and 60 Minutes During Earth Escape, Mars Capture and Escape

b. The development of one 700-K engine would be far more important for the EMPIRE Project, since it would permit at least a nuclear powered escape booster which would reduce the weight of the (otherwise chemically powered) ship to about one-half the weight of an all-chemical ship.

c. If only one engine of 30- to 60-minute operational lifetime can be developed, however, the most attractive thrust level, from an overall vehicle systems point of view would be 200 to 250 K, since it could provide nuclear drive for M-1, M-2 and M-3, and thereby reduce the departure weight to 22-20 percent of the chemical vehicle.

d. The ideal mission engine would be one which has an operational life of 10 to 40 hours, ready restart capability, and a specific impulse in the 860 to 900 sec range at a thrust level between 30 and 60 K. Since this engine is not suitable for powering the escape booster, its consideration implies the development of two instead of one nuclear engine systems for EMPIRE.

Because point c might represent the direction in which a decision by NASA could be made, the importance of clustering nuclear engines at sufficient distance from each other ("open" cluster) was recognized early in this study program. A request was made to Rocketdyne to study the feasibility of an open cluster arrangement from the engine performance and reactor control points of view. On the basis of their results, a cluster of four 200- to 250-K engines at technically reasonable distance is feasible. Their findings are reported in detail in the Addendum to this report.

8.10 CHEMICAL ENGINE SYSTEMS FOR CREW AND SERVICE VEHICLE. The chemical propulsion fulfills the following requirements:

a. Mars and Venus mission M-4 whenever graphite reactor engines are used for M-2 and M-3.

b. Certain special all-chemical Venus missions.

c. Abort during orbital launch to escape.

d. Spin for artificial gravity.

e. M-5 whenever M-4 is nuclear.

f. Possible contribution to mid-course correction.

g. Propulsion for auxiliary vehicles such as the space taxis, landers, scouts, etc.

Categories a and b use oxygen-hydrogen, pump-fed, relatively high thrust engines. In thrust rating they are not larger than engines currently being developed, such as the J-2 under development at Rocketdyne Division of NAA (200K) and the M-1 under development at Aerojet-General Corp. (1000 to 1500-K range). They do, however,

take advantage of some advanced features, such as higher chamber pressures and larger area ratios, in order to realize the combination of smaller overall dimensions coupled with higher vacuum performance. There is no pressing reason to use any nozzle design other than 70 or 80 percent bell. Table 8-5 summarizes typical LO_2/LH_2 engine dimensions for an area ratio of 150:1, 80 percent bell, which corresponds to an approximate vacuum specific impulse of 455 seconds:

Table 8-5. LO_2/LH_2 Engine Dimensions

THRUST (LB)	CHAMBER PRESSURE (PSIA)	EXIT DIAMETER (FT)	OVERALL LENGTH (FT)
75 K	1000	7.4	13.0
75 K	2000	5.2	10.0
200 K	1000	12.0	21.0
200 K	2000	8.5	16.0
800 K	1000	24.0	37.0
800 K	2000	17.0	26.0
1500 K	1000	33.0	50.0
1500 K	2000	23.4	35.0

From Table 8-5 it can be seen that for the small engine (75 K) the higher chamber pressure is probably an unnecessary complication, while for the large engine (1500 K) the higher chamber pressure has a significant effect on engine dimensions.

The 75-K LO_2/LH_2 engine used for chemical M-4 (category a above) has an operating time of approximately five minutes with no restart requirement. This is a conventional operating time and causes no new nozzle development.

Some category b LO_2/LH_2 engines (all-chemical Venus missions) require burning times of about one hour (200 K, M-2 engine). This can be accomplished with a long-life nozzle or a series of two or more engines burning in succession.

The essential construction of the nozzle is a combination of a regeneratively cooled chamber, throat and bell portion with a radiation-cooled bell extension.

Categories c through g encompass a group of essentially small, more or less self-contained, propulsion systems employing storable, hypergolic propellants. Figures 8-31 and 8-32 are schematic representations of two such systems. The main elements of each system are a pressure-fed chamber and nozzle assembly, positive-expulsion propellant tanks, pressurizing gas storage, and engine controls. The figures also indicate how sets of propellant storage and feed systems are arranged to feed different

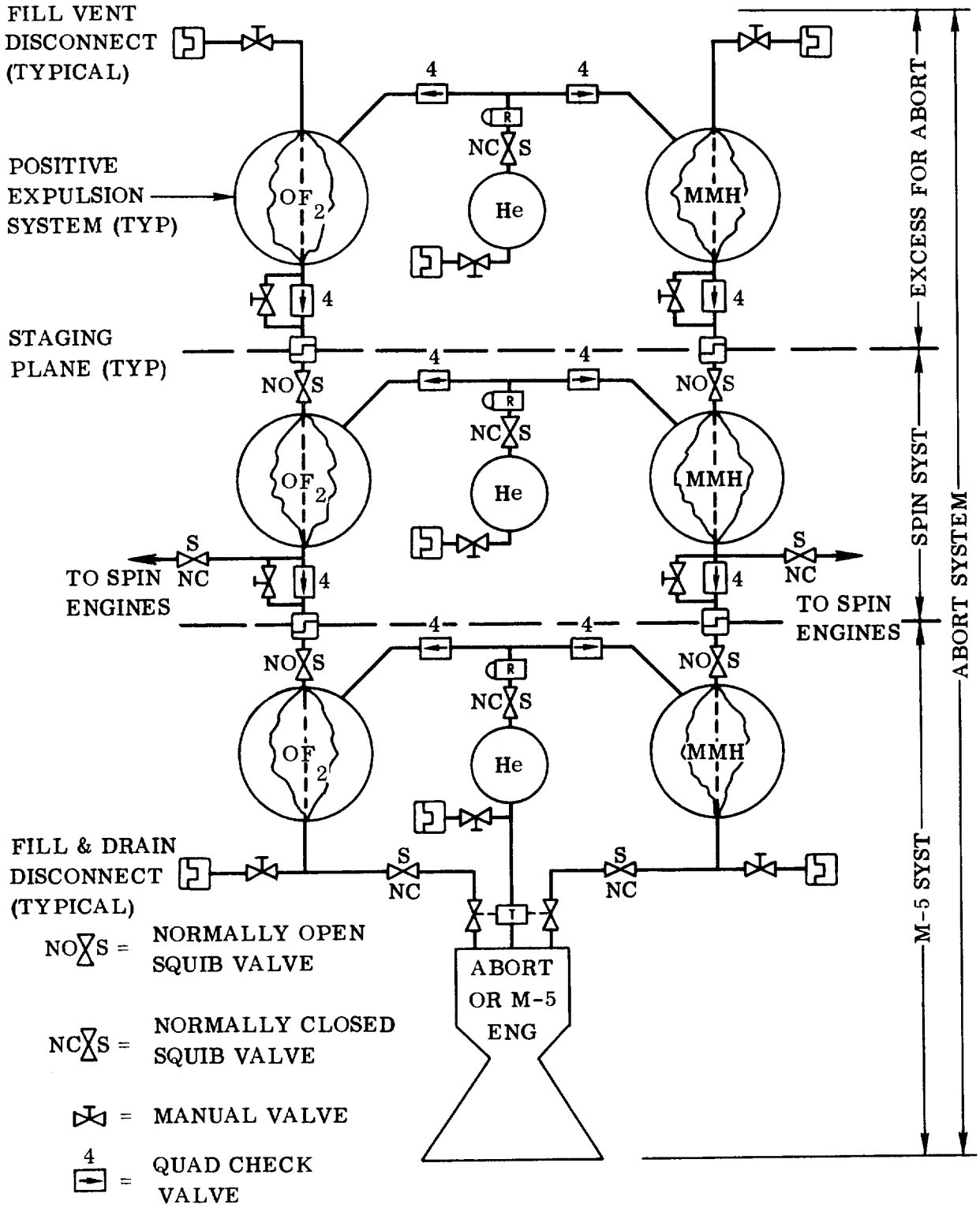

Figure 8-31. OF_2/MMH Abort, Spin and M-5 System as Used with a Nuclear Maneuver 4

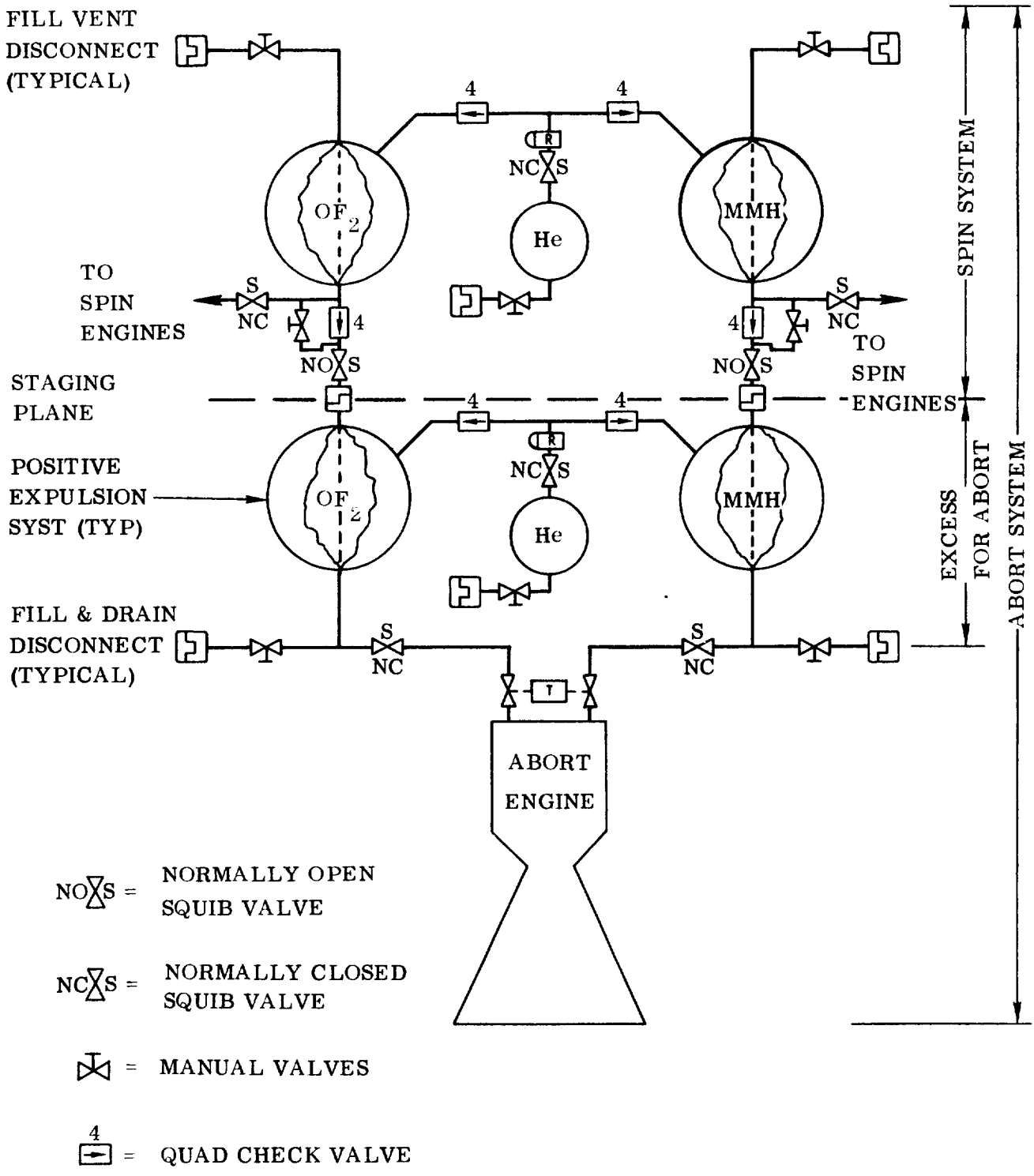

Figure 8-32. OF_2/MMH Abort and Spin System as Used With a Chemical (LO_2/LH_2) Maneuver 4

chambers at different times, thereby allowing the vehicle to use and/or jettison portions of the total system on an operations-and-time-selected basis. The engines, in general, have a variable thrust capability either by throttling (in the larger engines) or on-off pulsing (in smaller engines).

Figure 8-31 shows, in particular, the combined abort, spin, and M-5 system using oxygen difluoride and monomethyl hydrazine (OF_2/MMH) propellant combination and helium gas for pressurization. In the event of an abort, all tanks feed the large abort/M-5 engine. If, when Maneuver 1 is complete, the abort system has not been used, one set of loaded propellant tanks, representing the excess of the abort requirement above spin plus M-5, is jettisoned. At the same time, the tanks feeding the spin system are pressurized to deliver propellant to the valves of the spin engines, and the M-5 tank isolation valves are closed. Following the final de-spin, and prior to nuclear Maneuver 4, the spin system propellant tankage is jettisoned. Following the nuclear M-4, the M-5 system is used to essentially separate the re-entry capsule from the nuclear stage. The expended M-5 system, including the engine, is then jettisoned from the EEM.

Figure 8-32 defines a combined abort and spin system as used with a chemical M-4. In this case there is no need for a Maneuver 5, and the entire abort engine assembly and its controls are jettisoned, along with the tanks containing the excess propellant, upon the completion of M-1. The spin system is used in exactly the same manner as in the previous system, and is jettisoned after the final de-spin and prior to initiation of M-4.

The arrangement and use of components in the above-described systems is indicative of how the requirements of categories f and g could be met. These requirements have not, as yet, been formulated in enough detail to permit a complete definition of the systems; however, if the energy requirements are large, a pump-fed LO_2/LH_2 system might well replace the storable, hypergolic, pressure-fed system.

The use of oxygen difluoride as oxidizer with monomethyl hydrazine as fuel is based on work done by Reaction Motors Division of Thiokol Corporation with this combination. It has demonstrated a delivered specific impulse of 404 seconds in test firings of a 10,000-pound thrust engine and is fully hypergolic in the back pressure range of the tests. In addition to its high performance, it also has a high bulk density (1.244 gm/cc) and good space storability:

	Boiling Point	Freezing Point
OF_2	-229° F	-371° F
MMH	+188° F	-62° F

The low boiling point of OF_2 may impose a more difficult requirement on the positive expulsion system than the higher boiling points of present storable oxidizers such as nitrogen tetroxide (N_2O_4), but single-cycle, metallic-type diaphragms can be used if necessary.

The functions and arrangements of the various storable propellant systems described above are not in any way altered by using other storable hypergolic combinations such as the one in current use in the Titan II. In fact, advantage could be taken of a fringe benefit of OF_2; namely, its capability of being substituted for N_2O_4 in an existing system since the volumetric mixture ratios of OF_2 and N_2O_4 with the hydrazine fuels are numerically equal. The OF_2 combination gives a better than 70 percent increase in payload capability and would therefore represent considerable growth potential.

8.11 ECOLOGICAL LIFE SUPPORT SYSTEM. For design and weight analysis purposes a hydrogen reduction and electrolytic water decomposition system has been adopted as the reference system in this study. This system and the ecological systems for the EEM and the MEV are discussed in detail in Section 10.

8.12 COMMUNICATION SYSTEM. The convoy requires the following communication systems:

a. Convoy ⇄ Earth.

b. Intra-Convoy (vehicle to vehicle).

c. Taxi ⇄ Convoy vehicle.

d. Internal communication (intercom)

e. Communication between convoy vehicle and auxiliary vehicles, especially the MEV.

The intra-convoy communication system can be standardized to communicate with Earth at close distance (some 10 Earth radii or more) in terms of voice and picture transmission, and to communicate with the MEV as well as with the taxis, the Lander, and the Returner.

For long distance communication and tracking the convoy will communicate with NASA's Deep Space Instrumentation Facility at JPL and with the deep space communication facility which may be developed in connection with the Apollo Program.

No effort was spent on the intra-convoy communication system or the intercom system, since these are expected to offer no particular problems which cannot be solved even within the existing state of the art.

By far the greatest load imposed on the communication system will be that of data processing and data transmission to Earth. These data will come primarily from the auxiliary vehicles during the capture period. Among these, the Mapper is obviously the one that will impose the heaviest individual load on the system.

In recognition of the great importance which data handling and data transmission has for the "yield" of the tremendous effort of an EMPIRE mission, a subcontract was given to IBM to perform a preliminary study of the problems of scientific data compaction, data processing, and storage weight within the framework of the mission objectives planning presented in Section 5 and the principle of vehicle convoy operation. The IBM report is presented in Appendix I at the end of this volume.

8.13 NAVIGATION SYSTEM. The navigation system envisioned consists of a stellar-monitored four-gimbal all-inertial platform, a digital guidance computer, and associated equipment. The navigation system is discussed in Paragraph 6.9.

8.14 FUEL CONSERVATION

8.14.1 Introduction. Fuel conservation studies are concerned with the following areas:

a. Transportation of large quantities of hydrogen (packages of 100,000 to 600,000 lb) into orbit.

b. Orbital storage of hydrogen (and oxygen) prior to departure.

c. Orbital storage of hydrogen (and oxygen) during the mission, taking varying heliocentric distance and arbitrary vehicle attitudes into account.

d. Thermodynamics of the life support system.

e. Thermodynamic problems connected with the location of the mission command module in the M-4 hydrogen tank.

The heat protection must be independent of the vehicle's attitude in order to:

a. provide proper insulation on the launch pad;

b. provide proper shielding in the satellite orbits of Earth and target planet, where the vehicle is subject to thermal radiation from planet as well as from Sun;

c. permit random rotational motion of the vehicle during heliocentric transfer, and

d. make the materiel shield (which is required anyway) serve two purposes, by designing it simultaneously as a reflector shield.

Nevertheless, a certain shadow shielding capability (which by its very nature is attitude sensitive) is of interest, because it offers flexibility in emergency situations -- e.g., damage to the surface shield, periods of extreme irradiation (at close distance over the daylight side of Venus or during close perihelion passages), or periods of overload or repair of the hydrogen liquefaction unit.

The hydrogen must be stored in liquid form at various vapor pressures (roughly from 1 atm down to very low values, as characterizes subcooled fluids), or in solid/liquid (slurry), or in solid form.

8.14.2 HYDROGEN SOLIDIFICATION. The specific rate of evaporation (fraction of the total weight of cryogenic fluid per day) for an individual tank is given by

$$\frac{w_v}{W} = \frac{q}{A}\frac{A}{V}\frac{24}{Q_{g\rho}} \quad (1/\text{day}) \qquad (8\text{-}7)$$

where w_v is the daily fluid weight lost by evaporation, W is the total fluid weight initially in the tank, q/A is the specific heat flux density (Btu/ft^{2}hr), A is the area through which heat flux takes place, V is the tank volume, Q is the heat required to evaporate 1 lb of the fluid (Q is not necessarily the heat of evaporation), and $g\rho$ is the specific weight of the fluid. It is seen that, among other things, the specific rate of evaporation is inversely proportional to the value of Q. The heat of evaporation of hydrogen is Q_v = 225 cal/g-mole = 202.5 Btu/lb. At very low vapor pressure (0.07 kg/cm^2 ~ 1 psi) the melting temperature of H_2 is 13.96°K. At 1 atm vapor pressure, the H_2 temperature is 20.39°K. Thus, assuming H_2 is stored at 1 atm vapor pressure, its temperature first must be lowered by 6.43°K to cause fusion. Inspection of the specific heat of H_2 in this temperature range shows a value of about 3.9 cal/g-mole°°K. The enthalpy which must be removed is therefore 6.43 × 3.9 = 25.1 cal/g-mole. To this, the heat of fusion (28 cal/g-mole) must be added. The total enthalpy sink available under these conditions is 28 + 25.1 = 53.1 cal/g-mole = 26.55 cal/g = 47.79 Btu/lb. The quantity of heat required to evaporate 1 lb of H_2 is thus $Q = Q_t + Q_v$ = 250.3 Btu/lb. Therefore, the specific rate of evaporation is, for the solid hydrogen, 0.81 of the rate for the liquid hydrogen (everything else being constant). Conversely, the storage time ratio is 1/0.81 = 1.235.

Solidification of large quantities of hydrogen can contribute significantly to the long storage times required for interplanetary missions by increasing the storage period by approximately 23.5 percent. Moreover, transportation of solid H_2 greatly reduces the losses in case of meteoric punctures, until these can be sealed. It also eliminates sloshing. It is doubtful that the hydrogen can be completely solidified, because of unavoidable heat leaks. However, a heavy slurry should be achievable. The heat sink provided by H_2 solidification is not sufficient, though very helpful, and must be complemented by other means.

LH_2 is solidified with least energy penalty when the process is carried out on the ground, by either of the following two methods:

a. Adiabatic boiloff. Approximately 24 percent of a given quantity of LH_2 at 1 atm initial vapor pressure must be evaporated to solidify the rest.

b. Helium refrigeration. Very cold helium gas is circulated through heat exchanger coils immersed in the liquid hydorgen.

Method b has two disadvantages. The temperature of solid H_2 is 6.43°K, and that of He is 4.2°K. Thus, the gaseous He must be close to the fusion point itself if it is to solidify the H_2 in a reasonable time period (about 2 days per 150,000 lb H_2) or within acceptable power requirements. The second disadvantage is that the cooling coils can not be removed once the hydrogen is solidified. Therefore, the method of adiabatic boil-off is suggested.

Complete solidification by boiloff on the ground appears uneconomical. The most attractive approach appears to be the following:

a. Formation of hydrogen slurry by adiabatic boiloff on the ground to provide pre-launch standby capability for isothermal absorption of unavoidable heat inputs, to eliminate the need for venting the payload tank during ascent (while it is a slurry, the vapor pressure remains constant), and to minimize evaporation losses during H_2 solidification in orbit.

b. Solidification by adiabatic boiloff in orbit shortly before vehicle assembly. Thereby the dynamic simplifications due to absence of sloshing are used to advantage during the assembly process.

8.14.3 Insulation or Radiation Shielding. In the computation of the heat transfer rates through a series of radiation shields wrapped concentrically about a cylindrical hydrogen tank, the model shown in Figure 8-33 was used. Assuming the tank spins fast enough that its surface temperature is approximately the same on all sides, then the value of this temperature is, in interplanetary space,

$$T_S = \left[\frac{\alpha_S I_\odot + \frac{E}{A} \frac{\sigma \epsilon}{(n+1)(2-\epsilon)} T_w^4}{\sigma \frac{E}{A} \left(\epsilon_S + \frac{\epsilon}{(n+1)(2-\epsilon)} \right)} \right]^{\frac{1}{4}} \qquad (8\text{-}8)$$

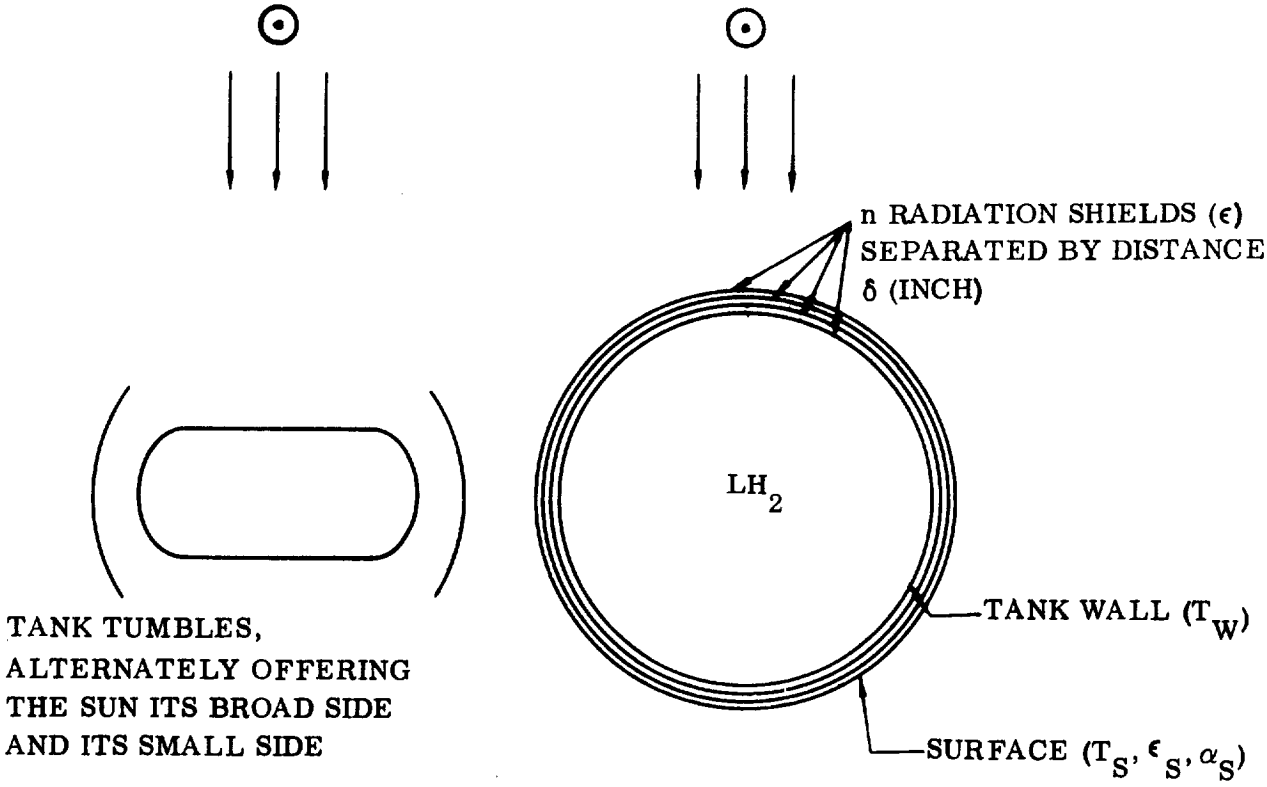

Figure 8-33. Tank Model

where, for a cylinder, the ratio of emitting to absorbing area is $E/A = \pi$. The wall temperature, T_w, has been set equal to that of liquid hydrogen; σ is the Stephan-Boltzmann constant. The value of T_S is plotted in Figure 8-34 for three limiting solar distances.

The heat transfer rate across the tank wall is, in interplanetary space,

$$q_w = \frac{E}{A} \frac{\sigma \epsilon}{(n+1)(2-\epsilon)} (T_S^4 - T_w^4) \qquad (8\text{-}9)$$

which is plotted in Figure 8-35.

The effective heat conductivity of the radiation shield is given by

$$k = \frac{q_w}{T_S - T_w} \; n\,\delta \; \left(\frac{\text{Btu}}{\text{hr ft °R}}\right) \qquad (8\text{-}10)$$

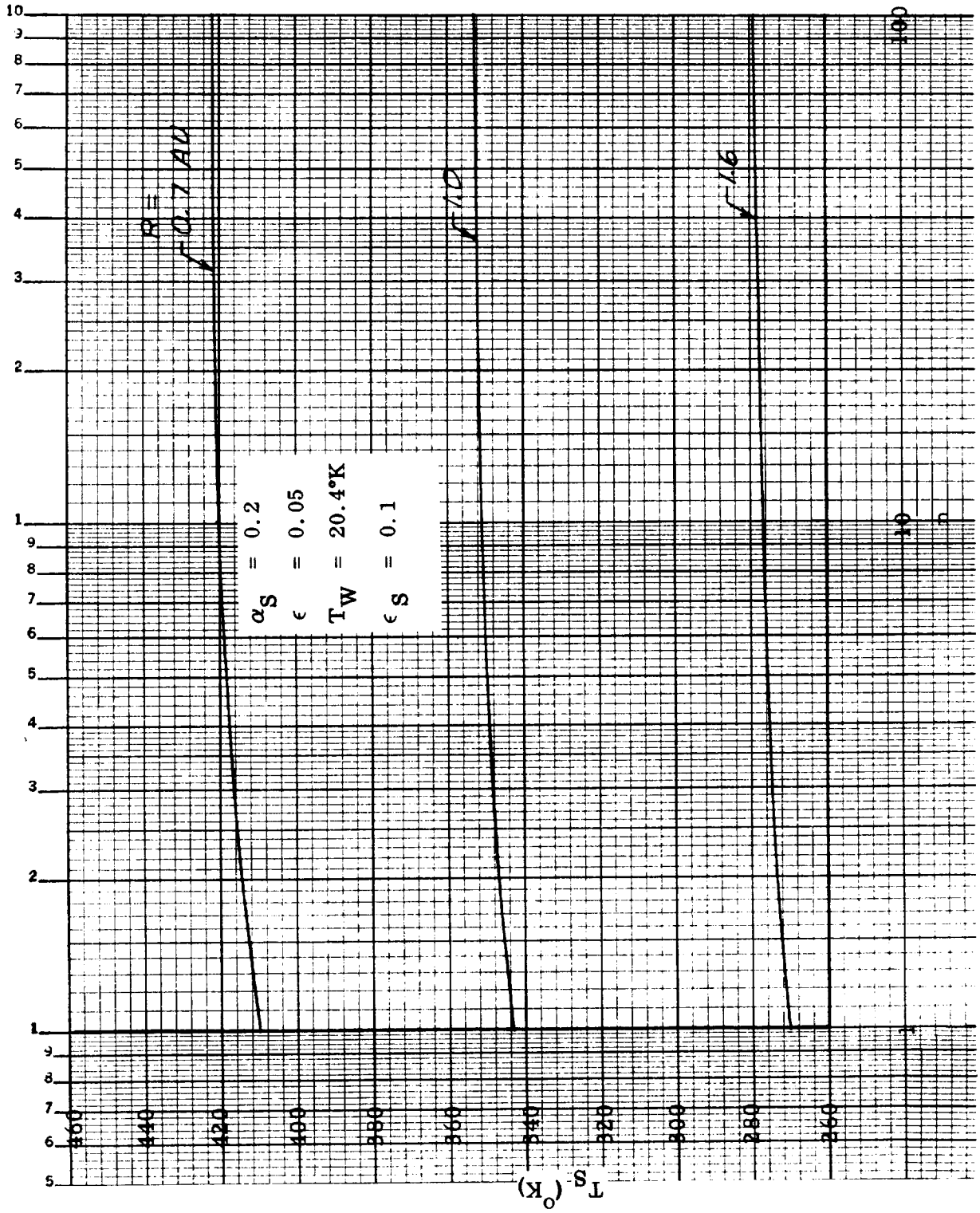

Figure 8-34. Surface Equilibrium Temperature Versus Number of Radiation Shields for Three Different Heliocentric Distances

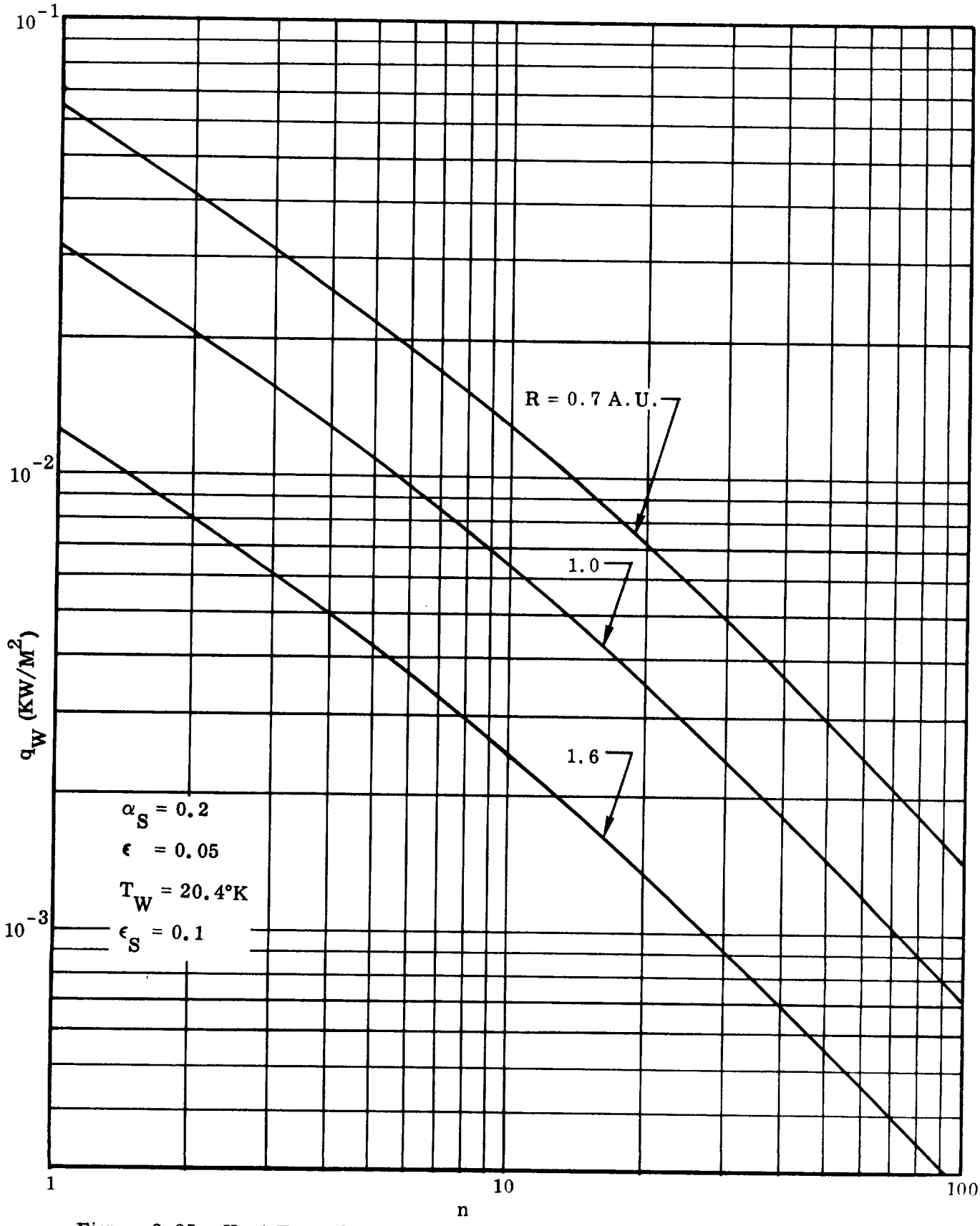

Figure 8-35. Heat Transfer Rate Across Hydrogen Tank Wall Versus Number of Radiation Shields for Three Different Heliocentric Distances

The value of k is plotted in Figure 8-36 and compared with the heat conductivity of various insulators.

The above value of q_w does not include the effect of heat conduction through spacers and other leaks. This heat influx can become considerable, but it is met very well accessible to evaluation until the vehicle design has sufficiently progressed.

Superinsulators consist essentially of a large number of radiation shields (up to 100). They are not open-ended as is envisioned for wrap-around radiation shields. Therefore, the space separating these shields minimizes conductive and convective heat transfer through the gas. Their specific weight is very low ($w_{sp} \approx 5$ lb/ft^3), whereas for wrap-around radiation shields the specific weight is approximately

$$w_{sp} \approx 0.1\ n\ (\text{lb/ft}^3) \tag{8-11}$$

The weight of the insulation is a function of its heat conductivity, time of operation, and the permissible boiloff, among other things:

$$\frac{w_{ins}}{S} = \frac{24\ k\ W_{sp}}{Q} \quad \frac{t_{(days)}}{W_{boil\text{-}off}/S} \quad (T_S - T_w) \tag{8-12}$$

where Q is the total heat absorbed to evaporate one unit weight of hydrogen, S is the surface area, and t is the time of operation.

Figure 8-37 shows the variation of solar distance and solar constant during a 410-day capture mission in 1972/73 according to the mission profile shown in Figure 8-38. The effect of the planetary irradiation has been neglected, because the value depends very much on distance or eccentricity of the capture orbit. This portion is roughly only 3 percent of the total accumulated mission value. The time integral of the solar constant for the mission is

$$\int_0^{410} S\ dt \approx 600\ \text{kw days/m}^2 \approx 55.8\ \text{kw days/ft}^2$$

Since 1 kw day = 20,600 K cal and since LH_2 absorbs approximately 125 K cal/kg (224.5 Btu/lb), this energy, which is offered to the space ship by the Sun alone, would evaporate $20,600 \times 600/125 \approx 100,000$ kg/m^2 = 20,400 lb/ft^2 during the mission, if the entire energy were absorbed by the vehicle. Since fuel tanks are jettisoned, the vehicle has no constant surface area or planform area. Figure 8-39 shows the hydrogen weight per unit surface area as indicated by the convoy vehicle design studies. It is

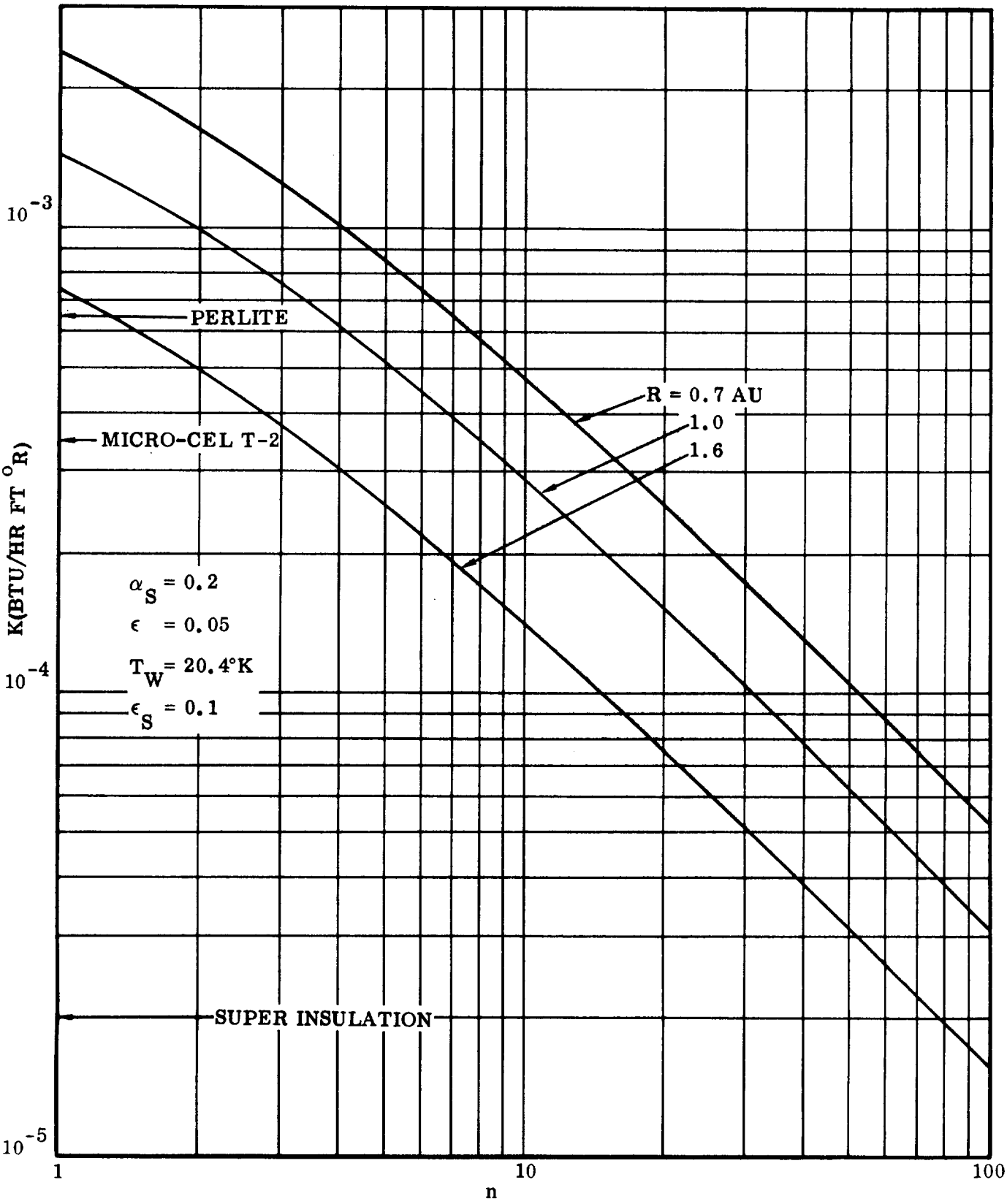

Figure 8-36. Effective Heat Conductivity of Radiation Insulation Versus Number of Radiation Shields for Three Different Heliocentric Distances

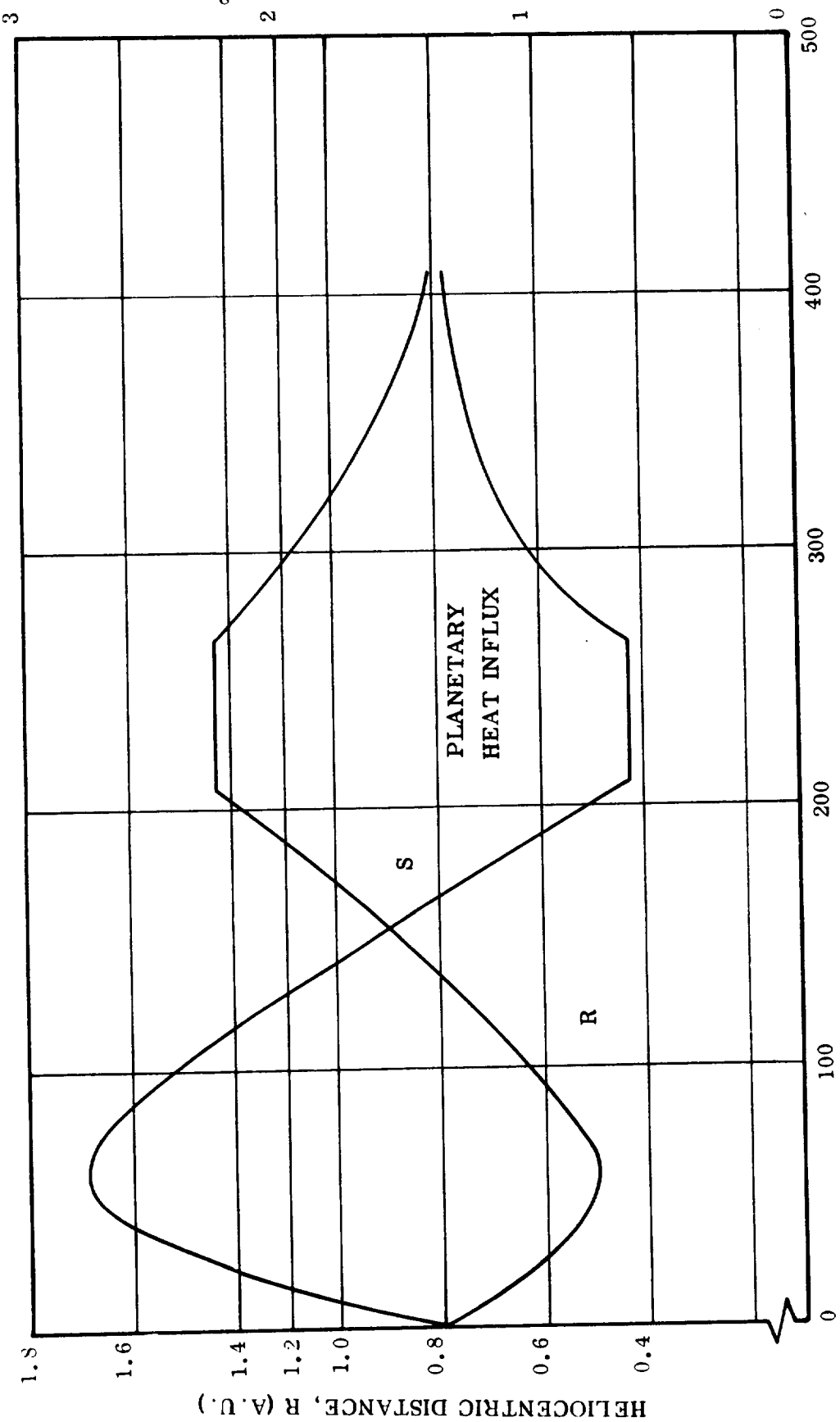

Figure 8-37. Distance and Solar Constant Variation During a 410-Day Capture Mission to Mars (1973)

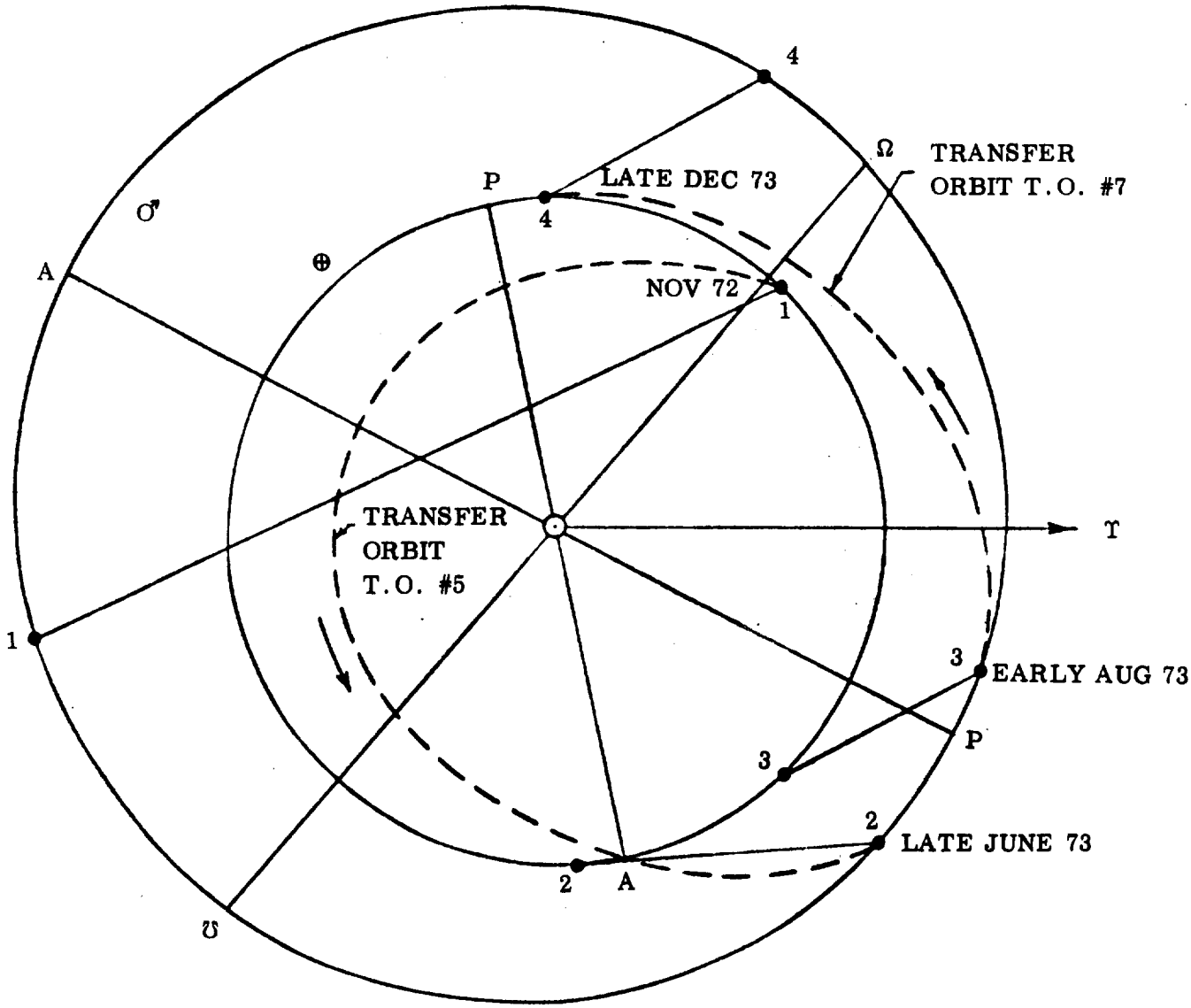

Figure 8-38. Characteristic Mission Profile (M.P. 57) for Mission Window of June-August 1973 Mars Capture

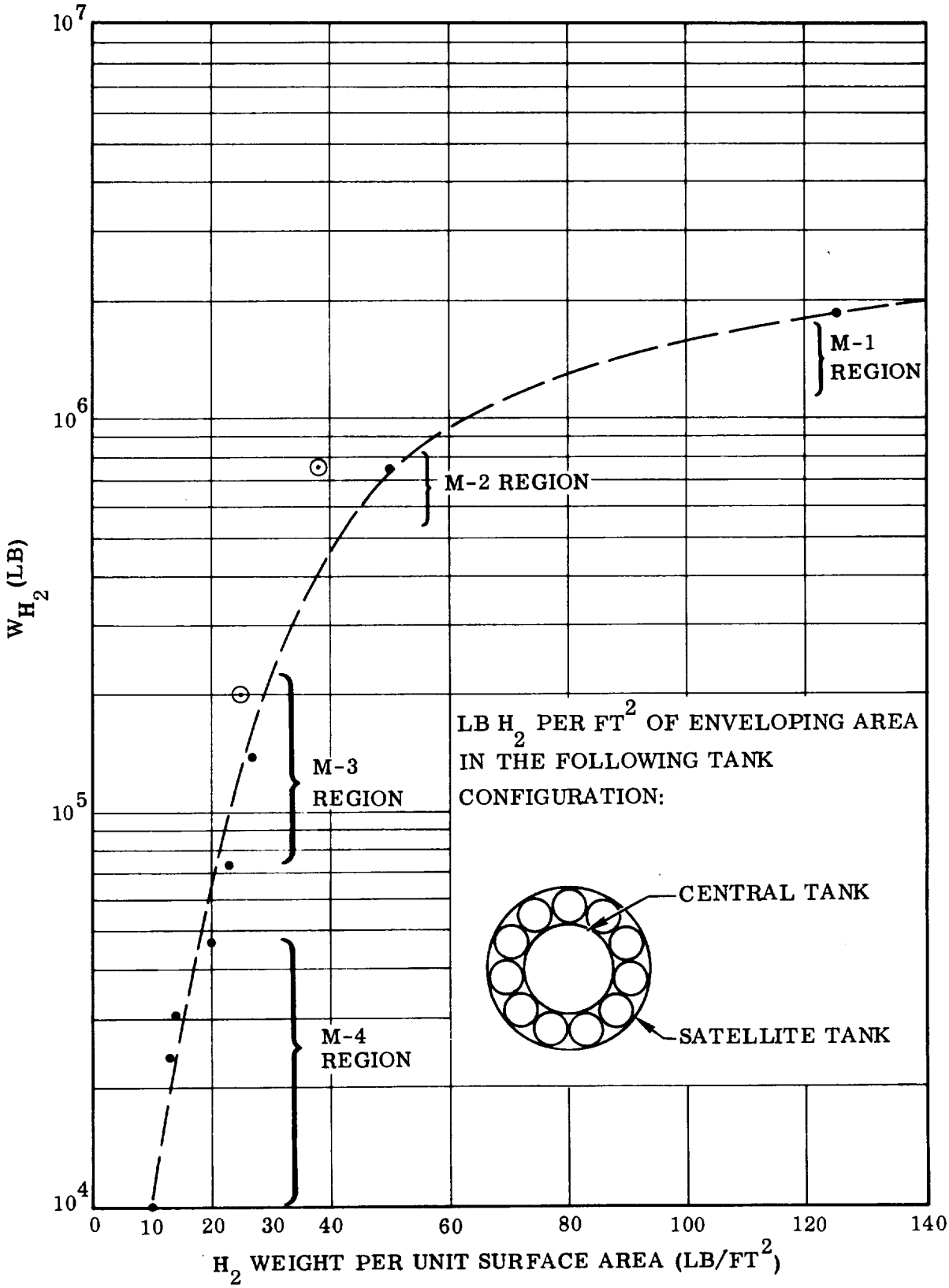

Figure 8-39. Hydrogen Weight Per Unit Surface Area In Convoy Vehicle Tanks and Tank Clusters

seen that the hydrogen weight per unit planform area is of the order of 25 to 45 lb/ft^2 for M-4, 50 to 85 lb/ft^2 for M-3 and 85 to 110 lb/ft^2 for M-2. For the M-2 tank section the storage time for the mission profile shown in Figure 8-38 is 210 days; for the M-3 tankage, 260 days; and for the M-4 tankage, 410 days. It is of importance to note that mission profiles which lead to a close perihelion passage on the outgoing leg show a disadvantage compared to those which have a perihelion passage on the return leg, because the former mission profile requires the protection of a much larger quantity of hydrogen (hence, of a larger surface area).

The first term in Equation 8-12) has the magnitude

$$\frac{24\, k\, w_{sp}}{Q} = \frac{24 \times 2 \times 10^{-5} \times 5}{224.5} = 1.07 \times 10^{-5} \quad \text{to}$$

$$\frac{24 \times 2 \times 10^{-5} \times 5}{250.1} = 9.6 \times 10^{-6}\ \frac{lb^2}{ft^4\ day\ °R}$$

for the two boundary cases of liquid and solid hydrogen. For a mean value of $T_S - T_w$ = 350°R and $W_{boiloff}/A$ = 1 lb/ft^2, the second term in Equation 8-12 becomes,

for M-2: $$\frac{t}{W_{boiloff}/A}\ (T_S - T_w) = 7.35 \times 10^4\ \frac{day\ ft^2\ °R}{lb}$$

for M-3: $$9.1 \times 10^4\ \frac{day\ ft^2\ °R}{lb}$$

for M-4: $$1.435 \times 10^5\ \frac{day\ ft^2\ °R}{lb}$$

Based on the data presented in Figure 8-39, an evaporation of 1 lb/ft^2 corresponds to an H_2 evaporation loss of 4 to 2 percent for M-4, 2 to 1.2 percent for M-3, and 1.2 to 0.9 percent for M-2. For these values, and under the other assumptions implied in the above numbers, the insulation weight becomes

for M-2: 0.79 to 0.705 lb/ft^2

for M-3: 0.975 to 0.874 lb/ft^2

for M-4: 1.59 to 1.38 lb/ft^2

for liquid and solid hydrogen, respectively.

The specific weight (W_{sp}) of 5 lb/ft^3 implies a total of approximately 50 radiation shields. Figure 8-36 shows that this number is approximately correct for 1 A.U., should be higher for R = 0.7 A.U., and could be lower for 1.7 A.U. This result implies the desirability of being able to vary the heat shield thickness (hence, its weight) consistent with the requirements for meteorite protection. The specific weight of 5 lb/ft^3 is about correct for the super insulation. Multiplying the above values by a factor of 1.2 for attachment and detachment provisions (the heat shield section covering the tanks about to be emptied in a main propulsion maneuver is jettisoned at the start of this maneuver), one obtains the weights shown in Figure 8-40 for the three propulsion sections as a function of the boiloff per square foot. For comparison, the average weight of the metal tank structure per unit surface is shown in Figure 8-41. The weight range obtained for the combined heat and meteoroid shield for various tank arrangements in convoy vehicles has also been indicated in Figure 8-40. The figure shows that the shields provide for an average H_2 boiloff loss of the order of 0.7 to 1 lb/ft^2 for M-4, 0.4 to 0.7 lb/ft^2 for M-3 and 0.35 to 0.5 lb/ft^2 for M-2. Absolute H_2 weights, H_2 boiloff weight losses, and percentage H_2 weight losses for the time period during which the shields are connected with the vehicle are as follows:

Propulsion Section	H_2 Weight Range (10^3 lb)	(10^3 kg)	H_2 Weight Loss (10^3 lb)	(10^3 kg)	Loss Range (Percent)
M-4	10-40	4.5-18.2	0.15-1.6	0.068-0.73	1.5-4
M-3	180-280	82-127	2.52-5.6	1.15-2.54	1.4-2
M-2	350-730	590-332	1.05-4.3	0.478-1.95	0.3-0.59

A loss of 1 lb H_2/ft^2 in M-4, which is carried through the entire mission period during which a total of 55.8 kw days/ft^2 is offered by the Sun (cf. Equation 8-12), corresponds approximately to 1/20,000 of the hydrogen evaporated if the entire solar radiation offered were absorbed by the (liquid) hydrogen. This is a very good insulation factor, but difficult to achieve in practice, since this figure neglects unavoidable heat leaks through conduction from hot or warm portions of the vehicle, the effect of shield damage and the possible cool-down losses for the nuclear engines. So many unknowns are as yet in the picture, with no firm design and operational sequence and with a variety of mission profiles still under consideration, that it is premature to arrive at firmer loss values at this time than those given above. In particular, an optimization of the trade-off between tank structure weight and insulation weight as functions of tank pressure remains to be made. Based on the hydrogen planform area loading (hydrogen weight per unit planform area) values given above, it is apparent that for a total loss of 1 percent, the H_2 boiloff losses must be kept to 0.25-0.45 lb/ft^2 planform area for M-4, to 0.5-0.85 lb/ft^2 for M-3, and to 0.85-1.1 lb/ft^2 for M-2. Assuming, as a representative value, that the "direct" boiloff loss (i.e., the loss caused by heat penetration of the radiation shield proper) is 0.67 of

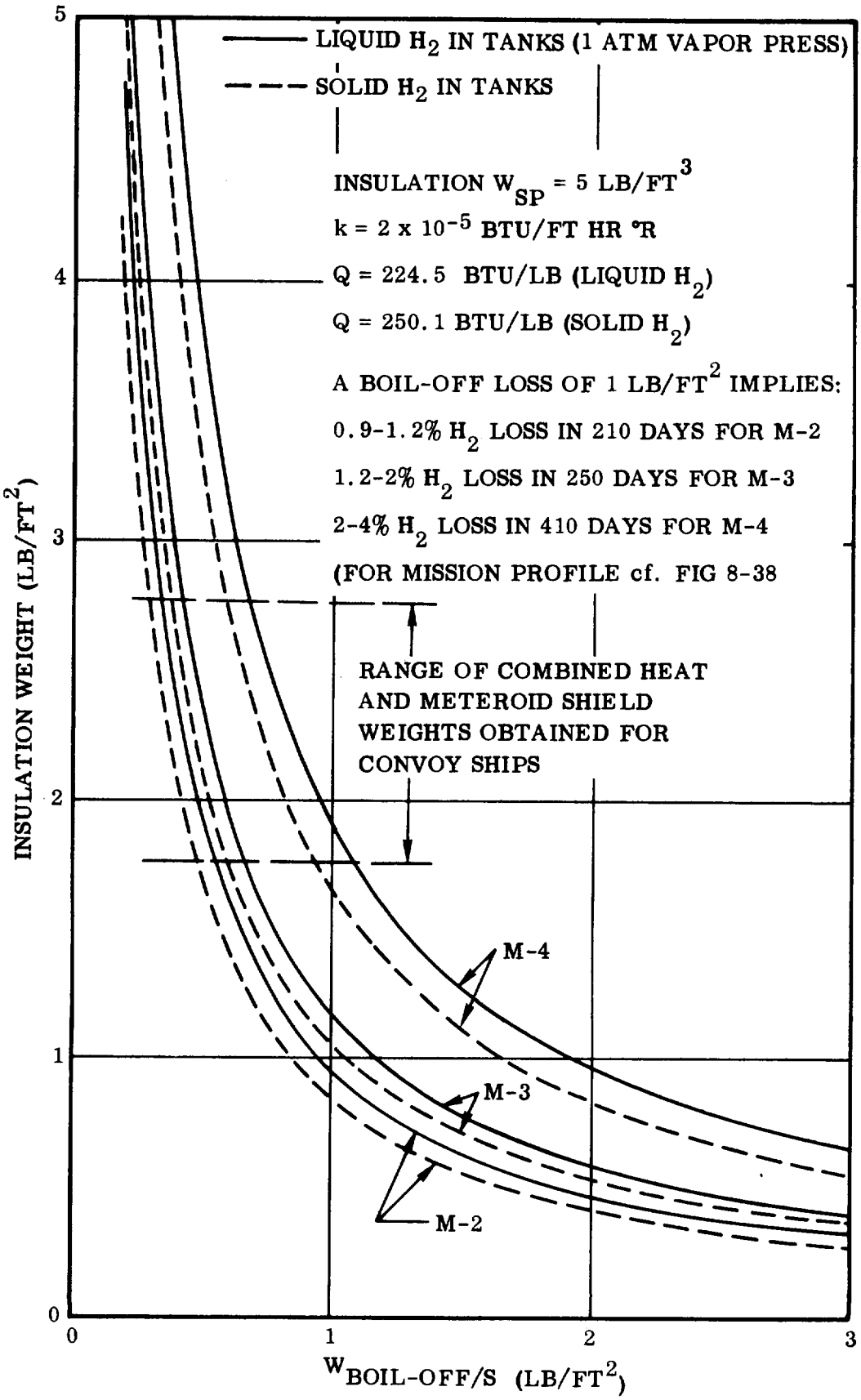

Figure 8-40. Variation of Heat Shield Insulation Weight Versus Boil-off Weight

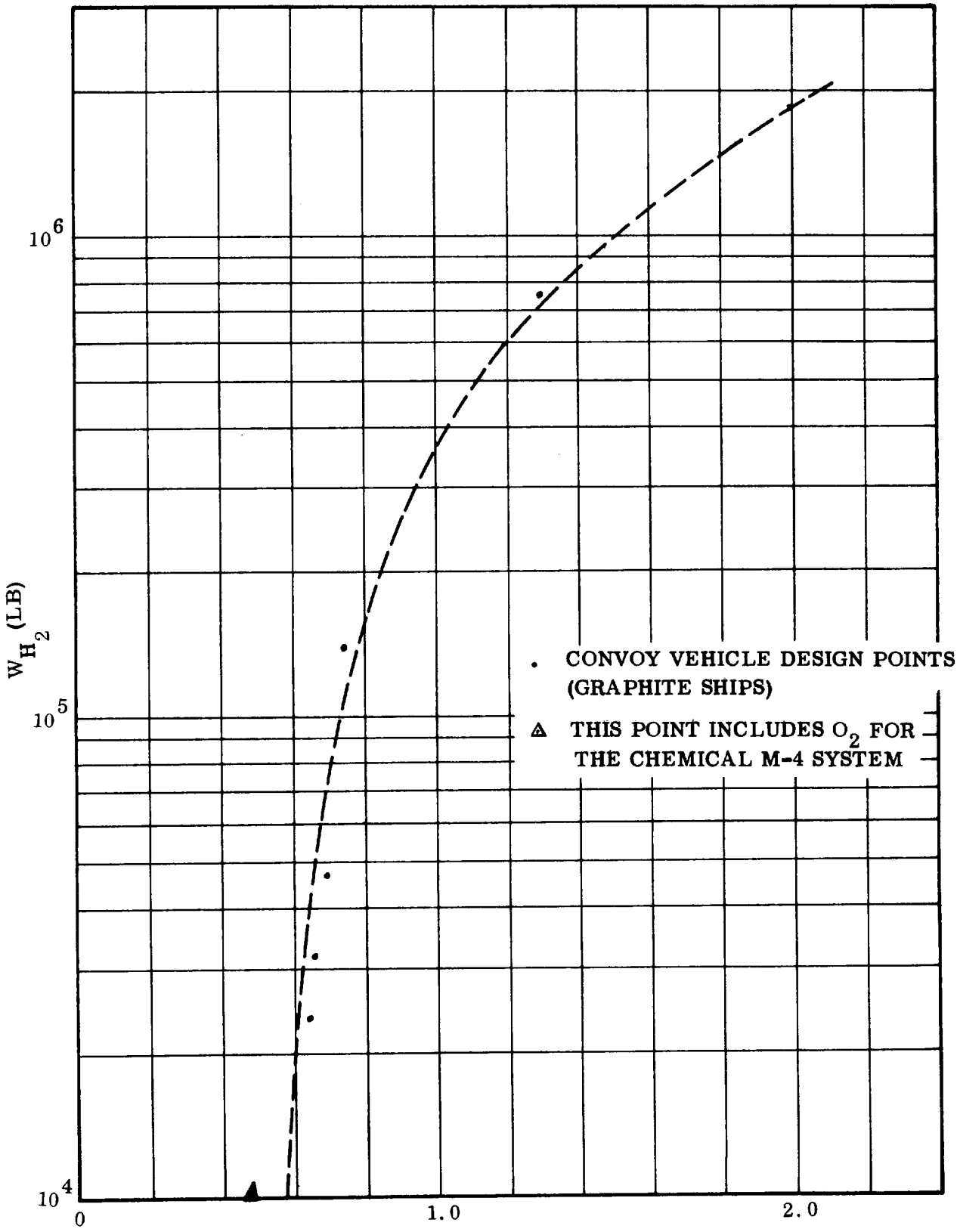

Figure 8-41. Metal Average Weight Per Unit Tank Surface Area in Convoy Vehicle Tanks and Tank Clusters

the total loss from all sources, it follows that the direct loss must be limited to 0.165-0.3 lb/ft^2 for M-4, to 0.3-0.56 lb/ft^2 for M-3, and to 0.56-0.725 lb/ft^2 for M-2. Inspection of Figure 8-40 shows that these objectives are not met for M-4 or for M-3, whereas the objective for M-2 appears to be met well. From this, and inspection of Figure 8-40, the following tentative conclusions can be drawn:

a. The thermal protection provided by a combination heat and meteoroid shield of the weight range indicated in Figure 8-40 is probably adequate, provided the heat conductivity of this shield can be kept in the range of $2 \times 10^{-5} \leq k \leq 2.5 \times 10^{-5}$ Btu/hr ft°R. In that case the meteorite protection requirements are the cominant factor for M-1.

b. The same combined heat and meteoroid shield is (thermally) probably insufficient for M-2 if the H_2 boiloff loss is to be kept at one percent of the total H_2 contained in the M-2 tanks at departure.

c. The same heat and meteoroid shield is inadequate for holding the hydrogen composition losses in M-4 to one percent of the M-4 hydrogen weight at departure.

d. The lower the boiloff per unit area is to be by means of heat shield insulation, the more effective it is to freeze or at least to sub-cool the hydrogen at departure. At $W_{boiloff}/S$ below 0.5 lb/ft^2 the difference in insulation weight required for initially liquid or initially solid hydrogen becomes very large.

8.14.4 Hydrogen Liquefaction. Figure 8-40 shows that if the direct losses are reduced for M-3 and M-4 to meet the requirements for a one-percent total loss, the insulation shield weight will rise sharply.

From the table in the preceding section it follows that a reduction of the direct loss to 0.67 percent means that the evaporation losses for M-4 and M-3 must be reduced by the following amounts:

M-4: 83-1330 lb (38-600 kg) or 0.2-3.2 lb/day (0.091-1.6 kg/day)

M-3: 1310-3730 lb (595-1700 kg) or 5.05-14.3 lb/day (2.2-6.5 kg/day)

With a heat of fusion and a hydrogen enthalpy difference between a liquid of zero and one atm vapor pressure of 14 K cal/kg (25.6 Btu/lb) and 12.55 K cal/kg (22.55 Btu/lb), respectively, or a total of Q = 26.55 K cal/kg (48.15 Btu/lb), the above daily evaporation rate corresponds to the following heat flux rates into the hydrogen:

M-4: 0.00415 Btu/day = 0.00105 K cal/day = 0.051 watt

M-2: 0.0665 Btu/day = 0.0167 K cal/day = 8.1 watt

Total: 0.7065 Btu/day = 0.0182 K cal/day = 8.151 watt

The evaporated hydrogen could be compressed isentropically, ducted into a radiator, condensed, and returned into the tank. However, since the radiator size varies inversely to the fourth power of the temperature, the radiator becomes unmanageably large and, in addition, seriously restricts the freedom of attitude of the convoy vehicle. In a heat pump system, higher radiator temperatures are possible.

An on-board heat pump system should be able to operate between 1 and 4 percent overall efficiency and would, therefore, require a power of between 0.2 to 0.82 kw.

With progressing cryogenic technology over the next ten years, flyable lightweight F_2, O_2 and H_2 liquefaction units will become feasible. One step in this direction is the proposal for a mobile hydrogen liquefaction unit made by Malaker and Daunt (Cross-Malaker Laboratories, Mountainside, New Jersey, "The Thermalord V-Engine Hydrogen Liquifier, a New and Novel Design of a Mobile, Hydrogen Liquefaction System," December, 1959). Their system, called Thermalord, is described as a continuously operating, high-efficiency, low-maintenance production unit. Although capable of producing 95 percent para-hydrogen, it can also be used as a closed-cycle hydrogen liquefaction unit without ortho-para conversion. When applied in this manner to re-liquify evaporated para-hydrogen in a spacecraft, the ortho-para conversion catalysts and associated plumbing can be omitted with corresponding gains in running economy and weight. A simplified flow diagram of the H_2 liquefaction unit is shown in Figure 8-42. The temperature and pressure levels are preliminary and may be subject to change after further study and development to optimize operating conditions. The system involves a closed hydrogen cycle which is repeatedly subject to partial liquefaction. In this form it reliquefies the hydrogen which evaporates in the storage tanks. Specifically, the system may operate as follows. The closed-cycle gaseous hydrogen (GH_2) is compressed from approximately 1 atm absolute to 15 atm by a compressor. The compressor head operates at a rejection temperature of 100°K. Crankcase and mechanical parts operate at higher temperature. The gas passes through Heat Exchanger I (H.E.I) to the Stirling cycle refrigerator where it is cooled to 32°K. The Stirling cycle refrigerator rejects at 100°K. The high-pressure gas then passes through the Joule-Thomson Heat Exchanger II (H.E.II) to the Joule-Thomson Expansion Valve at which about 50 percent of the H_2 is liquefied. The liquid hydrogen (LH_2) is ducted into the Evaporator-Interchanger in which the heat load of the evaporated GH_2, which is to be reliquefied, is absorbed. In this process the closed-cycle hydrogen is re-evaporated and is led through the low pressure side of H.E. I and II back to the compressor to start a new partial liquefaction cycle. The hydrogen (para-hydrogen) which evaporates in the storage tanks is ducted to the heat sink provided for it in the Evaporator-Interchanger. There it is liquefied at the inlet pressure at which it arrives from the tanks, then passes through a LH_2 pump to raise the pressure to the necessary liquefactor discharge pressure required to feed the LH_2 back into the storage tank. After emerging from the pump, the LH_2 is subcooled by a second passage through the Evaporator-Interchanger and subsequently leaves the liquefactor to be ducted back into the storage tank.

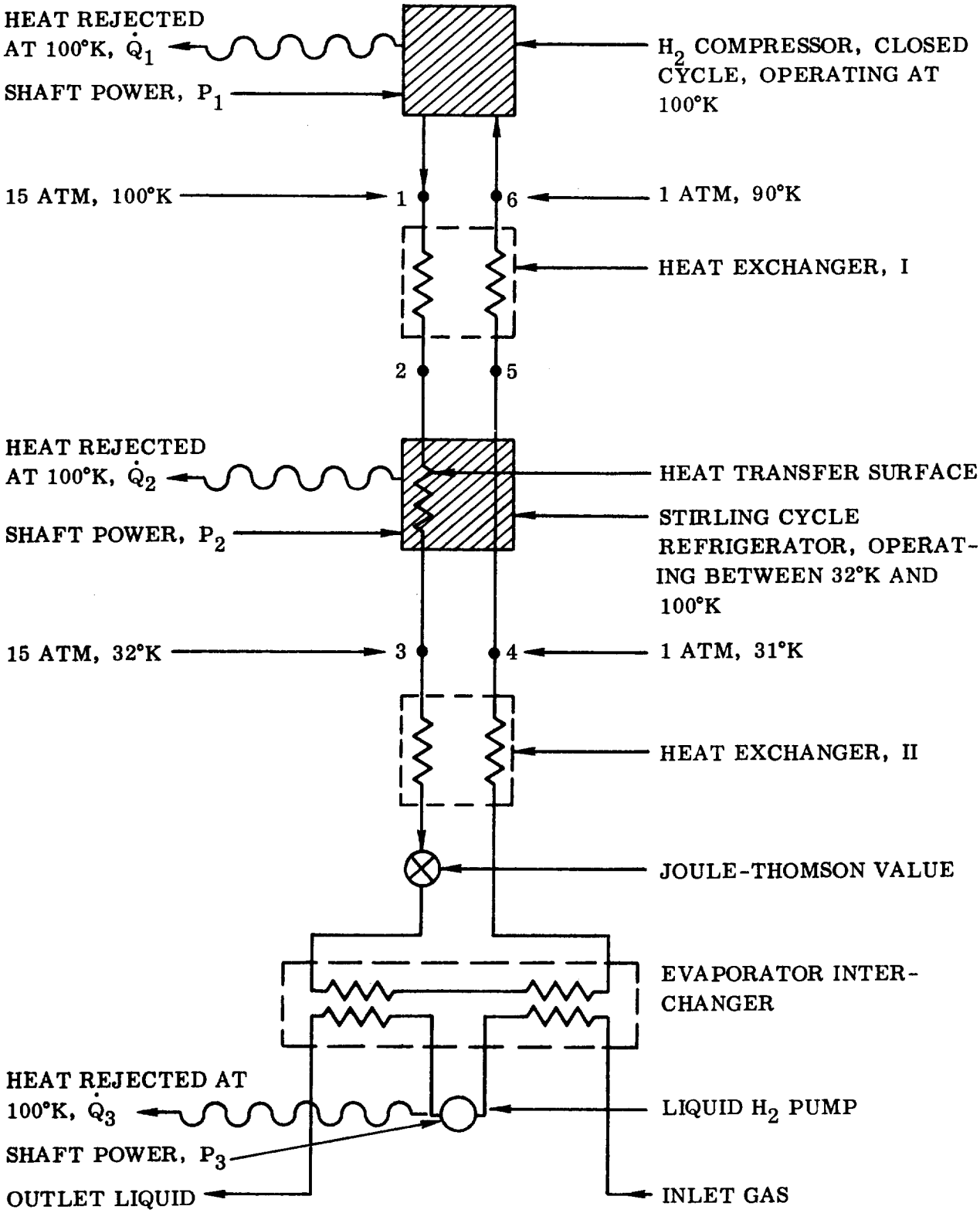

Figure 8-42. Simplified Flow Diagram of the Malaker-Daunt Thermalord H_2 Liquefaction Unit

Daunt and Malaker have made a preliminary analysis of liquefactor weight and power requirements for several capacities (lb GH_2 to be reliquefied per 24 hr). The results are presented in Table 8-6.

Table 8-6. Principal Data of Stirling Cycle H_2 Liquefaction Units

Capacity (lb (kg) H_2 liquefied in 24 hrs): 1)	50(22.7)	150(67.1)	300(136.5)
Estimated power requirements: 2)			
GH_2 flow through Compressor (scfm)	14.5	40	75
Shaft power, P_1, to Compressor (h.p.)	1.5	4.1	7.5
Heat rejected, Q_1, by Compressor at 100°K (kw)	0.45	1.2	2.1
Shaft power, P_2, to Stirling Refrigerator (h.p.)	3.6(2.25)	10(6.1)	18.6(11.4)
Heat rejected, Q_2, by Stirling Refrigerator at 100°K (kw)	3.1(2.0)	8.75(5.5)	16.5(10.2)
Liquefaction Coefficient at T value	0.5	0.5	0.5
Shaft power to LH_2 pump (h.p.)	0.15	0.15	0.15
Total shaft power (h.p.)	5.25(3.90)	14.25(10.35)	26.25(19.05)
(kw)	3.91(2.91)	10.6(7.7)	19.6(14.2)
Total heat rejected at 100°K (kw)	3.55(2.45)	9.95(6.7)	18.6(12.3)
Estimated weights (lb) and volumes (ft^3): 3)			
Compressor	120	200	300
Stirling Refrigerator	150	275	350
Heat Exchangers, Evaporator	250	350	450
LH_2 pump	30	35	40
Controls	100	100	100
Total weight (lb)	650 (450)	960 (760)	1190 (990)
Total volume (ft^3)	15	30	45

1) Numbers in parentheses are in kilograms.

2) Estimated power requirements are based on a relative efficiency of 20 percent for the Stirling Cycle Refrigerator. Numbers in parentheses are based on 33 percent. Actual efficiency is expected to lie between these two extremes.

3) Data are based on normal engineering practice. Numbers in parentheses are the anticipated figures to be obtained by the use of special lightweight materials.

Based on these data an analysis of the liquefaction system, using a higher heat rejection temperature (inlet temperature 300°K), has been made for a wider range of liquefaction capacities, especially in the direction of lower capacities. The results are shown in Figure 8-43. The total average liquefaction requirement indicated above is 8.1 kg/day. However, it is obvious that peak loads of two to three times this amount will occur. Therefore, the capacity of the liquefaction unit should be of the order of 22 kg H_2/24 hrs. The weight of this unit is approximately 900 lb (400 kg).

By comparison, M-3 at a representative planform area load of 75 lb/ft^2 and a representative hydrogen weight of 250,000 lb yields a planform area of approximately 3300 ft^2. The surface area is close to 14,000 ft^2. It is apparent that an increase in heat shield weight of even 1 lb/ft^2 adds many times the weight of the liquefaction unit. Actually, approximately 2 lb/ft^2 would have to be added to reduce the direct evaporation rate to 0.67 percent of the total. Therefore, a significant superiority of the liquefaction unit is indicated on the basis of weight alone.

The advantages of a spaceborne liquefaction unit are particularly apparent for long mission periods. Weight and power requirements impose certain limitations on its applicability in terms of a minimum vehicle weight in which such a unit can be conveniently carried and in terms of the vehicle's secondary power sources which must be large enough to provide the necessary power for the practically continuously operating liquefaction unit. With an increasing rate of evaporation, the refrigeration capability of the unit must grow likewise, drawing more electrical power. The over-all weight of this system increases rapidly, not only because of the weight of refrigerator unit and power source, but also because of the increasing radiator area which the electrical power unit needs as a result of its limited efficiency. For this reason alone (aside from the need for meteoroid protection) a combination of reflector shielding and refrigeration is most attractive in the majority of cases. The longer the storage time and the smaller the specific rate of evaporation, the more worthwhile will be the addition of a refrigerator unit.

It should be added that such units, if somewhat overdimensioned, will play an important role in emergency cases where, due to damage of reflector shield systems, the heat flux density increases to a critical extent. For weight minimization, an M-3 and a separate smaller M-4 unit could be considered. If regular or unexpected deterioration of the reflector shield system makes itself felt critically in the course of a manned interplanetary mission, the liquefaction unit which served the hydrogen tanks for the excape maneuver near the target planet would be retained, rather than jettisoned, to handle the increased evaporation rate in the Earth capture tank.

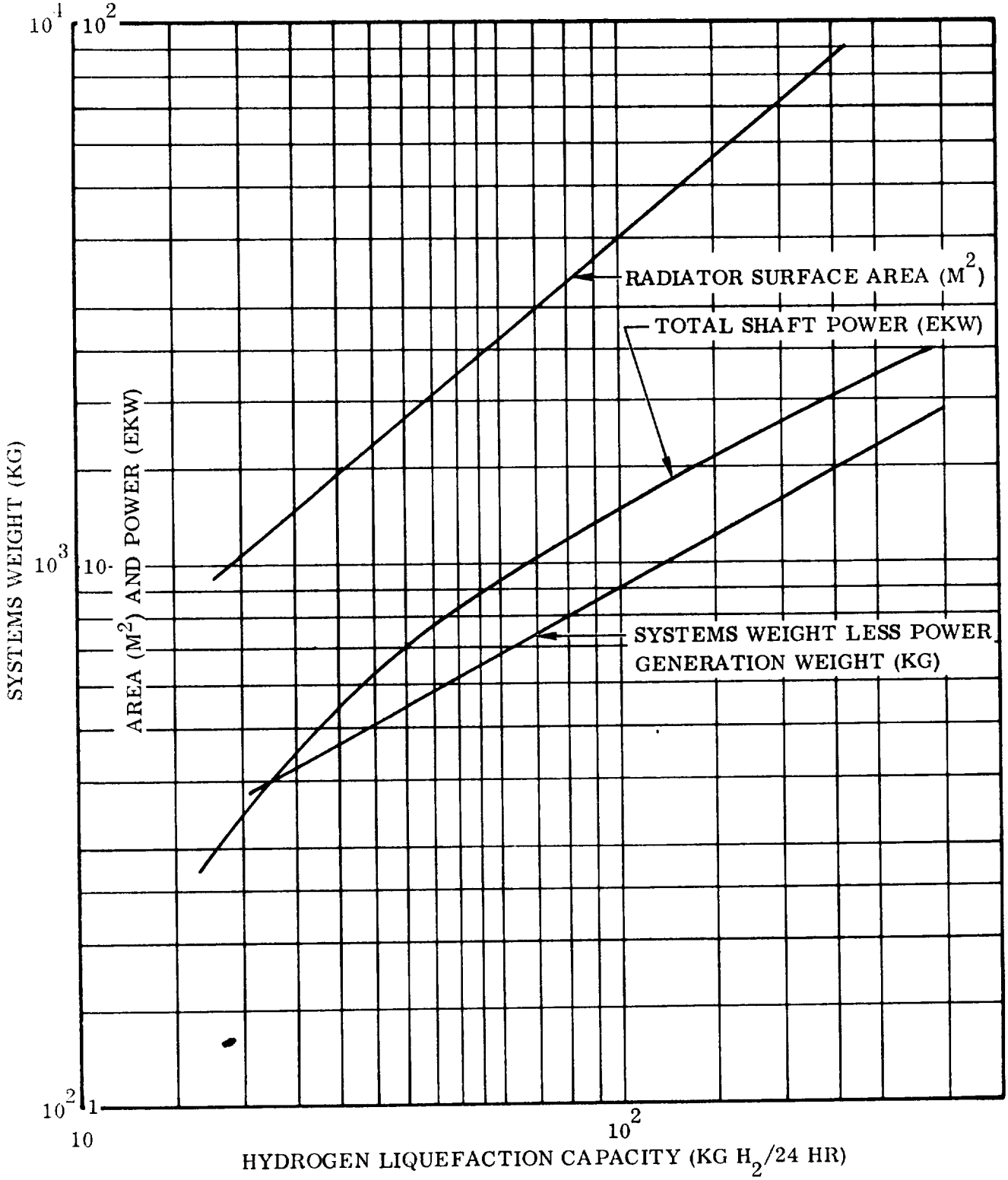

Figure 8-43. Hydrogen Liquefaction Systems Data (Stirling Cycle)

8.14.5 Shadow Shielding. Shadow shielding offers added flexibility by providing easily jettisonable radiation heat protection at periods of peak radiative heat flux. Referring back to Figure 8-37, it can be seen that for mission profiles of this type a shadow shield during the outgoing transfer would make the addition of a liquefaction unit to M-3 unnecessary since, in the shadow, the combined heat and meteorite protection shield would be amply adequate. The shadow shield could in this case be jettisoned prior to M-2 and would, therefore, not affect the mass ratio of any maneuver except M-1. An important benefit of the shadow shield lies in the fact that it connects the incident solar radiation to infrared radiation which can be reflected by the tank insulation far more effectively than the blue, violet, ultraviolet and X-ray portion of the solar spectrum.

A few shadow shield configurations are shown in Figure 8-44. The shield system in Figure 8-44(a) is located at some distance from the tank and faces the radiation source with a plane foil (front foil, Figure 8-45) which is highly reflective on both sides. The radiation emitted by the inside illuminates a V-shaped second foil (V-foil) which also is highly reflective on the inside and outside. The V-foil will therefore reflect most of the incident infrared radiation into the inside and emit very little radiation through the surfaces facing the cryogenic tank. The reflective energy is absorbed by a black foil occupying the center plane of the V-shaped interior. The equilibrium temperature of the black foil is higher than that of the V-foil. Acting as a heat source, it extends into the shadow side behind the V-foil from where its black surface readily emits thermal radiation essentially in the direction normal to the direction of the cryogenic tank. By draining the heat out of the triangular space in this manner with a highly conductive black foil, the interior portion of the black foil is cooled, re-radiation back to the V-foil is minimized; therewith, the temperature and radiation intensity of the outside of the V-foil (toward the tank) is kept low. Although the planes of the V-foil are inclined with respect to the line of sight to the tank, thereby reducing the configuration factor of these planes, the configuration factor of the black foil is still smaller. The black foil, therefore, represents the logical place for radiating the energy into space. Countless reflections resulting in gradual absorption of the entire initially absorbed energy by the concentric shield system is thereby avoided. The initially absorbed heat of the front foil is re-radiated into space as promptly as possible, in a direction which minimizes illumination of the tank. The comparatively largest emitting area facing the tank is the outside of the V-foil. Due to its inclination, the configuration factor is reduced. It could be further reduced by reducing the apex angle, but this can be done only at a weight penalty, since not only the area of the V-foil but also of the black foil increases. In general, the configuration factor of the V-foil is less important than that of the black foil, since the former turns a highly reflective surface to the tank, and hence emits very little radiation in the first place. The outside of the V-foil is somewhat illuminated by the black foil. Again, the configuration factor is small. Radiation from the black foil is at a low incidence angle. The radiation is infrared and is almost entirely reflected away from the tank by the V-foil. The tank is shielded from black foil by a small vertical end foil.

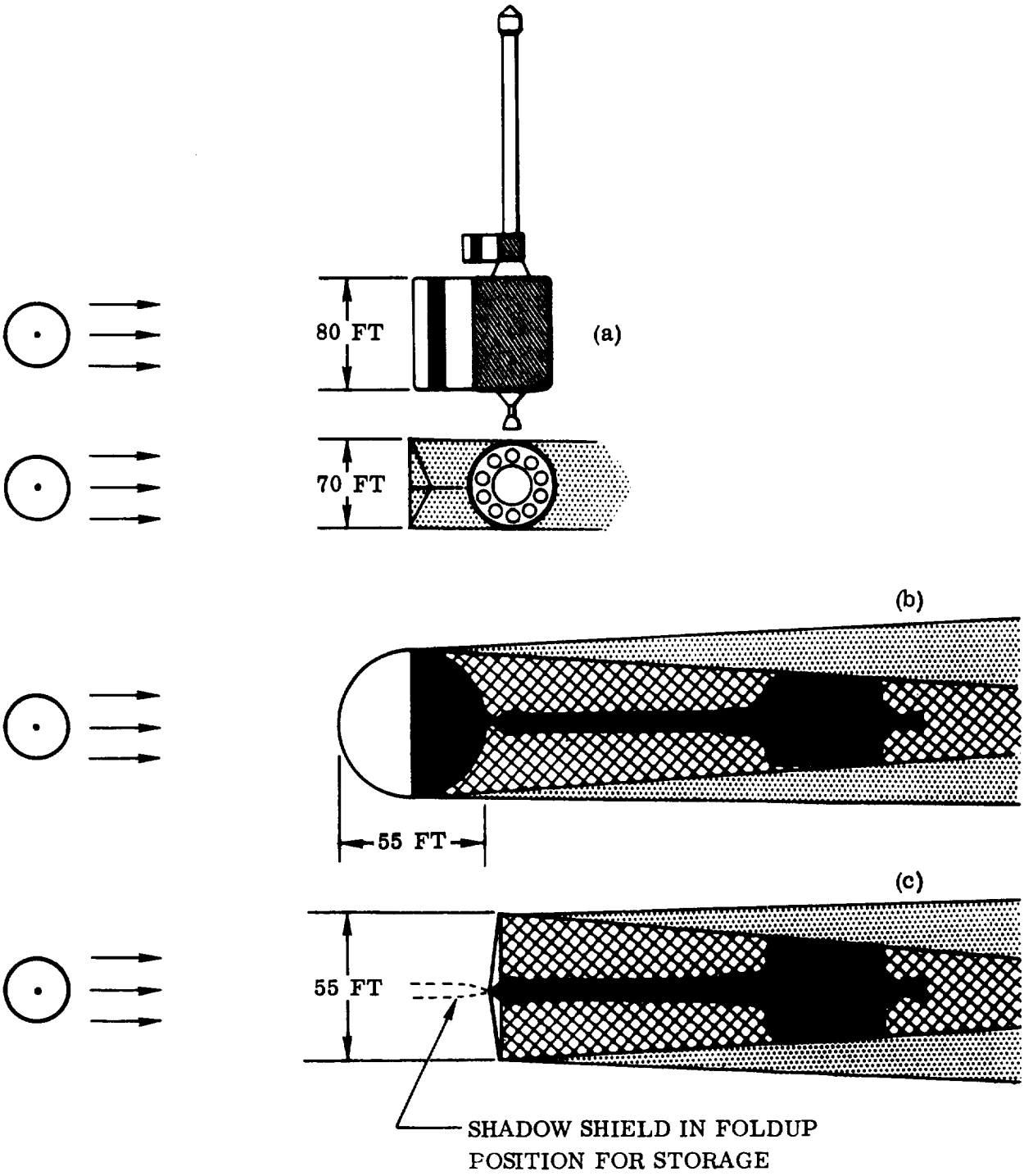

Figure 8-44. Three Shadow Shield Configurations

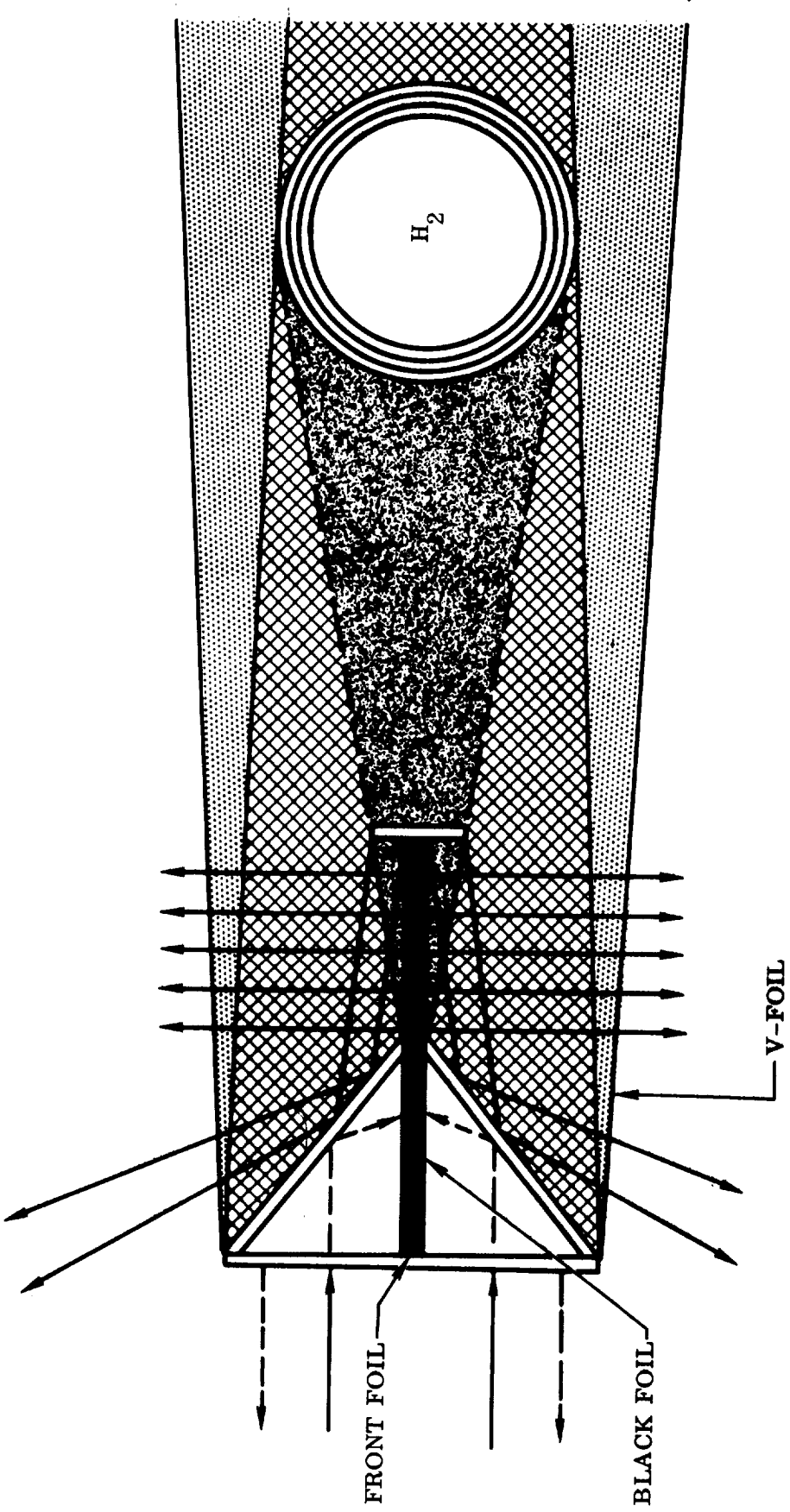

Figure 8-45. Shadow Shield

There remains some radiation directed toward the cryogenic tank. It comes from the V-foil. It is infrared radiation, sharply reduced in intensity below the amount of radiation which a third or even a fourth foil would receive in a concentric shield system. The shadow shield of the type shown in Figure 8-44(a) does not necessarily probibit tumbling of the space ship, provided it is roll controlled. If the weight of the shadow shield described above is too high, a simpler shield, consisting of the front foil only, can be employed as an effective shield system.

Simpler configurations are shown in Figure 8-44(b) and (c). It was not possible in the available study period to evaluate shadow shield systems in relation to insulation and hydrogen liquefaction systems.

8.15 SCIENTIFIC PAYLOAD WEIGHT AND POWER ESTIMATES FOR AUXILIARY VEHICLES

8.15.1 Introduction. Each Mars and Venus convoy is provided with a complement of auxiliary vehicles which carry much of the scientific instrumentation for making measurements in interplanetary space and in the vicinity of the planet. The types of auxiliary vehicles for the Mars and Venus missions are listed in Table 5-5, Section 5.

In addition to equipment carried by auxiliary vehicles, some instrumentation is installed on convoy vehicles, as described in Section 8.15.3.

8.15.2 Marens and Venens. Environmental satellites are placed in elliptical orbits about the planet, one each as follows: a) equatorial, b) 45° inclined, and c) polar orbit. The same three types of orbits are used for both Mars and Venus; in the latter case, if the pole of rotation is not established then the orbital plane of Venus is arbitrarily assumed to be its equatorial plane. Elliptical eccentricity is selected to put the periapsis below the trapped radiation belt and somewhat above the sensible atmosphere, and the apoapsis well above the radiation belt.

Since at present there is no direct evidence of the presence or intensity of trapped radiation belts for Mars or Venus, it is proposed for the present that instrumentation be assumed which is suitable for terrestrial environment.

Table 8-7 lists nine proposed experiments which are derived in part from experiments currently under development for the Arents satellite which is being built for ARPA by GD/A, and in part from earlier study of the Prospector vehicle requirements for lunar exploration.

Table 8-7. Marens and Venens Scientific Experiments

	NAME	WEIGHT (LB)	POWER (WATTS)
1.	Electrostatic spectrometer	8.2	2.00
2.	Electron scintillation spectrometer	8.8	1.00
3.	Proton scintillation spectrometer	12.1	1.00
4.	Low energy ionization chamber	7.3	1.44
5.	High energy ionization chamber		
6.	Cerenkov counter	15.0	2.00
7.	Modified boron trifluoride counter	18.0	0.93
8.	Micrometeorite gage*	3.0	0.50
9.	Magnetometer	7.0	4.00
	TOTAL	79.4 LB	12.87 WATTS

Weight and power estimates are based on current or recent state-of-the-art designs. Figure 8-46 shows the energy range of radiation detectors No. 1 to 7 for measuring electrons, protons, heavy nuclei, and neutrons.

Table 8-8 lists weight and power requirements for Marens and Venens components. It is assumed that orbital injection is provided by a separate booster, not specified. Estimates are based in part on Arents design, with modifications to allow for the greater communication distance (Mars or Venus to Earth) compared with Arents distance to Earth, and for the lesser solar cell irradiance in both cases, compared with Arents distance to the Sun.

For Marens, the distance of 1.67 A.U. at Mars aphelion leads to a factor of $(1/1.67)^2$ or 0.359 times Arents solar irradiance; for Venens, the possibility of requiring an Earth-Venus trajectory which extends in part as far as 1.2 A.U. from the Sun leads to a factor of $(1/1.2)^2$ or 0.694 times Arents solar irradiance.

Table 8-8 allows 50 watts for telemetry transmitter and signal conditioner, about three times the Arents requirement. Considerable redesign is required to provide adequate communication with such a modest power increase. The improvements include a) changing frequency from 136 MC to 2200 MC, b) providing greatly increased gain for satellite-borne and Earth-based antenna, c) making satellite antenna directional, d) redesign signal conditioner, etc. Not allowed for in Table 8-8 is a redesign of the solar cell system to provide paddle orientation towards the Sun (not in present Arents), which permits about a factor of 4 improvement via power production, but which also requires an additional weight (not yet evaluated) for paddle control.

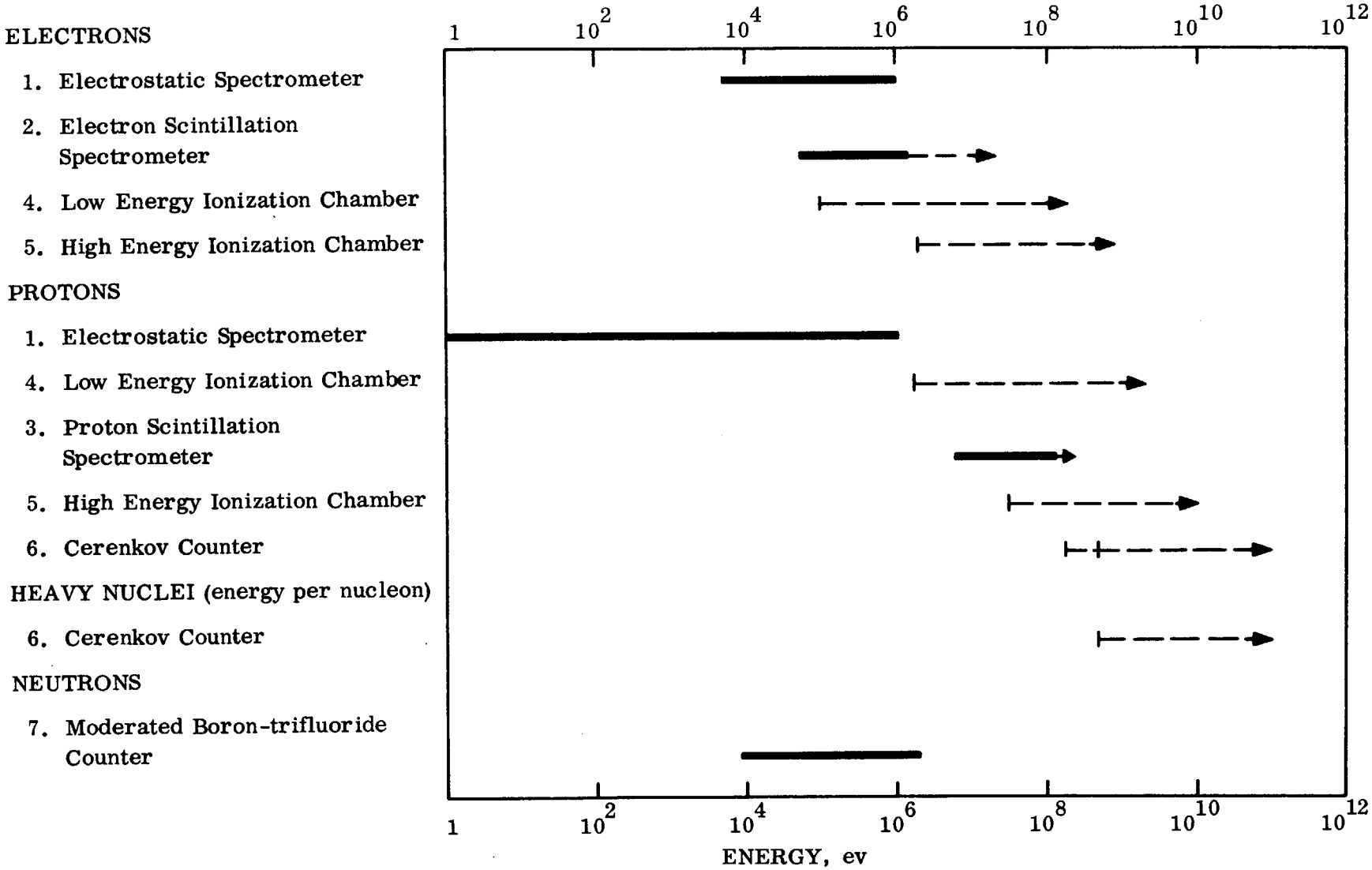

Figure 8-46. Energy Range of Nuclear Radiation Detectors

Table 8-8. Weight and Power Requirements Summary for Marens and Venens

	MARENS			VENENS		
COMPONENT	WEIGHT	LB	POWER (WATTS)	WEIGHT	LB	POWER (WATTS)
Structural		97			82	
Satellite body	40			35		
Solar paddle mechanism	30			20		
Experiment supports	5			5		
Magnetometer boom system	22		5	22		
Electrical		375			215	
Solar cell battery, including substrate	300			150		
Storage battery	40			30		
Converter/regulator	20		13	20		13
Switches and timer	5			5		
Wiring	10			10		
Telemetry		174			174	
Transmitter	20		50	20		50
Signal conditioner	13			13		
Recorder system	20		5	20		5
Antenna System	100		5	100		5
Transducers	1			1		
Wiring	20			20		
Aspect indicator		5			5	
Scientific experiments		80	13		80	13
TOTAL		731	91		556	91

AOK63-0001

8.15.3 C^2 (Convoy Companion) Probe and CSV (Convoy Service Vehicle) Probe. The scientific experiments provided for Marens and Venens are also operated in interplanetary space, with essentially the same weight and power estimates for each experiment as shown in Table 8-7.

A summary is provided in Table 8-9 of the weight and power requirements for C^2. It is assumed that the same experiments are carried as in Marens and Venens, but communication is required only to the convoy spacecraft, so a telemetry capability is assumed comparable with Arents design. However, the same solar cell irradiance factors discussed in Section 8.15.2 must be applied to solar cell requirements. Since no planetary shadowing is experienced, a storage battery is omitted. The propulsion system and its guidance components are not included.

Table 8-10 is a summary of weights and power requirements for the same group of experiments, carried as a probe installed on booms attached to the CSV. Power is supplied by cables from the CSV, and data are provided directly to the CSV by cable; both cables are contained within the boom system.

8.15.4 Deipro and Phopro (Deimos Probe and Phobos Probe). Impact probes of the Ranger-Surveyor type are directed toward the Martian satellites Deimos and Phobos. The choice between "hard," "rough," and "soft" landing must be based on the weights and capabilities of the respective required propulsion and guidance systems. It is assumed here that only hard or rough landings of the Ranger type are attempted.

Scientific experiments include magnetometer, telescope and camera for surface viewing, gamma ray spectrometer for detection of surface radioactivity, and seismometer. Only the seismometer is designed to survive the impact by separate packaging with a retrorocket and balsa wood impact-limiting cushion. The corresponding landing capsule for Ranger, including telemetry, propulsion system, batteries, and auxiliary mechanisms, weighs 300 pounds.

8.15.5 Lander. The Mars Lander is similar in objectives to Surveyor. Its purpose is to make a soft landing on selected sites of Mars and report environmental conditions to the orbiting convoy spacecraft. It most important experiment is the optical viewing system, consisting of television cameras with varied fields of view. The Surveyor TV system utilizes five separate cameras and requires 11 watts.

Table 8-11 lists suggested scientific experiments and equipment for Mars Lander. The total power requirement of 240 watts is not required at any one time; the peak load is approximately 100 watts. Additional tabulation of other Lander components is not yet completed; by comparison with Marens (based on solar cell provision of electrical power), Lander weighs about 4,000 pounds exclusive of propulsion, guidance, and special landing equipment.

Table 8-9. Weight and Power Requirements Summary for C^2 (Convoy Companion)

	MARS			VENUS		
COMPONENT*	WEIGHT	LB	POWER (WATTS)	WEIGHT	LB	POWER (WATTS)
Structural		72			59	
Satellite body	30			21		
Solar paddle mechanism	15			11		
Experiment supports	5			5		
Magnetometer boom system	22		5	22		5
Electrical		123			76	
Solar cell battery, including substrate	100			53		
Converter/regulator	8			8		
Switches and timer	5			5		
Wiring	10			10		
Telemetry		33			33	
Transmitter	4		17	4		17
Signal conditioner	13			13		
Antenna system	1			1		
Transducers	1			1		
Wiring	14			14		
Scientific experiments		80	13		80	13
TOTAL		308	35		248	35

*NOTE: Requirements are not included for propulsion (compressed gas) system and guidance system (including attitude intelligence, autopilot).

Table 8-10. Weight and Power Requirements Summary for CSV (Convoy Service Vehicle) Probe

COMPONENT	WEIGHT LB	POWER (WATTS)
Structural	86	
Probe body	15	
Experiment supports	5	
Probe boom system	44	10
Magnetometer boom system	22	5
Electrical	43	
Converter/regulator	8	
Switches and timer	5	
Wiring	30	
Scientific experiments	80	13
TOTAL	209	28

Table 8-11. Mars Lander Scientific Experiments

	WEIGHT (LB)	POWER (WATTS)
Optical		
Color comparator	5	5
Albedo meter	1	0.1
Spectroscope	40	10
TV Camera system	10	11
Electrical		
Electrical permittivity meter	1	0.1
Conductivity meter	1	4
Electric field meter	2	0.1
Magnetometer	7	4
Magnetic susceptibility meter	3	0.1
Metal particle detector	10	1
Mechanical		
Gravimeter	5	2
Seismometer	8	4
Hardness meter	1	10

Table 8-11. Mars Lander Scientific Experiments, (Continued)

	WEIGHT (LB)	POWER (WATTS)
Trafficability meter	2	10
Micrometeorite gage	3	0.5
Atmospheric pressure gage	1	0.1
Core drill	50	100
Sample scales	6	3
Mechanical arm and hammer	25	20
Sample transport system	5	5
Thermal		
Thermometer	1	0.1
Change of state test	1	1
Specific heat test	1	1
Conductivity test	2	20
Radiation		
Same as Marens	70	8.4
Biochemical	150	20
TOTAL	411	240.5

As a first approximation, a Venus Lander has the same purpose as a Mars Lander. Because of the more unfavorable environment on Venus, such as much higher surface temperature and pressure, it is not possible to undertake the same range of environmental experiments withou giving the Lander additional protection, including heat insulation, air conditioning, and provisions against wind damage (toppling, hard landing, dust bombardment). It is possible that Venus measurements to be made during the next decade will verify the presence of an environment so hostile that no suitable soft landing can be attempted. Prior to landing a complicated surface probe, a more rugged probe, similar to Ranger, is landed.

8.15.6 Mars Mapper. The principal function of the Mapper is the determination of Martian surface features in the maximum possible detail. The Mapper obtains data on the following characteristics:

a. Gross topography and surface inclination.

b. Surface topography with highest resolution (visible light, preferably in color).

c. Surface topography with lower resolution (infrared and ultraviolet light).

Resolution in the visible spectrum should be of the order of 1 to 100 meters (3 to 300 feet). Lower resolution photography is also required for gross identification and relative location of high-resolution details.

Additional related measurements are also provided by the Mapper. These include certain meteorological and aerophysical data, such as surface albedo, atmospheric opacity at various wavelengths, surface temperature, and meteorite measurements.

The bulk of the mapping data is stored or transmitted to Earth for subsequent analysis. Only those portions which are needed for on-the-spot decisions, such as data for possible landing sites, are extracted and presented to the crew for immediate analysis.

For reasons of maximum control and reliability, the Mapper remains connected with the Crew Vehicle during the capture period about Mars. Access is provided for repairs or adjustments, and data transmission is simplified between the Mapper optical system and the Crew Vehicle data storage system. Prior to Mars departure, the Mapper is released in orbit and continues to send data to the departing convoy and eventually to Earth, at reduced resolution.

8.15.6.1 Mars Mapper Orbits. For most effective mapping, the Mapper requires a polar orbit. A circular orbit at an altitude y = 662 km (357 n. mi.) has the following characteristics:

$$r/r_{oo} = 1.2$$

$$r = y + r_{oo} = 3972 \text{ km}$$

$$T = 2\pi \sqrt{r^3/K} = 7.593 \text{ sec} = 2.109 \text{ hr}$$

$$n = 24.623 \text{ hr (Mars day)}/T = 11.67 \text{ rev./Mars day}$$

where

r = radius of Mapper orbit

r_{oo} = radius of Mars = 3310 km

T = sidereal period of Mapper

K = gravitational constant = 4.2906×10^4 km^3/sec^2

n = number of Mapper revolutions/Mars day.

The plane of the Mapper orbit is oriented to make an angle of approximately 45 degrees with the radius vector between Mars and the Sun in order to provide shadow detail for map interpretation (Figure 8-47). Thus, either midmorning or midafternoon illumination is obtained.

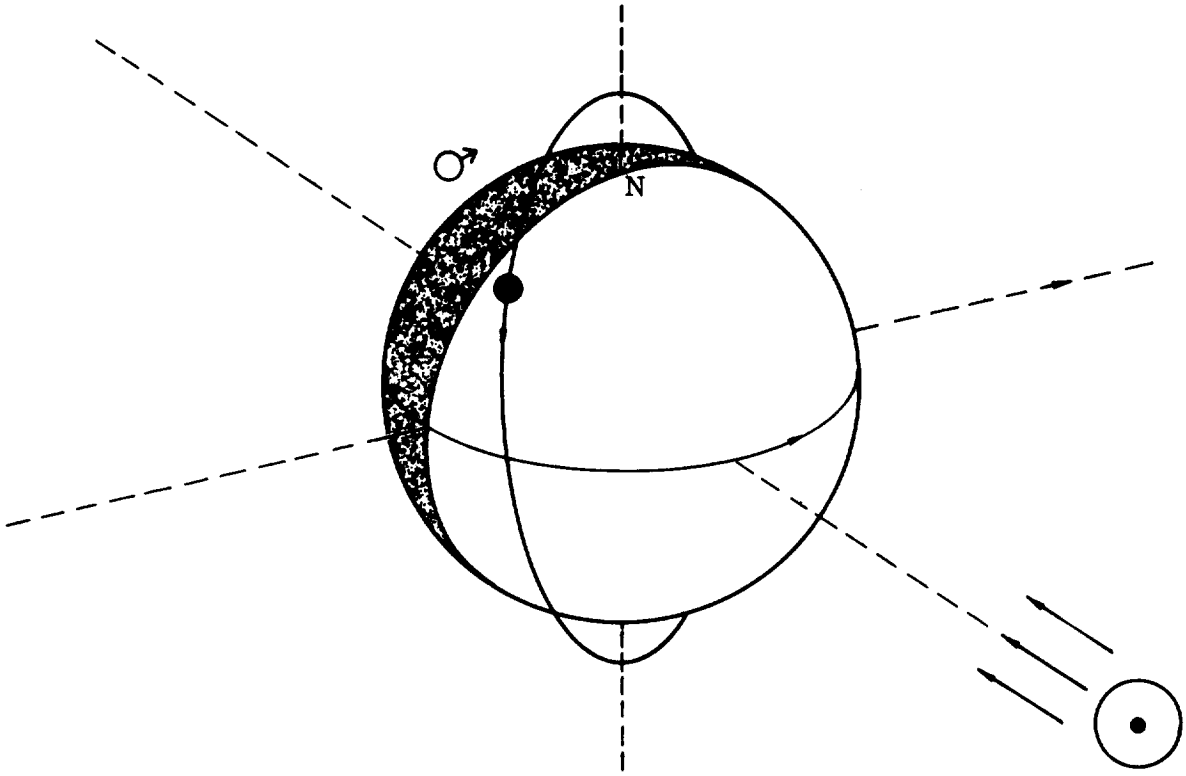

Figure 8-47. Mars with Mapper ● in Polar Orbit at $r/r_{oo} = 1.2$ (y = altitude = $0.2\ r_{oo} = 662$ km). Solar ⊙ illumination at 45° with Mapper orbit plane (mid-morning shadows). Inclination of polar axis (25.2°) not shown.

In the midmorning case, to allow for daily advance in shadow angle as the mapping proceeds, the Mapper orbit is started with its plane at an angle with the solar radius vector somewhat smaller than 45°, and the mapping ends with the angle an equal amount larger than 45°. With midafternoon illumination the sequence is reversed. For a mapping time of 50 Earth days out of the Martian year of 687 days, the total angle advanced is $(50/687) \times 360° = 26.2°$, so that the angle varies between $45° + (26.2°/2) = 58.1°$, and $45° - (26.2°/2 = 31.9°$. For an alternative mapping time of 10 days, the angle advances by $(10/687) \times 360° = 5.2°$, so that the angle varies between $45° + (5.2°/2) = 47.6°$, and $45° - (5.2°/2) = 42.4°$.

8.15.6.2 Mars Mapping. For a Mapper sidereal period of the order of two hours, the separate strips of Martian surface of constant width w ($w << 2\pi r_{oo}$ = equatorial circumference), as recorded by the Mapper optical system, form a spaced pattern, separated at the equator and overlapping at the poles. The illuminated (daytime) portions of the strips terminate near each pole (within 25.2° of the pole).

To estimate the overlapping (overmapping) it is assumed that the strip pattern is continued until the entire equatorial region is mapped just once, with strips immediately adjacent at the equator. For simplicity it is also assumed that the polar axis is not tilted. Each illuminated strip has an area πr_{oo} w from north south pole; the number of such strips crossing the equator is $2\pi r_{oo}/w$. Therefore the total mapped area A_m (including non-equatorial regions mapped more than once) is

$$A_m = \pi\ r_{oo}\ w \times 2\pi\ r_{oo}/w = 2\pi^2\ r_{oo}^2$$

which is independent of w. Comparing this area with the surface area ($A_{\sigma'}$) of Mars gives an overmapping factor (f) for the entire planet:

$$f = A_m/A_{\sigma'} = 2\pi^2\ r_{oo}^2/(4\pi\ r_{oo}^2) = \pi/2 = 1.57.$$

In order to provide additional overlapping of adjacent areas for map matching, $f = \pi$ is estimated as a practical value. Terrestrial photogrammetric practice calls for overlapping of from 40 to 100 percent; i.e., the ratio of area photographed to actual surface area is from 1.4 to 2. Using $f = \pi$ is equivalent to providing 100 percent overlap at the Martian equator.

8.15.6.3 Quantity of Mapping Information. If the Mars map is reduced to digital data for recording and/or transmission, the number of binary bits of data is computed as follows:

$$N = (A_{\sigma'}/s^2)\quad f\quad \log_2\quad n$$

where

N = number of bits of information

$A_{\sigma'}$ = surface area of Mars = 1.38×10^{14} meter^2

s = length of surface resolution, meters

$n = \log_2 10 = 1/\log_{10} 2 = 3.322$

f = overlapping and overmapping factor = π

Numerical values are summarized in Figure 8-48.

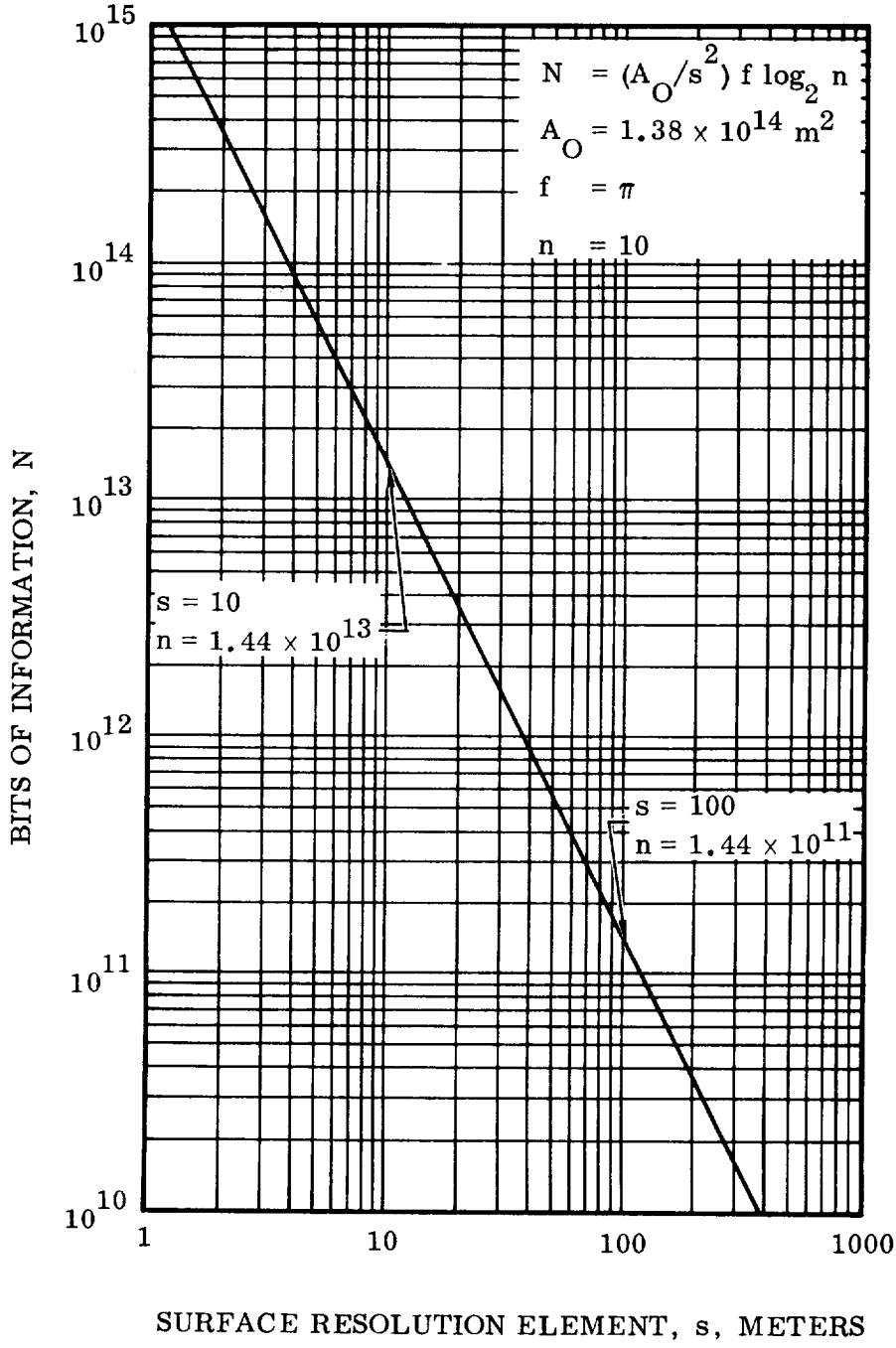

Figure 8-48. Information Requirements for Mapping Mars

8.15.6.4 Map Data Recording. Digitalized map data are recorded and stored for return to Earth or for transmission to Earth by telemetry. The following estimate indicates the magnitude of the storage requirements.

Recording on film in two dimensions is limited by film resolution, usually expressed in lines per millimeter. Silver halide film is currently easily capable of 200 lines/mm resolution; Kodak High Resolution Plates for microphotography currently can provide 1,500 lines/mm. However, silver halide emulsions require shielding from nuclear radiation. Xerox type (electrostatic) and Ozalid type (diazo dye coupling) processes show promise of providing even higher resolution in the near future (3,000 to 5,000 lines/mm). A conservative value q = 10^3 lines/mm = 10^6 lines/meter is assumed.

The required film area (A_f) is

$$A_f = N/q^2$$

where the number of bits of information is as estimated in Section 8.15.6.3. At s = 10 meter surface resolution, N = 1.44×10^{13} bits. Thus, A_f = 14.4 m^2 = 155 ft^2 which is a very modest requirement, even after making allowances for additional film area for data coding and film packaging.

8.15.6.5 Mars Mapper Optics. The optical resolution of a telescope limited by Fraunhofer diffraction is given by

$$s = 1.22\ (y\ \lambda/d) \times 10^{-7}$$

where the resolution(s) and the aperture diameter (d) are in meters, the object distance (y) is in kilometers (altitude) and the wavelength (λ) is in angstrom units. Figure 8-49 illustrates the theoretical resolution obtainable from telescopes of several apertures using orange light (λ6000). At 662 km altitude, a 0.3-m 9(0.984-ft) aperture has an ideal resolution of 1.61 m (5.24 ft), while a 1-m (3.28-ft) aperture has a resolution of 0.485 m (1.59 ft).

D. H. Robey (A Rocket Borne Video Telescope for Observing Mars, Astronautica Acta, Vol. 5, pp. 313-327, 1959) describes a 0.3-m aperture telescope system with telescope weighing about 23 kg (50 lb). Assuming a weight scaling of aperture to the 2.5 power, an aperture increase to 1 meter increases telescope weight by a factor of $(1/0.3)^{2.5}$ or about 20. Thus a 1-meter aperture telescope weighs about 450 kg (1000 lb). Since this weight is excessive, a 0.3-m aperture is tentatively selected. The above weight estimates apply only to the optical system and telescope frame, excluding shock mounting, stable platform, optical detecting and scanning system, and electronic and electrical controls.

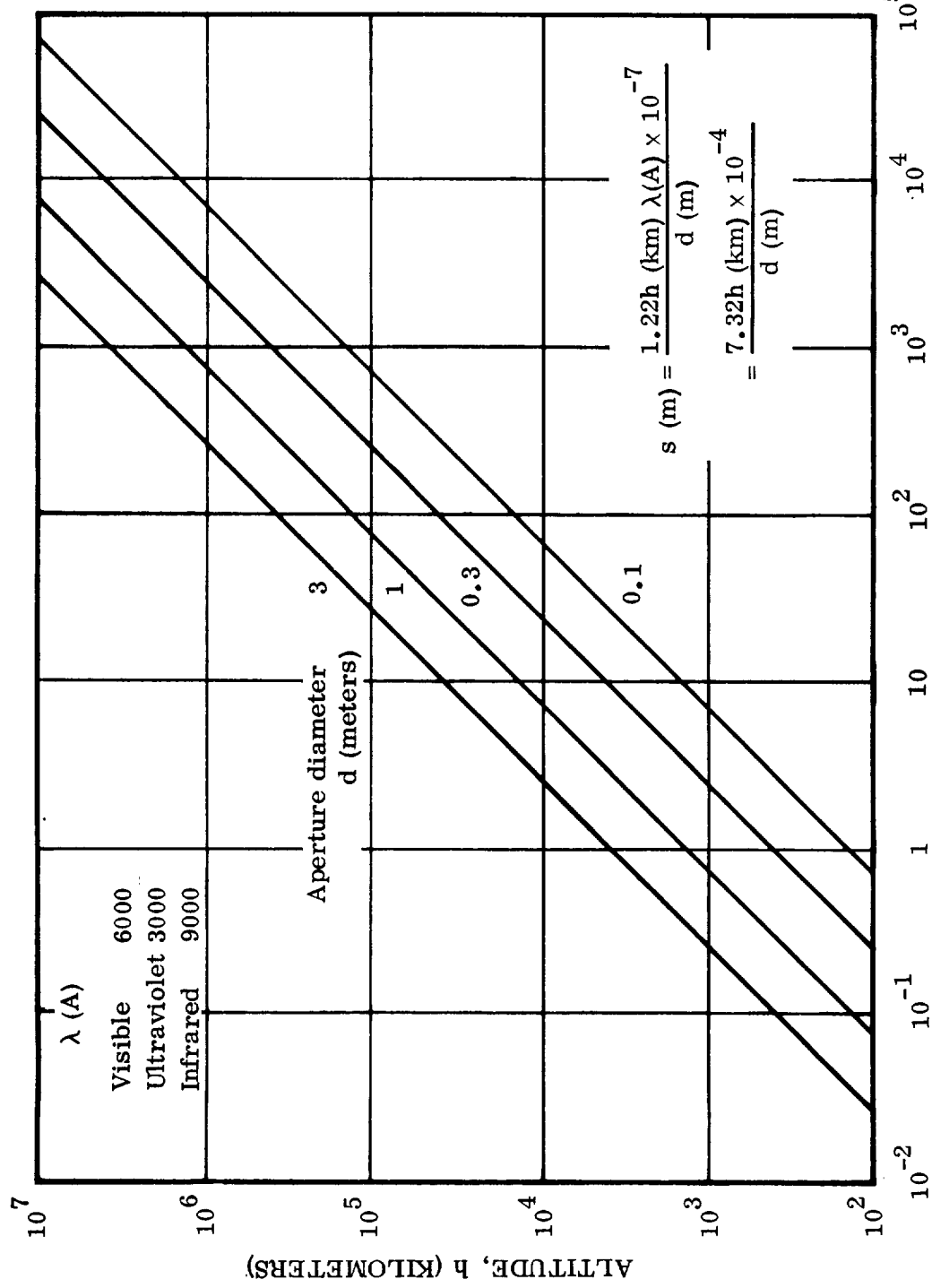

Figure 8-49. Optical Resolution of a Telescope for Visible Light (λ 6,000)

8.16 ELECTRICAL POWER SUPPLY

8.16.1 Power Requirements. The principal power consummers in the convoy vehicle are:

Life support system
Hydrogen liquefaction system
Data processing and storage system
Data transmission system
Radar mapper

The main life support system, based on CO_2 removal by reverse water gas reaction and O_2 production by electrolysis has a power requirement of close to 5 ekw for a crew of eight persons (cf. Section 10).

The hydrogen liquefaction system, for a capacity of 24 kg H_2 liquefaction per day requires a power supply of about 5 ekw (cf. Paragraph 8.14).

As pointed out in Paragraph 7.1.2 of the IBM report in the Appendix, it is difficult to select the proper data processing system at this early phase of the study. The processing requirements are not yet defined and therefore IBM was asked to provide broad parametric coverage of processing capability (in instructions per second) and its correlation with power, weight and volume. The power correlation is presented in Figure 7.1.2.2 in the Appendix; these data are not based on advanced design features such as micro-module and thin film techniques and are therefore probably conservative, relative to the years 1973 to 1975. Selecting an instruction speed of 8×10^5 per second, Figure 7.1.2.2 indicates a power requirement of 4 ekw.

For the data transmission (communication) system the power required was determined on the basis of the equation

$$P_{spec} = 1.9 \cdot 10^{-19} \frac{R^2 \lambda^2}{D_T^2 + R_R^2} \frac{w}{\text{Bits/sec}} \qquad (8\text{-}7)$$

where R, λ, D_T and D_R are the transmission distance, wavelength, diameter of transmitter antenna, and diameter of receiver antenna, respectively, all in meters. The factor 1.9×10^{-19} is the result of defining (among other constants) the systems noise temperature to be 40°K, the energy constrast of 6, and the efficiencies of the transmitter as 0.5 and of the receiver antenna as 0.55. The above equation was derived in the IBM report "Technical Proposal, Data Handling System Study for Project EMPIRE", December 6, p1962.

From the mission profile figures for 1973 and 1975, shown in Paragraph 6.4, it follows that the distances between vehicle and Earth do not exceed approximately 1 A.U. (1.495×10^{11} m). According to the present and near-future state of the art, the largest ground antenna diameter available can be expected to be 100 m. For the on-board transmitter antenna a diameter of 10 m was assumed. Selecting a frequency of 10 kmc (hence, $\lambda = 0.03$ m) it follows

$$P_{spec} = 1.71 \cdot 10^{-5} \frac{w}{Bit/sec}$$

The Mapper is estimated to have an information rate of 8×10^5 bits/sec (cf. Appendix, Section 3). However, for the Mars moon probes, temporarily a higher information rate is considered, namely, 6.7×10^7 bits/sec for the last 600 flight seconds of Deipro and 1.25×10^8 bits/sec for the last 1100 flight seconds of Phopro. Therefore, a maximum information rate of 10^8 bits/sec is selected for the communication system, resulting in a power requirement of 1.71 ekw.

The prime power requirement for the radar mapping system (applied to Venus or Mars, cf. classified addendum of this report) is plotted in Figure 8-50. The required power increases sharply with altitude and, therefore, requires operation of the radar at low altitude (400-600 km). A radar Mapper altitude of 400 km is selected at an associated prime power requirement of 5 ekw.

These data are summarized in Table 8-12 and 4 ekw added to cover many smaller power drainages and emergencies. There are promising aspects about the use of high resolution radar and associated altimeter (instead of optical means) to map Mars. However, in the present set-up, no provisions have been made to integrate the radar and its operational requirements into the scientific payload and into the capture operations near Mars. Therefore, the associated power figure is put in parenthesis. It follows that the convoy ships should each be equipped with at least one 30 ekw unit plus one backup unit, or a combination of backup systems.

8.16.2 Main Power Generation Systems. Table 8-13 resents a comparison of various types of electric power generators for space vehicles. Of these, a number are out of the question as main systems, because their power level and their power specific weight is too high (photovoltaic systems).

The ever-present Sun suggests the use of solar collector systems for planetary ships in the inner solar system. The amount of kilowatts offered by the Sun during a Mars round-trip is considerable as is shown in Paragraph 8-14. Solar collector systems have the advantage of being free of radiation problems, and they are probably lighter than nuclear power sources in the medium power range from 1-20 ekw. However, they have the disadvantages of requiring stringent attitude control and of being dependent

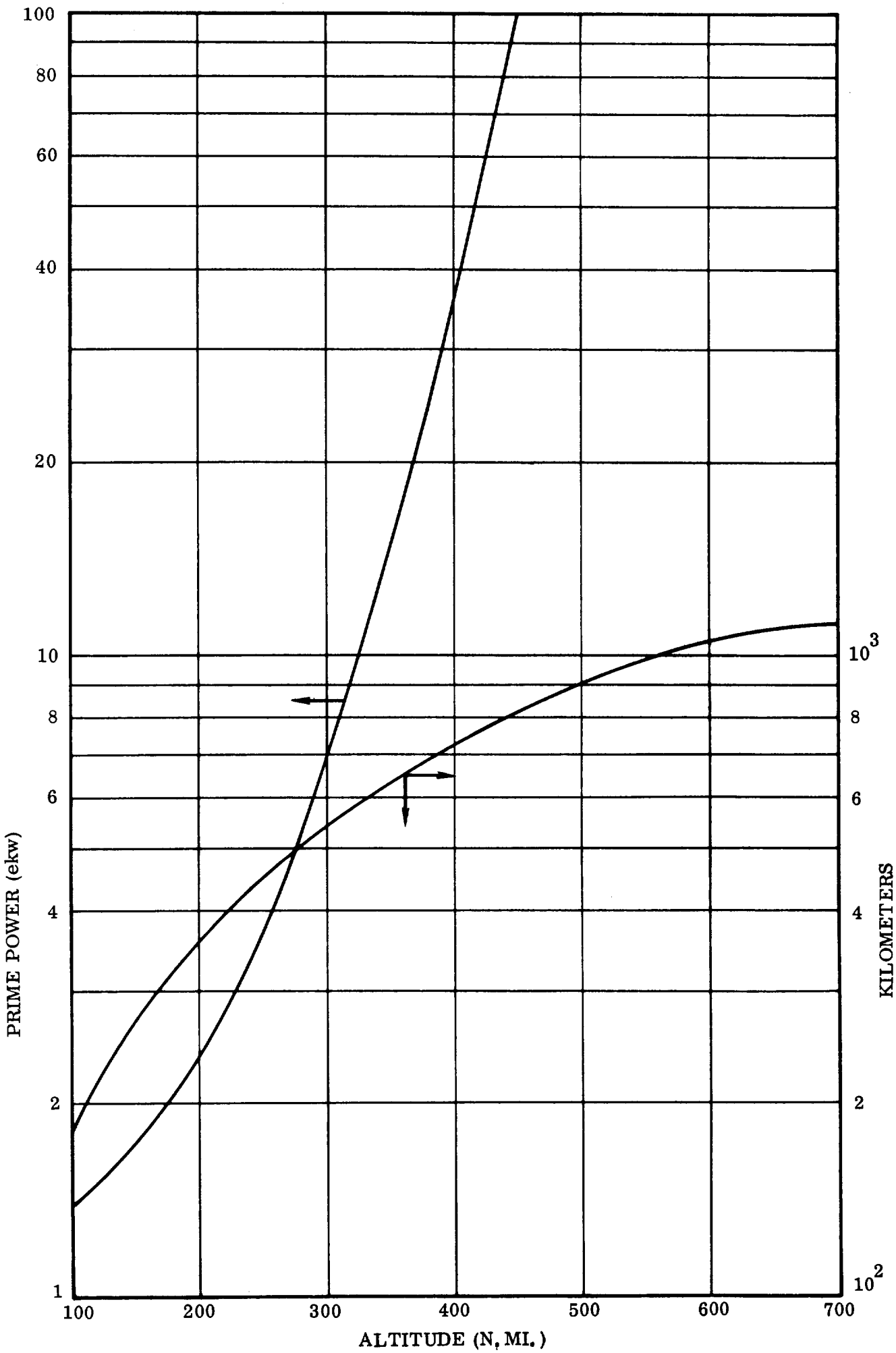

Figure 8-50. Prime Power Requirement for Radar Mapping System

Table 8-12. Principal Power Requirements (Convoy Vehicle)

	VENUS CONVOY SHIP	MARS CONVOY SHIP
	POWER (ekw)	
Ecological life support system (8 persons	5	5
Hydrogen liquefaction system	5	5
Data processing and storage system	4	4
Data transmission system	2	2
Radar Mapper	5	(5)
Miscellaneous and Emergency	4	4
TOTAL (ekw)	25	20 (25)
TOTAL (thermal kw)	111	89 (111)

upon the availability of solar radiation, which could become a problem during the capture period. During a Mars mission, the solar distance may vary between 0.7 and 1.6 A.U. (i.e., by a factor of 5); during a Venus mission the extremes presently considered range from 0.7 to 1.3 A.U. (i.e., by a factor of almost 3.5). It is of importance to note that the performance, expressed as energy flux per unit area through the solar image at the focus of a three-dimensional parabolic collector (the focal solar constant) is independent of solar distance for a given aperture, since the effect of varying solar distance and varying apparent area of the solar disk (both varying with $1/R^2$) cancel each other out (Ehricke, K.A., Solar Propulsion, Handbook of Astronautical Engineering, H. H. Koelle ed., McGraw-Hill, New York, 1961, p. 21-80). This is an attractive feature of the solar collector for interplanetary flight in the inner solar system, because the operation of the boiler is not subject to significant variations as the result of varying solar distance. Of course, the collector intercepts a larger amount of solar radiation nearer the Sun; but for a heater (boiler) sized for the solar image at the maximum distance to be encountered during the journey, this simply means that the additional energy intercepted would bypass the boiler through the larger solar image. The value of the focal solar constant is close to 4 kw/cm^2 (compared to 0.136 w/cm^2 solar constant at 1 A.U.). This value assumes 100 percent efficiency of the collector. Deviations from ideal parabolic shape and surface roughness cause the solar image to be spread over a larger surface. Other effects are reradiation of energy from the heater surface and the obscuration of the center of the primary parabaloid reflector by the heater. The most effective heater is a cavity absorber. Taking this heater and considering the effect of the losses mentioned

Table 8-13. Comparison of Various Types of Electrical Generators for Space Vehicles

TYPE OF ELECTRICAL GENERATION SYSTEM	ANTICIPATED POWER RANGE	ABILITY TO WITHSTAND ENVIRONMENTAL CONDITIONS				SIMPLICITY	RELIABILITY	COMPATABILITY WITH ION OR PLASMA PROPULSION	POSSIBILITY OF 2 – 3 YEAR LIFE	REMARKS
		VIBRATION	ACCELERATION	METEOROIDS	TEMP. VARIATIONS					
Radio isotope Thermo electric	1-100 W	Good	Good	Excellent	Fair	Good	Good	No	Poor	Already developed.
Solar Photo-Voltaic	1-1000 W	Good	Excellent	Good	Fair	Excellent	Excellent	No	Excellent	Proven excellent operation in space.
Solar-Thermionic Vacuum Type	30 W - 1 KW	Good	Good	Good	Excellent	Fair	Good	Requires voltage step-up	Good	No prototypes tested to date. Estimates are for anticipated results.
Solar-Thermionic Gas Filled Type	30 W - 30 KW	Good	Good	Fair	Good	Fair	Good	Requires voltage step-up	Excellent	" " "
Solar Thermoelectric	30 W - 30 KW	Good	Good	Good	Fair	Fair	Excellent	"	Excellent	Material development not completed.
Solar Turbine Generators	1 KW - 30 KW	Good	Good	Poor	Good	Poor	Good	Good	Fair	Rotational inertial changes bother navigation.
Atomic - Turbine-electromagnetic generators	3 KW - 1 MW	Good	Good	Poor	Excellent	Poor	Good	Good	Fair	Rotational inertia bothers vehicle control.
Atmoic - Turbine Electrostatic generator	3 KW	Good	Good	Poor	Excellent	Poor	Good	Excellent	Fair	This type of generator lighter than electromagnetic.
Atomic - Thermionic with coolant	3 KW - 3 MW	Good	Good	Poor	Excellent	Fair	Good	Requires voltage step-up	Good	Most promising large, long life, light weight system.
Atomic - Thermionic without coolant and with small rocket thrust	3 KW - 100 KW	Good	Good	Good	Good	Good	Good	Jet thrust to replace ion or plasma	Good	Ideal for communications satellite.

above, as well as the fact that the reflectivity of the collector will not be larger than 0.9, it appears that the combined collector-heater efficiency (i.e., the ratio of thermal power withdrawn from the heater to the total intercepted by the collector) will not be larger than 0.6. This will yield a cavity radiation equilibrium temperature of about 1800°K (2800°F) if the surface quality of the reflector equals that of the very best searchlights commercially available. If a concentrated effort is devoted toward solar collector development it appears likely that, by the reference period (1973-75), a surface quality roughly comparable to poor commercial searchlights will be available. This would mean a cavity radiation equilibrium temperature of roughly 1500°K (2200°F). For comparison, the maximum temperature theoretically attainable in the focus of a perfect parabolic mirror is 5100°K. The solar temperature is close to 5750°K. From $T = (q/\sigma)^{1/4}$ with $\sigma = 5.775$ kw/cm^2 °K^4 one finds that 5100°K correspond to an absorbed heat flux density (at black body conditions) of 3.9 kw/cm^2. At 1500°K, the equivalent heat flux density through the solar image is reduced to 2.91 kw/cm^2. The diameter of the solar image is $f\beta$ where f is the focal length and β the angular diameter of the Sun. At 1.3 and 1.6 A.U., β is about 14 and 10 minutes of arc, respectively. At a rim angle of 60° the ratio of parabolic reflector diameter D to focal length is D/f = 2.3. For these conditions the thermal power absorbed by the cavity heater is

$$P_{thermal} = 2.91\frac{\pi}{4} f^2 \beta^2 = 2.91\frac{\pi}{4} D^2 \frac{\beta^2}{(D/f)^2} = 0.431\, D^2 \beta^2 \text{ (kw)} \qquad (8\text{-}8)$$

This relation is plotted in Figure 8-51. To obtain the collector required for a given amount of electric kilowatts (ekw), the conversion efficiency of the electric power generation system must be known. The present efficiency of a turbogenerator system is around 0.17. By 1970 an increase in efficiency to about 0.27 can be expected. This means the reactor planform area must be 3.6 as large, and the diameter 1.93 times as large as shown in the figure, to obtain the associated electric power output. A 10-meter (32.8 ft) diameter collector (read 5.15 m on the graph) will therefore, at best, yield by 1970 a power of 20 ekw (0.7 A.U.), 10 ekw (1 A.U.), 5.8 ekw (1.3 A.U.) and 3.8 ekw (1.6 A.U.). For a rim angle of 60 degrees, the ratio of surface to planform area for a paraboloid is 1.09. The surface area of a 10 m parabolic mirror of 60 degrees rim angle is, therfore, 8.55 m^2 or 92 ft^2. Collectors of this magnitude have not been built at the quality assumed here. However, by 1970, this appears quite feasible, especially if the collector can be rigid. Further assuming an aluminum honeycomb structure with a double skin, an area weight of 0.4 to 0.5 lb/ft^2 appears attainable. If lightweight plastic foams are used, reflector weights of the order of 0.15 to 0.2 lb/ft^2 may be obtained during the sixty.

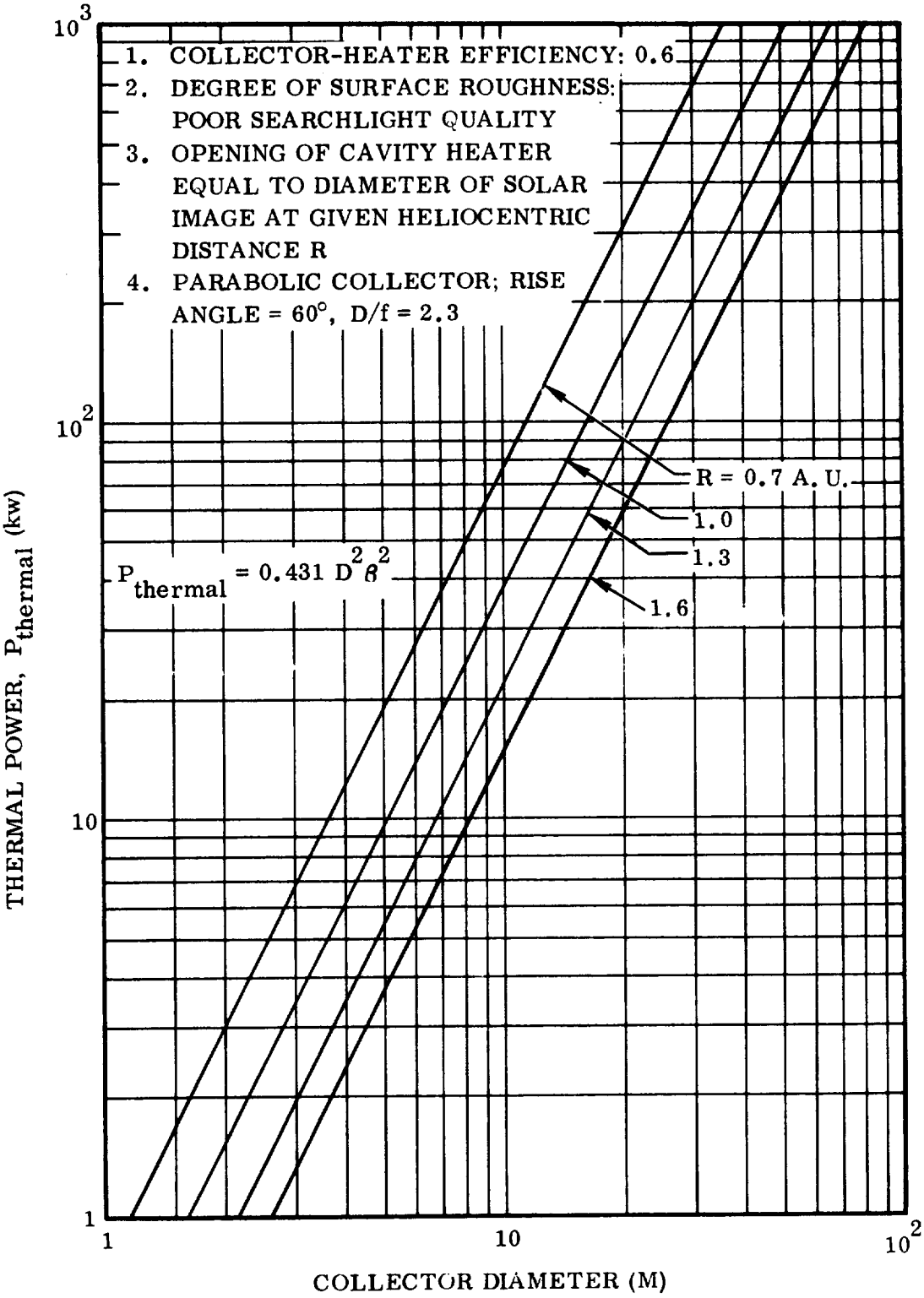

Figure 8-57. Effective Energy Flux Absorbed by a Cavity Heater at the Focus of a Parabolic Collector at Several Heliocentric Distances

Any comparison of solar-power systems depends upon the efficiency of the conversion system. Thermoelectric converters (thermocouples) whose efficiency is about 6 percent could conceivably grow to some 13 percent by 1970, and the maximum operating temperature increased from 1200°F to 2000°F. The Stirling engine offers considerable promise due to its high operating efficiency. Solar-Stirling engine systems offer minimum weight at a temperature range between 1256°F (melting point of LiH thermal storage unit) and 150°F (wet radiator using water coolant). In this range the engine will operate at 30 percent efficiency or better.

For operation in the capture orbit, thermal storage must be available, using the heat of fusion of materials. Lithium hydride (LiH) with a melting point of 1256°F (688°C) has the highest capacity with 685 w-hr/kg (312 w-hr/lb or 1132 Btu/lb). The second best appears to be silicon with 394 w-hr/kg. However, its melting point is very high (1700°K, 2600°F) and difficult to obtain within the range of expected reflector qualities. Moreover, silicon is very difficult to contain over long periods of time. LiH melts at a comparatively low temperature, but it expands 16 percent by volume upon melting, necessitating a mechanism to insure against excessive pressures and withdrawal of solid material from chamber walls. LiH will dissociate at high temperatures, and therefore requires increasingly high operating pressures. However, for a moderately high temperature system, LiH is a highly satisfactory material. The radiant energy which is concentrated by the collector passes through the aperture of the cavity heater and impinges upon an absorber surface converting the radiant energy to thermal energy. A liquid metal circulating system transfers heat to the reservoir assembly which contains many stainless steel cones filled with LiH.

Aside from the collector, the radiator is an important weight item. It has been shown frequently that, for minimum radiator weight per unit of power output, the radiator temperature should be 0.75 that of the source temperature. In solar-thermal systems, however, the necessity for a lightweight collector demands a high efficiency system with a lower radiator temperature, for reasons of thermodynamic efficiency. In practice, optimum radiator temperatures will depend a great deal on specific converter characteristics, as shown in Table 8-14.

Table 8-14. Optimum Radiator Temperatures for Minimum System Weights at the 3 ekw Power Level

SOLAR ENERGY CONVERTER	SOURCE TEMP °K	SOURCE TEMP °F	RADIATOR TEMP °K	RADIATOR TEMP °F
Thermoelectric	894.3	1150	304ω4	250
Turboalternator	922.2	1200	588.9	600
Stirling Engine	922.2	1200	338.9	150
Thermionic Emitter	1300	1700	866.6	1100

The energy conversion system can use one of several cycles. Generally, the most attractive cycle for turboalternator systems is the Rankine cycle because of its superior efficiency compared to the Brayton cycle, although the Brayton cycle works with a gaseous (one-phase) working fluid, such as argon or helium, whereas the Rankine cycle works with two-phase liquids, including water, mercury and rubidium. The Brayton cycle efficiency even at a T_{max}/T_{min} ratio of 6 is only about 0.2. Rankine cycles may be developed from about 0.17 to 0.27, as pointed out before; but this remains to be demonstrated. With the Stirling cycle, which in the ideal case equals the Carnot cycle, efficiencies of the order of 0.3 appear far more easily attainable. In fact, the Allison Research Dept. of General Motors built, in 1954, a 20-cu in. displacement engine which used hydrogen as working fluid and delivered 40 hp (29.8 hw) at the predicted efficiency of 36 percent with a maximum cycle temperature of 1300°F (Welsh, H.H., Poste E. A., and Wright, R.B., The Advanced Stirling Engine for Space Power, Allison Research Dept., Rep. EDR 1456, Indianapolis, Indiana, 1959). The temperature-entropy and the pressure-volume diagram for the ideal Stirling engine are shown in Figure 8-52. The ideal cycle consists of two isothermal and two isochoric processes. Heat is added to the cycle during isothermal expansion 3-4 and the initial isochoric process, 2-3; it is removed during isothermal compression 1-2 and the final isochoric process 4-1 ("The Philips Air Engine", The Engineer, vol. 148, no. 4795, December 19, 1947, pp. 572-574). To duplicate the Carnot efficiency, the heat which is normally rejected in the final process, 4-1, must be stored and returned to the gas during the initial isochoric process, 2-3, Heat which is added to, or removed from an isochoric process is the product of specific heat (c_v) and the temperature difference. Since both the initial and the final isochoric process operate at the same isotherms and the ideal c_v is constant, the heat involved is ideally the same for both processes. The heat is stored in the regenerator. The heat storage capacity of the regenerator must be at least about 10 times as great as the quantity of heat which must be transferred into the system. Therefore, the regenerator assumes great importance in the operation of the engine. The mechanical arrangement consists of two pistons in a cylinder and three heat exchangers (heater, generator, cooler). The lower piston does the compression and expansion work. The upper piston is used to transfer the working fluid from the lower to the upper spaces through the heat exchangers. No valves are used. By proper design of the heat exchangers and phasing of the pistons, the working fluid can be displaced through the heat exchangers in such a manner that the processes of the ideal cycle are simulated. The crank mechanism permits the reduction of torsional vibrations to negligible low values. By attaching a balanced alternator to each contrarotating crankshaft, all torsional moments are cancelled; and, since all rotating members have a contrarotating counterpart, the wet system gyrocouple is zero.

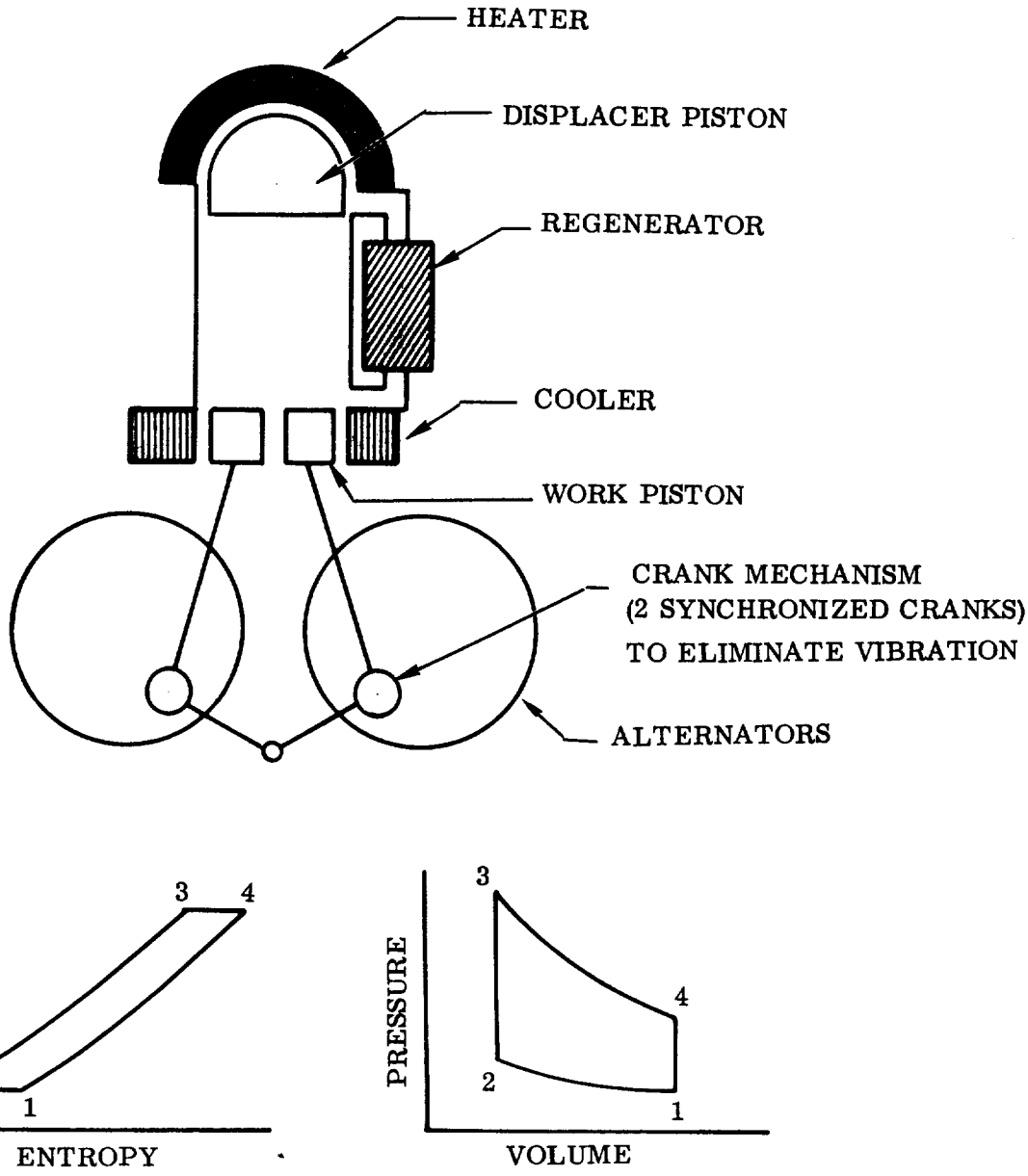

1-1: TEMPERATURE CONSTANT; ISOTHERMAL COMPRESSION
2-3: VOLUME CONSTANT; HEAT RETURNED TO CYCLE BY REGENERATOR
3-4: TEMPERATURE CONSTANT; ISOTHERMAL EXPANSION
4-1: VOLUME CONSTANT; HEAT REJECTED TO REGENERATOR

Figure 8-52. The Stirling Engine

The excellent thermodynamic properties of hydrogen make it first choice as working fluid in the Stirling cycle. Helium, the second device, results in an efficiency decrease of about 12 percent. Since hydrogen diffuses through most confining materials, especially at the high temperatures involved, helium is the more practical choice for long duration space applications. The limiting factor for the Stirling system is that it operates with the (reciprocating) Stirling engine. The Stirling cycle is not suitable for turbo machinery due to the constant volume processes involved. Reciprocating engines can be competitive to turbines only at the lower power level, perhaps up to about 10 ekw. The main difficulties with the Stirling engine for long-time operation are problems of engine lubrication, and preventing the oil from clogging the regenerator or contaminating the helium working fluid. Stirling engines may require more maintenance work by the crew and for this reason should not be connected with a nuclear power source.

Figure 8-53 shows the power specific weight versus power output for a number of systems (solar and nuclear). The nuclear systems are represented by the developments taking place in the SNAP program. Of these the SNAP-8 system, which is to furnish 30 ekw is of particular interest. It may be possible to hold the weight of this system to 3000 lb, including shielding. It is of interest, however, that if a solar-Stirling engine system delivering 10 ekw can be built for 85 lb/kw, it would actually weigh less to install three 10-ekw units of this type than one SNAP-8. This would not be true for the solar turbo-alternator system. Figure 8-54 shows a plot of radiator heat rejection per unit area as function of the radiator temperature. The SNAP systems operate at a temperature which, on the hot side, is about 1300°F. At a mean radiator temperature of 500°F (535°K) and a systems efficiency of 0.2, 120 kw must be rejected in the SNAP-8 system. The resulting radiator area is 110 m^2 (1185 ft^2) or roughly two squares of 24.5 ft (7.45 m) length and width each. It should be noted that this does not take the effect of solar radiation into account. This effect is negligible at Mars distance. At Earth distance, a side which is fully exposed to the Sun and absorbs about 0.08 km/cm^2 emits only 72.5 percent of the amount of energy which it would emit in the shade (always based on 535°K radiator temperature). Near Venus the solar illuminated side of the radiator would emit slightly less than half of its nominal energy value. Thus, in the case of such relatively low radiator temperature, an attitude control problem definitely exists during certain portions of the mission to Venus and Mars, not only for solar-powered but also for nuclear-powered systems. The attitude requirement can be reduced somewhat by providing the radiators with "blinders", i.e., with vertical fins at the rim which restrict the attitude portion at which the Sun can illuminate the radiator. But this involves a weight penalty. Another factor entering the weight considerations is the fact that above about 400°F it is necessary to change from aluminum to steel which at first (i.e., at 500°F and 600°F) increases the radiator weight, rather than reducing it. At 700°F the area specific weight begins to fall below that of an aluminum radiator at 400°F.

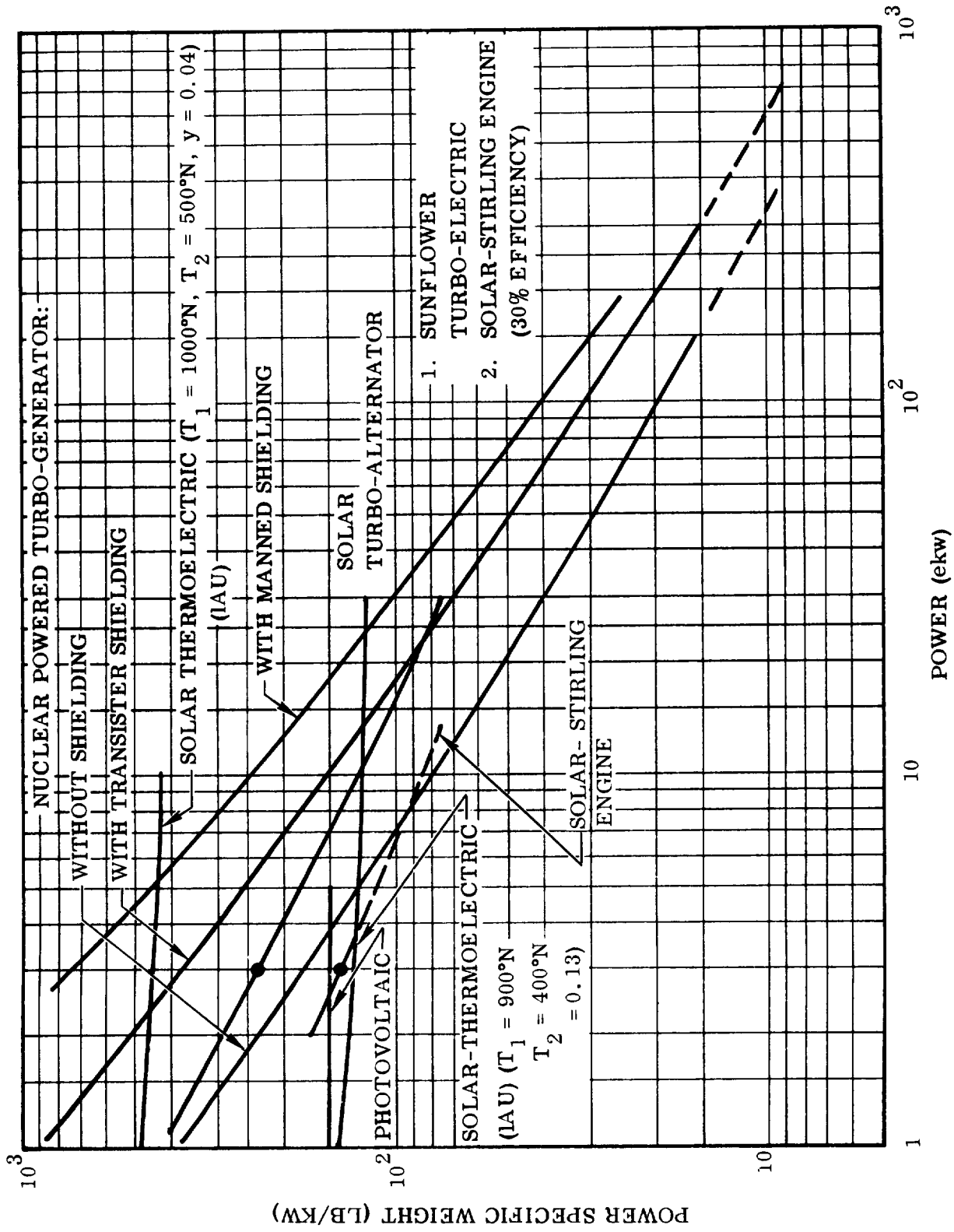

Figure 8-53. Power Specific Weight Versus Power Output Estimated for 1965

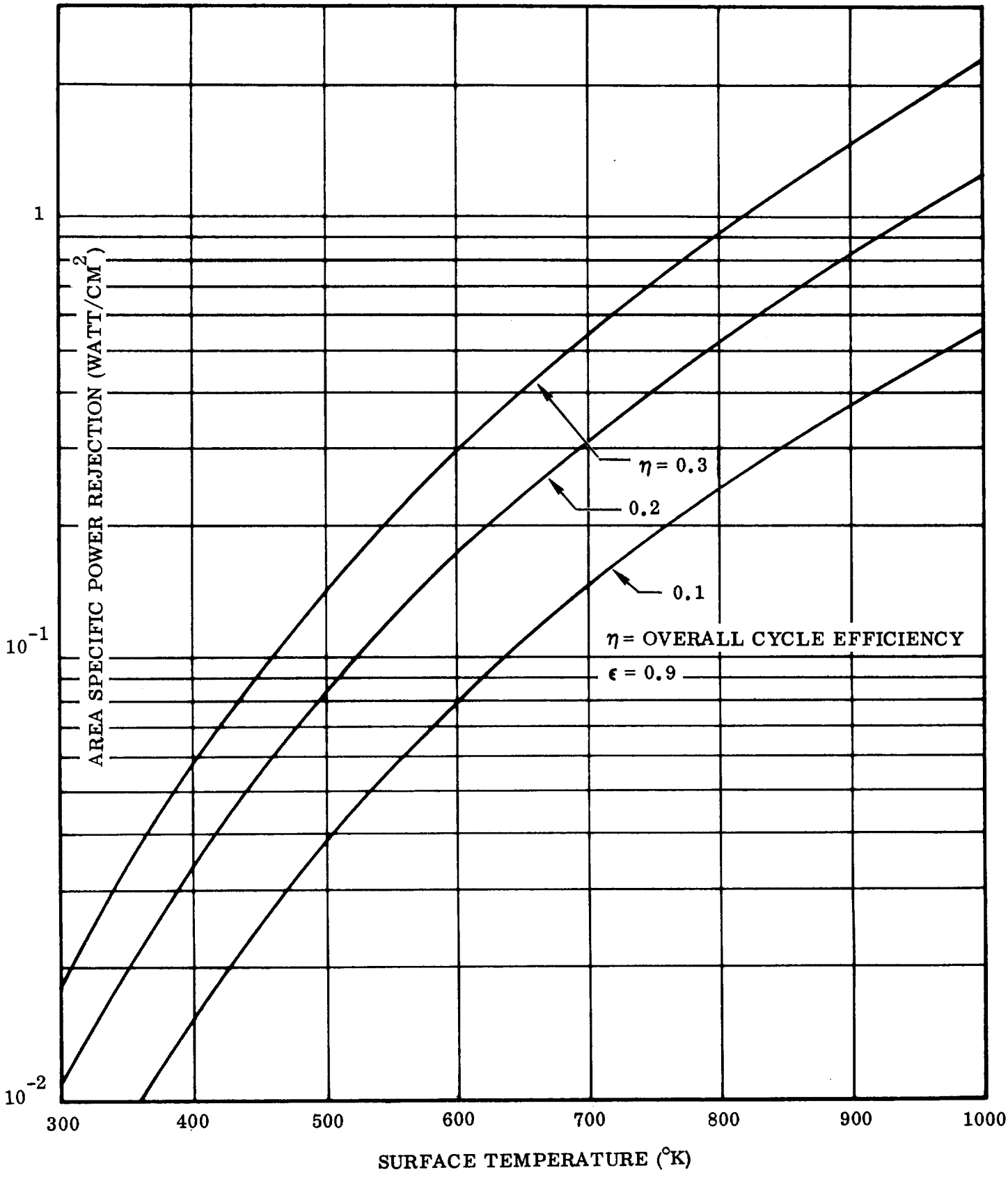

Figure 8-54 Area Surface Power Rejection

At this higher temperature the radiator performance is also less affected by solar irradiation. Now the solar effect near Earth reduces the radiator performance less than one percent and near Venus by about 10 percent. The required radiator area is now 40 m^2 (430 ft^2), if the overall cycle efficiency were the same. Actually, the higher heat sink temperature will cause a reduction by at least 3 to 4 percent. Assuming $\eta = 0.16$, the rejection rate is reduced to 0.22 watt/cm^2, resulting in a radiator area of about 55 m^2 (590 ft^2). Thus, the optimization of the system weight must, in the final analysis, consider radiator size, cycle efficiency, and effect of solar irradiation. All three are functions of the radiator temperature. The first and third parameter tend to raise the radiator temperature, the second tends to lower it.

It is concluded that for the main power supply system either two SNAP-8 systems or a larger number of solar-Stirling engine systems of smaller individual power output could be taken. From the weight standpoint they seem to be comparable. At this point of the study, a total of 8000 lb is set aside for electric power generation, corresponding nominally to two SNAP-8 systems and four solar-Stirling units at 4 ekw each as spares and emergency systems.

8.17 MARS LANDER, RETURNER, AND MANNED MARS EXCURSION VEHICLE (MEV). These three vehicles are considered to belong to the same family for reasons of economy and reliability. The lander is the smallest, highest, and relatively simplest of the three. It should be developed as an extension of the entry capsule of the voyager. The Returner's payload section resembles more that of the Surveyor, of course with additional instrumentation for biological and atmospheric observations (cf. Section 5). Generally, the Voyager should be planned with the Lander, the Returner and even the MEV in mind.

The function of landers is comparable to that of the Surveyor and the Prospector for our Moon. Additional measurements would pertain to the atmosphere, listening for sounds of moving objects, and skylight. A few landers will be earmarked in advance for descent to certain areas known now, or on the basis of Mariner and Voyager flights, to be of particular scientific or astronautic interest. A few additional landers will remain at the disposal of the crew to be sent to selected sites on the basis of the information obtained from the mappers.

The purpose of the instrumented returners is primarily to furnish soil and air samples to the crew. Their range of environmental measurements can, therefore, be more limited, since these are provided by the landers.

The aspects of a Manned Excursion Vehicle (MEV) with a crew of one to two persons have been studied. The highly desirable implications of a successful manned excursion to the surface of Mars must be put in best possible harmony with the overall mission plan. Therefore, the MEV should be designed such that it can be used as returner

if the crew decides not to land after all. This means the MEV should be modularized in three sections: propulsion, automatic instrumentation section, and pilot module containing also all the instrumentation and scientific equipment vehicle is predicated on the presence of man.

The configuration shown in Figure 8-55 is based on the philosophy that the vehicle should be usable either as Returner (unmanned, instrumented) or as MEV, carrying one person, if the decision is made during the capture period to engage in a manned landing for a brief period. In the latter case, an inhabitable (but unmanned) MEV will be sent down first to be available to the man who follows in a second MEV, landing nearby, should his vehicle be damaged. Prior to dispatching either of these two vehicles, Landers will have been sent to the surface to explore the feasibility of a successful landing. The vehicle uses C1 F_3/UDMH which are suited for the low night-time temperatures on Mars. (C1 F_3: F.P. = -105.4°F; UDMH: F.P. = -71°F). Since the temperature may drop as low as -100°F, heating provisions for the UDMH would have to be made.

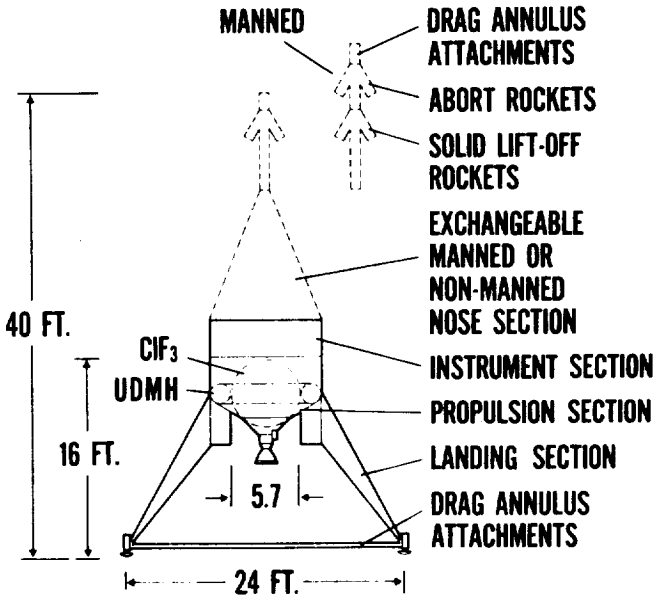

Figure 8-55. Mars Returner and Manned Mars Excursion Vehicle (MEV)

A sequence of pictures (Figure 8-56) illustrates the principle of descent and landing investigated for the MEV, the Returner, and possibly the Lander. The vehicle descends and lands gently. The drag body is of annular shape. If used to the point of touchdown, the descending amuclus does not obstruct the vehicle. A desirable aspect of using the drag body to touchdown is that the need for retrothrust is eliminated.

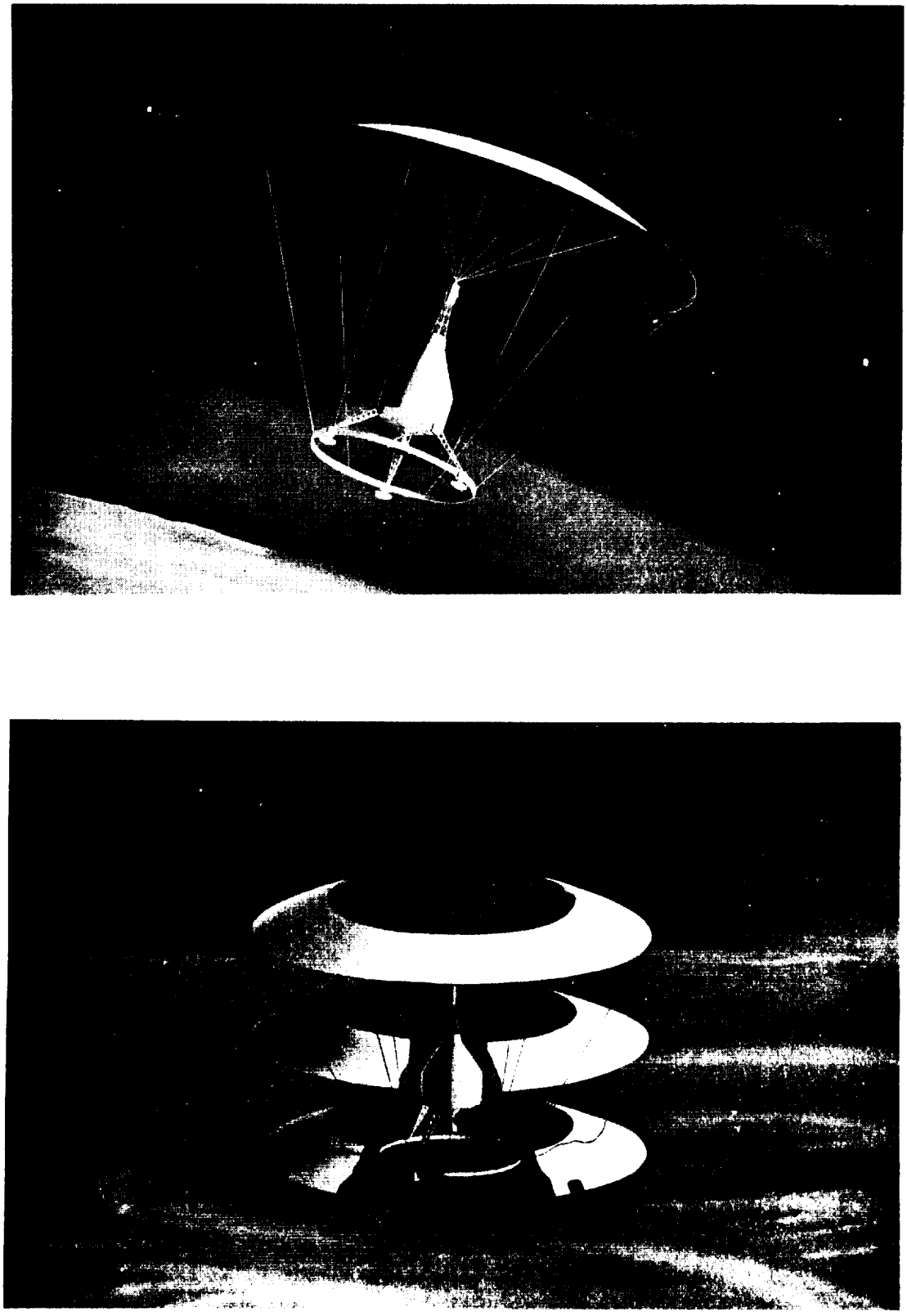

Figure 8-56. Descent and Landing of MEV, Returner, and (Possibly) Lander

This is especially desirable in the case of manned landing. Should winds render this approach impractical, the drag body may be used to close surface proximity. Then the vehicle is cut loose and allowed to fall essentially freely, while a small liquid propellant system in a tower above the nose section provides attitude control for the touchdown.

A weight breakdown is presented in Table 8-15.

Table 8-15. Principal Data Mars Excursion Vehicle (MEV)

Altitude of return orbit	1070 km
Ideal velocity for return	4.5 km/sec
*Return payload	3,000 lb
*Useful propellants	14,000 lb
ClF_3 10,900 lb r = 3.03 d = 1.38	
UDMH 3,600 lb I_{sp} = 280/325/(300)	
*Wet inert weight	1,100 lb
Gross weight (takeoff)	*18,600 lb = 7,600 lb**
*Weight left on Mars	3,400 lb
Gross weight (descent)	22,000 lb = 9,000 lb**
*Transport weight	22,500 lb
Area of drag annulus	9,000 ft^2

*Earth ** Mars

For ascent, the vehicle is equipped with a set of nose rockets designed to pull it off the ground before the (hypergolic) main propulsion system is ignited (Figure 8-57). This approach offers an opportunity to eliminate long landing legs from the vehicle, since the main propulsion system can now be closer to the ground. This reduces the weight and brings both crew and instrument compartment closer to the ground (Figure 8-58).

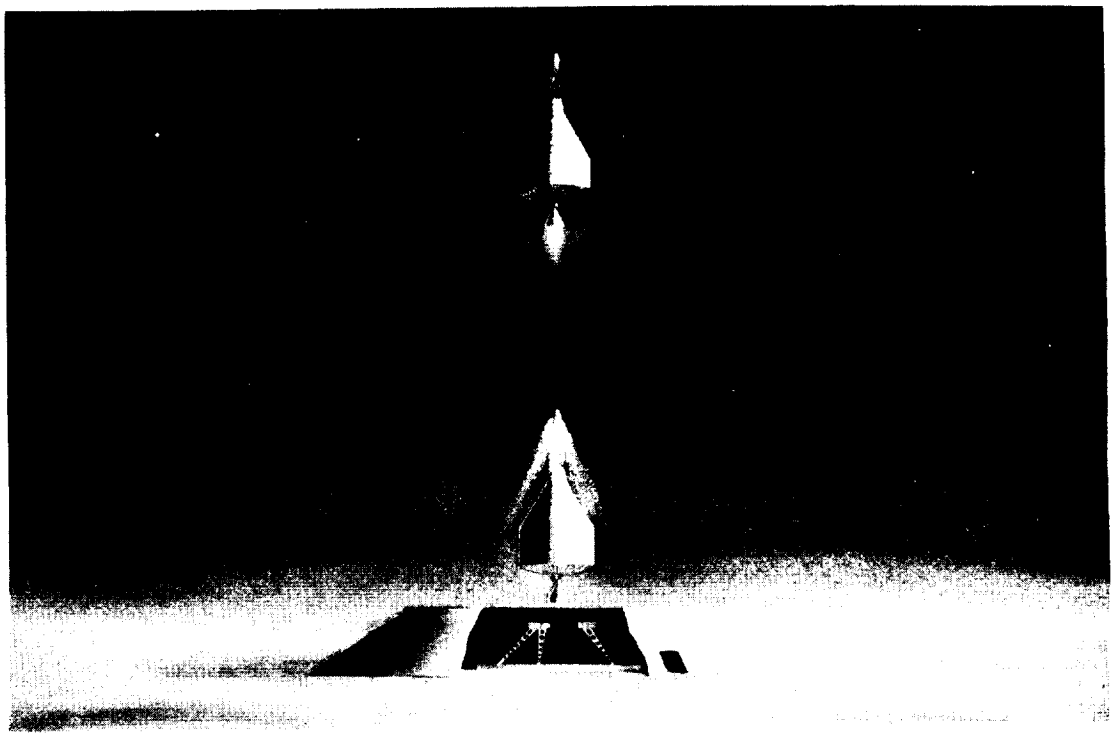

Figure 8-57. Two-Step Launch of MEV
1. Lift-Off by Nose Rockets
2. Acceleration by Main Propulsion System

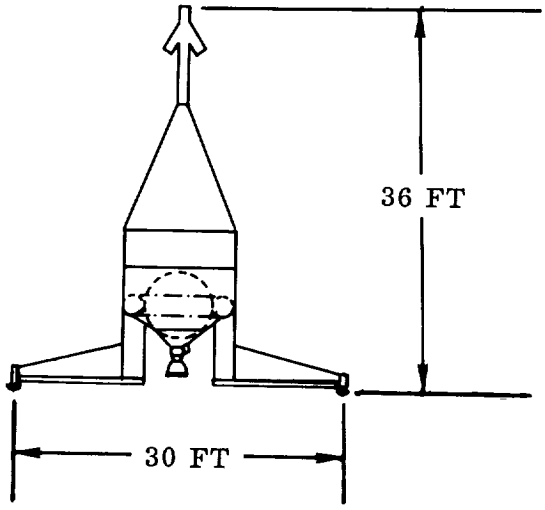

Figure 8-58. Alternate MEV Configuration

8.18 Weights. The following weight designations were used throughout this study. All weights with lower case subscripts refer to a particular stage only. Capital subscripts refer to the overall vehicle.

W_A = Gross weight at ignition ($W_A = W_B + W_P$)

W_B = Burnout weight of total vehicle ($W_B = W_b + W_\lambda$)

W_b = Burnout weight of particular stage (wet inert wt.)

W_j = Jettison weight other than W_b

W_c = Vehicle gross weight during heliocentric coast to and from target planet

W_s = Vehicle weight vehicle a satellite of earth or target planet

W_E = Atmospheric entry weight

W_p = Propellant weight (useful)

W_λ = Payload weight ($W_\lambda = W_A - W_p + W_b$)

λ= Payload weight fraction ($\lambda = W_\lambda / W_A$)

Λ= Propellant weight fraction ($\Lambda = W_p/W_A$

b= Burnout weight fraction ($b = W_b/W_A$)

$\lambda + \Lambda + b = 1.0$

W_N = Net weight ($W_N = W_p + W_b$)

x = Mass Fraction ($x = W_p/W_N$)

μ = Mass Ratio ($= W_A/W_B$)

The weight survey presented here is a summary of the weight evaluation conducted on the interplanetary vehicles to Mars and Venus.

8.18.1 Reference Vehicles (AZM-072). Prior to this study there had been a considerable amount of interplanetary mission data gathered and documented in Convair/ Astronautics Report No. AZM-072, dated 11 March 1959. The vehicles outlined in AZM-072 were used as a starting point for this study and a summary weight analysis was completed for four-and eight-person vehicles to Mars and an eight-person vehicle to Venus. The Earth orbital departure weight characteristics for these vehicles are

shown in Table 8-16. Additional weight, center of gravity, moment of inertia, and mass distribution data can be obtained from Report No. AOK 62-0003, dated 23 August 1962.

8.18.2 Earth Orbital Booster and Interplanetary Ship Evaluation. During the early part of the study several different M-1 booster (Earth orbit escape maneuver) and interplanetary ship configurations were evaluated.

The main booster configurations evaluated were clustered tanks, multiple tanks in parallel, and single tanks. Based on a constant propellant weight of 38.82 metric tons, the single tank arrangement was lighter than the multiple tanks in parallel by 18 metric tons and lighter than the clustered tank arrangements by 23.64 metric tons.

Booster mass fractions varied from 0.85 to 0.915 for propellant weights from 109 to 1,364 metric tons, respectively, when the 318.18-metric ton nuclear reactor was used. When Phoebus-type nuclear reactors were used, the mass fractions varied from 0.75 to 0.945 for propellant weights from 213 to 2,273 metric tons, respectively. Figures 8-59 and 8-60 show mass fraction versus useable propellant weights for the 318.18-metric ton and Phoebus-type boosters. Although the single tank booster arrangement was sufficient for most configurations it became essential to incorporate additional side tanks for the higher propellant loads in order to minimize tank length.

The interplanetary ship is defined as Maneuver 2, Maneuver 3, and Maneuver 4. M-2 and M-3 configurations evaluated were cylindrical tanks clustered about a central spine, torus tanks clustered about a central spine, cylindrical tanks clustered about a central tank, and single tank arrangements. Based on a constant propellant weight of 394 metric tons, the single tank arrangement and the cylindrical tanks clustered about a central tank were of equivalent weight; they were approximately 6.5 metric tons lighter than the cylindrical tanks clustered about a central spine. Since tanks clustered about a central tank were of equivalent weight to the single tank, without sacrificing interchangeability, this configuration was selected as the most favorable. This configuration also yielded lower L/D ratios and thus resulted in less meteor shielding weight (7.5% of propellant weight rather than the 9.5% when clustered about a spine). Mass fraction curves for M-2 and M-3 are shown in Figure 8-59 and 8-60 for the metal carbide ships and the graphite ships, respectively. (The graphite ships have Phoebus for M-1, Phoebus for M-2, Phoebus or advanced Nerva for M-3 and LO_2/LH_2 engines for M-4. The metal carbide ships have a 318.18 M.T. booster for M-1 and one 900-sec mission engine for M-2, M-3, and M-4.) More detailed weight analyses of the orbital escape booster and interplanetary ships are documented in GD/A Report No. AOK 62-0004, dated 6 September 1962.

Where graphite ships are considered, M-4 is achieved by chemical (LO_2/LH_2) stage. When M-4 energy requirements are not excessive, the chemical version is as much as 227 metric tons lighter than a nuclear version. However, two different types of

Table 8-16. Weight Characteristics Summary at Earth Orbital Departure

Vehicle No.*	4M-1-1	8M-1-1	8V-1-1
Payload Weight (Metric Tons)	26.00	39.00	48.00
Hardware Weight (Metric Tons)	71.00	90.00	59.00
Propellant Weight (Metric Tons)	648.00	803.00	439.00
Gross Weight (Metric Tons)	745.00	932.00	546.00
Longitudenal C.G. (Centimeters from Aft End)	4,440	5,179	4,186
Lateral C.G.	0	0	0
I_{roll} (Kg - M - Sec^2 x 10^6)	2.628	2.628	2.075
I_{yaw} (Kg - M - Sec^2 x 10^6)	59.884	100.544	70.395
I_{pitch} (Kg - M - Sec^2 x 10^6)	58.224	97.916	68.320
R (Gravity Radius - Meters)	91.44	96.32	92.35

* The following vehicle numbering system has been incorporated throughout this study:

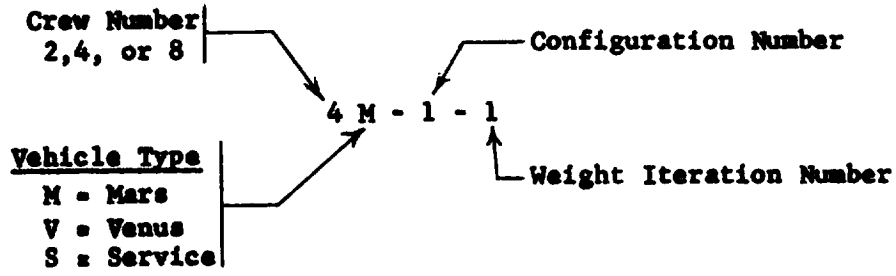

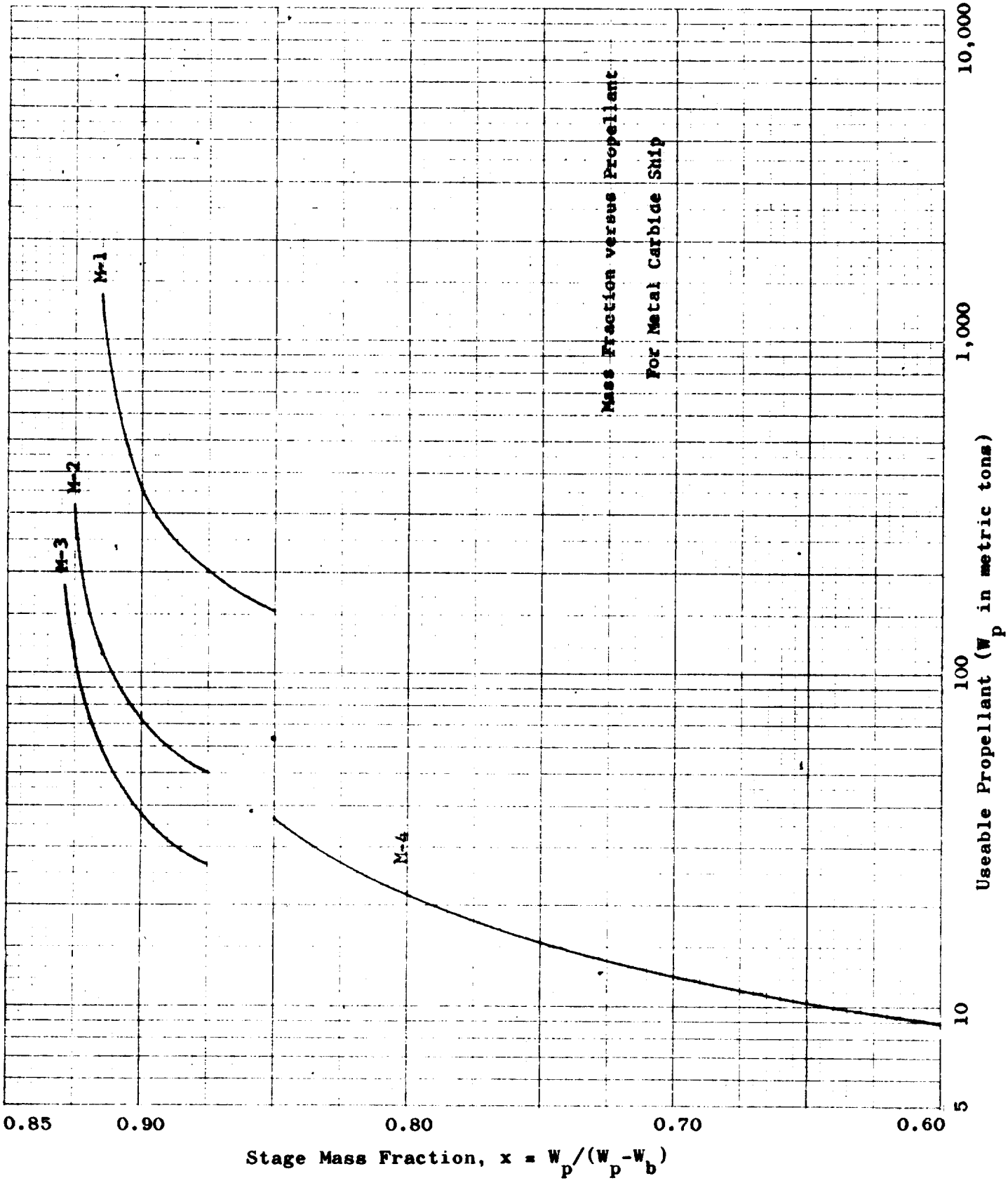

Figure 8-59. Mass Fraction vs Propellant for Metal Carbide Ship

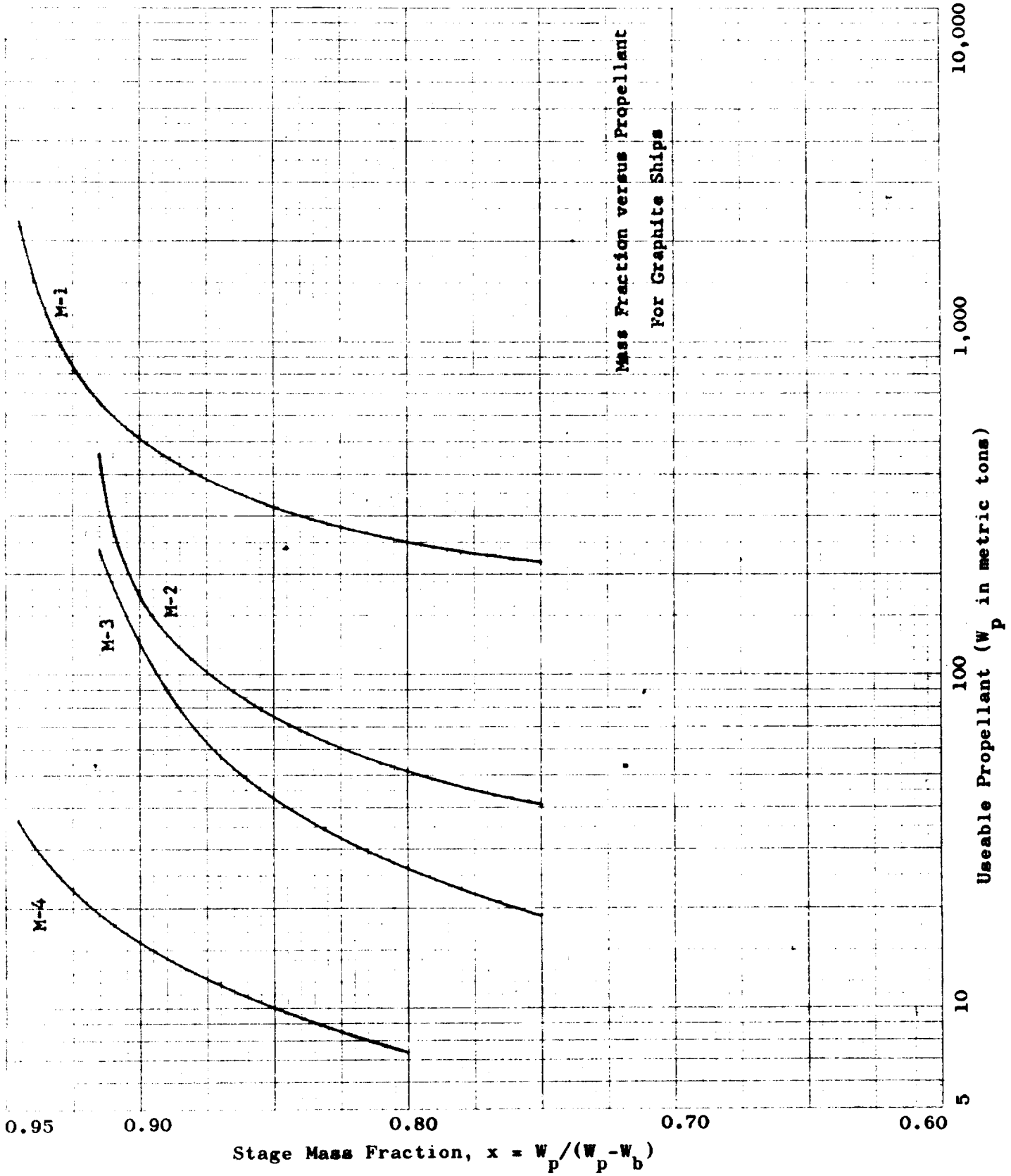

Figure 8-60. Mass Fraction vs Propellant for Graphite Ships

M-4 propellant tankages resulted out of the metal-carbide ship studies. When the propellant requirements are greater than 22 metric tons the propellant tank is wrapped around the life supporting system command module and utilizes the LH_2 as radiation shielding. When the propellant requirements are less than 22 metric tons the propellant is located between the life supporting system and the mission engine. These various configurations and their effect on overall weight will be discussed in more detail in the following paragraph. Mass fraction curves for M-4 are also shown in Figures 8-59 and 8-60 for the metal carbide and graphite ships, respectively.

8.18.3 Radiation Shielding Evaluation. The radiation shielding constitutes a large percent of the overall life supporting system weight. (The life supporting system is defined as those items not directly sustaining life, such as space suits, taxi capsules, living quarters, etc.) Therefore, an attempt was made to obtain the optimum radiation shielding configuration. Since this evaluation was conducted early in the study when the final trajectory data were unavailable, the evaluation was based on data obtained from Report No. ASO 1-4, dated 30 July 1962. Although the final configuration weights vary from the overall weights arrived at here the weight delta's would shift correspondingly. Following is a list of data used in this evaluation:

a. Specific impulse of all stages equals 830 sec

b. No allowance made for future growth

c. No allowance made for velocity increases

d. Mass fraction of first stage equals 0.86

e. Mass fraction of second stage equals 0.90

f. Mass fraction of third stage equals 0.92

g. Mars arrival date is 13 December 1973

Radiation protection was assumed to be equivalent to ten feet of hydrogen so the configurations varied from all carbon to all hydrogen with various combinations of carbon/hydrogen. The configuration with the command module completely submerged in M-4 propellant (henceforth designed as vehicle 8M-14) proved to be the lightest weight. It was approximately 58 metric tons lighter than the next lightest configuration and 92 metric tons lighter than the heaviest configuration. It was selected for more detailed analysis. For the more detailed analysis the following data were used:

a. Specific impulse of the first stage equals 845 sec

b. Specific impulse of all other stages equals 900 sec

c. A 5% allowance in 4th stage was added for future growth

d. Required volocities were increased by 3% in all stages

e. Mass fraction of the first stage equals 0.86

f. Mass fraction of the second stage equals 0.90

g. Mass fraction of the third stage equals 0.92

h. Mars arrival date is 13 December 1973

Based on the new data a vehicle gross weight of approximately 781 metric tons was obtained. A graph of vehicle gross weight versus Mars arrival date (figure 8-61) was made to determine if the arrival date was optimum. A graph of total ΔV and gross weight versus Mars arrival date was also made (Figure 8-62) which shows that minimum weight does not necessarily mean minimum energy but rather a careful selection of individual stage-energy combinations. Additional weight data involving the radiation shielding evaluation is documented in General Dynamics/Astronautics Report No. AOK 62-0006, dated 5 September 1962.

8.18.4 Metal Carbide - Graphite Ship Comparison. During the first half of the study it became apparent that the metal carbide reactor might not be available for the early missions, so weights were investigated utilizing the graphite reactors (Phoebus and Nerva type). Detailed back-up information comprising a large number of tables is available. The principal results are as follows: The graphite reactors costs approximately 400 metric tons if a chemical stage is used on M-4 and an additional 100 metric tons if M-4 is a nuclear stage. On some of the later missions this difference was reduced but still remained greater than 100 metric tons with a chemical M-4.

8.18.5 Crew Sizes. Crew size was not designated for this study so vehicles were sized for two, four, and eight persons. The difference in gross weight between a two-and four-person vehicle was approximately 87 metric tons and the difference between four and eight persons was approximately 105 metric tons. This resulted in an increase in people of 400% (two to eight persons) with less than 25% increase in gross weight. The basic reason for this is that much of the life support system is not dependent upon crew size. This also indicated that large weight reductions would have to be achieved by means other than reduction in crew size.

8.18.6 Weight Reduction Studies. When the graphite reactors were incorporated into the design, there was a substantial increase in weight due to the increase in structure weight and decrease in specific impulse. Since it had already been determined that large weight reductions would have to be achieved by means other than crew reduction, investigation was made of weight reduction by capture in elliptic rather than circular orbit and weight reduction by configuration changes involving jettisoning of the meteoroid protection shield prior to the powered maneuver substituting boron-filled polyethylene for carbon as radiation protection, and substituting chemical for nuclear propulsion in M-4. For this comparison A four-person vehicle was selected with a constant 390-day mission time. Detailed weight tables are available upon request, which reflect the weight data and weight breakdown for the vehicles involved. Figures 8-63 and 8-64 summarize the results of the study. The largest single weight reduction is obtained by increasing the ellipticity of the capture

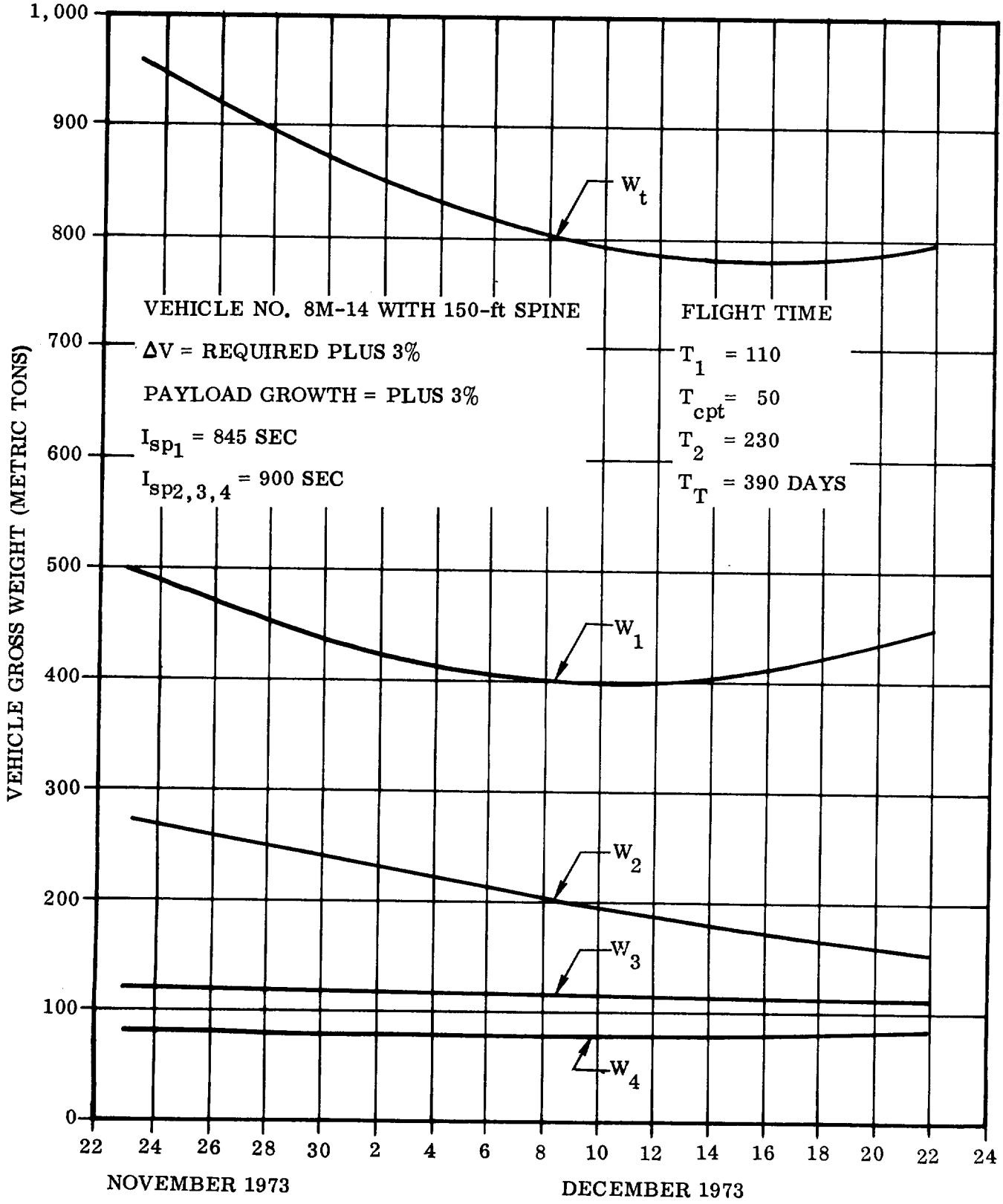

Figure 8-61. Gross Weight Vs. Mars Arrival Time

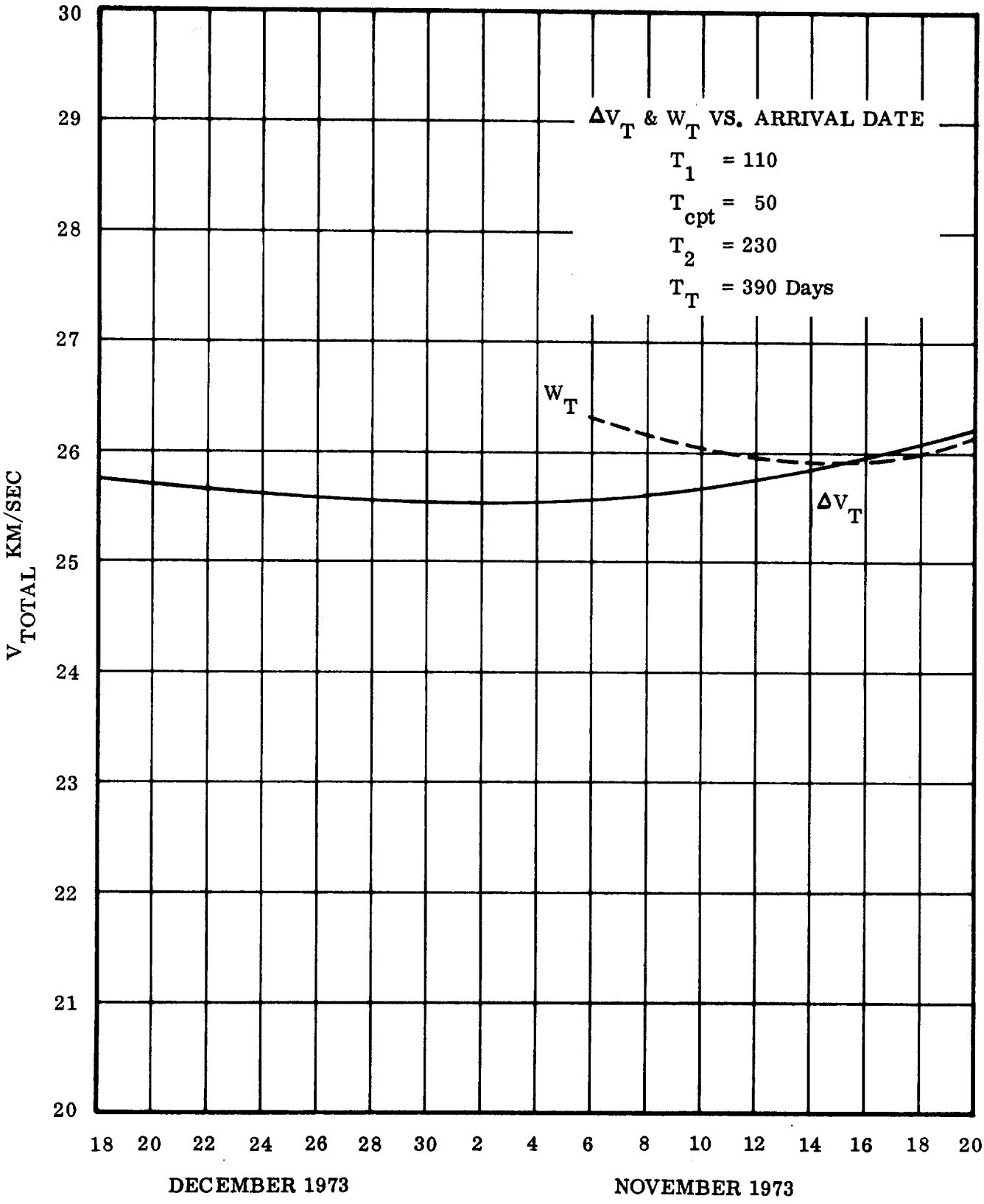

Figure 8-62. Mars Arrival Date Versus ΔV_T

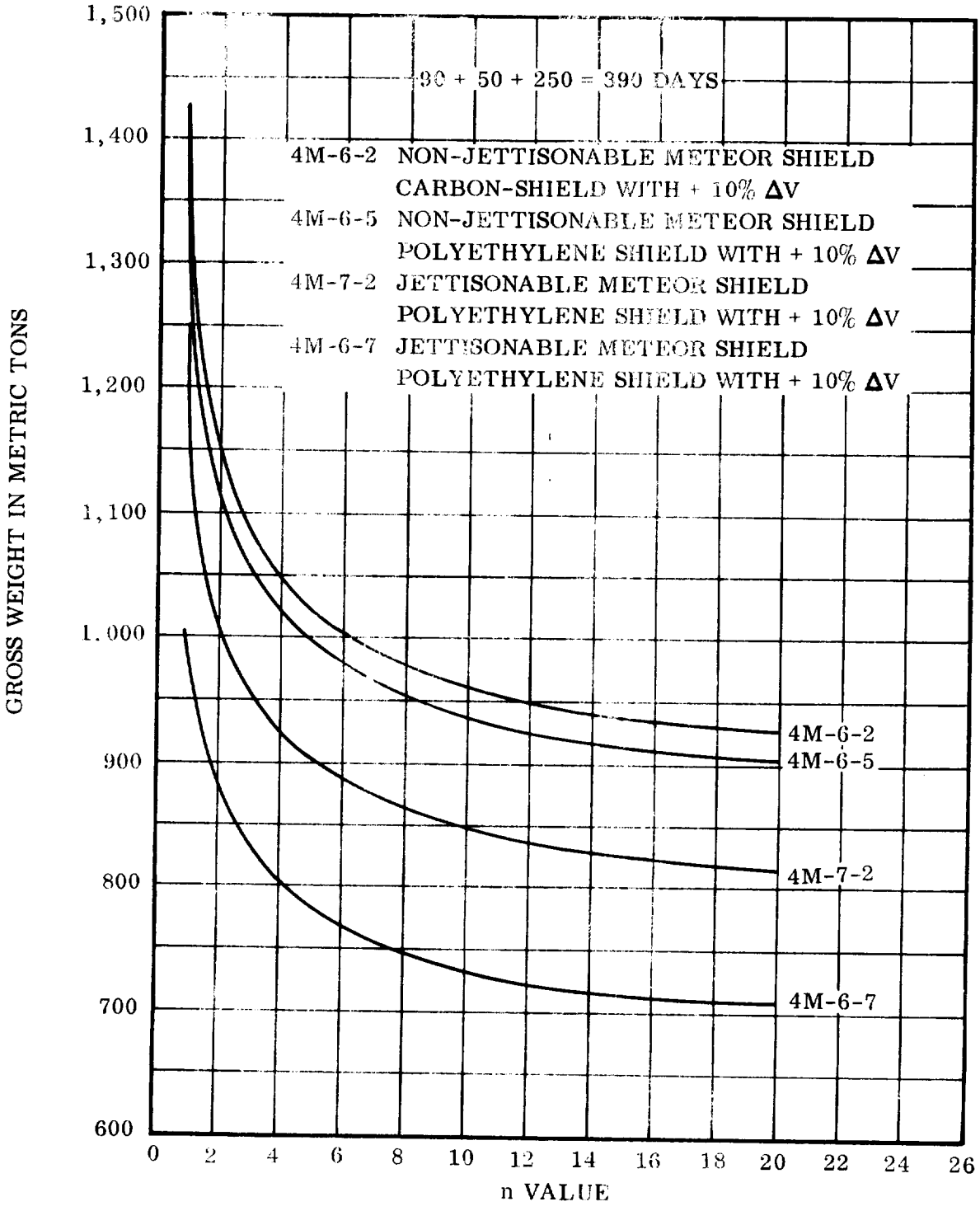

Figure 8-63. Gross Weight Vs. N Value For Various Conditions of 4 Man Vehicle

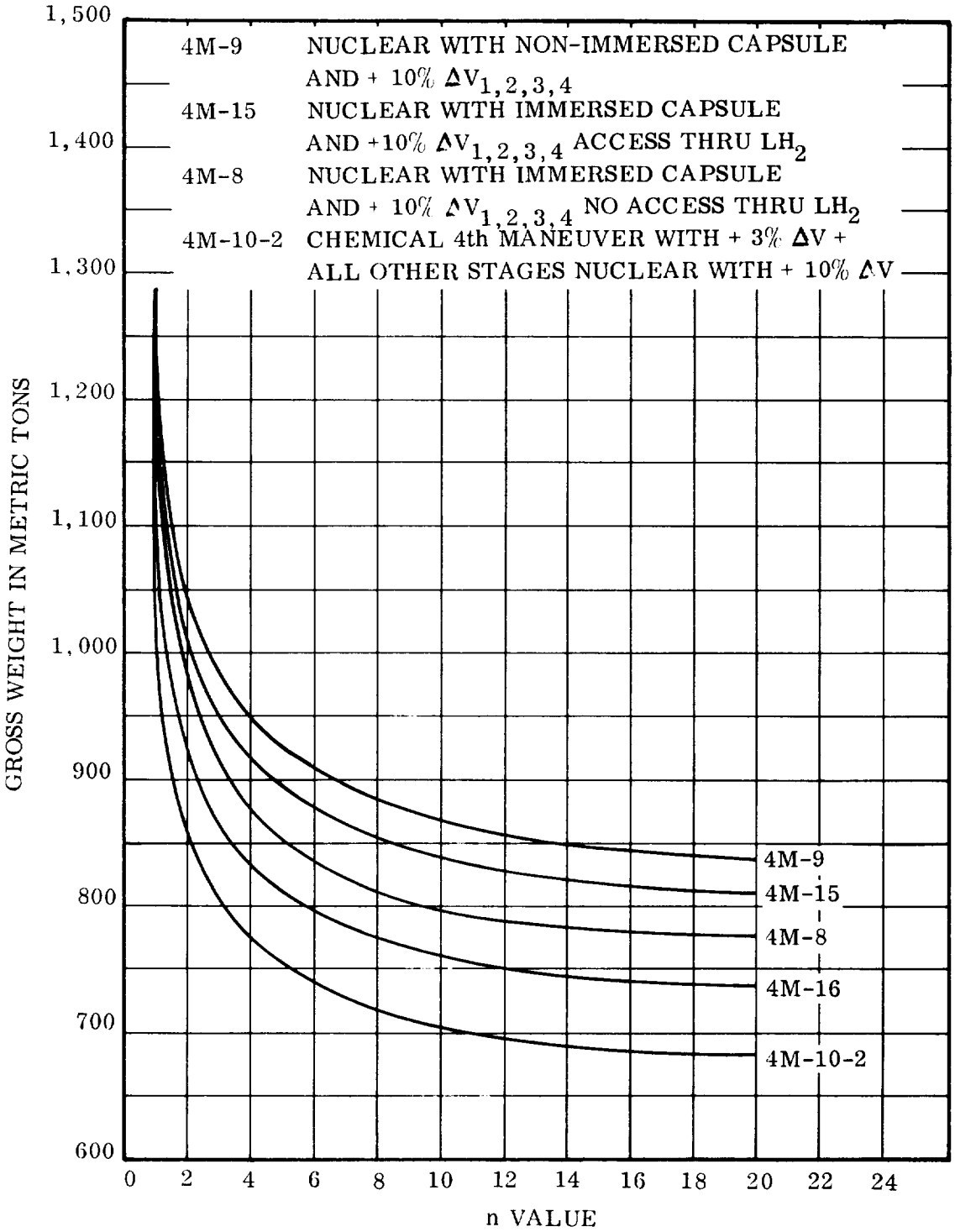

Figure 8-64. Gross Weight Vs. N Value (Jettisonable Meteor Shield and Boron Filled Polyethylene Shield)

orbit ($n = {}^{r}A/{}^{r}p$). Due to the type of mission involved, most weights are quoted for n=1.0. There were also substantial weight gains from jettisoning the meteor shield prior to engine firing and by substituting boron-filled polyethylene for the carbon radiation shielding. These two changes were incorporated into the design criteria for the balance of the study. It was also found that, when M-4 energy requirements are not excessive, a weight savings can be obtained by using a chemical rather than nuclear M-4 propulsion system. The reduction in I_{sp} was more than compensated by the reduction in shielding requirements and gravitational loss. During the final mission analysis an attempt was made to minimize M-4 energy requirements so that a chemical propulsion system could be utilized on all graphite ships.

8.18.7 Life Support System Weights. Since the various life supporting system configuration comparisons are documented in paragraph 8.4, only the standard dry version (L-28) will be summarized here. L-28 was used in the final 1973 and 1975 Mars Mission studies and in the final 1973 Venus mission studies. The standard wet or submerged version (L-27) was not used in the final analysis because the M-4 propellant requirements were less than 22 metric tons.

The weight summary for the eight-person life support system (Table 8-17) compares the Mars and Venus systems. For this study the life support system was divided into two basic parts: (a) the life supporting system (lodging quarters, taxi's, spin system, instrumentation, etc.); and (b) the ecological system (those items that directly sustain life, such as food, water, atmospheric system, etc).

Since the crew size is the same for both Venus and Mars the life supporting system varies only by the weight of the miscellaneous items, which are a function of man-days and include such items as personal kits, clothing, air filters, cleaners, sponges, etc.

The ecological system varies considerably because for Venus a 150-day long mission duration was selected on the basis of longer outgoing flights than were later selected. The food weights are based on a man-day consumption of 0.91 kg. Water is based on a total of 13.61 Kg/man, continuously recycled (3.17 kg/man for food and drink plus 10.44 kg/man for cleaning). There has also been 163.30 kg added in reserve for a total ecological system potable water weight of 272.16 kg. There is also 272.16 kg of water in the life supporting system. The water from both systems is stored in the floor of the command module and thus provides four inches of radiation shielding. The CO_2 reduction, O_2 regeneration is an H_2 reduction plus electrolysis system. The atmosphere is O_2 N_2 supercritically stored with a 1.25 margin of safety. All major systems have redundant units to ensure a more reliable mission.

8.18.8 1973 and 1975 Mars Mission Studies. Weight analyses have been completed on a multitude of two-, four-, and eight-person Mars interplanetary vehicles. Summary weights for the eight-person vehicles utilizing a dry (L-28) life support system are shown for several different Mars mission windows for both graphite and

Table 8-17. Weight Summary - Life Support System (8 Person)

	MARS*	VENUS*
LIFE SUPPORTING SYSTEM		
Command Module & Water	8,482.32	8,482.32
Spine Module	1,905.12	1,905.12
Mission Module	3,039.12	3,039.12
Taxi's & Propellant	430.92	430.92
Growth (Jett.)	4,263.84	4,263.84
Sub-system	2,268.00	2,268.00
Spin Structure	907.20	907.20
Spin Prop. (Lost During Coast)	453.60	453.60
Taxi Propellant (M2-3)	90.72	90.72
Misc. Lost in Orbit	390.10	521.64
Taxi Propellant (M1-2)	90.72	90.72
Spin Propellant (M1-2)	2,494.80	2,494.80
Guidance & Control	335.66	335.66
Miscellaneous	403.70	526.19
SUB-TOTAL	25,555.82	25,809.85
	(350 Days - 150 Day Res.)	(500 Days - 150 Day Res.)
ECOLOGICAL SYSTEM		
Food & Containers	3,991.68	5,443.20
Preparation Units	22.68	22.68
Storage Units	163.30	204.12
Water & Containers	272.16	272.16
Urine Stills & Accessories	1,061.42	1,415.23
Waste Collection & Material	762.05	1,061.42
CO_2 Reduction - O_2 Regeneration	889.06	1,106.78
Pressure System	3,492.72	4,626.72
Thermal Control	1,192.97	1,270.09
Contingency	1,106.78	1,814.40
SUB-TOTAL	12,954.02	17,236.80
TOTAL LIFE SUPPORT SYSTEM	38,510.60	43,046.65

*Weights are in Kilograms

metal-carbide ships. Propellant weights, jettisoned weights, and total weights shown were obtained by the same method used in Section 8.18.6. The mid-course correction propellants have been included in the M-2 and M-4 propellant weights. This value approached 45 metric tons for some of the more expensive missions. Table 8-18 summarizes the pertinent data used in the weight analysis of the 1973 and 1975 Mars missions. Tables 8-19 through 8-22 summarize the total weight, propellant weight, and jettisoned weight for each ship.

8.19.9 1973 Venus Mission Studies. A 1973 Venus mission of r/r_{ooo} = 20 and n = 1.0 was selected for a preliminary weight analysis of an eight-person graphite ship and metal-carbide ship. This mission was also used to study a four-person ship using chemical LO_2/LH_2 engines for all maneuvers. For the chemical ship study, r/r_{ooo} = 20 was held constant for three cases and n was varied from 1 to 2.33 to 4.0. Then r/r_{ooo} was decreased from 20 to 1.10 for three cases and n was varied from 1.0 to 4.0 to 20.0. Figure 8-65 shows the variation in gross weight with changes in r/r_{ooo} and n values.

8.18.10 Weight Determination Method. Due to the short study time involved (6 months) and the vast amount of information that must be covered in order to fairly evaluate all aspects of the program, the weights were derived by a combination of detail calculations, mass ratio and structural factor equations, and estimations. The following method of analysis was generally used to determine vehicle gross weight. Vehicles that were detailed at different times during the study (such as 8M-14 and 8M-19) to recheck mass fractions, structural factors, and meteor shielding percentages are naturally not included in this method.

Step 1: The required mass ratio (μ) was determined from performance data.

Step 2: The Earth entry weight was determined (crew, re-entry vehicle, and separation propulsion when required).

Step 3: The M-4 burnout weight (W_{B4}) was calculated or estimated, depending upon the amount of information available.

Step 4: The M-4 propellant weight was determined from the equation: $W_{p4} = W_{b4}(\mu-1)$.

Step 5: The weight jettisoned prior to M-4 was determined. This weight included the life support system, redundant equipment and systems, M-4 meteor shield, etc.

Having emphasis placed on the derivation of realistic weights during the first five steps for each configuration, since this was the area that would vary the gross weight of a particular vehicle. Maneuvers 1, 2, and 3 were fairly fixed for a particular version. Most of the weights derived during the first five steps were accompanied by configuration layouts and preliminary stress analysis.

Table 8-18. Weight Data For 1973 and 1975 Mars Missions

Year	73	73	73	73	73	73	75	75
Vehicle No.	8M-22-3	8M-23-3	8M-22-1	8M-23-1	8M-22-4	8M-23-4	8M-22-2	8M-23-2
Type Vehicle	Graphite	Metal	Graphite	Metal	Graphite	Metal	Graphite	Metal
Mission	1	1	2	2	3	3	1	1
n Value	1	1	1	1	1	1	1	1
r/r_{oo}	1.3	1.3	1.3	1.3	1.3	1.3	1.3	1.3
M-1 Engine	4 Phoebus	1 700K	4 Phoebus	1 700K	4 Phoebus	1 700K	4 Phoebus	1 700K
M-2 Engine	1 Phoebus	Uses M-4	1 Phoebus	Use M-4	1 Phoebus	Use M-4	1 Phoebus	Use M-4
M-3 Engine	1 Adv. Nerva	Uses M-4	1 Phoebus	Use M-4	1 Nerva	Use M-4	1 Nerva	Use M-4
M-4 Engine	1 LO_2/LH_2	1 Mission	1 LO_2/LH_2	1 Mission	1 LO_2/LH_2	1 Mission	1 LO_2/LH_2	1 Mission
1	1.789	1.789	1.960	1.960	1.789	1.789	2.774	2.774
2	2.363	2.456	2.020	2.091	1.717	1.777	1.646	1.746
3	2.825	2.561	2.850	2.850	2.850	2.850	2.162	2.126
4	2.421	1.546	4.177	2.075	4.177	2.075	3.778	1.979
1, 2	4.227	4.394	3.959	4.098	3.072	3.179	4.566	4.843
3, 4	6.839	3.959	11.904	5.910	11.904	5.914	8.168	4.207
1, 2, 3, 4	28.908	17.396	47.128	24.219	36.569	18.801	37.302	20.374
W_{A1}*	1,270,081	1,053,716	1,386,656	1,270,082	1,041,466	897,674	1,104,517	982,498
W_{A2}	572,081	478,139	562,912	549,810	462,672	412,458	287,719	273,476
W_{A3}	192,871	161,753	232,017	203,305	232,969	203,576	152,546	139,210
W_{A4}	13,608	15,104	23,678	20,821	23,678	20,820	20,956	19,641

* All weights are in kilograms

Table 8-19. Weight Summary For 1973-1 Mars Mission

$n = 1.0 \qquad r/r_{ood} = 1.30$

	Total Weight*	Propellants*	Jettisoned*
8M-22-3 (Graphite)			
Earth Departure	1,270,081	603,515	94,485
Maneuver 2	572,081	330,221	36,288
Orbit Mars	205,572	--	12,701
Maneuver 3	192,871	124,649	14,969
Mars Earth Transfer	53,253	--	39,645
Maneuver 4	13,608	7,575	--
Final Burnout	6,033	--	--
		1,065,960	198,088
8M-23-3 (Metal Carbide)			
Earth Departure	1,053,712	492,156	83,417
Maneuver 2	478,139	283,500	22,680
Orbit Mars	171,959	--	10,206
Maneuver 3	161,753	98,794	7,893
Mars Earth Transfer	55,066	--	39,962
Maneuver 5	15,104	5,352	--
Final Burnout	9,752	--	--
		879,802	164,158

*All weights are in kilograms

Table 8-20. Weight Summary For 1973-2 Mars Mission

$n = 1.0 \quad r/r_{ooo} = 1.30$

	Total Weight*	Propellant*	Jettisoned*
8M-22-1 (Graphite)			
Earth Departure	1,386,656	721,859	101,879
Maneuver 2	562,918	284,407	31,298
Orbit Mars	247,213	--	15,196
Maneuver 3	232,017	150,595	18,099
Mars - Earth Transfer	63,323	--	39,645
Maneuver 4	23,678	17,600	--
Final Burnout	6,078	--	--
		1,174,461	206,117
8M-23-1 (Metal Carbide)			
Earth Departure	1,270,082	621,886	98,386
Maneuver 2	549,810	308,448	24,676
Orbit Mars	216,686	--	13,381
Maneuver 3	203,305	131,998	10,524
Mars - Earth Transfer	60,783	--	39,962
Maneuver 4	20,821	10,796	--
Final Burnout	10,025	--	--
		1,073,128	186,929

*All weights are in kilograms

Table 8-21. Weight Summary For 1973-3 Mars Mission

$n = 1.0 \quad r/r_{ooo} = 1.30$

	Total Weight*	Propellants*	Jettisoned*
8M-22-4 (Graphite)			
Earth Departure	864,562	409,782	71,714
Maneuver 2	383,066	159,894	17,600
Orbit Mars	205,572	--	12,701
Maneuver 3	192,871	124,649	14,969
Mars - Earth Transfer	53,253	--	39,645
Maneuver 4	13,608	7,575	--
Final Burnout	6,033	--	--
		701,900	156,629
8M-23-4 (Metal Carbide)			
Earth Departure	713,966	333,396	54,069
Maneuver 2	326,501	143,111	11,431
Orbit Mars	171,959	--	10,206
Maneuver 3	161,753	98,794	7,893
Mars - Earth Transfer	55,066	--	39,962
Maneuver 4	15,104	5,352	--
Final Burnout	9,752	--	--
		580,653	123,561

*All weights are in kilograms

Table 8-22. Weight Summary For 1975-1 Mars Mission

$n = 1.0 \qquad r/r_{ood} = 1.30$

	Total Weight*	Propellant*	Jettisoned*
8M-22-2 (Graphite)			
Earth Departure	1,104,517	728,346	88,452
Maneuver 2	287,719	112,946	13,563
Orbit Mars	161,210	--	8,664
Maneuver 3	152,546	82,102	9,843
Mars - Earth Transfer	60,601	--	39,645
Maneuver 4	20,956	15,014	--
Final Burnout	5,942	--	--
		938,408	160,167
8M-23-2 (Metal Graphite)			
Earth Departure	982,498	628,236	80,786
Maneuver 2	273,476	117,029	9,390
Orbit Mars	147,057	--	7,847
Maneuver 3	139,210	73,710	5,897
Mars - Earth Transfer	59,603	--	39,962
Maneuver 4	19,641	9,707	--
Final Burnout	9,934	--	--
		828,682	143,882

* All weights are in kilograms

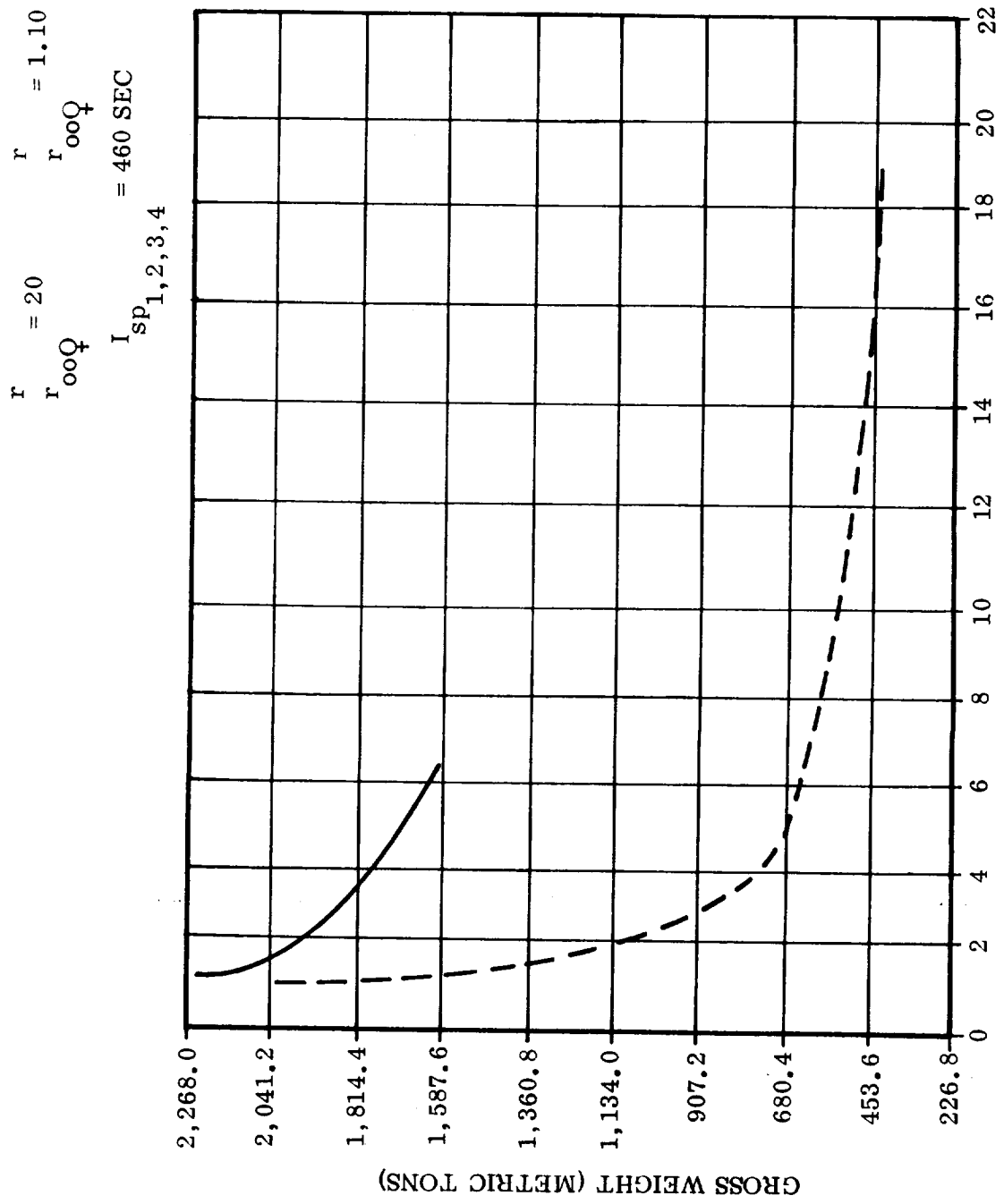

Figure 8-65. Gross Weight Vs. n Value 4 Person Venus Ship

Step 6: Having obtained the return coast weight, M-3, M-2, and M-1 propellant weights and hardware weights were derived by the equation:

$$W_p = \frac{W_{payload}\,(\mu-1)}{(1 - \text{Struct. Factor})-\text{Struct. Factor}\,(\mu)} \qquad (8\text{-}9)$$

and

$$W_H = W_p\,(\text{Structural Factor}) \qquad (8\text{-}10)$$

At various intervals a configuration was designed in more detail so that a check could be made against structural factors to assure that factors were not out of reason.

SECTION 9

CREW AND LIFE SUPPORT

9.1 INTRODUCTION. Studies of the crew and its life support system have covered the following areas:

a. Crew size and composition.

b. Crew distribution in convoy.

c. Basic design parameters for LSS layout and design.

d. Selection of ecological system.

e. Generation of artificial gravity.

f. Protection against corpuscular space radiation.

The first three aspects are covered in this section. The fourth is discussed in Section 10, the fifth in Section 11, and the last in Section 12. Compare also the discussion of the life support module design in Section 8.

9.2 CREW SIZE. An analysis made in 1959, of the derivable crew size and composition for fast manned interplanetary missions, led to a recommendation of eight persons as a representative figure (Ref. 9-1). The data and conclusions were re-examined and discussed with Prof. Strughold, and Dr. Clamann and his associates in several visits to the USAF School of Aerospace Medicine. As a result, the crew size of eight was retained as a likely number for a single individual crew, i.e., for the case where the convoy consists of one crew vehicle and one or two service vehicles. If several crew vehicles are involved, functions such as medical and certain scientific activities would not have to be duplicated in all ships. In this study the approach was taken that crew members could be exchanged and, if necessary in emergencies, entire crews would be lodged in the life support system of a sister ship.

The functions can be divided into two groups:

Group I Vehicle (V) Related Functions

- V-1 Flight Operations
- V-2 Configuration and Weight Control
- V-3 Maintenance
- V-4 Repair

Group II Mission (M) Related Functions

- M-1 Clinical Supervision
- M-2 Biological Research Direction
- M-3 Space-Physics Direction
- M-4 Planetary Reconnaissance Direction
- M-5 Data Transmission
- M-6 Orbital and/or Surface Excursions in Planetary Activity Sphere

Vehicle-related functions V-1 through V-4 determine the minimum crew size. These are the vehicle-oriented crew members who would have to be present in each ship even if there were no other task or function connected with the mission. Therefore, they must be self-sufficient in relation to the vehicle-related functions. The number of vehicle-oriented participants in the flight grows in direct proportion to the number of crew vehicles involved, at least for the numbers (one to four) under consideration here. For a very large convoy of crew vehicles it will eventually become possible to share certain maintenance and repair specialists among several ships.

In reality, there are at least some mission-related functions connected with each flight. Inasmuch as all crew members will at one time or another participate in mission-oriented tasks, the forementioned crew members therewith become primarily vehicle-oriented crew members. The crew size required by the mission-related functions does not increase in proportion to the number of vehicles, but in proportion to the number of tasks which must be performed by specialists and to the number of tasks which require direction of the other crew members by a specialist. The crew members responsible for mission-related functions contribute, therefore, work of their own as well as direction of other crew members in carrying out delicate experiments and investigations which may not be repeatable during the particular mission. The primarily mission-oriented crew members, in turn, will assist in vehicle-related tasks under the direction of the primarily vehicle-oriented crew members; with two reservations: The Flight Surgeon should not be exposed to hazardous assignments at any time during the mission; the director of scientific reconnaissance operations at the target planet should be ineligible to perform hazardous tasks prior to departure from the target planet.

The Commander and Deputy Commander are selected from the primarily vehicle-oriented part of the crew. It is assumed for practical reasons that these two men are equivalent in their capacity as expedition leaders, since it appears unfeasible (or perhaps not even desirable, psychologically) in such a limited crew size to shield or prevent the Commander from becoming involved in hazardous tasks, except for surface excursions from which he should be excluded. A representative crew composition, based on the assumption that nuclear reactors will be used for either electrical power generation, propulsion, or for both, is presented in Table 9-1.

Table 9-1. Representative Crew Composition for Fast Interplanetary Reconnaissance Capture Missions With Nuclear Vehicles. (All crew members are trained orbital and cislunar astronauts.)

ASTRO-NAUT NO.	REPRESENTATIVE PROFESSIONS	SPECIALIZATION	PRIMARY TECHNICAL RESPONSIBILITY	ORGANIZATIONAL RESPONSIBILITY
1	Engineer	Mechanical	Structure; all mechanical equipment and subsystems.	One Commander
2	Engineer	Electrical	All electrical equipment and subsystems; wiring; power distribution.	One Deputy Commander
3	Engineer-Physicist	Nuclear-Electronic	Nuclear equipment; reactor control; isotope systems; radiation protection (in cooperation with the flight physician).	At least one of this group will be involved in the surface excursion (if any) and serves as Excursion Commander, if more than one person is involved.
4	Engineer-Astronomer	Electronic	Communication; navigation; guidance and navigation equipment; meteor radar; data processing equipment.	
5	Engineer-Physicist	Electronic		
6	Physicist-Geophysicist	Instrumentation Space Physics	On-board scientific instrumentation; on-board observatory; operational readiness of auxiliary vehicles prior to deployment.	Directs space physical research during transfer and capture period.
7	Astronomer-Geologist	Planetology Meteorology Geophysics		Directs scientific reconnaissance operations concerned with the target planet.
8	Physician Biologist	Medicine Surgery Dentistry Radiology Psychiatry Biology Medical Technology	Monitoring bio-technical systems in LSS; food and sanitary control; health and morale of crew; biological and astro-clinical research	Flight Surgeon; directs clinical and biological research en route; directs target-planet oriented biological research

The most important duty function is control. The control room, which is part of the heavily shielded command module, is occupied at all times. Having capacity to seat three persons, it will never be occupied by less than two persons. They represent the 25 percent of the crew which is always in a state of maximum alert. Theirs is the initial response in any emergency situation or unexpected event; they alert part or all of the remaining crew.

The control duties are divided into two parts:

C-V (Vehicle-oriented):

Systems monitoring
Regular checkouts
Monitoring of vehicle-oriented work schedules and crew activities.
Planning and initiation of unscheduled maintenance or repair activities.
Routine monitoring of sanitary conditions.

C-M (Mission-oriented):

Routine navigational tasks.
Data recording and processing.
Data transmission and other communication with Earth.
Monitoring of critical environmental conditions (especially solar activity, corpuscular radiation intensity, meteor detection radar).
Monitoring of routine scientific measurements.
Monitoring of, and communication with other convoy vehicles.

The two crew members on control duty complement one another. The presence of two members permits temporary absence of one, if warranted by extraordinary circumstances. No crew member will be on duty in any one of these functions (C-1 or C-2) longer than two hours, except in emergencies or (possibly) under special conditions during the capture period. The maximum control duty period for a crew member is four hours, in which case nominally two hours are spent on vehicle-oriented control duty (C-V) and two hours on mission-oriented control duty (C-M). Exempted from this duty cycle are the Commander and the Flight Surgeon. A representative control duty schedule for the remaining six crew members is shown in Figure 9-1. This schedule is the backbone and frame of reference for all other on-board schedules. Each of the six crew members spends eight hours on control duty. Another four hours will be spent on maintenance, repair and scientific activities which cannot be scheduled in detail at this time, and which probably will have to be scheduled as warranted. Certainly the schedule controlling the residual four hours will be different during the capture period from the one in force during heliocentric transfer. Thus, the work day of the six "scheduled" crew members is 12 hours long;

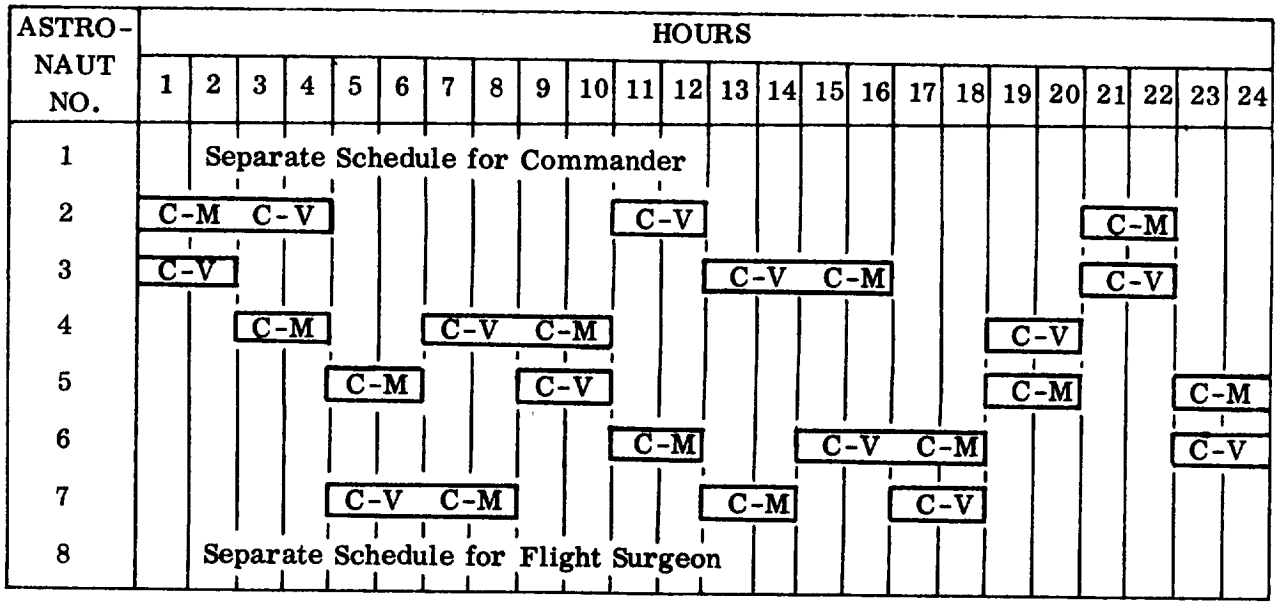

Figure 9-1. Representative Control Duty Schedule for an Eight-Man Crew in One Vehicle

a busy schedule is probably the most efficient antidote against psychological and morale problems of the crew during the year-long mission period. The residual 12 hours are divided into rest (recreation, athletics and personal activities) and sleep. Sleeping hours are flanked on both ends by at least one rest hour each, to enable each crew member to adjust his sleeping period according to his personal needs. Generaly, the sleeping time will be at least six hours. Placing at least one hour of rest prior and one hour following the sleeping period, to include time for personal hygiene and food intake, requires one rest-sleep period of no less than eight hours for each crew member. This condition is satisfied in the schedule shown in Figure 9-1. Where 10-hour periods appear between control duties (Astronauts No. 3, 6 and 7) some of this time may be spent on other duties, serving the additional four hours previously mentioned. Generally, however, it is assumed that the residual four-hour work period and the residual four-hour rest period (in addition to six hours sleep and one hour rest at each end of the sleeping period) will be scheduled informally, as required.

A crew of eight permits near-optimization of the functions of not only the scheduled crew members, but also of the Commander and the Flight Surgeon. Moreover, in emergencies or cases of sickness or death of one of the scheduled crew members, the Commander and Flight Surgeon can be scheduled into the cycle.

If the crew is reduced to six, all crew members must be included in the schedule. Standby capacity is zero. It is doubtful that the Flight Surgeon can, in practice, be incorporated into a rigid schedule for long periods of time. If, in a six-person crew,

one crew member is incapacitated and must be removed from the duty cycle, the rest and/or sleep period of the other crew members must be reduced by two hours for four of the five available crew members if a two-man duty is to be maintained in the command module at all times (Figure 9-2). Conditions would become critical during the capture period, where the work load is particularly high. Thus, the crew should contain at least seven persons.

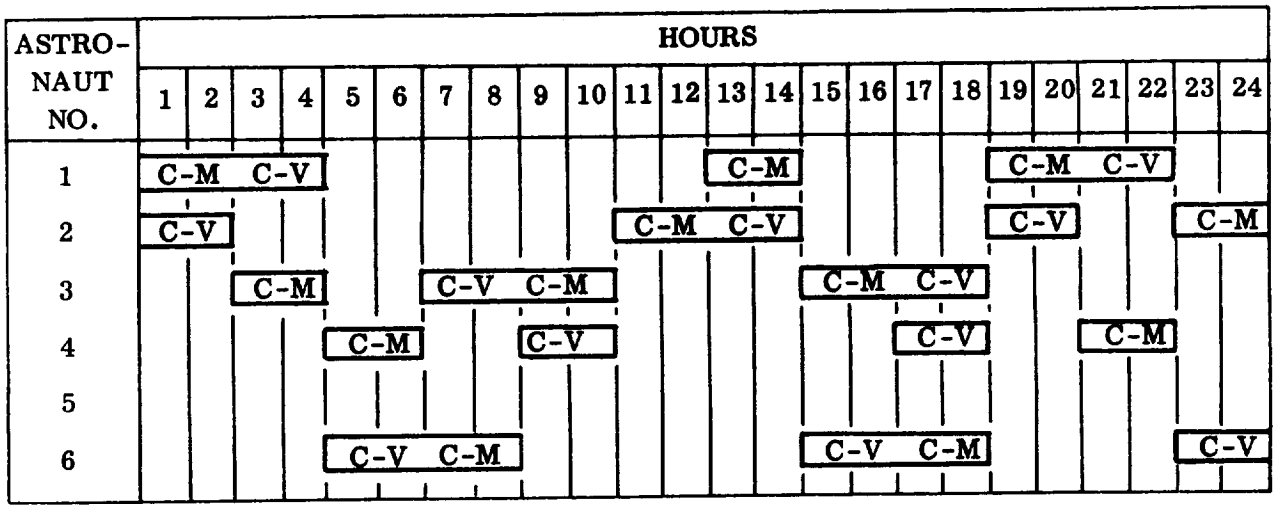

Figure 9-2. Representative Control Duty Schedule for a 6-Man Crew With One Crew Member Incapacitated

If the number of crew members is reduced to four, the strain becomes considerable if two members are to be on duty at all times. The maximum period between control duty is six hours (Figure 9-3). The crew members will, therefore, rarely sleep more than five hours. To attain even this limited sleeping period, crew members must be on duty for up to six hours at a time. This is considered inconsistent -- for the mission periods in question -- with the demands for highest alertness and reliability of the crew members, and should be accepted only under emergency conditions. Here again, if one crew member becomes incapacitated, a schedule which provides for two men on duty can not be maintained for more than a very few days. As an alternative, therefore, reducing the number of men on duty from two to one must be considered.

Figure 9-4 shows that under these conditions, the individual crew members have a nine-hour period between two duty periods of three turns each. In this case, however, the convoy should include at least two crew vehicles, each with a four-man crew, so that mission-oriented functions can be shared to reduce the work load for the individual crew member on duty. For example, the third, fourth and fifth of the C-M functions need not be duplicated in both vehicles.

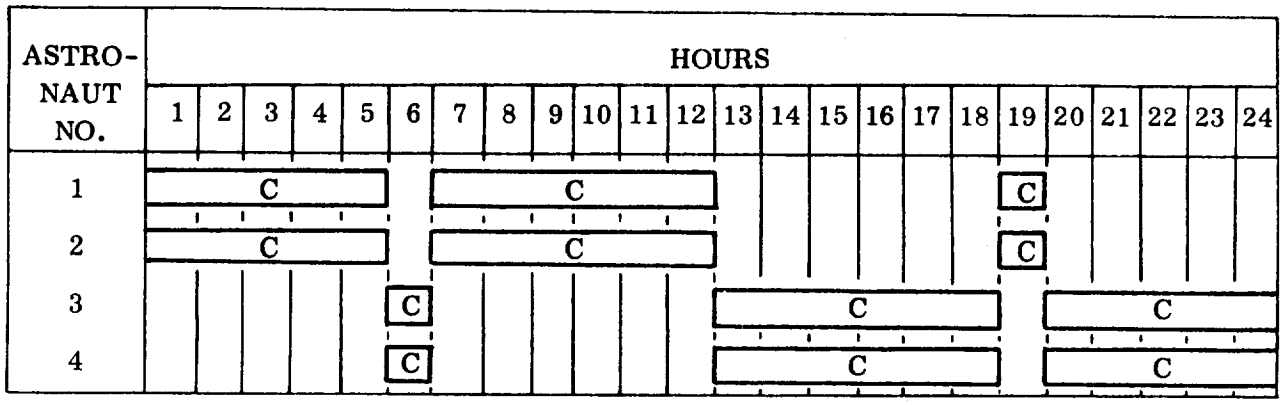

Figure 9-3. Control Duty Schedule Required for a 4-Man Crew if Two Crew Members are to be on Duty at All Times

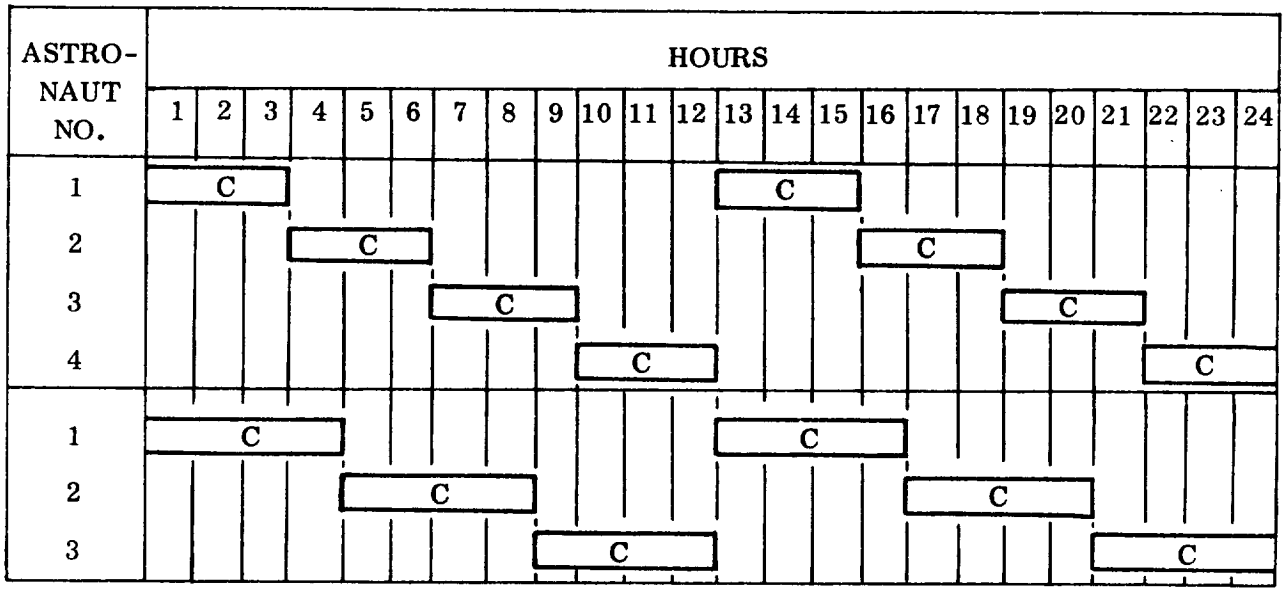

Figure 9-4. Control Duty Schedule for Crew Sizes of Four and Three

If the crew size is reduced to three, the conditions associated with four crew members (with one member always on duty) remains the same, except that for each crew member the duty period is lengthened by one hour and the interval between duty periods reduced correspondingly. Here again, two or three crew ships should participate. Otherwise, a crew size of three is not considered realistic.

It is concluded that a crew size of eight men per crew ship is adequate, since it permits the Commander and the Flight Surgeon to stay outside the regular duty cycle. In emergencies, or during the descent of one or two persons to the surface of the target planet, the Commander and Flight Surgeon participate in the cycle. If the convoy contains only one crew ship, a crew size of eight is considered adequate for handling one or two service ships en route.

If the surface excursion is to involve more than two persons, the additional personnel should be added to the crew.

If two crew members are to be on control duty at all times, the crew per vehicle should be no less than seven, to permit at least the Flight Surgeon to stay outside a rigid duty schedule.

A crew size of six is considered too small (at least for capture missions) for a continuous duty strength of two men, since this number contains no reserve for sickness of a crew member, or for possible excursions to the surface of the target planet.

A crew size of four to five per vehicle appears acceptable only if the convoy contains at least two crew ships and if no surface excursion is planned, as in the case of a Venus mission.

Crew sizes of three or less are considered incompatible with any practical combination of vehicle- and mission-oriented functions, and belong only in the category of emergency conditions.

9.3 CREW DISTRIBUTION. The crew operates a convoy of ships. The individual space ships would be either crew ships or serveice ships, or a combination carrying both crew and cargo. To some extent, of course, they are a combination in any case. The key difference implied by making the distinction here is that the crew vehicle or combination vehicles carries a complete LSS, whereas the service vehicle does not. It carries merely a spare Earth Entry Module (EEM) which also serves as temporary LSS for a crew boarding the service vehicle for limited periods of time. The distinction, therefore, implies the difference between crew distribution over the entire convoy (combination ships) and crew concentration in one (or a limited number) of the convoy ships.

A number of possible combinations of crew distribution in the convoy are shown in Table 9-2. Of these, all alternatives involving combination ships have been discarded primarily for two reasons: First, in cases such as B, D, J, and M the number of LSS is doubled, compared to cases A, C, G, and K without reducing their capacity which, for protection against emergencies, must be laid out for the entire expedition crew. Secondly, in cases such as F and N the number of vehicles which must return to Earth is a maximum. This means, also, that a maximum number of vehicles must be successfully launched out of the target planet capture orbit. If the launch of any one of these vehicles fails -- except perhaps at a sufficiently early phase so that the other ships could be stopped and a rescue operation from the convoy carried out -- the crew of the incapacitated ship would have to be left behind: not a desirable prospect. An additional reason for rejecting B and F is that the regular number of crew members is too small.

Table 9-2. Possible Combinations of Crew Distribution in Convoy

COMBI-NATION	CREW SIZE	NO. OF PERSONS PER LSS		NO. OF LSS REQUIRED	CONVOY VEHICLES REQUIRED		
		REGULAR	EMERGENCY		CREW	SERVICE	COMBI-NATION
A	6	6	6	1	1	1	
B	6	3	6	2			2
C	8	8	8	1	1	1	
D	8	4	8	2			2
E	8	4	8	2	2	1 or 2	
F	8	2	4	4			4
G	12	12	12	1	1	1	
H	12	6	12	2	2	1 or 2	
J	12	6	12	2			2
K	16	16	16	1	1	1	
L	16	8	16	2	2	1 or 2	
M	16	8	16	2			2
N	16	4	6	4			4

The remaining combinations consist of those which contain the entire crew in one vehicle (A, C, G, K) and those which distribute the crew over two vehicles (E, H, L). In both cases separate crew and service vehicles can be left behind, since the two crew vehicles serve as emergency vehicles for one another. Therefore, both life support systems must be laid out for the full crew strength of both ships. This is a decided weight disadvantage compared to having the crew in one LSS (as in the cases A, C, G, and K) which is separable and transferrable to the accompanying service ship in case of an emergency. The underlying assumption of this reasoning is, of course, that the LSS itself would not be severely damaged and that the only reason for transfer would be damage of the vehicle. This assumption appears justified in view of the heavy protection of command module and service module, in which the crew can survive even if all mission modules are destroyed or have to be jettisoned. The heavily shielded portions of the LSS could be destroyed only by an internal explosion or by a large meteorite hit, both very unlikely events. The chances that the crew would survive such an occurrence is even less likely.

Regarding failure of vital equipment inside the LSS, it is considered mandatory that the LSS be equipped with sufficient spares to permit the crew to repair any non-catastrophic failure without having to abandon the LSS. Therefore, pending a further detailed failure analysis of the LSS, it is tentatively assumed for the present that LSS destruction can be disregarded as a cause of crew transfer. If the LSS modules are transferrable (in an emergency) to the accompanying service vehicle, no spare LSS

is required and a significant weight penalty can be eliminated. It is realized, of course, that the service vehicle has to carry enough fuel to accommodate the LSS at any time. The fuel weight savings are derived from the fact that on the outbound leg of the trip, the service vehicle does not have to carry auxiliary vehicles (especially the manned excursion vehicles for a Mars flight) plus the LSS. The assumption is that if an emergency occurs (during the outbound flight), necessitating a transfer of the LSS, the payload of the service vehicle will be reduced by the mass equivalent of the LSS; spares and/or auxiliary vehicles (even the excursion vehicles, if necessary) will be sacrificed.

Unfortunately, it is not possible to carry a low-mass LSS on the service vehicle, since the bulk of the LSS is the command module and the ecological system, which together account for approximately 50,000 out of 85,000 pounds (eight-man system). Taking into account the other necessary items, such as the spine module, spin propellant, power generation and other subsystems, a "low-mass" LSS to be carried on the service vehicle without mission modules would be hardly 10,000 pounds lighter than the LSS on the crew vehicle. If a spare LSS is to be carried on the service vehicle in addition to its regular payload, the total payload weight on the outgoing leg of the flight would be nearly doubled, since the regular payload of the service vehicle is close to 100,000 pounds, most of which will be left in the planet's activity sphere.

Another cause of weight penalty for two-vehicle crew distribution is connected with the radiation pattern of the reactors which power the nuclear engines. Under presently considered ground rules these reactors are heavily shielded, at the end opposite the exhaust nozzle, to provide a shadow-shielded area in which the crew is located, adequately protected from excessive neutron and gamma radiation. The reactor side walls are not shielded. This results in a gamma radiation pattern of the type shown in Figure 9-5 for the NERVA engine. The gamma radiation dose at a 10-foot distance from reactor center is seen to be 2×10^8 rad/hr. The gamma intensity at the same distance from the reactor of a 200-k thrust engine is 5×10^8 rad/hr (cf. Addendum of this Report). The resulting gamma radiation intensity for a 30-minute thrust duration is shown in Figure 9-6 as a function of distance. The neutron flux density in the immediate vicinity of the unshielded side walls of the 200-k engine reactor is of the order of 10^{15} n/cm^2 sec (cf. Addendum). At distances that are large compared to the reactor dimensions the reactor can, in the first approximation, be regarded as a point source and the inverse square law can be applied. On this basis the neutron flux is shown in Figure 9-7 as a function of distance. The neutron flux is correlated with the roentgen equivalent (per) man (rem = rad $\times$ RBE; RBE = relative biological effectiveness) in Table 9-3, based on data in Ref. 9-2. Assuming the radiation consists of thermal neutrons, the biological effect of the neutron radiation even at 30,000 feet (about 9 km) distance is still 1875 mrem or 1.875 rem. The RBE factor of neutrons between the thermal energy level and 0.005 mev is of the order of 2.2 to 2.8 for continuous low-dose exposures; for acute high-dose rate exposure the RBE is lower.

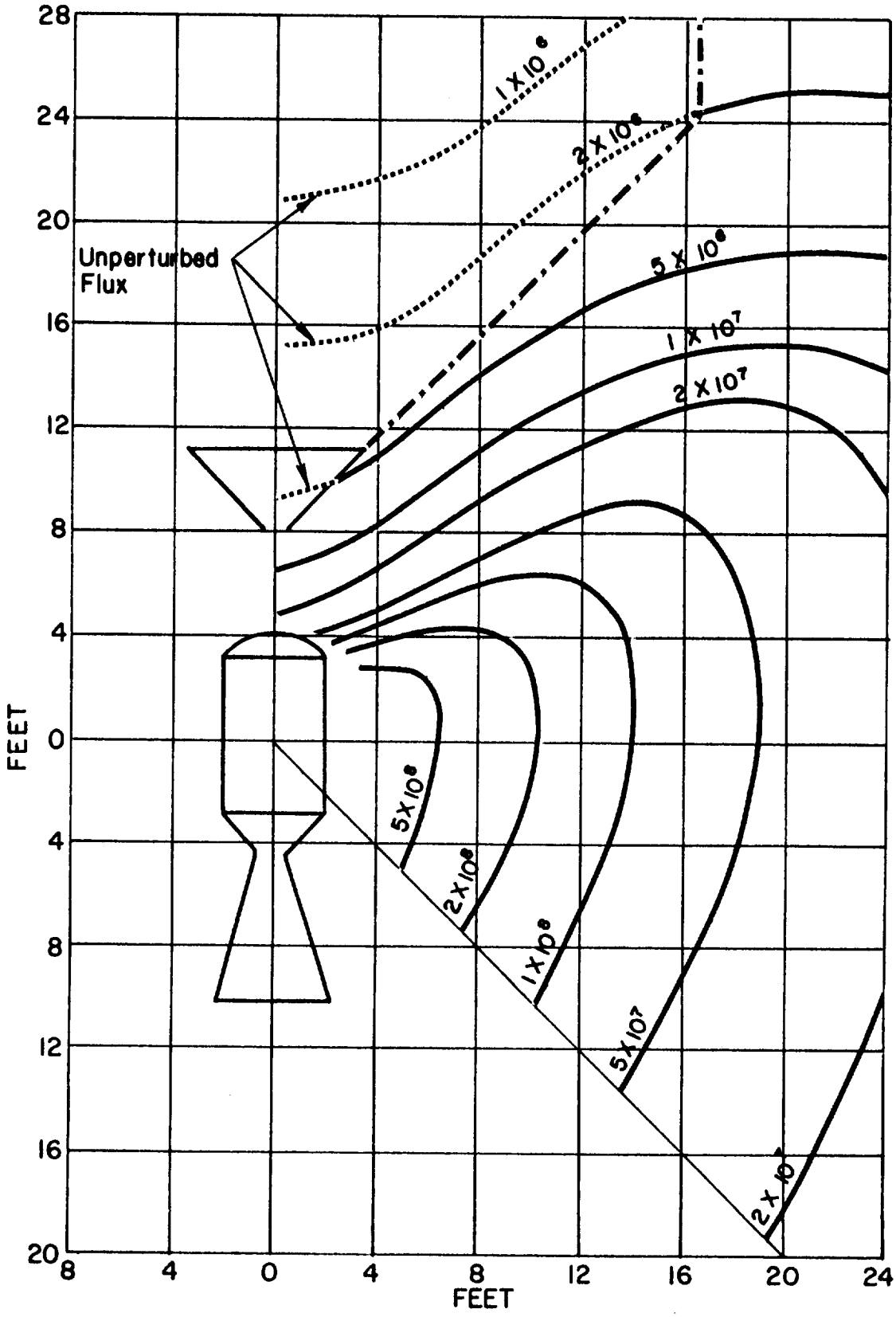

Figure 9-5. Shielded NERVA Engine - Operational Dose Rate (Rad/hr) (Ethylene Dosimeter)

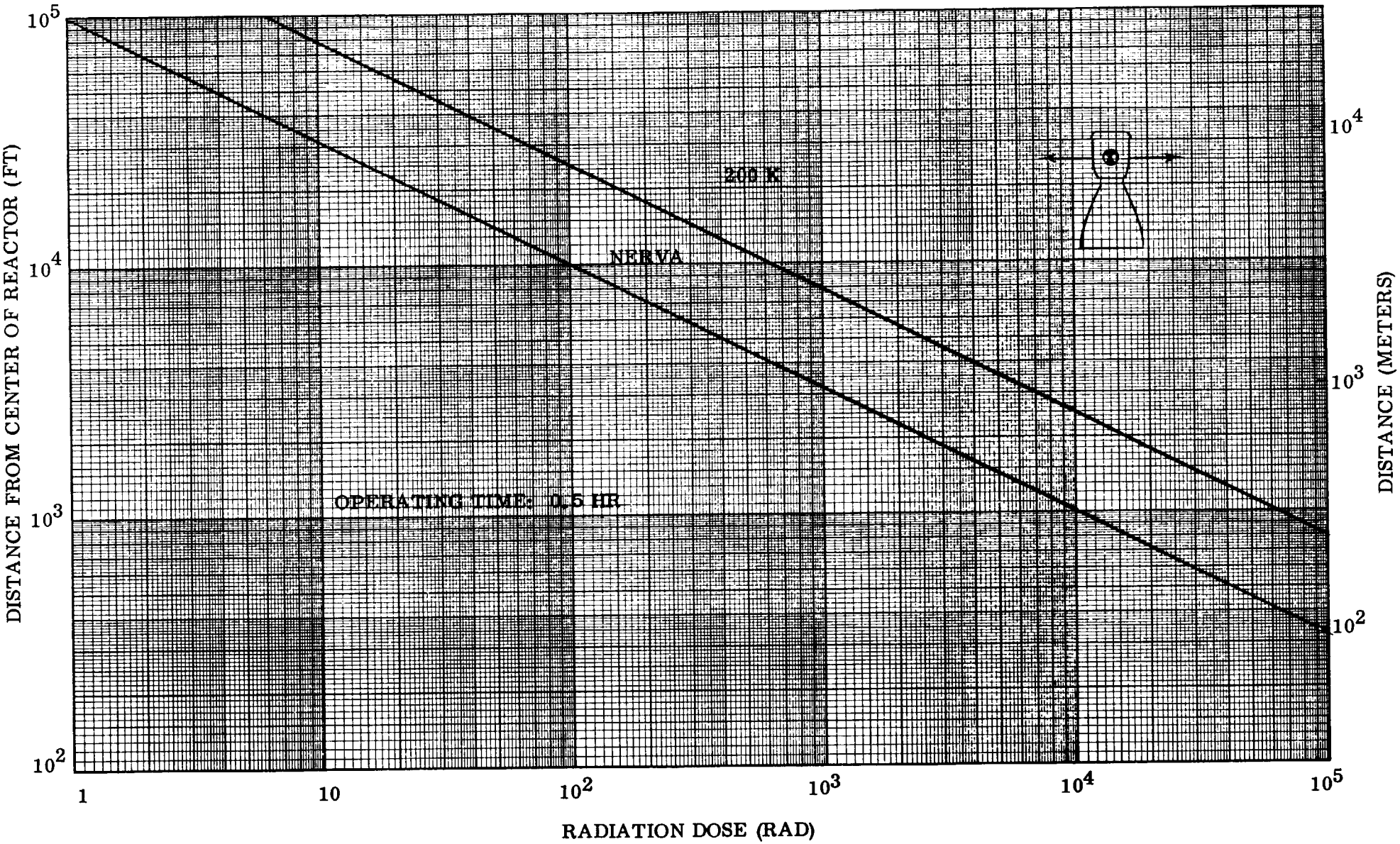

Figure 9-6. Gamma Radiation Dose Normal to Reactor Axis for 30 Minutes Operating Time for NERVA and a 200 k Thrust Engine

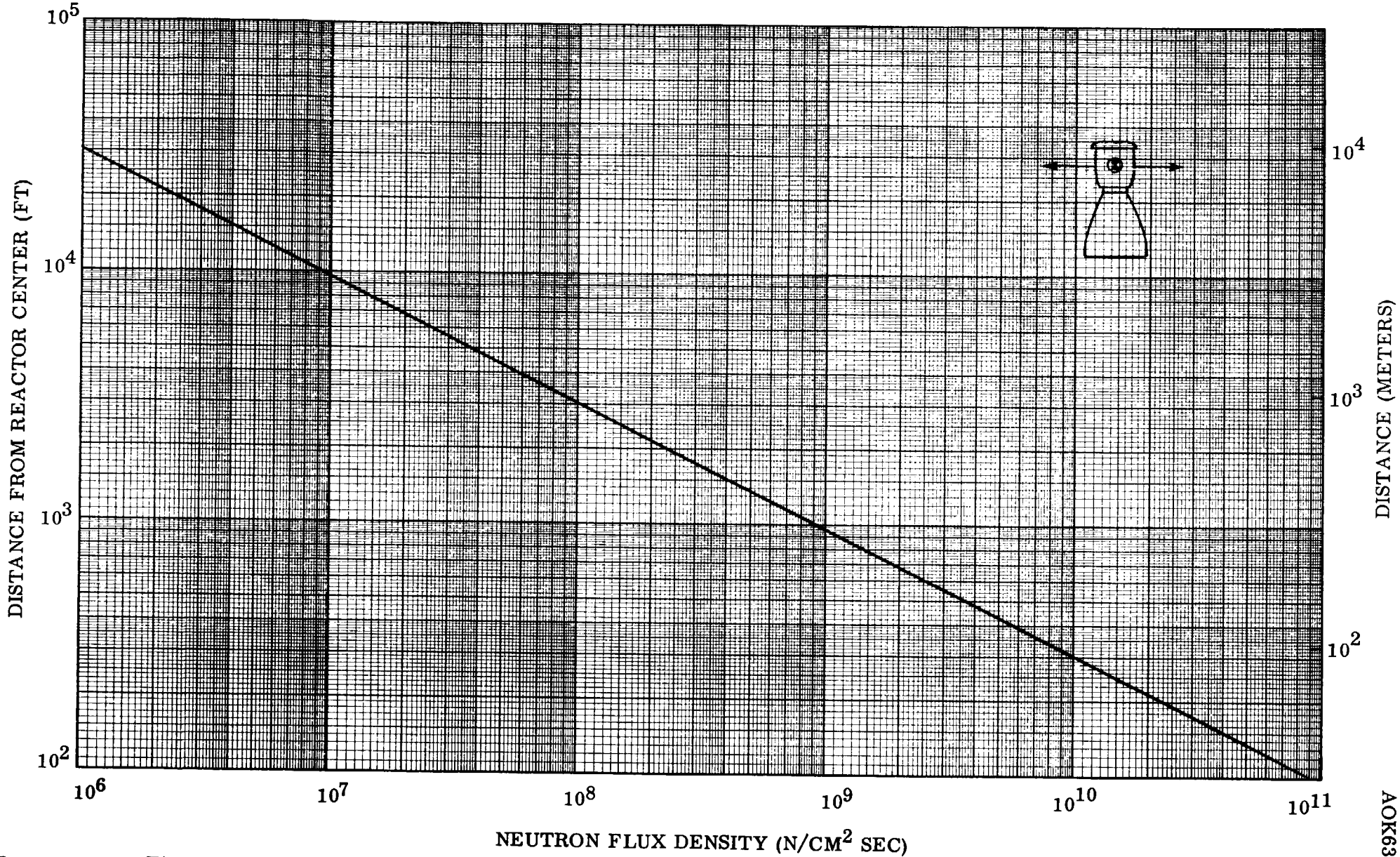

Figure 9-7. Neutron Flux Density Normal to Reactor Axis of a Nuclear Engine of 200,000-lb Thrust.

AOK63-0001

Table 9-3. Biological Effect of Neutron Radiation

NEUTRON ENERGY (MEV)	MREM* PER 30 MINUTES (NEUTRON/CM^2 SEC)
2.5×10^{-8} (thermal)	1.875×10^{-3}
10^{-4}	2.4×10^{-3}
4×10^{-3}	2.2×10^{-3}
2×10^{-2}	4.5×10^{-3}
0.1	1.5×10^{-2}
0.5	4.15×10^{-2}
1.0	6.125×10^{-2}
2.5	6.125×10^{-2}
5.0	6.8×10^{-2}
7.5	7.5×10^{-2}
10.0	7.5×10^{-2}

* Mrem = milli-roentgen-equivalent-man

Assuming an RBE of 1.5, the radiation dose rate corresponding to 1.875 rem is approximately 1.25 rad, or about one percent of the total trip dose. At the same distance the gamma intensity is 70 rad. The exact amount of rads to which the crew would be exposed under these conditions depends upon the shielding effectiveness of the material surrounding the Earth Entry Module (serving as the abort module, in which the crew is located during departure), and on the number of engines attached to the escape booster. The Earth Entry Module (EEM) is not strongly shielded and the escape boosters may be powered by as many as four 200-k engines. It is apparent, therefore, that a considerable weight penalty is involved either by shielding the reactor side walls or, even more so, by providing added shielding of the EEM. The other alternative is to keep the crew vehicles a considerable distance apart (10-20 km) during powered flight maneuvers (Earth escape as well as other powered maneuvers). This implies considerable maneuvering, if the convoy is to be drawn closer together during subsequent coast phases and then separated again prior to the subsequent powered maneuver.

For these reasons it is considered simpler and more efficient to house the entire mission crew in one LSS. The service vehicle, whose payload section is less sensitive, must be lined up behind the crew vehicle.

Another advantage of this arrangement lies in the additional safety it offers to the crew. After lining up the service vehicle behind the crew vehicle prior to a powered maneuver, the crew vehicle engine(s) will be started prior to those of the service vehicle. Therefore, it is not possible, in case of a crew-vehicle launch failure, for the service vehicle to pass the crew vehicle at close distance and expose the crew to dangerously high radiation flux densities.

As a result of these considerations, the following arrangements appear most attractive at this point of the study:

a. The entire expedition crew is assembled in one interplanetary spaceship, to 1) optimize the utilization of the heavy life support system; 2) minimize the chance of losing part of the crew due to launch failure of one of the crew ships during departure from the target planet; 3) minimize the shielding weight penalty for protecting the crew against reactor radiation from one or several sister crew ships; and 4) minimize the fixed-duty-schedule strain which increases with decreasing number of crew members in a ship. For the present, this conclusion is based on consideration of crew sizes between 7 and some 15 to 16 persons. (All do not necessarily have to return in one Earth Entry Module; several EEM's can be attached to the LSS.) The above conclusion has not yet been examined for significantly larger crews.

b. The crew ship is accompanied by a number of service vehicles (as many as are required for the mission assignments in the target planet capture orbit). During powered flight periods (if the ships have nuclear drives) the service vehicles are constrained to motion in the wake of the crew ship, which enjoys maximum protection from reactor radiation. The start of service vehicle engines is contingent upon successful start of the crew-vehicle engines. The service ships are subject to remote routine checkouts from the LSS, which serves as a "blockhouse" for service vehicle monitoring and control. Maintenance and repair, to the extent that it requires human participation, is accomplished by periodic visits of crew details during the coast period. The number of service ships and the amount of direct crew attention they require may alter (increase) the crew size beyond eight. This remains to be determined by a more detailed study. One service ship will accompany the crew ship on its return flight to Earth. During the return coast mode the service ship will have almost no payload and, therefore, will be able to accommodate the LSS if transfer of the latter should become necessary because of severe damage to vital parts of the crew vehicle, such as a loss of spin propellant, Earth capture retro propellant (where such maneuver is part of the mission sequence), hydrogen liquefaction unit, electrical power supply units, or the spine.

9.4 CREW-RELATED DESIGN CRITERIA. The crew-related design criteria which influence the type of life support systems, their size, necessary equipment, weights and so forth are, in summary:

a. Investigate life support systems (LSS) for a crew of 2, 4, 6, and 8 persons (male, 25-40 years of age, maximum weight 175 pounds) on a fast round-trip reconnaissance flight to Venus or Mars.

b. Mission period generally lies between 350 and 430 days, involving a capture period of 30 to 50 days in an orbit about the target planet.

c. The expedition crew will number no less than 8 persons, nor more than 16.

d. Based on the considerations in Paragraph 9-2, the entire mission crew will occupy one LSS. The LSS will be transferrable to an accompanying service ship in cases of emergencies.

e. The parameters to be monitored in the LSS, continuously or at regular intervals, are listed in Table 9-4.

f. Basic metabolism per day (Ref. 9-3)

		Consumption (lb/d)				Elimination (lb/d)					
		O_2	H_2O	Dry	Total	CO_2	H_2O		H_2O Breakdown:		
Age	Cal/d			Food				Resp.	Persp.	Urine	Feces
25	1760	1.2	3.4	1.2	5.8	1.5	3.9	0.55	0.78	2.3	0.23
40	1641	1.1	3.1	1.1	5.3	1.4	3.6	0.5	0.72	2.2	0.22

g. Maximum and nominal average daily activity, and associated metabolic rate, are tabulated in Table 9-5. Table tennis has been selected as a typical game suitable for maintenance of overall body coordination in terms of muscular response, equilibrium, and orientation. The value of 1400 Btu/hr refers to 1-g conditions. Less energy might be required under low-g conditions, but this effect might be compensated for by a greater effort to maintain position (more flailing of arms and legs, etc). Due to the comparatively high metabolic rate during the recreational period, the total rate of 2800 cal/person-day appears to represent the maximum normal metabolic rate at artificial gravity of 0.4 g or less and for a vehicle crew of no less than 7 persons. During special periods (e.g., capture period), the composition will change (less sleep, more physical work, less recreation).

h. Nitrogen intake is assumed to equal nitrogen output. However, allowance for gas leakage during the mission is made. This allowance corresponds to a daily leakage of 42 pounds of oxygen (rough estimate-to be refined on the basis of a given space ship design and daily activity plan involving a given number of egresses and entrances).

Table 9-4. List of LSS Parameters Requiring Continuous or Periodic Monitoring

1. Physical
   - Temperature
   - Pressure
   - Humidity
   - Dust and particles (crumbs)
   - Air ionization
   - Radiation level
   - Thrust acceleration during powered maneuvers
   - Centrifugal acceleration about all three axes during coast periods

2. Biological
   - Organisms (bacteria, spores, viruses; Flight Surgeon to make swabs of each crew member and check under microscope, initially twice per week; later once per week)
   - Metabolism
   - Algae or duck weed system (if any)
   - Regular check-ups of crew members
   - Provisions for monitoring and caring for crew members who may have to be isolated from the rest for any reason

3. Chemical
   - Atmosphere composition (N_2, O_2, O_3, CO, CO_2)
   - Water condition
   - Food condition
   - Drug management
   - Odor control
   - Toxicology (foods and gases)
   - Control of fuels and vapors
   - Fire control
   - Control of absorbents
   - Trace elements media

4. Operational
   - Internal supply conditions
   - Condition of cabin spaces (cleanliness and orderliness)
   - Physical and mental tasks
   - Radiation-exposure control and management by Flight Surgeon and Nuclear Engineer
   - Operational schedule and equipment control by Commander and Flight Surgeon
   - Emergency preparedness

Table 9-4. List of LSS Parameters Requiring Continuous or Periodic Monitoring (Continued)

5. Mars Surface Excursion
   Preparation of excursion crew by Flight Surgeon
   Medical monitoring of excursion crew by Flight Surgeon
   Close cooperation with Flight Surgeon in orbit, if excursion crew finds alien life
   Isolation of alien life carried into orbit by instrumented returner or in the manned excursion vehicle and sterilization of crew prior to transfer back into crew ship. Contact between returning surface vehicle and crew ship may have to be avoided.

Table 9-5. Maximum Daily Activity and Associated Metabolic Rate (Ref. Condition Figure 9-1)

ACTIVITY		PERIOD (HOURS)	BTU/ HR	CAL/ HR	TOTAL	
BASIC	DETAIL				BTU	CAL
Work	Control duty	8	440	110	3520	880
	Maintenance and repair duty	2	800	200	1600	400
	Scientific activity (seated)	2	420	105	840	210
Recreation	Rest (sitting)	2	400	100	800	200
	Rest (lying)	1	320	80	320	80
	Light exercise	1	900	225	900	225
	Heavy exercise (level of table tennis	1	1400	350	1400	350
Sleep	Sleep	7	260	65	1820	455
Total		24			11,200	2800

Nominal Average Metabolic Rate Adopted: 2500 cal/person-day

i. Basic specifications set for the layout of the main system (in the crew vehicle) are an eight-man crew, a nominal mission duration of 430 days, a 5.5 psia O_2-N_2 (rather than O_2-He) atmosphere, and an oxygen system consisting of a regular and an emergency oxygen supply. The main system will be fully integrated in the Command Module and the Spine Module. At least the oxygen and water cycles will be closed. The waste cycle may be open (including fecal water). It will be operable in the range between zero and one g.

j. Typical clothing allowances for the crew members are:

Flight coveralls
Cotton shorts
Cotton undershirts
Cotton socks
Handkerchiefs
Nylon-fabric shoes with tennis-shoe type soles
Towels
Body sponge

A typical weight break-down is presented in Table 9-6. Although a shirtsleeve environment is assumed, pressure suits will be provided for emergencies and for certain maintenance and repair activities. They are counted as part of the operational equipment.

Table 9-6. Basic Crew Weights

ITEM		WEIGHT LB	WEIGHT KG
1. Eight persons at 175 lb (79.5 kg)		1400	636
2. Clothing			
Coveralls	2.5 lb		
Underwear (shorts, shirt)	0.25 lb		
Sox (1 pair), handkerchief	0.25 lb		
Shoes (flight type)	3.0 lb		
Total for 1 set	6.0 lb		
6 sets per person for 8 persons		290	132
3. Towels and sponges		15	6.8
4. Personal sanitation kit			
10 lb/person fixed weight		80	36.4
1 lb/person-week (65 weeks)		520	236.6
5. Personal effects (12.5 lb/person)		100	45.5
Total Basic Crew Weight	Approx.	2405	1093.3

k. The Earth Entry Module will carry an independent open-cycle ecological system sized for eight persons for two days. The system is composed of gaseous O_2-N_2 storage, lithium hydroxide (LiOH) for CO_2 removal, and a water-boiler heat exchanger for thermal control. Food, water and wastes are stored.

l. The Mars Excursion Vehicle also is equipped with an independent ecological system which is sized for a two-man crew for seven days. The system will be open cycled, consisting of gaseous O_2-N_2 storage, LiOH for CO_2 removal, thermal control by a glycol space radiator and a water boiler heat exchanger. Food and water are stored. Wastes are also stored, to prevent contamination of the Martian world.

m. Since non-organic ecological systems are better understood and predictable at this time, a non-organic system is selected for the purpose of weight analysis and LSS layout. This system is a combination of catalytic reduction of CO_2 to H_2O with the aid of hydrogen, and of electrolytic decomposition of H_2O to gain breathing oxygen. Studies of the merits and characteristics of photosynthetic gas exchanger (PGE) systems are continued concurrently in an attempt to arrive at the best possible comparison of hydrogen reduction systems, PGE systems, and combination systems containing inorganic as well as organic phases.

n. Aside from a busy schedule, roominess and the availability of privacy is recommended as an important prerequisite for keeping the crew in a well-balanced condition. This consideration has governed the layout of the LSS complex. The Command Module and the Spine Module are the heart and indispensible core of the LSS complex. The Mission Modules provide the desired roominess. However, they can be jettisoned if necessary and therewith offer to the Commander added weight flexibility in cases of emergency.

SECTION 10

ECOLOGICAL LIFE SUPPORT SYSTEM

10.1 INTRODUCTION. The results of preliminary design and comparison of several ecological systems for the life support systems of crew vehicles for interplanetary missions are presented. The life support modules of the vehicle (cf. Section 8) consist of a command module, a service module (spine module), and a number of mission modules. In addition, an Earth Entry Module (EEM) and a manned Mars Excursion Vehicle (MEV) are to be considered. The command module houses the main life support system, minimum necessary living quarters, and, through the spine module, provides access to the EEM and to the MEV. The mission modules contain sensible heat rejection and other equipment, as well as more spacious living quarters.

The main life support system is designed to accommodate a crew of 6 to 12 for 400 to 500 days. Additional life support equipment is required for the full crew for two days in the EEM and for a crew of two for approximately a week in the MEV (cf. Section 9).

The fundamental criteria used in selecting the life support subsystems were overall weight penalty, volume, and reliability. The various subsystems which perform a given function were compared, with each subsystem being charged with power and heat rejection weight penalties. The subsystem exhibiting the lowest overall weight penalty, with acceptable reliability, was then selected. The subsystems selected were then combined to form a single lightweight life support system.

10.2 SUMMARY OF THE ECOLOGICAL SYSTEM DESIGN FOR THE CREW VEHICLE, THE EARTH ENTRY MODULE (EEM) AND THE MARS EXCURSION VEHICLE (MEV). The system was designed to be as simple and light as possible while maintaining a large factor of safety and reliability. The parameters for the weight summary are: eight men for 430 days for the main vehicle, two men for one week for the descent capsule, and eight men for one day (plus one day reserve) for the re-entry capsule.

The hydrogen reduction (reverse water gas process) and electrolysis method of carbon dioxide removal and oxygen regeneration is recommended for the main life support system. Of the carbon dioxide removal systems considered, this method is lowest in weight, low in volume and power requirements, and high in reliability. A redundant system should be included for reliability. Lithium hydroxide was selected to remove carbon dioxide in the EEM and in the MEV. LiOH is highly reliable and is lightest in weight for the short mission durations of these systems.

Oxygen to make up losses and leakage is stored as water for the main mission. An electrolysis unit plus a backup unit is used to liberate the oxygen from the water. A gaseous storage or supply large enough to provide two recompressions of the command

module is also carried as part of the main system. Oxygen storage in the form of water was chosen because of its light weight and storability. The nitrogen supply for the main system is carried as a gas since the quantity is fairly small and since this method has significant storability and reliability advantages.

Gaseous O_2 and N_2 storage was chosen for the MEV and the EEM for storability and reliability reasons.

If the command module is located inside the Maneuver-4 hydrogen tank. The tentative thermal control system selected for the main life support system rejects all sensible heat in the command module to the hydrogen shielding by blowing cabin air over the wall. The system is sized to accommodate the entire crew plus all other command module sensible heat sources. All latent heat generated in the entire vehicle is removed in an air-glycol heat exchanger located in the command module. The glycol transports the heat to a glycol-hydrogen heat exchanger located upstream of the cryostat. A ventilation system is used to ensure air circulation between modules. Sensible heat rejection in the mission modules is handled by an air-glycol heat-exchanger/space-radiation system which is sized to handle all other sensible heat sources. The EEM utilizes a water boiler heat exchanger for dehumidification and heat rejection. In the MEV, dehumidification and heat rejection is accomplished by an air-glycol heat-exchanger/space-radiator system when possible and by a water boiler heat exchanger when the space radiator becomes inoperable.

The food and wastes are stored in a cryogenic refrigerator which utilizes the liquid hydrogen surrounding the command module as a cold source. This unit is lighter than a comparable size thermo-electric refrigerator and does not require power for operation. The MEV and EEM do not require refrigerators, since food storable at room temperatures can be used for such short missions. Urine, wash water, and atmospheric condensate are recovered and reprocessed for reuse. A comparison of two waste-water reprocessing units was carried out; since the performance and power required is approximately equal for both, a vacuum distillation centrifugal still was chosen for the main vehicle system because its requirements for expendables (filters, liners, water losses, etc.) are about 30 percent less than those of a comparable vapor compression still.

Summaries of system weights are shown in Tables 10-1 through 10-3.

Table 10-1. Ecological Life Support System Weight Summary (Crew Vehicle)

ITEM	WEIGHT (Lb)	VOLUME (Ft^3)	POWER (Watts)
1. Environmental Control and Heat Rejection Equipment Summary			
CO_2 Reduction – O_2 Regeneration Unit (Hydrogen), Reduction with Redundant Unit	1458	20.8	2880
O_2 Supply & Pressurization System (Water Storage + Electrolysis + Gaseous Storage for two Recompress.)	3245	50.0	675
N_2 Supply & Press. System (Gaseous Storage)	2870	54.4	--
2. Main LSS Thermal Control System			
Main Dehumid. System – W/Redundant	40	--	37
Sensible Heat Reject System, Weight Unavailable Until Total Heat Load Known			
Ducting	15	--	--
Instrumentation	50	--	30
Trace Contam. Removal	42	4	160
Odor Removal	344	11.0	--
3. Miscellaneous			
Air Filters	40	6.5	--
Personal Kits and Clothing	760	--	--
Clothing Dry Cleaner	20	2	--
Cabin Cleaning Equipment	111	--	--
Personal Sanitation	12	--	--
Subtotal	9007	138.7	3782
Contingency 10%	900	13.9	378
TOTAL (Items 1, 2, and 3)	9907	152.6	4160

Table 10-1. Ecological Life Support System Weight Summary (Crew Vehicle) (Cont)

ITEM	WEIGHT (Lb)	VOLUME (Ft^3)	POWER (Watts)
4. Food, Water and Waste Management Weight Summary			
Food			
Food and Containers	7500	350*	--
Food Storage (Refrigerator)	328	520	--
Food Preparation Unit	25	2	200
Water Supply and Recovery System			
Potable Water Supply	200	3.2**	--
Potable Water Storage Container	12	3.5	--
Waste Water Storage Container	18	7	--
Main Urine Still and Accessory			
Fixed Weight	200	4	--
Variable Weight	1600	50*	100
Secondary Urine Still	120	3	75
Piping, Pumps, Etc.	25	2	25
Waste Material			
Two Feces and Urine Collector Units	20	5	--
Feces Bags, Urine Bags, Paper, Etc.	480	24*	--
Miscellaneous	340	20*	--
Subtotal	10,868	546.5	400
Contingency 10%	1,087	54.7	40
TOTAL (Item 4)	11,955	601.2	440
GRAND TOTAL	21,902	753.8	4600

* Stored in Refrigerator

** Stored in Potable Water Storage Container

Table 10-2. Ecological Life Support System Weight Summary (Earth Entry Module)

ITEM	WEIGHT (Lb)	VOLUME (Ft^3)	POWER (Watts)
1. CO_2 Removal, LiOH	67	2.0	--
2. O_2-N_2 Supply	127.3	1.5	--
3. Thermal Control			
Latent Heat Rejection	75	0.75	37
Sensible Heat Rejection	*		
4. Odor Removal	2	0.04	--
5. Instrumentation	30.8	--	0.9
6. Miscellaneous			
Air Filters	5	0.1	--
Personal Sanitation	2	--	--
Personal Equipment	10	--	--
Subtotal	319.2	4.75	37.9
Contingency 10%	31.9	0.47	3.8
TOTAL (Items 1 through 6)	351.1	5.22	41.7

* Sensible heat rejection equipment not included as total sensible heat load is undefined.

Table 10-2. Ecological Life Support System Weight Summary (Earth Entry Module) (Cont)

ITEM	WEIGHT (Lb)	VOLUME (Ft^3)	POWER (Watts)
7. Food			
Food and Containers	20	1.5**	--
Food Preparation Unit	--	--	--
Food Storage	1.5	2.0	--
8. Water Supply and Recovery System			
Potable Water Supply	200	3.2***	--
Potable Water Storage	12	3.5	--
Piping, Pump, etc.	10	1.5	15
Urine and Condensate Container	12	3.5	--
9. Waste Material			
Feces and Urine Collector	10	2.5	--
Feces Bags, Urine Bags, Paper	2	0.5	--
Feces and Waste Storage Container	0.5	1.0	--
Subtotal	268.0	14.5	15
Contingency 10%	26.8	1.5	1.5
TOTAL (Items 7, 8, and 9)	294.8	16.0	16.5
GRAND TOTAL	645.9	21.22	58.2

** Stored in Refrigerator

*** Stored in Potable Water Storage Container

Table 10-3. Ecological Life Support System Weight Summary (Mars Excursion Vehicle)

ITEM	WEIGHT (Lb)	VOLUME (Ft^3)	POWER (Watts)
1. CO_2 Removal, LiOH	212	6.5	--
2. O_2-N_2 Supply	434	5.1	--
3. Odor Removal	6	0.12	--
4. Thermal Control			
Latent Heat Rejection	*		
Sensible Heat Rejection	*		
5. Instrumentation	49	--	21
6. Miscellaneous			
Air Filters	15	0.3	--
Personal Sanitation	7	--	--
Personal Equipment	14	--	--
Subtotal	737	12.02	21
Contingency 10%	74	1.2	2
TOTAL (Items 1 through 6)	811	13.22	23

* Sensible and latent heat rejection equipment weights not included as total sensible heat load and amount of time that space radiator is inoperable is not known

Table 10-3. Ecological Life Support System Weight Summary (Mars Excursion Vehicle) (Cont)

ITEM	WEIGHT (Lb)	VOLUME (Ft^3)	POWER (Watts)
7. Food			
Food and Containers	31	3**	--
Food Storage	2	4	--
Food Preparation Unit	10	1	--
8. Water Supply and Recovery System			
Potable Water Supply	200	3.2***	--
Potable Water Storage Container	12	3.5	--
Piping, Pump, etc.	10	1.5	15
Urine and Condensate Storage Container	12	3.5	--
9. Waste Material			
Feces and Urine Collector	10	2.5	--
Feces Bags, Urine Bags, Paper, etc.	2	0.5	--
Feces and Waste Storage Container	0.5	1.0	--
Subtotal	289.5	17.5	15
Contingency 10%	29.0	1.8	1.5
TOTAL (Items 7, 8, and 9)	318.5	19.3	16.5
GRAND TOTAL	1129.5	32.52	39.5

** Stored in Food Storage Container
*** Stored in Water Storage Container

10.3 ENVIRONMENTAL CONTROL

10.3.1 General. Specific subsystems for environmental control for the crew vehicle life support system and the MEV life support system were compared on the basis of weight, volume, power requirements, cooling requirements, and reliability. Only subsystems of adequate reliability were considered in this study. A total weight penalty for each subsystem was determined by charging each with weight penalties for its power and cooling requirements.

The design parameters for internal atmospheric and environmental control used for this study are listed in Table 10-4. The weight penalty for power provided by a SNAP 8 nuclear power supply is at least 45 lb/kw* and at least 10 lb/kw when provided by a SPUR nuclear power supply based on average power loads.

Table 10-4. Design Parameters for Internal Atmosphere and Environmental Control – All Life Support Systems

CONDITION	NORMAL QUANTITY
Clothing	Shirtsleeves
Heat Output	
Latent	175 Btu/Man Hour
Sensible	288 Btu/Man Hour
O_2 Consumption	1.87 Lb/Man Day
CO_2 Production	2.32 Lb/Man Day
CO_2 Concentration	1.33 mol %
Pressure	5.5 psia
O_2 Partial Pressure	180 mm Hg (nominal)
Temperature	68° F
Relative Humidity	50%
Water Intake	6.94 Lb/Man Day
Food Intake (80% Dehydrated)	2.0 Lb/Man Day
Water, Sanitation	3.0 Lb/Man Day (recycled)
Water Output (Feces, Urine, Water Vapor)	7.66 Lb/Man Day
Fecal Solids Output	0.29 Lb/Man Day

* This is an optimistic estimate in the course of the study, higher weights were brought to our attention (cf. Section. 8, Electrical Power Generation) which indicate that the power specific weight of a 30 ekw SNAP-8 system might be as high as 88 lb/kw. The presence of men in the maintenance system, and advancements in the state of the art, are likely to result in lower weights by 1973/75.

10.3.2 Atmosphere Composition Control

10.3.2.1 CO_2 Removal and O_2/N_2 Supply and Pressurization Systems

10.3.2.1.1 CO_2 Reduction/O_2 Regeneration Systems (Crew Vehicle). A variety of CO_2 removal and O_2/N_2 supply and pressurization systems were investigated. Due to the length of the mission, only schemes which combined CO_2 removal with O_2 regeneration were considered for the main life support system. Some of these schemes were obviously unreliable or overly heavy and bulky and were eliminated immediately. The systems which appeared the most feasible for a mission of this type were compared on the basis of weight, volume, power, and heat rejection. A breakdown of system weight, volume, power, and heat rejection is shown in Table 10-5 for the photosynthetic, LiOH electrolysis, Sabatier-electrolysis, and hydrogen reduction electrolysis systems (Refs. 10-1 through 10-4, respectively). These various systems are compared on a total weight penalty basis (including power and cooling weight allowances) using a SNAP 8 nuclear power supply in Figure 10-1 and a SPUR nuclear power supply in Figure 10-2.

Photosynthetic gas exchangers utilizing mass algae cultures can be used for oxygen regeneration. Oxygen is produced when carbon dioxide, algae nutrients, and energy in the form of light are added to a 3 percent algae suspension in water; the photosynthesis process absorbs about 17 percent of the applied light. If the light is supplied by fluorescent lights the conversion efficiency from electric power to light output is about 20 percent. Consequently, large amounts of power are required for the reaction, resulting in a large cooling penalty. If a solar collector is used to provide the light, little cooling as power is required. However, the collector is quite bulky and is only operable when solar-oriented. Also, light intensity is reduced considerably at the orbit radius of Mars. This complicates the design problem by requiring a considerably larger reflector than would be necessary in the vicinity of Earth. About 0.11 lb of nutrients must be added to the culture per man-day. However, more than this amount of nutrients is available in feces and urine, although the processing of this material to produce usable nutrients remains a problem. Algae is a byproduct of the photosynthetic reaction and can be used in limited amounts as food. In the weight comparison, the photosynthetic systems were not credited with weight for the food produced and the reduced waste storage required, for the following reasons.

a. Stored wastes are serving double duty as radiation shielding for the main LSS vehicle; thus, little weight savings is realized from using the waste as a nutrient for the algae, as other shielding would have to be added to replace it.

Table 10-5. CO_2 Reduction/O_2 Regeneration Systems – Weight, Volume and Power Requirements (One Man Basis)

SYSTEM DESCRIPTION	COMPONENT WEIGHT (Lb/Man)	EXPENDABLE MAT'L. WT. (Lb/Man Day)	SYSTEM VOLUME (Ft^3/Man)	SYSTEM POWER* (kw/Man)	SYSTEM HEAT (kw/Man)
Photosynthetic					
(a) Electric Illumin.	255	0	6.15	5.5	3.20
(b) Solar Collector (1 A.U.)	227	0	9.45**	1.7	0.51
LiOH Electrolysis	275	0.34 (H_2O)	0.70	1.4	1.40
Microbial-Electrolysis	110-130	---	2.2-2.4	0.35	---
Sabatier-Electrolysis	120	0.50 (H_2O)	---	0.553	0.41
Hydrogen Reduction (CO_2 - H_2)	75	0.30 (H_2O)	1.30	0.36	0.133

* Cooling Power Not Included
** Folded Collector Volume

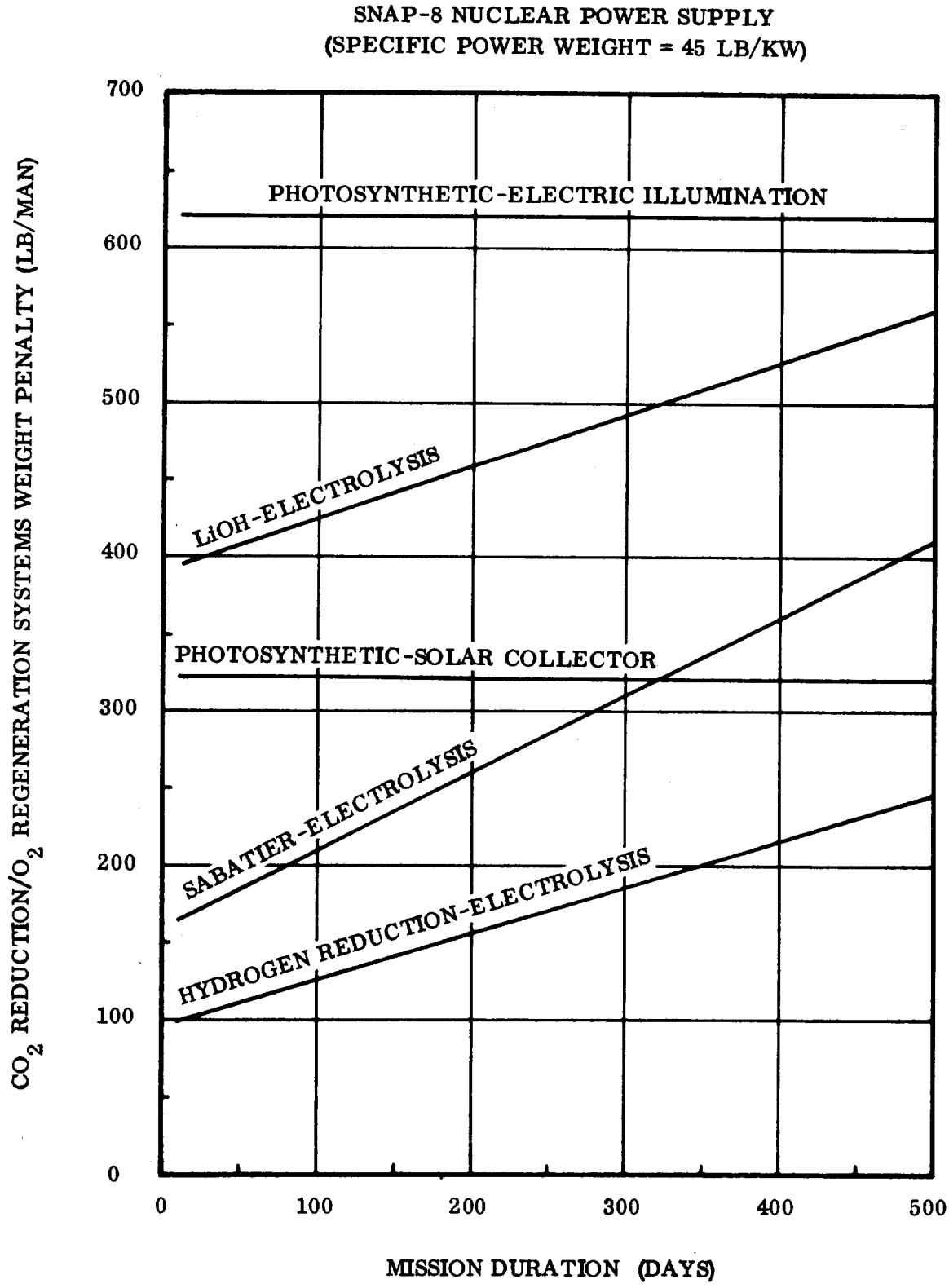

Figure 10-1. CO_2 Reduction/O_2 Regeneration Systems Comparison One-Man Basis

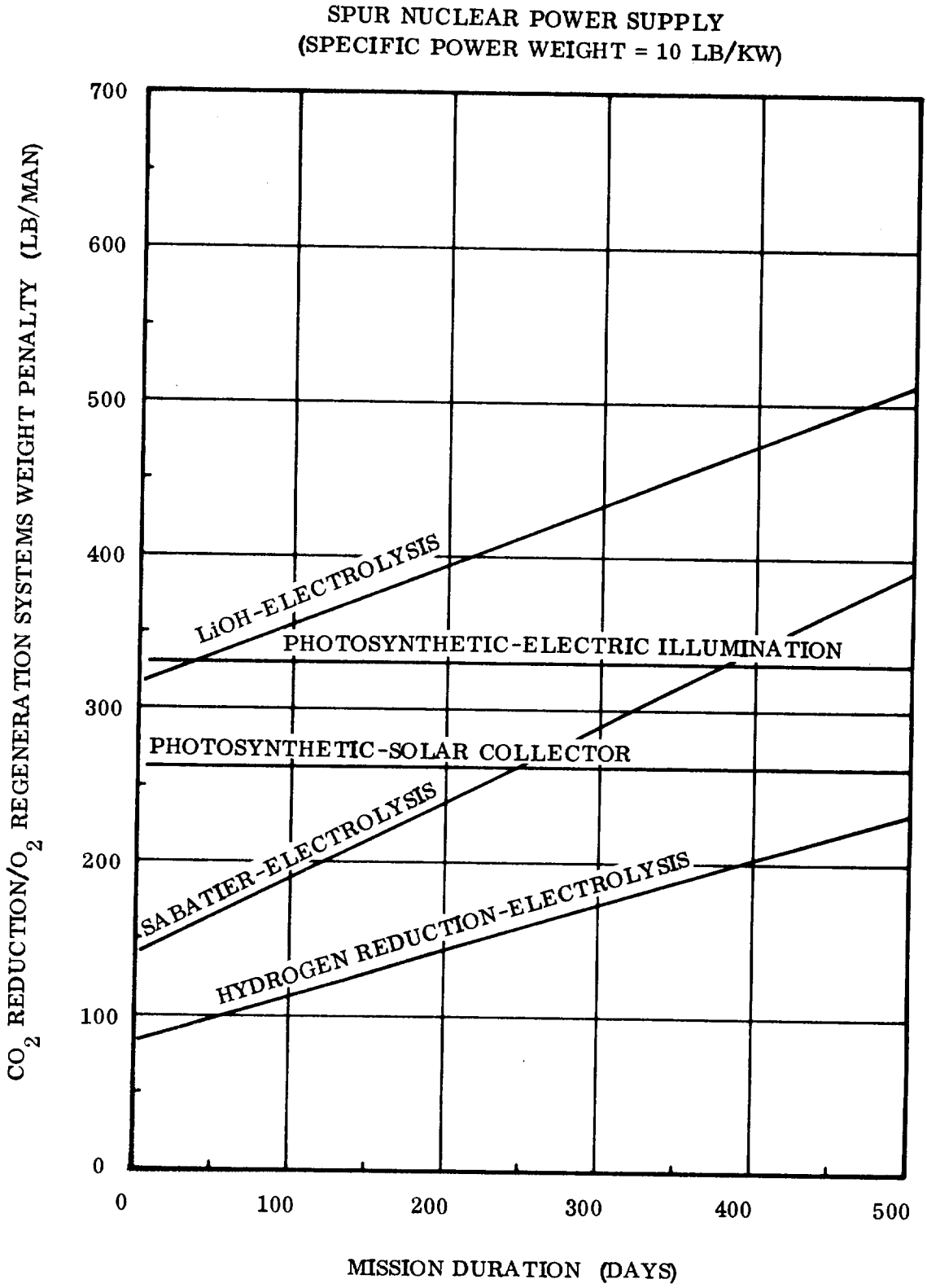

Figure 10-2. CO_2 Reduction/O_2 Regeneration Systems Comparison One-Man Basis

b. The weight savings gained by using some of the algae for food will tend to be equalized by the weight of the equipment required to process the waste for nutrient use and the excess algae into edible form. Waste processing methods have not been established, and the weight of the necessary equipment cannot be accurately estimated. Regarding use of algae as food, the algae cultures developed to date seem to be rather delicate, and the food value from any particular batch may vary widely with environmental conditions. Consequently, a fairly large weight penalty would probably be required for culture instrumentation if the use of algae as a major food source were contemplated.

The LiOH-electrolysis system for oxygen regeneration consists of flowing CO_2 into a LiH-CO_2 reactor where LiOH and carbon are produced. The LiOH is then reduced to LiH and oxygen. A molecular sieve is used to concentrate the CO_2. In the Sabatier-electrolysis process, hydrogen and CO_2 are passed over a catalyst at temperatures of 300°F to 500°F to form methane and water. The water is reduced electrolytically to H_2, which is returned to the reaction chamber, and O_2, which is passed into the cabin. The methane and some of the carbon dioxide are dumped overboard. Insufficient water is produced by the basic Sabatier reaction to supply the daily metabolic oxygen requirements and the necessary amount of hydrogen to sustain the reaction. Makeup water must be supplied from a storage source since the excess water produced metabolically is used to close the water cycle and is unavailable for use to counter the methane loss. A molecular sieve system is used to concentrate the CO_2.

In a modified Sabatier reaction another reactor is used to reduce the methane (CH_4) to carbon and hydrogen. The hydrogen is then returned to the Sabatier reactor. In this manner, the hydrogen which is dumped overboard in the methane in the unmodified Sabatier process, is saved and used to sustain the reaction. Consequently, makeup water to supply additional hydrogen is not required. This system has an added penalty of 5 lb and 40 watts per man. The overall additional weight penalty, including power, of 7 lb/man more than the unmodified Sabatier process is so small that separate curves are not shown for this process.

In the hydrogen reduction or reverse water gas reaction system, carbon dioxide is reduced to free carbon and water. This is done by passing CO_2 and H_2 over a catalyst at 1350°F and at low pressure to form CO and H_2O. The CO is then passed over a catalyst with H_2, which is returned to the reduction chamber, and O_2, which is passed into the cabin. Although makeup H_2O is required for this reaction (since not enough O_2 is available from metabolic CO_2 alone to provide the daily O_2 requirement), more than enough could be obtained from metabolic water. Again, however, the metabolic water is used to make up losses in the water recovery processes to close the water cycle.

10.3.2.1.2 CO_2 Removal System – MEV and EEM Life Support System (LSS). Because of the relatively short duration of the mission of these two systems (approximately one week for the MEV and two days for the EEM), the most appropriate CO_2 removal system is found to be a LiOH adsorption system for each. Such a system is very simple, highly reliable, has low power requirements, and requires very little heat rejection. LiOH is non-regenerable and one pound absorbs a minimum of 0.7 lb of CO_2.

10.3.2.1.3 Oxygen and Nitrogen Supply and Pressurization Systems – Crew Vehicle. Various methods of O_2 and N_2 storage systems were investigated for the main system. Oxygen and nitrogen are required to make up gas lost from the vehicle due to leakage, air lock operation, and accidental decompression. Approximately 5 lb/day of oxygen and 3 lb/day of nitrogen are lost by leakage from the vehicle. This leakage value was estimated by revising Mercury capsule leakage with scaling factors introduced to account for the much larger surface area of the interplanetary vehicle and the advance in the state of the art of vehicle pressure shell construction.

Enough gas is supplied to provide two repressurizations of the emergency capsule in the event of accidental decompression. An allowance was not made for gas lost through air lock operation in this study.

The storage systems considered were a high-pressure gaseous O_2 and N_2 storage system, a supercritical cryogenic O_2 and N_2 storage system, and a combination water-electrolysis/O_2-storage system. A weight comparison of the O_2 storage systems is shown in Figure 10-3, and a comparison of N_2 storage systems is shown in Figure 10-4.

The weight penalty for gaseous O_2 storage for the container, complete with controls and ullage, is 1.405 lb/lb O_2 stored. The weight penalty for supercritical O_2 storage for complete container and ullage is 0.615 lb/lb O_2 stored. In the water-electrolysis/O_2-storage system, enough H_2O is stored to provide the required O_2 upon electrolysis; 2.25 lb of H_2O yields about 2 lb of oxygen when electrolyzed. Water storage is quite simple and costs about 0.04 lb/lb H_2O. A hardware weight penalty for one operating electrolysis unit and one redundant unit to supply the daily leakage O_2 makeup is about 42 lb. Approximately 0.675 kw of power is required and 0.15 kw of heat must be rejected. A weight penalty of 184 lb for enough gaseous oxygen to provide two emergency capsule repressurizations must be included because the system contains no stored gas and hence cannot be used directly to recompress the cabin. Some weight benefit for this system may also accrue from limited use of the water for radiation shielding, although the water is used up during the flight. This factor, however, was not considered in the system comparisons.

The weight penalty for gaseous N_2 storage for container, complete with controls for ullage, is 1.705 lb/lb of N_2.

The weight penalty for supercritical N_2 storage is 0.745 lb/lb of N_2.

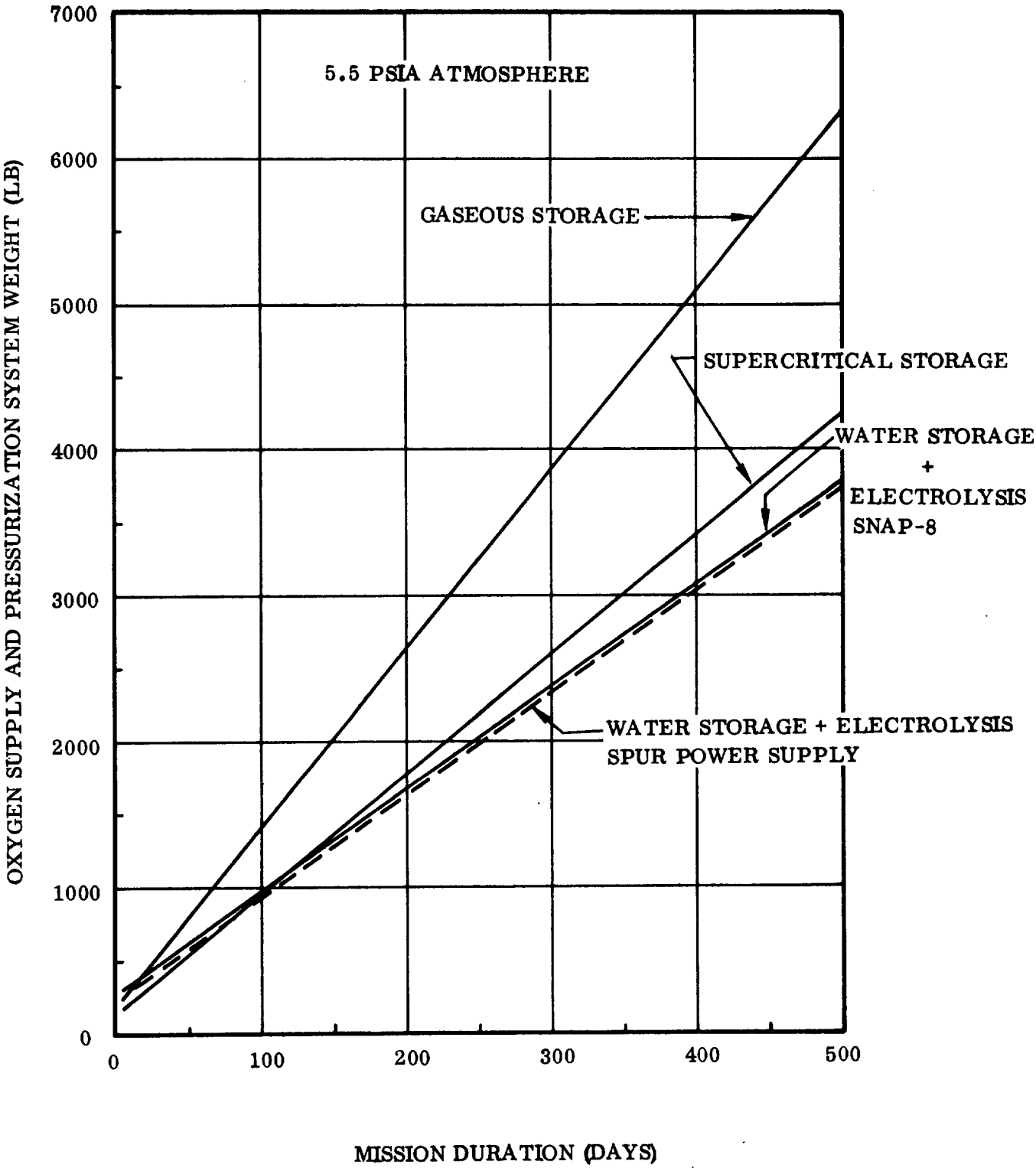

Figure 10-3. Oxygen Supply and Pressurization System Weight Comparison

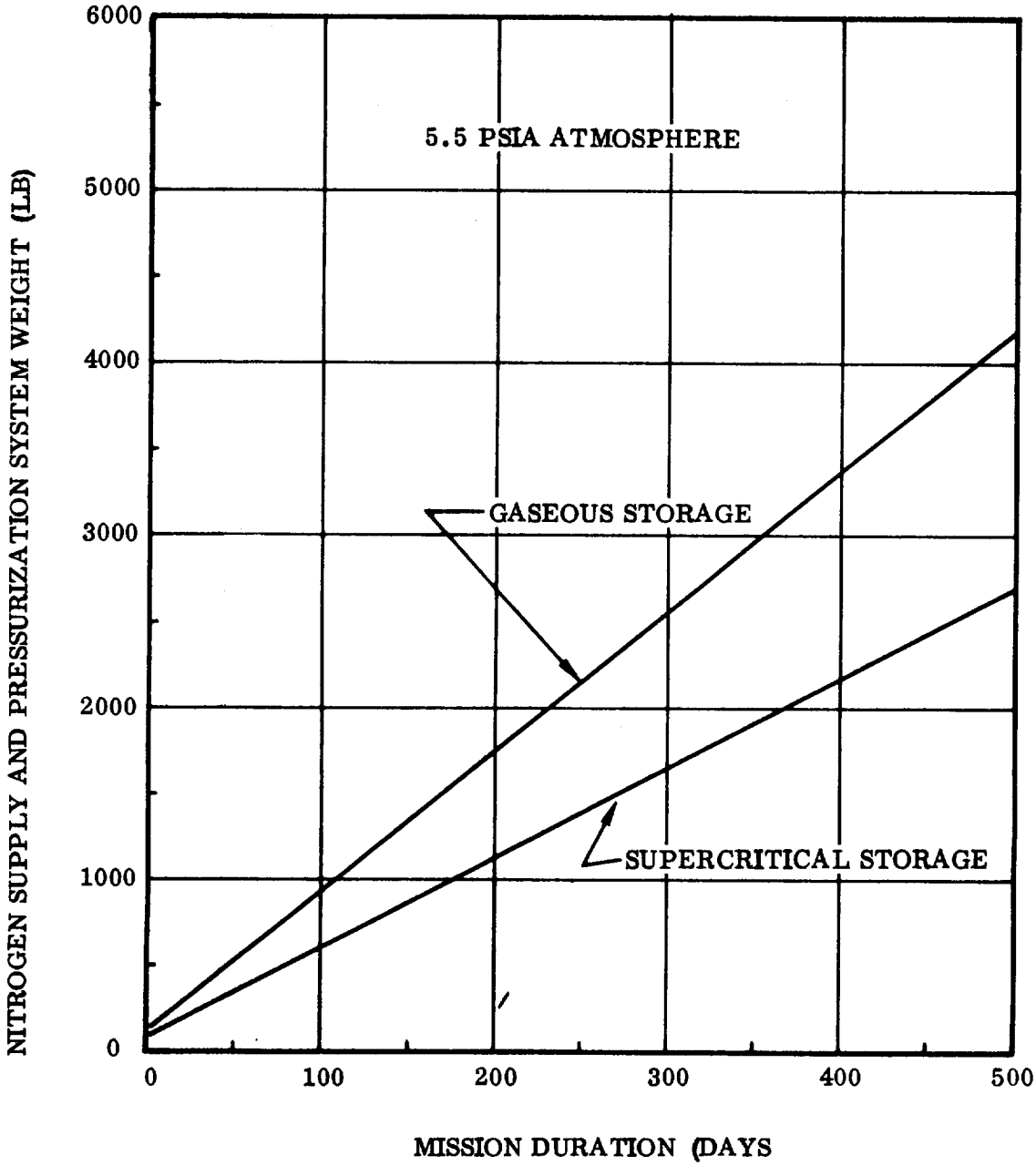

Figure 10-4. Nitrogen Supply and Pressurization System Weight Comparison

10.3.2.1.4 Oxygen and Nitrogen Supply and Pressurization Systems – MEV and EEM. The amount of stored oxygen and nitrogen required for the one-week, manned-descent mission and the two-day re-entry period is relatively small compared to the main mission. The weight penalty incurred by gaseous storage is not much larger than that of supercritical storage for these short mission times. Both types of storage have very high reliability and very good zero-g operation, and occupy roughly the same volume. However, the storability of gaseous O_2 and N_2 is much better than that of supercritical. Supercritical storage is only feasible where the boiloff can be used for metabolic or leakage makeup.

In the case of the MEV and the EEM, the O_2 and N_2 supply must be stored for several hundred days. For this reason, gaseous storage would appear to be the appropriate method.

10.3.2.2 Odor Removal. Removal of odors and other heavy organic atmosphere wastes will be accomplished in the main LSS, the MEV, and the EEM by use of high-flow-rate filtration through activated charcoal. It is estimated that about 0.1 lb of charcoal per man-day will be required to perform this function. It should be noted that the possibility exists that the charcoal in the main LSS may be reactivated to an extent by exposure to a vacuum and perhaps low-level heating. However, this was not considered in estimating system weight requirements.

10.3.2.3 Trace Contaminant Removal. Low-molecular weight trace gases from various sources such as flatus, urine, tobacco smoke, volatile material in electronic equipment, etc., will be oxidized by a catalytic burner. The major gases to be considered, – CO, H_2, CH_4, NH_3, and H_2S – present a toxic and sometimes an explosive hazard unless the concentration is kept to a minimum. Figure 10-5 shows the power required and weight of electrically heated, platinum-plated, nichrome wire catalyst, housed in a cylindrical container. Cabin air is passed over the catalyst and heated to about 500°F. Approximately 30 to 50 lb of air per hour can be treated in this manner. Toxic trace gas removal efficiency is in the 90 to 98 percent range, according to the manufacturer. For safety, two toxin burners would be carried and used alternately, or one used only in case of failure of the other.

The MEV and the EEM will utilize a similar catalytic burner which weighs approximately four lb and requires 50 watts. The air flow throughout this burner is approximately 1.6 lb/hr.

10.3.3 Atmosphere Thermal Control

10.3.3.1 Heat Rejection and Dehumidification. A general investigation has been conducted for the interplanetary vehicle thermal control system. Generalized parametric cooling system weight penalty expressions have been devised. These weight penalties are presented below. Since electronic and electrical loads, power supply details, and

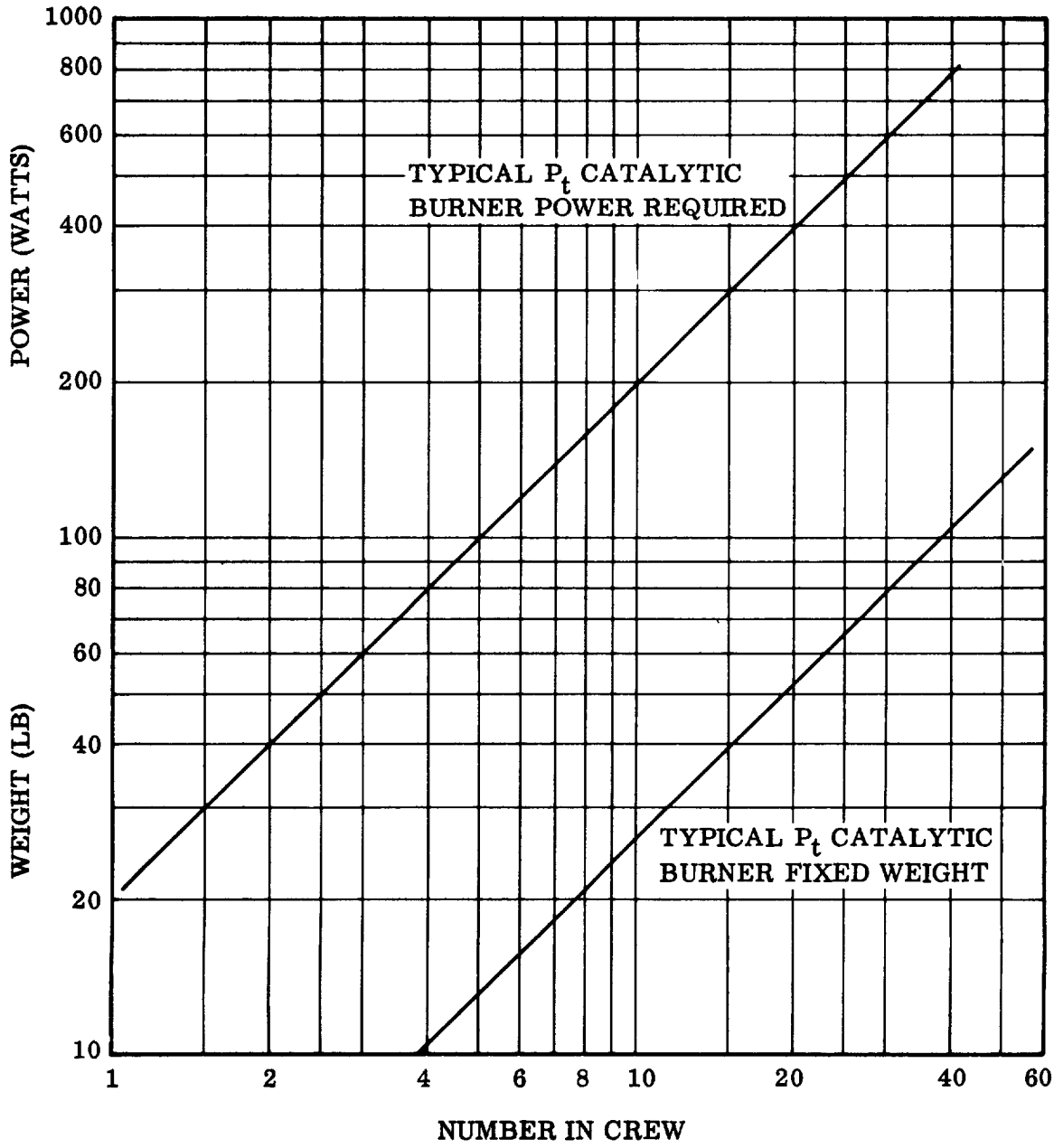

Figure 10-5. Catalytic Burner, Weight and Power Required

crew size have not yet been defined, no specific weight determinations for the complete thermal control system have been established.

a. Sensible Heat Rejection Via Air-Glycol Heat Exchanger to a Space Radiator. For a system of this type, air is passed through an air-glycol heat exchanger where the sensible heat is transferred to the glycol. The glycol in turn rejects this heat while flowing through the radiator tubes. The weight penalty, assuming the air entering the exchanger is heated by electronics or other equipment to 120°F, is:

$$\frac{Ws}{Q} = 0.00745 + 0.00885\ (m + nt)\ \frac{\text{Lb of equipment}}{\text{Btu/hr}}$$

where: Ws = weight penalty for sensible cooling (lb)

Q = sensible heat load (Btu/hr)

m = fixed power generation weight (lb/hr)

n = variable power generation weight (lb/watt-hr)

t = duration of operation (hr)

b. Dehumidification Via an Air-Glycol Heat Exchanger to a Space Radiator. For a system of this type, cabin air passes through an air-glycol heat exchanger where it is cooled below its dew point and a portion of the entrained water vapor is condensed. The condensate is removed from the air stream by a water separator and stored. The latent heat of condensation is picked up by the cool glycol and transported to the radiator where it is rejected. The weight penalty for this system, assuming the cabin air to be at 70°F, is:

$$\frac{W_D}{\dot{w}_{H_2O}} = 21.5 + 26.2\ (m + nt)\ \frac{\text{Lb of equipment}}{\text{Lb/hr of } H_2O}$$

where: W_D = weight penalty for dehumidification (lb)

$\dot{w}_{H_2O}$ = weight of water to be removed (lb/hr)

c. Glycol Cooling by a Space Radiator. The weight penalty for removing heat from any glycol loop and rejecting it through a radiator, assuming a glycol temperature drop across the radiator from about 120°F to 35°F, is:

$$\frac{W_G}{Q_G} = 0.0073 + 0.0013\ (m + nt)\ \frac{\text{Lb of equipment}}{\text{Btu/hr}}$$

where: W_G = weight penalty for cooling glycol (lb)

Q_G = heat load to be removed from glycol (Btu/hr)

d. Sensible Heat Rejection Via an Air-Hydrogen Heat Exchanger. The weight penalty for removing sensible heat from cabin air by passing the air through a heat exchanger where it goves up its heat to hydrogen, assuming an initial air temperature of 70°F, is:

$$\frac{W_s}{Q} = 0.0050 + 0.0021\ (m + nt)\ \frac{\text{Lb of equipment}}{\text{Btu/hr}}$$

where: W_s = weight penalty for sensible heat rejection (lb)

Q = sensible heat load (Btu/hr)

e. Heat Rejection and Dehumidification by a Water Boiler Heat Exchanger. Heat rejection and dehumidification is accomplished in a water boiler heat exchanger by extracting the heat from the cabin air and using it to vaporize water under a low pressure. About one pound of water is required per 1000 Btu to be removed. A water boiler which will handle a two-thermal-kw cooling load weighs about eight pounds and occupies a volume of approximately 3/4 cubic foot. For preliminary design purposes, these numbers can be scaled linearly.

10.3.3.1.1 Command Module Heat Rejection and Dehumidification. The heat rejection and dehumidification systems for both the crew vehicle and the EEM are located in the command module if the latter is surrounded by a liquid hydrogen shield; or in the spine module in the case of "dry" shielding (cf. Section 8). A schematic representing a preliminary design of these systems with liquid #2 shielding is shown in Figure 10-6. It is assumed that all sensible heat in the command module will be rejected to the liquid hydrogen radiation shield through the cabin walls. A blower system is required to circulate the air over the walls, thus promoting convective heat transfer. The air can be contained close to the cabin wall by a thin shell of material and the cabin air temperature controlled by regulating the amount of air blown over the cabin walls.

The latent heat from the crew and processes is removed by passing a portion of the cabin air through an air-glycol heat exchanger. The heat is transferred to the glycol and carried by a heat transport loop to a glycol-hydrogen heat exchanger for the main mission and to a water boiler for the re-entry portion of the mission. Since personnel can be located in the mission module during most operating conditions, a ventilating system circulates air between the command and mission modules. Latent heat generated in either area is removed by the command module dehumidification equipment. Hence, no similar equipment is required for the mission module.

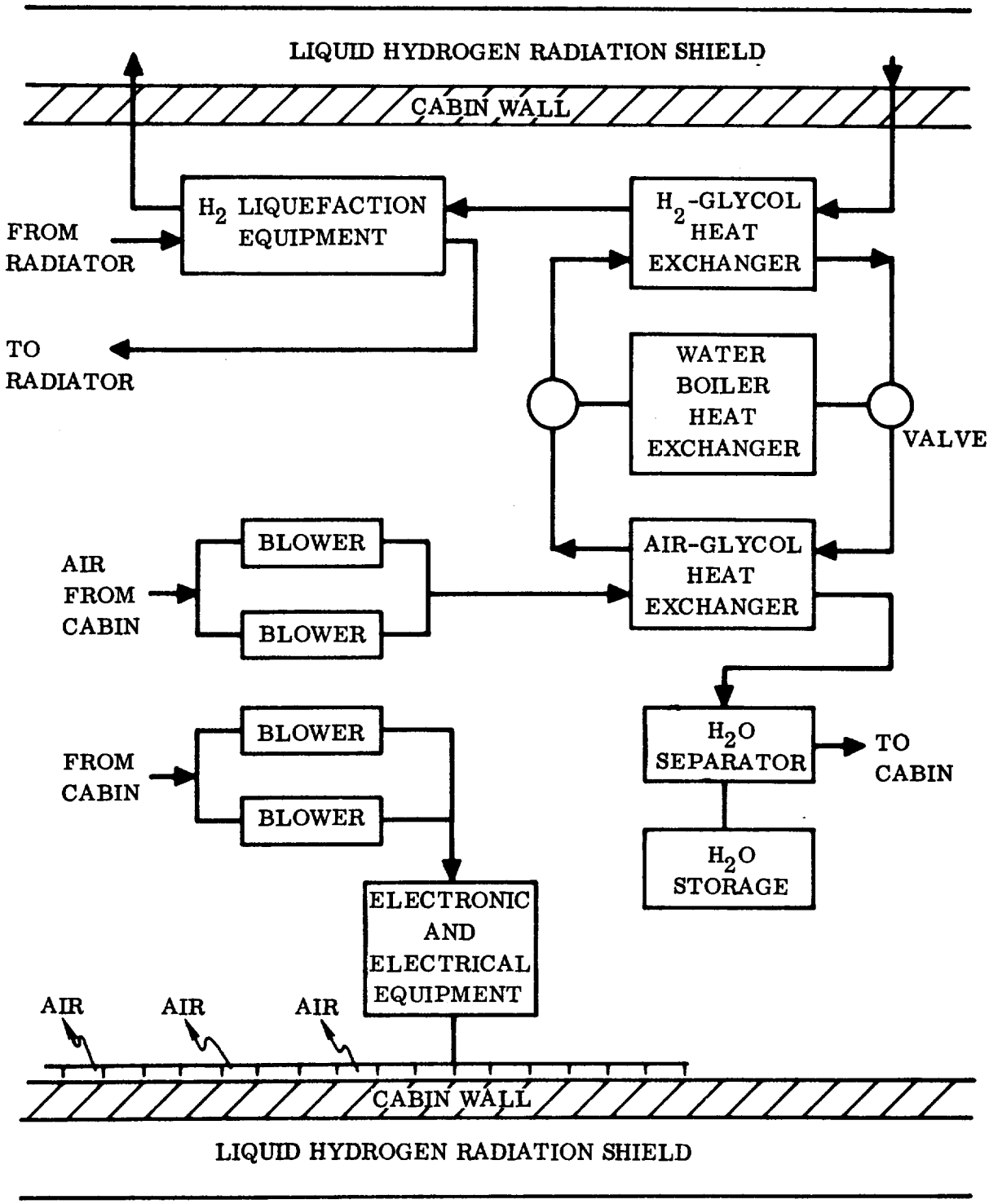

Figure 10-6. Command Module and Earth Entry Module Thermal Control System

During Earth entry, both the sensible and latent heat are rejected through the air glycol heat exchanger to the water boiler. Hydrogen boiloff is reliquefied by a cryostat or similar equipment. The heat from the reliquefying process is rejected to a space radiator.

10.3.3.1.2 Mission Module Heat Rejection. Sensible heat from equipment located in the mission module is removed by flowing the air through an air-glycol heat exchanger, which in turn transports the heat to a space radiator where it is rejected. A schematic of the system is shown in Figure 10-7. All crew-generated, sensible, and latent heat is charged to the command module system if LH_2 is used for shielding. In a "dry" shielding system, the arrangement shown in Figure 10-7 is typical for both command and mission module heat rejection systems.

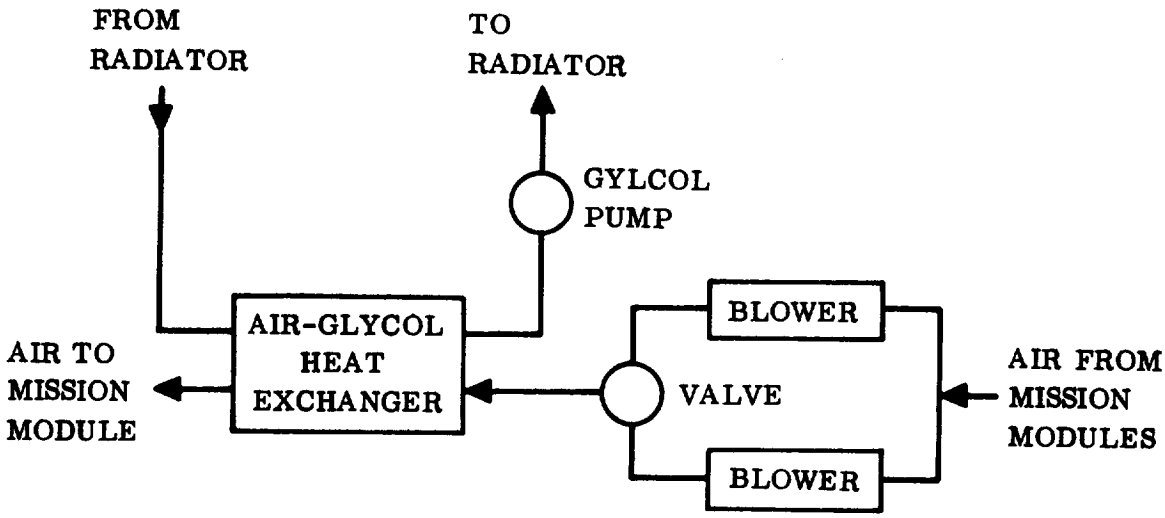

Figure 10-7. Crew Vehicle Mission Modules Thermal Control System

10.3.3.1.3 Mars Excursion Vehicle. Dehumidification and heat rejection is accomplished in the MEV by taking air from the cabin and from the crew's pressure suits and passing it through a heat exchanger where it gives up its heat to cold glycol. Moisture is condensed from the air, is separated in a water separator, and stored in a small tank. The heat is removed from the glycol by rejection from a space radiator whenever possible and by rejection to a water boiler heat exchanger when the radiator is inoperable. The cool dry air is passed back to the cabin and the suits. A schematic of this system is shown in Figure 10-8.

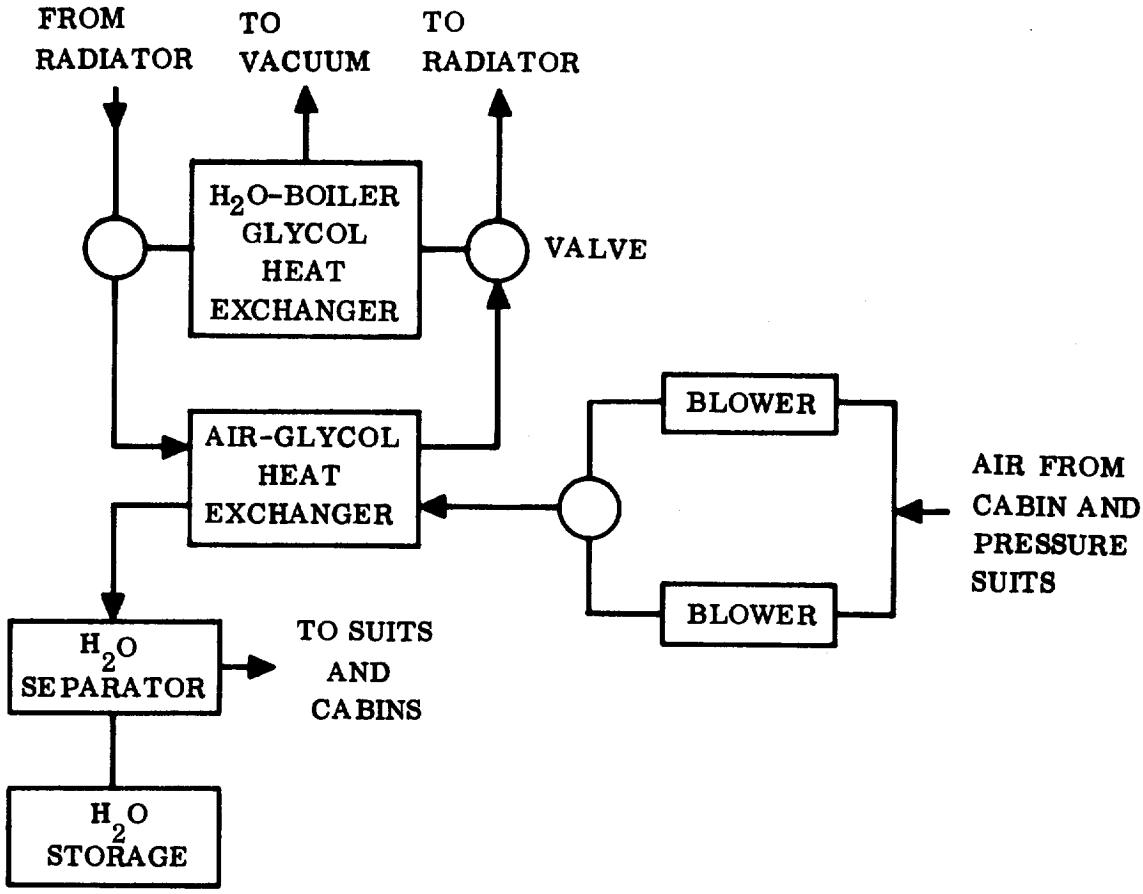

Figure 10-8. Mars Excursion Vehicle Thermal Control System

10.4 FOOD, WATER, AND WASTE MANAGEMENT

10.4.1 Food Supply, Storage, and Preparation

10.4.1.1 Food Supply. The food requirements postulated for this mission are two pounds per man per day on a dry basis. Of this two pounds, 20 percent is hydrated and 80 percent is dehydrated. The hydrated food contains approximately 1.0 lb of water. An additional 10 percent of food weight is required for containers. Figure 10-9 shows the total weight penalty for food, packaging, refrigerator, and heat rejection on a man-day basis. For this mission, a cryogenic refrigerator will be packaged in two-inch-diameter cylinders, seven inches long, for ease of handling and heating. Food and drink will be chosen to provide a 2000- to 2500-calorie-per-day, medium residue diet. Snacks such as candy, nuts, raisins, etc., could be included to increase morale as well as provide nourishment. Both hot and cold water will be available to hydrate food and drink.

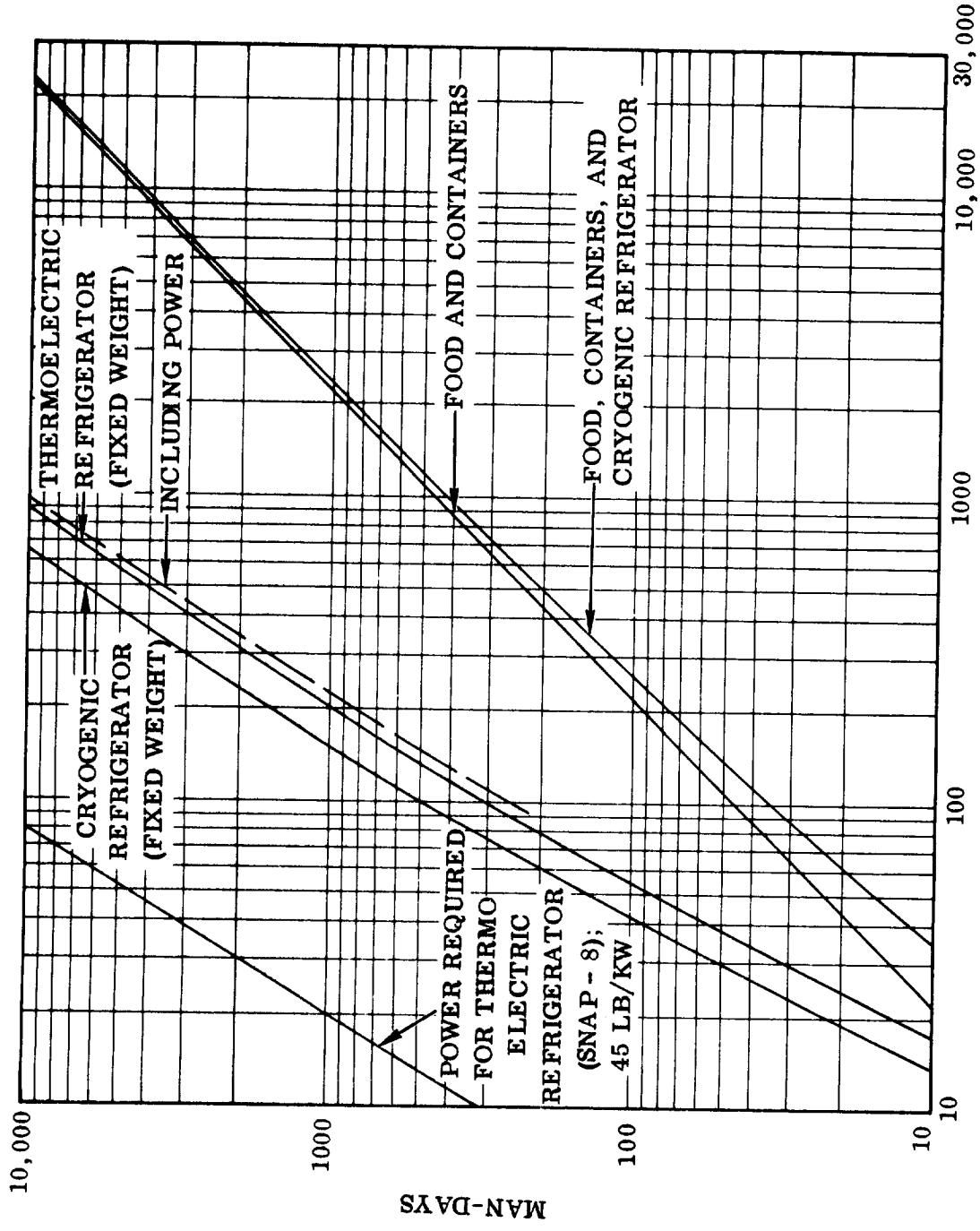

Figure 10-9. Food Supply and Storage Penalty

The MEV will not require a refrigerator. The food provided (two lb/man-day) will be both hydrated and dehydrated; however, the hydrated food will be vacuum packed and will not require freezing.

Provided for Earth entry will be food bars which do not require heating or hydration. The weight of food required in this form is 1.2 lb/man-day including packaging.

10.4.1.2 Food Storage Facilities. As mentioned previously, a cryogenic refrigerator or storage box utilizing LH_2 will be used. All food will be stored in this refrigerator, and, as the food is used, the available space will be used to store feces and other perishable waste (e.g. empty food containers). Figure 10-10 shows the refrigerator volume required for food and waste storage. As can be seen, the waste requires a greater storage volume (approximately 45 percent) than the food; therefore, the refrigerator must be sized to accommodate the waste. Gaseous hydrogen will be channeled through passages in the refrigerator walls prior to recycling through the cryostat. A freezer temperature of about -7°F will be maintained. This temperature is sufficiently low to resist bacteria growth in feces and other wastes, which would generate toxic gases if allowed to grow. The refrigerator contains a three- to five-gallon tank for chilling water to about 45°F. This tank is continuously replenished from the main pressurized potable water tank. The refrigerator also contains a defroster drawer where food is placed one day prior to eating. This drawer is kept at about 45°F.

Since no power is required to operate the box, the weight penalty is a function of size only. The weight, which varies with mission man-days, is shown in Figure 10-9. It may be feasible to burn paper wastes, thus eliminating the handling of these wastes as well as reducing the size of the storage box. However, the box weight is fairly small, so this possibility has not been considered in detail for the preliminary study.

The Mars Excursion Vehicle will not require a refrigerator for the one week mission. Food, as mentioned in Paragraph 10.3.2.1.1, will be selected which does not require freezing. Food will be stored in a small container which weighs approximately two pounds.

The Earth Entry Module will not require a refrigerator to store food. Food will be stored in a container of approximately 1.5 pounds.

10.4.1.3 Food Preparation. A food warmer using either electrical power or electronic compartment rejected heat is planned for this mission to warm hydrated food prior to consumption. This unit also contains a water tank and water heater from which hot water to prepare the dehydrated food and drink is obtained. Water is supplied under pressure from the main potable water storage tank.

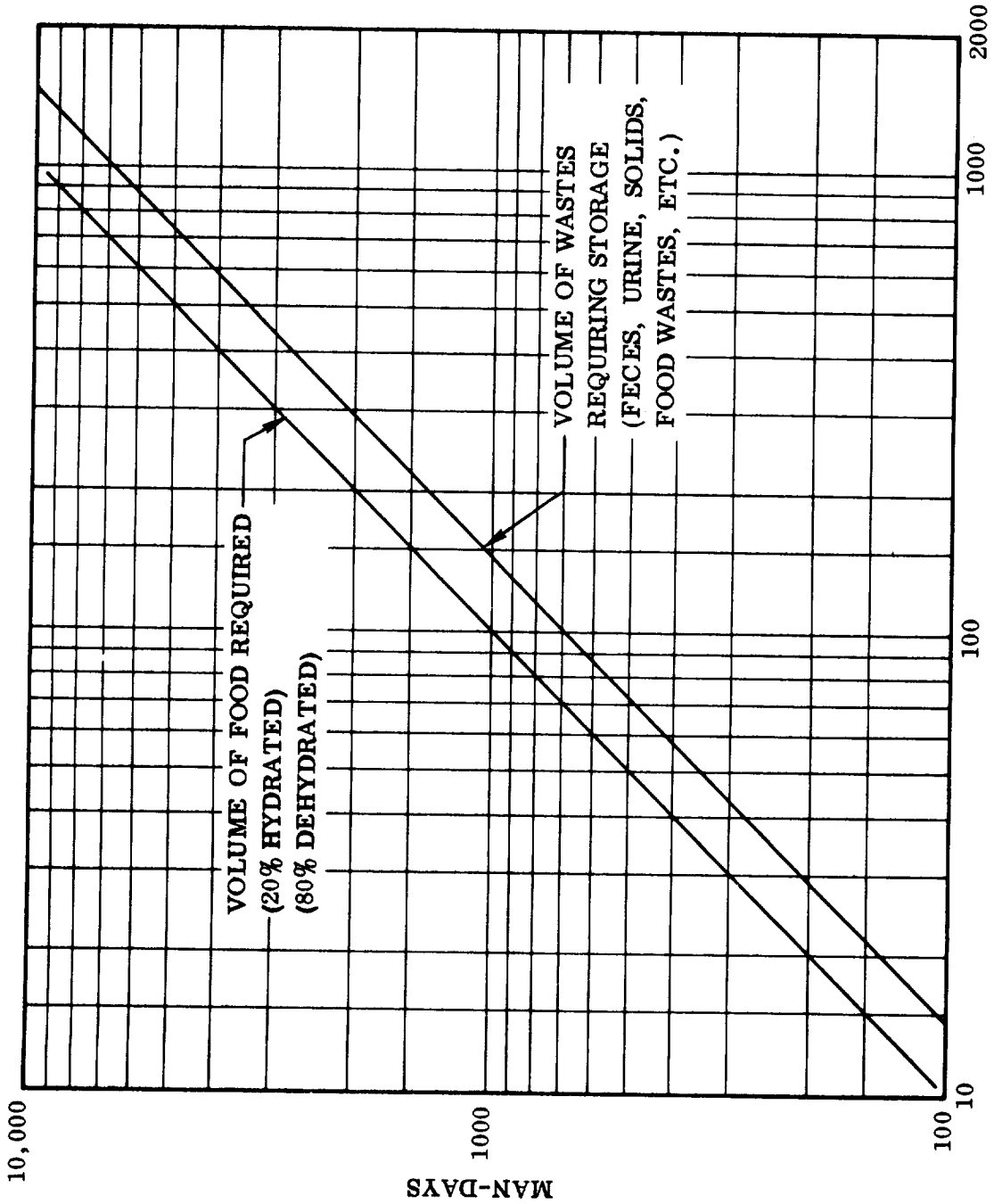

Figure 10-10. Refrigerator Volume Requirements

Hydrated food will be stored in cylindrical containers. One day before eating, it must be placed in the defrosting section of the refrigerator. If it is to be eaten warm, several hours before eating it must be placed in the heating unit to ensure uniform warming. The unit has the capability of heating the food to approximately 140°F in three hours. A unit for heating 10 food tubes simultaneously and providing adequate hot water for dehydrated foods will weigh about 25 pounds. If electric power is used for heating, an average power level of about 200 watts will be required for eight men.

Dehydrated foods and beverages will be packaged in lightweight cylindrical bags which have nipples at one end to facilitate both injecting water and ejecting the hydrated food into the crewmember's mouth. The procedure would be to break the seal on the nipple, inject the water (hot or cold as the case may be), allow a short period for hydration, then insert the nipple in the mouth and squeeze the bag to eject the food or drink.

Some solid hydrated foods will be carried in individually wrapped, bite-size pieces. Such food would consist of candy, nuts, raisins, meat chunks, etc., to be defrosted then eaten, or heated then eaten in the case of meat.

The MEV will have a simple food preparation unit which provides hot water for preparation of dehydrated food and permits warming of hydrated food. The unit will be operated by dissipated electronic heat and will weigh about 10 pounds.

The EEM will not require a food preparation unit.

10.4.2 Water Management

10.4.2.1 Water Requirements. The total water intake per man per day is an average of 3160 milliliters (6.94 lb). This water is taken into the body in the food and drink provided. The hydrated food provided contains approximately 460 milliliters (1.00 lb) per man-day. Of the total remaining water requirement, approximately 2060 milliliters (4.53 lb) is required to reconstitute the dehydrated food and beverages, leaving 640 milliliters (1.41 lb) available as drinking water.

For personal sanitation, approximately three pounds per man per day has been allowed. This includes water for bathing, cleaning, etc.

The water requirement for the MEV is approximately 10 lb/man-day. The higher drinking water allowance required by personnel in pressure suits will be made up by reduced sanitation requirements. This water would be stored and used as needed.

Approximately 10 lb/man-day will be provided in the EEM. All water provided will be at storage temperature. As in the MEV, the majority of water will be for drinking.

10.4.2.2 Water Recovery from Wastes. For a mission of this size, the weight penalty for expending water far exceeds the penalty for equipment and power to reprocess water, so the recoverable system is the only one discussed. Waste water sources are fecal water, atmospheric condensate, urine, and wash water. Recovery of water from feces is not feasible and the small quantity available from this source is not necessary for maintaining the water balance. The atmospheric condensate may be reclaimed directly from the air dehumidifier and passed through activated charcoal and bacterial filters to produce potable water. Urine and wash water may be mixed for processing.

The most practicable methods for recovering potable water from urine and wash water are to use either a vacuum distillation unit or a vapor compression still. Both use rotating (centrifugal) boilers to permit zero-g operation. Figure 10-11 shows the weight comparison between these two systems. The process loads for each case are 4.13 lb/man-day, which is the maximum urine output, plus 6.0 lb/man-day, which is the maximum wash water usage. Thus a total process load of 10.17 lb/man-day is allowed, although the average value based on normal urine output and wash water consumption is only 6.17 lb/man-day. This excess capacity will permit reprocessing of atmospheric condensate if it becomes excessively contaminated. The fixed weight includes the water recovery apparatus, fixed weight of auxiliary power chargeable to water recovery and fixed weight of heat rejection chargeable to the system. The variable (time-dependent) weight includes expendable filters, purge losses, and expendable plastic containers for urine transfer and for residue transfer from the still. While it is not necessary to recover 100 percent of the water contained in urine and wash wastes, the water cycle is closed only if net losses are no greater than the gain from body metabolic processes. In this study, based on still efficiency information, it is assumed all metabolic water is required to maintain water balance and distillation losses. Table 10-6 shows the significant quantities involved in establishing a water balance. It is assumed that the recovery apparatus would operate 22 hours of each 24-hour day, allowing two hours for maintenance and removal of distillation residue.

A standby centrifugal vacuum distillation unit is recommended to assure acceptable reliability. This unit need be used only in the emergency situation of prolonged or unrepairable malfunction of the primary unit; this unit would process the urine and 1.5 lb/man-day of wash water, which gives a process load of 5.67 lb/man-day. The fixed weight of the stand-by unit for eight men is about 130 pounds.

The MEV would not utilize a recovery system as such. The urine and wash water would be collected and processed in the main vehicle upon return.

During Earth entry, water will not be recovered. Urine and atmospheric condensate will be collected and stored in the re-entry capsule.

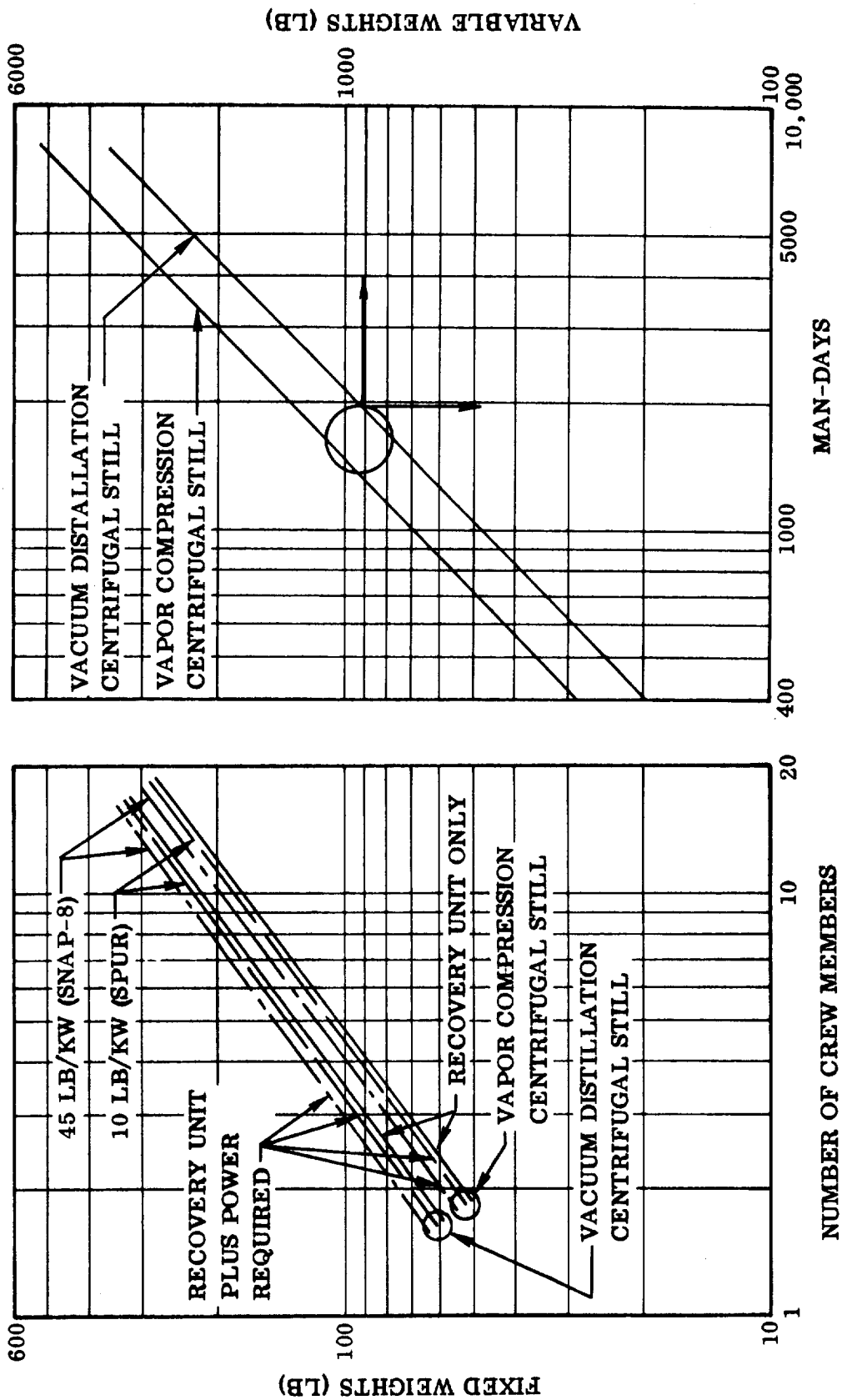

Figure 10-11. Water Recovery Unit Weights (Process Load 10.17 Lb/Man-Day)

Table 10-6. Water Management Balance

For Man

WATER SOURCE TO BODY	(LB/MAN-DAY)	WATER LOSSES FROM BODY	(LB/MAN-DAY)
Intake in food and drink	6.94	Urine	3.17
Metabolic produced	0.72	Fecal	.27
		Respiration and perspiration	4.22
	7.66		7.66

Balance

WATER SOURCE	(LB/MAN-DAY)	WATER CONSUMED	(LB/MAN-DAY)
Urine	3.17	For food and drink	6.94
Atmospheric condensate	4.22	Lost in urine residue	.07
Fecal water	0.27	Lost in feces	.27
Subtotal	7.66	Subtotal	7.28
Wash water recoverable	3.00	Wash water used	3.00
Total	10.66	Total	10.28

10.66	Provided
10.28	Consumed
0.38	NET GAIN

10.4.2.3 Water Storage. The reserve supply of water in the vehicle of 400 pound is sufficient for approximately five days usage by eight men at the average consumption rate. Waste is processed continuously, but any repairs of the recovery system would require storage of waste water while the malfunction is corrected. The maximum waste water accumulation cannot significantly exceed the potable water initially provided. It is proposed that two potable water containers of 200-pound capacity each and one waste water container of 400-pound capacity be provided. One 200-pound capacity container is in the EEM for use during re-entry and in the case of emergency. The other 200-pound capacity container is for potable water storage for the crew vehicle. These containers could be the collapsible type to minimize storage volume when empty; it is estimated that these containers would weigh a total of approximately 45 pounds.

A water supply of 200 pounds is stored in the potable water tank on the MEV. It could be filled prior to usage, which would require a larger potable storage tank in the main vehicle, or be filled at the start of the mission. If filled at the start of the mission, it could be purified if necessary prior to usage during the mission. The excess water reprocessing capability discussed above permits the latter method. A waste storage water tank of 200-pound capacity would be required to collect urine and wash water in the MEV during the excursion. It is not planned to process the waste water until return to the crew vehicle; then it will be passed through the crew vehicle water recovery system.

As mentioned above, the EEM contains a 200-pound capacity potable water storage tank. This tank can be used for supply to the crew vehicle system in emergency. Before re-entry, if the water has not been utilized it should be reprocessed to purify it.

10.4.3 Waste Management

10.4.3.1 Waste Material Summary. The waste materials and weight summary are shown in Table 10-7.

10.4.3.2 Feces and Urine Collection Units. Feces and urine are collected in one of two zero-g collection units, each of which weighs approximately 10 pounds. Since the weight is relatively little, it is felt that two collection units are desirable, considering both the length of the voyage and the size of the crew. The feces, toilet paper, and urine are collected in separate disposable bags, which are then stored in the refrigerator. The urine is transferred to the water recovery unit and the used urine bag is stored in the refrigerator. Approximately two feces collection bags and six urine collection bags are required per man per day.

10.4.3.3 Other Wastes. Food containers, food residue, napkins, kleenex, towels, disposable filters, vomit receptable, etc. are stored in the refrigerator after usage. The estimated compacted volume of all waste products is 0.047 ft^3/man-day. Calculating voids and allowing for waste paper receptacles, etc., the volume of waste storage required is found to be 0.145 ft^3/man-day, as shown in Figure 10-10.

Table 10-7. Waste Quantities and Weight Summary

ITEM	AVG LB/MAN-DAY
(1) Feces and urine solids	0.29
(2) Fecal water lost	0.27
(3) Unreclaimed fecal water	0.08
(4) Food packaging and residue	0.22
(5) Expendable air filters	0.11
(6) Expendable sanitary supplies	
Feces bags and paper	0.07
Urine collector bags	0.03
Disposable towels and napkins	0.04
(7) Expendable supplies for water recovery	
Evaporator liner	0.01
Filters	0.16
(8) Miscellaneous, vomit bags, etc.	0.10
WASTE TOTAL WEIGHT	1.35 lb/man-day

10.4.4 Instrumentation. A basic set of instrumentation to measure cabin and equipment temperatures, cabin total pressure, oxygen and CO_2 partial pressures and humidity will be an integral part of the crew vehicle life support system. A similar basic system will be included in the MEV. This basic instrumentation package is estimated to weigh 30 pounds with about a 10-watt, continuous power requirement. The crew vehicle instrumentation package will be located in the EEM and will serve both areas. Radiation monitoring equipment must be provided for the main life support system and the MEV system. In addition, trace contaminant sensing will be provided for the main life support system by a gas chromatograph. A breakdown of the instrumentation in each of the vehicles is shown in Table 10-8.

Table 10-8. Interplanetary Vehicle Instrumentation

COMPONENT	WEIGHT (LB)	DC POWER (WATTS)	AC POWER (WATTS)
Crew Vehicle and EEM Life Support Systems			
Temperature System	25.0	--	---
Humidity Sensors	0.8	0.2	0.3
PO_2 Sensor	2.0	0.2	---
PCO_2 Sensor	2.0	0.2	---
Cabin Pressure Gauge	3.0	--	---
Gas Flow Monitoring	6.0	--	---
Alarm Systems	7.0	*(50 main 20 re-entry)	---
Radiation Monitoring Equip	20.0	10.0	10.0
Gas Chromatograph	15.0	5.0	5.0
Subtotals	80.8	15.6	15.3
Mars Excursion Vehicle (MEV)			
Temperature System	15.0	--	---
Humidity Sensor	0.8	0.2	0.3
PO_2 Sensor	2.0	0.2	---
Cabin Press Gauge	3.0	--	---
Gas Flow Monitoring	6.0	--	---
Radiation Monitoring Equip	20.0	10.0	10.0
Alarm System	2.0	*(20)	---
Subtotals	48.8	10.4	10.3
Total for Crew Vehicle (if MEV is attached to Crew Vehicle)	129.6	26.0	25.6

* Note alarm power is not continuous.

10.5 MISCELLANEOUS

10.5.1 Air Filters. The air-conditioning ducting will be supplied with filters at each air inlet to prevent debris of any sort from entering the duct system. The weight penalty for these filters is approximately five pounds/man.

10.5.2 Personal Kits. Each man will carry on board a personal kit which will contain an electric shaver, comb and brush, dental tape, dental gum, Kleenex, and various other toilet articles. The weight penalty for these kits is approximately 10 lb/man + 1 lb/man-week. In addition, each man will be allowed approximately 25 pounds for clothing and other personal articles.

10.5.3 Clothing Dry Cleaner. The crew's clothing will be "dry cleaned" by placing the clothing in a small, sealed compartment which is opened to the vacuum of space. The volatile body oils are vaporized and pass out to space. After a day, the overboard vent valve is closed and the clothing removed. A "dry cleaner" of this type is estimated to weigh approximately 10 pounds for four men or 20 pounds for eight men.

10.5.4 Cabin Cleaning Equipment. Equipment for cabin cleaning will consist of items such as small vacuum cleaners, disposable towels, waste cans, etc. Additional cleaning facilities should be located in the air lock so that the outside of the crew's space suits may be cleaned of any foreign matter. An antiseptic, impregnated sponge and a vacuum-cleaner-type device should be sufficient for this purpose. About 25 pounds of cleaning supplies plus about 0.2 lb/man-day of expendable cleaning supplies are recommended.

10.5.5 Personal Sanitation. Cleansing of the body in a weightless state can be performed with a water- and soap-saturated cloth or sponge. To facilitate the transfer of water, it is advisable to use a thin sponge which has the capacity for holding water by capillary action. To save the weight and volume of disposable sponges, a device for saturating, washing, and drying sponges will be provided. Each crew-member will have a minimum of 15 sponges which weigh approximately 0.10 pound each. The water which is extracted from the sponge after use is recovered, as stated previously.

SECTION 11

ARTIFICIAL GRAVITY FOR INTERPLANETARY SHIPS

11.1 NEED FOR ARTIFICIAL GRAVITY. It would be rather presumptious at this early date to make a decision whether gravity will be mandatory for crews during missions of long duration. This gravity question continues to be of considerable discussion among spacecraft designers and medics. Opinions are not conflicting for the very short-termed space missions or for short-duration intermittent phases such as those needed for mid-course corrections, emergency operations, or other maneuvers where a nonrotating body is required. Continuous operation over periods of months or years is in question and is the condition that confronts interplanetary spaceship designers. Many problems of long-term space flight would be eliminated if gravity were eliminated; however, new problems would be created.

If gravity is provided, the design of much of the equipment aboard the vehicle is simplified because it can be built by long-adopted engineering practices where gas convection and liquid flow are natural. Testing of such equipment can be accomplished easily on Earth with reduction of gravity accounted for by appropriate formulae. During the unavoidable short periods of weightlessness, auxiliary equipment utilizing positive expulsion, or like means, may be substituted for the long-term equipment. Man, the prime factor aboard the spaceship, benefits in that he maintains his equilibrium -- he has an "up" and "down" to orient himself. When he exhales, the warm gases rise due to weight differences between warm and cool air; therefore, he does not rebreathe stale air. Also, his body heat does not have to be blown away with fans, and during fan shutdown he does not boil in his own heat.

A gravity environment simplifies normal living requirements such as food retention and waste disposal. Gravity eliminates the tendency of unattached objects to drift toward the air-conditioning outlets. Operation of the ecological system (pumping of liquids, such as in the water reduction and the algae-cycle systems) is also simplified. Even though a person is normal and in perfect health upon departure from the earth, he may in time produce secretions in the sinus cavities; if normal drainage by gravity is not available, then congestion and infection may develop.

There are many advantages of a gravity environment even if it is not mandatory for the crew's well-being and efficiency. However, there are also disadvantages such as the weight required for spin-up and spin-down propellant and hardware; biomedical problems associated with Coriolis acceleration if high rotational velocities are required; and navigation, directional communication, and celestial observations, which are difficult from a rotating body. (A nonrotating companion ship, such as that planned as part of the interplanetary convoy overcomes these latter difficulties.)

Since there is no conclusive answer to the gravity question at this time, and there appears to be none forthcoming in the near future, artificial gravity inclusion into the design of the crew vehicle is regarded as the safest, most practical solution. It is better to incorporate gravity provisions into the design philosophy at the onset, and remove them later, if possible, than to be confronted with the problem of suddenly adding thousands of pounds of weight to a fixed vehicle design. However, creating a concept that is least affected by the inclusion of gravity appears most logical and is the course taken in this study.

11.2 METHOD FOR PROVIDING GRAVITY. The only practical, known method of creating gravity in space by artificial means is to rotate the body (or combined bodies) about its (or their) common center of mass. The centrifugal acceleration thereby created varies proportionally with the distance outward from the center, and with the square of the rotational velocity (Figure 11-1).

Several methods for providing artificial gravity by centrifugal acceleration are shown in Figure 11-2. Method A shows the vehicle spinning about its own center of mass. This method is employed in the present 8M-14 and 8M-19 designs, and is the simplest in operation of the methods shown. The system is especially effective when the vehicle's center of mass is located far from the crew quarters, such as during the outbound coast phase where maximum propellant weight is stored at the aft end of the spaceship.

In Method B, a joining cable separates the crew modules from the propulsion section. Centrifugal acceleration keeps the connecting cable taut. This method is useful where a low rpm accompanied with high g-level and low Coriolis acceleration is sought. The method is somewhat complicated since the crew modules must be separated, during gravity operations, and rejoined prior to main firing or mid-course correction.

Method C joins two central spined vehicles, at their bases, to form one rigid body. This method provides a very suitable rotation arm and is especially attractive for cases where the center of mass of each individual vehicle is very close to its crew modules. This method of creating gravity requires mating fittings and joining apparatus. Mating is an added maneuver which, if not carefully executed, could produce tragic results. The vehicles must be separated for mid-course correction, subsequently rejoined for gravity, and then separated again for main stage firing. These operations enter into the mission reliability, add weight to the system, and depend upon the availability of a sister ship for mating. Combining the vehicles produces a very large mass moment of inertia which in turn requires more spin-up propellant to produce a required gravity level than spinning about the individual vehicle's own center of mass. In spite of these objections, this method appears very attractive for the 8M-14 vehicle's return home after Maneuver 2 and 3 propellants have been expended, when extremely high rotational velocities would otherwise have to be encountered.

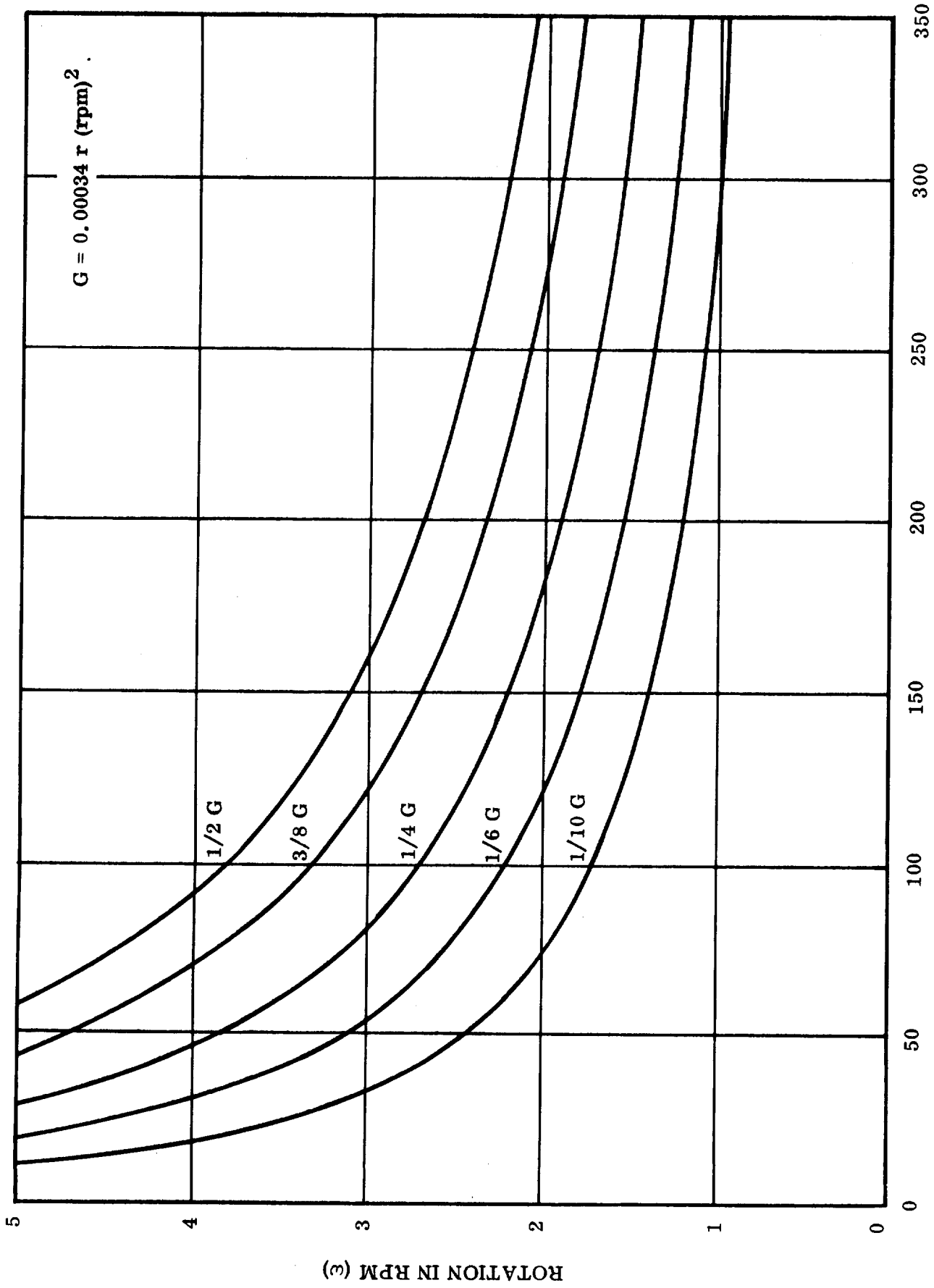

Figure 11-1. Gravity Level

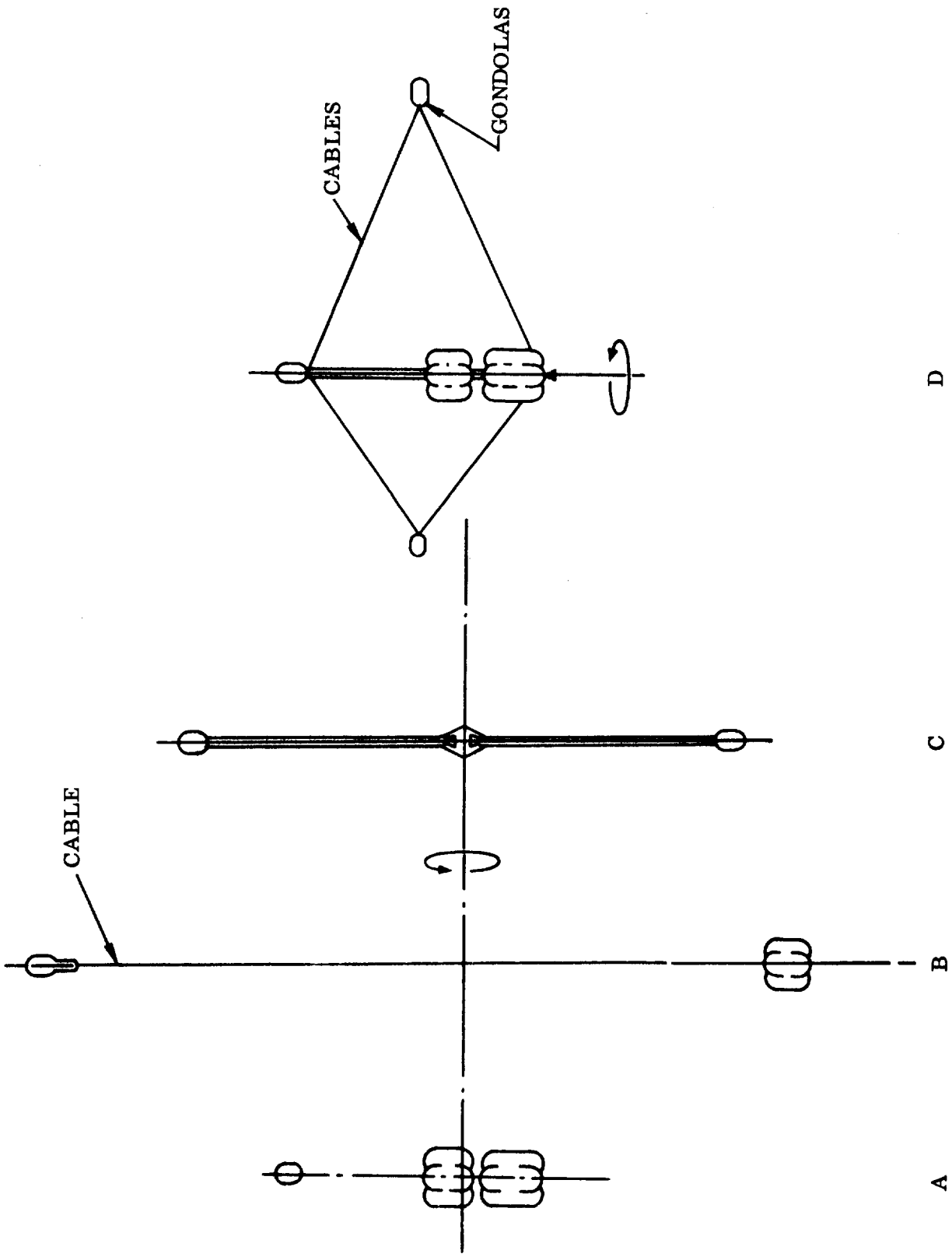

Figure 11-2. Methods of Producing Gravity for Interplanetary Spaceships

In Method D, three cable-spaced crew gondolas are placed at the ends of cables and rotated around the roll axis of the main vehicle. The large rotational radius inherent in the cable arrangement provides high g-level with low rpm and low ratio of Coriolis to vertical acceleration. With a counter-rotating platform at the central hub, navigation, pointing antennas and celestial observations could be operational during periods of gravity. With the design's triangular cable arrangement it would be possible to fire the low-thrust mission engine while providing gravity for the crew members in the gondolas. Small communication cars traverse the cables for transporting the crew between the central hub and the gondolas.

Since solar flares and other high sources of radiation are major hazards on deep-space flights, a shelter must be readily available. Making such provisions in each of the three gondolas appears far too expensive in weight, and communication car service appears too slow. These considerations, plus uncertainties in cable-clamping technology, have at present set this method aside.

Method A has been given prime consideration for the 8M-14 and 8M-19 vehicles. It is a straightforward operation with greatest simplicity. However, Method A is not satisfactory for 8M-14 return coast phase; during this period the center of rotation is located too close to the crew modules. Method C has been adopted for this return phase, since its spin-up design is compatible with that of Method A operation.

11.3 CORIOLIS ACCELERATION. This acceleration is a phenomenon created when a body is moved along the radial axis of a spinning system. The Coriolis acceleration acts perpendicular to the direction of the body's motion and is caused by the fact that the circumferential velocity is a function of distance from the center while the angular velocity is not. While walking toward or away from the center of a rotating system a person tends to veer sideways. The magnitude of the effect depends upon the system's period of rotation and on the (radial) velocity of the person's motion toward or away from the hub. Coriolis acceleration may become rather annoying to a crew member if the spacecraft is designed to produce his vertical acceleration by rotation of a short radius which, in general, results in the requirement of high rpm. In the design of the interplanetary spaceship it is, therefore, necessary to keep the ratio of Coriolis to centrifugal acceleration small. This requirement is met if sufficient vertical acceleration is produced by a slow period of rotation (on the order of 1 or 2 rpm) which requires comparatively large distances between the LSS and the center of mass. But the inherent distance between the center of mass and the crew modules becomes critically short, in some cases, during return coast when the propellant is expended.

Moving from one floor to another in the crew modules or moving one's hand up or down while operating controls produces Coriolis acceleration in the spin plane that is forward when moving toward the hub and aft when moving away. Figure 11-3 shows the effect

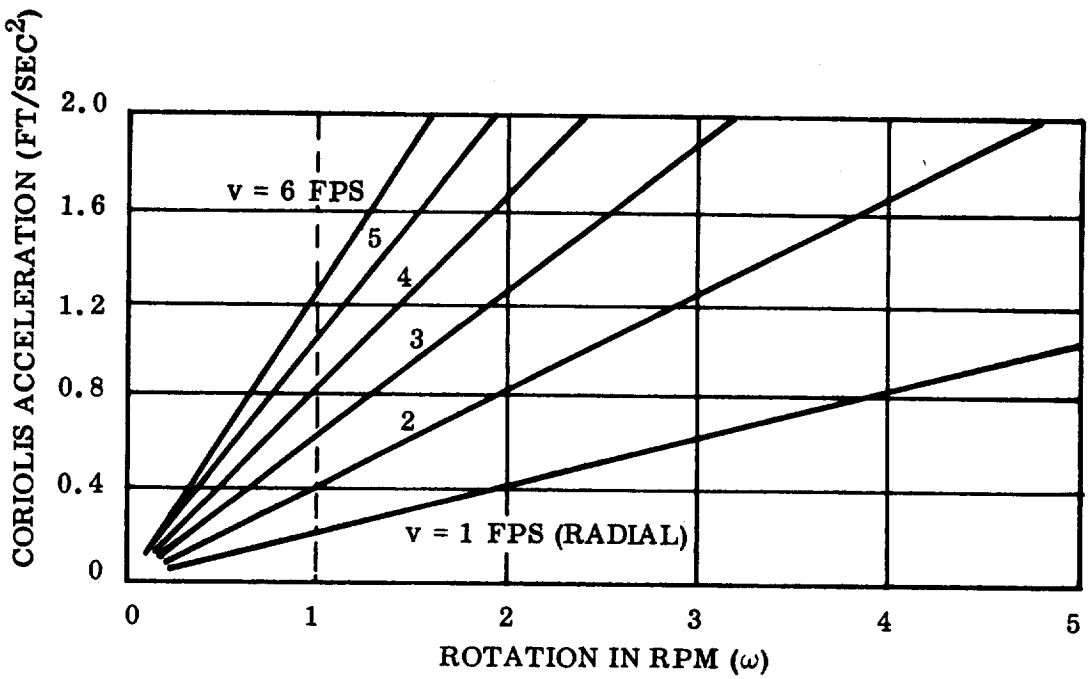

Figure 11-3. Coriolis Acceleration

of Coriolis acceleration as a function of the space lab's rpm. Coriolis acceleration (a_c) may be derived from the formula:

$$a_c = \frac{4\pi}{T} v$$

where

T = period of revolution (sec)

v = radial velocity (ft/sec).

In terms of rpm and g-level, $G_c = 0.0065$ (rpm) v.

For example (see Figure 11-3), a crew member in a spacecraft that is rotating at 2 rpm raises his hand vertically 3 ft/sec toward an object 3 feet directly above. If he did not restrain his motion, his hand would tend to veer ($S = \frac{1}{2} at^2 = \frac{1}{2} \times 1.26 (1)^2 =$ 0.63 ft or 7.5 inches) to the side of the object.

Although Coriolis acceleration will be present at any angular velocity, its effect is more noticeable at lower gravity levels. For example, the 8M-14 spaceship, when rotating at 4.9 rpm with a rotational radius of 31 feet, produces 0.25 g in the command module. At 4.9 rpm the Coriolis acceleration accompanying a 3 ft/sec radial velocity is about 0.1 g, or 38 percent of the vertical acceleration. Under these conditions, a crew member supposedly jumping vertically would in reality veer off at an angle of about 22 degrees with his vertical. If liquid were poured from a pitcher it would leave the spout at a 22 degree angle. These examples represent an extreme case, as shown in Figure 11-4. However, as shown, the Coriolis effect can be considerable with short rotational radii.

A crew member would find both physical and mental compensation necessary to produce the desired motion while moving about in the rotating spaceship. The degree of compensation depends upon his velocity normal to the rotation vector, and upon the rotation vector itself. The effect is negligible for either slowly rotating systems or for slow man motions.

It is believed that the tolerable level of Coriolis acceleration will be a deciding factor when determining the limits of rpm and rotational radius. Rotation creates a disturbing set of medical problems associated with the organs of balance. If a man or an animal is rotated and the axis of his vertibular apparatus is changed, as in nodding or tilting the head, some highly disturbing results take place. Very few individuals can tolerate much of this; some vomit, and others have had to go to bed to recover.

Current research has done much to define the psychophysiology of the problem. The adverse effects of rotation vary greatly from one individual to another. Professional dancers and acrobats appear to be the least affected. It has shown, however, that animals and man have a fairly rapid ability to adapt to the effects of rotation. At present, rotational velocity of approximately 4 to 5 rpm appears to be the maximum tolerable for most qualified crew members.

11.4 GRAVITY PROVISIONS FOR 8M-14 AND 8M-19 VEHICLES. After Earth departure and injection maneuvers the Mars spaceship begins its spin-up operations. A small jet mounted at the extreme distance from the center of mass provides the impulse for the spin-up maneuver. During this period the ship's mass moment of inertia and thrust reaction arm are at their greatest. Even though the thrust arm is greatest it does not compensate for the system's large inertia; therefore, the greatest

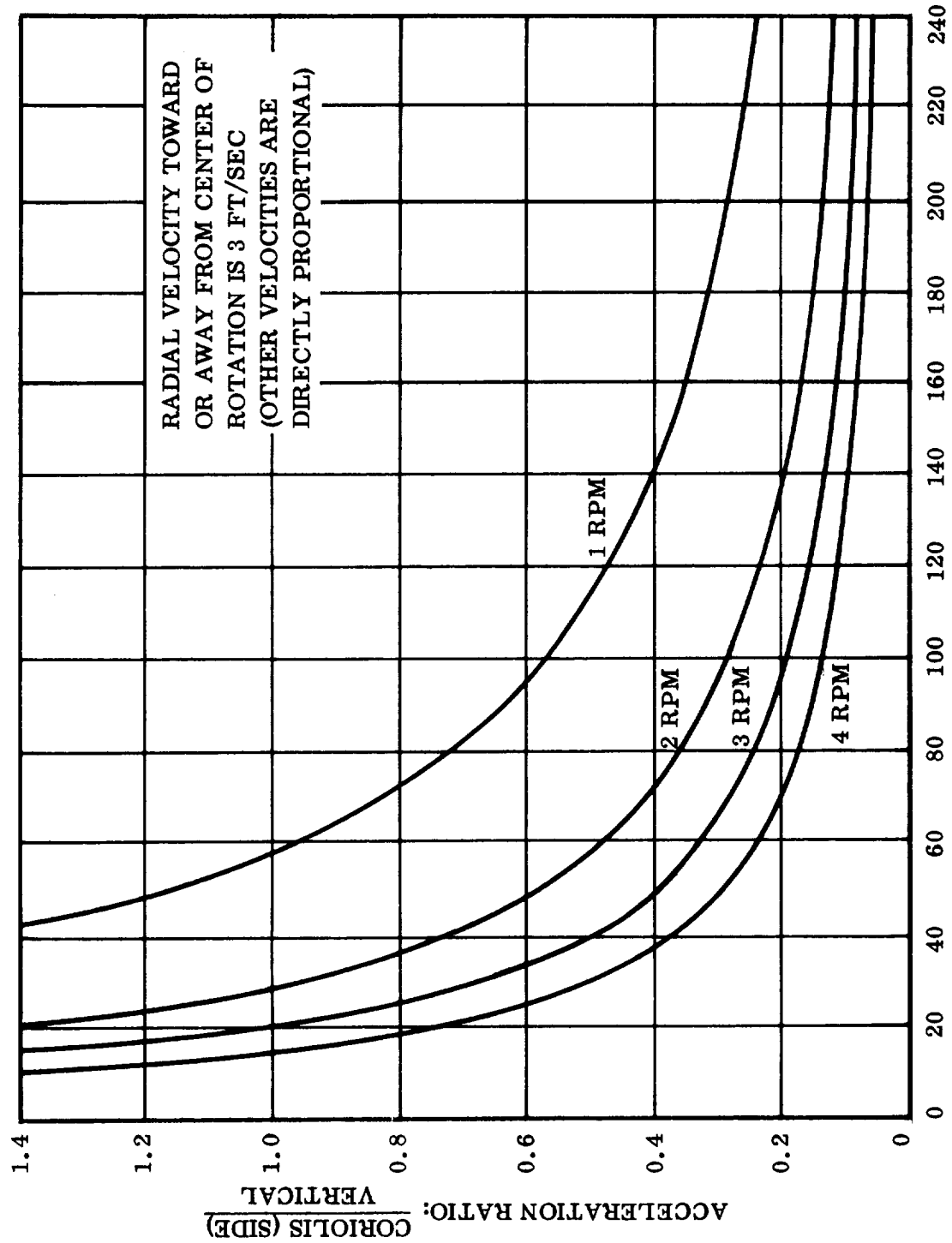

Figure 11-4. Ratio of Coriolis (Side) to Vertical Accelerations

amount of propellant for any spin-up operation is expended during this period. Spin-down is a reverse operation required prior to spaceship propulsion maneuvers. All spin-up and spin-down operations during the mission are similar except for the return trip, when the 8M-14 vehicle's radius of rotation reaches a critically low level (13 ft) which requires an unacceptable 7.5 rpm for 0.25 g at the commander's location. During this period it appears most feasible to join two crew vehicles of the convoy, base to base, and rotate the two as a unit. This method, although it requires five times the propellant per vehicle, reduces the rotation to a desirable 2 rpm.

For the return phase of the 8M-19 (graphite) vehicle, where separate propulsion modules are used, there is a choice of expending the propulsion tank and structure of Maneuver 3 (depart Mars) or retaining it. By retaining it, the center of mass is 20 ft further aft. This reduces the rotational rate from approximately 3 to 2-3/4 rpm, but requires about 23 percent more spin-up propellant. The gain in performance is trivial with respect to the increased propellant required; since the 3 rpm is acceptable, retaining the M-3 structure does not appear to be wise.

Tables 11-1 and 11-2 tabulate spin-up summaries for the 8M-14 and 8M-19 vehicles, respectively.

Table 11-1. Spin-Up Summary For 8M-14 Vehicle

	SINGLE VEHICLE			JOINED VEHICLES
	OUTBOUND	MARS ORBIT	RETURN	RETURN
G	0.25	0.25	0.25	0.25
G'	0.35	0.49	0.82	0.29
r	73	31	13	175
rpm	3.15	4.86	7.50	2.05
R_c	.25	.38	.59	.16
J_o	152×10^6	45×10^6	2.3×10^6	288×10^6
d	143	101	83	245
G. Wt.	900,350	450,650	174,800	349,600
W_P	1010	645	79	* 393
W_{P_T}	4040	1290	316	* 1570

*NOTE: Propellant required by each of the joined vehicles

where:

G = gravity level in commander's position of command module

G' = gravity level in center of mission modules

r = radius of rotation to commander's deck (ft) from C.G.

rpm = rotational velocity to provide gravity level

R_c = ratio: Coriolis (side) to vertical acceleration G at 3 fps radial vel.

J_o = mass moment of inertia of rotating system (sl-ft^2)

d = distance to spin-up rockets (ft) from C.G.

G.Wt = total vehicle weight (lb)

W_p = weight of propellant for one spin-up or -down (lb); I_{sp} = 320 sec

W_{P_T} = total weight of propellant for two spin-up cycles during outbound and return and one during Mars capture period

= 6900 lb

Table 11-2. Spin-Up Summary For 8M-19 (Graphite) Vehicles

	OUTBOUND	MARS ORBIT	RETURN	RETURN WITH M-3 STRUCTURE
G	0.25	0.25	0.25	0.25
G'	0.23	0.22	0.19	0.20
r	193	144	78	98
rpm	1.95	2.26	3.08	2.73
R_c	.15	.18	.24	.21
J_o	210.8×10^6	75.2×10^6	25.9×10^6	41.3×10^6
d	213	164	98	118
G.Wt.	1,317,450	619,300	212,400	259,400
W_p	635	340	253	313
W_{P_T}	2540	680	1012	1252

where:

G = gravity level in commander's position of command module

G' = gravity level at shop floor in spine

r = radius of rotation to commander's deck (ft) from C.G.

rpm = rotational velocity to provide gravity level

R_c = ratio: Coriolis (side) to vertical acceleration G at 3 fps radial vel.

J_o = mass moment of inertia of rotating system (sl-ft^2)

d = distance to spin-up rockets (ft) from C.G.

G.Wt. = total vehicle weight (lb)

W_p = weight of propellant for one spin-up or -down (lb); I_{sp} = 320 sec

W_{P_T} = total weight of propellant for two spin-up cycles during outbound and return and one during Mars capture period

= 4232 lb

11.5 SPIN-UP MECHANICS. Since the spaceship is in a zero-g environment during its nonpropulsive flight, the only gravity created within the capsule is produced by the centrifugal force of the vehicle rotating about its own center of mass, or, if joined with another body, about their common center of mass. The artificial acceleration created as a function of angular velocity and rotating radius arm is formalized by equating centrifugal force, $F = m\omega^2 r$, to $F = ma$; ie:

$$a = \omega^2 r$$

where a = acceleration (ft/sec^2)

ω = angular velocity (rad/sec)

r = radius of rotation to gravity deck (ft)

To express the artificial acceleration in terms of earth gravity ratio "G" and rpm

$$G = \frac{a}{32.2} = \frac{(0.1047\ rpm)^2 r}{32.2}$$

$$= 0.00034\ r\ (rpm)^2$$

Figures 11-5 and 11-6 are plots of G-levels versus rpm for various rotational radii inherent in the 8M-14 and 8M-19 vehicles, respectively.

11.6 SPIN-UP PROPELLANT REQUIREMENTS. The propellant required for spin-up is:

$$W_p = \frac{I_t}{I_{sp}}$$

where W_p = propellant required for spin-up (lb)

I_{sp} = specific impulse of spin-up propulsion (sec)

I_t = total impulse (lb-sec) = F (thrust) x t (time)

Spin-up torque is:

$$T = J_o \alpha$$

where: T = spin-up torque (ft-lb)

= F (thrust) x d (acting arm)

J_o = mass moment of inertia about the center of rotation ($sl\text{-}ft^2$)

α = angular acceleration (rad/sec)

$$= \frac{\omega_f - \omega_i}{t}$$

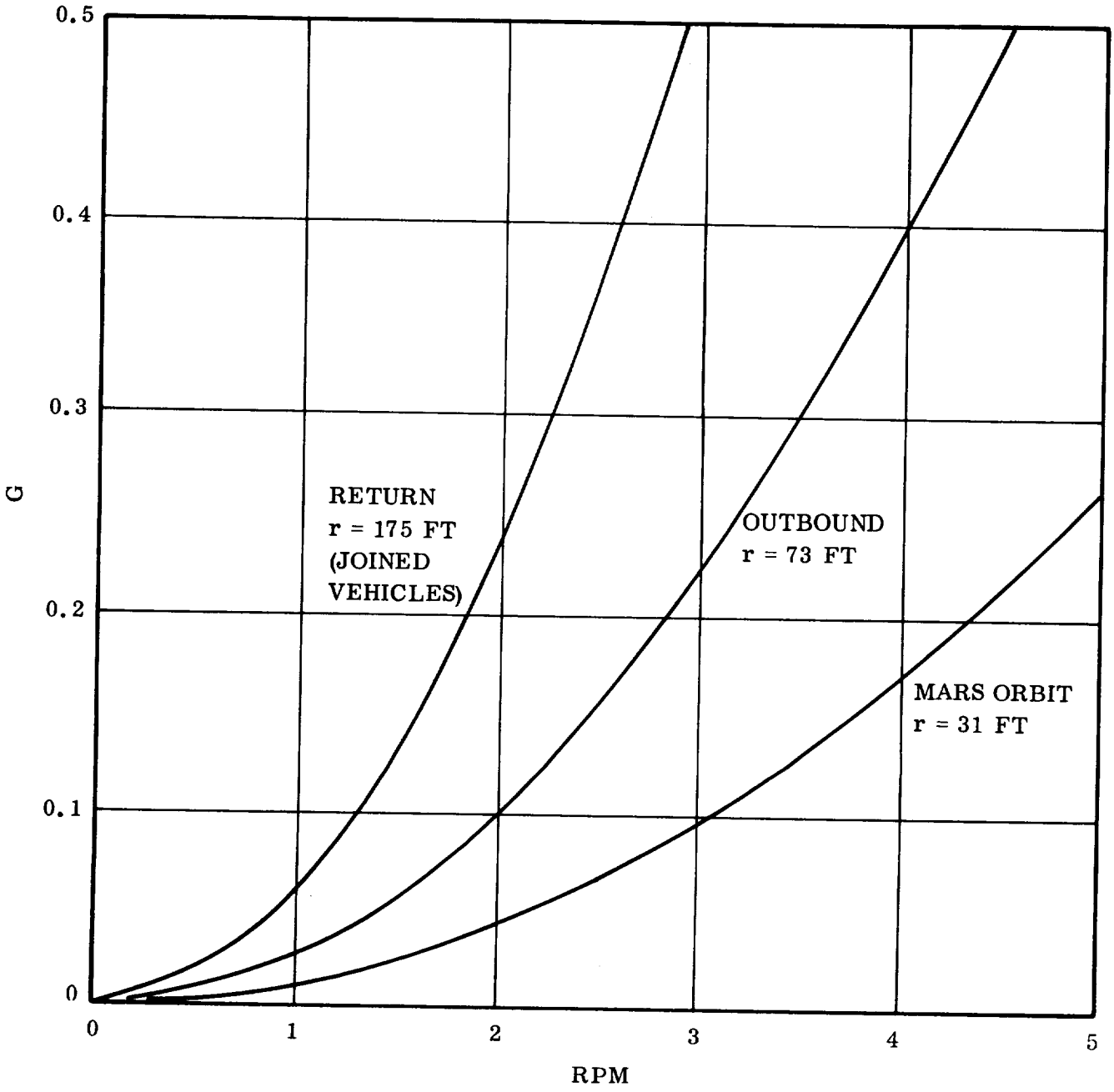

Figure 11-5. Gravity in Command Module of 8M-14 Vehicle

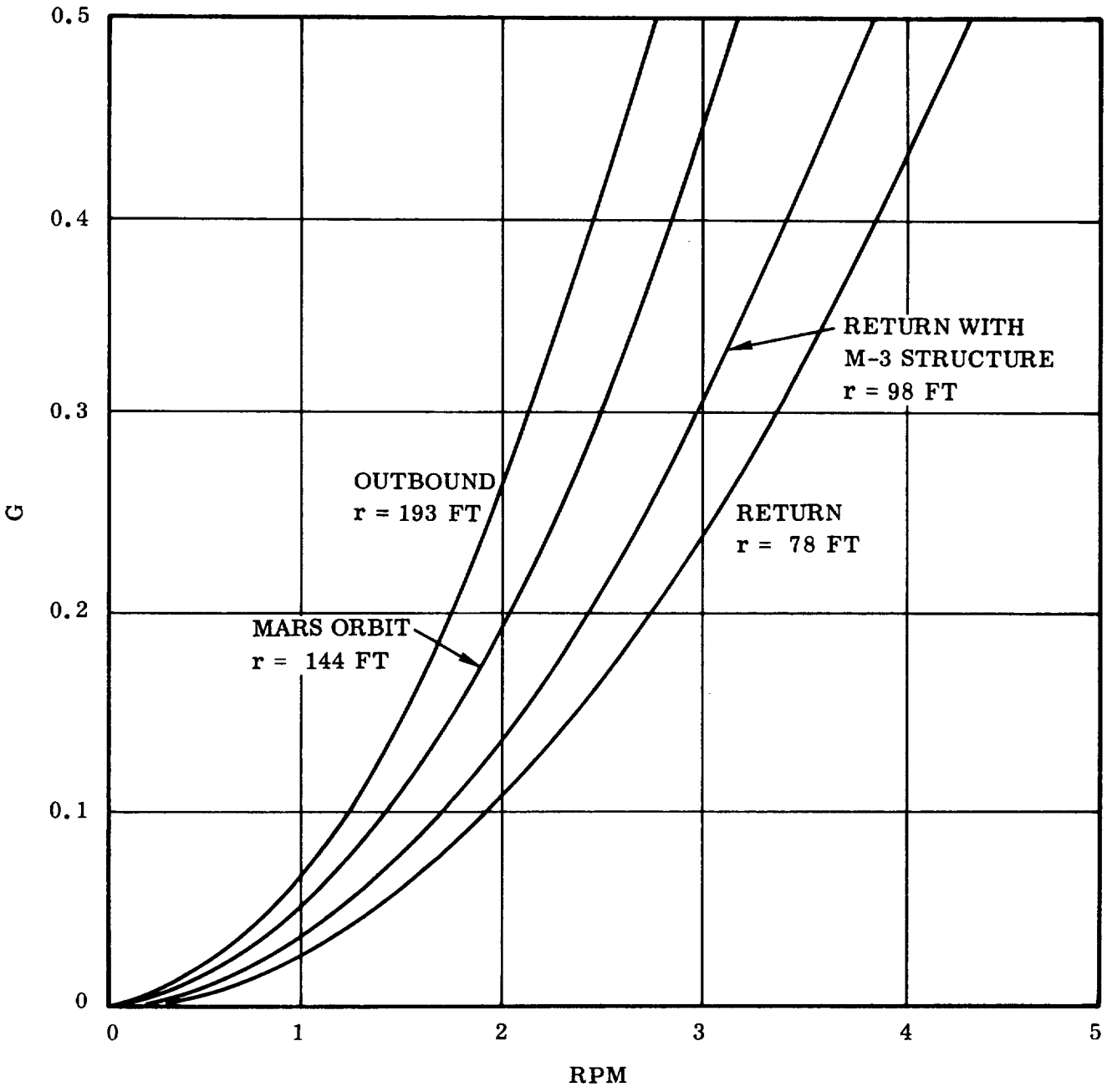

Figure 11-6. Gravity in Command Module of 8M-19 (Graphite) Vehicle

and ω_f = final rotational velocity (rad/sec)

ω_i = initial rotational velocity (rad/sec)

thus, $Fd = J_o \frac{\omega_f - \omega_i}{t}$

or $Ft = \frac{J_o}{d} (\omega_f - \omega_i)$,

then, from $Ft = I_t = W_p \times I_{sp}$,

$$W_p = \frac{J_o}{d\, I_{sp}} (\omega_f - \omega_i)$$

NOTE: If the initial rotational velocity is zero and the final velocity is in rpm, then

$$W_p = 0.1047 \frac{J_o}{d \times I_{sp}} (\text{rpm})$$

Spin-up propellant weight as a function of specific impulse is plotted for 8M-14 and 8M-19 vehicles in Figures 11-7 and 11-8, respectively. A 0.25 g at the commander's position in the command module has been assumed, for uniformity in comparison of the plots. Two spin-up and two spin-down operations are included for outbound and return phases of the mission, and one spin-up and spin-down cycle is included for Mars orbit.

As expected, the higher specific impulse requires less weight; however, storability and other factors must be considered. An I_{sp} of 320 sec is the basis for weights shown on the summary sheets.

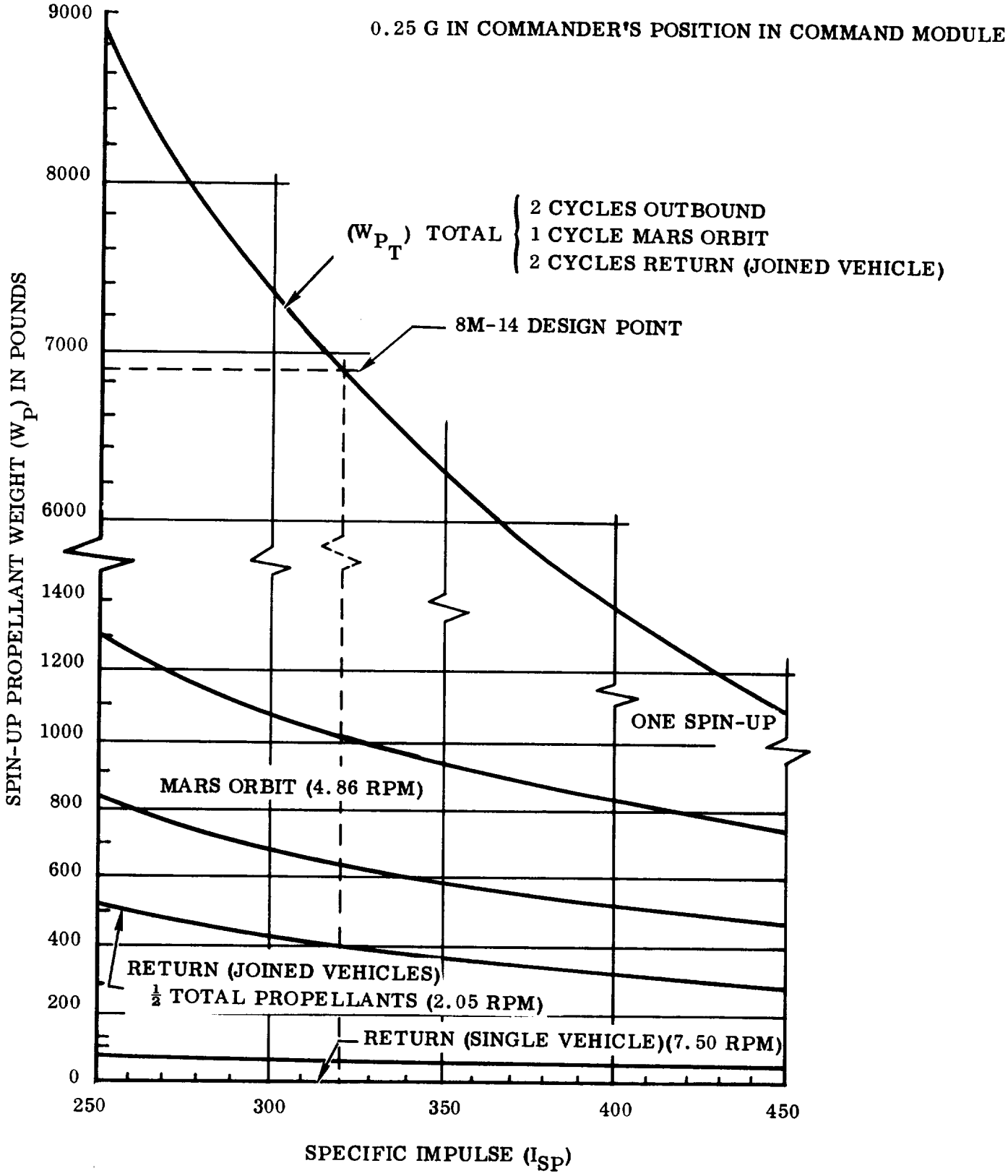

Figure 11-7. Spin-up Propellant Weight for 8M-14 Vehicle

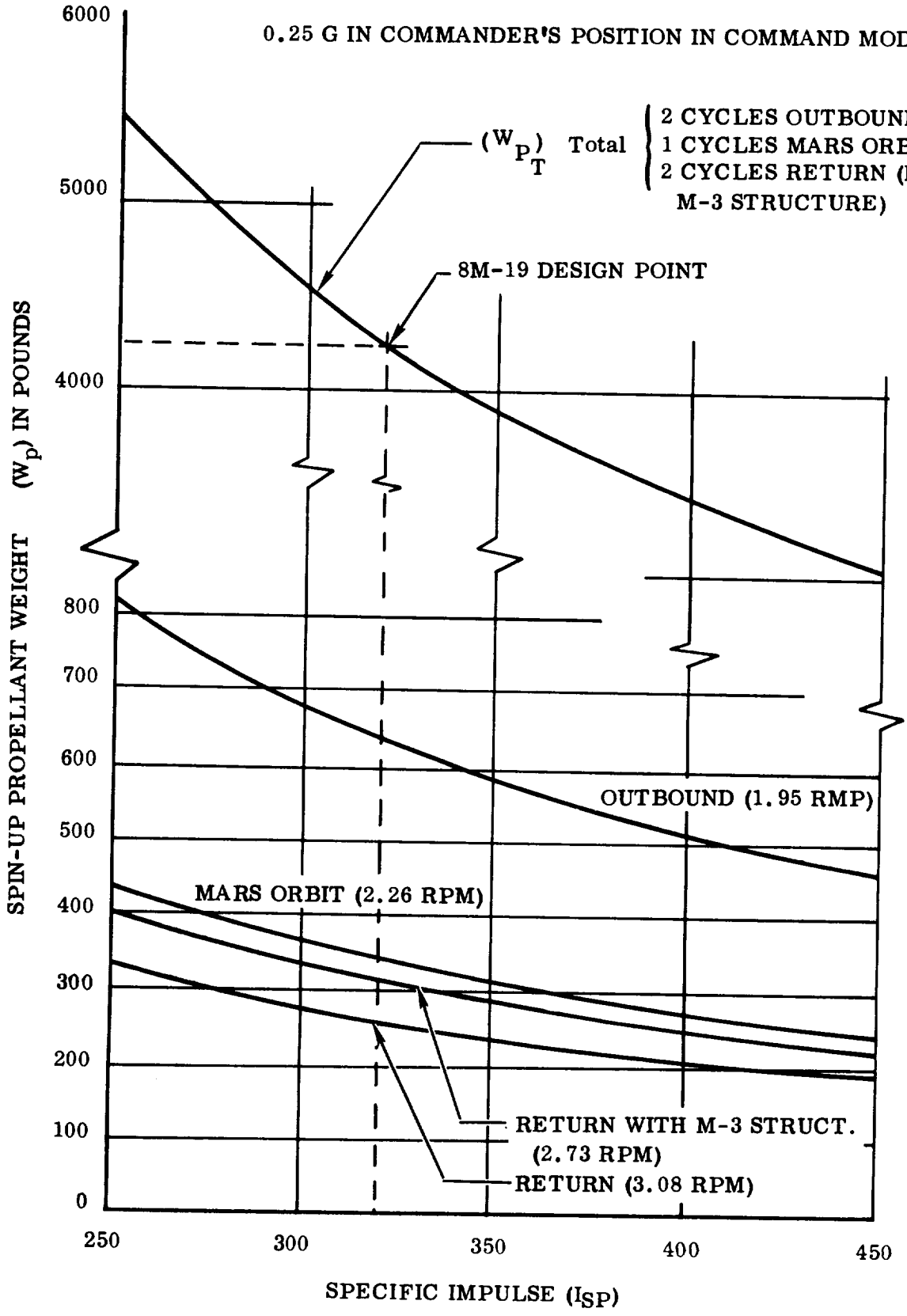

Figure 11-8. Spin-up Propellant Weight for 8M-19 (Graphite) Vehicle

SECTION 12

RADIATION PROTECTION

12.1 INTRODUCTION. The shielding philosophy, in general, is to provide a radiation shelter large enough to house all crew members in emergencies, and also while they sleep if this is desired. At other times the crew is exposed to radiation through a wall of about 0.4 gm/cm^2 of aluminum-fiberglass. Carbon wool, in lieu of fiberglass, is also being considered.

The desirability of sleeping inside the flare shelter is related to how important it is to eliminate some of the low energy, heavy cosmic ray primaries. If this should be worthwhile the crew will still have to contend with a somewhat higher dose from lighter, but more numerous, secondaries.

12.2 RADIATION DOSE DETERMINATION. The radiation dose from the model class 3+ solar flare was determined from the General Dynamics/Fort Worth solar flare shielding study (Ref. 4-17) which calculates the differential energy loss at a point target in rads. However, the point-target definition is less realistic than Schaefer's (Ref. 12-1) spherical body phantom, as it overestimates the dose. The point target definition may also, on occasion, be an order of magnitude higher than a volume-target energy deposition calculation in which self-shielding by other parts of the body phantom is considered (Ref. 12-2). After discussing this with Dr. R. K. Wilson, it was decided to divide by two the dose rates given in Ref. 4-17. No attempt was made to give the dose in rem although with the present 19 gm/cm^2 of boron-filled polyethylene shielding, the average relative biological effectiveness (RBE) of emergent solar flare radiation is probably about 1.5 (Ref. 12-2).

The Freden and White spectrum (Ref. 4-36) was used for calculating doses from trapped protons (Ref. 4-17). Since the particles which filter through shielding from trapped protons tend to be hard, there is little distinction between the point-target and volume-target dose definition. The former might be one-third higher than the latter. Since the electron component in the Mev range was neglected in the dose calculations, it was decided to use the point-target dose given in Ref. 4-17. The resulting dose rate is about 0.16 rads/hr for 19 gm/cm^2 of polyethylene.

The data in Table 12-1 gives the resulting relative mean radiation dose in terms of a unit dose at 1 A.U. from a selected model class 3+ solar flare for each Martian and Venusian trip indicated. The mean relative dose per day is also given. It can be seen, for example, that the Venusian trip on 17 February 1974 has a mean relative dose rate (MRDR) of 0.00930 compared to a MRDR of 0.00755 for a Martian trip on 4 November 1973.

If the selected shielding for the Martian trip proved acceptable, then the shielding for the Venusian trip might have to be increased by an amount which would reduce the model flare MRDR to a comparable value. The ratio of the Mars/Venus MRDR is about 0.82. A polyethylene flare shield of 19 gm/cm^2 would have to be increased to about 22 gm/cm^2 for the Venusian trip.

However, these calculations are for the active year 1958. If a correction is introduced for the expected decrease in solar activity in 1972-73, the mean dose/trip can be reduced by at least 50 percent since the expected SS numbers range from 20 to 40. Assuming the number of class 3+ flares is proportional to the smoothed SS number gives less than one class 3+ flare per year. Assuming the rate of major flare occurrence also decreases in the same manner, it is found that the MRDR for the 1972-74 period is only 10 to 20 percent of the 1958 value. However, to be conservative, this estimate has been increased to 33 1/3 percent of the 1958 value in Table 12-1.

As a matter of interest, the radiation dose limits for Apollo are shown in Table 12-2 (Ref. 12-2).

Figures 12-1 through 12-4 show the dose distributions calculated for the Martian and Venusian trips referred to in Table 12-1. Trips can be identified by the total number of days. The mean dose is also shown in terms of a unit dose at one A.U. from one class 3+ flare. Thus, the radiation dose per trip for the 369-day Venusian mission is equivalent to 3.431 class 3+ flares at the Earth's distance.

Figure 12-5 shows the assumed tissue dose from the model solar flare (10 May 1959) as a function of polyethylene shield mass density. The cosmic-ray type flare of 23 February 1956 is also shown. Figure 12-6 shows the estimated radiation dose rate from the most intense part of the Van Allen trapped-particle belt.

Table 12-1. Radiation Dosage for Selected Mars/Venus Trips

Leave Earth	Arrive Venus/Mars	Stay Time (Days)	Leave Venus/Mars	Arrive Earth	Trip Time (Days)	MRDR*	Mean Dose (Rad/Day)		Dose/Trip (Rad)	
							1958	1973	1958	1973
25 Oct 1973	17 Feb 1974 Venus	10	27 Feb 1974 Venus	29 Oct 1974	369	0.00930	1.013	0.338	374	125
16 Dec 1973	17 Feb 1974 Venus	36	25 Mar 1974 Venus	29 Dec 1974	372	0.00920	1.003	0.334	373	125
18 May 1973	4 Nov 1973 Mars	10	14 Nov 1973 Mars	13 June 1974	391	0.00755	0.824	0.271	322	107
7 Mar 1973	25 Sept 1973 Mars	39	3 Nov 1973 Mars	1 June 1974	451	0.00783	0.854	0.285	385	128

* MRDR - Mean relative dose rate (rads per normalized flare per day)

MRDR at Earth distance = 0.00995

MRDR at Venus distance = 0.01901

MRDR at Mars distance = 0.00429

Table 12-2. Radiation Dose Limits for Apollo *

Critical Organ	Max. Perm. Total Dose (Rem)	Max. Perm. Dose (Rad/Day) ***	RBE (Rem/Rad)	Mean Yearly Dose (Rad)	Maximum Emergency (Rad) **
Skin of Whole Body	1,630	78	1.5	233	500
Blood Forming Organs	271	19.4	1.0	54	200
Feet, Hands, and Ankles	3,910	199	1.4	559	700
Eyes	271	9.7	2	27	100

* Design doses a factor of four lower

** Skin erythema level

*** Based on 14 days trip time

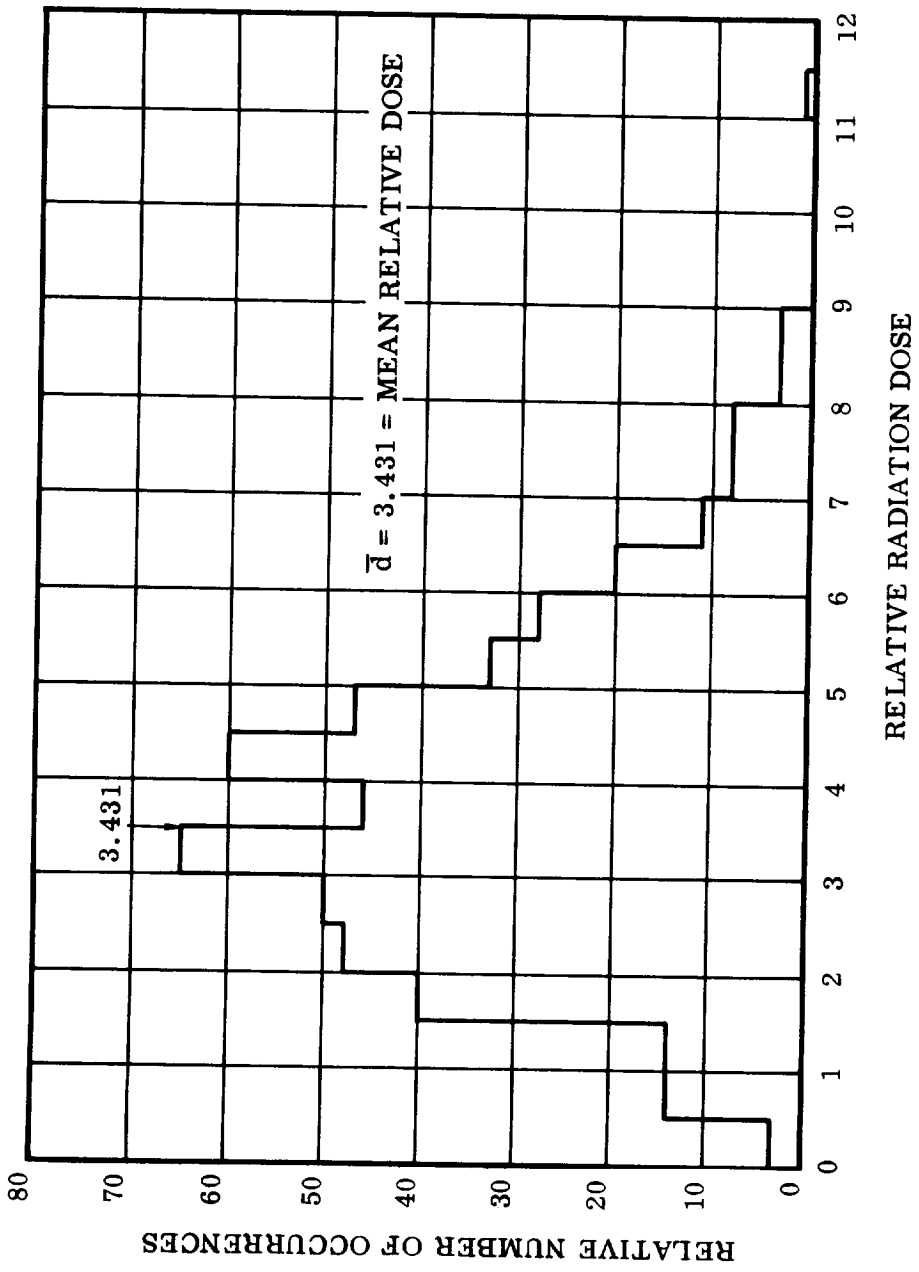

Figure 12-1. Dose Distribution for 1973 Earth-Venus Mission Window (369 Days, 500 Trips)

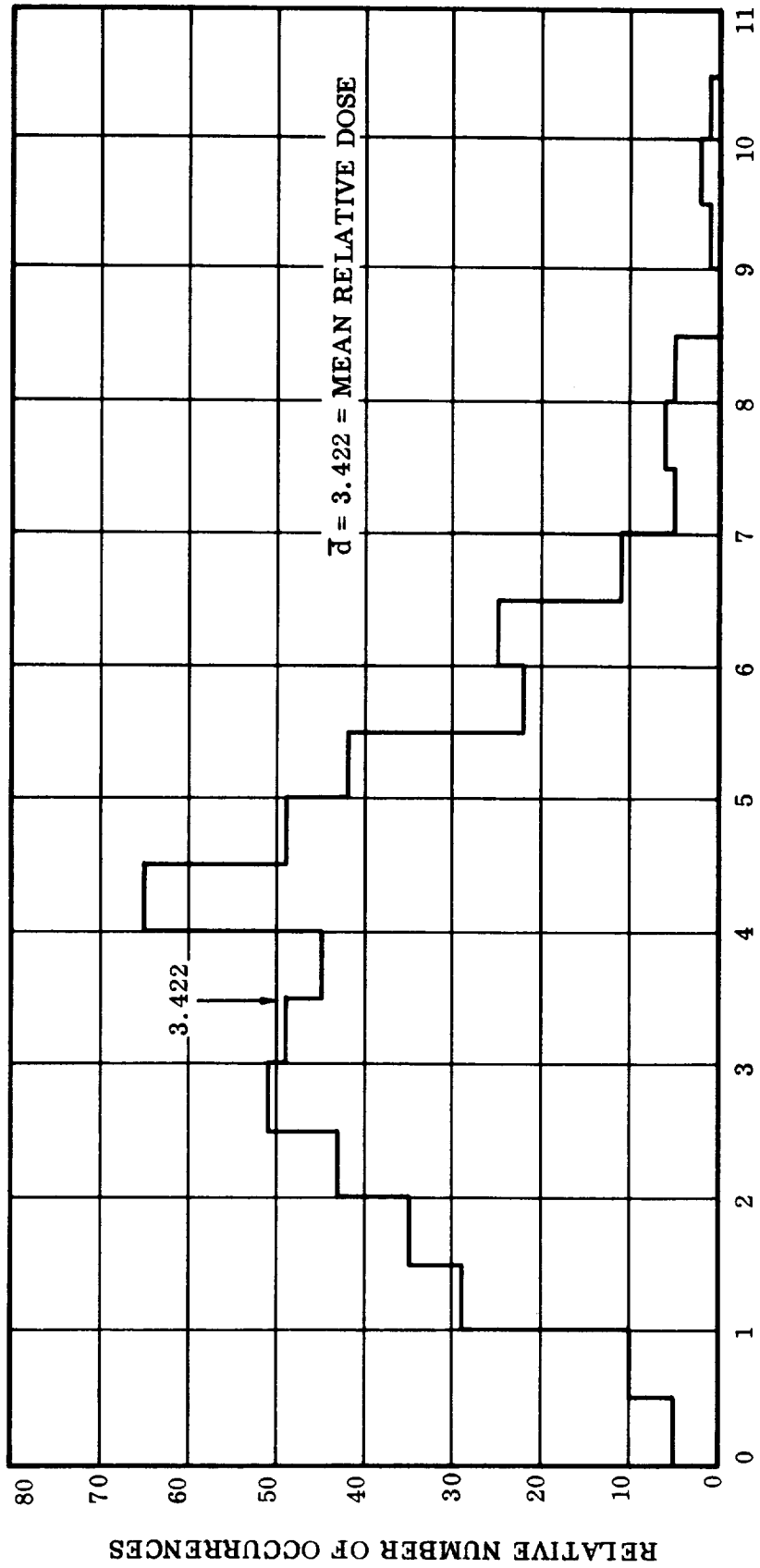

Figure 12-2. Dose Distribution for 1973 Earth-Venus Mission Window (372 Days)

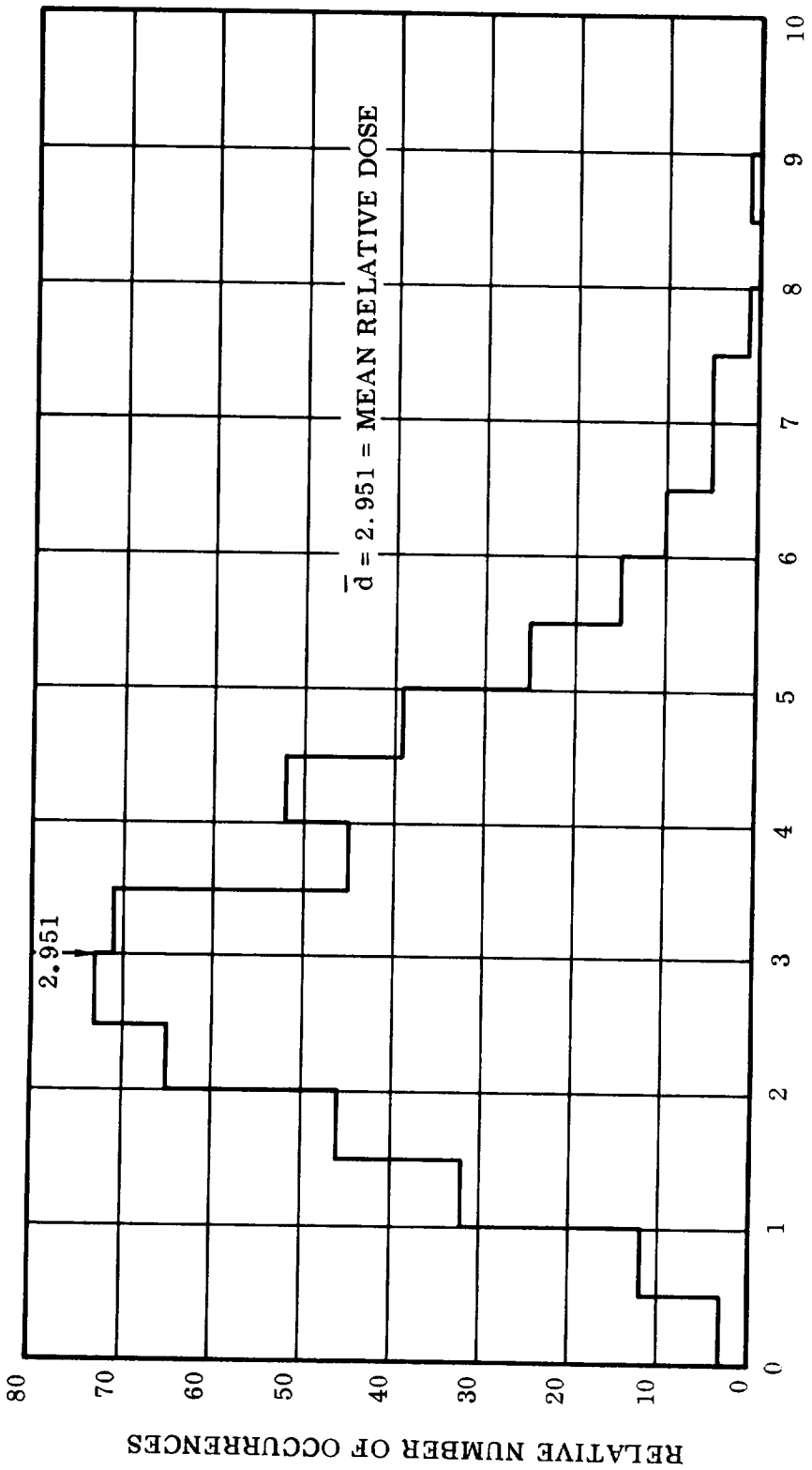

Figure 12-3. Dose Distributions for 1973 Earth-Mars Mission Window (392 Days, 500 Trips)

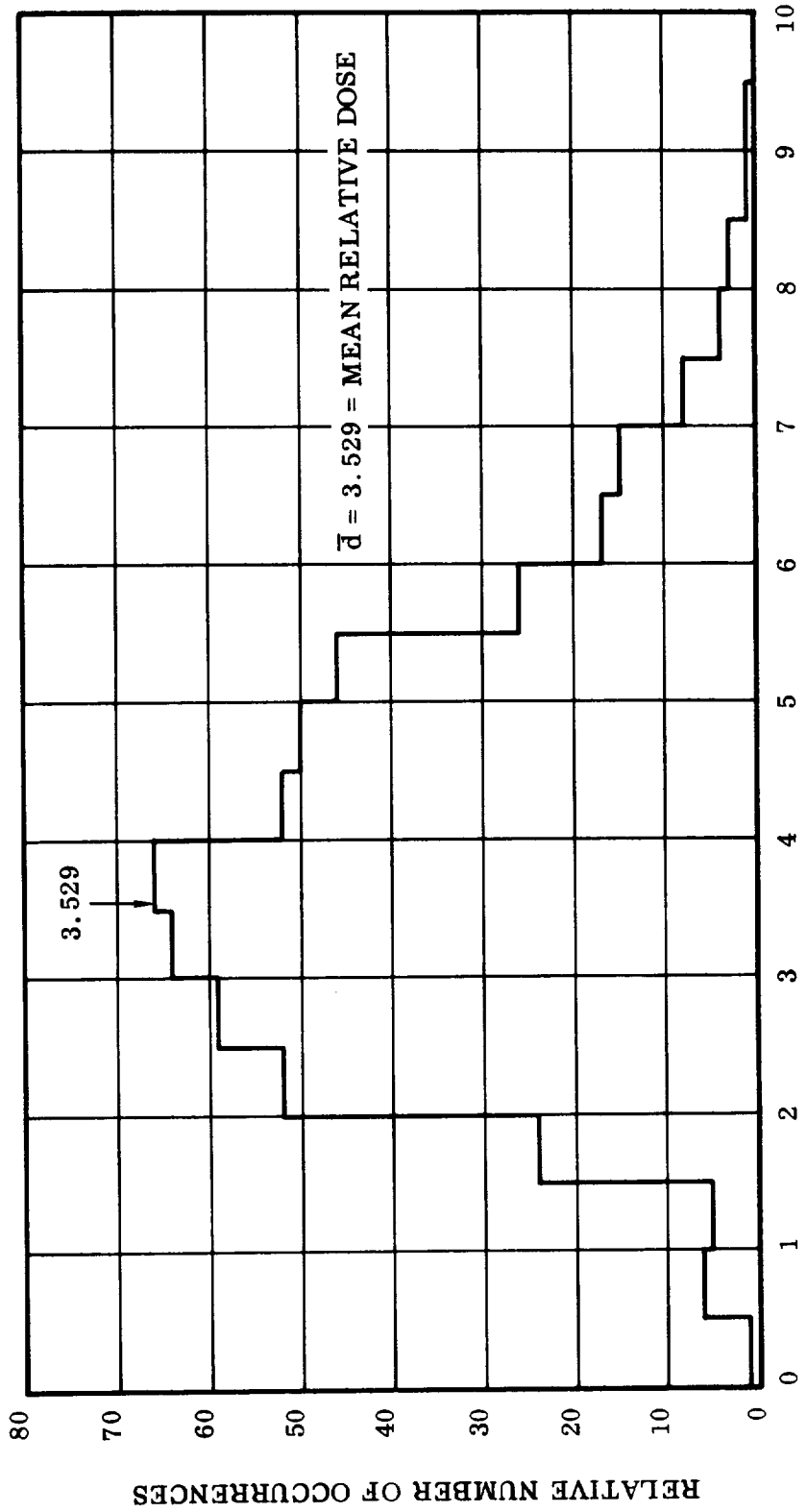

Figure 12-4. Dose Distribution for 1973 Earth-Mars Mission Window (451 Days, 500 Trips)

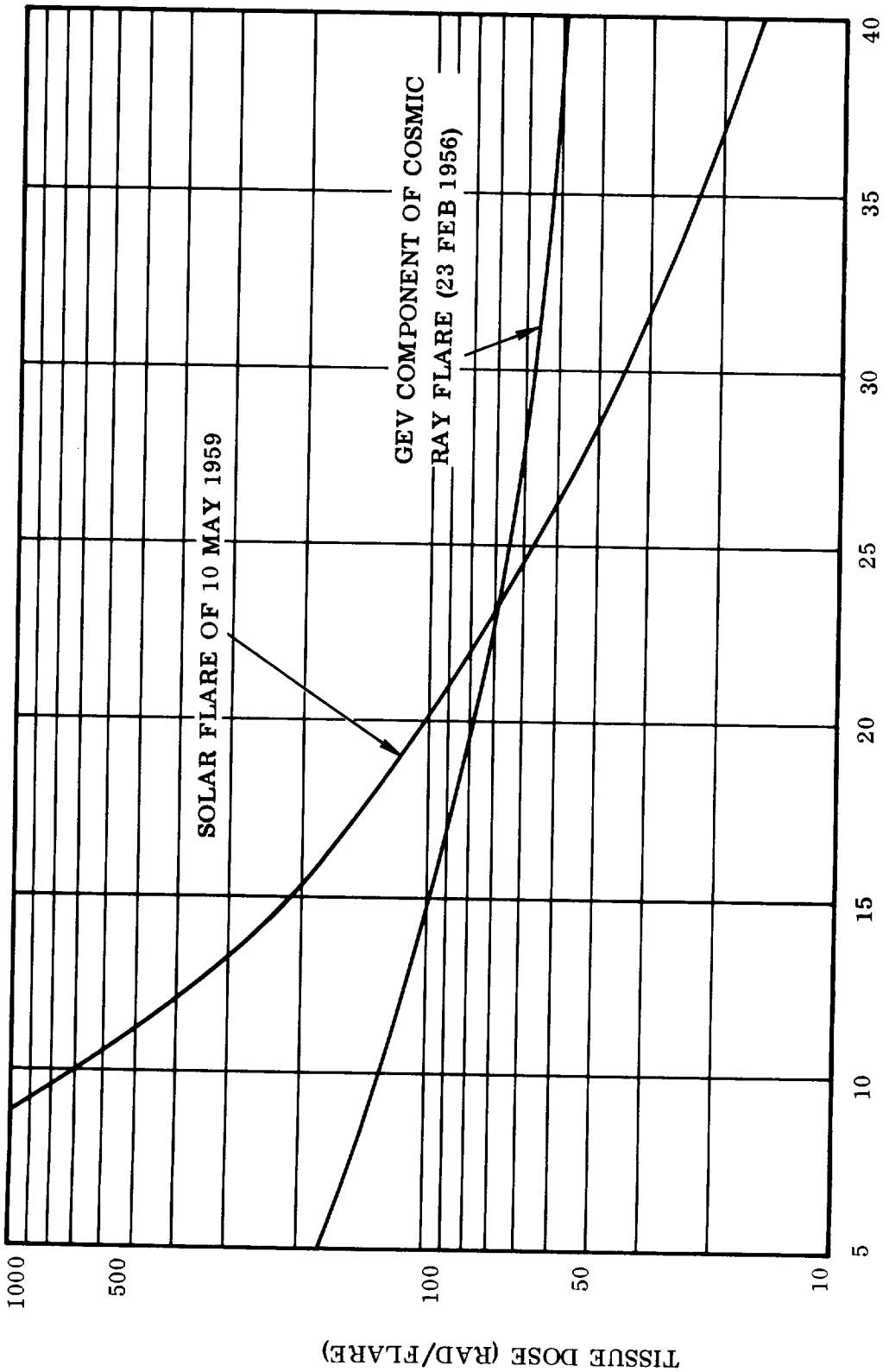

Figure 12-5. Assumed Tissue Doses from Model Solar Flare and Cosmic Ray Type Flare as Functions of Shield Mass Density

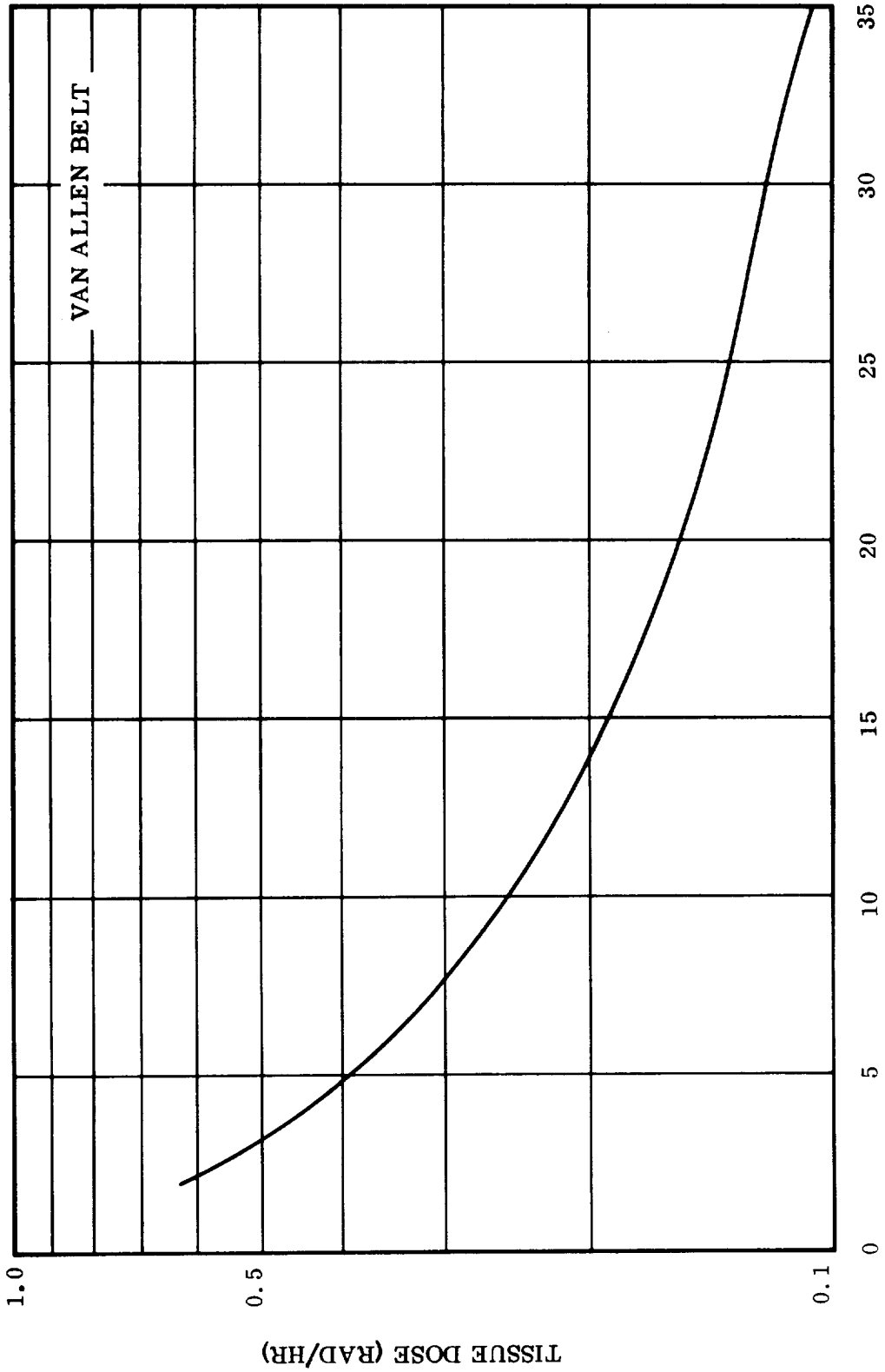

Figure 12-6. Estimated Radiation Dose Rate From Van Allen Belt

PART III

SYSTEMS INTEGRATION, OPERATIONS, PLANNING

SECTION 13

MISSION MODES

Several different mission modes are available for fast manned interplanetary reconnaissance missions, in addition to direct flights which require more potent propulsion systems than are presently considered to be most likely available in 1973 or 1975. These likely propulsion systems are:

a. Advanced chemical engines (e.g., high-pressure O_2/H_2 which, with expansion ratios of 150 or higher, could provide a specific impulse of about 455 seconds).

b. Certain types of nuclear engines (NERVA and one second-generation nuclear engine. The vital importance of nuclear propulsion for interplanetary flight is generally recognized by now and requires no elaboration at this point).

Unless a Post-Saturn Earth Launch Vehicle (ELV) of 10^6 lb payload or better into a near-Earth orbit is available (and in a number of cases even then) some form of orbital assembly is required. A convoy of several vehicles is considered. If the vehicles are nuclear powered, the entire crew is located in one vehicle (crew vehicle) to avoid the problems (in terms of shielding or intra-convoy navigation or both) associated with the strong side radiation of the nuclear reactors. The crew vehicle is accompanied by at least one (preferably two) service vehicles which serve as carriers for auxiliary vehicles, for propellant reserves and spares (including a spare Earth Entry Module), and which serve as secondary vehicles for the crew in case the crew vehicle is incapacitated. In this case, the entire life support module is transferred to one of the service vehicles.

Taking the crew vehicle as example, because it is the most important ship of the convoy (and the vehicle whose design serves as model for the service vehicles), the various mission modes are briefly discussed. The crew vehicle consists of the following modules:

a. Earth entry module (EEM) which also serves as abort capsule for the crew during departure or return.

b. Propulsion system for abort and for spin-up and spin-down of crew vehicle en route to provide a measure of artificial gravity.

c. Life support module (LSM) which is the principal crew abode during mission. The LSM consists of the command module, a number of mission modules, a utility module, and space taxis.

d. A number of propulsion modules (stages) for each of the principal mission maneuvers.

Each of these modules is interchangeable with the corresponding modules (if carried) of the other ships. Individual propellant tanks in each module can be replaced by one attached to one of the service vehicles. The entire LSM or LSM/EEM system is transferable from the crew vehicle to a service vehicle. Prior to each major powered maneuver the crew does "house cleaning," eliminating all weight no longer needed at the end of the respective coast period, of which there are three: Earth to target planet, target planet capture, and target planet to Earth. By far the largest weight reduction takes place prior to the Earth recapture maneuver, laid out to "erase" the interplanetary flight history and substitute for it Apollo entry conditions (reduction of relative orbital energy from $\epsilon > 0$ to $\epsilon = -0.04$). Prior to this maneuver, the entire LSM (about 88,000 lb for a crew of 8) is jettisoned and the terminal payload (the one slowed down to $\epsilon = -0.04$) consists essentially of EEM and crew. Its weight (about 9800 lb) and the hyperbolic velocity excess at Earth return determine primarily the terminal propellant consumption.

The general arrangement of the crew vehicle is shown in Figure 13-1 (Mars mission in 1973 or 1975 with a crew of eight; cf. OVAM weights, Table 13-1). The vehicle has nuclear propulsion for Earth escape, Mars capture and Mars escape. For the limited Earth capture maneuver it is equipped with chemical (O_2/H_2, I_{sp} = 455 sec) propulsion. The configuration for the first maneuver consists of one or two tanks (shown, 60 ft dia.), powered by an open cluster of four nuclear engines. Ten propellant tanks and one nuclear engine are used in the Mars capture maneuver. Mars escape again uses ten propellant tanks, and one smaller nuclear engine. The long spine separating the LSM from the chemical propulsion system is retained during the return coast to permit generation of artificial gravity by slow tumbling, but is jettisoned, together with the LSM, just prior to the Earth capture maneuver.

Due to the comparatively small quantities of hydrogen retained as part of the chemical propulsion system, following Mars escape, little crew protection can be provided by its use as a shield against corpuscular space radiation. The layout of a "dry" LSM version is shown in Figure 13-2. Radiation shielding is provided by 7.6 inches of boron-filled polyethylene over the command module, except for the floor which consists of 4 inches of polyethylene and 4 inches of water. The life support equipment, food storage and shop compartments are stacked vertically above the command module and surrounded by four external mission modules and two space taxis. All floors within the vehicle are designed as pressure bulkheads so that compartments penetrated by meteoroids can be readily isolated. A combined separation interface and EEM docking arrangement is provided at the end of the LSM for jettisoning the LSM while retaining the EEM prior to Earth capture.

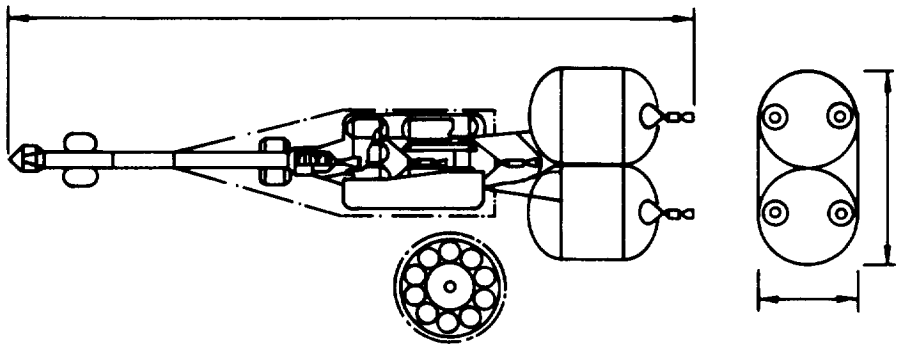

Figure 13-1. Propellant Tank Arrangement (8M-22)

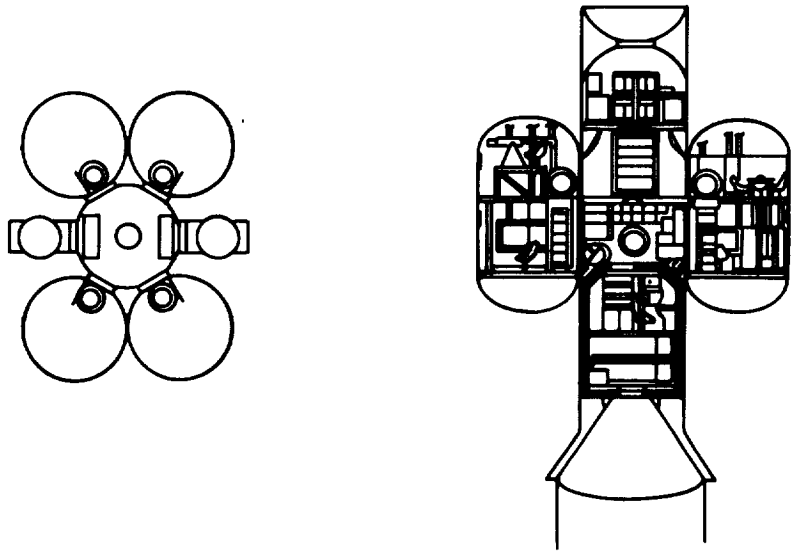

Figure 13-2. Interior Arrangements (L-28)

The four basic mission modes, aside from direct flight, are:

a. Orbital vehicle assembly mode (OVAM)

b. Interorbital vehicle assembly mode (IVAM)

c. Capture orbit vehicle assembly mode (COVAM)

d. Combination of (b) and (c) (IVAM/OVAM)

The mission modes differ essentially in the place in which the individual planetary ship is assembled. The principal trade-offs involved are:

a. More Earth-Orbital work, but departure with complete, basically self-sufficient planetary ships; mating and/or fueling of very massive modules.

b. Large Earth-escape modules and correspondingly high thrust requirements (which cause more problems all around, but particularly when nuclear engines are involved).

c. Large numbers of assembly flights with C-5 (at corresponding reduction of the probability of success of a given number of supply flights), or requirement for a larger Post-Saturn ELV sooner.

versus

a. Less orbital work, possibly none other than gathering individual convoy ships in the rendezvous orbit, if the total departure weights can be broken down into packages which represent individual departure ships in a weight range which can be delivered into orbit by the given available ELV.

b. Smaller thrust units required for Earth escape.

c. Disengagement of a Post-Saturn ELV development program from at least the first manned planetary reconnaissance mission, should a conflict exist between the two development schedules.

d. More work for the crew (which departs in ships which are not self-sufficient for the entire trip) in mating modules (albeit of considerably smaller mass) en route to the target planet or in the capture orbit.

e. A greater number of vehicles to depart from the Earth rendezvous orbit, since each ship is now transported in two to four sections.

Mission mode a calls for the complete assembly of a given planetary ship in Earth orbit, either by injecting the complete vehicle (only partially fueled, and fueling thereafter in orbit) or by orbital mating of fully fueled and otherwise operational modules. If each ship is assembled by mating two modules, a natural division is into Earth escape booster and planetary ship proper, each package weighing between 6×10^5 and over 10^6 lb.

Mission modes b, c, and d do not require the assembly in Earth orbit of self-sufficient vehicles. Rather, each planetary ship is separated into two (modes b and c) or four (mode d) modules which are launched by a larger convoy of independent ships and are mated en route as required. Assuming two-impulse transfer orbits between the planets, the following propulsion modules are needed for a crew vehicle; Earth escape (M-1), target planet capture (M-2), target planet re-escape (M-3) and Earth recapture (M-4).

The energy requirement for each of these maneuvers varies as a function of time. The variations can be considerable, even during a constellational period. Therefore, the four mission modes are compared for a specific, typical, capture mission to Mars in 1975 (Table 13-1). The operational sequence is illustrated in Figure 13-3. OVAM requires assembly of the complete vehicle in the EAO. In the particular example, this requires the assembly of a ship of some 2.4×10^6 lb orbital departure weight. The departure weights (hence, the departure thrust, i.e., the size or number of nuclear engines required by the Earth escape booster) are greatly reduced. In terms of orbital departure weight there is little difference between IVAM and COVAM. The difference lies in the mission phase during which the assembly of the respective vehicle modules must occur and also in the mass of the modules which have to be mated. IVAM requires mating during the interplanetary transfer period, COVAM during the capture period. The latter causes a stronger mission interference, since capture is the most valuable period of the entire mission and should be utilized to the maximum extent for planetary reconnaissance. On the other hand, the masses of the modules to be mated are significantly smaller in the case of COVAM than of IVAM, which may facilitate the mating operation for the limited number of crew members available and which may improve the probability of avoiding significant damage during mating.

In an all-out attempt to minimize the Earth orbital departure weight, one can combine IVAM and COVAM. In this case, four orbital launch vehicles are needed for a single crew or an equivalent payload weight. Since the mission would be flown with at least one crew vehicle and one service vehicle (carrying auxiliary vehicles for the planetary exploration and other cargo, as well as serving as backup vehicle for the crew) a fleet of eight vehicles would be required for sending the equivalent of two complete vehicles on the mission. The number of orbital operations in heliocentric space and near the target planet is maximized. Even in this case the weight of the heaviest of the four vehicles approaches 700,000 lb (i.e., far exceeds the delivery capability of a Saturn C-5 ELV). In fact, this capability is exceeded by all four vehicles, so that a considerable amount of Earth orbital rendezvous operations would still be needed. Under these

Table 13-1. Example of a Capture Mission to Mars and Comparison of Weight Distribution for Different Mission Modes (8-Man Crew)

Earth Departure Window	9 March through 29 March 1975
Arrival Mars	4 November 1975
Transfer Period, T_1	240 to 220 days
Mars Departure Window	4 December through 24 December 1975
Transfer Period, T_2	260 days
Maximum Capture Period	50 days
Capture Orbit	Circular, 1.3 Mars radii distance
Propulsion	Nuclear: M-1 through M-3 Chemical: M-4

Maneuver	M-1	M-2	M-3	M-4
v_∞^*	0.3705	0.1774	0.2082	0.3842
Isp (sec)	846	846	820	455
Mass ratio	2.774	1.646	2.162	3.778

Vehicle Weight (10^3 lb)

	OVAM	IVAM		COVAM		IVAM/COVAM			
Earth Dep.	2,435	1,300.4	1,069	957	1,290.1	466.6	387.6	681.8	537.6
Transfer		355.4	278			133.6	107.4	202.7	155.4
M-2	634.3	634.3		241	358.1	241		358.1	
Capt. Orbit Mars	355.4	355.4		146.5	217	146.5		217	
M-3	336.3	336.3		336.3		336.3			
Transfer	133.6	133.6		133.6		133.6			
Jettison LSS	87.4	87.4		87.4		87.4			
M-4	46.2	46.2		46.2		46.2			
Earth Entry	13.1	13.1		13.1		13.1			

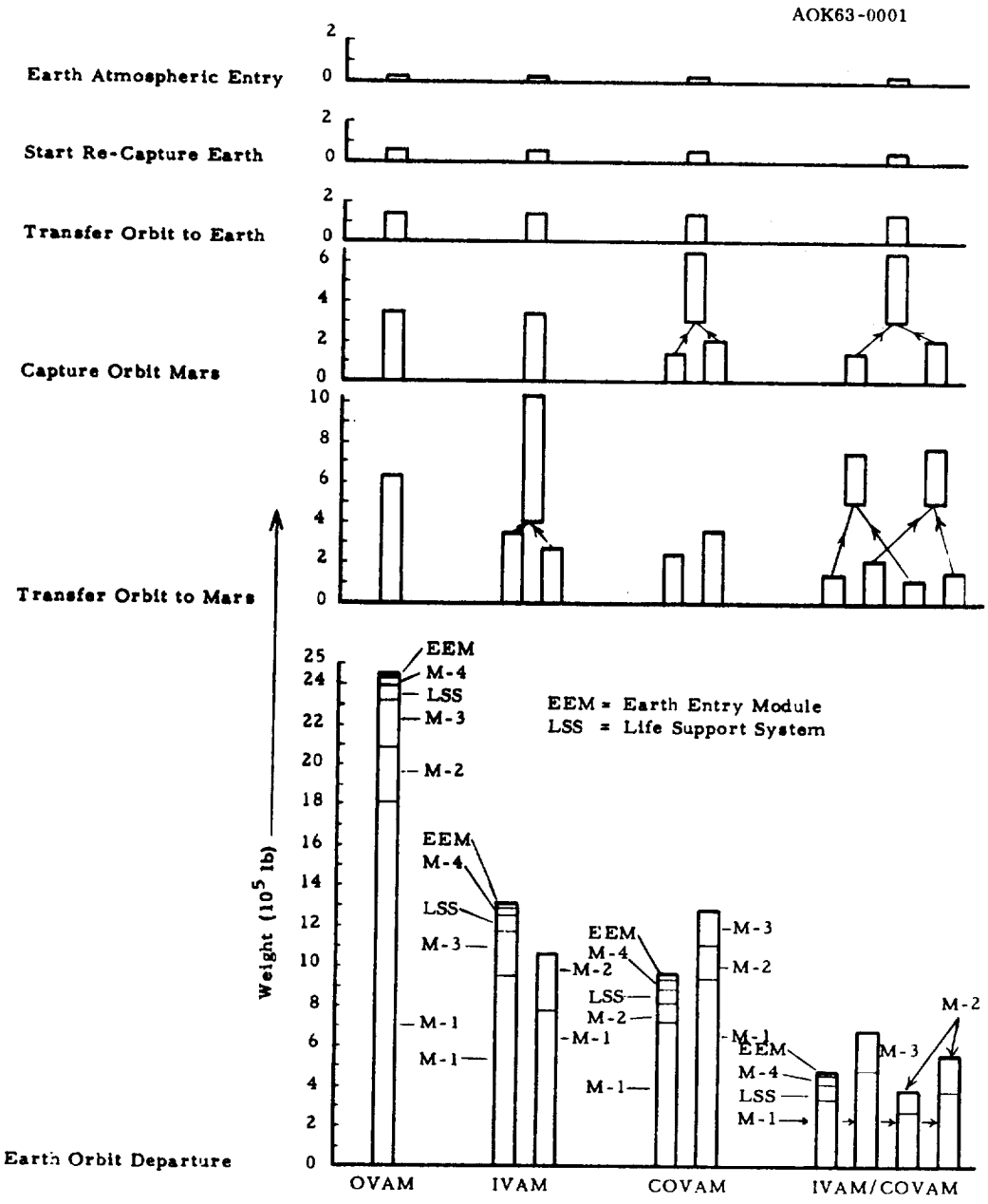

Figure 13-3. Comparison of Mission Modes for a Mars Mission 1975

conditions an IVAM/COVAM combination would not be attractive. If, however, a Post-Saturn ELV of higher payload capability (say, 700,000 lb) were postulated, IVAM/OVAM would make it possible to completely prepare all orbital operations other than gathering the convoy cluster would be required. To achieve the same for IVAM or COVAM alone, the hypothetical Post-Saturn ELV would require 1.3 to 1.5 million lb payload capability.

Each of these mission modes has advantages and disadvantages whose relative importance can be appraised only within a given frame of reference in terms of the expected state-of-the-art for launch vehicles and propulsion systems, practical experience gained in future rendezvous operations in Projects Gemini and Apollo, and so forth. The above example points out the considerable variety of approaches which can be taken. They lead to a wide range of orbital departure weights which are correlated with a corresponding variation of the extent of orbital operations and their sequencing in the course of the mission. Thus, superimposed over the flight dynamic effect on orbital departure weights, which correlates vehicle size with mission profile and the location and width of specific mission windows (set of launch windows at Earth and target planet) on the time scale, is the influence of operational choices on the orbital departure weight of individual vehicles. The variety of flight operational alternatives offers flexibility and freedom of choice among vital parameters affected by the expected state-of-the-art in space technology as well as in orbital operations. The orbital departure weight of individual vehicles may be reduced by a factor of three to four by proper choice of the mission mode, given an adequate incentive for such reduction, while retaining a given mission profile and mission window. By a proper combination of low energy mission profile (such as attainable by a fly-by mission, by a capture, or by long mission periods), of mission window (launch year and time of year), of target planet (Venus less expensive than Mars), and of mission mode, the orbital departure weight of the individual vehicle can be varied within even wider limits.

Other factors which may influence the choice of the mission mode lie in the realm of space physics and in the characteristics of planetary orbits. Increasing solar activity in the second half of the seventies will make the radiation problem (hence, the shielding weight problem) more acute, temporarily, for Venus or Mars runs after 1975. Moreover, an increase in mission energy requirement from 1973 through 1977 is indicated. This will cause an increase in launch weights.

SECTION 14

PRE-LAUNCH AND LAUNCH OPERATIONS

14.1 PRE-LAUNCH AND EARTH-TO-ORBIT OPERATIONS. The system studies for handling the interplanetary vehicle on the ground assumes that the vehicle must be transported, after manufacturing and checkout, to the launch complex from a remote manufacturing facility (see Figure 14-1). One restriction on the choice of the manufacturing site is that it must be adjacent to a body of water so that water transportation methods may be used.

Due to the size of the individual modules, transportation will necessarily be by water. Although a few sections of the interplanetary vehicle (spine, taxi capsules, re-entry module) are small enough to be shipped either by air or land, it is proposed that the complete vehicle be packaged by modules and carried on a C-2 class cargo ship to the launch complex. This ship would be capable of carrying one complete interplanetary vehicle. Choice of an inland manufacturing site with access by navigable rivers would necessitate loading the modules on barges which would be towed to AMR by tug.

Trailers provide the packaging for the modules and also perform the transfer functions between the manufacturing site and dock and at the launch complex. The docks at each end of the transportation route are constructed to provide roll-on/roll-off capabilities for the trailers. The M-1 and M-4 modules are carried on a self-propelled pneumatic trailer and are supported by a cradle at each end of the module. The M-2 and M-3 modules are carried on trailers which are self-powered units made up of a tubular steel chassis and frame, mounted on rubber-tired, hydraulically operated castors. The three tanks of the M-2 and M-3 modules are mounted on their "spines" and carried on the trailer by supporting the "spine" at several points.

At the launch complex, storage facilities for four complete vehicles are provided, including checkout facilities for two vehicles. The Interplanetary Test and Checkout Area provides this. Here the simulation of the completely assembled configuration will be made in a horizontal position prior to a complete system checkout. The two parallel checkout areas are located on either side of a row of checkout equipment. The complete vehicle is assembled with the modules supported on their trailers and positioned in tandem in their proper order. Alignment rails fixed on the floor of the checkout area assure proper positioning of each trailer and its module, and increase the ease of operations for mating each segment of the vehicle.

Mobile work platforms are necessary to provide access for each module while in the horizontal position. A 10-ton overhead crane services the whole Test and Checkout Area. This area is located within the Post-Saturn Vertical Assembly Building and has two assembly and checkout stalls on either side. A 50-ton bridge crane spanning the

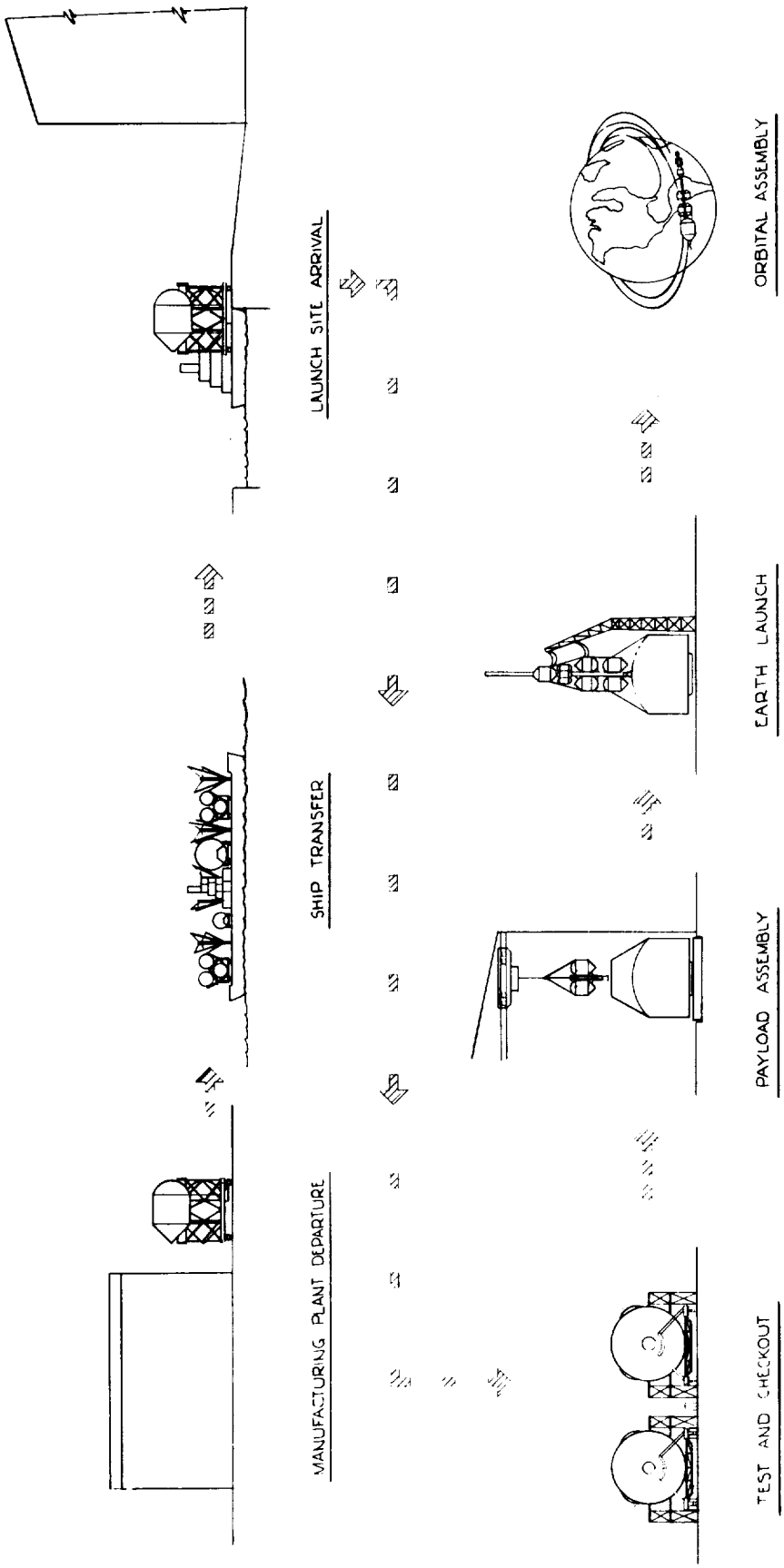

Figure 14-1. Pre-launch and Launch Operations

width of the Interplanetary Checkout Area and the Post-Saturn stalls provides the capability for transferring the Interplanetary modules to the Post-Saturn vehicle. Transfer of a module can be accomplished by simultaneously lifting each end of the module from its trailer with individual hoists to a sufficient elevation. By raising one hoist and then lowering the other, the module is rotated from a horizontal to a vertical position. By moving the hoist to a position over the Post-Saturn vehicle, the module can then be lowered and assembled as the payload for the booster. Final checkout, as well as assembly of the thermal/meteoroid shield, is accomplished in the Post-Saturn Vertical Assembly Building with the modules placed on the launch vehicle.

Two Post-Saturn launch vehicles (400-ton minimum payload capability) are necessary to place one interplanetary vehicle into earth orbit. One vehicle carries the M-2, M-3, and M-4 sections of the space vehicle packaged in that ascending order. The spine is placed above the M-4 section and acts as the nose of the payload. The M-1 section is launched as a separate payload on another Post-Saturn launch vehicle.

Propellant loading of the interplanetary vehicle is conducted at the launch pad, utilizing the storage facilities provided for the Post-Saturn vehicle. Hydrogen requirements of approximately 350 tons per payload necessitate expanding the Post-Saturn production and storage facilities proportionally. Propellant transfer operations are made within one hour. Boil-off of the hydrogen is kept to a minimum by providing a closed cycle, cold helium atmosphere in the space between the thermal/meteorite shield and the hydrogen tanks. The propellant transfer lines and the helium service lines are retained within the umbilical tower.

The Post-Saturn vehicle has been considered as the primary earth launch vehicle. It is conceivable that a Saturn C-5 vehicle could boost the modules of the interplanetary vehicle into an assembly orbit, but because of the many additional launches necessary, the complexity of the operations increase and the desirability of such a system is reduced. Assuming a payload capability of 250,000 lb for the Saturn C-5 vehicle, a total of eight launches and seven rendezvous operations would be necessary to place one interplanetary vehicle in its assembled orbital configuration. By adding the additional launches necessary to place the whole convoy in orbital readiness, it is apparent that not only would the system be more complex due to rendezvous necessities but also that the Saturn launch facilities would be more than overtaxed (see Figure 14-2).

Rather, a supplemental use of the Saturn vehicle has been considered. Replacement of a tank of the interplanetary vehicle damaged prior to earth orbit departure, providing maintenance and checkout requirements during orbital pre-launch operations and inserting the manned Apollo-type capsule into its rendezvous position are some of the operations which would require use of the Saturn launch booster.

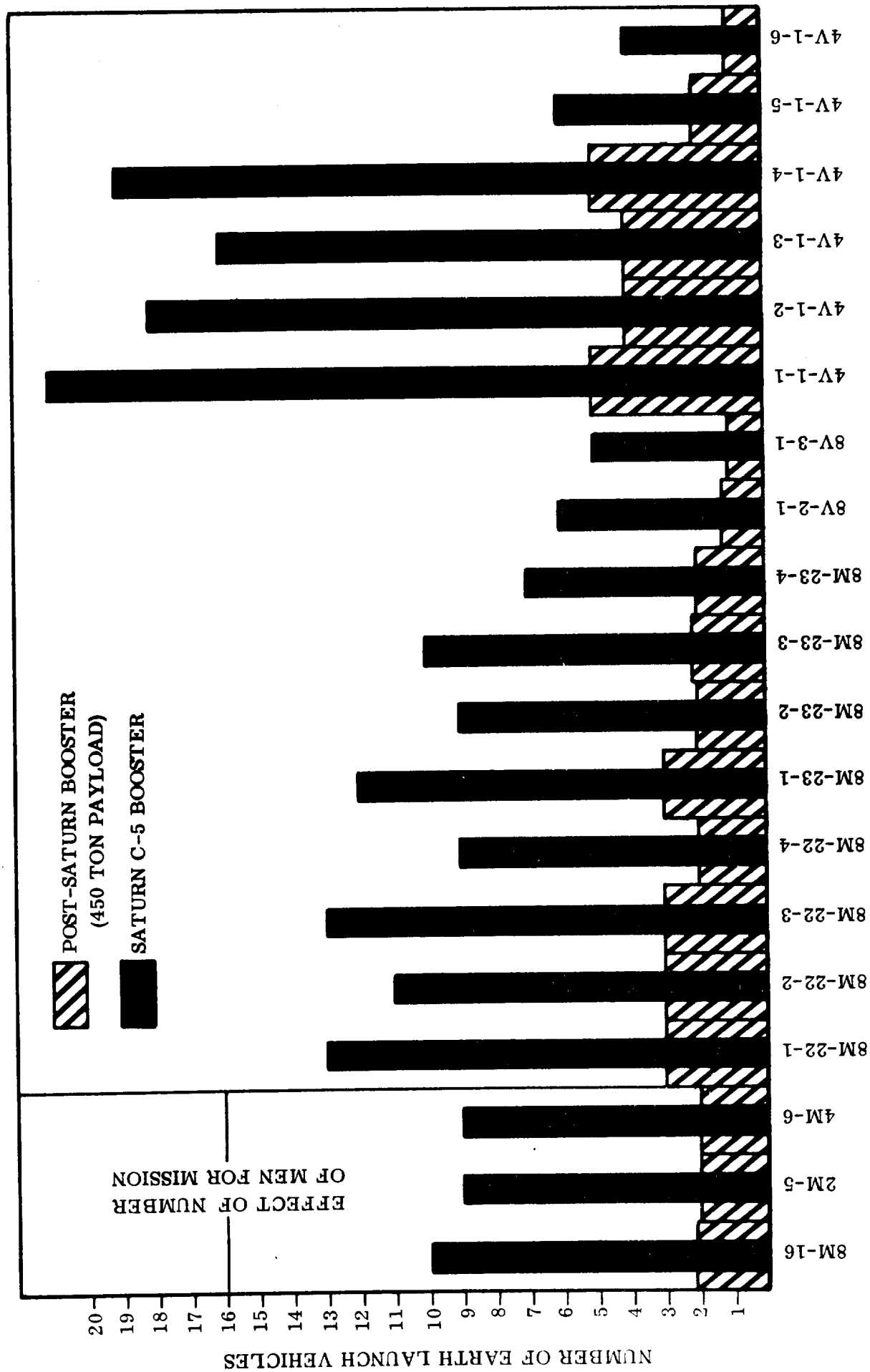

Figure 14-2. Comparison of Launch Vehicle Requirements

14.2 ORBITAL PRE-DEPARTURE OPERATIONS. The M-2, M-3, and M-4 payload is inserted into a 325 km earth orbit. After release by the earth launch vehicle and jettisoning of the aerodynamic fairings, the M-4 section and the spine must be released from the M-3 section, inverted, and reassembled with the spine fixed to the M-3 section. The M-1 payload is inserted into a lower parking orbit where, at the proper time, an auxiliary propulsion unit on the payload can inject it into the assembly orbit and assist in the rendezvous with the M-2 section.

The manned re-entry capsule is launched into the assembly orbit by a Saturn vehicle, and mated with the M-4 section of the interplanetary vehicle. Placed there prior to the arrival of the M-1 section, man will be available to monitor the rendezvous operations. A complete inspection, as well as functional checks, will be made on the vehicle after the assembly operations are completed. Man, with the use of the space taxi capsules, will perform these functions and conduct the final countdown checkout. Strategic emplacement of TV cameras and earth tracking stations will aid in the orbital pre-departure operations and act as a back-up system for the space crew. Prior to orbital launch, a Saturn C-5 tanker replenishes propellants and ecological supplies used during orbital operations.

SECTION 15

SPACE MATING

15.1 INTRODUCTION. For future spaceship operations, there exists a requirement for a positive joining system for mating large heavy bodies. The system must satisfy mating requirements for bodies with weights ranging from several hundred to about a million pounds. Reliability of the interplanetary mission depends upon the capability of propellant tank exchange enroute. Such tanks for the Mars capture maneuver weigh approximately 150,000 lb.

Space mating in the vicinity of Earth is somewhat more complicated than that during interplanetary flight for two reasons: one, the weights and sizes of the mating bodies are, in general, larger; second, the two bodies tend to be disturbed by the Earth's attraction since they are in different orbits. If the bodies are side by side they collide at their nodal points approximately every 45 minutes unless held separated by rocket thrust. If the orbits are in the same plane but one above the other, then they have different orbital velocities. However, if mating time is relatively short, say within a half hour for final joining, then it makes little difference whether it is orbital or interplanetary mating.

This section will deal with the operations performed between a rendezvous separation of 160 feet and the final mating of the two bodies.

The classical method with small light weight, rugged bodies is to utilize small rockets to bring the two vehicles together. Then by clamping or other attachment methods, the two bodies are joined. The difference between the joining of these small bodies and that of large heavy structures is the impact energy. The larger heavy bodies have disproportionately lighter structure which calls for closely controlled precision contact and great positive joining force for final connection. The joining force must be adequate to provide sufficient pressure at the contact areas for a suitable time period until latching takes place.

With man aboard the spaceship, his services and resources should be utilized, especially since he has decision-making ability during inspection periods and in cases of failure. Since small interconvoy taxis are also available for inspection and transportation during the interplanetary mission, they also should be utilized. They can serve as space tugs during mating operations. By attaching the tugs to the pursuit body, their attitude control and propulsion systems could be utilized and it would be unnecessary to duplicate this equipment on the pursuit body. The space tugs could provide a couple of hundred pounds of thrust for maneuvering purposes, for rectilinear translation, and for rotation and roll control, but final contact pressure would be grossly inadequate. During the pre-contact period, special docking devices must be in operation to provide range,

velocity, and rate vector information. Even so, at final contact, the bodies may impact at an intolerable velocity, producing devastating damage to both bodies.

To overcome the inadequacies of the reaction propulsion operation, and to provide added versatility, cable and winch systems are provided as part of the tugs. Thus, by reaction thrust tending to separate the mating bodies and the cable winching the two together, a very accurately controlled contact rate and velocity can be obtained. Range may be measured by cable length.

15.2 SYSTEM OPERATION. When the pursuit body approaches within 200 feet of the spaceship, the two space tugs, with cables attached to appropriate fittings at the mating site, travel to the pursuit body. They attach themselves to it by means of latches to special lugs designed for the purpose. After attachment, the reaction jets on the tugs position the body for pull-in. When the bodies are aligned and the cables taut, the winches pull, imparting acceleration and velocity to the bodies (toward each other). Each body accelerates proportional to its mass. When the bodies are accelerated to a reasonable velocity, the winches stop pulling and the two bodies drift slowly toward each other. Attitude control units maintain orientation during this coast period. The slack cables are wound on the winch drums at the same rate the two bodies are converging.

When the bodies are a short distance apart, the tugs fire their retardation rockets and the pursuit body slows to a zero velocity relative to the spaceship. The winch cables become taut and attitude control rockets on the spaceship and on the tugs keep the bodies oriented. An alignment inspection is made at this point; then, with the reaction rockets operating, the winch reels in the cable until the vehicles contact. At this time the reaction rockets are shut-off. A final alignment check is made and then the winches cinch the pursuit body into its mating position where latches are engaged. After a final check, the tugs and cables are disengaged and the tugs return to their docks. Propellant drain lines, pressure lines, and electrical harnesses are connected by remote control, and the two bodies are mated.

The following description of a Maneuver 2 (Mars capture) propellant tank (from a service vehicle) being mated to the 8M-14 vehicle during its outbound journey to Mars is a typical example of space mating operations. (Figure 15-1 shows the pertinent information regarding the two body systems.)

The acceleration of the tank (a_t) is

$$a_t = \frac{2P}{M_t} = \frac{2 \times 1000}{4660} = 0.43 \text{ ft/sec}^2.$$

Tank velocity (v_t) at the end of one-second cable pull:

$$v_t = 0.43 \times (1) = 0.43 \text{ ft/sec}.$$

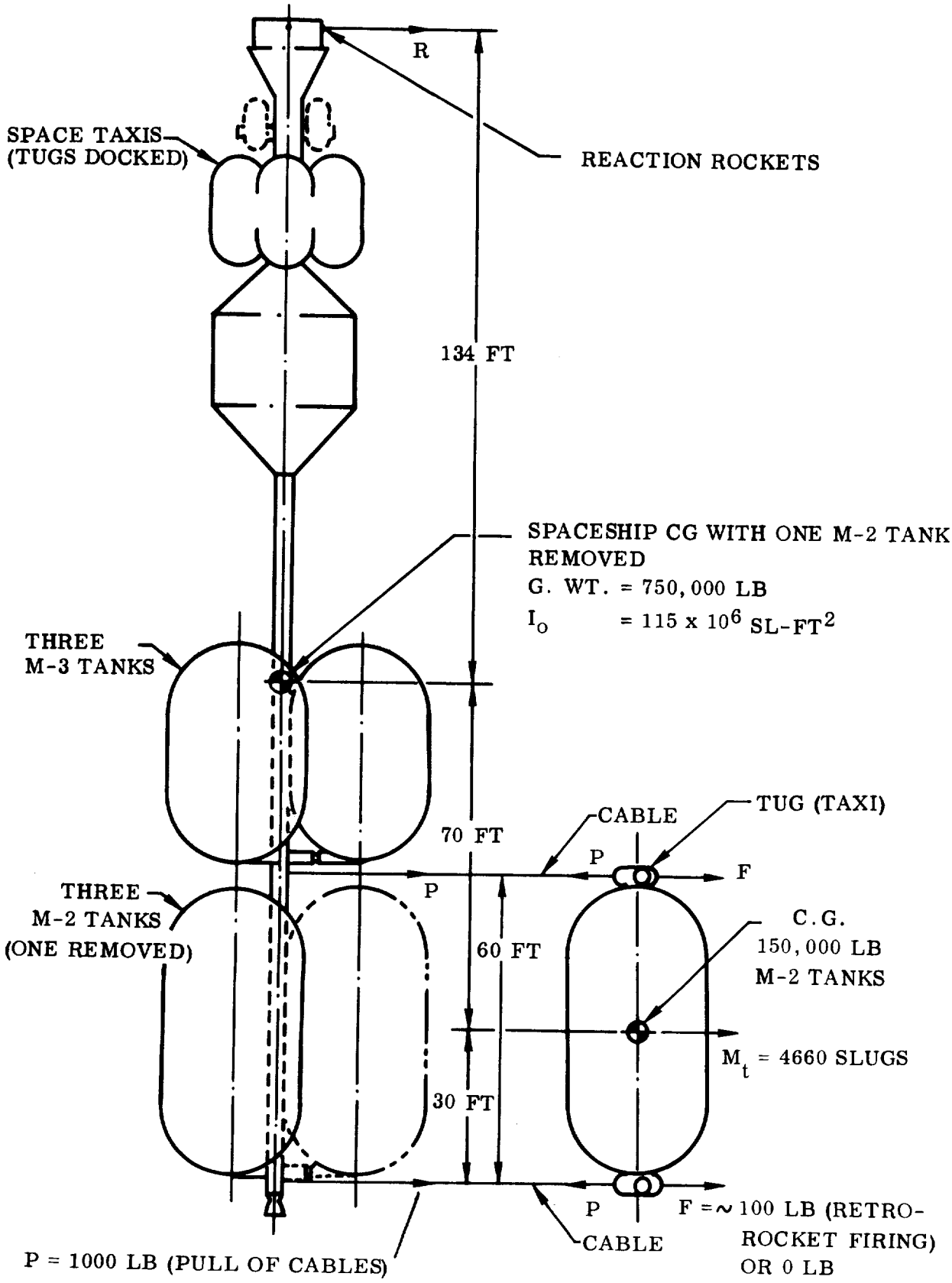

Figure 15-1. Mating M-2 Tank With 8M-14 Spaceship

Spaceship linear acceleration (a_s) resulting from cable reactions:

$$a_s = \frac{R + 2P}{M_s} \qquad R = 1.04P$$

$$= \frac{3.04 \times 1000}{23,300}$$

$$= 0.13 \text{ ft/sec}^2.$$

Spaceship velocity (v_s) at end of one-second pull:

$$v_s = 0.13 \times (1) = 0.13 \text{ ft/sec.}$$

Relative velocity (v_1) of tank and spaceship moving toward each other:

$$v_1 = v_t + v_s = 0.43 + 0.13 = 0.56 \text{ ft/sec.}$$

The relative distance (d_1) the two bodies move toward each other during the acceleration period is:

$$d_1 = \frac{1}{2} at^2 = \frac{1}{2} (0.43 + 0.13) (1)^2 = 0.28 \text{ ft.}$$

Time to reduce separation distance of bodies (measured to center lines of bodies: tank 30 ft dia., spaceship cradle 5 ft from center) from 160 to 40 ft:

$$t_2 = \frac{d}{v} = \frac{120}{0.56} = 214 \text{ sec (3.6 min)}$$

Braking rockets of F = 100 lbs each retard the tank's velocity to zero with respect to the spaceship. The tank's deceleration is:

$$a'_t = \frac{2F}{M}$$

$$= \frac{2 \times 100}{4660}$$

$$= 0.043 \text{ ft/sec}^2.$$

Time (t) to reduce relative velocity from 0.56 ft/sec to zero:

$$t = \frac{0.56}{0.043} = 13 \text{ sec.}$$

The distance traveled during retardation period is

$$d_3 = \frac{1}{2} a t^2 = \frac{1}{2} \times 0.043 (13)^2 = 3.62 \text{ ft.}$$

During the 120-ft reel-in period the cable has negligible tension. It is wound on the winch drum at a constant rate of a little over 1/2 ft/sec. At approximately 20 feet from contact, the tug's 100-lb retro-rockets keep firing until the cable becomes tensioned. Then the thrust is reduced to 25 percent of the retardation thrust level, providing just sufficient thrust to keep the cables taut and allow controlled motion by the winch.

At this time, the spaceship's rocket fires to counteract the rotational moment created by the tugs' cable pull of 25 pounds each. The spaceship's stabilizations system would respond with 26 pounds of retro-thrust acting on the opposite side of the C.G. from the cable pull but in the same direction. Thus, having all forces acting in the same direction the spaceship and tank would translate with an acceleration of $\frac{76}{900,000/32.2} = 0.0027$ ft/sec^2 in the direction of the cable pull.

Although the total forces acting to accelerate the spaceship are about 50 percent greater than those acting to accelerate the tank, the mass of the spaceship is about five times as great as the tank's. Therefore, even though the forces on the spaceship are acting to accelerate it toward the tank, the cable will remain taut during the pre-contact period with the entire system translating rectilinearly. During the 60-sec inspection and 122-sec pre-contact period, the velocity change imparted to the system is $\Delta v = 0.0027 \times 182 = 0.5$ ft/sec. The total side velocity imparted is 0.63 ft/sec.

At this point in the mating operation, an inspection is necessary to make sure the two bodies are in exact position for mating. Following the inspection period, with the rockets still firing, the winches slowly pull the two bodies toward contact. Just prior to contact the electric winches are reduced in speed so that the actual contact velocity is at an extremely slow rate (about 0.01 ft/sec). However, the average velocity for the last six feet may be 0.09 ft/sec.

At contact, all rocket motors cease firing. The tank is held against its cradle by the tensioned cables. After a contact position inspection, the winches tension their cables to seat the tank firmly into its final mated position. Latches are engaged; then the tugs can relieve their cable tension and disconnect themselves from the tank. The tugs having completed their task, return to their parking place near the manned modules. A typical example of the history of tank mating with a winch system is shown in Figure 15-2.

Electric and fuel line connections are mated automatically after the tank is latched into position.

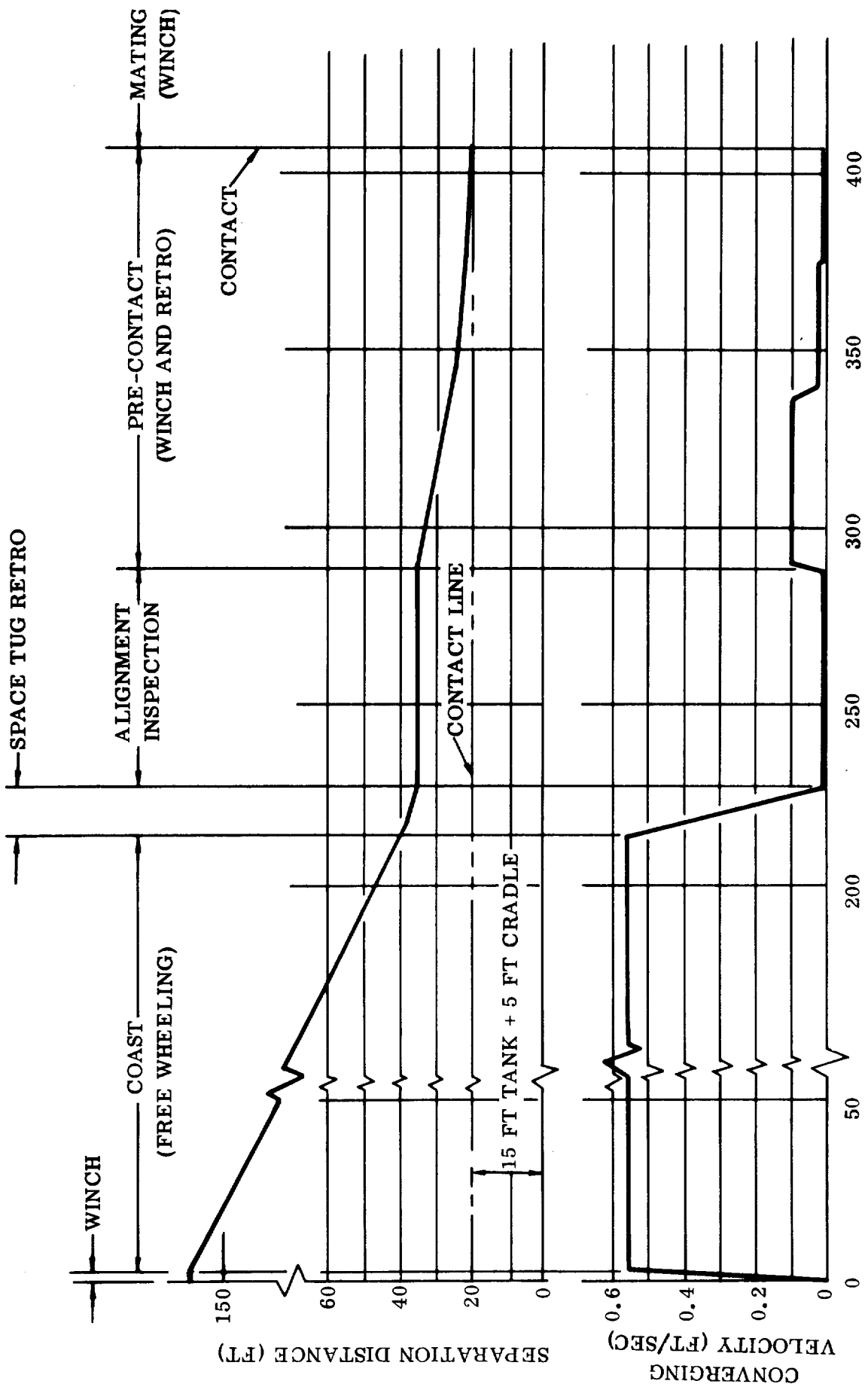

Figure 15-2. History of M-2 Tank Mating With 8M-14 Vehicle

The amount of propellant required to mate tank and spaceship, with

$$W_p = \frac{Ft}{I_{sp}} \text{ and } I_{sp} = 320 \text{ sec (storable) is shown in Table 15-1.}$$

Table 15-1. Propellant Weight Required for Mating

PERIOD	TUG (each) THRUST	TUG (each) TIME	TUG (each) W_p	SPACESHIP THRUST	SPACESHIP TIME	SPACESHIP W_p
Initial Velocity	———	winch	———	1040	1	3.2
Retardation	100	13	4.1	———	none	———
Inspection	25	60	4.7	26	60	4.9
Pre-contact	25	122	9.6	26	122	9.9
W_p Total (lb)			18.4			18.0

Total for 2 tugs and spacecraft = 55 lb.

NOTE: If approximately 50 % more propellant is added for inclusion of of lateral maneuvering and roll control during alignment periods, then the total propellant would be about 80 lb.

If a contra-rotating rocket were not employed to stabilize the spaceship, the vehicle would rotate. For example, as a result of the 1 sec. cable pull the vehicle would rotate with an angular acceleration of,

$$\dot{\omega} = \frac{T}{I_o} = \frac{140 \text{ P ft-lb}}{115 \times 10^6 \text{ sl-ft}^2}$$

$$= \frac{140 \times 1000}{115 \times 10^6}$$

$$= 0.00122 \text{ rad/sec}^2.$$

During the 214 sec required to travel the 120-ft distance, the spaceship would rotate about its own center of mass

$$\theta = \frac{1}{2} \dot{\omega} t^2 = \frac{1}{2} \times 0.00122 \ (214)^2$$

$$= 1600° = 4.5 \text{ revolutions}$$

which is an entirely acceptable situation since spaceship orientation would be lost and the connecting cables tangled.

15.3 RETRO-ROCKETS PLACED AT SPACESHIP CABLE CONNECTIONS. Instead of utilizing the spaceship's spin-up rockets for attitude stabilization during the tank mating maneuver, rockets could be placed at the cable connection points as part of the cable assembly. With these, sufficient reaction would be available to prevent rotation or translation of the spaceship. Their reaction thrust could be regulated by the tension of the cable. These rockets would provide the bulk of the reactive force, leaving lag errors and damping to the ship's attitude control system.

The advantage of this system is its elimination of rotation and linear motion of the spaceship. Its disadvantages lie in its complication to the tug's cable-and-winch system and in the weight of the added hardware. Also, additional propellant is required because this system always completely counteracts vehicle motion. Instead of 18 lb of propellant expended at the spaceship, the weight expended would be:

Initial velocity	(2) × 1000 lb for 1 sec	6.3 lb
Retardation	(no reaction at spaceship)	0
Inspection	(2) × 25 lb for 60 sec	9.4
Pre-contact	(2) × 25 lb for 122 sec	19.2
		34.9 lb

15.4 WINCH SYSTEM. The winch mechanism is located in the lower portion of the space taxis with the required cable stored on its drum. The winch turns freely during the reel-out period and has a friction brake capable of stopping the winch when the desired cable length has been dispensed. An electric motor with a gear system is engaged for tow-in of the cable.

The reel is about 12 inches in diameter and is constructed with a laminated fiberglass outer shell reinforced by a fiberglass core of approximately 8 lb/cu. ft. The winch drum is grooved and the system is provided with a lead block for self-winding capabilities. A summary of winch system characteristics is presented in Table 15-2.

Table 15-2. Winch and Cable System

Cable length	200 ft
Cable diameter	0.312 in.
Cable breaking strength (flexible 6 × 19)	9000 lb
Cable assembly	40 lb
Cable material	Steel
Drum diameter	12 in.
Drum length	12 in.
Electric motor power	1/8 HP
Reel-in velocity	0.01 to 3 ft/sec
Maximum run-out velocity	3.5 ft/sec
Maximum cable drag during run-out	1.5 lb
Braking time	2.9 sec
Braking load	390 lb
Total system weight	70 lb

SECTION 16

SEQUENCE OF EVENTS

The establishment of a "sequence of events" model is of fundamental importance for mission and operations analysis. To arrive at a complete model of a manned planetary roundtrip mission at this time is difficult because of the many alternatives which are still in the picture. As an initial step, a detailed sequence of events model has been set up for ground operations, earth departure, orbital predeparture operations, outgoing heliocentric transfer, planet arrival, and capture period. This is regarded as the first of a number of "sequence of events" models (Table 16-1).

Table 16-1. Sequence of Events Model No. 1

m = minute, H = hour, D = day, W = week, M = month, Y = year; c/o = checkout

OPERATION	TIME	CREW	MODE	TIME	PHASE	TIME	CUMUL. TIME FROM 1ST OPERA.	CUMUL. TIME FROM EARTH DEP.
1. Component Manuf. & Test	40W	Participates part time in test & assembly operations	Manufacturing	17M	GROUND			
2. Subsystem Ass'y & c/o Auxil. Vehicle Ass'y & C/O	28W							
3. Transport to Launch range	2W	--	Transport	0.5M	OPERATIONS			
4. Convoy Vehicle Stage Integration 5. LSS Modules & service modules integration	8W	Participates intimately in all ass'y operations & conducts integral systems test	Final Ass'y & Flight qual.	3M				
6. Complete convoy vehicle integral systems test	4W							
7. Disassembly into submits for orbit transport	2W	Crew devotes time for final mission preparations	Pre-launch	3M				
8. Standby (storage)	≤7W							
9. ELV Mating & Launch Qual Tst	2W					2Y	2Y	0

10. Transport to Launch Pad 11. Fueling, pressure & oper readiness of submit 12. Launch countdown	1W							
13. Ascent into parking orbit 14. Payload separ.	5m 1m	No participation	Ascent	6m	ORBITAL PREDEP OPERA			
15. Parking	1D	No participation	Coast	1D				
16. Transfer into Departure orbit	1.6H	No participation	Transfer	1.6H				
17. Rendezvous 18. Submit station keepg. 19. Docking, mating & checkout	1D 1D 3D	No participation No participation	Orbital Ass'y	5D				
20. Supplementary Logistics Support 21. Convoy Vehicle Coast 22. Crew joins convoy 23. Convoy Mission Readiness Test	2W $\lesssim$3M 1D 1W	No participation No participation Start of premission duty cycle Pre-Miss. duty cycle	Dep. Orbit Coast	$\lesssim$3M				
						100D	2.33Y	0

Table 16-1. Sequence of Events Model No. 1 (Continued)

m = minute, H = hour, D = day, W = week, M = month, Y = year; c/o = checkout

OPERATION	TIME	CREW	MODE	TIME	PHASE	TIME	CUMUL. TIME FROM 1ST OPERA.	CUMUL. TIME FROM EARTH DEP.
24. Convoy vehicles aligned. Crew veh leads 25. Final count-down	1.5H	Crew in Apollo Capsule in abort-ready state. GO/NO GO vehicle control	Orbital Pre-launch	1.5H	EARTH			
26. Convoy orbital launch	9m	" " " " "	Maneuver M-1	49m				
27. Escape Booster retro-jettisoning (attitude controlled)	10m	" " " " "			DEPARTURE			
28. Realignment relative to crew vehicle (acting as reference vehicle)	30m	Crew occupies command module for rad. belt transfer						
29. Convoy launch analysis	1H					41D	2.33Y	0
30. Convoy c/o (Service veh. by remote monitoring)	1D	Following Rad. Belt Crossing, crew occupies entire LSS						
31. Reference veh. navigating	2D	Weightless conditions continue throughout escape mode	Midcourse correction in hyperbolic orbit					

32. Convoy realigning (crew vehicle leads)	1D							4.1D
33. Jettisoning of abort fuel weight excess if any	1H	~0.4g environment established Routine operations by crew	First Coast	40D	OUTGOING HELIOCENTRIC TRANSFER			
34. Crew vehicle Spin up	1H							
35. Data Transmission to Earth	80D							
36. Vehicle c/o & maintenance								
37. Spin Down	1H							
38. Convoy correction	2m	Crew in LSS. Weightless condition exists	First Heliocentric. Correction	1.1D				
39. Correction Analysis	1H							
40. Reference vehicle indiv. vernier	1H							
41. Reference vehicle vernier analysis	1M							
42. Convoy alignment w/r to reference vehicle (convoy intercept)	1D							
43. Crew vehicle spin up	1H	0.4g environment restored	Second coast	110D				
44. Data trans. to earth	110D	Routine Crew operations						
45. Convoy veh c/o & Maint.								
46. Auxil veh. c/o & Read.								
47. Spin Down	1H							

Table 16-1. Sequence of Events Model No. 1 (Continued)

m = minute, H = hour, D = day, W = week, M = month, Y-= year; c/o = checkout

OPERATION	TIME	CREW	MODE	TIME	PHASE	TIME	CUMUL. TIME FROM 1ST OPERA.	CUMUL. TIME FROM EARTH DEP.
48. Convoy correction	2m	Crew in LSS						
49. Ref. vehicle correct on anal.	4D	Weightless Condition	Second Heliocentric					
50. Ref. vehicle vernier correction	1H			11D				
51. Ref. vehicle vernier correction analysis	6D							
52. Convoy realignment	1D		Correction Midcourse					
53.) As 43. 54.) 44. 55.) 45. 56.) 46.	70D	0.4g environment restored	Third Coast	70D				
57.) As in first & 58.) second helioc. 59.) correction 60.) 61.)	2D	Weightless Condition	Planet Homing	2D			3Y	238D
62. Excess weight) jettisoning)	0.5D	Weightless	Hyperbolic Arrival					
63. Convoy c/o)			Coast	3D				

64. Reference vehicle navigation 65. Convoy alignment	2D 0.5D				Planet Arrival	3.5D		
66. Convoy capture 67. Captive analysis 68. Ref veh cor. 69. Cor. analysis 70. Convoy align.	30m 1H 1M 6H 4H	Crew on stations	M-2 Maneuver	0.5D				241.5D
71. Boarding service vehicle 72. Deployment of Marens or Venens 73. Start mapping 74. Complete c/o & return readiness assurance test of vehicles to return to Earth. 75. Deploy 2 Landers & Floaters	1D 10D	Following c/o of Return vehicles crew is occupied with control of auxiliary vehicles, data handling & observations. Service vehicle which is aux. veh. carrier, will not spin. Crew vehicle will not spin, since it carries the Mapper if enough propellant is available to provide temporary relief to			C A P T U R E P E R I O D			
76. Determine landing site for first Returner 77. Decide on whether manned excursion positive or negative 78. Deploy first Returner (or MEV, w/o crew) 79. Deploy second returner (or MEV with crew)	10–30D		Planet Reconnaissance	20–40 D		20–50 D		263-293D

Table 16-1. Sequence of Events Model No. 1 (Continued)

m = minute, H = hour, D = day, W = week, M = month, Y = year; c/o = checkout

OPERATION	TIME	CREW	MODE	TIME	PHASE	TIME	CUMUL. TIME FROM 1ST OPERA.	CUMUL. TIME FROM EARTH DEP.
80. Deploy residual Landers 81. Recovery of Returners or MEV's 82. Deployment of Phopro and Deipro	10-30D	crew from prolonged weightlessness						
83. Recover Returns and/or MEV 84. Jettisoning of excess weight	2D							
85. Launch countdown 86. Departing convoy vehicles aligned Crew vehicle leads	1D							

The return flight is analogous to the outgoing flight. Prior to Earth capture maneuver, if there is a powered retro-maneuver, the entire LSS, except for this EEM is jettisoned. Crew stays in EEM from retro-maneuver to atmospheric entry and landing on Earth.

SECTION 17

EMERGENCY AND RESCUE

17.1 MALFUNCTIONS AND DAMAGE. At this point in time, space technology can hardly be expected to provide the confidence level required for a manned planetary capture mission. That the requirements for interplanetary flight can be met, however has been demonstrated in the case of the successful U.S. Venus probe and may be demonstrated again a few months from now with the USSR Mars probe. Although the convoy vehicles and their auxiliary vehicles, as well as the operational requirements of a manned capture mission, are much more complex, the presence of human intelligence and resourcefulness in the control circuit will contribute decisively to mission success, provided

a. such environmental conditions (physiologically as well as psychologically) are reliably furnished as needed to keep the crew in top condition throughout the mission

b. the vehicle design philosophy places a premium at permitting the crew a maximum degree of accessibility, parts exchangeability and override control within the technological system.

In other words, the crew must be able to rely confidently on two factors: Proper functioning of all the automatic control equipment on which they must rely during the execution of maneuvers; Proper monitoring and accessibility of all this equipment to crew members to assure that its proper functioning is assured during those critical periods in which the crew must rely on it rather than on their own sensory perceptions.

Often, actions or decisions depend vitally on correct appraisal of what happened and of the degree of damage or failure. A rapid and reliable failure diagnostic system is of vital importance. It will be tied into the data processing system.

If these requirements are met, then there are few components and subsystems which must have a degree of reliability normally associated with a nonmanned flight of same duration and complexity. The emphasis on reliability in most cases is rather determined by the need to keep monitoring and maintenance work commensurate with the size of the crew and a reasonable weight allowance for spares.

A significant exception are all nuclear components. Crew accessibility in a number of cases will not be possible (except under self-sacrificial conditions). The use of robots, remotely controlled from the command module is

seriously considered. A comprehensive nuclear engine malfunction analysis is presented in the Rocketdyne contribution in the classified Addendum to this report.

The first step in an analysis of emergencies is to survey the failures or malfunctions which could possibly occur, their relative importance and eventually their probability of occurrence as well as, where possible, the portion of the mission during which they are most likely to occur. Starting out with the principal subsystems of the overall convoy vehicle system, these subsystems are:

Propulsion System	Main propulsion
	Secondary propulsion (abort, attitude control, spin control, midcourse correction, LSS transfer propulsion system)
Navigation System	Optical trackers All-inertial guidance system Range and range rate measuring system Computer system Autopilot system
Communication System	Main communication and data transmission system Emergency communication system
Biotechnical System	Crew modules - Command module, Utility ("Spine") modules, Mission modules Earth entry module (EEM) Mars excursion vehicle (MEV) Ecological life support system Taxicapsules
Auxiliary (Electrical) Power System (APS)	Main supply systems (e.g. 1 or 2 SNAP-8 systems) Emergency supply systems (solar-Stirling engine system; O_2/H_2 powered Stirling engine system; possibly solar cell-battery combination for "last-ditch" defense against short-duration all-out power failures; it is up to the design to make this a near-impossibility)

Special Systems	Hydrogen liquefaction system Non-manned auxiliary vehicles Returner Lander Floater Marens/Venens Phopro; Deipro Convoy Companion (C^2) Data compaction and processing system

Emergencies can be divided into two categories: Emergencies which endanger crew survival (survival emergencies), and; Emergencies which endanger all or part of the mission objectives.

Disregarding presently the special systems, it can be stated that "complete destruction" (defined here as destruction beyond repairability with the resources available to the crew) of any of these systems with the exception of the communication system represents a survival emergency as far as the ship is concerned to which the crew is attached, and, in the case of the biotechnical system, even in a most general sense. Among the special systems, failure of the data processing system, if it involves complete destruction of the failure diagnostic system, may be regarded as a survival emergency in the sense, at least, that it would force the crew to change ships. Destruction of the data processing system would be a comparatively lesser emergency if it involves loss of some or even all the capability of handling the information influx from the auxiliary vehicles during capture. However, complete destruction would require an explosion, a collision with a major meteor, or similar improbable occurrences. Outright destruction of the biotechnical system would involve death of the crew. On the other hand, destruction of the electronic communication system may not mean more than an inconvenience for several reasons. First, manned spacecraft will be equipped with a complete spaceborne navigation system so that communication with Earth for velocity and distance measurement will not be required primarily. Second, it is a simple matter, and involves little weight, to carry an extra transmitter for speech or even only Morse signal transmission to Earth. Finally, the crew can make use of sunlight to transmit light flashes notifying the Earth of the nature and extent of their emergency. For this purpose a planar reflector, or a set of two such reflectors can be used, depending on whether Earth, as seen from the space ship, is in conjunction with, or opposition to, the Sun. A 3-ft planar reflector transmits from lunar distance flashes which can be seen with the unarmed eye and therefore are distinctly visible by optical tracking. Over a distance of the order of 1 to 1.5 astronomical units a reflector diameter of the order of 100 to 150 ft can be picked up as a star of less than 10th magnitude. By oscillating the reflector, Morse signals can be flashed. In order to assure reception of such signals at all times, unhindered by clouds or by daylight, optical tracking must be carried out by properly equipped satellites, attitude-controlled and directed from the

surface to keep the proper section of the sky under observation. These reflectors can be light compared to their size, consisting of a silver- or aluminum-coated polyethylene foil which is kept in tension by an inflated circular tube. However, the 150-ft diameter version would probably weigh around 500 lb. This is many times the weight of an emergency transmitter, including battery power.

Failures in the life support system can be tolerated for a limited period of time. Although long-term conditions in the cabin, such as temperature, humidity, oxygen content, and carbon dioxide content must be balanced carefully for minimum physiological stress, the human organism nevertheless can stand considerable deviations from these conditions for a limited period of time, except for the cabin pressure proper. During this time period the cause of failure must be removed. If this is not possible, the crew will die unless a secondary life support system is available.

This leaves as the key subsystems, as far as flight safety is concerned, the navigation system, the auxiliary power system, and the propulsion system. Of these, only the auxiliary power system can effectively be hardened against failure, because in contrast to the other two systems, auxiliary power sources can be decentralized for the various subsystems which they supply so that failure in one power source does not paralyze all subsystems. In addition to this, a separate emergency auxiliary power system should be provided for the life support system and one central emergency power system which is cut in automatically as soon as one of the power sources for the other subsystems fails. The emergency power systems must be simple and reliable, such as solar cells or batteries or a Stirling engine system.

Navigation system and propulsion system cannot be decentralized. The navigation system consists essentially of optical equipment (Sun and star seekers), stellar map matching equipment, attitude control, autopilot and all-inertial guidance including the on-board computer. If any one of these components fails, the navigation system cannot function. Although loss of the ability to navigate is serious, it can be tolerated temporarily, if the failure can be eliminated. If this is not possible, it becomes necessary to rely on the Earth through the communication link which, in replacing the navigation system, becomes now an equally important key subsystem. Alternately, a complete secondary navigation system must be provided. The same applies to the main propulsion system, only to a higher degree, since there is no other subsystem which can take over on an emergency basis. It is of crucial importance to design utmost simplicity and reliability into the propulsion system. Aside from this, added safety can be provided only by a secondary propulsion system.

The possibility of small failures or accidents in a manned spacecraft is virtually limitless. In many cases the crew members can cope with the resulting situation more or less in routine fashion, since they will most likely have

undergone thorough terrestrial and orbital flight training. Selecting the more critical irregularities, one can, without entering into a mass of specific details, define a number of areas of principal emergency situations in which deep-space vehicles may be involved. These are summarized in Table 17-1. Here the term "secondary vehicle" refers to the service vehicle which would be used by the crew as "back-up" crew vehicle and to which the crew vehicle LSS would be transferred if necessary (cf. Sect. 9).

In Table 17-1, the first 15 cases deal with situations which can be handled by the crew. In 7 of these, namely, 1, 4, 5, 7(b), 10(a) and 10(b), 13(a) and 13(c), and 14, it appears outright necessary to use the secondary vehicle as an independent spacecraft. In 3 cases, namely, 2, 7(a), 13(b), this is a conditional necessity. In most other cases, certain subsystems of the secondary vehicle are utilized. Table 17-1, therefore, indicates a strong need for a secondary vehicle. The last 5 cases in the table deal with the next higher (hence, less probable) state of emergency in which the secondary vehicle is of no help. The most extreme case is of course the explosive destruction of the life support system (from the inside, or by a meteor impact), which will cause instantaneous death of the crew (case No. 16). Explosion of propellant or working fluid is extremely unlikely, since it could hardly be caused by anything but a major meteor impact. If such violent destruction of the tanks occurs, its effect on the life support system and the crew will depend largely upon the space ship configuration. In a chemical spacecraft the life support system is usually anticipated to be close to the propellant tanks. In this case violent destruction of the tanks might destroy life support system and crew. If the life support system is separated from the tanks by a long boom or an even longer towing cable, it may not be at all affected. The last three cases, Nos. 18 to 20, deal with cases which would render the crew helpless, but permit the possibility of help from the Earth.

17.2 EMERGENCY AND RESCUE ORBITS. A discussion of these cases involves consideration of orbits and orbit changes the crew vehicle may negotiate.

The first three cases in Table 17-1 refer to Earth-Moon operations, i.e., to cases in which the vehicle has not yet attained hyperbolic velocity. If elliptic transfer orbits are used, there is no danger that the crew is lost to the Earth, and terrestrial rescue operations are always more readily possible than in interplanetary flight. Spaceborne action for a propulsion system failure, involving loss of maneuverability, depends very much on the type of propulsion system and configuration of the vehicle. For multistage vehicles, the last ("upper") stage is the logical secondary vehicle and if this fails, rescue operations from the Earth become necessary, unless either a separate emergency stage is designed into the vehicle or a sister ship is provided for emergencies. Protection against damage of the life support system (case 2, Table 17-1) depends on the design or number of

Table 17-1 Areas of Principal Emergencies in Deep-Space Vehicles

Flight Phase	No.	Failing Primary System	Effect	Action
Cislunar transfer	1	Propulsion system (P.S.)	Loss of maneuverability	Depends on type of vehicle used (cf. text) Rescue operations from Earth
	2	Life support system (L.S.S.)	Temporary (permanent) loss of inhabitability	Change to emergency L.S.S. or to secondary vehicle, either until damage can be repaired or for the rest of trip Control primary vehicle from secondary vehicle
	3	Auxiliary power system (A.P.S.) Navigation system (N.S.) or Communication system (C.S.)	Partial or total incapacitation	Use emergency equipment Continue mission
Earth escape	4	Propulsion system	Escape maneuver not successful or not desired	(*a*) If engine fails during acceleration period, immediate transfer to secondary vehicle and slow-down required to avoid radiation belt (*b*) If engine is damaged during hyperbolic coasting, transfer to secondary vehicle and slow-down required as soon as radiation conditions permit to enter either emergency return ellipse or emergency ellipse which keeps crew outside radiation belt (cf. Fig. 34.4 and text)
	5	Life support system	L.S.S. damaged or parts malfunctioning	Slow-down with reversed thrust into geocentric orbit outside radiation belt. Repair life support system. If possible, start again for target planet; otherwise return vehicle into low-altitude orbit
	6	A.P.S. or N.S. or C.S.	Partial or total incapacitation	Continue in hyperbolic orbit, if there is reasonable chance that equipment can be repaired. Meanwhile, use emergency equipment; otherwise discontinue escape and establish suitable geocentric orbit for replacement
Heliocentric transfer orbit to target planet or back to Earth	7	Propulsion system damaged	(*a*) Uncertain to function next capture maneuver (*b*) Certain not to function	Ready for abandoning primary vehicle in preparing capture maneuver. If P.S. does not function, change to secondary vehicle and carry out capture. If captured by target planet, stay time may be reduced as much as propulsive energy permits Use primary vehicle as long as possible. Abandon prior to entering emergency orbit to Earth
	8	Life support system damaged or malfunctioning	System must be abandoned	Use emergency system in secondary vehicle. Continue mission. Control primary vehicle from secondary vehicle, if possible
	9	A.P.S. or N.S. or C.S.	Partial or total incapacitation	Continue mission in primary vehicle, using emergency systems and secondary vehicle equipment
Capture target planet	10	Propulsion system	(*a*) Capture maneuver incomplete (*b*) Capture not successful	(*a*) If propulsion system unusable, stay in elongated orbit until departure with secondary vehicle into return orbit to Earth (*b*) Rapid transfer to secondary vehicle. Slow-down to elongated capture orbit. Determine best emergency orbit to Earth. Then escape for correct injection into the determined transfer orbit
	11	Life support system	System must be abandoned	Control primary vehicle from secondary vehicle Possibly shorten capture period for earlier return to Earth
	12	A.P.S. or N.S. or C.S.	Partial or total incapacitation	Like No. 9

Table 17-1 Areas of Principal Emergencies in Deep-Space Vehicles (cont'd)

Flight Phase	No.	Failing Primary System	Effect	Action
Capture Earth	13	Not enough propellant	(*a*) Capture not successful	(*a*) Ready for abandoning primary vehicle in preparing capture maneuver. Use primary vehicle as long as possible. Then rapid transfer to secondary vehicle for final maneuvering close to Earth
		For capture or engine failure during capture	(*b*) Propellant system uncertain to function	(*b*) Like No. 7(*a*)
			(*c*) Propellant system certain not to function	(*c*) Like No. 7(*b*)
	14	Life support system	Damage or breakdown of system	Abandon primary vehicle. Change to secondary vehicle for arrival maneuver
	15	A.P.S. or N.S. or C.S.	Partial or total incapacitation	Like No. 9
Anywhere	16	Life support system	Explosive destruction	Death of crew
	17	Propellant or working fluid tanks	Explosive destruction	Effect depends on vehicle configuration (cf. text)
Heliocentric transfer orbit to target planet	18	Systems incapacitation	Loss of primary and secondary maneuverability	Effect on crew depends on vehicle configuration (cf. text)
Satellite of target planet	19	Systems incapacitation	Inability to leave target planet	Extremely critical, but not necessarily fatal, depending on transfer orbit used (cf. text), provided life support system and communication with Earth remain intact
Approach to Earth	20	Systems incapacitation	Inability to enter capture maneuver	Extremely critical, but not necessarily fatal if Earth could be notified and has rescue vehicle standing by to intercept paralyzed spacecraft (cf. text)

gency orbit keeps the vehicle outside the radiation belt (Fig. 17-1). This orbit requires less energy. The impulse to raise the peri-apsis distance above the radiation belt is best given at the apo-apsis, as pointed out before. The resulting orbit requires expensive rescue operations from the Earth. The same two types of emergency orbits will have to be considered for cases Nos. 5 and 6 in the table.

In interplanetary space, the crew has three alternatives as far as orbit changes are concerned:

a. to cut the mission period short and return to Earth as quickly as possible, i.e. commensurate with the propulsive energy available,

b. to "sit out" a prolonged capture period and wait for pick-up from Earth during the next favorable constellation,

c. to enter a heliocentric emergency orbit and wait for pick-up from Earth.

Case (a) applies only to cases where the emergency occurs during the outgoing transfer or during the capture period.

If the emergency occurs during outgoing transfer, the least expensive way to proceed is to stay in the transfer orbit and change the mission from capture to fly-by. This is largely due to the rule that, if at all possible, maneuvers for changing the heliocentric orbital elements should be carried out during the hyperbolic encounter with a planet, rather than in heliocentric space. The larger the target planet's mass, the greater the energy saving.

Thus, if a need to cut the mission short becomes apparent while en route to Venus or Mars, the crew will not avoid the target planet, (provided, the mission period reduction so obtained is adequate but, to the contrary, it will attempt to approach the planet as closely as possible and at closest distance will carry out its heliocentric orbit change. It may, of course, not be possible to carry out all the required changes during the encounter. Then the higher energy requirements of heliocentric maneuvers must be accepted.

After these discussions, the maneuvers during capture by the target planet (Nos. 10 to 12 in table) and Nos. 13 to 15 are self-explanatory. It may be pointed out in view of the wide variety of transfer orbits possible (Figs. 17-2 and 17-3) that in case of trouble on the way to the target planet and perhaps even during the capture period, it may in some cases be advisable to hang on to the planet and wait for a rescue mission from Earth. Assume, for example, an expedition starts to Mars in transfer orbit 3 and reports severe failures en route, but retains ability of capture maneuver near Mars. If this occurs during the first one or two months of the trip and if a stand-by system is maintained on Earth or in orbit, (herein lies the significance of a direct

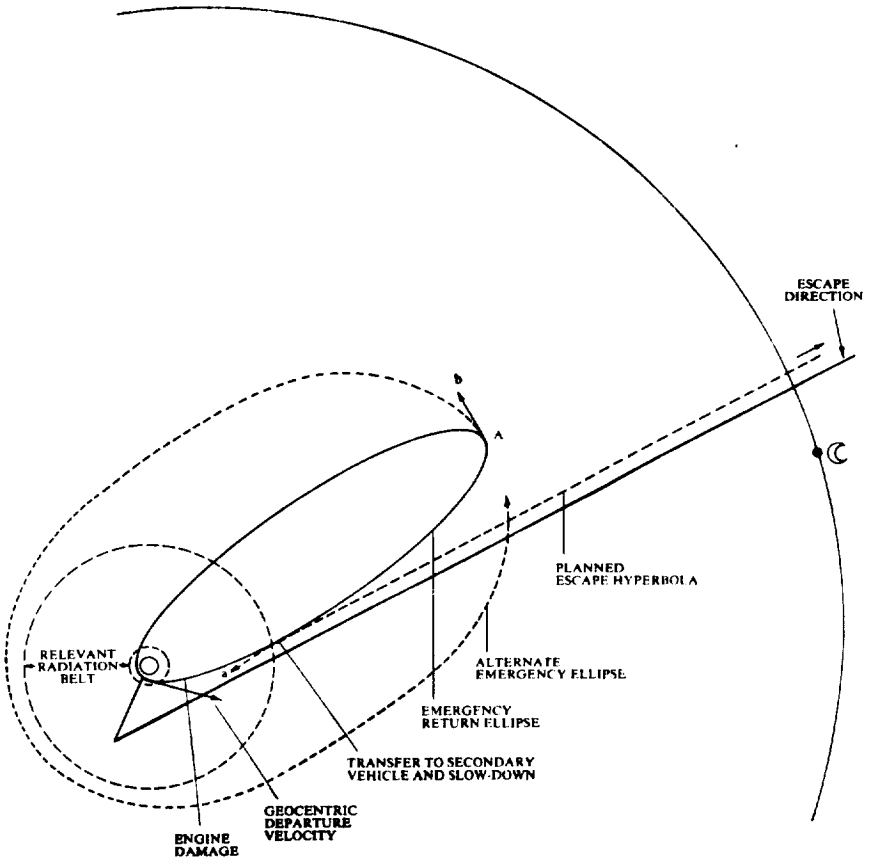

Fig. 17-1 Emergency Orbit during Earth Escape

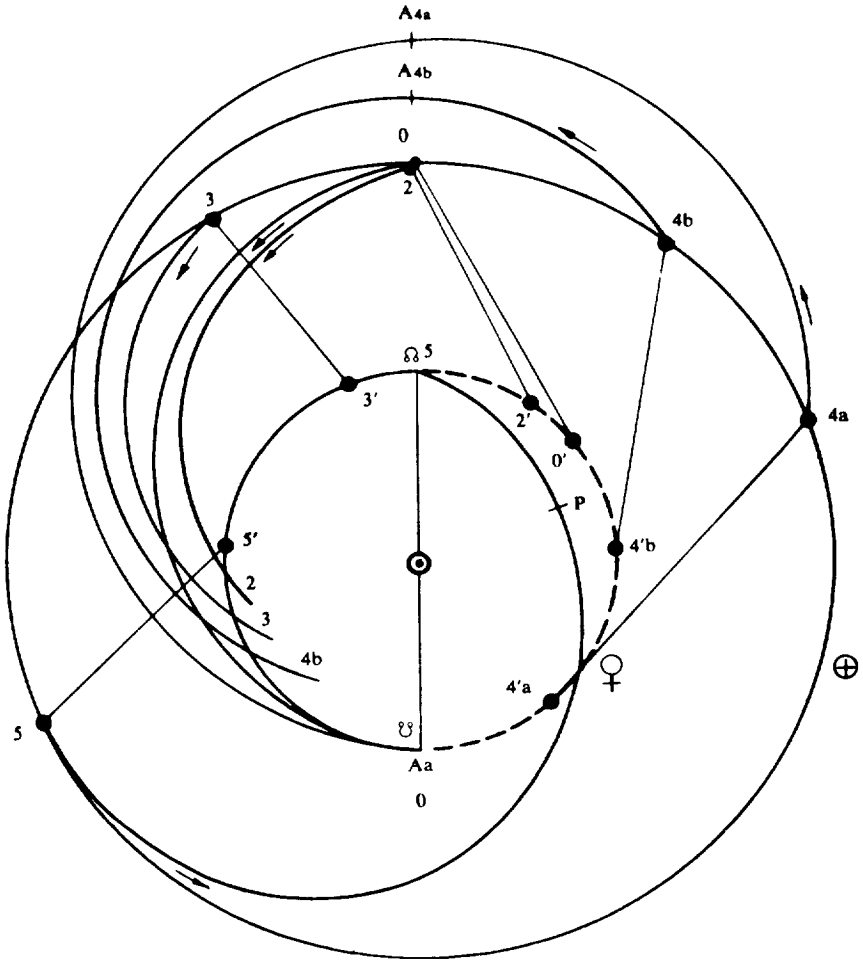

Fig. 17-2 Earth-Venus Transfer Orbit Alternatives for Emergencies during Outgoing Transfer or for Earth-Based Rescue Operations.

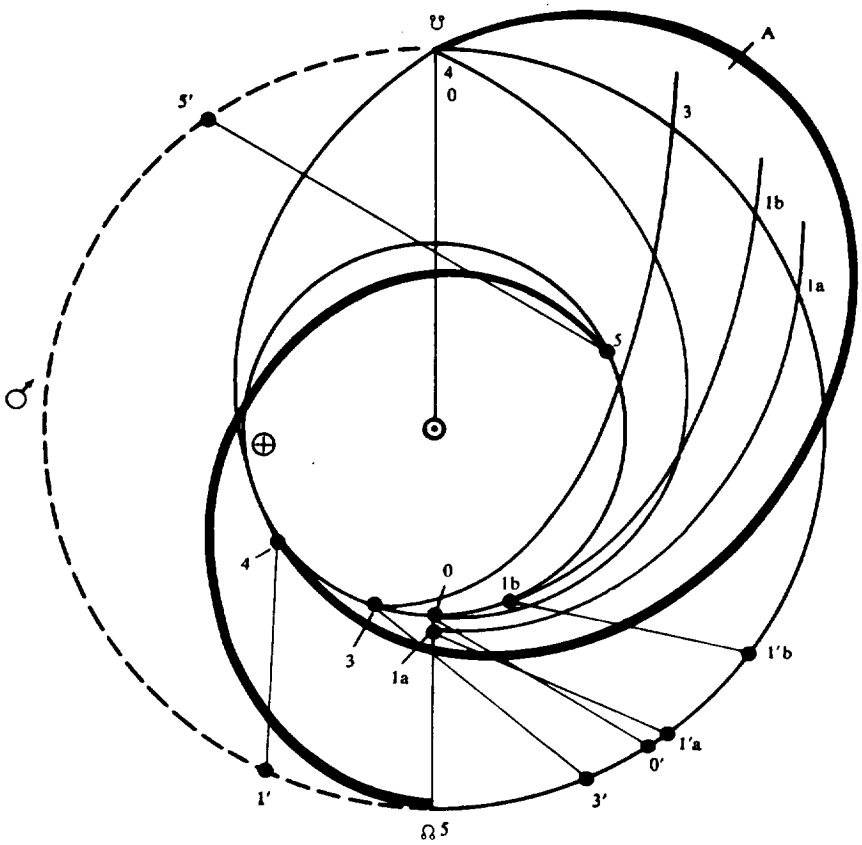

Fig. 17-3 Earth-Mars Transfer Orbit Alternatives for Emergencies during Outgoing Transfer or for Earth-Based Rescue Operations.

vehicles involved. An emergency life support system exists in the EEM of the crew ship or the spare Earth Entry Modules carried by the service vehicles. They do not carry a complete secondary LSS for reasons discussed in Sect. 9. The use of small survival capsules for individual crew members may be advantageous in cases where single vehicles are used, if the vehicle stays within the Earth's gravitational field. If the crew must abandon ship, they may be rescued by an emergency vehicle from the Earth within practical stay times in the survival capsule. The most economic protection against failure in the auxiliary power system, navigation system, or communication system in cislunar operations are simple emergency systems. Communication with Earth requires little power and can, at little weight penalty, be amended by using reflected sunlight as discussed before. Visibility from the Earth can be ascertained by means of not too large silver-coated polyethylene balloons (50 to 100 ft diameter). Therefore, navigational aid from Earth can well be ascertained.

Conditions are greatly aggravated in interplanetary flight. Help from Earth, either navigationally or vehicularly, is much more difficult to arrange. A single chemical stage is inadequate because of the energy requirements likely to be involved in heliocentric maneuvering. Simple survival capsules are useless and would only prolong the agony of hopelessness, because of the distances and flight times involved. Thus it is especially in interplanetary flight that secondary vehicles become necessary. Failure areas Nos. 4, 5, and 6 (Table 17-1) deal with the first orbital phase of interplanetary flight, namely, escape from the Earth's gravity field. For No. 4 two importantly different cases may arise. If the propulsion fails during acceleration into the hyperbolic escape path, then the failure occurs while the vehicle is still in the immediate vicinity of the Earth. At this moment the exact elliptic orbit will not be known right away and may involve longer stay time in the radiation belt, e.g. if the apo-apsis lies at, say, 8 or 10 Earth radii, than the crew can tolerate. Within a few minutes after premature propulsion cutoff (assumed to be given at about 180 km or 100 n. miles altitude), the vehicle will be several hundred miles out and rapidly enter the region of steeply increasing radiation intensity. To avoid this risk, the crew has little choice but to abandon the primary ship and slow themselves down in the abort module (EEM) as rapidly as possible. If, on the other hand, injection into the hyperbolic orbit is as planned and the propulsion system is damaged during the subsequent hyperbolic coast period (a much less likely case), then the crew may have to wait until the radiation belt is crossed before being able to transfer to the secondary vehicle (whether or not this is required depends on the arrangement of primary and secondary vehicle) (Fig. 17-1). As soon as possible (the sooner this is done, the less propellant it will cost), slow-down into a suitable elliptic orbit must be effected. A suitable orbit is one whose apo-apsis lies in cislunar space (this side of the Moon), 30 to 40 Earth radii away (if at that distance the radiation level is down to tolerable values). While the vehicle coasts through the apo-apsis, an exact orbit determination can be made, terrestrial emergency stand-by measures arranged, and path corrections be made, if necessary, to assure correct peri-apsis location between radiation belt and atmosphere where the return maneuver into a low-altitude satellite orbit can be effected. An alternate emer-

Earth-to-planet flight capability, so that time-consuming orbital operations can be avoided) then it would still be time for the rescue vehicle to transfer to Mars along orbit 1b and arrive before the crew in the damaged vehicle. If it is too late for this maneuver, a rescue operation along an orbit of the type 5 (without or with canting (the latter case is faster)) can be attempted. These possibilities are, of course, particularly valuable in emergency cases such as Nos. 18 to 20, involving the system's incapacitation to the extent that neither primary nor secondary vehicle is maneuverable.

17.3 CONCLUSIONS. The preceding discussion leads to a number of conclusions, the most important of which are summarized here.

1. Crew must be thoroughly integrated into the systems design to provide it with a maximum of accessibility for monitoring, maintenance and repair. This requires above all an advanced intra-vehicle check-out system with comprehensive failure diagnostic capability.

2. Emphasis is, for safety reasons, on emergency systems (such as auxiliary power, communication, life support system) and on decentralization (auxiliary power systems).

3. This design philosophy and the ensuing weight increase represent a characteristic distinction from the missile where emphasis is on weight minimization and equipment concentration.

4. The indicated need for a secondary propulsion system, navigation system, and life support system, hence, also for a secondary auxiliary power system add up, in effect, to the requirement for a secondary vehicle.

5. In augmenting the vehicular capability of the expedition by the addition of one or more secondary vehicles the payload weight per person is raised considerably. However, if the secondary vehicles are used as service vehicles before the advent of an emergency, the provision of one or more secondary vehicles is as economical as possible under the circumstances. It also emphasizes the need for high-energy propulsion systems.

6. The purpose of the secondary vehicle is to retain maneuverability of the crew, so that emergency orbits can be entered and the flight continued on an austere basis if necessary, after emergency abandonment of the crew vehicle.

7. The energy requirement for interplanetary secondary vehicles can be reduced greatly if the change into a different heliocentric orbit is carried out during the hyperbolic encounter with a planet rather than in heliocentric space.

8. Even for interplanetary operations to Venus and Mars, rescue operations from the Earth are possible, using nuclear heated propulsion systems for the orbital stage and preferably launching this stage by means of a chemical booster from the Earth's surface. This would cut orbital preparations short. Thus, in the extreme case of systems incapacitation, all hope is not necessarily lost. Crews from Earth will have practical and powerful means to come to the aid of the crew in distress in the depth of space.

SECTION 18

PRINCIPAL DEVELOPMENT TASKS, SCHEDULES AND A PRELIMINARY COST ESTIMATE

The information presented in this section is based on the following ground rules:

a. Mars capture mission 1975-1.

b. Convoy vehicles are powered by nuclear engines (M-1 by a cluster, M-2 by a single 200 k engine, M-3 by an advanced NERVA); M-4 is powered by a high-pressure O_2/H_2 system.

c. The Apollo entry mode is used. Hence, there are no requirements or costs included for the development of hyperbolic atmospheric entry.

d. The OVAM mission mode is used; i.e., the convoy vehicles are mated and/or fueled in Earth orbit and made self-sufficient prior to departure.

e. The main development of the SNAP-8 power generation system will not be charged to EMPIRE.

f. The development of an advanced NERVA (taken here as meaning primarily higher I_{sp}) and of a 200-k engine and its cluster development will be charged to EMPIRE.

g. For the labor in orbit the following cost figure is adopted for the late 1960's and early 70's:

   Transport cost into orbit and return: \$100,000/man.
   Average stay of man in orbit: 30 days.
   Actual labor hours: $\sim$ 1/3 of stay $\approx$ 10 days $\approx$ 250 hours.
   Resulting labor cost: \$400/man-hour.

   Assume, admittedly with some arbitrariness, that an average of one metric ton (2,200 lb) of working equipment is associated with the man (transport cost \$660,000/lb). 1 man-year costs, therefore: \$100,000 × 12 = \$1.2 million plus equipment. The average number of men is put at 15. Hence, with equipment, this work force costs \$19 million/year in direct labor or, 8 men for 4 years: \$40 million per year.

The principal development tasks are listed in Table 18-1. The associated development periods are shown in Figure 18-1. The complete schedule is presented in Figure 18-2. Details are listed in Tables 18-2 through 18-12. Further explanations of a number of items listed in Table 18-2 as well as in Figure 18-3 are presented subsequently.

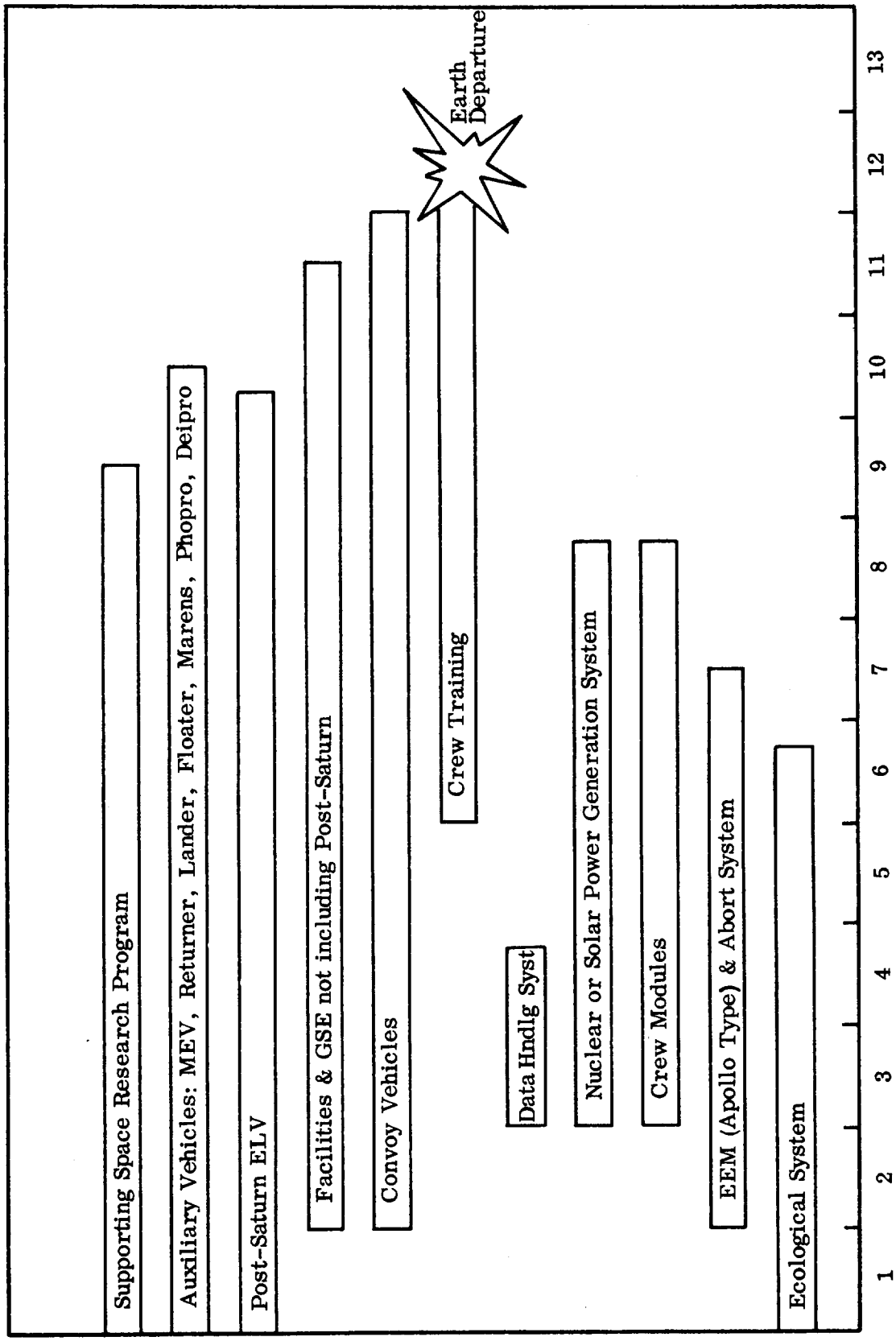

Figure 18-1. Development Periods for a Number of Principal Subsystems and Systems

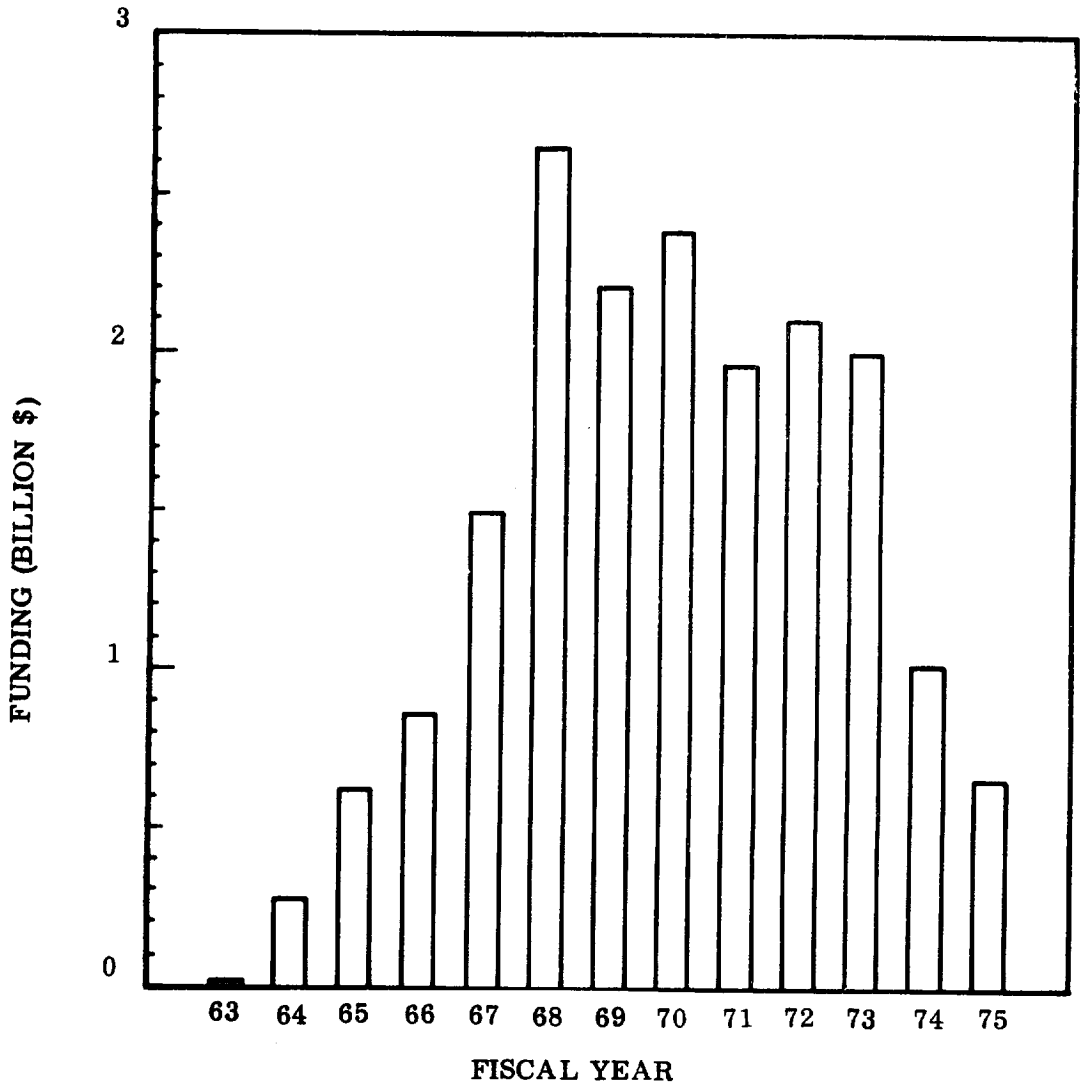

Figure 18-2. EMPIRE Program Funding Plan NO. 1

A preliminary cost breakdown of the EMPIRE Program is presented in Table 18-2 based on a capture Mission to Mars (Mission Profile 1975-1) using graphic reactor powered stages, except for M-4 which operates on O_2/H_2. Subsequently explanations are presented for the individual items.

Item	Explanations
1	Preliminary design and systems studies of principal vehicles, engines, ecological systems as well as mission modes and other key pace setters. Purpose of the preparatory studies is to provide basis for NASA evaluation and top level decisions.
2	Studies and basic research to provide the basis for full program go-ahead decision and numerous decisions in the course of the program development phase.
3	Development assumes a nominally non-organic system. Organic system development is back-up. Development is distributed over six fiscal years, FY 64 - 69. In the latter part of FY 69 and in the subsequent fiscal years, follow-on engineering and improvement funds are assumed to be spent.
4	Earth Entry Module and Abort System: Apollo entry conditions assumed. Hence most of development cost capsule is assumed to be carried by Apollo Program. Cost charged to EMPIRE Program consists of three major portions: (a) capsule modification for 8-man crew and integration into interplanetary ship; (b) addition of an abort propulsion system; (c) ground and flight testing of capsule and abort system. Development essentially completed through FY 69. Improvement and follow-on engineering funding allowed. Production figures include procurement and maintenance (primarily spares). Operation costs include the cost of Earth launch vehicles plus 10% for handling. After December 1969, operation costs pertain to handling and maintaining the EEM only. Launch costs are charged to the larger systems (e.g. Convoy vehicle sections) under development.

5 Crew modules are defined as consisting of command module, utility modules and mission modules. The command module is taken as containing everything including data processing equipment. The most expensive utility module installation, the ecological system, is not included in the utility module cost, but accounted for separately. The furnishings of the mission modules are comparatively inexpensive.

6 It is assumed that SNAP-8 will be developed under separate program, so that only modification, test and systems integration costs are incurred. Since the various power generation systems to be incorporated into crew and service vehicles have not been firmly selected a total of about 3% of the complete budget or $60 million has been summarily set aside for funding the electrical power generation systems development for Project EMPIRE and distributed over the relevant fiscal years consistent with the overall program objectives. A total of $110 million has been set aside for procurement and operation.

7 A total of $500 million has been set aside for the entire complex of data compaction, data storage, data display, data transmission system to Earth, guidance system, stellar navigation system and internal vehicle checkout and malfunction diagnosis system as well as for the associated instrumentation. Also included are the on-board tracking system (for meteorites and for auxiliary vehicles during capture), ship-to-ship and ship-to-taxi capsule communication. This includes development, production and operational costs.

8 Crew training involves complete training (except for the final flight tests in 1973) of three complete crews of eight men each. It is assumed that the direct expenses per man incurred to the Government are of the order of $100,000 per year in the average (including travel cost, per diem, moving of families, university courses, outfitting with pressure suits, etc.). This amounts to about $17 million for the entire period, taken as seven years. In addition there is the special training for the mission proper, involving facilities, instructors and equipment, including orbit training. This is funded with $5 million average amount per crew per year for four years. In addition, 12 persons (1.5 crews) will participate in the training during the December 1973 to July 1964 period. A total of $10 million is charged to this period as directly crew related expenses (e.g. transportation to and from orbit, etc.).

9.1 A high-pressure O_2/H_2 thrust system is assumed at 50K thrust which can be throttled to about 18K. Based on an evaluation of engine manufacturers' data and on the development costs of the Centaur engine (RL-10) and the Saturn C-1/S-II engine (J-2), a first unit cost of $15 per lb F (thrust) has been adopted, a cost of $5 per lb F for the first 15 units and a development cost of $100 million through Qualification Testing.

9.2 The structure includes thrust frame, tanks, insulation and meteoric protection, attitude control and the boom ("neck") connecting the propulsion unit proper with the LSS during return flight. Although propulsion is chemical, the neck is needed during earlier periods of nuclear propulsion and is retained during return transfer to keep the distance between c.g. and LSS large enough so that acceptable artificial gravity conditions can be generated by slow tumbling. The development program includes all ground testing, i.e., static component testing, vibration testing, environmental testing (vacuum chamber operation of valves, meteoroid jettisoning mechanism and other functions), as well as test articles for static firing, transportation and assembly tests of the entire convoy vehicle.

The flight test program includes the hardware for the orbital flights indicated in the schedule chart in the lines headed M-4, M-3, M-2, M-1 as well as spares, Earth launch vehicles (ELV), and labor (orbital and ground). The flight test program cost is broken down in Table 18-8.

9.3 The M-3 propulsion section is treated in the same manner as the M-2 section. The development schedule suggested is compatible with Aerojet estimates for the development of a second generation NERVA engine (classified). The production and operational figures of the M-3 program are included in the flight test program figures, since practically all M-3 hardware produced,outside of ground test requirements, serves the flight test program. Mission flight hardware is not included in the flight test program figures.

9.4 M-2 is treated according to the ground rules outlined for M-3. The development schedule for this propulsion section assumes a development schedule for the 200 k engine which is 2 years longer than the schedule suggested by Rocketdyne in the classified addendum of this report. The engine development cost is estimated in relation to the expected NERVA development cost (about $1 Billion) and the experience

gained in its development, which should be applicable to a large degree. For the breakdown of the light test program costs cf. Table 18-8.

9.5 M-1 is treated according to the ground rules outlined for M-3. The development schedule again is based on an engine cluster development which is about two years longer than the one suggested by Rocketdyne. It is assumed that no ground firing tests will be made with the engine cluster due to the great influence of the environment (air versus vacuum) on the operation and controllability of the cluster. Therefore, the cluster development will consist of proper shielding and control modifications of the 200 k single engine system, cold flow tests and vibration tests with the cluster. Hot runs will be made in orbit.

10.1 Tooling cost is based on an approximate value of 20 percent of the production cost. The production cost for a crew vehicle is almost a quarter-billion dollars. The cost of the auxiliary vehicles together is of the same order of magnitude (for a breakdown of these figures cf. Table 18-10). Therefore $0.1 B was allocated for tooling.

10.2 Launch facilities include the establishment of three launch sites and modification of Saturn C-1 and C-5 launch sites to accept large volume payloads.

10.3 Mississippi Test Site facilities include a Post-Saturn heavy tank test facility.

10.4 The Nevada Test Site figures assume that all 200 k engine test facilities are charged to the EMPIRE Program.

10.5 and 10.6 Assembly and checkout facilities must be established for the convoy vehicles as well as for the auxiliary vehicles. The facilities must be so located that C-5 as well as Post-Saturn launch complexes are readily accessible. They must be close to each other, since the auxiliary vehicles represent the payload of the service vehicle and must, therefore, be attached during a composite systems checkout to which each convoy vehicle is subjected before it is dissassembled into the sections which will separately be transported into orbit.

10.7 The orbital assembly and launch operation facility is envisioned first as an adjunct to the manned space station (Mod-1 through Mod-3) and later (beginning 1972) as connected with the convoy vehicle assembly operation exercises. Its purpose is to develop the orbital

technology of handling the large convoy vehicle sections in orbit, of fueling, exchanging parts and tanks etc; and, in this process, to develop a team of well-trained orbital engineers and technicians who will assist the mission crews in their orbital training and who will represent the U.S. orbital launch team which is responsible for handling, together with the mission crew, the pre-launch operations for the final mission in 1975.

Table 18-1. Principal Development Tasks

		FY	CY
1a	Preparatory Studies (Industry)	64, 65, 66	July 63 - Dec. 65
1b	NASA Centers: In-House Study and Industry Evaluation	63, 64	July 63 - June 64
1c	NASA HQ Evaluation and Key Decisions	63, 64	
2	Supporting Studies and Research	64 - 74	
3	Ecological System	64 - 69	July 63 - Feb. 68
	Systems evaluation	64 - 65	
	Prime system selection		July 65
	Design and manufacture	65 - 66	
	First system built for testing		Dec. 66
	Ground Testing and Test evaluation	66, 67	
	First system delivered for installation into EEM for ground testing		May 67
	First operational system delivered for installation into orbital Mod-1		Feb. 68
4	EEM (Apollo type) and Abort System	65 - 70	July 64 - Dec. 69
	Design		July 65
	Manufacturing		July 66
	Ground and Ballistic Tests		July 67
	PFRT engine system		Nov. 67
	Orbital and Entry Tests		Nov. 68/69
	System Operational		Dec. 69
5	Crew Modules	66 - 71	July 65 - March 71
	Design Mod-1		July 66
	Manufacturing Mod-1		Jan. - June 67
	Design Mod-2		July 67
	Ground testing Mod-1		Aug. 67 - July 68
	Manufacturing Mod-2		Jan. - June 68
	Ground Testing Mod-2		Aug. 68 - July 69
	Design Mod-3		67/68
	Mod-1 Orbital		Nov. 68

Crew Modules (Continued)

	Manufacturing Mod-3	68/69
	Ground Testing Mod-3	69
	Mod-2 Orbital	Nov. 69
	Mod-3 Orbital	July 70
	Crew Modules Operational	1st Quarter 71
6	Nuclear or Solar Power Generation System 65 - 71	July 64 - Dec. 70
	Design	64/65
	Component testing	65/66
	System Manufacturing	66
	Delivery of first unit for Mod-1 installation for ground testing	Jan. 67
	Independent systems testing	67
	Delivery of first operational unit for installation into orbital Mod-1	March 68
	Additional development effort (reliability, wt. reduction, etc.)	68, 69, 70
7	Data Handling System 65 - 67	July 64 - March 67
	Pre-Design	64/65
	Advanced Development	65/66
	Subsystems specification	Dec. 66
	Design	67
	Manufacturing	68/69
	Quality testing	70
	Delivery of flight articles for installation into Convoy vehicles and auxiliary vehicles	1st Quarter 67
8	Crew Training 69 - 75	July 68 - March 75
	Selection	July 68
	Basic Training	Oct. 68 - Jan. 71
	Flight Training	Feb. 71 - March 73
	Interplanetary Launch "Dress Rehearsal"	March/April 73
	Mission Simulation Flights	Nov. 73 - July 74
	Mission Departure	March 75

9	Convoy Vehicles	65 - 73	July 64 - June 74
9.1	M-4 Propulsion Unit	65 - 70	July 64 - Dec. 69
	PFRT		July 68
	Qual. Testing		July 69
9.2	M-4 Propulsion Structure	65 - 71	July 64 - July 71
	Orbit test of part of convoy structure attached to Mod-1		Nov. 68
	M-4 orbit flight tests (4)		June 69 - March 71
9.3	M-3 (Nuclear)	65 - 71	June 64 - June 72
	Pre-Design and Preliminary Studies		June 64 - June 66
	Design and prototype manufacturing		July 65 - June 67
	Structural testing and Systems testing		June 67 - April 68
	Nevada ground testing		May 68 - May 69
	Manufacturing of flight article		June 69 - July 70
	Final assembly and checkout		Aug. 70 - Dec. 70
	M-3 flight tests (2)		Feb. 71 - Nov. 71
	M-3 plus M-4 flight test (1)		March 72
9.4	M-2 (Nuclear)	65 - 73	June 64 - April 73
	Pre-Design and Preliminary Studies		June 64 - June 67
	Design and prototype manufacturing		July 66 - June 68
	Structural and systems testing		June 68 - March 69
	Nevada ground testing		April 69 - April 70
	Manufacturing of flight article		May 70 - April 71
	Final assembly and checkout		May 71 - Sept. 71
	M-2 flight tests (2)		Nov. 71 - June 72
	M-2 + M-3 + M-4 flight tests (2)		Nov. 72 - March 73
9.5	M-1 (Nuclear)	65 - 74	June 64 - June 74
	Pre-Design and Preliminary Studies		June 64
	Design and prototype manufacturing		
	Structural testing and systems testing		
	Manufacturing of flight article		
	Final assembly and checkout		
	M-1 flight tests (2)		
9.6	Convoy flight tests (2 or 3)	72 - 73	Nov. 73 - June 74

10	Facilities and GSE	63 - 74	June 63 - June 74
	Tooling		June 64 - Dec. 67
	ELV Launch and Checkout facilities		June 65 - March 69
	Nevada test site		June 64 - June 68
	Convoy Vehicle Assembly and C/O Facility (AMR)		June 66 - Dec. 68
	Auxiliary Vehicle Assembly and C/O Facility (AMR)		June 67 - Dec. 69
	Orbital Assembly and Launch Oper.		Jan. 69 - March 75
	World-Wide Tracking Net		June 66 - Dec. 68
	Deep Space Instrumentation Facility		July 68 - Dec. 72
11	Post Saturn	64 - 74	Jan. 63 - June 73
	Studies		Jan. 63 - June 65
	Full go-ahead		July 65
	Design completed		Dec. 66
	Component and subsystem development completed		June 68
	Battleship testing and captive firing		July 68 - Dec. 69
	Flight tests (5)		Jan. 70 - June 71
	Integration into EMPIRE Launch Progr.		Aug. 71
	Operational		Aug. 73
12	Mars Excursion Vehicle Returner Lander and Other Auxiliary Vehicles	64 - 73	Jan. 63 - June 73
	Studies		May 63 - Dec. 63
	Design		1964
	Prototype manufacturing		1965
	Ground testing		1966
	Flight article manufacturing		1966
	First Voyager launch		Spring 67
	MEV Sub-system testing and hot firing tests		July 67 - Dec. 68
	Second Voyager launch		Spring 69
	MEV Ballistic Tests		1968/69
	Third Voyager launch		Summer 71
	Manned lunar landing test flight with MEV, Returner, Lander		Nov. 72
	All auxiliary vehicles operational		June 1973

4-28 Hermann J. Schaefer and Abner Golden, Microphocal Alpha Irradiation as a Means of Simulating Exposure to Heavy Nuclei, J. Am. Med., Vol 27, p322, 1956.

4-29 T.C. Evans, The Effect of Small Daily Doses of Fast Neutrons on Mice, Radiology, Vol 50, p811, 1954.

4-30 H.J. Curtis, Some Specific Considerations of the Potential Hazard of Heavy Primary Cosmic Rays, Paper presented at joint ORNL and NASA MSC Symposium in Gatlinburg, Tennessee, 5-7 November 1962.

4-31 N.M. Kocharian, G.S. Saakian, and Z.A. Kirokosian, J. Exptl. Theoret. Phys. Vol 35, p933-942, USSR, 1959.

4-32 S.F. Singer, Cosmic Ray Effects at High Altitudes, J. Av. Med., Vol 27, p111, 1956.

4-33 B. Peters, Progress in Cosmic Ray Physics, Vol 1, p209, North-Holland Publiching Company, Amsterdam, 1957.

4-34 Preliminary Results from Explorer XII, NASA News Release No. 62-14, Washington, D.C., 19 January 1962.

4-35 B.J. O'Brien, J.A. Van Allen, C.D. Laughlin, and L.A. Frank, Absolute Electron Intensities in the Heart of the Earth's Outer Radiation Zone, J. Geophys. Res., Vol 67, pp397-403, 1962.

4-36 S.C. Freden, and R.S. White, Particle Fluxes in the Inner Radiation Belt, J. Geophys. Res., Vol 65, pp1377-1383, 1960.

4-37 F.L. Whipple, A Comet Model II, Ap. J., Vol 113, pp464-474, 1951.

4-38 I.S. Astapovich, New Material on the Fall of the Large Meteorite of 30 June 1908 in Central Siberia, Ap. J., Vol 10, No. 4, pp564-486, 1933.

4-39 V.G. Fesenkov, On the Cometary Nature of the Tunguska Meteorite, Ap. J., Vol 5, No. 4, pp441-600, 1962.

4-40 Nikolous B. Richter, Statistik und Physik der Kometen, Johann Ambrosius Barth/Verlag/Leipzig, p117, 1954.

4-41 J.G. Portor, Catalogue of Cometary Orbits Equinox 1950, Mem. Brit. Astron. Association, Vol 39, No. 3, June 1961.

4-42 Fred L. Whipple and Gerald S. Hawkins, Encyclopedia of Physics, Vol L11, "Meteors," Edited by S. Flugge, Springer-Verlag, Berlin, P554, 1959.

4-43 L.G. Jachia, Ap. J., Vol 121, p521, 1955.

4-44 Peter M. Millman, A Provisional List of Major Meteor Showers, Sky and Telescope, p96, January 1955.

4-45 John A. Wood, Stony Meteorite Orbits, M.N.R.A.S. Vol 122, pp79-88, 1961.

4-46 K.A. Ehricke, Space Flight, Vol I, D. Van Nostrand Company, New York.

5-1 Y. Mintz, Energy Budget and Atmospheric Circulation of A Synchronously Rotating Planet, Icarus, Vol 1, pp172-173, 1962.

5-2 C.H. Mayer et al, 3.15-cm Observations of Venus in 1961, Proc. XIth Internat. Astrophys, Colloquium, Liege, 1962.

5-3 F.D. Drake, 10-cm Observations of Venus in 1961, Publ. National Radio Astronom, Obs., Vol 1, p165, 1962.

5-4 W.K. Victor et al, Radar Exploration of Venus, Jet Propulsion Laboratory, Technical Report No. 32-132, Pasadena, 1961.

6-1 J.H. Lambert, Beitraege zum Gebrauch der Mathematik, Teil 3, 1772.

6-2 F.K. Gauss, Theoria Motus Corporum Coelestium, Article 88-94, C.H. Davis trans., Little, Brown, Boston.

6-3 J.V. Breakwell, R.W. Gillespie, and S.E. Ross, Researches in Interplanetary Transfer, ARS Journal, Vol 3, No. 2, February 1961.

6-4 K.A. Ehricke, Space Flight, Vol 2, "Dynamics", D. Van Nostrand Company, Princeton, N.J., 1962.

6-5 S. Ross, et al., A Study of Interplanetary Transportation Systems, First Report, Contract NAS8-2467, George C. Marshall Space Flight Center, Document No. 3-17-62-1, Lockheed Missiles and Space Company, Sunnyvale, Calif., 2 June 1962.

6-6 W.C. Riddell and R.E. Seiley, Interplanetary Flight Departure and Arrival Parameters, Vol I, Rep. No. AG1212, General Dynamics/Astronautics, 27 July 1962.

6-7 K.A. Ehricke, Mission Map Parameters: Hyperbolic Excess Velocity, Inclination, Path Angle, Perihelion Distance and Transfer Angle, Vol I, "Earth-Venus-Earth, 1972 to 1982", Contract NAS8-5026, NASA, George C. Marshall Space Flight Center, General Dynamics/Astronautics, Report AOK63-0004, January 1963.

6-8 K.A. Ehricke, Mission Map Parameters: Hyperbolic Excess Velocity, Inclination, Path Angle, Perihelion Distance and Transfer Angle, Vol II, "Earth-Mars-Earth, 1972 to 1982", Contract NAS8-5026, NASA, George C. Marshall Space Flight Center, General Dynamics/Astronautics, Report AOK63-0005, January 1963.

6-9 W.R. Fimple, Optimum Midcourse Plane Changes for Ballistic Interplanetary Trajectories, United Aircraft Corporation-Research Laboratories, Report A-110058-3, June 1962.

6-10 R.J. Trumpler, Observation of Mars at 1924, Lick Observatory Bull., Vol 13, pp19-45, 1924.

6-11 G. Houtgast, Indication of the Magnetic Field of the Planet Venus, Nature, Vol 175, pp678-79, 1955.

6-12 H.J. Gordon, A Study of Injection Guidance Accuracy as Applied to Lunar and Interplanetary Missions, Jet Propulsion Lab, Technical Report No. 32-90, May 1961.

6-13 R.M. Leger, Effects of Launching Time on Space Navigation Problems, General Dynamics/Astronautics, San Diego, California, presented at the Institute of Navigation Meeting, USAF Academy, Denver, Col., June 1960.

6-14 H.J. Gordon, A Study of Injection Guidance Accuracy as Applied to Lunar and Interplanetary Missions, Jet Propulsion Lab, Technical Report No. 32-90, 15 May 1961.

The following documents were also used as references for Section 6, although they are not specifically referred to in the text.

6-15 A.R.N. Noton, E. Cutting, and F.L. Barnes, Analysis of Radio-Command Mid-Course Guidance, Jet Propulsion Lab, Technical Report No. 32-28, 28 September 1960.

6-16 D.P. Harry, and A.L. Friedlaender, Exploratory Statistical Analysis of Planet Approach--Phase Guidance Schemes, Using Range, Range-Rate and Angular-Rate Measurements, NASA TND-268, March 1960.

6-17 P.J. de Fries, Analysis of Error Progression in Terminal Guidance for Lunar Landing, NASA TND-605, July 1961.

6-18 D.P. Harry, and A.L. Friedlaender, An Analysis of Errors and Requirements of an Optical Guidance Technique for Approaches to Atmospheric Entry with Interplanetary Vehicles, NASA TRR-102, 1961.

9-1 K.A. Ehricke, A Systems Analysis of Fast Manned Reconnaissance Flight to Venus and Mars, Part I, "Mission Philosophy, Life Support, Scientific Reconnaissance and Prototype Vehicle Layout," General Dynamics/Astronautics, Report AZM-072, March 1959.

9-2 H. Etherington, editor, Nuclear Engineering Handbook, p7-84, McGraw-Hill Book Company, New York, 1958.

9-3 A.B. Konecci, Manned Space Cabin Systems, Advances in Space Sciences, Academic Press, 1959.

10-1 Strategic Lunar System, Space Research Laboratories, Litton Industries, SR 192, AFBMDTR 60-16, February 1960.

10-2 M.G. Del Duca, F.D. Miraldi, and A.D. Babinsky, Oxygen Regeneration Systems for Manned Space Application, Thompson-Ramo Wooldridge Inc., WADD Technical Report 60-574, August 1960.

10-3 S.H. Dole and A.R. Thomplin, The Sabatier Reaction for Inorganic Recovery of Oxygen in Manned Space Capsules, Rand Corporation, WADD Technical Report 60-574, August 1961.

10-4 M.G. Del Duca, A.D. Babinsky, and F.D. Miraldi, Selected Methods for Atmosphere Control in Manned Space Flights, Thompson-Ramo Wooldridge Inc., 1961 SAE National Aeronautics Meeting, New York, New York, 352 C.

12-1 H.J. Shaefer, Dosimetry of Proton Radiation in Space, U.S. Naval School of Aviation Medicine, Pensacola, Florida, Report No. 19, June 1961.

12-2 R.K. Wilson, Shielding Problems for Manned Space Missions, GD/Fort Worth Nuclear Aerospace Research Facility, FZM-2721, 17 October 1962.

APPENDIX

DATA HANDLING SYSTEM

In view of the important role which data handling, data compaction, and data transmission play in the overall mission operation, a subcontract was let to IBM to conduct a preliminary investigation of the aspects and problems of data handling, data processing and storage weight as well as power forecasting within the frame of reference of the mission objectives and basic operational concepts as described in Section 5. Pertinent sections from the report documenting the results of this study are presented here in unabridged form, although some parts are repetitive with respect to Section 5 of this report. All figure and paragraph references within this Appendix refer to the Appendix itself and not to the basic report.

SECTION 3

Scientific Data Handling

This section discusses the scientific experiments to be performed during the EMPIRE mission. These experiments will be carried out by a number of auxiliary probe vehicles that will be deployed from the main convoy while it is in a capture mode around Mars. Estimates of the actual scientific measurements to be made, the sensors required for these measurements and expected data rates for each experiment are discussed in section 3.1. A discussion of various weight considerations for scientific data acquisition are presented in section 3.2. A discussion of data compaction as well as detailed descriptions of several possible data compactors is presented in section 3.3. Section 3.4 presents several alternate approaches to scientific data processing, storage, and transmission that might be adopted for the EMPIRE mission.

Major emphasis has been placed on the mapper auxiliary vehicle throughout this portion of the study. This is due to the fact that the mapper data represents a major percentage of the scientific data to be acquired.

3.1 Description of Sceintific Experiments

The following sections present a preliminary description of the scientific experiments to be performed by the various auxiliary vehicles. Estimated data rates for each of the experiments are also presented where sufficient information is available to define the experiment in detail. It is recognized that many of these experiments and their associated data rates will change drastically as the various auxiliary vehicle designs are more thoroughly investigated. However, the data presented in this section provide a base line for estimating the cost of the scientific data acquisition, processing, transmission, and storage systems. These costs are discussed in some detail in section 3.2.

Data for the measurement and sensor tabulations was derived primarily from Jet Propulsion Laboratory technical reports for the Ranger and Mariner spacecraft, and from the final report for task number 0850, IBM Independent Research and Development Program.

3.1.1 Mapper

3.1.1.1 Mission

The primary scientific mission of the mapper vehicle is the determination of planetary surface features in maximum possible detail. In particular, the mapper will establish the following planetological characteristics:

(1) Gross topology and surface inclination

(2) Surface topology with best possible resolution

(3) Surface infrared topology (low resolution)

(4) Surface ultraviolet topology (low resolution)

3.1.1.2 Data Acquisition

To accomplish the above objectives, the mapper vehicle will be equipped with the following:

(1) Visual mapping system

(2) Infrared mapping system

(3) Ultraviolet mapping system

(4) High accuracy time reference

The visual mapping and the associated time reference systems impose by far the most stringent requirement on the data transmission, processing, and storage systems and have therefore been analyzed in some detail. A summary of expected data rates from the mapper vehicle is presented in table 3.1.1. The assumptions used, and the analysis performed to determine visual mapping data rates, are discussed in section 3.1.1.4. Infrared and ultraviolet data rates were estimated from known data rates from the Tiros II weather satellite.

3.1.1.3 Visual Mapping System Data Rates

For analysis purposes, the following assumptions regarding the visual mapping system are made:

(1) Television image tube systems (i.e., vidicons, image orthicons, etc.) will be used for direct surface mapping of Mars. Systems involving electronic scanning of photographic film were not considered for this analysis since the storage of film in space environments as well as automatic dry processing of film are felt to be only marginally acceptable from a reliability viewpoint. It should be noted, however, that a system using photographic film provides greatly increased resolution capabilities and probably should not be ignored in future study of the mapping problem.

(2) Projected state-of-the-art advances in image tube systems will permit 2000 line scanning of a single image tube. Restrictions on tube face sizes and scan linearity of present day systems limit scan resolution to 400 to 600 lines across the viewing surface.

(3) The mapper vehicle will be placed in a circular polar orbit. Further study of non-polar, and/or non-circular orbits, would be necessary to determine data rates for other ephemerides.

(4) The mapper control system selected for analysis is one that provides for non-overlapped still "pictures" along the orbital track. This control system results in a strip of pictures one-half the planet circumference in length and of varying width for each full orbit of the mapper vehicle.

From the above assumptions, it can be shown that the mapper resolution is given by:

$$S = \frac{W}{K_S} \qquad (1)$$

Measurement	Sensor	Bits/Second
Visual Mapping	Television Image Tube System	8×10^5
Infrared Mapping	Infrared Radiometer	100
Ultraviolet Mapping	Ultraviolet Radiometer	100
Time Reference	Time Code Generator	17
Mapper Position	Convoy Tracking System	30

TABLE 3.1.1

MAPPER DATA ACQUISITION

Where S = Mapper resolution in meters

W = Width of strip "seen" by mapper in meters

K_S = Scan resolution = 2000 lines

It can also be shown that for complete (100%) mapping of the plantet, the mapper must "see" strip of width W at the equator where W is:

$$W = \frac{2\pi R_{OO}}{T} \times T_{sid} \tag{2}$$

R_{OO} = Circular radius of the planet

T = Total time available for mapping

T_{sid} = Siderial period of mapper

Mapper resolution at the equator is therefore:

$$S = \frac{2\pi R_{OO}}{T K_S} \times T_{sid} \tag{3}$$

$$S = \frac{2\pi R_{OO}}{T K_S} \times \sqrt{\frac{(R_{OO} + y)^3}{K}} \tag{4}$$

Where y = satellite altitude

K = the gravitational constant

Figure 3.1.2 shows mapper resolution as a function of radial distance $(R_{OO} + y)$ for various stay times T, with a scan resolution of 2000 lines. These curves indicate that for reasonable satellite altitudes (greater than 100 K_m), the best resolution possible is on the order of 25 meters for a stay time of 30 days. It should be emphasized that these curves are derived for a single image tube system and are computed based on 100% mapping of the planet. Better resolutions are, of course, possible if mapping of less than 100% of the planet surface is accepted, or if multiple image tube systems within one mapper vehicle are provided.

Returning to the assumptions regarding mapper control systems operation, it can be shown that the mapper data rate (B) is given by:

$$B = \frac{\text{Area of Planet}}{\text{Stay Time} \times S^2} \times \text{Gray Scale Coding}$$

$$B = \frac{4\pi (R_{OO})^2}{\text{Stay Time} \times S^2} \times B_O \qquad (6)$$

Where B_O = Gray Scale Coding

Data acqusition bit rate as a function of stay time for various resolutions with a Gray Scale Coding of 4 bits have been plotted for Mars in figure 3.1.3. These curves represent mapping of 100% of the planet surface area. Resolutions shown do not consider systems implementation. Achievement of these resolutions may require multiple image tube systems or mapping of less than the entire planet surface area.

3.1.1.4 Visual Mapping System Analysis

The mapper control system analyzed in the previous section was postulated as providing complete coverage of the planet with no overlap of pictures. To achieve non-overlapping pictures of the planet, the following major restrictions are placed on the mapper:

(1) The mapper must be placed in a circular polar orbit such that synchronism with the Mars day is achieved after a finite number of orbits.

(2) The field of view of the mapper must be chosen to coincide exactly with the synchronous period. For example, if an orbit is attained such that synchronism is achieved after 180 orbits, the mapper field of view must be 2 degrees.

(3) The mapper control system must automatically change the width of each picture as the vehicle changes latitudes.

If any or all of these criteria are not met, the mapper must produce redundant information. As an example of the amount of redundancy that may be produced, consider the requirement to change the frame width with latitude.

Postulating a control system that does not shrink the frame width but continuously maps a strip one half the planet circumference in length and a constant width W, it can be shown that if the mapper is in synchronous orbit and has an appropriate field of view, the total data acquired is:

$$D_1 = \pi R_{oo} \times 2\pi R_{oo} \times K_d \qquad (7)$$

Where D_1 = Total data acquired

K_d = Data bits per unit area

The useful data acquired by the mapper under these conditions is:

$$D_2 = 4\pi R_{oo}^2 \times K_d \tag{8}$$

The ratio of total data acquired to useful data is thus:

$$\frac{D_1}{D_2} = \frac{2\pi^2 R_{oo}^2 K_d}{4\pi R_{oo}^2 K_d} = \pi/2 \tag{9}$$

The redundancy introduced by this less sophisticated but more easily mechanized control system model is therefore $\pi/2$. This factor would effect all data rate, storage, and transmission curves presented throughout this report.

Similar comments may be made relative to the achievement of synchronous orbits and attitude stability. The study of such deviations, and the effect such deviations would have on overlap requirements and therefore on data rates, storage, and transmission is, however, beyond the scope of this report.

From the data presented in figures 3.1.2 and 3.1.3, a realistic estimate of mapper data rates can be established. Assuming a convoy stay time of 20 days and a minimum mapping resolution of 20 meters, with a gray scale coding of 4 bits, the mapper data rate is from figure 3.1.3 on the order of 8×10^5 bits per second. From figure 3.1.2 under these same conditions, it is obvious that the mapper must be provided with two image tube systems.

The selection of 20 day stay times, 20 meter resolution, and 4 bit gray coding, are quite consistent with the expressed mission objectives of the mapper. Therefore, a data rate of 8×10^5 bits per second will be used throughout this section as representative of the mapper visual data acquisition system.

3.1.2 Lander

3.1.2.1 Mission

The basic scientific mission of the Mars lander vehicle is the determination of biological and planetological characteristics of the planet. The Venus lander would have a similar mission, however, due to the expected hostile environment of the planet there exists some doubt as to the feasibility of such a mission. For this reason, only the Mars lander vehicle is considered here. The specific scientific objectives of the lander are to perform:

(1) Biological experiments to establish the existence of, and to define the chemistry and morphology of extra-terrestrial life.

(2) Detailed observations of the planet surface including:

(a) Organic soil analysis

(b) High resolution photography

(c) Soil microscopy

(d) Biochemical soil analysis

(e) Culture studies

(f) Ultraviolet surface examinations

(g) Planetary biological contamination studies

(h) Chemistry of planetary organisms

3.1.2.2 Data Acquisition

Many of the scientific experiments to be conducted by the lander vehicle require complex instrumentation to retrieve surface samples, prepare cultures and microscope sections, etc. Much of this instrumentation is yet to be developed and therefore no reliable estimates of data acquisition rates can be made. Moreover, some of this instrumentation will undoubtedly require two way transmission of information, control signals from the convoy to the lander, and data from the lander to the convoy.

As with the mapper satellite, however, it is expected that the major data transmission and storage requirements will be generated by the visual data acquired by a television camera system.

This system will be required to not only provide pictures of the Mars landscape in the near vicinity of the lander, but may also be used to aid the convoy crew in the remote control of lander mechanical devices such as core sampling drills, biological organism detectors, etc. A first approximation to the television system data rate can therefore be made on the assumption that:

(1) The television system will be used continuously while the lander is deployed on the surface of the planet. During times when the convoy is within transmission distance the television system will most likely be controlled by the convoy crew for

detailed tasks, and at all other times the system will be used for landscape viewing.

(2) The average frame rate of the television system will be of the order of one frame per second.

(3) The resolution requirements for the television system will be no greater than normal television (i.e., 500 lines).

Assuming a 4 bit gray scale, the expected data rate for the lander television system will be of the order of 10^6 bits per second. This figure will be used throughout the remainder of this section as representative of the lander data rate.

3.1.3 Returner

3.1.3.1 Mission

The scientific objectives of the returner vehicle are identical to those of the lander. The only exception to this could arise from the fact that the returner will bring back samples of the planetary surface to the convoy including samples of foreign and perhaps hostile biological organisms. For this reason, the returner scientific mission may stress biological contamination studies to a far greater extent than the lander mission.

3.1.3.2 As with the lander vehicle, it may be assumed that the major data acquisition source on the returner vehicle will be the television camera system. Therefore, a data rate of 10^6 bits per second is assumed to be representative of the returner throughout the remainder of this section.

3.1.4 Floater

3.1.4.1 Mission

The primary scientific objective of the floater mission is to determine planetary atmospheric characteristics. The characteristics to be investigated include:

(1) Air composition

(2) Thermal structure

(3) Pressure, density, specific heat ratio, and lapse rate as functions of altitude

(4) Insulation as function of altitude

(5) Radiation intensity (upper atmosphere)

(6) Wind circulation

(7) Cloud cover

3.1.4.2 Data Acquisition

Typical scientific measurements and sensors required to accomplish The above goals are summarized in table 3.1.4. Also shown are estimates of the data acquisition rates for each of these measurements. These estimates are based on an assumed data readout rate of one per second for each measurement. This data readout rate represents the maximum possible rate consistent with the measurements being taken. In practice, these rates will be of the order of 1/10 to 1/100 of the values given depending upon the final sensor selection and on expected data values as determined by unmanned planetary probes.

Floater position as determined by tracking measurements made by the convoy vehicles will be used to determine wind direction and velocity. Data rates for this position determination are assumed to be equivalent to instrumentation radar data rates (i.e., 30 bits per second). The total floater data rate of 182 bits per second includes this position data.

3.1.5 Environmental Satellites (Marens, Venens)

3.1.5.1 Mission

The major scientific goals of the environmental satellites is the determination of the following planetary characteristics:

(1) Magnetic fields

(2) Energy spectrum and distribution of radiation belts

(3) Neutron albedo

3.1.5.2 Data Acquisition

Typical scientific measurements and sensors required to define these characteristics are summarized in table 3.1.5. Also summarized are estimates of data acquisition rates for each of these measurements. The estimated data rates are again based on a data readout rate of one per second per measurement, which represents the maximum possible. In the case of the Marens vehicle, the actual data readout rate may prove to be 1/10 to 1/100 of this value depending upon the intensity of the Mars trapped radiation belts. In the case of the Venens vehicle, a one per second readout rate will most

Measurement	Sensor	Bits/ Second
Wind direction and velocity	Convoy tracking system	30
Air pressure and density	Ionization gage	35
Air composition	Mass spectrometer	28
Air temperature	Thermistor	8
Relative humidity	Thermistor	8
Sky and ground brightness	Radiometer	8
Spectral absorption	Ultraviolet spectrometer	14
Radiation intensity	Electrostatic analyzer	14
Altitude	Radar altimeter	20
Time reference	Time code generator	17
	Total	182

TABLE 3.1.4

FLOATER DATA RATES

Measurement	Sensor	Bits/ Second
Particle radiation intensity	Solar plasma analyzer	8
	Electron scintillation spectrometer	14
	Proton scintillation spectrometer	14
	Low energy ionization chamber	14
	High energy ionization chamber	14
	Cerenkov counter	10
	Boron triflouride counter	14
Cosmic dust detection	Micrometeorite gage	* 4
Magnetic field intensity	Magnetometer	8
Time reference	Time code generator	17
Satellite position	Convoy tracking system	30
	Total	147

* For one gage only

TABLE 3.1.5

ENVIRONMENTAL SATELLITE DATA RATES

likely be required due to the anticipated high level of intensity of the Venus trapped radiation belts.

3.1.6 Manned Excursion Vehicle (MEV)

3.1.6.1 Mission

The scientific mission requirements for the manned excursion vehicle have not been defined beyond those elements which are identical to the lander and returner vehicles. For the purpose of this study, it is therefore assumed that the manned excursion vehicle will present data acquisition, processing, storage, and transmission requirements similar to those for the returner vehicle.

3.1.6.2 Data Acquisition

The data acquisition source with the highest rate for the MEV will most likely be an image tube system. The data rates to be expected for this system will, however, be less than those for either the lander or returner vehicles since the remote control functions anticipated for the lander and returner television systems can be accomplished by the crew of the MEV. The expected data rates for the MEV are therefore almost a function only of the amount of data acquired in landscape viewing. This will result in 1/2 to 1/10 of the data acquired by the more sophisticated lander and returner television systems. Expected data rates for the MEV are therefore of the order of 10^5 bits per second.

3.1.7 Mars Satellite Probes (Phopro/Deipro)

3.1.7.1 Mission

The major scientific goals of the Phopro/Deipro vehicles, in addition to the general investigation of the orbital dynamics of the two Mars satellites, are determination of the following:

(1) Each satellite's surface features through television mapping

(2) Seismic activity on each satellite

(3) Surface radiation

(4) Magnetic field characteristics

3.1.7.2 Data Acquisition

Typical measurements and sensors required to gain scientific knowledge about the two Mars satellites are summarized in tables 3.1.6 and

3.1.7. The estimates shown for data rates were derived, with the exception of the television data rate, by assuming a readout rate of one per second per measurement. It should be noted that the seismometer data rate begins some time after probe impact and that all other data transmission ceases at probe impact. The television picture data rate was derived in the following manner:

(1) It is assumed that at least one picture with a resolution of the order of 100 meters is required.

(2) It is also assumed that this picture should, if possible, include the entire satellite being "photographed."

(3) Probe weight restrictions will prohibit the carrying of more than one image tube system.

(4) Probe terminal velocities will be of the order of 5,000 feet per second.

With these assumptions and the additional assumption that the probe(s) image tube system provides a 1/2 degree field of view and a gray scale coding of 4 bits, the television system data rates are for Phopro approximately 1.25×10^8 bits per second and for Deipro approximately 6.7×10^7 bits per second. These rates will be in effect for only the final 1100 seconds of the Phopro mission and the final 600 seconds of the Deipro mission.

Measurement	Sensor	Bits/Second In Transit	Bits/Second Post Impact
Magnetic field intensity	Magnetometer	8	
Surface radiation	Gamma ray spectrometer	14	
Seismic activity	Seismometer		100
Surface features	Television camera	* 1.25×10^8	
Time reference	Time code generator	17	
Probe trajectory	Convoy tracking system	30	

* Final 1100 seconds of mission

TABLE 3.1.6

PHOBOS PROBE DATA ACQUISITION

Measurement	Sensor	Bits/Second	
		In Transit	Post Impact
Magnetic field intensity	Magnetometer	8	
Surface radioactivity	Gamma ray spectrometer	14	
Seismic activity	Seismometer		100
Surface features	Television camera	* 6.7×10^7	
Time reference	Time code generator	17	
Probe trajectory	Convoy tracking system	30	

* Final 600 seconds of mission

TABLE 3.1.7

DEIMOS PROBE DATA ACQUISITION

3.2 Data Systems Costs

The following sections describe the cost in terms of weight that must be paid for acquisition of scientific data. In particular, section 3.2.1 defines storage weight costs for data storage on-board the auxiliary vehicles; section 3.2.2 defines storage weight costs for data storage on-board the convoy; section 3.2.3 defines communications system weight costs for transmission of scientific data from the convoy to Earth; and section 3.2.4 discusses weight costs for auxiliary vehicle to Earth data communications. Weight costs have not been determined for auxiliary vehicle to convoy communications systems since information on exact convoy and auxiliary vehicle trajectories is required to permit even preliminary predictions.

3.2.1 Data Storage in Auxiliary Vehicles

To establish the requirements for data storage in individual auxiliary vehicles, it is necessary to examine the time available for transmission of data from the auxiliary vehicles to the convoy and/or from the auxiliary vehicles to Earth. Figure 3.2.1 presents the ratio of shadow time to total orbital period between a satellite in circular orbit around Mars and a distant observer. Shadow time refers to the time the planet itself interferes with transmission of data to the distant observer. This figure represents the case of the mapper or Marens satellites in circular orbit around Mars, and can be used to determine storage requirements for data being transmitted directly to Earth.

Figure 3.2.2 presents a similar curve for the ratio of visible time to total orbital time between a fixed point on the surface of Mars and a satellite in circular orbit around Mars. This is representative of the case for a Mars lander, returner, or floater and a convoy vehicle in circular orbit. Similar curves may be obtained for shadow time between two satellites in circular or non-circular orbit. However, the computations required are quite extensive and have therefore not been attempted in the present study.

The actual on-board storage time requirements for the Mars mapper have been estimated as one hour for the case of the convoy vehicles in elliptic orbit. Figure 3.2.3 presents storage system weight as a function of mapper stay time for various mapping resolutions assuming one hour of data storage. Data for these curves was derived from information presented in section 7 of this report and from the data of figure 3.1.3.

Specific storage weights for other auxiliary vehicles can be derived by comparison of the data rate tables of section 3.1 and the shadow time curves presented here with weight criteria and curves presented in section 7. This was not done for vehicles other than the mapper, since it is felt that

the mapper data rates present the greatest, single data system design challenge, and because the other auxiliary vehicles have not been studied in sufficient depth to establish firm data rate requirements.

3.2.2 Convoy Data Storage

The major cost element to be determined for storage of scientific data on-board the convoy vehicles is the weight of the storage media and recording system selected. In the usual case, scientific data would be stored on-board the convoy vehicles only as long as is required to re-transmit this data to Earth. Figure 3.2.4 presents the weight of the recording system and bulk storage media on-board the convoy for mapper data only, as a function of mapper stay time, and mapper resolution for constant convoy to Earth re-transmission rates of 10^6 bits per second. These curves were derived from information presented in section 7of this report and from figure 3.1.3. The storage media is assumed to be magnetic tape. The magnetic tape itself is the major weight contributing factor.

Table 3.2.5 presents data storage weight requirements assuming no re-transmission of data to Earth.

3.2.3 Data Communications - Convoy to Earth

Estimate of communications system weights as a function of data rate and distance have been presented in section 4 of the report. From the weight curves of figure 4.9 for a communication distance of one astronomical unit, and from the mapper data rate curves of figure 3.1.3, convoy communication system weight as a function of mapper stay time have been shown in figure 3.2.6. This curve was derived assuming that the convoy would not store any data, but would simply function as a communication relay point for all mapper data. In actual practice, the convoy vehicles would most likely function as both a data storage center and data transmission relay center, since continuous communication cannot be guaranteed. The actual system's weight for both the convoy communication system and the convoy storage system will probably lie somewhere between the curves of figure 3.2.6 and table 3.2.5.

3.2.4 Data Communications - Auxiliary Vehicle to Earth

Direct communication of scientific data from individual auxiliary vehicles to Earth becomes of prime importance after the EMPIRE convoy has left the Mars capture mode. Direct auxiliary vehicles to earth communications may also be of importance for data acquisition backup during the convoy Mars capture mode. For this reason, data communications system weight costs must be assessed for reduced data transmission rates.

Figure 4.9 presents communication system weights for distances up to 2 astronomical units as a function of bit rate. This curve and the data presented in section 3.1 can be used to determine optimum communication system weights for reduced data rates that will permit the transmission of meaningful scientific data after completion of the main convoy mission.

Mapper Resolution Meters	Storage Weight Pounds
200	62
100	188
50	682
20	4,200
10	16,600

TABLE 3.2.5

STORAGE WEIGHTS - MAPPER DATA ONLY

FOR

NO RETRANSMISSION OF DATA

3.4 Scientific Data Handling System Analysis

From the material presented in this section as well as sections 4 and 7, a number of alternate approaches to the scientific data handling problem are apparent. Several of these are discussed below, however, no detailed trade-off studies have been made, and therefore no recommendations for final data handling system configuration are presented.

Alternate I

Transmission of data from auxiliary vehicle to convoy with minimum storage on-board auxiliary vehicles. Minimal transmission of data from convoy to earth with all data retained in storage on the convoy vehicle.

This alternate presents several advantages, including:

(1) Reliability of scientific data if the convoy returns safely to Earth.

(2) Optimization of convoy communications system weight since data transmission from the convoy to Earth is a backup or secondary source of final data.

(3) Independence from data communication systems reliability and possible transmission problems arising from sunspot activities, etc.

The risks involved and the penalties paid by this alternate include:

(1) Possible loss of the greatest percentage of the scientific data acquired if the convoy fails to return.

(2) Weight penalty for on-board convoy storage of all data.

(3) Relative inflexibility of mission objectives and operational plans since no detailed Earth-based study of data can be expected.

Conclusion I

If the weight advantage that communication is predicted to have over storage holds true, large weight penalties will be encountered in this mode.

Alternate II

Transmission of data from auxiliary vehicles to convoy with minimum storage on-board auxiliary vehicles. Re-transmission of all data at best possible rate from convoy to Earth with only buffer storage on-board convoy.

The advantages of this alternate include:

(1) Optimization of convoy bulk storage requirements since the primary final data source is the convoy to Earth communication system.

(2) Flexibility in mission objectives and operational plans due to Earth-based analysis of data.

The disadvantages of this alternate are:

(1) Weight penalties paid for reliable, wide band convoy to Earth data communications systems.

(2) Dependence upon communications system reliability.

There are, of course, a multitude of alternates available other than those described above. The analysis of these alternates and trade-off studies of weight cost versus reliability versus mission operational flexibility should be initiated at an early date if realistic development times are to be achieved for the scientific data handling system. It must be pointed out, however, that the detailed trade-off studies necessary to determine the optimum data handling system are dependent upon thorough analysis of all auxiliary vehicle scientific mission objectives, measurements to be made, and orbital trajectories. This information must be available before the data handling system can be optimized.

References

Ehricke, Krafft A., " Space Flight", Volume I, Enrironment and Celestial Mechanics

Ehricke, Krafft A., "A Study of Early Manned Interplanetary Missions", Intermediate Report Number 1, Missions and Operations Studies, ASO 1-4, GD/Astronautics July 30, 1962

Ehricke, K. A., "Objectives and Deployment of Auxiliary Vehicles. Communication Link Distribution, Effect of Capture Period on Auxiliary Vehicle Deployment. Representative Composition of an 8-Person Crew", Memorandum to Dr. D. H. Garber, October 30, 1962

Garber, Dr. D. H., "Trip Report, Visit to JPL on Planetary Experiments, September 19, 1962

Garber, Dr. D. H., "Interplanetary Studies Scientific Payload Estimates - Preliminary", ASO 1-6

Wyckoff, R. C., "Scientific Experiments for Mariner R-1 and R-2", JPL 32-315, July 15, 1962

"Planetary Studies", XI, from JPL Space Programs Summary 37-16

Adamski, D. F., "The Lunar Seismograph Experiment: Ranger 3, 4, 5", JPL TR 32-272, June 1, 1962

"Scientific Experiments for Ranger 3, 4, 5", JPL TR 32-199 (Revised), October 1, 1962

Eimer, Manfred, "Measuring Lunar Properties from a Soft-Lander", JPL TR 32-282, July 1962

Steinhoff, E. A., "A Possible Approach to Scientific Exploration of the Planet Mars", RAND Corporation, January 12, 1962

IBM Federal Systems Division, "Sensor Signal Compression for Space Telemetry", Final Report Independent Research and Development Program Task 0850, December 1961

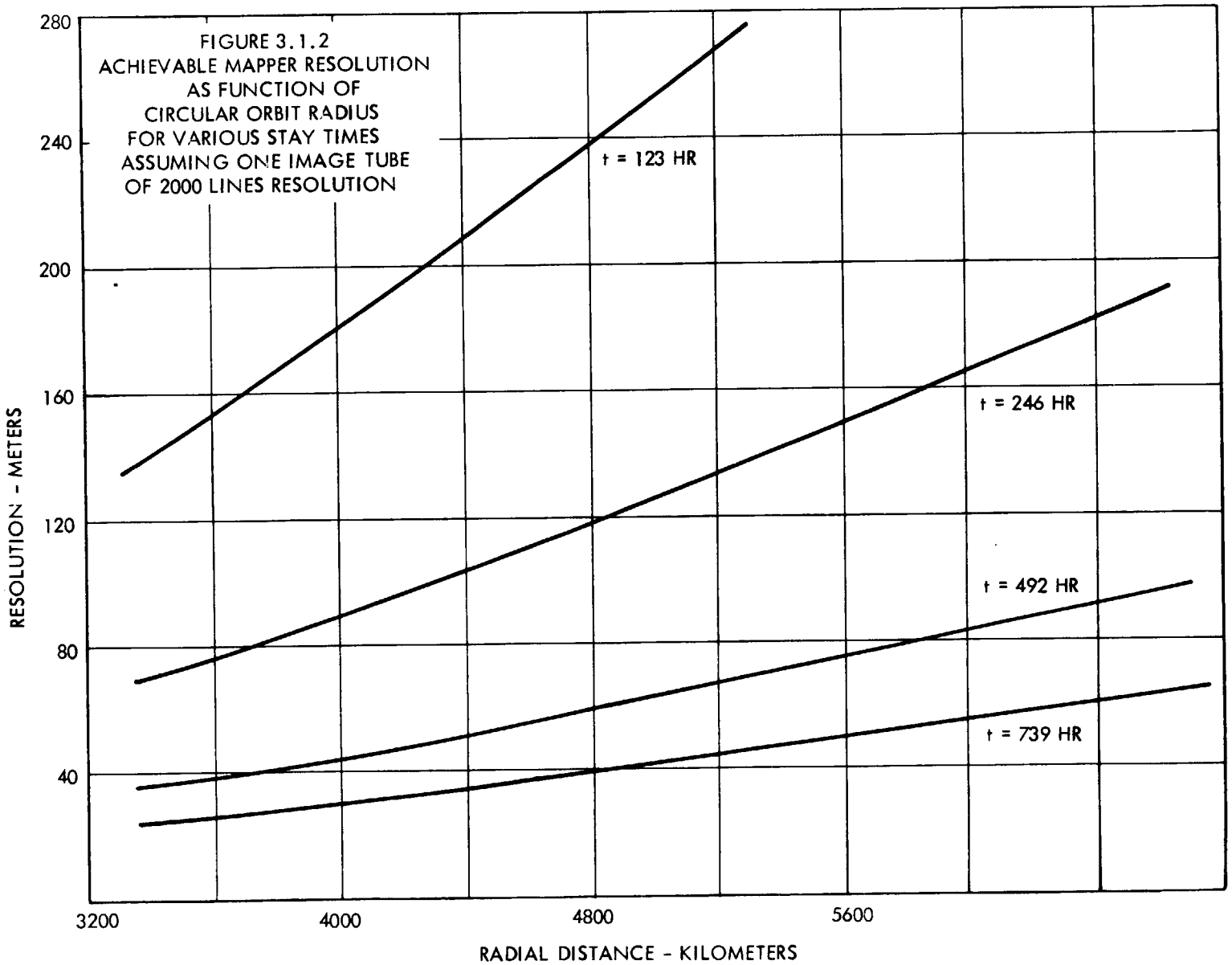
FIGURE 3.1.2
ACHIEVABLE MAPPER RESOLUTION
AS FUNCTION OF
CIRCULAR ORBIT RADIUS
FOR VARIOUS STAY TIMES
ASSUMING ONE IMAGE TUBE
OF 2000 LINES RESOLUTION
t = 123 HR
t = 246 HR
t = 492 HR
t = 739 HR
RESOLUTION - METERS
280
240
200
160
120
80
40
3200
4000
4800
5600
RADIAL DISTANCE - KILOMETERS

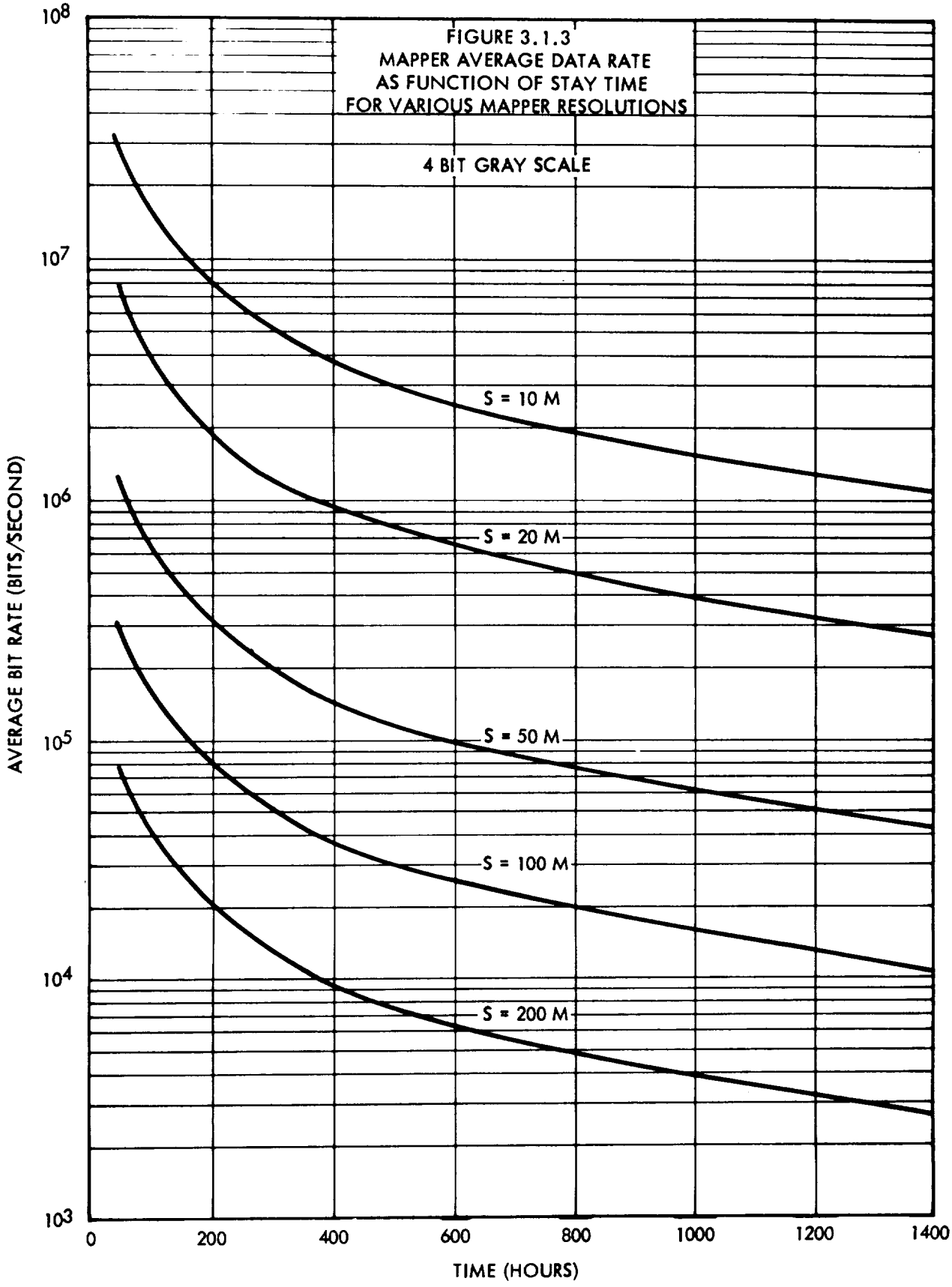
FIGURE 3.1.3
MAPPER AVERAGE DATA RATE
AS FUNCTION OF STAY TIME
FOR VARIOUS MAPPER RESOLUTIONS
4 BIT GRAY SCALE
S = 10 M
S = 20 M
S = 50 M
S = 100 M
S = 200 M
AVERAGE BIT RATE (BITS/SECOND)
10^8
10^7
10^6
10^5
10^4
10^3
0
200
400
600
800
1000
1200
1400
TIME (HOURS)

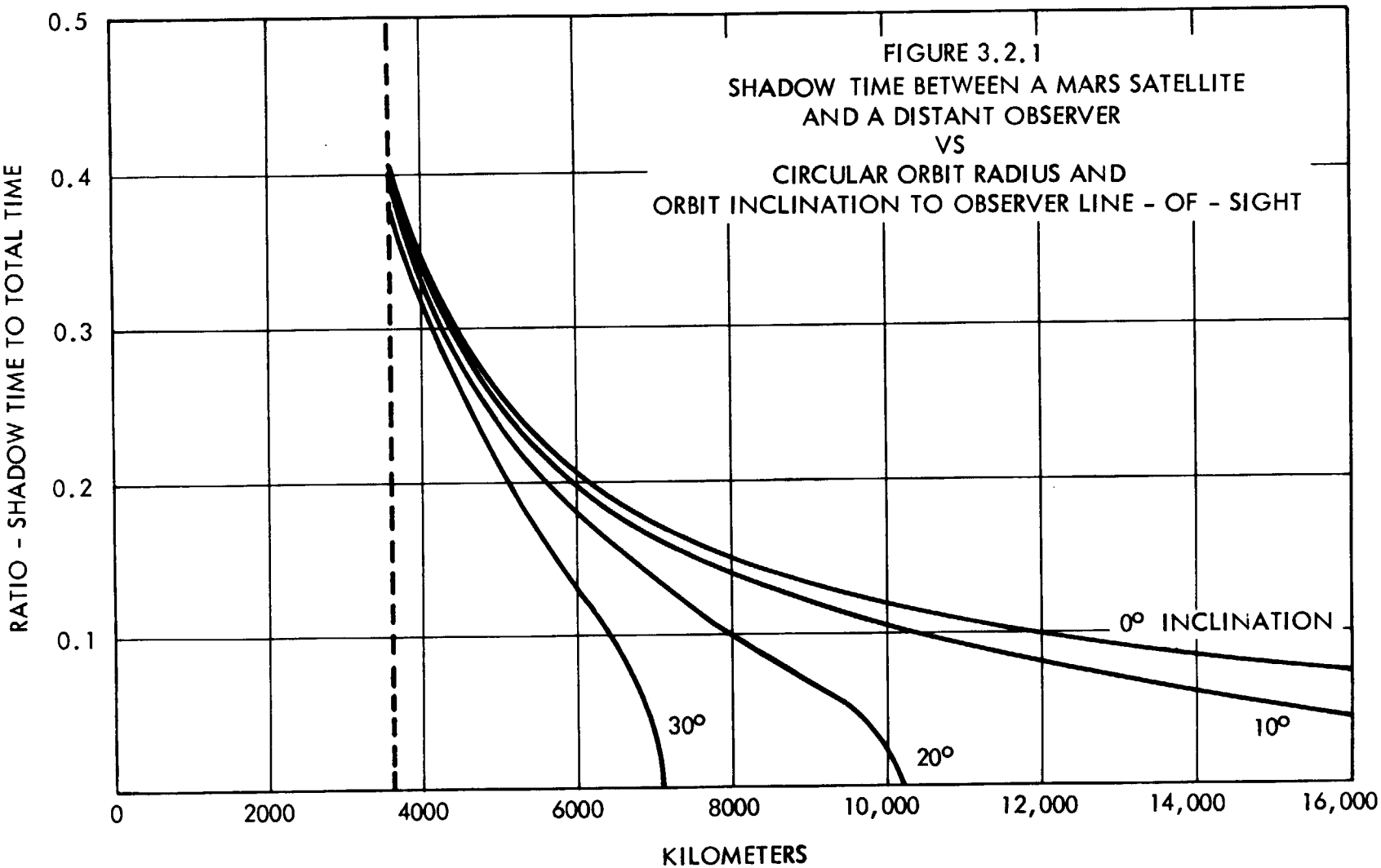
FIGURE 3.2.1
SHADOW TIME BETWEEN A MARS SATELLITE
AND A DISTANT OBSERVER
VS
CIRCULAR ORBIT RADIUS AND
ORBIT INCLINATION TO OBSERVER LINE - OF - SIGHT
RATIO - SHADOW TIME TO TOTAL TIME
0.5
0.4
0.3
0.2
0.1
0
2000
4000
6000
8000
10,000
12,000
14,000
16,000
KILOMETERS
0° INCLINATION
10°
20°
30°

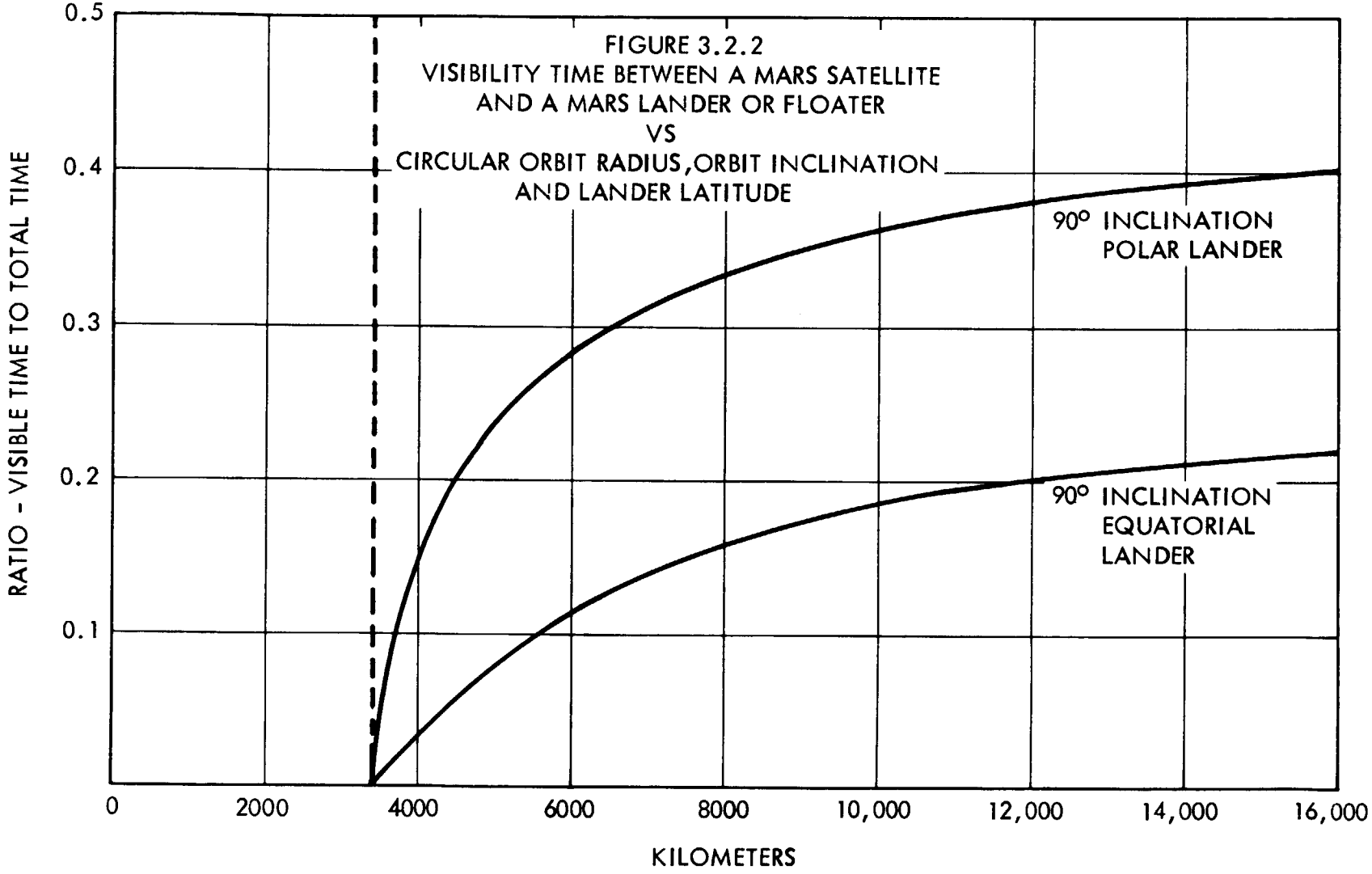
FIGURE 3.2.2
VISIBILITY TIME BETWEEN A MARS SATELLITE
AND A MARS LANDER OR FLOATER
VS
CIRCULAR ORBIT RADIUS, ORBIT INCLINATION
AND LANDER LATITUDE
RATIO - VISIBLE TIME TO TOTAL TIME
0.5
0.4
0.3
0.2
0.1
0
2000
4000
6000
8000
10,000
12,000
14,000
16,000
KILOMETERS
90° INCLINATION
POLAR LANDER
90° INCLINATION
EQUATORIAL
LANDER

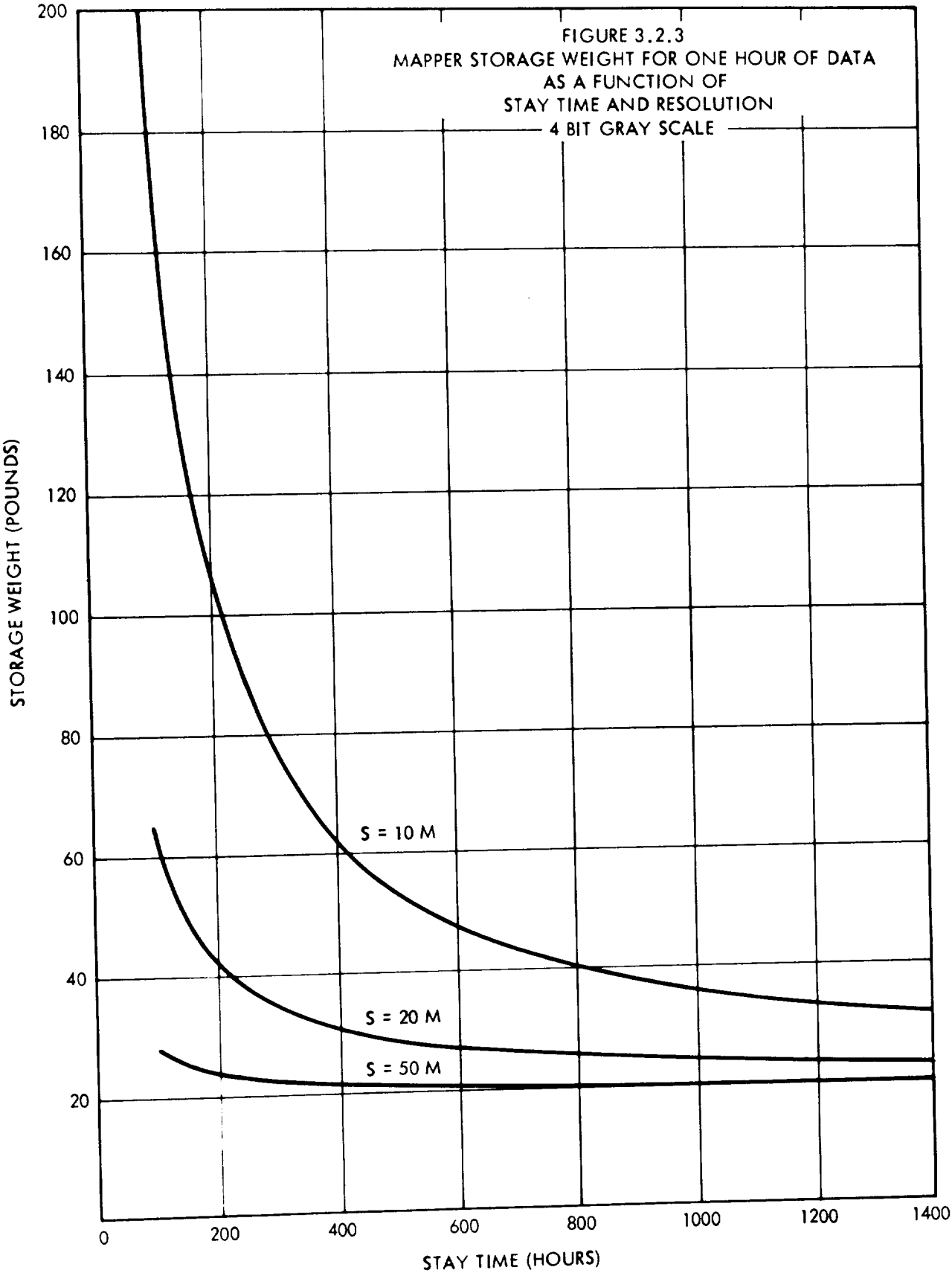
FIGURE 3.2.3
MAPPER STORAGE WEIGHT FOR ONE HOUR OF DATA
AS A FUNCTION OF
STAY TIME AND RESOLUTION
4 BIT GRAY SCALE
STORAGE WEIGHT (POUNDS)
200
180
160
140
120
100
80
60
40
20
0
200
400
600
800
1000
1200
1400
STAY TIME (HOURS)
S = 10 M
S = 20 M
S = 50 M

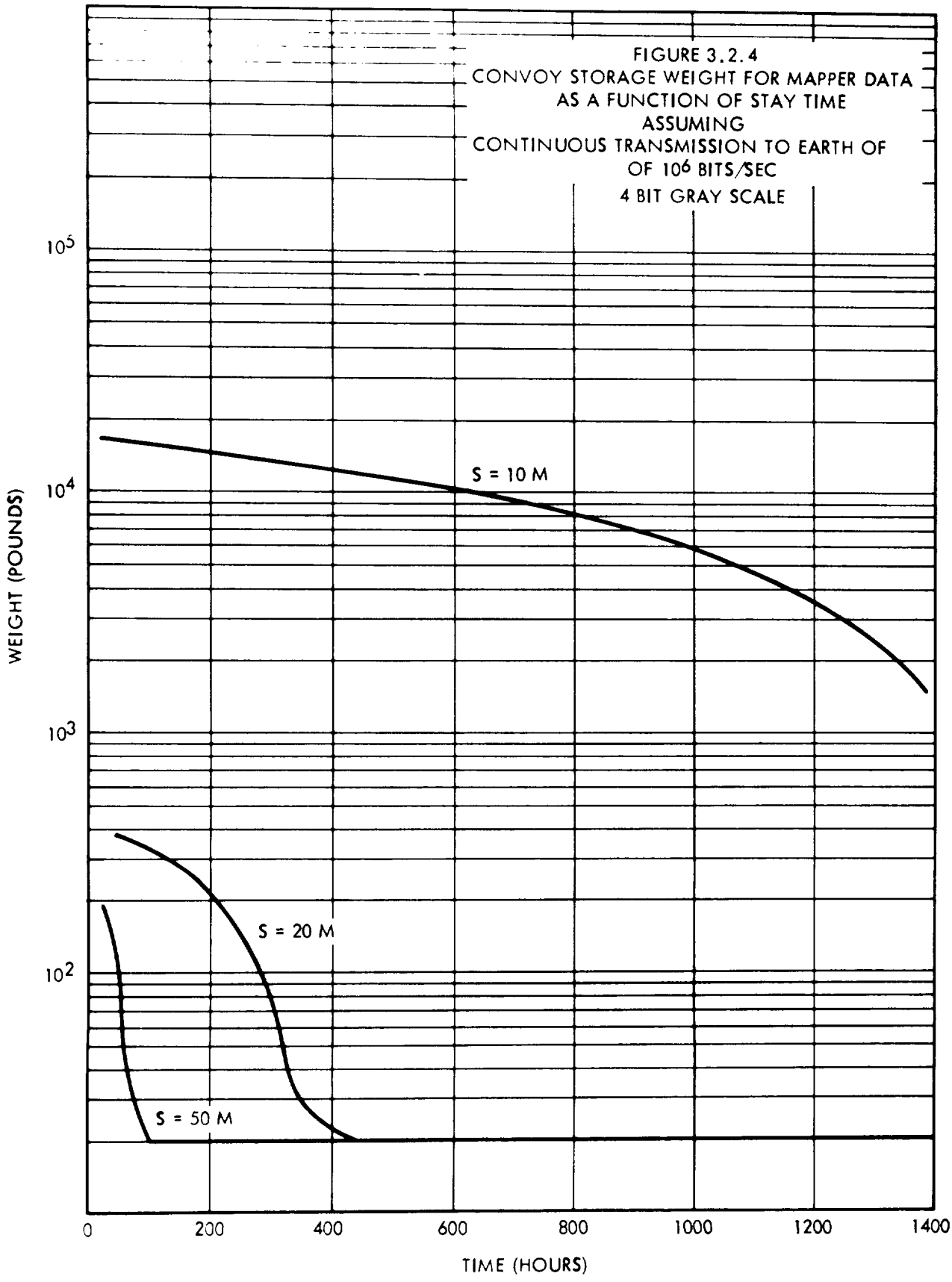
FIGURE 3.2.4
CONVOY STORAGE WEIGHT FOR MAPPER DATA
AS A FUNCTION OF STAY TIME
ASSUMING
CONTINUOUS TRANSMISSION TO EARTH OF
OF 10⁶ BITS/SEC
4 BIT GRAY SCALE
WEIGHT (POUNDS)
10⁵
10⁴
10³
10²
S = 10 M
S = 20 M
S = 50 M
0
200
400
600
800
1000
1200
1400
TIME (HOURS)

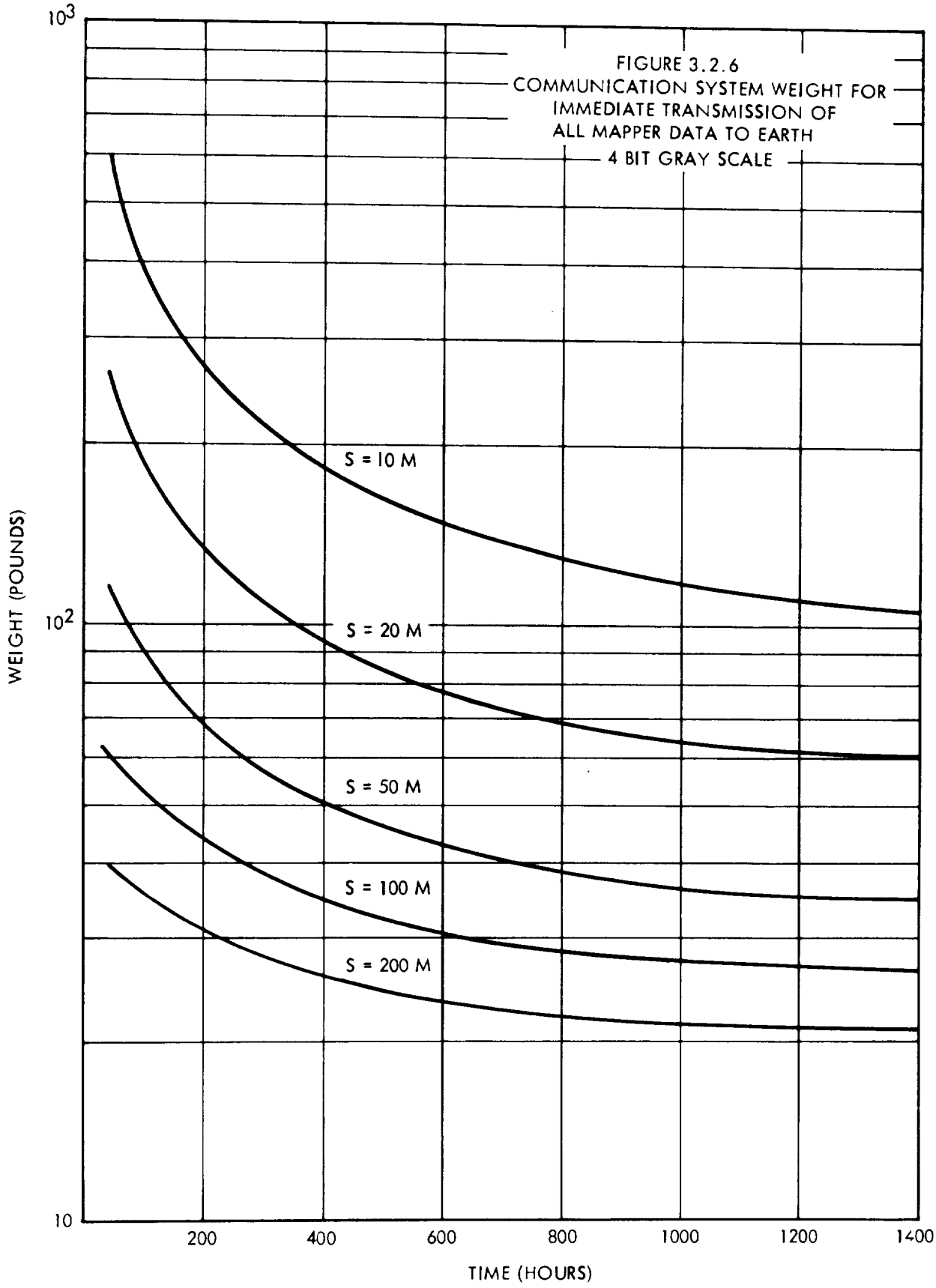
FIGURE 3.2.6
COMMUNICATION SYSTEM WEIGHT FOR
IMMEDIATE TRANSMISSION OF
ALL MAPPER DATA TO EARTH
4 BIT GRAY SCALE
WEIGHT (POUNDS)
10^3
10^2
10
S = 10 M
S = 20 M
S = 50 M
S = 100 M
S = 200 M
200
400
600
800
1000
1200
1400
TIME (HOURS)

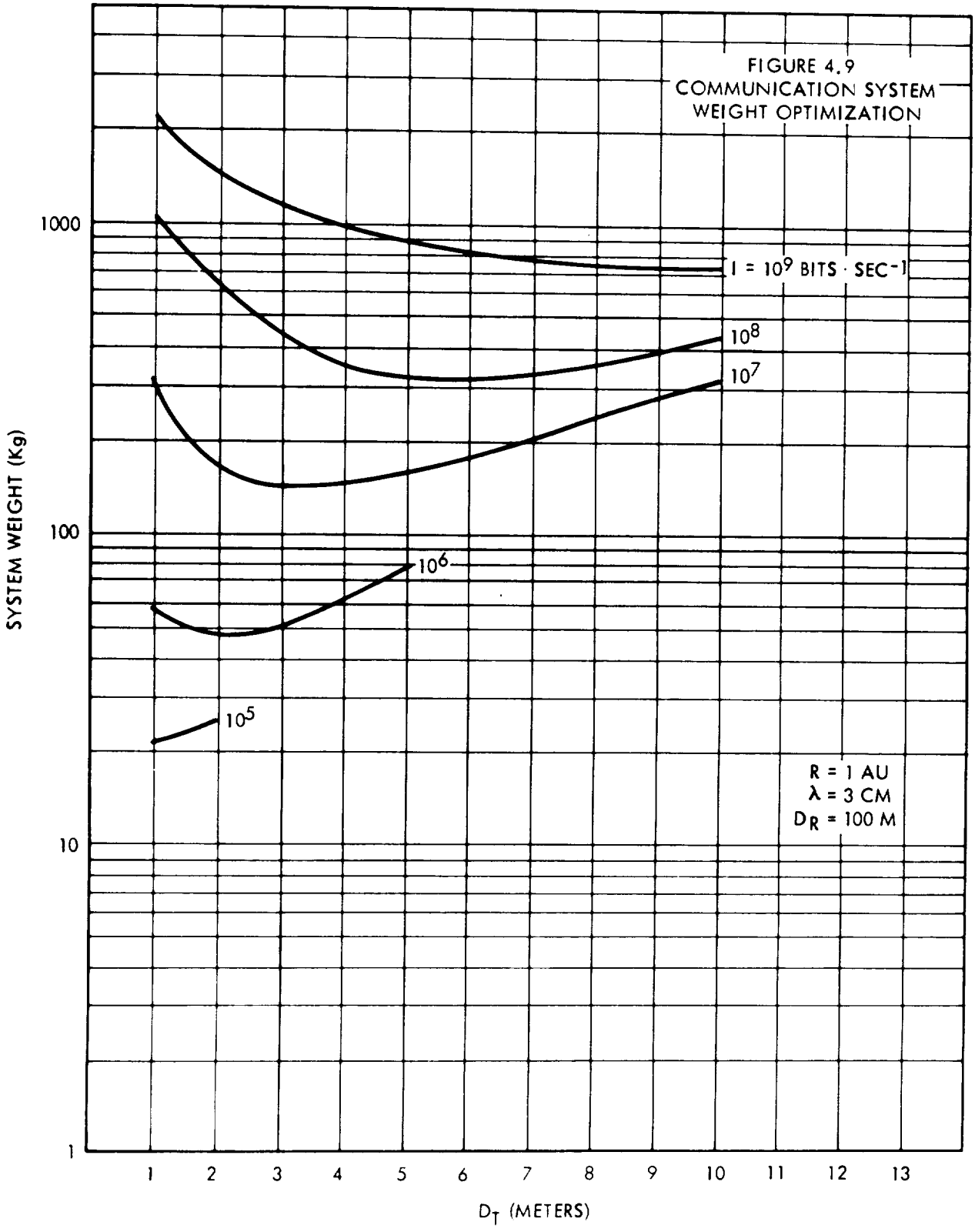
FIGURE 4.9
COMMUNICATION SYSTEM
WEIGHT OPTIMIZATION
I = 10^9 BITS · SEC^-1
10^8
10^7
10^6
10^5
R = 1 AU
λ = 3 CM
D_R = 100 M
SYSTEM WEIGHT (Kg)
1000
100
10
1
1
2
3
4
5
6
7
8
9
10
11
12
13
D_T (METERS)

SECTION 7

Data Processing and Storage Weight and Power Forecasts

The part that miniaturization will play in the electronics industry, and the time period in which it will begin to play its part, have been the subject of considerable conjecture. It is such a swiftly changing field that it is difficult to make predictions that hold their value. The factor introduced by interconnections between very small elements is especially difficult to estimate. This section discusses the feasibility of microminiaturized data processors in terms of weight, power, and volume as a function of various parameters.

7.1 Forecasts of Weight, Power, and Volume of Data Processors

The principal objective of microminiaturization is to effect a great reduction in the weight and volume of electronic equipment. Data, based on microminiaturization equipment development work in progress, shows that reduction in weight, power, and volume of from two to five orders of magnitude appear feasible. The applicability of microminiaturization is, however, largely limited to logic type circuitry at the present time and little is being done with the power dissipation and insulation requirements for high-voltage components. Thus, the total system may not show the gains predicted. Another factor that must be considered is maintenance. As components are made smaller, they must be combined into replaceable units composed of larger groups of components. These units are generally not similar to one another and thus there is an increase in the number of spares that must be carried. The difficulty of interconnection becomes greater as the assemblies become smaller, and it appears that there may exist a point of diminishing returns as far as volume reduction is concerned.

The greater reliability that is demanded for our systems is another factor which affects considerably the equipment complexity. And, as the equipment complexity increases, so do the weight and volume.

7.1.1 Weight, as a Function of Calendar Year of Development (1965-1975)

The past two decades have seen a striking increase in the sophistication and performance capability required of both airborne and ground data processing equipment. Microelectronics, accordingly, is needed to reduce the weight and volume of present day equipments and to anticipate the needs for reductions in physical size and weight of equipments of the future. The approximate weight relationships of various technologies and the projected calendar year of development for each are shown in figures 7.1.1.1 and 7.1.1.2.

Integrated logic types of technology are probably the more advanced of the many microminiaturization schemes that are being developed. These are technologies where resistive, capacitive and conductive elements, within the limits of existing technologies, can be deposited by vacuum evaporation techniques on common substrates. The semiconducting elements are then connected by placing uncased semiconductor elements on the substrates or by wiring in uncased units.

Micro-module types of technology in which assemblies are built up by stacking wafers are also in process of development. All the components are packaged within the stacks and interconnections between wafers are usually made by riser-wire techniques.

Multi-layer magnetic film structures representing large scale circuit assemblies have been processed but the fabrication techniques require years of refinement before economical yields can be obtained. The simplicity of the logic units in the multi-layer structures will make it possible to fabricate lower cost units as well as improve the reliability potential.

The relationships in 7.1.1.1 are based upon 1,000 circuit models (excluding power and chassis) and those in 7.1.1.2 are based upon 10,000 circuit models (excluding power and chassis). Note the proportionately greater increase in weight of the micro-module type of technology in figure 7.1.1.2. This is due to a choice of circuits that do not have the signal rejuvenation qualities of the circuits employed in other technologies. As a result, more amplifiers must be used thus resulting in a proportionate increase in weight.

7.1.2 Weight, Power, and Volume as a Function of Speed in Instructions Per Second

The choice of what type and capability of data processor to be used in EMPIRE is a difficult one. A number of criteria such as processing capability, reliability, and availability, ease of programming, weight, and physical size must be considered before a particular data processor configuration can be selected.

The selection is further complicated by the necessity of making a choice between different equipment organization concepts. For a given application, one may select a single, very high-speed data processing system or one may select a combination of several smaller processing systems.

The very high speed data processing system has been characterized by more powerful instruction sets, rapid advances in access time and size of storage devices, increased component reliability, improved machine organization, and increased emphasis on ability to perform simultaneous operations.

On the other hand, a combination of smaller processing systems, better referred to as a multiprocessor, has advanced various configurations of processors as total processing systems for fulfilling the requirements of either large, or small and expanding systems. Such a total system also possesses the advantages of high processing capability, reliability, availability, maintainability, and non-disruptive growth.

Specific recommendations of an equipment configuration cannot be made without a detailed system analysis and evaluation. In view of the fact that the processing requirements have not been defined, a broad spectrum of processing capability in instructions per second and the relationship to weight, power, and volume are shown in figures 7.1.2.1, 7.1.2.2, and 7.1.2.3. Data processors having capabilities approximately equivalent to that of last generation and present generation ground based equipment, and a multiprocessor about 11 or 12 times more powerful than present large scale ground based computers as follows:

The graphs are based upon a multiprocessor (48 bit word length) which includes the following elements:

4 - 16,000 word memories

4 - Processors

2 - Arithmetic units

2 - Input output units

1 - Operating console and maintenance unit

The single computer graphs were based upon a system consisting of the following elements:

Basic computer including:

Extended performance indexing

Floating point-single precision

Floating point-double precision

Clock

4 - Anciliary equipment channels

1 - 32,000 word memory

2 - Input output synchronizers

Power figures for the micro-module and thin film types of technologies were not available. It can, however, be assumed the power per elementary logic unit in most of the microminiaturized technologies is steadily decreasing from that used in the representative large computer systems in production today. This is borne out by the power curve drawn for the integrated logic technology where lower power consumption per logic unit is a reality.

7.1.3 Weight and Volume as a Function of Word Length

The computing systems presently in existence which are labeled "general purpose" are normally capable of accomplishing all common computing and data processing functions, but the facility with which they do each function varies widely. To say that a computing system is good, bad, or better than any other system, is obviously meaningless unless the purpose(s) for which the systems are to be used are specified.

Cognizance of this application sensitivity has long been taken by computer engineers resulting in the "scientific" systems, the "commercial" systems, and more recently, "real-time" control systems. The process of choosing or designing the computer best suited for the "real-time" control job in EMPIRE is one that must be done carefully. One of the computer characteristics that can affect this choice is word length, and, word length can, in turn, affect the weight, power, volume, and speed of the computer complex.

As the word length of a computer grows the logical capability of the computer usually has a corresponding growth. There is also a corresponding increase in weight, power, and volume.

In figure 7.1.3, the weight of a computer logically similar to present large scale ground based computers is plotted against its 36-bit word length. The weight is based upon integrated logic type of technology. If the word length is doubled, with the assumptions that the same speed is maintained and the logical capability is increased (by making use of the additional bits), the weight can generally be expected to triple. If the word length is doubled, with the assumptions that the same speed is maintained and that the logic remains compatible with the present machine, the weight will more than double. If there is only a requirement for logical compatibility but not speed, the weight will be approximately 1.75 times that of the 36-bit machine.

The effect of doubling the word length has a similar effect to that discussed above on the power and volume of the computer.

7.1.4 Weight, Power, and Volumes as a Function of Memory Size

In recent years, much work has been done in the field of core storage units to improve their speed, reduce their cost, reduce their size, and increase

their capacity, and generally make them keep pace with the rapidly progressing computer technology. Considerable pressure for improvement of core storage units continues, because it is generally conceded that storage units limit the speed of computers.

Improvement programs are many and varied and include the following:

- Research in new core materials
- Improved core geometries
- New addressing techniques
- New driving techniques
- Automatic assembly methods

Some new core materials and new addressing techniques have decreased the size of the memories and increased their speeds. Further reductions in size and therefore weight will be realized. Figure 7.1.4 gives some indication of the weights of memories ranging in size from 8,000 to 65,000 36-bit words of storage that can be expected in the time period from 1965 through 1975. There are now, and there will be, cooling problems caused by increased packing density and higher speeds. Some of the temperature problems, in some instances, have been alleviated by liquid cooling of the arrays. Further significant reductions in the power dissipation per core can forestall usage of such elaborate cooling methods.

7.2 Forecast of Weight and Volume of Bulk Storage Devices

Increased speed and capacity as well as reduced weight and volume of high-speed bulk storage devices, are key requirements for the airborne data processing systems of the future. This section examines briefly and compares the present state-of-the-art against what is projected in high-speed storage devices for the 1965-1975 time period.

High-speed digital data storage devices are considered in two categories:

High speed read-write storage characterized by the many core storage units available today, and

Mechanical storage units including drums, disks, and tapes

7.2.1 Weight as a Function of Calendar Year of Development

The present major efforts to improve bulk storage services can be reasonably expected to result in significant improvements in this field.

Thin magnetic film devices have been under active development for the past six years. Relatively few successful storage devices using this technology have been announced. It seems true, however, that thin magnetic films have the potential to reduce the weights, and increase the speeds as well, of the bulk storage device field. Significant flexibility in design and construction is also possible. This flexibility is due to deposition techniques for producing the film and etched circuitry techniques for wiring arrays.

The curve shown in figure 7.2.1.1 is an indication of how significant the reduction in weight might be. As an example, a 65,000 36-bit memory (over 2.3 million bits) is expected to weigh about 20 to 25 percent of a corresponding memory made out of cores.

Cryogenic storage offers considerable promise with several companies having active research programs in this field. Recent successes in the fabrication of cryogenic storage planes have indicated that this technology may well take a dominant position in high speed storage devices in the 1970's. Like thin magnetic films, this technology is particularly adaptable to microminiaturizing and the simultaneous fabrication of storage elements and logic.

The innovation of the disk file, introduced in 1955, represented a large step forward in producing bulk storage in a dense package and at low cost. The developments in magnetic recording heads are particularly

important for increasing bit and track densities and, in turn, paving the way for a substantial increase in storage capacity. The in-contact recording on magnetic tapes has always permitted higher density recording than has been possible with heads maintained at a fixed distance for the recording surface. Although closer spacing is not the only parameter permitting denser recording, it bears an important relation to maximum recording density of any head-surface combination.

Magnetic tapes have a higher recording density than any other computer oriented technology in use, and they weigh less than other rotating storage devices. The curves shown in figure 7.2.1.2 therefore show only the progress that is expected in improving the densities of present day tapes. The weight forecast is based upon densities of approximately 4500 bits per inch. This may be conservative as experimental work has shown that bit densities up to 40,000 bits per inch and track densities up to 500 per inch may be feasible with magnetic recording techniques.

7.2.2 Forecast Weight of Bulk Storage Devices as a Function of Recording and Reading Rates

Over the major range of high-speed devices, down to 500×10^{-9} second cycle time, cores will continue to dominate. New addressing and wiring techniques, as well as new materials will contribute to implementing the advanced state of the device technology indicated in figure 7.2.2.1 and 7.2.2.2. The two figures differ only in that the 36-bit word capacity versus the cycle time are plotted figure 7.2.2.1, and the total bit capacities versus the cycle time are plotted in figure 7.2.2.2.

At the extremely high speeds approaching 10×10^{-9} seconds, the thin magnetic-film technology and the Esaki-diode technology can be expected to be competitive. In general, the cryogenics technology is expected to implement storage devices with speeds and capacities indicated. Cryogenic storage devices will not be economically competitive below 1000 words. At this capacity, however, 20×10^{-9} second cycle time will be achieved. It will be noted that the speeds expected from cryogenics surpass those expected from other technologies. The principal impediment to wide-scale use of cryogenics is the necessity for the controlled environment. The further development of extremely reliable closed-cycle refrigeration systems, themselves occupying little volume and weight, will further insure the broad applicability of cryogenics.

The weight of the high-speed storage devices are usually closely related to their bit capacities. Reference should be made to figure 7.2.1.1 where the weight-capacity relationship is shown for both core and thin film storage units. The cryogenics technology was not plotted in Figure 7.2.1.1 because of the large volume and weight of the closed-cycle refrigeration systems.

As for future mechanical storage devices, it is expected that moving magnetic surface recording devices will dominate the field without any other mechanical storage technology in serious contention. In terms of capacity and random access time, drums, disks, strip-files and tapes form a continuous spectrum of devices over a wide range as shown in figure 7.2.2.3.

There are three major approaches that are being taken presently to improve the access times in figure 7.2.2.3. These are:

- Faster mechanical accessing
- Denser recording techniques
- Multiple access stations

Faster mechanical accessing may be accomplished by faster rotational speed, improved power sources, reduction of travel distances, and directions and reductions of the movable mass. Denser recording techniques contribute to improved access time by reducing the amount of head travel necessary to cover a given number of information tracks, or by reducing the required storage area which, in turn, permits faster rotational speeds. Multiple access stations in their simplest form may consist of a single fixed head per track on either a drum file or a disk file. This approach eliminates the necessity for positioning heads and reduces the initial access time. However, multiple access stations impose severe restrictions on the design and operation of the mechanical hardware.

The capacities of rotating magnetic storage devices will improve as will the access times through the 1965-1975 time period. The relationship of the capacities of these devices as a whole to their access time is shown on figure 7.2.2.3. No attempt was made to predict the weight of storage devices other than tapes. These were shown in figure 7.2.1.2.

7.2.3 Weight and Volume as a Function of Real-Time Input-Output Capability

The "real-time" control processor(s) used in EMPIRE will require a great deal of flexibility in the input-output control units. Because of the large volumes of data that we can assume will be transferred to and from the processor(s), the control units will have perhaps as many as four independent channels through which data will be transferred. Each of these channels may, in turn, have as many as four separate input-output operations proceeding simultaneously, each under the supervision of one of the channels. Once started, the channels would operate independently of the main program.

If four present-day tape drives were attached to a channel, it would be possible to exchange information with a computer at a rate of 250,000 characters per second with all four drives running simultaneously. In the 1965-1975 time period, the increased density of data on tape would enable one channel to exchange information at a rate of over 1,500,000 characters per second.

Other storage devices or "real-time" buffers through which data would be exchanged between the computer and the outside world at possibly different rates could be substituted for the tapes in our example. The number of devices, buffers, and even the rates of exchange all affect the logical complexity of an input-output control unit. In figures 7.1.2.1, 7.1.2.2, and 7.1.2.3, it was assumed that four channels of input-output capability existed and the associated weights, powers, and volumes are plotted for each of the processors. It can roughly be assumed that half of the weight, power, and volume of each processor is due to the input-output control units and to the large number of channels included in each. The weights could, of course, be reduced if less capability was required in the input-output control units.

7.2.4 Selection of Storage Devices

The types and amount of storage required for a processor depend on the nature of the application. Some applications require internal storage alone; others rely heavily on secondary storage; still others need a combination of the two. Some of the factors that affect the storage requirements are outlined below:

7.2.4.1 Type of Processing Performed

The type of processing performed varies greatly. Certain scientific or engineering problems involving extensive calculations can utilize large internal storage. Large internal storage is classified as that which is an integral part of the computer, and that which is directly controlled and automatically accessible. Magnetic core storage units usually fall in this category. Processing is fastest if all the instructions and data are contained in internal memory.

Certain applications rely more heavily on secondary storage. Secondary storage is classified as that which is not an integral part of the processor, but is directly connected and controlled by it. Tapes, drums, and disks are examples of secondary storage units. The processor(s) used in one or more areas in EMPIRE will rely heavily on secondary storage and involve limited computation. The secondary storage in EMPIRE will be used to store data temporarily until the data can be transmitted to some main processor in the fleet or back to Earth.

7.2.4.2 Time Limit Between Occurrence of Events

The time limit between the occurrence of events and the need for information about those events is a factor that must be considered in selecting storage devices. Tight time schedules may require that one or perhaps even more units of storage be available at all times. Thus, it may be necessary for the processor to have the capability of transmitting to secondary storage and to some external location simultaneously through many channels. The frequency and the nature of the references to storage and the transmission to external areas affect the selection of storage devices.

7.2.4.3 Data Volume

Data volume is a most important factor in selecting efficient storage methods. Huge volumes of data impose restrictions upon the system designer in that he must use storage methods with low unit cost and weight. This, in turn, usually means that access times to storage will be slower.

7.2.4.4 Other Factors

There are factors which affect the choice of storage. Reliability, weight, and volume must also be given serious consideration in selecting storage devices.

The nature of the application must be analyzed thoroughly before a choice of processor(s) and associated storage devices can be made.

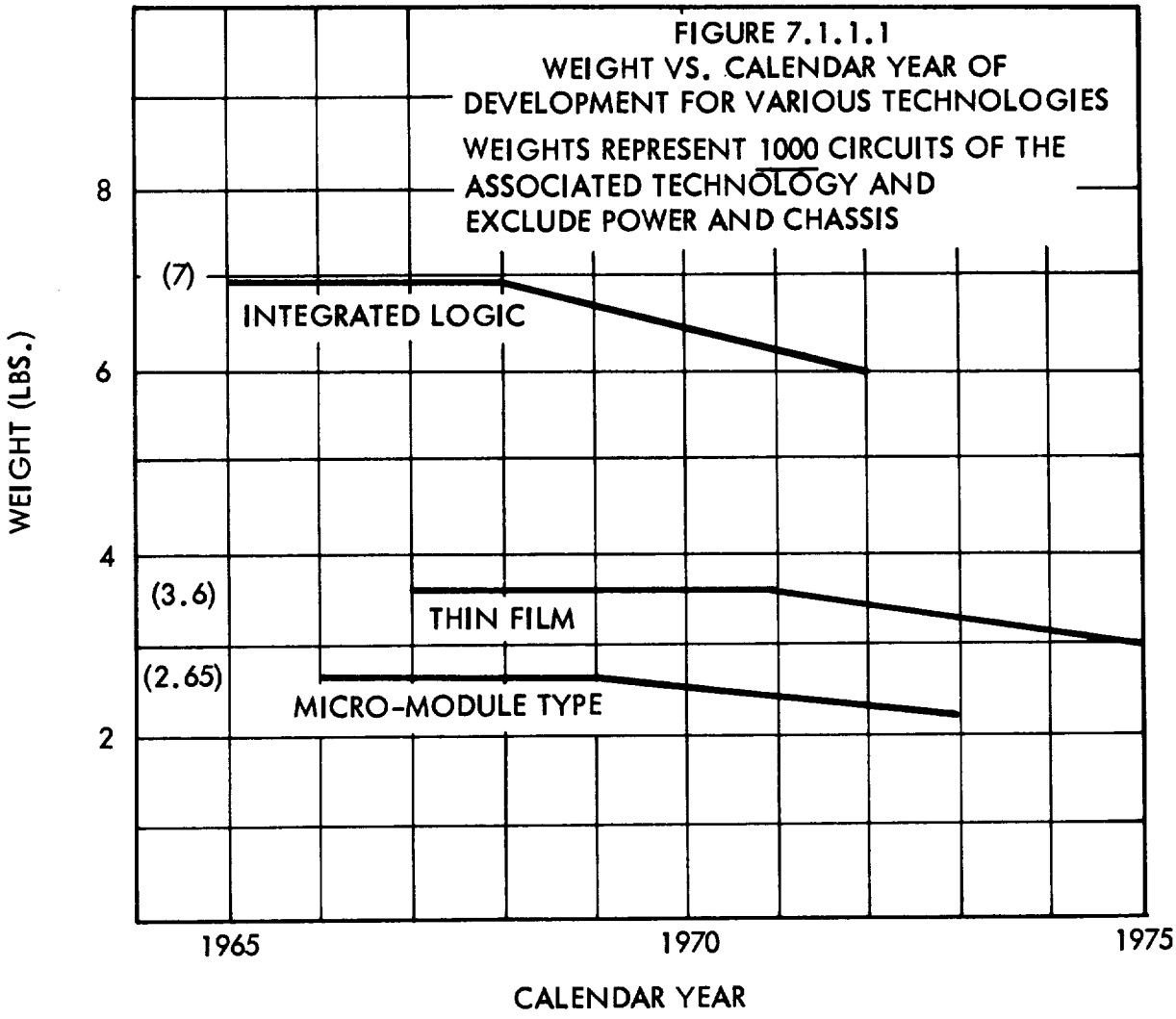
FIGURE 7.1.1.1
WEIGHT VS. CALENDAR YEAR OF
DEVELOPMENT FOR VARIOUS TECHNOLOGIES
WEIGHTS REPRESENT 1000 CIRCUITS OF THE
ASSOCIATED TECHNOLOGY AND
EXCLUDE POWER AND CHASSIS
WEIGHT (LBS.)
8
6
4
2
(7)
INTEGRATED LOGIC
(3.6)
THIN FILM
(2.65)
MICRO-MODULE TYPE
1965
1970
1975
CALENDAR YEAR

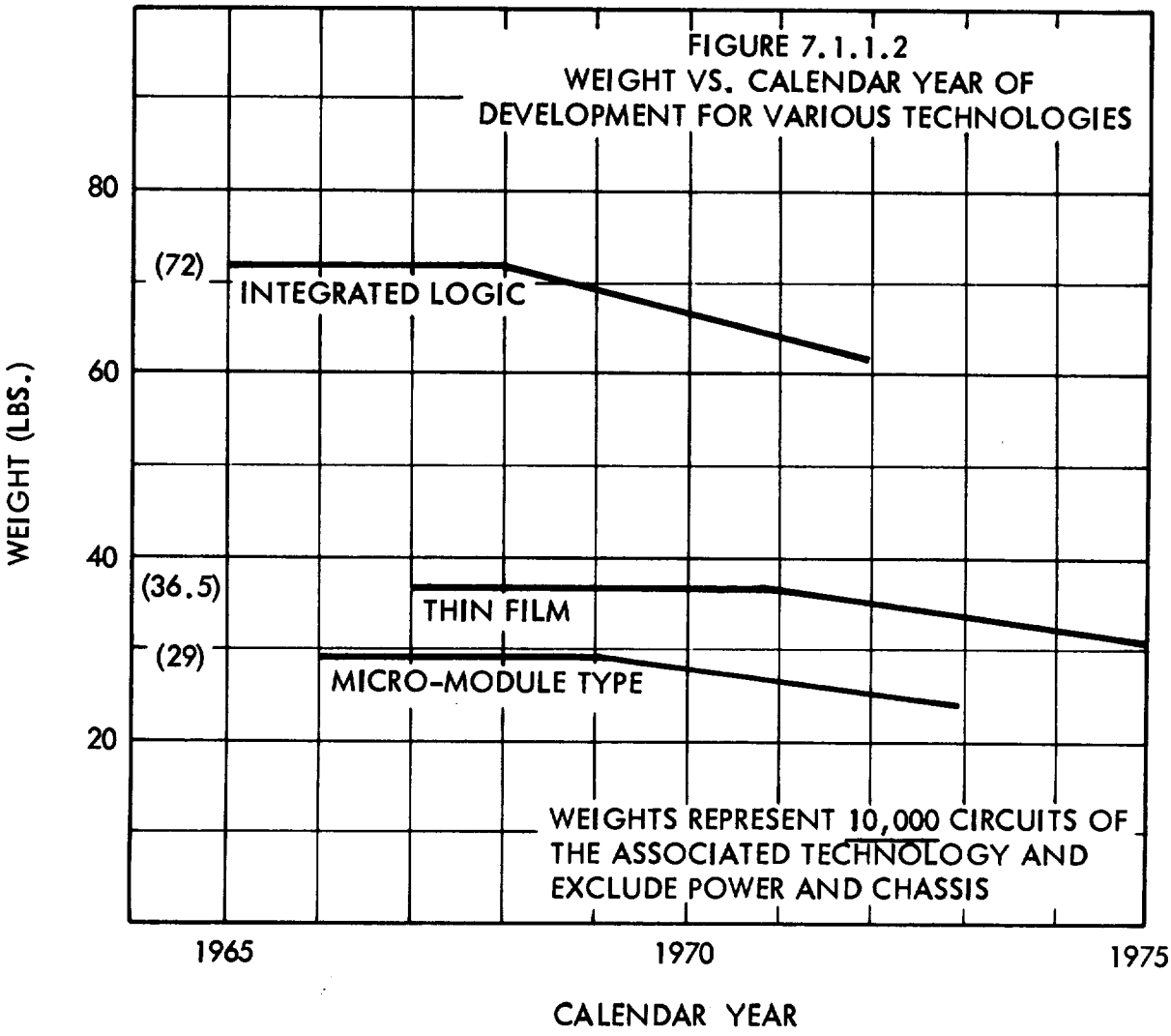
FIGURE 7.1.1.2
WEIGHT VS. CALENDAR YEAR OF
DEVELOPMENT FOR VARIOUS TECHNOLOGIES
80
60
40
20
(72)
INTEGRATED LOGIC
(36.5)
THIN FILM
(29)
MICRO-MODULE TYPE
WEIGHTS REPRESENT 10,000 CIRCUITS OF
THE ASSOCIATED TECHNOLOGY AND
EXCLUDE POWER AND CHASSIS
WEIGHT (LBS.)
1965
1970
1975
CALENDAR YEAR

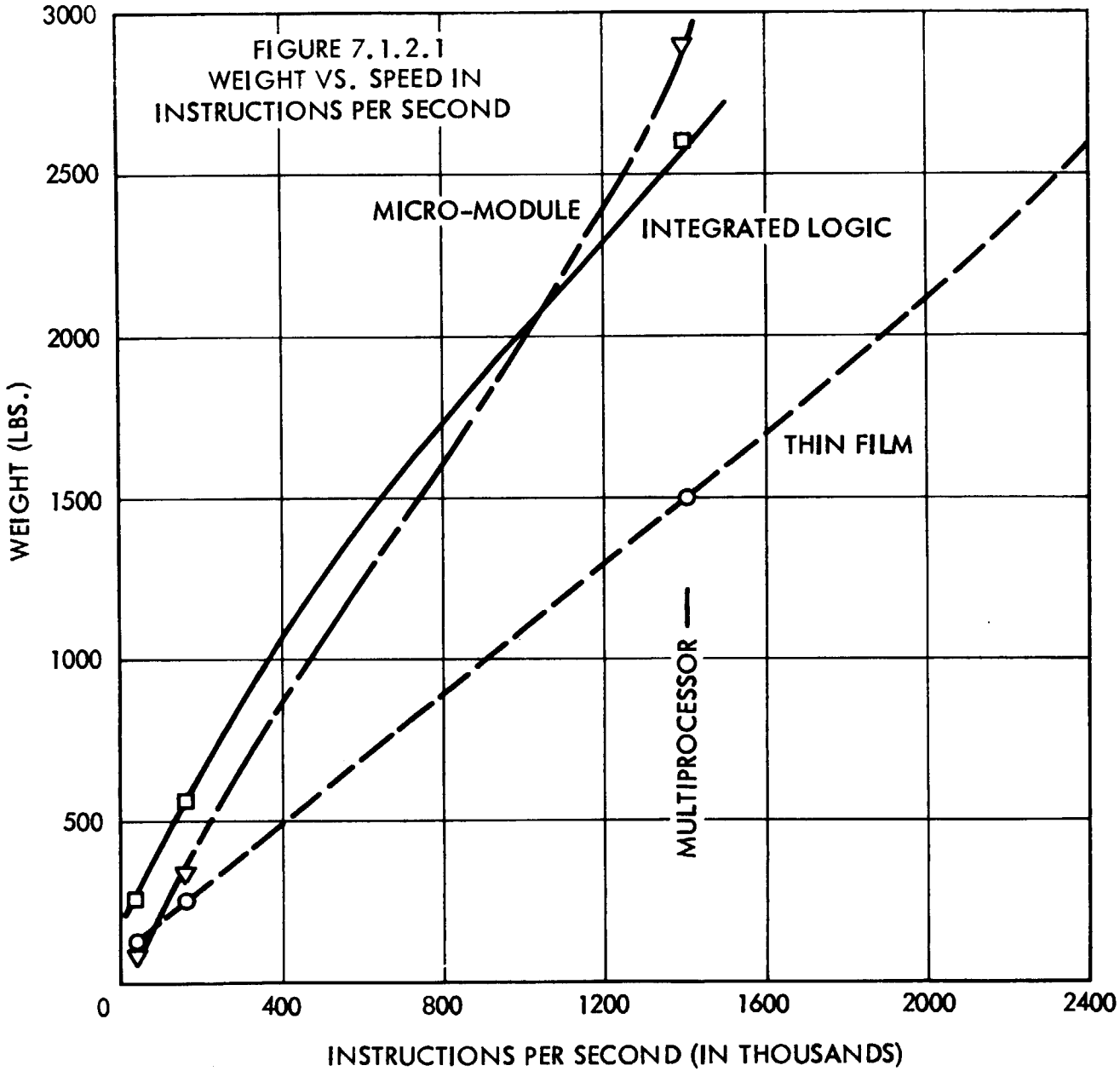
FIGURE 7.1.2.1
WEIGHT VS. SPEED IN
INSTRUCTIONS PER SECOND
MICRO-MODULE
INTEGRATED LOGIC
THIN FILM
MULTIPROCESSOR
WEIGHT (LBS.)
3000
2500
2000
1500
1000
500
0
400
800
1200
1600
2000
2400
INSTRUCTIONS PER SECOND (IN THOUSANDS)

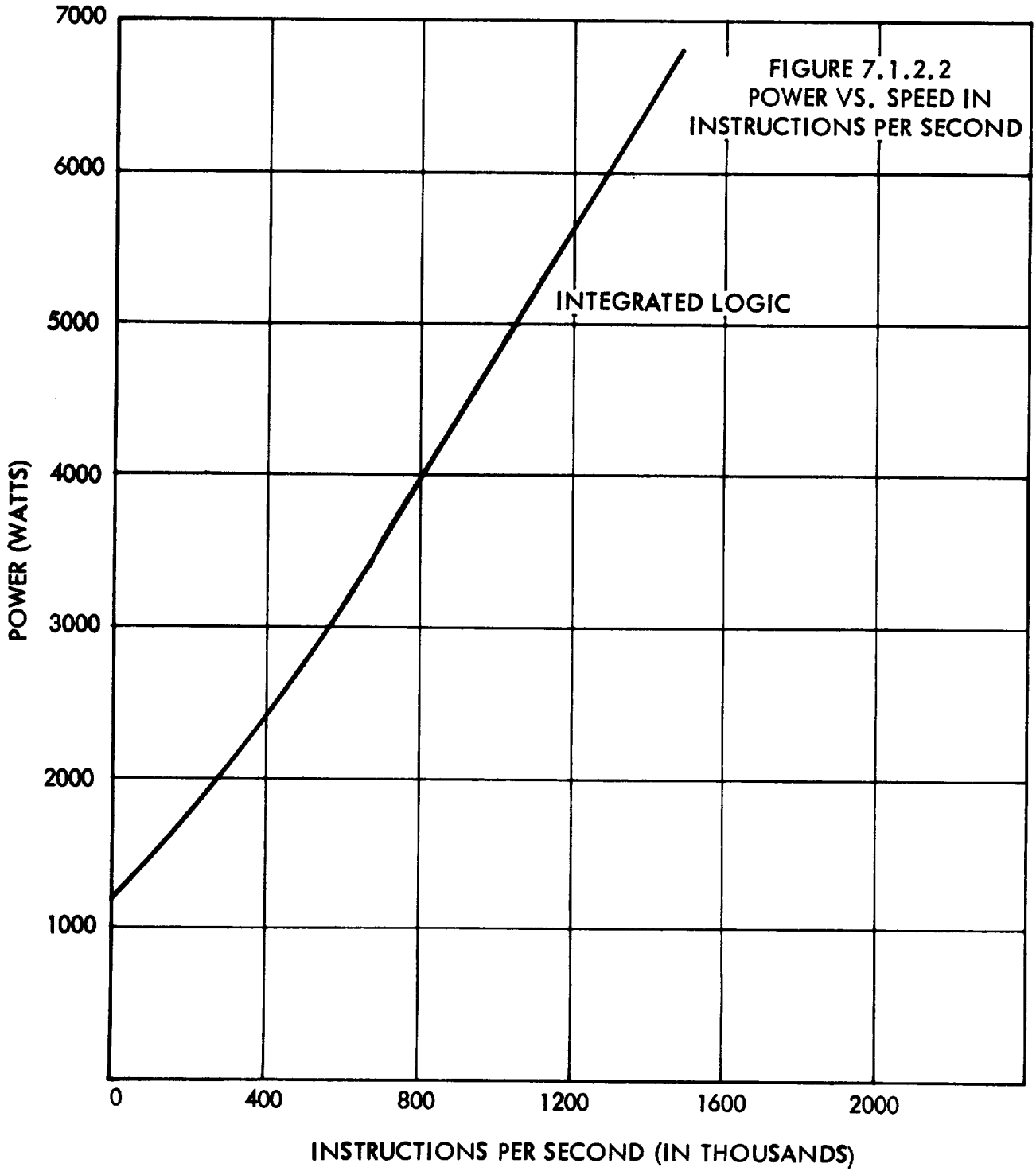
FIGURE 7.1.2.2
POWER VS. SPEED IN
INSTRUCTIONS PER SECOND
INTEGRATED LOGIC
POWER (WATTS)
7000
6000
5000
4000
3000
2000
1000
0
400
800
1200
1600
2000
INSTRUCTIONS PER SECOND (IN THOUSANDS)

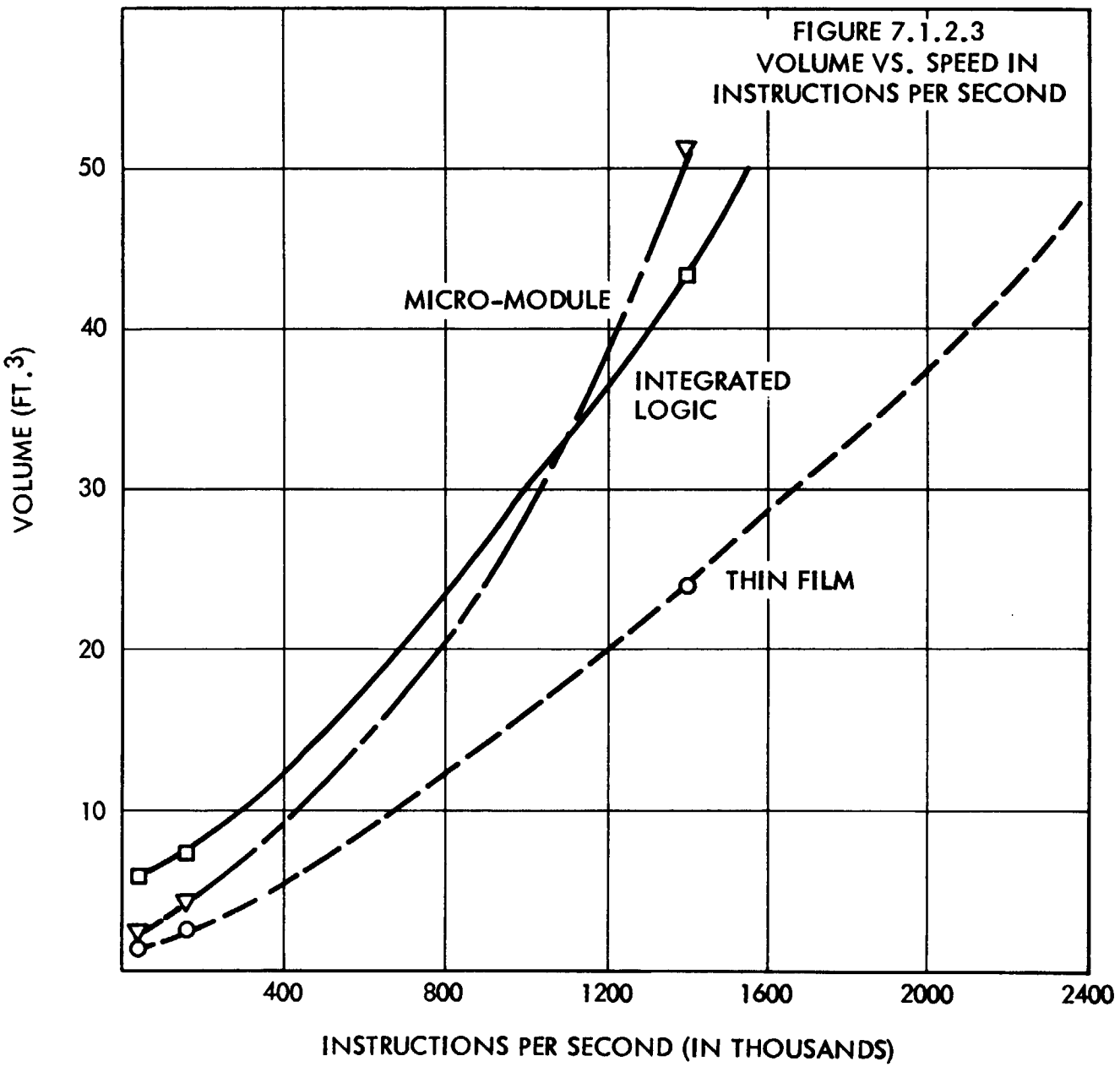
FIGURE 7.1.2.3
VOLUME VS. SPEED IN
INSTRUCTIONS PER SECOND
MICRO-MODULE
INTEGRATED
LOGIC
THIN FILM
VOLUME (FT.3)
50
40
30
20
10
400
800
1200
1600
2000
2400
INSTRUCTIONS PER SECOND (IN THOUSANDS)

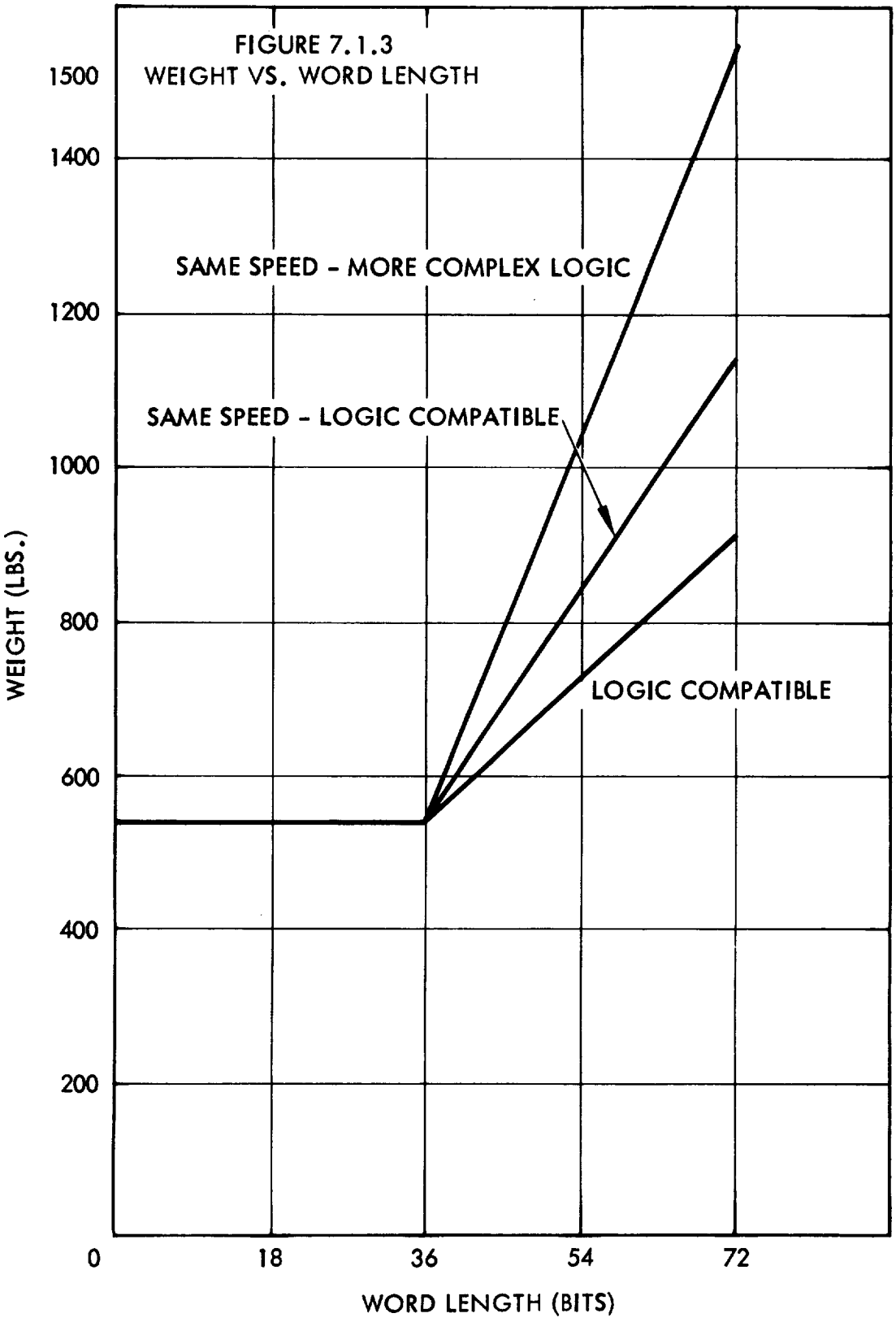
FIGURE 7.1.3
WEIGHT VS. WORD LENGTH
1500
1400
1200
1000
800
600
400
200
0
18
36
54
72
WEIGHT (LBS.)
WORD LENGTH (BITS)
SAME SPEED - MORE COMPLEX LOGIC
SAME SPEED - LOGIC COMPATIBLE
LOGIC COMPATIBLE

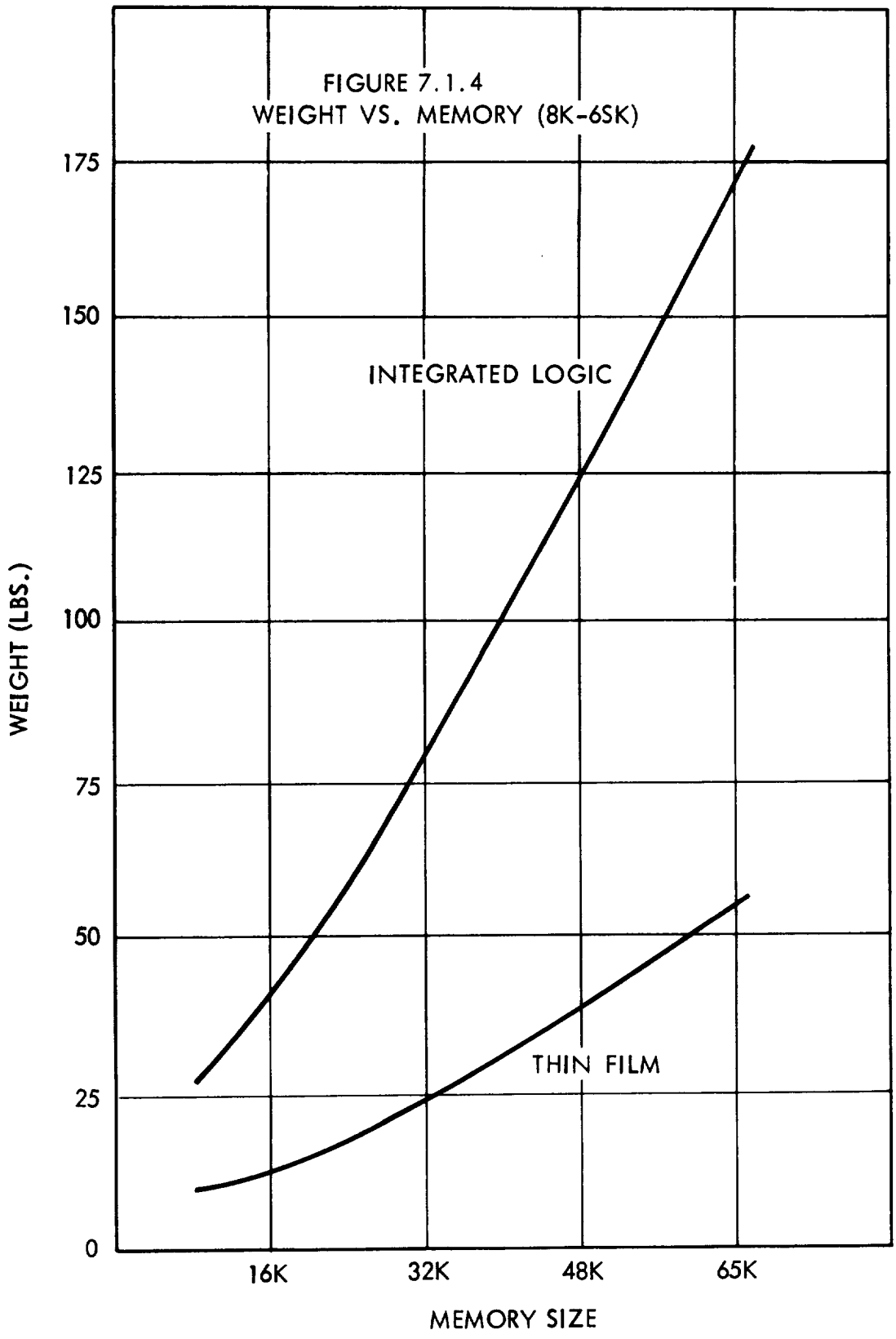
FIGURE 7.1.4
WEIGHT VS. MEMORY (8K-6SK)
175
150
125
100
75
50
25
0
WEIGHT (LBS.)
INTEGRATED LOGIC
THIN FILM
16K
32K
48K
65K
MEMORY SIZE

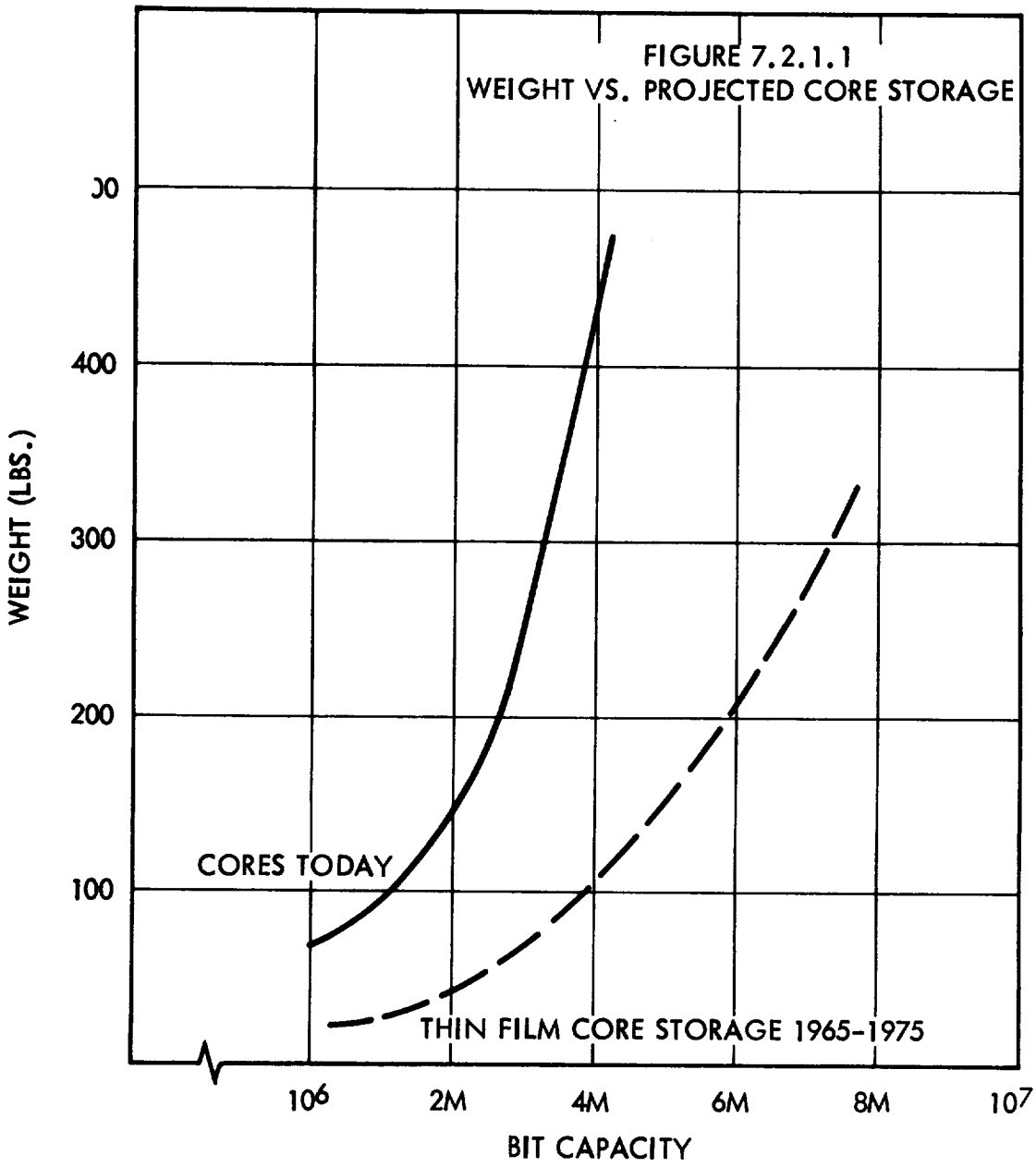
FIGURE 7.2.1.1
WEIGHT VS. PROJECTED CORE STORAGE
500
400
300
200
100
WEIGHT (LBS.)
CORES TODAY
THIN FILM CORE STORAGE 1965-1975
10^6
2M
4M
6M
8M
10^7
BIT CAPACITY

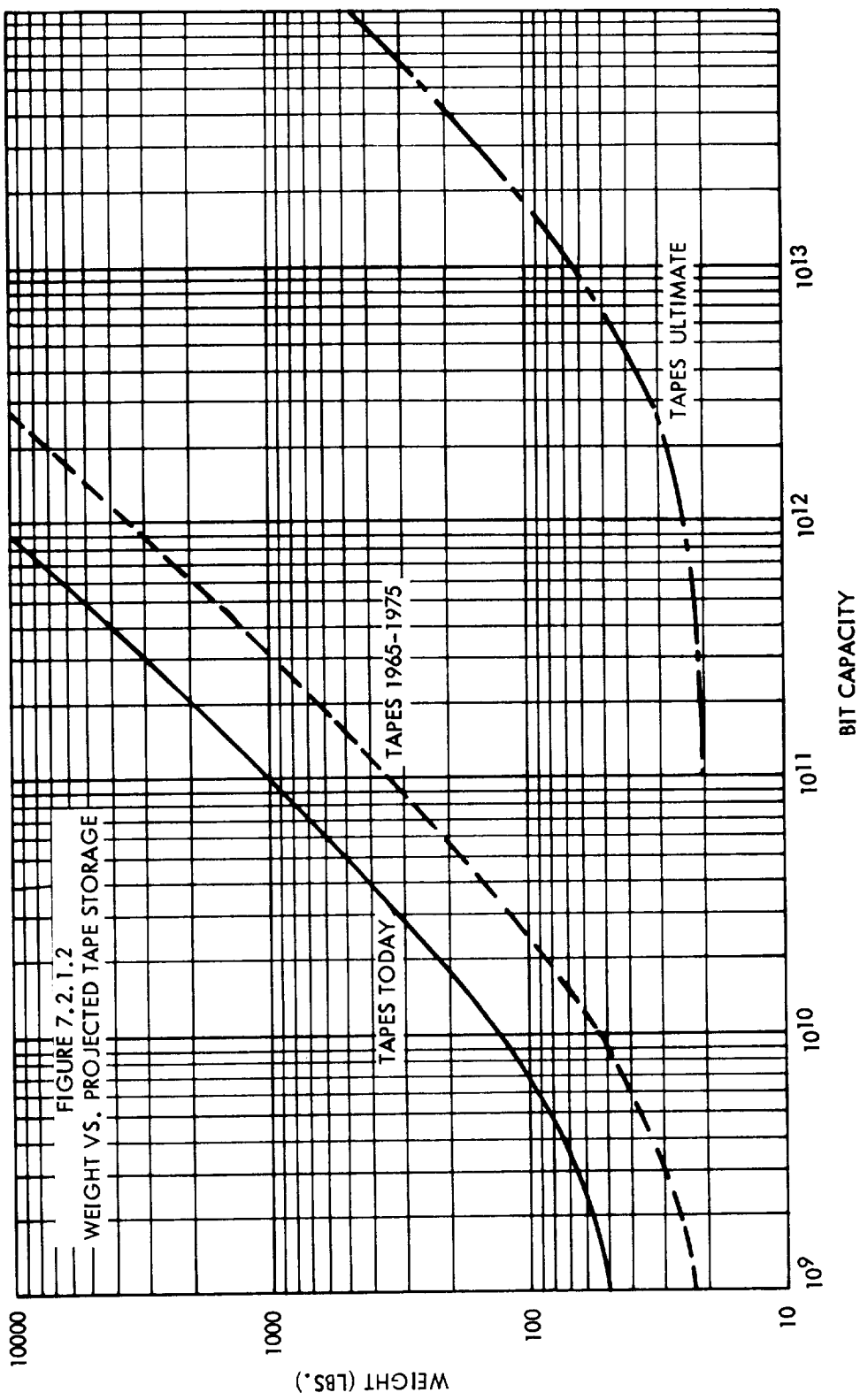
FIGURE 7.2.1.2
WEIGHT VS. PROJECTED TAPE STORAGE
TAPES TODAY
TAPES 1965-1975
TAPES ULTIMATE
WEIGHT (LBS.)
10000
1000
100
10
10^9
10^{10}
10^{11}
10^{12}
10^{13}
BIT CAPACITY

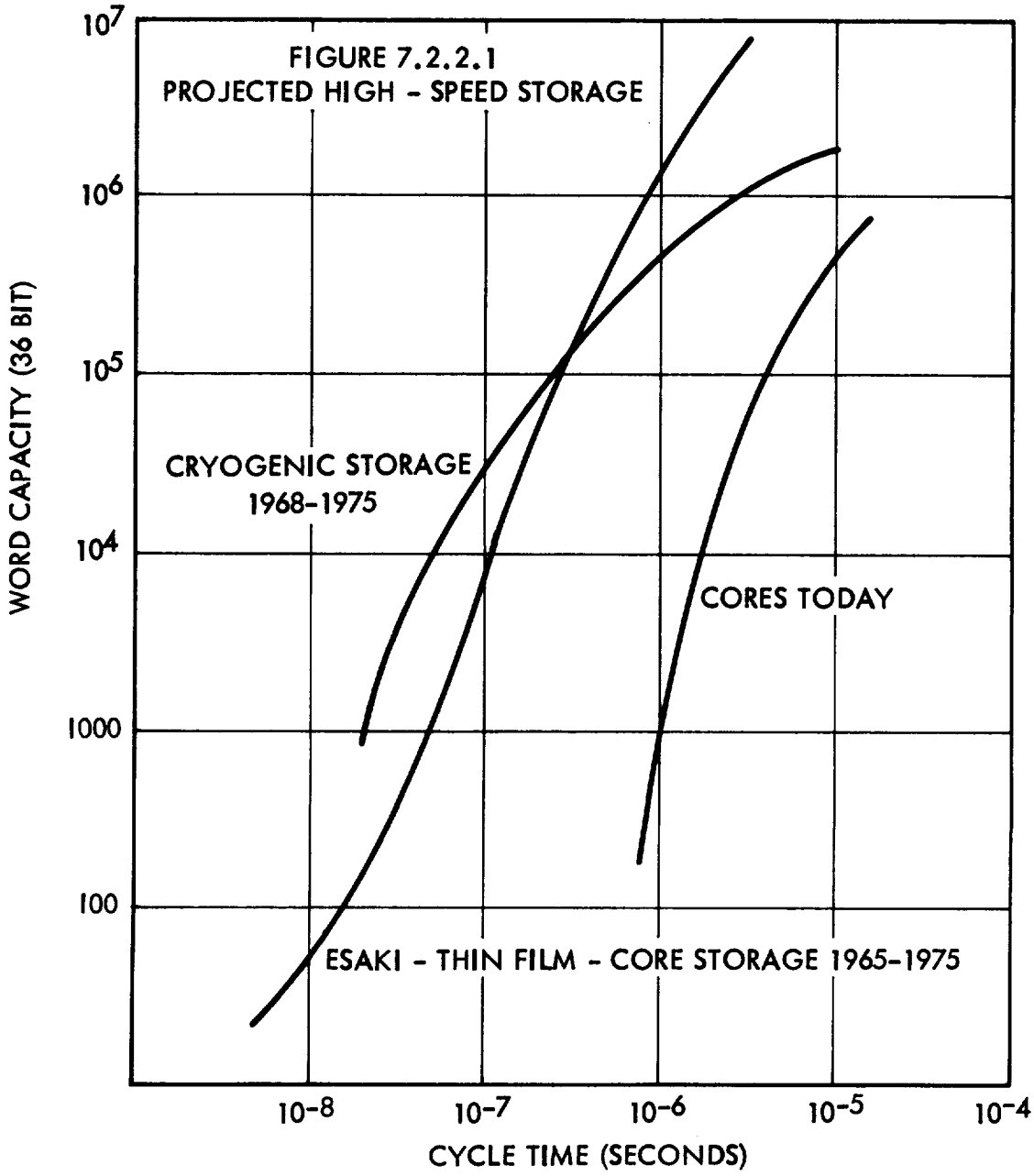
FIGURE 7.2.2.1
PROJECTED HIGH - SPEED STORAGE
WORD CAPACITY (36 BIT)
10^7
10^6
10^5
10^4
1000
100
CRYOGENIC STORAGE
1968-1975
CORES TODAY
ESAKI - THIN FILM - CORE STORAGE 1965-1975
10^{-8}
10^{-7}
10^{-6}
10^{-5}
10^{-4}
CYCLE TIME (SECONDS)

FIGURE 7.2.2.2
PROJECTED HIGH - SPEED STORAGE

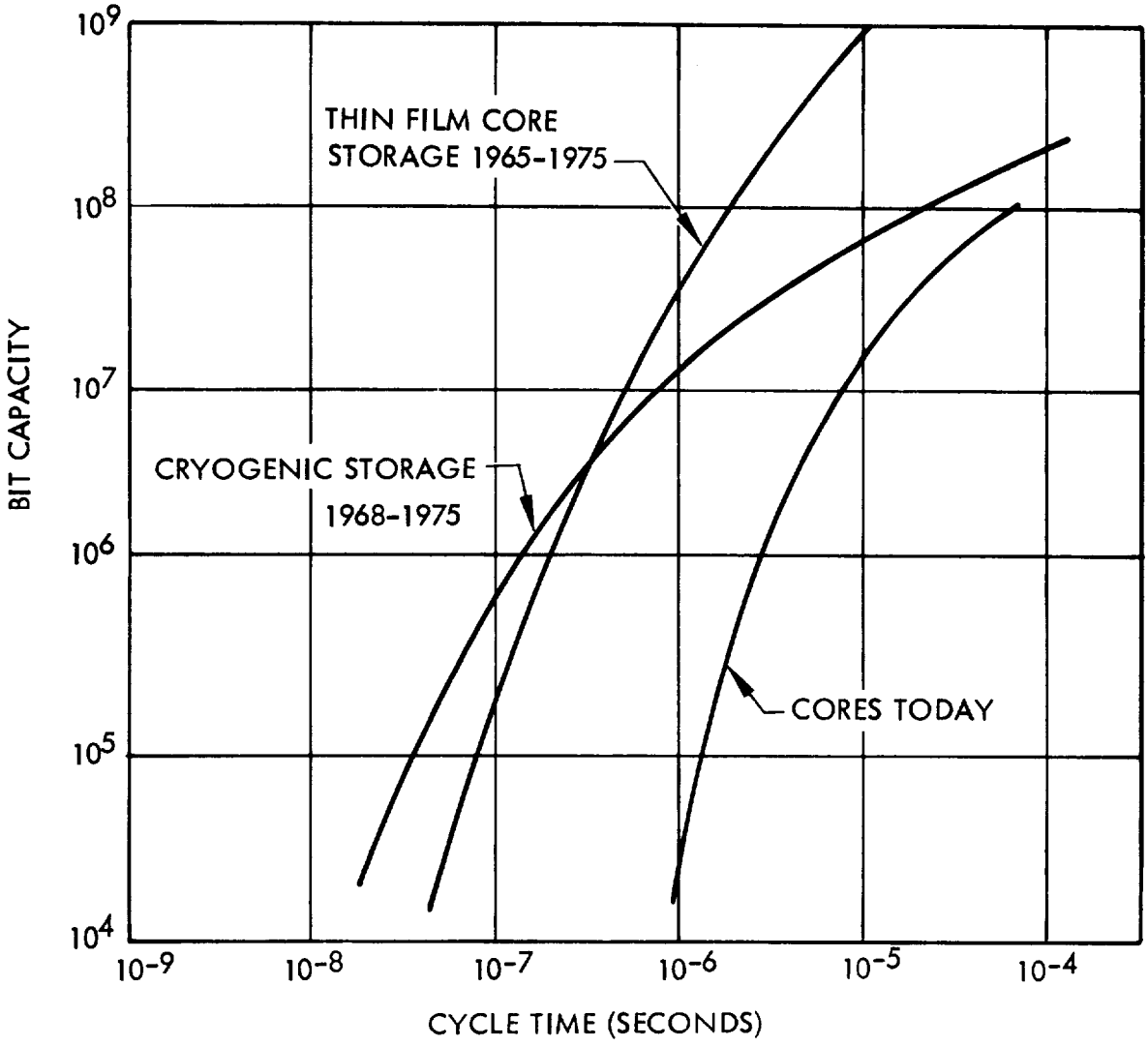

FIGURE 7.2.2.3
PROJECTED MECHANICAL STORAGE

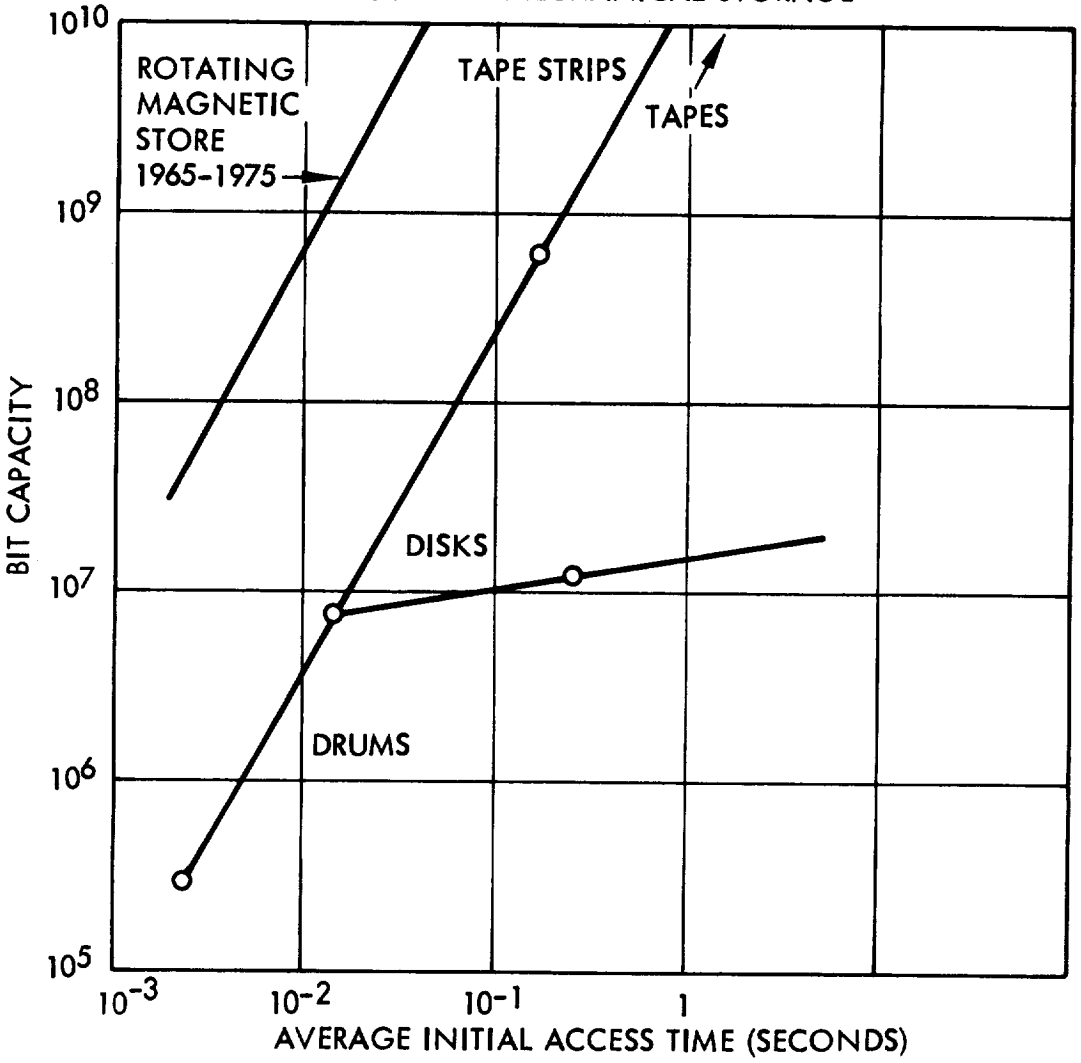

ERRATA

p. 1-5/6 4th line from top, change "would have to be fly-by" to "would have to be elliptic, or mission would have to be fly-by".

p. 2-1 4th line from bottom, change "elliptic" to "ecliptic"

p. 6-1 Eq. 6-1 and the paragraph following Eq. 6-1, change all designations "mu" to "u".

p. 6-45 Add to caption of Figure 6-34: "Mission Profile 1975-1".

p. 6-59 Eqs. 6-26 and 6-28: Change γ to J.

p. 6-61 Line 7 from bottom, change "15 radii" to "20 radii".

p. 6-71 Sentence preceding Eq. 6-42, change reference to Figure 6-49 to Figure 6-48.

p. 7-10 The mass ratio symbol "μ" in Eqs. 7-11 and 7-12 should have primes as in Eq. 7-13.

p. 7-11 The 6th line from the top (1st line of new paragraph), "μ ' " should read "μ" and "velocity charge" should read "velocity change".

p. 7-43 Dividing line should be added in Eq. 7-42.

p. 7-44 Eq. 7-43 $\frac{\Delta V^*}{V_\infty^*}$ the term on the left hand side should be in parantheses.

p. 8-60 Change title of Paragraph 8.9.4 to "Thrust Section for Nerva Follow-on Engines".

p. 8-78 Figure 8-39, only the circled points in figure are based on the tank configuration shown in Figure 8-39.

p. 8-85 Figure 8-42, change "Joule-Thompson Value" to "Joule-Thompson Valve".

p. 8-109 Lines 3 and 4 following Table 8-12, change sentences in parantheses to "(i.e. the solar energies varies by a factor of 5)" and "(i.e. solar energies varies by almost a factor of 3.5)".

p. 8-111 Line 12 from bottom, change "reactor" to "collector".

p. 8-112 Figure 8-57 has been turned upsidedown before lettering. A new figure will be supplied. As printed in the report, the figure should be read by turning the report by 180 degrees and by marking the abscissa from $1\text{-}10^2$ and the ordinate from $1\text{-}10^3$ and reversing the designations of r on the curves.

p. 8-117 Figure 8-53, temperatures for the solar-thermoelectric systems are given in degrees Kelvin. The efficiencies of the associated efficiency figures should be designated by the greek letter Eta.

p. 18-14 Table 18-2: Years listed in line on top are fiscal years.

p. 18-26 Table 18-9: Reference to Table 18-8 in FLIGHT TEST OBJECTIVE column should be to Table 18-7 instead.

TABLE OF CONTENTS

APPENDIX: Data Handling System (IBM)

SECTION 19

REFERENCES

2-1 D.O. Muhleman, D.B. Holdridge, and N. Block, The Astronomical Unit Determined by Radar Reflections From Venus, Jet Propulsion Lab, Technical Report 32-221, 8 March 1962.

2-2 Planetary Coordinates For the Years 1960-1980, prepared by H.M. Nautical Almanac Office, William Clower and Sons, Ltd, London, 1958.

2-3 K.A. Ehricke, Space Flight, Vol II, "Dynamics" p980, p1045, D. Van Nostrand Co., Inc., Princeton, N.J., 1962

3-1 K.A. Ehricke, Space Flight, Vol I, "Environment and Celestial Mechanics," pp113-259, Van Nostrand, 1960.

3-2 Gerard P. Kuiper, editor, The Atmospheres of the Earth and the Planets, second edition, pp306-405, "Planetary Atmospheres and Their Origin," University of Chicago Press, 1952.

3-3 Gerard P. Kuiper and Barbara M. Middlehurst, editors, The Solar System, Vol 3, "Planets and Satellites," University of Chicago Press, 1952.

3-4 Harold C. Urey, The Planets, Their Origin and Development, Yale University Press, 1952.

3-5 Harold C. Urey, Science in Space, pp199-217, "The Planets," McGraw-Hill, 1961.

3-6 Patrick Moore, A Guide to the Planets, revised edition, Norton, 1960.

3-7 Seymour L. Hess, Advances in Space Science and Technology, Vol 3, pp151-193, "Mars as an Astronautical Objective," Academic Press, 1961.

3-8 Patrick Moore, A Guide to Mars, second edition, Macmillan, 1958.

3-9 Gerard de Vaucouburs, Physics of the Planet Mars, Faber and Faber, 1954.

3-10 Earl C. Slipher, The Photographic Story of Mars, Northland Press, Flagstaff, 1962.

3-11 Carl Sagan, The Planet Venus, Science Vol 133, p849-858, 24 March 1961.

3-12 Patrick Moore, The Planet Venus, second edition, Macmillan, 1959.

3-13 D.O. Muhleman, D.B. Holdridge, and N. Block, The Astronomical Unit Determined by Radar Reflections from Venus, Astronomy Journal, Vol 67, pp191-203, May 1962.

3-14 G.H. Pettengill, H.W. Briscoe, J.V. Evans, E. Gehrels, G.M. Hyde, L.G. Kraft, R. Price, and W.B. Smith, A Radar Investigation of Venus, Astronomy Journal, Vol 67, pp181-190, May 1962.

3-15 William W. Kellogg and Carl Sagan, The Atmospheres of Mars and Venus, National Academy of Sciences - National Research Council, Publication No. 944, 1961.

3-16 Joseph W. Chamberlain, Upper Atmospheres of the Planets, Astrophysics Journal, Vol 136, pp582-593, September 1962.

3-17 Gerhard F. Schilling, Limiting Model Atmospheres of Mars, Rand Report No. R-402-JPL, August 1962.

3-18 Handbook of Geophysics, United States Air Force, revised edition, Macmillan, 1960.

3-19 Hubertus Strughold and Oskar L. Ritter, Solar Irradiance from Mercury to Pluto, USAF Aerospace Medical Center (ATC) , School of Aviation Medicine, Brooks Air Force Base, Texas, Report No. 60-39, February 1960.

3-20 Michael H. Briggs and John P. Rivill, The Chemistry of Mars. Part II. "The Surface," J. Brit. Interplanetary Soc, Vol 17, pp459-461, November-December 1960.

3-21 William M. Sinton, Further Evidence of Vegetation on Mars, Science, Vol 130, pp1234-1237, 6 November 1959.

3-22 Harold C. Urey, The Atmospheres of the Planets, Handbuchder Physik, Vol 52, pp364-418, Springer-Verlag, 1959.

3-23 Harold C. Urey and A.W. Brewer, Fluorescence in Planetary Atmospheres, Proc. Roy. Soc., Vol A241, pp37-43, 23 July 1957.

3-24 Carl Sagan, Is the Martian Blue Haze Produced by Solar Protons? Icarus, Vol 1, pp70-74, May 1962.

3-25 Hyron Spinrad, Spectroscopic Temperature and Pressure Measurements in the Venus Atmosphere, Publ. Astronom. Soc. Pac., Vol 74, pp187-201, June 1962.

3-26 N.A. Kozyrev, Izv. Krym. Astr. Obsv., Vol 12, p169, 1954.

3-27 Gerard P. Kuiper, The Threshold of Space, "The Atmosphere and the Cloud Layer of Venus," Pergamon Press, 1957.

3-28 Gordon Newkirk, Jr., The Airglow of Venus, Planet. Space Sci., Vol 1, pp32-36, January 1959.

3-29 J.L. Weinberg and Gordon Newkirk, Jr., Airglow of Venus: A Re-examination, Planet. Space Sci., Vol 5, pp163-164, June 1961.

3-30 B. Warner, The Emission Spectrum of the Night Side of Venus, Monthly Not. Roy. Astronom. Soc., Vol 121, pp279-283, October 1960.

3-31 Carl Sagan, Structure of the Lower Atmosphere of Venus, Icarus, Vol 1, pp151-169, September 1962.

3-32 Hyron Spinrad, A Search for Water Vapor and Trace Constituents in the Venus Atmosphere, Icarus, Vol 1, pp266-270, October 1962.

3-33 Carl Sagan, The Radiation Balance of Venus, Jet Propulsion Laboratory, Technical Report No. 32-34, 15 September 1960.

3-34 Georg Joos, Theoretical Physics, second edition, Blackie, 1951.

3-35 Donald H. Robey, A Rocket Borne Video Telescope for Observing Mars, Astronautica Acta, Vol 5, pp313-327, 1959.

4-1 E.N. Parker, Kinetic Properties of Interplanetary Matter, Planet, Sci., Vol 9, pp461-475, 1962.

4-2 D.E. Billings, IAU Symposium No. 16, Cloudcraft, New Mexico, USA, August 1961.

4-3 H. Bachman, Z. Astrophys., Vol 44, No. 1, p56, 1957.

4-4 P.J. Coleman, Jr. and coworkers, Interplanetary Magnetic Fields, Science, Vol 138, p1095, 7 December 1962.

4-5 M. Neugebauer, W. Snyder Conway, Solar Plasma Experiment, Science, Vol 138, p1099, 7 December 1962.

4-6 G.E. Moreton, New Observations of Flare-Initiated Solar Atmosphere Disturbances, Lockheed Solar Observatory, Lockheed Aircraft Corporation, Burbank, California.

4-7 E.N. Parker, Acceleration of Cosmic Rays in Solar Flares, Phys. Rev., Vol 107, No. 3, pp830-836, 1957.

4-8 Herbert Friedman, Variations of Solar Emission, Ultraviolet and X-ray Regions of the Spectrum, Paper No. 1443-60, 15th Annual ARS Meeting, Washington, D.C., 1960.

4-9 E.N. Parker, Our Present Knowledge of Interplanetary Conditions, SAE-AFSOR Astronautic Symposium, 12-14 October 1960.

4-10 Constance Warwick, National Bureau of Standards List of IGY Flares With Normalized Values of Importance and Area, IGY Solar Activity Report Series, Number 17, Boulder, Colorado, 1 May 1962.

4-11 Solar-Geophysical Data, Part B, CRPL-F 186, NBS Central Propagation Laboratory, Boulder, Colorado, 29 February 1960.

4-12 C.M. Minnus, An Estimate of the Peak Sunspot Number in 1968, J. Atm. Terr. Phys., Vol 20, pp94-99, 1961.

4-13 Constance Warwick and Marion Wood Haurwitz, A Study of Solar Activity Associated with Polar-Cap Absorption, J. Geophys. Research, Vol 67, No. 4, p1317, 1962.

4-14 Private communication from D.K. Bailey of the NBS, Boulder, Colorado.

4-15 D.H. Robey, Radiation Shielding Requirements for Two Large Solar Flares, Astronautica Acta, Vol VI, No. 4, pp206-224, 1960.

4-16 Shielding Problems in Manned Space Vehicles, Annual Report - 1960, Lockheed Nuclear Products, Marietta, Georgia, NR-140, September 1961.

4-17 A Study of Space Radiation Shielding Problems for Manned Vehicles, General Dynamics/Fort Worth, Texas, FZK-144, 8 June 1962.

4-18 James A. Earl, Cloud Chamber Observations of Primary Cosmic Ray Electrons, Phys. Rev. Letters, Vol 6, No. 3, p125, 1961.

4-19 Peter Meyer, and R. Vogt, The Primary Cosmic Ray Electron Flux during a Forbush-Type Decrease, J. Geophys. Res., Vol 66, No. 11, p3950, 1961.

4-20 Peter Meyer, and R. Vogt, Electrons in the Primary Cosmic Radiation, Phys. Rev. Letters, Vol 6, No. 4, p193, 1961.

4-21 W.R. Webber, Progress in Elementary Particle and Cosmic Ray Physics, Vol 6, "Time Variations of Low Rigidity Cosmic Rays During the Recent Sunspot Cycle," 1961.

4-22 E.L. Fireman, Distribution of Helium-3 in the Carbo Meteorite, Nature, Vol 181, p1725, 1958.

4-23 J.R. Winckler, Primary Cosmic Rays, Rad. Research, Vol 14, p521, 1961.

4-24 E.N. Parker, The Hydrodynamic Theory of Solar Corpuscular Radiation and Stellar Winds, Astrophys. J., Vol 132, p821, 1960.

4-25 Scott E. Forbush, Cosmic-Ray Intensity Variations During Two Solar Cycles, J. Geophys. Research, Vol 63, -651, 1958.

4-26 L. Woltjer, Hydromagnetic Equilibrium and Cosmic Magnetic Fields, Leiden University Observatory, 1959.

4-27 R.E. Carter and N.P. Knowlton, Jr., Hematological Changes in Humans Exposed to Low-Level Gamma Radiations, LA 1092, 1950.

13	Supporting Space Research Program	64 - 72	July 63 - Dec. 71
	Near-Earth Micro-Meteoroid research		Jan. 64 - Dec. 65
	Cis-Martian Meteoroid probes		July 64 - Dec. 66
	Cis-Venusian Meteoroid probes		July 64 - Dec. 66
	Mariner launches		
	Voyager launches		

Table 18-2. EMPIRE Program Development Cost Plan No. 1 (Billions of Dollars)

No.			Dev.	Prod.	Oper.	Total	63	64	65	66	67	68	69	70	71	72	73	74	75
1	Preparatory Studies (Industry)		.006			.006		.002	.003	.001									
2	Supporting Studies and Research					.560		.002	.003	.020	.050	.100	.100	.100	.100	.050	.020	.010	.005
3	Ecological System	Dev.	.660			.845		.006	.030	.100	.300	.130	.035	.025	.015	.015	.004		
		Prod.		.185								.070	.015	.015	.015	.015	.020	.035	
4	Earth Entry Module	Dev.	.101						.006	.010	.020	.030	.020	.010	.010				
	and Abort System	Prod.		.232		.470					.023	.014	.020	.030	.030	.030	.015	.060	.010
		Oper.			.137						.068	.045	.002	.003	.003	.003	.002	.010	.001
5	Crew Modules	Dev.	.315							.010	.100	.100	.041	.022	.012	.010	.010	.010	
	(incl. Command Module)	Prod.		.062		.850						.018	.008	.018	.018				
		Oper.			.473							.183	.132	.146	.007	.005			
6	Nuclear or Solar	Dev.	.059					.001	.004	.010	.020	.015	.006	.002	.0003	.0003	.0003	.0001	
	Electrical Power	Prod.		.170		.239						.020	.025	.025	.025	.025	.025	.020	.005
	Generator System	Oper.			.010														
7	Data Handling System					.500		.001	.002	.010	.040	.060	.100	.100	.050	.050	.050	.035	.002
8	Crew Training					.0870							.0025	.0175	.0174	.0174	.0174	.0124	.0024
9	Convoy Vehicle Propulsion																		
	Sections	Total				4.3415													
9.1	M-4 Propulsion Unit	Dev.	.100					.001	.005	.020	.020	.025	.020	.009					
	(hi-p_c O_2/H_2)	Prod.		.035		.1042							.0005	.0005	.0005	.0005	.0005	.0005	.0005
		Oper.			.0007								.0001	.0001	.0001	.0001	.0001	.0001	.0001
9.2	M-4 Structure and Tests	Dev.	.115						.015	.025	.030	.020	.015	.010					
	Structure/GSE	Prod.		.0473		.4113						.01155	.0055	.0055	.00275	.0055	.0055	.0110	
		Oper.			.043							.001	.0005	.0005	.0003	.0005	.0005	.001	
	Test Program					.206					.010	.030	.050	.050	.040	.026			
	M-4 Total					.7215													
9.3	M-3 Propulsion Section:																		
	Structure/GSE					.160			.010	.015	.030	.050	.040	.015					
	Advanced NERVA Development					.330			.006	.010	.050	.100	.060	.050	.020	.014	.010	.010	
	Flight Test Program					.700								.210	.220	.220	.150		
	M-3 Total Development					1.190													
9.4	M-2 Propulsion Section																		
	Structure/GSE					.170			.006	.020	.030	.030	.040	.030	.010	.004			
	200 k engine					.400			.040	.050	.080	.100	.070	.040	.020				
	Flight Test Program					.620									.110	.220	.220	.070	
	M-2 Total Development					1.190													

Table 18-2. EMPIRE Program Development Cost Plan No. 1 (Billions of Dollars) (Continued)

No.		Dev.	Prod.	Oper.	Total	63	64	65	66	67	68	69	70	71	72	73	74	75
9.5	M-1 Propulsion Section																	
	Structure/GSE				.247			.006	.010	.010	.020	.040	.060	.060	.030	.010	.001	
	200 k Engine Cluster				.200						.030	.050	.070	.030	.010	.008	.002	
	Flight Test Program				.793									.100	.100	.400	.193	
	M-1 Total Development				1.240													
10	Facilities and GSE																	
10.1	Tooling (Convoy and Auxiliary Vehicles incl. propulsion systems)				.100			.001	.030	.050	.019							
10.2	Launch Facilities				1.0						.200	.300	.400	.100				
10.3	Mississippi Test Site				.600					.100	.200	.200	.100					
10.4	Nevada Test Site				.100			.005	.015	.040	.040							
10.5	Convoy Vehicle Assembly and Checkout Facility (AMR)				.100					.020	.060	.020						
10.6	Auxiliary Vehicle Assembly and Checkout Facility (AMR)				.100						.020	.060	.020					
10.7	Orbital Assembly and Launch Operations				1.0							.100	.100	.150	.200	.200	.200	.05
10.8	World-Wide Tracking Net				.30					.050	.100	.150						
10.9	Deep Space Instrument Facility				.20							.040	.050	.050	.050	.010		
11	Post-Saturn				4.0	.001	.005	.010	.100	.300	.500	.500	.600	.700	.600	.450	.200	.034
	SUB-TOTAL I (rounded out)				15.4	.001	.018	.152	.456	1.441	2.341	2.227	2.514	1.911	1.701	1.628	.881	.110
12	Mars Excursion Vehicle																	
	Ground/Structure/LSS/GSE				.402	.001	.001	.010	.020	.050	.100	.100	.050	.020	.020	.020	.010	
	Propulsion				.070		.005	.008	.020	.017	.015	.003	.002					
	Flight Test Program				.200					.010	.020	.030	.050	.050	.040			
	Scientific Payload				.100			.010	.010	.015	.020	.030	.010	.005				
	Total				.772													
13	Lander																	
	Structure/Guidance/GSE				.100					.005	.010	.020	.030	.020	.015			
	Propulsion				.050					.001	.005	.010	.020	.010	.004			
	Flight Test Program				.100								.005	.050	.045			
	Total				.250													

Table 18-2. EMPIRE Program Development Cost Plan No. 1 (Billions of Dollars) (Continued)

No.		Dev.	Prod.	Oper.	Total	63	64	65	66	67	68	69	70	71	72	73	74	75
14	Mapper				.200			.010	.020	.030	.040	.050	.030	.015	.005			
15	Marens, Floater, Phopro, Deipro				.300				.010	.030	.040	.050	.060	.070	.030	.010		
16	Service Module				.100							.005	.010	.040	.020	.010		
	SUB-TOTAL II				1.622	.001	.006	.038	.090	.158	.250	.298	.267	.280	.179	.040	.010	
	SUB-TOTAL III = I + II				17.022	.002	.024	.190	.546	1.599	2.591	2.525	2.781	2.191	1.880	1.668	.891	.110
	Convoy mission launch cost:																	
	Hardware				1.53										.500	.500	.300	.230
	Fuel transportation into orbit				.195													.195
	Hardware transportation into orbit				.110													.110
	1 Spare LSS transported into orbit (0.030 + 0.080)				.110													.110
	Total				1.517													
	GRAND TOTAL				18.539	.002	.024	.190	.546	1.599	2.591	2.525	2.718	2.191	2.380	2.168	1.191	0.755

Table 18-3. Cost Data of Key Subsystems of the Convoy Vehicle
(Billions (B) of Dollars)

ITEM	PROCUREMENT	MAINTENANCE & SPARES
Earth Entry Module (EEM) & Abort System (sensors and separation mechanism; in the graphite ships, the chemical M-4 propulsion system is used for abort)	.010/unit fully equipped (available FY-69) . .005/unit partly equipped	Spares cost assumed to be 50% of cost of capsules procured per annum, except for mission use (FY 74 and 75)
Ecological Life Support System	.010/unit (beginning FY-68) Procurement cost for lunar base not included	.025 B per annum in orbit for FY 69-72. Maintenance costs beyond FY-72 no longer charged to EMPIRE
Crew Modules (without EEM & Abort System and without Ecological system; but incl. Data Handling, Guidance & Communication System, including cost to install the Ecol. System)	.018/complete unit 1 Command Mod. (.012) 2 Utility Mod. (.002) 4 Mission Mod. (.004) Partly equipped Command Module: .006 Command Module (Mod-1) delivery in early FY-69; Mod-2, early FY-70 Mod 3, end of FY-70	Spares cost assumed to be 25% of cost of modules procured per annum, except for mission use
Communication, Data Handling, Vehicle Checkout, Guidance, Celestial Navigation	Included in Command Module Cost	
M-4 Propulsion Section	1st unit: .0038 Av. cost 1st 10 units: .00325	10% Spares
M-3 Propulsion Section	1st unit: .010 Av. cost 1st 10 units: .0086	10% Spares
M-2 Propulsion Section	As M-3	10% Spares
M-1 Propulsion Section	1st unit: .026 Av. cost first 10 units: .023	10% Spares

Table 18-4. Procurement and Maintenance of Ecological System, Earth Entry Module and Abort System and Crew Modules

	FY	TOTAL	67	68	69	70	71	72	73	74	75
Ecological System	Proc.	0.090		0.020	0.010	0.010	0.010	0.010	(0.020)	(0.010)	
	Maint.	0.095		0.050	0.005	0.005	0.005	0.005		(0.025)	
	Total	0.18									
Earth Entry Module	Proc.	0.0895	0.015	0.010	0.010	0.020	0.020	0.020	0.010	(0.040)	0.010
& Abort System	Maint.	0.122	0.008	0.004	0.010	0.010	0.010	0.010	0.050	0.020	
	Total	0.12115									
Crew Modules: Mod 1	Proc.	0.036		0.006	0.006	0.012	0.012				
(Com. Mod partly	Maint.	0.016		0.002	0.002	0.006	0.006				
equipped) plus	Total	0.052									
Utility Modules											
Add 2 Mission Mod.	Proc.	0.006			0.002	0.002	0.002				
(To get Mod-2)	Maint.	0.0015			0.0005	0.0005	0.0005				
	Total	0.0075									
Add 2 Mission Mod	Proc.	0.0006				0.002	0.002	0.002			
(To get Mod-3)	Maint.	0.0015				0.0005	0.0005	0.0005			
	Total	0.0075									
Complete Mod-3	Proc.	0.040		0.010					(0.020)	(0.010)	
	Maint.	0.005		0.0025						(0.0025)	
	Total	0.055									
Communication & Data Handlg. Syst.	Procurement & Maintenance Cost included in Mod-1 and Mod-3 cost										

( ) = for mission use

Table 18-5. Crew Module Flight Test Program and Associated Earth Launch Vehicles

1.	Mid 1968:		
	Mod-1 to space station	(35,000 lb)	ELV: 2 C-1
	EEM – Abort System space sta.	(26,000 lb)	ELV: 1 C-1 (pld. p/f)
2.	Mid 1969:		
	Add two mission modules to space station to get Mod-2	(3400 lb)	ELV: Ti-II
3.	Late 1969:		
	Add two mission modules to space station to get Mod-3	(3400 lb)	ELV: Ti-II
4.	1968:		
	Send spine (or neck) of Convoy Ship to orbit to become part of space station		ELV: Ti-II
5.	For M-4 Flight Tests (1969/71):		
	1 EEM – Abort System	(26,000 lb)	ELV: C-1 (Payload p/f)
6.	For M-3 Flight Tests (1971/72):		
	Command Module	(35,000 lb)	ELV: 2 C-1
7.	For M-2 Flight Tests and M-1 Flight Tests (1971/74):		
	Complete operational LSS		ELV: 3 C-1
	1 Spare		ELV: 3 C-1

Table 18-6. Procurement of Propulsion Section for Convoy Vehicle Flight Test Program

M-4 : 5 + 1 Spare

Direct costs : 1st unit 3.8M[1]
Av. cost of first 10 (86%): 3.25M

Procurement cost of M-4 : 1 x 3.8 + 5 x 3.25 = 20.05M = 0.02005[3]
0.020B

ELV[2] : (5 + 1) C-1 : 0.120B

M-3 : 5 complete M-3 + 1 spare + 1 set of M-3 tanks

Direct costs: 1st unit 10M
Av. cost of first 10 (86%) = 8.6M
1 set of tanks 1M

Procurement cost of M-3 : 1 x 10 + 5 x 8.6 + 1 = 53M = 0.053B

ELV : (11 + 1) C-5 50M = 0.550B

M-2 : 7 + 1 spare = 8

Direct costs: 1st unit 10M
Av. cost of first 10 (86%): 8.6M

Procurement cost of M-2 : 8 · 8.6 = 0.069B 0.07B

ELV : (6 + 1) C-5 50M = 0.350B; 1 Post-Saturn (0.100B)

M-1 : 7 + 1 spare = 8

Direct costs 1st unit 10M (Airframe) + 3.6 · 4.6
(4 Phoebus) = 26.5M = 0.0265B

Av. cost first 10 (86%) = 23M

Procurement cost of M-1 : 8 x 23 = 184M = 0.184B

1 M = Millions (of dollars)

2 ELV = Earth Launch Vehicle

3 B = Billions (of dollars)

Table 18-7. DEVELOPMENT PROGRAM FOR M-4 THROUGH M-1

Phase	Technological Objective	Program Objective
Experimental Design		1. Preliminary Design Verification
Basic Tests	Struct. material selection Insulation material selection Selection of special manufacturing methods Long duration tests at extreme conditions Flight simulator computer program Vacuum tests etc.	2. Firming up Module Configuration 3. Overall Vehicle Systems Integration and Configuration Determination 4. Preliminary Manufacturing Concept Verification
Experimental Tests	Down-scaled model testing Experimental manufacturing Partial airframe structural testing Duct size and configuration testing Fatigue and leakage testing Insulation testing Stage or tank separation testing Transportation testing Weighing system selection tests Antenna configuration testing and selection etc.	5. Preparing Integral Test and Facilities Plan 6. Preparing a GSE Plan 7. Preparing a Tooling and Quality Assurance Plan
Final Design		1. To assure that design approach and component and subsystem selection support operational and performance requirements of module or vehicle. 2. To promote reliability and develop a realistic reliability program for the development.
Component Development Tests	Design Verification: Laboratory testing: Component testing; Small parts structural, vibration, temperature and pressure testing; vacuum testing; parts compatibility testing	

Phase	Technological Objective	Program Objective
Subsystem Qual. Tests	Thrust structure testing; Flow testing; Tanking testing; Corrosion testing; Tank static structural testing; Propellant utilization testing; Pneumatic system testing; H_2-liquefaction unit testing; Flight control system testing; Retro-rocket system testing; Autopilot testing; Telemetry and communication testing; Range safety command testing; data handling systems testing; electrical power unit testing; Centrifuge tests; dynamic structural testing; Interstage compatibility testing; GSE testing.	1. Design Criteria Verification under ambient conditions 2. Overall Vehicle System Compatibility 3. Verification of Reliability and Manufacturing Quality Assurance Procedures 4. Verification of expected Weight and Subsystem Performance
System Qual. Tests	Environmental testing of module or entire vehicle: Vacuum effects Cryogenic effects Nuclear radiation effects Shock, vibration and load effects Electromagnetic interference control Pre-Flight testing: Propulsion Test Vehicle (PTV) Flight Acceptance Firing (FAF) with flight articles Stage integration, payload integration and Combined Systems Test (CST)	1. Design Criteria Verification under simulated environmental conditions. 2. Determination of off-design criteria (safety factors, reliability). 3. Final verification of overall structural integrity, inter-module compatibility. 4. Final verification of GSE Operational capability 5. Verification of flight test readiness of module or vehicle.

Phase	Technological Objective	Program Objective
System Qual. Tests (Continued)	GSE testing (part of environmental and and pre-flight testing)	
Flight Tests	Components or Sub-systems tested on airplanes or missiles (e.g. zero-g or extended orbital component tests). Vehicle or module flight testing	1. Operational integration of ELV and module or vehicle in terms of checkout, pre-launch, launch and separation in parking orbit. 2. Demonstrate engine start in orbit and capability of controlled flight operations. 3. Demonstrate capability of prolonged coasting in orbit (100 days or more) with subsequent launch into a specified mission profile within a specified launch window. 4. Where applicable demonstration of engine restart 5. Demonstrate capability of module or vehicle to communicate and rendezvous with target body in "assembly orbit". 6. Demonstrate interchange of individual LH_2 tanks, LSS modules or entire LSS module systems between two simulated convoy vehicles in orbit, to check out emergency operations during interplanetary transfer.

Phase	Technological Objective	Program Objective
Flight Tests (Continued)		7. Demonstrate orbital fueling a module or attaching small additional tanks of LH_2 to attain higher performance, as might be required in the case of a launch delay on an interplanetary mission.
		8. Demonstrate mating of modules to a larger vehicle (contact between vehicle modules and establishment of interconnections) (Orbit Integration Test)
		9. Demonstrate proper handling of nuclear hazards, especially attitude controlled separation of a "hot" nuclear stage from the rest of the vehicle, following burnout (Combined Flight Test)
		10. Demonstrate emergency shut-off and engine separation of a nuclear engine
		11. Demonstrate overall operational mission readiness by prolonged test flights in cislunar space, lunar capture round trip and translunar flight test mission.

Table 18-8. Convoy Vehicle Development Flight Test Program (Billion $) (Direct Cost)

Test Article	EEM	Crew Modules	M-4	M-3	M-2	M-1	Total
Flight Article Hardware	0.047	0.120	0.020	0.030	0.070	0.184	0.494
Earth Launch Vehicles Overall Launch costs:							
Titan II	0.020	0.016					0.036
Titan III	0.080						0.080
Saturn C-1		0.260	0.120				0.380
Saturn C-5				0.550	0.350		0.900
Post-Saturn					0.100	0.400	0.500
Orbital Engineering Labor ($400/hr)	-	0.040 (8 men/4 yr)	-	0.010 (8 men/1 yr)	0.013 (10 men/1 yr)	0.018 (10 men/1 yr)	0.081
Surface Engineering Labor (incl. aux. personnel) ($25,000/yr = $12.50/hr) (100% overhead included)	0.010 (400 Engr./ 1 yr)	0.010 (400 Engr./ 1 yr)	0.030 (400 Engr./ 3 yr)	0.045 (600 Engr./ 3 yr)	0.030 (600 Engr./ 2 yr)	0.090 (2000 Engr./ 2 yr)	0.205
Propellants (test articles and LH_2 only)(H_2 propellant utilization factor for orbit operations: 4; LH_2 Cost: $0.25/lb) Most of evaporation takes place on Earth. Therefore, no additional transport costs of LH_2 in orbit assumed.			20,000 lb/unit 10 flights 80,000 x 4 = 320,000 lb: 0.00008	200,000 lb/unit 8 flights 1,600,000 x 4 = 6,400,000 lb: 0.0016	300,000 lb/unit 7 flights 2,100,000 x 4 = 8,400,000 lb: 0.00021	700,000 lb/unit 5 flights 3,500,000 x 4 = 14,000,000 lb: 0.0035	0.008
Contingency	0.016	0.110	0.035	0.063	0.055	0.097	0.376
Total Direct Cost	0.173	0.556	0.206	0.700	0.620	0.793	3.048
Total No. of Flights	3 Ballistic 4 Orbital	3 Orbital	10 Orbital & Cislunar	8 Orbital & Cislunar	7 Orbital & Cislunar	5 Orbital & Cislunar	40

Table 18-9. Flight Test Plan for Convoy Vehicle Propulsion Sections
(1975-1 Mission)

GROUP	NO. OF PROGRAMMED FLIGHTS	FLIGHT TEST OBJECTIVE (TABLE 18-8)	M-4 (#1 through #8)	M-3	M-2	M-1
I.	3 Test Flights	1.-4.	#1: C-1+M-4(p/f)	C-5+M-3(p/f) +C-5 tanker	C-5+M-2(p/f) +C-5 tanker	Post-Saturn+M-1(p/f) +Post-Saturn tanker
			#2: C-1+M-4(p/f)	C-5+M-3(p/f) +C-5 tanker	C-5+M-2(p/f) +C-5 tanker	Post-Saturn+M-1(p/f) +Post-Saturn tanker
			#3: C-1+M-4(p/f) +C-1 tanker	C-5+M-3(p/f) +C-5 tanker	C-5+M-2(p/f) +C-5 tanker	Post-Saturn+M-1(p/f) +Post-Saturn tanker
			2 M-4's reusable for 2nd Test Series	2 M-3's reusable for 2nd Test Series	2 M-2's reusable for 2nd Test Series	No M-1 reusable for 2nd Test Series
II.	3 Test Flights	5.-9. or 10.	#4: Orbit M-4 fueled by 1st C-5 tanker	Orbit M-3 fueled by 1st C-5 tanker	Orbit M-2 p. fueled by Post-Saturn tanker	
			#5: Orbit M-4 fueled by 2nd C-5 tanker	Orbit M-3 fueled by 2nd C-5 tanker	Orbit M-2 p. fueled by Post-Saturn tanker	
			#6: Orbit M-4 fueled by 3rd C-5 tanker	Orbit M-3 fueled by 3rd C-5 tanker	Orbit M-2 p. fueled by Post-Saturn tanker	
			1 M-4 reusable	1 M-3 reusable		
			Orbit M-4 fueled by C-1 tanker	Orbit M-3 fueled by C-5 tanker		
III.	2 Operational Test Flights	11.	#7: C-5+LSS+LH_2 C-5+SM+LH_2	C-5+M-3(f)+M-4(p/f) C-5+M-3(f)+M-4(p/f)		Post-Saturn+M-2(f)+M-1(p/f) Post-Saturn+M-2(f)+M-1(p/f)
				1 Post-Saturn Tanker		
			No jettisoning of LSS, M-4 and M-3 engine (only tanks). M-2 and M-1 jett.			
			#8: C-5+M-3(f)	Post-Saturn+M-2(f)+M-1(p/f) Post-Saturn Tanker (fuels M-1, M-4)		

p. fueled = partly fueled
p/f = partly fueled
f = fully fueled
jett. = jettisoned

Table 18-10. Cost of Convoy Vehicles and Their Principal Payload (All stages powered by graphite reactor engines except 17-4 which uses hi-p_c O_2/H_2)

1. Crew Ship

Life Support System (Crew Modules)	0.030
Earth Entry Module & Abort System	0.010
M-4	0.00325
M-3	0.0086
M-2	0.0086
M-1	0.1840
Total	0.24445 ≈ 0.245B

2. Service Ship

Service Module			0.226
2 MEV's	@ 0.030B	= 0.060B	
4 Landers	@ 0.020B	= 0.080	
1 Mapper	@ 0.020B	= 0.020	
3 Marens	@ 0.010B	= 0.030	
5 Floaters	@ 0.004B	= 0.020	
1 Phopro	@ 0.008B	= 0.008	
1 Deipro	@ 0.008B	= 0.008	
Earth Entry Module & Abort System (Spare)			0.010
M-4			0.00325
M-3			0.00860
M-2			0.00860
M-1			0.1840
Total			0.4404 ≈ 0.440B

Weightwise the crew and service vehicle are comparable:

	Cost
Hardware weight	366,000 lb @ $ 80/lb = 0.029B
LH_2	2,070,000 lb @ $ 80/lb = 0.065B
1 single LSS (0.030B)	100,000 lb @ $ 80/lb = 0.008B

Above costs is assumed to comprise orbit transportation, mating and orbital launching.

Thus, 1 crew ship: 0.245 + 0.029 + 0.065 = 0.339B
1 service ship: 0.440 + 0.029 + 0.065 = 0.534B

Assembly of 3 ships in orbit plus transportation of 1 spare LSS into orbit. Total procurement and launch operation cost:

1 crew ship	0.339B
2 service ships	1.068
1 spare LSS (0.030 + 0.080)	0.110
	1.517B

Table 18-11. Earth Launch Vehicle Cost Data
(in Billions (B) of Dollars)

Titan II		$ 0.004 B/launch
Titan IV		$ 0.020 B/launch
Saturn C-1		$ 0.020 B/launch
Saturn C-5	Total cost effectiveness:	$ 0.050 B/launch
	$ 200/lb payload in orbit	
	Total payload in orbit: 250,000 lb	
Post-Saturn	Total cost effectiveness:	$ 0.080 B/launch
	$ 80/lb payload in orbit	
	Total payload in orbit: 10^6 lb	

Table 18-12. Procurement of Earth Launch Vehicles (incl. Spares)
(up to, but excluding Mission Launch Preparations)

ELV	PROGRAM	FY 66	67	68	69	70	71	72	73	74
Titan II	EEM (Ballistic)		3							
	Mod-2				1					
	Neck of Convoy									
	Ship to orbit		1							
	Mod-3					1				
Titan III	EEM (Orbital)		2	2						
Saturn C-1	Mod-1		2							
	EEM Abort Syst. for Space Station		1							
	M-4 Tests			1						
	M-3 Tests					2				
	M-2 & M-1 Tests					3	3			
	Operational Tests						1			
Saturn C-5	M-3 Tests					3	3			
	M-2 Tests							3	3	
	M-1 Tests							1		
	Operational Tests								3	3
Post-Saturn								3	2	

	Programmed	Spares	Total
Titan II	6	2	8
Titan III	4	1	5
Saturn C-1	13	3	16
Saturn C-5	18	5	23
Post-Saturn (reusable)	4	1	5

Figure 18-3. Project EMPIRE: Mars Mission 1975-1 Development Schedule Milestones; Chemo-Nuclear (Graphite) Convoy Vehicle